

ΔΕΛΤΙΟ ΤΗΣ ΕΛΛΗΝΙΚΗΣ ΓΕΩΛΟΓΙΚΗΣ ΕΤΑΙΡΙΑΣ
Τόμος XLIII, No 5

BULLETIN OF THE GEOLOGICAL SOCIETY OF GREECE
Volume XLIII, No 5

ΕΙΚΟΝΑ ΕΞΩΦΥΛΛΟΥ - COVER PAGE

Γενική άποψη της γέφυρας Ρίου-Αντιρρίου. Οι πυλώνες της γέφυρας διασκοπήθηκαν γεωφυσικά με χρήση ηχοβολιστή πλευρικής σάρωσης (EG&G 4100P και EG&G 272TD) με σκοπό την αποτύπωση του πυθμένα στην περιοχή του έργου, όσο και των βάθρων των πυλώνων. (Εργαστήριο Θαλάσσιας Γεωλογίας & Φυσικής Ωκεανογραφίας, Πανεπιστήμιο Πατρών. Συλλογή και επεξεργασία: Δ.Χριστοδούλου, Η. Φακίρης).

General view of the Rion-Antirion bridge, from a marine geophysical survey conducted by side scan sonar (EG&G 4100P and EG&G 272TD) in order to map the seafloor at the site of the construction (pylons and piers) (Gallery of the Laboratory of Marine Geology and Physical Oceanography, University of Patras. Data acquisition and Processing: D. Christodoulou, E. Fakiris).

ΔΕΛΤΙΟ ΤΗΣ ΕΛΛΗΝΙΚΗΣ ΓΕΩΛΟΓΙΚΗΣ ΕΤΑΙΡΙΑΣ
Τόμος XLIII, No 5

BULLETIN OF THE GEOLOGICAL SOCIETY OF GREECE
Volume XLIII, No 5

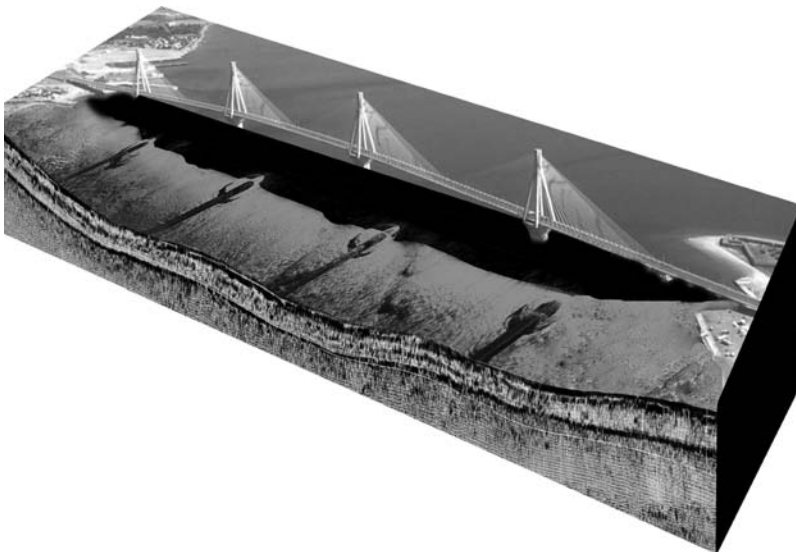


**12ο ΔΙΕΘΝΕΣ ΣΥΝΕΔΡΙΟ
ΤΗΣ ΕΛΛΗΝΙΚΗΣ ΓΕΩΛΟΓΙΚΗΣ ΕΤΑΙΡΙΑΣ**

ΠΛΑΝΗΤΗΣ ΓΗ:
Γεωλογικές Διεργασίες και Βιώσιμη Ανάπτυξη

**12th INTERNATIONAL CONGRESS
OF THE GEOLOGICAL SOCIETY OF GREECE**

PLANET EARTH:
Geological Processes and Sustainable Development



ΠΑΤΡΑ / PATRAS 2010

ISSN 0438-9557

Copyright © από την Ελληνική Γεωλογική Εταιρεία
Copyright © by the Geological Society of Greece

12ο ΔΙΕΘΝΕΣ ΣΥΝΕΔΡΙΟ
ΤΗΣ ΕΛΛΗΝΙΚΗΣ ΓΕΩΛΟΓΙΚΗΣ ΕΤΑΙΡΙΑΣ

ΠΛΑΝΗΤΗΣ ΓΗ:
Γεωλογικές Διεργασίες και Βιώσιμη Ανάπτυξη

Υπό την Αιγίδα του
Υπουργείου Περιβάλλοντος, Ενέργειας και Κλιματικής Αλλαγής

12th INTERNATIONAL CONGRESS
OF THE GEOLOGICAL SOCIETY OF GREECE

PLANET EARTH:
Geological Processes and Sustainable Development

Under the Aegis of the
Ministry of Environment, Energy and Climate Change



ΠΡΑΚΤΙΚΑ / PROCEEDINGS

ΕΠΙΜΕΛΕΙΑ ΕΚΔΟΣΗΣ

Γ. ΚΟΥΚΗΣ

Πανεπιστήμιο Πατρών

Α. ΖΕΛΗΛΙΔΗΣ

Πανεπιστήμιο Πατρών

Ι. ΚΟΥΚΟΥΒΕΛΑΣ

Πανεπιστήμιο Πατρών

Γ. ΠΑΠΑΘΕΟΔΩΡΟΥ

Πανεπιστήμιο Πατρών

Μ. ΓΕΡΑΓΑ

Πανεπιστήμιο Πατρών

Β. ΖΥΓΟΥΡΗ

Πανεπιστήμιο Πατρών

EDITORS

G. KOUKIS

University of Patras

A. ZELILIDIS

University of Patras

I. KOUKOUVELAS

University of Patras

G. PARATHEODOROU

University of Patras

M. GERAGA

University of Patras

V. ZYGOURI

University of Patras

PATRAS, May 2010

ΕΛΛΗΝΙΚΗ ΓΕΩΛΟΓΙΚΗ ΕΤΑΙΡΕΙΑ



ΔΙΟΙΚΗΤΙΚΟ ΣΥΜΒΟΥΛΙΟ

(που εξελέγη στη Γενική Συνέλευση των μελών της Εταιρείας το Μάρτιο του 2010)

ΠΡΟΕΔΡΟΣ

Απόστολος ΑΛΕΞΟΠΟΥΛΟΣ

ΑΝΤΙΠΡΟΕΔΡΟΣ

Αλεξάνδρα ΖΑΜΠΕΤΑΚΗ-ΛΕΚΚΑ

ΓΕΝ. ΓΡΑΜΜΑΤΕΑΣ

Ευγενία ΜΩΡΑΪΤΗ

ΕΙΔ. ΓΡΑΜΜΑΤΕΑΣ

Δημήτριος ΓΑΛΑΝΑΚΗΣ

ΤΑΜΙΑΣ

Ασημίνα ΑΝΤΩΝΑΡΑΚΟΥ

ΕΦΟΡΟΣ

Χαράλαμπος ΚΡΑΝΗΣ

ΜΕΛΗ

Κωνσταντίνος ΒΟΥΔΟΥΡΗΣ

Χρυσάνθη ΙΩΑΚΕΙΜ

Αθανάσιος ΓΚΑΝΑΣ

GEOLOGICAL SOCIETY OF GREECE



BOARD OF DIRECTORS

(elected at the General Assembly of the members of the Society on March 2010)

PRESIDENT

Apostolos ALEXOPOULOS

VICE-PRESIDENT

Alexandra ZAMBETAKIS-LEKKAS

GENERAL SECRETARY

Evgenia MORAITI

EXECUTIVE SECRETARY

Dimitrios GALANAKIS

TREASURER

Asimina ANTONARAKOU

TRUSTEE

Charalambos KRANIS

MEMBERS

Konstantinos VOUDOURIS

Chyssanthi IOAKIM

Athanasios GANAS

ΟΡΓΑΝΩΤΙΚΗ ΕΠΙΤΡΟΠΗ 12ου ΔΙΕΘΝΟΥΣ ΣΥΝΕΔΡΙΟΥ



ΠΡΟΕΔΡΟΣ

Γεώργιος ΚΟΥΚΗΣ, Καθηγητής Πανεπιστημίου Πατρών

ΑΝΤΙΠΡΟΕΔΡΟΣ

Αβραάμ ΖΕΛΗΛΙΔΗΣ, Καθηγητής Πανεπιστημίου Πατρών

ΓΕΝΙΚΟΣ ΓΡΑΜΜΑΤΕΑΣ

Ιωάννης ΚΟΥΚΟΥΒΕΛΑΣ, Αν. Καθηγητής Πανεπιστημίου Πατρών

ΕΙΔΙΚΟΣ ΓΡΑΜΜΑΤΕΑΣ

Γεώργιος ΠΑΠΑΘΕΟΔΩΡΟΥ, Αν. Καθηγητής Πανεπιστημίου Πατρών

ΤΑΜΙΑΣ

Μαρία ΓΕΡΑΓΑ, Λέκτορας Πανεπιστημίου Πατρών

ΜΕΛΗ

Νικόλαος ΚΟΝΤΟΠΟΥΛΟΣ, Καθηγητής Πανεπιστημίου Πατρών

Νικόλαος ΛΑΜΠΡΑΚΗΣ, Καθηγητής Πανεπιστημίου Πατρών

Νικόλαος ΣΑΜΠΑΤΑΚΑΚΗΣ, Αν. Καθηγητής Πανεπιστημίου Πατρών

Ευθύμιος ΣΩΚΟΣ, Επ. Καθηγητής Πανεπιστημίου Πατρών

Δημήτριος ΠΑΠΟΥΛΗΣ, Λέκτορας Πανεπιστημίου Πατρών

Μιχαήλ ΣΤΑΜΑΤΑΚΗΣ, Καθηγητής Εθνικού και Καποδιστριακού
Πανεπιστημίου Αθηνών

Απόστολος ΑΛΕΞΟΠΟΥΛΟΣ, Καθηγητής Εθνικού και Καποδιστριακού Πανεπι-
στημίου Αθηνών, Πρόεδρος Ε.Γ.Ε.

Κωνσταντίνος ΠΑΠΑΒΑΣΙΛΕΙΟΥ, Αν. Καθηγητής Εθνικού και Καποδιστριακού
Πανεπιστημίου Αθηνών, Γενικός Δ/ντής Ι.Γ.Μ.Ε.

Κωνσταντίνος ΜΑΚΡΟΠΟΥΛΟΣ, Καθηγητής Εθνικού και Καποδιστριακού
Πανεπιστημίου Αθηνών, Δ/ντής Γεωδυναμικού Ινστιτούτου Ε.Α.Α.

Εμμανουήλ ΜΑΝΟΥΤΣΟΓΛΟΥ, Αν. Καθηγητής Πολυτεχνείου Κρήτης

Σπυρίδων ΠΑΥΛΙΔΗΣ, Καθηγητής Αριστοτελείου Πανεπιστημίου Θεσσαλονίκης

Κωνσταντίνος ΠΑΠΑΚΩΝΣΤΑΝΤΙΝΟΥ, Πρόεδρος ΕΛ.ΚΕ.Θ.Ε.

Γραμματεία Συνεδρίου

Συνέδρα

Ηρ. Πολυτεχνείου 92, 26442 Πάτρα • Τηλ.: 2610 432.200 • Fax: 2610 430.884

URL: www.synedra.gr • E-mail: synedra@synedra.gr

ORGANIZING COMMITTEE OF THE 12th INTERNATIONAL CONGRESS



PRESIDENT

George KOUKIS, Professor, University of Patras

VICE-PRESIDENT

Abraham ZELILIDIS, Professor, University of Patras

GENERAL SECRETARY

Ioannis KOUKOUVELAS, Assoc. Professor, University of Patras

EXECUTIVE SECRETARY

George PAPTAEODOROU, Assoc. Professor, University of Patras

TREASURER

Maria GERAGA, Lecturer, University of Patras

MEMBERS

Nikolaos KONTOPOULOS, Professor, University of Patras

Nikolaos LAMBRAKIS, Professor, University of Patras

Nikolaos SABATAKAKIS, Assoc. Professor, University of Patras

Eythimios SOKOS, Assist. Professor, University of Patras

Dimitrios PAPOULIS, Lecturer, University of Patras

Michael STAMATAKIS, Professor, National and Kapodistrian
University of Athens

Apostolos ALEXOPOULOS, Professor, National and Kapodistrian University of Athens.
President of G.S.G.

Constantinos PAPAASSILEIOU, Assoc. Professor, National and Kapodistrian University of
Athens, Gen. Director of I.G.M.E.

Konstantinos MAKROPOULOS, Professor, National and Kapodistrian University of Athens,
Director of Institute of Geodynamics, N.O.A.

Emmanouil MANOUTSOGLU, Assoc. Professor, Technical University of Crete

Spyridon PAVLIDES, Professor, Aristotle University of Thessaloniki

Konstantinos PAPACONSTANTINOY, President of H.C.M.R.

Congress Secretariat

Synedra

Iroon Polytechniou 92, GR 26442 Patras • Ph.: +302610 432.200 • Fax: +302610 430.884
URL: www.synedra.gr • E-mail: synedra@synedra.gr

ΧΟΡΗΓΟΙ
ΤΟΥ 12ου ΔΙΕΘΝΟΥΣ ΣΥΝΕΔΡΙΟΥ ΤΗΣ ΕΛΛΗΝΙΚΗΣ ΓΕΩΛΟΓΙΚΗΣ ΕΤΑΙΡΕΙΑΣ



Υπό την Αιγίδα του
ΥΠΟΥΡΓΕΙΟΥ ΠΕΡΙΒΑΛΛΟΝΤΟΣ, ΕΝΕΡΓΕΙΑΣ & ΚΛΙΜΑΤΙΚΗΣ ΑΛΛΑΓΗΣ

και τη Συμβολή των
ΤΜΗΜΑ ΓΕΩΛΟΓΙΑΣ ΠΑΝΕΠΙΣΤΗΜΙΟΥ ΠΑΤΡΩΝ
ΙΝΣΤΙΤΟΥΤΟ ΓΕΩΛΟΓΙΚΩΝ ΚΑΙ ΜΕΤΑΛΛΕΥΤΙΚΩΝ ΕΡΕΥΝΩΝ
ΓΕΩΤΕΧΝΙΚΟ ΕΠΙΜΕΛΗΤΗΡΙΟ ΕΛΛΑΔΑΣ

ΚΟΙΝΩΦΕΛΕΣ ΙΔΡΥΜΑ
ΙΩΑΝΝΗ Σ. ΛΑΤΣΗ

ΠΑΝΕΠΙΣΤΗΜΙΟ ΠΑΤΡΩΝ

ΟΡΓΑΝΙΣΜΟΣ ΑΝΤΙΣΕΙΣΜΙΚΟΥ
ΣΧΕΔΙΑΣΜΟΥ ΚΑΙ ΠΡΟΣΤΑΣΙΑΣ

ΑΚΤΩΡ Α.Τ.Ε.

ΕΜΒΕΛΕΙΑ Α.Ε.

ΕΛΛΗΝΙΚΑ ΛΑΤΟΜΕΙΑ Α.Ε.

ΟΜΙΛΟΣ ΤΕΧΝΙΚΩΝ ΜΕΛΕΤΩΝ
(ΟΤΜ) Α.Τ.Ε.

ΓΕΦΥΡΑ Α.Ε.

ΓΕΝΙΚΗ ΜΕΛΕΤΩΝ Ε.Π.Ε. «ΙΣΤΡΙΑ»

ΣΥΝΔΕΣΜΟΣ ΜΕΤΑΛΛΕΥΤΙΚΩΝ
ΕΠΙΧΕΙΡΗΣΕΩΝ

ΔΕΛΦΟΙ-ΔΙΣΤΟΜΟΝ Α.Μ.Ε.

ΓΕΩΜΗΧΑΝΙΚΗ Α.Τ.Ε.

Α.Ε. ΤΣΙΜΕΝΤΩΝ ΤΙΤΑΝ

ΕΛΑΦΟΣ ΣΥΜΒΟΥΛΟΙ
ΜΗΧΑΝΙΚΟΙ Α.Ε.

ΓΕΩΣΚΟΠΙΟ Α.Τ.Ε.

Η Οργανωτική Επιτροπή του 12ου Διεθνούς Συνεδρίου της Ελληνικής Γεωλογικής Εταιρείας ευχαριστεί θερμά τα ανωτέρω Ιδρύματα, Ινστιτούτα Ερευνών, Οργανισμούς, Τεχνικές και Μελετητικές Εταιρείες για την οικονομική υποστήριξη και συμβολή τους στην οργάνωση και υλοποίηση του Συνεδρίου.

SPONSORS
OF THE 12th INTERNATIONAL CONGRESS OF THE GEOLOGICAL SOCIETY OF GREECE



Under the Aegis of the
MINISTRY OF ENVIRONMENT, ENERGY AND CLIMATE CHANGE

and the Contribution of the
DEPARTMENT OF GEOLOGY, UNIVERSITY OF PATRAS
INSTITUTE OF GEOLOGY AND MINERAL EXPLORATION
GEOTECHNICAL CHAMBER OF GREECE

JOHN S. LATSIS, PUBLIC BENEFIT
FOUNDATION

UNIVERSITY OF PATRAS

EARTHQUAKE PLANNING AND
PROTECTION ORGANIZATION

AKTOR S.A.

EMBELIA S.A.

HELLENIC QUARRIES S.A..

CONSULTING ENGINEERING
COMPANY (OTM) S.A.

GEFYRA S.A.

GENERAL CONSULTING LTD "ISTRIA"

GREEK MINING ENTERPRISES
ASSOCIATION

DELFI-DISTOMON BAUXITE S.A.

GEOMECHANIKI S.A.

TITAN CEMENT COMPANY S.A.

EDAFOS ENGINEERING
CONSULTANTS S.A.

GEOSCOPIO S.A.

The Organizing Committee of the 12th International Congress of the Geological Society of Greece expresses its grateful thanks to the above Foundations, Institutes, Organizations, Construction and Consulting Companies for their substantial support.

ΕΠΙΣΤΗΜΟΝΙΚΗ ΕΠΙΤΡΟΠΗ – SCIENTIFIC COMMITTEE



Η Οργανωτική Επιτροπή ευχαριστεί θερμά τους κριτές για τη συμβολή τους στην κρίση όλων των εργασιών. Κάθε εργασία κρίθηκε από δύο κριτές για την απόκτηση Πρακτικών υψηλού επιστημονικού επιπέδου. Η Οργανωτική Επιτροπή δεν έχει ευθύνη για το περιεχόμενο και τις απόψεις που εκφράζονται στις εργασίες από τους συγγραφείς.

The Organizing Committee expresses sincere thanks to the reviewers for their contribution in evaluating and approving of the submitted papers. Each paper has passed through two reviewers, producing Proceedings of high scientific level. The Organizing Committee is not responsible for the content and the views expressed by the authors in the papers.

Alexopoulos A., Alexopoulos I., Alexouli A., Anagnostou C., Antonarakou A., Argyraki A., Avramidis P., Bersezio R., Bogdanov K., Caputo R., Christanis K., Christaras B., Christidis G., Depountis N., Drakatos G., Dresnier Th. Drinia H., Economou G., Fassoulas C., Ferentinos G., Fermeli G., Filippidis A., Fountoulis I. Frey M.L., Gaki – Papanastassiou K., Ganas A., Georgakopoulos A., Geraga M., Godelitsas A., Hatzipanagioutou K., Iliopoulos I., Ioakim C., Kalavrouziotis I., Kaleris V., Kallergis G., Kamberis E., Karakaisis G.F., Karakitsios V., Karastathis V., Karipi S., Katagas C., Kati M., Katsonopoulou D., Kiliass A., Kiratzi A., Kitsou D., Kokkalas S., Kollaman H., Kondopoulou D., Konispoliatis N., Konstantinou C., Kontopoulos N., Koroneos A., Koukis G., Koukouvelas I., Lambrakis N., Laskou M., Lekkas E., Loupasakis C., Lykousis V., Magganas A., Manoutsoglou E., Marinou P.V., Markopoulos Th., Migiros G., Mladenova Th., Mountrakis D., Mposkos E., Mylonakis G., Nakov R., Nikolaou N., Oprsal I., Papadimitriou E., Papadimitriou P., Papadopoulos T., Papaioannou Ch., Papamarinopoulos S., Papanastassiou D., Papanikolaou D., Papatheodorou G., Papazachos C.B., Papoulis D., Paraskevopoulos P., Parcharidis I., Pavlides S., Pavlopoulos A., Pe – Piper G., Perdikakis V., Perrakis M., Perraki Th., Petalas C., Pomoni – Papaioannou F., Pomonis P., Ritolo S., Rokka A., Rondoyanni Th., Roumelioti Z., Rozos D., Ruiz – Ortiz P.A., Sabatakakis N., Sachpazi M., Sakellariou D., Scordilis Em., Seifert Th., Skarpelis N., Skias S., Sokos E., Soulios G., Soupios P., Stamatakis M., Stamatelopoulou - Seymour K., Stamatis G., Stiros S., Stournaras G., Syrides G., Theodorou G., Theodosiou I., Torok A., Tranos M., Triantafyllou M.V., Tsapanos T.M., Tselentis G-A., Tsiambaos G., Tsikouras B., Tshipoura – Vlahou M., Tsirambides A., Tsokas G., Tsolis–Katagas P., Tsombos P., Tsourlos P., Tucker M.E., Tulipano L., Tzani A., Varnavas S., Vavelidis M., Voudouris K., Voulgaris N., Xypolias P., Zagana E., Zambetakis – Lekkas A., Zelilidis A., Zouros N., Zygori V.

ΔΟΜΗ ΤΩΝ ΠΡΑΚΤΙΚΩΝ / SCHEME OF THE PROCEEDINGS



ΤΟΜΟΣ 1 / VOLUME 1

Εναρκτήρια Ομιλία / Opening Lectures
Κεντρικές και Θεματικές Ομιλίες / Special and Keynote Lectures
Γενική και Τεκτονική Γεωλογία / General and Structural Geology
Νεοτεκτονική και Γεωμορφολογία / Neotectonics and Geomorphology

ΤΟΜΟΣ 2 / VOLUME 2

Παλαιοντολογία, Στρωματογραφία και Ιζηματολογία /
Palaeontology, Stratigraphy and Sedimentology.
Γεωαρχαιολογία / Geoarchaeology
Γεώτοποι / Geosites
Διδακτική των Γεωεπιστημών / Teaching of Earth Sciences
Θαλάσσια Γεωλογία και Ωκεανογραφία / Marine Geology and Oceanography

ΤΟΜΟΣ 3 / VOLUME 3

Τεχνική Γεωλογία και Γεωτεχνική Μηχανική /
Engineering Geology and Geotechnical Engineering
Φυσικές Καταστροφές / Natural Hazards
Αστική Γεωλογία / Urban Geology
Γ.Σ.Π. στις Γεωεπιστήμες / G.I.S in Earth Sciences

ΤΟΜΟΣ 4 / VOLUME 4

Υδρογεωλογία και Υδρολογία / Hydrogeology and Hydrology
Γεωφυσική / Geophysics
Σεισμολογία / Seismology

ΤΟΜΟΣ 5 / VOLUME 5

Ενεργειακές Πρώτες Ύλες και Γεωθερμία / Energy resources and Geothermics
Γεωχημεία και Κοιτασματολογία / Geochemistry and Ore Deposit Geology
Βιομηχανικά Ορυκτά και Πετρώματα / Industrial Minerals and Rocks
Ορυκτολογία και Πετρολογία / Mineralogy and Petrology

ΤΑ ΣΥΝΕΔΡΙΑ ΤΗΣ Ε.Γ.Ε.

- 1ο ΔΙΗΜΕΡΟ, ΑΘΗΝΑ, 1983, Δελτίο XVII
- 2ο ΔΙΗΜΕΡΟ, ΑΘΗΝΑ, 1984, Δελτίο XIX
- 3ο ΣΥΝΕΔΡΙΟ, ΑΘΗΝΑ, 1986, Δελτίο XX
- 4ο ΣΥΝΕΔΡΙΟ, ΑΘΗΝΑ, 1988, Δελτίο XXIII
- 5ο ΣΥΝΕΔΡΙΟ, ΘΕΣΣΑΛΟΝΙΚΗ, 1990, Δελτίο XXV
- 6ο ΣΥΝΕΔΡΙΟ, ΑΘΗΝΑ, 1992, Δελτίο XXVIII
- 7ο ΣΥΝΕΔΡΙΟ, ΘΕΣΣΑΛΟΝΙΚΗ, 1994, Δελτίο XXX
- 8ο ΣΥΝΕΔΡΙΟ, ΠΑΤΡΑ, 1998, Δελτίο XXXII
- 9ο ΣΥΝΕΔΡΙΟ, ΑΘΗΝΑ, 2001, Δελτίο XXXIV
- 10ο ΣΥΝΕΔΡΙΟ, ΘΕΣΣΑΛΟΝΙΚΗ, 2004, Δελτίο XXXVI
- 11ο ΣΥΝΕΔΡΙΟ, ΑΘΗΝΑ, 2007, Δελτίο XXXX



THE CONGRESSES OF G.S.G.

- 1st MEETING, ATHENS, 1983, Bull. XVII
- 2nd MEETING, ATHENS, 1984, Bull. XIX
- 3rd CONGRESS, ATHENS, 1986, Bull. XX
- 4th CONGRESS, ATHENS, 1988, Bull. XXIII
- 5th CONGRESS, THESSALONIKI, 1990, Bull. XXV
- 6th CONGRESS, ATHENS, 1992, Bull. XXVIII
- 7th CONGRESS, THESSALONIKI, 1994, Bull. XXX
- 8th CONGRESS, PATRAS, 1998, Bull. XXXII
- 9th CONGRESS, ATHENS, 2001, Bull. XXXIV
- 10th CONGRESS, THESSALONIKI, 2004, Bull. XXXVI
- 11th CONGRESS, ATHENS, 2007, Bull. XXXX

ΠΡΟΛΟΓΟΣ



Η Γη είναι ένας πλανήτης με συνεχή και δυναμική εξέλιξη στην ιστορία του. Η γνώση και κατανόηση από τον άνθρωπο της εξέλιξης αυτής είναι μεγάλης σημασίας για τον εντοπισμό, την εκμετάλλευση και τη χρήση των φυσικών πόρων, καθώς και για την ανάδειξη και αντιμετώπιση των περιβαλλοντικών προκλήσεων-προβλημάτων από τη χρήση των πόρων αυτών.

Η περιβαλλοντική αυτή διάσταση απαιτεί μια ολοκληρωμένη, πολυ-επιστημονική θεώρηση του Πλανήτη, που θα περιλαμβάνει τη μελέτη όλων των παραγόντων, όπως της λιθόσφαιρας, της υδρόσφαιρας, της ατμόσφαιρας και της βιόσφαιρας, οι οποίοι συνδέονται μεταξύ τους σε πολύ σημαντικά συστήματα. Τα συστήματα αυτά απαιτούν τη συνεργασία, χωρίς σύνορα και περιορισμούς, των φυσικών επιστημών, όπως η Γεωλογία, η Βιολογία, η Χημεία και η Φυσική. Έτσι μόνο θα κατανοήσουμε τον Πλανήτη μας, θα αναδείξουμε τα περιβαλλοντικά προβλήματα και θα δημιουργήσουμε ενημερωμένες-ευαισθητοποιημένες κοινωνίες, οι οποίες θα μπορούν να αποφασίσουν για το παρόν και το μέλλον του.

Σήμερα είναι γεγονός ότι υπάρχει μια εμπεριστατωμένη άποψη σχετικά με την εξελικτική πορεία της Γης στη διάρκεια των 4,6 δισεκατομμυρίων ετών της ύπαρξής της. Παράλληλα αποτελεί κοινή συνείδηση ότι η ισορροπία του πλανήτη από την καθημερινή πίεση των έξι (6) περίπου δισεκατομμυρίων ανθρώπων που φιλοξενούνται σε αυτόν, είναι πλέον εύθραυστη. Ειδικότερα όσον αφορά στις Γεωεπιστήμες, υπάρχει σοβαρή γνώση σχετικά με τις **Γεωλογικές Διεργασίες**, που έχουν λάβει χώρα στα πλαίσια της ιστορίας αυτής με τη δημιουργία των ορέων και των ωκεανών, τους σεισμούς, την ηφαιστειακή δραστηριότητα, καθώς και την εκδήλωση εξωγενών φαινομένων, όπως οι κατολισθήσεις, οι πλημμύρες, οι ξηρασίες, τα τσουνάμι.

Όσον αφορά στη **Βιώσιμη Ανάπτυξη**, είναι γνωστό ότι τις τελευταίες δεκαετίες η τεχνολογική εξέλιξη και η πληθυσμιακή έκρηξη επέβαλαν μια αλόγιστη και χωρίς σχεδιασμό υπερεκμετάλλευση των φυσικών πόρων, με αποτέλεσμα την υποβάθμιση του περιβάλλοντος για πρώτη φορά στην ιστορία του Πλανήτη μας.

Έτσι, μερικά από τα ερωτήματα που τίθενται επιτακτικά και αναμένουν απαντήσεις από την επιστημονική κοινότητα, δεδομένου ότι εκφράζουν την αγωνία όλης της ανθρωπότητας, είναι τα εξής: α) Οι ανθρώπινες δραστηριότητες έχουν προκαλέσει πράγματι επικίνδυνες τροποποιήσεις του περιβάλλοντος και μάλιστα μη αναστρέψιμες ή οι κλιματικές μεταβολές που παρατηρούνται σήμερα αποτελούν φυσικές διακυμάνσεις; β) Ειδικότερα η βιομηχανική ανάπτυξη και η υπερκατανάλωση ενεργειακών πρώτων υλών αποτελούν κίνδυνο για το περιβάλλον ή θεωρούνται μηδαμνής επίδρασης σε σχέση με τις ηφαιστειακές εκρήξεις και τις αλλαγές των ρευμάτων στους ωκεανούς, οι οποίες προκαλούν δραματικές αλλαγές στο περιβάλλον;

γ) Είναι ακόμα δυνατή μια Βιώσιμη Ανάπτυξη και εάν ναι, ποιο είναι το είδος αυτής στα όρια αντοχής και αποδοχής του πλανήτη μας;

Στα παραπάνω ερωτήματα και προβληματισμούς η επιστήμη της Γεωλογίας έχει να προσφέρει πολλά, δεδομένου ότι οι φυσικές διεργασίες κατά τη διάρκεια της εξέλιξης της Γης έχουν καταγραφεί στους εδαφικούς και βραχώδεις γεωλογικούς σχηματισμούς, χωρίς επηρεασμούς από τις παρεμβάσεις του ανθρώπου. Έτσι οι ανθρώπινες παρεμβάσεις της σύγχρονης εποχής μπορούν να διαχωριστούν και να επισημανθούν, ώστε να αντιμετωπιστούν σωστά. Γενικότερα, η γνώση και κατανόηση της εξέλιξης της Γης μέσα από τις φυσικές διεργασίες μπορούν να συμβάλουν στην αποτύπωση των ρυθμών αλλαγής της Γης στο γεωλογικό χρόνο. Επιπλέον οι ρυθμοί αλλαγής και οι διεργασίες, που είναι υπεύθυνες για αυτούς, μπορούν παράλληλα να αποτελούν δείκτες πρόγνωσης για την πορεία του πλανήτη στο μέλλον. Με άλλα λόγια, το παρελθόν και γενικότερα η γεωλογική ιστορία του Πλανήτη μπορεί να αποτελέσει το «κλειδί» για το παρόν και το μέλλον αυτού.

Συμπερασματικά, η συμβολή της Γεωλογίας και γενικότερα των Φυσικών Επιστημών στην κοινωνία μας είναι πολύ σημαντική για τη γνώση της εξέλιξης της Γης, την έρευνα και αξιολόγηση των φυσικών πόρων, την εκτίμηση των περιβαλλοντικών επιπτώσεων λόγω εκμετάλλευσης των πόρων αυτών, καθώς και την πρόγνωση-αντιμετώπιση των διάφορων φυσικών επικινδυνοτήτων από γεωλογικές διεργασίες και καταστροφικά καιρικά φαινόμενα.

Το 12ο Διεθνές Συνέδριο της Ελληνικής Γεωλογικής Εταιρίας με τίτλο «**Πλανήτη Γη: Γεωλογικές Διεργασίες και Βιώσιμη Ανάπτυξη**» διοργανώνεται από το Τμήμα Γεωλογίας του Πανεπιστημίου Πατρών και πραγματοποιείται στο Συνεδριακό και Πολιτιστικό Κέντρο του Πανεπιστημίου από τις 19 έως 22 Μαΐου 2010. Το Δελτίο της Ελληνικής Γεωλογικής Εταιρίας περιλαμβάνει τα Πρακτικά του Συνεδρίου σε πέντε (5) τόμους των 2.992 σελίδων συνολικά. Οι τόμοι αυτοί καλύπτουν όλο το φάσμα των Γεωεπιστημών σε θέματα της βασικής και εφαρμοσμένης έρευνας. Στα πρακτικά περιλαμβάνονται 267 συνολικά εργασίες από 605 συγγραφείς, όλες στην Αγγλική γλώσσα, δίνοντας έτσι τη δυνατότητα διεθνούς προβολής και χρήσης του επιστημονικού Δελτίου της Εταιρίας. Οι επίσημες γλώσσες του Συνεδρίου είναι η Ελληνική και η Αγγλική.

Στο Συνέδριο υπάρχει σημαντικός αριθμός εργασιών από τον ευρύτερο γεωγραφικό μας χώρο, έχουν δε δηλώσει συμμετοχή πολλοί αξιόλογοι επιστήμονες από την Ελλάδα και το εξωτερικό, καθώς και νέοι ερευνητές και φοιτητές.

Όλες οι εργασίες που δημοσιεύονται, υπεβλήθησαν σε επιστημονική κρίση από εξωτερικούς κριτές, ακολουθώντας τη διαδικασία που είναι διεθνώς καθιερωμένη στα επιστημονικά περιοδικά. Πολλοί αναγνωρισμένοι επιστήμονες, Έλληνες και ξένοι, όλων των ειδικοτήτων, συμμετείχαν στη διαδικασία αυτή. Εκ μέρους της Οργανωτικής Επιτροπής τους ευχαριστώ για τη συμμετοχή και τη συμβολή τους με το σοβαρό έργο που προσέφεραν στην απόκτηση Πρακτικών υψηλού επιπέδου.

Οι επιστημονικές εργασίες εντάχθηκαν σε επιμέρους θεματικές ενότητες, στις οποίες διαχωρίστηκαν τα Πρακτικά και αποτέλεσαν αντικείμενο στις αντίστοιχες Συνεδρίες. Τα κείμενα των ειδικών και προσκεκλημένων ομιλιών, που καλύπτουν το ευρύτερο αντικείμενο της κάθε ενότητας και παρουσιάζουν υψηλού επιπέδου θεώρηση σχετικά με την υφιστάμενη γνώση, τις νέες απόψεις και τάσεις της έρευνας, αποτέλεσαν ιδιαίτερη ενότητα.

Στο Συνέδριο αυτό δίνεται ιδιαίτερη έμφαση στις Γεωλογικές Διεργασίες και τη Βιώσιμη Ανάπτυξη. Όπως αναφέρθηκε διεξοδικά παραπάνω, η κατανόηση της εξέλιξης του πλανήτη Γη μέσα από τις γεωλογικές διεργασίες επιτρέπει στον άνθρωπο να αξιολογήσει τις διάφορες δραστηριότητές του, όπως την αναζήτηση, εκμετάλλευση και χρήση των φυσικών πόρων, καθώς και την κατασκευή διαφόρων έργων υποδομής, χωρίς να προκαλεί επικίνδυνες μεταβολές στο φυσικό και το ανθρωπογενές περιβάλλον. Έτσι μόνο μπορεί να εξασφαλιστεί η Βιώσιμη Ανάπτυξη και να προβλεφθεί η πορεία του Πλανήτη.

Η έγκαιρη εκτύπωση και παράδοση των τόμων του Συνεδρίου στους συνέδρους και στην επιστημονική κοινότητα, καθώς και η γενικότερη οργάνωση του Συνεδρίου γίνεται με την οικονομική στήριξη πολλών φορέων, δημόσιων και ιδιωτικών. Εκφράζονται θερμές ευχαριστίες στο Υπουργείο Περιβάλλοντος, Ενέργειας και Κλιματικής Αλλαγής, που έθεσε το Συνέδριο υπό την αιγίδα του, καθώς και στο Τμήμα Γεωλογίας του Πανεπιστημίου Πατρών, το Ι.Γ.Μ.Ε., και το ΓΕΩΤ.Ε.Ε. Θερμές ευχαριστίες εκφράζονται επίσης στο Κοινοφελές Ίδρυμα Ιωάννη Σ. Λάτση, το Πανεπιστήμιο Πατρών, αλλά και σε ιδιωτικές Τεχνικές και Μελετητικές Εταιρίες, που με τόση προθυμία ανταποκρίθηκαν στην πρόσκλησή μας.

Τέλος, θα ήθελα να εκφράσω τις προσωπικές μου ευχαριστίες στους συναδέλφους της Οργανωτικής Επιτροπής για την αμέριστη βοήθειά τους και την άριστη συνεργασία στη συλλογική αυτή προσπάθεια, καθώς και στο Γραφείο Οργάνωσης Συνεδρίων «*Συνέδρα*», όπως επίσης στους φοιτητές του Τμήματος Γεωλογίας, που αγάλιασαν και βοήθησαν στην οργάνωση του Συνεδρίου με απαράμιλλο ζήλο.

Πάτρα, 14 Απριλίου 2010

Γεώργιος Χρ. Κούκης
Πρόεδρος
της Οργανωτικής Επιτροπής

PROLOGUE



Earth is a dynamic Planet that has been continuously changing and evolving throughout its whole history. Knowledge and understanding of the evolution processes is of crucial importance not only to explore and take advantage of the natural recourses that our planet provides, but also to access the degree of environmental impacts that the exploitation of these causes.

This environmental aspect demands to consider a comprehensive and multi-scientific view of our Planet, which involves the study of lithosphere, hydrosphere, biosphere and atmosphere. All the above are closely connected together to form very important and complex natural systems, which need the close cooperation of all sciences involved, such as Geology, Biology, Chemistry and Physics. This is the most effective way to understand our Planet, to consider the environmental problems and enforce societies to become informed and conscious of its present and future.

Nowadays an almost complete and comprehensive knowledge about the evolution of Earth during the 4.6 billion years of its age has been gained. In parallel, it is common sense that our Planet's equilibrium is fragile due to environmental pressures that human causes, since Earth's population exceeds 6 billion people.

In the field of Geo-Sciences, in special, there has been gained sufficient experience about the **Geological Processes** that have been taken place during Earth's history and are evident in the formation of mountains and oceans, by the manifestation of earthquakes, by volcanic activity, as well as in natural phenomena as landslides, floods, droughts and tsunamis.

Concerning **Sustainable Development**, it is well known that during the last decades technological evolution and population growth have imposed an unreasonable and sometimes without design overconsumption of natural resources, which leads to gradual degradation of the environment for the first time in our Planet's history.

Thus, some of the "hot" questions that have been arisen and need to be answered by the Scientific Community, since they express the concern of the whole humanity, are: a) Human activities have indeed caused dangerous and non-reversible modifications of the environment or present climatic changes are a result of normal and natural fluctuations? b) Industrial development and overconsumption of natural recourses are a "red flag" for the environment or they can be considered as of minor effect when compared with volcanic eruptions and changes in the regime of ocean current circulation, which cause dramatic environmental changes? c) Is Sustainable Development still achievable and, if yes, in which form and within our Planet's bearing thresholds?

In the above questions Scientific Community can offer a lot, regarding that natural processes

during Earth's evolution have been imprinted on soil and rock geological formations, without any influence by human activities. Present human actions can be clearly distinguished and identified in order to be treated in the right way. The deep knowledge and understanding of Earth's evolution through natural processes can contribute to imprint the rates of Earth's changes through geological time. The changing rates and the processes responsible for them also contribute to obtain indices to predict similar phenomena for the future. In other words the Past and, generally, the geological history of our Planet is the "key" for the Present and Future.

In conclusion, the contribution of Geology and generally of Natural Sciences in our society is very important to understand Earth's evolution, to assist the research and assessment of natural resources, as well as to estimate the environmental impacts from their exploitation. Furthermore, they can provide solutions to the direction of the prevention and confrontation of natural hazards that are triggered by Geological Processes and catastrophic climatic events.

The 12th International Congress of the Geological Society of Greece entitled "**Planet Earth: Geological Processes & Sustainable Development**" is organized by the Department of Geology of the University of Patras in Greece and is held at the Conference and Cultural Center of the University between the 19th and 22nd of May 2010. The *Bulletin of the Geological Society of Greece* includes the Congress's Proceedings in 5 Volumes of 2.992 pages. These volumes cover the whole spectrum of Geo-Sciences in themes of basic and applied research. They include 267 research papers by 605 authors, all written in English making them easily accessible and promoted internationally. Official languages of the Congress are Greek and English. Many renowned scientists from Greece and abroad participate, covering scientific issues from our broad geographic region, as well as new researchers and students.

All submitted papers were reviewed by external reviewers, following the procedure that is established in scientific magazines. Many renowned scientists, Greek and foreigners, of all specialties, participated in this process. On behalf of the Organizing Committee I would like to thank them for their participation and contribution to acquire Proceedings of high quality.

The research papers were included in specific thematic units to which the Proceedings were divided and covered each Congress's session. Special and Keynote lectures about currently acquired knowledge, new insights and modern research trends for each area of interest comprised a special thematic unit.

This Congress focuses on Geological Processes and Sustainable Development. As it was mentioned above, the understanding of Earth's evolution through geological processes allows human to assess his activities, such as investigation and exploitation of natural resources and construction of Infrastructure Works, without causing serious and dangerous damages to the natural and human environment. This is the only way to secure sustainable development and forecast Earth's future.

The on-time production and delivering of the proceedings to the participants and scientific community, as well as the organization of the Congress is sponsored by many public and pri-

vate Organizations, Services and Companies. I would like to express my special thanks to the Ministry of Environment, Energy and Climate Change, which held the Congress under its aegis, as well as to the Department of Geology of the University of Patras, the Institute of Geology and Mineral Exploration (I.G.M.E.) and the Geotechnical Chamber of Greece for their contribution to organize this Congress. Special thanks are also expressed to the Public Benefit Foundation “John S. Latsis”, to the University of Patras and to many private technical and consulting companies which willingly accepted our invitation.

Finally, I would like to personally thank the colleagues of the Organizing Committee for their generous help, support and cooperation to this teamwork, the Congress Organizing firm “Synedra”, as well as the students of the Department of Geology for their precious contribution.

Patras, 14 of April 2010

George Ch. Koukis
President
of the Organizing Committee

ΠΕΡΙΕΧΟΜΕΝΑ / CONTENTS



ΤΟΜΟΣ 1 / VOLUME 1

Εναρκτήρια Ομιλία / Opening Lectures
Κεντρικές και Θεματικές Ομιλίες / Special and Keynote Lectures
Γενική και Τεκτονική Γεωλογία / General and Structural Geology
Νεοτεκτονική και Γεωμορφολογία / Neotectonics and Geomorphology

ΕΝΑΡΚΤΗΡΙΑ ΟΜΙΛΙΑ / OPENING LECTURE

Zerefos C.S.: The “Anthropocene” in the Mediterranean 2

ΚΕΝΤΡΙΚΕΣ ΟΜΙΛΙΕΣ / SPECIAL LECTURES

Foscolos, A.E.: Climatic Changes: Anthropogenic Influence or Naturally Induced Phenomenon 8

Makris, J.: Geophysical studies and tectonism of the Hellenides 32

Papazachos, B.C., Karakaisis, G.F., Papazachos, C.B., Scordilis E.M.: Intermediate Term
Earthquake Prediction Based on Interevent Times of Mainshocks and on Seismic Triggering 46

Rausch, R., Schüth, C., Kallioras, A.: Groundwater Resources Management in Arid Countries 69

ΘΕΜΑΤΙΚΕΣ ΟΜΙΛΙΕΣ / KEYNOTE LECTURES

Νεοτεκτονική και Γεωμορφολογία – Neotectonics and Geomorphology

Papanikolaou, D.: Major Paleogeographic, tectonic and geodynamic changes from the last
stage of the Hellenides to the actual Hellenic Arc and Trench System 72

*Παλαιοντολογία, Στρωματογραφία και Ιζηματολογία – Paleontology, Stratigraphy
and Sedimentology*

Dermitzakis, M.D.: The Status of Stratigraphy in the 21st Century 86

Γεωαρχαιολογία – Geoarchaeology

Mariolakos, I.D.: The forgotten geographical and physical – oceanographic knowledge of the
Prehistoric Greeks 92

Papamarinopoulos, S.P.: Atlantis in Spain (Part I, II, III, IV, V, VI) 105

Γεώτοποι – Geosites

Zouros, N.: Geodiversity and Sustainable Development: Geoparks - A new challenge for Research
and Education in Earth Sciences 159

Διδακτική των Γεωεπιστημών – Teaching Earth Sciences

Makri, K., Pavlides, S.B., Kastanis, N.: An analysis of Geological Textbooks, at 1830-1930 169

Θαλάσσια Γεωλογία και Ωκεανογραφία – Marine Geology and Oceanography

Ferentinos, G.: The contribution of Marine Geology to the Socio-economic Development of Greece:

Marine Resources, Infrastructure, Environment Sustainability, Cultural Heritage. A brief account of the 30 years contribution of the laboratory of Marine Geology and Physical Oceanography	176
<i>Τεχνική Γεωλογία και Γεωτεχνική Μηχανική – Engineering Geology and Geotechnical Engineering</i>	
Tsiambaos, G.: Engineering Geological Behaviour of Heterogeneous and Chaotic Rock masses	183
<i>Υδρογεωλογία και Υδρολογία – Hydrogeology and Hydrology</i>	
Soulios, G.: Springs (Classification, Function, Capturing)	196
<i>Σεισμολογία – Seismology</i>	
Makropoulos, K.C.: Earthquakes and Preventive Measures	216
<i>Ενεργειακές Πρώτες Ύλες και Γεωθερμία - Energy Resources and Geothermics</i>	
Christanis, K.: Energy Resources of Greece: Facts and Myths	224
<i>Γεωχημεία και Κοιτασματολογία – Geochemistry and Ore Deposit Geology</i>	
Varnavas, S.: Medical Geochemistry. A key in the Precautionary Measures against the Development of Cancer and other Diseases	234
<i>Ορυκτολογία και Πετρολογία – Mineralogy and Petrology</i>	
Katagas, Ch.: Wandering about Mineralogy and Petrology	247
<hr/>	
ΓΕΝΙΚΗ ΚΑΙ ΤΕΚΤΟΝΙΚΗ ΓΕΩΛΟΓΙΑ / GENERAL AND STRUCTURAL GEOLOGY	
Argyriadis, I., Midoun, M., Ntontos, P.: A new interpretation of the Structure of Internal Hellenides	264
Kilias, Ad., Frisch, W., Avgerinas, A., Dunkl, I., Falalakis, G., Gawlick, H.-J., Mountrakis, D.: The Pelagonian nappe pile in Northern Greece and FYROM. Structural Evolution during the Alpine Orogeny: A new approach	276
Kokinou, E., Kamberis, E., Sarris, A., Tzanaki, I.: Geological and Magnetic Susceptibility Mapping of Mount Giouchta (Central Crete)	289
Kurz, W., Wölfler, A., Handler, R.: Cenozoic Tectonic Evolution of the Eastern Alps – A reconstruction based on ⁴⁰ AR/ ³⁹ AR Mica, Zircon and Apatite Fission track and Apatite (U/TH) – HE Thermochronology	299
Marsellos, A.E., Kidd, W.S.F., Garver, J.I., Kyriakopoulos, K.G.: Exhumation of the Hellenic Accretionary Prism – Evidence from the Fission Track Thermochronology	309
Migiros, G., Antoniou, Vas., Papanikolaou, I., Antoniou, Var.: Tectonic setting and deformation of the Kallidromo Mt, Central Greece	320
Papageorgiou, E.: Crustal Movements along the Hellenic Volcanic Arc from DGPS measurements	331
Papageorgiou, E., Tzanis, A., Sotiropoulos, P., Lagios, E.: DGPS and Magnetotelluric constraints on the Contemporary Tectonics of the Santorini Volcanic Complex, Greece	344
Papoulia, J., Makris, J.: Tectonic processes and crustal evolution on/offshore western Peloponnese derived from active and passive seismics	357
Spanos, D., Koukouvelas, I., Kokkalas, S., Xypolias, P.: Patterns of Ductile Deformation in Attico – Cycladic Massif	368

Tselepidis, V., Rondoyanni, Th.: A contribution to the Geological Structure of Chios Island, Eastern Aegean Sea	379
Xypolias, P., Chatzaras, V.: The nature of Ductile deformation in the Phyllite – Quartzite unit (External Hellenides)	387

NEOTEKTONIKH KAI GEOMORFOLOGIA / NEOTECTONICS AND GEOMORPHOLOGY

Caputo, R., Catalano, S., Monaco, C., Romagnoli, G., Tortorici, G., Tortorici, L.: Middle – Late Quaternary Geodynamics of Crete, Southern Aegean, and Seismotectonic Implications	400
Gaki – Papanastassiou, K., Karymbalis, E., Maroukian, H.: Recent Geomorphic changes and Anthropogenic Activities in the Deltaic Plain of Pinios River in Central Greece	409
Gaki – Papanastassiou, K., Karymbalis, E., Maroukian, H., Tsanakas, K.: Geomorphic evolution of Western (Paliki) Kephalaria Island (Greece) during the Quaternary	418
Kokkalas, S.: Segmentation and Interaction of Normal Faults in Central Greece	428
Metaxas, Ch.P., Lalechos, N.S., Lalechos, S.N.: Kastoria “Blind” Active Fault: Hazardous Seismogenic Fault of the NW Greece	442
Mourtzas, N.D.: Sea level changes along the coast of Kea Island and Paleogeographical coastal reconstruction of Archaeological sites	453
Nomikou, P., Papanikolaou, D.: A comparative morphological study of the Kos – Nisyros – Tilos volcanosedimentary basins	464
Papanikolaou, M., Papanikolaou, D., Triantaphyllou, M.: Post – Alpine Late Pliocene – Middle Pleistocene uplifted Marine sequences in Zakynthos Islands	475
Pavlidis, S., Caputo, R., Sboras, S., Chatzipetros, A., Papathanasiou, G., Valkaniotis, S.: The Greek Catalogue of Active Faults and Database of Seismogenic Sources	486
Tranos, M.D., Mountrakis, D.M., Papazachos, C.B., Karagianni, E., Vamvakaris, D.: Faulting deformation of the Mesohellenic Trough in the Kastoria – Nestorion Region (Western Macedonia, Greece)	495
Tsanakas, K., Gaki-Papanastassiou, K., Poulos, S.E., Maroukian, H.: Geomorphology and Sedimentological processes along the coastal zone between Livanates and Agios konstantinos (N. Evoikos Gulf, Central Greece)	506
Vassilopoulou, S.: Morphotectonic analysis of Southern Argolis Peninsula (Greece) based on Ground and Satellite Data by GIS Development	516
Zygouri, V.: Probabilistic Hazard Assessment, using Arias Intensity Equation, in the eastern part of the Gulf of Corinth (Greece)	527
Ευρετήριο συγγραφέων / Author index	537



ΤΟΜΟΣ 2 / VOLUME 2

Παλαιοντολογία, Στρωματογραφία και Ιζηματολογία /
Palaeontology, Stratigraphy and Sedimentology

Γεωαρχαιολογία / Geoarchaeology

Γεώτοποι / Geosites

Διδακτική των Γεωεπιστημών / Teaching Earth Sciences

Θαλάσσια Γεωλογία και Ωκεανογραφία / Marine Geology and Oceanography

ΠΑΛΑΙΟΝΤΟΛΟΓΙΑ, ΣΤΡΩΜΑΤΟΓΡΑΦΙΑ ΚΑΙ ΙΖΗΜΑΤΟΛΟΓΙΑ / PALAEOLOGY, STRATIGRAPHY AND SEDIMENTOLOGY

Anagnostoudi, Th., Papadopoulou, S., Ktenas, D., Gkadri, E., Pyliotis, I., Kokkidis, N., Panagiotopoulos, V.: The Olvios, Rethis and Inachos Drainage System Evolution and Human activities influence of their future evolution	548
Avramidis, P., Panagiotaras, D., Papoulis, D., Kontopoulos, N.: Sedimentological and Geochemical characterization of Holocene sediments, from Alikes Lagoon, Zakynthos Island, Western Greece	558
Antonarakou, A.: Plankton Biostratigraphy and Paleoclimatic implications of an Early Late Miocene sequence of Levkas Island, Ionian Sea, Greece	568
Bellas, S., Keupp, H.: Contribution to the late Neogene stratigraphy of the Ancient Gortys area (Southern Central Crete, Greece)	579
Codrea, V., Barbu, O., Jipa-Murzea, C.: Upper Cretaceous (Maastrichtian) land vertebrate diversity in Alba district (Romania)	594
Dimiza, M.D., Triantaphyllou, M.V.: Comparing living and Holocene coccolithophore assemblages in the Aegean marine environments)	602
Drinia, H., Koskeridou, E., Antonarakou, A., Tzortzaki, E.: Benthic Foraminifera associated with the zooxanthellate coral <i>Cladocora</i> in the Pleistocene of the Kos Island (Aegean Sea, Greece): sea level changes and palaeoenvironmental conditions	613
Drinia, H., Pomoni-Papaioannou, F., Tsapas, N., Antonarakou, A.: Miocene Scleractinian corals of Gavdos Island, Southern Greece: Implications for tectonic control and sea level changes	620
Kafousia, N., Karakitsios, V., Jenkyns, H.C.: Preliminary data from the first record of the Early Toarcian oceanic anoxic event in the sediments of the Pindos Zone (Greece)	627
Karakitsios, V., Triantaphyllou, M., Panoussi, P.: Preliminary study on the slump structures of the Early Oligocene sediments of the Pre-Apulian zone (Antipaxos Island, North-western Greece)	634
Kourkounis, S., Panagiotakopoulou, O., Zelilidis, A., Kontopoulos, N.: Texture versus distance of travel of gravels on a stream bed: a case study from four streams in NW Peloponnese, Greece	643
Koutsios, A., Kontopoulos, N., Kalisperi, D., Soupios, P., Avramidis, P.: Sedimentological and Geophysical observations in the Delta Plain of Selinous River, Ancient Helike, Northern Peloponnesus Greece	654
Kyriakopoulos, K., Karakitsios, V., Tsioura-Vlachou, M., Barbera G., Mazzoleni, P., Puglisi, D.: Petrological characters of the Early Cretaceous Boeothian Flysch, (Central Greece)	663

Makrodimitras, G., Stoykova, K., Vakalas, I., Zelilidis, A.: Age determination and Palaeogeographic reconstruction of Diapondia Islands in NW Greece, based on Calcareous Nannofossils	675
Maneta, V., Voudouris, P.: Quartz megacrysts in Greece: Mineralogy and Environment of Formation	685
Manoutsoglou, E., Batsalas, A., Stamboliadis, E., Pantelaki, O., Vakalas, I., Zelilidis, A.: The Auriferous submarine fans sandstones of the Ionian zone (Epirus, Greece)	697
Moumou, Ch., Vouvalidis, K., Pechlivanidou, S., Nikolaou, P.: The Fluvial action of the Karla basin streams in a natural and man-made environment	706
Pavlopoulos, A., Kamperis, E., Sotiropoulos, S., Triantaphyllou, M.: Tectonosedimentary significance of the Messinia conglomerates (SW Peloponnese, Greece)	715
Photiades, A., Pomoni-Papaioannou, F.A., Kostopoulou, V.: Correlation of Late Triassic and Early Jurassic Lofer – type carbonates from the Peloponnesus peninsula, Greece	726
Sigalos, G., Loukaidi, V., Dasaklis, S., Alexouli-Livaditi, A.: Assessment of the Quantity of the material transported downstream of Sperchios River, Central Greece	737
Svana, K., Iliopoulos, G., Fassoulas, C.: New Sirenian findings from Crete Island	746
Triantaphyllou, M.V.: Calcareous nannofossil Biostratigraphy of Langhian deposits in Lefkas (Ionian Islands)	754
Triantaphyllou, M.V., Antonarakou, A., Drinia, H., Dimiza M.D., Kontakiotis, G., Tsolakis, E. Theodorou, G.: High resolution Biostratigraphy and Paleocology of the Early Pliocene succession of Pissouri Basin (Cyprus Island)	763
Zambetakis – Lekkas, A.: On the occurrence of primitive <i>Orbitoides</i> species in Gavrovo – Tripolitza platform (Mainalon Mountain, Peloponnesus, Greece)	773
Zidianakis, G., Iliopoulos, G., Fassoulas, C.: A new late Miocene plant assemblage from Messara Basin (Crete, Greece)	781
Zoumpoulis, E., Pomoni-Papaioannou, F., Zelilidis, A.: Studying in the Paxos zone the carbonate depositional environment changes during Upper Cretaceous, in Sami area of Kefallinia Island, Greece	793

ΓΕΩΑΡΧΑΙΟΛΟΓΙΑ / GEOARCHAEOLOGY

Economou, G., Kougemitrou, I., Perraki, M., Konstantinidi-Syvridi, E., Smith, D.C.: A Mineralogical study of some Mycenaean Seals employing Mobile Raman Microscopy	804
Katsonopoulou, D.: Earth Science Applications in the field of Archaeology: the Helike example	812
Mariolakos, I., Theocharis, D.: Geomythological approach of Asopos River (Aegina, Greece)	821
Mariolakos, I., Nikolopoulos, V., Bantekas, I., Palyvos, N.: Oracles on faults: a probable location of a “lost” oracle of Apollo near Oroviai (Northern Euboea Island, Greece) viewed in its Geological and Geomorphological context	829
Melfos, V., Voudouris, P., Papadopoulou, L., Sdrolia, S., Helly, B.: Mineralogical, Petrographic and stable isotopic study of Ancient white marble quarries in Thessaly, Greece - II. Chasanbali, Tempi, Atrax, Tisaion Mountain	845
Rathossi, C., Pontikes, Y., Tsolis-Katagas, P.: Mineralogical differences between ancient sherds	

and experimental ceramics: Indices for Firing conditions and Post - burial alteration	856
Stiros, S., Kontogianni, V.: Selection of the path of the Eupalinos aqueduct at Ancient Samos on the basis of Geodetic and Geological / Geotechnical criteria	866

ΓΕΩΤΟΠΟΙ / GEOSITES

Antonelou, A., Tsikouras, B., Papoulis, D., Hatzipanagiotou, K.: Investigation of the formation of speleothems in the Agios Georgios Cave, Kilkis (N. Greece)	876
Dotsika, E., Psomiadis, D., Zanchetta, G., Spyropoulos, N., Leone, G., Tzavidopoulos, I., Poutoukis, D.: Pleistocene Palaeoclimatic evolution from Agios Georgios Cave speleothem (Kilkis, N. Greece)	886
Fassoulas, C., Zouros, N.: Evaluating the influence of Greek Geoparks to the local communities	896
Haidarlis, M., Sifakis, A., Brachou C.: Geoconservation legal status and Geopark establishment in Greece	907
Illiopoulos, G., Eikamp, H., Fassoulas, C.: A new Late Pleistocene mammal locality from Western Crete	918
Theodosiou, Ir.: Designation of Geosites – Proposals for Geoparks in Greece	926
Theodosiou, Ir., Athanassouli, E., Epitropou, N., Janikian, Z., Kossiaris, G., Michail, K., Nicolaou, E., Papanikos, D., Pashos, P., Pavlidou, S., Vougioukalakis, G.: Geotrails in Greece	939
Vaxevanopoulos, M., Melfos, V.: Hypogenic features in Maronia Cave, Thrace, Greece. Evidence from morphologies and fluid inclusions	948
Zisi, N., Dotsika, E., Tsoukala, E., Giannakopoulos, A., Psomiadis, D.: Palaeoclimatic evolution in Loutra Arideas Cave (Almopia Speleopark, Macedonia, N. Greece) by stable isotopic analysis of fossil bear bones and teeth	958
Zouros, N., Valiakos, I.: Geoparks management and assessment	965

ΔΙΔΑΚΤΙΚΗ ΤΩΝ ΓΕΩΕΠΙΣΤΗΜΩΝ / TEACHING EARTH SCIENCES

Fermeli, G., Dermitzakis, M.: The contribution of Museums’ digitalized Palaeontological collections to the scientific literacy of compulsory education students: the case of an interactive multimedia production of the Palaeontological and Geological Museum of the University of Athens	978
Fermeli, G., Vitsas, T., Foundas, P., Sokos, E., Alexandropoulou, S., Papatheodoropoulos, P., Germenis, N., Nikolaidis, A., Zevgitis, T.: The use of Educational seismographs in the Seismology School Network “EGELADOS”	989
Katrivanos, D.E., Makri, K.: Perception of first-year geology students on the Tectonic Plates Theory	999
Kritikou, S., Malegiannaki, I.: Following the traces of Naxian emery – an implementation of environmental education in geodidactics	1007

ΘΑΛΑΣΣΙΑ ΓΕΩΛΟΓΙΑ ΚΑΙ ΩΚΕΑΝΟΓΡΑΦΙΑ / MARINE GEOLOGY AND OCEANOGRAPHY

Iatrou, M., Papatheodorou, G., Geraga, M., Ferentinos, G.: The study of Heavy Metal concentrations in the Red Mud deposits at the Gulf of Corinth, using multivariate techniques	1018
---	------

Lycourghiotis, S., Stiros, S.: Sea surface topography in the Gulf of Patras and the Southern Ionian Sea using GPS	1029
Perissoratis, C., Ioakim, Chr.: Research projects to study the Sea floor and Sub-bottom sediments funded by the recent European Commission Framework Programs: The IGME Participation	1035
Sakellariou, D., Fountoulis, I., Lykousis, V.: Evidence of cold seeping in Plio-Pleistocene sediments of SE Peloponnes: The fossil carbonate chimneys of Neapolis Region	1046
Sakellariou, D., Sigurdsson, H., Alexandri, M., Carey, S., Rousakis, G., Nomikou, P., Georgiou P., Ballas, D.: Active tectonics in the Hellenic Volcanic Arc: The Kolumbo submarine volcanic zone	1056
Thomopoulos, K., Geraga, M., Fakiris, E., Papatheodorou, G., Ferentinos, G.: Palaeoclimatic and Palaeoceanographic evolution of the Mediterranean Sea over the last 18ka	1064
Xeidakis, G., Georgoulas, A., Kotsovinos, N., Delimani, P., Varaggouli, E.: Environmental Degradation of the coastal zone of the West part of Nestos River Delta, N. Greece	1074
Ευρετήριο συγγραφέων / Author index	1085



ΤΟΜΟΣ 3 / VOLUME 3

Τεχνική Γεωλογία και Γεωτεχνική Μηχανική /
Engineering geology and Geotechnical Engineering
Φυσικές Καταστροφές / Natural Hazards
Αστική Γεωλογία / Urban Geology
Γ.Σ.Π. στις Γεωεπιστήμες / GIS in Earth Sciences

ΤΕΧΝΙΚΗ ΓΕΩΛΟΓΙΑ ΚΑΙ ΓΕΩΤΕΧΝΙΚΗ ΜΗΧΑΝΙΚΗ / ENGINEERING GEOLOGY AND GEOTECHNICAL ENGINEERING

Angelopoulos, A., Soulis, V.J., Malandraki, V.: Geological and geotechnical behaviour of Evinos Dam following the impoundment	1094
Antonioni, A.A., Tsiambaos, G.: Engineering geological aspects for the microzonation of the city of Volos, Greece	1104
Chatziangelou, M., Thomopoulos, Ach., Christaras, B.: Excavation data and failure investigation along tunnel of Symbol Mountain	1112
Christaras, B., Papathanassiou G., Vouvalidis, K., Pavlides, S.: Preliminary results regarding the rock falls of December 17, 2009 at Tempi, Greece	1122
Christaras, B., Syrides, G., Papathanassiou, G., Chatzipetros, A., Mavromatis, T., Pavlides, Sp.: Evaluating the triggering factors of the rock falls of 16 th and 21 st December 2009 in Nea Fokea, Chalkidiki, Norderh Greece	1131
Depountis, N., Lainas, S., Pyrgakis, D., Sabatakakis, N., Koukis, G.: Engineering Geological and geotechnical investigation of landslide events in wildfire affected areas of Iliia Prefecture, Western Greece	1138

Diasakos, N., Amerikanos, P., Tryfonas, G., Vagioutou, E., Baltzois, V., Bloukas, S., Tagkas, Th., Malandrakis, E., Poulakis, N., Kalogerogiannis, G., Tsirigotis, N.: Tunnel excavation in clayey-marly formations: The case of Kallidromo Tunnel	1149
Hagiou, E., Konstantopoulou, G.: Environmental planning of abandoned Quarries rehabilitation – A methodology	1157
Karagianni, A., Karoutzos, G., Ktena, S., Vagenas, N., Vlachopoulos, I., Sabatakakis, N., Koukis, G.: Elastic Properties of Rocks	1165
Kouki, A.: Mineralogical composition and fabric as related to the mechanical behavior of the fine – grained Plio – Pleistocene sediments of Achaia, Greece	1169
Kouki, A., Rozos, D.: The fine – grained Plio – Pleistocene deposits in Achaia – Greece and their distinction in characteristic geotechnical units	1177
Kouki, A., Rozos, D.: Engineering – Geotechnical conditions in Patras ring road wider area, Greece. Compilation of the relevant map at scale of 1:5000	1184
Kozyreva, E.A., Khak, V.A.: The anthropogenic changes in the Geological Environment in the South of East Siberia	1192
Kynigalaki, M., Kanaris, D., Nikolaou, N., Kontogianni, V.: Buildings’ damage at Horemi Village, Arkadia, Greece: evaluation of the Geotechnical conditions at shallow depths	1202
Lainas, S., Koulouris, S., Vagenas, S., Depountis, N., Sabatakakis, N., Koukis, G.: Earthquake-induced rockfalls in Santomeri Village, Western Greece	1210
Loupasakis, C., Rozos, D.: Land subsidence induced by the overexploitation of the aquifers in Kalochori village – new approach by means of the computational geotechnical engineering	1219
Loupasakis, C., Spanou, N., Kanaris, D., Exioglou, D., Georgakopoulos, A.: Geotechnical investigation of the rock slope stability problems occurred at the foundations of the coastal byzantine wall of Kavala city, Greece	1230
Marinos, P.V.: Engineering geological behaviour of rock masses in underground excavations	1238
Marinos, P.V.: New proposed GSI classification charts for weak or complex rock masses	1248
Marinos, P.V., Tsiambaos, G.: Strength and deformability of specific sedimentary and ophiolitic rocks	1259
Moraiti, E., Christaras, B., Brauer, R.: Landslide in Nachterstedt of Germany	1267
Mourtzas, N., Gkiolas, A.: Tunneling in ophiolitic series formations: Tunnels of the new high-speed railway double track line - section Lianokladi – Domokos	1272
Mourtzas, N.D., Symeonidis, K., Passas, N., Alkalais, E., Kolaiti, E.: Slope stabilization on Chalkoutsí – Dilesi road, at Pigadakia location, Attica Prefecture	1286
Parcharidis, I., Fomelis, M., Kourkouli, P.: Slope instability monitoring by space-borne SAR interferometry: Preliminary results from Panachaiko Mountain (Western Greece)	1301

ΦΥΣΙΚΕΣ ΚΑΤΑΣΤΡΟΦΕΣ / NATURAL HAZARDS

Bizoura, A., Lykoudi, E., Spyridonos, E., Manoutsoglou, E.: Assessment of the vulnerability degree of different lithological formations in the catchment area of Agia Eirini Gorge, Western Crete	1314
--	------

Diakakis, M.: Flood history analysis and its contribution to flood hazard assessment. The case of Marathonas, Greece	1323
Gournelos, T., Nastos, P.T., Chalkias, D., Tsagas, D., Theodorou, D.: Landslide movements related to precipitation. Analysis of a statistical sample from the Greek area	1335
Kadetova, A.V., Kozireva, E.A.: The potential natural hazards to be considered in the design and exploitation of the aerial rope-way in the “Gora Sobolinaya” mountain-skiing resort (Southern Pribaikalia, Russia)	1341
Kalantzi, F., Doutsou, I., Koukouvelas, I.: Historical landslides in the Prefecture of Ioannina – collection and analysis of data	1350
Lekkas, E.: Macroseismicity and geological effects of the Wenchuan earthquake (Ms 8.0r - 12 May 2008), Sichuan, China: Macro-distribution and comparison of EMS ₁₉₉₈ and ESI ₂₀₀₇ intensities	1361
Papathanassiou, G., Pavlides, S.: Probabilistic evaluation of liquefaction-induced ground failures triggered by seismic loading in urban environment; case studies from Greece	1373
Papathanassiou, G., Valkaniotis, S., Chatzipetros, Al., Pavlides S.: Liquefaction susceptibility map of Greece	1383
Poyiadji, E., Nikolaou, N., Karmis, P.: Ground failure due to Gypsum dissolution	1393
Rozos, D., Lykoudi, E., Tsangaratos, P., Markantonis, K., Georgiadis, P., Rondoyanni, Th., Leivaditi, A., Kyrousis, I.: Evaluation of soil erosion and susceptibility to landslide manifestation as a consequence of wildfire events affected the Zacharo municipality, Peloponnesus, Greece	1406

ΑΣΤΙΚΗ ΓΕΩΛΟΓΙΑ / URBAN GEOLOGY

Apostolidis, Em., Koutsouveli, An.: Engineering geological mapping in the urban and suburban region of Nafplion city (Argolis, Greece)	1418
Georgiou, Ch., Galanakis, D.: Neotectonic study of urban and suburban Nafplio area (Argolida-Greece)	1428
Karastathis, V.K., Karmis, P., Novikova, T., Roumelioti, Z., Gerolymatou, E., Papanastassiou, D., Liakopoulos, S., Giannouloupoulos, P., Tsombos, P., Papadopoulos, G. A.: Liquefaction risk assessment by the use of Geophysical techniques: The test area of Nafplion city, Greece	1438
Karmis, P.D., Giannouloupoulos, P., Tsombos, P.: Geophysical investigations at Nafplion city, Greece. Hydrogeological implications	1447
Koukoulis, A., Karageorgiou, D.E.: Radon: Geoinformation for the planning of urban – suburban regions. The case of Nafplion city, Greece	1457
Loupasakis, C., Galanakis, D., Rozos, D.: Rock slope stability problems in natural sightseeing areas - an example from Arvanitia, Nafplio, Greece	1465
Mitropoulos, D., Zananiri, I.: Upper Quaternary evolution of the Northern Argolis Gulf, Nafplio area	1474
Nikolakopoulos, K., Tsompos, P.: Remote sensing applications in the frame of “Urban Geology” project	1486

Photiades, A.: Geological contribution to the tectono- stratigraphy of the Nafplion area (NW Argolis, Greece)	1495
Sabatakakis, P., Koukis, G.: Aqueous environment and effects on the civil areas: The case of Nafplio	1508
Tassiou, S., Vassiliades, E.: Geochemical study of the urban and suburban area of Nafplion city, Argolidha Prefecture, Hellas	1520
Tsombos, P.I., Zervakou, A.D.: The “Urban Geology” project of IGME: The case study of Nafplio, Argolis Prefecture, Greece	1528
Zananiri, I., Chiotis, E., Tsombos, P., Hademenos, V., Zervakou, A.: Geoarchaeological studies in urban and suburban areas of the Argolis Prefecture	1539
Zananiri, I., Zervakou, A., Tsombos, P., Chiotis, E.: Visualization of datasets from urban geology studies using Google Earth: The case study of Nafplio, Argolis Prefecture	1549
Zervakou, A.D., Tsombos, P.I.: GIS in urban geology: The case study of Nafplio, Argolis Prefecture, Greece	1559

Γ.Σ.Π. ΣΤΙΣ ΓΕΩΕΠΙΣΤΗΜΕΣ / G.I.S. IN EARTH SCIENCES

Bathrellos, G.D., Skilodimou, H.D., Chousianitis, K.G.: Soil erosion assessment in Southern Evia Island using USLE and GIS	1572
Golubović Deliganni, M., Parcharidis, I., Pavlopoulos, K.: Karstic landscape study based on Remote Sensing Data: the case of Ksiromero region, Aitolokarnania - Western Greece	1582
Iliia, I., Tsangaratos, P., Koumantakis, I., Rozos, D.: Application of a Bayesian approach in GIS based model for evaluating landslide susceptibility. Case study Kimi area, Euboea, Greece	1590
Karageorgiou, M.M.D., Karymbalis, E., Karageorgiou, D.E.: The use of the Geographical Information Systems (G.I.S.) in the geological – mineralogical mapping of the Paranesti area	1601
Sboras, S., Ganas, A., Pavlides, S. : Morphotectonic analysis of the neotectonic and active faults of Beotia (Central Greece), using G.I.S. techniques	1607
Kynigalaki, M., Nikolaou, N., Karfakis, J., Koutsouveli, An., Poyiadji, El., Pyrgiotis, L., Konstantopoulou, G., Bellas, M., Apostolidis, Em., Loupasakis, K., Spanou, N., Sabatakakis, N., Koukis, G.: Digital engineering geological map of the Athens Prefecture area and related Database Management System	1619
Nikolakopoulos, K., Gioti, Ev., Skianis, G., Vaiopoulos, D.: Ameliorating the Spatial Resolution of Hyperion Hyperspectral Data. The case of Antiparos Island	1627
Rozos, D., Bathrellos, D.G., Skilodimou, D.H.: Landslide susceptibility mapping of the Northeastern part of Achaia Prefecture using Analytical Hierarchical Process and GIS techniques	1637
Skianis, G.Aim., Gournelos, Th., Vaiopoulos, D., Nikolakopoulos, K.: A study of the performance of the Modified Transformed Vegetation Index MTVI	1647
Tsangaratos, P., Koumantakis, I., Rozos, D.: GIS-Based application for geotechnical data managing	1656
Ευρετήριο συγγραφέων / Author index	1667



TOMOS 4 / VOLUME 4

Υδρογεωλογία και Υδρολογία / Hydrogeology and Hydrology
Γεωφυσική / Geophysics
Σεισμολογία / Seismology

ΥΔΡΟΓΕΩΛΟΓΙΑ ΚΑΙ ΥΔΡΟΛΟΓΙΑ / HYDROGEOLOGY AND HYDROLOGY

Christaras, B.: Could water co-management contribute to Peace, in Middle East?	1672
Christoforidou, P., Panagopoulos, A., Voudouris, K.: Towards a new procedure to set up groundwater threshold values in accordance with the provisions of the EC Directive 2006/118: A case study from Achaia and Corinthia (Greece)	1678
Dimitrakopoulos, D., Vassiliou, E., Tsangaratos, P., Ilija, I.: Environmental management of mine water, considering European Water Legislation. Case study of Megalopolis mines	1688
Gkioungkis, I., Mwila, G., Pliakas, F., Kallioras, A., Diamantis, I.: Hydrogeological assessment of groundwater degradation at the Eastern Nestos river delta, N.E. Greece	1697
Karalemas, N., Lekkas, S.: Operational mechanism of karst spring “Logaras”, near the village “Skortsinou”, Arcadia, (Peloponnesus)	1707
Karapanos, E., Burgess, W., Lambrakis, N.: Groundwater flow modelling of the alluvial aquifer in the Mouria area, SW Greece	1716
Katsanou, K., Stratikopoulos, K., Zagana, E. Lambrakis, N.: Radon changes along main faults in the broader Aigion region, NW Peloponnese	1726
Kelepertzis, E., Argyraki, A., Daftsis, E., Ballas, D.: Quality characteristics of surface waters at Asprolakkas River Basin, N.E. Chalkidiki, Greece	1737
Koukidou, I., Panagopoulos, A.: Application of feflow for the simulation of groundwater flow at the Tirnavos (Central Greece) alluvial basin aquifer system	1747
Kounis, G.D., Kounis, K.G.: Infiltration, effective porosity, transmissibility and critical yield of water wells in the carbonate fissured aquifers of Attica – A contribution to the regional and managerial hydrogeology	1758
Kounis, G.D., Kounis, K.G.: Relationship between the transmissibility of the “Athens Schists” and the percentage of their competent rock component	1767
Maramathas, A., Gialamas, J., Pambuku, A., Beshku, H., Vako, E.: Brackish karst springs simulation with “modkarst” model under not enough data conditions (the case of the “Potami” spring at Himara Albania)	1777
Mariolakos, I., Spyridonos, E.: Remarks on the karstification in the wider area of the Upper Messinia closed hydrogeological basin (SW Peloponnesus, Greece)	1785
Matiatos, I., Alexopoulos, A., Zouridakis, N.: Use of stable isotopes in the determination of the mean altitude of recharge and the investigation of function mechanism of spring waters in Argolis Peninsula (Greece)	1792
Mertzanides, Y., Economou, N., Hamdan, H., Vafidis, A.: Imaging sea water intrusion in coastal	

zone of Kavala (N. Greece) with electrical resistivity tomography	1802
Mertzanides, Y., Ziannos, V., Tsobanoglou, C., Kosmidis, E.: Telemetry network for monitoring quality of irrigation water in Kavala (N. Greece)	1812
Nikas, K., Antonakos, A., Kallergis, G., Kounis, G.: International hydrogeological map of Europe: sheet D6 “Athina”	1821
Papafotiou, A., Schütz, C., Lehmann, P., Vontobel, P., Or, D., Neuweiler, I.: Measurement of preferential flow during infiltration and evaporation in porous media	1831
Raco, B., Dotsika, E., Psomiadis, D., Doveri, M., Lelli, M., Zisi, N., Papakonstantinou, K., Lazaridis, A.: Geochemical investigation of aquifer pollution from waste management. The case of Komotini landfill (Greece)	1840
Rozos, D., Sideri, D., Loupasakis, C. Apostolidis, E.: Land subsidence due to excessive ground water withdrawal. A case study from Stavros - Farsala site, West Thessaly Greece	1850
Skordas, K., Tziritis, E., Kelepertsis, A.: Groundwater quality of the hydrological basin of Amyros River, Agia area Thessaly, Greece	1858
Stamatis, G.: Groundwater quality of the Ag. Paraskevi/Tempi valley karstic springs - application of a tracing test for research of the microbial pollution (Kato Olympos/NE Thessaly)	1868
Zagana, E., Lemesios, I., Charalambopoulos, S., Katsanou, K., Stamatis, G., Lambrakis, N.: Environmental – hydrogeological investigations on the clay deposits in the broad area of Mesologgi – Aitoliko lagoons	1878

ΓΕΩΦΥΣΙΚΗ / GEOPHYSICS

Aidona, E., Kondopoulou, D., Alexandrou, M., Ioannidis, N.: Archaeomagnetic studies in Kilns from N. Greece	1888
Alexopoulos, J.D., Dilalos, S.: Geophysical research for geological structure determination in the region of South Mesogheia (Attica)	1898
Arvanitis, A.A., Stampolidis, A.D., Tsokas, G.N.: Contribution of geophysical methods to the investigation of geothermal conditions in the Southwestern part of the Strymon Basin (Macedonia, Northern Greece)	1907
Chailas, S., Tzanis, A., Kranis, H., Karmis, P.: Compilation of a unified and homogeneous aeromagnetic map of the Greek mainland	1919
Skarlatoudis, A.A., Papazachos, C.B.: Implementation of a non-splitting formulation of perfectly matched layer in a 3D – 4 th order staggered-grid velocity-stress finite-difference scheme	1930
Tzanis, A.: A Matlab program for the analysis and interpretation of transient electromagnetic sounding data	1941
Vargemezis, G., Fikos, I.: Large scale vertical electrical soundings survey in Anthemountas River Basin for evaluating hydraulic communication between sub basin aquifers	1953
Vargemezis, G., Tsourlos, P., Mertzanides, I.: Contribution of deep electrical resistivity tomography technique to hydrogeological studies: Cases from areas in Kavala (North Greece)	1962
Zananiri, I., Kondopoulou, D., Spassov, S.: The application of environmental magnetism techniques for pollution assessment in urban and suburban areas in Greece: State of the art and case studies	1972

Adamaki, A.K., Tsaklidis, G.M., Papadimitriou, E.E., Karakostas, V.G.: Evidence for induced seismicity following the 2001 Skyros mainshock	1984
Astiopoulos, A.C., Papadimitriou, E., Karakostas, V., Gospodinov, D., Drakatos, G.: Seismicity changes detection during the seismic sequences evolution as evidence of stress changes	1994
Chousianitis, K., Agalos, A., Papadimitriou, P., Lagios, E., Makropoulos, K.: Source parameters of moderate and strong earthquakes in the broader area of Zakynthos Island (W. Greece) from regional and teleseismic digital recordings	2005
Kapetanidis, V., Papadimitriou, P., Makropoulos, K.: A cross-correlation technique for relocation of seismicity in the Western Corinth Rift	2015
Karakaisis, G.F., Papazachos, C.B., Scordilis, E.M.: Seismic sources and main seismic faults in the Aegean and surrounding area	2026
Karakonstantis, A., Papadimitriou, P.: Earthquake relocation in Greece using a unified and homogenized seismological catalogue	2043
Karakostas, V.G., Papadimitriou, E.E., Karamanos, Ch.K. Kementzetzidou, D. A.: Microseismicity and seismotectonic properties of the Lefkada – Kefalonia seismic zone	2053
Karakostas, V.G., Papadimitriou, E. E., Tranos, M.D., Papazachos, C.B.: Active seismotectonic structures in the area of Chios Island, North Aegean Sea, revealed from microseismicity and fault plane solutions	2064
Karamanos, Ch.K., Karakostas, V.G., Seeber, L., Papadimitriou, E.E., Kiliias, A.A.: Recent seismic activity in Central Greece revealing local seismotectonic properties	2075
Kaviris, G., Papadimitriou, P., Makropoulos, K.: Anisotropy study of the February 4th 2008 swarm in NW Peloponnesus (Greece)	2084
Leptokaropoulos, K.M., Papadimitriou, E.E., Orlecka–Sikora, B., Karakostas, V.G.: Seismicity rate changes in association with time dependent stress transfer in the region of Northern Aegean Sea, Greece	2093
Moshou, A., Papadimitriou, P., Makropoulos, K.: Moment tensor determination using a new waveform inversion technique	2104
Paradisopoulou, P.M., Papadimitriou, E.E., Karakostas, V.G., Lasocki, S., Mirek, J., Kiliias, A.: Influence of stress transfer in probability estimates of $M \geq 6.5$ earthquakes in Greece and surrounding areas	2114
Popandopoulos, G., Baskoutas, I.: Space regularity manifestation of the temporal variation of seismic parameters: Possibility for the strong seismic activity assessment	2125
Roumelioti, Z., Kiratzi, A.: Incorporating different source rupture characteristics into simulations of strong ground motion from the 1867, M7.0 earthquake on the Island of Lesbos (NE Aegean Sea, Greece)	2135
Roumelioti, Z., Kiratzi, A.: Moderate magnitude earthquake sequences in Central Greece (for the year 2008)	2144
Scordilis, E.M.: Correlations of the mean time and mean magnitude of accelerating preshocks with the origin time and magnitude of the mainshock	2154

Segou, M., Voulgaris, N., Makropoulos, K.: On the sensitivity of ground motion prediction equations in Greece	2163
Serpetsidaki, A., Sokos, E., Tselentis, G-A.: Study of the 2 nd December 2002 Vartholomio earthquake (Western Peloponnese), M5.5 aftershock sequence	2174
Sokos, E., Pikoulis, V.E., Psarakis, E.Z., Lois, A.: The April 2007 swarm in Trichonis Lake using data from a microseismic network	2183
Tsapanos, T.M., Koravos, G.Ch., Plessa, A., Vythoulkas, N.K., Pitsonis, I.S.: Decay parameters of aftershock sequences globally distributed	2193
Votsi, I., Limnios, N., Tsaklidis, G., Papadimitriou, E.: Semi-Markov models for seismic hazard assessment in certain areas of Greece	2200
Ευρετήριο συγγραφέων / Author index	2211



ΤΟΜΟΣ 5 / VOLUME 5

Ενεργειακές Πρώτες Ύλες και Γεωθερμία / Energy resources and Geothermics
Γεωχημεία και Κοιτασματολογία / Geochemistry and Ore Deposit Geology
Βιομηχανικά Ορυκτά και Πετρώματα / Industrial Minerals and Rocks
Ορυκτολογία και Πετρολογία / Mineralogy and Petrology

ΕΝΕΡΓΕΙΑΚΕΣ ΠΡΩΤΕΣ ΥΛΕΣ ΚΑΙ ΓΕΩΘΕΡΜΙΑ / ENERGY RESOURCES AND GEOTHERMICS

Fotopoulou, M., Siavalas, G., İnaner, H., Katsanou, K., Lambrakis, N., Christanis, K.: Combustion and leaching behavior of trace elements in lignite and combustion by products from the Muğla basin, SW Turkey	2218
Karageorgiou, D.E., Metaxas, A., Dimitriou, D., Arapogiannis, E., Varvarousis, G.: Contribution of lignite in the Greek economy	2229
Karageorgiou, D.E., Metaxas, A., Karageorgiou, M.M.D., Papanikolaou, G., Georgakopoulos, A.N., Vrettos, K.: Development of lignite in Crete. Comparison of basins, possibilities of exploitation	2236
Kolios, N., Arvanitis, A., Karydakis, G., Koutsinos, S.: Geothermal drilling activity in the Akropotamos Area (Macedonia, Northern Greece)	2246
Mertzanides, Y., Kargiotis, E., Mitropoulos, A.: Geological and geophysical data of “Epsilon” field in Prinos oil basin	2257
Metaxas, A., Varvarousis, G., Karydakis, Gr., Dotsika, E., Papanikolaou, G.: Geothermic status of Thermopylae - Anthili area in Fthiotida Prefecture	2265
Metaxas, A., Georgakopoulos, A.N., Karageorgiou, D.M.M., Papanikolaou, G., Karageorgiou, E.D.: CO ₂ Content of Greek lignite: the case of Proastio Lignite deposit in Ptolemais Basin, Northern Greece	2274
Oikonomopoulos, I., Perraki, Th., Tougiannidis, N.: FTIR study of two different lignite lithotypes from Neocene Achlada lignite deposits in NW Greece	2284

Papanicolaou, C., Triantafyllou, G., Pasadakis, N., Foscolos, A.E.: Adsorption of phenols from olive oil mill wastewater as well as n and p from a simulated city wastewater liquid on activated Greek lignites	2294
--	------

ΓΕΩΧΗΜΕΙΑ ΚΑΙ ΚΟΙΤΑΣΜΑΤΟΛΟΓΙΑ / GEOCHEMISTRY AND ORE DEPOSIT GEOLOGY

Alexandratos, V.G., Behrends, T., Van Cappellen, P.: The influence of reductive dissolution of iron oxides by S(-II) on uranium mobility	2310
Argyraiki, A., Petrakaki, N.: Heterogeneity in heavy metal concentrations in the soil of a firing range area at Kesariani, Athens, Greece	2319
D' Alessandro, W., Brusca, L., Martelli, M., Rizzo, A., Kyriakopoulos, K.: Geochemical characterization of natural gas manifestations in Greece	2327
Demetriades, A., Birke, M., Locutura, J., Bel-lan, A.B., Duris, M., EuroGeoSurveys Geochemistry Expert Group: Urban geochemical studies in Europe	2338
Demetriades, A., Reimann, C., Birke, M., Salminen, R., De Vos, W., Tarvainen, T., EuroGeoSurveys Geochemistry Expert Group: Geochemical Atlases of Europe produced by the EuroGeoSurveys Geochemistry Expert Group: State of progress and potential uses	2350
Kyriakopoulos, G.K.: Natural degassing of carbon dioxide and hydrogen sulphide and its environmental impact at Milos Island, Greece	2361
Papastergios, G., Filippidis, A., Fernandez-Turiel, J.L., Gimeno, D., Sikalidis, C.: Natural and anthropogenic effects on the soil geochemistry of Kavala Area, Northern Greece	2373
Psomiadis, D., Dotsika, E., Albanakis, K., Zisi, N., Poutoukis, D., Lazaridis, A.: Comparison of sampling techniques for isotopic analysis of shallow marine carbonates	2383
Serelis, K.G., Kafkala, I.G., Parpodis, K., Lazaris, S.: Anthropogenic and Geogenic contamination due to heavy metals in the vast area of Vari, Attica	2390
Stefanova, M., Marinov, S.P.: Organic geochemistry of humic acids from a Neogene lignite sample, Bulgaria	2398
Tombros, S.F., St. Seymour, K., Spry, P.G., Bonsall, T.A.: The isotopic signature of the mineralizing fluid of the Lavrion carbonate-replacement Pb-Zn-Ag district	2406
Triantafyllidis, S., Skarpelis, N.: Geochemical investigation and modelling of an acid pit lake from a high sulfidation ore deposit: Kirki, NE Greece	2417

ΒΙΟΜΗΧΑΝΙΚΑ ΟΡΥΚΤΑ ΚΑΙ ΠΕΤΡΩΜΑΤΑ / INDUSTRIAL MINERALS AND ROCKS

Anagnostou, Ch.: Bauxite resource exploitation in Greece vs sustainability	2426
Arvanitidis, N.D.: New metallogenetic concepts and sustainability perspectives for non-energy metallic minerals in Central Macedonia, Greece	2437
Fadda, S., Fiori, M., Pretti, S., Valera, P.: Volcanic – sedimentary metal deposition in Paleomargin environment: A “ Protore ” occurrence in Central Sardinia (Italy)	2446
Kitsopoulos, K.: Immobile trace elements discrimination diagrams with zeolitized volcanics from the Evros - Thrace - Rhodope volcanic terrain	2455

Lampropoulou, P., Tzeveleku, Th., Papamantellos, D., Stivanakis, V., Papaefthymiou, S.: Human interferences to the environment, consequences and care	2465
Laskaridis, K., Patronis, M.: “Karystía líthos”: a timeless structural ornamental stone	2475
Leontakianakos, G., Baziotis, I., Ekonomou, G., Delagrammatikas, G., Galbenis, C.T., Tsimas, S.: A Case study of different limestones during quick lime and slaked-lime production	2485
Manoutsoglou, E., Panagopoulos, G., Spyridonos, E., Georgiou, A.: Methodology for optimal determination of new drilling program in an active open pit: Example from an active sulfate open pit in Altsi, Lasithi Prefecture, Eastern Crete	2492
Mpalatsas, I., Rigopoulos, I., Tsikouras, B., Hatzipanagiotou, K.: Suitability assessment of Cretaceous limestones from Thermo (Aitoloakarnania, Western Greece) for their use as base and sub-base aggregates in road-construction	2501
Papastamatiou, D., Skarpelis, N., Argyraki, A.: Air quality in mining areas: The case of Stratoni, Chalkidiki, Greece	2510

ΟΡΥΚΤΟΛΟΓΙΑ ΚΑΙ ΠΕΤΡΟΛΟΓΙΑ / MINERALOGY AND PETROLOGY

Baziotis, I., Mposkos, E.: Geochemistry and tectonic setting of eclogite protoliths from Kechros Complex in East Rhodope (N.E. Greece)	2522
Bourliva, A., Michailidis, K., Sikalidis, C., Filippidis, A., Apostolidis, N.: Municipal wastewater treatment with bentonite from Milos Island, Greece	2532
Bourouni, P., Tsikouras, B., Hatzipanagiotou, K.: Petrological investigation of carbonate rocks from the Ionian Zone (Etolokarnania, Western Greece)	2540
Christidis, G.E., Skarpelis, N.: Clay mineralogy of the sedimentary iron-nickel ore of Agios Ioannis, NE Boeotia: new data and implication for diagenetic modifications	2553
Christidis, G.E., Katsiki, P., Pratikakis, A., Kacandes, G.: Rheological properties of Palygorskite- Smectite suspensions from the Ventzia Basin, W. Macedonia, Greece	2562
Christidis, G.E., Perdikatsis, V., Apostolaki, Ch.: Mineralogy of the Saharan Aeolian Dust in Crete: Examples from the period 2004-2009	2570
Çina, A.: Mineralogy of chromitite, Bulqiza ultramafic massif, Albanian ophiolitic complex	2577
Fadda, S., Fiori, M., Pretti, S., Valera, P.: Manganese mineralisations at the base of Miocene sediments in Northern Sardinia (Italy)	2588
Filippidis, A., Papastergios, G., Apostolidis, N., Filippidis, S., Paragios, I., Sikalidis, C.: Purification of urban wastewaters by Hellenic natural Zeolite	2597
Georgiadis, I.K., Koronaios, A., Tsirambides, A., Stamatakis, M.: Textural and petrological study of modern sands from the Vertiskos Unit of Serbomacedonian Massif (Macedonia, Greece)	2606
Karipi, S., Tsikouras, B., Rigopoulos, I., Hatzipanagiotou, K., Pomonis, P.: Insights into hydrothermal activity in the Iti Ophiolite (Central Greece)	2617
Kitsopoulos, K.: Magma generation and mixing in the earliest volcanic centre of Santorini (Akrotiri Peninsula). Mineral chemistry evidence from the Akrotiri Pyroclastics	2625
Koutsopoulou, E., Tsolis-Katagas, P., Papoulis, D.: Heavy metals in stream sediments affected by a landfill and associated impact on groundwater quality	2635

Lykakis, N. Kiliyas, S. P.: Epithermal Manganese Mineralization, Kimolos Island, South Aegean Volcanic Arc, Greece	2646
Michailidis, K., Trontzios, G., Sofianska, E.: Chemical and mineralogical assessment of clays from Peloponnese (S. Greece) and their evaluation for utilization in ceramics industry	2657
Mposkos, E., Baziotis, I.: Study of the metamorphic evolution of a carbonate – bearing metaperidotite from the Sidironero Complex (Central Rhodope, Greece) using P-T and P(T)- X_{CO_2} Pseudosections	2667
Papadopoulos, A., Christofides, G., Papastefanou, C., Koroneos, A., Stoulos, S.: Radioactivity of granitic rocks from Northern Greece	2680
Persianis, D., Katsikis, J., Karageorgiou, D.E.: The genetic hypothesis of the uraniferous mineralization, Eastern Chalkidiki (Northern Greece)	2692
Ploumis, P., Chatzipanagis, I.: Geological, petrological and tectonic features characterizing the commerciality of the marbles of Southern Vermion Mountain	2702
Rigopoulos, I., Tsikoura, B., Pomonis, P., Karipi, S., Hatzipanagiotou, K.: Quantitative analysis of Asbestos fibres in ophiolitic rocks used as aggregates and hazard risk assessment for human health	2712
Solomonidou, A., Dominic Fortes, A., Kyriakopoulos, K.: Modelling of volcanic eruptions on Titan	2726
Stamatakis, M., Stamatakis, G.: The use of diatomaceous rocks of Greek origin as absorbents of olive-oil wastes	2739
Theodosoglou, E., Koroneos, A., Soldatos, T., Zorba, T., Paraskevopoulos, K.M.: Comparative Fourier Transform infrared and X-Ray powder diffraction analysis of naturally occurred K-feldspars	2752
Tzamos, E., Filippidis, A., Kantiranis, N., Sikalidis, C., Tsirambides, A., Papastergios, G., Vogiatzis, D.: Uptake ability of zeolitic rock from South Xerovouni, Avdella, Evros, Hellas	2762
Vasilatos, Ch., Vlachou-Tsipoura, M., Stamatakis, M.G.: On the occurrence of a volcanic ash layer in the Xylokastro Area, North Peloponnesus, Greece: Mineralogy and geochemistry	2773
Voudouris, P., Magganas, A., Kati, M., Gerogianni, N., Kastanioti, G., Sakelaris, G.: Mineralogical constraints to the formation of vein-type zeolites from Kizari area, Thrace Northern Greece	2786
Ευετήσιο συγγραφέων / Author index	2799

12ο ΔΙΕΘΝΕΣ ΣΥΝΕΔΡΙΟ ΤΗΣ ΕΛΛΗΝΙΚΗΣ ΓΕΩΛΟΓΙΚΗΣ ΕΤΑΙΡΙΑΣ
ΠΛΑΝΗΤΗΣ ΓΗ: Γεωλογικές Διεργασίες και Βιώσιμη Ανάπτυξη

12th INTERNATIONAL CONGRESS OF THE GEOLOGICAL SOCIETY OF GREECE
PLANET EARTH: Geological Processes and Sustainable Development



ΕΝΕΡΓΕΙΑΚΕΣ ΠΡΩΤΕΣ ΥΛΕΣ ΚΑΙ ΓΕΩΘΕΡΜΙΑ
ENERGY RESOURCES AND GEOTHERMICS

COMBUSTION AND LEACHING BEHAVIOR OF TRACE ELEMENTS IN LIGNITE AND COMBUSTION BY-PRODUCTS FROM THE MUĞLA BASIN, SW TURKEY

**Fotopoulou M.¹, Siavalas G.¹, İnaner H.², Katsanou K.³, Lambrakis N.³,
and Christanis K.¹**

¹ Section of Earth Materials, Department of Geology, University of Patras, 26500 Rio-Patras - Greece,
mariafot@gmail.com, siavalas@upatras.gr, christan@upatras.gr

² Department of Geological Engineering, Dokuz Eylul University, Buca-Izmir-Turkey,
hulya.inaner@deu.edu.tr

³ Section of Applied Geology and Geophysics, Department of Geology, University of Patras, 26500
Rio-Patras - Greece, katsanou@upatras.gr, nlambrakis@upatras.gr

Abstract

The Muğla Basin is one of the most well-documented coal basins of Anatolia, SW Turkey. Previous studies mainly focused on coal geology, as well as on the environmental impacts from trace elements emitted into the atmosphere during coal combustion. However, the environmental impacts from coal utilization also include groundwater contamination from hazardous trace elements leached from exposed lignite stockpiles or ash disposal dumps. In the present study a comparative assessment of the combustion, as well as the leaching behaviour of trace elements from sixteen lignite, fly ash and bottom ash samples under various pH conditions is attempted. The samples were picked up from three regions in the Muğla Basin, namely, these of Yeniköy, Kemerköy and Yatağan.

Proximate and ultimate analyses were performed on all samples. Quantitative mineralogical analysis was carried out using a Rietveld-based full pattern fitting technique. The elements Ag, As, B, Ba, Be, Co, Cr, Cu, Fe, Ga, Hf, Li, Mn, Mo, Ni, Pb, Sr, U, V and Zn were grouped according to their volatility during combustion and their leachability in the various types of samples. The pH of the leaching agent little affected the leaching trends of most elements and the mode of occurrence proved to be the major factor controlling primarily combustion and to a lesser extent leaching. The elements were classified into 7 classes with increasing environmental significance with Mo, Sr and V being the most potentially hazardous trace elements in the Muğla region.

Key words: *bottom ash, fly ash, leachability, lignite, mobility, Muğla, trace elements, Turkey, volatility.*

1. Introduction

The last decades countries using “conventional” fuels for electricity generation, are attempting to develop a friendlier to the environment, energy policy. The study of the behavior of trace elements, particularly of the hazardous atmospheric pollutants - HAPs (As, Be, Cd, Cl, Cr, Co, F, Hg, Mn, Ni, Pb, Se, Sb and U), is necessary for the prediction and the prevention of environmental impacts, induced by coal combustion and the disposal of the wastes (Finkelman, 1994; Finkelman and Gross, 1999). The behavior of trace elements in combustion can be assessed studying their geochemical and mineralogical characteristics (Clarke and Sloss, 1992; Meij, 1995).

There is an extensive literature concerning the determination of HAP behaviour during coal combustion (e.g. Finkelman, 1994; Vassilev et al., 2005). All these studies are based on the fact that an element is enriched in the produced fly and bottom ash due to the escape of the volatile matter during combustion. Elements depleted in comparison to the feed coal are considered volatile and potential HAPs. The volatility of an element depends on its properties but also on its mode of occurrence. The mode of occurrence of an element can vary not only in different coals but sometimes even in coals from the same deposit. Therefore, it is necessary to study the behavior of the elements for each coal deposit separately.

Apart from atmospheric emissions, coal utilization involves environmental hazards concerning waste disposal. The impacts are related to the mobilization of toxic metals after the deposition of fly and bottom ash at dump sites. The behavior of an element after the exposure of the waste under the atmospheric conditions can be predicted considering its mode of occurrence, but an experimental study using leaching tests provides direct evidence for the most susceptible to mobilization elements. There are two major types of leaching tests concerning their set up: Column tests, which better simulate field conditions, and batch tests, which provide evidence for the maximum potential mobility of an element. Batch tests are more widely applied due to their relatively rapid and reliable results but can easily be misinterpreted if only absolute values are to be considered (Siavalas et al., 2007; Baba et al., 2008; Hesbach et al., 2009).

The lignite mining activities in Turkey appear to have serious repercussions in underground waters. Several studies showed that certain trace elements are dissolved from ash dumping sites and pass into the groundwater (e.g. Demirak et al., 2005). Taking into consideration the fact that Turkish lignite displays low calorific value, high ash yield and sulphur content, further research is required to investigate the environmental impacts caused by their exploitation (İnaner and Nakoman, 2005).

The present work aims to investigate the combustion and leaching behaviour of trace elements in lignite, fly ash and bottom ash from the regions of Yatağan and Milas in Muğla Basin. The main focuses are the conditions, under which trace elements are able to escape from the organic and inorganic fraction of lignite, fly- and bottom ash and to be transported in the terrestrial and aquatic environment constituting environmental hazard.

2. Regional and geological setting

Muğla Basin is located on the Eastern coast of the Aegean Sea, in southwest Anatolia (Fig. 1). The coal fields are of Miocene age. The basin's margins consist of the formations of the Menderes Massif and the Lycian nappes.

Muğla Basin is separated into two sub-basins: Yatağan and Milas (Fig. 1). The NW-SE oriented Yatağan Sub-basin hosts the lignite deposits of Turgut, Eskihisar, Bagyaka, Tinaz and Bayır, while the sub-basin of Milas includes the lignite deposits of Ekizköy, Sekköy, Cakıralan, Karacahisar, Husamlar and Alatepe (Fig. 1). Open-cast mines operate in the Eskihisar, Bagyaka, Tinaz, Sekköy, Ekizköy, Husamlar, and Cakıralan coal fields. The Alatepe coal field has been exploited by underground mining methods. Bayır, Turgut, and Karacahisar coal fields are to be exploited by underground mining methods in the future. Most of the lignite production supplies three thermal power plants (Fig. 1), these of Yatağan, Yeniköy and Kemerköy with 630, 420 and 630 MW installed capacity, respectively (Querol et al., 1999; İnaner et al., 2008). Electrostatic precipitators and desulphurization units are installed in all 3 power plants and solid wastes are removed and stored by hydro-transportation. Ash-dumping sites have been afforested by authorities of thermal power plants.

The Yatağan thermal power plant produces approximately 5 kt of fly and bottom ash per day. The produced solid wastes are transported to a schist and karstic marble disposal site. The Yeniköy thermal power plant produces daily 4.5 kt of fly and bottom ash. The produced solid wastes are transported

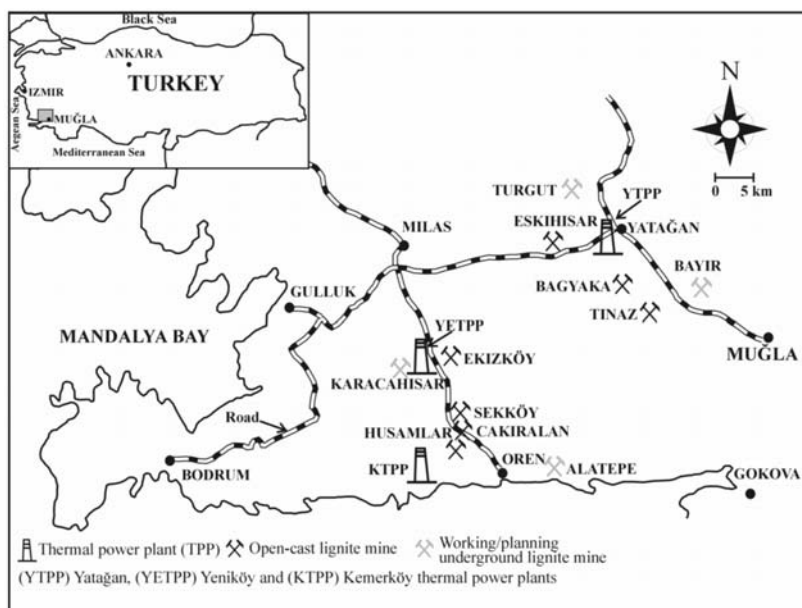


Fig. 1: Thermal power plants and major lignite fields in Muğla Basin (İnaner et al., 2008, modified).

to the disposal site, which is located on alluvial deposits and limestone. The Kemerköy thermal power plant produces c. 6 kt of fly and bottom ash per day. The produced solid wastes are transported to a karstic and fractured dolomitic and cherty limestone disposal site (Baba and Kaya, 2004).

3. Experimental

Sixteen samples of lignite, fly ash and bottom ash were collected from mines and thermal power plants in the areas of Milas and Yatağan, in Muğla province. The lignite samples were described macroscopically according to the nomenclature of ICCP (1993). Proximate analysis carried out following ASTM procedures, included the determination of moisture, ash yields, volatile matter and fixed carbon content. In addition, mineralogical analysis was performed in all samples. The contents of C, H, N and S of lignite and lignite combustion by-products were determined using the Carlo Erba EA1108 CHNS analyzer. Quantitative mineralogical analysis was carried out using a Bruker D8 Advance X-ray diffractometer, which is equipped with the detector LynxEye®, whereas the mineralogical phases were quantified using a routine, which is based on the Rietveld method with the Topas software. All samples were digested in acid solutions using a Milestone microwave oven. The contents of Ag, As, B, Ba, Be, Co, Cr, Cu, Fe, Ga, Hf, Hg, Li, Mn, Mo, Ni, Pb, Se, Sr, U, V and Zn in the digested lignite, fly- and bottom ash samples were determined using an ELAN 6100 Perkin Elmer® instrument (Inductively Coupled Plasma-Mass Spectrometry, ICP-MS). Batch leaching experiments took place under pH 5 and 8.5 to estimate the mobility of trace elements from lignite and its by-products.

4. Results

4.1 Proximate analysis

The lignite belongs to the matrix lithotype. Moisture ranges from 14.0 to 36.5 wt.%, ash yield from 8.4 to 50.3 wt.%, where the highest ash yields concern the feed coal samples of the area. The calorific

Table 1. Quantitative mineralogical analysis of bulk coal samples, low-temperature (400°C) ash, fly ash and bottom ash samples. GoF (x^2): Goodness of Fit factor.

	<i>Quartz</i>	<i>Feldspars</i>	<i>Clays</i>	<i>Muscovite</i>	<i>Zeolites</i>	<i>Calcite</i>	<i>Sulphides</i>	<i>Sulphates</i>	<i>Gehlenite</i>	<i>Mullite</i>	<i>Lime</i>	<i>Fe oxides</i>	<i>Other oxides</i>	<i>Amorphous matter</i>	<i>GoF (x^2)</i>
TR-L1	19.2						80.8								1.5
TR-L2	11.7	19.4	11.6	39.3			9.4	8.5							1.1
TR-L3	39.0	14.2	28.7	18.1			7.1								1.6
TR-L3a	49.4		27.6	23.0			6.2	5.8							1.6
TR-L4	13.5	14.7	35.4	33.8			2.5								1.6
TR-L5	8.9	4.0	58.8	2.5		20.5	1.6	6.1							1.2
TR-L6	12.1	5.7	47.3	11.7		18.7	1.6	14.4							1.2
TR-L1 LTA	7.7	10.7	4.8					71.6				5.1			1.5
TR-L2 LTA	6.2	4.0	66.0					19.2				5.1			1.2
TR-L3 LTA	9.8	4.7	52.6					33.0							1.5
TR-L3a LTA	23.0		4.3					72.8							1.6
TR-L4 LTA	5.4	3.4	74.7					11.8				2.0			1.3
TR-L5 LTA	10.3	4.5	45.8			22.5		15.5				1.4			1.3
TR-L6 LTA	11.8	6.6	40.2			21.6		17.7				2.1			1.4
TR-AF1	3.2	3.2	0.7					5.8	7.5	2.4	4.0	2.3	4.1	66.8	2.3
TR-AF2	10.1	18.2						3.6	4.8	5.6	0.7	5.2		51.8	1.2
TR-AF3	4.1	1.5						14.7	12.2	0.8	4.6	3.9		58.2	1.5
TR-AF4	7.5	9.5						1.3	2.2	3.3	0.8	2.3		73.1	1.2
TR-AF5	6.4	6.6						6.0	7.0	2.5	2.6	4.0		64.9	1.3
TR-AB1	2.1	4.7			4.7	3.5			23.6			1.3		60.1	1.4
TR-AB2	3.7	9.9			12.7	7.6		3.6	20.2			2.8		39.4	1.8
TR-AB3	5.1	20.5			9.0	2.3			8.9		1.2	2.5	1.2	49.4	1.4
TR-AB4	10.9	13.5			4.6				2.2	1.8	0.6	1.5		65.0	1.6

value ranges from 10.6-20.9 MJ/kg (on moist, ash-free basis). The content of volatile matter ranges from 44.1 to 67.1 wt.% and of fixed carbon from 5.6 to 29.0 wt.%. According to these results the Muğla lignite is classified as low to medium-grade, humic, ortho- to meta-lignite (ECE-UN, 1998).

The fly ash is composed of fine-grained particles and the volatile matter content ranges from 0.6 to 1.1 wt.%. The volatile matter content in bottom ash ranges from 0.7 to 8.5 wt.%.

4.2 Mineralogical analysis

The accuracy of the quantitative mineralogical analysis was checked using the Goodness of Fit (GoF) rule, where the more the GoF value approaches 1 the better fit was achieved (Bish and Post, 1992). This value ranges between 1.1 and 2.3 with an average of 1.4 for the studied samples indicating that a good fit was achieved (Table 1).

The inorganic constituents of coals may be introduced into the peat either as clastic material or may derive from authigenic precipitation. However, in the study of bulk coal samples due to high noise/signal ratio caused by the organic matter, it is hard to determine some mineral phases. For this reason mineralogical analyses were also performed on ash derived after low temperature (400°C) ashing (LTA) in order to remove the organic matter without altering much the mineralogical composition (Table 1).

According to the combined results from both bulk samples and LTAs the most common mineralogical components in the Muğla lignite are quartz, feldspars, carbonates, clay minerals mainly illite and kaolinite, all being common in coals worldwide (Diessel, 1992).

The major minerals in fly ash samples are quartz, anhydrite and aluminosilicate minerals such as feldspars, mullite and gehlenite. There are also ferrous and calcium oxides such as magnetite, hematite, maghemite, portlandite and lime. The mineralogical composition of bottom ash samples is somewhat different to that of the fly ash. Ghelenite is the dominant phase being more stable at low temperatures. Calcite content is also higher probably due to the contribution of lignite particles in the bottom ash. Quartz and aluminosilicates are present at lower contents than in the fly ash. Moreover, minerals from the zeolite group were determined at relatively high contents (16 wt.%, on average). The zeolites form from the reaction of glass with water in the combustion chamber (Karayiğit et al., 2000). Bassanite and corundum are occasional minerals.

Furthermore, the content of amorphous matter in fly and bottom ash samples was determined in ZnO spiked samples. Amorphous matter content in the fly ash ranges from 51.8 to 71.3 wt.% being higher than the respective in the bottom ash, which ranges from 39.4 to 65.0 wt.% (Table 1).

4.3 Chemical composition

In the lignite samples C ranges from 42.2 to 52.5 wt.%, N from 1.2 to 1.4 wt.%, H from 5.7 to 7.8 wt.% and total S from 2.7 to 7.9 wt.%, on a dry basis. The content of C in fly ash samples ranges from 0.2 to 0.3 wt.%, of H is about 0.1 wt.%, of N is below 0.1 wt.% and of total S from 0.4 to 1.4 wt.%. Finally, the content of C ranges from 0.5 to 1.9 wt.%, of H from 0.0 to 0.7 wt.%, of N below 0.1 wt.% and of S from 0.0 to 1.3 wt.% in the bottom ash.

The Fe concentration in the lignite samples ranges from 0.2 to 1.7 wt.% being probably related to pyrite; it is also possible to participate in clay minerals. The average concentrations of Ag, As, Cd, Cr, Ga, Li, Mo, Ni, Pb, Sr, U, V and Zn in the lignite samples are higher than the average world coal concentration (Table 2). The determination of Hg and Se is not accurate, due to their high volatility and the results for these elements are treated with skepticism.

Strontium exceeds 100 mg/kg in the lignite, while the concentrations of many elements as Ba (21-227 mg/kg), Mn (23-173 mg/kg), Ni (9-153 mg/kg) and V (59-163 mg/kg) display a wide range among the bulk samples. The contents of As, B, Co, Cr, Cu, Ga, Li, Mo, Pb, U, Zn have contents vary from 1 mg/kg to 100 mg/kg, whereas these of Ag, Be, Cd, Hf, Hg are <1 mg/kg. The elements Ag, As, B, Ba, Be, Cd, Co, Cr, Cu, Fe, Ga, Hf, Li, Mn, Ni, Mo, Zn display strong correlation with the ash yields suggesting an inorganic affinity, whereas the weak correlation of B, Mo, Sr, V, U and ash yield indicates an intermediate affinity (organic–inorganic) for these elements.

Element concentrations in fly ash samples were compared to those corresponding to the average crust composition (Table 2). It appears that As, B, Li, Mo, Ni, Pb, U, V and Zn are enriched. The concentrations of Ag, Cd, Cu, Ga present higher values in comparison to these of the crust, but not as high as the elements that were mentioned before. Barium, Co, Cr, Hf, Mn, and Sr display lower average concentrations in the fly ash samples than in the crust (Table 2).

The Fe content ranges from 0.9 to 2.9 wt.% in bottom ash with an average of 1.6 wt.%. Mn, Sr, V and Zn have contents higher than 100 mg/kg, while the contents of Ag, Be, Cd, Co, Cr, Cu, Ga, Hf, Hg, Li, Mo, Ni, Pb, Se and U range lower than 100 mg/kg. The elements As, B, U, V and Zn display very high average values in the bottom ash. Beryllium, Co, Cu, Hf, Mn, and Sr display lower

Table 2. Average concentrations (in mg/kg, if not otherwise stated) of trace elements in Muğla lignite, fly and bottom ash in comparison to worldwide coal (Clarke and Sloss, 1992) and upper crust average values (Seredin and Finkelman, 2008).

<i>Element</i>	<i>Lignite</i>	<i>Fly ash</i>	<i>Enrichment Factor</i>	<i>Bottom ash</i>	<i>Enrichment Factor</i>	<i>Crust</i>	<i>Worldwide coals</i>
Fe (%)	0.7	2		1.6			
Ag	0.1	0.3	0.63	0.3	0.61	0.1	0.1
As	21	131	1.56	24	0.29	1	7.6
B	38	167	1.07	100	0.64	10	56
Ba	86	296	0.84	280	0.80	425	150
Be	0.5	3	1.29	2	1.10	3	1.2
Cd	0.4	2	1.04	0.6	0.37	0.2	0.2
Co	4	17	1.07	15	0.93	25	4.2
Cr	35	93	0.66	76	0.54	100	15
Cu	12	65	1.32	52	1.04	55	15
Ga	8	32	0.93	24	0.70	15	5.5
Hf	0.4	2	1.07	2	0.95	20	1.2
Hg	0.4	-	-	-	-	0.08	0.1
Li	13	71	1.30	58	1.06	20	10
Mn	77	314	0.98	295	0.93	950	153
Mo	10	29	0.69	17	0.42	2	2.2
Ni	40	100	0.62	93	0.57	75	9.0
Pb	10	41	1.03	17	0.44	13	6.6
Se	-	-	-	-	-	0.05	1.0
Sr	370	294	0.20	372	0.25	375	120
U	30	56	0.47	64	0.53	2	2.9
V	124	255	0.52	242	0.49	135	22
Zn	61	220	0.89	131	0.53	70	18

contents in the bottom ash compared to the crust (Table 2). The ash samples are enriched in most of the trace elements due to the loss of volatile elements during combustion.

4.4 Behavior of elements during combustion

In order to estimate the mobility of the studied elements, the relative enrichment factor (EF) was calculated using a formula introduced by Meij (1995) (Table 2). It constitutes a measure of the concentration of an element in the bulk coal sample and its produced ash (Meij & te Winkel, 2009; Vejehati et al., 2009). Elements with $EF > 0.7$ are considered enriched, these with $EF < 0.5$ non-enriched, and these with $0.5 < EF < 0.7$ slightly enriched. According to the calculated EFs B, Mo, Sr, U and V are the most volatile elements, whereas Ag, As, Be, Cd, Cr, Ga, Ni, Pb and Zn display medium volatility. Barium, Co, Cu, Hf, Li and Mn are non-volatile elements.

4.5 Leaching

The concentration of an element in the leachate solutions is a function of both total element concentration in the sample and leaching behavior. For this reason the calculation of indices, which in-

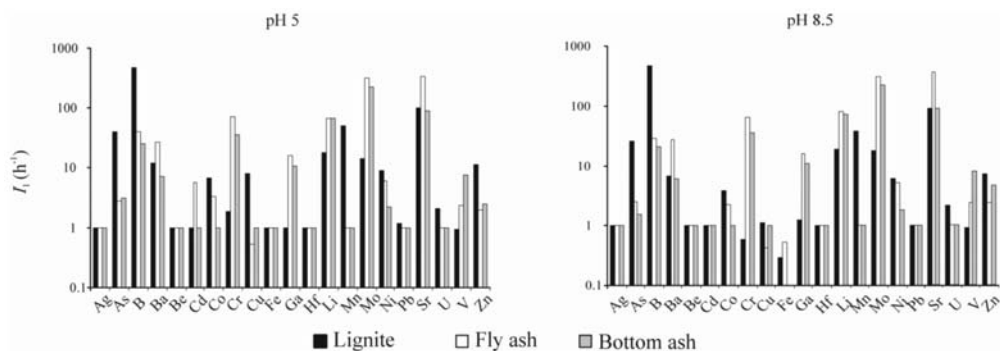


Fig. 2: Element Leaching Intensities (I_l) in the Muğla lignite, fly ash and bottom ash.

volve total element concentration is a common practice used to describe the leaching behavior of an element.

In the present study the Leaching Intensity (I_l) was calculated in order to describe the leaching rate with respect to the leaching time (Wang et al., 1999):

$$I_l = \frac{\alpha_x \times V \times 10^3}{A_x \times M \times t} \quad (\text{eq. 1})$$

where α_x the concentration of an element x in the leachate (mg/ml), V the total volume of the leachate solution (ml), A_x the concentration of the element x in the original sample (mg/g), M the sample weight (g) used for the leaching experiment and t the leaching time (h). The stronger the I_l , the highest the leaching rate of an element. The leachability of an element is distinguished in four classes according to its I_l . Strong leachability display elements with $I_l \geq 5$, medium with $1 \leq I_l < 5$, weak with $0.5 \leq I_l < 1$ and very weak with $I_l < 0.5$ (Wang et al., 1999).

Arsenic, B, Ba, Cu, Li, Mn, Ni, Zn and Sr have strong leachability at all pH values in lignite samples except for Cu and Zn which reduce their leachability under alkaline conditions from strong to medium. Chromium displays medium leachability under acidic and alkaline conditions (Fig. 2). Boron, Ba, Cr, Ga, Li, Mo, Ni, Sr have strong leachability at all pH values in the fly ash samples, whereas As, Co, V and Zn have medium leachability with Co leachability turned to weak under alkaline conditions. Finally, B, Ba, Cr, Ga, Li, Mo, Sr, V display strong leachability at all pH values in bottom ash samples and As, Ni, Zn have medium leachability, except for Zn which increases its leachability to strong under alkaline conditions.

5. Discussion

Volatility and leachability are considered the major properties, which define the environmental significance of an element. The former predicts the combustion behaviour and the latter the potential release of an element from the dump sites and the hazard for groundwater contamination. Both properties were divided into three classes including high, moderate and low volatile/leachable elements (Fig. 3).

High volatile elements are Sr, Mo, U and V, whereas the volatility of most of the elements seems to be moderate. Manganese, Li, Ba, Cu, Co and Hf are the least volatile elements. The correlation of element concentrations and mineralogical composition indicates that the most volatile elements in

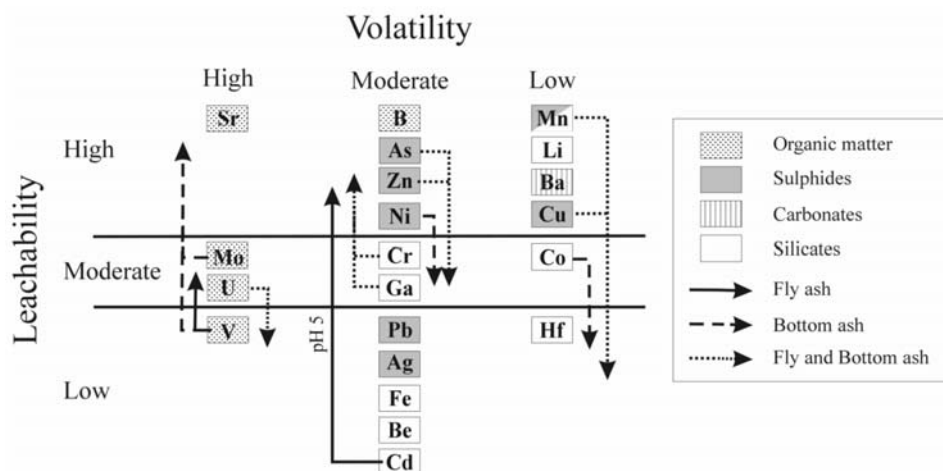


Fig. 3: The mode of occurrence and the classification of the elements according to their combustion and leaching behaviour in the Muğla lignite. Arrows indicate the shift of leaching behaviour in the ash samples.

the Muğla lignite display a mixed affinity between mineral and organic matter probably forming organometallic compounds or being adsorbed on the organic matter (e.g. Wang et al., 1999). Sulphide-bound elements display a moderate volatility except from Cu (Fig. 3), whereas elements affiliated to the carbonates and the silicates appear to be low or non-volatile.

All elements display almost the same leaching behaviour for the same sample type under both initial pH values of the leaching agent except from Cd, which proves to be highly mobile in the fly ash under pH 5. The elements B and Sr seem to be the most mobile elements in the lignite indicating that the organic affinity is responsible for the high leaching rate of an element, as well. However, other organically-bound elements such as U and V display moderate and low mobility in the lignite suggesting that the mode of occurrence of an element is not the exclusive factor influencing an element's mobility. This is also supported by the fact that other elements such as As, Ba, Cu, Li, Mn, Ni and Zn with different modes of occurrence seem to be high mobile in the lignite. Most of them display an affinity to the sulphide phase but others like Ba and Li are related to other phases (Fig. 3). The elements affiliated with the silicate phase are low or non-mobile.

Generally, most of the elements are redistributed during combustion due to volatilization and recondensation reactions participating either on the surface or in the matrix of the ash particles. Elements distributed on the ash surface tend to be more mobile but most of the trace elements are less likely to be released due to their adsorption on less soluble aluminosilicates and oxide phases in fly ash and bottom ash samples (Yuan, 2009). The elements Sr, B, Li, Ba, Pb, Ag, Fe, Be and Hf do not display a shift in their leaching behaviour during the transition from the lignite to the ash state. The surface distribution seems to be the most probable reason for the high mobile and organically-bound elements (Sr, Mo, B). These three elements are usually among the most mobile in both coal and the produced ashes (e.g. Wang et al., 1999; Georgakopoulos et al., 2002; Praharaj et al., 2002; Ward et al., 2009). Especially Mo is mobile under all pH values between 2 and 8.5 (Siegel, 2002). The majority of the elements, affiliated to the sulphide phase in the lignite, displays a profound decrease in their leachability in both fly and bottom ash. The breakdown of sulphides and the formation of stable secondary oxides or other more complex compounds is considered responsible for this change. Particularly for As the decrease of its mobility in the ash state has also been reported from other

coals worldwide and is due to the formation of the arsenate oxyanion, which reacts with calcium to form calcium arsenate (Jones, 1995). However, although Ca acts as an immobilizing agent for other elements such as B, its action in the Muğla ashes seems to be limited, probably due to its low concentration as suggested by the low calcite and lime contents in the lignite and ash, respectively. Elements with increased mobility in the ash samples are Cr, Ga and V, whereas Cd increased its mobility in the fly ash under acidic conditions.

Aside volatility and leachability the total concentration of an element has to be considered in order to discuss the environmental significance of a certain element. When compared to the average of coals worldwide the Muğla lignite is enriched in As, Cr, Mo, Ni, Sr, U, V and Zn. In the fly and bottom ash samples all elements are enriched compared to the average upper crust concentrations. Additionally, it has been shown that certain elements including As, Mn, Mo and Pb are susceptible for soil contamination in Yatağan region, although high Mn concentrations are attributed to the use of fertilizers in the area (Baba, 2002).

6. Conclusions

Muğla lignite is a low rank coal of medium to poor quality, thus the estimation of environmental impacts from its utilization is necessary. Trace element and mineralogical analyses reveal that the mode of occurrence of the elements is the major factor controlling their combustion behaviour with the most volatile being these, exhibiting a mixed organic/inorganic affinity (Sr, Mo, U, V and B). Sulphide related elements are next in the volatility string, whereas elements bound to the silicate minerals seem to be the less volatile.

The mode of occurrence also controls the leaching behaviour but other factors such as the physico-chemical properties of individual elements have to be considered. The majority of elements display identical leaching behaviour under both acidic and alkaline environments. Additionally, the change of state from lignite to ash affects mostly the behaviour of elements affiliated to the sulphide phase decreasing their leaching rates.

Based on both combustion and leaching behaviour all trace elements in the Muğla lignite can be distinguished in the following classes with increasing environmental concern:

- Ia: non-volatile/non-mobile elements - Co, Cu, Hf,
- Ib: non-volatile/lignite mobile elements - Ba, Mn, Li,
- IIa: moderately volatile/low mobile - Ag, Be, Fe, Pb,
- IIb moderately volatile/lignite mobile - As, Ni, Zn,
- III moderately volatile/high mobile - B, Cd, Cr, Ga,
- IVa: high volatile/low mobile - U and
- IVb: high volatile/high mobile - Mo, Sr, and V.

7. References

- Baba, A., 2002. Geochemical assessment of environmental effects of ash from Yatağan (Muğla-Turkey) thermal power plant. *Water, Air, and Soil Pollution*, 144, 3-18.
- Baba, A. & Kaya A., 2004. Leaching characteristics of solid wastes from thermal power plants of western Turkey and comparison of toxicity methodologies. *Journal of Environmental Management*, 73, 199-207.

- Baba, A., Gurdal, G., Sengunalp, F. & Ozay, O., 2008. Effects of leachant temperature and pH on leachability of metals from fly ash. A case of study: Can thermal power plant, province of Canakkale, Turkey. *Environmental Monitoring and Assessment*, 139, 287-298.
- Bish, D.L. & Post, J.E., 1993. Quantitative mineralogical analysis using the Rietveld full-pattern fitting method. *American Mineralogist*, 78, 932-940.
- Clarke, L.B. & Sloss, L.L., 1992. Trace elements-emissions from coal combustion and gasification. London, IEA Coal Research, 111.
- Demirak, A., Balci, A., Dalman Ö. & Tüfekci, M., 2005. Chemical investigation of water resources around the Yatağan thermal power plant of Turkey. *Water, Air and Soil pollution* 162, 171-181.
- Diessel, C.F.K., 1992. Diessel, C.F.K., 1992. Coal-Bearing Depositional Systems. Springer Verlag, Berlin. 721 pp
- Economic Commission for Europe-United Nations (ECE-UN), 1998. International Classification of In-Seam Coals. United Nations, Geneva. 42 pp.
- Finkelman, R.B., 1994. Modes of occurrence of potentially hazardous elements in coal: levels of confidence. *Fuel Processing Technology*, 39, 21-34.
- Finkelman, R.B. & Gross, P.M.K., 1999. The types of data needed for accessing the environmental and human impacts of coal. *International Journal of Coal Geology*, 40, 90-101.
- Georgakopoulos, A., Filippidis, A., Kassoli-Fournaraki, A., Fernández-Turiel, J.L., Llores, J.F. & Mousty, F., 2002. Leachability of major and trace elements of fly ash from Ptolemais Power Station, Northern Greece. *Energy Sources*, 24, 103-111.
- Hesbach, P., Kim, A.G., Abel, A. & Lamey, S., 2009. Serial batch leaching procedure for characterization of coal fly ash. *Environmental Monitoring Assessment*, in press (available online).
- İnaner, H. & Nakoman, E., 2005. Properties of lignite deposits in Western Turkey. Abstract Book 57th Annual Meeting of the ICCP, Patras, 11.
- İnaner, H., Nakoman, E. & Karayığit, A.I., 2008. Coal resource estimation in the Bayir Field, Yatağan-Muğla, SW Turkey. *Energy Sources, Part A*, 30, 1000-1015.
- International Committee for Coal Petrology (ICCP), 1993. International Handbook of Coal Petrography, Supplement, Commission I, 19.
- Jones, D.R., 1995. The leaching of major and trace elements from coal ash. In: Environmental Aspects of Trace Elements in Coal, Swaine, D.J. and Goodarzi, F. (eds). The Netherlands, Kluwer Academic Publishers, 221-262.
- Karayığit, A.I., Gayer, P. A., Querol, X. & Onacak, T., 2000. Contents of major and trace elements in feed coals from Turkish coal-fired power plants. *International Journal of Coal Geology*, 44, 169-184.
- Meij, R., 1995. The distribution of trace elements during the combustion of coal. In: Environmental Aspects of Trace Elements in Coal, Swaine, D.J. and Goodarzi, F. (eds). The Netherlands, Kluwer Academic Publishers, 111-127.
- Meij, R. & te Winkel, B.H., 2009. Trace elements in world steam coal and their behaviour in Dutch coal-fired power stations: A review. *International Journal of Coal Geology* 77, 289-293.
- Praharaj, T., Powell, M.A., Hart, B.R. & Tripathy, S., 2002. Leachability of elements from sub-bituminous coal fly ash from India. *Environment International*, 27, 609-615.
- Querol, X., Alastuey, A., Plana, F., Lopez-Soler, A., Tuncali, E., Toprak, S., Ocakoglu, F., & Koker, A., 1999. Coal geology and coal quality of the Miocene Mugla basin, southwestern Anatolia, Turkey. *International Journal of Coal Geology*, 41, 311-332.
- Seredin, V. and Finkelman, R., 2008. Metalliferous coals: A review of the main genetic and geochemical types. *International Journal of Coal Geology*, 76, 253-289.

- Siavalas, G., Zilakou, S., Kalaitzidis, S., Chatziapostolou, A., Bouzinos, A. & Christanis, K., 2007. Trace element lechability from lignite and combustion by-products under certain pH conditions. *Proceedings of the 10th International Conference on Enviromental Science and Technology*, Kos Island, 5-7 September.
- Siegel, F.R., 2002. *Environmental Geochemistry of Potentially Toxic Metals*. Springer-Verlag, Berlin-Heidelberg, Germany, 218 pp.
- Vassilev, S.V., Vassileva, C.G., Karayigit, A.I., Bulut, Y., Alastuey, A. & Querol, X., 2005. Phase-mineral and chemical composition of composite samples from feed coals, bottom ashes and fly ashes at the Soma power station, Turkey. *International Journal of Coal Geology*, 61, 35-63.
- Vejahati, F., Xu, Z. & Gupta, R., 2009. Trace elements in coal: Associations with coal and minerals and their behavior during coal utilization – A review. *Fuel*, in press (available online).
- Wang Y., Ren D. & Zhao F., 1999. Comparative leaching for trace elements in raw coal, laboratory ash, fly ash and bottom ash. *International Journal of Coal Geology*, 40, 103-108.
- Ward, C. R., French, D., Jankowski, J., Dubikova, M., Li, Z. & Riley K. W., 2009. Element mobility from fresh and long-stored acidic fly ashes associated with an Australian power station. *International Journal of Coal Geology*, 80, 224-236.
- Yuan, C.G., 2009. Leaching characteristics of metals in fly ash from coal-fired power plant by sequential extraction procedure. *Microchimica Acta*, 165, 91-96.

CONTRIBUTION OF LIGNITE IN THE GREEK ECONOMY

**Karageorgiou D. E.¹, Metaxas A.¹, Dimitriou D.¹, Arapogiannis E.¹
and Varvarousis G.¹**

¹ *Institute of Geology and Mineral Exploration, Olympic Village, Entrance C 136 77 Acharnae Greece
dek@igme.gr*

Abstract

The objective of the present work is the assessment of the lignite contribution to the energy balance of Greece, according to the creation processes and the chronological classification.

The lignite deposits known so far in Greece have been discovered and researched from the scientists of IGME in the course of evolution since 1948 (Greek Geological Survey), 1950 (Institute of Geology and Surface Research), 1973 (National Institute of Geological and Mineral Exploration) and finally in its current form in 1976 (Institute of Geology and Mineral Exploration) and are divided into (a) “productive”, (b) future “productive” and (c) no financial interest in power generation. A project, co-financed by the Greek Government and the European Union, is currently implemented, aiming at the recovery of the latter in non-electrical purposes with very good results in the first stage of research.

According to the works carried out so far it has been observed that lignite formation started in Greece during Eocene and continued to date.

From 1950 until today there is an upward trend in lignite reserves. Lignite generates electricity at a rate 63% today with higher rates 79.3%, during 1994.

In Greece 41% of lignite deposits were created during Miocene. However, only 13% of these deposits that contribute to electricity generation derive from economically exploitable reserves.

In Greece, due mainly to use of lignite for electricity production, the cost of Kw/h for both domestic use and for industrial is below the European Union average.

Key words: *lignite, energy balance, chronological classification and electricity.*

1. Introduction

The objective of the present work is the assessment of the lignite contribution to the energy balance of Greece, according to the creation processes and the chronological classification.

Furthermore, it was observed that lignite creation in Greece started during Eocene and that 41% of the lignite deposits were formed during Miocene. However, only 13% of the deposits contributing to electricity generation derive from economically exploitable reserves.

2. Chronological Classification

The lignite deposits known so far in Greece have been discovered and researched from the scientists of IGME in the course of evolution since 1948 (Greek Geological Survey), 1950 (Institute of



Fig. 3: Map of Up. Miocene – L. Pliocene Greek lignite bearing basins.

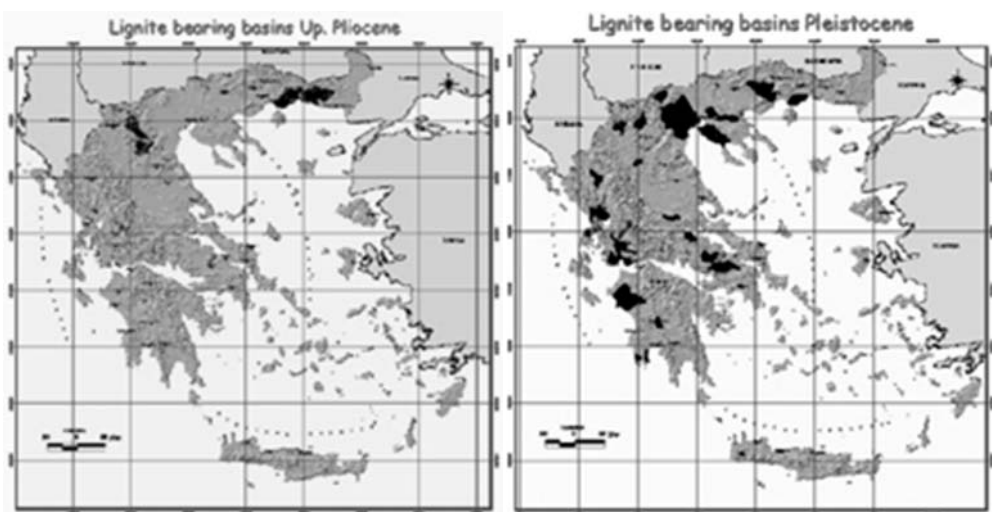


Fig. 4: Map of Up. Pliocene Greek lignite bearing basins. **Fig. 5:** Map of Pleistocene Greek lignite bearing basins.

Geology and Surface Research), 1973 (National Institute of Geological and Mineral Exploration) and finally in its current form in 1976 (Institute of Geology and Mineral Exploration) and are divided into (a) “productive”, (b) future “productive” and (c) no financial interest in power generation. A project, co-financed by the Greek Government and the European Union, is currently implemented, aiming at the recovery of the latter in non-electrical purposes with very good results in the first stage of research (Fanara and Chatzigiannis, 1999).

According to the studies implemented so far, the chronological classification of the Hellenic territory is illustrated in figs 1,2,3,4 and 5. In Greece, lignite formation started during Eocene and continued to date (Metaxas et al., 2007).

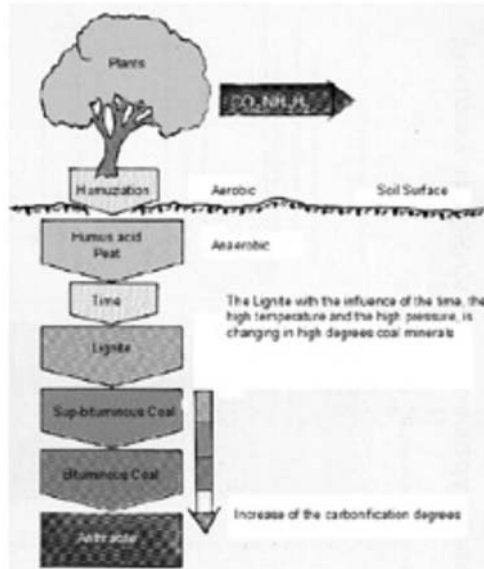


Fig. 6: General view of lignite formation.

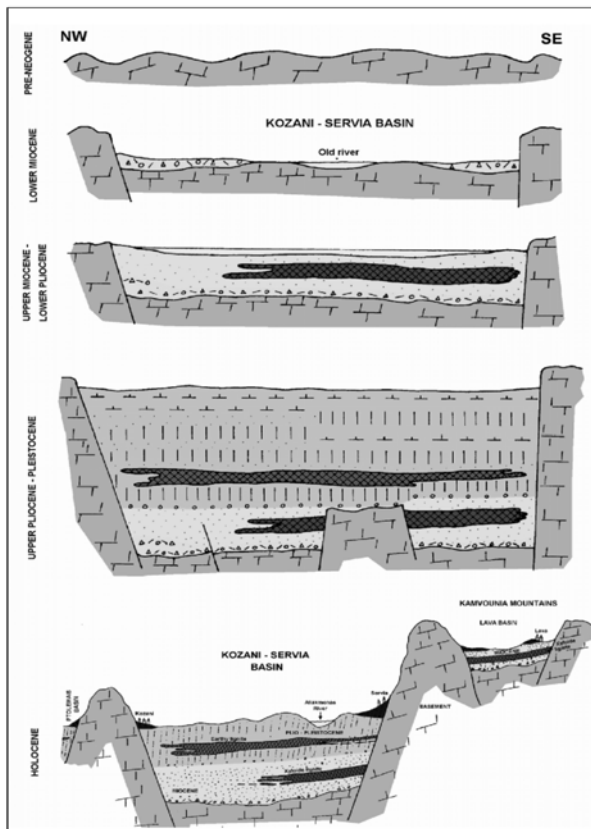


Fig. 7: Different phases of the Kozani – Servia lignite bearing basin.

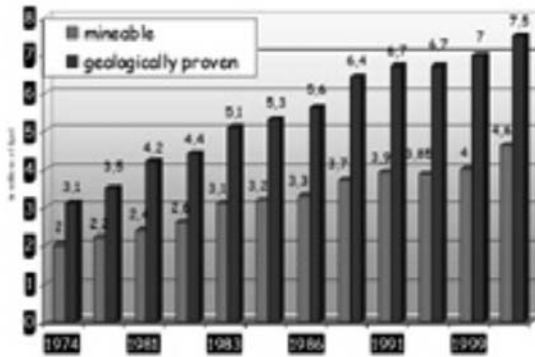


Fig. 8: Greek lignite mine able and geological proven reserves.

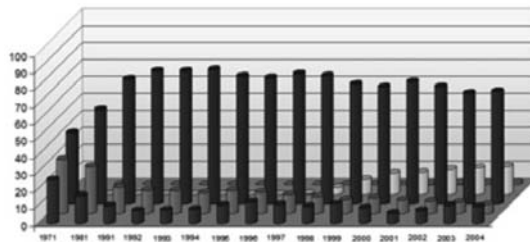


Fig. 9: The contribution of the lignite in the electricity in Greece.

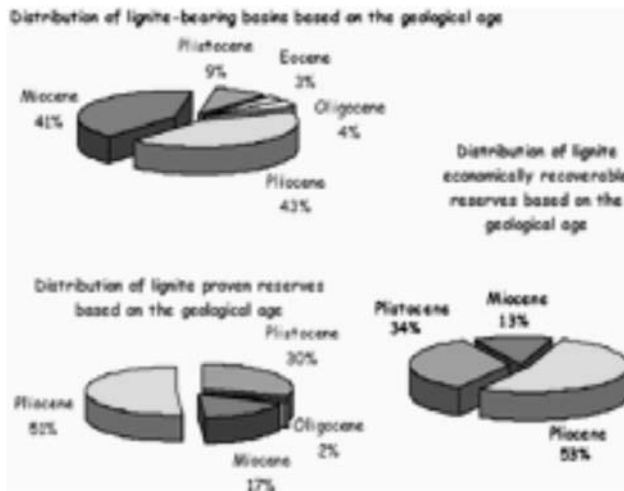


Fig. 10: Distribution of Greek lignite bearing basins reserves.

A schematic representation of the general creation way of lignite is given in figure 6, while in figure 7 is schematically given the creation of the lignite-bearing basin Kozani – Servia.

3. Participation of Lignite in the Energy Balance

From 1950 to date, there was an upward trend in the participation of the lignite reserves (Fig. 8) As indicated in figure 9, lignite contributes to electricity generation at a percentage of 63% today, comparison with highest ever level of 79.3%, recorded during 1994 (Leontidis et al., 2005).

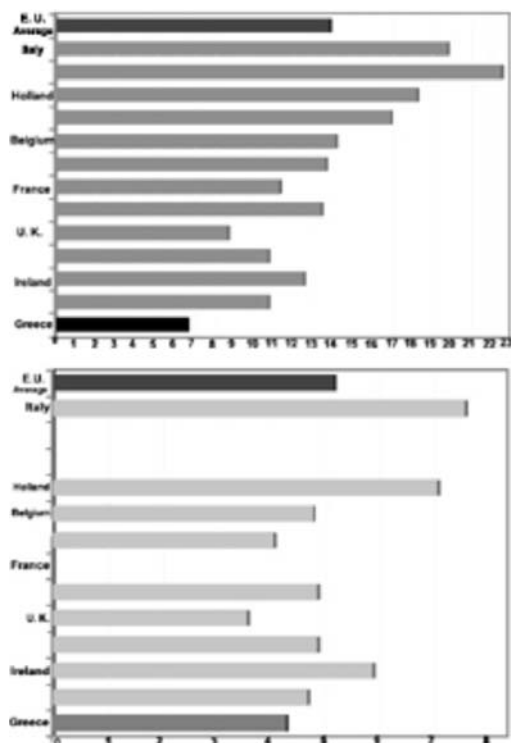


Fig. 11: Prices of Kw/h in €, for industrial and domestic use in E.U.

According to figure 10 although around 41% of lignite deposits in Greece was formed during Miocene and only 9% during Pliocene, 30% out of the economically exploitable reserves of electricity generating lignite belongs to Pliocene, (Koukouzas et al., 1997; Kotis, 2002)

In Greece, due mainly to the use of lignite for electricity production, the cost of Kw/h for both domestic use 6,7€, and for industrial 4,3€, is below the European Union average 13.9€ and 5.2€ respectively (Karageorgiou and Metaxas, 2006) (Fig.11).

4. Conclusions

The known lignite deposits in Greece, have been discovered and researched by the scientists of Institute of Geology and Mineral Exploration (I.G.M.E.),

Lignite formation started in Greece during Eocene and continued to date.

Lignite generates electricity at a rate 63% today with higher rates 79.3%, during 1994.

In Greece although 41% of lignite deposits were formed during Miocene and only 9% during Pliocene, the electricity generating lignite belongs mostly to Pliocene, at a rate 30% of the economically exploitable reserves.

In Greece, due mainly to the use of lignite for electricity production, the cost of Kw/h for both domestic use 6.7€, and for industrial 4.3€, is below the European Union average 13.9€ and 5.2€ respectively.

5. References

- Fanara, E. and Chatziyiannis, G., 1999. Lignite Deposits and Mines of Greece. *Athens I.G.M.E.*
- Karageorgiou, D., E., Metaxas, A., 2006. Contribution of Greek Lignite in the Production of Electricity and in the Environmental Protection. *Proceedings XVIIIth Congress of the Carpathian – Balkan Geological Association pp.255-257. Belgrade, Serbia.*
- Kotis, Th., 2002. The deposits of lignite in the basins Florina, Megalopoli, Elassona, Drama, *Athens IGME 8pp. (In Greek).*
- Koukouzas, C., Foskolos, A.,E., Kotis, T., 1997. Research and exploration of coal in Greece. A view to the future, *Energy Sources, 19, 335-347pp.*
- Leontidis, M., Roubos, Ch., Vlachou, A., 2005. Hundred Years Lignite. *P.C.E. 6th publication, pp.50 (in Greek) 3–169.*
- Metaxas A., Karageorgiou, D.,E., Varvarousis, G., Kotis, Th., Ploumidis, M., and Papanikolaou, G., 2007. Geological evolution – stratigraphy of Florina, Ptolemaida, Kozani and Saradaporo graben. *Proceedings 11th International Conference of Geological Society of Greece pp. 161-172. Athens Greece.*

DEVELOPMENT OF LIGNITE IN CRETE. COMPARISON OF BASINS, POSSIBILITIES OF EXPLOITATION

**Karageorgiou D. E.¹, Metaxas A.¹, Karageorgiou M. M. D.²,
Papanikolaou G.³, Georgakopoulos A. N.⁴, Vrettos K.¹**

¹*Institute of Geology and Mineral Exploration, Olympic Village, Entrance C 136 77,
Acharnae, Greece, dek@igme.gr*

²*Geographer, 62 Amissou str. 17123 N. Smyrni, Athens, Greece, melaxroini_ka@yahoo.gr*

³*Geologist, Department of Geology, National & Kapodistrian University of Athens, Greece,
geopapgr@gmail.com*

⁴*Aristotle University of Thessaloniki, Department of Mineralogy-Petrology-Economic Geology,
Laboratory of Economic Geology, 54124 Thessaloniki, Greece, ageorgak@geo.auth.gr*

ABSTRACT

The island of Crete has been thoroughly explored, by various organizations, for the presence of lignite deposits, in order to examine the possibility of energy independence for the island and thus reduce the cost of consumed electric energy. Research showed that lignite generates in fluvial – lacustrine environments in many places in Crete and lignite deposits have been investigated and exploited from time to time. In the present study all lignite occurrences of the island are recorded and their generation and depositional environment is analysed. Lignite horizons from different basins are compared and correlated. An evaluation of results from previous studies is attempted, regarding both surface information and depth data, derived from borehole projects. Finally, areas suitable for lignite exploitation in the production of electricity or other uses are presented.

Key words: lignite origin, lignite deposits, electricity, exploitation, Crete, South Greece.

1. Introduction

Exploratory works carried out in the island of Crete have shown the presence of lignite deposits in several areas. In some of them small-scale exploitation took place in the past.

The electric power consumed in the island of Crete reaches 3050Gw/h per year and is either transported from the mainland or produced in Steam Electric Stations using oil.

The aim of this study is to present the lignite deposits recorded by investigations carried out by Institute of Geology and Mineral Exploration of Greece (IGME) in the island of Crete (fig.1) regarding both surface information and depth data. An analysis of the origin and depositional environments is attempted, given that they are mainly located in fluvial-lacustrine environments with successive sea transgressions. Moreover, the lignite horizons from different basins are correlated. This study can contribute to the reduction of the electric power costs and achieve energy independence for the island of Crete.

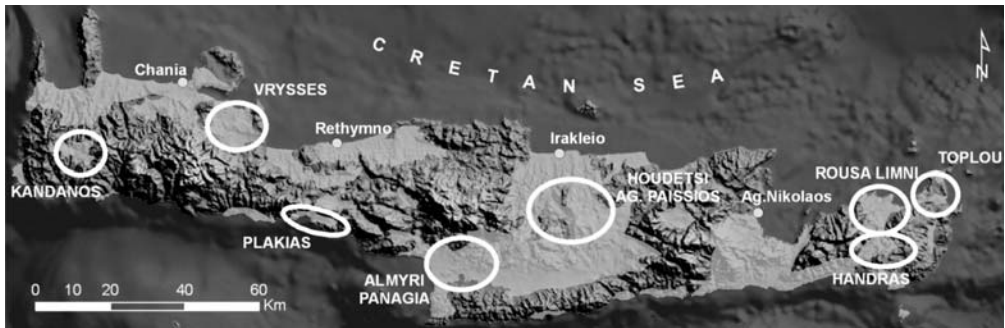


Fig. 1: Neogene's and Quaternary lignite areas of Crete Island.

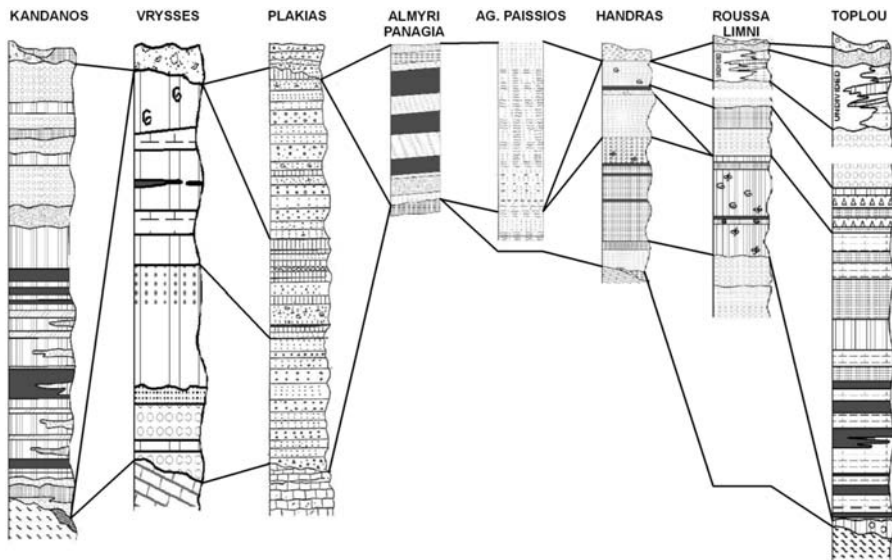


Fig. 2: Stratigraphic correlation of the lignite areas of Crete Island.

2. Geological setting

In the island of Crete the lignite deposits are located into the Miocene fluvial-lacustrine formations, with exception of Kandanos to the West and Almyri Panagia in the Central and South part of the island basins. (Karageorgiou, 1952).

Lignite was deposited into fluvial-lacustrine formations consisting of clays, sands and marls. Fossils - *neritina*, *potamites*, *melanopsis*, etc. – are observed into these formations (Vetoulis, 1952). Frequent sea transgressions are also observed separating the lignite beds.

The general stratigraphic column of the lignite basins is described below:

- **Bedrock:** consists of the rocks of the formations of Tripolis zone (Jurassic to Middle Eocene Limestones, Flysch of Upper Eocene to Oligocene), Pindos zone (Upper Cretaceous Limestones, Flysch of Paleocene to Eocene), as well as of the ophiolitic complex of the internal zones.
- **Formation of the Base:** consists of a polymict conglomerate, breccias, sands, red clays, with thickness ranging from a few centimetres to some tens of meters. It overlies the bedrock and

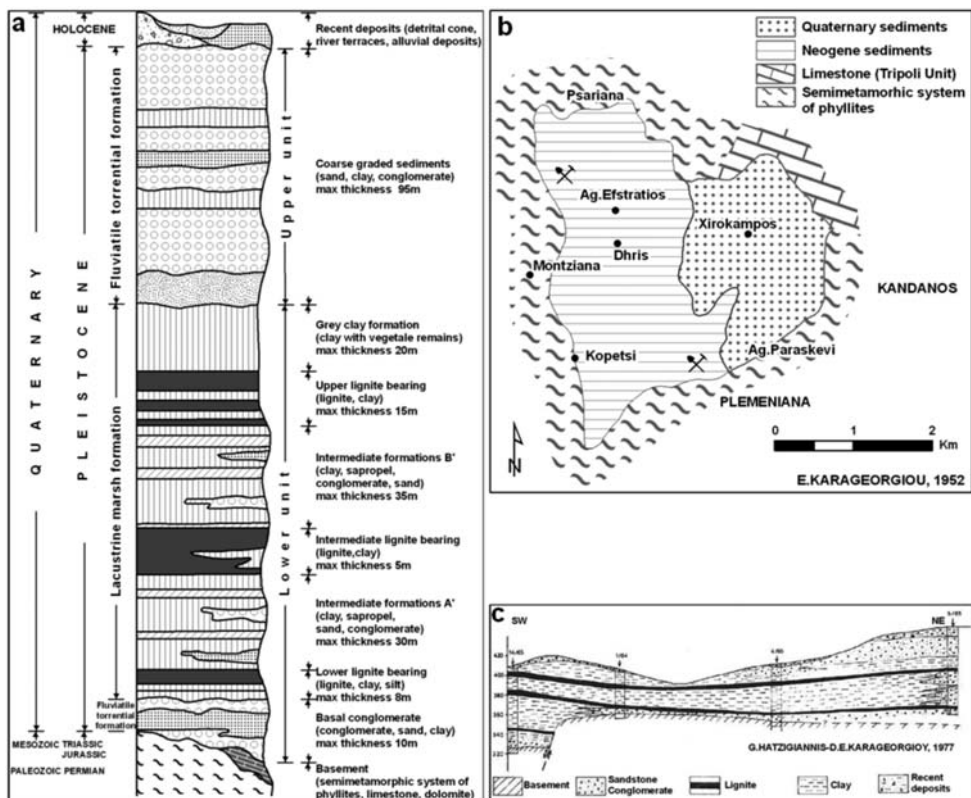


Fig. 3: (a): Stratigraphic column of Kandanos area; (b): Geological map of Kandanos area; (c): Geological section of boreholes in Kandanos area.

smooths its erosions. In the areas of Almyri Panagia and Handra these sediments are of marine origin and different age: Upper Pliocene and Miocene respectively.

- Lacustrine-marshy and fluvial-lacustrine phase: consists of marls, clays, sands and silts and hosting lignite beds of various thicknesses. This phase is of Miocene age apart from the areas Almyri Panagia and Kandanos, which are of Pleio-Pleistocene age.
- Fluvial-torrential or marine formations: closing the Neocene series. The marine formations consist of a transgression conglomerate and sands, clays with *Ostrea*, *Pecten*, etc. fossils and the fluvial-torrential formations of sands, clays, conglomerates and breccias.
- Recent formations: alluvial deposits, talus cones, clays, sands, unconsolidated conglomerates (Fig. 2).

3. Areas of Interest

3.1 Kandanos

The area is located to the South-West of Chania city at a distance of 60 km., occupying an extent of about 10km². Only the West - North West part of 1km² area has been investigated in the past, (Karageorgiou, 1951) since it is of great geological interest and Germans have exploited the lignite of this section during the period 1940-1944.

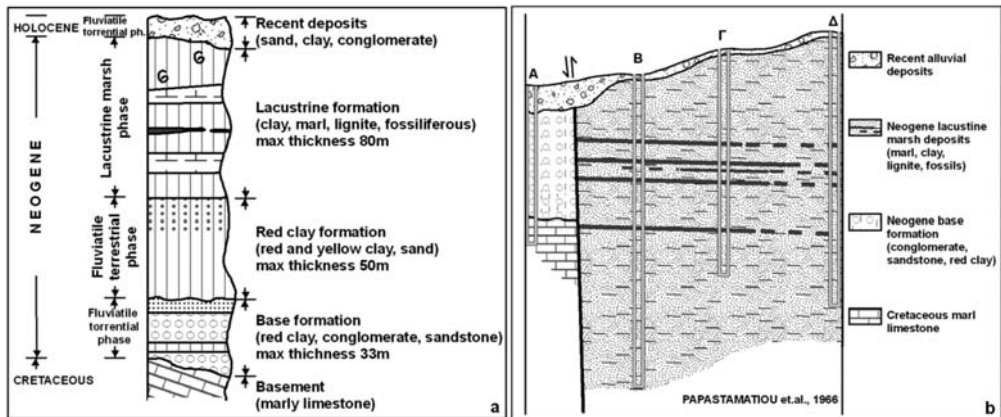


Fig. 4:(a): Stratigraphic column of Vrysses area; (b): Geological section of boreholes in Vrysses area.

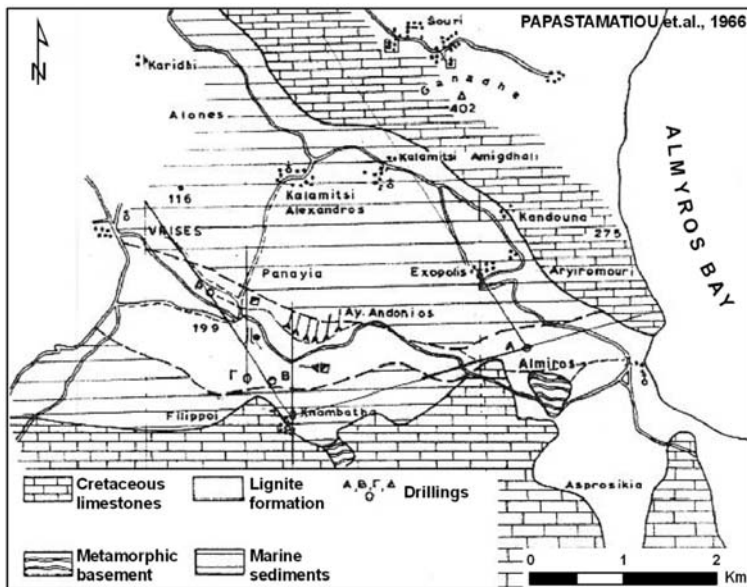


Fig. 5: Geological map of Vrysses area.

The geological formations (Chatziagiannis and Karageorgiou 1977) observed in the area are shown in the stratigraphic column (Fig. 3a) and the geological map (Fig. 3b).

Three main lignite beds are located in Kandanos area (Fig. 3c) having 9 million tons as potential reserves. These lignite beds can be exploited by open-pit mining with an exploitation ratio ranging from 2.3 to 11/1. The Gross Calorific Value [on an a.r. (as received) basis] is of 1700Kcal/Kg.

The region should be systematically investigated as a whole in order to increase the exploitable lignite reserves.

3.2 Vryses

This area is located east of Chania city at a distance of 20 km. The geological formations observed in the area are shown in the stratigraphic column (Fig. 4a) and the geological map (Fig. 5).

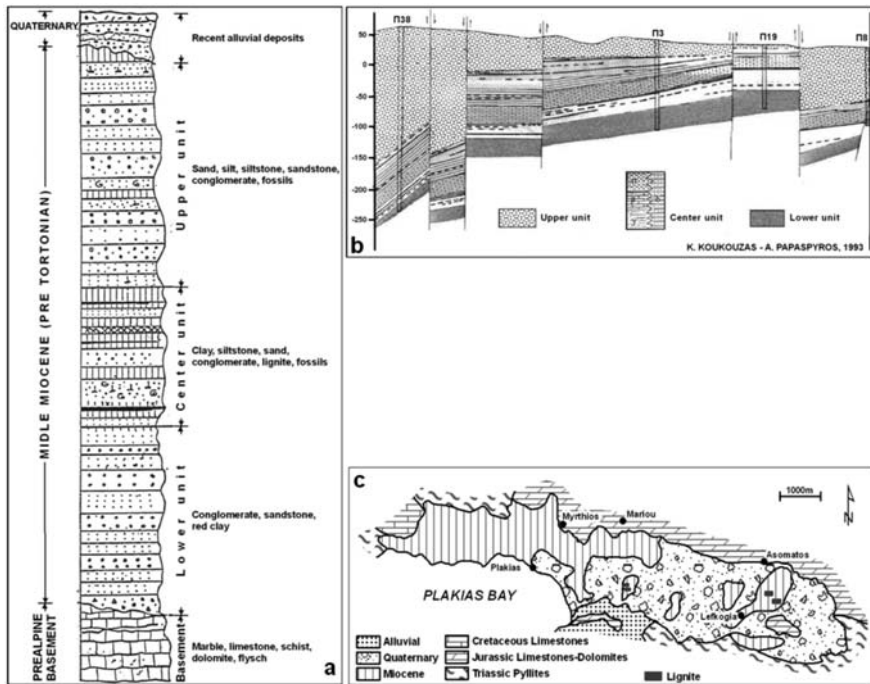


Fig. 6: (a): Stratigraphic column of Plakias area; (b): Geological section of boreholes in Plakias area; (c): Geological map of Plakias area.

Four lignite beds (Fig. 4b) were located in the area of Vryses Apokoronou. Previous investigations (Papachristos, 1952) demonstrated that there is apparent economic interest in the region.

3.3 Plakias – Lefkogia

The area is located south of Rethymno city at a distance of 35km, occupying an area of 10km² and has been repeatedly exploited in the past. From the extended mineralogical and geological investigation of the area carried out by I.G.M.E. (Koukouzas and Papaspyros 1993) 2.3 m. tons of strongly tectonized mineable lignite were located with an average Net Calorific Value [on an a.r. (as received) basis] >2.000 Kcal/Kg as illustrated in Fig. 6b. The geology of the area is shown in the stratigraphic column (Fig. 6a) and the geological map (Fig. 6c).

3.4 Almyri Panagia

The area is located to the south of Iraklio city at a distance of 40 km occupying an area of 8Km².

Restricted investigation including drilling of a few boreholes of small depth was carried out in the past (Papastamatiou et al., 1966). Four lignite beds were located (Fig. 7) having geological reserve in the order of 4.5 million tons and thickness of lignite beds varying from 2.70m to 5.20m (Papaspyros 1993). The geology of the area is shown in the stratigraphic column (Fig. 8a) and the geological map (Fig. 8b).

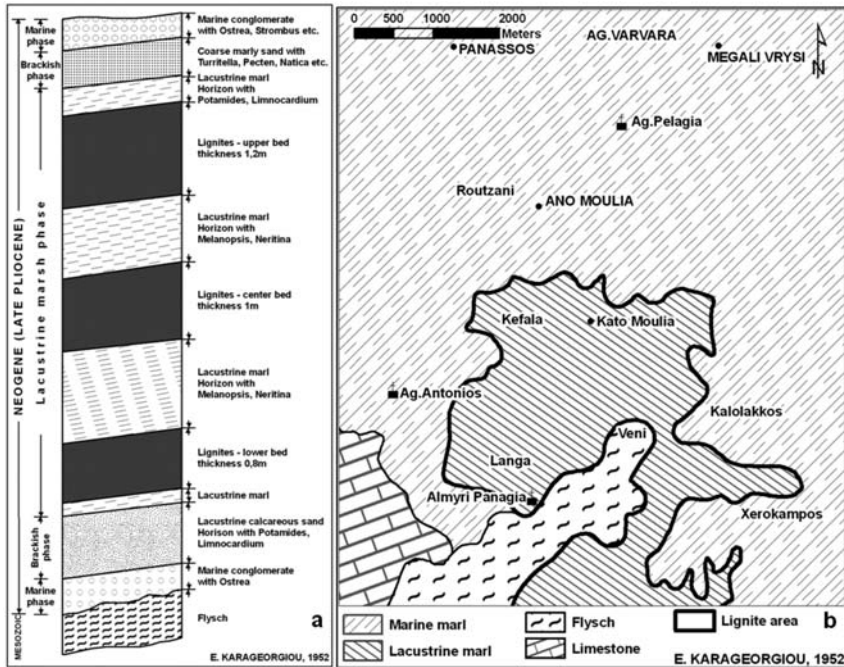


Fig. 7: (a): Stratigraphic section of lignite outcrop in Almyri Panagia area; (b): Geological map of Almyri Panagia area.

3.5 Agios Paisios – Houdetsio

The area is located to the South-East of Iraklio city and at a distance of 20 km, occupying an area of 18km².

The area is covered by lacustrine sediments of Miocene age with overlying marine Miocene formations (Koukouzas and Pappaspyros 1984). The lacustrine sediments occupy much greater extent than the aforementioned (the 18km²).

3.6 Handras

The area is located to the South of Sitia city at a distance of 20 km, occupying an area of 4,5km².

During Miocene three sea transgressions took place in the area alternating with two fluvial-marshy phases including the lignite beds of 30cm average depth (Maratos, 1952). Apart from the surface observation (Figs 8a, 8b) no other exploratory work was implemented in the area.

3.7 Roussa Limni

It is located at the margins of Sitia city occupying an extent of about 35km². Besides the geological mapping (Fig. 9b) and surface recordings, no further investigation was carried out in the area. The surface observation leads to the conclusion that the marine deposition of the sediments was interrupted by a small period of deposition of lacustrine-lacustrine-marshy sediments of 6m thickness, resulting in lignite generation without any economic interest (Fig. 9a). At the margins of the basin,

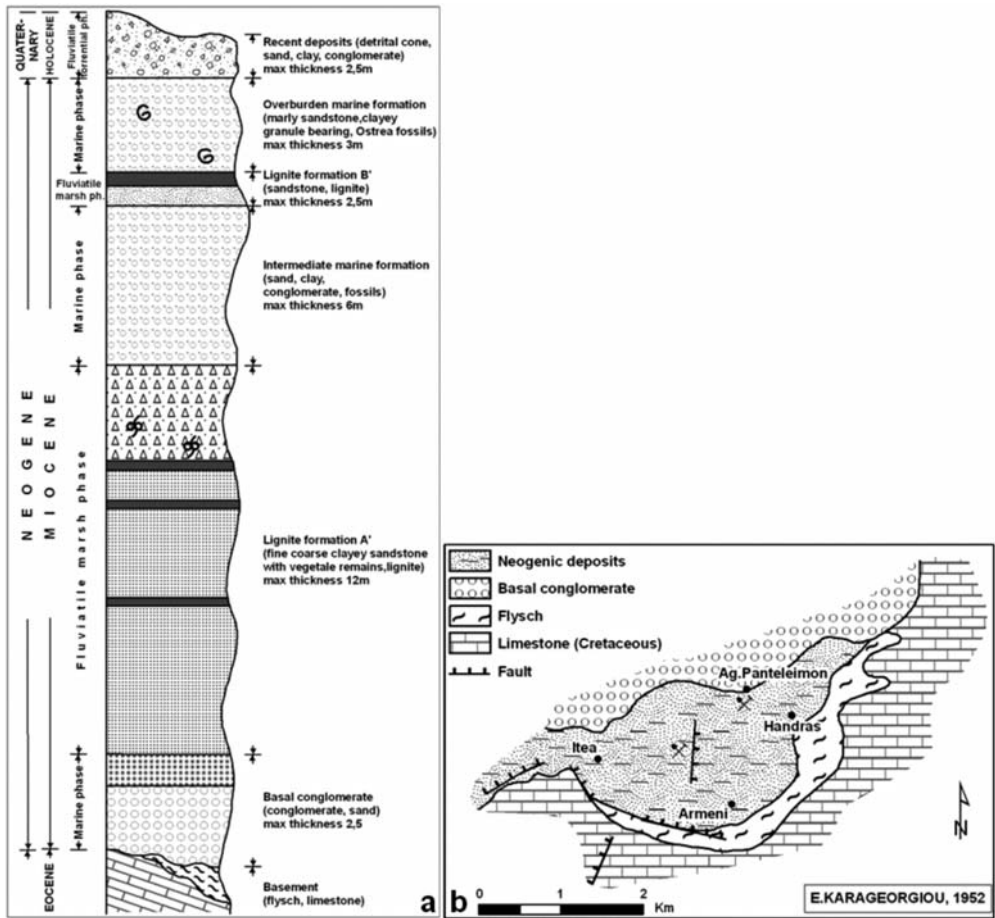


Fig. 8: (a): Stratigraphic column of Handras area; (b): Geological map of Handras area.

to the west of Sitia city, a small occurrence of lacustrine Pliocene formations is observed with potential lignite deposition (Karageorgiou, 1978).

3.8 Toplou monastery

It is located East of Sitia city at a distance of 18 km, occupying an area of 20km². The development of the geological formations in the area is similar to this of Lake Roussa area (Fig. 10b). The drilled borehole for irrigation of the cultivations provides the only evidence for the existence of lignite beds in the area where a lignite seam of 40 m thickness was found at a depth of about 70m (Fig. 10a). In order to confirm the occurrence of “blind” lignite deposit, this area should be further investigated (Karageorgiou, 1978).

4. Possibility of lignite deposits use

According to the data from the Public Power Corporation (P.P.C.), the electricity needs in Crete amount annually to 3050Gw/h. To produce this energy, two units of 300MWatt each are required.

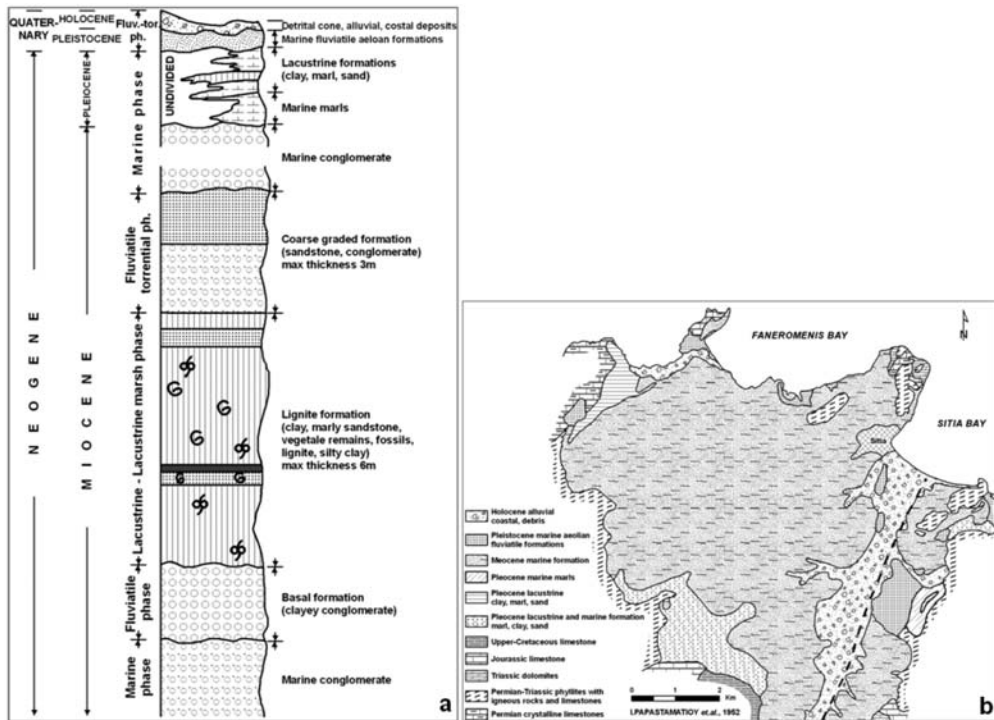


Fig. 9: (a): Stratigraphic column of Roussa Limni area; (b): Geological map of Roussa Limni area.

Burning oil produces the higher percentage. According to data obtained from the investigations so far on the island, a unit of 150Mwatt can be constructed and run with the existing lignite reserves. These reserves will increase if the potential lignite reserves of the island of Crete will be explored more systematically. At least 25% of the electricity consumed can be covered by the use of lignite instead of oil as fuel with lower costs and hence lower prices paid by the consumer. On the other hand carbon dioxide and other heat-trapping gases are declared as pollutants and endanger public health and welfare. Man-made CO₂ released into the atmosphere is a significant contributor to the greenhouse gas effect and related global warming. This fact must be taken into account in an island with important tourist industry. With plans to drastically reduce the venting of CO₂ through capture at the source [Carbon Capture and Storage (C.C.S.) Technology], vast volumes of CO₂ will need to be sequestered and it is expected that CO₂ capture and storage in the subsurface and monitoring are going to be of major importance in the future. Pilot Projects concerning carbon sequestration are under development worldwide. In the case of Crete, storage-related research should be done, in the sea at great depths or below evaporitic horizons, in order to estimate the CO₂ storage capacities. In parallel, other methods than the conventional ones for the lignite exploitation and combustion can be applied to reduce the environmental impact. As an example the in situ combustion is mentioned.

In the recent years an investigation was carried out by the Institute of Geology and Mineral Exploration (I.G.M.E.) under the Community Support Framework programs, on the possible uses of lignite in other applications than electricity production (I.G.M.E. Final Report: Study and Research of selected Solid Fuel deposits for application in other than electricity uses, ISBN 978-960-87453-2-2, 2008).

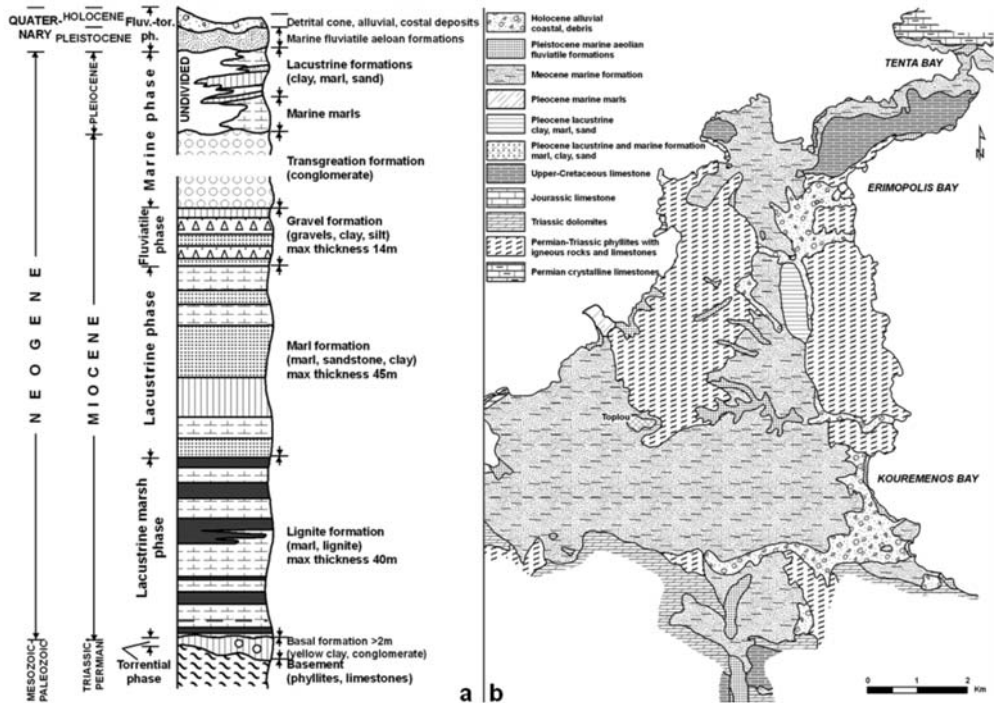


Fig. 10: (a): Stratigraphic column of Toplou area; (b): Geological map of Toplou area.

It was concluded that Crete lignites may be suitable for use as additives in drilling mud, as a soil improvement product and as a pollutant-removing material contributing to the increase of their economic value.

5. Conclusions-Results

Lignite basins mainly of Miocene age develop in the island of Crete. The total reserves of these basins amount 25,000 million tons. Among these reserves some millions tons can be exploited. Since the electric power requirements in the island of Crete reaches 3.050 Gw/h annually, mostly covered by the use of oil, lignites exploitation can contribute to a dependency reduction of at least 25%. This lignite exploitation can be achieved using new technologies in order to reduce the impact on the environment and offer cheaper and cleaner energy. In this purpose a more systematic investigation of the lignite deposits in the island of Crete is necessary. The use of lignites in other than electricity production applications is also possible.

6. References

- Chatzigiannis, G. and Karageorgiou D.E., 1977. Mineralogical reconnaissance in Kandanos lignite basin, Chania region, Crete. I.G.M.E. Athens p.14 (in Greek).
- I.G.M.E. Final Report: Study and Research of selected Solid Fuel deposits for application in other than electricity uses, ISBN 978-960-87453-2-2, 2008.
- Karageorgiou, D.E., 1978. Geological and Mineralogical reconnaissance of the Neocene basins of the

- Lassithi region, Inland Crete. I.G.M.E. Athens p.6 (in Greek).
- Karageorgiou, E.D., 1951. Geological reconnaissance of the lignite area of Kandanos – Psariana, in Crete inland. I.G.S.R. Athens p.6 (in Greek).
- Karageorgiou, E.D., 1952. Geological reconnaissance of the lignite areas of Crete inland. I.G.S.R. Athens p.20 (in Greek).
- Koukouzas, K. and Papaspyros, A., 1984. Mineralogical reconnaissance of lignite in the areas Toplou, Handra of Lassithi region and Houthetsio of Iraklion region. I.G.M.E. Athens p.7 (in Greek).
- Koukouzas, K. and Papaspyros, A., 1993. Lignite exploration of Plakia basin of Rethymnon, Crete. I.G.M.E. Athens p.82 (in Greek).
- Maratos, G., 1952. The appearances of lignite in Lassithi region. I.G.S.R. Athens p.6 (in Greek).
- Papachristos, G., 1952. Lignite exploration of Vrises Apokoronou and Fournes basins of Chania Crete. I.G.S.R. Athens p.10 (in Greek).
- Papaspyros, A., 1993. Lignite exploration of Almyri Panagia area of Iraklion region. Crete. I.G.M.E. Athens p.78 (in Greek).
- Papastamatiou, J., Vetoulis D., Brousoulis, J., 1966. Lignite exploration of Almyri Panagia basin, of Vryses Apokoronou basin and of Kandanos basin, Crete. I.G.S.R. Athens p.30 (in Greek).
- Vetoulis, D., 1952. Lignite exploration of Iraklion basins, Crete. I.G.S.R. Athens p.15 (in Greek).

GEOTHERMAL DRILLING ACTIVITY IN THE AKROPOTAMOS AREA (MACEDONIA, NORTHERN GREECE)

Kolios N.¹, Arvanitis A.², Karydakis G.³ and Koutsinos S.¹

¹ Institute of Geology and Mineral Exploration, Regional Branch of Central Macedonia, 54626, Thessaloniki, Greece, kolios@thes.igme.gr

² Institute of Geology and Mineral Exploration, Division of Geothermal Energy and Thermal Mineral Waters, Entrance C, Olympic Village, 13677, Acharnae, Attica, Greece, arvanitis@igme.gr

³ Institute of Geology and Mineral Exploration, Division of Works and Drilling, Entrance C, Olympic Village, 13677, Acharnae, Attica, Greece, grigorios_karydakis@hotmail.com

Abstract

The Akropotamos area constitutes a new geothermal field located in the eastern coastal zone of the Strymonikos Gulf in Macedonia (Northern Greece). After a detailed and systematic reconnaissance study including water temperature measurements at the heads of the existing irrigation and water supply wells, 6 new geothermal wells were constructed. This geothermal drilling program was performed by the Institute of Geology and Mineral Exploration during October 2003 - February 2006. Temperature and fluid conductivity logs were carried out into these boreholes during their drilling and after their completion. Well AKR-1 has a depth of 275 m and produces thermal waters at a temperature of 83°C with artesian flow rate 150 m³/h and large amounts of dissolved CO₂. Well AKR-2 of 410 m yields 25 m³/h of waters at 46°C. Well AKR-3 was drilled down to 515 m and the temperature of 88.9°C was measured at 498 m. This well yields about 200 m³/h CO₂-rich geothermal fluids at a temperature of 90°C with artesian flow. Next to this borehole, well AKR-4 was drilled at 180 m penetrating a shallow aquifer with waters reaching 49.7°C. During pumping test with constant flow rate, this well yielded 40 m³/h water of 48°C. Well AKR-5, 422 deep, was drilled in the western part of the study area close to the Strymon river's mouth. The temperature of 27.8°C was recorded at 280 m into this borehole. The last well AKR-6 was drilled down to 545 m in the eastern part of the field. The temperature of 38°C was recorded at depth of 503 m. Pumping tests were performed in wells AKR-2 and AKR-4. This geothermal drilling project has resulted in the official characterization of the Akropotamos - Kavala area as a "proven low enthalpy geothermal field".

Key words: Akropotamos, Macedonia, geothermal field, geothermal wells, Strymonikos Gulf, Kavala, CO₂.

1. Introduction

The Akropotamos area constitutes a new low enthalpy geothermal field located in the eastern coastal zone of the Strymonikos Gulf in Macedonia (Northern Greece). During 2002-2006 the Institute of Geology and Mineral Exploration (I.G.M.E.) of Greece performed a systematic geothermal investigation in the area extended between the mouth of the Strymon river and the Eleftheres thermal springs (Fig. 1). After a detailed and systematic reconnaissance study including evaluation of geological and tectonic setting of the wider area, water temperature measurements at the heads of the

existing irrigation and water supply wells and geophysical surveys, six (6) new production geothermal wells were constructed at depths of 180-545 m and produce waters up to 90°C. This drilling activity proved the existence of one of the most important low enthalpy geothermal fields of Greece in the area. This paper presents the results of the geothermal drilling project in the Akropotamos - Kavala field supported financially by the 3rd Community Support Framework 2000-2006 (Operational Programme “Competitiveness”).

2. Geological and tectonic setting

The Akropotamos geothermal area belongs to the wider area of the Strymon basin. This basin is a typical post-orogenic graben. It has been formed between the Serbomacedonian Massif (SMM) to the west and the Rhodope Massif (Pangeon Unit) to the east and it has been filled with Neogene and Quaternary sediments of a total thickness reaching about 4000 m. Various depositional palaeoenvironments (continental, fluvial, fluviolacustrine, lacustrine-marshy, marine, brackish, deltaic) were created during Neogene-Quaternary and their succession make the stratigraphy very complicated (Syrides, 2000). The typical stratigraphic column of the basin consists of the older Miocene formations (basal conglomerates and breccias, alternations of clays, sandstones, dark brown marls, lignite layers, petroliferous limestones), 700-800 m Pliocene sediments (layers of clays, conglomerates, travertines, marls, red clays, sandstones, siltstones, limestones, lignites) and 900-1000 m of Pleistocene deposits (alternations of sands, clays, sandstones, marls, siltstones, conglomerates and limestones) (Lalechos, 1986; P.P.C., 1988). The Strymonikos Gulf (or Orfanos Gulf) can be considered as an offshore extension of the Strymon basin southeastwards separated from the continental Strymon basin by a horst (tectonic uplift) close to the present estuary of the Strymon river. Noussinanos (1991) considers the northern part of the Orfanos Gulf to correspond to a post-Alpine basin in a shallow marine environment (“shallow water”) and the southern part of the Orfanos Gulf to belong to a “transitional” environment. According to Lalechos (1986) during Miocene there was no connection between a lake prevailed extended to the continental basin and the Miocene Sea of the Orfanos Gulf because of a probable barrier from the metamorphic basement. Sediments composed of marls with intercalation of anhydrite layers and deeper layers of hard sandstones and limestones were revealed in a cross-section of a road next to the sea and these formations can be correlated with offshore well APOLLONIA-1 (AP-1) drilled in the Strymonikos Gulf (Fig. 1) indicating that during Pliocene a fault had separated the continental area of the Strymon basin and the Orfanos Gulf (Lalechos, 1986). Oil exploration borehole AP-1 of 3146 m depth has penetrated Pleistocene-Holocene deposits (0-1250 m), Pliocene sediments (1250-1875 m) and Miocene formations (1875-3146 m). Holocene - Pleistocene deposits consist of alternating sands, clays and sandstones with locally lignite intercalations and fragments of Bivalvia (Lamellibranchia). Pliocene - Miocene sediments are composed of alternating sandstones, siltstones, clays and marls. Alternations of dolomites, sandstones, limestones and anhydrites dominate near the base of Miocene formations (Lalechos, 1986). In borehole AP-1 the temperatures of 59-67 and 121-130°C were registered at depths of 1335 and 3146 m respectively and the average geothermal gradient is estimated to be 36.5°C/km. During the Upper Miocene, the South Kavala Ridge (tectonic uplift in a NW-SE direction, South-East of the Akropotamos area, Fig. 1) emerged to separate the Prinos - Kavala basin from the Orfanos Gulf (Pollak, 1979).

The Akropotamos area lies close to the “Strymon line”, which is the tectonic contact between the Serbomacedonian and Rhodope Massifs. Therefore, the geological basement of this area consists of gneisses, amphibolites and schists belonging to the Serbomacedonian Massif (Kerdylia series) to the West and marbles (dominant rock type) and schists belonging to the Pangeon Unit (Rhodope Mas-

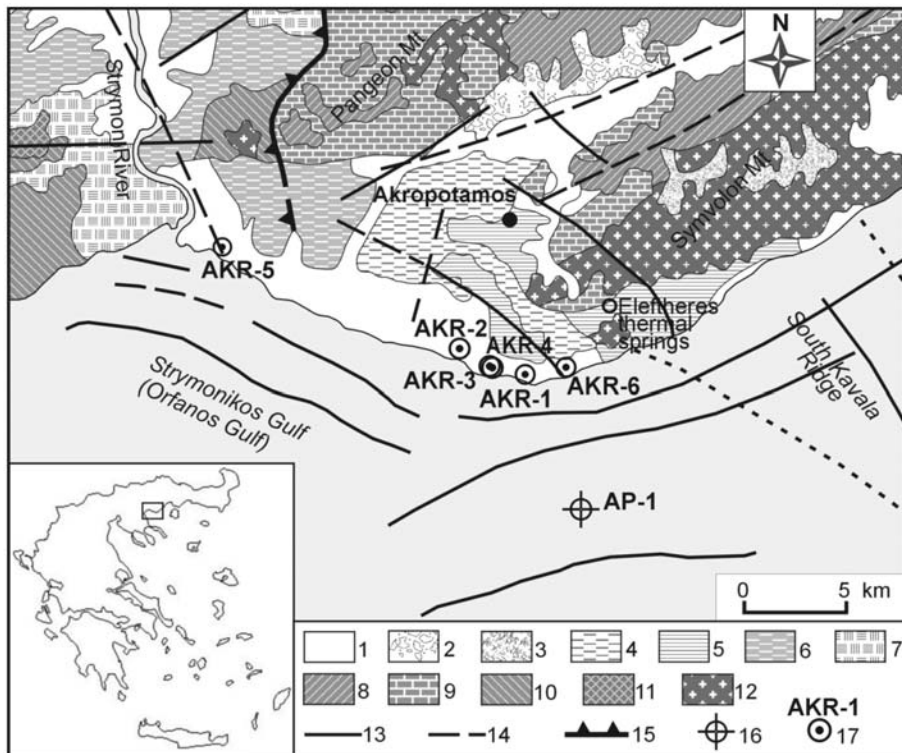


Fig. 1: Simplified geological map of the Akropotamos area with the sites of geothermal wells [1: Alluvial deposits in valleys and coastal deposits, 2: Alluvial fans and older talus cones - Scree, 3: Pleistocene lacustrine and continental deposits: clays, loams, sands, conglomerates, 4: Pleistocene marine deposits: marls, clays, sands, conglomerates, coastal terraces, 5: Pliocene marine deposits: conglomerates, sands, clays, marls, marly limestones, 6: Mio-Pliocene lacustrine and terrestrial sediments: conglomerates, sands, marls, clayey material, marly limestones and clays, 7: Mio-Pliocene marine deposits: the above-mentioned detrital sediments, 8: Amphibolites, gneisses, schists with marble intercalations (Rhodope Massif), 9: Marbles or crystalline limestones (Rhodope massif), 10: Amphibolites, gneisses, schists with marble intercalations (Serbomacedonian Massif), 11: Gneisses (Serbomacedonian Massif), 12: Tertiary granitoids, 13: Fault, 14: Probable fault, 15: Strymon tectonic line, 16: Oil exploration borehole, 17: Geothermal well]. The compilation of this map is based on the geological map of Greece at a scale of 1:500,000 (I.G.M.E., 1983) with some additional tectonic structures derived from the 1:500,000-scale seismotectonic map of Greece (I.G.M.E., 1989) and some modifications according to Lalechos (1983) and Pollak (1979).

sif) to the East. Tertiary granitoids have intruded into the crystalline rocks of the basement (Eleftheriadis G. et al., 2001). The oldest Miocene sediments of the Akropotamos area consist of lacustrine and fluvial-lacustrine deposits with conglomerates, sands, coarse-grained sandy marls and sandstones with a total thickness more than 500 m. Eastwards thick laminated biogenic limestones of Middle Miocene age of high secondary porosity are located. The sedimentary series was developed uniformly towards the Pliocene. Pliocene sediments consist of travertine deposits, sands and clays of marine origin and calc-sandstones. Southwards the entire series is covered by recent coastal and fluvial - torrential deposits and scree.

The fault pattern of the Akropotamos area is dominated by NW-SE and NE-SW faults. The NW-SE faults with a greater population are activated as oblique sinistral normal faults and they have high

dip angles. The NE-SW faults are very common in the area, probably related to the Kavala-Xanthi-Komotini fault zone (Mountrakis and Tranos, 2004). These faults are activated as oblique dextral-normal faults. During Lower Quaternary the wider area of Akropotamos was affected by NW-SE and NE-SW striking faults. Two main tectonic blocks are observed in this area: the Akropotamos horst and the Pieria graben (east of the investigation area). The wider area was activated due to the presence of the North Anatolian Fault Zone.

The thermal springs of Eleftheres located about 3 km east-northeast of the study area constitute the only geothermal manifestation in the wider area. Their water temperature is 38.7-53°C. These springs are situated in the Marmaras river Valley occurring in a NNW-SSE direction in the Symvolon granitoid (Miocene granodiorite) although the marbles of the Pangeon Unit dominate in the area. The presence of the springs is related to a fault or intersecting faults (P.P.C. and E.N.E.L., 1979; Gavrielides, 1990).

3. Geothermal drilling activity in the Akropotamos area

3.1 General

A detailed and systematic reconnaissance study was carried out in the Akropotamos area extended between the mouth of the Strymon river and 3 km west of the Eleftheres thermal springs. This study was performed during 2002-2003 including evaluation of geological and tectonic setting of the wider area, water temperature measurements at the heads of the existing irrigation and water supply wells, water sampling and chemical analyses and geoelectric surveys. Based on the results of this research, 6 exploration - production geothermal wells were constructed by I.G.M.E in the investigation area during the period October 2003 - February 2006. The sites of these wells are shown on the map of Figure 1: The results of this drilling activity are presented as follows.

3.2 Geothermal well AKR-1

Geothermal well AKR-1 was drilled in the coastal zone, south of the national road Thessaloniki - Nea Peramos - Kavala. The coordinates of the drilling site are X:504423 and Y: 4507391 (Greek Grid, GGRS1987). Its elevation is approximately 9 m a.s.l. This well was drilled during October-December 2003. It has a depth of 275 m. Pliocene and Miocene sediments were penetrated. These sediments consist of chaotic conglomerates, clayey-marly formations, fractured limestones and calcareous conglomerates. The geothermal reservoir is located at 240-275 m depth composed of calcareous conglomerates. The lithologic column and the mechanical diagram with the main construction features of well AKR-1 are shown in Fig. 2. The wellbore was drilled at a diameter of 15'' to a depth of 40 m and drilling was then continued at a diameter of 9 5/8'' down to the final depth of 275 m. The casing of this borehole has a diameter of 10 3/4'' at 0-40 m and 6 5/8'' at 0-275 m. Screens were placed at 233-275 m. The well was cemented from the surface to 40 m depth. Well AKR-1 produces about 150 m³/h waters of 83°C with artesian flow. The electrical conductivity of water is 7718 µS/cm. The produced geothermal fluids contain significant quantities of carbon dioxide (CO₂).

3.3 Geothermal well AKR-2

Geothermal well AKR-2 was constructed at a distance of 3.2 km WNW of well AKR-1 in the coastal zone. Its coordinates are X: 501353 and Y: 4508475 (Greek Grid, GGRS1987) and its elevation is approximately 7 m. It was drilled during January-April 2004. The total drilled depth was 422 m and the borehole was cased down to 410 m. The section from the surface to 45 m was drilled at a diam-

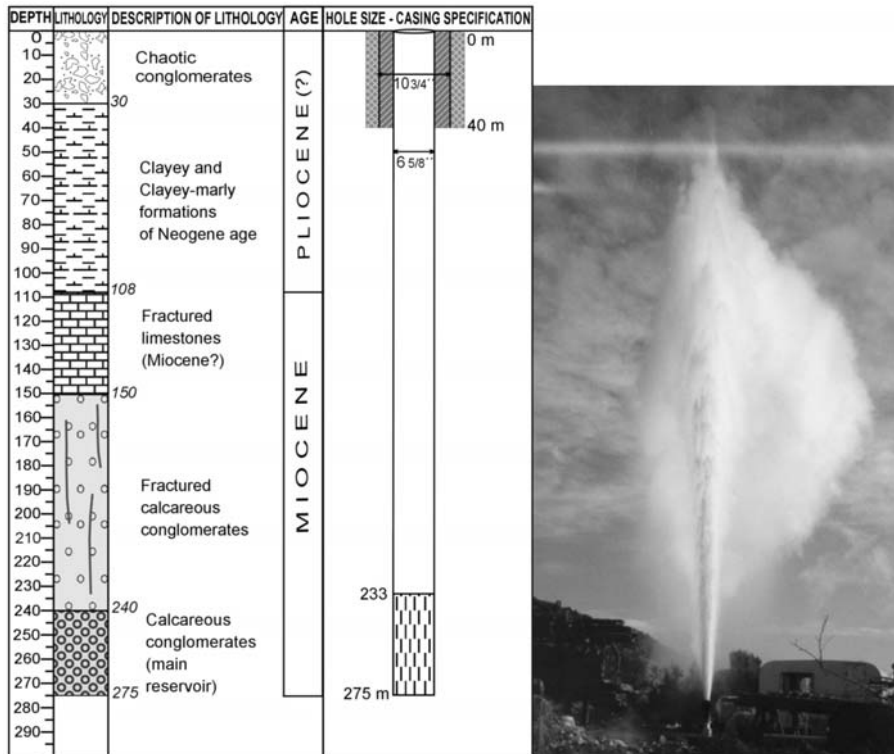


Fig. 2: (left): Lithologic column and mechanical diagram of geothermal well AKR-1; (right): Photo showing the artesian flow rate of geothermal well AKR-1.

eter of 15'' and drilling continued at a smaller diameter (9 5/8'') below 45 m. The casing of this borehole has a diameter of 10 3/4'' at 0-45 m, 6 5/8'' at 0-48 m and 5'' at 48-410 m. Screens were placed at 294-410 m. The borehole was cemented from the surface to 100 m depth.

Well AKR-2 penetrated a sedimentary sequence composed of sands, pebbles, gravels, unconsolidated calcareous conglomerates, unconsolidated clayey sandstones, clays, marls and coarse-grained sandstones. The geothermal aquifer is located at depths of 282-422 m composed of coarse-grained sandstones. Temperature and water conductivity logs were performed in borehole AKR-2. The temperature of 48°C was measured at 360 m (Fig. 3). Considering that the mean annual surface temperature of the area is 16.8°C, the average geothermal gradient is calculated to be 8.70 °C/100 m from the surface to 360 m depth. The results of water conductivity logs recorded in this borehole at various dates are shown in Fig. 4. Measurements dated 20/4/2004 and 25/5/2004 showed an enormous increase between 70 and 190 m depth and the maximum value reached 15800 µS/cm at 130 m on 20/4/2004. This indicates a probable intrusion of sea water into the unconsolidated calcareous conglomerates located at 65-120 m depth influencing a large part of this well. This increase was not recorded on 29/4/2004 and the electrical conductivity rose gradually down to 344 m reaching 3680 µS/cm.

A 24-hour pumping test at a constant flow rate of 25 m³/h was performed. The final drawdown was measured at 44.6 m. The static water level was 7 m before pumping. The water temperature remained constant at 46°C during the pumping test and the electrical conductivity of the pumped water was 3334-3600 µS/cm.

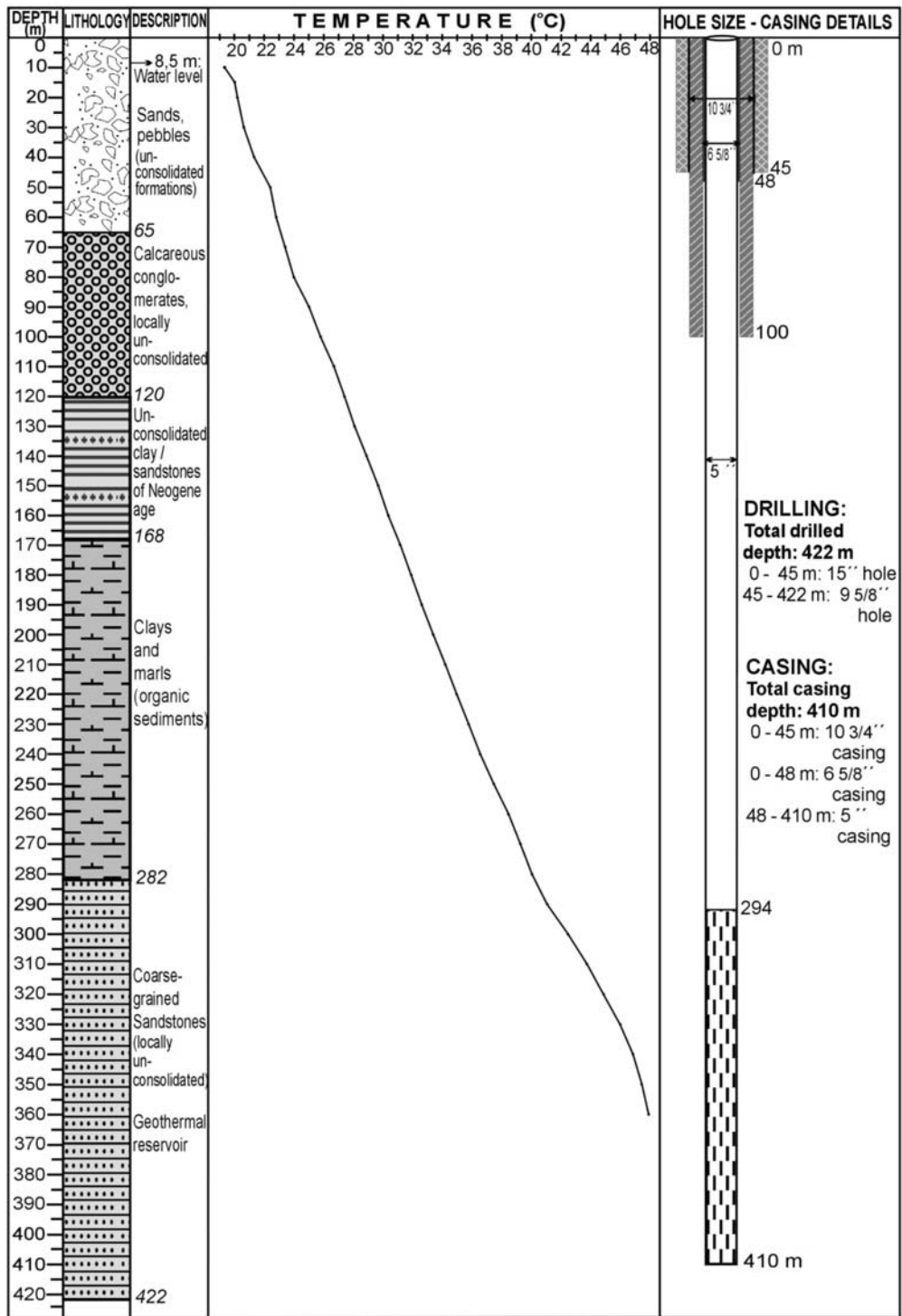


Fig. 3: Geothermal well AKR-2.

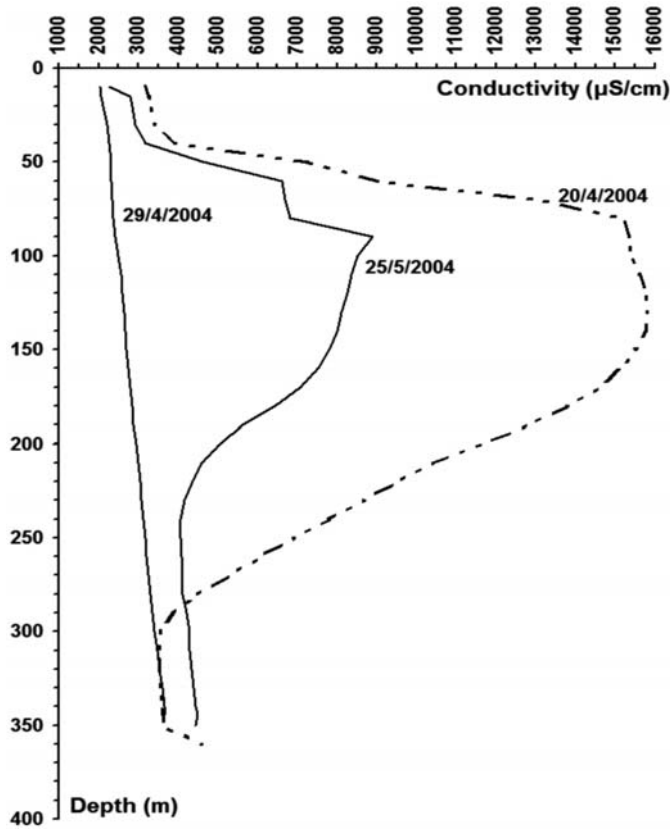


Fig. 4: Water conductivity logs in geothermal well AKR-2.

3.4 Geothermal well AKR-3

Geothermal well AKR-3 was drilled at a distance of 1.62 km southeast of well AKR-2 in the coastal zone (Fig. 1). Its coordinates are X: 502858 and Y: 4507783 (Greek Grid, GGRS1987) and its elevation is approximately 2 m. It was constructed during May-October 2004. The total well depth is 515 m. Sands, clays, sandstones and conglomerates were penetrated. The lithology of this borehole is shown in Fig. 5. A deep geothermal aquifer is located at 480-515 m depth. This aquifer is made up of sandy sandstones and contains geothermal fluids of about 90°C. A shallow aquifer composed of coarse-grained sandstones and conglomerates is located at 102-185 m depth containing thermal waters of 48-49°C. Microfossils have been found at depths of 96-102, 258-270, 360-372, 480-492 and 510-515 m. Among them, the presence of *Tectochara escheri* (Charophyta) found in the lower layers of this borehole (486-515 m depth) is of special interest and suggests a Miocene to Middle Pliocene age for these strata. The total casing depth is 515 m. Screens were placed from 440 to 515 m depth (Fig. 5). Temperature and water conductivity logs were performed in this borehole at different times. The maximum measured temperature was 88.9°C at depth of 498 m. Considering that the mean annual surface temperature of the area is 16.8°C, the average geothermal gradient is calculated to be 14.48°C/100 m from the surface to 498 m depth. All conductivity measurements show a significant increase between 100-230 m depth and the maximum

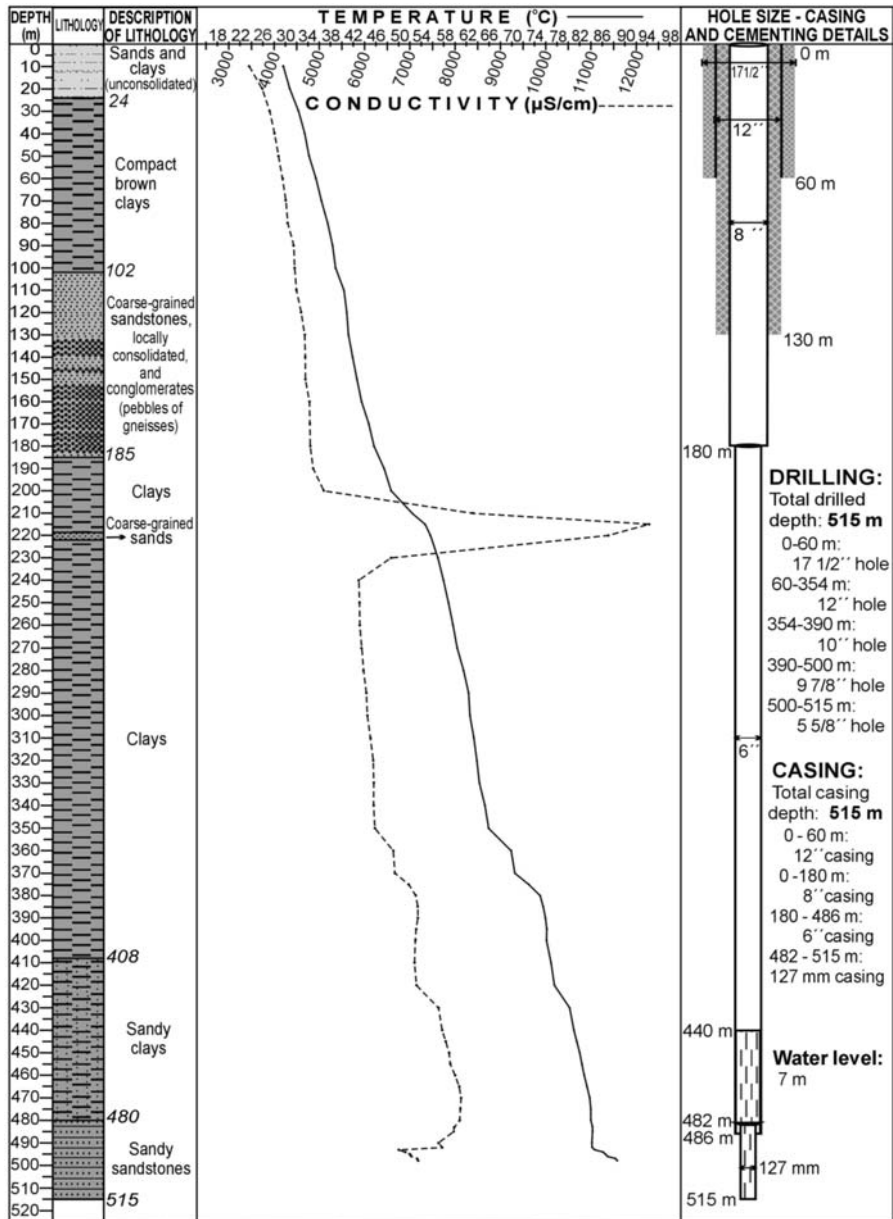


Fig. 5: Geothermal well AKR-3.

value was 14000 μS/cm at 215 m registered on 9/9/2004. This indicates the presence of brackish water in a shallow aquifer. This brackish water has a temperature of 48-50°C. Fig. 5 shows the conductivity vs. depth curve based on logs carried out on September 27, 2004. Well AKR-3 produces about 200 m³/h waters of 90°C with artesian flow. The electrical conductivity of water is 5858 μS/cm. The produced geothermal fluids contain significant quantities of CO₂.

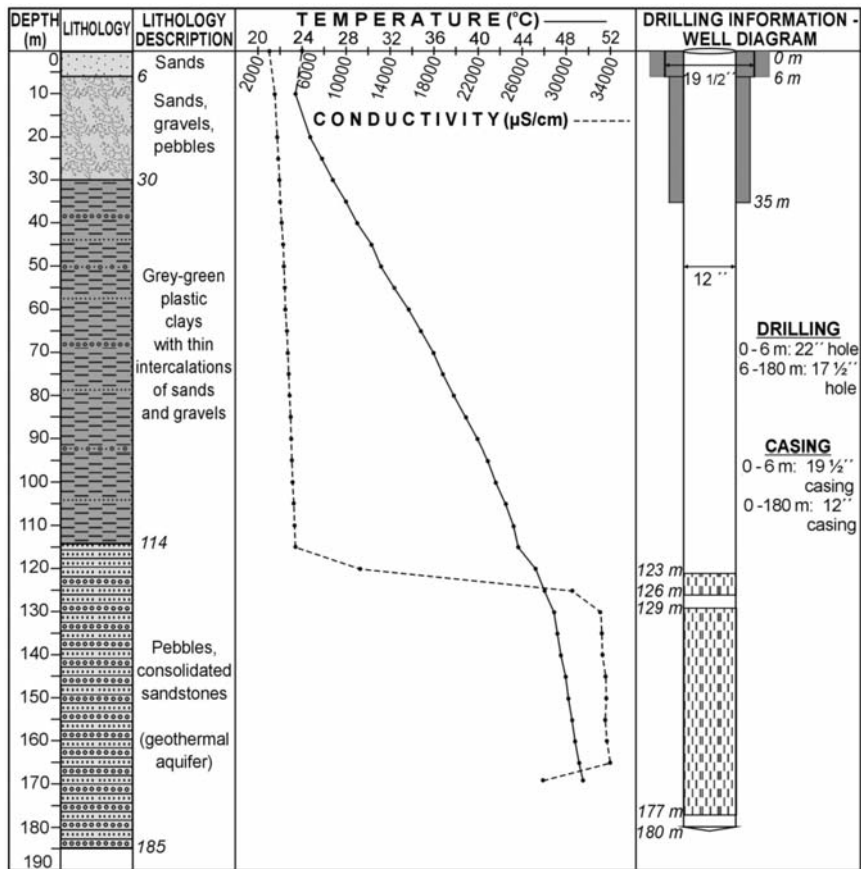


Fig. 6: Geothermal well AKR-4.

3.5 Geothermal well AKR-4

Geothermal well AKR-4 was drilled next to well AKR-3, only a few meters away (Fig. 1). Its coordinates are X: 502862 and Y: 4507796 (Greek Grid, GGRS1987). It was constructed during April-June 2005. The total well depth is 180 m. Borehole AKR-4 penetrated a sedimentary sequence composed of sands, gravels, pebbles, grey-green plastic clays with thin intercalations of sands and gravels and finally pebbles and consolidated sandstones (Fig. 6). The latter sediments located at 114-185 m depth make up a hot aquifer containing waters of 46-49.7°C. Temperature and water conductivity logs were performed in borehole AKR-2 on September 12, 2005. The maximum temperature of 49.7°C was measured at depth of 168.86 m. Considering that the mean annual surface temperature of the area is 16.8°C, the average geothermal gradient is calculated to be 19.48°C/100 m between the surface and 168.86 m depth. Water conductivity log showed a rapid and high increase below 115 m depth and the maximum value of 34000 µS/cm was recorded at 165 m depth (Fig. 6). This increase in water conductivity indicates a high percentage of seawater in the shallow geothermal aquifer due to probable seawater intrusion into this aquifer. Step-drawdown and constant-rate pumping tests were carried out after the completion of the well. The static water level was 3 m before pumping. A step-drawdown test was performed on June 23, 2005. The well was pumped for 2 hours each in two steps at discharge rates of 28 and 40 m³/h respectively and the total drawdown was 32.77 m at the end of the test. The

24h constant-rate pumping test was performed at a flow rate of 40 m³/h and the drawdown at the end of this test was 37.12 m. The water temperature was increased from 47°C (in the beginning of the constant-rate test) to 48°C (after 16 hours pumping) and remained constant until the end of this test. Electrical conductivity of the pumped water was 36990-37360 µS/cm.

3.6 Geothermal well AKR-5

Well AKR-5 was drilled 2.2 km southeast of the Strymon river estuary at a small distance from the coast. Its coordinates are X: 489165 and Y: 4514004 (Greek Grid, GGRS1987) and its elevation is about 1.5 m. Well AKR-5 was drilled down to 422 m and penetrated a sedimentary sequence composed of unconsolidated sands (0-45 m depth), coarse-grained sands (45-50 m), alternations of compact sands and clays of Neogene age (50-180 m), alternations of Neogene compact sands and clays with dominant clay material (180-280 m), aquifer sands (280-320 m), clays (320-330 m), aquifer sands derived from gneisses (330-350 m), clays (350-380 m) and impermeable organic material (380-422 m). The wellbore was drilled at a diameter of 17½'' from the surface to 12 m depth and drilling then continued at smaller diameters below 12 m (drilling was 11'', 9 7/8'', 7 ½'' and 5 5/8'' in diameter at depths of 12-48, 48-218, 218-330 and 330-422 m respectively). Well AKR-5 was cased down to 422 m and 12'', 10'', 8'', 6'' and 4'' casings were set at depths of 0-12, 0-48, 0-218, 170-290 and 278-422 m correspondingly. The total casing length is 542 m. The annular space around the outside of the 12'' surface casing was cemented. The annular space between the 12'' and 10'' casings from the surface to 12 m depth was cemented too. Cementing was also performed around the outside of the 8'' casing down to 60 m depth. Screens were placed at depths of 280-340, 355-363, 375-383 and 416-418 m. Temperature and water conductivity logs were performed in borehole AKR-5 on October 11, 2005. The static water level was 3.2 m below the surface. The temperature of 27.8°C was measured at depth of 280 m. Considering that the mean annual surface temperature of the area is 16.8°C, the average geothermal gradient is calculated to be 3.93°C/100 m from the surface to 280 m. Water conductivity log showed a gradual increase with depth. Electrical conductivity values ranged from 10138 to 19500 µS/cm at depths of 4-280 m. Below 120 m the water conductivity values were higher than 18000 µS/cm indicating the influence of seawater on the sandy aquifers.

3.7 Geothermal well AKR-6

Well AKR-6 was drilled 1.9 km east of well AKR-1 and approximately 3 km SW of the Eleftheres thermal springs (Fig. 1). Its coordinates are X: 506291 and Y: 4507527 (Greek Grid, GGRS1987) and its elevation is about 13 m. It was constructed during October 2005-February 2006. Well AKR-6 was drilled down to 545 m depth and penetrated a sedimentary sequence composed of scree and travertine limestones (0-42 m depth), Neogene sandy clays (42-96 m depth), unconsolidated conglomerates and breccias alternating with marls (96-135 m), clays and marls (135-174 m), sandy clayey-marly sediments (174-192 m), flyschoid formations (192-246 m), consolidated organic clays and sandy clays (246-486 m), grey-green clays and fine-grained sands (486-492 m), fine-grained sands (492-516 m), clays with gravels and small pebbles (516-522) and finally grey-green clays with fine-grained sands and gravels (522-545 m). The wellbore was drilled at a diameter of 22'' from the surface to 6 m depth and drilling then continued at smaller diameters below 6 m (drilling was 17'', 9 7/8'' and 5 5/8'' in diameter at depths of 6-117, 117-492 and 492-545 m respectively). Well AKR-6 was cased down to 545 m and 19½'', 10'', 6'' and 4'' casings were set at depths of 0-6, 0-117, 102-492 and 485-545 m correspondingly. The total casing length is 573 m. The annular space around the outside of the 19½'' surface casing was cemented. Cementing was also performed around the outside of the 10'' casing down to 60 m depth. Screens were placed at depths of 497-515, 521-533

and 539-545 m. Temperature and water conductivity logs were performed in AKR-6 at various dates. The temperature of 38°C was recorded at 503 m depth and the average geothermal gradient is calculated to be 4.2°C/100 m from the surface to this depth. The conductivity logs have registered values higher than 6600 $\mu\text{S}/\text{cm}$ reaching up to 36940 $\mu\text{S}/\text{cm}$.

4. Conclusions

In the Akropotamos area, the preliminary geothermal investigation resulted in a drilling program including the construction of 6 exploration - production wells (AKR-1, AKR-2, AKR-3, AKR-4, AKR-5 and AKR-6). All these wells were drilled in the coastal zone of the Strymonikos Gulf at depths of 180-545 m. The main geothermal interest is focused on the area between wells AKR-2 and AKR-1 along the coastal zone (Fig. 1), where geothermal waters of 46-90°C are produced from depths of 130-515 m. Two geothermal aquifers have been recognized in this area: (a) a shallow aquifer at 100-185 m depth containing high-conductivity (14000-38000 $\mu\text{S}/\text{cm}$) waters of 46-49.7°C and (b) a deeper reservoir at 240-515 m containing lower conductivity (3600-8160 $\mu\text{S}/\text{cm}$) waters of up to 90°C. Wells AKR-1 and AKR-3 produce about 150 and 200 m^3/h CO_2 -rich waters of 83 and 90°C respectively with artesian flow. The Akropotamos area has been characterized officially as “a proven low temperature geothermal field” and its boundaries have been defined by a Ministerial Decision (Official Gazette 1058/B / 02.06.2009) based on the geothermal study carried out by I.G.M.E.

5. References

- Eleftheriadis, G., Frank, W. and Petrakakis, K., 2001. $^{40}\text{Ar}/^{39}\text{Ar}$ Dating and Cooling History of the Pangeon Granitoids, Rhodope Massif (Eastern Macedonia, Greece). Bull. Geol. Soc. Greece XXXIV/3, *Proceedings of the 9th International Congress*, Athens, 911-916.
- Institute of Geology and Mineral Exploration (I.G.M.E.), 1983. Geological map of Greece, scale 1:500000. Athens.
- Institute of Geology and Mineral Exploration (I.G.M.E.), 1989. Seismotectonic map of Greece with seismological data, scale 1:500000. Athens.
- Mountrakis, D.M. and Tranos, M.D., 2004. The Kavala-Xanthi-Komotini fault (KXKF): a complicated active fault zone in Eastern Macedonia - Thrace (Northern Greece). *Proceedings, 5th International Symposium on Eastern Mediterranean Geology, Thessaloniki, Greece, 14-20 April 2004*, Ref: S1-19.
- Noussinanos, Th., 1991. Classification of Hydrocarbon basins of NE Greece. *Mineral Wealth*, 73, 33-56.
- Syrides, G., 2000. Neogene marine cycles in Strymon basin, Macedonia, Greece. Geological Society of Greece, Special Publications, *Proceedings, International Interim Colloquium RCMNS, Patras, Greece, May 1988*, 217-225.
- Gavrielides, G., 1990. Study of the subsurface aquifer conditions of the Eleftheres curative springs. *Proceedings of the 2nd Congress on the thermal mineral waters (Thessaloniki, Greece, 1988)*, Hellenic Association of Municipalities and Communities of Curative Springs and Spas, Thessaloniki, 155-166.
- Lalechos, N., 1986. Correlations and Observations in Molassic Sediments in Onshore and Offshore Areas of Northern Greece. *Mineral Wealth*, 42, 7-34.
- P.P.C. (Public Petroleum Corporation), 1988. Evaluation of deep oil boreholes. Athens, pp. 0-53.
- P.P.C (Public Power Corporation / Geothermal Department) and E.N.E.L.(Ente Nazionale per l' Energia Elettrica), 1979. Geothermal reconnaissance study of Macedonia and Chalcidice, General Report, GR/R-4.
- Pollak, W.H., 1979. Structural and lithological development of the Prinos - Kavala basin, Sea of Thrace, Greece. *Annales Géologique des Pays Helléniques, Tome hors serie*, 2, 1003-1011.

GEOLOGICAL AND GEOPHYSICAL DATA OF “EPSILON” FIELD IN PRINOS OIL BASIN

Mertzanides Y.¹, Kargiotis E.¹, Mitropoulos A.¹

¹Department of Oil and Gas Technology, Technological Educational Institute of Kavala, 65404, Kavala–Greece, mertzan@gmail.com

Abstract

The Epsilon field, is located at the centre of Prinos oil basin (N. Aegean, Greece), 11 km NW of the island of Thassos and 4 km NW of the Prinos field, the first productive oil field in the Aegean Sea. The taphrogenetic basin of Prinos has been widely studied, due to its hydrocarbon reservoirs. Extensive geophysical survey, started at early 1970 's, led to a number of drilling jobs, which confirmed the existence of hydrocarbons in the area. The combined geological information, derived from the analysis of lithological, stratigraphic and geochemical data of the basin, suggested a structural and depositional model, strongly related to the Miocene tectonics and sedimentation. The new geophysical and drilling data from Epsilon oil field, are correlated to that already known, completing the model of the basin. Pay zone is found to be below an evaporitic sequence, consisting predominantly of salt, with anhydrite, clay and sandstone intercalations. These upper Miocene aged evaporites extend, varying in thickness, throughout Prinos basin. Reservoir consists mainly of sandstone with intercalations of claystone and trace of siltstone. The geology of the structure and the initial productivity, were positive for further drilling operations in Epsilon field.

Key words: Prinos taphrogenetic basin, anticline, evaporites, Epsilon oil field, drilling data.

1. Introduction

The Epsilon oil field is located in the north Aegean Sea between the Greek mainland and the island of Thassos, approximately 11 km S-SE of the city of Kavala. It belongs to the taphrogenetic basin of Prinos, the only area with productive hydrocarbon fields in Greece (Fig. 1). Geophysical (seismic) exploration in the area at large, started in 1970 and resulted to a number of drillings. The first well was drilled in 1971, 20 km east of Thassos island but encountered very low gravity oil (Proedrou and Sidiropoulos, 1992). In 1972-1973 the next two wells were drilled west of the island and led to the discovery of South Kavala gas field in 52 m of water depth. The main reservoir was a turbiditic sand package, contained in between a sequence of evaporites. It consisted mainly of methane and small quantities of ethane, propane and butane (Proedrou and Sidiropoulos, 1992; Proedrou, 2001). The fourth drilling attempt, was at the end of 1973, at the centre of Prinos basin and led to the discovery of Prinos oil field in a water depth of approximately 30 m. The oil was present in stacked turbiditic sandstones, in four reservoir units. It was waxy, containing a high proportion of asphaltenes, sulphur and H₂S (Proedrou and Sidiropoulos, 1992). Four delineation wells in 1975-1977 (Proedrou and Sidiropoulos, 1992) and a 3-D seismic survey followed by interpretation in 1993-1995, confirmed the presence of North Prinos oil field. The five wells that were drilled in 1976, 1994, 1996, 2004 and 2009, kept the field in production till today.

The Epsilon oil field was discovered in late 2000, in a water depth of 30-40 m. The well E-1 drilled in 2001 but it was suspended and re-entered in 2002 as E-1A. Technical problems led to re-drilling in 2002 and the well was sidetracked as E-1As.

This work presents geological and geophysical data from Epsilon oil field in Prinos basin. Data were given from KAVALA OIL SA, as part of the project ARCHIMEDES II: “Rock ‘n’ oil-The Kavala band”, supervised by Department of Oil and Gas Technology, Technological Educational Institute of Kavala. The project was co-financed by the European Social Fund (75%) and Greek national resources (25%), under the Framework of the Third Community Support Framework 2000-2006, Operational Program for Education and Initial Vocational Training, Priority Action Line 2 – Promotional Improvement of Education and Vocational Training within the framework of Lifelong Training, Measure 2.2 – Reformation of Studies Programmes, Expansion of Higher Education, Action 2.2.3 – Postgraduate Studies Courses, Research Scholarships, Action Category 7 - Enhancement of Research Groups in Technological Educational Institutes.

2. Prinos basin model

2.1 Geotectonic evolution

The extensive exploration for hydrocarbons in the offshore area at large of Thassos island and the study of the well drilling data that followed on, since 1970, brought the information for understanding the geotectonic evolution of the area. A detailed description of this information and a complete model for the geology and the depositional model of Prinos basin can be found in literature (Pollak, 1979; Proedrou, 1979; 1988; Proedrou and Sidiropoulos, 1992; Georgakopoulos, 1998; 2000; Proedrou, 2001; Proedrou and Papaconstantinou, 2004; Kiomourtzi, 2007; 2008; 2009). According to this model, the Prinos basin is a result of the post-alpine tectonism that started in early to middle Miocene and led to the breaking of the Aegean plate and to the subsidence of the pre-alpine Rhodope massiv under the sea level. This gravity tectonics was responsible for the genesis of grabens and horsts in North Aegean. A number of gravity, often echelon, faults with NE-SW and NW-SE direction formed the taphrogenetic basin of Prinos. Its length is approximately 38 km, from Nestos river delta in NE, to offshore south Kavala ridge in SW. Its width is approximately 20 km, from Thassos island in SE, to the opposite mainland in NW. It is subdivided into two sub-basins, separated by a topographic basement high, in Ammodhis area (Fig. 1). The Nestos sub-basin is located at the north part and the Prinos sub-basin, deeper than the previous, at the south part. The taphrogenetic basin is structured by roll-over anticlines, formed by NW-striking and SW-dipping faults which are related to the trapping mechanism (Fig. 2). These faults, still active today, activated during sedimentation (syngenetic faults) and resulted in the dome-like anticlines of Prinos, North Prinos, Epsilon, Ammodhis and South Kavala (Fig. 1).

The NE part of Prinos basin was probable close by the first time of its formation, while the SW basement started to uplift by messinian period, forming the south Kavala ridge (Fig. 1). The basin was gradually isolated from the open sea and changed into a lagoon.

2.2 Stratigraphy

The stratigraphy model of the taphrogenetic basin has been presented by Pollak (1979) and Proedrou (1979) (Fig. 3). According to this, the generalized stratigraphic column is divided into three series:

- The Pre-Evaporitic Series.
- The Evaporitic Series.
- The Post-Evaporitic Series.

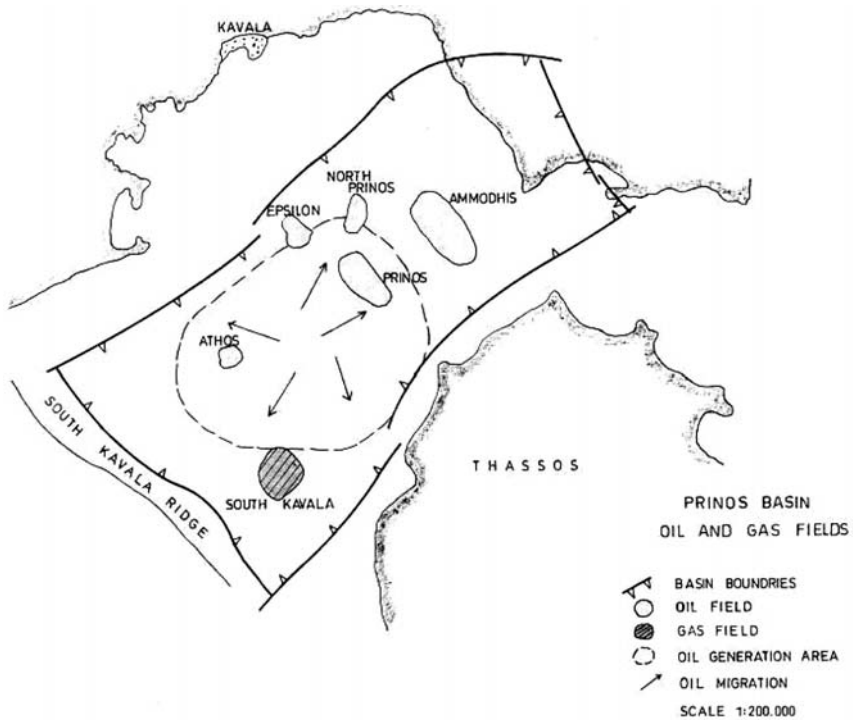


Fig. 1: The Epsilon oil field is located in the middle and north part of the basin of Prinos (N. Aegean Sea). Along with Prinos field, Prinos North field and South Kavala gas filed are the only productive hydrocarbon fields in Greece. The oil generation and the migration paths are shown. Figure from Proedrou and Papaconstantinou (2004).

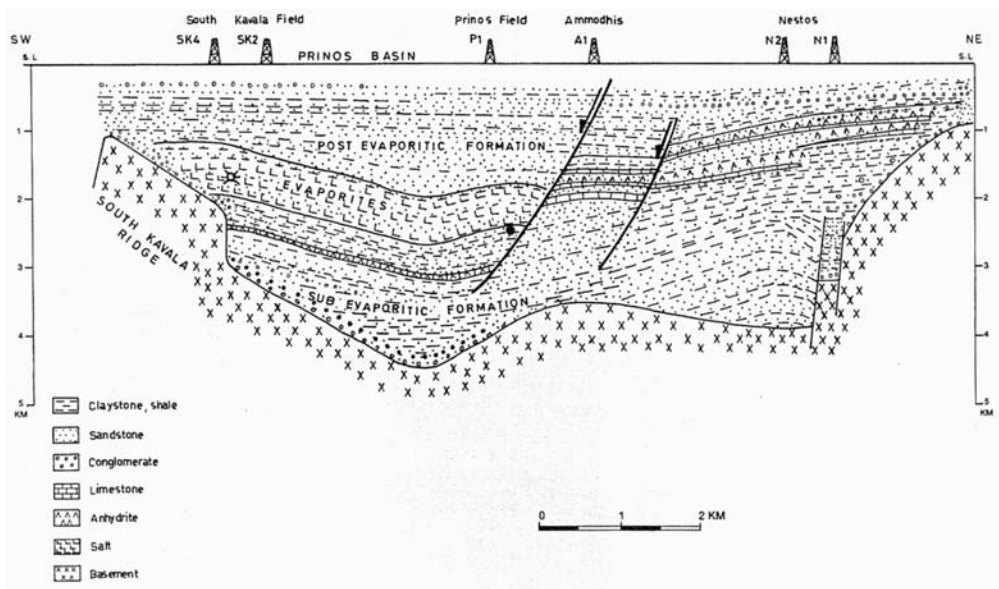


Fig. 2: Simplified cross section of the Prinos basin parallel to the long axis. The roll-over syngenetic faulting formed the dome-like anticlines. Depths in kilometres below mean sea level. Figure from Proedrou and Sidiropoulos (1992).

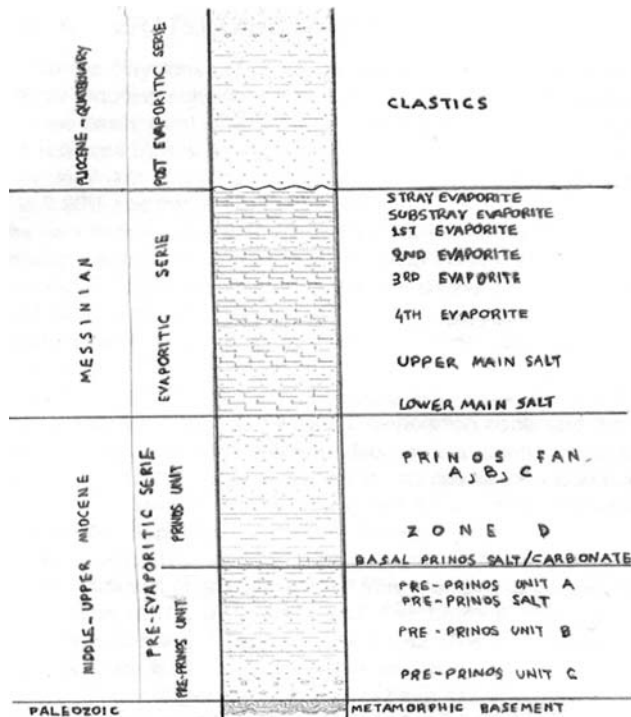


Fig. 3: Generalized chronostratigraphic column of Prinos basin. Figure from Proedrou and Sidiropoulos (2004).

The Palaeozoic basement is composed of metamorphic rocks: gneiss, quartzite and dolomitic marble. The Pre-Evaporitic Series, closely related to Miocene tectonics, begins with continental deposits: conglomerates with large basement components, sandstones, feldspatic, mainly immature, claystones and thick coal seams. These continental deposits originated from the NE and SW parts of the basin, decrease in thickness towards the centre of the sub-basins. They are followed by marine deposits of shales with interbedded sandstones, coarser at the periphery of the basin, which overlay the older ones with an unconformity. Above these units, a zone of limestone, dolomite and anhydrite layers alternated with clastics follows. Towards the centre of the basin, to the deeper parts, the anhydrite is replaced by a few metres thick layers of salt. At the top of the Pre-Evaporitic Series, at Prinos sub-basin, there is an extended deposition of dark gray claystone, the zone D. It is petrolierous and strong carbonaceous, with sandstone intercalations. The following Prinos sub-marine fan, consists entirely of turbiditic fan deposits, which were deposited along the downthrown side of a fault escarpment. The present facies, are representative of the turbidite facies classification of Walker and Mutti (1973). At Nestos sub-basin, the equivalent zone is the pro-deltaic varves (Proedrou and Papaconstantinou, 2004).

The Evaporitic Series, closely related to Messinian “Salinity Crisis” of the Mediterranean Sea (Hsu, 1972), consists of two facies, in each of the two sub-basins. In the northern one, anhydrite and limestone layers 3-5 m thick, alternate each other and with sandstone, claystones and marls, too. The series in the southern part, consists of 7-8 salt layers with increasing thickness towards the base of the section, which alternate with clastics and has a total thickness up to 800 m. The salt is white, gray, crystalline, often intercalated by anhydrite and dolomite layers (Proedrou and Papaconstantinou, 2004).

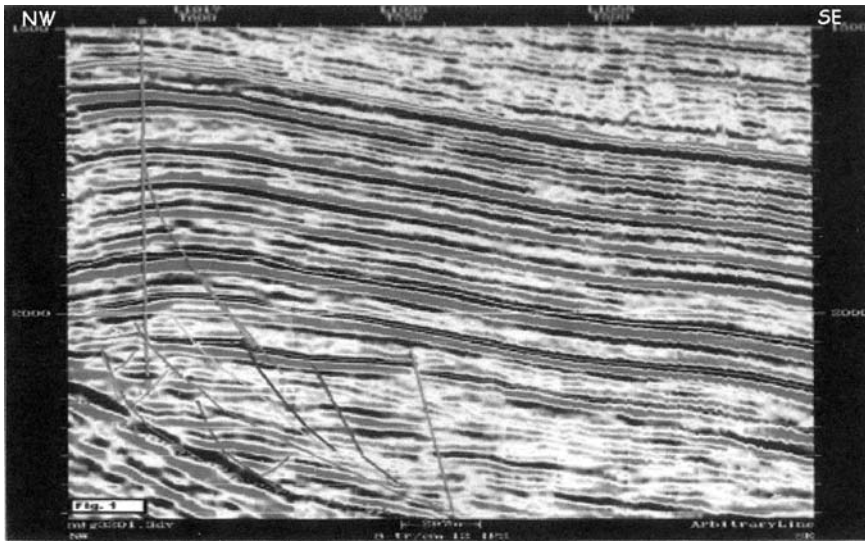


Fig. 4: NW-SE seismic section across the wells E-1 and E-1As in Epsilon oil field of Prinos basin. The anti-clinal structure with the downthrown faults are well illustrated from the seismic reflectors.

The Post-Evaporitic Series is pure clastic and marine origin, as indicated by the presence of a great number of Pliocene foraminifera and algae. Towards the top, coarse clastic sediments with abundant rests of molluscs point out to a deltaic, according to the seismic, prograding sequence. A transgression followed with deposition of marine clastic sediments (Proedrou and Papaconstantinou, 2004).

These three series reflect the different sedimentological conditions of each period and generally, increase in thickness towards the centre of the sub-basins.

2.3 Reservoirs

Hydrocarbon fields in Prinos basin are related to rollover anticlines, which are in front of syngenetic NW-SE striking downthrown faults or surrounded by downthrown faults. Prinos oil field, Prinos North oil field and South Kavala gas field belong to the former and Ammodhis and Epsilon fields to the latter case (Proedrou and Papaconstantinou, 2004).

Reservoirs are mainly sandstones and secondly siltstones, that resulted from the uppermost Miocene depositions from deltaic, marine and turbiditic environments. The evaporites cover the whole basin, keeping hydrocarbons below them, except from an upward movement of hydrocarbons in South Kavala and Ammodhis fields, probable due to fault activation. Generally, porosity and permeability is decreasing with increasing depth, due to weight overlay, clay content and dolomitization (Proedrou and Papaconstantinou, 2004).

3. Epsilon field data

3.1 Seismic section

The Epsilon oil field is located in the middle of the Prinos basin axis, close to the north slope of the basin, approximately 4.2 km W-NW of the Prinos oil field (Fig. 1). The 3-D seismic survey that took place the period 1993-1997, indicated the existence of a new hydrocarbon field in the area.

The first well, E-1, was drilled in 2001 and confirmed the results of the geophysical research, but as mentioned in section 1, technical reasons dictated the redrilling in 2002, originally with E-1A and finally with E-1As wells.

The discovery of Epsilon oil field brought some new data for the already well studied Prinos basin. In Fig. 4, the NW-SE seismic section across the wells E-1 and E-1As is shown. The anticlinal structure of Epsilon field with the downthrown faults are well illustrated from the seismic reflectors.

3.2 Drilling data

According to the E-1 well drilling data, as recorded by KAVALA OIL S.A., the Evaporitic Series started at 1895 m (all depths T.V.D.). The 40 m thick stray evaporite zone consisted predominantly of anhydrite and salt with claystone, limestone and sandstone. The 1st evaporite horizon was found at 2096 m depth. It consisted of salt and traces of anhydrite. The salt was colourless, white or milky white, translucent, firm or crystalline. The anhydrite was white, soft to moderately firm, cryptocrystalline and occasionally microstalline. The thickness of the horizon was about 34 m. The 2nd evaporite horizon was found at 2195 m depth in well E-1 and at 2195.5 m depth in well E-1A (KOP from well E-1 was at 2135 m). It consisted of salt with anhydrite intercalations and had a thickness of about 50 m. The salt was again colourless, white, tan, transparent, firm, well crystalline, occasionally with succrosic texture and anhydritic. The anhydrite again it was white, soft to moderately firm, cryptocrystalline and occasionally microstalline. There were also traces of gray, soft plastic and soluble clay. The 3rd evaporite horizon was found at depths of 2321.5 m in well E-1 and 2319 m in well E-1A. It was composed of salt with clay and sandstone intercalations. The salt was similar to the 1st and 2nd evaporite, except that sometimes it was anhydritic with up to 10 % anhydrite with traces of gypsum. The claystone was gray, soft, highly washable and calcareous. The thickness of this horizon was 30-34 m. The 4th evaporite was met at depths of 2483.5m in well E1, 2476.5 m in well E-1A and 2479.5 m in well E-1As. It consisted of salt and anhydrite, up to 10%. The salt was colourless, white to off white, milky white, soft to firm, with succrosic texture, crumbly, well crystalline and occasionally microcrystalline. The anhydrite was milky white, soft to moderately firm, pasted and occasionally cryptocrystalline. The thickness of this series was 46-50 m.

The Upper Main Salt (UMS) zone was found at 2633 m deep in E-1 well, while in wells E-1A and E-1As at 2630 m deep and had a thickness of 50-57 m. The Lower Main Salt (LMS) was at depths of 2769 m, 2775.5 m and 2777 m at wells E-1, E-1A and E-1As, correspondingly and had a thickness of 30-42.5 m. Both UMS and LMS zones were becoming thicker from the NW to the SE, towards E-1As well.

The cap rock (claystone 70-90% with sandstone intercalations and traces of siltstone), was found at depths of 2799 m in E-1, 2816m in E-1A and 2819 m in E-1As and had a thickness of 13.5-15 m. The top reservoir was at 2813 m, 2831 m and 2833 m in the three wells, respectively. The reservoirs had a total maximum thickness of 77.5 m at E-1As well. They consisted of latest Miocene fan deposits, where sandstone was prevalent (60-70%) with claystone intercalations (30-40%) and traces of siltstone. Sandstone was non-consolidated, colourless, translucent transparent, occasionally smoky white, fine to medium, subangular and subrounded, pyritic in part. Claystone was gray, soft to moderated firm, blocky, silty, grading to high siltstone and calcareous to high calcareous in part. Sandstones were cemented and had porosities that varied from 5-20%. The permeabilities varied from 8-10 md in reservoirs of E-1, to 10-15 md in E-1As. In Fig. 5, a 3-D structure map of Epsilon oil field, contoured at the top of the reservoir is shown.

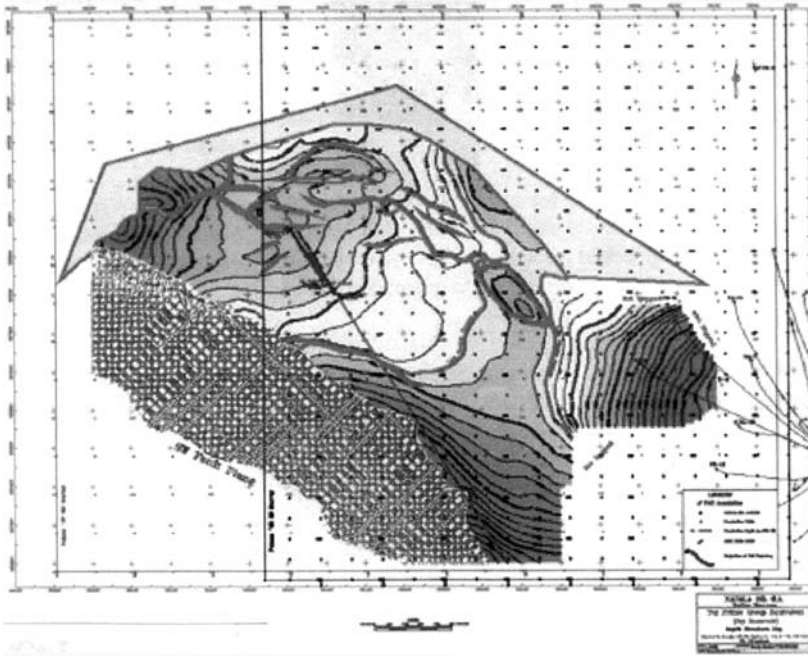


Fig. 5: A 3-D structure map of Epsilon field, contoured at the top of the reservoir.

Epsilon oil is aromatic-asphaltic type with 36.5^o API at 18^o C and with sulphur content less than the 4% of Prinos oil. The average initial pressures for the producing zones were approximately 6000 psi. Total reserves at place of Epsilon field were initially estimated to more than 40· 10⁶ bbl.

4. Conclusions

The Prinos basin is the only productive hydrocarbon area in Greece and the Epsilon oil field is the latest field brought to production. Following the general structure of the taphrogenetic basin, it is a dome-like anticline formed by NW-striking and SW-dipping syngenetic faults also related to the trapping mechanism. Guided from the seismic survey of 1993-'97, three drillings took place in 2001-'02 that confirmed the existence of the new hydrocarbon field. The drilling data were in agreement to the geotectonic evolution and depositional model of Prinos basin. The quality and quantity characteristics of initial production led to plans for further drilling operations in Epsilon field.

5. Acknowledgements

The authors would like to thank Mr. Costas Papaconstantinou, Managing Director of KAVALA OIL SA, for the permission to publish this work.

6. References

Georgakopoulos, A., 1998. Study of source rocks of the petroliferous Prinos-Kavala oil bearing basin using organic geochemical methods. *Bull. Geol. Soc. Greece*, vol. XXXII, n.3, *Proceedings of the 8th International Congress*, Patras, May, pp.325-333. (In Greek with English abstract).

- Georgakopoulos, A., 2000. Lithology and stratigraphy of the Neogene Prinos-Kavala basin, Northern Greece. *Proceedings R.C.M.N.S. Interim Colloquium*, Patras 1998. (Ed.) G.D. Koufos & Ch.E. Ioakim, *Mediterranean Neogene Cyclostratigraphy in marine-continental palaeoenvironments*, Geol. Soc. Greece Sp. Publ. No 9, pp.79-84.
- Hsu, K.J., 1972. Origin of saline giants: a critical review after the discovery of the Mediterranean evaporite. *Earth-Science Review*, v. 8, pp.371-396.
- Kiomourtzi, P., Pasadakis, N. and A. Zelilidis, 2007. Geochemical Characterization of Satellite Hydrocarbon Formations in Prinos-Kavala Basin (North Greece). *Bull. Geol. Soc. Greece*, vol. XXXX, n., pp.839-850.
- Kiomourtzi, P., Pasadakis, N. and A., Zelilidis, 2008. Source Rock and Depositional Environment Study of the Three Hydrocarbon Fields in Prinos-Kavala Basin (North Aegean). *The Open Petroleum Engineering Journal*, vol.1, pp.16-30.
- Kiomourtzi, P., Zelilidis, A. and N., Pasadakis, 2009. Organic geochemical study of the Kalirahi formation (Prinos-Kavala Basin). *3rd AMIREG International Conference: Assessing the Footprint of Resource Utilization and Hazardous Waste Management*, Athens, Greece.
- Pollak, W.H., 1979. Structural and lithological development of the Prinos-Kavala basin, sea of Thrace, Greece. *Annex Geologique pays Hellenic tome hors serie*, fasc II, VIIth International Congress on Mediterranean Neogene, Athens, Greece, pp.1003-1011.
- Proedrou, P., 1979. The Evaporite formation in the Nestos-Prinos graben in the northern Aegean sea. *Ann. Geol. Pays Hellen.*, Tome hors serie 1979, fasc. II, VIIth International Congress on Mediterranean Neogene, Athens, Greece, pp.1013-1020.
- Proedrou, P., 1988. New age determination of the Prinos basin. *Bull. Geol. Soc. Greece*, vol. XX, n.2, pp.141-147.
- Proedrou, P., and T. Sidiropoulos, 1992. Prinos field – Greece, Aegean basin, structural traps. *Treatise of petroleum Geology atlas of oil and gas fields*, AAPG, pp.275-291.
- Proedrou, P., 2001. South Kavala gas field-Taphrogenetic Prinos basin. *Bull. Geol. Soc. Greece*, vol. XXXIV, n.3, pp.1221-1228.
- Proedrou, P., and C.M., Papaconstantinou, 2004. Prinos basin – A model for oil exploration. *Bull. Geol. Soc. Greece*, vol. XXXVI, n.1, pp.327-333.
- Walker, R.G., and E. Mutti, 1973. Turbidite facies and facies associations, in G.V. Middleton and A.H. Bouma, eds, *Turbidites and deep water sedimentation: SEPM Pacific Section Short Course*, Anaheim, California, pp.119-157.

GEOHERMIC STATUS OF THERMOPYLAE - ANTHILI AREA IN FTHIOTIDA PREFECTURE

Metaxas A.¹, Varvarousis G.¹, Karydakis Gr.¹, Dotsika E.², Papanikolaou G.³

¹ *Institute of Geology and Mineral Exploration, Entrance C' Olympic Village 13677 Acharnae – Greece*

² *Laboratory of Archaeometry, Institute of Materials Science N.C.S.R “Demokritos”,
15310 Aghia Paraskevi - Greece*

³ *Geologist, Postgraduate student, Faculty of Geology and Geoenvironment, National & Kapodistrian
University of Athens, geopapgr@gmail.com*

Abstract

The purpose of this study was the discovery, identification and evaluation of directly exploitable geothermal fields, in the Thermopylae - Anthili area (100km²).

After the evaluation and the processing of any preexisting data, followed the surface works, such as further geological mapping, tectonic and stratigraphic correlations and analyses, geothermal impressions, observations at 30 recorded points (springs, drillings, wells) regarding water sampling, chemical analyses, temperature, pH and conductivity measurements, special sampling for Br and isotopes analyses. The in depth works that took place concern geophysical prospecting, loggings, small and large diameter drillings. All the data were digitized and processed in a GIS environment.

After correlating all the data collected for the region, a geological - geothermal model was constructed. According to this model, water percolates through permeable formations, joints and faults, gets mixed with the existing salt water, warms up and then ascends to the surface through faults and concentrates on proper reservoirs. Specifically, the region of Damasta where two areas of hot water reservoirs have been identified is of particular geothermal interest. The first, located in Triassic–Jurassic limestones (more than 600m deep), presents the greatest interest in terms of temperature and capacity, while the second (found on the surface and up to 350m deep) is located in Quaternary sediments and the upper formations of the underlying Late Cretaceous limestone.

Key words: *geothermy, reservoir, geothermal gradient, isothermal lines, Central Greece.*

1. Introduction

Geothermy as an alternative form of energy, is sustainable and does not pollute the environment. It should also be mentioned that Greece, according to the European Union standards, has to increase the use of alternative energy sources to 18% of the total energy consumption by 2020. Any geothermal energy exploitation will bring social, financial and environmental benefits, in both regional and national level.

A research about the geothermal field of Spercheios area was made to identify if there is any geothermal interest in the geological formations of the basin and then to estimate if there is any ability of these new fields to be exploited. In this framework of the Spercheios basin research (Metaxas

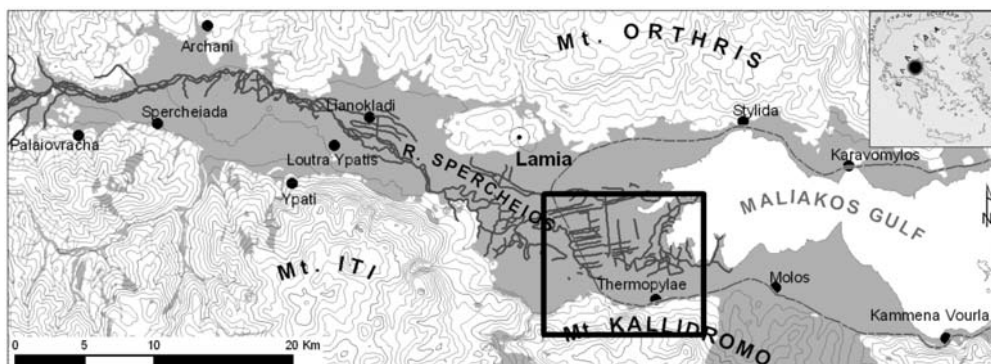


Fig. 1: Indicative map of Spercheios Basin (in black frame the Thermopylae-Anthili area).

et.al., 2008), a significant geothermal field was found near Thermopylae – Anthili, in the close area of Damasta (Fig. 1) that is described below.

Spercheios basin is located in central Greece and in terms of administration belongs to the Fthiotida prefecture, where reside the headquarters of the region of Central Greece. The basin's surface is approximately 700km², while of the wider research area is 2400km². It ranges from Maliakos bay in the East to Tymfristos mountain on the West. To the North the basin is defined by Mount Orthris and to the South by mountains Iti and Kallidromo (Fig. 1).

Geothermal energy in Spercheios basin has been known since ancient times. For example the Ypati baths are mentioned in inscriptions of the 4th century B.C. and seem to have been dedicated to the goddess Aphrodite. During the Turkish Occupation they were known as “Patratzik Baths”.

The only use of geothermal energy so far, is for spa therapy.

2. Methodology

After the evaluation and the processing of previous studies (Garagunis, C. N., 1976; Stamatakis, 1987) and any preexisting data, as were the geological mapping (Marinos et al., 1963, 1967) and the recorded temperature measurements of the water samples by surface-active hot springs, drillings and wells (Dounas et al., 1978), an widespread thermal anomaly was observed in Spercheios that occupies the entire basin and extends beyond it.

The survey in Spercheios basin, determined that the Thermopylae-Anthili area, namely the close area of Damasta presents the greatest geothermal interest. The results of this study is the outcome of numerous surface works in the area such as further geological mapping, tectonic and stratigraphic correlations and analyses, geothermal impressions, observations at 30 recorded points (springs, drillings, wells) regarding water sampling, chemical analyses, temperature, pH and conductivity measurements, special sampling for Br and isotopes analyses. The in depth works that took place concern geophysical prospecting, loggings, small and large diameter drillings. All the data were digitized and processed in a GIS environment. After correlating all the data collected for the region, a geological - geothermal model was constructed.

3. Thermopylae-Anthili area

The surface warm water events occur along faults in the areas of Kammena Vourla, Thermopylae, Psoroneria, Ypati, Platystomo, Palaiovracha, Archani (Metaxas et al., 2008).

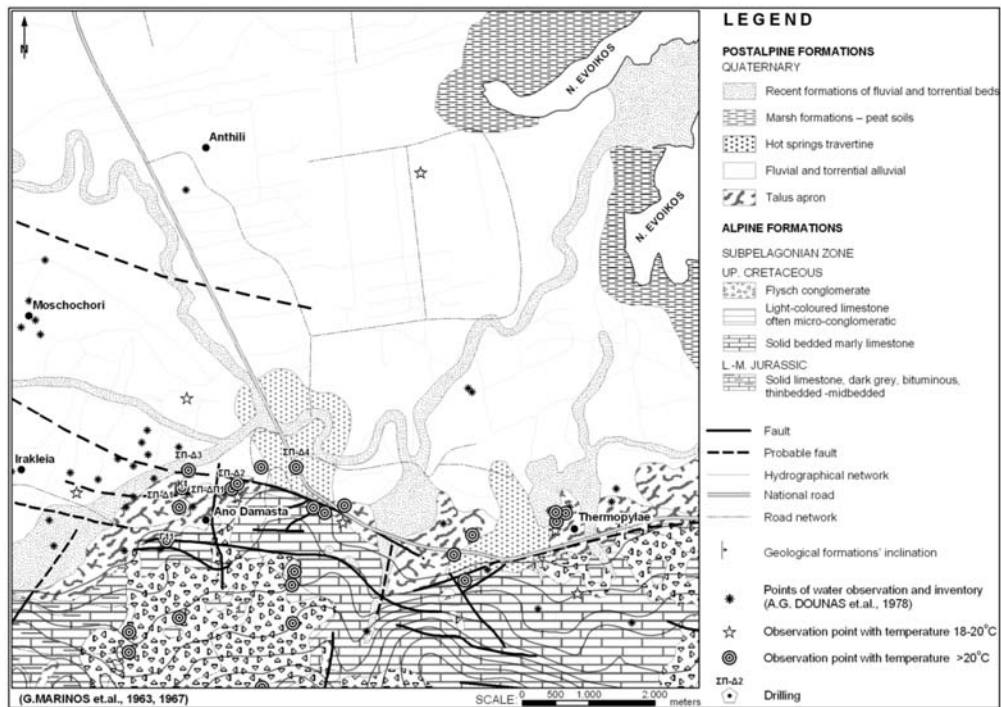


Fig. 2: Geological map of Thermopylae-Anthili area.

The area of Thermopylae - Anthili is located in the southeastern part of the Spercheios basin and covers an area of 100km². The synthesis of geological mappings (Fig. 2) indicated that the background consists of flysch and limestones (Upper Cretaceous), parts of the schist-chert formation with ophiolites and limestones (Triassic – Jurassic) of the Subpelagonian zone. The sediments of the area are mainly recent formations of river and torrent beds, older fluvial and torrential deposits, slope debris and hot springs' travertine, mainly in the Thermopylae and Psoroneria areas. In coastal regions, particularly at the mouth of Spercheios river, recent marsh formations with peat are observed. The basin's clastic sediments and the layers of limestone and dolomite are permeable formations and are able to hold significant quantities of geothermal fluids. The impermeable formations of ophiolites and flysch as well as the fine-grained clastic materials, mainly located in the eastern part of the basin, are considered the permeable formations' cap preventing thus any direct heat loss.

The intense tectonics observed in the basin, the vertical faults, the joints and any form of discontinuity, are contributing to the upward movement of hot fluids that reach the surface. Warm water, during its ascent through the faults towards the surface, is mixed with cold water table aquifers, leading to changes in both its temperature and its chemical composition. The temperature across the basin is irregular and significant fluctuation is observed from place to place. The main directions of the region's faults are E-W and NW-SE while the recent ones are vertical to the old ones: NE-SW and N-S.

In Thermopylae-Anthili and namely in the close area of Damasta, were also carried out several small and large diameter drillings (Fig. 2) that were part of this project (Metaxas et al., 2008) in order to determine the geothermal field for immediate use, and its qualitative and quantitative parameters.

Specifically in Damasta, a productive drilling was made and based at its rate $C = 435\text{m}^2/\text{sec}^5$ was

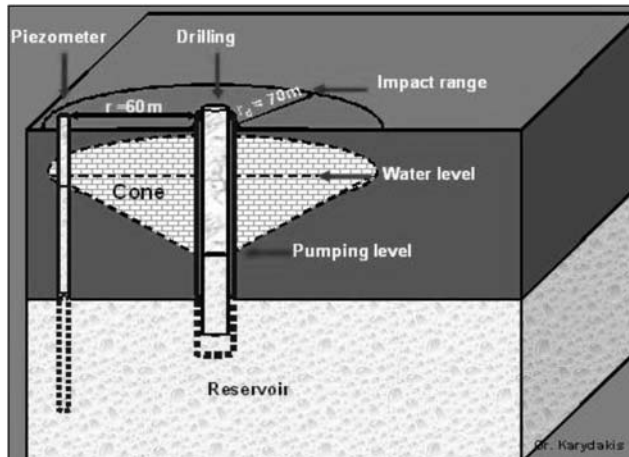


Fig. 3: Impact range r_d and drop cone of the drill level.

characterised as efficient, and its specific capacity that is over $40(\text{m}^3/\text{h})/\text{m}$ is considered quite good for a constant pumping flow of $115\text{m}^3/\text{h}$ and a temperature of 43.6°C . The range of the effect should be considered to be at least 100m on a constant supply of $115\text{m}^3/\text{h}$ (Fig. 3) and the reservoir has a high permeability, is semi-confined and has also a high pressure drop factor.

Observations at 30 recorded points (springs, drillings, wells) showed that temperatures in the area range from 19.4°C to 43.6°C .

The geochemical and isotopic study of the hot water in the Thermopylae - Anthili region (Dotsika et. al. 2008), showed that according to the concentration of the total dissolved solids (TDS), it is classified as salt water, with greater concentration in Psoroneria area (Damasta). In terms of acidity (pH) the water is neutral to slightly alkaline (Psoroneria) and according to the Waterlot chart, the potability is not appropriate. From the Piper chart it seems that warm water is sodic, chloride, sea water and comes from calcareous and siliceous rocks.

The ionic values of the water (Dotsika et. al. 2008) show that the solutions are chemically charged, with the concentration of the chlorine salt at 16000 mg/L . The water specimens from the region of Thermopylae are of Na-Cl, Na- HCO_3 and Ca- HCO_3 type.

The use of silica geothermometer shows that the temperature of the source of the hot water is around $107,5^\circ\text{C}$.

The water's chemistry generally indicates the underground course followed through the rocks and the exchange of the chemical elements among them. Indeed, the calcium, bicarbonates and magnesium levels show the exchange between water and rock under the influence of high temperatures. The isotopic values of the waters from Thermopylae, Damasta and Psoroneria show the penetration of the sea in the deep geothermal reservoir (Dotsika et al., 2008). To estimate the temperature in the deep reservoir based on the above mentioned data, the use of the K-Mg geothermometer is recommended; and gives probable temperatures of $80-85^\circ\text{C}$.

From the analysis and evaluation of all previous data and information, it seems that the geothermal model of the area is the one presented in Figure 4. In this figure, surface water percolates through the raised part of the area which consists of limestones and other formations; and also through faults, cracks and joints and discontinuities into deeper formations. The percolated water is heated and mixed with the existing salt water which penetrated during earlier times, altering the water's tem-

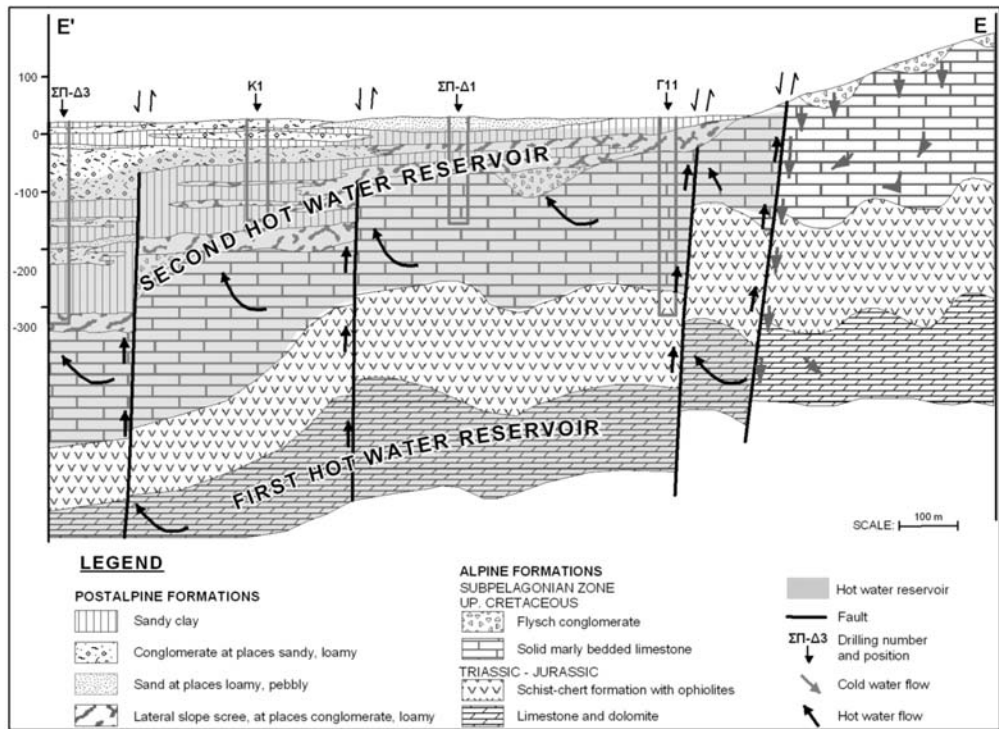


Fig. 4: Geological-Geothermal model of Damasta area.

perature and chemical composition. Finally, through different faults, the water rises again to the surface in the form of hot springs. While rising, part of the water gets trapped in the Triassic-Jurassic limestones & dolomites, which lie beneath the impermeable cover of the schist-chert formation and the ophiolites. The rest of the water continues to rise and another part of it gets trapped in the Upper Cretaceous limestones that lie below the sediments as well as in the sandy and generally coarse-grained clastic quaternary formations, which are below the fine-grained clastics (clays, sludges) that function as impermeable cover.

From the above mentioned data derives the conclusion that the area has a special geothermal interest with two hot water reservoirs. The first is located in the quaternary sediments and the Upper Cretaceous limestone and is located between just under the surface on the South and 350m deep to the North. The second one is located in the Triassic - Jurassic limestone beyond 600m deep and presents the greatest interest in terms of temperature and potentiality.

According to the financial research program in the area of Spercheios and the available resources, it was impossible to explore the deeper reservoir. Because of this, we describe in details only the second -shallower- reservoir.

It appears (Fig. 5) that the most important factor that determines the temperature change, in relation to the depth of the second -shallower- reservoir, are the regional tectonics. High temperatures are occurring just under the surface, on the basement's slopes, and reach 350m deep in a relatively short distance due to the faults presence. In drilling ΣΠ-Δ2 (Fig. 5) was observed a characteristic horst, where in both sides the vertical temperature is sinking because of the faults.

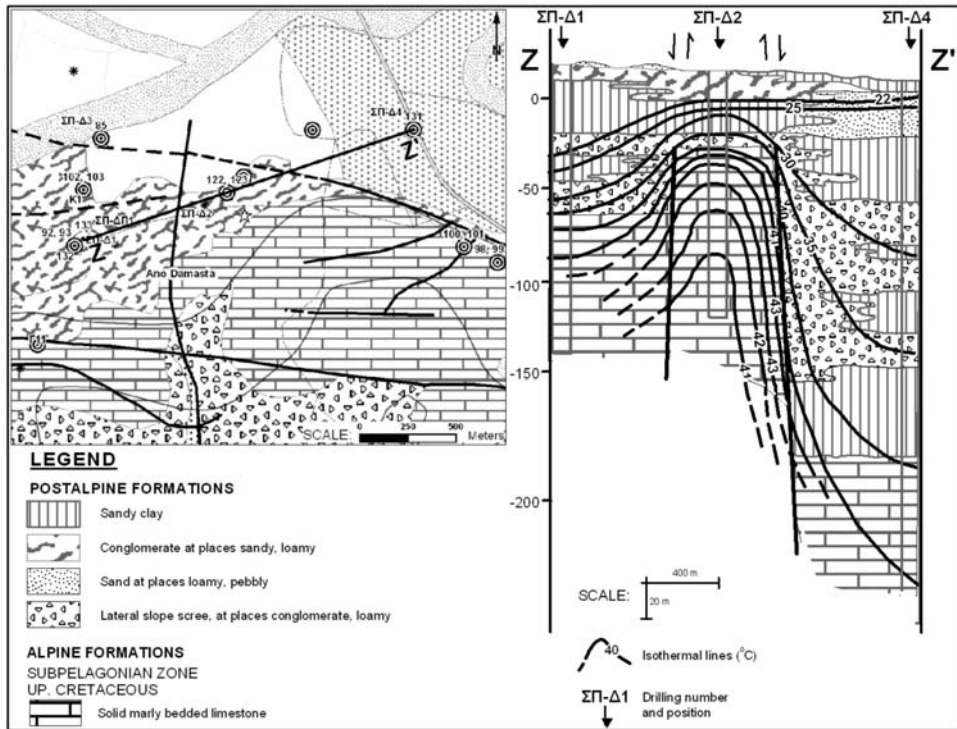


Fig. 5: Geological map of the Damasta area and correlation section Z-Z' with isothermal lines.

Generally, due to the presence of faults, a gradual increase in the depth of high temperatures is observed from the basement (South) towards the basin (from South to North - Northeast). Higher temperatures seem to occur in debris cones above the basement and also inside the basement in the Upper Cretaceous limestone.

The second-shallow reservoir is a hot water table aquifer in the close area of Damasta that has been identified in quaternary basin sediments, especially in coarse-grained clastics, conglomerates, gravel conglomerates, sands, etc., which are often interrupted by clay, as well as in the Upper Cretaceous limestone below quaternary basin sediments. Its main volume and higher temperatures are specified in the Upper Cretaceous limestone, that is fragmented, faulted and karstified, as well as in the overlying limestone debris (breccia, conglomerates, etc.).

The sediments have a standard thickness and expansion because of their fluvial / fluvial-torrential origin. There is a continuous change and movement of river and torrent beds and as a result there is a continuous change in the sediment composition and granulometry.

The high temperatures are starting to appear round about the surface in the southern region, whereas while going north the depth where the hot water table aquifer appears, increases significantly (Fig. 6). This is mostly due to the large and deep faults of NW-SE and N-S direction that exist in the area, and less to those of E-W direction.

In Figure 6 we can see the contour lines of the hot water aquifer's roof, taking into account the temperature of 25°C. It should be noted that after the edging fault the depth increases significantly to -90m absolute altitude in the NE part of the region and to -130m absolute altitude in the NW part, primarily because of the vertical fault of N-S direction.

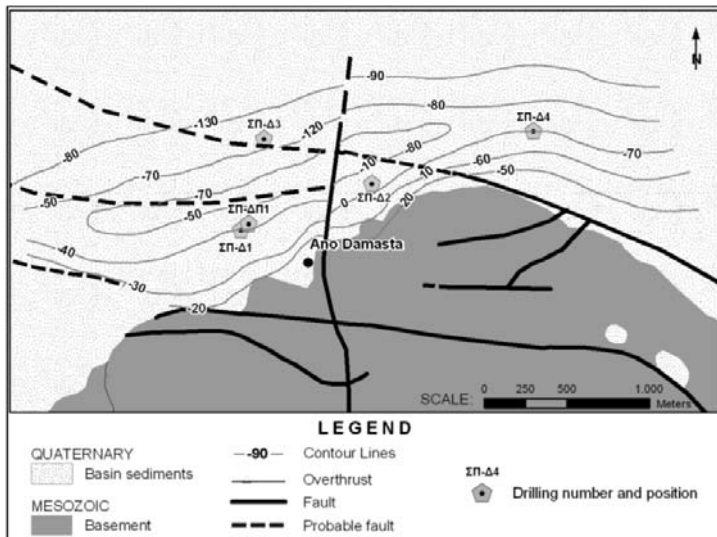


Fig. 6: Map of contour lines for the roof of the hot aquifer (25°C).

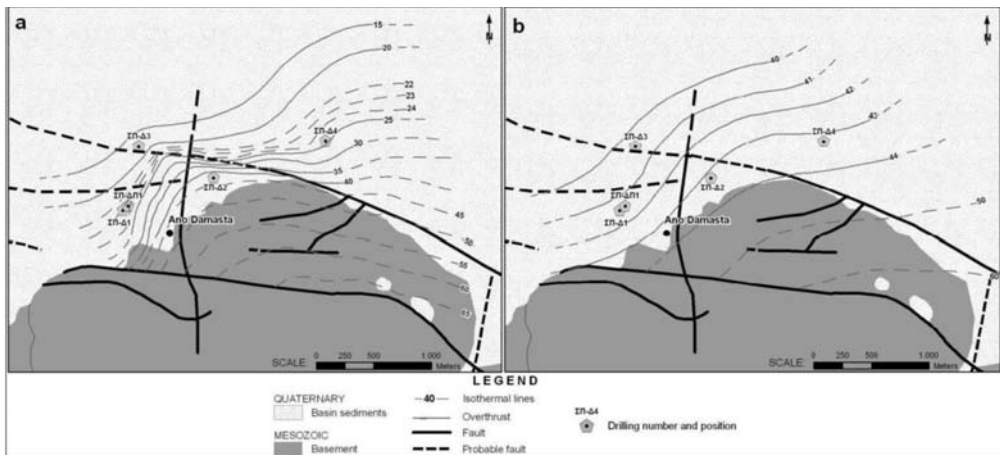


Fig.7: (a): Map of isothermal lines at 50m deep; (b): Map of isothermal lines of the highest temperature.

Taking into account all facts of the close Damasta area and by observing the isothermal lines that were drawn for every 50m depth (Fig. 7a), we see that higher temperatures are found in the southern region and gradually reduce towards North-Northeast. These range from 20-45°C depending on the depth of the basin. In the basement, between the two edging faults, although we have no information from drillings, the trend of the lines shows that much higher temperatures of 50-65°C are to be expected. We present a map of isothermal lines of the highest temperature that appears in the area (Fig. 7b). It is an area that should be investigated, with future programs, in order to verify or reject the above mentioned theory.

Taking into consideration all the above mentioned factors, the map of the equivalent curves for the average gradient was composed (Fig. 8) for the Damasta region.

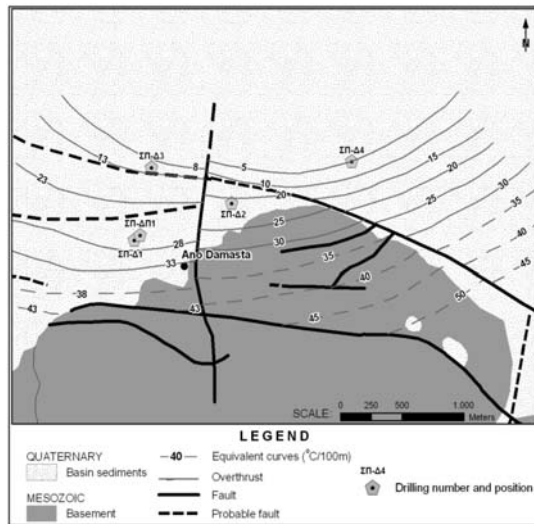


Fig. 8: Map of equivalent curves for the average geothermal gradient.

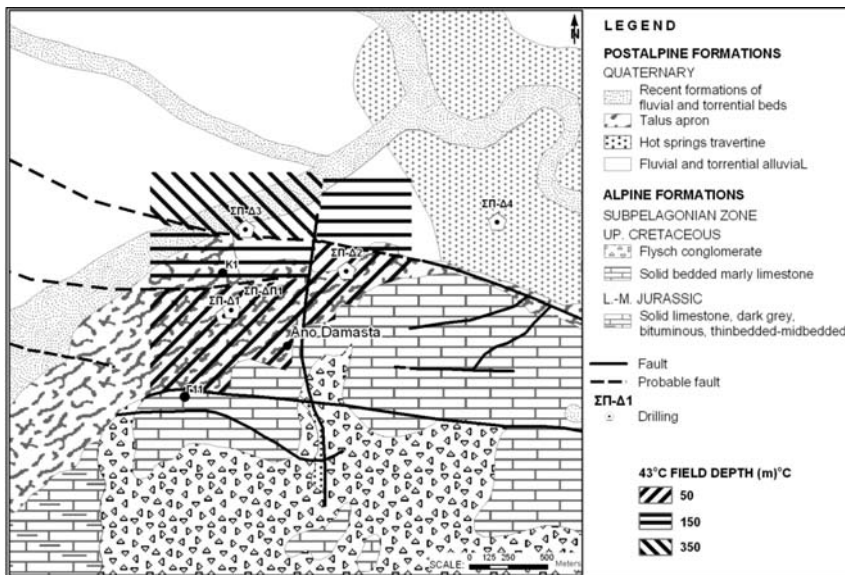


Fig. 9: Map of geothermal fields in Damasta area.

In the map (Fig. 8) the higher values are located South and the lower ones to the North. In the sediments temperature is ranging from 35°C/100m to 5°C/100m and in the basement is estimated at 35-50°C/100m.

After the process and evaluation of all the data and information that the research provided, some geothermal fields, of 43.5°C in relation to the depth, have been identified (Fig. 9). This map shows that the most important part, with the higher temperatures and the lower depths, is in the Southern region. Gradually going north the same reservoir deepens due to the tectonics that are observed in the region.

4. Results and discussions

The following new data and results from the presented study can be summarised and further interpreted to the following:

- The thermal anomaly observed in Spercheios is extensive, occupies the entire basin and extends beyond it.
- The surface warm water events occur along the faults observed in the region.
- From the geochemical study of the Damasta area, warm water is salty (sea water), sodic, chloride, neutral to slightly alkaline and non potable.
- The temperature of the hot water source is 107.5°C according to the silicate geothermometer and the K-Mg geothermometer while the temperatures of the deep reservoir are 80-85°C.
- In Damasta area, there are two reservoirs of hot water. The one (second one) is in the quaternary sediments and the Upper Cretaceous limestone and is located between just under the surface on the South and 350m deep to the North. The first and more interesting reservoir, in terms of temperature and capacity, is found in the Triassic-Jurassic limestone at depths exceeding 600m.
- The geothermal gradient of the second reservoir inside the sediments is ranging from 35°C/100m to 5°C/100m and in the basement is estimated at 35-50°C/100m.
- The constant pumping flow to the assigned geothermal field is 115m³/h with a temperature of 43.6°C, the reservoir has a high permeability and is semi-confined.

There should be a deep drilling research program to identify and explore the deeper reservoir as well as a shallow drilling program to explore the southern part of the study area and enhance the determination of the quantitative and qualitative parameters of the already known reservoir.

Some examples for future exploitation of the geothermal energy in the area when the conditions are favourable are: agricultural applications (greenhouses, etc.), fish farming, desiccation of agricultural products, house heating, and others like indoor swimming pools and SPA therapy that can become an attraction for winter as well as summer tourists.

5. References

- Dotsika, E., Duriez A., Metaxas A., Karydakis Gr., Varvarousis G., Marlin C., 2008. Isotopic and geochemical study of hot water in Spercheios basin, Athens, 111.
- Dounas, G.A., et. al., 1978. Hydrogeological research of Sperchios basin – annex – inventory of water points, *Hydrological and hydrogeological researches*, N.26, I.G.M.E., Athens, p.105
- Garagunis, C., 1976. Geothermal areas in the Maliac Gulf region in Greece. Proceedings of the Int. Congress on Thermal Waters, Geothermal Energy and Volcanism of the Mediterranean Area, vol. 1, Athens p.241-274
- Marinos, G., Anastopoulos J., Maratos G., Melidonis N., Andronopoulos B., 1963. Geological map of Greece, Stilis sheet, scale 1:50.000, I.G.M.E., Athens.
- Marinos, G., Papastamatiou J., Maratos G., Melidonis N., Andronopoulos B., Tataris A., Betoulis D., Katsikatsos G., Maragoudakis N., Lalechos N., 1967. Geological map of Greece, Lamia sheet, scale 1:50.000, I.G.M.E., Athens.
- Metaxas, A., Varvarousis G., Karydakis Gr., 2008. Geothermical research of Spercheios basin, I.G.M.E., Athens, p.193.
- Stamatakis, M., 1987. Boron distribution in hot springs, volcanic emanations, marine evaporates and sedimentary rocks of Cenozoic age in Greece, phd dissertation, University of Athens, 459pp.

CO₂ CONTENT OF GREEK LIGNITE: THE CASE OF PROASTIO LIGNITE DEPOSIT IN PTOLEMAIS BASIN, NORTHERN GREECE

**Metaxas A.¹, Georgakopoulos A.N.², Karageorgiou D.M.M.³,
Papanikolaou G.⁴ and Karageorgiou E.D.¹**

¹ *Institute of Geology and Mineral Exploration, Entrance C Olympic Village, 136 77, Acharnae Greece, dek@igme.gr*

² *Department of Mineralogy-Petrology-Economic Geology, Laboratory of Economic Geology, Aristotle University of Thessaloniki, 54124 Thessaloniki, Greece, ageorgak@geo.auth.gr*

³ *Geographer, 62 Amissou str. 17123 N. Smyrni, Athens, Greece, melaxroini_ka@yahoo.gr*

⁴ *Geologist, Department of Geology, National & Kapodistrian University of Athens, Greece, geopapgr@gmail.com*

Abstract

Lignite is an important energy source for Greece, which severely relies on this fossil fuel for electricity generation over the years. The lignite combustion, however, releases a significant amount of carbon dioxide to the atmosphere per unit of energy generated, more than does the combustion of other fossil fuels. On the other hand, there is a growing concern over the possible consequences of global warming due to the increase of carbon dioxide in the atmosphere (a major greenhouse gas). Additionally, there is also a need for accurate estimates of carbon dioxide emissions.

There are many factors resulting in the increase of CO₂ content in lignite such as their formation and depositional environment, the possible presence of fossils, and their rank.

In the present paper the CO₂ content of the Proastio lignite deposit, Ptolemais Basin, is studied, in relation to the depositional palaeo-environment. An interpretation of CO₂ variation with depth, age and surrounding rocks is also attempted.

CO₂ content of Proastio deposit is compared with this of other lignite deposits in the Ptolemais Basin, of various types and ages. Finally, the effect of CO₂ content in the combustion of lignite is studied, while the possibility of the geological storage of the emitted carbon dioxide is explored after its capture from the Thermal Power Plants (CCS technology).

Key words: *lignite, carbon dioxide, Proastio, Ptolemais, NW Greece, carbon storage.*

1. Introduction

There are a number of adverse environmental effects of coal mining and burning, especially in power stations. These effects include release of carbon dioxide, a greenhouse gas, which causes - according to the IPCC [Intergovernmental Panel on Climate Change] - climate change and global warming. Coal combustion is the largest contributor to the human-derived CO₂ in the air.

In Greece, approximately 38% of the annual CO₂ emissions, i.e. 53 t of a total of 140 t, derive from lignite combustion for the production of electric power. From P.P.C. data's it knows that for each pro-

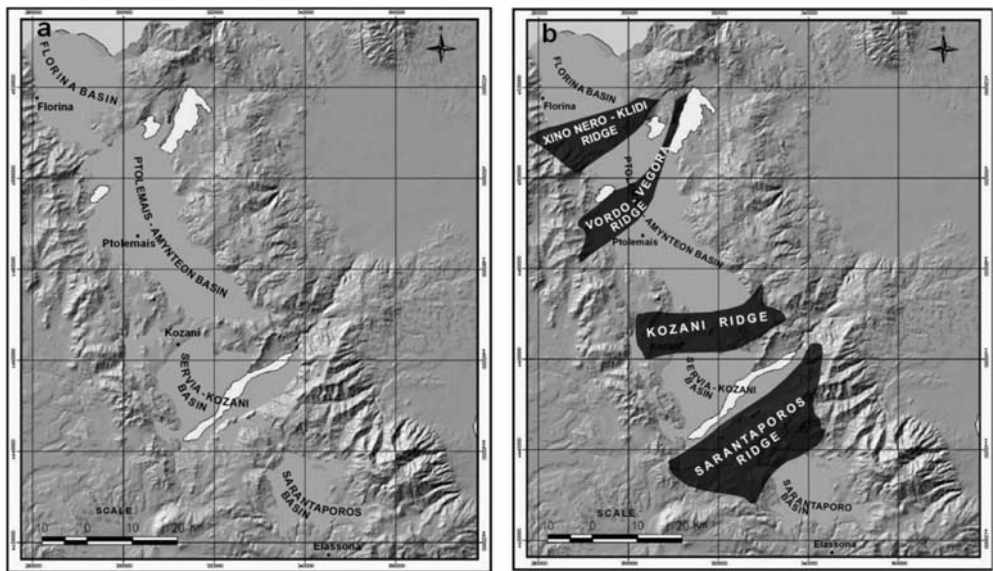


Fig. 1: (a): Map of Florina-Ptolemais Kozani and Sarantaporo basins; (b): Map of Graben with ridges.

duced MW/h in the Thermal Power Plants, 1.2-1.3 t CO₂ are emitted in the atmosphere. To meet the enhancement of the annual energy demand that is expected to increase significantly until the year 2030, the use of fossil fuels (lignite, hydrocarbons) is necessary apart from the use of Renewable Energy Sources (R.E.S.), a fact resulting in an increase of CO₂ emission from 18 Gt in 1980 to 40 Gt in 2030. The Hellenic lignite, constituting the main electric power generation source in the country, contains varying CO₂ amounts depending mostly on the age of deposition, the depositional environment and the lignite features. The elevated CO₂ content of the Proastio lignite and the Upper Pliocene lignite in general, is mainly due to the great amount of fossils, the CaCO₃ saturations and the thin intercalated marl layers. Carbon dioxide, a greenhouse colourless, inorganic gas is generated as a by-product of the combustion of fossil fuels or the burning of vegetable matter, among other chemical processes. Small amounts of carbon dioxide are emitted from volcanoes and other geothermal processes such as hot springs and geysers and by the dissolution of carbonates in crystal rocks. The Pliocene lignite deposits hosted in the Ptolemais Basin display high CO₂ contents (Metaxas et al., 2007) resulting in the emission into the atmosphere of 0.6-0.7 t CO₂ per ton of lignite burned in the thermal power plants. A representative deposit of this age is that of Proastio, which, in terms of total reserves, is the second one after the Southern Field deposit.

2. Geological setting

The Ptolemais Basin is located in the North-Western Greece and constitutes part of the Monastir-Ptolemais-Kozani-Servia tectonic trench (Fig.1a). It is a discontinued geological unit due to occurrence of recent tectonic disturbances of great scale, which were activated in Neogene and Quaternary times. The elongated and deep basins (Metaxas et al., 2007) of Ptolemais-Ardasa-Vegoritida, etc. as well as the tectonic ridges of Xyno Nero, Bordo-Filota, etc., disrupted the continuity of various lignite-bearing regions (Fig. 1b).

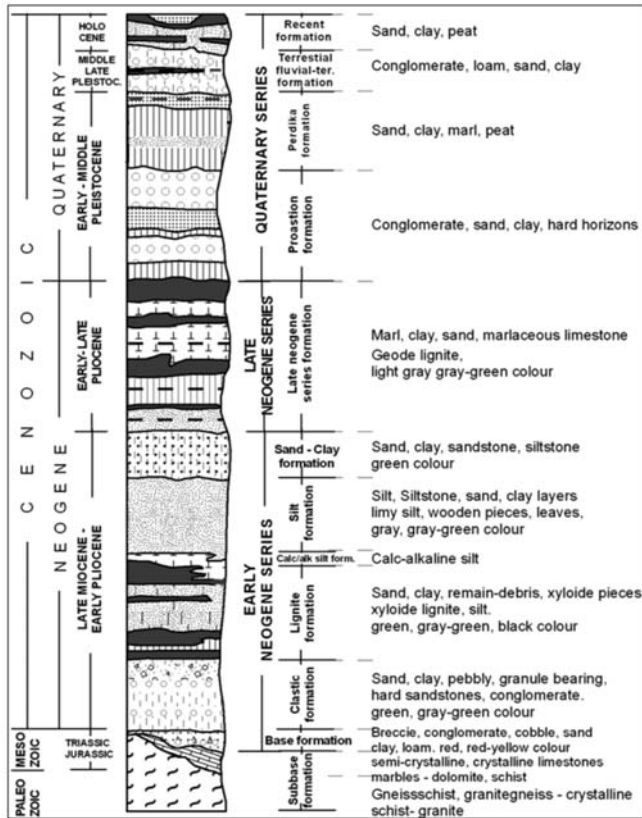


Fig. 2: Synthetic stratigraphic column of the Florina, Ptolemais-Amynteon, Kozani, Sarantaporo Graben.

The area of Proastio is located at a distance of about 5 km to the S-SE of Ptolemais city. It is not an independent geological unit and is attributed to the geological unit of Ptolemais basin.

The stratigraphic structure of the sedimentary series, the lithofacies analysis of the geological formations and the geological structure of the lignite deposits in general, were based on the data obtained from the study of borehole cores (Kotis et al., 2001).

The overview of the geological setting of the broad Ptolemais basin (Metaxas et al., 2007) is showing in the stratigraphic column (Fig. 2).

During Upper Miocene-Lower Pliocene, the Ptolemais Basin was supplied with materials from the North and West. The rocks in these basin margins are metamorphic, such as gneisses, schists, etc. This is one of the main reasons that calcium carbonate display low contents in these formations. Fossils occur rarely into these formations due to the small concentration of CaCO_3 during this period. The aforementioned feeding is due to the ascension of the basement of the Florina Basin during Mio-Pliocene, in relation to Ptolemais Basin, which is going on up to now. Moreover, it seems that the ascension of the western margins of Ptolemais Basin was quicker and higher compared to the eastern ones. The sediments deposited during this period are coarser in Florina Basin and the western margins of Ptolemais Basin (coarse-grained sands, conglomerates, etc.) compared to these deposited at the eastern margins (clays, silts, etc.). Lignite deposition of this type could not form in the West and North of the trench due to the aforementioned rea-

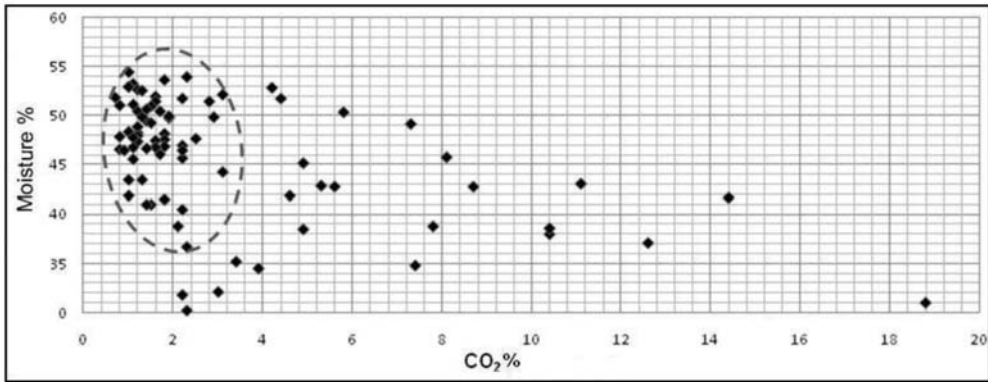


Fig. 3: Correlation between CO₂ and moisture.

sons and in addition to the quick flow and great volume of transported materials. During Upper Pliocene, when lignite of Ptolemais type was deposited, the feeding of the Ptolemais Basin took place from the East. Further ascension of Florina Basin impeded deposition of Pliocene lignite in this basin as well as a quicker ascension of the eastern margins of Ptolemais Basin and subsidence of the central area and the western margins. Thus, this lignite type occurs in the central and the western parts of Ptolemais Basin. Given that the feeding took place from the eastern bedrock, where carbonate rocks such as limestone, semi-metamorphic marble etc., occur, high concentrations of CaCO₃ and fossils are included into the sediments of this period resulting in, respectively, high CO₂ amounts released from the lignite of Ptolemais type. Another factor of CaCO₃ deposition is the environment of lignite formation of this type. Sediments of biochemical type with increased CaCO₃ are observed due to the smooth environment where the time required for creation and deposition of these sediments is ensured. Furthermore, capture of CO₂ by the plants through the solutions took place resulting in CaCO₃ deposition.

The lignite deposit of Proastio is remarkable and second in terms of total volume of deposit after the South Field. This deposit can be developed and exploited securing the supply of two units of 600 MW for 43 years.

The formations observed in the area (Kotis et al., 2001) are described in the stratigraphic column of Fig. 3. The maximal cumulative thickness of the lignite seam is 360 m and this of lignite 81 m. The average moisture of lignite is 45.8%, the ash yield [on dry basis] 29.7%, the volatile matter content 40.0%, while the fixed carbon [on dry basis] ranges from 31.4 to 35.1%. The average combustible sulphur is 0.63% and the total 1.19%. The elemental analysis of the fuel (d.b.) gave a Carbon content of 50.7%, Hydrogen content 4%, Nitrogen content 1.39%, Oxygen content 10.61%. The Gross calorific value (G.C.V.) is of 2485 kcal/kg while the net calorific value (N.C.V.) 2085 kcal/kg.

Geological reserves are estimated to 370 m. tn. and mineable reserves to 273 m. tn, with an average exploitability relation [(Overhead deadwood + Intermediate deadwood) / lignite, (Y+E)/Λ=9,88:1] and average ash content [on dry basis] 27.8%.

3. CO₂ Content In The Ash

The content in carbonate minerals constitutes a very important factor for the qualitative differentiation of the lignite beds. During lignite combustion into the steam power plants these minerals are split in carbon dioxide and oxide of the respective element, for example CaCO₃ → CaO + CO₂↑.

The higher the CO₂ content, the worse the lignite quality, because a part of the power (425 kcal/kg)

is absorbed to break down the carbonates (endothermic reaction) thereby reducing the amount of energy produced. Thus, determining the quantity of CO₂ released by the decay of carbonate minerals is essential for characterising the actual coal.

Until around 1980, there was no need to calculate the CO₂ content in the evaluation of the deposits. For this reason no measurements and information exist before this date. After 1980 the CO₂ content is taken into account in the calculations referred to in the evaluation of each deposit, based on the ash (Kolovos et al., 2002; 2002; 2002; 2003, Sotiropoulos et al., 2005).

The ash yield of each sample is due to the presence of various fossils shells, apart from the inorganic materials comprised into lignite and the thin barren layers (clay, marls, etc.) collected with lignite during sampling.

The only concern previously considered during the sampling of lignite layers was the thickness of the barren layer, if consisting of clay, not to exceed 5% of the length of the core - sample.

The other criterion in the evaluation of the deposits was the relatively low ash yield on dry basis (35%) in the mineable bed. But today, after implementation of chemical analyses it was proved that in many layers, where ash is less than the above limit, adding CO₂, exceeds 45 to 50% and the exploitable reserve decreases down to the 1/3 of the initially calculated reserve without the CO₂.

As a result, several operational problems are created, even black out of the station, depending on the specifications of the lignite combustion unit. Furthermore, problems are created in the exploitation and the overall design of a mine as well as in the use, transportation, combustion, etc.

Re-evaluation of several lignite deposits is suggested, mainly of those assessed before 1980, using new datasets, taking into consideration the CO₂ and the specifications of the combustion plants to be fed by the specific lignite deposit. If for example a station can use lignite having thermal capacity up to 1280 kcal/kg, the N.C.V. of the mineable lignite seams should be taken into account for the evaluation.

The ash yield on an as-received basis varies widely due not only to the different content in inorganic matter, but also to the different moisture of the samples. Moisture varies even for lignite samples of the same composition. Thus, in order to compare the values of ash yield and therefore of CO₂, it is appropriate to refer them to a fixed percentage of moisture or to a dry and ash free basis. Figure 3 shows that as the moisture increases, the CO₂ decreases on an as-received basis.

4. Origin of CO₂

During the exploration of the Proastio deposit, a specific sampling of lignite was carried out, depending on the reaction to the hydrochloric acid (HCl, density 1:10), as well as on the fossils contained and the thin marl or clay layers included.

The samples of the pure or clayey lignite are not reacting to the hydrochloric acid (no bubbling) and their average CO₂ content ranges on an as-received basis is about 1.5% (Fig. 4). This amount of CO₂ is mainly due to CaCO₃ dissolved from the surrounding carbonate rocks by surface and karstic waters feeding the palaeomires.

Only the fossils included in the lignite samples react to the HCl (strong bubbling) and the average CO₂ values are c. 7%. These values vary from sample to sample, depending on the fossils content. In this category, the CaCO₃ reaches values up to 40%.

Samples with thin marl or clay layers are classified to the third category. They display very strong reaction to the HCl (very strong bubbling); the average CO₂ value is about 9%, while CaCO₃ exceeds 45% (Fig. 5).

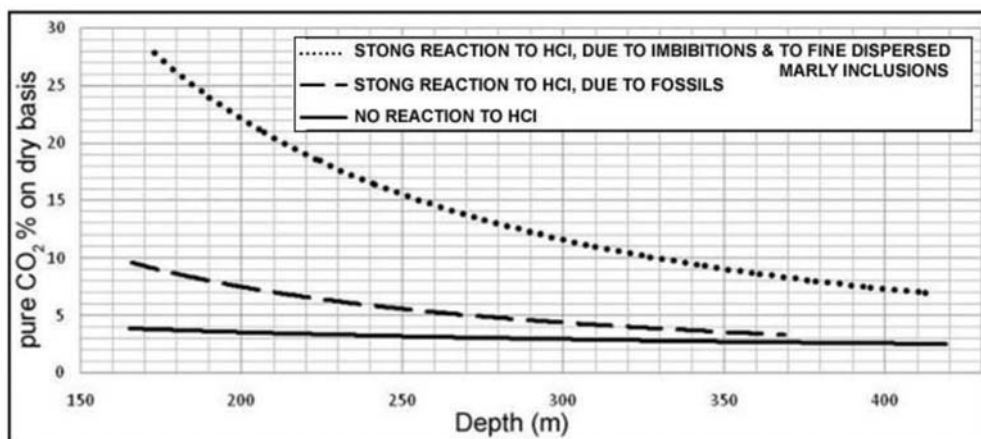


Fig. 4: Correlation between pure CO₂ and depth.

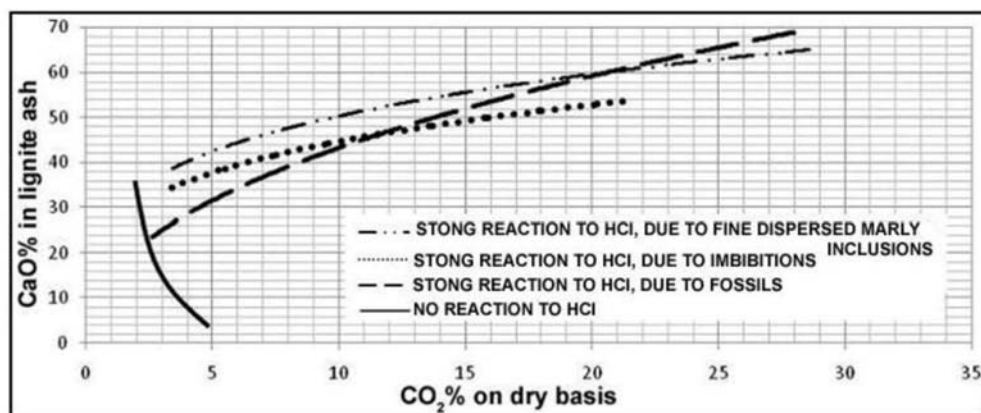


Fig. 5: Correlation between CaO content in lignite ash and CO₂ content (on dry basis).

The marl layers hosted into the lignite beds are mainly due to changes of the depositional environment, the feeding from the surrounding rocks and the vegetation type (abstraction of CO₂ from the plants for the photosynthesis resulting to CaCO₃ precipitation).

In Proastio area and beneath a depth of 210 m, the CO₂ content decreases drastically in all categories of lignite samples, as well as the CaCO₃ content below 11% (Fig. 6).

One of the main reasons is the feeding environment. During the deposition period of the deeper lignite beds (Miocene/Pliocene boundary), the feeding took place from North and West where the surrounding rocks are metamorphic (gneiss, schist). Almost stable relation of CO₂ is observed in the lignite free from saturations, marl layers and fossils, compared to the combustible (Fig. 7) and fixed carbon (Fig. 8), with however a small decrease when CO₂ increases. Conversely, a great decrease in lignite beds with fossils and marl layers is observed. The greater decrease of the permanent carbon is mainly observed in the lignite with CaCO₃ saturations. Almost stable relation between O₂ and CO₂ is observed in the lignite samples including fossils or thin marl layers, with a small increase of O₂ when CO₂ increases. On the contrary, in samples not reacting to HCl or with CaCO₃ saturations,

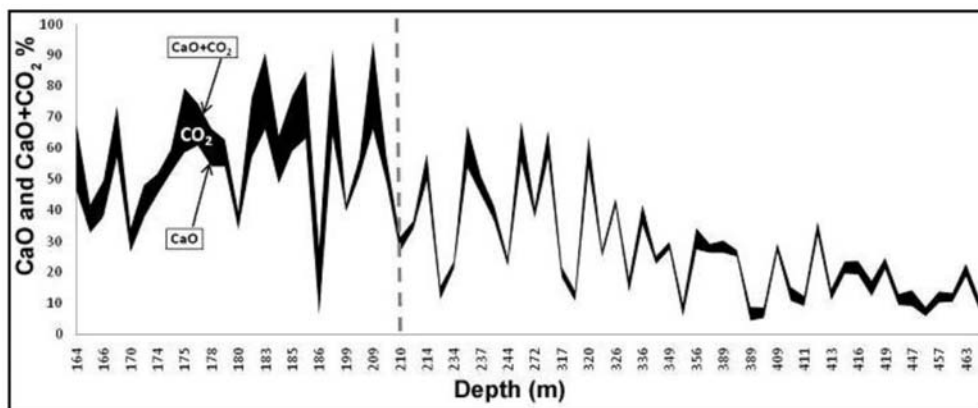


Fig. 6: Correlation between CaO, CaO+CO₂ and depth.

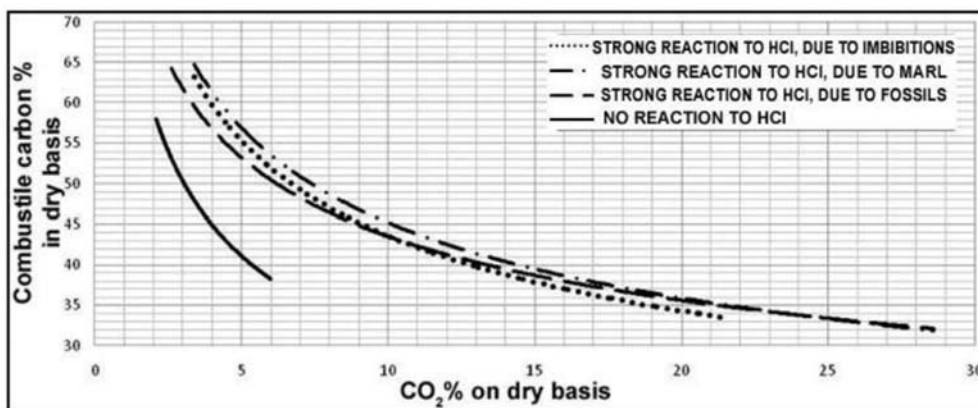


Fig. 7: Correlation between combustible carbon and CO₂ on dry basis.

the O₂ decreases when CO₂ increases with greater decrease in the saturations (Fig. 9).

The above described situation is the same in all Pliocene lignite deposits of Ptolemais Basin. In the Proastio deposit the average CO₂ value on dry basis of the mineable lignite is 3.8%, while the geological lignite ranges from 1.3 to 14.4%, with an average value 4.5%.

Conversely, the respective CO₂ in the Miocene xylite-rich lignite deposits of Ptolemais and Florina Basins is from 0.8% to 2.2% (Anatoliko-Karyohori).

Based on all the aforementioned, and taking into consideration the fact that lignite constitutes the main resource for electric power generation in Greece, it is obvious that the CO₂ capture and storage (CCS) technology should be applied in the near future.

5. Current Situation of the CCS Technology

The CCS technology began developing in the 1990's, when the first large-scale storage of CO₂ started in the underwater reservoir of Sleipner, Norway (North Sea). Other large-scale (industrial) projects were carried out in Weyburn, Canada, and in Salah, Algeria. In all these cases, either there

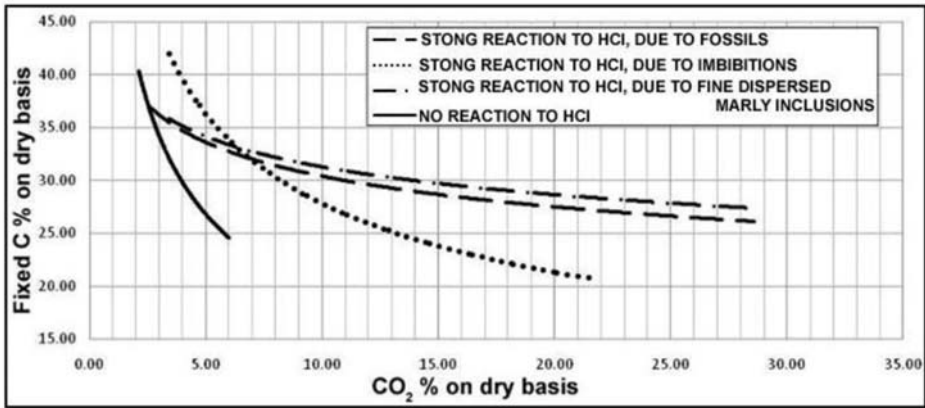


Fig. 8: Correlation between fixed carbon and CO₂ on dry basis.

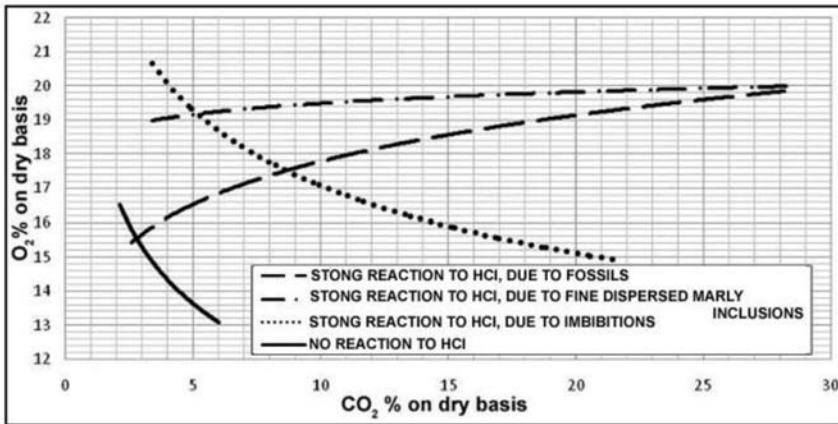


Fig. 9: Correlation between O₂ and CO₂ on dry basis.

is no cost for pure CO₂ from other gases, or there is economic benefit from the improved extraction of hydrocarbons. The Intergovernmental Panel on Climate Change suggested in 2005 that CCS could achieve 55 per cent of the global mitigation effort while reducing costs by 30 per cent or more compared with a non-CCS solution. The European Commission found in 2008 that the costs of meeting its climate change commitments to 2030 will be 40 per cent higher, at €60 billion (\$95 billion), if CCS is not included. The Pew Center on Climate Change, concluded in 2007 that building 30 CCS demonstration projects for \$30 billion would save the US \$80 to \$100 billion in subsequent mitigation costs. This tranche of CCS demonstration projects will be expensive, but in the medium term they will bring considerable savings to society (Aarnes et al., 2008).

The CCS technology in electric power stations or other industries, which require the capture of CO₂, is currently at the stage of pilot applications, such as in the Schwarze Pumpe (Berlin) and Ketzin, Germany, where capture and storage technologies are tested in units of 30 MWe with lignite fuel. In the Schwarze Pumpe the capture of CO₂ takes place before combustion using the Oxyfuel technology. According to the officers of VATTENFALL, which is responsible for the unit, the technology for “clean lignite stations” with capture and storage of CO₂ will be rentable in a decade at a cost

equivalent of the CO₂ emissions rights market.

Interdisciplinary research groups examine the role of coal in a world where constraints on carbon dioxide emissions are adopted to mitigate global climate change. The future of coal in a carbon-constrained world, will evaluate the technologies and costs associated with the generation of electricity from coal along with those associated with the capture and sequestration of the carbon dioxide produced coal-based power generation. Growing electricity demand in Greece and in the world will require increases in all generation options (renewable, coal, and nuclear) in addition to increased efficiency and conservation in its use. Coal will continue to play a significant role in power generation and as such carbon dioxide management from it will become increasingly important. A study, which examines all interrelated technical, economic, environmental and political challenges, must be undertaken the soonest possible. The final report, addressed to the Hellenic Government, but also to the industry and the academic leaders, will help to meet this urgent scientific challenge. Additionally, an aggressive R&D effort in the relatively near term will yield significant dividends down the road, and should be undertaken immediately. A significant charge on carbon emissions is needed to increase the economic attractiveness of new technologies that avoid carbon emissions and specifically to lead to large-scale CCS in the coming decades. A large-scale demonstration project of the technical, economic and environmental performance of an integrated CCS system is needed in Greece over the next decade with government support. This is important for establishing public confidence for a large-scale sequestration program anticipated in the future.

Cost constitutes the great problem in the implementation of the CCS, followed by the monitoring and authorization. CCS technology should reduce costs by 2 to 4 times (30-15 €/t CO₂) to be economically viable. Improving and standardizing the relevant technology can address this challenge. Something similar was also observed in the case of the flue-gas desulphurization plants of the thermal power stations, in which the cut down of cost was remarkable.

6. Conclusions

The CO₂ emissions from lignite combustion to generate electric energy contribute 38% to the greenhouse effect since for each MW/h 1.2-1.3 t of CO₂ is emitted.

The CO₂ lignite content varies and depends on the age, the deposition environment and the lignite type in general.

The Pliocene lignite deposits display higher CO₂ contents compared to the Miocene ones.

The CO₂ content in the Upper Pliocene lignite in Ptolemais Basin, for example in the Proastio deposit, is mainly due to the great amount of fossils and the CaCO₃ saturation.

The Proastio lignite deposit is noteworthy and can feed two units of 600MW for 43 years.

It was observed that with increasing CO₂ the fuel elements of lignite are reduced such as the permanent and combustible coal, the O₂ etc.

The amounts of CO₂ emissions during lignite combustion must be determined.

Re-evaluation of the lignite deposits assessed before 1980 is necessitated since CO₂ contents were not taken into account. As it was proven, several lignite beds with TEX ≤ 35% were considered exploitable, while adding CO₂ they became non-exploitable given that ash exceeded 50% and thus the estimated deposit was reduced to 1/3 causing problems in the exploitation planning, transportation, combustion, production.

CCS is the critical enabling technology because it allows significant reduction in CO₂ emissions while allowing lignite to meet future energy needs. Taking into consideration that lignite will be for the next few decades the main resource for electric power generation in Greece, it is clear that the CCS technology should be applied, which to be economically viable has to reduce the cost of capture 2 to 4 times (30-15 €/t of CO₂).

7. References

- Aarnes, J., et al. 2008. Guidelines for geological storage of CO₂: selection and qualification of sites and projects. 9th International Conference on Greenhouse Gas Control Technologies, Washington DC, USA.
- Kolovos, N., Georgakopoulos, A., Filippidis, A., Kavouridis, C. 2002. Environmental Effects of Lignite and Intermediate Steriles Coexcavation in the Southern Lignite Field Mine of Ptolemais, Northern Greece. *Energy Sources*, 24(6): 561-573.
- Kolovos, N., Georgakopoulos, A., Filippidis, A., Kavouridis, C. 2002. The Effects on the Mined Lignite Quality Characteristics by the Intercalated Thin Layers of Carbonates in Ptolemais Mines, Northern Greece. *Energy Sources*, 24(8): 761-772.
- Kolovos, N., Georgakopoulos, A., Filippidis, A., Kavouridis, C. 2002. Utilization of lignite reserves and simultaneous improvement of dust emissions and operation efficiency of a Power Plant by controlling the calcium (total and free) content of the fed lignite. Application on the Agios Dimitrios Power Plant, Ptolemais, Greece. *Energy & Fuels*, American Chemical Society, 16: 1516-1522.
- Kolovos, N., Sotiropoulos, D., Georgakopoulos, A. 2003. Lignite Recovery in Multi-Seam Open-pit Mining Operations in Northern Greece. In: Proceedings IIIrd International Scientific Conference on Modern Management of Mine Producing, Geology and Environmental Protection “Surveying Geology-Ecology-Management” SGEM 2003, Section II: Technology and Technical Equipment for the Open-pit Mining of Mineral Resources. June 2003, Varna city, Bulgaria, p. 59-65.
- Kotis, Th., Ploumidis, M. and Dimitriou, D., 2001. Geological and Mineral Deposit Research of Lignite in the area of Proastion Ptolemais Basin. I.G.M.E. p. 1-68, Athens (in Greek).
- Metaxas, A., Kotis, Th., G. Varvarousis, Ploumidis, M., Karageorgiou, D. E., Papanikolaou, G. 2007. Geological Evolution – Stratigraphy of Florina, Ptolemais, Kozani and Saradaporo Graben. 11th I.C.G.S.G. Vol.XXXX/1 pp. 161-172 Athens.
- Sotiropoulos, D., Georgakopoulos, A., Kolovos, N. 2005. Impact of free-calcium oxide content of the fly ash on dust and sulfur oxide emissions in a lignite-fired Power Plant. *Journal of the Air and Waste Management Association*, 55: 1042-1049.

FTIR STUDY OF TWO DIFFERENT LIGNITE LITHOTYPES FROM NEOCENE ACHLADA LIGNITE DEPOSITS IN NW GREECE

Oikonomopoulos I.¹, Perraki Th.¹, and Tougiannidis N.²

¹ National Technical University of Athens, School of Mining & Metallurgical Engineering, Division of Geosciences, 9 Heroon Politechniou St., GR-15773 Zografou, Greece. giannis@metal.ntua.gr, peraki@metal.ntua.gr

² Institute of Geology and Mineralogy, University of Cologne. GeoNikolas@gmx.de

Abstract

The FTIR spectra for both Neogene xylite and matrix lignite samples from Achlada NW Greece show significant differences, which are mainly evident in aliphatic stretching region (3000-2800 cm⁻¹) where the intensities of the vibrations are reduced in matrix lignite lithotype compared to xylite one. The intense bands in the region 3402-3416 cm⁻¹ are attributed to -OH stretching of H₂O and phenol groups. The bands at ~3697 cm⁻¹ and ~3623 cm⁻¹ as well as at ~538 cm⁻¹ and 470 cm⁻¹, which are more evident in the FTIR spectra of matrix lignite, are attributed to higher content of clay minerals in the samples of this lithotype. The stretching vibration appears at ~1032 cm⁻¹ is intense in all matrix lignite samples and it is broadening in the xylite ones. The FTIR spectra of all samples confirm the progressive elimination of aliphatic vibrations from xylite lithotype to matrix lignite one and the appearance of clay minerals in the latter. As a whole the FTIR spectra of both xylite and matrix lignite confirm the significant differences between these two lignite lithotypes.

Key words: FTIR, Neocene, lignite, xylite, Achlada, Greece.

1. Introduction

At the end of diagenesis the polycondensed organic residue, called lignite in coal swamps, also contains varying amounts of largely unaltered refractory organic material (Killops and Killops, 1993). Therefore, the organic structure of coal can be regarded as consisting of heterogeneous aromatic structures, with aromaticity increasing from low rank (lignite, brown coal) to high rank coals (semi-anthracite, anthracite). The term lignite refers to the maturity stage of coals, while the terms xylite and matrix refer to lignite lithotype. Fourier Transform Infra Red (FT-IR) method is a widely used analytical technique for determining the different functional groups of coal structures. Infrared (IR) spectroscopy has been extensively employed in the characterization of the mineral and organic matter of coals (Guiliano et al., 1990; Cloke et al., 1997; D' Alessio et al., 2000; Georgakopoulos et al., 2003; Kalaitzidis, 2007; e.t.c).

In Greek lignites a limited number of studies have been published up to now, using FTIR method for coal characterization. Georgakopoulos et al. (2003) resulted in the presence of phenolic and alcoholic C-O bonds as well as C-O-C bonds with aliphatic carbons (strong peak at 1032 cm⁻¹) concerning the initial xylite sample BEX from Vevi region. In the same study the FT-IR spectra of lignite and humic clay samples, from Apofysis-Amynteo lignite deposits NW Greece, revealed the great

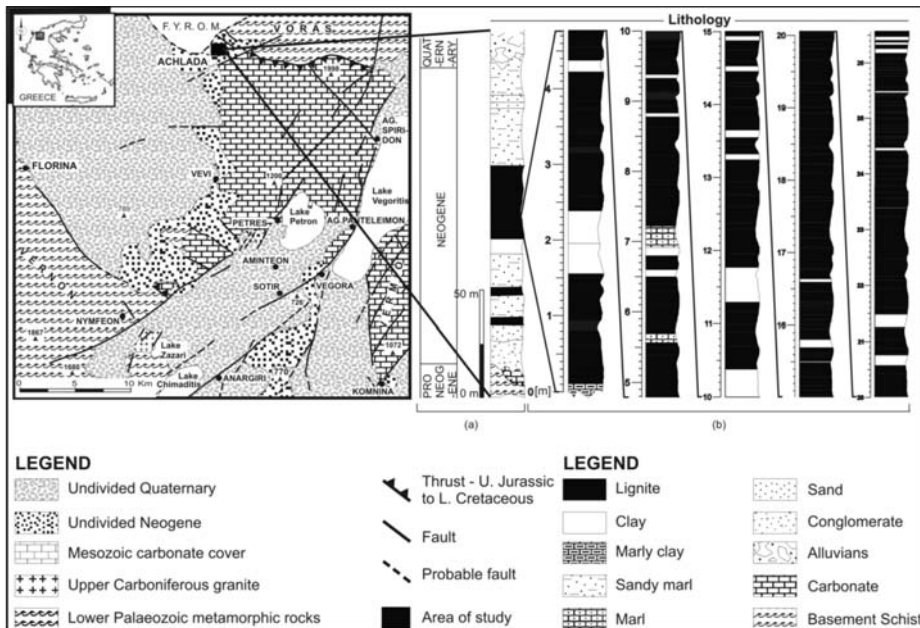


Fig. 1: Geological map of the Florina Basin with the location and generalized lithological column (a) of the studied area (after Pavlides & Mountrakis 1987) and (b) of Achlada lignite deposits, NW Greece.

abundance of C=O and C-O-R structures ($1800-1000\text{ cm}^{-1}$ region) as well as clay and silicate minerals in the $3600-3800\text{ cm}^{-1}$ and $400-600\text{ cm}^{-1}$ region, respectively.

No study has been published concerning the investigation by FTIR method of the organic beds of Achlada lignite deposits, Florina sub-basin, NW Greece.

The present study is part of a research of both xylite and matrix lignite aimed at their structural characterization by Fourier transform infrared spectroscopy (FTIR) and focuses on their significant differences. X-ray diffraction (XRD), thermo-gravimetric (TG/DTG) and differential thermal analysis (DTA) were also employed for this purpose.

2. Geological setting

The studied samples obtained from the lignite-bearing sequence of Neocene Achlada lignite deposits, which are located at the east margins of Florina sub-basin, NW Greece.

The Neocene-Quaternary sediments that fill the basin, overlay unconformably both Palaeozoic metamorphic rocks and Mesozoic crystalline limestones and consist of conglomerates, sands, marls, sandy marls, clays, lignite beds, lateral fans and alluvial deposits (Pavlides and Mountrakis, 1987).

3. Methods

Lithological features of each of the studied samples were macroscopically described and the lignite lithotype determined according to guidelines established by the International Committee for Coal and Organic Petrology (I.C.C.P., 1993), as well as by Taylor et al. (1998). Samples with less than 10% by volume woody tissues were logged as matrix lignite, whereas those of immiscibly woody tissues were classed as xylite.

Several xylite and matrix lignite samples were examined using the FTIR method of analysis. The IR measurements were carried out using a Fourier Transform Infra Red (FT-IR) spectrophotometer (Perkin Elmer GX-1). The FT-IR spectra, in the wavenumber range from 4000 cm^{-1} to 400 cm^{-1} , were obtained using the KBr pellet technique. The pellets were prepared by pressing a mixture of the sample and of dried KBr (sample:KBr, approximately 1:200), at 8 tons/ cm^2 . Bands were identified by comparison to published studies (Wang and Griffith, 1985; Lide, 1991; Sobkowiak and Painter, 1992; Van Krevelen, 1993; Mastalerz and Bustin, 1995, 1996; Ibarra et al., 1996; Cloke et al., 1997; Koch et al., 1998; Das, 2001; e.c.t). Bands assignments used in this paper are listed in table 1.

Peak areas representing the hydroxyl group region (3100-3700 cm^{-1}), aliphatic stretching region (2931-2855 cm^{-1}), aromatic carbon (peaks at 1618 and 1606 cm^{-1}), aliphatic bending region (1509-1371 cm^{-1}), cellulose and lignin region (1300-1000 cm^{-1}) and the aromatic out-of-plane region (900-700 cm^{-1}) were measured. Additionally, intense vibrations at 3698 cm^{-1} , 3620 cm^{-1} , 531 cm^{-1} and 469 cm^{-1} are attributed to clay and silicate minerals.

The same xylite and matrix lignite samples were also examined by means of X-ray diffraction (XRD) analysis, as well as thermo-gravimetric (TG/DTG) and differential thermal (DTA) analysis. X-ray power diffraction patterns were obtained using a Bruker D-8 Focus diffractometer, with Ni-filtered $\text{CuK}\alpha_1$ radiation ($\lambda=1.5405 \text{ \AA}$), operating at 40 kV, 30mA, while TG/DTG/DTA were obtained simultaneously using a thermal analyzer (Mettler, Toledo 851) at a heating rate of 10°C/min, at air atmosphere and temperature range 25°C-1200°C.

4. Results and Discussion

4.1 FTIR study of xylite and matrix lignite samples

Representative FT-IR spectra of xylite and matrix lignite samples are shown in figure 2. The spectra differ significantly in the peaks due to mineral matter, as well as to phenolic (C-O) and aliphatic carbon (C-H) groups.

Both representative spectra show typical infrared characteristics of the organic matter of low-rank coals, including aliphatic C-H stretching bands at 2924 cm^{-1} and 2856 cm^{-1} , C=C or C=O aromatic ring stretching vibrations at ~1610 cm^{-1} and at ~1506 cm^{-1} , as well as aliphatic C-H stretching bands, at 1455 cm^{-1} , 1370 cm^{-1} and 822 cm^{-1} .

Due to the fact that the present functional groups are different for xylite and matrix lignite samples it is more convenient to describe them separately.

Studying the FTIR spectra of the representative xylite sample (Fig. 2a), from the Achlada lignite deposits in NW Greece, the following conclusions resulted:

- The broad band at 3392 cm^{-1} is attributed to -OH stretching vibrations of hydrogen-bonded hydroxyl groups of absorbed water of clay minerals as well as to -OH of phenol groups.
- The strong peak at ~2931 cm^{-1} is due to asymmetric aliphatic C-H stretching vibrations of methylene (-CH₂).
- The band at ~1606 cm^{-1} is attributed either to C=O or C=C aromatic ring stretching vibrations.
- The band at ~1505 cm^{-1} is due to C=O stretching vibrations.
- The band at ~1454 cm^{-1} is attributed to symmetric aliphatic C-H vibration of methylene (CH₂) and methoxyl (OCH₃).
- The peak at ~1370 cm^{-1} is due to symmetric aliphatic C-H bending vibration of methyl groups (OCH₃).
- The band at ~1265 cm^{-1} are attributed to C-O stretching vibrations.

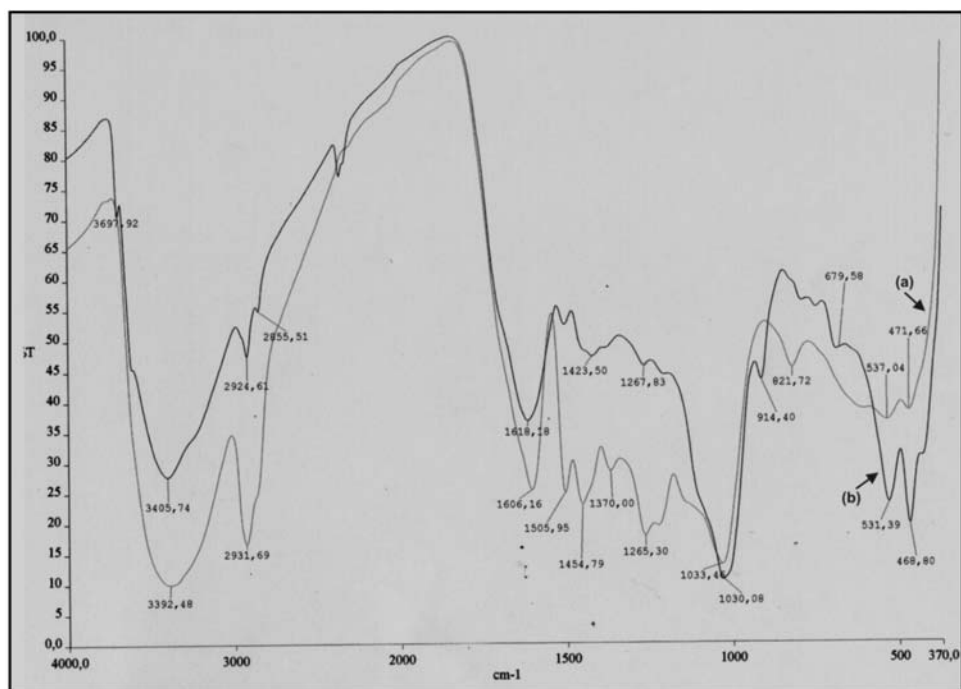


Fig. 2: FTIR spectra of representative xylite (a) and matrix lignite (b) samples.

- The peak at $\sim 1033\text{ cm}^{-1}$ is due to C-O-H bonds in cellulose as well as to C-O stretching vibrations of aliphatic ethers (R-O-R') and alcohols (R-OH).
- The band at $\sim 821\text{ cm}^{-1}$ is due to out-of-plane-aryl ring with isolated C-H groups.

In the FT-IR spectra of the matrix lignite samples bands corresponding to the most abundant minerals were detected confirming the occurrence of clay minerals (e.g. kaolinite bands at $\sim 3698\text{ cm}^{-1}$, 3620 cm^{-1} , 1030 cm^{-1} , 915 cm^{-1} , 531 cm^{-1} , and 469 cm^{-1}). The small peaks at $\sim 3698\text{ cm}^{-1}$ and 3620 cm^{-1} can be assigned to the crystal water which exists in clay minerals of the matrix lignite samples (Geng et al., 2009).

Studying the FTIR spectra of the representative matrix lignite sample (Fig. 2b), from the Achlada lignite deposits in NW Greece, the following conclusions resulted:

- The small peak at $\sim 3698\text{ cm}^{-1}$ arises from the in-phase symmetric stretching vibration of the OH groups, either "outer" or "inner" surface OH of the octahedral sheets, which form weak hydrogen bonds with the oxygen of the next tetrahedral layer (Balan et al., 2001). The peak at $\sim 3620\text{ cm}^{-1}$ is due to the stretching vibrations of the "inner OH groups" lying between the tetrahedral and octahedral sheets (Madejova, 2002; Geng et al., 2009).
- The broad band at $\sim 3406\text{ cm}^{-1}$ is attributed to -OH stretching vibration of absorbed water either of clay minerals or of the organic matter of the matrix lignite sample.
- The bands at $\sim 2925\text{ cm}^{-1}$ and $\sim 2855\text{ cm}^{-1}$ are attributed to asymmetric and symmetric aliphatic $-\text{CH}_2$ stretching vibrations respectively.
- The strong band at $\sim 1618\text{ cm}^{-1}$ is attributed either to C=O or C=C aromatic ring stretching vibrations, as well as to OH bending vibrations of adsorbed water.

Table 1. Characteristic FTIR bands of functional groups of low rank coals.

<i>Wavenumber (cm⁻¹)</i>	<i>Assignment</i>
3400	O-H stretching vibrations of hydrogen-bonded hydroxyl groups in polymeric association
2930	Asymmetric aliphatic C-H stretch vibrations–methylene (CH ₂)
2850	Symmetric aliphatic C-H stretch vibrations–methylene (CH ₂)
1610	Aromatic ring (C=C in plane) stretching symmetric
1510	C=O stretching vibrations
1458	Asymmetric aliphatic C-H deformation of methylene and methoxyl
1430-1420	aromatic C=C stretching vibrations
1370	Symmetric aliphatic C-H bending of methyl groups CH ₃
1266	C-O stretch vibration (in lignin-gualacyl ring with C-O stretch)
1224	C-O stretch vibration (in lignin-gualacyl ring and C-O stretch)
1031	C-O-H deformation in cellulose
822	Aromatic out-of-plane-rings with 2 neighboring C-H groups
~534	Si-O-Al ^{VI} vibrations (Al in octahedral co-ordination) of clay minerals
~468	Si-O-Si bending vibrations of clay minerals

- The ~1030 cm⁻¹ and 1013 cm⁻¹ bands arise from the Si-O-Si and Si-O-Al^{VI} vibrations, respectively.
- The ~914 cm⁻¹ band arises from the bending vibrations of “inner” OH groups of Al-OH-Al of kaolinite structure.
- The band at ~680 cm⁻¹ could be related to aromatic out-of-plane C-H vibrations, rather than to mineral matter (Georgakopoulos, 2003).
- The band at ~531 cm⁻¹ originates from Si-O-Al^{VI} vibrations (Al in octahedral co-ordination), while the band at ~469 cm⁻¹ is attributed to the Si-O-Si bending vibrations (Van Jaarsveld et al., 2002; Madejova, 2003).

The main FTIR absorption bands of both xylite and matrix lignite samples are summarized in table 1.

The comparative FT-IR spectroscopy of xylite and matrix lignite lithotypes showed that:

- An intense and broad hydroxyl band of the xylite sample with a maximum at ~3392 cm⁻¹, was displaced relatively to the matrix lignite band which appears at ~3406 cm⁻¹. The latter peak is accompanied by two other small peaks around 3698 cm⁻¹ and 3620 cm⁻¹ due to mineral matter, which is more abundant in the matrix lignite.
- The predominant FTIR feature for xylite samples (Fig. 2b), in contrast to matrix lignite ones, is the high intensity of aliphatic C-H stretching vibration at ~2931 cm⁻¹, which appears at slightly lower wavenumbers (2925 and 2856 cm⁻¹), in matrix lignite samples.

Significant differences of the containing functional groups are also present in the 1700-1100 cm⁻¹ region. More specifically:

- The stretching vibrations at ~1506 cm⁻¹ due to C=O structures tend to decrease in matrix lignite. As far as, the bands at this region (~1506 cm⁻¹) practically disappear at the stage of bi-

kaolinite and gypsum (Fig. 3aA), while anhydrite is present in both heated samples (Fig. 3bA,B). Illite (+muscovite) is identified by the sharp diffraction peaks at $d_{001} \approx 10 \text{ \AA}$ and $d_{003} \approx 3.34 \text{ \AA}$, while kaolinite by its typical peaks at $d_{001} \approx 7.1 \text{ \AA}$ and $d_{002} \approx 3.5 \text{ \AA}$. In the same figure gypsum is identified by its characteristic peak at $d_{020} \approx 7.56 \text{ \AA}$. Minerals in minor contribution such as quartz at $d_{101} = 3.34 \text{ \AA}$ and $d_{100} = 4.26 \text{ \AA}$ and calcite at $d_{104} \approx 3.03 \text{ \AA}$ have been detected, too. It is important to be mentioned that the formation of anhydrite, in the heated samples at $d_{020} \approx 3.49 \text{ \AA}$ and $d_{210} \approx 2.85 \text{ \AA}$ indicates the presence of gypsum in raw materials.

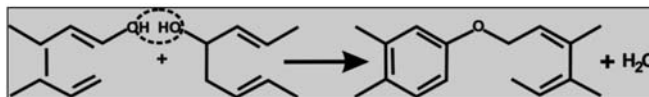
From the X-ray diagrams (Fig. 3a) it becomes clear that clay minerals are present in the matrix lithotype, while in the xylite one these are absent. This observation confirms the FTIR results, in which the typical bands of clay minerals are absent from xylite spectrum. This may be attributed to the nature of xylite samples that prevent the water movement through the xylite mass.

In addition, the samples were heated up to 550°C for 2 hours, in a static oven (Fig. 3b). Samples were then cooled at room temperature and examined by X-ray power diffraction (XRD). A decrease in the intensity of the characteristic diffraction pattern at $d \approx 7.57 \text{ \AA}$, due to the collapse of gypsum, as well as the presence of typical peaks at $d \approx 3.50 \text{ \AA}$ and $d \approx 2.85 \text{ \AA}$ (Fig. 3b), indicates clearly the presence of anhydrite for both xylite and matrix lignite lithotypes.

4.3 TG/DTG and DTA study of xylite and matrix lignite samples

The thermal study results of the Achlada low rank coal samples examined after heating up to 1200°C , at a rate of $10^\circ\text{C}/\text{min}$, are shown in Fig. 4a,b. The TG curves of the examined samples showed a continuous weight loss during heating up to $\sim 650^\circ\text{C}$ and 900°C , for xylite and matrix lignite samples, respectively. More specifically:

- The steep slope of the xylite TG curve, in the temperature range from 200°C to 500°C , due to the rapid weight loss is attributed to the high devolatilization rate of organic matter.
- In the same temperature range, a big and sharp devolatilization peak observed at the DTG curve indicates the high devolatilization rate of xylite lithotype comparing to matrix one. This sharp peak at $\sim 380^\circ\text{C}$ (Fig. 4a) can be attributed to cellulose content of xylite sample (Charland et al., 2003). Taking into consideration that this peak height can provide a relative measure of the reactivity, the xylite seemed to be more reactive, as far as its decomposition rates were higher than those corresponding to the matrix lignite (Vamvuka et al., 2004). On the other hand, the bulk of the burning process for matrix lignite occurred mainly between 450°C and 600°C .
- An endothermic peak at $\sim 380^\circ\text{C}$ (DTA curve) is associated with the decomposition of cellulose, while the decomposition of lignin is characterized by an exothermic one, in the temperature range from 200°C to 400°C (Fig. 4a).
- Xylite samples present higher weight loss up to 1000°C (67.35% wt), comparing to matrix lignite ones (37.66% wt). The water that is evolved during pyrolysis arises from OH of constituent water as well as from the condensation of phenols (MacPhee et al., 2004), as it is shown in the following equation:



The thermogravimetric curves of the Achlada low rank coal samples examined show that:

- The first peak of DTG curve at 100°C , which is associated with sample drying phase (Fig. 4b).

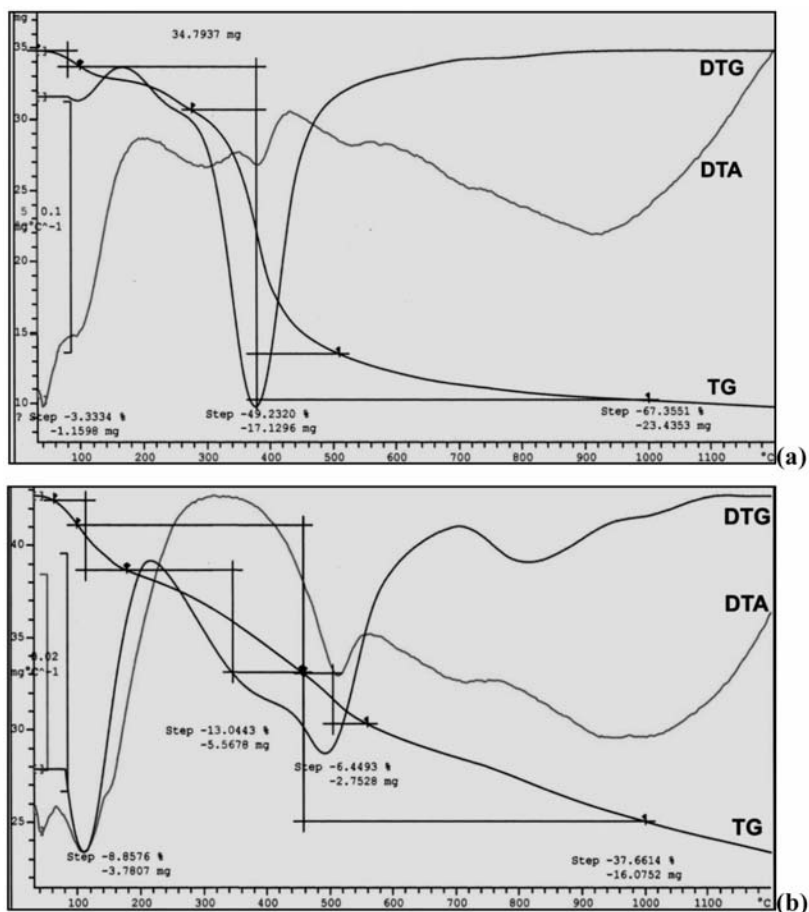


Fig. 4: TG/DTG/DTA diagrams of representative xylite (a) and matrix lignite (b) samples.

- In the temperature range from 200°C to 560°C, the weight loss is less than in xylite sample and this is indicated by the slight slope of the TG curve.
- The TG curve of the matrix lignite samples showed a continuous weight loss during heating up to ~900°C, originated from the lignin content, that is quite difficult to decompose, as well as from the presence of inorganic material.
- The exothermic peak in the temperature range from 200°C to 400°C of DTA curve is characteristic of lignin and can be attributed to the destruction of aliphatic grouping, CH groups, carbohydrate components and to some extent of oxygeneous (alcoholic, phenolic) and amino groups (Kucerik et al., 2004).
- The endothermic peak at ~500°C is attributed to the dehydroxylation of the kaolinite, (due to the loss of OH groups, surrounding the Al^{VI} atoms) and the progressive transformation from the octahedral co-ordinated Al, in kaolinite, to a tetrahedral co-ordinated form, in metakaolinite, through the breaking of OH bonds (Van Jaarsveld et al., 2002). A part of the weight loss in this temperature range comes from the decomposition of siderite according to the reaction

$\text{FeCO}_3 \rightarrow \text{FeO} + \text{CO}_2$. Chlorite and illite (+muscovite) give endothermic peaks at higher temperatures.

5. Conclusions

Studying the xylite and matrix lignite lithotypes from the organic beds of Achlada lignite deposits, Florina sub-basin, NW Greece, by FT-IR spectroscopy, in combination with X-ray diffraction and thermoanalytical methods (TG/DTG and DTA), the following conclusions were taken:

- The FTIR spectra of all samples confirm the progressive elimination of aliphatic vibrations from xylite lithotype to matrix lignite one and the appearance of clay minerals in the latter.
- The aliphatic stretching regions at $3000\text{-}2800\text{ cm}^{-1}$ and $1700\text{-}1100\text{ cm}^{-1}$, where the vibrations of C-H and C-O groups at $\sim 1458\text{ cm}^{-1}$, 1370 cm^{-1} , 1267 cm^{-1} and 1224 cm^{-1} are present, reduced in matrix lignite.
- The vibrations corresponding to the occurrence of clay minerals ($\sim 3697\text{ cm}^{-1}$, 3620 cm^{-1} , 1034 cm^{-1} , 915 cm^{-1} , 531 cm^{-1} , 469 cm^{-1} and 435 cm^{-1}), are more evident in matrix lignite samples and very weak in xylite ones.
- According to X-ray analysis the minerals present in the matrix lignite are mainly illite (+muscovite), kaolinite, and gypsum, while in the xylite samples these minerals are absent. The formation of anhydrite in the heated samples indicates the presence of gypsum in both raw materials.
- The TG/DTG/DTA curves of xylite lithotype present higher weight loss comparing to matrix lignite lithotype, as well as a sharp DTG peak at $\sim 380\text{ }^\circ\text{C}$, accompanied with an endothermic peak of DTA curve, that is characteristic of cellulose decomposition. In contrast, the lignin decomposition is characterized by an exothermic peak in the temperature range from $200\text{ }^\circ\text{C}$ to $400\text{ }^\circ\text{C}$.

6. Acknowledgments

The authors would like to thank D. Tsiakalos and S. Papadakis for their staunch support during the laboratory work, as well as both the mining engineers Th. Balis and O. Grammenopoulos of the Achlada lignite mine for their support during the sampling.

7. References

- Balan, E., Marco Saita, A., Mauri, F., and Calas, G., 2001. First-principles modeling of the infrared spectrum of kaolinite. *American Mineralogist*, 86, 1321-1330.
- Charland, J.-P., MacPhee, J.A., Girou, L., Price, J.T., Khan, M.A., 2003. Application of TG-FTIR to the determination of oxygen content of coals. *Fuel Processing Technology*, 81, 211-221.
- Cloke, M., Gilfillan, A., and Lester, E., 1997. The characterization of coals and density separated coal fractions using FTIR and manual and automated petrographic analysis. *Fuel*, 76(13), 1289-1296.
- D'Alessio, A., Vergamini, P., Benedetti, E., 2000. FT-IR investigation of the structural changes of Sulcis and South Africa coals under progressive heating in vacuum. *Fuel*, 79, 1215-1220.
- Das, T.K., 2001. Thermogravimetric characterization of maceral concentrates of Russian coking coals. *Fuel*, 80, 97-106.
- Geng, W., Nakajima, T., Takanashi, H., Ohki, A., 2009. Analysis of carboxyl group in coal and coal aromaticity by Fourier transform infrared (FT-IR) spectrometry. *Fuel*, 88, 139-144.

- Georgakopoulos, A., Iordanidis, A., and Karma, V., 2003. Study of Low Rank Coals Using FTIR Spectroscopy. *Energy Sources*, 25, 995-1005.
- Guiliano, M., G. Mille, P. Doumenq, Kister, J., and Muller, J.F., 1990. Study of various rank demineralised coals and maceral concentrates: Band assignment of FTIR spectra after resolution enhancement using Fourier deconvolutions. In H. Charcosset (eds), *Advanced Methodologies in Coal Characterization, Coal Science and Technology*, 15, pp. 399-417, Amsterdam, Elsevier.
- Ibarra, J.V., Munoz, E., and Moliner, R., 1996. FTIR study of the evolution of coal structure during the coalification process. *Org. Geochem*, 24, 725-735.
- International Committee for Coal and Organic Petrology (ICCP), 1993. International Handbook of Coal Petrography. Supplement, Commission 1, 19 pp.
- Kalaitzidis, S., 2007. Peat-forming and evolution of peatlands in Greece. Phd Thesis, University of Patras, 350 p.
- Killops, S.D. and Killops, V.J., 1993. An introduction to organic geochemistry. New York, Longman, 265 p.
- Koch, A., Krzton, A., Finqueneisel, G., Heintz, O., Weber, J., and Zimny, T., 1998. A study of carbonaceous char oxidation in air by semi-quantitative FTIR spectroscopy. *Fuel*, 77(6), 563-569.
- Kucerík, J., Kovár, J., Pekar, M., 2004. Thermoanalytical investigation of lignite humic acids fractions. *J. Thermal Analysis Calorimetry*, 76(1), 55-65.
- Lide, D.R., 1991. CRC Handbook of Chemistry and Physics. Boston: CRC Press.
- MacPhee, J.A., Giroux, L., Charland, J.-P., Gransden, J.F., Price, J.T., 2004. Detection of natural oxidation of coking coal by TG-FTIR-mechanistic implications. *Fuel*, 83, 1855-1860.
- Madejova, J., 2002. FTIR techniques in clay mineral studies. *Vibrational Spectroscopy*, 944, 1-10.
- Madejová, J., 2003. FTIR techniques in clay mineral studies. *Vibrational Spectroscopy*, 31(1), 1-10.
- Mastalerz, M. and Bustin, R.M., 1995. Application of reflectance micro-Fourier transform infrared spectrometry in studying coal macerals: comparison with other Fourier transform infrared techniques. *Fuel*, 74(4), 536-542.
- Mastalerz, M. and Bustin, R.M., 1996. Application of reflectance micro-Fourier Transform infrared analysis to the study of coal macerals: an example from the Late Jurassic to Early Cretaceous coals of the Mist Mountain Formation, British Columbia, Canada. *Int. J. Coal Geol.*, 32, 55-67.
- Pavlidis, S. and Mountrakis, D., 1987. Extensional tectonics of northwestern Macedonia, Greece, since the late Miocene. *J. Struct. Geol.*, 9/4, 385-395.
- Sobkowiak, M. and Painter, P., 1992. Determination of the aliphatic and aromatic CH contents of coals by FT-IR: studies of coal extracts. *Fuel*, 71(10), 1105-1125.
- Taylor, G.H., Teichmuller, M., Davis, A., Diessel, C.F.K., Littke, R., and Robert, P., 1998. Organic Petrology. Gebruder Borntraeger, Berlin and Stuttgart, 704 p.
- Vamvuka, D., Kastanaki, E., Lasithiotakis, M., Papanicolaou C., 2004. Combustion behavior of xylite/lignite mixtures. *Carbon*, 42, 351-359.
- Van Jaarsveld, J., Van Deventer, J., Lukey, G., 2002. The effect of composition and temperature on the properties of fly ash and kaolinite-based geopolymers. *Chemical Engineering J.*, 89, 63-73.
- Van Krevelen, D.W., 1993. Coal. Typology - Physics - Chemistry - Constitution, (3rd ed.). Amsterdam, Elsevier, 979 p.
- Wang, S.H. and Griffiths, P.R. 1985. Resolution enhancement of diffuse reflectance IR spectra of coals by Fourier self-deconvolution 1. C-H stretching and bending modes. *Fuel*, 64, 229-236.

ADSORPTION OF PHENOLS FROM OLIVE OIL MILL WASTEWATER AS WELL AS N AND P FROM A SIMULATED CITY WASTEWATER LIQUID ON ACTIVATED GREEK LIGNITES

Papanicolaou, C.¹, Triantafyllou, G.², Pasadakis, N.², Foscolos, A, E.²

¹ Institute of Geology and Mineral Exploration, 3rd Entrance Olympic Village, Acharnai, 13677 Greece

² Department of Mineral Resources Engineering, Technical Univ. of Crete, Akrotiri, Chania73100

Abstract

Organic petrology and detailed physicochemical properties has been undertaken on twenty six Greek low rank coals (peat, peaty lignites, lignites of both matrix and xylite-rich lithotypes, and sub-bituminous coals in order to evaluate the increase of their adsorptive surface area by pyrolysis.

The results show that surface area of activated coal samples increased substantially and in some more than the commercial one. The increase in surface area was higher the higher the carbon content and the lower the ash content.

The adsorption capacity of phenols and the decrease of COD (Chemical Oxygen Demand) in olive oil mill wastewater disposals were measured in selected samples as well as the decrease of COD and the adsorption of nitrogen and phosphorus from a solution which simulates city waste disposals were measured in 14 selected Greek lignites and 1 commercially available activated lignite sample (HOK).

The maximum recorded adsorption of phenol was 30.6 mg/g of activated lignite while the commercial one (HOK) adsorbed 16 mg/g of activated lignite. The COD reduction was 1262 mg of COD/g of activated lignite while in the commercial one the reduction was 439 mg of COD/g of activated lignite. The maximum adsorption of N and P from the simulated city waste liquid was 6.41 mg/g of activated lignite and 2.52 mg/g of activated lignite, respectively. while the commercial one (HOK) adsorbed 2.84 mg/g and 2.42 mg/g, respectively. Finally, the COD reduction was 50.28 mg/g of activated lignite and 34.92 mg/g for the commercially one (HOK).

The results show that Greek activated lignites can be used successfully for cleaning industrial and city wastes. These findings open the door for the economic exploitation of small to medium size lignite deposits in Greece, which are widespread in Greece.

Key words: Activated lignite, adsorption, olive oil mill wastes, city waste liquids.

1. Introduction

Research on activated lignite started some thirty five years ago (Fraser, 1972) while its application for environmental purposes started fifteen years later (Klose and Heschel, 1987) and continuous to date (Navarro et al., 2006). Activated lignite is used in the treatment of waste water (Engelhard and Lenz, 1997; Olson and Stepan, 2000; Stepan et al., 2001) and industrial wastes (Khan et al., 1981; Allen et al., 1997; Dabrowski et al., 2005; Galanakis et al., 2006).

Table 1. Estimated OOMW volumes generated from olive oil processing (Niaounakis and Halvadakis, 2006).

<i>Country</i>	<i>OOMW, m³/y</i>	<i>Olive cake, m³/y</i>
Spain	2.8x10 ⁶	1.6x10 ⁶
Italy	2.4x10 ⁶	1.6x10 ⁶
Greece	1.4x10 ⁶	0.8x10 ⁶
Tunisia	0.55x10 ⁶	0.3x10 ⁶

Optimization of manufacturing conditions for the production of activated lignites is discussed by Karacan et al., (2006) while its commercialization for various environmental purposes have been undertaken by a large number of industries.

In the present study an effort was undertaken to clean olive oil mill wastewaters (OOMW), which are slightly acidic and associated with high biochemical oxygen demand (BOD) and chemical oxygen demand (COD). The phytotoxic effect of OOMW is partially attributed to organic fraction (phenolics and related substances) which is present in notable concentrations and inhibits the growth of certain microorganisms (Paredes et.al., 1986). The phenolic content (phenols, flavonoids or polyphenols) along with long chain fatty acids produce methanogenic toxicity and therefore the option of discharging OOMW to land should be carefully considered (Hamdi, 1992; D' Annibale et al., 2004; Mekki et al., 2007) the adsorption of phenols. This problem is very serious in the Mediterranean area which accounts for almost 95% of the world oil production (Al Malah et al., 2000). The estimated OOMW volumes generated from olive oil processing is presented in Table 1.

In the present research work 28 composite lignite samples from 12 coal basins in Greece have been activated in order to measure their surface area. Experiments were conducted on 14 selected raw and activated lignite samples plus one commercially activated lignite sample which was used as a reference point. The aim of the research study was to relate the adsorption of phenols and COD from olive oil mill wastewater, since Greece produces a large amount of OOMW, Table 1, and furthermore to investigate the adsorption of nitrogen and phosphorus from a simulated city waste water by activated Greek lignite samples.

2. Materials and Methods

Twenty-eight composite samples of peat, peaty lignites and lignites, of both matrix and xylite-rich lithotypes according to ICCP (1993, Figure 1 and Table 2), have been analyzed using a wide variety of coal characterization methods.

For proximate, ultimate and calorific values, the samples were ground to <100 mesh (150 μ m) and analyzed following the procedures outlined by ASTM (1978, 1989a, 1989b). Sulphur was determined by LECO apparatus as outlined by Foscolos and Barefoot (1970).

For petrographic composition, the coals were crushed to a maximum particle size of 850 μ m (20 mesh), mounted in epoxy resin and then ground and polished. Maceral analysis based on 500 points was performed using a LEICA DMRX microscope coupled to a Swift automatic point counter attached to a mechanical stage. The terminology and descriptions for macerals used in this paper is that recommended by the International Committee for Coal Petrology (ICCP, 1963; 1971; 1993, 2001; Sýkorova et al., 2004).



Fig. 1: Location of studied samples.

Adsorption studies were carried out on 28 composite samples from various coal basins. All samples were crushed to an appropriate size particle (-2.0,+1.00 mm) and then physically activated by pyrolysis. Subsequently, a given quantity of lignite is dried at 110° C and placed into the reactor under nitrogen flow (150 ml/min) for 30 min, in order to remove the air. Afterwards, the samples were pyrolyzed in two steps at 400°C for 2 hours and 700°C for another 2 hours under N₂ and CO₂ gases respectively, following procedure outlined in Zhang et al. 2005. Surface area measurements of non-activated and activated lignites were calculated using the BET (Brunauer, Emmet and Teller) method with N₂ as absorbent gas and a NOVA (Quantachrome) surface analyzer. All samples were degassed under vacuum for 12 hours at 300°C in order to determine their BET specific surface area (S_{BET}).

For the study of the adsorption of olive mill wastewater 14 raw and activated lignites were used along with commercially activated lignite (AC) in 24h-adsorption experiments to test their sorption capacity. Experiments were performed at room temperature using a model glass fixed column in a continuous recycling operation. Adsorptive materials were washed out with 2L distilled water before the experiment process. Olive oil wastewater was placed into a 10L tank. It was provided at the bottom of the column by a Percom N-M peristaltic pump (fixed at 20 rpm) and recycled into the tank with a flow rate of 0.5 ml/s. For the phenol measurements 15 ml of wastewater samples were taken at 0, 0.5, 1, 2, 4, 8, and 24h intervals, while COD was measured at 0, 4, 12 and 24 h. The sorption capacity (q) was defined as: $q = (C_w^0 - C_w^1) / C_a^0$, whereas C_w⁰, C_w¹ are the concentrations of the ad-

Table 2. Location of samples and lithotypes.

Code Name	Origin	Lithotypes
TH1	Thessaly	Peat with clay particles
TH2	Thessaly	Peat with clay particles
TH3	Thessaly	Matrix brown coal, clay - rich, friable
TH4	Thessaly	Matrix brown coal, with plant remnants
TH5	Thessaly	Matrix brown coal, with plant remnants
TH6	Thessaly	Xylite brown coal
TH7	Thessaly	Xylite brown coal
TH8	Thessaly	Matrix brown coal, xylitic, with plant remains
MT1	Macedonia	Mixed peat, clay - rich, black colour
MT2	Macedonia	Mixed peat, clay - rich, black colour
MT3	Macedonia	Mixed peat, clay - rich, black colour
MT4	Thrace	Matrix brown coal, stratified, clay - rich, friable
MT5	Thrace	Matrix brown coal, stratified, clay - rich, cluster bands containing xylitic fragments
MT6	Thrace	Matrix brown coal, stratified, clay - rich, cluster bands containing xylitic fragments
MT7	Thrace	Matrix brown coal, stratified, clay - rich, cluster bands containing xylitic fragments
MT8	Thrace	Matrix brown coal, stratified, cohesive at places, presence of micas
PP1	Peloponnese	Matrix brown coal, stratified, xylitic at places
PP2	Peloponnese	Matrix brown coal, xylitic
PM1	Peloponnese	Matrix brown coal, stratified, clay-rich
I1	Epirus	Matrix brown coal
I2	Epirus	Matrix brown coal, clay rich
KP1	Crete	Subbituminous, lustreous appearance
KP2	Crete	Subbituminous, mat / lustreous appearance
KP3	Crete	Brown matrix coal, layered at places, mat / glossy
KP4	Crete	Organic matter bearing clay, layered, cohesive in some places
KP5	Crete	Mixture of KP1 and KP2 at a ratio 1:2

sorbate in the wastewater (mg/L) at zero and interval time, while C_a^o , is the mass per volume ratio of adsorbent versus wastewater (g/L). Total phenol content was determined colorimetrically using the Folin-Ciocalteu reagent (Atanassova et al., 2005; Folin and Ciocalteu, 1927).

The adsorption of N and P from a city wastewater disposal was carried out using the following simulated liquid, Aivazidis, 2000. 20g. of peptone along with 20g of sugar, 4.76 ml of glacial acetic acid, 5.62g of KH_2PO_4 and 6.48g of urea $(NH_2)_2CO_3$ were transferred to one liter of distilled water.

30 ml of this solution were transferred to 3 liters of distilled water. This final solution was used for measuring COD decrease as well as N and P adsorption by activated lignite samples. Nitrogen and phosphorus measurements were carried out using a Hanna C214 Multiparameter Bench Photometer for Wastewater Treatment Application along with the special reagents. For the adsorption of N and P measurements were carried out at 0.5, 3, 6 and 12 hours intervals while for COD measurements the intervals were 3, 6, and 12 hours respectively.

3. Results and Discussion

3.1 Proximate and Ultimate Analysis and Calorific Values

Table 3 shows the data obtained from the proximate and ultimate analysis together with the calorific values. Proximate analysis indicates that the samples of peat and peaty lignites: I1 and I2 (Epirus), PM1, PP1 and PP2 (Peloponnesus), TH1, TH2 and TH3 (Thessaly), as well as the samples MT1, MT2 and MT3 (Macedonia, N. Greece) to have high volatile content ranging from 66 to 76.8 %, while its fixed carbon content to vary from 23.2 to 35.6 %. High values are recorded for oxygen and nitrogen, which fluctuate from 25.6 to 34.6 % and from 2.1 to 3.7 %, respectively. These results are indicative of their low maturity. Also the samples I1 and I2 are characterized from their high sulfur content, 6.6 to 6.5 %, which attributed to the presence of pyrite (Papanicolaou, 2001).

For the samples with higher maturity TH4, TH5, TH6, TH7, TH8 (Thessaly), MT4, MT5, MT6, MT7, MT8 (Thrace), as well as for the xylite rich samples AA and BB (Macedonia, N. Greece) their volatile matter content ranges from 49.8 to 61.9 %, while their fixed carbon content fluctuates between 38.1 to 50.2 %. Oxygen content ranges from 23.4 to 30.3 %, while nitrogen concentration varies from 0.5 to 1.7 %, which indicates different maturation. The latter is also ascertained from the higher calorific values (Table 2). Noteworthy is the presence of high sulfur content, 14.9 to 18.8 % on the samples MT4, MT5 and MT6 (Macedonia) and 5.5 and 7.1 % from the samples MT7 and MT8 (Thrace). These values are attributed to the presence of pyrite, which is also indicative of their depositional environment (Papanicolaou, 2001).

Sub-bituminous coals, KP1, KP2, KP3 and KP5 (Crete), are also characterized by their high sulfur values, which range from 6.9 to 19 % due to the presence of pyrite, as well as their high calorific values, up to 26.5 MJ/kg. Sample KP4 is a carbonaceous clay sample intercalating the coal seams.

Finally, the samples PM1, PP1 and PP2 (Peloponnesus), are characterized by high volatile content, >62 %, relatively high sulfur content >5.5 % and relatively low calorific values that range from 20.6 MJ/kg to 20.8 MJ/kg.

3.2 Maceral Composition

Maceral composition of the studied samples is presented in Table 4. In general huminite is the predominant maceral group, whereas liptinite and inertinite occur with very low values. Peat and peaty lignite samples differ in more than one maceral sub-group. Peat from Thessaly (TH1, TH2, TH3), have low concentrations of telohuminitic ranging from 15.3 to 17.6 vol.%, while their detrohuminite fluctuates from 69.2 to 72 vol.% (Fig. 2). Noteworthy is the fact that within the detrohuminitic components the ratio of attrinite to densinite is quite high. On the other hand peat and peaty lignite samples from Macedonia (MT1, MT2, MT3), though they have similar telohuminitic concentrations, as the previously mentioned samples from Thessaly, their ratio of attrinite to densinite is much lower. Peaty lignite samples from Epirus (I1, I2), are characterized by higher telohuminitic content than the peat and peaty lignite samples from Thessaly and Macedonia. Moreover, these samples have less de-

Table 3. Results of proximate and ultimate analysis and calorific values of lignite samples (except ash values are on dry and free ash basis).

Location	Ash	Vol. Mat.	C _{Fixed}	C	H	O	N	S	Cal. Val.
	wt.-%								MJ/kg
Thessaly									
TH-1	47.6	66.0	34.0	55.7	5.6	33.8	2.7	2.2	21.6
TH-2	58.8	66.3	33.7	55.1	5.7	34.6	2.7	1.8	18.82
TH-3	37.4	66.9	33.1	59.7	5.0	30.5	3.1	1.6	22.7
TH-4	24.4	55.4	44.6	65.4	4.7	24.0	1.4	4.5	25.1
TH-5	39.6	61.2	38.8	63.5	5.5	28.0	1.7	1.3	24.5
TH-6	45.4	58.8	41.2	60.8	5.6	30.3	1.5	1.8	23.6
TH-7	17.3	56.9	43.1	65.8	5.0	25.1	1.5	2.6	25.5
TH-8	38.1	57.3	42.7	64.4	5.7	25.0	1.4	3.0	25.4
Greek Macedonia & Thrace									
AA	8.7	59.2	40.9	67.9	5.9	23.4	0.5	2.2	27.6
BB	13.2	57.6	42.4	64.6	4.1	26.2	1.1	3.9	23.6
MT-1	52.5	64.4	35.6	58.3	5.5	29.0	2.1	5.1	21.8
MT-2	41.5	67.9	32.1	61.6	5.4	25.7	2.3	5.1	23.6
MT-3	40.2	67.5	32.5	62.4	4.8	27.6	2.5	3.1	23.2
MT-4	52.8	53.2	46.5	52.6	5.2	26.4	0.9	14.9	20.1
MT-5	43.0	49.8	50.2	51.3	4.8	24.4	0.8	18.8	19.4
MT-6	48.0	52.3	47.7	53.6	5.0	25.6	1.0	14.9	20.3
MT-7	51.0	54.5	45.5	62.0	5.8	25.7	1.1	5.5	24.1
MT-8	64.6	61.9	38.1	56.5	6.4	29.3	0.7	7.1	17.6
Crete									
KP-1	30.2	51.5	48.5	66.6	4.9	20.4	1.0	7.1	26.5
KP-2	52.8	54.2	45.8	60.3	4.8	22.1	0.9	11.9	23.7
KP-3	72.0	61.7	38.3	52.1	4.6	26.3	1.2	15.8	17.5
KP-4	83.2	81.1	18.9	41.6	5.4	32.7	1.2	19.0	11.7
KP-5	30.1	52.3	47.7	66.6	5.0	20.9	0.9	6.9	26.6
Epirus									
I-1	48.5	74.9	25.1	58.5	3.5	29.3	3.5	6.6	19.9
I-2	51.5	76.8	23.2	57.5	3.7	30.1	3.7	6.5	19.7
Peloponnese									
PM-1	39.5	66.4	33.6	58.1	4.0	30.8	1.6	5.6	20.6
PP-1	43.4	64.7	35.3	57.2	4.3	31.0	1.5	6.0	20.8
PP-2	36.1	62.0	38.0	59.6	4.2	28.6	1.5	6.1	20.8

Table 4. Maceral composition of the studied samples (vol.-%, on mineral matter free basis).

Location	Textinite	Ulminite	Telohuminitite	Attrinitite	Densinite	Detrohuminite	Gelohuminite	Huminitite	Liptinitite	Inertinite
Thessaly										
TH-1	2.8	14.8	17.6	66.4	2.8	69.2	4.4	91.2	8.8	-
TH-2	3.6	13.6	17.2	64.1	6.8	70.9	2.4	90.5	9.5	-
TH-3	3.0	12.3	15.3	62.5	9.5	72.0	2.5	89.8	6.2	4.2
TH-4	1.8	25.4	27.2	37.8	22.0	59.8	2.2	89.2	4.8	0.6
TH-5	1.1	29.8	30.8	31.3	26.0	57.3	4.2	92.3	7.1	-
TH-6	0.4	32.2	32.6	34.6	26.0	53.8	4.6	91.0	9.0	-
TH-7	3.2	48.4	51.6	18.6	19.2	40.8	3.4	95.8	4.2	-
TH-8	-	38.6	38.6	30.0	22.2	49.8	4.2	92.8	7.7	-
Greek Macedonia & Thrace										
AA	7.0	45.0	52.0	15.0	14.0	29.0	3.0	84.0	16.0	-
BB		72.0	72.0	5.0	2.0	7.0	3.0	82.0	18.0	-
MT-1	2.1	13.5	15.7	48.7	19.7	68.4	3.9	88.0	8.0	4.0
MT-2	2.6	18.8	21.4	41.3	22.4	63.7	3.7	88.0	6.6	4.6
MT-3	1.6	17.0	18.6	37.0	28.6	65.6	2.6	87.6	7.2	5.0
MT-4		55.2	55.2	23.5	6.2	29.7	9.9	94.8	5.2	-
MT-5		63.7	63.7	16.6	8.3	24.9	6.4	95.0	4.4	0.6
MT-6	2.5	51.7	54.7	23.3	10.0	33.3	5.3	92.8	5.9	1.3
MT-7	1.1	54.0	55.1	22.6	12.7	35.3	4.3	94.7	5.1	0.2
MT-8		69.4	69.4	15.7	5.0	20.7	4.2	94.3	5.7	-
Crete										
KP-1		71.0	71.0	12.0	8.8	20.8	3.4	95.2	4.8	-
KP-2		72.4	72.4	14.7	4.8	19.5	5.2	97.1	2.9	-
KP-3		53.0	53.0	30.3	5.1	35.4	4.7	93.1	6.9	-
KP-4		40.6	45.9	39.8	6.1	45.9	4.5	91.0	9.0	-
KP-5		54.5	54.5	27.7	8.5	36.2	4.6	95.3	4.7	-
Epirus										
I-1	1.5	43.0	44.4	25.0	16.0	41.0	2.2	87.6	4.5	3.4
I-2	1.6	28.6	30.1	34.5	21.3	55.8	1.8	87.7	5.9	6.4
Peloponnese										
PM-1		16.0	16.0	27.5	26.0	53.5	13.4	82.9	15.7	1.4
PP-1		18.6	18.6	43.2	17.0	60.2	6.2	85.0	7.5	7.5
PP-2		25.0	25.0	32.0	19.0	51.0	11.0	87.0	8.0	5.0

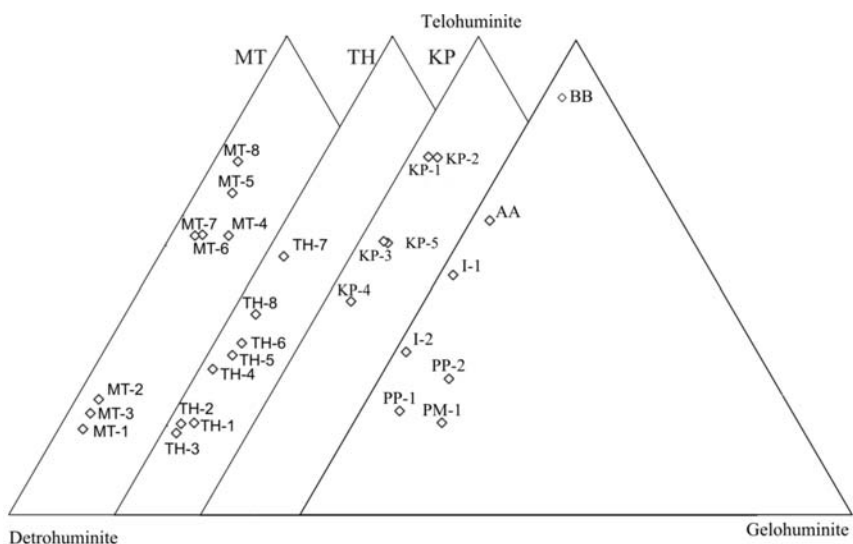


Fig. 2: Ternary plot of huminite maceral subgroup contents.

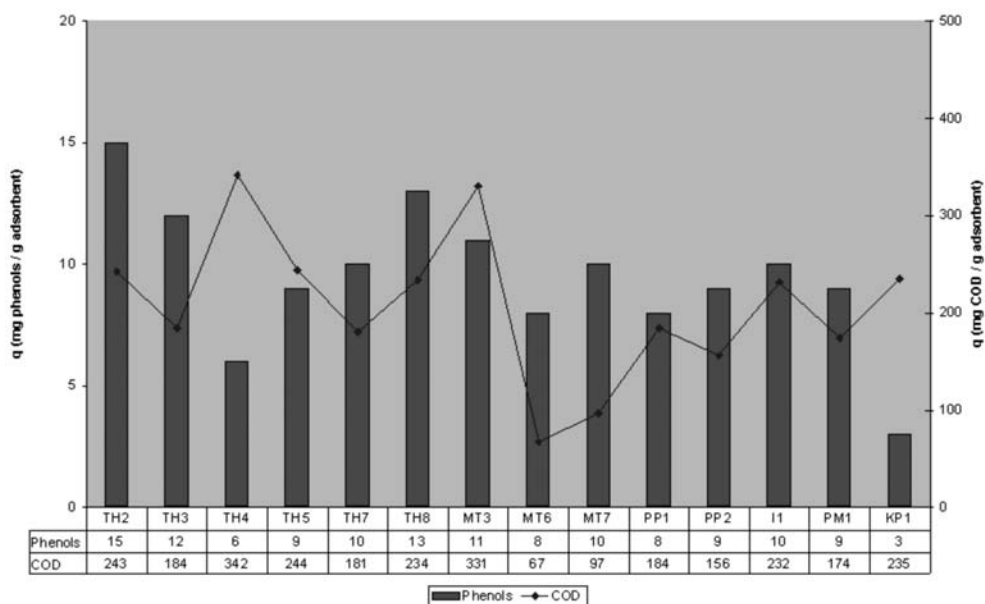


Fig. 3: Sorption capacity q (mg adsorbate / g adsorbent) of phenols and COD for the 14 raw lignite samples at the end of the 24h experiments.

trohuminitic and gelohuminitic content while their inertinitic concentration is higher than their equivalent samples from Thessaly and Macedonia.

Lignite samples from Thessaly TH4, TH5, TH6 and TH8 are characterized by relatively high telohuminitic content ranging from 30.8 to 38.6 vol.%, while detrohuminitic components are higher fluctuating from 49.8 to 59.8 vol.%.

Table 5. Surface area (BET) in m²/g of bulk and activated lignites.

Location	Bulk sample	Activated sample	Location	Bulk sample	Activated sample
Thessaly			Crete		
TH1	3.1	158.5	KP1	3.1	241.2
TH2	14.0	112.1	KP2	5.2	144.3
TH3	3.1	226.5	KP3	8.6	82.5
TH4	4.3	247.4	KP4	10.8	50.1
TH5	7.6	189.7	KP5	5.7	125.1
TH6	11.5	145.6	Epirus		
TH7	3.6	271.3	I1	3.6	186.4
TH8	5.0	202.2	I2	4.3	164.1
Eastern Greek Macedonia & Thrace			Western Greek Macedonia		
MT1	3.0	140.9	AA		299.2
MT2	4.2	168.2	BB		412.4
MT3	3.7	233.9	Western Peloponnese		
MT4	6.8	155.1	PM1	8.7	227.6
MT5	16.8	161.3	PP1	5.1	207.6
MT6	6.9	194.1	PP2	3.4	184.8
MT7	8.7	118.3			
MT8	23.8	88.6			

Lignite samples from western Peloponnesus PM1, PP1, and PP2 have much lower telohuminitic components than the ones from Thessaly ranging from 16 to 25 vol.-%, while their detrohuminic components are relatively similar varying from 51.0 to 60.2 vol.-%. Moreover, the samples from western Peloponnese are also characterized from higher liptinite and inertinite macerals. Samples TH7 and TH8 from Thessaly and MT4, MT5, MT6, MT7 and MT8 from Thrace, as well as all the samples from Crete have high telohuminitic components mainly as eu-ulminite. The difference amongst these samples lies upon the range of detrohuminite concentration. The concentration in samples from Thessaly, TH7 and TH8 varies from 40.8 to 49.8 vol. %, while those from Thrace MT7 and MT8, fluctuate from 20.7 to 35.3 vol.% and those from Crete have wider ranges, which varies from 19.5 to 45.9 vol.% (Table 3).

Finally, the two samples AA and BB, from western Macedonia are characterized by their high telohuminitic components and liptinite macerals and their low detrohuminic components and the absence of inetrinite macerals.

3.3 Surface area measurements

Surface area measurements on non-activated and activated lignite have been measured following the BET method. The results are presented in Table 5 and indicate that in all samples the activation process has increased their surface area substantially, e.g. KP1 from Crete, TH3, TH4 and TH7 from Thessaly.

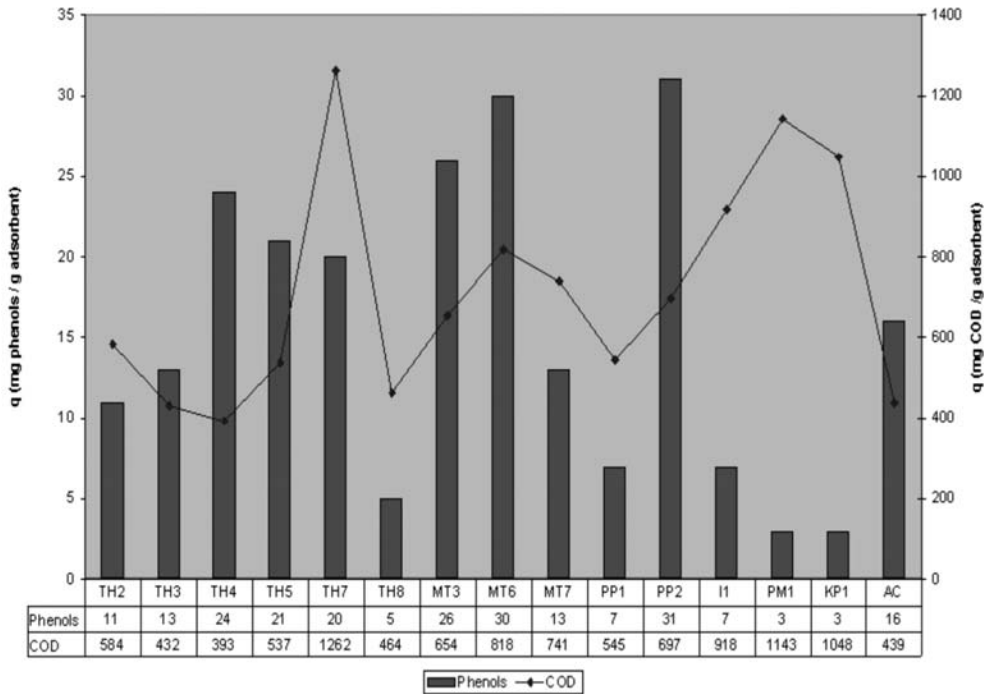


Fig. 4: Sorption capacity q (mg adsorbate / g adsorbent) of phenols and COD for the 15 activated lignite samples at the end of the 24h experiments.

3.4 Adsorption studies

The adsorption capacity q (mg adsorbate/g adsorbent) of phenols from the olive mill waste water was estimated according to the reduction of total phenols and COD at the end of 24 hours experiment for 14 raw and activated lignite samples as well as for one commercially available one (AC).

From the raw lignites, samples TH2, TH8, TH3, I1 and MT3 have q values over 10 mg of phenol /g lignite which are relatively good while the q value of the commercially available activated lignite (AC) is 15 mg of phenol/ g lignite (Figure 4). As far as the COD reduction only two samples MT6 and MT7 have values, 67 mg COD/g lignite and 97 mg/g lignite which are lower than the AC sample 439 mg COD/g lignite. From the activated lignite, samples PP 2, MT6, MT3 and TH4 have q values of over 26 mg/g act. lignite while the commercial AC yield a value of 16 mg/g act. lignite (Figure 5). As far as COD values are concerned, samples TH7, PPI and KP1 have better values, 1262 mg/g act. lignite, 1143 mg/g act. lignite and 1048 mg/g act. lignite respectively, than AC sample which has 271 mg/g act. lignite.

Data concerning the decrease of COD, nitrogen and phosphorus from the simulated city wastewater disposal following the adsorption from raw and activated lignite samples are shown in Figures 5, 6 and 7, respectively.

The decrease of COD demand in raw lignite samples at a half hour interval, Fig.5, indicates that samples KP1, MT6, MT8, I1 and TH4 with q values 7.5 mg/g, 7.3 mg/g, 7.2 mg/g, 7.0 mg/g and 6.7 mg/g, respectively yield higher values than the commercially activated sample, AC, whose value was

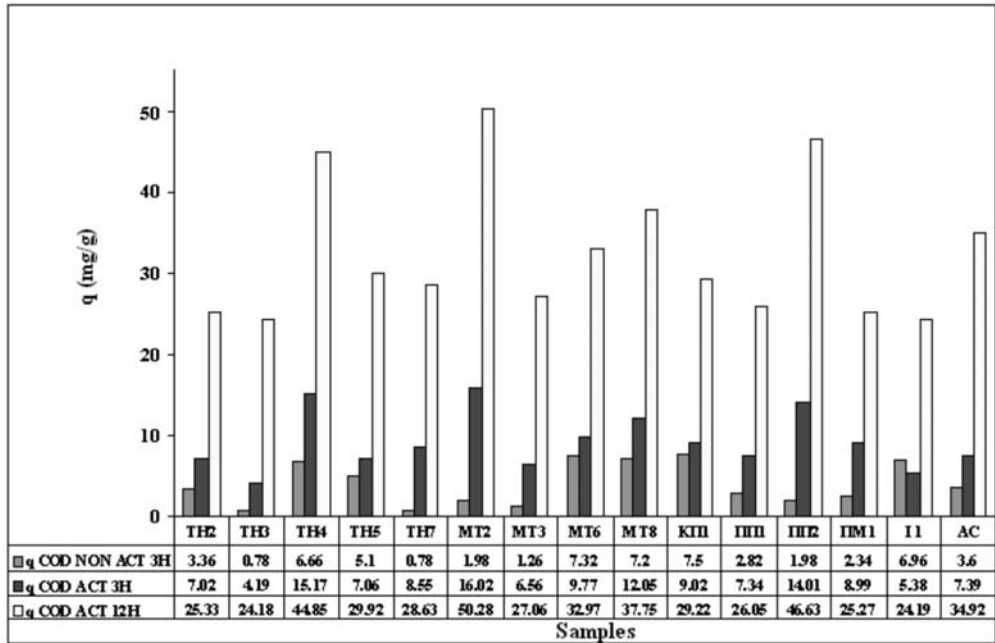


Fig. 5: Decrease in COD demand in mg/g from a simulated wastewater liquid in both raw lignite samples after half an hour interval and activated lignite samples after 3 hours and 12 hours interval.

3.6 mg/g. The decrease, in q value, of COD in activated lignite samples at the time interval of 3 hours, Fig. 5, was in the following order:

$$MT2 > TH4 > PP2 > MT8 > MT6 > KP1 > PM1 > TH7 > AC$$

while at 12 hour interval the order was:

$$MT2 > PP2 > TH4 > MT8 > AC > MT6 > TH5 > TH5 > KP1 > MT3$$

The decrease in q value for nitrogen adsorption at the end of 12 hours, Fig. 6, was in the following order:

$$MT2 > I1 > PM1 > TH4 = PP1 > PP2 > TH7 > MT8 > MT6 > AC$$

The decrease in q value for phosphorus adsorption at the end of 12 hours, Fig. 7, was in the following order:

$$I1 > AC > TH4 > PP2 > MT8 > PM1 > TH5$$

From the above experimental data it is more than obvious that a large number of Greek activated lignite samples can be used successfully to clean industrial and city wastewaters since they behave better than the commercially available one AC (HOK) produced by Rheinbraun Brennstoff GmbH (RBB).

Table 1 shows that every year 1.4×10^6 m³ of OOMW is produced in Greece. Since 1 m³ of OOMW contains 1.8 g/l of phenols it is calculated that the amount of phenols contained in the 1.4×10^6 m³ amounts to 2520 tons. Given that sample PP1 adsorbs 30 mg of phenols/g of activated lignite then to clean the annual effluent of OOMW requires 84000 tons of this type of lignite per year. Assuming that we have a small mineable lignite deposit of 5000000 tons then upon activation the amount left is

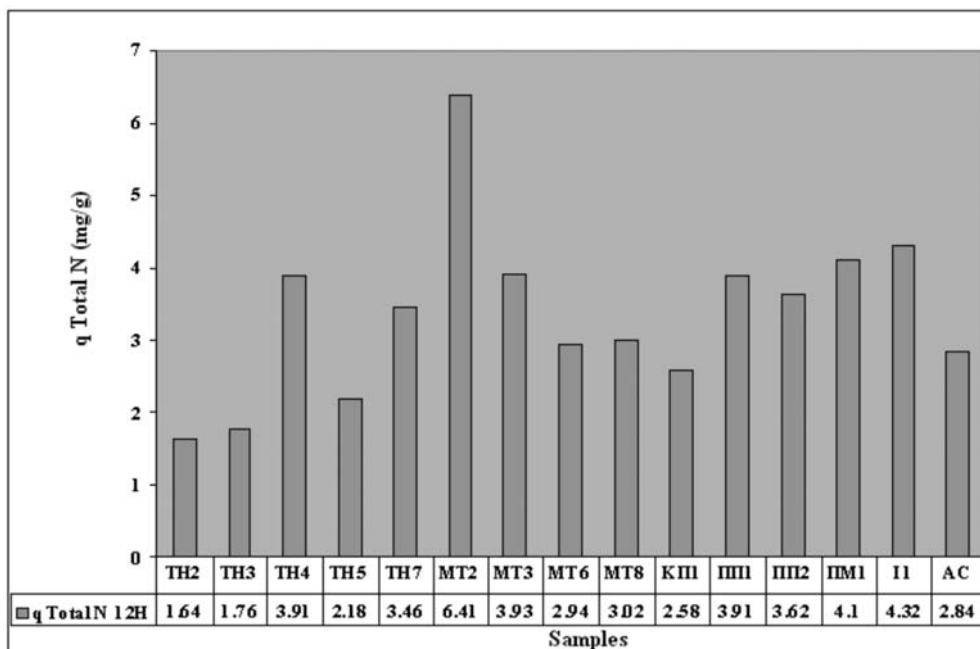


Fig. 6: Nitrogen adsorption in mg/g on activated lignite samples from a simulated wastewater liquid after 12 hours contact.

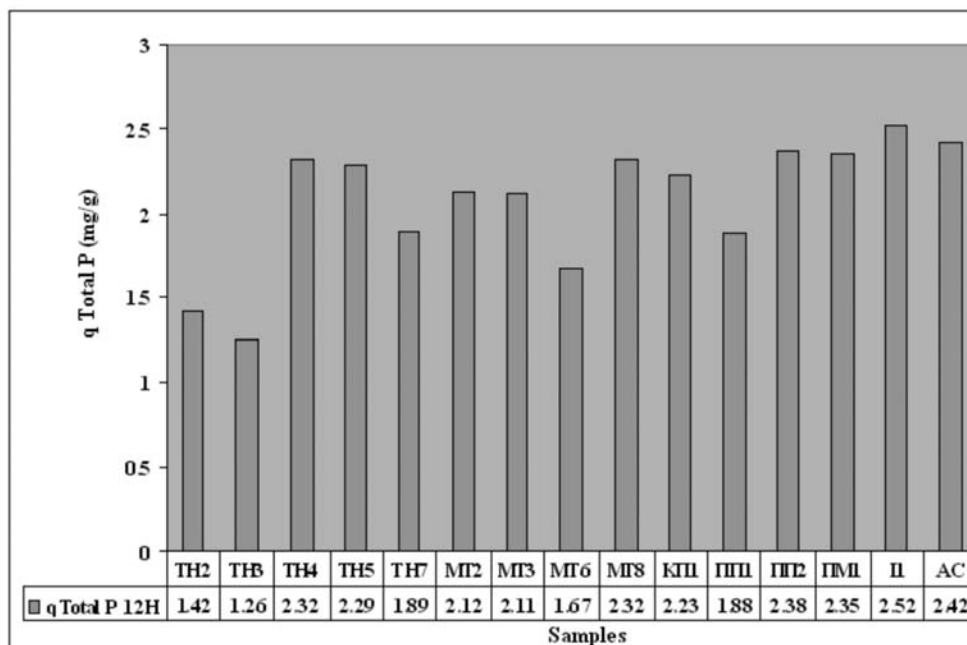


Fig. 7: Phosphorus adsorption, in mg/g on activated lignite samples from a simulated wastewater liquid after 12 hours contact.

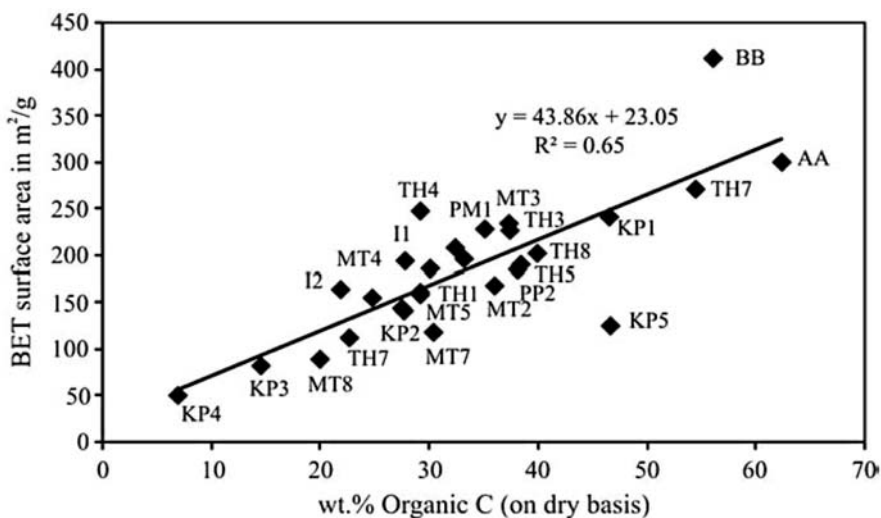


Fig. 8: Relationship between surface area of physically activated lignite samples (m²/g) and their carbon content on dry samples.

roughly 2500000 tons since more than 50% of its weight is lost during the activation process. This implies that such a deposit can satisfy the cleaning process of OOMW in Greece for 30 years.

The 84000 tons of contaminated by phenols activated lignite can be used for the production of valuable by-products (Roig et. al., 2006; Oreopoulou and Russ, 2007). Activated lignite which is saturated with phenols can not be applied in soils as fertilizers because it inhibits the growth of certain bacteria (Paredes et al., 1986).

4. Conclusions

Surface area measurements have been conducted on 28 activated Greek brown coal samples. The results show that some lignite samples such as AA and BB (from northern Macedonia) and TH7 and TH4 from Thessaly, central Greece) have high surface area equal or better than that of the commercial activated carbon sorbents.

Surface area of activated lignite samples is inversely proportional to ash and proportional to carbon content of lignite samples.

The use of activated lignite samples as adsorptive materials for cleaning olive mill wastewater contaminants and consequently for environmental purpose was successful. Maximum recorded adsorption of phenol was recorded on sample PP1 with a value of 30.6 mg/g of activated lignite while the commercial one (AC) adsorbed 14 mg/g of activated lignite. The maximum COD reduction was recorded on sample TH7 with a value of 1262 mg /g of activated lignite while in the commercial one the reduction was 439 mg /g of activated lignite.

Based upon the results obtained from the study of a simulated wastewater disposal liquid, a substantial number of Greek activated lignite samples reduce COD as well as nitrogen and phosphorus content more efficiently than the commercially available activated lignite HOK which produced by Rheinbraun Brennstoff GmbH (RBB).

5. Acknowledgments

This research was funded by EU and the Greek Ministry of Development through the 3rd Community Support Framework, Competitiveness Operational Programme.

6. References

- Aivazides, A. 2000. *Technologia Diachirissis Ygron Apovlition, Panepistimiako Sygramma Dimokritio Panepistimio Thrakis, Xanthi* p. 56 (Translation in Greek of the “Handbuch zur Schott-Anaerob-Testeinheit“, 1987. Shott Glaswerke Mainz, Geschäftsbereich Chemie, Apparate-u. Anlagebau, Bio-prozesstechnik, 56 p.
- Al-Malah, K., M.O.J. Azzam and N.I. Abu-Lail 2000. Olive mills effluent (OME) Waste water post-treatment using activated clay. *Separation and Purification Technology*, 20, pp. 225-234.
- Allen, S. J., Whitten, L. J., Murray, M., Duggan, O. 1997. The adsorption of pollutants by peat, lignite and activated chars. *Jour. of Chemical Technology and Biotechnology*, 68, pp. 442-452.
- American Society for Testing and Materials (ASTM) 1978. Annual book of ASTM standards. Part 26. Proximate analysis of coal and coke. D3172-3173, ultimate analysis of coal and coke, D 3174-3176. ASTM Philadelphia, PA : 380, 390-391.
- American Society for Testing and Materials (ASTM) D3174, 1989. Standard method of ash in the analysis sample of coal and coke from coal. 1989 Annual Book of ASTM Standards, Part 26, Gaseous Fuels: Coal and Coke. ASTM, Philadelphia, PA, pp. 291-294.
- American Society for Testing and Materials (ASTM) D3302, 1989. Standard method of total moisture in coal. 1989 Annual Book of ASTM Standards, Part 26, Gaseous Fuels: Coal and Coke. ASTM, Philadelphia, PA, pp. 326- 332.
- Atanassova, D., P. Kefalas and E. Psillaki (2005). Measuring the antioxidant activity of olive oil mill wastewater using chemiluminescence. *Environ. International*, 31,2, pp. 275-280.
- Dabrowski, A., Podkoscielny, P., Hubicki, Z., Barczak, M. 2005. Adsorption of phenolic compounds by activated carbon: A Critical Review. *Chemosphere*, 58, pp. 1049-1070.
- D' Annibale, A., Casa R., Pieruccetti, F., Ricci, M., Marabotini, R. 2004. Lentula edodes removes phenols from olive mill wastewater ; impact on durum wheat (*Triticum durum* Desf.) grainability. *Chemosphere* 54: 887-894.
- Engelhard, J., Lenz, U. 1997. Lignite coke in water and waste gas clean-up Proceedings of the 11th International Conference on Coal Research, Calgary, Alberta, Canada September 9-12, 1997, pp. 355-368.
- Folin, O. and V. Ciocalteu (1927) ‘On tyrosine and tryptophan determination in protein. *J. of Biology and Chemistry*, 73, pp. 627-50.
- Foscolos, A.E., Barefoot, R.R., 1970. A rapid determination of total organic and inorganic carbon in shales and carbonates— A rapid determination of total sulphur in rocks and minerals. *Geol. Surv. Can.* pp. 70-11.
- Fraser, K. M. 1972. Sorptive mode of activated lignite char. Ph. D. Thesis Libr. Univ. of Calgary, 91 p.
- Galanakis, C., Dimou, D., Pasadakis, N., Papanicolaou, C., Gekas, V. 2006. Adsorption of olive mill wastewater on raw and activated Greek lignites. Protection and Restoration of the Environment VIII, Chania 2006: http://www.ath.aegean.gr/srcosmos/generic_pinakas.aspx?pinakas=publications&author_name=Galanakis%20C
- Hamdi, M., Ellouz, R. 1993. Treatment of detoxified olive mill wastewaters by anaerobic filter and aerobic fluidized bed process. *Environ. Technol.* 14 (2) : 183-188.
- International Committee for Coal Petrology (ICCP), 1963. International Handbook of Coal Petrography,

- 2nd edition. Centre National de la Recherche Scientifique, Paris, France.
- International Committee for Coal Petrology (ICCP), 1971. International Handbook of Coal Petrography, 1st supplement to 2nd edition. Centre National de la Recherche Scientifique, Paris, France.
- International Committee for Coal Petrology (ICCP), 1993. International Handbook of coal petrography, 3rd supplement to 2nd edition. Centre National de la Recherche Scientifique, Paris, France.
- International Committee for Coal and Organic Petrology (ICCP), 2001. The new inertinite classification (ICCP System 1994). *Fuel* 80, 459-471.
- Karacan, F., Ozden, U., Karacan, S. 2006. Optimization of manufacturing conditions for activated carbon from Turkish lignites by chemical activation using response surface methodology. *Applied Thermal Engineering*, 27 (7) SPEC. ISS., May 2006 pp. 1212-1218.
- Khan, K.A., Suidan, M.T., Cross, W.H. 1981. Anaerobic activated carbon filter for the treatment of phenol-bearing wastewater. *J. Water Pollut. Control Fed.: Vol/Issue: 53:10*, pp. 1519-1532.
- Klose, E., Heschel, W. 1987. Zur eignung von braunkohlenkoksen fuer die aktivkohleherstellung. *Chemische Technik (Leipzig)* 39 (2), pp.70-74.
- Mekki, A., Dhoub, A., Sayadi, S., 2007. Polyphenols dynamics and phytotoxicity in a soil amended by olive mill wastewaters. *J. Environ. Manag.* 84: 134-140.
- Niaounakis, M., Halvadakis, C., P. 2006. Olive Processing Waste Management: Literature Review and Patent Survey, 2nd Edition, Series 5, Elsevier Publication 498 p. ISBN-10 0-08-044851-8.
- Navarro, M.V., Murillo, R., Lopez, J.M., Garcia, T., Callen, M.S., Mastral, A.M. 2006. Modeling of activated carbon production from lignite. *Energy and Fuels*, 20 (6) pp. 2627-2631.
- Olson, E.S., Stepan, D.J. 2000. Subtask 1.5-Activated carbon from lignite for water treatment. U S. Department of Energy, National Energy Technology Laboratory, Technical Report, 20 p., Cooperative Agreement No. DE-FC26-98FT40320.
- Oreopoulou, V., Russ, W. {eds} 2007. Utilization of by-products and treatment of waste in the food industry. (Integrating Safety and Environmental Knowledge into Food Studies Towards Sustainable Development. Springer. Science+ Business Media LLC. 316 p. ISBN-10 0-387-33511-0, Library of Congress Control Number 2006928132.
- Papanicolaou, C., 2001. Atlas of Greek Coals, Libr. Inst. of Geol. and Miner. Explor., Athens, Greece, (in Greek), 426 p.
- Paredes, M.J., Monteoliva-Sanochez M., Moreno E., Perez J., Ramos-Cormenzana A. and Martinez J. (1986). Effect of waste waters from olive oil extraction plants on the bacterial population of soil, *Chemosphere* 15: 659-664.
- Roig, A., Cayuela, M.L., Sanchez-Monedero, M.A., 2006. An overview on olive mill wastes and their valorization methods. *J. Waste Manag.* 26: 960-969.
- Stepan, D.J., Moe, T.A., Hetland, M.D., Laumb, M.L. 2001. JV –Task 15- Powdered activated carbon from North Dakota lignite: An option for disinfection by-product control in water treatment plants. U S. Department of Energy, National Energy Technology Laboratory, Technical Report, 41 p. Cooperative Agreement No. DE-FC26-98FT40321.
- Sykorova, I., Pickel, W., Christanis, K., Wolf, M., Taylor, G.H., Flores, D. 2005. Classification of huminite. -ICCP System 1994. *Intern. J. of Coal geol.* 62 (1-2 SPEC.ISS.), PP. 85-106.
- Zhang, S., Yan, Y., Yongjie, J. Y., Li, T., Ren, Z., 2005. Upgrading of liquid fuel from the pyrolysis of biomass. *Bioresour. Technol.* 96, 545-550.

12ο ΔΙΕΘΝΕΣ ΣΥΝΕΔΡΙΟ ΤΗΣ ΕΛΛΗΝΙΚΗΣ ΓΕΩΛΟΓΙΚΗΣ ΕΤΑΙΡΙΑΣ
ΠΛΑΝΗΤΗΣ ΓΗ: Γεωλογικές Διεργασίες και Βιώσιμη Ανάπτυξη

12th INTERNATIONAL CONGRESS OF THE GEOLOGICAL SOCIETY OF GREECE
PLANET EARTH: Geological Processes and Sustainable Development



ΓΕΩΧΗΜΕΙΑ ΚΑΙ ΚΟΙΤΑΣΜΑΤΟΛΟΓΙΑ
GEOCHEMISTRY AND ORE DEPOSIT GEOLOGY

THE INFLUENCE OF REDUCTIVE DISSOLUTION OF IRON OXIDES BY S(-II) ON URANIUM MOBILITY

Alexandratos V. G.¹, Behrends T.¹ and Van Cappellen P.^{1,2}

¹ Utrecht University, Faculty of Geosciences, Department of Earth Sciences – Geochemistry P.O. Box 80.021, 3508 TA Utrecht, The Netherlands, vasso@geo.uu.nl, behrends@geo.uu.nl, pvc@geo.uu.nl

² Georgia Institute of Technology, School of Earth & Atmospheric Sciences, Atlanta, Georgia 30332-0340, USA pvc@eas.gatech.edu

Abstract

This study investigates possible redox transformations of uranium under transient redox conditions. Specific focus lies on the fate of U as reductive dissolution of iron oxyhydroxides by S(-II) is initiated. In batch experiments sulfide was incrementally added to a lepidocrocite suspension containing adsorbed U(VI). The partitioning of uranium was monitored during the progressing transformation of lepidocrocite into FeS. Synchrotron-based X-ray absorption spectroscopy was used to resolve the oxidation state of uranium. Upon addition of sulfide intermediate release of U from the solid to the solution was observed. The mobilization of U was followed by immobilization in later stages. XAS reveals that this immobilization coincides with reduction of U(VI) to U(IV). Consequently, reduction of U(VI) and precipitation of U(IV) solids, due to a shift from oxic to sulfate reducing conditions is possible. However, kinetic effects might lead to an intermediate mobilization of U that should be considered for the risk assessment of nuclear waste repositories and the remediation of sites, contaminated with radionuclides.

Key words: uranium mobilization, reductive dissolution, iron mineral transformation, redox transitions, iron sulfides, X-ray absorption spectroscopy.

1. Introduction

In recent years the fate of uranium in natural environments has received great attention due to the high potential of uranium migration beyond the designated waste disposal sites. Uranium contamination poses great health risks to an affected community both as a heavy metal and with the exposure to radiation as it decays. Uranium transport is mainly associated with its higher oxidation state of U(VI), considered as the uranium species with the highest solubility. In recent years, the approach of uranium immobilization as a possible in situ remediation pathway has driven numerous studies to investigate abiotic and microbial processes that induce reduction of U(VI) to U(IV), leading to uranium precipitation and thus removal from aquatic systems. Subsurface environments specifically, are characterized by ongoing changes in redox conditions that may influence not only the mobility of uranium species but also induce changes in iron mineralogy with which uranium is closely associated. The interrelationship between redox transformations of uranium and iron are very relevant in many natural environments and a subject of major importance for the remediation of sites contaminated with radionuclides and the risk assessment of nuclear waste repositories.

Among soil minerals, iron oxides/oxyhydroxides are considered as primary sorbents for uranium due to their high reactive surface areas. Uranium sorption has been studied on goethite (e.g. Duff, 1996; Gabriel et al., 1998; Hsi and Langmuir, 1985; Giammar and Herring, 2001), on hematite (e.g. Bargar et al., 2000; Ho and Miller, 1986; Liger et al., 1999), on ferrihydrite (e.g. Waite et al., 1994; Morrison et al., 1995), on magnetite (Sagert et al., 1989) and green rust (O'Loughlin et al., 2003). In the above studies, inner-sphere complexation of uranium species with the iron mineral surfaces has been widely supported, indicating the strong sorption behavior among uranium and iron oxides. However, iron oxides can significantly influence uranium transport not only by providing reactive surfaces for uranium adsorption but they can also catalyze the reduction of U(VI) by Fe(II) (Liger et al., 1999; Lloyd et al., 2002). Mixed valence iron oxides have been proposed to be able to reduce U(VI), which has been attributed to the presence of sorbed Fe²⁺ (e.g. Charlet et al., 1998; Fredrickson et al., 2000; O'Loughlin et al., 2003).

Open questions still remain regarding the fate of uranium once iron oxides undergo mineral transformation with changes in the redox regime. It is known that in oxic environments uranium adsorption typically competes with carbonate complexation in solution, while under anoxic conditions reduction of U(VI) to U(IV) occurs, forming insoluble minerals (De Pablo et al., 1999; Ragnarsdottir and Charlet, 2000). Consequently, once uranium occurs in the environment as adsorbed onto iron oxides, changes in the redox regime, from oxic to anoxic, may not necessarily lead to the mobilization of uranium. However, kinetic effects might lead to the release of solid bound uranium which is not predicted by equilibrium thermodynamics. One of the most critical aftermaths of iron oxide dissolution would be the release of important -previously sorbed- pollutants such as uranium.

Overall results from previous studies lead to the hypothesis that U(VI) adsorbed to iron oxides might be mobilized when the reductive dissolution of Fe(III) is faster than the reduction of U(VI) and Fe outcompetes U as an oxidant for S(II). Here, we experimentally investigate the possibility of U mobilization upon reductive dissolution of iron oxides with adsorbed U(VI) by S(II), and evaluate whether U(VI) can be reduced. Efforts begin with an ideal abiotic system, imposed to anoxic conditions, where sulfide was incrementally added to a lepidocrocite suspension with preadsorbed U(VI). Lepidocrocite (γ -FeOOH) was chosen for these experiments as a highly reactive iron oxide mineral which is also found in environments of altering redox conditions (Canfield, 1989). Our main purpose is to characterize the redox state and binding environment of uranium that is associated with lepidocrocite during the reaction with sulfide. Additionally the level of competition between uranium and iron reduction by sulfide will be addressed and as well as further role it could play in uranium transport within natural environments.

2. Background Information

During diagenesis it has been shown that bacteria play a key role in the dissolution of iron oxides by using Fe(III) as an electron acceptor and resulting in the production of Fe(II) (e.g. Lovely et al., 1991), which can be expressed by the following reaction:



However, bacteria are also known to rapidly produce H₂S in organic-rich soil, which also acts as an Fe(III) reductant (Jorgensen, 1977; Canfield, 1989; Krom et al., 2002). The kinetics of reductive dissolution of iron oxides by S(-II) are well established and show a dependency on the degree of reactivity of the available iron minerals in the soil (Poulton et al., 2004; Poulton 2003; Yao and Millero, 1996; Peiffer et al., 1992; Dos Santos Afonso and Stumm, 1992). Either by using geochemical mod-

els or through experiments, the above mentioned studies have emphasized the significance of pH, dissolved sulfide and Fe(II) concentrations in solution and the controlling factor of mineral surface area on the rates of iron oxide dissolution.

In contrast to iron oxides, very little is known about the kinetics of U reduction by S(-II). As previously mentioned the abiotic reduction of U(VI) has been connected to the presence of Fe(II), however uraninite (UO₂) which has a very low solubility ($K_{sp} = 10^{-60.6}$; Langmuir 1978) is mostly known to form either by iron reducing bacteria (Lovley et al., 1991) or by sulfate reducing bacteria (Lovley et al., 1993; Payne et al., 2004). Nevertheless, data from several field studies from areas such as the Biscay Bay, the Cariaco Trench, the Black Sea and the Framvaren Fjord, where anoxic conditions, and thus, sulfide concentrations were extreme, gave no evidence for U(VI) reduction (Chaillou et al., 2002; Anderson et al., 1989). The reduction of U(VI) to U(IV) by a strong reductant such as H₂S should be possible, based on thermodynamics, and can possibly be expressed by the following reaction stoichiometry:



However, most studies that achieved uranium reduction by sulphide did so only by manipulating physical or chemical parameters in laboratory experiments, e.g. by using strong sorbents that would catalyze reduction, by increasing uranium or sulfide concentrations in solution (Kochenov et al., 1977; Mohagheghi et al., 1984). Thus, evidence indicates that homogeneous reduction of U(VI) by S(-II) is kinetically hindered.

3. Methods

In a pH stat reactor U(VI) acetate was added to a lepidocrocite suspension. Synthetic lepidocrocite was produced according to the Schwertmann and Cornell (2000). Measured surface area of produced lepidocrocite was 78 m²/g (N₂-BET analysis). No mineral phases other than lepidocrocite were identified by powder X-ray diffraction (XRD).

After adsorption equilibrium variable amounts of S(-II) (in the form of sodium sulfide solution) were added and the partitioning of uranium, changes in iron redox state, and iron oxide mineralogy were monitored. The pH during the reduction experiments was 8, the ionic strength was adjusted to 0.1 M by adding NaCl solution. Concentrations of dissolved elements were obtained with the use of ICP-MS or standard photometric methods after filtrating aliquots of the suspension. Depending on the macroscopic observations, fractions of the suspension were collected. The solids were recovered by centrifugation and freeze dried for X-ray adsorption spectroscopy (XAS).

For XAS solid samples were prepared as pellets and air tight sealed to avoid oxidation of reduced iron or uranium by oxygen during transportation. Collection of spectra took place at the FAME BM30M beamline, at the ESRF in Grenoble, France. XAFS spectra were recorded in the fluorescence mode at the U L_{III}-edge (~17.17 keV) in a cryostat at about 30K. For energy calibration a Y foil (k-edge) was used. Titanium reduced uranium was used as a U(IV) standard and a known U(VI)-iron oxide sample for U(VI). Both X-ray absorption near-edge structure (XANES) and extended X-ray absorption fine structure (EXAFS) spectroscopy were utilized to gain insight on the oxidation state and local environment of uranium bound to the mineral surface throughout the reduction process.

All experiments and XAFS sample collection and preparation took place in an O₂-free glovebox which instead contained a gas mixture of N₂ (95%) and H₂ (5%). The glovebox was additionally equipped with a Pd catalyst and an O₂ monitor, in order to maintain and control oxygen levels below 1 ppm. All glassware used (DURAN® ISO laboratory bottles) were previously checked for possi-

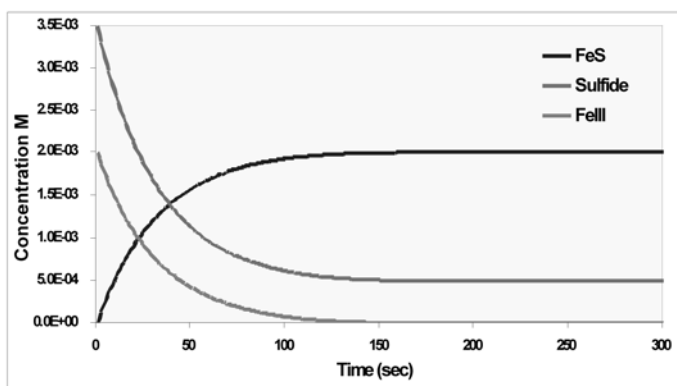


Fig. 1: Model of lepidocrocite reductive dissolution caused by sulfides.

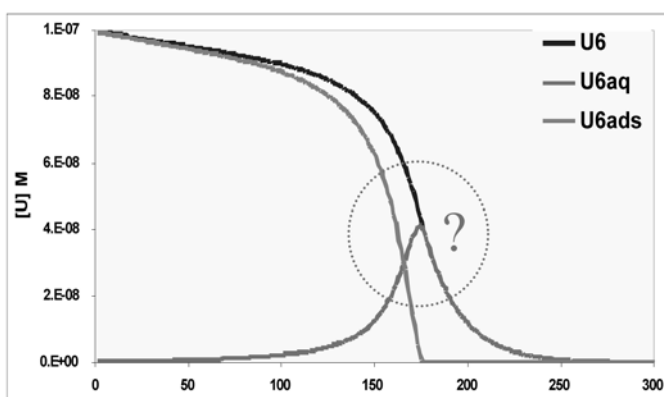


Fig. 2: Evolution of U(VI) concentration and speciation over time. The reduction of U(VI) leading to the decrease of U(VI) concentration, once U(VI) is released into solution, is fictive -indicated with question mark- and included in the model for illustrative purpose.

ble uranium uptake; in repeated blank absorption experiments no uranium was lost from solution. All chemicals used were of reagent grade and no further purification was performed.

In order to illustrate the role of kinetics on the mobility of uranium during reductive dissolution of iron oxides geochemical modelling was used. The rate of lepidocrocite dissolution was estimated based on the rate law and kinetic constants reported in past studies (Peiffer et al., 1991). Due to shrinking of the particles and consumption of S(II) the rate of lepidocrocite dissolution decreases with progressing reaction. For simplicity it was assumed that all produced Fe(II) precipitates as FeS. The process of complete reduction of lepidocrocite after addition of sulfide is shown in Fig. 1.

Additionally, possible pathways for the fate of U(VI) sorbed on the iron oxide mineral surface were modeled (Figure 2). The dissolution of lepidocrocite results in the release of U(VI) back into solution. U(VI) adsorption onto lepidocrocite was calculated with a simple K_d model. The K_d value was derived from adsorption isotherms which were performed prior to the dissolution experiments (data not shown). Adsorption onto FeS was not taken into account. For illustrating the possibly only temporal nature of U mobilization in such system re-immobilization by reduction of U(VI) was included in the calculations. In this case, relative rapid homogenous reduction of dissolved U(VI) by S(II) was assumed.

4. Results and Discussion

Mineral transformation from lepidocrocite to iron sulfide occurred by the very first sulfide injection in the lepidocrocite-uranium system, an effect that was visible by the color change of the suspension from orange to black. All added S(II) was consumed within the first two hours after the initial sulfide injection, as shown in Figure 3. During this period of time, electron transfer is assumed to be taking place from the Fe(III) solid phase (lepidocrocite) to the sulfides that are interacting with the substrate surface. In all experiments, a second sulfide injection took place two hours after the first one, maintaining the same total concentrations of sulfide added. Consumption of S(II) occurred after the second injection as well, with the exception of experiments for which S(II) remained in excess in solution at the concentration level of ~ 3 mM (shown in Fig.3).

The progressive formation of amorphous FeS is assumed to dominate after the second sulfide addition, which would follow the reductive dissolution pathway described in detail by Afonso & Stumm, (1992). Due to the fact that in these series of experiments sulfides have been added incrementally, the effects of this reduction for the system lepidocrocite-U can be observed as they follow every new sulfide addition. Reaction of lepidocrocite and S(-II) was a relatively fast process and completed within less than one hour, which agrees with the findings of Peiffer et al.(1991) and Poulton (2004). The consumption of S(-II) was predominantly coupled to the production of Fe(II). A notable increase in Fe(II) concentrations in both solution and solid were observed (data not shown). In all experiments Fe(II) produced is in analogy to the amount of sulfides added. In experiments where S(-II) was added in excess (e.g. Fig.3), almost all Fe(II) is produced by the very first sulfide addition.

Prior to sulfide addition to the system, the concentration of dissolved uranium (U(aq)) was below detection limits indicating the strong adsorption onto lepidocrocite (Fig. 3). Instant mobilization of U(VI) was observed with every sulfide addition. Preliminary results suggested that the instantaneous mobilization and elevated concentrations of uranium in solution after sulfide addition might be due to 1) a loss of sorption sites during iron mineral transformation 2) competition between uranium and Fe(II) for reactive surface sites, 3) possible formation of uranium complexes with sulfides in solution (e.g. polysulfides).

After the instantaneous increase in U(aq) concentration, induced by S (-II) addition, U(VI) concentration in solution decreased, however, approached a level significantly higher than before S(-II) addition. The decrease in U(aq) in the first hour after S(-II) addition was correlated with the S(-II) concentration. This suggests that the instantaneous mobilization of uranium might be due to formation of complexes with sulfide in solution. The elevated uranium concentrations remaining in solution after all S(-II) has been consumed after the first injection can be explained by a loss of sorption sites due to iron reduction or the competition with Fe(II) for reactive surface sites; U(VI) shows a lower affinity for Fe-SH than for Fe-OH groups. The release of uranium observed in all experiments reaches $\sim 5\%$ of the total uranium added to the suspensions. Aqueous speciation of released U is believed to be UO_2^{2+} .

The decrease in U(aq) concentration after one hour of reaction time with sulfide was not accompanied with a decrease in S(-II) concentration. This re-immobilization might be caused by reduction of uranium. XANES spectra, shown in Figure 4, showed successive transformation of U(VI) into U(IV) with time. Reduction of U(VI) is in the time scale of days. We have data that supports the hypothesis that the uranium reductant is most likely not $\text{S(-II)}_{\text{aq}}$ but FeS. Hence, formation of FeS might be required for sustainable immobilization of U. Evidence for sorption and reduction of U(VI) by the crystalline sulfides galena and pyrite has been given by Wersin et al. (1994).

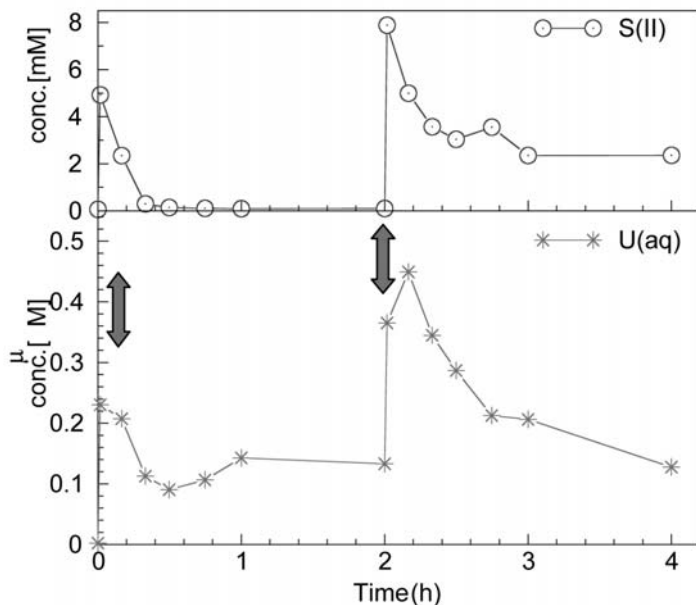


Fig. 3: Top graph shows the kinetics of S(II) consumption. The graph below shows the phase distribution of uranium in response to sulfide addition. Red arrows indicate the timings of S(II) additions.

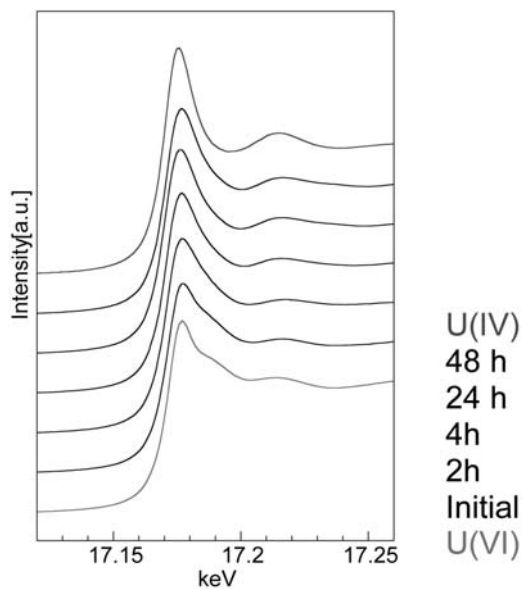


Fig. 4: XANES spectra showing reduction of uranium as a function of time (hours). Samples taken from the same suspension as a function of time, starting from the initial conditions (prior to sulfide additions) and following with samplings of 2, 4, 24 and 48 hours. XANES spectra are compared to standards of U(IV) (Titanium reduced uranium, with blue) and U(VI) (adsorbed to hematite, with red).

Linear combination of spectra indicated an approximate 15% presence of U(IV) in the solid sample reacted for two hours with S(-II) and an increase of 45% for the solid of 48 hours of reaction. A similar trend of progressive U(VI) reduction was observed for sample series of all other experiments.

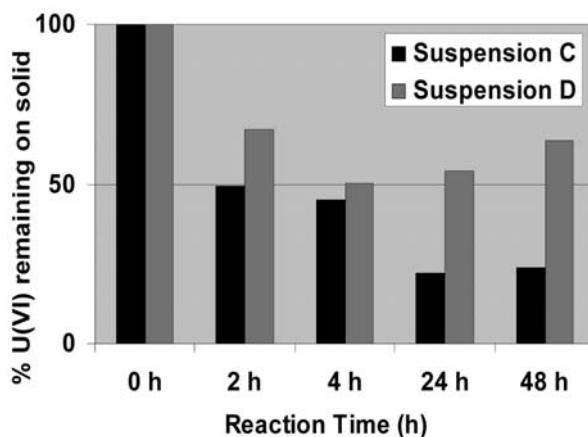


Fig. 5: Chart with U(VI) percentages remaining in association with the solid from two suspensions reacted with 8 mM S(-II) in “C” and 5 mM S(-II) in “D”. Results are derived using coordination numbers from EXAFS fitting.

Uranium reduction is reflected in EXAFS fitting results by the decrease of axial oxygens. Coordination numbers were used to derive and compare percentages of U(VI) still remaining within the solid fraction of the collected time-series experiments. Figure 5 illustrates two of the experiments performed, indicated as “C” and “D”. To these suspensions 8 mM and 5 mM of S(-II) were added respectfully. Results show a dramatic decrease of U(VI) in suspension with the higher amount of sulfide. The formation of uraninite made its appearance much later within the duration of the experiments (data not shown). EXAFS spectra indicate U-U interactions, which are more prominent in suspensions reacted with higher amounts of S(-II) and with a greater presence of FeS. This gives us some indication that FeS is the dominant reductant for U(VI) in these systems and interactions between U(VI) with FeS might be of significant importance for controlling the mobility in environments with ongoing microbial sulfate reduction.

5. Acknowledgments

Authors are grateful to Dr A. Scheinost from the FZR for his assistance in the collection and analyses of XAS data as well as O. Proux and the people from the FAME beamline at the ESRF for technical support. We also thank the ESRF for funding XAS experiments but also the EU for financial support (FUNMIG).

6. References

- Afonso, M., dos Santos and Stumm Werner, 1992. Reductive Dissolution of Iron(III) (Hydr)oxides by Hydrogen Sulfide. *Langmuir*, 8, 1671-1675.
- Anderson, RF, Fleisher, MQ., LeHuray, AP., 1989. Concentration, oxidation state and particulate flux of uranium in the Black Sea. *Geochim. Cosmochim. Acta*, 53, 2215-2224.
- Bargar, J. R., Reitmeyer, R., Lenhart, J. J and Davis, J.A., 2000. Characterization of U(VI)-carbonato ternary complexes on hematite: EXAFS and electrophoretic mobility measurements. *Geochimica et Cosmochimica Acta*, 64, No. 16, pp. 2737–2749, 2000.
- Behrends, T. and Van Cappellen, P., 2005. Competition between enzymatic and abiotic reduction of ura-

- nium(VI) under iron reducing conditions. *Chemical Geology* 220, pp. 315-327.
- Canfield, D.E., 1989. Reactive iron in marine sediments. *Geochim. Cosmochim. Acta* 53, 619–632
- Chaillou, G., Anschutz, P., Lavaux, G., Schäfer, J. and Blanc, G., 2002. The distribution of Mo, U, and Cd in relation to major redox species in muddy sediments of the Bay of Biscay. *Marine Chemistry* 80: 41-59
- Charlet, L., Silvester, E., and Liger, E., 1998c. N-compound reduction and actinide immobilisation in surficial fluids by Fe(II): the surface Fe(III)OFe(II)OH degrees species, as major reductant. *Chemical geology*, vol.151 iss.1-4, pg.85 -93.
- De Pablo, J., Casas, I., Gimenez, J., Molera, M., Rovira, M., Duro, L., and Bruno, J., 1999. The oxidative dissolution mechanism of uranium dioxide. I. The effect of temperature in hydrogen carbonate medium. *Geochim. Cosmochim. Acta* 63, 3097-3103.
- Duff, M.C. and Amrhein, C., 1996. Uranium(VI) adsorption on goethite and soil in carbonate solutions. *Soil Sci. Soc. Am. J.* 60, 1393.
- Fredrickson, J.K., Zachara, J.M., Kennedy, D. W., Duff, M. C., Gorby, Y. A., Li, S. M. W., and Krupka, K.M., 2000. Reduction of U(VI) in goethite (alpha-FeOOH) suspensions by a dissimilatory metal-reducing bacterium. *Geochim. Cosmochim. Acta* 64, 3085-3098.
- Gabriel, U., Gaudet, J. P., Spadini, L., and Charlet, L., 1998. Reactive transport of uranyl in a goethite column: an experimental and modeling study. *Chem. Geol.*, 151, 107-28.
- Giammar, D.E and Herring, J.G., 2001. Time scales for sorption-desorption and surface precipitation of uranyl on goethite. *Environ. Sci. Technol.* 35, 3332-3337
- Hsi C.-K. D. and Langmuir, D., 1985. Adsorption of uranyl onto ferric oxyhydroxides: Application of the surface complexation site-binding model. *Geochim. Cosmochim. Acta* 49, 1931–1941.
- Ho, C. H. and Miller, N. H., 1986. Adsorption of uranyl species from bicarbonate solution onto hematite particles. *J. Colloid Interf. Sci.* 110, 165–171.
- Jørgensen, B. B., 1977. The sulfur cycle of a coastal marine sediment (Limfjorden, Denmark). *Limnol. Oceanogr.* 5, 814–832.
- Krom, M. D., Mortimer, R. J. G., Poulton, S. W., Hayes, P., Davies, I. M., Davison, W., and Zhang, H., 2002. In-situ determination of dissolved iron production in recent marine sediments. *Aquatic Sciences* 64, 282-291.
- Langmuir, D., 1978. Uranium solution-mineral equilibria at low temperatures with application to sedimentary ore deposits. *Geochim. Cosmochim. Acta* 42, 547–569.
- Liger, E., Charlet, L. and Van Cappellen, P., 1999. Surface catalysis of uranium (VI) reduction by iron(II). *Geochim. Cosmochim. Acta*, 63, 2939-2955.
- Lloyd, J. R., Chesnes, J., Glasauer, S., Bunker, D. J., Livens, F. R., and Lovley, D. R., 2002. Reduction of actinides and fission products by Fe(III)-reducing bacteria. *Geomicrobiology Journal* 19(1), 103-120.
- Lovley, D. R., Phillips, E. J. P., Gorby, Y. A., and Landa, E. R., 1991. Microbial reduction of uranium. *Nature* 350, 413-416.
- Lovley, D. R., Roden, E. E., Phillips, E. J. P., and Woodward, J. C., 1993. Enzymatic Iron and Uranium Reduction by Sulfate-Reducing Bacteria. *Mar. Geol.* 113, 41–53.
- Mohaghghi, A., Updegraff, D. M., Goldhaber, M. B., 1984. The role of sulfate-reducing bacteria in the deposition of sedimentary uranium ores. *Geomicrobiology Journal*. 4(2): 153-173
- Morrison, S. J., Spangler, R. R., and Tripathi, V. S., 1995a. Adsorption of U(VI) on Amorphous Ferric Oxyhydroxide at High-concentrations of Dissolved Carbon (IV) and sulphur (VI). *Journal of Contaminant Hydrology* 17, 333-346.

- Morse, J. W. and Choppin, G. R., 1991. The chemistry of transuranic elements in natural waters. *Rev. Aquatic Sci.* 4, 1-22.
- O'Loughlin, E.J., Kelly, S.D., Cook R. E., Csencsits R., Kemner K.M., 2003. Reduction of uranium(VI) by mixed iron(II)/iron(III) hydroxide (green rust): Formation of UO₂ nanoparticles. *Environ. Sci. Technol.* 37, 721-727.
- Payne, T. E., Davis, J. A., and Waite, T. D., 1994. Uranium Retention by Weathered Schists – The role of Iron Minerals. *Radiochimica Acta*, 297 -303.
- Poulton, S. W., M. D. Krom, and R. Raiswall, 2004. A revised scheme for the reactivity of iron (oxy-hydr)oxide minerals towards dissolved sulfide. *Geochim. Cosmochim. Acta* 68:3703–3715.
- Poulton, S.W., 2003. Sulfide oxidation and iron dissolution kinetics during the reaction of dissolved sulfide with ferrihydrite. *Chemical Geology*, 202, 79-94.
- Peiffer, S., Afonso, M., Wehrll, B., Gachter, R., 1992. Kinetics and Mechanism of the Reaction of H₂S with Lepidocrocite. *Environ. Sci. Technol.*, 26, 2408-2413.
- Ragnarsdottir, KV., and Charlet, L., 2000. Uranium behaviour in natural environments. In Cotter-Howells JJ, Batchelder M, Campbell L, Valsami-Jones E, eds, *Environmental Mineralogy: Microbial Interactions, Antropogenic Influences, Contaminated Lands and Waste Management*, Series 9. Mineralogical Society of Great Britain and Ireland, London, UK, pp 333–377.
- Sagert, N. H., Ho, C. H., and Miller, N. H., 1989. The Adsorption of Uranium(VI) onto a Magnetite Soil. *Journal of Colloid and Interface Science* 130, 283-287.
- Schwertmann, U. and Cornell, R. M., 1991. Iron Oxides in the Laboratory – Preparation and Characterization; VCH: New York, Chapters 5-6, pp 61-84.
- Waite, T. D., Davis, J. A., Payne, T. E., Waychunas, G. A., and Xu, N., 1994. Uranium(VI) adsorption to ferrihydrite: Application of a surface complexation model. *Geochim. Cosmochim. Acta* 58, 5465–5478.
- Wersin, P. Jr., Peresson, P., Redden, G., Leckie, J. O., Harris, D. W., 1994 Interaction between aqueous uranium (VI) and sulfide minerals: Spectroscopic evidence for sorption and reduction., *Geochim. Cosmochim. Acta* 58, 2829-2843.
- Yao, W. and Millero, F. J., 1996. Oxidation of hydrogen sulfide by hydrous Fe(III) oxides in sea water. *Mar. Chem.* 52, 1–16.

HETEROGENEITY IN HEAVY METAL CONCENTRATIONS IN THE SOIL OF A FIRING RANGE AREA AT KESARIANI, ATHENS, GREECE

Argyrazi A.¹ and Petrakaki N.¹

¹ University of Athens, Department of Economic Geology and Geochemistry, 15784 Athens, Greece, argyrazi@geol.uoa.gr

Abstract

Heterogeneity in metal concentrations is a typical characteristic of contaminated sampling targets, with consequences in the estimation of measurement uncertainty and the spatial delineation of contamination. Heterogeneity of contamination is site specific and is linked to the type and origin of the contaminants. In this paper we present a case study on a completed firing range, at Skopeftirio Park in Kesariani, Athens, Greece. The study focused on two heavy metals in the soil with contrasting properties. Lead, an element with high concentrations due to the previous land use of the park and Cr, an element with concentrations close to the natural background at this site. Forty nine top soils samples (0-10cm) were collected from an area of 0.7 km² by using a 40m x 40m grid. Duplicate samples were collected from 8 randomly selected sampling sites, 5 m away from the original sampling location and were analyzed in duplicate for the estimation of measurement uncertainty. Elemental concentrations were measured by AAS after an aqua-regia acid attack. Robust analysis of variance applied on duplicate measurements separated the total variability of the results into three components, representing the analytical, sampling and geochemical variances for the two elements in soil. It was shown that the combined sampling and analytical variance for the Pb has a high proportion in the total (53.5%) reflecting the extreme small-scale spatial variation of Pb contamination. For Cr, the proportion is lower (17%) indicating a more homogeneous distribution of elemental concentrations.

Key words: *geochemical sampling, measurement uncertainty, heterogeneity, ANOVA, contaminated soil, heavy metals.*

1. Introduction

Sampling is an integral part of the measurement process in geochemistry. However, only recently appropriate attention has been given to this process in terms of the errors and uncertainty that it generates. Uncertainty of measurement, according to metrological terminology is defined as a parameter, associated with the result of a measurement that characterizes the dispersion of the values that could reasonably be attributed to the measurand (ISO, 1993). The idea of devising methods for the estimation of sampling uncertainty analogous to the methods already in use for the estimation of analytical uncertainty has been suggested (Ramsey, 1994; Thompson and Ramsey, 1995). The analogy is limited by three important differences from analytical practice (Ramsey and Thompson, 2007) namely: (i) the heterogeneity of sampling targets plays a role during assessment of sampling uncertainty, while this (ideally) does not play a role during assessment of analytical uncertainty, (ii) practical difficulties obstruct the estimation of sampling bias, (iii) analytical variations can be observed directly, but sampling variation cannot be observed directly because there will always be interfering analytical variations.

However, through recent research, methodology has been developed for estimating uncertainty from sampling empirically by using techniques based on randomized replicated experiments. In such techniques, the utilization of analysis of variance, often abbreviated as ANOVA, has a central role. In the instance of contaminated land investigations, where the objective of the measurement is defined in terms of contaminant concentration in the sampling target and not simply in the laboratory sample, the act of taking a sample introduces uncertainty in the reported result. Possible sources of error and uncertainty during sampling operations may include cross-contamination and imperfect stabilization of samples resulting in bias or additional variability, but the most significant source of uncertainty is heterogeneity of the sampling target and its effects, such as random variability and selection bias. Furthermore, studies of environmental systems have shown that effects caused by heterogeneity often outweigh between-sampling operator and between-sampling protocol differences in concentration results (Ramsey and Argyraki, 1997) and uncertainty on the measurements is greatly affected by the heterogeneity of contamination, which in turn is linked to the type and origin of the contaminants. It has been shown that the higher the heterogeneity of contamination the higher the levels of the estimated measurement uncertainty (Taylor et al., 2005). Work on contaminated land with different characteristics also confirmed that heterogeneity is site specific.

In this paper we present a case study on a completed firing range, at the Skopeftirio Park in Kesariani, Athens, Greece. The study focused on two heavy metals in soil with contrasting properties. Lead, an element with high concentrations in surface soil due to the previous land use of the park as shooting range and chromium, an element with concentrations close to the natural background which is controlled by local geology. The objective of this work is to present an application of analysis of variance (ANOVA) technique to sampling uncertainty estimation and to discuss the heterogeneity in heavy metal concentrations in soil with reference to sampling quality as well as fitness for purpose of the used sampling protocol.

2. Site description

The study area is situated in the Skopeftirio Park of the Municipality of Kesariani, about 3km east of Athens centre. The Skopeftirio Park has a total area of 0.7 km² of almost flat topography. The vegetation within the park includes coniferous trees and grass areas. Park amenities include playgrounds and a gun-shooting club which is fenced and isolated from the rest of the park area. The park has a long history mostly related to the 2nd World War when it was used as an execution place by the Nazis. The area has been also used for military purposes over the years. Recently it has been declared as a historical monument of modern Greece by the Ministry of Culture. After the 50's, different parts of the park have been used as shooting ranges for recreational purposes. Some of these areas have been remediated while others are left in their original state. The previous use of the later is evidenced by small spherical lead shots lying on the ground. Lead shots remaining on the surface soil are eroded over time, releasing Pb into the soil (Petraiki, 2009).

Geologically, the area belongs to the Athens Unit which lithologically comprises solid, white, platform carbonates as well as some pelagic clastic sediments including bodies of basic and ultrabasic rocks and volcano-sedimentary tuffs (Papanikolaou et al., 2004). These basic and ultrabasic rocks are naturally enriched in Cr and contribute to the geochemical fingerprint in the park soil with respect to the concentrations of this metal.

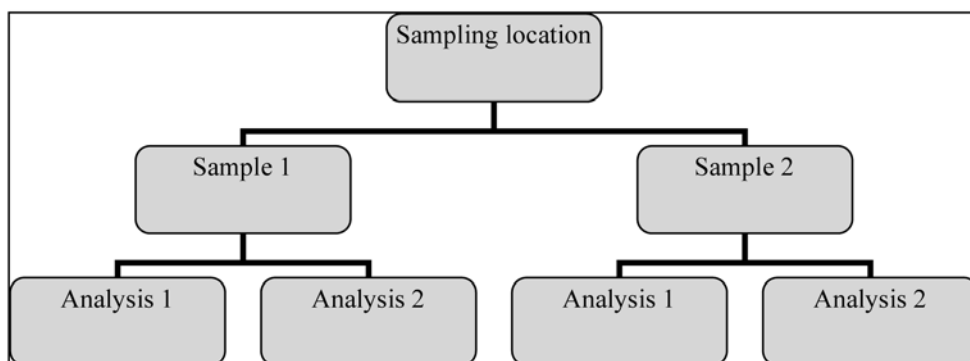


Fig. 1: Schematic balanced design of sampling and analytical duplicates.

3. Methods

3.1. General

When investigating a single sampling target of contaminated land, by applying duplication on sampling and analysis, ANOVA can be applied to the measurement of a parameter on the duplicated samples for estimating the random component of uncertainty (Ramsey and Ellison, 2007). Although a higher level of replication can be used, duplication is the most effective form of replication in sampling studies. Research has shown that a minimum of eight duplicates is required to provide sufficiently reliable estimates of uncertainty (Lyn et al., 2007). The experimental design of this method is the balanced two-stage nested design (Fig. 1).

Based on this, two independent estimates of the population variance can be made, the between sample variance estimate, $s^2_{sampling}$ and the within sample (between analysis) variance estimate, $s^2_{analytical}$. The sum of these represents the measurement variance, s^2_{meas} :

$$s^2_{meas} = s^2_{sampling} + s^2_{analytical}$$

and the standard uncertainty (u) can be estimated as:

$$u = s_{meas} = \sqrt{(s^2_{sampling} + s^2_{analytical})}$$

Subsequently, the estimate of the total variance in the sampling target is given by:

$$s^2_{total} = s^2_{geochemical} + s^2_{sampling} + s^2_{analytical}$$

where:

$s^2_{geochemical}$ = the variance estimate between sampling locations

It should be noted here that because classical ANOVA is a parametric statistical method, it relies on the assumptions of normality of the distribution of the studied parameter and homoscedasticity of the variances. The obtained variance estimates become less reliable when these assumptions do not hold. The first assumption is not met in many instances, particularly in the case of environmental contaminants where analyte concentrations often display log-normal distributions. Furthermore, in order for homoscedasticity to hold, ANOVA assumes no change of the variance within the concentration range. Thus, the estimation of uncertainty by this method is only applicable close to the mean value of the sample's concentration but does not apply in instances of wide range of concentration where a change in measurement precision with concentration is expected. To overcome the problems with non-normally distributed data the use of robust statistics has been suggested (AMC, 1989; Ramsey, 1998). Robust ANOVA treats outlying values by down-weighting them rather than rejecting them.



Fig. 2: Map of Skopeftirio Park at Kesariani in Athens, showing the sampling points [open circles] of surface soil.

3.2. Sampling and chemical analysis

Forty nine top soil samples (0-10cm) were collected from the study area based on a 40m x 40m regular grid. The exact sampling points were located using a GPS (Fig. 2). A hand auger was used to collect a three-fold composite sample over a 1m² area at each sampling point. The sampling precision was estimated by taking sampling duplicates at 5m distance away from the initial sampling point in random direction, in order to reproduce variability accurately so that a realistic estimate of the sampling repeatability variance could be made. A total number of 8 sampling duplicates were also collected.

Test portions of all soil samples weighing 0.250 g each were prepared for chemical analysis by AAS in order to measure the concentrations of Pb and Cr. Analytical duplicates were prepared for each sampling duplicate, for the estimation of sampling and analytical precision. Reagent blanks and three certified soil reference materials were analysed at random positions between the sample test portions for the estimation of analytical bias.

4. Results and discussion

The statistical interpretation of analytical measurements focused on the study of two elements with contrasting properties at this site; Pb and Cr. These elements were selected so that comparisons of the results of the applied sampling methodology could be made. The statistical interpretation of the data was made after applying the quality control procedures discussed below. The frequency distribution for the mean Pb concentration at each sampling point show a positive skew and approaches a log-normal distribution. The concentration of Pb is generally high with an arithmetic mean of ~300µg g⁻¹ and a maximum of ~2400µg g⁻¹ in the soil. The distribution of Cr is less skewed with a mean of ~140µg g⁻¹. The descriptive statistics for Pb and Cr concentrations in the sampled area are summarised in Table 1.

Table 1. Descriptive statistics for Pb and Cr in $\mu\text{g g}^{-1}$ based on the 49 collected samples.

<i>Statistic</i>	<i>Pb</i>	<i>Cr</i>
Mean	309	137
Median	114	136
Standard deviation	491	22
Minimum	30	96
Maximum	2394	198

Table 2. Measured concentrations of Pb and Cr ($\mu\text{g g}^{-1}$) in sampling (S1, S2) and analytical (A1, A2) duplicates.

<i>Cr</i>				
Sample	S1A1	S1A2	S2A1	S2A2
C6	112	117	128	133
E12	125	132	150	142
G11	134	135	144	143
H19	169	178	166	156
I3	110	114	119	108
K11	128	129	121	125
K15	167	171	162	149
M8	105	109	119	118
<i>Pb</i>				
C6	564	557	168	198
E12	42	66	78	108
G11	378	347	90	120
H19	1336	1313	1887	2008
I3	78	78	42	54
K11	120	60	84	102
K15	72	78	48	48
M8	48	54	60	54

Sampling and analytical quality control was applied to estimate only the random measurement errors of Pb and Cr. For this purpose a nested design of sample and analytical duplicates was used. Robust analysis of variance was applied to the concentrations measured for the sampling and analytical duplicates (Table 2) so as to estimate separately the geochemical, sampling and analytical variances (s^2_{geochem} , s^2_{samp} , s^2_{anal}) respectively. The technique was implemented using the computer program ROBAN. EXE, adapted from a published program (AMC, 1989) and available from the (UK) Royal Society of Chemistry web site.

The total variance is:

$$s^2_{\text{total}} = s^2_{\text{geochem}} + s^2_{\text{samp}} + s^2_{\text{anal}}$$

where:

s^2_{total} = the total variance

s^2_{geochem} = the geochemical variance

s^2_{samp} = the sampling variance

s^2_{anal} = the analytical variance

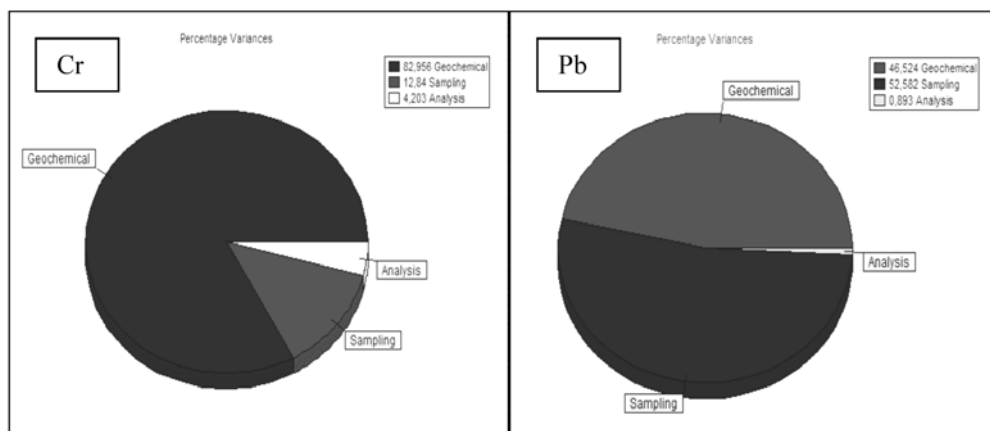


Fig. 3: Relative importance of measurement errors from sampling and analysis and geochemical variability, in the park of Skopectirio, both expressed as proportions of total variance. Robust ANOVA estimates were used.

The proportions of the variances in the total variance were then calculated and displayed as pie charts (Fig. 3). The pie chart for the Cr variance in soil using the duplicate data shows that the analytical precision is acceptable as it contributes 4% to the overall variance and less than 20% to the measurement variance (Ramsey, 1993). Similarly the combined sampling and analytical precision was also acceptable contributing less than 20% to the overall variance.

For the Pb data, the analytical variance (0.9% over total variance) is well within the 4% limit but the high sampling variance of 52.6% of total, makes the measurement precision to be over the 20% acceptable for spatial interpretation of the concentration estimates. However, the mean concentration results can be interpreted within their stated uncertainties. The apparently high proportion of sampling error, in this case, is due primarily to the relatively low geochemical variance of Pb (46.5% of total variance).

The measurement uncertainty (u_R) caused by random variations (under reproducibility conditions) can be estimated from the combination of the sampling and analytical variance described above giving the measurement variance (s_{meas}) as:

$$u_R = s_{meas} = \sqrt{(s_{smp}^2 + s_{anal}^2)}$$

To express the extended random uncertainty (U_R) with a coverage factor $k = 2$ (for 95% confidence) this gives:

$$U_R = k u_R = 2s_{meas}$$

As uncertainty relative to the mean concentration x becomes:

$$Ur\% = 200 s_{meas} / x$$

Where x is the estimated mean concentration of the analyte in the site. At this site the relative random uncertainty estimated from the 8 duplicate samples is 15% and 169% for Cr and Pb respectively. The interpretation of this, assumes that it does not change as a function of concentration. The great difference between the uncertainties estimated for Cr and Pb is attributed to the differences in concentrations between the duplicate samples for each element. Specifically, the within location (sampling) variance for Pb is greater than the between location (geochemical) variance, while the opposite is observed for Cr. This in turn is related to the origin of Cr and Pb in the park soil and the subsequent de-

gree of heterogeneity in heavy metal concentrations in the soil for the same spatial scale.

Lead which is dispersed in soil after the erosion of lead-shots is present within the park area only in few hot-spots, the dimensions of which may be smaller than the 5m distance separating the sampling duplicates. This extreme small-scale spatial variation is characteristic for Pb contamination in the site, contributing to the great magnitude of measurement uncertainty. For Cr, the relative measurement uncertainty is lower indicating a more homogeneous distribution of elemental concentrations. This is explained by the geological origin of this element which is dispersed in soil following the pedological processes influencing the release of the metal and its mobilization from the underlying basic rocks into the soil. Thus, the variability of the element in soil is captured by the 40 m distance separating the sampling locations. It should be noted that the analytical variance is insignificant compared to that of sampling for both Pb and Cr, indicating that chemical analysis is not a major source of error during the measuring process.

The estimates of random uncertainty for the sampling protocol used in the survey allow the assessment of its 'fitness-for-purpose' for this sampling target. 'Fitness-for -purpose' is defined as the property of data, produced by a measurement process that enables a user of the data to make technically correct decisions for a stated purpose (Thompson and Fearn, 1990). For Cr, since the proportion of measurement uncertainty contributes less than the empirical limit of 20% to the total variance, logistical factors, related mostly to the ease of applying the sampling protocol, have the main role in the selection of the most appropriate sampling scheme for the objective of estimating the mean metal concentration in the soil. For the particular field the optimal sampling scheme for this objective appears to be the regular grid because it is fast and simple to set up and should therefore be least prone to location errors. The grid size of 40m is also judged appropriate for delineating the Cr concentrations across the site. On the contrary for Pb, the used sampling protocol is judged as not fit-for-purpose because the magnitude of sampling variance exceeds that of geochemical variance. As a consequence it does not allow the realistic spatial interpretation of the Pb data across the site. In this instance a different sampling protocol has to be applied in order to delineate the element's concentration within the sampled area. Triangular grids are usually performing better when the aim is to delineate contamination hot-spots within an area.

5. Conclusions

This survey demonstrated that it is possible to estimate uncertainty in field sampling by using ANOVA following a nested design of sampling and analytical duplicates on an area of contaminated land. The heterogeneity of the elemental concentration within the sampling target affects the magnitude of precision and makes the sampling variance the dominant factor in the estimation of measurement uncertainty.

The performance of the sampling protocol has been evaluated and compared with criteria based on fitness-for-purpose considerations. The 40m x 40m grid used in this trial proved to be fit-for-purpose for Cr but suspect for Pb, using a fitness-for-purpose criterion of 20%. The main factor affecting the suitability of the sampling protocol is the degree of heterogeneity of the sampling target. A large degree of variation on the estimated mean was observed for Pb, showing the significant role of soil variability on the outcome of analytical measurements on site investigations. Estimates of the uncertainty associated with the sampling protocol could be made. In the instance of Pb, the large sampling precision dominates the total uncertainty. The main reason is the great variability in Pb concentration at the sample target related to its origin from the lead shots. This is contrasted to the more homogeneously distributed Cr concentration in soil related to the local geology.

6. References

- Analytical Methods Committee. 1989. Robust Statistics – How not to reject outliers, Part 1, Basic Concepts, *Analyst*, 114, 1693-1697.
- ISO 1993. *Guide to the Expression of Uncertainty in Measurement (GUM)*. Geneva (2nd printing 1995).
- Lyn, J.A., Ramsey, M.H., Coad, D.S., Damant, A.P., Wood, R., Boon, K.A. 2007. The duplicate method of uncertainty estimation: are eight targets enough?, *Analyst*, 132, 1147-1152.
- Papanicolaou, D., Lozios, S., Soukis, K. and Skourtsos, E. 2004. Geological structure of the allochthon system of Athens. *Proceedings of the 10th Conference of the Greek Geological Society*, Thessaloniki, vol. XXXVI, 1550-1559.
- Petrakaki, N. 2009. Geochemical distribution of Pb in shooting range soils: The case of Kesariani's shooting range, *MSc Thesis*, University of Athens, Athens (in Greek)
- Ramsey M.H. and Ellison S.L.R. (eds) Eurachem/EUROLAB/CITAC/Nordtest/amc Guide. 2007. *Measurement uncertainty arising from sampling; a guide to methods and approaches*, Eurachem.
- Ramsey, M.H. 1993. Sampling and analytical quality control (SAX) for improved error estimation in the measurement of Pb in the environment using robust analysis of variance, *Applied Geochemistry*, Suppl. Issue No.2, 149-153.
- Ramsey, M.H. 1994. Error estimation in environmental sampling and analysis, in: B. Market, Ed. *Environmental Sampling for Trace Analysis*, VCH, Weinheim, p. 93-108.
- Ramsey, M.H. 1998. Sampling as a source of measurement uncertainty: techniques for quantification and comparison with analytical sources, *Journal of Analytical Atomic Spectrometry*, 13, 97-104.
- Ramsey, M.H. and Argyraki, A. 1997. Estimation of measurement uncertainty from field sampling: Implications for the classification of contaminated land, *The Science of the Total Environment*, 198, 243-257.
- Ramsey, M.H. and Thompson, M. 2007. Uncertainty from sampling, in the context of fitness for purpose, *Accreditation and Quality Assurance*, 12, 503-513.
- Taylor, P.D., Ramsey, M.H., Potts, P.J. 2005. Spatial contaminant heterogeneity: quantification with scale of measurement at contrasting sites, *Journal of Environmental Monitoring*, 7, 1364-1370.
- Thompson, M. and Fearn, T. 1990. What exactly is fitness for purpose in analytical measurement?, *Analyst*, 121, 273-278.
- Thompson, M. and Ramsey, M.H. 1995. Quality concepts and practices applied to sampling – an exploratory study, *Analyst*, 120, 261-270.

GEOCHEMICAL CHARACTERIZATION OF NATURAL GAS MANIFESTATIONS IN GREECE

D'Alessandro W.¹, Brusca L.¹, Martelli M.¹, Rizzo A.¹ and Kyriakopoulos K.²

¹ Istituto Nazionale di Geofisica e Vulcanologia, sezione di Palermo, via U. La Malfa 153, 90146 Palermo, Italy, w.dalessandro@pa.ingv.it

² National and Kapodistrian University of Athens, Dept. of Geology and Geoenvironment, Panepistimioupolis, 157 84 Ano Ilissia, Greece, ckiriako@geol.uoa.gr

Abstract

The Greek region is characterized by intense geodynamic activity with widespread volcanic, geothermal and seismic activity. Its complex geology is reflected in the large variety of chemical and isotopic composition of its gas manifestations.

Basing on their chemical composition the gases can be subdivided in three groups, respectively CO₂, CH₄ or N₂-dominated. On oxygen-free basis these three gases make up more than 97% of the total composition. The only exceptions are fumarolic gases of Nisyros that contain substantial amounts of H₂S (up to more than 20%) and one sample of Milos that contains 15% of H₂. CO₂-dominated gases with clear mantle contribution in their He isotopic composition (R/R_a corrected for air contamination ranging from 0.5 to 5.7) are found along the subduction-related south Aegean active volcanic arc and on the Greek mainland close to recent (upper Miocene to Pleistocene) volcanic centers. These areas are generally characterized by active or recent extensive tectonic activity and high geothermal gradients. On the contrary, gases sampled in the more external nappes of the Hellenide orogen have generally a CH₄- or N₂-rich compositions and helium isotope composition with a dominant crustal contribution (R/R_a corr < 0.2).

The chemical and isotopic characteristics of the emitted gas display therefore a clear relationship with the different geodynamic sectors of the region. Gas geochemistry of the area contributes to a better definition of the crust-mantle setting of the Hellenic region.

Key words: natural gas manifestations, gas chemistry, He- and C- isotope composition.

1. Introduction

The Hellenic territory has a very complex geodynamic setting deriving from a long and complicated geological history. Many of the geologic features of Greece are still argument of strong debate and Zeilinga de Boer (1989) defined its geodynamic situation as "The Greek enigma". The Hellenic territory is also the site of intense seismic activity (Burton et al., 2004) and enhanced geothermal gradient (Fytikas and Kolios, 1979). This together with the presence of an active volcanic arc favours the existence of many cold and thermal gas manifestations.

Until now only scarce data on chemical and isotopic composition of these gas manifestations have been published. Furthermore these data are either limited to single volcanic/geothermal systems

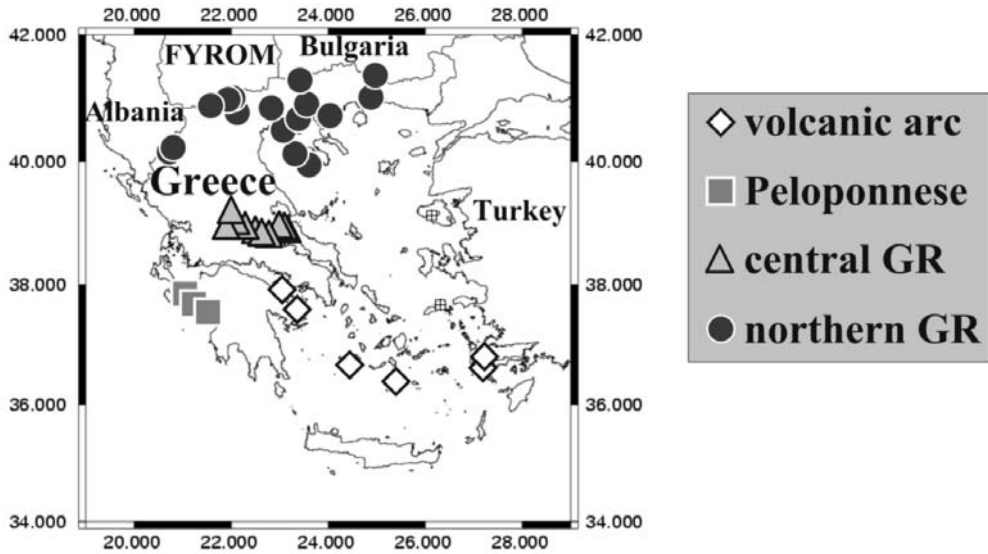


Fig. 1: Geographic distribution of the sampled gas manifestations.

(Marini and Fiebig, 2005; D'Alessandro et al., 2008) or if considering geographically wider areas they refer only to their chemical (Minissale et al., 1989; 1997) or to their noble gas isotopic (Shimizu et al., 2005) composition. In the present study both the chemical and the isotopic composition (C, He) of 52 samples collected along the whole Hellenic territory has been analysed in an attempt to reveal possible relationships with the geodynamic situation.

2. Study area and methods

2.1 Geological setting

The Aegean region is a concentrate of the main geodynamic processes that shaped the Mediterranean region: oceanic and continental subduction, mountain building, high-pressure and low-temperature metamorphism, backarc extension, post-orogenic collapse, metamorphic core complexes, gneiss domes are the ingredients of a complex evolution that started at the end of the Cretaceous with the closure of the Tethyan ocean along the Vardar suture zone (Jolivet and Brun, 2008).

The Greek and west Anatolian region was affected by a Tertiary and Quaternary volcanism with an orogenic signature. The oldest products are of upper Eocene-Oligocene age and are exposed in limited volumes in the northern part of Greece. The volcanic activity reached a climax in the Lower Miocene and was exhausted by the Middle Miocene (Yilmaz et al., 2001).

The Paleogene Hellenide orogeny of Greece and its eastward continuation into western Turkey resulted from collision of the Apulian microcontinental fragment in the Eocene to Oligocene with the Pelagonian, Rhodope, and Serbo-Macedonian fragments, which had previously accreted to the southern margin of Eurasia in the Cretaceous. Subsequent extension in the Aegean was rapid, likely due

to subduction rollback over residual oceanic crust of the African plate, whereas Anatolia had been bounded by African continental crust south of Cyprus since the Early Miocene. This regional extension and the thermal effects of asthenospheric upwelling, related to changes in the geometry of subducting slabs, have been interpreted as causing magma genesis principally within the lithospheric mantle (Pe-Piper and Piper, 2002).

At the south Aegean Volcanic Arc the volcanic activity started during the Upper Pliocene (Fytikas et al., 1986) and is still active today mainly in the form of solfatar activity. The calc-alkaline volcanic activity of Southern Aegean region developed in various volcanic centers from Sousaki to Nisyros through Methana-Poros, Milos and Santorini. The volcanic products are dominated by lava domes and lava flows with associated minor pyroclastic breccias and felsic ignibritic covers (Mitropoulos et al., 1987). The final activity of this orogenic cycle is characterized by the presence of K-rich shoshonites and latites with ultrapotassic character.

2.2 Sampling and analytical methods

A total of 52 samples were collected along the whole Hellenic territory (Fig. 1). Free gas samples were taken from natural gas manifestations like fumarolic discharges, soil gases, mofettes, gas bubbling in cold or thermal waters and also from wells drilled either for groundwater or carbon dioxide abstraction or for geothermal exploration. Water for dissolved gas analyses were collected in glass vials sealed underwater.

Fumarolic gas discharges and soil gases were collected at a depth of 50 cm through steel or nylon tubes connected to a syringe while bubbling gases were collected through inverted funnels. Samples were then stored into glass flasks equipped with vacuum stopcocks.

Gas concentrations were measured at INGV in Palermo using the GC Perkin Elmer Clarus 500 equipped with Carboxen 1000 columns, HWD and FID detectors with methanizer. The gas samples were injected through an automated injection valve with a 1000 μ L loop. Calibration was made with certified gas mixtures. Analytical precision (1σ) was always better than $\pm 5\%$. The detection limits were about 1 ppm vol. for CH₄, 2 ppm vol. for H₂, 6 ppm vol. for He, 20 ppm vol. for CO₂, 200 ppm vol. for O₂ and 500 ppm vol. for N₂. He concentrations less than 6 ppm were determined during He isotopic analysis with a detection limit of about 0.1 ppm. Dissolved gases in water samples were extracted using the head-space equilibration method according to Capasso and Inguaggiato (1998).

Analyses of carbon isotopes of CO₂ were carried out by using a Finnigan Delta plus mass spectrometer. Values of carbon isotope of CO₂ are expressed in $\delta\text{‰}$ vs. V-PBD, accuracy being 0.1 $\delta\text{‰}$. The method proposed by Capasso et al. (2005) was used for determination of the $\delta^{13}\text{C}$ of total dissolved inorganic carbon (TDIC). The theoretical equilibrium composition of a free CO₂ gas phase was calculated considering the fraction of all dissolved carbon species (H₂CO₃, HCO₃⁻ and CO₃²⁻) and the relative fractionation factors.

The He-isotope ratio in the gas samples was analysed directly from the sample bottles after purification in the high-vacuum inlet line of the mass spectrometer. The isotope composition of dissolved He was analysed by headspace equilibration, following the method proposed by Inguaggiato and Rizzo (2004). He isotopes were measured with a modified double-collector mass spectrometer (VG 5400-TFT). ³He/⁴He ratios, determined against an air standard, are referred here to the atmospheric ratio ($R_a = 1.386 \times 10^{-6}$) as R/R_a . Measured values were corrected for the atmospheric contamination of the sample on the basis of its ⁴He/²⁰Ne ratio (Sano and Wakita, 1985) determined with a quadrupole mass spectrometer (QMS, VG Quartz).

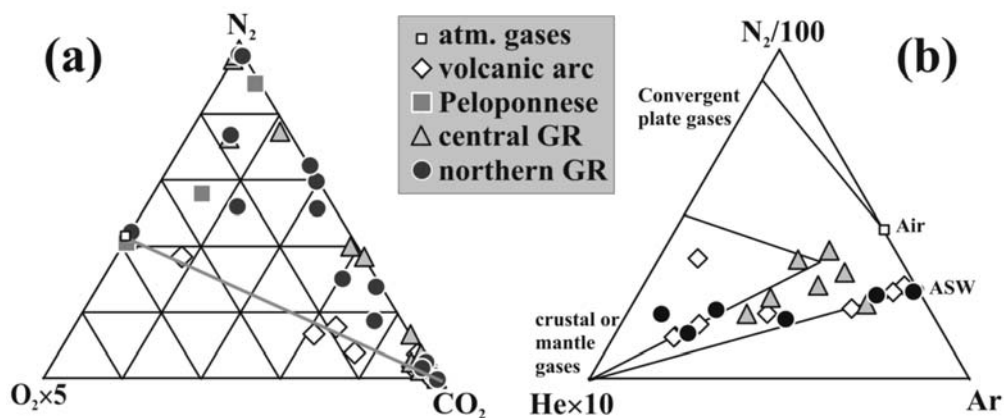


Fig. 2: a) O_2 - N_2 - CO_2 triangular plot and b) He - N_2 - Ar triangular plot. Symbols as in Fig. 1 refer to the geographical distribution of the sampling sites.

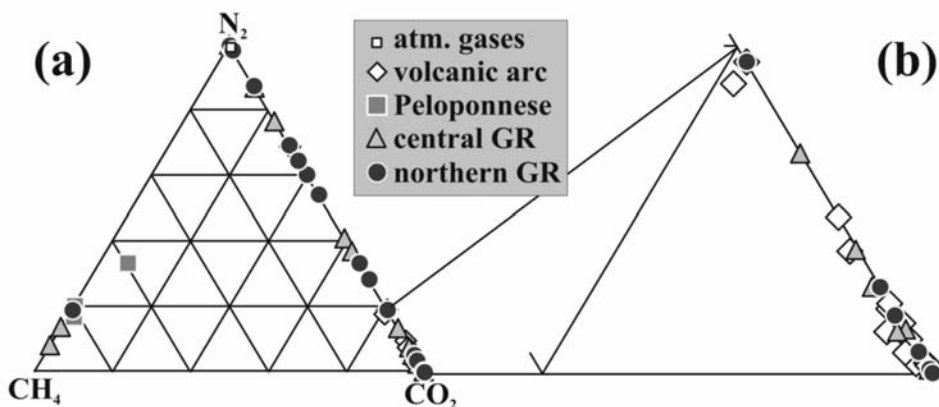


Fig. 3: a) CH_4 - N_2 - CO_2 triangular plot. b) enlargement of the CO_2 vertex. Symbols as in Fig. 1 refer to the geographical distribution of the sampling sites.

3. Results and discussion

3.1 Chemical composition of the gases

The results of the chemical analyses are listed in Table 1. They are reported as dry gases excluding water vapour, which is significant only in the fumarolic gas samples of Nisyros. The gas samples display a very large variability in chemical composition. Helium ranges from 0.4 up to 2940 ppm and shows a fair positive correlation with N_2 . Only 21 samples have detectable H_2 (> 2 ppm) concentrations ranging from 5 up to 149000 ppm. Oxygen concentrations range from below the detection limit (< 200 ppm – 11 samples) up to 193000 ppm. The concentrations of N_2 , CH_4 and CO_2 range from 600 to 978000, from less than 1 to 915000 and from 27 to 993000 ppm respectively. The last three species represent always the main gas component and all the samples can be subdivided in N_2 , CH_4 and CO_2 dominated gases. On oxygen-free basis these three gases represent generally more than 97% of the total composition. The only exceptions are fumarolic gases of Nisyros that contain substantial amounts

Table 1. Chemical and isotopic composition of gas samples.

sample	lat	long	date	He	H ₂	O ₂	N ₂	CH ₄	CO ₂	δ ¹³ C(CO ₂) ‰ vs PDB	R/Ra	He/Ne	R/Ra c	±1σ
		dd-mm-yy	ppm	ppm	ppm	ppm	ppm	ppm	ppm	%c				
Nisyros (PP9S)	36.583	27.166	10-10-07	30	16000	1600	8100	1760	743000	-0.6	5.69	22	5.76	0.048
Nisyros (AM) 36.582	27.164	11-10-07	33	9230	500	6200	6200	805	809000	-0.4	5.78	40	5.82	0.063
Nisyros (S4)	36.578	27.169	12-10-07	27	6200	1100	4900	4400	792000	-0.9	5.72	12	5.86	0.048
Thermia (Kos)	36.814	27.192	25-07-08	43	< 2	38400	89600	427	847000	n.d.	n.d.	n.d.	n.a.	n.a.
Palea Kameni	36.399	25.380	07-05-96	1.1	3580	750	6400	4	980000	-1.1	3.34	4	3.52	0.053
Santorini Kameni B	36.404	25.396	06-10-07	7	11700	40800	178000	119	759000	0.5	3.35	2	3.81	0.023
Milos Mad 1	36.694	24.482	12-10-07	69	< 2	2800	73000	4880	896000	-0.9	3.37	38	3.39	0.034
Milos C3 (Fyriplaka)	36.668	24.492	01-06-07	8	1870	145000	581000	471	264000	-1.5	n.d.	n.d.	n.a.	n.a.
Milos 1 (Sinopi)	36.727	24.428	05-09-08	50	< 2	9200	39100	2640	944000	n.d.	2.97	13	3.02	0.004
Milos 2 (Adamas)	36.725	24.451	12-08-08	15	13	425	20700	1400	966000	-1.3	3.04	6	3.15	0.004
Milos 3 (Paleochori)	36.670	24.501	12-08-08	14	29	3800	12500	7450	957000	-0.4	n.d.	n.d.	n.a.	n.a.
Milos 6 (Paleochori)	36.668	24.501	05-09-08	80	149000	52100	144000	11000	657000	-0.7	n.d.	n.d.	n.a.	n.a.
Methana (MET 46)*	37.598	23.406	11-06-06	0.5	106	< 200	4900	42	966000	-1.0	2.34	3	2.48	0.034
Methana (Pausanias)*	37.638	23.360	23-06-06	0.5	< 2	5600	30900	17	970000	-2.0	2.06	2	2.22	0.063
Methana (Thiafy) *	37.597	23.405	24-06-06	20	29	6700	42200	717	942000	-1.4	2.55	22	2.57	0.022
Sousaki well	37.933	23.087	03-06-06	1.3	22	270	4900	61	987000	-1.5	0.64	7	0.62	0.013
Sousaki cave	37.935	23.087	03-06-06	37	< 2	1000	25700	10800	966000	-1.7	0.20	120	0.19	0.005
Loutra Kilini	37.857	21.111	28-05-07	212	19	600	167000	803000	17100	-15.4	0.05	12	0.03	0.002
Katakolo mare	37.645	21.319	28-05-07	454	< 2	53600	190000	741000	2300	n.d.	0.08	119	0.08	0.007
Katakolo volcano 3	37.642	21.316	28-05-07	247	466	35900	317000	563000	69100	-5.1	0.04	43	0.04	0.001
Termopotamos	38.858	23.049	09-11-05	0.4	< 2	6200	26500	298	949000	-2.9	0.87	2	0.85	0.045
Ipatis	38.897	22.277	14-09-06	74	5	8400	52400	4600	929000	-5.2	n.d.	n.d.	n.a.	n.a.
Ipatis 2	38.894	22.281	14-09-06	139	< 2	< 200	25400	5400	958000	n.d.	0.06	974	0.06	0.001
Kammena Yourla	38.774	22.776	27-03-08	861	< 2	5100	762000	1783	232000	-9.4	0.48	222	0.48	0.010
Psoroneria 1	38.803	22.497	27-03-08	827	< 2	4000	407000	612	588000	-6.0	0.07	455	0.07	0.003
Psoroneria 2	38.804	22.495	27-03-08	890	< 2	< 200	367000	643	624000	-5.3	0.08	660	0.08	0.003
Amplas	38.922	22.052	28-03-08	57	24	600	81600	915000	100	n.d.	0.05	56	0.04	0.001
Archani #	38.983	22.162	28-03-08	25	< 2	5540	961000	33900	27	n.d.	n.d.	n.d.	n.a.	n.a.

Table 1. Continued

sample	lat	long	date	He	H ₂	O ₂	N ₂	CH ₄	CO ₂	δ ¹³ C(CO ₂) ‰ vs PDB	R/Ra	He/Ne	R/Ra c	±1σ
		dd-mm-yy	ppm	ppm	ppm	ppm	ppm	ppm	ppm	%				
Platystomo #	38.972	22.097	26-06-09	103	34	425	853000	135000	1100	-24.3(°)	0.10	15.7	0.09	0.002
Gialtra	38.850	22.987	29-03-08	397	<2	39000	864000	954	130000	-10.7	0.44	81	0.44	0.014
Edipos 2	38.855	23.049	29-03-08	1.8	<2	<200	2600	861	991000	-3.0	0.42	55	0.42	0.005
Ilion	38.852	23.128	29-03-08	102	<2	800	75500	1632	919000	-2.6	0.25	341	0.25	0.006
Termopiles	38.793	22.528	28-03-08	213	<2	<200	133000	745	855000	-5.8	0.17	544	0.17	0.010
Smokovo	39.130	22.012	11-10-08	103	28	<200	136000	850000	100	n.d.	0.05	55	0.04	0.007
Termopigi	41.281	23.363	05-10-04	33	<2	800	13600	622	978000	-2.1	0.60	110	0.60	0.004
Pozar	40.971	21.914	27-05-08	475	<2	61700	652000	1	289000	-5.1	0.72	68	0.72	0.006
Promachoi	40.991	21.980	27-05-08	259	<2	34700	820000	<1	118000	-7.4	1.27	30	1.27	0.012
Nimfopetra	40.689	23.355	30-05-08	2540	15	2700	968000	1680	5400	n.d.	0.05	304	0.05	0.000
Elefiere	40.736	24.091	30-05-08	27	<2	800	51700	526	919000	-0.8	0.48	19	0.47	0.004
Nigrita	40.898	23.554	30-05-08	1.2	<2	<200	1300	26	988000	-1.7	0.33	20	0.32	0.003
Sani	40.102	23.313	31-05-08	597	8	<200	192000	814000	3300	n.d.	0.63	2823	0.63	0.005
Amarantos	40.175	20.731	02-06-08	7	<2	192700	777000	10	1200	n.d.	n.d.	n.d.	n.a.	n.a.
Pikrolimni #	40.830	22.827	29-05-08	313	<2	19300	328000	22	653000	-6.4(°)	0.33	5	0.31	0.005
Souroti #	40.467	23.086	30-05-08	45	<2	3390	283000	951	712000	-3.0(°)	0.35	5	0.33	0.009
Doumbia #	40.530	23.320	30-05-08	537	<2	9890	536000	789	453000	-5.1(°)	0.40	12	0.39	0.014
A. Paraskevi #	39.924	23.590	31-05-08	6	22	1780	601000	915	396000	-1.4(°)	n.d.	n.d.	n.a.	n.a.
Kabasilos #	40.106	20.708	02-06-08	1320	<2	1420	978000	2320	16700	-10.3(°)	0.14	307	0.14	0.005
XNT-1 (Thermes)	41.348	25.012	26-08-08	2940	<2	<200	631000	1010	346000	-2.5	0.43	218	0.43	0.004
Marina 2	40.861	21.491	04-03-07	25	<2	4600	35400	1660	950000	-0.3	0.24	31	0.24	0.003
Mesochori 2	40.872	21.528	01-06-08	1.7	60	<200	3100	353	992000	-1.5	0.66	6	0.64	0.005
Kampos	40.903	21.488	01-06-08	0.4	<2	<200	600	22	993000	-1.7	0.46	3	0.40	0.003
Ikaria (Ag. Kyr. I)	37.628	26.308	01-10-06	58	<2	86600	860000	<1	35900	-19.6	n.d.	n.d.	n.a.	n.a.

R/Ra_a is the Helium isotopic ratio normalised to the atmospheric ratio while R/Ra_c is the same ratio corrected for air contamination considering the measured He/Ne values. ± 1σ error of the R/Ra_c value. * Analyses previously published in D' Alessandro et al, 2008. # Dissolved gas sample. °Theoretical equilibrium values of CO₂ calculated from the measured total dissolved inorganic carbon. n.d. not determined, n.a. not applicable.

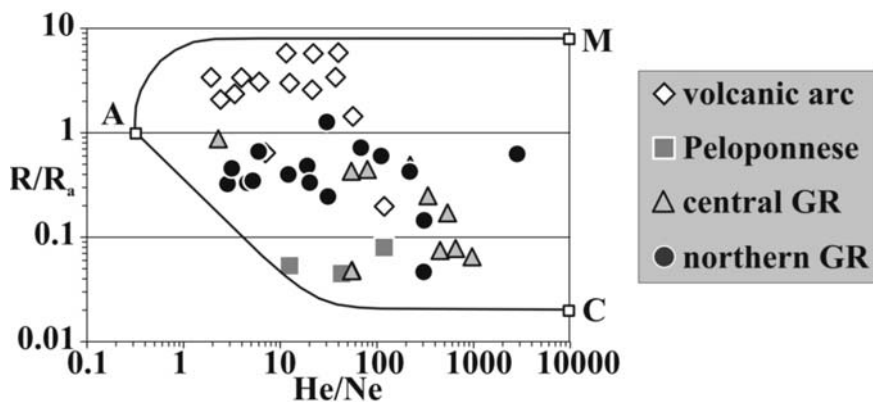


Fig. 4: R/R_a vs. He/Ne plot of the natural gas manifestations of Greece. A, M and C represent three possible end-members: atmospheric air, MORB-like mantle and crust. The mixing lines between A and M and between A and C are also plotted.

of H_2S (up to more than 20%) and one sample of Milos that contains 15% of H_2 .

The O_2 - N_2 - CO_2 triangular plot (Fig. 2a) reveals that only few samples plot close to the point representing atmospheric air excluding important contaminations for most samples. Furthermore most samples display N_2/O_2 ratios much higher than the atmospheric one indicating that the atmospheric component deriving from meteoric recharge has probably been modified by redox reactions in the subsoil. Great contributions of N_2 deriving from slab-sediments can be ruled out by the N_2/Ar ratios, which are generally close to the atmospheric, or the air-saturated water ratios (Fig. 2b). Furthermore most of the samples show a strong contribution of helium deriving either from a crustal or a mantle source.

The CH_4 - N_2 - CO_2 triangular plot (Fig. 3a) shows that only 6 samples display a CH_4 -dominated composition comprising all 3 samples collected in the Peloponnese, two samples of central Greece and one of northern Greece. N_2 - and CO_2 -dominated gases display on the same plot a mixing line (Fig. 3a). To the latter group, the most abundant (32 samples), belong all the samples collected along the active south Aegean volcanic arc (Fig. 3b) except one sample of Milos (Fyriplaka) contaminated with atmospheric air (Fig. 2a). Most of the N_2 -dominated gases were collected in northern Greece (Fig. 3a).

3.2 Isotopic composition of the gases

The results of the isotopic analyses are listed in table 1. He isotopic values, expressed as $^3He/^4He$ ratio normalised to the atmospheric one ($R_a = 1.386 \times 10^{-6}$), range from 0.03 to 5.78 R/R_a . Measured values corrected for the atmospheric contamination of the sample on the basis of its $^4He/^{20}Ne$ ratio (Sano and Wakita, 1985) display a similar range (R/R_a corr 0.03 – 5.86). Such a wide range is indicative of different sources for the helium in the studied gases.

In Figure 4 the measured R/R_a values are plotted against the $^4He/^{20}Ne$ ratio together with the characteristic composition of three possible sources, the atmosphere (A), a MORB-like mantle (M) and the crust (C). The plot excludes strong atmospheric contaminations because only few samples display low $^4He/^{20}Ne$ ratios close to the characteristic end-member of atmospheric air. Samples col-

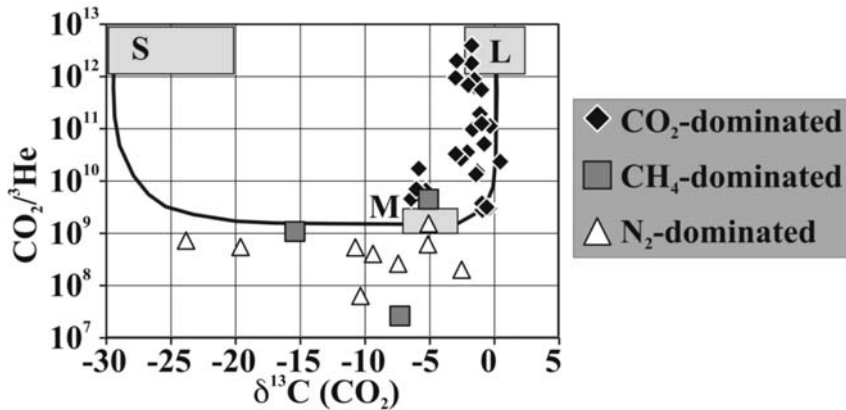


Fig. 5: $\text{CO}_2/{}^3\text{He}$ vs. $\delta^{13}\text{C}(\text{CO}_2)$ plot of the natural gas manifestations of Greece. The endmember compositions for sediments (S), MORB-like mantle (M) and limestones (L) are $\delta^{13}\text{C}(\text{CO}_2) = -30\text{‰}$, -5‰ and 0‰ ; and $\text{CO}_2/{}^3\text{He} = 1 \cdot 10^{13}$, $2 \cdot 10^9$ and $1 \cdot 10^{13}$, respectively (Sano and Marty, 1995).

lected along the volcanic arc display the highest mantle contribution with all but the samples collected at Sousaki having values above 1 R/R_a . A few samples, among which are all those collected in the Peloponnese, display a prevailing crustal imprint ($R/R_a < 0.2$). Most of the samples display intermediate helium isotopic composition (R/R_a between 0.2 and 1) evidencing contributions of both deep sources (mantle and crust).

The carbon isotopic composition of CO_2 in the free gas samples ranges from -19.6 to $+0.5 \delta^{13}\text{C} \text{‰}$ (vs. V-PDB). For the dissolved gas samples the theoretical isotopic composition of gaseous CO_2 in equilibrium with the liquid phase has been calculated from the following measured parameters, temperature, $\delta^{13}\text{C}$ of the total dissolved inorganic carbon, dissolved CO_2 concentration and alkalinity, considering all fractionation factors between gas and all dissolved carbon species (Zhang et al., 1995). The obtained values range from -24.3 to $-1.4 \delta^{13}\text{C} \text{‰}$. All CO_2 -dominated gases display a narrower range spanning from -6.4 to $+0.5 \delta^{13}\text{C} \text{‰}$ and in this group the samples collected along the volcanic arc have still narrower range (-2.0 - $+0.5 \delta^{13}\text{C} \text{‰}$).

Considering the $\delta^{13}\text{C}(\text{CO}_2)$ values and the $\text{CO}_2/{}^3\text{He}$ ratios (Fig. 5), samples collected along the volcanic arc plot on the mixing line between the mantle and the limestones end-members. This pattern further excludes important contributions from organic sediments to the fluids deriving from the descending slab. A small contribution from organic sediments can be detected in the CO_2 -dominated gases of mainland Greece deriving probably from crustal sources. On the contrary CH_4 - and N_2 -dominated gases display sometimes a strong organic contribution and low $\text{CO}_2/{}^3\text{He}$ ratios probably due to CO_2 -depleting processes (carbonate precipitation, CO_2 reduction, etc.).

3.3 Geographical distribution

Measured R/R_a values of the Greek gas manifestations display an increasing trend going from north to south and from west to east (Fig. 6). A similar trend has been previously also evidenced by Shimizu et al. (2005) for the south Aegean volcanic arc. Based on the ${}^{87}\text{Sr}/{}^{86}\text{Sr}$ ratios of the least evolved rocks, they attributed this pattern to increasing crustal contamination of ascending magma.

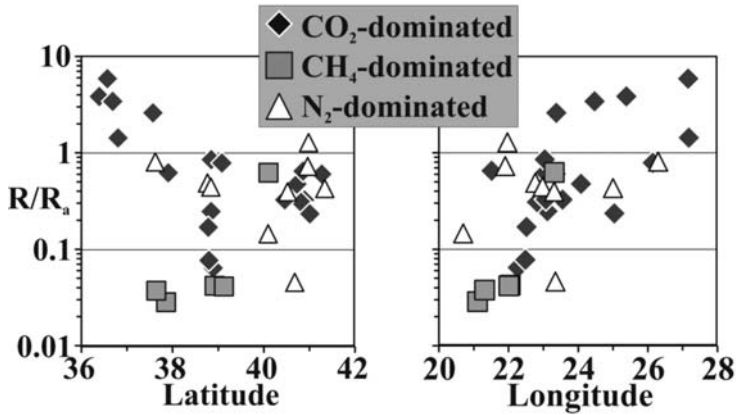


Fig. 6: Variation of measured R/R_a values of the Greek gas manifestations vs. latitude (left) and longitude (right) of the sampling site.

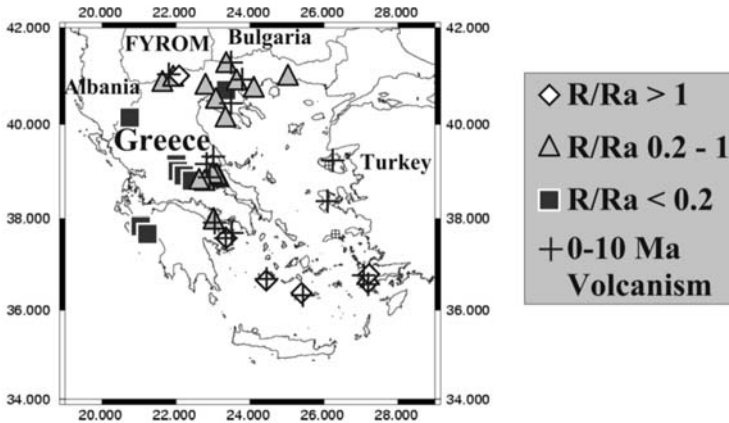


Fig. 7: Relationships between He isotopic compositions measured in the natural gases and the recent volcanic manifestations of the Hellenic territory.

Crustal contamination along the volcanic arc could be due to several processes. For example, Pe-Piper and Piper (2005) subdivided the arc in an older part comprising Methana and Milos and a more recent part comprising Santorini and Nisyros. Volcanism is considered to be slowly decreasing in the western sector, and the ascent of new magma from the mantle, being currently much lower than in the eastern part, supports a lower ^3He flux. A further significant difference between the eastern and western parts of the arc is in the type of volcanism. Santorini and Nisyros (in the east) are both characterized by central stratovolcanoes with large calderas and frequent eruptive activity during historical time (Pe-Piper and Piper, 2002). This volcanic environment facilitates the easy and rapid ascent of mantle fluids, and a corresponding lower probability of crustal contamination. In contrast, Methana and Milos (in the west) exhibit numerous monogenic centres accompanied by lower eruptive rates (Fytikas et al., 1986), which is compatible with a higher crustal contamination in the emitted fluids.

Gases with a clear crustal imprint in their He isotopic composition ($R/R_a < 0.2$) are found almost exclusively in the western part of Greece. In this area where the more external nappes of the Hellenide orogen crop out, the thickness of the crust reaches the highest values of the Hellenic region (> 40 km).

Gases with intermediate He isotopic composition ($R/R_a 0.2 - 1$) have been collected across the most internal terrains of the Hellenide orogen. In this area crustal thinning, due to extensive tectonics, favoured the recent (< 10 Ma) volcanic activity and either direct or magma-mediated mantle fluids ascent. This area is also the site of enhanced geothermal gradient (Fytikas and Kolios, 1979). Noteworthy almost all sites where gas samples with intermediate He isotopic composition (Fig. 7) have been collected fall close to recent volcanic centers and/or within the zones of highest geothermal gradient.

4. Conclusions

The 52 gas manifestations sampled along the whole Hellenic territory can be subdivided, on the basis of their chemical composition, in CH_4 - N_2 - and CO_2 -dominated. The former two groups, almost all collected in the western part of the country, display also very low R/R_a values (< 0.2) highlighting their crustal origin. This region is characterised by a high crustal thickness (up to > 40 km) and absence of recent (< 10 Ma) volcanic manifestations. On the contrary samples collected in the eastern part of Greece, where instead the crust is thinner (20 – 30 km) and recent volcanic manifestations are widespread, the gases have generally CO_2 -dominated composition and intermediate R/R_a values (0.2 – 1) evidencing a significant contribution from a mantle source. Finally, a strong mantle contribution was found in the samples collected along the south Aegean active volcanic arc, which all display a CO_2 -dominated composition and high R/R_a values (1 – 5.8). CO_2 carbon isotopic composition and the $\text{CO}_2/{}^3\text{He}$ ratio of the latter gases evidence a mixing between a mantle and a limestone source excluding any contribution from sedimentary material. This is also confirmed by the measured N_2/Ar ratios, which are all close either to the atmospheric or to the air-saturated water ratio. A small contribution from sedimentary material, probably of crustal origin, can be highlighted in the CO_2 -dominated gases of continental Greece.

5. Acknowledgments

We kindly acknowledge all the Greek colleagues that helped us either in the field or with precious informations about the sampling sites. Among them we remember E. Dotsika, Prof. N. Lambrakis, S. Karakatsanis, K. Katsanou, N. Kolios, M. Margaritopoulos, G. Michas, G. Papadakis.

6. References

- Burton, P.W., Xu, Y., Qin, C., Tselentis, G., Sokos, E., 2004. A catalogue of seismicity in Greece and the adjacent areas for the twentieth century. *Tectonophysics*, 390, 117-127.
- Capasso, G. and Inguaggiato, S., 1998. A simple method for the determination of dissolved gases in natural waters. An application to thermal waters from Vulcano Island. *Applied Geochemistry* 13, 631-642.
- Capasso, G., Favara, R., Grassa, F., Inguaggiato, S., Longo, M., 2005. On-line technique for preparation and measuring stable carbon isotope of total dissolved inorganic carbon in water samples ($\delta^{13}\text{C}_{\text{TDIC}}$). *Annals Geophysics* 48, 159-166.
- D'Alessandro W., Brusca L., Kyriakopoulos K., Michas G., Papadakis G., 2008. Methana, the westernmost active volcanic system of the south Aegean arc (Greece): insight from fluids geochemistry. *Journal of Volcanology and Geothermal Research* 178, 818-828.

- Fytikas, M. and Kolios, N., 1979. Preliminary heat flow map of Greece. In: Cermak, V., Rybach, L., (eds) *Terrestrial heat flow in Europe*. Springer-Verlag, pp 197–205.
- Fytikas, M., Innocenti, P., Manetti, R., Mazzuoli, R., Peccerillo, A. Villari, L., 1984. Tertiary to Quaternary evolution of volcanism in the Aegean region. In: J.E. Dixon and A.H.F. Robertson (Editors), *The Geological evolution of the Eastern Mediterranean*. Geol. Soc. London, Spec. Publ., 17:687-699.
- Fytikas, M., Innocenti, F., Kolios, N., Manetti, P., Mazzuoli, R., 1986. The Plio-Quaternary volcanism of the Saronikos area (western part of the active Aegean volcanic arc). *Annales Geologique des Pays Helleniques* 33, 23-45.
- Inguaggiato, S. and Rizzo, A., 2004. Dissolved helium isotope ratios in groundwaters: a new technique based on gas-water re-equilibration and its application to Stromboli volcanic system. *Applied Geochemistry* 19, 665-673.
- Jolivet, L. and Brun, J.P., 2008. Cenozoic geodynamic evolution of the Aegean. *International Journal of Earth Sciences* doi: 10.1007/s00531-008-0366-4.
- Matini, L. and Fiebig, J., 2005. Fluid geochemistry of the magmatic-hydrothermal system of Nisyros (Greece). In: The geology, geochemistry and evolution of Nisyros volcano (Greece). Implications for the volcanic hazards (Hunziker, J.C. and Marini, L. eds.), *Memoires de Geologie*, 44, 121-163.
- Minissale, A., Duchi, V., Kolios, N., Totaro, G., 1989. Geochemical characteristics of Greek thermal springs. *Journal of Volcanology and Geothermal Research* 39, 1-16.
- Minissale, A., Duchi, V., Kolios, N., Nocenti, M., Verrucchi, C., 1997. Chemical patterns of thermal aquifers in the volcanic islands of the Aegean arc, Greece. *Geothermics*, 26, 501-518.
- Mitropoulos, P., Tarney, J., Saunders D., Marsh N., 1987. Petrogenesis of cenozoic volcanic rocks from the Aegean Island Arc. *Journ. Volcanology and Geothermal Research*, 32, 177-193.
- Pe-Piper, G. and Piper, D.J.W., 2002. *The Igneous Rocks of Greece*. Stuttgart, Borntraeger, 645 p.
- Pe-Piper, G., Piper, D.J.W., 2005. The south Aegean active volcanic arc: relationships between magmatism and tectonics. In: *The south Aegean active volcanic arc* (Fytikas, M., Vougioukalakis, G.E. eds.) – Developments in Volcanology 7, 113-133.
- Sano, Y. and Marty, B., 1995. Origin of carbon in fumarolic gas from island arcs. *Chemical Geology* 119, 265-274.
- Sano, Y. and Wakita, H., 1985. Geographical distribution of $^3\text{He}/^4\text{He}$ in Japan: implications for arc tectonics and incipient magmatism. *Journal of Geophysical Research* 90, 8729–8741.
- Shimizu, A., Sumino, H., Nagao, K., Notsu, K., Mitropoulos, P., 2005. Variation in noble gas isotopic composition of gas samples from the Aegean arc, Greece. *Journal of Volcanology and Geothermal Research* 140, 321–339.
- Zeilinga de Boer, J., 1989. The Greek enigma: is development of the Aegean orogene dominated by forces related to subduction or obduction? *Marine Geology* 87, 31-54.
- Zhang, J., Quay, P.D., Wilbur, D.O., 1995. Carbon isotope fractionation during gas-water exchange and dissolution of CO_2 . *Geochimica et Cosmochimica Acta* 59, 107-114.

URBAN GEOCHEMICAL STUDIES IN EUROPE

**Demetriades A.¹, Birke M.², Locutura J.³, Bel-lan A.B.³, Duris M.⁴
and EuroGeoSurveys Geochemistry Expert Group⁵**

¹ Institute of Geology and Mineral Exploration, 1 Spirou Louis Street, Entrance C, Olympic Village,
136 77 Acharnae, Attiki, Hellas, ademetriades.igme.gr

² Bundesanstalt für Geowissenschaften und Rohstoffe, Stilleweg 2, D-30655 Hannover, Germany,
Manfred.Birke@bgr.de

³ Instituto Geologico y Minero de España, 23 Rios Rosas, ES-28003 Madrid, Spain,
j.locutura@igme.es, a.bel-lan@igme.es

⁴ Czech Geological Survey, Klárov 3, CZ-118 21 Praha 1, Czech Republic, miloslav.duris@geology.cz

⁵ EuroGeoSurveys Geochemistry Expert Group, Rue Joseph II 36-38, 1000 Brussels, Belgium,
www.eurogeosurveys.org; Chairperson: Reimann C., Geological Survey of Norway,
39 Leiv Eirikssons, 7040 Trondheim, Norway, Clemens.Reimann@ngu.no

Abstract

Urban soil is generally contaminated to a variable degree depending on its proximity to contamination sources. Traffic is one of the main sources of urban contamination; lead (Pb) from the use of leaded petrol, zinc (Zn) and cadmium (Cd) from tyre wear, antimony (Sb) from break pads, and the platinum group elements (PGEs) from the wear of catalytic converters, are some typical elements that often reach high concentrations in the urban environment. Lead was also a key ingredient in white paint, and in towns with a high proportion of white wooden houses very high concentrations were found in soil. Crematoria can or have emitted mercury (Hg). Coal and heavy oil fired municipal power and heating stations emit sulphur (S), silver (Ag), vanadium (V), bromine (Br) and barium (Ba). The use of impregnated wood may have resulted in high concentrations of arsenic (As), especially in kindergartens (nursery schools) and playgrounds. Building materials (plaster and paint) may also contain high concentrations of organic contaminants, especially polychlorinated biphenyls (PCBs), which again end up in urban soil. Coal and wood burning, the use of diesel fuel, and the production of coke, all lead to the emission of polycyclic aromatic hydrocarbons (PAHs). There exist countless other sources of local contamination in towns, and there is thus every reason to be concerned about the quality of the urban environment, and the suitability of soil for sensitive land uses, such as schools, playgrounds, parks and vegetable gardens. Contaminated urban soil may contaminate indoor dust and, therefore, to an increased human exposure to toxic chemicals. Consequently, the distribution of toxic contaminants in urban soil needs to be documented and known by city administration to avoid costly mistakes in land use planning, and further spreading of highly contaminated materials.

The EuroGeoSurveys 'Geochemistry' Expert Group during the compilation of a proposal to the Directors for a European wide urban geochemistry project, using a harmonised sampling and analytical methodology, it discovered that many urban geochemical studies have been performed in Europe by National Geological Surveys, which are not known to the wider geoscientific community. Since, the results of these studies are directly related to our quality of life, the EuroGeoSurveys 'Geo-

chemistry' Expert Group decided to publish at least one case study from each country in a book, which will be available in the second half of 2010. A concise description of some of these studies will be given in this paper.

Key words: urban geochemistry, toxic chemical elements, contamination, soil, dust, Europe.

1. Introduction

The town is a heterogeneous complex structure that has been developed by humans as a necessity for protection, collaboration, trade, *etc.*, and is growing, changing, but also decaying, and its build-up is never completed. Since, urban areas in Europe are growing, the quality of their environment is becoming an important issue in the 21st century, following the serious degradation with the release of many toxic chemical elements and compounds by industrial processes, beginning from the industrial revolution, with a peak after the Second World War, as well as the modern style of living.

Industries were, and still are, variously located within the urban structure of many European towns. Since, the 1970s an attempt is, however, being made in many countries to develop industrial estates outside the urban structure. But, within the urban environment remain brownfield sites, and the enormous effort of their redevelopment in order to reduce the pressure on greenfield sites. However, this does not solve the contamination problem that has been developed over tens or hundreds of years in many urban centres, which may apparently be exacerbated in the not too distant future. At the beginning of the 20th century about 15% of the world's population was living in towns, and recent projections indicate that by the year 2030 the urban population will be two times as large as the rural. This increase will consume an important natural resource, *soil*; part of it will be completely lost through sealing, and the other will most likely lose its multi-functionality, because of contamination and compaction.

In comparison to atmosphere and water bodies, many contaminants are not diluted in soil, but are accumulated over time. In many cases, soil functions as a sink, with both inorganic and organic substances being adsorbed on soil colloids (*e.g.*, humic matter, clay minerals, iron and manganese hydroxides). Often, toxic substances are converted in soil to other, more stable, insoluble forms. Besides soil composition, the types of substances that accumulate in soil are governed by pH, redox conditions, and micro-organisms. A characteristic of urban areas is the wide distribution of fly ash and construction materials with neutral to basic pH values. Such conditions increase the immobilisation of many substances in urban soil. If soil conditions change, however, these substances can be remobilised and may enter ground or surface water.

Due to heterogeneity and continuous change of urban areas, it is important to understand, therefore, the distribution of chemical elements in the various environmental compartments (soil, atmosphere, road dust, house dust, water), and the methods for distinguishing human induced geochemical anomalies, *i.e.*, areas with chemical element concentrations above the natural geochemical baseline variation. The variable character of the natural geochemical baseline of chemical elements is an important concept that should be understood by decision-makers and planners; in simple terms, it means that elevated element concentrations, may be geochemically anomalous in one environment, whilst they can be part of the natural baseline concentrations in another; this continental scale natural geochemical baseline variation is well portrayed in the EuroGeoSurveys' "*Geochemical Atlas of Europe*" (<http://www.gtk/publ/foregsatlas/>). Therefore, geochemical maps of urban areas are needed to display the geographical distribution of chemical elements and compounds, in order to allow reliable recognition of contaminated areas.

Since, many health related problems are linked to the state of the urban environment, the European citizens are entitled to know the quality of not only the land their houses are built on, but also that of schools, parks, playgrounds, recreation areas, and workplaces. Estate agents would like to know the quality of the land they are marketing, and insurance brokers the potential risks on their customers.

2. Geochemical state of urban land

Concentrations of many potentially harmful elements (PHEs) are enhanced in the urban environment as a result of atmospheric and terrestrial contamination and the nature of urban ground, which is often disturbed and in-filled and frequently bears little relation to the residual soil, bedrock and superficial cover of the surrounding rural hinterland. Even in completely undisturbed urban areas, such as parks, many PHEs signatures are elevated in comparison to the rural natural geochemical baseline concentrations, due to atmospheric contamination, littering, urban surface run-off and other factors. Hence, it is necessary to establish the overall urban geochemical signature, so that areas of concern within a town can be highlighted, and detailed site investigation and contamination studies can be assessed in terms of the urban geochemical profile in addition to the rural baseline chemical element variation. It should be noted that systematic urban surveys do not replace the need for site-specific contaminated land investigations, but such data provide the citywide framework and context to more detailed assessments.

Urban soil is generally contaminated to a variable degree depending on its proximity to contamination sources. Traffic is one of the main sources of urban contamination; lead (Pb) from the use of leaded petrol, zinc (Zn) and cadmium (Cd) from tyre wear, antimony (Sb) from break pads, and the platinum group elements (PGEs) from the wear of catalytic converters, are some typical elements that often reach high concentrations in the urban environment. Lead was also a key ingredient in white paint, and in towns with a high proportion of white wooden houses very high concentrations were found in soil. Crematoria can or have emitted mercury (Hg). Coal and heavy oil fired municipal power and heating stations emit sulphur (S), silver (Ag), vanadium (V), bromine (Br) and barium (Ba). The use of impregnated wood may have resulted in high concentrations of arsenic (As), especially in kindergartens (nursery schools) and playgrounds. Building materials (plaster and paint) may also contain high concentrations of organic contaminants, especially polychlorinated biphenyls (PCBs), which again end up in urban soil. Coal and wood burning, the use of diesel fuel, and the production of coke, all lead to the emission of polycyclic aromatic hydrocarbons (PAHs). There exist countless other sources of local contamination in towns, and there is thus every reason to be concerned about the quality of the urban environment, and the suitability of soil for sensitive land uses, such as schools, playgrounds, parks and vegetable gardens. Contaminated urban soil may contaminate indoor dust and, therefore, to an increased human exposure to toxic chemicals. Consequently, the distribution of toxic contaminants in urban soil needs to be documented and known by city administration to avoid costly mistakes in land use planning, and further spreading of highly contaminated materials.

Next to soil, other natural materials could be sampled, as road dust, house dust, and attic dust. The chemical composition of each of these materials reveals a specific aspect of the urban environment. Road dust characterises mainly the current active sources of contamination. House dust is the material that children especially come mostly in contact with, and is characteristic of the narrow local home contamination. Attic dust, although not of direct concern to the quality of the home environment, it preserves a long record of past contaminating sources. Surface and ground water is an additional medium of concern that is closely associated with the quality of life of the population in some urban areas.

Of concern in the home environment are the levels of natural radon, which are based on geological factors, relation to mines and mine tailings, as well as the concentration of radium and radon in water supplies. Radon gas can penetrate houses from many sources and in different ways. In general, high levels of radon are associated with granite, igneous rocks, shale, slate, dirty quartz sedimentary rocks, phosphate deposits and some beach sands, which may contain high levels of radon progenitors, *i.e.*, uranium, or thorium. The most important contributor to indoor radon is the soil from which radon can be drawn through large and small subsurface gaps in the house foundations. A map of radon distribution should be produced to help planners and builders to site houses, or housing estates, on ground with low radon emission, and/or to reduce natural radon penetration in the home environment.

3. National Geological Surveys and urban issues

Soil contamination is becoming a key issue, and urban planning needs soil that is fit for human use, and is a matter that should be tackled efficiently. At European level, an initiative called “*Soil and Land Alliance of European Cities and Towns*” has been founded with the aim to make an active contribution to sustainable use of soil in communities [http://www.soil-alliance.org/e_manifesto.htm]. Production of a high quality compatible database on the geochemistry of urban soil is time consuming and costly, and especially if information down to the property level is required, since such systematic studies demand the use of the same sampling, sample preparation and analytical methodology, as well as data presentation. Existing urban soil geochemical databases from various sources have problems of data comparability, because different approaches to sampling, sample preparation and chemical analysis have been used.

Each European urban area has its own unique development, which is a result of many variables linked to historical, social, economic, cultural, geographical and climatic issues. Differences in living habits, land use practices, and use of building materials, may have resulted in different ways contaminants are stored in the various types of natural soil. Such a European wide comparison of the geochemistry of urban areas, using exactly the same methodology in all the investigation steps, will document the local peculiarities, and possible mistakes that have been made in one region do not need to be “transferred” to another. It is, therefore, strongly believed that there is a lot to be learned by such a well-coordinated European comparison of the geochemical state of the urban environment, and city administrators and planners will have at their disposal a high quality database for efficient urban planning.

Such systematic work in urban areas can only be carried out by national Geological Surveys, because they have the scientific expertise for such studies, and the infrastructure to maintain the required Geographical Information System databases to be accessed by each citizen. Something that has already been demonstrated by the production of the Geochemical Atlas of Europe (Salminen *et al.*, 2005; De Vos, Tarvainen *et al.*, 2006), and the pending Geochemical Atlas of Agricultural and Grazing land soil, which has started in 2008 (EGS Geochemistry, 2008; Reimann *et al.*, 2009).

4. Methods

4.1 General

Since, it is important to have comparable results across Europe, a field sampling manual for urban geochemical investigations in Europe is under compilation by the EuroGeoSurveys Geochemistry Expert Group, and should be released in 2010. Some of the principles have, however, been agreed,

and are described herein. The average sampling density should be 4 soil samples/km². In order to cover the urban area uniformly, it is proposed to collect soil samples from the central nodes of a 500 x 500 m grid. The sampling density can, however, be varied in sections of the town where contamination is suspected to the central nodes of a 250 x 250 m grid (16 samples/km²), and in the surrounding rural area to the central nodes of a 1000 x 1000 m grid (1 sample/km²).

There was a lively discussion with respect to the thickness of soil to be sampled, and whether single or composite samples should be collected. The different proposals were 0-2 cm, 0-5 cm, 0-10 cm and 0-20 cm. It was finally decided to collect surface soil samples down to a depth of 10 cm, after removal of surface litter, since this will give the best impression of anthropogenic impact. There is still disagreement, however, between single or composite soil samples. Collection of composite soil samples from four to five sub-sites up to a distance of 10 m around the central node is considered that it will give greater reproducibility and representativeness. This could be argued as suitable for natural situations, but in areas where humans have intervened for tens or hundreds of years, as is the case of urban environments, the variation could be enormous even at very short distances, since the principles governing the distribution of elements in the natural environment are no longer applicable. Hence, a composite soil sample may end-up diluting a significant point pollution target. Single spot soil samples have the advantage of representing precisely the site from which they have been collected. Reproducibility may not be good, but this is expected, because there are no rules about the spatial distribution of human induced contamination.

Soil samples should be collected from parks, playgrounds, sport fields and schoolyards, because these are the areas used by children and teenagers alike. Extensively used sites are preferred as, for example, in a grass covered park the most suitable site shall be where the grass has been worn through continuous use.

All field teams shall be provided with the same sampling equipment, purchased from the same source. At each sample site, GPS coordinates and field observations shall be recorded, and digital photographs taken; the recommendation is to take four general landscape photographs of the surrounding environment (North-East-South-West), and a site photograph showing details of soil texture.

Soil samples to be air dried and sieved to <2 mm (the standard fraction used in soil sciences) and pulverised to <0.063 mm prior to laboratory analysis. It is suggested to firstly analyse the samples by an aqua regia digestion. Total element concentrations (XRF or multi-acid-extraction) should be measured as well. A weak extraction would provide valuable information about availability, needed for the toxicological evaluation of the results. Because most weak extractions are quite element specific, it will not be easy to decide which one to use. Probably the Canadian “water extractable” standard, developed for the North-American geochemical mapping programme, is the best choice. All chemical analyses for a particular suite of parameters must be carried out in one laboratory only. All samples need to be randomised, and quality control samples (standards and duplicates) included at regular intervals (one in ten). Finally, all samples shall be submitted to the laboratory as one single batch.

Additional standard information needed for soil samples includes: pH, organic matter (*e.g.*, LOI as a proxy), and grain size analysis.

5. Results

Urban geochemical results are presented concisely from Berlin (Germany), Lavrion (Hellas), Madrid (Spain) and Prague (Czech Republic). There are many other case studies from Naples (Italy), Ljubljana (Slovenia), Trondheim, Bergen and Oslo (Norway), Stassfurt (Germany), and many others that

will be published in a book entitled “*Mapping the chemical environment of urban areas*” (Johnson *et al.*, 2010).

5.1 Berlin, Germany

About 4000 topsoil samples (0-20 cm) were taken in industrial and suburban areas of Berlin at a variable density between 20 and 40 samples/km² in densely populated and industrial parts of the city, and at a lower density (1-2 samples/km²) in the suburbs (Birke & Rauch, 1997, 2000; Birke *et al.*, 2000). The soil samples were air dried, sieved through a 2 mm nylon screen, and milled with an appropriate mill (planetary ball mill with agate grinding jars) to a grain size of <63 μm . The <2 mm fraction was analysed for 11 major elements (Si, Al, Fe, Mg, Ca, Na, K, P, S, total C, TOC) and 41 trace elements (Ag, As, B, Ba, Be, Bi, Br, Cd, Ce, Co, Cr, Cs, Cu, F, Ga, Ge, Hg, I, In, La, Mn, Mo, Nb, Ni, Pb, Rb, Sb, Se, Sn, Sr, Ta, Te, Th, Ti, Tl, U, V, W, Y, Zn, Zr). Electrical conductivity and pH were also determined. Hydrocarbons, aromatics, volatile halogenated compounds and polychlorinated dibenzodioxins and dibenzofurans (PCDD/PCDF) were analysed only in topsoil from the central part of Berlin. For the urban Berlin area the estimated median value is 0.98 ng ITE/kg for PCDD/F's.

The spatial distribution of Al, K, Si, Na, Rb, Zr, Nb, Co, Sc, and Ti is mainly of geogenic origin, *i.e.*, related to the chemical composition of parent material.

Industrial areas tend to be characterised by contamination of top- and sub-soil with respect to Cu, Cd, Zn, Hg, Pb and Sn. Industrial and commercial areas often display considerably elevated values for Mo, Ni, As, Ag, Cr, Sb, Sr, TOC, Fe, Mn, Mg, P and, especially, Pb and Hg.

Wooded areas show no great enrichment, except for Cd and Zn. In the area around Berlin, strong and extensive anomalies occur near iron and steel industries and construction materials industries, as well as in the vicinity of sewage treatment plants. There is local heavy-metal pollution (Hg, Cd, Zn) from the sewage treatment plants north and south of Berlin.

Urban geochemical studies in Berlin, and other German cities, have shown that toxic elements (*e.g.*, Cd, Cu, Cr, Hg, Ni, Pb, Zn and As) are enriched in soil by 1.8 to 8.9 times the natural geogenic concentrations (Table 1).

Especially in the polluted soil of old industrial sites, peak values of 2050 times the geogenic background were measured for Cu, 1780 times for Hg, and 1638 times for Cd. This means that, taking a soil of 1.2 g/cm³ density and the median concentration values from Berlin as an example of a large

Table 1. Topsoil element concentrations in Berlin (in mg/kg; n=3,746)

<i>Element</i>	<i>Arithmetic mean</i>	<i>Highest mode</i>	<i>Element</i>	<i>Arithmetic mean</i>	<i>Highest mode</i>
As	4.4	2.4	F	280	200
B	17.6	13.0	Hg	0.29	0.04
Be	1.14	1.0	Ni	8.1	2.7
Cd	0.65	0.08	Pb	85.8	21.7
Co	1.9	<1.0	Sb	2.92	2.1
Cr	28.7	12.2	Sn	7.6	1.6
Cu	53.1	6.0	Zn	166	19.3

city, the topsoil (0-20 cm depth) contains about 834 tonnes (t) As, 74 t Cd, 5,366 t Cr, 6,660 t Cu, 40.6 t Hg, 1,646 t Ni, 16,377 t Pb and 27,580 t Zn.

5.2 Lavrion, Hellas

Lavrion is a town 55 km to the south-east of Athens. Historically is a unique place, together with its surroundings, in the classical history of Hellas, since the mining of argentiferous galena provided the financial means for the Golden Age of Pericles during the 5th Century B.C. Almost two-and-a-half thousand years later (1865-1989 A.D.) was again a centre for mining and ore-smelting activities. Such a unique place in World history deserved a unique integrated environmental impact study, leading to recommendations for the necessary remediation measures that must be taken in order to make the area safe for habitation (Demetriades *et al.*, 1997; Demetriades, 1999a, b, c, d, e, 2010; N.T.U.A., 1999).

The following sample types were collected from an area of 7 km², covering the urban and suburban parts of Lavrion: (i) parent rocks (n=140), (ii) metallurgical processing residues (n=62), (iii) overburden including residual soil from 0-5 cm (n=224), (iv) house-dust (n=127), (v) metallurgical processing wastes and residual soil for particle-size analysis (n=21), (vi) ground water (n=15), (vii) metallurgical processing wastes for particle characterisation (n=31), and (viii) overburden from drill-hole core and vertical profiles (n=165). In addition, biomedical samples (n=235) collected during the last cross-sectional epidemiological study in March 1988, and soil samples for an agronomy study (n=583) were also utilised.

To begin with, the geochemistry of parent rocks, which depicts the natural levels of elements at the archetype state was studied (Table 2). Subsequently, human intervention followed with the exploitation of the mineral resources of the greater Lavrion area and the Lavreotiki peninsula, which had severe effects on the chemistry of soil. The enormous amount and expanse of metallurgical wastes in the Lavrion urban area contributed, together with other factors (aerial, fluvial, *etc.*), in the contamination of soil by Pb, Zn, As, Sb, Cd, Cu, Hg, *etc.* The geochemical investigation of the soil cover revealed the intensity and extent of contamination (Table 2). House dust is also severely contaminated (Table 2). Use of a sequential extraction method has given information about the geochemical behaviour, leachability, mobility and potential bioaccessibility of chemical elements in soil and house dust. These parameters were significant in the assessment of the effects of environmental contamination on the health of the local population.

Exposure to local environmental pressures is indicated by high Pb concentrations in child blood (5.98-60.49 µg/100 mL, mean 19.43 µg/100 mL, n=235), and deciduous teeth (0.97-153.26 µg/g, mean 9.88 µg/g, n=82), as well as by high As levels in 24 hour urine As (0.53-77.23 µg/24h, mean 8.59 µg/24h, n=261) (Stavrakis *et al.*, 1994), and total As in urine (9.7-1279 µg/L, mean 163.1 µg/L, n=65) (Demetriades *et al.*, 2008). The child blood-Pb levels, together with the geological, geochemical, metallurgical processing wastes and land use variables, were used in the risk assessment and subsequent environmental management scheme for the Lavrion urban area.

The percentage proportion of the Lavrion urban-suburban area with potentially hazardous element concentrations to human health is: (a) 100% for As, Pb, Cd and Zn, (b) 90 to 99% for Ag, V and Sb, (c) 45 to 68.8% for Cu and Mo, and (d) 13.8 to 33% for Ba, Ni and Cr. It is concluded, therefore, that the multi-element contamination of the Lavrion overburden/soil and house dust is extremely high, and presents an unacceptable risk on the quality of life of the local population, and is also potentially hazardous to plants and animals. Hence, it is highly urgent to rehabilitate the whole area by suitable remediation techniques.

Table 2. Statistical parameters of inorganic elements in samples of surface soil, house dust, parent rocks and metallurgical processing wastes, Lavrion, Hellas (values in mg/kg).

Element	Overburden samples, including residual soil (n=224)				House dust (n=127)	Parent rocks (n=140)	Metallurgical processing wastes (n=62)
	Min.	Max.	Mean	Median	Median	Median	Median
Ag**	1.4	204.6	17.8	12.1	4.81	0.5	18.9
As	50	24,000	2,194	1,290	750	15.6	2492
Ba	64	4,555	663.2	479	473	210	243
Be**	0.2	2.7	1.1	1	0.5	0.5	0.5
Cd	4	925	68	38	16.3	0.5	20.6
Co	3	106	17.7	16	8.1	20.5	23.8
Cr	2	1,083	264.2	183	114	20	73.2
Cu	43	4,445	357	186	179	25	630.5
Mo**	1.7	108.9	6.9	4.9	4.1	0.5	3.6
Ni	40	591	141.4	127	84	54.5	38.5
Pb	810	151,579	11,578	7,305	3,091	22	20,750
Sb ^{§**}	<6.8	567	121	121	-	2.5	189
V	26	325	86.1	75	42.5	9	46.3
Zn	591	76,310	10,872	6,668	3,044	57	39,800

[§]Overburden: Sb (n=90); **Rock: Ag, Mo (n=155); Be, Sb (n=48).

5.3 Madrid, Spain

The Madrid investigation was a multi-media urban geochemical study that covered an area of 400 km², *i.e.*, (1) 1730 top soil samples (0-20 cm) were collected at a density of 4 samples/km² from public gardens, buildings sites, *etc.*; the <180 µm fraction was analysed for major and trace elements by ICP-AES following (a) partial extraction by hot HNO₃+HCl acid (leach for 6 hours at 100°C), (b) a hot tetra-acid digestion (nitric, perchloric, fluorhydric, chloridric), and also (c) total contents by INAA (48 elements), (2) 248 soil samples at a density of 0.6 samples/km² were taken for the determination of organic compounds, such as volatile halogens, extractable halogen organic compounds (EOX), PAHs, and PCBs, (3) 302 pavement and sidewalk dust at a density of 0.75 samples/km² were collected by sweeping a surface of 15-20 m², and the <180 µm fraction was analysed for major and trace elements, and (4) 25 leaf samples were collected from plants and after ashing at 550°C total element concentrations were determined for 48 elements by ICP-AES and INAA.

The levels of most organic compounds were always below the detection limits of analytical methods, except EOX that showed some local contamination of small extension and intensity.

Overall the soil geochemical and dust patterns were of lithogenic origin, except locally where they

are disturbed by human factors due to the allochthonous nature of transported materials. The most significant anthropogenic signatures in soil with respect to total element contents were (a) Cu, Pb, Zn, P, Ni, Sb, Ag, (\pm Cd, Co, Cr) patterns that are ascribed to industrial and airport activities and fertilisation with sewage sludge, (b) Br, Organic Matter, Cr, (\pm Sb, Co, Pb, P, Mo) have a strong relationship with traffic and burning of liquid and solid fuels, and (c) Au has its own pattern, as it does not show any correlation with other elements. Geochemical patterns from partial extraction analyses are similar to those from total extraction, although the levels are lower; for some contaminants, however, patterns are more distinct, as is the case of W, which delineates more clearly pollution from the airport and some metal industries. An interesting observation was the distortion of natural geochemical patterns from the waste demolition dumps in the suburban area of Madrid, and the localised contamination by metallic elements.

Settled dust had contamination signatures from traffic, and fuel combustion, but also it delineated some new anomalies of industrial origin at the south-eastern, eastern and northern parts of Madrid.

The conclusion of this study was that Madrid has a similar contamination problem as other large industrial cities, and that the collected information would be useful for the establishment of a monitoring network for the detailed study of local polluted areas.

5.4 Prague, Czech Republic

The soil geochemical survey of Prague covered an area of 550 km² at a density of 1 sample/km² (Duris, 1999; Zimova *et al.*, 2001). The whole study area was divided into 1 km² grid cells, which were subsequently subdivided into 4 quadrants for sampling purposes. From each 1 km² cell a composite sample was made by taking a surface soil sub-sample (0-20 cm) from each quadrant. The soil samples were air dried (\approx 20°C), sieved through a 180 μ m nylon screen, and ground to <75 μ m for analysis. In addition, pavement dust was collected at selected road junctions in 1996 and 1999.

Concentrations of some inorganic and organic pollutants in soil are tabulated in Table 3. The Prague results show that Pb has elevated concentrations over the whole urban area, and the highest levels are in the city centre together with Cu and Hg. Similar patterns are observed with respect to PAHs and PCBs.

Changes of Pt, Pd and Pb concentrations in pavement dust at selected road junctions from 1996 to 1999 are shown in Table 4. It is indeed interesting to observe the drop in Pb, since the introduction of unleaded petrol, but also the rise of Pt and Pd from the use of catalytic converters.

Table 5 shows the concentrations of selected elements in child body tissues. Since, the Prague environment has elevated levels of contaminants in soil, the urban geochemical survey results are being evaluated from the public health risk point of view.

6. Conclusions

These urban geochemical studies have provided a comprehensive geochemical data base that permits differentiation between the natural geochemical background and local anthropogenic contamination.

It is also quite apparent from these studies that toxic element concentrations in topsoil vary considerably in an urban environment. Elevated values primarily reflect land use and the type and volume of industrial production.

The above studies have also shown that different sampling, sample preparation and analytical meth-

Table 3. Statistical parameters of inorganic and organic pollutants in surface soil (0-20 cm), Prague (values in mg/kg, unless otherwise stated).

<i>Element</i>	<i>Minimum</i>	<i>Maximum</i>	<i>Arithmetic mean</i>	<i>Geometric mean</i>	<i>Median</i>
Sb	0.1	8.6	1.3	1.6	0.9
As	7	102	18	16	16
Be	<0.8	3	1.5	1.4	1.4
Sn	<7	60	8	6.6	4
Cr	48	187	83	82	82
Cd	<0.4	9.1	0.5	0.5	0.4
Cu	<7	152	45	39	37
Ni	<7	103	32	29	31
Pb	13	420	74	62	58
Hg	<0.03	2.45	0.33	0.25	0.23
Tl	<0.05	0.89	0.15	0.13	0.14
V	14	89	37	36	35
Zn	41	912	201	173	167
PAHs ($\mu\text{g}/\text{kg}$)	211	95176	8379	3699	3319
PCBs ($\mu\text{g}/\text{kg}$)	3	7527	118	43	39

Table 4. Changes of Pt, Pd and Pb from 1996 to 1999 in pavement dust at selected road junctions in Prague.

<i>Road junction</i>	<i>Pt ($\mu\text{g}/\text{kg}$)</i>		<i>Pd ($\mu\text{g}/\text{kg}$)</i>		<i>Pb (mg/kg)</i>	
	<i>1996</i>	<i>1999</i>	<i>1996</i>	<i>1999</i>	<i>1996</i>	<i>1999</i>
Argentinská, Plynární	103	222	6	91	410	376
Spojovací Konevova	77	317	7	191	360	312
Žitná, Mezibranská	171	502	32	164	690	427
V Botanice, Zborovská	72	44	15	18	344	132
Barr. most (Smíchov)	41	983	5	329	785	335
Vítězné náměstí	25	61	5	17	414	271
Pod mag. U Bulhara	89	362	13	119	335	348

Table 5. Concentrations of Cd, Cu, Hg, Pb and Zn in child body tissues (in $\mu\text{g}/\text{L}$). It is noted that the WHO upper admissible limit for Pb in child blood is 100 $\mu\text{g}/\text{L}$.

<i>Body tissue</i>	<i>Statistics</i>	<i>Cd</i>	<i>Cu</i>	<i>Hg</i>	<i>Pb</i>	<i>Zn</i>
Blood	Median	0.15	1058	0.57	33	5202
	Minimum	0.015	511	0.04	8	2500
	Maximum	3.6	2074	7.8	247	8900
Urine	Median	0.235	10.1	0.25	3.73	547
	Minimum	0.035	0.799	0.01	0.16	54
	Maximum	5.91	460	87.5	36.2	2952

ods have been used, making, therefore, very difficult the comparison of results. Since, it is very important at the European level to have results that are compatible, the EuroGeoSurveys Geochemistry Expert Group, with the approval of Survey Directors, will be carrying out in 2010-11 an urban geochemical survey in at least ten cities with exactly the same methodology of sampling, sample preparation, laboratory analysis and map plotting.

In conclusion, the distribution of toxic contaminants in urban soil needs to be documented and results made known to town authorities for planning purposes in order to avoid costly mistakes in land use planning, and further spreading of highly contaminated materials.

7. Acknowledgments

This is a combined effort by the members of the EuroGeoSurveys Geochemistry Expert Group (<http://www.eurogeosurveys.org/>), who compiled the introductory parts of this paper in 2007, and all colleagues are thanked for their input. The paper is published by permission of the General Director of the Hellenic Institute of Geology and Mineral Exploration.

8. References

- Birke, M. & Rauch, U., 1997. Geochemical investigations in the Berlin metropolitan area. *Zeitschrift für Angewandte Geologie* 43(1), 58-65.
- Birke, M. & Rauch, U., 2000. Urban geochemistry: investigations in the Berlin metropolitan area. *Environmental Geochemistry and Health* 22, 233-248.
- Birke, M., Rauch, U. & Raschka, H., 2000. *Geochemical investigations in urban areas: megacities, mining districts, waste disposals and industrial zones*. Report (0120667), Federal Institute for Geosciences and Natural Resources, Berlin, 66 pp.
- Demetriades, A. (Editor), 1999a. *Geochemical atlas of the Lavrion urban area for environmental protection and planning; Volume 1, Explanatory text*. Project "Soil rehabilitation in the Municipality of Lavrion", EU LIFE programme Contract No.: 93/GR/A14/GR/4576. Institute of Geology and Mineral Exploration, Athens, Hellas, Open File Report E8272, 365 pp.
- Demetriades, A. (Editor), 1999b. *Geochemical atlas of the Lavrion urban area for environmental protection and planning; Volume 1A, Tables and figures*. Project "Soil rehabilitation in the Municipality of Lavrion", EU LIFE programme Contract No.: 93/GR/A14/GR/4576. Institute of Geology and Mineral Exploration, Athens, Hellas, Open File Report E8272, 210 pp.
- Demetriades, A. (Editor), 1999c. *Geochemical atlas of the Lavrion urban area for environmental protection and planning; Volume 1B, Appendix reports*. Project "Soil rehabilitation in the Municipality of Lavrion", EU LIFE programme Contract No.: 93/GR/A14/GR/4576. Institute of Geology and Mineral Exploration, Athens, Hellas, Open File Report E8272, 176 pp.
- Demetriades, A. (Editor), 1999d. *Geochemical atlas of the Lavrion urban area for environmental protection and planning; Volume 2, Geochemical Atlas*. Project "Soil rehabilitation in the Municipality of Lavrion", EU LIFE programme Contract No.: 93/GR/A14/GR/4576. Institute of Geology and Mineral Exploration, Athens, Hellas, Open File Report E8272, 222 pp.
- Demetriades, A. (Editor), 1999e. *Environmental management plan for the rehabilitation of soil in the Lavrion urban area; Volume 4*. Project "Soil rehabilitation in the Municipality of Lavrion", EU LIFE programme Contract No.: 93/GR/A14/GR/4576. Institute of Geology and Mineral Exploration, Athens, Hellas, Open File Report E8272, 155 pp.
- Demetriades, A., 2010. The Lavrion urban geochemical study. In: C.C. Johnson, A. Demetriades, R.T. Ottesen & J. Locutura (Editors), *Mapping the urban chemical environment*. Wiley, London (in preparation).

- Demetriades, A., Stavrakis, P. & Vergou-Vichou, K., 1997. *Exploration geochemistry in environmental impact assessment: examples from Greece*. In: P.G. Marinos, G.C. Koukis, G.C. Tsiambaos & G.C. Stourmaras (Editors), *Engineering Geology and the Environment*. Balkema, Rotterdam, Volume 2, 1757-1762.
- Demetriades, A., Vergou, K. & Vlachoyiannis, N., 2008. *The contamination of Lavreotiki peninsula and the urban environment of Lavrion from the mining-metallurgical wastes and the effects on the health of the local population*. Proceedings of the 9th Scientific Meeting of S.E. Attiki, Lavrion Attiki, 13-16 April 2000. Society of Studies of South-east Attiki, Kalivia Thorikon, Hellas, 573-624 (text in Hellene).
- De Vos W., Tarvainen T. (Chief Editors), Salminen R., Reeder S., De Vivo B., Demetriades A., Pirc S., Batista M.J., Marsina K., Ottesen R.T., O'Connor P.J., Bidovec M., Lima A., Siewers U., Smith B., Taylor H., Shaw R., Salpeteur I., Gregorauskiene V., Halamic J., Slaninka I., Lax K., Gravesen P., Birke M., Breward N., Ander E.L., Jordan G., Duris M., Klein P., Locutura J., Bel-lan A., Pasieczna A., Lis J., Mazreku A., Gilucis A., Heitzmann P., Klaver G. and Petersell V. 2006. *Geochemical Atlas of Europe. Part 2 - Interpretation of Geochemical Maps, Additional Tables, Figures, Maps, and Related Publications*. Geological Survey of Finland, Espoo, 692 pp. Available online at: <http://www.gtk.fi/publ/foregsatlas> (last accessed on 17/1/2010).
- Duris, M., 1999. Geochemical and ecological survey of the Prague agglomeration. In: D.A. Lovejoy (Editor), *Heavy metals in the environment: An integrated approach conference presentations from the 1st international conference "metals in the environment"*. Institute of Geology, Vilna, Lithuania, 134-136.
- EGS Geochemistry, 2008 (EuroGeoSurveys Geochemistry Working Group). *EuroGeoSurveys Geochemical mapping of agricultural and grazing land soil of Europe (GEMAS) - Field manual*. Geological Survey of Norway, Trondheim, NGU Report 2008.038, 46 pp. Available online at: <http://www.ngu.no/en-gb/hm/Publications/Reports/2008/2008-038/> (last accessed on 17/1/2010).
- Johnson, C.C., Demetriades, A., Ottesen, R.T. & Locutura, J., 2010. *Mapping the urban chemical environment*. Wiley, London (in preparation).
- N.T.U.A., 1999. *Environmental characterisation of Lavrion site – Development of remediation techniques*. Volume 3, In: Soil Rehabilitation in the Municipality of Lavrion. Project "Soil rehabilitation in the Municipality of Lavrion", EU LIFE programme Contract No.: 93/GR/A14/GR/4576. National Technical University of Athens, Hellas, 175 pp.
- Reimann, C., Demetriades, A. Eggen, O.A., Filzmoser, P. & the EuroGeoSurveys Geochemistry Expert Group, 2009. *The EuroGeoSurveys geochemical mapping of agricultural and grazing land soils project (GEMAS) - Evaluation of quality control results of aqua regia extraction analysis*. Geological Survey of Norway, Trondheim, NGU Report 2009.049, 94 pp. Available online at: <http://www.ngu.no/en-gb/hm/Publications/Reports/2009/2009-049/> (last accessed on 17/1/2010).
- Salminen R. (Chief Editor), Batista M.J., Bidovec M., Demetriades A., De Vivo B., De Vos W., Duris M., Gilucis A., Gregorauskiene V., Halamic J., Heitzmann P., Lima A., Jordan G., Klaver G., Klein P., Lis J., Locutura J., Marsina K., Mazreku A., O'Connor P.J., Olsson S.Å., Ottesen R.T., Petersell V., Plant J.A., Reeder S., Salpeteur I., Sandström H., Siewers U., Steenfelt A. and Tarvainen T. 2005. *FOREGS Geochemical Atlas of Europe, Part 1: Background Information, Methodology and Maps*. Geological Survey of Finland, Espoo, 526 pp. Available online at: <http://www.gtk.fi/publ/foregsatlas> (last accessed on 17/1/2010).
- Stavrakis, P., Vergou-Vichou, K., Fosse, G., Makropoulos, V., Demetriades, A. & Vlachoyiannis, N., 1994. A multidisciplinary study on the effects of environmental contamination on the human population of the Lavrion urban area, Hellas. In: S.P. Varnavas (Editor), *Environmental Contamination*. 6th International Conference, Delphi, Greece, CEP Consultants, Edinburgh, 20-22.
- Zimova, M., Duris, M., Spevackova, V., Melichercik, J., Lepsi, P., Tesarova, B., Knotek, P., Kubinova, R. & Ronen, Y., 2001. Health risk of urban soils contaminated by heavy metals. *International Journal of Occupational Medicine and Environmental Health*, 14, 231-234.

GEOCHEMICAL ATLASES OF EUROPE PRODUCED BY THE EUROGEOSURVEYS GEOCHEMISTRY EXPERT GROUP: STATE OF PROGRESS AND POTENTIAL USES

**Demetriades A.¹, Reimann C.², Birke M.³, Salminen R.⁴, De Vos W.⁵,
Tarvainen, T.⁴ and the EuroGeoSurveys Geochemistry Expert Group⁶**

¹ *Institute of Geology and Mineral Exploration, 1 Spirou Louis Street, Entrance C, Olympic Village,
136 77 Acharnae, Attiki, Hellas, ademetriades.igme.gr*

² *Geological Survey of Norway, 39 Leiv Eirikssons, 7040 Trondheim, Norway, Clemens.Reimann@ngu.no*

³ *Bundesanstalt für Geowissenschaften und Rohstoffe, Stilleweg 2, D-30655 Hannover, Germany,
Manfred.Birke@bgr.de*

⁴ *Geological Survey of Finland, P.O.Box 96, FI-02151 Espoo,
Finland, reijo.salminen@gtk.fi, timo.tarvainen@gtk.fi*

⁵ *Geological Survey of Belgium, Jannestraat 13, B-1000 Brussels, Belgium,
walter.devos@naturalsciences.be*

⁶ *EuroGeoSurveys Geochemistry Expert Group, Rue Joseph II 36-38, 1000 Brussels, Belgium,
www.eurogeosurveys.org*

Abstract

An 'Atlas' is a collection of maps usually published in a book form. A 'Geochemical Atlas' is a thematic special purpose atlas with maps describing the geographical distribution of chemical elements and other physico-chemical parameters in different natural sample media, such as stream sediment, overbank or floodplain sediment, stream water, ground water, soil, plants, etc. Because our standard of living and health depend closely on the chemistry of near-surface materials, such atlases that provide data on the state of our environment are important for policy and decision makers, but also for researchers and citizens alike. The EuroGeoSurveys Geochemistry Expert Group is dedicated to provide harmonised multi-purpose geochemical data bases, and has already published the Geochemical Atlas of Europe, and is in the process of preparing the Atlas of Ground water Geochemistry of Europe, and the Atlas of Agricultural and Grazing Land Soils. An important aspect is that all raw data, quality control information, statistics, maps and interpretation texts are freely available for downloading through the internet.

Key words: *geochemical atlas, stream water, ground water, bottled water, soil, overbank sediment, floodplain sediment, harmonisation of methods, INSPIRE, REACH, Europe.*

1. Introduction

Let us start from the right beginning! *What is an Atlas?* According to Encyclopaedia Britannica (2010) an atlas is 'a collection of maps or charts, usually bound together'. *Where does this name come from?* The name is derived from a custom, which was initiated by Gerardus Mercator, the Flemish cartographer (1512-1594), in the 16th century who used the figure of the

Titan Atlas, holding the globe on his shoulders, as a frontispiece for his books of maps. *Who was the Titan Atlas?* According to Hesiod's Theogony, Atlas was the son of Titan Iapetus and the Oceanid Clymene (or Asia) and brother of Prometheus (creator of humankind). He was one of the Titans who took part in their war against Zeus (the chief deity of the Pantheon, the Hellenic Olympian Gods). Upon loosing the war, Zeus for his punishment condemned him to support the pillars that held heaven and earth apart. The place was probably the highest peak of the Atlas Mountains in north-west Africa.

The '*Atlas*' over time has evolved, and in addition to maps and charts, *Atlases* often contain pictures, tabular data, facts about areas, and indexes of place-names keyed to coordinates of latitude and longitude or to a locational grid with numbers and letters along the sides of maps. Thematic, or special purposes, *Atlases* deal primarily with a single subject, such as agriculture, geology, climate, history, industry, languages, population, religions, resources, or other characteristics of a geographical area. One such thematic category is '*Applied Geochemistry*', a discipline that can indeed produce many different thematic atlases, containing a multitude of maps showing the geographical distribution of chemical elements in different sample media, such as stream sediment, overbank or floodplain sediment, stream water, ground water, soil, plants, *etc.*

Why are Geochemical Atlases important? The answer is given by Darnley *et al.* (1995, p.X) '*Everything in and on the earth - mineral, animal and vegetable - is made from one, or generally some combination of, the 90 naturally occurring chemical elements. Everything that is grown, or made, depends upon the availability of the appropriate elements. The existence, quality and survival of life depend upon the availability of elements in the correct proportions and combinations. Because natural processes and human activities are continuously modifying the chemical composition of our environment, it is important to determine the present abundance and spatial distribution of the elements across the Earth's surface in a much more systematic manner than has been attempted hitherto*'. Systematic geochemical mapping is, therefore, considered as the best available method to document changes in the levels of chemical elements in materials occurring at or below the Earth's surface.

Where can Geochemical Atlases be used? The systematic geochemical information in the atlases can be used for (a) state of the environment reports, (b) mineral exploration, (c) agriculture, (d) forestry, (e) animal husbandry, (f) geomedicine or medical geology, (g) determination of natural background values for environmental risk assessment, *etc.* The list of end-users is, in fact, very long, when it is realised by policy makers and regulators that our living and working environment, and humans themselves, depend on the chemical composition of near-surface earth materials. What is required is education from the primary school age to university that our health and quality of life depend, to a large extent, on the chemical composition of our environment. When we understand how significant the above statement by Darnley *et al.* (1995) is, then we will begin to use efficiently the information in *Geochemical Atlases*.

2. The EuroGeoSurveys Geochemistry Expert Group

The EuroGeoSurveys Geochemistry Expert Group (EGS Geochemistry Group) has been in existence, under different names and forms of the association of European Geological Surveys, since 1986, *i.e.*, Working Group on Regional Geochemical Mapping (Western European Geological Surveys, WEGS), Geochemistry Task Group (Forum of European Geological Surveys, FOREGS), Geochemistry Working Group and finally Geochemistry Expert Group under EuroGeoSurveys, the Association of Geological Surveys of Europe (<http://www.eurogeosurveys.org/>).

The EGS Geochemistry Group has always been very active and forward in its proposals to the European Geological Survey Directors. It has carried out considerable research work on the harmonisation of sampling, sample preparation, laboratory analysis of samples, quality control of methods, and has produced many reports and publications, which can be viewed at <http://www.gtk.fi/publ/foregsatlas/> and <http://www.globalgeochemicalbaselines.eu/>.

Presently, the EGS Geochemistry Group has undertaken to carry out many significant projects, including (i) the geochemical mapping of agricultural and grazing land soil, (ii) geochemistry of ground water, (iii) urban geochemical mapping of selected cities, (iv) publication of a book on the chemistry of urban environments, and many other initiatives. An important aspect of all these projects is that of harmonisation of methodologies, since this is the only way to produce comparable results across political boundaries, and to comply with the European Union's INSPIRE directive (Infrastructure for Spatial Information in the European Community at <http://inspire.jrc.ec.europa.eu/>).

3. Geochemical Atlas of Europe

Since the 1950s Geological Surveys have been documenting the natural geochemical background variation of chemical elements in a variety of sample materials, mainly for mineral exploration purposes (Garrett *et al.*, 2008). The generated data at the national scale are often not comparable at the European scale (different sampling strategies, different materials and equipment used for sampling and sample preparation, different sample preparation protocols, different analytical protocols, *etc.*), and are, therefore, not able to provide a harmonised pan-European or Global geochemical 'baseline' (Bölviken *et al.*, 1996). A reference network is, therefore, needed, where local data can be tied into European and Global scale data. International collaboration assisted UNESCO to establish in 1988 the IGCP 259 'International Geochemical Mapping' project and presently the IUGS/IAGC 'Global Geochemical Baselines' project, the aims of which are to establish a harmonised global geochemical reference baseline for over 60 determinands in different sample media for environmental and resource applications (Darnley *et al.*, 1995; Darnley, 1997; Demetriades, 1998). The terrestrial surface of the Earth was divided into 5000 grid cells of 160 x 160 km (area 25,600 km²), and named the Global Reference Network (GRN). Although the proposed sampling density is low, approximately one sample site per five thousand square kilometres (1 site/5000 km²), applied geochemists have been using quite effectively such low-sample density surveys to cover large areas for the last forty years.

The EGS Geochemistry Expert Group, as an input to the global project, carried out the geochemical baseline survey in 26 European countries, according to an agreed field sampling protocol (Salminen, Tarvainen *et al.*, 1998). Samples of stream water, stream sediment, topsoil, subsoil, floodplain sediment and humus from approximately 800 drainage basins, identified on the Global Reference Network within Europe, were collected, using the agreed standardised field sampling methods (Demetriades *et al.*, 2008; Fedele *et al.*, 2008; Lima *et al.*, 2008).

Following sample preparation, all samples were sent to Slovakia for homogenisation and splitting into subsamples for analysis. All samples were subsequently analysed for the same suite of determinands at the same laboratory, since this is the only way to produce comparable results. Chemical analysis of all samples was completed in 2004, and data subsequently collated and examined for error, and determinand distribution maps plotted by the Geological Survey of Finland. Maps and introductory texts were published in Part 1 (Salminen *et al.*, 2005), and the interpretation, together with specialised papers, included in Part 2 (De Vos, Tarvainen *et al.*, 2006).

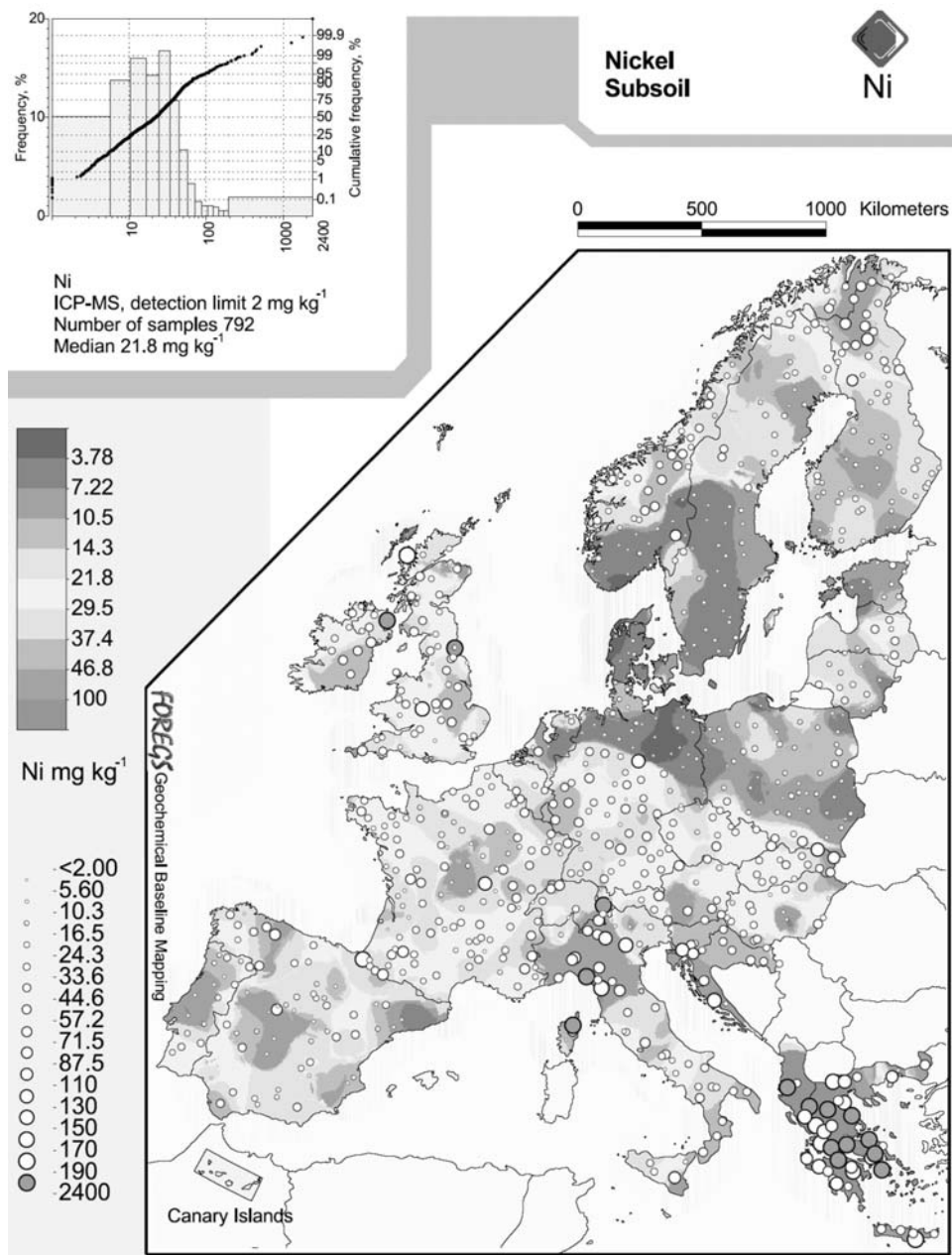


Fig. 1: Geochemical distribution of total Ni in the <math><2 \text{ mm}</math> fraction of soil >50 cm depth (Salminen *et al.*, 2005, p.357).

Both parts, including analytical data and photograph archive can be downloaded from URL <http://www.gtk.fi/publ/foregsatlas/>. The two volume atlas contains about 400 thematic maps describing the geochemistry of surface materials in Europe, and one example is given below.

3.1. Distribution of nickel (Ni) in subsoil

High Ni values in subsoil occur in areas with mafic/ultramafic substrate, such as Hellas, Albania, Liguria (Italy) and Corsica, N. Ireland (Antrim plateau basalt), central Norway and northern Scandinavia with greenstone belts (Fig. 1). There are pronounced differences in subsoil between northern (low) and southern (high) Europe. The break follows the maximum extent of glaciation, marking an important geochemical difference between old and strongly weathered soil (S. Europe), and young, coarse grained and less weathered soil (N. Europe). The large differences in Ni levels show that it is impossible to define one background range for the whole of Europe.

4. European Ground water Geochemistry

While the geochemistry of surface water is documented in the EuroGeoSurveys ‘*Geochemical Atlas of Europe*’ (Salminen *et al.*, 2005; De Vos and Tarvainen *et al.*, 2006), the geochemistry of ground water has not yet been documented in a comparable way at the European scale. Such data are, however, urgently needed in connection with the EU Water Directive. At present the European Environmental Agency anticipates to build up a database from each Member State’s water quality monitoring databases. The EGS Geochemistry Expert Group’s experience, however, with previous compilations of all geochemical data in Europe, has clearly demonstrated that this attempt will face serious problems of homogeneity of the collected data, based on various sampling and analytical methods. Since, the policy of EuroGeoSurveys is to provide data of high integrity and compatible across political boundaries, the EGS Geochemistry Expert Group proposed that the Geological Surveys themselves to use their own resources and to start a Europe-wide mapping of ground water quality following the ‘*Geochemical Atlas of Europe*’ example (low density sampling, harmonised equipment and sample protocol, all analysis carried out in one laboratory only, *etc.*). Because ground water is not a ‘simple’ sample medium, and all Geological Surveys cannot provide the necessary funds, in order to obtain a first and inexpensive approximation of ground water quality at the European scale, it was decided to sample bottled water, which could easily be purchased from supermarkets by each national representative and other colleagues. It was known that the storage and preservation conditions of bottled water in supermarkets across Europe undoubtedly varied, but it was considered a worth while effort to test if this water could provide an inexpensive first approximation to ground water quality. Therefore, available bottled waters in Europe were purchased from November 2007 to March 2008, and sent to Bundesanstalt für Geowissenschaften und Rohstoffe (BGR) in Germany for analysis.

All bottled waters were stored in refrigerators, and analysed by different methods for pH, EC, Ag, Al, As, B, Ba, Be, Bi, Ca, Cd, Ce, Co, Cr, Cs, Cu, Dy, Er, Eu, Fe, Ga, Gd, Ge, Hf, Hg, Ho, I, K, La, Li, Lu, Mg, Mn, Mo, Na, Nb, Nd, Ni, Pb, Pr, Rb, Sb, Sc, Se, Sm, Sn, Sr, Ta, Tb, Te, Th, Ti, Tl, Tm, U, V, W, Y, Yb, Zn, Zr, Br⁻, HCO₃⁻, Cl⁻, F⁻, NH₄⁺, NO₂⁻, NO₃⁻, PO₄³⁻, SO₄²⁻ and SiO₂. Duplicate bottled water samples were purchased from different supermarkets, and replicate and multiple analyses were performed for quality control purposes, and the estimation of measurement uncertainty. Since, bottle materials are known to affect the chemical composition of contained water, both glass and “plastic” bottles (polyethylene terephthalate, PET) of the same brand were purchased, and leaching tests were carried out. It was found that at a pH of 6.5 leaching of elements from bottle materials is negligible, but it becomes serious at a pH of 3.5, *i.e.*, PET bottles contaminated the contained water with Sb, and clear glass bottles with

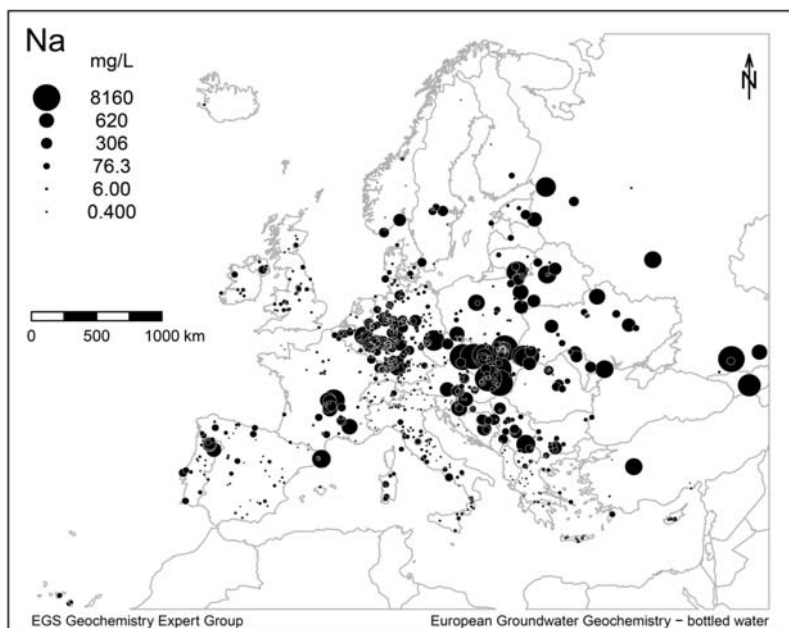


Fig. 2: Geochemical distribution of Na in bottled water (EGS, 2010).

Ce, Pb, Al, Zr, Ti, Hf, Th, La, Pr, Fe, Zn, Nd, Sn, Cr, Tb, Ag, Er, Gd, Bi, Sm, Y, Lu, Yb, Tm, Nb and Cu, whereas green bottles leach more Cr, Fe and Zr. A detailed account of all procedures followed, quality control results, and leaching tests will be given in the atlas, which is under preparation (EGS, 2010). Although the analytical results are in the process of verification an example is given below.

4.1 Distribution of sodium (Na) in bottled water

Sodium varies in bottled water from 0.4 to 8160 mg/L, with a median of 15.5 mg/L (n=884). The map of Na in bottled water shows high local variation (Fig. 2). This is a surprising observation. Given the high Na concentration in sea water, one may expect higher Na concentrations in coastal areas, rather than far inland. There are two possible explanations, *i.e.*, (i) it could be related to culture, a tendency towards stronger, more mineralised, ‘tasty’ mineral waters in Eastern Europe, but it could also be related to (ii) geology and the deep sedimentary basins that are exploited in those areas for mineral water, giving rise to Na-rich brines. The Carpathian Mountain Range, as well as the Dinarides, is marked by high Na values. The wells with the highest Na concentrations (up to 8160 mg/L) occur in Slovakia and Hungary. Wells abstracting water from Hercynian granite in France and Portugal also show somewhat increased Na concentrations, an indication of long residence time and water-rock interaction.

5. Geochemical Atlas of Agricultural and Grazing Land Soils

The geochemical atlas of agricultural and grazing land soils is under preparation (GEMAS). This is essentially a follow-up project of the ‘Geochemical Atlas of Europe’, but concentrating on soil, and the reasons for carrying out this project follow. The administration of REACH (Reg-

istration, Evaluation and Authorisation of Chemicals), the new European Chemicals Regulation adopted in December 2006 (http://ec.europa.eu/environment/chemicals/reach/reach_intro.htm/), and the pending EU Soil Protection Directive, require additional knowledge about ‘soil quality’ at the European scale. REACH specifies that industry must prove that it can produce and use its substances safely. Risks, due to the exposure to a substance during production and use at the local, regional and European scale, all need to be reliably assessed. In contrast to human-made organic substances that do not occur naturally in the environment, all industries dealing with natural resources will face in the near future a number of specific questions: (i) Most of their ‘products’ occur also naturally – the natural background variation needs to be established, in addition to a methodology to differentiate the industrial impact from the natural geogenic background; (ii) What is the ‘bioavailability’ of metals and other chemical elements in soil? and (iii) What is the long-term fate of metals and other chemical elements added to soil?

The GEMAS project will deliver good quality and comparable exposure data of metals in agricultural and grazing land soil; in addition soil properties known to influence the bioavailability and toxicity of metals (and other elements) will be determined in soil at the European scale.

The sampling at a density of 1 site/2500 km² was completed at the beginning of 2009 by collecting 2211 samples of agricultural soil (Ap-horizon, 0-20 cm, regularly ploughed fields), and 2118 samples from land under permanent grass cover (grazing land soil, 0-10 cm), according to an agreed field protocol (EuroGeoSurveys Geochemistry Working Group, 2008).

All samples were shipped to the laboratory of the Geological Survey of Slovakia for sample preparation, where they were air dried, sieved to <2 mm using a nylon screen, homogenised and split to subsamples for analysis. They are analysed for (1) 53 chemical elements following an *aqua regia* extraction, (2) pH in CaCl₂, TOC, LOI, grain size (on a selection of samples), total C and total S, (3) total concentrations of 39 elements by X-ray fluorescence, (4) Pb and Sr isotopes, (5) prediction of soil properties by mid infrared (MIR) measurements and (6) determination of K_d values for selected elements on selected samples. The *aqua regia* results were received in September 2009 and were subjected to a rigorous quality control procedure before their acceptance (Reimann *et al.*, 2009). Because of the complexity of the project, and confidentiality of results, the Geochemical Atlas will be ready by 2013, and an example is given below.

5.1 Distribution of strontium (Sr) in agricultural soil

Natural variation of Sr is large (4 orders of magnitude) and can be reliably mapped as is shown in Figure 3. Nature, geology and climate are the major driving forces for its distribution patterns, while anthropogenic anomalies, as input by fertilisers are not recognisable at this scale. It is clearly indicated that there is not one background value for a sizeable area. Strontium, together with other elements, shows substantially lower concentrations in North than in South European agricultural soil. Surprisingly, recent volcanism (Cyprus, Sicily, mainland Italy) and active fault zones and plate margins are often better indicated by Sr anomalies than some of the major limestone areas, except those of eastern Spain, southern France, Italy, and Paris Basin in France.

6. Conclusions

European wide geochemical maps are designed to reveal large continental scale geochemical anomalies or patterns; it is stressed that patterns of local significance cannot be observed in such low density sampling surveys. Nevertheless, continental scale geochemical surveys pro-

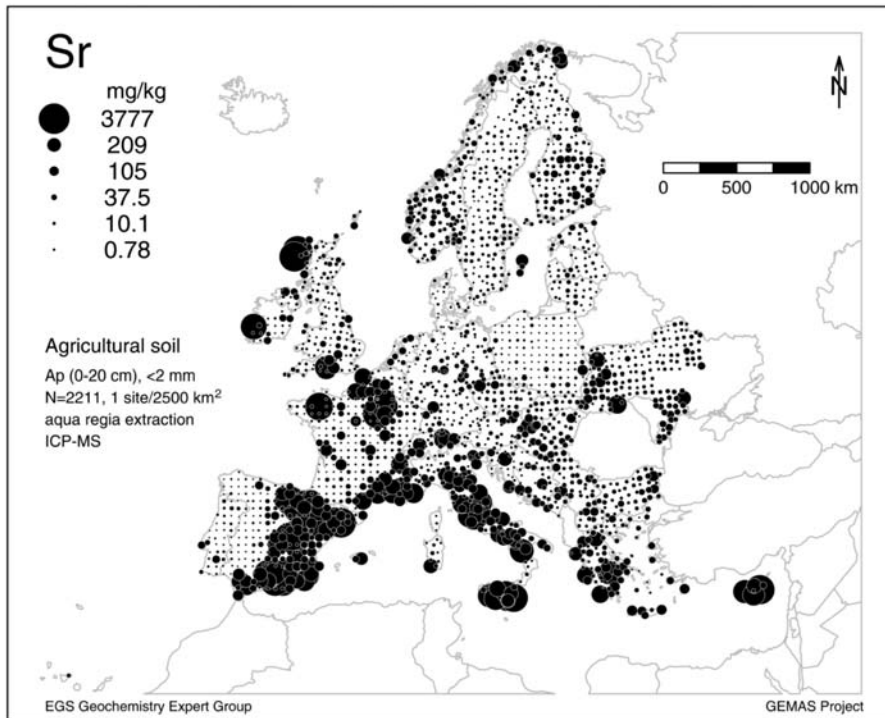


Fig. 3: Geochemical distribution of *aqua regia* extractable Sr in the <2 mm fraction of agricultural soil (0-20 cm) (Reimann *et al.*, 2009, Fig. 7, p.28).

vide us with invaluable information about the natural and human induced concentrations of chemical elements in sample media of the near-surface environment, where we live on, grow our crops, raise our livestock, and from which we extract our drinking water, and other raw materials, including mineral wealth. Our quality of life and health depend, in fact, on the chemical composition of water (surface or ground water) and soil, whether residual (developed directly on bedrock) or alluvial (transported by river water and deposited during flood episodes on floodplains).

The European wide projects, carried out by the EuroGeoSurveys Geochemistry Expert Group, have, therefore, demonstrated that low-density geochemical mapping can provide the needed information about the geochemical background variation in natural soil, stream water, ground water, stream and overbank or floodplain sediments. Thus, the EuroGeoSurveys ‘*Geochemical Atlases of Europe*’ provide European policy-makers, researchers, applied geochemists and citizens alike with sound data about the geochemical state of environmental media that our standard of living and health are closely related to. They also provide the ‘*geochemical baselines*’ against which the next generations will quantify changes, whether natural or human-made.

Production of such harmonised strategic baseline geochemical databases and maps is only possible, because of standardisation of all procedures of sampling, sample preparation, chemical analysis and data management across political boundaries. Without harmonisation of methods, it is impossible to produce meaningful continental scale geochemical databases and maps. It is, therefore, important for scientists working for the production of European wide databases and

maps to understand the concept of harmonisation of methods, and to apply it in their work. Otherwise, valuable time, effort and financial resources will be wasted in the production of incompatible data across political boundaries.

Finally, geochemical maps at a variety of scales are needed for different purposes (Reimann *et al.*, 2009). However, low density geochemical mapping lays the foundations for regional geochemistry and research in environmental sciences (Smith and Reimann, 2008). The relative importance of a variety of geochemical processes that govern the geochemistry at the Earth's surface can only be distinguished and evaluated from the study of continental or global scale maps, since many processes will not be recognised at the too detailed local scale.

10. Acknowledgments

This is a combined effort by members of the EuroGeoSurveys Geochemistry Expert Group, *i.e.*, *Austria*: Albert Schedl, Heinz Reitner, Edith Haslinger, Peter Filzmoser; *Belgium*: Walter De Vos; *Bosnia & Herzegovina*: Hazim Hrvatovic; Neven Miosic, Ferid Skopljak, Natalija Samardzic; *Bulgaria*: Valeri Trendavilov; *Croatia*: Josip Halamić, Ajka Šorša, Stjepan Husnjak; *Czech Republic*: Miloslav Duris; *Cyprus*: Zomenia Zomeni; *Denmark*: Vibeke Ernstsen; *Estonia*: Jaan Kivisilla, Walter Petersell; *Finland*: Timo Tarvainen, Mikael Eklund; *France*: Ignace Salpeteur; *F.Y.R.O.M.*: Trajce Stafilov; *Germany*: Manfred Birke, Rainer Hoffmann, Jens Utermann; *Hellas*: Alecos Demetriades; *Hungary*: Gyozo Jordan, Ubul Fugedi, Laszlo Kuti; *Ireland*: Patrick O'Connor, Fionnuala Ni Mhairtin, Vincent Gallagher; *Italy*: Benedetto De Vivo, Annamaria Lima, Stefano Albanese, Enrico Dinelli, Domenico Cicchella, Paolo Valera; *Latvia*: Aivars Gilucis; *Lithuania*: Virgilija Gregorauskiene; *Luxembourg*: Robert Maquil; *Netherlands, The*: Gerben Mol; *Norway*: Clemens Reimann, Rolf Tore Ottesen, Tore Volden, Ola A. Eggen, Arnold Arnoldussen; *Poland*: Anna Pasieczna, Aleksandra Dusza, Paweł Kwecko; *Portugal*: Maria Joao Batista, Cátia Prazeres; *Serbia*: Aleksandra Gulan, Dragana Vidojević; *Slovakia*: Igor Slaninka, Peter Sefcik, Daniela Mackovych, Silvester Pramuka; *Slovenia*: Mateja Gosar; *Spain*: Juan Locutura, Alejandro Bel-lan; *Sweden*: Madelen Andersson, Kaj Lax; *Switzerland*: Peter Hayoz, Reto Giulio Meuli; *Ukraine*: Boris I. Malyuk, Volodymyr Klos; *United Kingdom*: Dee Flight, Andreas Scheib, Mick Strutt, Paul McDonnell. The GEMAS project is sponsored by the European Association of Metals (Eurometaux - <http://www.eurometaux.org/>) for sample preparation and parts of the analytical work. The support of BGR for the provision of free analysis for all projects is acknowledged. The paper is published by permission of the I.G.M.E. General Director.

11. References

- Bölviken, B., Bogen, J., Demetriades, A., De Vos, W., Ebbing, J., Hindel, R., Langedal, M., Locutura, J., O'Connor, P., Ottesen, R.T., Pulkkinen, E., Salminen, R., Schermann, O., Swennen, R., Van der Sluys, J. & Volden, T., 1996. Regional geochemical mapping of Western Europe towards the year 2000. *Journal of Geochemical Exploration*, 56, 141-166.
- Darnley, A.G., 1997. A global geochemical reference network: the foundation for geochemical baselines. In: K. Marsina & K. Vrana (Editors), Environmental Geochemical Baseline Mapping in Europe. Special Issue, *Journal of Geochemical Exploration*, 60(1), 1-5.
- Darnley, A.G., Björklund A., Bölviken, B., Gustavsson, N., Koval, P.V., Plant, J.A., Steenfelt, A., Tauchid, M., Xuejing, X., Garrett, R.G. & Hall G.E.M., 1995. *A global geochemical database for environmental and resource management*. Final report of IGCP Project 259. Earth Sciences,

19, UNESCO Publishing, Paris, 122 pp.

- Demetriades, A., 1998. Global Geochemical Baselines: A fundamental international project for environmental management. *Bulletin of the Geological Society of Greece*, 32(1), 321-329.
- Demetriades, A., De Vivo, B., Ander, E.L., Bidovec, M., Lima, A., Pirc, S., Reeder, S., Siewers, U., Smith, B., Albanese, S., Batista, M.J., Bel-Ian, A., Birke, M., Breward, N., De Vos, W., Duris, M., Gravesen, P., Gregorauskiene, V., Halamic, J., Jordan, G., Lax, K., Locutura, J., O'Connor, P.J., Pasieczna, A., Slaninka, I., Tarvainen, T., Gilulis, A., Heitzmann, P., Klaver, G., Klein, P., Lis, J., Marsina, K., Mazreku, A., Ottesen, R.T., Petersell, V., Salminen, R., Salpeteur, I., Sandstrom, H., Shaw, R., Steenfelt, A. & Taylor, H., 2008. The EuroGeoSurveys Geochemical Atlas of Europe: Stream water geochemistry. In: G. Migiros, G. Stamatis & G. Stournaras (Editors), *Proceedings 8th International Hydrogeological Congress of Greece – 3rd MEM Workshop on fissured rocks hydrology*. Geological Society of Greece, Athens, Volume 1, 237-250.
- De Vos W., Tarvainen T. (Chief Editors), Salminen R., Reeder S., De Vivo B., Demetriades A., Pirc S., Batista M.J., Marsina K., Ottesen R.T., O'Connor P.J., Bidovec M., Lima A., Siewers U., Smith B., Taylor H., Shaw R., Salpeteur I., Gregorauskiene V., Halamic J., Slaninka I., Lax K., Gravesen P., Birke M., Breward N., Ander E.L., Jordan G., Duris M., Klein P., Locutura J., Bel-Ian A., Pasieczna A., Lis J., Mazreku A., Gilucis A., Heitzmann P., Klaver G. & Petersell V. 2006. *Geochemical Atlas of Europe. Part 2 - Interpretation of Geochemical Maps, Additional Tables, Figures, Maps, and Related Publications*. Geological Survey of Finland, Espoo, 692 pp. Available online at: <http://www.gtk.fi/publ/foregsatlas/> (last accessed on 17/1/2010).
- EuroGeoSurveys Geochemistry Working Group, 2008. *EuroGeoSurveys Geochemical mapping of agricultural and grazing land soil of Europe (GEMAS) - Field manual*. Geological Survey of Norway, Trondheim, NGU Report 2008.038, 46 pp. Available online at: <http://www.ngu.no/en-gb/hm/Publications/Reports/2008/2008-038/> (last accessed on 17/1/2010).
- EGS (EuroGeoSurveys), 2010. *EuroGeoSurveys Geochemistry Expert Group's European Ground water Geochemistry Part I: Bottled Water*. Schweizerbart'sche Verlagsbuchhandlung, Stuttgart, in press.
- Encyclopaedia Britannica, 2010. *Encyclopædia Britannica 2010 Ultimate Reference Suite DVD*. Encyclopædia Britannica, Chicago.
- Fedele, L., Plant, J.A., De Vivo, B. & Lima, A., 2008. The rare earth element distribution over Europe: geogenic and anthropogenic sources. *Geochemistry: Exploration, Environment, Analysis*, 8(1), 3-18.
- Garrett, R.G., Reimann, C., Smith, D.B. & Xie Xuejing, 2008. From geochemical prospecting to international geochemical mapping: a historical overview. *Geochemistry, Exploration, Environment, Analysis*, (Arthur Darnley issue), 8, 205-217.
- Lima, A., Plant, J.A., De Vivo, B., Tarvainen, T., Albanese, S. & Cicchela, D., 2008. Interpolation methods for geochemical maps: a comparative study using arsenic data from European stream waters. *Geochemistry: Exploration, Environment, Analysis*, 8(1), 41-48.
- Reimann, C., Demetriades, A., Eggen, O.A., Filzmoser, P. & the EuroGeoSurveys Geochemistry Expert Group, 2009. *The EuroGeoSurveys geochemical mapping of agricultural and grazing land soils project (GEMAS) - Evaluation of quality control results of aqua regia extraction analysis*. Geological Survey of Norway, Trondheim, NGU Report 2009.049, 94 pp. Available online at: <http://www.ngu.no/en-gb/hm/Publications/Reports/2009/2009-049/> (last accessed on 17/1/2010).
- Reimann, C., Matschullat, J., Birke, M., & Salminen, R., 2009. Arsenic distribution in the environment: the effects of scale. *Applied Geochemistry*, 24, 1147-1167.
- Salminen R. (Chief Editor), Batista M.J., Bidovec M., Demetriades A., De Vivo B., De Vos W.,

Duris M., Gilucis A., Gregorauskiene V., Halamic J., Heitzmann P., Lima A., Jordan G., Klaver G., Klein P., Lis J., Locutura J., Marsina K., Mazreku A., O'Connor P.J., Olsson S.Å., Ottesen R.T., Petersell V., Plant J.A., Reeder S., Salpeteur I., Sandström H., Siewers U., Steenfelt A. and Tarvainen T. 2005. *FOREGS Geochemical Atlas of Europe, Part 1: Background Information, Methodology and Maps*. Geological Survey of Finland, Espoo, 526 pp. Available online at: <http://www.gtk.fi/publ/foregsatlas/> (last accessed on 17/1/2010).

Smith, D.B. & Reimann, C., 2008. Low density geochemical mapping and the robustness of geochemical patterns. *Geochemistry, Exploration, Environment, Analysis*, (Arthur Darnley issue), 8, 219-227.

NATURAL DEGASSING OF CARBON DIOXIDE AND HYDROGEN SULPHIDE AND ITS ENVIRONMENTAL IMPACT AT MILOS ISLAND, GREECE

Kyriakopoulos G.K.

*National and Kapodistrian University of Athens, Dept. of Geology and Geoenvironment, Panepistimioupolis,
157 84 Ano Ilissia, Greece, ckiriako@geol.uoa.gr*

Abstract

The Aegean region represents an active convergent zone, where continental micro-plates exhibit a complex interaction between the African and the Eurasian plates. The calc-alkaline volcanic activity of the Southern Aegean region developed in various volcanic centers from Soussaki to Nisyros through Methana-Poros, Milos and Santorini. Milos Island has been an active volcano till the middle of Quaternary and is at present characterized by a high enthalpy geothermal system. The volcanism started 3.5 Ma ago and still continues up today in the form of post-volcanic manifestations.

Most quiescent volcanoes released large amounts of CO₂ and H₂S through fumarolic activity and soil diffuse degassing. Numerous small fumaroles occur in various places, mainly at Kalamos and Adamas volcanic areas. Also along the southern coast of the island there are volcanic gas manifestations in the sea. Gases were sampled from fumaroles at Kalamos area as well as from north east part of Adamas village. Furthermore many soil gases were sampled at 50 cm depth and analyzed for their chemical composition. Apart from atmospheric gases (N₂ and O₂), which sometimes contaminate the samples, the main gas phase is CO₂. Sometimes also H₂S, CH₄ and H₂ are present in high amounts while CO and He are always present in trace amounts. The He isotopic composition highlights a significant mantle component.

CO₂ and H₂S concentrations higher than in the normal atmosphere can be stimulating for plant growth until certain levels and detrimental above them. As for many active geothermal areas of the world also H₂S and CO₂ concentrations measured in the area of Milos could be of concern for human health.

Key words: *Volcanic gases, Health hazard, Environmental impact, South Aegean Volcanic Arc, Milos Island.*

1. Introduction

A volcanic gas is a relatively heterogeneous mixture, mainly dominated by steam (up to 99 % v/v), where a large number of other gas compounds are dispersed: SO₂, H₂S, HCl, HF, H₂, N₂, CO, CO₂, CH₄ and other hydrocarbons, noble gases, COS, etc. with contents that may range from ppbv or ppmv to few % v/v. The determination of gas species at low to very low concentrations is not only an analytical challenge, being some compounds in trace amounts to be considered useful indicators of impending eruptive events (e.g. Chiodini et al., 1993; Giggenbach, 1996; Delmelle & Stix, 2000). The yearly flux of carbon from sub-aerial volcanoes in volcanic arcs has been estimated at 13.5% (range of 5-25%),

of the mid-ocean ridge flux of 2.1×10^{10} moles of carbon (Marty and Jambon, 1987).

Mörner and Etiope (2002) have recently evidenced that the contribution of geothermal systems to lithospheric carbon degassing, although at present poorly constrained, is probably higher than volcanic degassing. An accurate quantification of CO_2 and CH_4 fluxes from low-enthalpy geothermal systems would therefore add important data for the accurate quantification of their contribution to the earth's carbon budget and to the global climate change. Both gas species have in fact important greenhouse effects and prediction of future climate scenarios rely heavily on a better quantification of their fluxes between all geochemical spheres.

H_2S is a toxic gas producing multiple effects. It is colourless gas with unpleasant odour of bad eggs. In nature large amounts are produced during processes of biological decomposition. A major part of the atmospheric hydrogen sulphide is of natural geothermal origin. Air pollution is of anthropogenous type as well. Industry is the main source - coke ovens, cellulose production, artificial fibers, natural gas and oil-product refining.

Contact of man with this gas is affected through the respiratory system. Scanty information exists on possible penetration through the digestive tract. The gas is absorbed by the organism through the lungs. In the liver and kidneys it is transformed into tiosulphates and sulphates. It is eliminated through the lungs, urine and fecal matter. Health effects are as follows - low concentrations may irritate the mucous tissues and cause conjunctivitis, and high concentrations may cause serious damages of the respiratory organs.

The aim of this paper is present the geochemical characterization of the main fumarole degassing and the soil gases of Milos Island geothermal field. Possible impact on the surrounding environment and on human health is also discussed.

2. Geological setting

The Aegean region represents an active convergent zone, where continental micro-plates exhibit a complex interaction under the influence of the overall N-S convergence between the African and the Eurasian plates. Apart from the compressional trench zone, the rest of the Aegean region is dominated by an extensional regime as evidenced by predominantly extensional fault plane and the presence of numerous normal faults (Mckenzie, 1972; Angelier et al., 1977; Dewey and Sengor, 1979). The volcanic arc lays ca. 150 km above the subduction zone, which forms an amphitheatre-like conical plane, with a maximum depth of 190 km at the central part of the South Aegean Volcanic Arc. (Spakman et al., 1988; Truffert et al., 1992; Papadopoulos et al., 1986; Papazachos, 1990), (Fig. 1).

The stratigraphy of Milos Island is composed, from the bottom to the top, by altered crystalline metamorphic basement, Neogene sediments, old volcanic tuffaceous formations, ignimbrites, old rhyolitic rocks, old dacitic and andesitic members, pyroclastic rocks, younger tuffs, lahar in different places, younger volcanics of acid composition and quaternary formations. Regarding its geological characteristics, the intensively eroded crystalline metamorphic basement appears in a very limited area (SE coastline). A not continuous series of Mio-Pliocene marine sediments is lying above the crystalline basement; it begins with reddish conglomerates and ends up with well-bedded limestones, which at places turn to sandstones (Fytikas, 1977).

From Upper Pliocene Milos was affected by an extensive volcanism, which lasted until late Quaternary (Fytikas et al., 1986). The composition of Milos volcanic rocks shows a calcalkaline character ranging from andesites to rhyolites. The youngest Upper Pleistocene volcanic activity is concentrated in corre-

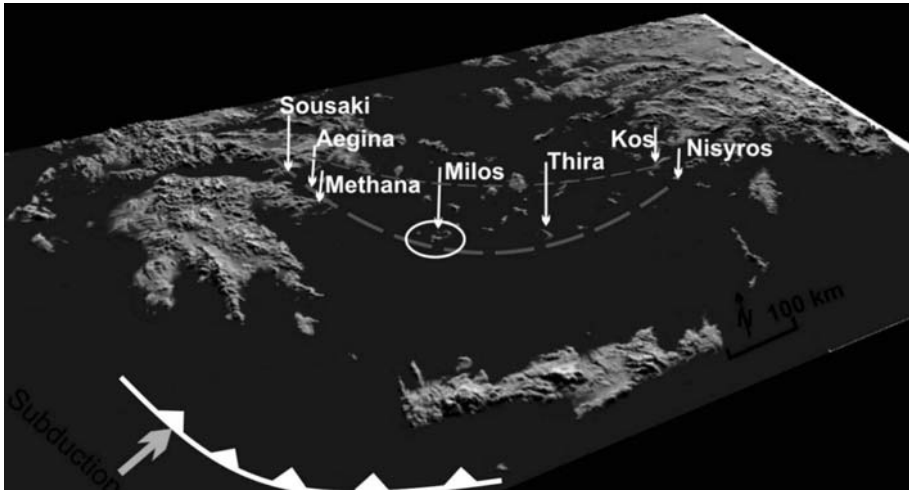


Fig. 1: Map of Greece showing Milos Island and the South Aegean Volcanic Arc.

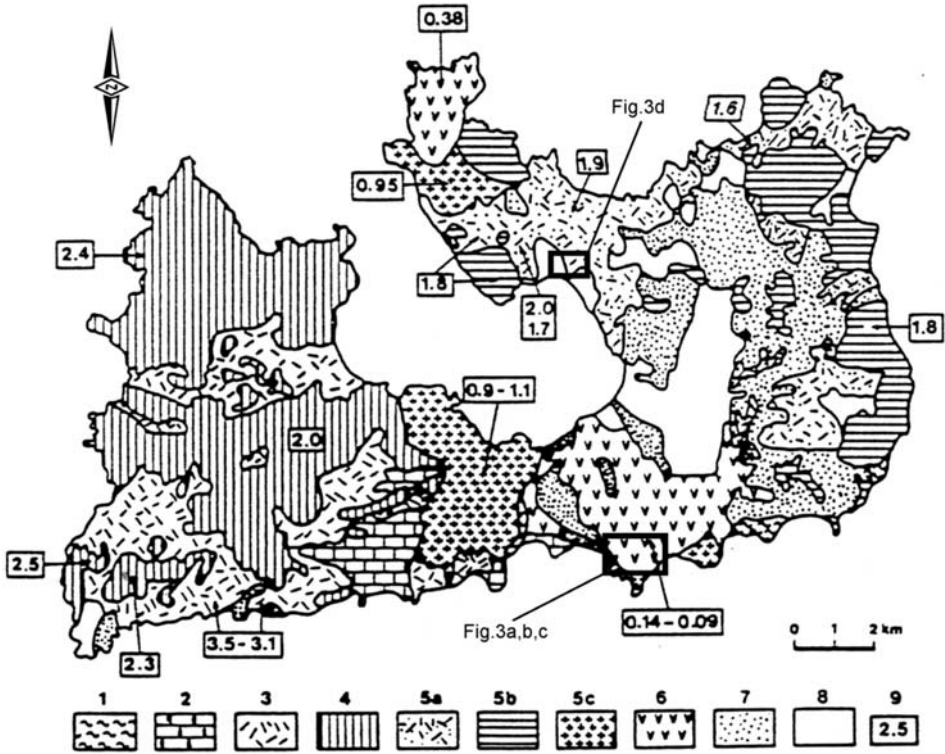


Fig. 2: Main geological units of Milos volcanic island (From Fytikas, 1976 modified). 1=Metamorphic basement; 2= Neogene sediments; 3= Basal pyroclastic series (Middle-Upper Pliocene); 4= complexes of domes and lava flows (Upper Pliocene); 5= Upper Pleistocene volcanics: pyroclastic series (5a), lava domes (5b) and Halepa and Plaka domes (5c); 6= Fyriplaka and Trachilas Rhyolitic complexes of Upper Pleistocene; 7= freatic activity products; 8= Quaternary sediments; 9= Radiometric ages from Angelier et al. (1977), Bigazzi and Radi (1981), Fytikas et al. (1976).

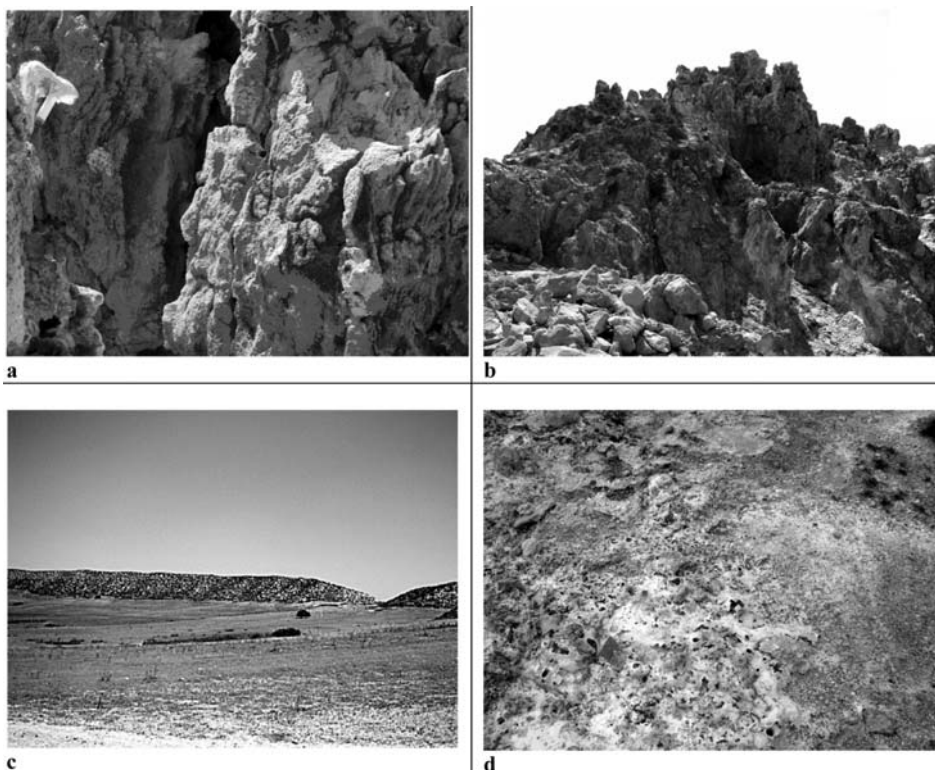


Fig. 3: a,b) Fumaroles at Kalamos degassing area, c) Crater of Fyriplaka volcano, d) Surface secondary minerals due to alteration phenomena of H_2S emanation, north of Adamas geothermal field. The locations of these photographs are noted on the map of Fig. 2.

spondence of the volcanic centres of Fyriplaka in the South and Trachilas in the North. In Trachilas the explosive activity began with the formation of a tuff ring mainly composed by pyroclastic surges; the surge deposits gradually pass to block and lapilli and finally to lava flows (Fytikas et al., 1986; Mitropoulos et al., 1987; Kelepertzis and Kyriakopoulos, 1991; Kyriakopoulos, 1998).

In the Fyriplaka area at least two tuff rings can be identified: a larger one (about 1500 m in internal diameter) and an inner and smaller one. The explosive activity leading to the formation of these tuff rings alternated with effusive episodes producing lava flows which ran to the NW and reached the sea inside the Gulf of Milos (Fytikas et al., 1986), Fig.2.

A decrease in the water content interacting with the magma is generally observed in the evolution of the eruptions: they usually start as phreatic and successively evolve into phreatomagmatic and magmatic activity; lava flows close the eruptive cycles (Fytikas et al., 1986).

3. Sampling and analytical methods

A total of 26 samples were collected from Kalamos and Adamas areas where intense gas emanation is occurring. The localities sites of the volcanic areas Kalamos and Fyriplaka in the south part and Adamas at the central part of the island are reported in Figure 3. Free gas samples were taken from natural gas manifestations like fumarolic discharges, soil gases, and mofettes and were collected at

a depth of 50 cm through steel or nylon tubes connected to a syringe while bubbling gases were collected through inverted funnels. Samples were then stored into glass flasks equipped with vacuum stopcocks. Furthermore 78 samples of soil gases were analysed in the field for CO₂ concentration with a portable IR spectrometer.

Gas concentrations were measured at INGV in Palermo using the GC Perkin Elmer Clarus 500 equipped with Carboxen 1000 columns, HWD and FID detectors with methanizer. The gas samples were injected through an automated injection valve with a 1000 µL loop. Calibration was made with certified gas mixtures. Analytical precision (1σ) was always better than ±5%. The detection limits were about 1 ppm vol. for CO and CH₄, 2 ppm vol. for H₂, 6 ppm vol. for He, 20 ppm vol. for CO₂, 200 ppm vol. for O₂ and 500 ppm vol. for N₂. Analyses of carbon isotopes of CO₂ were carried out by using a Finnigan Delta plus mass spectrometer. Values are expressed in ‰ vs. V-PDB, accuracy ±0.1 ‰.

4. Health hazard from volcanic gases

Regarding health hazard related of volcanic gases at least 455 million people worldwide live within potential exposure range of a volcano that has been active in recent times. The effects of SO₂ on people and the environment vary widely depending on (1) the amount of gas a volcano emits into the atmosphere; (2) whether the gas is injected into the troposphere or stratosphere; and (3) the regional or global wind and weather pattern that disperses the gas.

The volcanic gases that pose the greatest potential hazard to people, animals, agriculture, and property are sulfur dioxide, carbon dioxide, and hydrogen fluoride. Locally, sulfur dioxide gas can lead to acid rain and air pollution downwind from a volcano.

Because carbon dioxide gas is heavier than air, the gas may flow into in low-lying areas and collect in the soil. The concentration of carbon dioxide gas in these areas can be lethal to people, animals and vegetation, Table 1.

Table 1. Physiologic effects of human exposure to H₂S (Beauchamp et al. 1984; WHO 2003).

Exposure ppm	Effect/observation
0.01–0.13	Odor threshold
0.3	Distinct odor
2	Bronchial constriction in asthmatic individuals
3.5	Increased eye complaints
5–10	Increased blood lactate concentration, decreased skeletal muscle citrate synthase activity, decreased oxygen uptake
3.5–20	Eye irritation
20	Fatigue, loss of appetite, headache, irritability, poor memory
50	Marked irritant action on conjunctiva and respiratory tract
100–200	Olfactory paralysis
250	Prolonged exposure causes pulmonary edema
500–1,000	Immediate death

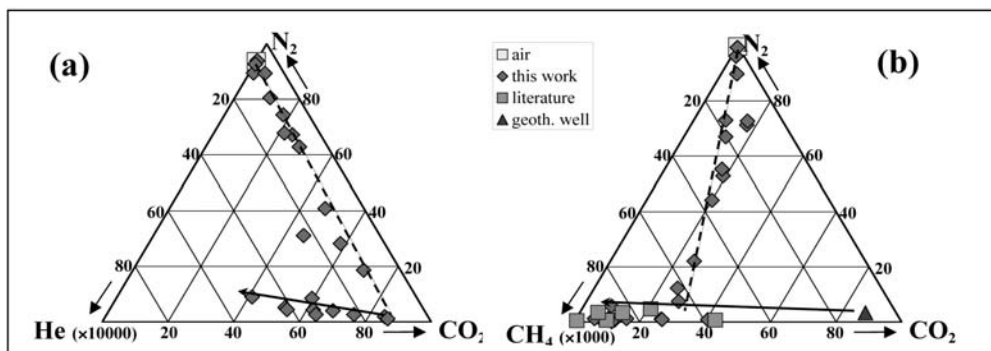


Fig. 4: – (a) He-N₂-CO₂ and (b) CH₄-N₂-CO₂ triangular plot of the gas samples collected at Milos. Dark gray squares and the geothermal well composition are from literature data. Dashed line shows the mixing between atmospheric air and geothermal gases. The arrows indicate CO₂ loss.

4.1 Hydrogen sulfide (H₂S)

Hydrogen sulfide (H₂S) is a colorless, flammable gas with a strong offensive odor. It is sometimes referred to as sewer gas. At low concentrations it can irritate the eyes and acts as a depressant; at high concentrations it can cause irritation of the upper respiratory tract and, during long exposure, pulmonary edema. A 30-minute exposure to 50 ppm results in headache, dizziness, excitement, staggering gait, and diarrhea, followed sometimes by bronchitis or bronchopneumonia, while concentrations above 500 ppm can be lethal within short time (Table 1). Continuous exposure to high concentration should be avoided. Moreover various studies (Loppi, 1996; Tretiach and Ganis, 1999) highlighted the adverse effects of volcanic/geothermal H₂S on nearby growing vegetation.

4.2 Carbon dioxide (CO₂)

Volcanoes release more than 130 million tonnes of CO₂ into the atmosphere every year. This colorless, odorless gas usually does not pose a direct hazard to life because it typically becomes diluted to low concentrations very quickly whether it is released continuously from the ground or during episodic eruptions. But in certain circumstances, CO₂ may become concentrated at levels lethal to people and animals. Carbon dioxide gas is heavier than air and the gas can flow into in low-lying areas; breathing air with more than 30% CO₂ can quickly induce unconsciousness and cause death.

5. Results and discussion

5.1 Geochemistry of the gases

Although Milos Island is not currently volcanically active, it is the site of intense old and recent hydrothermal processes. At the present time a high geothermal gradient (> 2,5 H.F.U.) occur. The high heat flow caused intense hydrothermal activity, which is responsible for many phreatic explosions. In some places the hydrothermal activity is expressed by the occurrence of many hot springs (30-85°C), fumaroles (98-102°C), hot grounds (100°C at a depth of 30-40cm) and submarine gas emissions, widespread on and around the island. Fyriplaka volcano is the expression of the most recent volcanic activity on the island and includes fumaroles, solfataras and hot grounds (Fytikas et al., 1986).

A preliminary survey of volcanic gas analyses shows that, with very few exceptions, the predominating constituents making up more than 95 % of the volcanic gas discharge are water vapor and

Table 2. Chemical composition of gas samples of Milos Island.

sample	type	date	He	H ₂	O ₂	N ₂	CO	CH ₄	CO ₂	H ₂ S	δ ¹³ C	R/Ra	He/Ne
			ppm	ppm	ppm	ppm	ppm	ppm	ppm	ppm	‰		
Milos C1 Fyriplaka	FG	1-06-2007	5	<2	194900	789400	3.7	3.6	1200	100	n.d.	n.d.	n.d.
Milos C2 Fyriplaka	FG	1-06-2007	8	492	168500	725600	6.3	171	97200	200	n.d.	n.d.	n.d.
Milos C3 Fyriplaka	FG	1-06-2007	8	1873	145500	581400	11	471	263600	2000	-1.5	n.d.	n.d.
Milos C4 Fyriplaka	FG	1-06-2007	8	91	187500	771100	3.4	20	10600	100	n.d.	n.d.	n.d.
Milos C5 Fyriplaka	FG	1-06-2007	5	29	182000	760900	4	46	40600	200	n.d.	n.d.	n.d.
Milos Fyriplaka	FG	20-06-2007	6	5	193800	777800	1	3.2	1500	n.d.	-0.1	n.d.	n.d.
Milos Adamas	SG	20-06-2007	12	596	101600	416000	3.9	986	482800	n.d.	0.3	n.d.	n.d.
Milos Paleochori 1	BG	21-06-2007	45	8	33300	119400	17	7533	838100	n.d.	n.d.	n.d.	n.d.
Milos Paleochori 2	BG	21-06-2007	69	<2	19000	85700	14	10100	874400	n.d.	n.d.	n.d.	n.d.
Milos Paleochori 3	BG	21-06-2007	49	<2	12000	62900	10	7929	901000	n.d.	-0.3	2.57	12.51
Milos Paleochori 4	BG	21-06-2007	37	<2	13800	52700	8	6615	905300	n.d.	n.d.	2.52	20.23
Milos Fyriplaka	FG	12-10-2007	8	432	142600	627400	6	334	226000	n.d.	n.d.	n.d.	n.d.
Milos Mad 1	BG	12-10-2007	69	<2	2800	73000	1	4877	896200	n.d.	-0.9	3.37	37.76
Milos Mad 2	SG	13-10-2007	7	237	166400	668500	5	109	160000	n.d.	1.6	n.d.	n.d.
Milos Paleochori	SG	22-10-2007	15	284	32800	315300	4	1593	650600	n.d.	-0.2	n.d.	n.d.
Milos M1	SG	21-03-2008	<5	1304	170000	680100	1.6	206	129600	n.d.	n.d.	n.d.	n.d.
Milos M2	SG	21-03-2008	10	486	152600	635600	1.8	313	201500	n.d.	1.7	n.d.	n.d.
Milos M3	SG	21-03-2008	<5	664	167300	672000	1	99	153300	n.d.	n.d.	n.d.	n.d.
Milos 1 Sinopi	BS	5-09-2008	50	<2	9200	39100	1.5	2636	944100	n.d.	n.d.	2.97	12.64
Milos 2 Adamas DEH	BG	12-08-2008	15	13	425	20700	1.5	1405	966100	n.d.	-1.3	3.04	6.14
Milos 3 Paleochori	BS	12-08-2008	14	29	3800	12500	3.2	7448	957000	n.d.	-0.4	n.d.	n.d.
Milos 4 Adamas	SG	5-09-2008	12	1418	50300	199300	3	1717	750600	n.d.	-0.7	n.d.	n.d.
Milos 5 Paleochori	BS	4-09-2008	26	6660	91600	348900	14	5167	511800	n.d.	n.d.	n.d.	n.d.
Milos 6 Paleochori	BS	5-09-2008	80	¹⁴ 910 0	52100	143800	13	11000	657400	n.d.	n.d.	n.d.	n.d.
Milos DEH	BG	10-06-2009	28	<2	4700	33400	1.6	2625	951200	n.d.	-0.4	n.d.	n.d.
Exploratory well (*)			n.d.	12000	11000	35000	n.d.	100	926000	15000	n.d.	n.d.	n.d.

Type: FG = fumarolic gas; SG = soil gas; BG = bubbling gas; BS = gas bubbling in sea water – n.d. = not determined. (*) data from Minissale et al. (1997)

species containing carbon and sulfur in their various oxidation states such as CO₂, CO, SO₂, S₈ and H₂S together with H₂. In the case of Milos gases, water vapour is an important component only of the fumarolic gases. In the present study only the dry gas composition (i.e. excluding water vapour) has been determined and the analytical results are shown in table 2. Apart from atmospheric gases (O₂ and N₂) deriving from air contamination, the main gas is CO₂. The O₂, N₂ and CO₂ contents evidence a clear mixing trend between two end-member represented by the atmospheric air and a CO₂-dominated geothermal gas. Isotopic composition of the CO₂-carbon, displaying values close to 0‰ (range from -1.5 to 1.6 ‰), indicates that the main CO₂ source may be the reaction between the acidic hydrothermal solutions with underlying Neogene limestone deposits (Fytikas, 1989) as well as from thermal decomposition of subducted marine sediments. But a contribution from mantle CO₂ cannot be excluded. Such contribution is strongly suggested by the isotopic composition of the helium whose values (R/R_a ranging between 2.5 and 3.4) highlights a mantle component of at least 50% for this gas.

The He-N₂-CO₂ triangular plot (Fig. 4a) shows two alignments. The first belongs to the mixing trend between atmospheric air and the geothermal gas. The second pointing towards the He vertex is probably due to processes responsible of CO₂ loss like carbonate precipitation or CO₂ dissolution in water. The last process is mostly evident in those gases which were collected from manifestations bubbling in sea-water.

The gas composition of one exploratory well (Table 2) evidences the enrichment in H₂S of the geothermal fluids at Milos. But this gas is partially lost in the shallow environment due to dissolution in condensing water vapour and oxidation processes. Such processes producing H₂SO₄-rich condensates are responsible of the low pH values (2.9) measured in the fumarolic condensate at Aghia Kyriaki, on the south coast of Milos (Dominico and Papastamataki, 1975). The CH₄-N₂-CO₂ triangular plot (Fig. 4b) further evidences the processes that bring to CO₂ loss and the mixing processes between geothermal and atmospheric gases.

Carbon dioxide in the soils of Milos shows a wide range of concentrations from 0.01 to 99.8 % (table 3). Concentrations sustained by biologic activity within the soils are generally less than a few %, while higher concentrations are clearly due to uprising geothermal fluids. Notably the highest concentrations were found at Adamas and Kalamos areas close to the sites of the most recent volcanic activity (Fig. 5).

5.2 Gas hazard and environmental impact

Volcanic/geothermal areas release huge amounts of gases, which apart from having important influences on the global climate could have a strong impact both on the local environment and on human health. Gases have both acute and chronic effects. Carbon Dioxide and Sulphur gases are the main gases responsible for acute mortality due to their asphyxiating and/or toxic properties. The problem has long been neglected until the “Lake Nyos” catastrophe in 1986, in which about 1700 people were killed by a volcanic CO₂ emission, attracted the worldwide attention of the mass media.

Gas hazard is largely underestimated because it acts also during quiescent periods and also in areas where volcanic activity is nowadays extinct. Furthermore, although the frequency of occurrence is relatively high, the number of victims of each lethal accident is generally low and often the real cause of death is not properly recognized. As a consequence, the recently published database of volcanic disasters and incidents of the 20th century (Witham, 2005), which attributed the death of 2000 persons and the injury of nearly 3000 to volcanic gases, is probably largely incomplete. The most dangerous gas species is CO₂, responsible of more than 90% of the victims and of the worst episodes

Table 3. Soil CO₂ concentrations at -50 cm depth (in vol %) of Milos geothermal field.

ID	LAT	LONG	ALTITUDE	CO ₂	ID	LAT	LONG	ALTITUDE	CO ₂
1	36.668	24.493	146	7.93	41	36.677	24.485	68	0.50
2	36.669	24.493	146	6.99	42	36.695	24.545	55	0.05
3	36.668	24.493	133	2.30	43	36.695	24.544	17	0.05
4	36.668	24.493	145	3.77	45	36.694	24.544	17	0.21
5	36.668	24.493	146	12.80	46	36.694	24.538	95	0.22
6	36.667	24.493	138	11.17	47	36.675	24.513	27	7.58
7	36.667	24.492	145	4.90	48	36.675	24.515	30	0.22
8	36.667	24.492	140	7.90	49	36.675	24.513	27	1.30
9	36.667	24.492	140	6.90	50	36.675	24.513	27	20.20
10	36.666	24.492	140	0.09	51	36.731	24.448	10	22.07
11	36.666	24.493	140	6.42	64	36.731	24.448	10	54.60
12	36.666	24.493	148	0.18	65	36.731	24.448	10	77.08
13	36.665	24.493	144	0.09	66	36.731	24.448	10	95.70
14	36.665	24.493	144	0.78	67	36.731	24.448	10	48.70
15	36.665	24.493	144	0.14	68	36.731	24.448	10	99.80
16	36.666	24.494	144	0.22	69	36.731	24.449	10	79.80
17	36.666	24.494	106	0.14	70	36.731	24.449	10	55.70
18	36.667	24.494	106	0.19	71	36.731	24.449	15	2.20
19	36.667	24.494	106	0.54	72	36.731	24.449	8	1.30
20	36.667	24.493	138	1.29	73	36.731	24.450	8	0.99
22	36.667	24.493	138	1.78	74	36.731	24.450	11	0.90
23	36.667	24.493	138	2.70	75	36.731	24.448	6	18.00
24	36.667	24.493	136	0.46	76	36.731	24.448	6	18.00
25	36.666	24.493	144	0.27	77	36.731	24.449	6	2.80
26	36.666	24.492	131	0.06	78	36.730	24.449	5	1.15
27	36.666	24.491	114	7.71	79	36.731	24.448	6	60.00
28	36.665	24.491	133	18.20	80	36.731	24.448	9	20.00
29	36.665	24.491	110	2.10	81	36.732	24.448	9	5.10
30	36.665	24.491	110	1.70	82	36.732	24.447	11	3.00
31	36.666	24.491	114	0.70	83	36.732	24.446	13	0.25
32	36.666	24.491	114	1.22	84	36.732	24.445	30	0.20
33	36.667	24.491	124	1.14	85	36.732	24.448	21	0.10
34	36.669	24.492	128	1.30	86	36.733	24.448	32	0.10
35	36.670	24.492	91	5.07	87	36.734	24.448	44	0.10
36	36.670	24.492	109	2.62	8	36.735	24.447	51	0.10
37	36.670	24.491	109	1.42	89	36.736	24.446	58	0.10
38	36.668	24.491	130	0.50	90	36.737	24.445	69	0.15
39	36.671	24.490	112	0.22	91	36.731	24.450	11	0.10
40	36.674	24.487	77	0.01	92	36.731	24.451	25	0.10

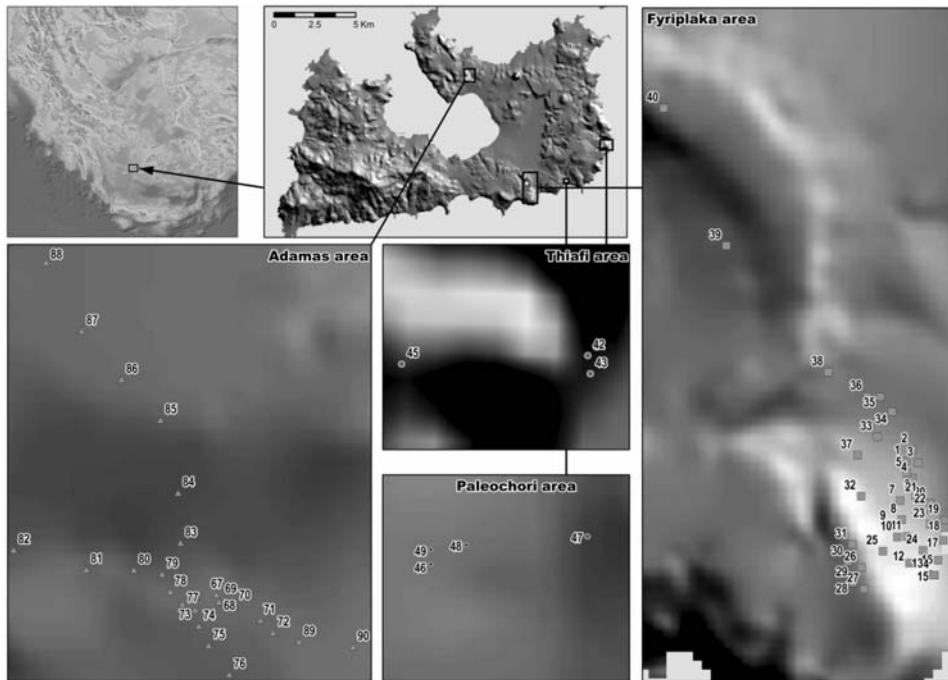


Fig. 5: Distribution of the soil gas sampling points of the four sampling areas on a shaded relief map.

(Lake Nyos and Lake Monoun, Cameroon and Dieng Plateau, Indonesia), but lethal episodes are also attributed to sulphur gases (SO_2 and H_2S).

Being heavier than air, CO_2 and H_2S can accumulate in topographic depressions and enclosures, and in areas with high fluxes their concentrations can exceed 10% and 100 ppm, respectively, which can be lethal to both animals and humans. At Milos Island hazardous concentrations of CO_2 (more than 90 %) and H_2S (up to 2000 ppm) are measured near the main emanation Kalamos and Fyriplaka areas.

People living in anomalous degassing areas are generally aware of the danger posed by gas accumulation, but nevertheless volcanic gases cause many fatalities each year worldwide (Witham, 2005). Even though the gas hazard at Milos appears restricted to limited areas, it should not be neglected, especially its effects on the most exposed people: children, workers involved in excavation activities and tourists who use public baths.

The H_2S dispersing in the surrounding atmosphere displays concentrations of some ppm that produces surely annoying smell and represents also a potential chronic health impact for the nearby living persons. Furthermore oxidizing reactions in the atmosphere transforms H_2S in SO_2 , locally increasing the acid burden through wet and dry deposition. Such processes are more intense during the summer season when high temperature and strong incoming solar radiation increases the formation of strong oxidant species like OH and O_3 .

Furthermore, where gas emanations are very high, the soils are altered and covered with thin layers of secondary minerals as alunite, magnesite and sulphur. In these areas, the extreme acidity of the fumarolic condensates, which is responsible of the high mobility of harmful elements during alteration processes, could negatively impact biota of the surrounding terrestrial and marine environ-

ments. Although such impact at Milos has not been studied yet, it is worth noting that vegetation around the hydrothermal manifestations is very stunted probably due to the bioaccumulation of the mobilized toxic elements.

6. Conclusions

The main gas manifestations at Milos show a typical hydrothermal composition. Excluding water vapour, the main gas species is represented by carbon dioxide. Its carbon isotopic composition points to a main origin from carbonate rocks although a significant mantle contribution cannot be ruled out. Other typical hydrothermal gases like hydrogen, methane and hydrogen sulphide display sometimes concentrations up to a few percent.

Soil gases show characteristic mixing trend between atmospheric air and deep geothermal gases. The latter implies their highest contents close to the fumarolic areas of Adamas and Kalamos. These areas show very high risk of gas hazard, and gas emissions could have a strong impact on the local environment.

7. Acknowledgements

The author would like to thank W. D'Alessandro for his helpful remarks and constructive guidance, Dr. E. Vassilakis for his assistance in elaborating GPS data and Dr. A. Marsellos for his fruitfully discussions and suggestions.

8. References

- Angelier, J., Cantagrel, M., Vilminot, C., 1977. Neotectonique cassante et volcanisme plioquaternaire dans l'arc egeen interne: l'île de Milos (Grece). *Bull. Soc. Geol. France*, 19, 119-121.
- Beauchamp, R.O., Jr, Bus, J.S., Popp, J.A., Boreiko, C.J., Andjelkovich, D.A., 1984. A critical review of the literature on hydrogen sulfide toxicity. *Crit Rev Toxicol* 13:25-97.
- Chiodini, G., Cioni, R., Leonis, C., Marini, L., Raco, B., 1993. Reactions governing the chemistry of crater fumaroles from vulcano island Italy, and implications for volcanic surveillance. *Appl. Geochem.*, 8, 357-371.
- Delmelle, P. and Stix, J., 2000. Volcanic Gases. In: *Encyclopedia of Volcanoes* (eds. H. Sigurdsson B. Houghton S. McNutt H. Rymer J. Stix), Academic Press, San Diego, 803-815.
- Dewey, J.F. and Sengor, A.M.C., 1979. Aegean and surrounding regions: complex multiplate and continuum tectonics in convergent zone. *Bull. Geol. Soc. Am.* 90, 84-92.
- Dominco, P. and Papastamataki, A. 1975. Characteristics on Greek geothermal waters. 2nd U.N. Symp. Dev. Use Geoth. Resources. S. Francisco.
- Fytikas, M. Giuliani, O. Innocenti, F. Marinelli, G., Mazzuoli, R., 1976. Geochronological data on recent magmatism of the Aegean Sea. *Tectonophysics*, 31, T29-T34.
- Fytikas, M., Innocenti, F., Kolios, N., Manetti, P., Mazzuoli, R., Poli, G., Rita, F., Villari, L., 1986. Volcanology and petrology of volcanic products from the island of Milos and neighbouring islets. *J. Volcanol. Geotherm. Res.* 28, 297-317.
- Fytikas, M., 1989. Updating of the geological and geothermal research on Milos Island. *Geothermics*, 18, 485-496.
- Giggenbach, W.F., 1996. Chemical composition of volcanic gases. In: *Monitoring and Mitigation of Volcano Hazards* (R. Scarpa, R.I. Tilling, editors) Springer, Berlin, pp. 221-256.

- Kelepertzis, A. and Kyriakopoulos, K., 1991. Mineralogy and geochemistry of the Mn-mineralization from Vani area of Milos island-its genesis problem. *Prakt. Acad. of Athens*, vol. 66, pp. 107-121.
- Kyriakopoulos, K., 1998. K-Ar and Rb-Sr isotopic data of white micas from Milos island geothermal boreholes field. *Annal. Geol. Pays Hell.* 38, p. 37-48.
- Loppi, S., 1996. Lichens as bioindicators of geothermal air pollution in Central Italy. *Bryologist* 99, 41-48.
- Marty, B. and Jambon, A., 1987. C^{13} He in volatile fluxes from the solid earth: implications for carbon geodynamics *Earth Planet. Sci. Lett.* 83, 16-26.
- Minissale, A., Duchi, V., Kolios, N., Nocenti, M., Verrucchi, C., 1997. Chemical patterns of thermal aquifers in the volcanic islands of the Aegean arc, Greece. *Geothermics*, 26, 501-518.
- Mitropoulos, P., Tarney, J., Saunders, D., Marsh, N., 1987. Petrogenesis of cenozoic volcanic rocks from the Aegean Island Arc. *J. Volcanol. Geotherm. Res.* 32, 177-193.
- McKenzie, D., 1972. Active tectonics of the Mediterranean region. *Geoph. J. R. Astr. Soc.*, 30, 55-71.
- Mörner, N.A., Etiope, G., 2002. Carbon degassing from the lithosphere, *Global Planet. Change* 33, 185-203.
- Papadopoulos, B.A., Kondopoulou, D.P., Leventakis, G.A., Pavlides, S.B., 1986. Seismotectonics of the Aegean Region. *Tectonophysics*, 124, pp. 67-84.
- Papazachos, B.C., 1990. Seismicity of the Aegean and surrounding area. *Tectonophysics*, 178, 287-308.
- Spakman, W., Wortel, M.J.R., Vlaar, N.J., 1988. The Hellenic subduction zone: a tomographic image and its geodynamic implications. *Geophys. Res. Lett.* 15, 60-63.
- Tretiach, M., Ganis, P., 1999. Hydrogen sulphide and epiphytic lichen vegetation: a case study on Mt. Amiata (Central Italy). *Lichenologist* 31, 163-181.
- Truffert, C., Chamot-Rooke, N., Lallemand, S., De Voogd, B., Huchon, P., Le Pichon, X., 1992. A crustal-scale cross section of the western Mediterranean ridge from deep seismic data and gravity modelling. *Geophys. J. Int.* 114, 360-372.
- Witham, C.S., 2005. Volcanic disasters and incidents: A new database. *J. Volcanol. Geotherm. Res.*, 148, 191-233.
- WHO, 2003. *Hydrogen sulphide: human health aspects*. Concise International Chemical Assessment Document 53, World Health Organization, Geneva, pp 26.

NATURAL AND ANTHROPOGENIC EFFECTS ON THE SOIL GEOCHEMISTRY OF KAVALA AREA, NORTHERN GREECE

**Papastergios G.¹, Filippidis A.¹, Fernandez-Turiel J.L.², Gimeno D.³,
and Sikalidis C.⁴**

¹Department of Mineralogy-Petrology-Economic Geology, Aristotle University of Thessaloniki, 54124, Thessaloniki, Greece, gpapaste@geo.auth.gr, anestis@geo.auth.gr

²Institute of Earth Sciences “Jaume Almera”, Consejo Superior de Investigaciones Científicas (CSIC), Lluís Solé i Sabarís, s/n – 08028, Barcelona, Spain, jlfernandez@ija.csic.es

³Department of Geochemistry, Petrology and Geological Exploration, University of Barcelona, Zona Universitària de Pedralbes, Martí i Franquès, s/n – 08028, Barcelona, Spain, domingo.gimeno@ub.edu

⁴Department of Chemical Engineering, Aristotle University of Thessaloniki, 54124, Thessaloniki, Greece, sikalidi@eng.auth.gr

Abstract

A total of 65 surface soils and 8 rock samples from the area surrounding the city of Kavala, Northern Greece, was collected and analyzed for their contents in 10 major and 32 trace elements. The extraction of the elements from the < 200µm soil fraction was based on the digestion of 0.1g of each sample with 2ml HNO₃. The analytical methods used were ICP-OES and ICP-MS and the elements determined were Al, Ca, Cl, Fe, K, Mg, Na, P, S, Si, Ag, As, B, Ba, Cd, Ce, Co, Cr, Cs, Cu, Ga, Ge, Hg, La, Li, Mn, Mo, Ni, Pb, Rb, Sb, Se, Sn, Sr, Th, Ti, U, V, W, Y, Zn and Zr. Comparisons between the concentrations of the surface soil samples and the surrounding rock samples indicate that the majority of major, as well as, of trace elements are found in the surface soils of Kavala with such concentrations that are considered as the product of natural processes such as the weathering of parent rocks and pedogenesis. However, there are some major elements (Cl, Na, S) and trace elements (Ag, As, Pb, V, Zn) that are present in the surface soils of the study area with elevated concentrations that cannot be regarded as the sole product of natural processes, but as the result of both, natural and anthropogenic activities, especially for the samples that are situated inside the industrial area of Kavala.

Key words: geochemistry, environment, soil, rock, Kavala, Greece.

1. Introduction

As it is known, soils and sediments are principal environmental sinks for both major and trace elements. Their content in soils is derived, either through natural processes such as the weathering of parent rocks, or through anthropogenic activities such as industry and agriculture. Since Potentially Toxic Trace Elements (PTTE) are regarded as one of the main sources of pollution in the environment, the study of their distribution is very important, especially from an environmental point of view, explicitly because many human activities mobilize and redistribute elements in the environment, often causing adverse effects. Elevated concentrations of PTTE in soils and sediments may re-

sult in an increased uptake of PTTE by crops and vegetables which, in turn, may have a negative effect on animals and human health (Hesterberg 1998; Fernandez-Turiel et al., 2001; Georgakopoulos et al., 2001; Kabata-Pendias and Pendias, 2001; Cui et al., 2005).

The objectives of this study were to describe the chemical dataset collected and to investigate the geochemical identity of the surface soils of the Kavala area, with the intention of identifying the possible elemental sources in the area, whether natural and/or anthropogenic. In order to reach this goal, several methods were applied. However, in this paper are presented the results of the comparison between the elemental concentrations of the surface soils and the surrounding rocks of the Kavala area.

2. Study area – Geological setting

The study area is the city of Kavala, its industrial zone and their surroundings (Fig. 1). The climate of the area shows general Mediterranean characteristics. The mean temperature is 4.0°C in January and 24.5°C in July, while the prevailing wind is from SE (H.N.M.S. 1978, Petalas et al., 2004). Land uses in the area may be divided into four categories: agricultural, uncultivated, industrial and residential (Fig. 1). The main industrial activities are the Phosphoric Fertilizer Industry (P.F.I.) and the Kavala Oil land facilities. The first industry produces phosphoric fertilizers, pesticides and other similar products and its main byproduct is phosphogypsum, while in the second industry oil desulfurization takes place. Other activities include some small enterprises that exploit and market local marbles and the Xifias Fishery enterprise which terminated its activities during the undertaking of the present research. Also, near the Kavala Oil land facilities and the Xifias Fishery, several uncontrolled landfill sites exist.

The study area is a part of the Rhodope massif and it consists of metamorphic and plutonic-eruptive rocks (Fig. 2). The main rock types in the area are: a) gneisses and schists, b) limestones and marbles, c) granitic and granodioritic rocks and d) sedimentary deposits. The intense plutonism of the Rhodope is represented by granites, granodiorites, monzonites, quartz monzonites and diorites of Eocene, Oligocene, and Miocene age (Kilias et al., 1999; Christofides et al., 2001, Pe-Piper and Piper 2002). Additionally, Pyrite-Blende-Galena (PBG), Au, Cu, Mn, and Fe mineralizations and ore deposits are widespread in the study area (Filippidis et al., 1996; Vavelidis et al., 1996, 1997) (Fig. 2).

3. Methodology

3.1 Sampling and sample preparation

In total, 65 surface soil samples were collected between November 2002 and January 2003 (Fig. 1). Surface soil was selected because it is very sensitive to anthropogenic influences. This kind of samples is well suited for gaining information on the long-term impact of trace metals accumulation (Ramsey, 1997, Fernandez-Turiel et al., 2001, Kabata-Pendias and Pendias, 2001). Along with the soil samples, 8 rock samples from the surrounding rocks of the study area were collected. An effort was made so all the major rock types present in the area were represented (Tables 1 and 2).

All soil samples were dried in an oven at 40°C. After sieving, the < 200µm fraction was used due to the fact that environmentally available trace elements mainly remain in this fraction (Fernandez-Turiel et al., 2001, Kabata-Pendias and Pendias, 2001, Papastergios et al., 2009). The rock samples were crushed and pulverized in an agate mortar and followed the same procedure as the soils did.

The elements analyzed were extracted with analytical grade, concentrated (65%) HNO₃. The HNO₃

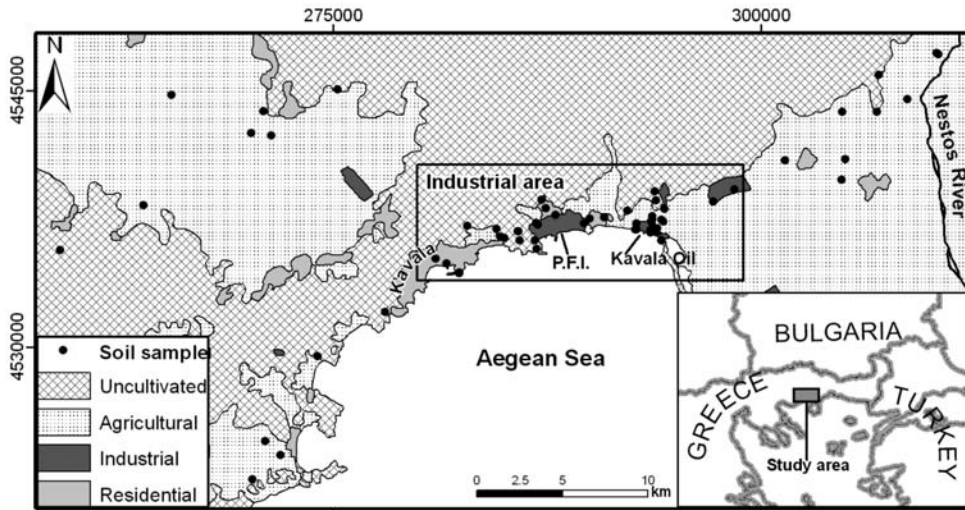


Fig. 1: Landuse/cover map of the study area and soil sample locations (modified from Papastergios, 2008).

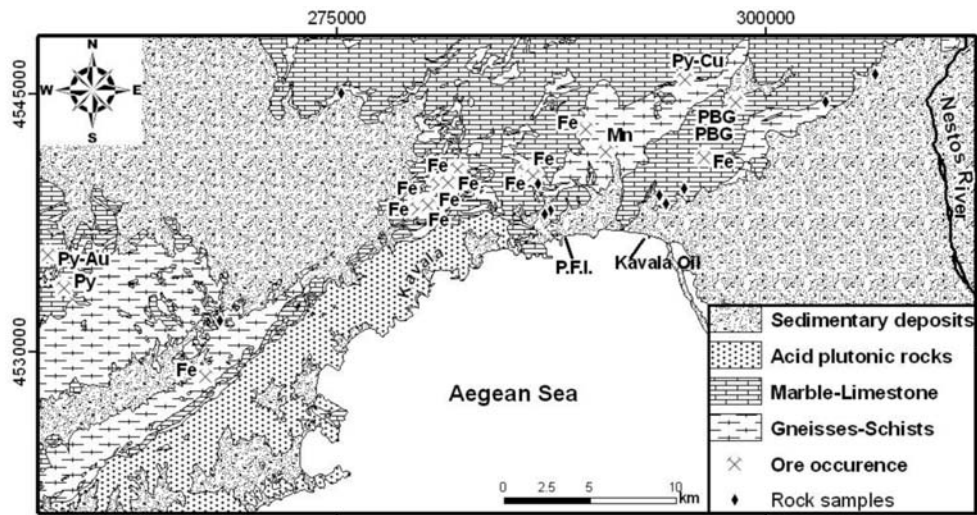


Fig. 2: Simplified geological map of the study area. Locations of rock samples and mineralizations are included (modified from Papastergios, 2008).

extraction procedure is a very strong acid digestion that puts in solution almost all elements that could become “environmentally available” (Walsh et al., 1997, Sastre et al., 2002). Analytical grade HNO_3 has been selected in order to work with extreme analytical conditions, and maintain, at the same time, the compatibility of the leachate with the input solution in ICP-MS and ICP-OES (direct determination after dilution). In the present work, a 0.1 g aliquot of each sample was placed into 14 mm diameter polyethylene tubes. Then, 2 ml of HNO_3 were added. All samples were placed in a rotary shaker for 24h. After the extraction procedure, the solution was filtered in 100 ml volume flasks. The volume flasks were made up volume with Milli-Q type deionized water of 18.2 $\text{M}\Omega/\text{cm}$.

3.2 Analytical methods

Ten major (Al, Ca, Cl, Fe, K, Mg, Na, P, S and Si), and 32 trace element (Ag, As, B, Ba, Cd, Ce, Co, Cr, Cs, Cu, Ga, Ge, Hg, La, Li, Mn, Mo, Ni, Pb, Rb, Sb, Se, Sn, Sr, Th, Ti, U, V, W, Y, Zn and Zr) concentrations were determined in all samples by Inductively Coupled Plasma – Optical Emission Spectrometry (ICP-OES) and Inductively Coupled Plasma – Mass Spectrometry (ICP-MS). A Perkin Elmer Optima 3200RL with a Perkin Elmer Autosampler AS-90+ was used for the ICP-OES analyses, while a Perkin Elmer Sciex Elan 6000 with a Perkin Elmer AS-91 automatic sampler was used for the ICP-MS analyses. The analyses were performed at the SCT-UB (Scientific Technical Services of the University of Barcelona), Barcelona (Spain). Details on ICP-MS analysis can be found in Fernandez-Turiel et al. (2000).

In order to check the quality of the results, the same methods were applied to the reference materials CANMET SO-1, SO-2, SO-3, SO-4, as well as to four replicates of a randomly selected sample. The methodology used, achieved precise analysis for practically all reference materials. Many elements exhibited Relative Standard Deviations (RSD) lower than 3%, and some around 1% (e.g., Ca, Mg, Fe, Al, Pb, Sr). Exceptions were Na, S, Cl, B, Cd, Ge, Hg, Sb and Se, probably due to their low concentrations (close to the quantification limits) in the reference materials. In regard to the extraction procedure's repeatability, many elements exhibited RSD values lower than 5%. Similarly, some of the worst values could be attributed to the low concentrations of these elements. Detailed results regarding the methodology used are given in Papastergios (2008).

4. Results and discussion

Before comparing the results between the soils and the surrounding rocks, the concentrations of the surrounding rocks were compared with similar rock types, in order to disclose any unusual concentrations. The average concentrations of carbonates, shales and granites, as given by Faure (1992) were used for these comparisons. The results revealed that, only Ag (in marbles and granites) and Cd and Co (in marbles) are found with, relatively, elevated concentrations. The rest of the elements, for all rock types of the study area, are found within normal ranges (Papastergios, 2008).

4.1 Major elements

Table 1 shows the average leached concentrations for the major elements of the surrounding rocks and the surface soils of the study area. The two most abundant elements for both the surrounding rocks and surface soils are Ca and Fe, with an average concentration of 124.64 g kg⁻¹ and 27.98 g kg⁻¹ for Ca and 8.28 g kg⁻¹ and 6.35 g kg⁻¹ for Fe, respectively. This came as no surprise, as marbles are the dominant rock type and Fe mineralizations are common, in the area (Fig. 2). Concerning the surrounding rocks, Mg and Al are the next two elements with high concentrations, around 2.3 g kg⁻¹ and they are followed by P, Cl, Na, Si and S, which all have concentrations lower than 1 g kg⁻¹. The order changes slightly, for the surface soils. After Ca and Fe, the elements with the highest concentrations are Al, Mg, Na and Cl with average concentrations between 4.5 and 1.0 g kg⁻¹. The rest of the elements (P, S and Si) have concentrations below 1.0 g kg⁻¹.

A series of comparisons were generated between the surface soil samples and the surrounding rocks samples (as a total and separately with each rock type) of the study area (Table 1). The aim of the comparisons was to identify whether the surrounding rocks of the study area could provide the surface soils of Kavala with their elemental content.

The results indicate that Al, Ca, Fe, K, Mg, P and Si are found in the surface soils of the present study

Table 1. Average leached concentrations for the major elements (in g kg⁻¹) of the surface soils and the surrounding rocks of the study area, and Enrichment Factors (EF) of the comparisons between the leached concentrations of the surface soils and the surrounding rocks.

Element	Rocks (total)	Marbles	Gneisses	Granites	Soils
Al	2.11	0.05	2.65	3.63	4.50
Ca	124.64	365.78	5.35	2.78	27.98
Cl	0.37	0.90	0.21	0.02	1.12
Fe	8.28	0.61	10.35	13.88	6.35
K	1.26	0.01	1.75	2.01	1.38
Mg	2.40	3.71	1.60	1.89	2.83
Na	0.31	0.30	0.10	0.53	1.88
P	0.56	0.53	0.70	0.44	0.72
S	0.15	0.29	0.07	0.09	0.68
Si	0.25	0.16	0.26	0.34	0.26
Enrichment Factors (EF)					
Element	Soils vs. Rocks (total)	Soils vs. Marbles	Soils vs. Gneisses	Soils vs. Granites	
Al	2.1	96.9	1.7	1.2	
Ca	0.2	0.1	5.2	10.1	
Cl	3.0	1.2	5.4	70.2	
Fe	0.8	10.4	0.6	0.5	
K	1.1	150.7	0.8	0.7	
Mg	1.2	0.8	1.8	1.5	
Na	6.1	6.2	19.6	3.6	
P	1.3	1.3	1.0	1.6	
S	4.5	2.3	9.6	7.9	
Si	1.0	1.6	1.0	0.8	

as a result of natural processes, such as the weathering of parent rocks and pedogenesis, since their Enrichment Factors (EF) are lower than 3 (Table 1). On the other hand, Cl, Na and S are found in the surface soil samples with concentrations that seem to be elevated (EF larger than 3) and that could not have been provided solely by the erosion of the surrounding rocks. In the case of S, potential sources could be the PBG ore occurrences and the Kavala Oil land facilities, with the second being, most likely, the case, especially since almost all elevated values are found in its vicinity. The S deriving from the desulphurization of the oil is stacked in opencast sites inside the Kavala Oil land facilities and hence, is freely transferred by the wind. Additionally, the samples with, both Cl and Na elevated values, are found in the same area (Papastergios 2008). In fact, almost all samples that show elevated values are common. According to Kabata-Pendias and Pendias (2001) elevated Cl values are connected with the usage of mineralized waters and/or fossil fuels (i.e., oil, carbon, gas etc). Although, the transfer of sea water aerosols and the deposition of NaCl particles on the surface soils cannot be excluded.

4.2 Trace elements

Table 2 shows the average leached concentrations for the trace elements of the surrounding rocks and the surface soils of the study area. For the calculation of the descriptive statistics, values that were below the detection limit for each element were substituted by half its detection limit. For the surrounding rocks, only Mn had an average concentration larger than 100 mg kg⁻¹ (269.45 mg kg⁻¹), while for the surface soils two elements (Mn: 524.2 mg kg⁻¹ and Zn: 147.68 mg kg⁻¹) had concentrations above 100 mg kg⁻¹. Elements with concentrations between 100 and 1 mg kg⁻¹ were Sr, Ti, Ba, Zn, Rb, Cr, Cu, Ni, Ce, Pb, Th, Y, V, B, Li, La, Co, As, W, Cs, U, Mo, Ga and Sn, for the surrounding rocks, while the respective elements for the surface soils were Ba, Ti, Pb, As, Sr, Ce, Cu, V, Rb, Cr, Ni, La, Y, B, Co, Th, Li, Ga, Zr and Cs. The rest of the elements, either for the surrounding rocks (Se, Zr, Cd, Sb, Hg, Ag and Ge) or the surface soils (U, Se, Ag, Cd, Sn, W, Sb, Mo, Hg and Ge), had concentrations that were below 1 mg kg⁻¹.

The comparisons between the surface soil samples and the surrounding rocks samples indicate that B, Ba, Cd, Ce, Co, Cr, Cs, Cu, Ga, Ge, Hg, La, Li, Mn, Mo, Ni, Rb, Sb, Se, Sn, Sr, Th, Ti, U, W, Y, and Zr are found in soils of the Kavala area with concentrations that could have been provided through natural processes, since they have EF that are lower than 3 (Table 2). On the contrary, Ag, As, Pb, V and Zn show elevated concentrations which must not be attributed to the weathering of parent rocks, alone. The PBG ore occurrences of the study area may be regarded as possible contributors. However, with the exception of few samples located in the west part of the study area, the rest of the samples are situated far away from the PBG ore occurrences and near the industrial area of Kavala. In fact, the samples that are situated inside the industrial area of Kavala have larger concentrations than those situated outside (Fig. 1, Table 3) and, moreover, most of the samples with the elevated concentrations are found in the direction the prevailing wind blows (Papastergios et al., 2004, 2007, Papastergios 2008). Furthermore, all of the aforementioned elements have been connected to anthropogenic activities such as the ones taking place in the study area (Kabata-Pendias and Pendias 2001); therefore, these activities must have contributed to the elevated concentrations of the former elements in the surface soils of the study area. Additionally, given that the elemental content of the surrounding rocks has been found to be within normal ranges, the influence of the anthropogenic activities on the surface soils of Kavala, especially near its industrial area seems very likely, particularly, since the majority of the elevated concentrations are found near that area.

The negative influence of the local anthropogenic activities has been suggested for organic pollutants (Grigoriadou et al., 2008a, b) and heavy metals in street dust and roadside soil along the major national road in Kavala's region (Christoforidis and Stamatis, 2009), by other researches as well. In fact, recently developed research, regarding the prefecture of Kavala, has reported that it has a higher rate of mortality (per 1000) by approximately 20% due to cancer, cardiac and pulmonary diseases than compared to the National average and that this observation could be linked to local environmental contamination activities (Theophanides et al., 2007).

5. Conclusions

The comparisons between the surface soil samples and the surrounding rocks of the study area indicate that the majority of the major elements (Al, Ca, Fe, K, Mg, P, Si), as well as of the trace elements (B, Ba, Cd, Ce, Co, Cr, Cs, Cu, Ga, Ge, Hg, La, Li, Mn, Mo, Ni, Rb, Sb, Se, Sn, Sr, Th, Ti, U, W, Y, Zr) are found in the surface soils of Kavala with such concentrations that are considered as the product of natural processes such as the weathering of parent rocks and pedogenesis. However, there are some elements, both major (Cl, Na, S) and trace (Ag, As, Pb, V, Zn) that are present in the

Table 2. Average concentrations for the trace elements (in mg kg⁻¹) of the surface soils and the surrounding rocks of the study area, and Enrichment Factors of the comparisons between the concentrations of the surface soils and the surrounding rocks.

Element	Rocks (total)	Marbles	Gneisses	Granites	Soils	Enrichment Factors (EF)			
						Soils vs. Rocks (total)	Soils vs. Marbles	Soils vs. Gneisses	Soils vs. Granites
Ag	0.07	0.07	0.07	0.07	0.64	9.3	9.5	9.0	9.4
As	1.85	1.96	1.77	1.81	55.06	29.8	28.0	31.0	30.3
B	5.33	5.50	8.62	1.86	8.02	1.5	1.5	0.9	4.3
Ba	32.82	19.59	39.25	39.62	97.24	3.0	5.0	2.5	2.5
Cd	0.41	1.01	0.15	0.05	0.58	1.4	0.6	3.8	12.7
Ce	8.27	2.62	12.47	9.72	23.78	2.9	9.1	1.9	2.4
Co	4.13	6.44	2.66	3.29	6.83	1.7	1.1	2.6	2.1
Cr	17.78	1.26	20.22	31.85	16.08	0.9	12.8	0.8	0.5
Cs	1.60	0.04	0.62	4.13	1.55	1.0	36.4	2.5	0.4
Cu	15.54	3.47	19.68	23.47	22.33	1.4	6.4	1.1	1.0
Ga	1.43	0.05	2.12	2.13	2.58	1.8	54.3	1.2	1.2
Ge	0.03	0.02	0.03	0.04	0.04	1.2	2.1	1.2	0.9
Hg	0.09	0.24	0.02	0.02	0.07	0.7	0.3	3.3	3.8
La	4.74	4.14	5.18	4.91	11.91	2.5	2.9	2.3	2.4
Li	4.96	0.26	5.15	9.45	5.65	1.1	21.6	1.1	0.6
Mn	269.45	72.02	340.87	395.45	524.20	1.9	7.3	1.5	1.3
Mo	1.44	0.08	1.76	2.49	0.28	0.2	3.5	0.2	0.1
Ni	11.10	18.08	6.35	8.85	14.90	1.3	0.8	2.3	1.7
Pb	8.08	4.16	11.63	8.44	62.36	7.7	15.0	5.4	7.4
Rb	18.04	0.22	22.58	31.32	16.69	0.9	77.2	0.7	0.5
Sb	0.12	0.06	0.15	0.13	0.30	2.6	4.9	1.9	2.3
Se	0.96	1.90	0.58	0.58	0.80	0.8	0.4	1.4	1.4
Sn	1.28	0.28	1.60	1.95	0.43	0.3	1.5	0.3	0.2
Sr	83.26	166.34	9.86	73.60	35.59	0.4	0.2	3.6	0.5
Th	6.10	0.40	10.23	7.68	5.65	0.9	14.1	0.6	0.7
Ti	75.31	1.64	144.85	79.44	74.52	1.0	45.5	0.5	0.9
U	1.52	0.17	0.49	3.90	0.90	0.6	5.4	1.8	0.2
V	5.57	1.09	7.75	7.88	18.42	3.3	17.0	2.4	2.3
W	1.85	5.29	0.18	0.07	0.43	0.2	0.1	2.3	6.5
Y	5.58	7.55	5.20	3.97	10.71	1.9	1.4	2.1	2.7
Zn	24.69	16.03	23.89	34.14	147.68	6.0	9.2	6.2	4.3
Zr	0.74	0.19	0.39	1.63	1.99	2.7	10.4	5.2	1.2

Table 3. Comparison between the soil samples that are inside the Industrial Zone (IZ) and those found outside (RS).

	IZ	RS		IZ	RS
element	average	average	element	average	average
Al*	4.35	4.81	Ge	0.03	0.05
Ca*	31.96	19.65	Hg	0.09	0.03
Cl*	1.57	0.18	La	9.94	16.05
Fe*	6.36	6.32	Li	5.88	5.16
K*	1.45	1.24	Mn	492.03	591.61
Mg*	3.09	2.31	Mo	0.36	0.11
Na*	2.60	0.37	Ni	14.98	14.73
P*	0.82	0.51	Pb	64.60	57.67
S*	0.93	0.15	Rb	15.60	18.99
Si*	0.25	0.28	Sb	0.32	0.26
Ag	0.83	0.22	Se	0.82	0.75
As	66.56	30.96	Sn	0.56	0.15
B	10.70	2.41	Sr	45.67	14.46
Ba	99.63	92.23	Th	5.14	6.73
Cd	0.61	0.52	Ti	85.68	51.13
Ce	19.64	32.44	U	0.85	1.00
Co	6.56	7.39	V	18.25	18.77
Cr	16.35	15.50	W	0.53	0.21
Cs	1.59	1.47	Y	9.65	12.93
Cu	26.81	12.94	Zn	192.73	53.30
Ga	2.72	2.30	Zr	1.98	2.01

IZ: samples inside the industrial zone. RS: samples outside the industrial zone (reference samples). Concentrations are expressed in mg kg^{-1} except for those elements marked with asterisk, which are expressed in g kg^{-1} .

surface soils of the study area with elevated concentrations that cannot be regarded as the sole product of natural processes. In these cases, it seems very likely that the anthropogenic activities taking place in the industrial area of Kavala have contributed, at least partly, to these elevated concentrations, especially for the samples situated inside the industrial zone of Kavala. Additional statistical treatment of the data presented herein would provide further insight in the relationships between the elemental content of the surface soils and the natural and anthropogenic processes taking place in the study area.

6. Acknowledgments

The authors would like to acknowledge the technical assistance provided by the personnel of the Faculty of Geology of the University of Barcelona, the SCT-UB and ICTJA-CSIC, Barcelona (Spain). Georgios Papastergios wishes to acknowledge the support of the Greek State Scholarships Foundation (IKY). This work was partially carried out in the framework of PEGEFA 2005SGR-00795 Research Consolidated Group, funded by AGAUR-DURSI, Generalitat de Catalunya. The constructive comments of an anonymous reviewer are greatly appreciated.

7. References

- Christoforidis A. and Stamatis N. 2009. Heavy metal contamination in street dust and roadside soil along the major national road in Kavala's region, Greece. *Geoderma*, 151: 257–263.
- Christofides G., Koroneos A., Soldatos T., Eleftheriadis G. and Kiliyas, A., 2001. Eocene magmatism (Sithonia and Elatia plutons) in the Internal Hellenides and implications for Eocene-Miocene geological evolution of the Rhodope Massif (Northern Greece). *Acta Vulcanologica*, 13: 73-89.
- Cui Y.J., Zhai R.H., Huang Y.Z., Qiu Y. and Liang J.Z., 2005. Exposure to metal mixtures and human health impacts in a contaminated area in Nanning, China. *Environment International*, 31: 784-790.
- Faure G. 1992. Principles and applications of inorganic geochemistry. N.Y. Macmillan Pub. Co. 626p.
- Fernandez-Turiel J.L., Llorens J.F., López-Vera F., Gómez-Artola C., Morell I. and Gimeno D., 2000. Strategy for water analysis using ICP-MS. *Fresenius' Journal of Analytical Chemistry* 368: 601-606.
- Fernandez-Turiel J.L., Aceñolaza P., Medina M.E., Llorens J.F. and Sardi F., 2001. Assessment of a smelter impact area using surface soils and plants. *Environmental Geochemistry and Health*, 23: 65-78.
- Filippidis A., Georgakopoulos A., Kassoli-Fournaraki A., Misaelides P., Yiakkoupis P. and Broussoulis J., 1996. Trace element contents in composite samples of three lignite seams from the central part of the Drama lignite deposit, Macedonia, Greece. *International Journal of Coal Geology*, 29: 219-234.
- Georgakopoulos, A., Fernandez-Turiel, J.L., Christanis, K., Kalaitzidis, S., Kassoli-Fournaraki, A., Llorens, J.F., Filippidis, A. and Gimeno, D., 2001. The Drama basin water: quality and peat/lignite interaction. *Environmental Geology*, 41: 121-127.
- Grigoriadou A., Schwarzbauer J. and Georgakopoulos A., 2008a. Molecular indicators for pollution source identification in marine and terrestrial water of the industrial area of Kavala city, North Greece. *Environmental Pollution*, 151: 231–242.
- Grigoriadou A., Schwarzbauer J. and Georgakopoulos A., 2008b. Organic geochemical parameters for estimation of petrogenic inputs in the coastal area of Kavala City, Greece. *Journal of Soils and Sediments*, 8: 253–262.
- H.N.M.S. (Hellenic National Meteorological Service), 1978. Climatic data of the Greek network, period 1930 – 1975, (in Greek), 100p.
- Hesteborg D., 1998. Biochemical cycles and processes leading to changes in mobility of chemicals in soils. *Agriculture Ecosystems and Environment*, 67: 121-133.
- Kabata-Pendias A. and Pendias H., 2001. Trace elements in soils and Plants, 3rd ed., CRC Press, New York, 413p.
- Kiliyas A.A., Falalakis G. and Mountrakis D.M., 1999. Cretaceous – Tertiary structures and kinematics of the Serbomacedonian metamorphic rocks and their relation to the exhumation of the Hellenic hinterland (Macedonia, Greece). *International Journal of Earth Sciences*, 88: 513-531.
- Papastergios G., Georgakopoulos A., Fernandez –Turiel J.L., Gimeno D., Filippidis A., Kassoli-Fournaraki A. and Grigoriadou A., 2004. Heavy Metals and Toxic Trace elements contents in selected areas of the Kavala Prefecture, Northern Greece, Bulletin of the Geological Society of Greece, 36(1): 263-272.
- Papastergios G., Filippidis A., Christofides G., Kassoli-Fournaraki A., Fernandez-Turiel J.L., Georgakopoulos A. and Gimeno D., 2007. Trace elements contents in uncultivated surface soils in the Kavala area, northern Greece, Bulletin of the Geological Society of Greece, 40(3): 1491-1498.
- Papastergios G., 2008. Environmental geochemical study of soils and sediments in coastal areas, east of Kavala (Macedonia, Greece) and production of geochemical maps via the use of GIS. (in Greek, with English summary), PhD, Aristotle University of Thessaloniki, Greece, 224p.
- Papastergios G., Fernandez–Turiel J.L., Georgakopoulos A. and Gimeno D. 2009. Natural and anthro-

- pogenic effects on the sediment geochemistry of Nestos River, northern Greece. *Environmental Geology*, 58: 1361–1370.
- Pe-Piper G. and Piper D.J.W., 2002. The igneous rocks of Greece, The anatomy of an orogen, Gebrüder Borntraeger, Berlin; 573p.
- Petalas C., Pliakas F., Diamantis I. and Kallioras A., 2004. Study of the distribution of precipitation in District of Eastern Macedonia and Thrace for the Period 1964-1998, (in Greek with English abstract), Bulletin of the Geological Society of Greece, 36(2): 1054-1063.
- Ramsey M.H., 1997. Sampling and sampling preparation. In: Gill, R., (Editor), Modern Analytical Geochemistry, An introduction to Quantitative Chemical Analysis Techniques for Earth, Environmental and Materials Scientists, Pearson Education Limited, England, 329p.
- Sastre J., Sahuquillo A., Vidal M. and Rauret G., 2002. Determination of Cd, Cu, Pb and Zn in environmental samples: microwave-assisted total digestion versus aqua regia and nitric acid extraction. *Analytica Chimica Acta*, 462: 59-72.
- Theophanides M., Anastassopoulou J., Vasilakos C., Maggos T. and Theophanides T., 2007. Mortality and pollution in several Greek cities. *Journal of Environmental Science and Health, Part A*, 42: 741-746.
- Vavelidis M., Christofides G. and Melfos V., 1996. The Au-Ag bearing mineralization and placer gold of Palea Kavala (Macedonia, N. Greece), Terranes of Serbia, The formation of the geologic framework of Serbia and the adjacent regions, Eds: Knežević V. and Krstić B., Belgrade 1996, 311-316p.
- Vavelidis, M., Melfos, V. and Eleftheriadis, G., 1997. Mineralogy and microthermometric investigations in the Au-bearing sulphide mineralization of Palea Kavala (Macedonia, Greece). In: Papunen H. (Editor). *Mineral deposits: Research and exploration, where do they meet?* Balkema, Rotterdam, 343-346.
- Walsh J.N., Gill R. and Thirwall M.F., 1997. Dissolution procedures for geochemical and environmental samples. In: Gill, R., (Editor), *Modern Analytical Geochemistry, An introduction to Quantitative Chemical Analysis Techniques for Earth, Environmental and Materials Scientists*, Pearson Education Limited, England, 329p.

COMPARISON OF SAMPLING TECHNIQUES FOR ISOTOPIC ANALYSIS OF SHALLOW MARINE CARBONATES

**Psomiadis D.^{1,2}, Dotsika E.¹, Albanakis K.², Zisi N.¹, Poutoukis D.³
and Lazaridis A.⁴**

¹ *Stable Isotope Unit, Institute of Materials Science, NCSR Demokritos, Agia Paraskevi Attiki, Greece, dapsom@ims.demokritos.gr, edotsika@ims.demokritos.gr, nzissi@ims.demokritos.gr*

² *Department of Physical and Environmental Geography, School of Geology, Aristotle University of Thessaloniki, Greece, albanaki@geo.auth.gr*

³ *General Secretariat for Research and Technology, Mesogion 14-18, 11510 Athens, Greece, dpoutoukis@gsrt.gr*

⁴ *Greek Ministry of National Education and Religious Affairs, Andrea Papandreou 37, Marousi 15180 Greece*

Abstract

Recent studies have widely used beachrock samples for isotopic and dating techniques; however the source matrix of the analyzed samples varied. Bulk rock material, skeletal fragments, allochems and pure cement have been used in different studies. Basic parameters of each technique are crucial for the accuracy and the reliability of the obtained results, affecting each time important agents. This study includes isotopic analyses ($\delta^{13}\text{C}$, $\delta^{18}\text{O}$) of marine carbonates (beachrocks) from the coasts of N. Greece (Thassos island). The sub-sampling was carried out along beachrock cores, following different procedures and protocols. The obtained results show in general expecting differences in isotopic composition of the samples. Experiments that included heating of the samples show an influence on oxygen isotope. Different separation and selection of sampling material affect majorly the isotope of carbon (^{13}C). Differences are attributed to the origin of the carbonate component of the analyzed material. The study indicates that a full-range of comparison experiments should be implemented in order to define in detail the analytical parameters that affect isotopic measurements. The results of that kind of studies will be used not only in stable isotope analyses but also in a variety of methods used in palaeoclimatic and palaeoenvironmental research.

Key words: *marine cements, beachrock, sampling, stable isotopes.*

1. Introduction

The rapid cementation of beach sediments in the intertidal zone leads to the formation of characteristic syndimentary lithified structures termed as beachrocks (Rey et al., 2004). Beachrock is a hard, rocky, coastal formation, lithified in the intertidal zone by carbonate cements. The importance of beachrocks can be rendered in three main topics: their impacts on coastal evolution (Cooper 1991), their role as sea-level indicators (Hopley, 1986; Caldas et al., 2006) and the information they contain regarding the coastal processes of cementation and palaeoenvironmental evolution (Longman, 1980; Vieira and De Ros, 2006).

There have been numerous mechanisms proposed for beachrock cementation by calcium carbonate (Scholten, 1972):

1. Abiotic precipitation from evaporation of sea water (Ginsburg, 1953; Emery et al., 1954; Stoddart and Cann, 1965; Moore and Billings, 1971; Milliman, 1974; Beier, 1985).
2. Abiotic precipitation from ground water (Russell, 1962, 1963; Deboo, 1962; Russell and McIntire, 1965).
3. Abiotic precipitation in the salt water-fresh water mixing zone (Schmalz, 1971; Moore, 1973).
4. CO₂ degassing from beach ground waters (Hanor, 1978).

Several studies have been carried out using the isotopic signature of carbonate cements in the marine-phreatic environment. Authors have used in the past stable isotopes (Beier, 1985; Chaves and Sial, 1998; Friedman, 2004; Holail and Rashed, 1992; Land, 1970; Vieira et al., 2006) based on whole-rock samples and isolated cement. The case of whole-rock sampling for isotopic analysis carries wide erroneous parameters which may lead to false isotopic fingerprints for the carbonate precipitates and thus to misleading conclusions on diagenetic environments and palaeoclimatic interpretations. For reference, Vieira et al. (2006) attempted to determine the origin of Holocene beachrocks in NE Brazilian coast by measuring the isotopic composition of bulk-rock samples after defining their cement petrography. The range of isotopic values reached up to 11.4‰ and 3.9‰ for $\delta^{13}\text{C}$ and $\delta^{18}\text{O}$ respectively, indicating “contaminated” samples by allogenic carbonates. Also, Land (1970) studied the diagenetic features between phreatic and vadose beachrocks from Bermuda, indicating a wide range of $\delta^{13}\text{C}$ values (2.2 to -6.8‰) and relatively lower differences in $\delta^{18}\text{O}$. Other studies used beachrock cement (e.g. Chaves and Sial, 1998; Calvet et al., 2003; Spurgeon et al., 2003; Friedman, 2004; Guerra et al., 2005) isolated by simple techniques, achieving lower range of isotopic values however showing wide differences between same environment of precipitation.

This study aims to compare the isotopic composition of specific levels inside a carbonate formation like beachrock. In particular, samples from the same level were analyzed, differing from each other on the sampled material. Bulk rock sample, macroscopic and microscopic selection, stirred and dried material are some of the selected methods of sample extraction for isotopic analysis. The results are plotted on diagrams and compared, in order to evaluate the reliability and suitability of sampling methods for isotopic analysis. Samples were taken from the same level of the formation in order to avoid differences of values originated in different precipitation conditions.

2. Setting of the study area

The studied beachrock used in this work is located in Thassos Island (N. Greece), in Northern Aegean Sea. The study area is located at the west coast of the island, between Skala Sotira and Skala Kallirachis villages (Fig. 1). The beach is 375 m long and reaches width of 25 m (Psomiadis et al., 2009a). Coastal sediments are fine to medium well graded sand with some gravels on the south side where a stream is discharging.

The prevalent rocks in the area are gneiss and marbles. The basins that end up to the study area include Holocene sediments, Miocene marbles, marbles and gneiss alternations and Maries gneiss (Mountrakis, 1985). Two local ephemeral streams end up to the study beach, with a total length of 26.48 km, which cross carbonate rocks and transfer similar sediments to the coast. The area of Thassos is characterized by coastal – marine climatic type, transitional to continental climate (high sum-

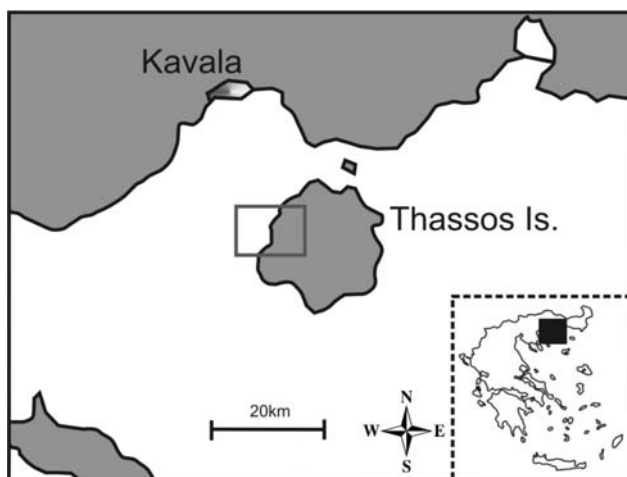


Fig. 1: Simplified map showing the area of study. The studied beachrock is located at the west coast of Thassos Island, between Skala Sotira and Skala Kallirachis villages.

mer temperature, storms), due to the slight distance of the island from the coast of Macedonia at the north. The average annual temperature is 15,8°C, the average annual precipitation is 770 mm and the prevalent wind direction is NW for the western part of the island (study area). The exposed beachrock is located in the swash zone and dips gently seawards (mean 5°), following the arrangement of the beach. The main body of the formation has a total length of 305 m and exposure width 2-10 m. The height of the beachrock at its underwater face reaches up to 70 cm. This face is quite steep and has been undercut in many places, resulting in cracking, collapsing, even in displacement of blocks of the formation. Ultra-sonic velocities recorded that deeper layers are less porous than surficial, indicating older age at the bottom (Psomiadis et al., 2009b). At the north end, a jetty separates the study beach from the prolongation of the coastline at the north.

3. Methods

3.1 General

Beachrock formation from S.Kallirachis beach (Thassos Island, N. Greece, Fig. 1) was drilled and two cores were used in the experimental procedure. The cores were 8 and 20cm long each and their diameter was 2.5cm. Whole-rock samples were separated from the cemented sediments. The different procedures of sample handling included specific parameters that may cause isotopic fractionation (e.g. temperature). The techniques are separated to mechanical and physico-chemical. The first group consists of a) whole-rock grinding, b) macroscopic separation by light grinding, vibration and selection of pale dry grapes, c) microscopic separation by stereo-microscopic selection of carbonate grains, and d) microscopic selection of quartz grains with carbonate cement coating. The physico-chemical procedures included a) whole-rock processing by light grinding, dilution in distilled water by stirring, extraction of CO₃⁻ solution and drying in room temperature (approx. 48h), and b) whole-rock processing by light grinding, dilution in distilled water by stirring, extraction of CO₃⁻ solution and drying in oven at 70°C for 24h. All samples were grinded to powder after processing and δ¹³C and δ¹⁸O isotopic ratios were measured (vs. PDB standard) on a Thermo Delta V Plus isotope ratio mass spectrometer equipped with a GasBench II device at Stable Isotope Unit, I.M.S., NCSR Demokritos,

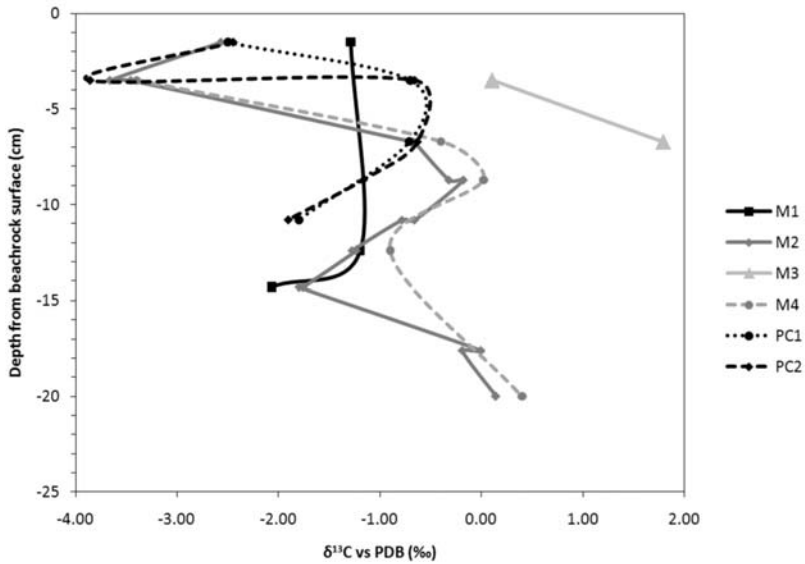


Fig. 2: Carbon isotopic variation of beachrock samples, processed by 6 different techniques (4 mechanical and 2 physicochemical). M1: whole-rock grinding, M2: macroscopic separation by light grinding, vibration and selection of pale dry grapes, M3: microscopic separation by stereo-microscopic selection of carbonate grains, M4: microscopic selection of quartz grains with carbonate cement coating, PC1: whole-rock processing by light grinding, dilution in distilled water by stirring, extraction of CO_3^{2-} solution and drying in room temperature (approx. 48h), PC2: whole-rock processing by light grinding, dilution in distilled water by stirring, extraction of CO_3^{2-} solution and drying in oven at 70°C for 24h.

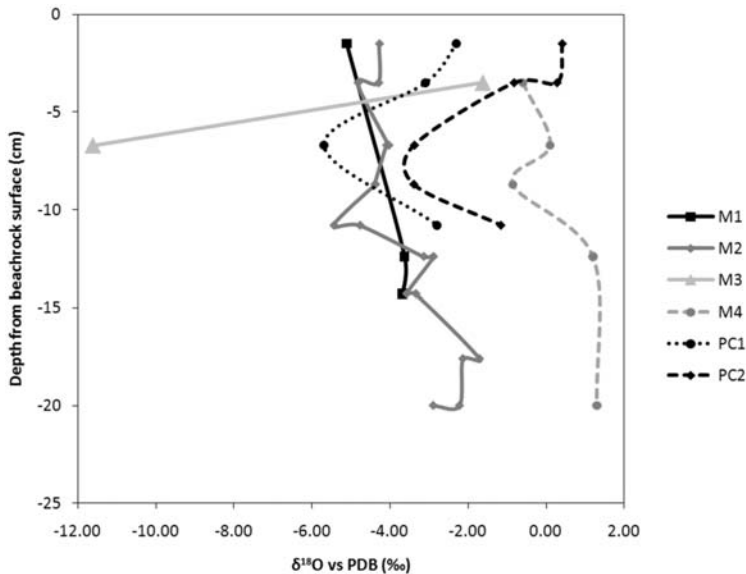


Fig. 3: Oxygen isotopic variation of beachrock samples, processed by 6 different techniques (4 mechanical and 2 physicochemical). Legend same as Figure 2. The two cores are correlated relatively to the beachrock surface, in order to have one reference depth for all samples. The number of samples per technique varies, depending on the physical or chemical tolerance of the material during the laboratory experimental processing.

Athens, after addition of H_3PO_4 for CO_2 production at 72°C . The standards used for comparison were NBS 19 and NBS 18 carbonates and an internal Carrara marble standard.

4. Conclusions-Results

Carbon and oxygen isotopic composition of the samples was plotted in diagrams versus their depth from beachrock surface (Fig. 2 and 3). Isotopic variation of $\delta^{13}\text{C}$ indicates a general similarity for most techniques, with a light divergence for M1 and a total alteration for M3. Except from the fact that these two techniques included the fewer samples, resulting in lower analytical resolution, their differentiation from the other techniques could be attributed to material composition (especially for M3) as the microscopic grain selection results in more thorough carbonate material separation for analysis. Regarding the oxygen isotopic variation, the observed alterations can be dissociated in two basic causes: either physicochemical implications through processing (temperature, PC1 vs PC2) or material composition (M1, M2 vs M4). In particular, the physicochemical techniques reach a good agreement in variation but they show an alteration ($\delta^{18}\text{O}$ enrichment in PC2), which is attributed to possible temperature effect on diluted and re-precipitated carbonate crystals during processing (Clayton, 1961). Techniques M1 and M2 gave similar results, whereas M4 follows same isotopic variation versus depth relatively to M1 and M2 but shows a $\delta^{18}\text{O}$ enrichment, probably due to different material composition (totally bulk material for M1 and M2 versus carbonate coating around quartz grains for M4). M3 is presented irregular to the other techniques in that case too.

In conclusion, isotopic composition of whole-rock beachrock samples is affected in different intensity by the experimental processing during preparation for analysis. Carbon and oxygen isotopes show different variation due to their sensitivity to physicochemical agents. The material composition affects greatly $\delta^{13}\text{C}$, while $\delta^{18}\text{O}$ is influenced mostly by temperature, and secondly by the purity of the carbonate material. Further research should focus on specific parameters like mineralogy of cement, affecting the isotopic fingerprint of carbonate cements.

5. Acknowledgments

The authors would like to thank Mr. Paltzoglou A. and Mr. Zafeiriadis C. for their handful assistance during drilling.

6. References

- Beier, J.A., 1985. Diagenesis of Quaternary Bahamian beachrock: petrographic and isotopic evidence, *Journal of Sedimentary Petrology*, 55 (5), 755-761.
- Caldas, L.H.O., Stattegger, K., Vital, H., 2006. Holocene sea-level history: Evidence from coastal sediments of the northern Rio Grande do Norte coast, NE Brazil. *Marine Geology*, 228, 39-53.
- Calvet, F., Cabrera, M.C., Carracedo, J.C., Mangas, J., Pérez-Torrado, F.J., Recio, C., Travé, A., 2003. Beachrocks from the island of La Palma (Canary Islands, Spain). *Marine Geology*, 197 (1-4), 75-93.
- Chaves, N.S., Sial, A.N., 1998. Mixed oceanic and freshwater depositional conditions for beachrocks of northeast Brazil: Evidence from carbon and Oxygen isotopes. *International Geology Review*, 40 (8), 748-754.
- Clayton, R.N., 1961. Oxygen isotope fractionation between calcium carbonate and water. *The Journal of Chemical Physics*, 34 (3), 724-726.
- Cooper, G.A., 1991. Beachrock formation in low latitudes: implications for coastal evolutionary models. *Marine Geology*, 98, 145-154.

- Deboo, P.B., 1962. A preliminary petrographic study of beach rock. *Natl. Coastal and Shallow Water Research Conf. (1st)*, 456-458.
- Emery, K.O., Tracey, J.I., Jr., Ladd, H.S., 1954. *Geology of Bikini and nearby atolls*. U.S. Geol. Survey Prof. Pap. 260-A, 265 pp.
- Friedman, G.M., 2004. Holocene chronostratigraphic beachrocks and their geologic climatic significance. *Geochemical Investigations in Earth and Space Science: A Tribute to Isaac R. Kaplan*, 125-142.
- Ginsburg, R.N., 1953. Beach rock in South Florida. *Journal of Sedimentary Petrology*, 23, 85-92.
- Guerra, N.C., Kiang, C.H., Sial, A.N., 2005. Carbonate cements in contemporaneous beachrocks, Jaguaribe beach, Itamaracá island, northeastern Brazil: Petrographic, geochemical and isotopic aspects. *Anais da Academia Brasileira de Ciencias*, 77 (2), 343-352.
- Hanor, J.S., 1978. Precipitation of beachrock cements: mixing of marine and meteoric waters vs. CO₂ degassing. *Journal of Sedimentary Petrology*, 48, 489-501.
- Holail, H., Rashed, M., 1992. Stable isotopic composition of carbonate-cemented recent beachrock along the Mediterranean and the Red Sea coasts of Egypt. *Marine Geology*, 106 (1-2), 141-148.
- Hopley, D., 1986. Beachrock as a sea-level indicator. In: Van de Plassche O (ed) *Sea-level Research*. Galliard Printers, Great Yarmouth, 157-173.
- Land, L.S., 1970. Phreatic versus vadose meteoric diagenesis of limestones: Evidence from a fossil water table. *Sedimentology*, 14, 175-185.
- Longman, M.W., 1980. Carbonate diagenetic textures from nearsurface diagenetic environments. *American Association of Petroleum Geologists Bulletin*, 64(4), 461-487.
- Milliman, J.D., 1974. *Marine Carbonates*. Springer-Verlag, Berlin, 375 pp..
- Moore, C.H., 1973. Intertidal carbonate cementation Grand Cayman, West Indies. *Journal of Sedimentary Petrology*, 43, 591-602.
- Moore, C.H., Jr., Billings, G.K., 1971. Preliminary model of beachrock cementation, Grand Cayman island, B.W.I. In: Bricker, O.P. (Ed.), *Carbonate Cements*. Johns Hopkins Press, Baltimore, MD, 40-43.
- Mountrakis, D., 1985. *Geology of Greece*. University Studio Press, Thessaloniki, 27-35 (in greek).
- Psomiadis, D., Tsourlos, P., Albanakis, K., 2009a. Electrical Resistivity Tomography mapping of beachrocks: application to the island of Thassos (N. Greece). *Environmental Earth Sciences*, 59(1), 233-240, doi: 10.1007/s12665-009-0021-9.
- Psomiadis, D., Vogiatzis, D., Albanakis, K., Christaras, V., Dotsika, E., Zisi, N., 2009b. Valuation of beachrock formation through ultrasonic pulse technique. A method to compare porosities in horizontal and vertical aspects. *Geophysical Research Abstracts*, Vol. 11, EGU2009-1472, Vienna, Austria.
- Rey, D., Rubio, B., Bernabeu, A.M., Vilas, F., 2004. Formation, exposure, and evolution of a high-latitude beachrock in the intertidal zone of the Corrubedo complex. *Sedimentary Geology*, 169, 93-105.
- Russell, R.J., 1962. Origin of beach rock. *Zeitschrift fur Geomorphologie*, 6, 1-16.
- Russell, R.J., 1963. Beach rock. *Journal of Tropical Geography*, 17, 24-27.
- Russell, R.J., McIntire, W.G., 1965. Southern hemisphere beach rock. *Geogr. Rev.* 55, 17-45.
- Schmalz, R.F., 1971. Formation of beachrock at Eniwetok Atoll, In: Bricker P (ed) *Carbonate Cements*. Johns Hopkins Press, Baltimore, MD, 17-24.
- Scholten, J.J., 1972. Beach rock: a literature study with special reference to the recent literature. *Zentralbl. Geol. Palaontol. Teil I*, 351-368.
- Spurgeon, D., Davis Jr., R.A., Shinnu, E.A., 2003. Formation of 'Beach Rock' at Siesta Key, Florida and

- its influence on barrier island development. *Marine Geology*, 200 (1-4), 19-29.
- Stoddart, D.R., Cann, J.R., 1965. Nature and origin of beach rock. *Journal of Sedimentary Petrology*, 56, 422-428.
- Vieira, M.M., De Ros, L.F., 2006. Cementation patterns and genetic implications of Holocene beachrocks from northeastern Brazil. *Sedimentary Geology*, 192, 207-230.
- Vieira, M. , Sial, A., de Ros, L., 2006. Origin of Holocene Beachrock Cements in Northeastern Brazil Revealed from Carbon and Oxygen Isotopes. *V South American Symposium on Isotope Geology*, IGCP 478, Montevideo, Uruguay.

ANTHROPOGENIC AND GEOGENIC CONTAMINATION DUE TO HEAVY METALS IN THE VAST AREA OF VARI, ATTICA

Serelis K.G.¹, Kafkala I.G.¹, Parpodis K.¹ and Lazaris S.²

¹ *Laboratory of Mineralogy-Geology, Agricultural University of Athens, 75, Iera Odos, 118 55 Athens, serelis@aua.gr, kafkala@aua.gr, kparpodis@yahoo.gr*

² *Agroland S. A. spyrosfaz@yahoo.com*

Abstract

The purpose of this work was to investigate the soil heavy metal contamination of the area between Koropi and Vari, in Attica, Greece and to determine their anthropogenic or/and geogenic-lithogenic origin. Soil samples were taken from two different depths of 23 uncultivated sampling sites. Determined heavy-metal concentrations ranged widely; mean values in several sites were elevated and much higher than the soil grand mean worldwide. The higher Co and Ni contamination was found in the lower soil depth (10-25cm), while for Cd, Zn, and Pb in the upper depth (0-10cm). These results, in connection with the performed Hierarchical Cluster Analysis and Principal Component Analysis, indicate that there are two contamination sources. The first, concerning Co-Ni, is a geogenic-lithogenic source and the second, concerning Zn-Cd and Pb, is considered as an anthropogenic source. Since in the study area there is no evidence of an existing anthropogenic source (e.g. an industry) and the parent material does not confirm and give reason for the elevated Zn, Cd and Pb contents, it could be concluded that this contamination was due to ancient metallurgical activities in the area.

Key words: *soil contamination, heavy metals, anthropogenic factors, geogenic- lithogenic factors, HCA, PCA, Vari, Attica.*

1. Introduction

Heavy metal soil contamination is a serious environmental problem, mainly due to its impact on human health (Fytianos et al., 2001, Imperato et al., 2003; Selinus et al., 2005; Girard et al., 2005; Shakeri et al., 2009; Zhuang et al., 2009; Singh et al., 2010). Heavy metals are found in the crust in less than 0.01% (Kabata-Pendias and Pendias, 2001). The existence of heavy metals in soils is attributed to both anthropogenic and geogenic (particularly lithogenic) factors. The main human activities resulted in environmental contamination are: mining and smelting, industrial activities, agricultural practices, fossil fuel combustion, waste disposal, transportation etc. and they have been discussed in numerous reports and publications (e.g. Alloway, 1995; Dudka and Adriano, 1997; Kabata-Pendias and Pendias, 2001; Wong et al., 2002; Girard et al., 2005; Selinus et al., 2005; Kribek et al., 2010).

The presence and distribution of heavy metals in soils is influenced mainly by the parent material, the chemical and physical soil properties, the metal speciation, and the climatic conditions. The mineral content of the parent material is one of the most important factors for the amount of trace elements in soils, irrespective of classification or the amount of weathering (Burt et al., 2003).

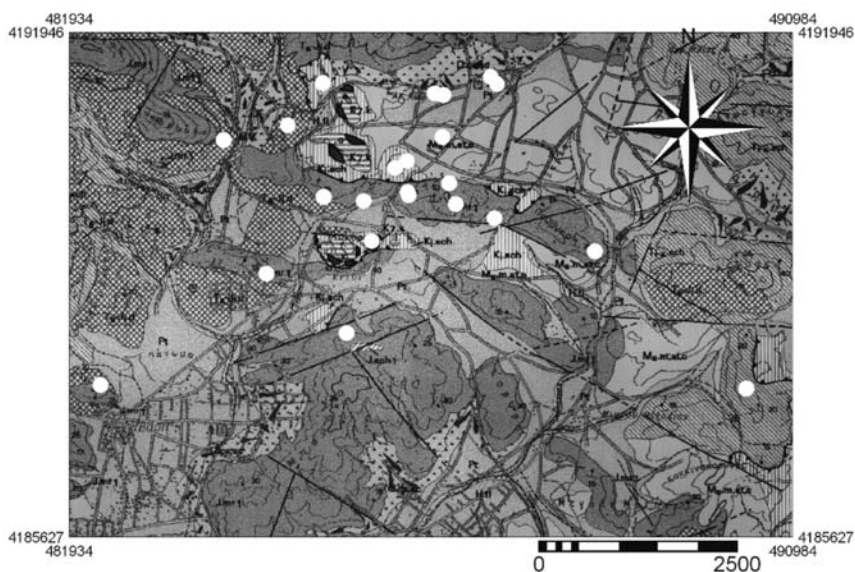


Fig. 1: Map showing the locations of the soil sampling sites. a) Ts-J1d, Pirnari dolomites, b) J.mr1, J.sch1: Lower marble, schists intercalations respectively, c) K1.sch, K1.K: schists, recrystallized limestones respectively, d) K7.k: limestones, e) O: ofiolites, f) Ms.m, st, c: marls, loams, sandstones, conglomerates, g) Pt: Pleistocene deposits, h) Q.cs, sc: Quaternary undivided old and new talus cones and scree (I.G.M.E. KOROPI-VARI sheet 2004 Geological map, 1:50.000).

Soil contamination can be distinguished according to the intensity, the number, and the distance of pollution sources. **“Diffuse” contamination** is the contamination due to 1) a numerous sources, which are poorly identified, 2) sources that are in long distances (dozens of kilometres and sometimes hundreds), 3) mobile sources (vehicles, airplanes etc.). Contamination of this kind is usually moderate. **“Punctual” contamination** is due to an identified source, often close to the contaminated soil. This kind of contamination could be due to industrial activities or a heavy vehicle circulation in highways. Referring to a small region, the displacement of a punctual contamination to a diffusive one is given by the following example: the atmospheric emissions by a Pb smelter are a punctual contamination for surrounding soils but they contribute to a diffusive contamination as they move away. In this case, we have a pollution zone “diffuse of proximity” around the source and in many kilometres (Robert, 1996 in Girard et al. 2005).

Our previous studies (Lazaris, 2008) showed that in the forest (uncultivated) area of Vari, Attica (Fig. 1) multiple contaminants co-exist; namely Pb, Cd, Ni, Co, and Zn were determined in the soil horizons. The purpose of this work is to determine the concentrations of the heavy metals Cd, Zn, Pb, Co, and Ni in the soil of the study area and to investigate whether the possible elevated concentrations found are due to anthropogenic or geogenic sources.

2. Materials and Methods

2.1 Study area and Sampling

The study area belongs to the Attic-Cycladic geotectonic zone of Greece. It is localized by a rectangular with X,Y coordinates of upper left corner [481934, 4191946] and lower right corner [490984, 4185627]. The lithologic formations of the study area are dolomites, marble, schists, lime-

stones, ofiolites (mafic rocks), marls, loams, sandstones, and quaternary deposits (Fig. 1). For centuries, the non-forest area was used for agricultural purposes, which through the years has been transformed to a light industrial one. The last few years though, there is an important urbanisation, legal and illegal. Soil sampling was conducted during October 2008. Twenty three sample sites were chosen (Fig.1) in uncultivated areas and soil was collected from two different depths in each sample site: i) 0-10cm (A depth) and ii) 10-25cm (B depth), making the number of samples forty six. The samples have been transported to the laboratory the same day and have been air-dried at room temperature for several days and passed through a 2mm stainless-steel sieve. Sub-samples were taken for further analysis.

2.2 Analytical Methods

Soil characteristics were determined following standard procedures. Measurement of soil pH in 1:1 (w/v) soil to deionised water agitated for 1 hour. Organic matter concentration was determined by the Wakley-Black method which is based on $K_2Cr_2O_7-H_2SO_4$ oxidation (Nelson and Sommers, 1982). The determination of total carbonate was performed as equivalent $CaCO_3$ percentage using a Bernard calcimeter (Allison and Moodie, 1965). Particle size distribution was determined by Hydrometer method (Bouyoukos, 1951). Heavy-metal concentrations were determined by extraction with Na_2EDTA (ethylenediamine tetraacetic acid) which extracts the exchangeable, carbonate-bound, Fe and Mn oxide-bounds, and a significant quantity of organic-bounds (Clayton and Tiller, 1979). The method involves shaking 10g of soil with 80cm³ of 0.005M EDTA (pH=6.0) in polypropylene tubes for 15 hours at 20°C. EDTA extraction procedure was chosen because it is widely accepted as a successful extractant and it is traditionally proposed for calcareous soils (Quevauviller et al. 1996; Quevauviller et al. 1998). The samples for the extraction procedure (Na_2EDTA) were centrifuged for 20min at 3000rpm ($\approx 1500g$) to compact most of the soil at the bottom of the tubes. The supernatant was filtered through a Whatman No 42 filter paper. The filtrates were analyzed for heavy metals using flame atomic absorption spectrometry (FAAS).

2.3 Statistical Processing

Descriptive statistics and multivariate statistical processing were performed. The data were classified into two groups according to their sample soil depth. Hierarchical Cluster Analysis (HCA) and Factor Analysis (FA) and namely the Principal Component Analysis (PCA) were applied with the use of SPSS 11.0.0 in order to obtain a visual interpretation of data and to detect similarities or differences among them. HCA is used to identify relatively homogeneous groups. The dendrograms were extracted using the Ward method and squared Euclidean distance and there has been a z standardization of the data. PCA analysis, a central tool in chemometrics, was performed using varimax rotation in order to make interpretable components. The component number was selected by using the Kaiser criterion (eigenvalue higher than 1).

3. Results- Discussion

Most soils of the study area are Alfisols and in particular suborder Xeralfs. Their mean organic matter content is 0.05 (A depth) and 0.04 (B depth), while mean pH value in both depths is 8.0. The soils are characterised as silty loamy, with clay mean values of 0.13 (A depth) and 0.18 (B depth) and corresponding silt values of 0.41 and 0.55 respectively (Table 1).

Heavy metal -EDTA extracted- concentrations ranged widely among sample sites (data not shown);

Table 1. Descriptive statistics of soil properties and heavy-metal concentrations (mg kg⁻¹) for A, B depths.

A	OM _A	pH _A	CaCO _{3A}	CLAY _A	SILT _A	Pb _A	Cd _A	Co _A	Ni _A	Zn _A
Min.	0.01	7.70	0.10	0.04	0.24	9.65	0.00	0.50	0.00	1.29
Max.	0.08	8.30	0.50	0.23	0.68	1779.12	1.78	15.98	18.58	23.22
Mean	0.05	8.01	0.11	0.13	0.41	169.35	0.60	7.19	6.98	6.21
Std. Dev.	0.02	0.13	0.12	0.06	0.13	381.37	0.47	4.54	4.57	4.88
B	OM _B	pH _B	CaCO _{3B}	CLAY _B	SILT _B	Pb _B	Cd _B	Co _B	Ni _B	Zn _B
Min.	0.01	7.7	0.01	0.08	0.34	10.66	0.00	0.14	0.00	0.40
Max.	0.07	8.4	0.38	0.32	0.70	1649.88	1.45	18.44	25.77	13.65
Mean	0.04	8.00	0.09	0.18	0.55	161.36	0.53	8.30	9.43	3.52
Std. Dev.	0.01	0.15	0.93	0.08	0.08	349.31	0.39	5.66	6.36	3.12
Grand mean*						25*	0.175**	7.90*	22*	64*
Geometric mean**										
OM=Organic Matter										

determined mean values of the measured heavy metals in several sites were elevated and much higher than the soil grand mean worldwide (Table 1), as they were reported by Kabada-Pendias and Pendias (2001). Maximum, minimum, and mean values of the examined elements of the entire study area are presented in Table 1. Significant differences and elevated standard deviations were observed.

The higher Co and Ni contamination is found in the lower depth (10-25cm) indicating that they are derived from the parent material, while for Cd, Zn, and Pb in the upper depth (0-10cm) probably due to anthropogenic sources.

It is well known that cobalt and nickel are concentrated in soil horizons rich in organic matter and clays (Van Hullebusch et al., 2006; Lin et al., 2008). They are immobile in alkaline conditions since their oxides, hydroxides, and carbonate forms are very insoluble, while in acid conditions dissolution and leaching are more likely to occur (Alloway, 1995). The study area is not an acidic one and therefore Co and Ni are in a rather immobile form indicating that leaching is difficult to occur. Therefore, it could be suggested that the higher contents in the B depth originate from the parent material; this suggestion is amplified by the presence of relicts of ofiolites, meta-mafic veins, and carbonate rocks (I.G.M.E. Geological map, issue Koropi, 1:50.000) in the area, which inherit the highest amounts of Co and Ni in soils in accordance with Alloway (1995) and Kabata-Pendias and Pendias (2001).

Zn and Cd are very mobile and bioavailable metals, and their higher contents in A depth suggest their anthropogenic origin. Specifically for lead, measured values were extremely high and in some sites were 80 folds higher than the worldwide grand mean, i.e. 1779.12 and 1649.88 mg kg⁻¹ compared to the grand mean of 25 mg kg⁻¹. This result indicates that in the case of lead the source of contamination is a punctual source. Since in these specific sample sites there is no evidence of an existing anthropogenic source (e.g. an industry) and the parent material does not confirm and give reason for

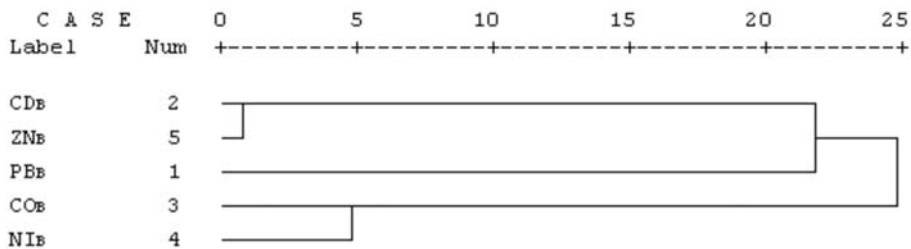


Fig. 3: Dendrogram for the descriptors using Ward Method (B depth).

Table 2. Principal Component Analysis (Varimax Rotation Method with Kaiser Normalization) for A depth.

	Component			
	1	2	3	4
OM _A	0.11	0.10	0.93	-0.07
pH _A	0.10	-0.62	-0.52	-0.47
CLAY _A	0.81	0.39	-0.22	0.11
SILT _A	0.95	0.09	0.06	0.09
Pb _A	0.20	-0.07	-0.03	0.90
Cd _A	0.92	0.14	0.06	0.24
Co _A	0.39	0.60	-0.21	0.47
Ni _A	0.16	0.90	0.15	-0.20
Zn _A	0.80	-0.12	0.48	0.01
% Variance	36.26	19.43	16.43	15.27
Cumulative %	36.26	55.69	72.12	87.39

Table 3. Principal Component Analysis (Varimax Rotation Method with Kaiser Normalization) for B depth.

	Component			
	1	2	3	4
OM _B	0.82	-0.09	0.14	0.04
pH _B	0.30	-0.88	0.07	0.02
CLAY _B	0.39	0.18	0.76	0.31
SILT _B	0.24	0.04	-0.92	-0.01
Pb _B	0.15	0.06	0.10	0.96
Cd _B	0.92	0.26	0.12	0.11
Co _B	0.37	0.79	0.15	0.30
Ni _B	0.30	0.65	0.56	-0.28
Zn _B	0.84	-0.03	-0.20	0.14
% of Variance	30.69	21.40	20.65	13.49
Cumulative %	30.69	52.09	72.74	86.23

clay, silt, Cd, and Zn. The second component, which explains the 19.43% of the total variance, shows high correlation to Ni and a moderate one to Co. The third component with a 16.43% of the total variance has a high factor loading for organic matter. The fourth component, accounting for the 15.27% of the total variance, has a very high factor loading for Pb.

Table 3 represents the four factors that are retained in the analysis and account for the 86.23% of the total variance in B depth. The first component accounts for the 30.69% of the total variance and is composed of very high factor loadings for Cd, Zn, and organic matter. The second component, explaining the 21.40% of the total variance, has a high factor loading for Co and a less high one for Ni. The third component with the 20.65% of the total variance has a high factor loading for clay. The fourth component explaining the 13.49% of the total variance has a very high positive factor loading for Pb.

The results of Hierarchical Cluster Analysis are in accordance with the results of Factor Analysis showing that there are two different contamination sources in the study area: the first source is connected to Cd, Zn, and Pb and is considered as the anthropogenic source, while Co and Ni originate from the second lithogenic source and are more correlated in depth B than in depth A, showing their probable lithogenic origin.

4. Conclusions

Measured EDTA extractable concentrations of Cd, Zn, Pb, Co and Ni ranged widely among sample sites and substantial differences were observed. The results of HCA and FA analysis of soil properties and heavy-metal concentrations satisfactorily describe the presence of the five heavy metals in the soil of the study area. The factors and the clusters excluded are in agreement with each other showing two sources of pollution. Firstly the lithogenic source, which provides the heavy metals Co and Ni, with higher concentrations in B depth (lower depth), and secondly the anthropogenic source, which provides the heavy metals Cd, Zn, and Pb, with higher concentrations in A depth. Determined lead concentrations were extremely high and in connection with its long lasting half-life in soils (740-5900y) this metal can threaten the health of animals and humans upon entering in food chain. Since there are not any minerals containing Pb in the lithologic formations of the area or any industries that would produce such concentrations, it could be concluded that probably in this sites there were ancient metallurgical activities. Indeed, this is in agreement with the findings of archaeological excavations which indicate that in the antiquity the area has been used as a workshop of metallurgy.

5. References

- Allison, L. E. and Moodie, C. D., 1965. Carbonate. In: CA Black (ed.) *Methods of Soil Analysis*, part 2. Agronomy 9: 1379–1400. Am Soc of Agron, Madison, Wisconsin, USA.
- Alloway B. J., 1995. Heavy metals in soils, 2nd Edition, Springer 1995, pp. 384.
- Bouyoukos, G.J., 1951. A recalibration of the hydrometer method of making mechanical analysis of soils. *Agron. J.* 43: 434-437.
- Burt, R., Wilson, M., Mays, M.D., Lee, C.W., 2003. Major and trace elements of selected pedons in the USA. *J. Environ. Qual.* 32:2109-2121 (2003).
- Clayton, P.M. and Tiller, K.G., 1979. A Chemical Method for the Determination of the Heavy Metal Content of Soils in Environmental Studies. In: *Paper No. 41*, CSIRO Australia, Melbourne Div. Soils Tech. (1979), pp. 1–17.
- Dudka, S., Adriano, D.C., 1997. Environmental impacts of metal ore mining and processing: a review. *Journal of Environmental Quality* 26: 590-602.
- Fytianos, K., Katsianis, G., Triantafyllou, P., Zachariadis, G., 2001. Accumulation of heavy metals in vegetables grown in an industrial area in relation to soil. *Bull. Environ. Contam. Toxicol.* 67: 423-430.
- Girard, M-C., Walter, C., Rémy, J-C., Berthelin, J., Morel, J-L., 2005. *Sols et environnement*, Éditions Dunod, Paris, 2005.
- Godin, P.M., Feinberg, M. H., Ducauze, C. J., 1985. Modelling of soil contamination by airborne lead and cadmium around several emission sources. *Environmental Pollution Series B, Chemical and Physical*, 10:2 (1985), pp. 97-114.
- I.G.M.E. KOROPi-VARI sheet 2004 Geological map 1:50.000. Department of geological maps of IGME, Athens, Greece.

- Imperato, M., Adamo, P., Naimo, D., Arienzo, M., Stanzione, D., Violante, P., 2003. Spatial distribution of heavy metals in urban soils of Naples city (Italy). *Environmental Pollution* 124 (2003) 247–256.
- Kabata-Pendias, A., and Pendias, H., 2001. Trace elements in soils and plants, 3rd Edition, CRC Press LLC, pp. 413.
- Kakavoyianni, O., 2003. A EH I Metallurgy Workshop of Silver in Lambrika, Attica (Koropi). *Archaeology & Arts* 94, 45-48 (in Greek with abstract in English).
- Kribek, B., Majer, V., Veselovsky, F., Nyambe, I., 2010. Discrimination of lithogenic and anthropogenic sources of metals and sulphur in soils of the central-northern part of the Zambian Copperbelt Mining District: A topsoil vs. subsurface soil concept. doi: 10.1016/j.gexplo.2009.12.005.
- Lazaris, Sp., 2008. Determination of heavy-metal contamination sources in soils of Koropi-Vari area, Attica. Master thesis, Agricultural University of Athens (in greek).
- Lin, C., Negev, I., Eshel, G., Banin, A., 2008. In situ accumulation of copper, chromium, nickel, and zinc in soils used for long-term waste water reclamation. *Journal of Environmental Quality* 37: 1477-1487.
- Mousoulos, P., 1976. Metallurgy of Pb. National Engineering School, Athens 1976 (in greek), pp. 125.
- Nelson, D.W. and Sommers, L.E., 1982. Total carbon, organic carbon, and organic matter, pp. 539-579. IN: A. L. Page, R. H. Miller, and D. R. Keeney (eds.) *Methods of Soil Analysis Part 2, Chemical and Microbiological Properties* Soil Science Society of American, Inc., Madison, WI.
- Quevauviller, Ph., Lachica, M., Barahona E., Rauret G., Ure, A., Gomez, A., Muntau, H., 1996. Interlaboratory comparison of EDTA and DTPA procedures prior to certification of extractable trace elements in calcareous soil. *The Science of the Total Environment* 178 (1996) 127-132.
- Quevauviller, Ph., Lachica, M., Barahona, E., Gomez, A., Rauret, G., Ure, A., Muntau, H., 1998. Certified reference material for the quality control of EDTA- and DTPA-extractable trace metal contents in calcareous soil (CRM 600). *Fresenius J Anal Chem* (1998) 360 : 505–511.
- Selinus, O., Alloway, B., Centeno, J. A., Finkelman, R. B., Fuge, R., Lindh, R., Smedley, P., 2005. *Medical Geology*, Elsevier Academic Press, 2005, pp. 812.
- Shakeri, A., Moore, F. and Modabberi, S., 2009. Heavy Metal Contamination and Distribution in the Shiraz Industrial Complex Zone Soil, South Shiraz, Iran. *World Applied Sciences Journal* 6 (3): 413-425.
- Singh, A., Sharma, R.K., Agrawal, M., Marshall, F.M., 2010. Health risk assessment of heavy metals via dietary intake of foodstuffs from the wastewater irrigated site of a dry tropical area of India. *Food and Chemical Toxicology* 48: 611-619.
- Van Hullebusch, E.D., Gieteling, J., Zhang, M., Zandvoort, M.H., Van Daele, W., Defrancq, J., Lens, P.N.L., 2006. Cobalt sorption onto anaerobic granular sludge: Isotherm and spatial localization analysis. *Journal of Biotechnology* 121: 227-240.
- Wong, S.C., Li, X.D., Zhang, G., Qi, S.H., Min, Y.S., 2002. Heavy metals in agricultural soils of the Pearl River Delta, South China. *Environmental Pollution* 119: 33-44.
- Zhuang, P., McBride, M.B., Xia, H., Li, N., Li, Z., 2009. Health risk from heavy metals via consumption of food crops in the vicinity of Dabaoshan mine, South China. *The Science of the Total Environment* 404: 1551-1561.

ORGANIC GEOCHEMISTRY OF HUMIC ACIDS FROM A NEOGENE LIGNITE SAMPLE, BULGARIA

Stefanova, M. and Marinov, S.P.

*Institute of Organic Chemistry Bulgarian Academy of Sciences, Sofia 1113 BULGARIA
maia@orgchm.bas.bg*

Abstract

Humic substances naturally occur in Miocene/Pliocene-aged lignite at very high concentrations. Here biomarkers in the bitumen-free extract of humic acids from Thracian lignite, Bulgaria, are studied. Applying methods of organic geochemistry a broad range of compounds are isolated and characterized. Species are classified according to abundance, possible source input and diagenetic transformation. A feature of humic acids derived from Thracian coal is the extremely high content of 16 α (H)Phyllocladane, ~60% of aliphatic fraction, or 1.6 wt.% of initial lignite. The high diterpenoids content, especially with abietane skeleton, proved the conifer contribution to the peat-forming helophytes, i.e. Cupressaceae s. str., Podocarpaceae, Araucariaceae, Taxodiaceae, Phyllocladus, Piceae. Tightly-trapped, linear long-chain fatty acids (FAs) are the main constituents of the acidic fraction of humic acids. Their distribution patterns indicate a dominant higher plant origin. The presence of α OH-FAs and hopanoid acids assumes bacterial activity in the plant material reworked. A hint for the input of plant biopolymers, i.e. cutin, suberin, is the relative high content of “even” carbon numbered ω OHFAs and α,ω -alkanedioic FAs. “Even” numbered short-chain ω OHFAs could originate from cutin-derived constituents of the needles of numerous species of gymnospermous families.

Key words: *Thrace, lignite, humic acid, biomarker, fatty acid, palaeoenvironment.*

1. Introduction

According to topographic, morphotectonic, lithologic and genetic characteristics Neogene coals in Bulgaria are divided into four coal-bearing provinces: Dacian, Thracian, Sofia, Strimon-Mesta (Šiškov, 1997). The Thracian is the largest one hosting the main energy resources of the country. Palaeobotanical data of the Thracian lignite supports the presence of Taxodiaceae issue remains (twigs, cones, wood, etc.) along with a floral composition being similar to this of the mires in temperate climates. The results from previous studies (Bechtel et al. 2005) indicated that the larger part of the Thracian coal deposits is derived from coniferous flora, which is the main source of resinous organic matter. The results confirmed a low Angiospermae/Coniferales ratio due to the high abundance of coniferous fragments in the lignite. The huge amounts of 16 α (H)-Phyllocladane the variety of tricyclic diterpanes and their polar counterparts proved the gymnosperm contribution at a molecular level (Stefanova et al., 1995). There were also some chemical indicators for the presence of angiosperm debris in the source material (Stefanova et al., 2002).

Humic substances naturally occur in Miocene/Pliocene lignites at very high contents (~70%) and could be considered representative for coal organic matter. The aim of the present study was to as-

sess biomarker assemblage of humic acid from Thracian coal-bearing province with the aim to enrich the information on coal precursors and maturation degree inasmuch humic substances are firmly involved in coal formation.

2. Geological setting

The Thracian coal-bearing province hosts three deposits, namely these of Maritza-East, Maritza-West (Early-Middle Miocene) and Elhovo (Pliocene) located in the Thracian depression, which is filled with sediments of the lower (Palaeogene) and upper (Neogene) coal-bearing molasse. Coal formation started in Late Oligocene and continued through Miocene into Pliocene. It took place in highly peneplaned coastal areas covered by eutrophic mires. Younger sedimentary sequences of varying thickness occur from west to east due to compensation from the formation of the Black Sea and gradual marine regression to this direction. The Maritza-East lignite deposit (maximum thickness 25 m) is a good example of the long-lasting peat accumulation in this region.

3. Methods

3.1 Bulk characteristics

One sample from Maritza-East lignite, seam “Trojanovo North”, was extracted for humic acids (HA) preparation. Some rank parameters of Neogene coals in Bulgaria were published in Šiškov (1997). Briefly, Maritza East lignites were described by the following characteristics, in %: R_1 – 0.20; W^r – 64.4; C^{daf} – 65.0, VM^{daf} – 55.8 and calorific value in MJ/kg, Q^{daf} – 22.31.

Isolation and fractionation of humic acids were described in a previous paper (Stefanova et al., 1993). To get an extractable portion (bitumen “free”) of humic acids, about 6 g were extracted with chloroform under 100 atm at 80°C (3 x 20 min) (Dionex equipment). Acids and neutrals were separated from the bitumen-“free” fraction on a SiO_2/KOH column (McCarthy and Duthie, 1962). Hydrocarbons, ketones and esters were separated from the other neutrals applying liquid chromatography and using for elution diethyl ether/petroleumether mixtures of increasing polarity (Grasset and Amblès, 1998; Váľkova et al., 2009). Acids were identified as methyl esters. Hydroxyl FAs were determined as TMS ethers/methyl esters after classical methylation of the acid fraction with trimethylsilyldiazomethane (Hashimoto et al., 1981).

3.2. GC-MS study

The products were analyzed by capillary GC using a Hewlett-Packard 6890 GC (split injector, 250°C; flame ionization Detector (FID), 300°C) with a fused silica capillary column (SGE BPX 5%, 30 m length, 0.25 mm id., 0.25 μ m film thickness) and helium as carrier gas. The GC was temperature programmed from 60 to 300°C at 5°C min⁻¹ (isothermal for 20 min final time). The GC-MS analyses were performed on a Trace GC Thermo Finnigan coupled to a Thermo Finnigan Automass (with the same GC conditions). The MS was operated in the electron impact mode with a 70eV’s ion source energy and the ion separation was operated in a quadripolar filter. The various products were identified on the basis of their GC retention times, their mass spectra (comparison with standards) and literature data. SIM was used for acids visualization: m/z 74 for linear fatty acids; m/z 98 for linear α,ω alkanedioic FAs; m/z 103 for α OH- and ω OH FAs; m/z 191 for hopanoic acids.

Table 1. Classification, abundance and source of biomarkers in neutral fraction (in rel.%).

<i>Classification</i>	<i>Abundance</i>	<i>Higher plants</i>	<i>Bacteria</i>	<i>Uncertain</i>
Acyclic alkanes: i.e. n-alkanes, ketones isoprenoids	19.37 19.06 0.31	17.98 0.31	? trace	1.08 -
Terpenoids: i.e. sesquiterpenoids diterpenoids sesterpenoids triterpenoids	77.88 0.41 68.75 0.40 8.32	0.41 68.75 - -	- - 0.40 0.32	- - - -
Total	97.25			

4. Results

For Thracian lignite HAS “free” bitumen amounted 110 mg/g TOC. After fractionation on SiO₂/KOH column the material was separated into neutrals (~ 1/3 of the applied sample), acids (~ 1/3) and polars (~ 1/3).

4.1 Neutral fraction

The main homologue series GC-MS registered in the neutral fraction are:

- Hydrocarbons with long chains, $nC_{23} \div nC_{33}$, maximizing at nC_{29} , with strong “even” carbon numbers domination, CPI 2.8;
- Ketones with long chains, $nC_{23} \div nC_{33}$, with nC_{29} in maximal content, CPI 4.0. One *iso*-ketone structurally related to phytol was registered as well;
- Diterpenoids were in a high preponderance due to the presence of huge amounts of tetracyclic diterpenoid 16 α (H)-Phyllocladane (Str.I);
- Tri-, sesqui-, and sesterpenoids were in subordinating quantities compared to diterpenoids;
- Hopanoids (Hs), i.e. 17 β -(H)22,29,30-trisnorhopane (H₂₇) and the range of H₂₉-H₃₁ 17 β (H), 21 β (H)-hopanes.

Table 1 presents a classification scheme, the abundance and possible sources of biomarkers in HA grouped according to Wang and Simoneit (1990).

4.2 Acidic fraction

The acidic fraction was composed by linear long chain fatty acids (*n*FAs), their functionalized analogues α - (α OH-FAs), ω - (ω OH-FAs) hydroxy fatty acids and dicarboxylic fatty acids (α,ω -di-FAs). Their patterns of distributions are illustrated in Figure 1. The following acid series were mass-spectrometrically identified:

- linear long chain FAs, methyl esters ($nC_{12} \div nC_{34}$), nC_{28} maximal, with “even” carbon number prevalence, 44.9 rel.% of acidic fraction (Str. III);

- linear long chain α,ω alkanedioic FAs, dimethyl esters (nC_{16} , nC_{20} – nC_{30}) with a distribution similar to *n*FAs, 3.18 rel.% (Str. IV);
- α OH-FAs as 2-(trimethylsilyloxy), methyl esters, nC_{22} – nC_{27} (nC_{23} in trace), 1.2 rel.% (Str. V);
- ω OH-FAs as trimethylsilyloxy, methyl ester derivatives, nC_{12} – nC_{28} , strongly maximizing at nC_{16} , 3.32 rel.% (Str. VI);
- dehydroabietic acid, methyl ester, 0.8 rel.% (Str. VII);
- hopanoic acids, methyl esters, i.e. $C_{32}\alpha\beta$, $C_{30}\beta\beta$ and $C_{31}\beta\beta$, < 1 rel.% (Str. VIII).

Apart from the above mentioned acids some alkylated phenols were detected as well. They probably were produced during accelerated “free” bitumen extraction under pressure or are end products of diagenetic transformations of lignin moieties. One diterpenoid ketophenol, totarol 3-one (Str. II), was highly abundant (5.2 rel.%) in the acidic fraction.

4.3 Data analysis

In some papers dedicated to humic substances organic solvent soluble portion of humic acids was named hymatomelanic acids. It is still contestable were hymatomelanic acids a separate group of compounds or could be considered as lipids. Their origin received special attention in the study of Lehtonen et al. (2001), where the achievements in the field were discussed.

4.3.1 Neutral fraction

The aliphatic hydrocarbons in the bitumen-free fraction comprise long chain *n*-alkanes from nC_{17} to nC_{35} , the major component being the nC_{29} alkane. They show a clear odd/even carbon number predominance indicating a dominant plant input (Kolattukudy, 1976).

Terpenoids at different ratios depending on plant communities compose aliphatic fraction (neutrals). A striking feature of Thracian lignite HA is the extremely high content of 16(H)-Phyllocladane (~60% of aliphatics or 1.6% of initial coal).

The identified diterpenoids demonstrated the presence of Gymnospermae in the coal-forming plant community of Maritza-East lignite. Furthermore, phenolic ketoditerpenoid indicated a specific input of organic matter from conifers of the Cupressaceae/Taxodiaceae or Podocarpaceae as the most abundant trees in the coal-forming mire (Stefanova et al., 2002).

Actually, biomarker assemblage of humic acids resembled biomarker compositions of Maritza-East lignite lithotypes and their polar constituents already described in previous paper (Stefanova et al., 1995). All data support strong Gymnospermae contribution to the palaeomire.

4.3.2 Acidic fraction

Acids demonstrate some novelty concerning humic acids structure. Our results proved the high ability of humic acids to retain hydrophobic species. We suppose that functionalised fatty acids are integrated parts of humic acids inherited from precursors.

Fatty acids are common constituents of humic acids. Their forms of linkage have been studied by several researchers in a suite of papers devoted to humic acids in soils, peat, lignite, etc. (Amblès, 2001; Grasset et al., 2002; Guignard et al., 2005; Deport et al., 2006; Válková et al., 2009). Except “free” fatty acids extraction, authors used thermochemolysis in the presence of different alkylation

reagents, i.e. TMAH, TEAAc, to distinguish strongly trapped and esterified FAs. It is worth noting that according to them the major part of FAs occurs as “free” constituents being trapped within the network.

Linear long chain FAs are the main constituents of the acidic fraction of humic acids, amounting about a half of GC amenable compounds. The distribution pattern of “free” *n*FAs presents a long mode maximizing at *n*C₂₈ with strong “even” carbon numbered dominance. Such a distribution indicates a dominant higher plant origin. In the samples under study there were not unsaturated and branched chain FAs.

One order less of magnitude was the content of α,ω -alkanedioic FAs with “even” carbon numbered dominance. Sources of long members could be suberin and cutin from higher plants or products of FAs microbial ω -oxidation. A hint for the input from plant biopolymers is the relative high content of “even” numbered ω OH-FAs (Fig.1). Actually hydroxyl FAs are the second in abundance. Allard (2006) published a comparative study on the chemical compositions of humic acids extracted from soil, agricultural soil and lignite deposits based on the data for bound lipids, carbohydrates and amino acids compositions. ω OH-FAs were determined only in soil humic acids being completely absent in lignite HAs. It should be emphasized that humic acids from Maritzsa-East lignite containing a high content of xylite-rich lithotype, are comparable with these of soil organic matter. “Even” numbered short-chain ω OH-FAs (C₁₂,C₁₄,C₁₆) have been reported as characteristic cutin-derived constituents of needles of numerous species of gymnospermous families (Oros et al., 1999). The data coincides well with the conclusions based on the diterpenoids assemblage assuming predominant gymnospermous contribution. The input of suberin is indicated by the presence of linear long-chain FAs, α,ω -alkanedioic FAs, ω OH-FAs and long-chain alcohols (not described here as registered in humin), all suberin building blocks (Kolattukudy, 1980).

α -OH-FAs are in a lowest content compared to the other linear FAs. According to Cranwell (1982) they are by-products of the α -oxidation of FAs and are not source specific biomarkers.

The presence of hopanoid acids assumed bacterial activity in the reworking process of the plant material. The dominance of $\beta\beta$ hopanoid acids is in agreement with the immaturity of the lignite sample.

5. Conclusions

Biomarker assemblage of humic acids from Maritzsa-East lignite, Bulgaria, proved a strong gymnospermous contribution to the palaeomire. A feature of the Thracian lignite HAs was the extremely high content of 16 α (H)-Phyllocladane (~60 % of aliphatics or 1.6 % of initial coal). The identified diterpenoids demonstrated the presence of Gymnospermae in the coal-forming plant communities. Phenolic ketoditerpenoids indicated a specific input of organic matter from conifers of the Cupressaceae/Taxodiaceae or Podocarpaceae as the most abundant trees in the coal-forming mire.

Tightly-trapped linear long-chain FAs were the main constituents of the acidic fraction of humic acids. Their distribution pattern indicated a dominant higher plant origin.

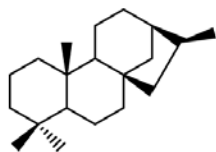
The presence of hopanoid acids assumed bacterial activity in the plant material reworked. A hint for the input from plant biopolymers, i.e. cutin, suberin, was the relative high contents of “even” carbon numbered ω OH-FAs and α,ω -alkanedioic FAs.

“Even” numbered short-chain ω OH-FAs could originate from cutin-derived constituents of needles of numerous species of gymnospermous families.

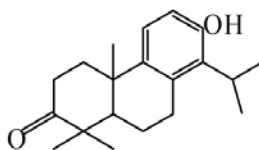
6. Acknowledgement

One of us (M.S.) would like to express her gratitude to Prof. A. Amblès and Dr. L. Grasset for the possibility to perform experiments in the University of Poitiers, France as well as for the fruitful discussions of the results.

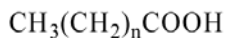
Appendix: Structures cited in the text



Str.I. 16 α (H)-Phyllocladane



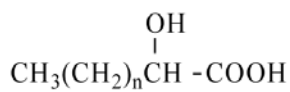
Str.II. Totarol-3-one



Str.III. Fatty acid



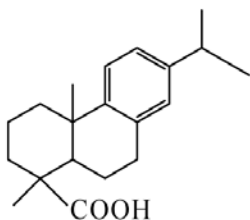
Str. IV. α,ω Dicarboxylic acid



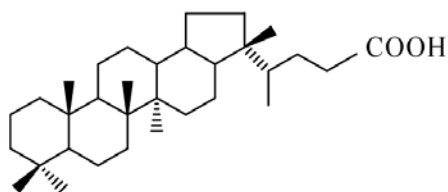
Str. V. α OH Fatty acid



Str. VI. ω OH Fatty acid



Str. VII. Dehydroabietic acid



Str. VIII. β C₃₂ Hopanoid acid

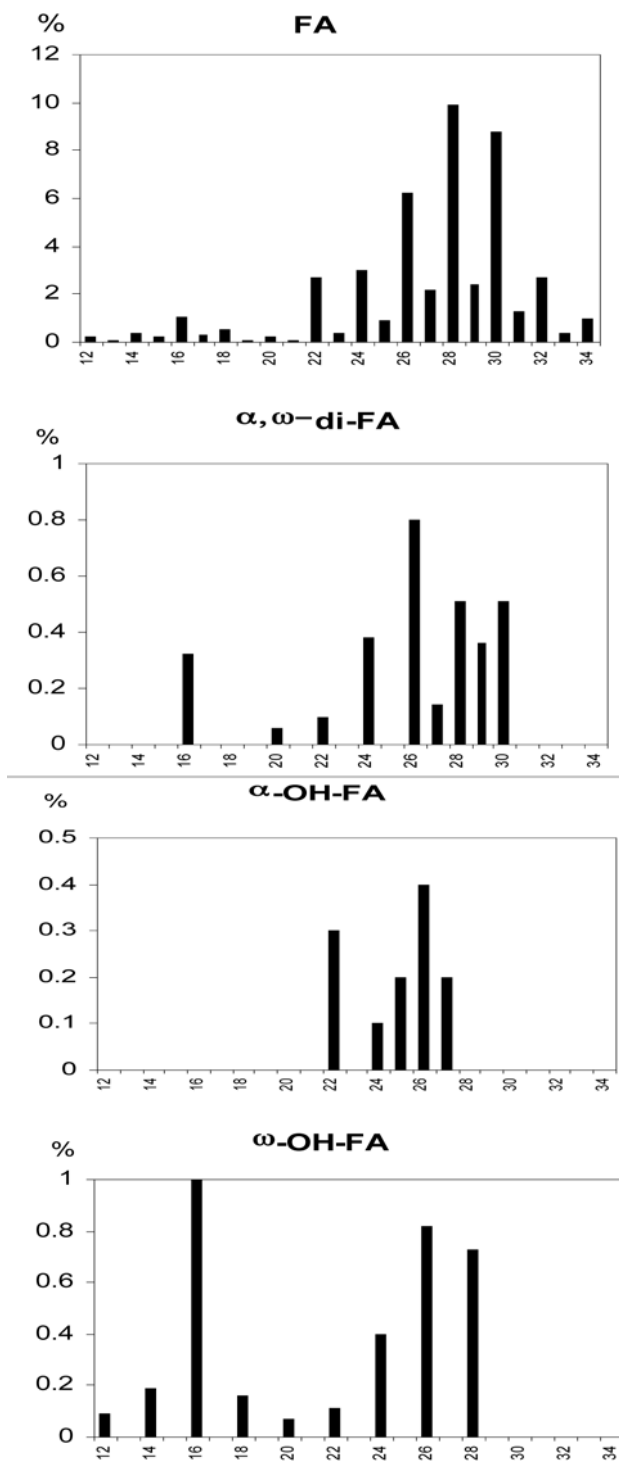


Fig. 1: Patterns of distributions of fatty acids (X axis numbers correspond to carbons in FAs chains).

7. References

- Allard, B. 2006. A comparative study on the chemical composition of humic acids from forest soil, agricultural soil and lignite deposit. Bound lipid, carbohydrate and amino acid distributions. *Geoderma* 130, 77-96.
- Amblès, A. 2001. Methods to reveal the structure of humic substances. In: Hofrichter, M., Steinbüchel, A. (Eds) *Biopolymers*. Wiley-VCH. v.1 pp. 325-348.
- Bechtel, A., Sachsenhofer, R.F., Zdravkov, A., Kostova, I., Gratzner, R. 2005. Influence of floralassemblage, facies and diagenesis on petrography and organic geochemistry of the Eocene Bourgas coal and the Miocene Maritza-East lignite (Bulgaria). *Organic Geochemistry* 36, 1498-1522.
- Cranwell, P.A. 1982. Lipids of aquatic sediments and sedimenting particules. *Prog. Lipid Res.* 21, 271-308.
- Deport, C., Lemée, L., Amblès, A. 2006. Comparison between humic substances from soils and peats using TMAH and TEAAc thermochemolysis. *Organic Geochemistry* 37, 649-664.
- Grasset, L., Amblès, A. 1998. Structural study of soil humic acids and humin using a new preparative thermochemolysis technique. *J. Anal. and Applied Pyrolysis* 47, 1-12.
- Grasset, L., Guignard, C., Amblès, A. 2002. Free and esterified aliphatic carboxylic acids in humin and humic acids from peat sample as revealed by pyrolysis with TMAH or TEAAc. *Organic Geochemistry* 33, 181-188
- Guignard, C., Lemée, L., Amblès, A. 2005. Lipid constituents of peat humic acids and humin. Distinction from directly extractable bitumen components using TMAH and TEAAc thermochemolysis. *Organic Geochemistry* 36, 287-297.
- Hashimoto N., Aoyama T., Shiori T. 1981. New methods and reagents in organic synthesis. 14. A simple efficient preparation of methyl esters with trimethylsilyl diazomethane (TMSCHN₂) and its application to gas chromatographic analysis of fatty acids. *Chemical Pharmaceutical Bulletin* 29, 1475-1478.
- Kolattukudy, P.E. 1976. Chemistry and biochemistry of natural waxes, Elsevier, Amsterdam.
- Kolattukudy, P.E. 1980. Biopolyester membranes of plants: cutin and suberin. *Science* 208, 990-1000.
- Lehtonen, K., Hänninen, K., Ketola, M. 2001. Structurally bound lipids in peat humic acids. *Organic Geochemistry* 32, 33-43.
- McCarthy, R.D., Duthie, A.H. 1962. A rapid quantitative method for the separation of free fatty acids from other lipids. *J. of Lipid Res.* 2, 117-119.
- Oros, D.R., Standley, L.J., Chen, X., Simoneit, B.R.T. 1999. Epicuticular wax composition of predominant conifers of western North America. *Z. Naturforsch.* 54c, 17-24.
- Šiškov, G.D. 1997. Bulgarian low rank coals: geology and petrology. In: Gayer, R. and Pešek, J. (eds), *Eur. Coal Geology and Technol. Geol. Soc. Spec. Publ.* 125, 141-148.
- Stefanova, M., Velinova, D., Marinov, S.P., Nikolova, K. 1993. The composition of lignite humic acids. *Fuel* 72, 681-684.
- Stefanova, M., Magnier, C., Velinova, D. 1995. Biomarker assemblage of some Miocene-aged Bulgarian lignite lithotypes. *Organic Geochemistry* 21, 1067-1084.
- Stefanova, M., Oros, D.R., Otto, A., Simoneit, B.R.T. 2002. Polar aromatic biomarkers in the Miocene Maritza-East lignite, Bulgaria. *Organic Geochemistry*, 33, 1079-1091.
- Válkova, D., Grasset, L., Amblès, A. 2009. Molecular compounds generated by RuO₄ oxidation and preparative off line thermochemolysis of lignite humic acids from South Moravia: implication for molecular structure. *Fuel* 88, 2113-2121.
- Wang, T.-G., Simoneit, B.R.T. 1990. Organic geochemistry and coal petrology of Tertiary brown coal. 2. Biomarker assemblage and significance. *Fuel* 69, 12-20.

THE ISOTOPIC SIGNATURE OF THE MINERALIZING FLUID OF THE LAVRION CARBONATE-REPLACEMENT PB-ZN-AG DISTRICT

Tombros S.F.¹, St. Seymour K.¹, Spry P.G.² and Bonsall T.A.²

¹ University of Patras, Department of Geology, Laboratory of Volcanology and Ore deposits, 26500 Patras, Greece, tompros@mailbox.gr, kstseymr@upatras.gr

² Iowa State University, Department of Geological and Atmospheric Sciences, 253 Science I, Ames, Iowa 50011-321, pgspry@iastate.edu.

Abstract

The Pb-Zn-Ag carbonate-replacement deposits in the Lavrion district are genetically related to a 7-10 Ma-old granodiorite, felsic dikes and sills. These deposits are hosted in the Upper and Lower marble and schists of the Cyclades Blueschist unit and occur along the major Legraina detachment fault. Carbonate-replacement orebodies occur as “mantos” and veins, dominated by base metal sulfides and Ag, Bi, Sn, Sb, As, and Pb sulfosalts. Calculated carbon and oxygen isotope compositions of the hydrothermal fluid range from $\delta^{13}\text{C}_{\text{CO}_2}$ of -13.7 to 0.8 per mil and $\delta^{18}\text{O}_{\text{H}_2\text{O}}$ of 4.2 to 27.4 per mil, at 400°, 350°, 320°, 300°, 250° and 200°C. These isotopic compositions reveal water-to-rock ratios ranging from 4.8 to 52.6%, which reflect intense interaction of the ore fluid with the host rock in a water-dominated, transitional closed to open hydrothermal system.

The range of $\delta^{34}\text{S}_{\text{H}_2\text{S}}$ for sulfides in the deposits were from -8.5 to 6.8 per mil, for similar temperatures, whereas for barite-fluorite veins from $\delta^{34}\text{S}_{\text{H}_2\text{S}}$ of -43.6 to -16.4 per mil, at 200°, 150° and 100°C. This range implies that there was contribution from a magmatic sulfur component exsolved from the Plaka pluton, as well as contribution from a metasedimentary component. Based on the iso-

topic signature of sulfur for barite, the $\log \frac{a_{\text{SO}_4^{2-}(\text{aq})}}{a_{\text{H}_2\text{S}(\text{aq})}}$ ranges from -6.7 to -7.6, comprising an increase

in the fluid influx. Isotopic temperatures based on pyrite-galena and sphalerite-pyrite pairs revealed at least three major events of carbonate-replacement ore deposition, (i) at ~ 360°, (ii) 320°-280° and (iii) 260°-200°C.

Key words: polymetallic ores, ore fluid, carbon, oxygen, sulfur isotopes.

1. Introduction

The Lavrion district is famous for the production of Pb (~ 1.4 Mt, at 20%) and Ag (~ 3.5 kt, at 400 g/t) since the Golden Age of Athens (Conofagos, 1980). Recent mining in this area was mainly conducted by Compagnie Française des Mines du Laurium (~ 0.9 Mt, at 3% Pb and 4.2 kt Ag, at 140 g/t, Conofagos, 1980). The area is considered as the northern part of the Cycladic Blueschist Belt, which is one of the most spectacular Alpine orogenic belts worldwide (Blake et al., 1981). Within this belt, various types of base and precious metal ores including skarn (i.e., Serifos, Lavrion and

rocks (Kaesariani schists), sandwiched between the Upper and Lower marbles, at the top (Fig. 1) (Marinos and Petrascheck, 1956).

During the Tertiary, it experienced two episodes of regional metamorphism. The first occurred at ~ 70 Ma, during collision between the Apulian microplate and Eurasia, and reached the blueschist to eclogite facies ($T_{\max} \approx 450\text{--}550^\circ\text{C}$ and a $P_{\max} \approx 12\text{--}18$ kbar; Bröcker and Pidgeon, 2007). This event was followed by an episode of greenschist to amphibolite facies metamorphism, at 25–18 Ma ($T_{\max} \approx 450\text{--}480^\circ\text{C}$ and $P_{\max} \approx 5\text{--}7$ kbars), which occurred as a result of isothermal decompression and exhumation (Wijbrans et al., 1993). Finally, contact metamorphism during Miocene was associated with the intrusion of the 8.3 to 11.9 Ma-old Plaka granodiorite and 7.3 Ma, felsic dykes and sills (Altherr and Siebel, 2002; Skarpelis et al., 2008).

The Cyclades Blueschist unit in the area is tectonically overlain by the “Upper unit” ophiolites i.e., a heterogeneous unit composed of unmetamorphosed Permian to Mesozoic sediments, intercalated ophiolitic fragments, Tertiary-greenschist facies rocks and Late-Cretaceous medium pressure-high temperature rocks (also called prasinites, Baltatzis, 1996; Photiades and Carras, 2001) (Fig. 1). It is separated from the Cyclades Blueschist unit by a detachment fault that formed during the early Miocene as back-arc extension dominated the Cyclades (Skarpelis, 2007). During this extensional period, granodioritic magmas intruded these units, and hornfels developed around the margins of the Plaka pluton (Skarpelis et al., 2008) (Fig. 1).

3. Types of Sulfide Mineralization and Their Paragenesis

There are several types of sulfide mineralization present in the Lavrion district, which are related to progressive decrease in temperature of formation: (i) *porphyry-style*, low-grade, molybdenite mineralization in the proximity of Plaka granodiorite, which occurs as quartz tension gashes and minor stockworks. It is associated with the potassic alteration assemblage of orthoclase-albite-sericite-biotite (Bonsall et al., 2007; Voudouris et al., 2008a, b), (ii) *Ca-Fe skarn*, hosted in schists and marbles located at the margins of Plaka pluton, with the assemblages magnetite and magnetite-hematite representing endoskarns (stage I), and pyrite-pyrrhotite and Fe-rich-sphalerite-pyrite-Ag-rich-galena (\pm arsenopyrite-bismuthinite-chalcopyrite-mackinawite-glaucodote-native bismuth-scheelite-tetradymite, $T \leq 581 \pm 3^\circ\text{C}$, Glatz, 1967) to form exoskarns (stage II) (Marinos and Petrascheck, 1956; Leleu et al., 1973; Economou et al., 1981; Bonsall et al., 2007), (iii) *breccia-porphyry* dike mineralization which contains minor amounts of arsenopyrite, pyrite, magnetite, pyrrhotite, Fe-rich sphalerite and chalcopyrite (stage I), galena, argentian tetrahedrite and tennantite, freibergite, wurtzite and enargite (stage II) and marcasite, argentian galena, and Bi-Cu-Ag-Pb-Sn-sulfosalts (stage III) (Economou and Sideris, 1976; Bonsall et al., 2007; Voudouris et al., 2008a, b) and (vi) *carbonate-replacement* Pb-Zn-Ag mantos, chimney-orebodies and veins (e.g., vein 80) with the generalized assemblage: pyrite, arsenopyrite, pyrrhotite, loellingite, rammelbergite, sphalerite (with Fe ≥ 10 wt. %), greenockite, niccolite, laggisite, gerdorsfite and chalcopyrite (stage I), pyrite, argentian chalcopyrite and tetrahedrite, enargite, luzonite, freibergite, wurtzite (with Fe ≤ 2 wt. %), and galena (stage II), marcasite, argentian galena, bournonite, miargyrite, pyrargyrite-proustite ($T \geq 192^\circ\text{C}$, Hall, 1966), stephanite, nuffeldite, argentite, polybasite, pearsite, chalcocite, stannite, petrukite, isotropic-orpiment ($T = 265 \pm 5^\circ\text{C}$, Hall and Yund, 1964), stibnite, native Bi, As and Au, covellite, and Bi-Cu-Ag-Pb-Sn-sulfosalts (cosalite, aikinite, lilianite, isotropic matildite, $T = 195 \pm 5^\circ\text{C}$, (Craig, 1967), bismuthite, ramdohrite, semseyite, wittichenite, emplectite and mummeite (stage III). These ores are related to carbonatization of the schists and silicification of the marbles, and late formation of vein and vuggy fluorite, siderite and barite. These hypogene stages were followed by a supergene

one (stage V) with more than fifty different minerals including, native Au and Ag (Skarpelis and Ardyraki, 2008).

4. Samples and Methods

Material for stable isotope studies was obtained from calcite intergrown with Pb-Zn-Ag sulfides, as well as smithsonite, cerussite, aragonite, and pyrite, sphalerite and galena, from the Ca-Fe skarns, carbonate-replacement ores. Additionally, late barite and gypsum, host marbles and Plaka granodiorite and associated porphyritic dikes and sills were sampled. Samples were collected from underground and surface locations at Plaka, Kamariza, Sounio, Esperanza, Adame, Avlaki, Villia, Megala Pefka, Christina, and Sounio deposits. All minerals analyzed were hand picked and checked under a binocular microscope to ensure a purity of >95 %. Isotopic compositions of oxygen and carbon were analyzed on a Thermo-Finnigan Delta-Plus XL mass spectrometer, at the Stable Isotope Research Facility, Indiana University. Carbon and oxygen in carbonates were liberated as CO₂ by treating the samples with 100 % phosphoric acid at 75°C (Clayton et al., 1989, in Lefticariu et al., 2006). Sulfur was released as SO₂ from sulfides and sulfates by heating samples to 1,100°C in the presence of CuO (Fritz et al., 1974, Lefticariu et al., 2006) and then, measured using a Finnigan MAT 252 mass spectrometer. The isotopic ratios are reported in standard δ notation per mil relative to V-SMOW for oxygen, V-PDB for carbon, and V-CDT for sulfur. Analytical precision was better than ± 0.05 per mil.

5. Conditions of Emplacement of the Plaka Pluton

In order to estimate the conditions of emplacement of the Plaka pluton, we have used the amphibole geobarometer (based on the variation in the Al^{IV} content of the amphibole as a function of pressure), utilizing the experimental calibrations of Schmidt (1992). The composition of the analyzed amphiboles varies from the crystals core to the rim from 1.21 (Al₂O₃ = 7.06 wt. %) to 0.87 (Al₂O₃ = 5.99 wt. %), which mirrors ascent of the granodiorite magma. The spectrum of the calculated pressure values ranges between 2.75 to 1.15 kbars. Temperatures of crystallization were calculated by using the Vyhnal et al. (1991) geothermometer which is a function of the pressure. The calculated temperatures range between 725° and 685°C for the above pressure values.

6. Carbon and Oxygen Isotopes

Twelve carbon and oxygen isotope analyses were obtained from calcite in the carbonate-replacement mineralization and five metamorphic calcite from the Upper and Lower Marbles. Ten additional isotopic values for calcite are from Bosnall et al. (2007) and fifteen of cerussite, late aragonite and phosgenite from Gilg and Boni (2004).

Calcite in carbonate-replacement from Kamariza, Villia, Esperanza, Adame and M. Pefka deposits displays values of $\delta^{13}\text{C} = -8.6$ to -3.1 and $\delta^{18}\text{O} = 18.4$ to 34 , $\delta^{13}\text{C} = -11.8$ to -8.3 and $\delta^{18}\text{O} = 34.0$ to 38.7 to, $\delta^{13}\text{C} = -13.5$ to -1.4 and $\delta^{18}\text{O} = 18.0$ to 28.6 , $\delta^{13}\text{C} = -12.0$ to -2.0 and $\delta^{18}\text{O} = 21.2$ to 26.1 , and $\delta^{13}\text{C} = -15.6$ and $\delta^{18}\text{O} = 18$ per mil, respectively. Based on the calcite-water and CO₂-water equations of Ohmoto and Rye (1979), the calculated isotopic values, for the same locations, were: $\delta^{13}\text{C}_{\text{CO}_2} = -6.7$ to -2.2 and $\delta^{18}\text{O}_{\text{H}_2\text{O}} = 8.9$ to 26.2 (at 400°, 350°, 320°, 300°, 250° and 200°C), $\delta^{13}\text{C}_{\text{CO}_2} = -9.3$ to -5.8 and $\delta^{18}\text{O}_{\text{H}_2\text{O}} = 4.2$ to 8.9 (at 300°C), $\delta^{13}\text{C}_{\text{CO}_2} = -10.8$ to -4.4 and $\delta^{18}\text{O}_{\text{H}_2\text{O}} = 13.7$ to 24.3 (at 320°C), $\delta^{13}\text{C}_{\text{CO}_2} = -9.2$ to 0.8 and $\delta^{18}\text{O}_{\text{H}_2\text{O}} = 16.2$ to 21.2 (at 350°C), and $\delta^{13}\text{C}_{\text{CO}_2} = -13.7$ and $\delta^{18}\text{O}_{\text{H}_2\text{O}} = 26.6$ per mil (at 300°C) (Fig. 2).

Calcite in the Upper and Lower marbles display measured isotope values of $\delta^{13}\text{C} = -6.7$ to -2.8 and

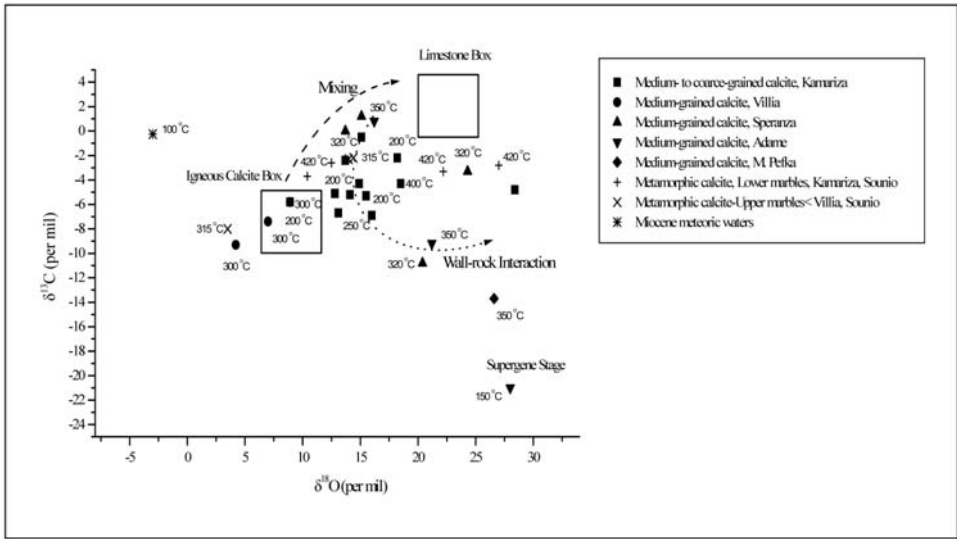


Fig. 2: Carbon versus oxygen isotope diagram for hydrothermal and metamorphic calcite showing stable isotope systematics of hydrothermal fluids from Kamariza, Villia, Speranza, Adame, M. Pefka, Lavrion deposits (the marine limestone and “igneous calcite” boxes after Bowman (1998) are indicated and the estimated $\delta^{18}\text{O}$ and $\delta^{13}\text{C}$ values of Miocene-age meteoric water for southern Europe from Zachos et al., 2001).

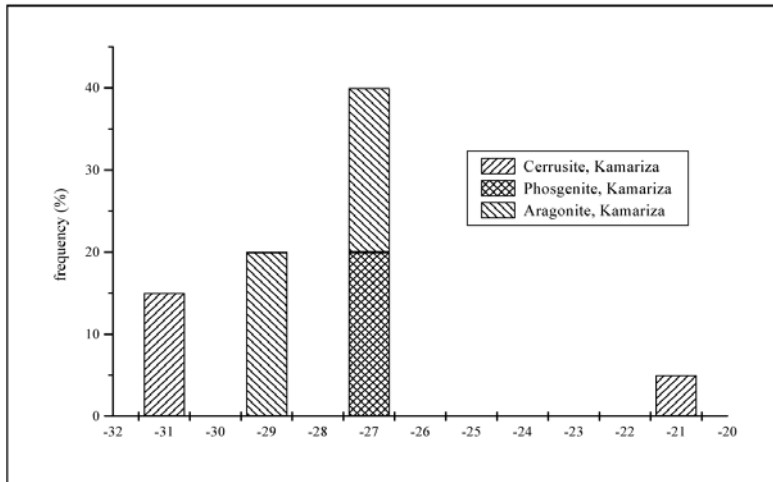


Fig. 3: Histogram of the frequency of the $\delta^{18}\text{O}_{\text{H}_2\text{O}}$ values of cerussite, aragonite and phosgenite from the Kamariza deposits.

$\delta^{18}\text{O} = 13.2$ to 29.8 per mil (Lower marble from Kamariza and Sounio deposits) and $\delta^{13}\text{C} = -10.9$ to -4.8 and $\delta^{18}\text{O} = 27.7$ to 28.4 per mil (Upper marble from Villia and Sounio). Based on the same equations of O’Neil et al., (1969) and Ohmoto and Rye (1979), the calculated isotopic values were: $\delta^{13}\text{C} = -3.7$ to -2.6 and $\delta^{18}\text{O} = 10.4$ to 27.0 (Lower marble, at 420°C ; obtained from Knoll, 1988), and $\delta^{13}\text{C} = -8.0$ to -2.3 and $\delta^{18}\text{O} = 3.5$ to 14.6 (at 315°C), $\delta^{13}\text{C} = -10.8$ to -4.4 and $\delta^{18}\text{O} = 13.7$ to 24.3 (at 320°C ; obtained from Knoll, 1988) (Fig. 2).

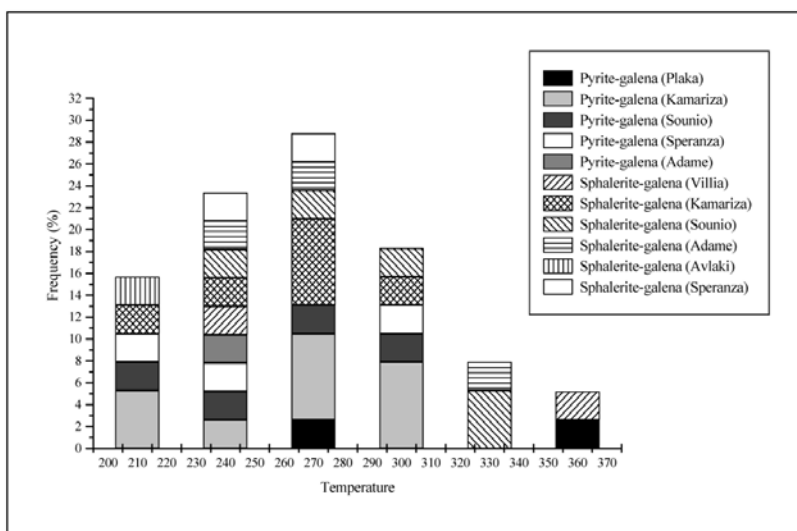


Fig. 4: Histogram of the frequency of the temperature values obtained by isotope geothermometry from the Plaka, Kamariza, Sounio, Speranza, Adame, Villia and Avlaki deposits.

Finally, the isotopic compositions of cerussite, aragonite and phosgenite range from $\delta^{18}\text{O} = -25.9$ to 24.6 (some of the measured values were adopted from Gilg and Boni, 2004, and are for the Kamariza and Adame deposits), $\delta^{18}\text{O} = 30.0$ to 33.0 and $\delta^{18}\text{O} = 27.1$ to 28.7 per mil (both from Kamariza). These correspond to isotopic calculated values of $\delta^{18}\text{O}_{\text{H}_2\text{O}}$ that range from 17.1 to 32.8, 26.2 to 27.3 and 27.0 to 29.0 per mil (at 100°C) (Fig. 3).

7. Oxygen and Hydrogen Isotopes

Oxygen and hydrogen isotope compositions of quartz from Plaka granodiorite range from 6.8 to 9.1 and from -70 to -78 per mil (one measured value was obtained by Altherr et al., 1988). These correspond to calculated $\delta^{18}\text{O}_{\text{H}_2\text{O}}$ fluid values of 5.3 to 5.9 per mil and -55 to -62 per mil, at 700°C. The $\delta^{18}\text{O}$ and δD values from quartz in skarn of 10.8 and -76 per mil corresponds to $\delta^{18}\text{O}_{\text{H}_2\text{O}} = 3.2$ per mil and $\delta\text{D}_{\text{H}_2\text{O}} = -67$, at 500°C (Baltatzis, 1981).

8. Sulfur Isotope Study and Temperature of Sulphide Deposition

Temperature determinations for primary sulphide deposition based on $\delta^{34}\text{S}$ isotopes, were obtained for the isotopic coexistence of the pyrite-galena and sphalerite-galena pairs according to the equations of Ohmoto and Lasaga (1982). The calculated temperatures during sulphide deposition range between 358° to 306°C for Plaka, to 359° to 225°C for Kamariza, 350° to 260°C for Villia, 300° to 225°C for Adame, 320° to 220° C for Sounio, 300° to 225°C for Speranza, and ~ 200°C for Avlaki (Fig. 4).

A $\delta^{34}\text{S}$ isotope value obtained from arsenopyrite in the skarn (high temperature mineralization, Plaka area) is 7.3 per mil, which corresponds to a calculated value of $\delta^{34}\text{S}_{\text{H}_2\text{S}}$ of 6.8 per mil (based on the arsenopyrite- H_2S equation of Ohmoto and Lasaga, 1982, at $T = 400^\circ\text{C}$, Economou et al., 1981) (Fig. 5). The $\delta^{34}\text{S}$ measured isotopic values of pyrite from Plaka, Villia, Kamariza, Sounio, Speranza and M. Pefka locations display a range of $\delta^{34}\text{S}$ values of -2.6 to 3.9, 4.3 to 5.7, ≈ 1.3 , -3.2 to -0.4, -1.8 to -0.9, -3.7 to 4.5, ≈ 0.4 and ≈ -2.7 per mil, respectively. Based on the equations for pyrite- H_2S of

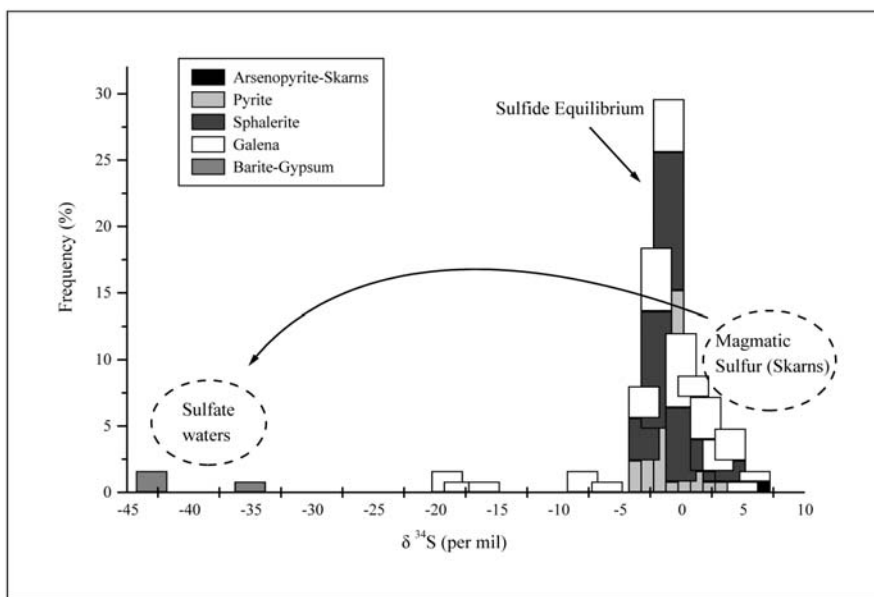


Fig. 5: Histogram of the frequency of the $\delta^{34}\text{S}_{\text{H}_2\text{S}}$ values of arsenopyrite, pyrite, sphalerite, galena, barite and gypsum from the Plaka, Sounio, Kamariza, M. Pefka, Spiliazeza, Speranza, Villia, Adame, Sounio, Christina, Avlaki deposits.

Ohmoto and Rye (1979) and Ohmoto and Lasaga (1982), the calculated $\delta^{34}\text{S}_{\text{H}_2\text{S}}$ values are -1.6 to 2.9, 3.2 to 4.6, ≈ 0.3 , -2.1 to 0.8, -2.8 to -0.2, -1.5 to 2.2, ≈ -0.7 and ≈ -1.2 per mil, in the fluid, at $T = 200^\circ, 250^\circ, 300^\circ, 320^\circ$ and 350°C (Fig. 5).

Values of $\delta^{34}\text{S}$ of sphalerite from Villia, Adame, Kamariza, Sounio, Spiliazeza, Speranza, Christina and M. Pefka exhibit a range from 4.2 to 4.8, -1.6 to 1.6, -3.7 to -1.1, -2.8 to -1.2, -3.9 to 1.3, 0.6 to 4.1, ≈ -1.4 and ≈ 9.4 per mil, respectively. The calculated values for the isotopic composition of the fluid (based on the sphalerite- H_2S equation of Ohmoto and Rye, 1979; Ohmoto and Lasaga, 1982) were $\delta^{34}\text{S}_{\text{H}_2\text{S}} = 3.9$ to 4.5, -1.8 to 1.4, -3.3 to -0.8, -2.4 to -0.7, -3.3 to -0.7, 0.4 to 3.7, ≈ -1.0 , and ≈ 9.1 per mil, at the same temperatures, respectively (Fig. 5). The $\delta^{34}\text{S}$ values for galena from Plaka, Villia, Adame, Kamariza, Sounio, Speranza, and Avlaki range from -3.3 to 4.1, 2.3 to 3.9, -3.4 to 1.5, -4.7 to -0.4, -5.0 to 2.6, 0.2 to 1.7 and 2.7 to 3.6 per mil, respectively. The calculated values (based on the galena- H_2S equation of Ohmoto and Rye, 1979; Ohmoto and Lasaga, 1982) were $\delta^{34}\text{S}_{\text{H}_2\text{S}} = -2.5$ to 6.0, 4.1 to 5.6, -1.8 to 1.6, -2.8 to 1.7, -8.5 to -1.1, 2.0 to 3.5 and -0.2 to 1.7 per mil, at the same temperatures (Fig. 5).

Finally, sulfur isotope compositions of barite and gypsum from the Kamariza and Sounio deposits reveal values of $\delta^{34}\text{S}$ which range from $\delta^{34}\text{S} = 17.3$ to 20.4 and ≈ 23.5 , and ≈ 0.2 per mil, corresponding to calculated $\delta^{34}\text{S}_{\text{H}_2\text{S}}$ of -19.5 to -16.4, ≈ -35.0 and ≈ -43.6 per mil (based on the barite- H_2S and gypsum- H_2S equations of Kusakabe and Robinson, 1977 and Ohmoto and Rye, 1979, at $T = 200^\circ, 150^\circ$ and 100°C) (Fig. 5).

Calculations of water-to-rock ratios were performed by assuming a closed system for the early mineralized stages, at $T \geq 300^\circ\text{C}$ (as evidenced by the occurrence of calcite veins mainly as stockworks), and an open system for the late ones, at $T \leq 300^\circ\text{C}$. Calculations were achieved by using the equa-

tions adopted from Taylor (1974). The calculated isotopic compositions reveal water-to-rock ratios with values of, 6.6 to 10.1% (for Villia), 8.5% (for Adame), 8.9 to 52.6% (for Kamariza), 29.6% (for Speranza), 40.3% (for Sounio) and 2.6% (for Plaka).

9. Discussion and Conclusions

Oxygen and carbon isotope data suggest multiple sources for the ore fluid, i.e., magmatic and metamorphic (Fig. 2). There is a recognizable depletion in $\delta^{13}\text{C}$ and $\delta^{18}\text{O}$ values which can be the result of interaction of modified high-temperature magmatic fluids with the hosts or to have formed under medium to high water-to-rock ratios, i.e., 4.8 to 52.6%. This depletion is also correlated to simple cooling of the fluid, from 400° to 150°C, which was caused by mixing of the Ag-bearing fluid with meteoric waters had entered the highly permeable carbonate-host.

The oxygen and hydrogen isotope compositions are consistent with magmatic water composition, and are similar to those characterizing the Tinos, Mykonos and Serifos granitoids and skarns (Tombros et al., 2007, 2008; Tombros, 2009 and St. Seymour et al., 2009a, b). However, granitoids in Lavrion area are weakly affected by alteration (e.g., silicification, propylitization, carbonatization, and sericitization, Bonsall et al., 2007) due to their interaction with the mineralizing fluids; as it was depicted from the $\delta\text{D}_{\text{H}_2\text{O}}$ values of the Plaka granitoid. For the early stages of Lavrion ores the calculated $\delta^{18}\text{O}_{\text{H}_2\text{O}}$ and $\delta\text{D}_{\text{H}_2\text{O}}$ isotopic values reflect the dominance of a magmatic component, whereas the late-stage fluids are consistent with isotopic exchange of the mineralizing fluid with Miocenic meteoric waters.

The mixing hypothesis of the fluid is also supported by the $\delta^{34}\text{S}_{\text{H}_2\text{O}}$ data: The calculated $\delta^{34}\text{S}_{\text{H}_2\text{O}}$ compositions of sulfides i.e., $\delta^{34}\text{S}_{\text{H}_2\text{O}} = -8.0$ to 9.0 per mil from the Lavrion deposits are interpreted to reflect a double source. The positive $\delta^{34}\text{S}_{\text{H}_2\text{O}}$ values could have been the result of the direct addition of magmatic volatiles to the hydrothermal fluid (e.g., $\delta^{34}\text{S}_{\text{H}_2\text{O}} = 6.8$ per mil from skarn-arsenopyrite). The negative $\delta^{34}\text{S}_{\text{H}_2\text{O}}$ values can be explained by the introduction of isotopically light sedimentary sulfur into the hydrothermal system from the enclosing metasedimentary rocks, at higher $\log f_{\text{O}_2}$ conditions. Sulfur isotope compositions $\delta^{34}\text{S}_{\text{H}_2\text{O}}$ of barite and gypsum from carbonate-replacement ores, range from -43.6 to -16.4 to per mil and reflect seawater sulfate values of Miocene (e.g., -40 to -20 per mil, Ohmoto and Rye, 1979).

Temperatures based on $\delta^{34}\text{S}$ pyrite-galena and sphalerite-pyrite pairs revealed at least three thermal pulses during deposition of the carbonate-replacement ore: (i) ~ 360°, (ii) 320°-280° and (iii) 260° to 200°C. Telescoping phenomena i.e., co-existence of minerals which belong to different paragenetic stages is apparent in the Lavrion ores. This can be explained by the protracted period of the ore-forming event of more than 2 Ma (10 to 8 Ma, Skarpelis, 2007). A primary closed, channelized hydrothermal system was operational in Lavrion in the early stages resulted in As-rich skarn deposits ($T \leq 500^\circ\text{C}$). Then, the hydrothermal system in the late stages of its evolution had opened ($T \geq 100^\circ\text{C}$), and resulted in the precipitation of fluorite-barite ores.

10. References

- Allherr, R., and Siebel, W. 2002. I-type plutonism in a continental back-arc setting: Miocene granitoids and monzonites from the central Aegean Sea, Greece. *Contributions to Mineralogy and Petrology*, 143, 397-415.
- Baltatzis, E. 1981. Contact metamorphism of a calcilicite hornfels from Plaka area, Lavrion, Greece. *Neues Jahrbuch für Mineralogie Monatshefte*, 11, 481-488.

- Baltatzis, E. 1996. Blueschist-to-greenschist transition and the P-T path of prasinites from the Lavrion area, Greece: *Mineralogical Magazine*, 60, p. 551-561.
- Baziotis, I., Proyer, A., and Mposkos, E., 2009, High-pressure/low-temperature metamorphism of basalts in Lavrion (Greece): Implications for the preservation of peak metamorphic assemblages in blueschists and greenschists: *European Journal of Mineralogy*, 21, 133-148.
- Bonsall, T.A., Spry, P.G., Voudouris, P., St. Seymour, K., Tombros, S., and Melfos, V. 2007. Fluid inclusion and stable isotope characteristics of carbonate replacement Pb-Zn-Ag deposits in the Lavrion district, Greece. In Andrews, C.J., et al., eds., *Mineral exploration and research: Digging deeper*, Irish Association for Economic Geology, Dublin, 283-286.
- Bowman, J.R. 1998. Stable-isotope systematics of skarns. In Lentz, D.R., ed., *Mineralized intrusion-related skarn systems*, *Mineralogical Association of Canada Short Course Series*, 26, 99-145.
- Bröcker, M., and Pidgeon, R.T. 2007. Protolith ages of meta-igneous and metatuffaceous rocks from the Cycladic Blueschist Unit, Greece: Results of a reconnaissance U-Pb zircon study. *Journal of Geology*, 115, 83-98.
- Conofagos, C. 1980. The Lavrion and the ancient Greek techniques for silver production. Athens, Ekdotiki Athinon, 458 p.
- Clayton, R.N., Goldsmith, J.R., and Mayeda, T.K. 1989. Oxygen isotope fractionation in quartz, albite, anorthite and calcite. *Geochimica et Cosmochimica Acta*, 53, 725-733.
- Craig, J.R. 1967. Phase relations and mineral assemblages in the Ag-Bi-Pb-S system. *Mineralium Deposita*, 1, 278-306.
- Economou, M., and Sideris, C. 1976. A mineralized brecciated granodiorite porphyry in the Laurium mines, Greece. *Neues Jahrbuch für Mineralogie Abhandlungen*, 128, 209-218.
- Economou, M., Skounakis, S., and Papathanasiou, C. 1981. Magnetite deposits of skarn type from the Plaka area of Laurium, Greece. *Chemie der Erde*, 40, 241-252.
- Fritz, P., Drimmie, R.J., and Norwick, K. 1974. Preparation of sulfur dioxide for mass spectrometer analysis by combustion of sulfide with copper oxide. *Analytical Chemistry*, 76, 164-166.
- Glatz, A.C., 1967. The Bi_2Te_3 - Bi_2S_3 system and the synthesis of tetradymite. *American Mineralogist*, 52, 161-170.
- Gilg, H.A. and Boni, M., 2004, Stable isotope studies on Zn and Pb carbonates: Could they play a role in mineral exploration? In: *Applied Mineralogy*, Developments in Science and Technology, Pecchio, M., Andrade, F.R.D., D'Agostino, L.Z., Kahn, H., Sant'Agostino, L.M., Tassinari, M.M.M.L., (eds), ICAM-BR, São Paulo, 2, 781-784.
- Hall, H.T., 1966. The systems Ag-Sb-S, Ag-As-S and Ag-Bi-S: Phase relations and mineralogical significance. PhD Thesis, Brown University, 240 p.
- Hall, H.T., and Yund, 1964. Equilibrium relations among some silver sulfosalts and arsenic sulfides. *American Geophysical Union Transactions*, 45, 1311-1321.
- Kalogeropoulos, S.I., and Mitropoulos, P. 1983. Fluid inclusion characteristics of fluorite from Lavrion (Greece). *Annales Geologiques des Pays Helleniques*, 31, 130-135.
- Knoll, O. 1988. Ore mineralogy and fluid inclusion studies of Pb-Zn-ores from Lavrion-Greece. MSc Thesis, Hamburg, University of Hamburg, 72 p.
- Kusakabe, M., and Robinson, B. 1977. Oxygen and sulfur isotope equilibria in the BaSO_4 - HSO_4^- - H_2O system from 110° to 350°C and applications. *Geochimica and Cosmochimica Acta*, 41, 1033-1040.
- Lefticariu, L., Pratt, L. M., and Ripley, E. M. 2006. Mineralogic and sulfur isotope effects accompanying the oxidation of pyrite in millimolar solutions of hydrogen peroxide at temperatures from 4 to 150 °C. *Geochimica et Cosmochimica Acta*, 70, 4889-4905.

- Leleu, M. 1966. Les gisements plombo-zincifères du Laurium (Grèce). *Sciences de la Terre*, 9, 293-343.
- Leleu, M., Morikis, A., and Picot, P. 1973. Sur des mineralisations de type skarn au Larium (Grèce). *Mineralium Deposita*, 36, 477-489.
- Marinos, G. and Petrascheck W.E. 1956. Larium: Geological and geophysical research. *Institute for Geology and Subsurface Research*, 4, 1-246.
- Melidonis, N.G., 1980. The geological structure and mineral deposits of Tinos Island (Cyclades, Greece): A preliminary study. *Institute of Geology and Mineral Exploration*, 13, 1-80.
- Ohmoto, H., and Lasaga, A.C. 1982. Kinetics of reactions between aqueous sulfates and sulfides in hydrothermal systems. *Geochemica Et Cosmochimica Acta*, 46, 1727-1745.
- Ohmoto, H., and Rye, R.O. 1979. Isotopes of sulfur and carbon: In Barnes, H.L. (ed.), *Geochemistry of hydrothermal ore deposits*, 2nd ed., New York, Wiley Interscience, 509-567.
- Papanikolaou, D., and Syskakis, D. 1991. Geometry of acid intrusive in Plaka, Laurion and relation between magmatism and deformation. *Bulletin of the Geological Society of Greece*, 25, 45-67.
- Photiades, A. and Carras, N. 2001. Stratigraphy and geological structure of the Lavrion area (Attica, Greece). *Bulletin of the Geological Society of Greece*, 34, 103-109.
- Salemink, J. 1985. Skarn and ore formation at Seriphos, Greece, as a consequence of granodiorite intrusion. *Geologica Untrajectina*, 40, 1-231.
- Skarpelis, N. 2002. Geodynamics and evolution of the Miocene mineralization in the Cycladic-Pelagonian Belt, Hellenides. *Bulletin of the Geological Society of Greece*, 34, 2191-2209.
- Skarpelis, N. 2007. The Lavrion deposit (SE Attica, Greece): geology, mineralogy and minor elements chemistry. *Neues Jahrbuch für Mineralogie Abhandlungen*, 183, 227-249.
- Skarpelis, N., and Ardyraki, A. 2008. Geology and origin of supergene ore at the Lavrion Pb-Ag-Zn deposit, Attica, Greece. *Resource Geology*, 59, 1-14.
- Skarpelis, N., Tsikouras, B., and Pe-Piper, G. 2008. The Miocene igneous rocks in the Basal unit of Lavrion (SE Attica, Greece): Petrology and geodynamic implications. *Geological Magazine*, 145, 1-15.
- Schmidt, M.W. 1992. Amphibole composition in tonalite as a function of pressure: an experimental calibration of the Al-in-hornblende barometer. *Contributions to Mineralogy and Petrology*, 110, 304-310.
- St. Seymour, K., Zouzias, D., Tombros, S.F., and Kolaiti, E. 2009a. The geochemistry of the Serifos pluton and associated iron oxide and base metal sulphide ores: Skarn or metamorphosed exhalite deposits?. *Neues Jahrbuch für Mineralogie Abhandlungen* (DOI: 10.1127/0077-7757/2009/0143).
- St. Seymour, K., Mastrakas, N., Tombros, S.F., Spry, P.G., Denes, G., and Kranidiotis, P. 2009b. Scheelite mineralization of the skarn deposit, at Tinos Island, Aegean Sea, Cyclades. *Neues Jahrbuch für Mineralogie Abhandlungen*, 186, 37-50.
- Tombros, St., 2009. Prospecting for Au-Ag-Te mineralization in the Cyclades, based on the example of Tinos Island. "Pythagoras II", Post-doctoral Fellowship, Operational Program for Educational and Vocational Training II (EPEAEK II), Univ. of Patras, 940 p.
- Tombros, S.F., Seymour, K., Spry, P.G., and Williams-Jones, A. 2008. Later stages of evolution of an epithermal system: Au-Ag Mineralizations at Apigania Bay, Tinos Island, Cyclades, Hellas (Greece). *Mineralogy and Petrology*, 94, 175-194.
- Tombros, S.F., Seymour, K., Williams-Jones, A., and Spry, P. 2007. The genesis of epithermal Au-Ag-Te mineralization, Panormos Bay, Tinos Island, Cyclades, Greece. *Economic Geology*, 102, 1269-1294.
- Vyhnal, C.R.; McSween, H.Y.Jr. and Speer, J.A. 1991. Hornblende chemistry in southern Appalachian granitoids: Implications for aluminium hornblende thermobarometry and magnetic epidote stability. *American Mineralogist*, 76, 176-188.

- Voudouris, P., Melfos, V., Spry, P. G., Bonsall, T., Tarkian, M., and Solomos, C. 2008a. Mineralogical and fluid inclusion study of the Kamariza carbonate-replacement deposit, Lavrion, Greece. *Mineralogy and Petrology*, 94, 85-106.
- Voudouris, P., Melfos, V., Spry, P. G., Bonsall, T., Tarkian, M., and Economou-Eliopoulos, M. 2008b. Mineralogical study and constraints on fluid evolution in the Plaka-related ore system, Lavrion, Greece. *Mineralogy and Petrology*, 93, 79-110.
- Wijbrans, J.R., Van Wees, J.D., Stephenson, R.A., and Cloetingh, S.A.P.L. 1993. Pressure-temperature-time evolution of the high-pressure metamorphic complex of Sifnos, Greece. *Geology*, 21, 443-446.
- Zachos, J., Pagani, M., Sloan, L., Thomas, E., and Billups, K., 2001, Trends, rhythms, and aberrations in global climate 65 Ma to present: *Science*, 292, p. 686-693.

GEOCHEMICAL INVESTIGATION AND MODELLING OF AN ACID PIT LAKE FROM A HIGH SULFIDATION ORE DEPOSIT: KIRKI, NE GREECE

Triantafyllidis S.¹ and Skarpelis N.²

¹ Nikoforou 19, 16675 Glyfada, Athens, Greece, statrib@gmail.com

² Faculty of Geology and Geoenvironment, University of Athens, Panepistimiopoli, 157 84 Zografou, Athens, Greece, skarpelis@geol.uoa.gr

Abstract

Open pit mining of a high sulfidation epithermal type deposit at Kirki (Thrace, NE Greece) resulted in the formation of an acid pit lake by infilling of the open cast by rain and drainage waters after mine closure. The acidic and oxidative pit lake waters show high concentrations of trace metals largely due to the high toxic metals content of the ore, the limited buffering capacity of host rocks and the direct exposure of the ore zone to weathering. The floor of the pit lake is covered by a fine-grained mineral precipitate that comprises mainly detrital minerals, originating from erosion of the rocks exposed on the walls of the open pit. Secondary anglesite, several species of the jarosite-group, rozenite, melanterite, gypsum, bukovskyite, beaverite, scorodite and minor goethite are also detected. The mineral precipitate presents significant heavy metal content indicating effective removal of metals from the acidic waters. The speciation/mass transfer computer code PHREEQC-2 and the MINTEQ database were employed for geochemical modelling of the equilibrium between the acidic pit lake waters and the secondary phases of the mineral precipitate.

Key words: Acid pit lake, mineral precipitate, high-sulfidation ore, geochemical modelling, Kirki.

1. Introduction

Pit lakes are unique water bodies. They are developed as a result of open cast mining. When the activity ceases, the open pit is back filled with groundwater and surface water (Lu et al., 2003). The rate of filling is defined by climatic and geologic conditions, as well as the regional hydrologic characteristics.

Assessment of the environmental risks of pit lake development is an imperative for the mining industry and the public, especially in cases of high sulfidation deposits that are characterized by high concentrations of toxic metals (Plumlee et al., 1999). Pit lakes forming from such deposits pose a significant threat to the environment since they are often acidic containing elevated concentrations of metals (e.g. Fe, Al, Pb, Cu, Zn, Mn, Cd) and metalloids (e.g. As, Sb), and show high acid generation potential and very low buffering capacity (Latanzi et al., 2008; Sperling & Grandschamp, 2008; Shevenell et al., 1999).

Quantification, prediction and evolution of pit lake systems require the use of numerical models (such as PHREEQC), which take into account the relevant thermodynamic, mineralogical and geochemical data, as well as other parameters such as changes in pit lake volume, effects of seasonal

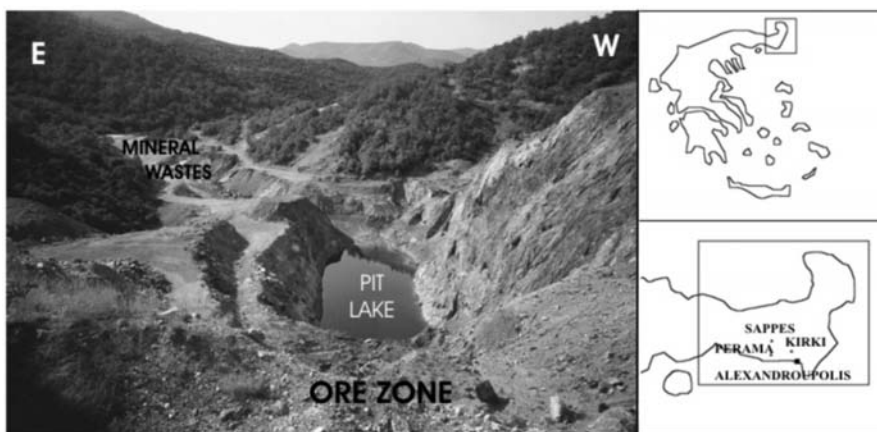


Fig. 1: View from north of the Kirki (Ag. Filippos) acid pit lake.

weather patterns, processes occurring on pit walls above the lake surface (Gimber et al., 2008). The aim of this paper is to provide information on the function of the small pit lake developed at the abandoned Kirki (Agios Filippos) high sulfidation mine. The results of this study can be used for future evaluation of various remediation options for the pit lake.

2. Site description

The Kirki (Agios Filippos) high sulfidation deposit is hosted into the Eocene-Oligocene volcano-sedimentary rock sequences of SE Evros county and is associated with orogenic calc-alkaline to shoshonitic magmatism. The high sulfidation epithermal type mineralization is developed between two sub-parallel fault zones that form the western and the eastern part of the open pit. The ore is rich in base-metals sulfides and various Pb- and As-bearing sulfosalts (Skarpelis, 1999). Galena shows the highest degree of weathering among other sulfides and sulfosalts. The low degree of oxidation of pyrite and sphalerite is reasonably explained by their rather chemical purity (Triantafyllidis & Skarpelis, 2004). Studies by Triantafyllidis (2006) showed that in the upper part of the oxidation zone sulfates, hydrosulfates and sulfoarsenates are the predominant secondary mineral phases. Anglesite is the major oxidation product, followed by lower proportions of osarizawaite, beaverite, linarite and beudantite (Triantafyllidis & Skarpelis, 2004). At lower levels of the oxidation zone, carbonates are additionally identified. Secondary carbonates include cerussite, hydrocerussite, smithsonite, azurite and rosasite. The mineralogy of efflorescences appearing on the walls of the open pit is indicative of highly acidic and oxidative conditions. Efflorescences of Fe-bearing (e.g. siderotile, copiapite, rhomboclase) and Cu-bearing sulfates (e.g. chalcantinite), arsenates (scorodite) and sulfoarsenates dominate over Pb and Zn sulfates.

Since mine closure in 1997, an acid pit lake has been formed by infilling of the open pit by rain and drainage waters (Fig. 1). The height of the water column fluctuates, depending on the annual rainfall. The waters from the pit lake show low pH, high Eh values and increased concentrations of dissolved toxic metals through the year (Triantafyllidis & Skarpelis, 2006). The topography of the mine prevents overflow and dispersion of acidic waters into the drainage system of the area.

A yellowish to orange-yellowish, fine-grained, unconsolidated mineral precipitate with an average thickness of 20cm covers the floor of the pit lake and yields significant heavy metal content. The mineral precipitate comprises mainly detrital quartz, dickite/kaolinite, pyrophyllite and feldspar, origi-

nating from erosion of the rocks exposed on the walls of the open pit. Semiquantitative analyses indicate that Fe-bearing sulfates (jarosite group minerals, melanterite, rozenite, butlerite), sulfoarsenates (bukovskyite) and arsenates (scorodite) dominate over other secondary minerals (e.g. anglesite, beaverite, wroewolfeite and gypsum) (Triantafyllidis & Skarpelis, 2006).

3. Sampling - analytical methods

Drill core samples down to a depth of 200m from the surface were used for the mineralogical investigation of secondary mineral phases. Samples of mineral precipitate from the open pit and efflorescences from the mine walls were collected and dried at room temperature. Water samples from the open pit were collected in September 2001, June 2003 and December 2004, applying standard sampling techniques. Temperature, pH and Eh were measured on site using a WTW pH 320/Set-2 electronic pH-meter. Water samples were filtered through a 0.45 µm Millipore filter and acidified with 1 M HNO₃. Details of the analytical technics implemented in this study can be found at Triantafyllidis (2006), Triantafyllidis & Skarpelis (2006) and Triantafyllidis et al. (2007).

4. Analytical data used

The physicochemical data for the pit lake waters, the geochemical data of the mineral precipitate, and the mineralogy of the precipitate are given in Tables 1, 2, and 3 respectively (Triantafyllidis & Skarpelis, 2006).

Table 1. Physicochemical characteristics of pit lake waters (Dissolved ions in mg/l, Eh in mV) (from Triantafyllidis & Skarpelis, 2006).

	pH	Eh	SO ₄	Cd	Co	Cu	Fe	Mn	Ni	Pb	Zn
September 2001											
Mean	3.1	235	2300	3.82	0.26	16.2	7.5	169.7	1.76	2.24	425.5
Stan. Dev.	0	1.58	130	0.07	0.01	0.25	0.26	3.4	0.03	0.03	1.22
June 2003											
Mean	2.9	248	1700	2.71	0.14	12.1	27.1	112.0	1.30	0.90	282.5
Stan. Dev.	0.06	4.62	75	0.06	0.01	0.13	1.04	1.91	0.04	0.02	3.4
Ag, Hg, As, Sb below detection											
Total Radioactivity: 16.48 – 151.62 pCi/l											

Table 2. Chemical analyses of the mineral precipitate (Major elements and Fe in wt %, trace elements in ppm) (from Triantafyllidis & Skarpelis, 2006)

	SiO ₂	Al ₂ O ₃	CaO	Cr ₂ O ₃	K ₂ O	MgO	Na ₂ O	P ₂ O ₅	TiO ₂	LOI
Min	30.9	12.72	0.4	0.02	1.82	0.6	0.16	0.1	0.43	11.4
Max	59.5	22.71	0.63	0.03	3.1	0.91	0.37	0.19	0.64	22.9
Mean	43.8	17.5	0.52	0.02	2.39	0.76	0.28	0.14	0.55	18.4
Stan. Dev.	12.1	4.4	0.09	0.01	0.58	0.14	0.09	0.03	0.1	5.16
LOI: Loss on ignition										

Table 2 continued.

	Fe	Pb	Zn	Cu	Mn	As	Cd	Ni	Sb	Co	Ag	Bi	U
Min	6.21	3219	3195	473	591	497	22	22	26	b.d.	7.2	84	b.d.
Max	20.78	6748	4789	958	2017	1582	46	31	38	20	11.3	136	11
Mean	11.38	5087	4231	710	1256	889	32	25	31	4	8.9	98	6
Stan. Dev.	5.91	1050	621	147	577	475	7.3	3	5.6	6.6	1,5	28	4.4
Hg: below detection limit b.d.: below detection													

Table 3. Semiquantitative analyses of secondary minerals identified in the mineral precipitate (from Triantafyllidis & Skarpelis, 2006).

Jarosite group minerals (jarosite, hydronium jarosite)	$(K, H_3O)Fe_3(SO_4)_2(OH)_6$	XXX
Wroewolfeite	$Cu_4(SO_4)(OH)_6 \cdot 2H_2O$	X
Beaverite	$PbCu(Fe, Al)_2(SO_4)_2(OH)_6$	XX
Gypsum	$CaSO_4 \cdot 2H_2O$	XX
Anglesite	$PbSO_4$	XX
Scorodite	$FeAsO_4 \cdot 2H_2O$	X
Bukovskiyite	$Fe_2(AsO_4)(SO_4)(OH) \cdot 7H_2O$	X
Goethite	$Fe(OH)_3$	XX
Melanterite	$FeSO_4 \cdot 7H_2O$	X
Rozenite	$FeSO_4 \cdot 4H_2O$	X
Butlerite	$FeSO_4(OH) \cdot 2H_2O$	X
Mineral abundances: XXX very abundant, XX medium, X low		

5. Application of PHREEQC geochemical code

The correlation between the chemistry of the acidic pit lake waters and the mineralogy of the mineral precipitate was investigated with the use of the geochemical code PHREEQC-2 (Parkhurst & Appelo, 1999) and in particular the 2.12 edition.

There are two basic approaches to geochemical modeling: chemical equilibrium and chemical kinetics, with the first, and most common, being employed in this study. In general, equilibrium models can be divided into the following categories: forward (reaction path models) and inverse.

Forward models are used for prediction of water chemistry evolution. In this case the starting water chemistry is defined and an attempt is made to model water evolution by precipitation of mineral phases. During each step the program transfers a small amount of mass from reactant to products. Then it calculates mass distribution among the products and saturation indices of pre-determined phases. Then, the program checks whether the water is supersaturated relative to those phases.

Inverse models are based on mass balance calculations for solid phase and dissolved species in a geochemical system. In this case, we examined the precipitation of the mineral phases identified in the pit lake after mixing of two different water types.

Table 4.

Physicochemical characteristics of the solutions used for PHREEQC modeling			
Solution 1 (meteoric waters)		Solution 2 (acidic pit lake waters)	
Temperature	25°C	Temperature	25°C
pH	6	pH	3
pε	4	pε	4
density	1gr/cm ³	density	1g/cm ³
		S (as SO ₄)	2300 mg/L
		Cu	16 mg/L
		Mn	170 mg/L
		Zn	425 mg/L
		Fe	7 mg/L
		Pb	2 mg/L
		Na	10 mg/L
		K	2 mg/L

6. Geochemical modeling

Thermodynamic data was taken from MINTEQ database (Allison et al., 1991). Imported parameters in the system involved: Fe (total), Pb, Zn, Cu, Mn, SO₄⁻² and pH. Cobalt was not taken under consideration since it is not included in the MINTEQ database. Several different scenarios were employed for the system “acidic pit lake waters – precipitate mineralogy”.

6.1 Forward modeling

The first scenario involved the possibility of direct precipitation of the identified secondary phases, as a result of supersaturation due to evaporation, or excessive input of toxic metals, sulfates and arsenates to the pit lake, at a given time period. Application of the PHREEQC geochemical code showed that direct precipitation is impossible largely due to the low heavy metal and sulfate load of the pit lake waters.

6.2 Inverse modeling

Inverse modeling was applied to verify hypotheses on the origin of the identified secondary phases in the mineral precipitate. Two cases were examined. The first case involved the study of the chemical characteristics of a theoretical solution that resulted after mixing slightly acidic meteoric water (Table 4, solution 1) with a potential acid drainage in several ratios, to check if that solution is in equilibrium with the secondary phases identified in the precipitate. For the second case, the acidic pit lake waters were used as the potential acid drainage (Table 4, solution 2). Once more, the behavior of mixing the slightly acidic rain water with the potential acid drainage in several ratios was investigated.

1st case: The potential acid drainage was based on thermodynamic data from MINTEQ database. The mineralogy of the Kirki high sulfidation deposit is very complex with a diversity of sulfides and sulfosalts and, unfortunately, for most of these minerals there is no data. This geochemical model showed that potential acid drainage with thermodynamic data only for pyrite, galena and sphalerite cannot sufficiently interpret the secondary mineralogy of the precipitate.

Table 5.

Saturation indices of secondary minerals in equilibrium with the acidic pit lake waters, based on the PHREEQC-2.12 geochemical code		
Mineral	Saturation index (MINTEQ)	Formula (MINTEQ)
Anglesite	0.66	PbSO ₄
Bianchite	-4.93	ZnSO ₄ ·x6H ₂ O
Cerussite	-1.62	PbCO ₃
Ferrihydrite	-1.58	Fe(OH) ₃
Goethite	2.82	FeOOH
Goslarite	-4.74	ZnSO ₄ ·x7H ₂ O
Hematite	10.64	Fe ₂ O ₃
H3O-jarosite	0.94	(H ₃ O)Fe ₃ (SO ₄) ₂ (OH) ₆
Jarosite	1.87	KFe ₃ (SO ₄) ₂ (OH) ₆
Na-jarosite	-0.89	NaFe ₃ (SO ₄) ₂ (OH) ₆
Larnackite	-3.42	PbOxPbSO ₄
Lepidocrocite	1.94	FeOOH
Maghemite	0.24	Fe ₂ O ₃
Magnetite	5.07	Fe ₃ O ₄
Melanterite	-5.91	FeSO ₄ ·x7H ₂ O
Smithsonite	-4.33	ZnCO ₃

2nd case: Development of this model with PHREEQC, for mixing of the aforementioned solutions in ratio 95:5 (95% solution 1 and 5% solution 2), leads to a final solution that is in equilibrium with the majority of the secondary phases identified in the pit lake mineral precipitate (e.g. anglesite, goethite, jarosite), as well as other secondary phases that cannot be detected with X-ray Diffraction (e.g. ferrihydrite) (Table 5).

It is worth mentioning that similar results arise with different mixing ratios (e.g. 99 to 1). Another characteristic of this model is the thermodynamic equilibrium of several secondary Fe phases, while the concentration of Fe in the acidic pit lake water are relatively low (7.5 to 27 mg/L).

7. Conclusions

The Kirki (Agios Filippos) high sulfidation deposit is rich in base metals sulfides (e.g. pyrite, galena, sphalerite) and sulfosalts (e.g. enargite, tennantite, jordanite). Lead and Cu-bearing sulfates and hydrosulfates dominate in the upper part of the oxidation zone of the Kirki deposit, whereas at lower levels supergene carbonates are present. During the last ten years, an acid pit lake was formed by infilling of the open pit by rain and drainage waters. The highly acidic pit lake waters show high concentrations of dissolved toxic metals. The pit lake waters are characterized by increased toxic metals concentrations as a result of:

- Oxidation of sulfides and sulfosalts and the partial release of their toxic load to the environment due to the presence of mildly acidic and oxidative meteoric and drainage waters.

- Washing and dissolution of soluble secondary phases (efflorescences) formed on the walls of the open pit.
- The direct contact of the highly acidic and oxidative waters of the pit lake with grains of sulfides and sulfosalts present at the level of pit lake water.

The model developed with PHREEQC for the Kirki pit lake system shows that meteoric waters plays a key role in deposition of secondary phases in the pit lake. In particular, mixing of slightly acidic meteoric waters with the acidic pit lake waters in ratio 95:5 or higher, may successfully lead to the formation of anglesite, goethite, jarosite group minerals, hematite and ferrihydrite. On the other hand, due to lack of thermodynamic data, there are no conclusions concerning beaverite, scorodite, bukovskyite, wroewolfeite and siderotile.

Finally, it is very important to state that the aforementioned model for the Kirki pit lake system is based on a critical limitation, being the organic activity within the pit lake waters. It is known that the role of aerobic bacteria is critical in the initial oxidation/weathering of primary sulfides and sulfosalts (Stokes, 1954; Walsh & Mitchell, 1972; Trafford et al., 1973; Ivarson & Sojak, 1978; Crepar et al., 1979; Evangelou, 1983), as well as their catalytic behavior in the formation of secondary phases present in pit lakes precipitates. Further study aims to shed light on the role bacteria play for the evolution of the Kirki pit lake system.

8. Acknowledgements

The research work was funded through the program “IRAKLEITOS - Fellowships for Research of National and Kapodistrian University of Athens - ENVIRONMENT”.

9. References

- Allison, J.D., Brown, D.S. & Novo-Gradac, K.J., 1991. MINTEQA2/PRODEFA2, A geochemical assessment model for environmental systems, Version 3.0 User's Manual, Environmental Research Laboratory, Office of Research and Development, US Environmental Protection Agency, EPA/600/3-91/021, Athens, Georgia, 30605, 92.
- Crepar, D.A., Knox, G.W. & Means, J.L., 1979. Biogeochemistry of bog iron in the New Jersey pine barrens. *Chemical Geology*, 24, 111-135.
- Enders, M.S., Knickerbocker, C., Tittle & Southam, G., 2006. The role of bacteria in the supergene environment of the Morenci Porphyry Copper Deposit, Greenlee County, Arizona. *Economic Geology*, 101, 59-70.
- Evangelou, V.P., 1983. Pyritic coal spoils: Their chemistry and water interactions. In S.S. Augustithis (eds), *Leaching and diffusion in rocks and their weathering products*, Theophrastus Publications S.A., Athens, Greece, 175-228.
- Kimber C., Preda, M., Scott, P. & McCombe, C., 2008. Geochemical Assessment and Modelling of Open Cut Pit, Mount Morgan, Queensland, Australia. In O. Totolo, (ed.) *Book of Proceedings, Water Resource Management 2008 (Africa WRM 2008)*, Gaborone, Botswana, Africa, 8-10 September, 2008, 248p.
- Ivarson, K.C. & Sojak, M., 1978. Microorganisms and ochre deposits in field drains of Ontario. *Canadian Journal of Soil Science*, 58, 1-17.
- Lattanzi, P., Da Pelo, S., Musu, E., Atzei, D., Elsener, B., Fantauzzi, M. & Rossi, A., 2008. Enargite oxidation: a review. *Earth Science Reviews*, 86, 62-88.
- Lu, M., Carlsson, E. & Ohlander, B., 2003. Limnological and geochemical comparisons of two sulphide

- mine lakes. In *Book of Proceedings of the 10th International Conference, Tailings and Mine Waste 03*, Vail, Colorado, 12-15 October 2003, Swetz and Zeitlinger B.V., Lisse, Netherlands, 523p.
- Parkhurst, D.L. & Appelo, C.A.J., 1999. User's guide to PHREEQC (version 2) - a computer program for speciation, batch-reaction, one-dimensional transport and inverse geochemical calculations. U.S. Geological Survey, Denver, Colorado, report 99-4259.
- Plumlee, G.S., Smith, K.S., Montour, M.R., Ficklin, W.H. & Mosier, E.L., 1999. Geologic controls on the composition of natural waters and mine waters draining diverse mineral-deposit types. In L.H. Filipek & G.S. Plumlee (eds.), *Reviews in Economic Geology, 6B. The Environmental Geochemistry of Mineral Deposits. Part B: Case Studies and Research Topics*, Society of Economic Geologists, 373-432.
- Skarpelis, N., 1999. The Agios Filippos ore deposit, Kirki (Western Thrace). A base metal part of a high sulfidation epithermal system. *Bulletin of the Geological Society of Greece*, 33, 51-60.
- Shevenell, L., Connors, K.A. & Henry, C.D., 1999. Controls on pit lake water quality at sixteen open-pit mines in Nevada. *Applied Geochemistry*, 14, 669-687.
- Sperling, E. & Grandschamp, C.A.P., 2008. Possible water uses in mining lakes: case study of Agua Claras, Brazil. 33rd WDEC International Conference, 375-380.
- Stokes, J.L., 1954. Studies in the filamentous iron bacterium *Sphaerotilus natans*. *Journal of Bacteriology*, 67, 278-291.
- Trafford, B.D., Bloomfield, C., Kelso, W.I. & Pruden, G., 1973. Ochre formation in field drains in pyritic soils. *Journal of Soil Science*, 24, 453-460.
- Triantafyllidis, S., 2006. *Environmental risk assessment of mining and processing activities and rehabilitation proposals in Evros and Rhodope prefectures (Thrace, NE Greece)*. Unpublished PhD Thesis (in Greek). National and Kapodistrian University of Athens, Faculty of Geology and Geoenvironment, Department of Economic Geology and Geochemistry, 307p.
- Triantafyllidis, S. & Skarpelis, N., 2004. A mineralogical approach to understanding dispersion of toxic elements around high sulfidation epithermal deposits: the case of Kirki, N. Greece. In Z. Agioutantis and K. Komnitsas (eds), *Proceedings of the 1st International Conference in Advances in Mineral Resources Management and Environmental Geotechnology (AMIREG)*, Hania, Greece, 739-744.
- Triantafyllidis, S. & Skarpelis, N. (2006) Mineral formation in an acid pit lake from a high-sulfidation ore deposit: Kirki, NE Greece. *Journal of Geochemical Exploration*, 88, 68-71.
- Triantafyllidis, S. & Skarpelis, N. & Komnitsas, K. (2007) Environmental characterization and geochemistry of Kirki, Thrace, NE Greece, abandoned flotation tailing dumps. *Environmental Forensics*, 8, 351-359.
- Walsh, F. & Mitchell, R., 1972. A pH-dependent succession of iron bacteria. *Environmental Science and Technology*, 6, 809-812.

12ο ΔΙΕΘΝΕΣ ΣΥΝΕΔΡΙΟ ΤΗΣ ΕΛΛΗΝΙΚΗΣ ΓΕΩΛΟΓΙΚΗΣ ΕΤΑΙΡΙΑΣ
ΠΛΑΝΗΤΗΣ ΓΗ: Γεωλογικές Διεργασίες και Βιώσιμη Ανάπτυξη

12th INTERNATIONAL CONGRESS OF THE GEOLOGICAL SOCIETY OF GREECE
PLANET EARTH: Geological Processes and Sustainable Development



ΒΙΟΜΗΧΑΝΙΚΑ ΟΡΥΚΤΑ ΚΑΙ ΠΕΤΡΩΜΑΤΑ
INDUSTRIAL MINERALS AND ROCKS

BAUXITE RESOURCE EXPLOITATION IN GREECE vs SUSTAINABILITY

Anagnostou Ch.

*Institute of Oceanography – Hellenic Center for Marine Research (HCMR), 46,7 km Athens – Sounio,
Mavro Lithari, 19013 Anavissos – Attikis, chanag@ath.hcmr.gr*

Abstract

In the central part of Greece bauxite ore deposits are systematically exploited since more than fifty years, initially by a French industrial group and since few years by a Greek investment group. This “economical” activity uses the non renewable mineral resources of bauxite, non renewable energy sources, as well as significant amount of water and it exports to the environment pollutants and byproducts. CO₂, NO_x, F, PAHs are diffused to the atmosphere, polluting the soil of the adjacent area. Big amount of red mud is deviated to the sea, covering an extended shelf area and parts of deeper marine areas. The aim of this work is to evaluate this “economic” activity using principles of the sustainability science. In its broadest definition, sustainability refers to the ability of a society to continue functioning into the future without being forced into decline through the exhaustion or overloading of key resources.

1. Introduction

Bauxite, the ore that contains a high concentration of aluminum hydroxide minerals, is the raw material for the aluminum industry. Bauxites generally consist of mixtures of the minerals gibbsite [Al(OH)₃], boehmite, and diasporite [AlO(OH)], clay minerals such as kaolinite [Al₂Si₂O₅(OH)₄], quartz (SiO₂) and anatase and rutile (TiO₂). The worldwide bauxite reserves, the bauxite production and the alumina (aluminum oxides-hydroxides) production are given in Table 1. Greece is the largest bauxite producer of the European Union. Bauxite offers high concentration of Al₂O₃ and is the most important commodity of Greek aluminum mining industry. The exploitation of bauxite ores in Greece began in 1925 in the Parnassus area (central Greece). The mineral industry of Greece is mainly export orientated, in order to meet the demand of the globalized mineral market.

At present time one company in Greece is activated in the elaboration of bauxite extracting pure alumina (aluminum oxide) and then from the alumina aluminum, the “Aluminum of Greece S. A., [AtE]”. Bauxite exploitation activities are the driving (D) forces acting as pressures (P) for the environment. Space is needed, non renewable mineral resources as well as energy resources and big amounts of fresh water are used. These activities release significant amount of byproducts in the environment, climate gas emissions, inorganic and organic pollutants, bauxite residues, etc. These pressures are the factors changing the state (S) of the environment, impacting (I) the human society. Changes in the state of the environment and impacts on the human society trigger responses (R). Authorities, investors, citizens groups, non governmental organizations (NGOs), scientists, called together “stakeholders” have to establish a common language to plan, to meet decisions and measures, to reorientate the development priorities and to apply progressively the sustainability principles.

Table 1. Bauxite reserves (in million metric tones), bauxite production (in thousand metric tones) and alumina production (in thousand metric tones) [Reference year 1998]
(American Bureau of Metal Statistics, Inc. Secaucus, NJ 1980, 1985 U.S. Geological Survey, Mineral Commodity Summaries, 1990–1998, modified)

Nr	Country	Bauxite Reserves	Country	Bauxite Production	Country	Alumina Production
1	Guinea	7,400,000	Australia	45,000	Australia	13,385
2	Brazil	3,900,000	Guinea	16,500	Un. States	5,090
3	Australia	3,200,000	Jamaica	12,606	Jamaica	3,411
4	Jamaica	2,000,000	Brazil	12,500	China	3,000
5	India	1,500,000	China	8,500	Brazil	2,756
6	China	720,000	India	6,000	Russia	2,300
7	Guyana	700,000	Venezuela	4,500	Venezuela	1,800
8	Suriname	580,000	Suriname	4,000	India	1,700
9	Venezuela	320,000	Russia	3,400	Suriname	1,600
10	Greece	300,000	Guyana	2,600	Irland	1,200
11	Russia	200,000	Greece	2,500	Greece	750

The aim of this work is to present this complicated net of human activities, behaviors and actions in the case study bauxite exploitation in Greece and to discuss if the logical DPSIR scheme (D=drivers, P=pressures, S=state, I=impact, R=response) can be introduced in the greek community as a whole and if the sustainability principles can find fruitful substratum in the Mediterranean country, called Greece.

2. Bauxites ore deposits in Greece

The major bauxite deposits of Greece are geological formations hosted within carbonate rocks of different geological ages of the Parnassos – Ghiona geotectonic zone - Hellenides (central Greece). Three bauxite horizons (B1, B2, B3) are distinguished, intercalated with shallow-water limestones of the Upper - Jurassic to Middle Cretaceous carbonate sequences of the Parnassos – Ghiona zone. The (paleo)geographical distribution of the three bauxite horizons (B1, B2, B3) shown in Fig. 1 indicates a displacement of the formation areas from the NE place of the older B1 bauxite horizon to SW direction where the younger B2 and B3 bauxite horizons are formed (Petraschek & Mack, 1978). The bauxite reserves of Greece are estimated in approximately 300 billion tons (Papastavrou, 1986). The economically most important bauxite formations occur in the upper (B3) horizon, which expands over extended distances as continuous layer of 1–10 m in thickness. This horizon shows a pisolithic and/or oolitic texture and a red to red-brown color (Valeton et al., 1987). The mineralogical composition of the bauxite formations of the Parnassos – Ghiona zone shows mainly boehmite or diaspore and in lesser amounts gibbsite, kaolinite, hematite, goethite (Valeton et al., 1987, Laskou, 2001, Laskou & Andreou, 2003). The average chemical composition of the bauxite samples is: 55% Al₂O₃, 20% Fe₂O₃, 3-5% SiO₂, 0.5-1.0% CaO, 2-2.5% TiO₂ and 10-14% loss of ignition. The average concentration of trace elements is: 450 ppm Ni, 700 -900 ppm Cr, 50-70 ppm Zn, 500-600 ppm Zr and 37 ppm Sr. (Valeton et al., 1987, Laskou & Economou-Eliopoulos, 2007).

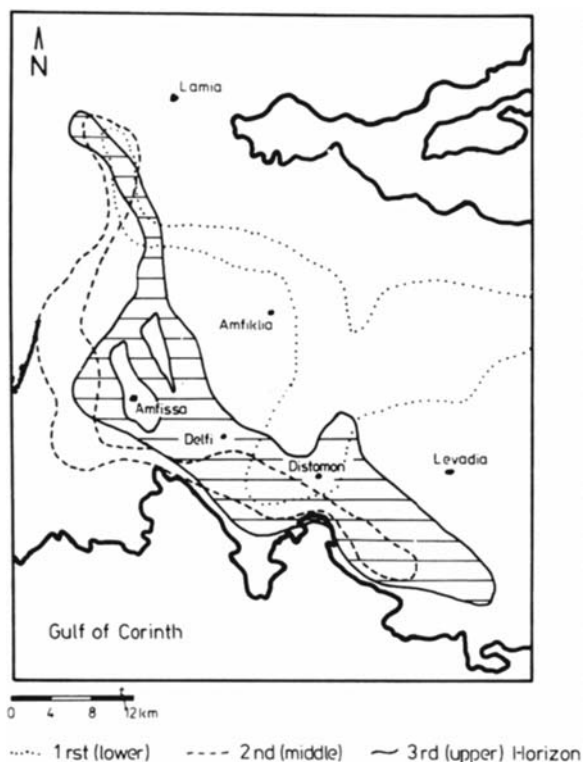


Fig. 1: Regional distribution of the 1st (B1), 2nd (B2), 3rd (B3) bauxite horizons in central Greece (Petraschek & Mack, 1978).

Greek bauxite offers high concentration of Al_2O_3 , low of CaO, low loss of ignition and low humidity comparing to the largest bauxite exporters of the globe (Guinea, Australia, Jamaica, Brazil and China). However Greek bauxite has the disadvantage of high SiO_2 concentration, which makes it difficult to process (Laskou & Andreou, 2003).

3. Bauxites mining in Greece

Three bauxite mining industries are active at present time in Greece, the S&B industrial minerals S.A., Delphi Distomo S.A. and ELMIN S.A. with a total production of ~2.500.000 tons/year. Approximately 900.000 tons/year (year 2005) are directly as bauxite exported. The main export targets of Greek bauxite are European Union countries as well as Russia, Ukraine and Romania. The main domestic bauxite consumer is “Aluminum of Greece S.A.” [AtE] subsidiary of the Delphi Distomo S.A., which consumes ~1,500,000 tons/year. The “Aluminum of Greece S.A.” [AtE] produces alumina and aluminum. In the mining of bauxite the extension and shape of the deposits are determined by field geology studies and if needed by core drilling. After the fixation of the bauxite mining sites and the establishing of the necessary infrastructure, the bauxite is broken up, often with the aid of explosives, and removed with conventional earthmoving equipment. It is then transported to the clients.

4. Bauxite industry in Greece

In Greece only one company is dealing with extraction of alumina (aluminum oxide) from bauxite and aluminum from alumina, the above mentioned “Aluminum of Greece S. A. [AtE]”, which is

sited in Antikyra bay, Gulf of Corinth. The “Aluminum of Greece S. A. [AtE]” was founded in 1960 and it started the production 1966. The first owner was PECHINEY (1960-2003). In 2004 “Aluminum of Greece S. A. [AtE]” was soled to ALCAN and ALCAN soled the company to MYTIL-NAIOS financial group (2005). The information about the history of the company, the procedures of alumina and aluminum extraction as well as about mineral ores and energy resources used, about byproducts accumulation and about future plans of the company, are gained from a recently carried out Technical Report of the “Aluminum of Greece S. A. [AtE]” company (Aluminum of Greece S. A. [AtE], 2007).

Extraction of alumina from the bauxite: Pure alumina (aluminum oxide) is extracted from bauxite by the Bayer process. In the Bayer process bauxite received from the mines is crushed, usually by a hammer mill to small particles and well blended. Lime (CaO) is added to assist in the extraction of alumina, to scavenge impurities, and later to enhance clarification. This mixture then flows to agitated storage tanks and is metered into high-temperature (~255°C) sodium hydroxide digesters (NaOH), where alumina is extracted from the bauxite as sodium aluminate (NaAlO₂). Pure alumina is then precipitated (by lowering temperature to 50-70°C) from the solution as a hydroxide [Al(OH)₃], filtered, washed, and then calcined to pure alumina (Al₂O₃) at 1100–1200°C.

Digestion	Precipitation	Calcination
AlO(OH)+NaOH → NaAlO ₂ +H ₂ O	NaAlO ₂ +2H ₂ O → Al(OH) ₃ + NaOH	2Al(OH) ₃ → Al ₂ O ₃ + 3H ₂ O

This procedure leaves behind the impurities as an insoluble residue, mainly consisting of hematite (Fe₂O₃), titania (TiO₂), and silica (SiO₂). For the production of one tone of alumina two tones of bauxite are needed. The “Aluminum of Greece S. A. [AtE]” produces more than 750,000 tones alumina yearly.

The extraction of alumina from the bauxite is supported from two smaller industrial units:

- a. The unit producing CaO (needed by the extraction procedure) from limestones coming from the geological formations exposed near the industrial field.
- b. A unit producing thermal energy, needed also for the procedure. Using as energy resource imported crude oil.

Extraction of aluminum metal from the alumina: Aluminum metal is extracted from the alumina electrolytically by the Hall–Heroult process. In this process, the purified alumina is dissolved in an electrolyte consisting mainly of molten at ~960°C cryolite (NaF·AlF₃). Consumable carbon anodes are employed, producing carbon dioxide and carbon monoxide, which escape from the cell while the molten aluminum accumulates at the cathodic bottom and is siphoned out periodically. The aluminum produced is normally 99.6–99.9% pure. The typical impurities are iron, silicon, titanium, vanadium, gallium, and manganese, coming from the anode but also from impurities in the alumina. The “Aluminum of Greece S. A. [AtE]” produces approximately 170,000 tones aluminum metal yearly.

Uses of Aluminum: The market for aluminum comprises containers and packaging [foil, plastic, and paper laminants and pouches are used for packaging a wide variety of food and nonfood products] building and construction [doors and windows are generally produced], transportation [commercial and military aircrafts, use of aluminum in automobiles to reduce weight, in marine service, in space vehicles], electrical [high voltage electrical transmission lines], consumer durables, machinery and equipment.

5. Bauxites exploitation activities and environment in Greece

5.1 Natural environment

The bauxite exploitation is a complicated human activity. It needs and it uses space, ore material resources, energy resources, water. The production procedure leads also to a huge amount of byproducts, which affect the environment and have significant impact to the humans health and the society. All the information on which is based this unit is the recently carried out Technical Report of the “Aluminum of Greece S. A. [AtE]” company (Aluminum of Greece S. A. [AtE], 2007).

Space: For the bauxite mining it is necessary to establish transport infrastructure in the mountains to reach the mining sites, which are changing the natural environment. The mining procedures result to harvesting of trees and local concentration of overburden, which are removed and set aside, contributing to environmental changes. No data are found about the area in which the mining activities are extended.

The industry itself occupied one field of 770,000 m², where the industrial plants are sited and a second field, in the same order of extension, where the employees of the industry are living. Both sites are plain areas near the sea, where olive trees were cultivated 50 years ago and are totally harvesting changed in industry field and residence area respectively. The company is owner of an expropriated 50 years ago extended area of 7,050,000 m².

Ore material resources: The “Aluminium of Greece S.A [AtE]” company obtains the bauxite mainly from the bauxite ore mining of the adjacent area (Delphi – Distomo S. A.) as well as a smaller amount imported from Africa (tropical bauxite). In the year 2006 the “Aluminium of Greece S.A [AtE]” consumed more than 1,760,000 tones bauxite.

Use of limestones for the production of CaO: The company uses yearly more than 125.000 tones of limestones (production of ~62,000 tones/year lime).

Energy resources: Table 2 gives a breakdown of the energy required from the “Aluminum of Greece S. A. [AtE]” to produce aluminum. The energy for mining and refining comes from fossil fuels. Crude oil is used also by the Beyer process (refining the ore) as well as by the Hall-Herout process (smelting). From Table 2 it can be seen, that smelting consumes ~90% of the total electric power. The company obtains the energy required from the National Energy Network of Greece in a tariff significant lower than this of the normal electricity consumer.. The sources covering the electricity requirements of the “Aluminium of Greece S. A. [AtE] are showing in Table 3.

Fresh water use: Water is commonly used throughout the aluminum industry for cooling, clearing and dissolving purposes. The “Aluminum of Greece S. A. [AtE]” consumed in the year 2006 ~4,000,000 m³ water to cover the industrial requirements and 225,000 m³ as potable water. The company gains this water quantity through exploitation of the ground water of the area.

Byproducts:

Climate gases emissions: The “Aluminum of Greece S. A. [AtE]” produces as byproducts climate gases emissions. The annual emission of CO₂ is more than 1.000.000 tons. The emission of CF₄ is ~8.2 t/y (CO₂ equivalent ~53.300 t/y), ~0.05 kgr/t Al and of C₂F₆ ~0.8 t/y (CO₂ equivalent ~7,500 t/y), ~0.005 kgr/t Al.

SO₂ emissions: The total SO₂ emission reaches~16,000 t/y, having as the main source the bad quality of crude oil, which contain ~2.7 – 3.00 % S.

Table 2. Energy required for the production of Aluminum of the “Aluminum of Greece S. A. [AtE]”.

	Electrical energy MWH/year	Thermal energy Crude oil t/year	Thermal energy Diesel m ³ /y
Mining and transportation of bauxite			~480
Refining ore (Bayer process)	~200,000		~250
Smelting (Hall–Herout process)	~2,300,000	~231,456	
Electrolysis [2.200.000 MWH/year]			
Other [115.000 MWH/year]			
General requirements	~10,000		
Total	~2,500,000	~231,456	~730

Table 3. Sources covered the electricity requirements of the “Aluminum of Greece S. A. [AtE]”.

Total electrical energy required	~2.500.000 MWH/year
Covered by: Coal burning (lignite)	50%
Hydropower	50%
Renewable energy sources	0%

NOx emissions: The total NOx emission reaches ~1390 t/y, having as source the thermal energy resources.

Fluoride emissions: The total (gaseous and particulate) emissions of fluoride from primary alumina electrolysis plants of the company “Aluminum of Greece S. A. [AtE]” reaches ~270 t/y, making 1.65 kg/t Al. Measurements carried out from the company in atmospheric particles show the presence of fluoride in distances more than 8 km from the industry. Indicative values of fluoride in the atmospheric particles are following:

- 0-2 km distance from the industry ~800 µg/week,
- 2-4 km distance from the industry ~80 µg/week,
- 4-6 km distance from the industry ~27 µg/week,
- 6-8 km distance from the industry ~20 µg/week,
- >8 km distance from the industry ~8 µg/week.

Benz (a) Pyrene emissions (BaP emissions): From the industry an important quantity of PAHs (PolyAromativHydrocarbons) is emitted in the atmosphere. Measurements carried out from the company in atmospheric particles show concentrations of total PAHs fluctuating from 5 -9 mg//m³ (measurements of 2006). Data available for Benz (a) Pyrene emissions of the company “Aluminum of Greece S. A. [AtE]”, show concentration from 0.05 – 0.5 mg/m³. PAHs and Benz (a) Pyrene are emitted in the atmosphere by paste plants, anode plants and primary smelters.

Bauxite residue deposited: The bauxite residue materials are defined as the materials remaining after the extraction of the alumina. It has a brown red color and a mud texture. The “Aluminum of Greece S. A. [AtE]” company produces an amount of approx. 700,000 t/y of this byproduct. All these amounts of red mud are canalized to the sea in a depth of 110 m and a distance from the coastline

of 2.200 m. In the red mud discharge area the submarine topography is totally changed. A number of six lobes on the shelf area are formed with an elevation from 7 m to 37 m. Through gravity mass movements a part of these deposits are moved to the deeper zone of the marine area (depths of 700 – 800 m). Indicative chemical composition of the red mud is showing below.

Fe ₂ O ₃	40-46 %	SiO ₂	7-12 %
Al ₂ O ₃	14-25 %	Na ₂ O	2.2-2.7 %
CaO	8-14 %	TiO ₂	6.0 %

The area covered from the red mud shows high heavy metals concentration. Using as reference sample a pre-industrial sample of a core of the red mud area the enrichment factor of some heavy metals is calculated. The enrichment factor for Cr is 44, for cobalt 11, for Ni 29, for As 64 and for Pb 25 Data stem from a report of the “Aluminum of Greece S. A. [AtE]”, based on studies carried out from the Hellenic Center of Marine Research (HCMR).

Spent pot lining and Hazardous waste deposited: The quantity of spent pot linings from electrolysis pot rooms deposited after removal of materials for reuse and recycling reaches 104.244 t/y, the amount of hazardous wastes deposited reaches 12.212 t/y (year 2006).

5.2 Social environment

The “Aluminum of Greece S. A. [AtE]” gives in its report (Aluminum of Greece S. A. [AtE], 2007) the information that provide a safe workplace for employees and gives emphasis on the prevention of accidents in the workplace. However no data are available for the Lost Time Incident (LTI), the number of lost time accidents, the fatalities and the employee exposure and health assessment.

6. Bauxites exploitation viewed under the sustainability framework

6.1 The European programme of Aluminium for Future Generations – The “Sustainable Development Indicators (SDI)”

The interest groups related to bauxite exploitation have to be committed to navigate all their activities following the general principle of the sustainability, i.e. “meeting the needs of the present, without compromising the ability of future generations to meet their own needs”. This means meeting the needs of modern society by

- taking seriously into account that bauxite ore resources and energy resources used, are not renewable and fresh water quantity is limited,
- reducing the environmental impact,
- demonstrating social responsibility towards employees, customers, local communities and society as a whole.

The European Aluminium Association (EAA) and its member companies, through the Aluminium for Future Generations programme, developed 34 measurable “Sustainable Development Indicators (SDI)” to be systematically tracked and transparently reported by the European aluminium industries, on a dynamical process and a future pathway towards sustainability. Sustainability is more than just an initiative it is a philosophy that have to run right through the industry influencing every activity and decision.

Shortly to mention the 34 measurable “Sustainable Development Indicators (SDI)” are related to the

-production [SDI 01.Total Production Alumina], -policy and management efforts (SDI 02. Sustainability mission statement; SDI 03.Plant certification, (ISO 14000, OSHAS, etc)], -competitiveness [SDI 04 Aluminium use per capita; SDI 05. R&D expenditure (R&D investment/year); SDI 06 R&D persons employed; SDI 07 Value added], -revenues and investments [SDI 08 Total revenue; SDI 09 Capital investments], -employee development and relations [SDI 10 Training performance (~hours for job training/person/year); SDI 11 Wage level; SDI 12 Total number of employees], -community relations [SDI 13 Community expenditure (for social, cultural, sports, and others); SDI 14 Community dialogue; SDI 15 Community health initiatives], -health and safety [SDI 16 Lost time incident rate (lost time accidents), SDI 17 Total recordable incident rate; SDI 18 Fatalities; SDI 19 Severity rate; SDI 20 Employee exposure and health assessment], -resource use at global level [SDI 21 Bauxite area mined; SDI 22 Mine rehabilitation rate], -resource use at european level [SDI 23 Energy consumption (electric energy/tonne of product in kWh), (other energy/tonne of product in MJoule); SDI 24 Renewable electric energy in %; SDI 25 Fresh water use (m³/tonne of product)], -emissions [SDI 26 Climate gases emissions (in kilogram of CO₂ equivalent per tonne produced); SDI 27 Fluoride emissions. (in kilogram per tonne produced); SDI 28 BaP emissions (Benz a pyrene emissions/tonne produced); SDI 29 Bauxite residue deposited (kgr/tonne of alumina produced); SDI 30 Spent pot lining and Hazardous waste deposited (kgr/tonne of alumina produced), product life cycle [SDI 31 Use phase; SDI 32 Aluminium recycling; SDI 33 Life Cycle; SDI 34 Recycling material flow].

6.2 The Greek programme of Aluminium for Future Generations – The “Sustainable Development Indicators (SDI)”

The only one aluminum company in Greece, the “Aluminum of Greece S. A. [AtE]” produces ~750,000 tons per year alumina [SDI 01], while the European total production (in 2005) reached the amount of 6.786.000 tons. 50% of the produced aluminum and 20-25 % of aluminum products are exported mainly in Europe. Unknown are the policy and management efforts of the company related to the sustainability mission statement of the company [SDI 02] and the plant certification, (ISO 14000, OSHAS, etc [SDI 03]).

The competitiveness indicators for the “Aluminum of Greece S. A. [AtE]” show 15,5 kg aluminium per capita [SDI 04], while for Europe the indicator is 24,2 kg/person, No data are found about the R&D expenditure (Research &Development investment/year) [SDI 05], R&D persons employed [SDI 06], Value added [SDI 07]. No data are found about revenues and investments [SDI 08], [SDI 09], employee development and relations [SDI 10], [SDI 11], [SDI 12], community relations [SDI 13], [SDI 14], [SDI 15], health and safety [SDI 16], [SDI 17], [SDI 18], [SDI 19] [SDI 20], resource use at global level [SDI 21], [SDI 22]. In the above mentioned “Sustainable Development Indicators” [SDI] we can add the total number of employees [SDI 12] reaching ~1000 persons.

Some important “Sustainable Development Indicators” [SDI] are calculated from the author for the production activities of the “Aluminum of Greece S. A. [AtE]”, related to resource use at European level and the emissions (Table 4). The electric energy consumption in kWh per ton of product [SDI 23] reaches the value of 14.706 kWh (for Europe 804.7 kWh, data for 2005). The calculation of the production of primary aluminum of 170,000 tons/year is taken into account. No renewable electric energy is used from the company [SDI 24]. The fresh water used (m³/tonne of product) [SDI 25] reaches the value of 23.5 m³/tonne of product (for Europe is 12.7 m³/tonne of product, data for 2005).

For the emissions the “Sustainable Development Indicator” [SDI] for the climate gases emissions is calculated (in kilogram of CO₂ equivalent per ton produced) [SDI 26]. The 1,000,000 tones of CO₂

Table 4. Sustainable Development Indicators of the European Aluminium Industry.

SDI Nr	“Sustainable Development Indicators” [SDI] European Aluminium Association	Europe 2005	AtE
	RESOURCE USE AT EUROPEAN LEVEL	804.7	14,706
SDI 23	Energy consumption (electric energy/tonne of product in kWh)	45.7	0%
SDI 24	Renewable electric energy in %	12.7	23.5
SDI 25	Fresh water use (m ³ /tonne of product)		
	EMISSIONS		
SDI 26	Climate gases emissions (in kilogram of CO ₂ equivalent per tonne produced)	134	5,294
SDI 27	Fluoride emissions. (in kilogram per tonne produced)	0.96	1.65
SDI 28	BaP emissions (Benz a pyrene emissions kgr /tonne produced)	1.11	-
SDI 29	Bauxite residue deposited (kgr/tonne of alumina produced)	706	~ 800
SDI 30	Spent pot lining and Hazardous waste deposited (kgr/tonne of alumina produced)	12.8	15.4

Source: European Aluminium Association: Sustainability of the European Aluminium Industry 2006

corresponds, according to US Environmental Protection Agency (<http://www.epa.gov/RDEE/energy-resources/calculator.html>) to approximately 900.000 CO₂ equivalent and gives the SDI 26 indicator ~5.300 kilograms of CO₂ equivalent per ton produced. The European middle value is 134 kilograms of CO₂ equivalent per ton produced (Table 4). The fluoride emissions indicator [SDI 27] is calculated in 1,65 kilograms per tonne produced (the European middle value is 0.96 kilograms per tonne produced). No significant data were available for the Benz-a-pyrene (BaP) emissions indicator [SDI 28].

The bauxite residue deposited indicator [SDI 29] is ~800 kgr/tonne of alumina produced (the European middle value is 706 kilograms per tonne produced). The spent pot lining and hazardous waste deposited indicator [SDI 30] is calculated in 15.4 kgr/tonne of alumina produced (the European middle value is 12.8 kilograms per tonne produced).

No data are found for the product life cycle, use phase [SDI 31], aluminium recycling [SDI 32], life cycle [SDI 33] and recycling material flow [SDI 34].

6.3 A plan for the aluminum industry in Greece based on the sustainability principles is needed

As it is mentioned above, at present time one company in Greece is activated in the elaboration of bauxite, the “Aluminum of Greece S. A., [AtE]”. These activities are the driving forces (D) acting as pressures (P) for the environment. Space is needed, non renewable mineral resources as well as energy resources and big amounts of fresh water are used. These activities release significant amount of byproducts in the environment. All these pressures are the factors changing the state (S) of the environment, impacting (I) the human society. The changes in the state of the environment and the

impacts on the human society trigger responses (R). Authorities, investors, citizens groups, non governmental organizations (NGOs), scientists, called together “stakeholders” have to establish a common language to plan, to meet decisions and measures. The “Sustainable Development Indicators” [SDI] shown in Table 4 indicate that the company has to change exploitation and elaboration practices in order to converge the company SDIs towards the European SDIs.

A reorientation of the development priorities and the progressively application of the sustainability principles gain importance in this procedure. The spiral D-P-S-I-R scheme is a logical tool to be applied. The only question remaining open is if the greek society is mature to participate in those procedures.

The companies, mainly the “Aluminum of Greece S. A., [AtE]” and the public authorities related to the mining and industrialization of bauxites have not any plans and any policies for the management of the unrenewable resources. For the protection of the environment no important measures are undertaken. The public services in local, regional and central levels are totally manipulated from the industry interest group. The scientific community of the most of the public services, research centers, universities, generally does not react to this situation. And if some scientists try to search the state of the environment in the area near the industry activity, the entrance in the industry field is forbidden (research team from the University of Patras). Even worse is the situation for researchers from the Hellenic Center of Marine Research (HCMR), who announce results of their measurements (Anagnostou & Hatjianestis, 2009). They are confronted with justiciable measures from the company, carrying out this procedure in “harmonical” collaboration with directors of the Research Center. Small citizen groups and initiatives as well as Non Governmental Organizations are the only “healthy” part of the greek society.

The company spends efforts for communication with local communities and authorities and some money to gain a positive resonance from the local community with expenditures for social, cultural, sports and other community activities and to form also a citizen revetment against the pressure of the Non Governmental Organizations and the citizen initiatives.

7. The way out

The educational and scientific research communities have to find the way first to emancipate themselves and then to play the leading role for the society, which is permanently in crisis (economical, societal, cultural). Managing the environment is not simple. Managing the natural resources, protecting the function of the nature, giving priority to the biodiversity, solving the survival problems of many human communities, all these are questions waiting for answers. Integration and participation are showing the way out.

8. References

- “Aluminum of Greece S. A. [AtE]”, 2007: Studies for the environmental impact in the industrial are of the company (in greek).
- American Bureau of Metal Statistics, Inc. Secaucus, NJ 1980, 1985 U.S. Geological Survey, Mineral Commodity Summaries, 1990–1998.
- Anagnostou, Ch. & Hatjianestis, I., 2009: Impact on the coastal system, land and marine area, from the industrial activities of the company “Aluminum of Greece S. A. [AtE]” (Antikyra bay, Corinthian Gulf). –Technical Report, Hellenic Center for Marine Research, p.42 (in greek).
- Laskou, M., 2001: Chromite in karst bauxites, bauxitic lateritesand bauxitic clays of Greece. In: Piestrzyn-

- ski, et al. (eds), Mineral Deposits at the Beginning of the 21st century, 6th Biennial SGA Meeting, Krakov, Millpress, Rotterdam, pp. 1091-1094.
- Laskou, M. & Andreou, 2003: Rare earth element distribution and REE-minerals from the Parnassos – Ghiona bauxite deposits, Greece. In: Eliopoulos, D. et al. (eds), Mineral Exploration and Sustainable Development, 7th Biennial SGA Meeting, Athens, Millpress, Rotterdam, pp. 89-92.
- Laskou, M. & Economou-Eliopoulos, M., 2007: The role of the microorganisms on the mineralogical and geochemical characteristics of the Parnassos – Ghiona bauxite deposits, Greece. *Journal of Geochemical Exploration*, 93 (2007) 67 -77.
- Papastavrou, S. 1986: Greek bauxites. Mineral Deposits Research, IGME – Internal Report (in Greek) Athens, 30 pp.
- Petraschek, W. E. & Mack, E., 1978: Palaeogeographie, Verteilung und Qualitaet der Bauxite im Parnass-Kiona-Gebiet, 4th Int. Congress ICSOBA 2: 526-539.
- Valeton, I., Bierman, M., Reche, R., Rosenberg, F., F., 1987: Genesis of nickel laterites and bauxites in Greece during the Jurassic and the Cretaceous and their relation to ultramafic rocks. *Ore Geology Reviews*, 2, 359-404.

NEW METALLOGENETIC CONCEPTS AND SUSTAINABILITY PERSPECTIVES FOR NON-ENERGY METALLIC MINERALS IN CENTRAL MACEDONIA, GREECE

Arvanitidis N. D.¹

¹ Institute of Geology and Mineral Exploration (IGME), Fragon 1, 52646 Thessaloniki,
narvanitidis@thes.igme.gr

Abstract

Greece's geology favours a potent and dynamic use of mineral resources, which became a major incentive of the country's mining business, and economic and social growth. Among the Non-Energy Metallic Minerals (NEMM) commodities, base and precious metals, in particular copper and gold, is becoming an increasingly important and rapidly growing target of the mining industry. In the region of central Macedonia, where most of their deposits are hosted, the NEMM occur in a wide range of genetic types related to Alpine orogenic and subduction related ore forming processes extending from Mesozoic to Cenozoic times, and culminating during the Tertiary (Arvanitidis and Amov, 2006). From the global metallogenetic point of view the post-Alpine Tertiary geodynamic systems in SE Europe are potential in producing high-grade ore deposits of base and precious metal sulphide minerals. The classification of NEMM mineralizations to specific genetic types, along with the geological knowledge available, is contributing (a) to more efficient exploration and prospect evaluation (b) to safer assessment of ore potential and economic perspectives (c) to rational management of resource production, and (d) in applying sustainable development practices.

1. Introduction

This paper focuses on the NEMM of central Macedonia in northern Greece (Diakakis and Stephanidis, 1994) using new metallogenetic aspects for implementing low-risk exploration campaigns, reducing environmental footprints and securing sustainable supply and use of commodities (Arvanitidis, 2003).

2. Regional Geology and Mineralizations

The sulphide mineral deposits in Greece are mainly located, in the Rhodope and Serbomacedonian zones. The western and central parts of the Rhodope zone consist mainly of Paleozoic high-metamorphic rocks, but its eastern part is dominated by Tertiary volcanics. The Tertiary volcanic belt extends through the northern Mediterranean, Romania, Bulgaria, Greece, Turkey and Iran and is characterized by subduction – related intermediate to felsic volcanics (Jankovic et al., 1980; Heinrich and Neubauer, 2002) (Fig. 1). The belt hosts numerous vein – type (e.g. Kirki, Madjarovo) and stratiform (e.g. Essimi) Pb – Zn sulphide mineralisations as well as epithermal gold (e.g. Konos, Perama; Michael et al., 1995; Voudouris et al., 2007) and porphyry copper deposits (Frei, 1995; Tobey et al., 1998). The highly metamorphosed carbonate and silicate rocks to the west, contain vein and massive sulphide replacement mineralisations, ranging from base metal (e.g. Thermes,

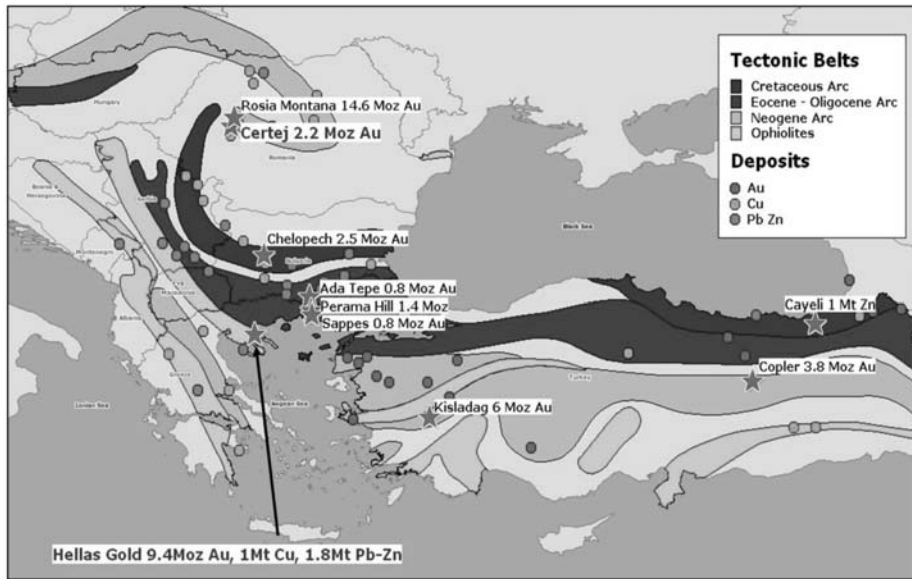


Fig. 1: Regional geotectonic map of southeast Balkan showing the major metallogenetic belts and related mineralization types (European Goldfields Inc, pers. Com.).

Madam) to polymetallic (e.g. Farasino, Pangeo) compositions, and stratabound karst – related Pb – Zn sulphide (e.g. Thassos) to manganese (e.g. Drama) deposits. The Serbomacedonian zone represents the accretionary back land beneath which the African plate was subducted. The zone is a complex metamorphic terrain of schists, gneisses and marbles that are often mineralized and intruded by Variscan granitic rocks. It trends NW, is some 500 km long, and is host to numerous deposits, including Olympias and Stratoni polymetallic deposits, and Skouries and Pontokerasia, porphyry copper in Greece, Sasa and Zletovo Pb – Zn deposits, and Bucim porphyry copper in the Former Yugoslav Republic of Macedonia, as well as the Lece polymetallic deposit in Serbia – Montenegro. In the case of the polymetallic and/or Pb – Zn sulphide replacement deposits such as Olympias, Stratoni and Madem Lakkos, they are controlled by a combination of the marble horizons, that contain the carbonates which were replaced and the deep – seated faults developed as part of the crustal re-working of the area and subsequent fluid movements along these. The porphyries are mainly part of the Variscan volcanism. The Skouries deposit is a typical representative of sub-alkaline copper porphyry forming a near-vertical pipe intruded into amphibolite and biotite schist country rock.

Genetic Types

NEMM mineralization in the region of central Macedonia comprises (Fig. 2).

Mesozoic mid-ocean types in terms of,

- Magmatic/ophiolites hosted chromite, Fe-Ni laterites and chalcopyrite-pyrite-pyrrhotite assemblages
- Volcano-sedimentary syngenetic deposits including VMS type stratiform base metal sulphides, stratified chalcopyrite-pyrite-arsenopyrite lenses, banded iron formations and scheelite (W) veins/disseminations
- Intrusion related porphyry type Mo stockwork veins and impregnations, and

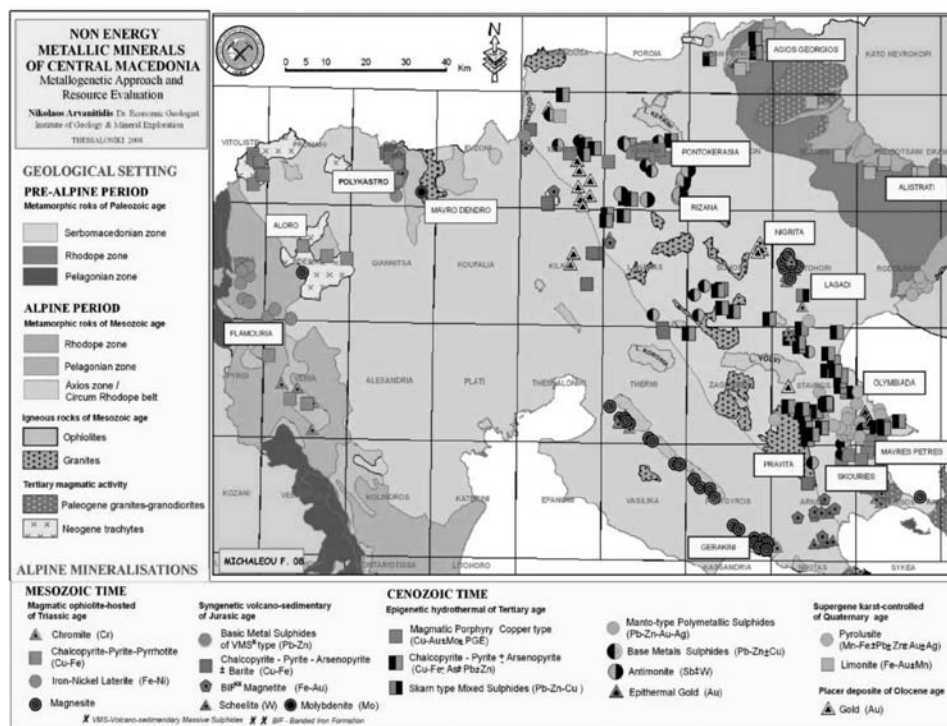


Fig. 2: Simplified geological map showing the main Alpine orogenesis related polymetallic mineralizations in the region of central Macedonia.

Cenozoic, mainly Tertiary, epigenetic, hydrothermal types of,

- Magmatic porphyry Cu-Au deposits containing elevated values of PGE and associated with calc-alkaline sub-volcanic intrusions (Eliopoulos and Economou-Eliopoulos, 1991)
- Hypothermal/Mesothermal chalcopyrite-pyrite-arsenopyrite veins hosted by amphibolites
- Skarn formations of Cu-Zn-Pb sulphides
- Manto type polymetallic (Pb-Zn-Au-Ag) massive sulphides
- Antimonite (Sb) - scheelite (W) veins (Kilias et al., 1995)
- Epithermal gold (Au) along with fault-controlled silicification and pyritization zones
- Supergene fault/karst-controlled mineralization of economic pyrolusitic manganese and gold bearing limonitic iron oxidations
- Placer gold deposits

4. Gold Mineralizations

Gold occurs in a wide range of genetic types, comprising magmatic, hypothermal / mesothermal, epithermal and supergene mineralization types (Arvanitidis, 2003; Melfos et al., 2003). All the main types of gold mineralization are linked to plate tectonic movements during the Tertiary.

Magmatic porphyry copper type deposits and mineralizations show economic gold grades. The Skouries gold-copper ore deposit (Frei, 1995; Tobey et al., 1998) is located 20km southwest of the

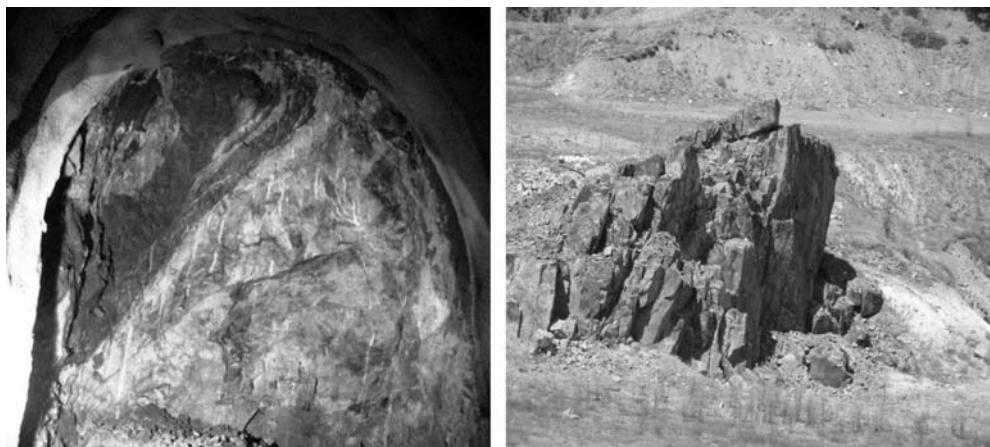


Fig. 3: Typical ore structures of manto-type stratabound sphalerite lens (left) in Mavres Petres mine and malachite impregnations in Skouries porphyry copper mineralization.

Olympias mine and the most representative example of this class (Fig. 3). It is a typical sub – alkaline copper porphyry forming a near – vertical pipe intruded into amphibolite and biotite schist country rock. The deposit is characterized by concentric alteration zones comprising an inner potassic zone, with stock work quartz veinlets and an outer propylitic zone, affecting mostly the host schists. Weak phyllic and argillic alteration is confined to vein haloes and faults. Mineralisations within the potassic zone primarily comprise chalcopyrite veinlets with subordinate bornite and disseminated chalcopyrite and bornite. Mineralisation within the propylitic zone contains disseminated pyrite, molybdenite and rare chalcocite. Gold mineralisation occurs as native gold associated with gangue minerals. It also occurs as blebs within sulphides and occurs in the ore during testing. An oxide zone occurs from surface to 30 to 50 meter depths and includes malachite, cuprite, secondary chalcocite and minor azurite, covellite, digenite and native copper. The total resources were estimated to 191,200,000 tonnes, with 0.82 g/t gold and 0.55 wt% copper, or in terms of total metal amounts, 5.03 Moz gold and 1.043.000 tonnes copper. Current reserves are estimated to 129,500,000 tonnes, with 0.89 g/t gold and 0.56 wt% copper, corresponding to metal amounts of 3.71 Moz gold and 725,000 tonnes copper (Hellas Gold, pers. com.).

Hypothermal / mesothermal manto-type polymetallic sulphides form high - grade gold ores (Kalogeropoulos et. al., 1989; Hellingwerf et. al., 1993; Kalogeropoulos et. al., 1996; Kiliyas et. al., 1996). The Olympias massive deposit, representing this class, is a stratabound replacement orebody occurring at the contact between marbles and overlying gneisses. Sulphide mineralisations comprises pyrite, arsenopyrite, sphalerite, galena, tetrahedrite – tenantite, boulangerite and chalcopyrite. Gold values are associated almost exclusively with arsenopyrite and pyrite. The total resources and nearly reserves, were estimated to 14,528,000 tonnes, with 9.31 g/t gold, 128.6 g/t silver, 4.18 wt% lead and 5.58 wt% zinc (Hellas Gold S.A., pers. com). Corresponding total amounts of metal contents are 4.35 Moz gold, 60.06 Moz silver, 607,000 tonnes Pb and 810,000 tonnes zinc. Further to the north, the Stratoni lead-zinc-silver deposits are also considered as carbonate replacement type mineralisations, with pyrite, galena, sphalerite, arsenopyrite and chalcopyrite as the main sulphide minerals. The entire resources are currently located in the Mavres Petres mine contained within a marble-hosted stratabound orebody adjacent to the east-west striking Stratoni Fault. The ore is also gold bearing, mostly associated with the arsenical pyrite and arsenopyrite. Quartz, calcite and minor

rhodochrosite form the gangue minerals. The total sulphide content prior to mining was estimated at 2.5 Mt (Hellas Gold, pers. com.).

Epithermal type deposits were emplaced within a broad volcanic belt, which developed first in Bulgaria and then moved south through northern Greece (Marchev et al., 2005) to the region of Thrace. The Konos - Sappes and Perama high sulphidation gold mineralizations (Michael et al., 1995; Voudouris et al., 2007; Michael, 2004), in strongly silicified and/or argillised felsic volcanics, make a typical representative of this class. A rhenium-rich molybdenite and rheniite Mo–Cu–Te–Ag–Au porphyry mineralization located in the Pagoni Rachi area shows close geotectonic setting affinities to the epithermal metallogenesis of the region (Voudouris et al., 2009).

The genetic link between porphyry coppers and large polymetallic manto style sulphide deposits can be incorporated into regional exploration strategies. The metallogenetic concept suggests that epithermal mineral assemblages exposed at the present land surface may indicate hidden base metal ore bodies at depth. These styles of mineralization, porphyry coppers and manto - style sulphides, have potential for substantial deposits (Hellingwerf et al., 1994). Gossans in the region have low economic potential due to erratic gold values and the necessity for costly beneficiation techniques (Dimitroula et al., 1995; Arvanitidis et al., 1996). The gossans develop on mineralized veins and thrusts, but the gossanous material tends to spread laterally, giving a false impression of the underlying mineralization. Parts of the gossans can be richer in gold, but these patches mainly constitute small scale exploration targets in west Rhodope.

5. Metallogenetic approach

The tectonic structure of Greece consists of elongated tecto-magmatic strips, representing successive subductions, such as the Serbo-Macedonian massif hosting the manto-type massive sulphide Olympias and Stratoni (Madem Lakkos and Mavres Petres orebodies) deposits, and the porphyry copper systems of Skouries, Fisoka, Vathi, Gerakario and Pontokerasia. The overall metallogenetic process of the area is part of the Alpine orogenesis, lasting from Mesozoic to Tertiary times, and associated geodynamic release of anomalous thermal and mechanical energy. The overwhelming evolution of the Tethyan Ocean, during Triassic to Jurassic times, was accompanied by extensive mid-ocean magmatic activity and new oceanic crust formation, including ophiolitic rocks and related mineralizations (Fig. 4). At a very early transitional stage of subducting oceanic crust movements and distal to mid-ocean ridge settings there were conditions of, probably back-arc, calc-alkaline volcano-sedimentary activity along with formation and deposition of syngenetic metallic minerals of VMS (due to later hydrothermal remobilization may sometimes be considered as “hybrid epithermal VMS”) and BIF types. The progressively collisional subduction and destruction of Tethys led to compressional tensions and mineralized ophiolitic slabs were thrust over onto Paleozoic continental margin of Serbo-Macedonian basement rocks. The imposed orogenic mechanism and the associated probably post-subduction extensional tectonics (Richards, 2003 and 2009; Marchev et al., 2005) inferred generated intra-continental syn-orogenic faults, formed rift-basins and activated extensive Tertiary magmatic belts of orogenic I-type plutonic and sub-volcanic rocks which during Miocene differentiated partly to back-arc volcanism (e.g. Aridea volcanic belt). The emerging metallogenetic activity of intensive hydrothermal solutions leads to ore formation of manto-type polymetallic sulphides, copper-gold porphyry systems, ISCG-type (Iron Sulphide Copper Gold) gold-bearing pyrite-chalcopyrite-arsenopyrite mineralizations and high sulphidation epithermal gold and Mo–Cu–Te–Ag–Au porphyries along with probably post-subduction extension and rift-basin volcanism further to the east in the region of Thrace (Voudouris et al., 2009). This metallogenetic framework has similar geochemi-

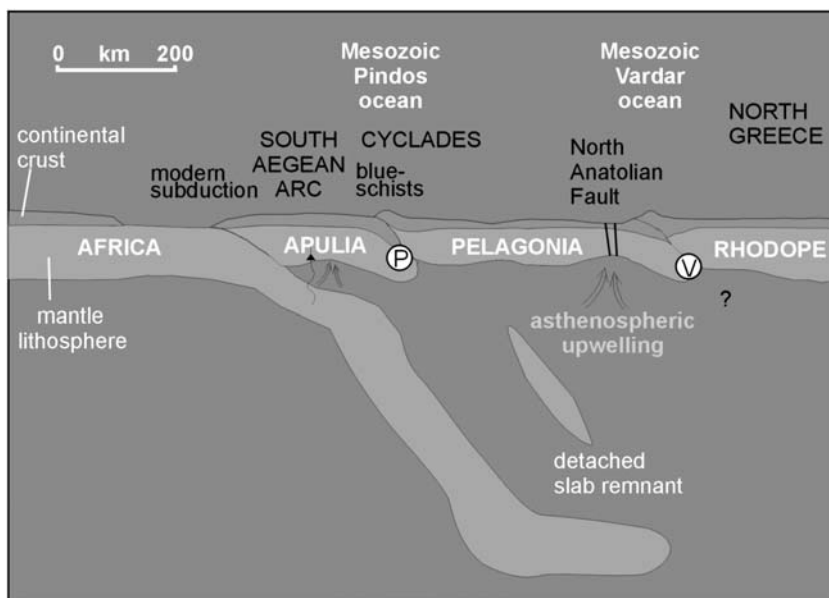


Fig. 4: The main mineralization types in northern Greece and southeast Balkan, and their genetic links to Tethys mid-ocean magmatic activity during Mesozoic and to subduction related orogenic belts during Tertiary (modified after, Pe-Piper, G. and Piper, D.J.W., 2001).

cal affinities with the copper-gold porphyries and the orogenic IOCG (Iron Oxide Copper Gold) type NEMM which at Archean-Proterozoic times are referred to as hybrid porphyry-IOCG style deposits (Weiher et al., 2008). Other typical and common features of the orogenic mineralizations, as the case is for the Tertiary Hellenic mineralizations, are their syn-tectonic and mesothermal characteristics. All previous types of sulphide minerals (particularly those hosted by Rhodope and Serbo-Macedonian marbles) were overimposed by post-Pliocene co-active supergene oxidation and karstification processes (Fig. 5). In spite of the manganese ore formation and the obvious iron enrichment of some occurrences, the metallic content and inter-related commodity grades of the primary sulphide deposits were not particularly affected during supergene oxidation.

6. Implication of new exploration concepts

The metallogenetic regime of orogenic and back-arc magmatic belts is globally one of the most dynamic geotectonic environments for the formation of potential polymetallic, porphyry and epithermal type gold deposits. It has been indicated that almost 50% of porphyry and epithermal type gold occurs in orogenic belts. In this respect, the Alpine or Tethyan orogenic setting makes a high priority target for exploration of Cenozoic NEMM resources and gold deposits in particular. This requires of course further and more systematic ore prospecting of selected regions and areas in Greece and the Balkan Peninsula using new technologies and methods. Based on the geodynamic, spatial and time compliant features of the mineralization types described above, to target and achieve NEMM resource sustainability the following conceptual tools could be applied:

- The local and regional aspects of the metallogenetic evolution which extend the geographical and geological potential of the NEMM resources with respect to transnational targets as for example is the Carpatho-Balkan belt (Jankovic et al., 1980; Heinrich and Neubauer, 2002).

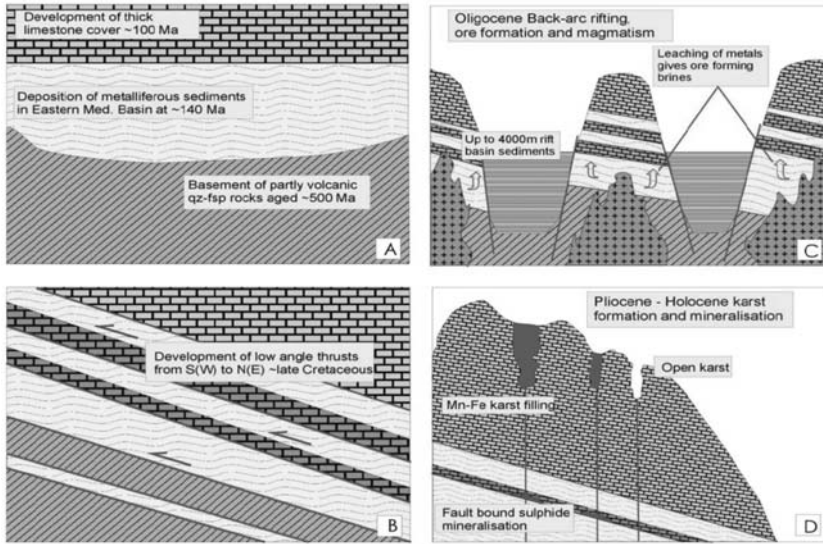


Fig. 5: Schematic integrated four phase mineralization and karst-forming model.

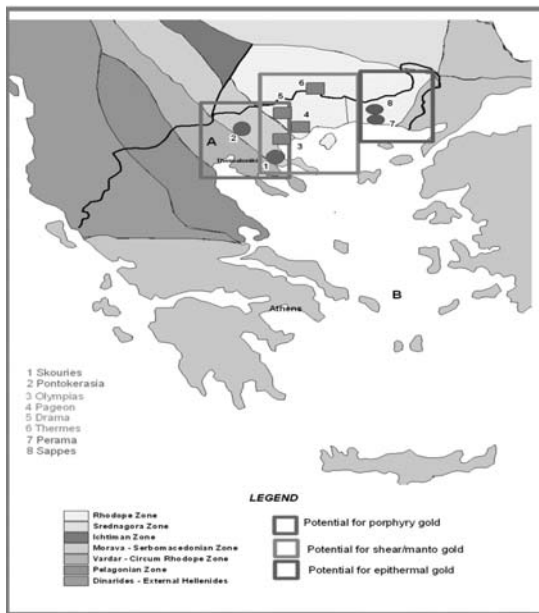


Fig. 6: Major gold potential exploration areas in Greece related to porphyry, manto-type and epithermal mineralization regimes and following the geotectonic and metallogenic evolution during Cenozoic time.

- The development and implementation of 3D/4D exploration models to locate deep seated mineral deposits in the known manto and porphyry type belts of Serbo-Macedonian zone and the IOCG like supergene assemblages of western Rhodope zone.
- The feasibility studies for the technoeconomical favourable presence of eco-efficient NEMM in the mentioned mineralization types, like for example the promising grades of PGE in the porphyry copper systems, which appear to become critical minerals and hot commodities for the European mining industry.

7. References

- Arvanitidis, N. D., Constantinides, D. C., Ashworth, K. L., Baker, J. H., Hellingwerf, R. H., and Epitropou N., 1995. Regional and local metallogenetic concepts in the SerboMacedonian and Rhodope Massifs, Northern Greece. *Proceedings of the third Biennial SGA meeting*, Prague, Pasava, Kribek and Zak (eds), Balkema, Rotterdam, 27-30.
- Arvanitidis, N.D., Tsamantouridis, P., and Dimou, E., 1996. Gold-bearing sulphide and gossans mineralization systems of the Myriophyto Region, central Macedonia, Greece, *Geologica Balcanica*, 26, 25-36.
- Arvanitidis, N., 2003. Gold deposits in Greece genetic types and economic perspectives, *Proceed. of the 7th Biennial SGA Meeting* on “Mineral Exploration and Sustainable Development” Athens, Millpress Roterdan, 941-943.
- Arvanitidis, N. D., and Amov, B., 2006. New geological and metallogenetic interpretation of lead isotopes from mineralizations in Greece, *Proceedings of XV III th Congress of the Carpathian-Balkan Geological Association*, Serbian Geological Society, Belgrade, 9-12.
- Diakakis, M., and Stefanidis, P., 1994. Mineral raw material atlas of central Macedonia, Greece, *IGME internal report*, Thessaloniki.
- Dimitroula M., Chatzipanagis I., Arvanitidis, N. D., and Economou, G. 1995. Gold mineralogy and geochemistry of the iron - manganese gossans in Thymaria area (Palea Kavala), Northern Greece, *XV Congress of the Carpatho - Balkan Geol. Ass.*, Athens, Spec. Publ. of the Geol - Soc of Greece, No 4/2, 704-709.
- Eliopoulos, D.G., and Economou-Eliopoulos, M., 1991. Platinum-group element and gold contents in the Skouries porphyry copper deposit, Chalkidiki Peninsula, northern Greece, *Economic Geology* 86, 740-749.
- Frei, R., 1995, Evolution of mineralizing fluid in the porphyry copper system of the Skouries deposit, northeast Chalkidiki (Greece): evidence from combined Pb-Sr and stable isotope data; *Economic Geology*, 90, p. 746-762.
- Heinrich, C. H., and Neubauer, Z. F., 2002. Cu – Au – Pb – Zn – Ag metallogeny of the Alpine – Balkan – Carpathian – Dinaride geodynamic province, *Mineralium Deposita*, 37, 533–540.
- Hellingwerf, R. H., Arvanitidis, N. D, and Constantinides D. C., 1993. The Olympias and Madem Lakkos massive sulphide deposits (Chalkidiki Peninsula/Greece): A new metallogenetic approach, *Abstracts of the Conference on Plate Tectonic Aspects of Alpine Metallogeny in the Carpatho - Balkan Region*, Budapest Proceedings, 20- 21.
- Hellingwerf, R. H., Arvanitidis, N. D., and Constantinides D. C., 1994. Ores, exploration tools and new targets in the eastern Chalkidiki peninsula, northern Greece, *Bulletin of the Geological Society of Greece vol. XXX/1*, 457-467.
- Jankovic, S., Petkovic, M., Tomson, I. N. and Kravcov, V., 1980, Porphyry copper deposits in the Serbo-Macedonian Province, southeastern Europe; in Jankovic, S. and Sillitoe, R.H., eds., *European Copper Deposits, Proceedings of International Symposium*, Bor, Yugoslavia, September 1979, Society for Geology Applied to Mineral Deposits (SGA), Special Publication 1, 96-101.
- Kalogeropoulos, S.I., Kiliass, S.P. Arvanitidis, N.D., 1996. Physicochemical conditions of deposition and origin of the carbonate-hosted base metal sulfide mineralization of the Thermes ore-field, Rhodope Massif, NE Greece. *Mineralium Deposita*, v. 31, p. 407-418.
- Kalogeropoulos, S.I., Kiliass, S.P., Bitzios, D., Nicolaou, M., Both R.A., 1989. Genesis of the Olympias carbonate-hosted Pb-Zn (Au, Ag) sulphide ore deposit, Eastern Chalkidiki Peninsula, N. Greece. *Economic Geology*, v. 84, p. 1210-1234.
- Kiliass S.P., Veranis N., Konnerup-Madsen J., 1995. The nature of the fluids associated with scheelite

- (+gold) mineralization, Metaggitsi-Pravita area, Central Chalkidiki Peninsula, N. Greece. In: Pasava, J., Kribek, B., Zak, and K. (eds.) *Mineral Deposits: From their origin to their environmental impacts*. Balkema/Rotterdam/Brookfield, pp. 877-880.
- Kiliyas, S.P., Kalogeropoulos, S.I., Konnerup-Madsen, J., 1996. Fluid inclusion evidence for the physico-chemical conditions of sulphide deposition in the Olympias carbonate-hosted Pb-Zn(Au,Ag) Sulphide ore deposit, E. Chalkidiki peninsula, N. Greece. *Mineralium Deposita*, v. 31, p. 394-406.
- Marchev, P., Kaiser-Rohrmeier, M., Heinrich, C., Ovtcharova, M., von Quadt, A., and, Raicheva, R., 2005. Hydrothermal ore deposits related to post-orogenic extensional magmatism and core complex formation: The Rhodope Massif of Bulgaria and Greece, *Ore Geology Reviews* 27, 53–89.
- Melfos, V., Vavelidis, M., Bogdanov, K., 2003. Occurrence, mineralogy and chemical composition of primary gold from Tertiary ore mineralization in the Rhodope Massif (Greece–Bulgaria). In: Eliopoulos, D., et al., (Eds.), *Mineral Exploration and Sustainable Development*. Millpress, Rotterdam, pp. 1201– 1204.
- Michael, C., Perdikatsis, V, Dimou, E., Marantos, I., 1995. Hydrothermal alteration and ore deposition in epithermal precious metal deposits of Agios Demetrios, Konos area, northern Greece. Proceedings XV Congress of the Carpathian–Balkan Geological Association, *Geological Society of Greece Special Publications no. 4*, pp. 778-782.
- Michael, C., 2004. Epithermal systems and gold mineralization in western Thrace (north Greece). *Bulletin of the Geological Society of Greece vol. XXXVI*, pp.416-423.
- Pe-Piper, G. and Piper, D.J.W., 2001: Late Cenozoic, post collisional Aegean igneous rocks: Nd, Pb and Sr isotopic constraints on petrogenetic and tectonic models. *Geological Magazine*, 138, 653-668.
- Richards, J.P. 2003, Tectonomagmatic precursors for porphyry Cu-(Mo-Au) deposit formation: Economic Geology and the Bulletin of the Society of Economic Geologists, v. 96, p. 1515– 1533.; Richards, J.P. 2009 Post-subduction porphyry Cu-Au and epithermal Au deposits: Products of remelting of subduction-modified lithosphere; *Geology; March 2009; v. 37; no. 3; p. 247-250*).
- Tobey, E., Schneider, A., Alegria, A., Olcay, L., Perantonis, G. and Quiroga, J., 1998, Skouries porphyry copper-gold deposit Chalkidiki, Greece: setting, mineralization and resources; in Porter, T. M., ed., *Porphyry and Hydrothermal Copper and Gold Deposits: a global perspective, PACRIM '98 Conference Proceedings*, Australian Mineral Foundation, p. 159-168.
- Voudouris, P., Papavasiliou, C., Alfieris, D., and Falalakis, G., 2007. Gold-silver tellurides and bismuth sulfosalts in the high-intermediate sulfidation Perama Hill deposit, western Tharce (NE Greece), *Geological Survey of Finland, Guide 53*.
- Voudouris et al, 2009. Rhenium-rich molybdenite and rheniite in the Pagoni Rachi Mo–Cu–Te–Ag–Au prospect, northern Greece: implications for the re geochemistry of porphyry-style cu–mo and mo mineralization ;*The Canadian Mineralogist Vol. 47, pp. 1013-1036 , 2009*.
- Weihed, P., Eilu, P., Larsen, R.B., Stendal, H., and Tontti, M., 2008. Metallic mineral deposits in the Nordic countries, *Episodes, Vol. 31, No. 1, 125-132*.

VOLCANIC – SEDIMENTARY METAL DEPOSITION IN PALEOMARGIN ENVIRONMENT: A “ PROTORE ” OCCURRENCE IN CENTRAL SARDINIA (ITALY)

Fadda S.¹, Fiori M.¹, Pretti S.², and Valera P.²

¹ *Istituto di Geologia Ambientale e Geoingegneria del CNR, 09100 Cagliari, Italy,
sfadda@unica.it, fiori@unica.it*

² *Dipartimento di Geoingegneria e Tecnologie Ambientali, Università di Cagliari, Italy,
paolo@paolov.net*

Abstract

Several metallogenic periods took place at different moments of the geological evolution of Sardinia, but at places they interacted: the close correlation between the metal parageneses in the Ordovician – Silurian sequences, outcropping in the central part of the island, and the veins and masses associated with the Hercynian magmatism is depicted. The volcanic-sedimentary mixed-sulphide lenses contained in Silurian occurrences show clear sedimentary structures, and the connection with coeval volcanics seems evident. These mineralizations are thought to be the protores for the subsequent metallogenic cycle related with the Hercynian orogenesis which had a strong effect as a promoter of the remoulding of preexisting mineral concentrations to give new ore- and industrial-minerals deposits. Several geochemical campaigns have covered the entire island, and wide areas of the Paleozoic basement, mostly localised in the internal zones, showed high base- and heavy-metals contents. A new prospecting programme has been started in Central Sardinia; it follows the ore-bearing horizon along the Ordovician-Silurian boundary with the purpose to better understand these primary metal depositions, their relationships with geodynamic structures, and ore mobilisation caused by the Hercynian granites. The geochemical anomalies along this horizon detected in the area of “Castello Medusa” support detailed prospecting works.

Key words: *protore, sulfides, Ordovician-Silurian, Sardinia.*

1. Introduction

The present shape, grade and composition of many Sardinian deposits are the final result of recurrent reworkings of original, not always economically interesting accumulations. Among the metallogenic epochs recognizable in the Paleozoic basement of the Sardinian microplate, one took place in the Upper Ordovician to Lower Devonian and yielded different types of deposits that share a common character: they are all syndepositional and partly volcano-sedimentary, at least as far as their protores are concerned (Pretti et al., 1990). These stratiform deposits are essentially located in the central part of the island, in one of the two main recognizable sedimentary areas, the “*internal trough*” (Fig. 1), where volcanics and tuffites are frequent and a Cu-Zn-Pb stratabound mineralization is well developed as a number of generally small, high-grade, mixed-sulphide lenses contained in Silurian black shales (Carmignani et al., 1994); these bodies show evident sedimentary structures

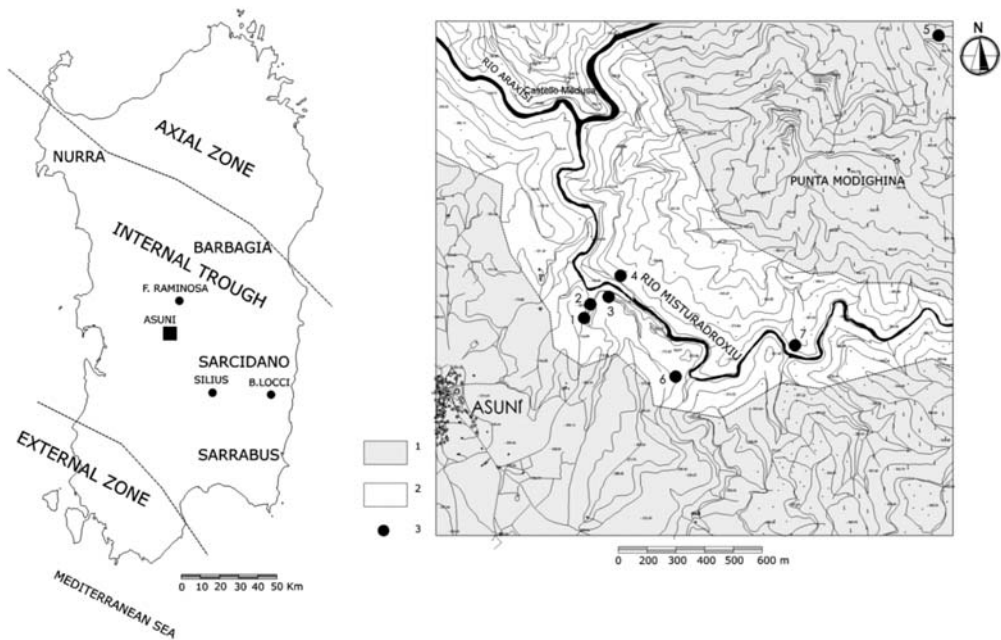


Fig. 1: Left: sketch map of Sardinia showing the three main structural areas; Right: topographic map of the area under study. 1) Silurian-Devonian complex: micaschists, phyllites, arenaceous phyllites; 2) Silurian-Devonian marbles, calcshists; 3) Sampling sites.

(load cast, slumping, diagenetic fracturing, etc). Another type which is characterized by its high Ag grade, at places with recoverable quantities of galena and minor sphalerite, is well known in the Sarrabus district (SE Sardinia), and oolitic iron ore accumulations interbedded with Silurian slates occur in the NW corner of the island (Nurra). The main ore-bearing horizon is made up of lavas and tuffitic rocks probably of Caradocian age. The products of this volcanic cycle, that may represent the cause of the metal supply, are covered almost everywhere by shales, black shales and limestone, of Silurian age. The above subaerial and submarine volcanism started during the Ordovician and exhausted in the Upper Silurian; The ore-bearing horizon seems to represent its upper part, and displays a comparatively modest thickness (50 to 100 m, Garbarino et al., 1980). However important phenomena of ore remobilisation, caused by the Hercynian folding, occurred in this horizon, so that it loosed its spatial continuity and was split and reworked in the nuclei of the folds. Numerous skarn deposits were generated by contact metamorphism of previous protores and/or metasomatic replacement, giving rise to new ore associations and textures (Marcello et al., 1994; Pretti et al., 1990).

A series of geochemical campaigns have covered the entire island, and several base- and heavy-metals showed high contents in numerous, and often wide areas of the Paleozoic basement of Sardinia. Most of these areas are localised in the internal zone.

A five-years prospecting programme was carried out during the eighties in the ambit of CNR-supported "Geodinamica" Project. About 250 samples were collected in the Barbagia region along the above stratigraphic sequences. All the samples have been analysed for Pb, Zn, and Cu by AAS and XRF (Tab. 1).

Table 1. M = average content in ppm; S = standard deviation; n = number of samples.

	M	S	n	Silurian metasediments (phyllites, black shales, skarn and met-alimestones)	M	S	n	Silurian meta-volcanics (metandesites, metarhyolites and their tuffs)
Cu	43	41	97		30	25	48	
Pb	16	9	97		18	9	48	
Zn	196	246	97		115	28	48	

Table 2. Analytical results of high metal spots from the sampled area, values in ppm.

	PA1A	PA2A	PA3A	PA3B	PA4A	PA4B	PA4C	PA4D	PA4E	PA5	PA6	PA7
Cu	13	8	65	661	16	94	265	329	19	6	15	225
Pb	7	14	6	21	1634	6	8	13	3	3	1612	7
Zn	2	1	21	8	11	40	11	32	24	3	8	7
As	7	23	13	16	6	5	1	1	1	15	5	5
Sb	0.15	2	2	1	1	2	1	1	3	0.4	1	14
Cd	2	0.1	1	1	1	4	1	4	0.1	0.4	1	0
Mo	0.01	0.01	4	3	1	11	10	0.22	0.22	0.01	1	12
Se	0.3	0.3	0.4	1	15	1	1	1	0.02	0.02	13	2
Te	0.009	0.06	0.005	0.03	1	0.2	0.1	0.05	0.005	0.005	1	1.4
Hg	3	2	5	2	4	2	2	2	1	3	4	52
Bi	0.4	0.7	1	1	123	6	2	1	0.3	0.05	122	131
Ni	12	5	95	25	15	94	64	43	19	23	13	5
Co	1	1	22	4	3	14	10	16	6	3	3	157
Ag	0.5	0.8	0.6	6	119	3	3	3	0.2	<0.005	103	7
Au	0.04	0.01	0.007	0.007	0.011	0.003	0.002	0.003	0.007	<0.001	0.009	0.053

The aim of this work is to examine some of these areas especially in the pre-Hercynian limestones and shales, in order to detect “spots” having rather high metal content; they could represent a “protore”. In the study area of *Castello Medusa* frequent transitions between different lithologies occur: tuffs, tuffites, clastic sediments, black shales, phyllites and limestones are observable; the area also hosts fluorite-galena-bearing veins, which have been exploited in the past. The following step is to recognize disseminated ore minerals and to match the composition of these “protore” with the compositions prevailing in the known ore bodies along the same NW-SE belt. Actually numerous indications of mineralization have been recognized during this field work, which was developed by following the stratigraphic and structural guides.

2. Geological setting

The internal trough, from Sarrabus to Barbagia and Nurra (Fig.1), includes the thickest Palaeozoic sequence of the Sardinia microplate and it is characterized by low grade metamorphism. Lithostratigraphic sequences of the various tectonic units in this zone are composed of a Middle Cambrian-Lower Ordovician pelitic-arenaceous substrate. During the Middle-Upper Ordovician period a subaerial volcanic complex formed and is principally recorded by intermediate-acid metavolcanics with subalkaline affinity. Upper Ordovician deposits are transgressive on the volcanic complex and are represented by terrigenous and, subordinately, carbonate metasediments. Subsequent deposition is recorded by Lower-Middle Silurian pelitic neritic metasediments and by Upper Silurian-Devonian pelagic platform carbonate deposits. The Hercynian deformational history in central Sardinia involved essentially two phases. The first was produced during collision-related shortening, the second deformational event, which appears largely extensional in character, deformed the earlier structures and produced open folds. This orogenic event took place approximately 350 to 290 Ma ago. During the Hercynian cycle tonalities, granodiorites and monzogranites, followed by post-tectonic leucogranites were emplaced, accompanied by porphyrites at the end of the cycle.

3. Sampling and analytical procedures

Data collected during the CNR “Geodinamica” Project have been chosen for a first matching with the results of the present study. Figure 1 shows the sampling pattern and sites along the Rio Misturatroxiu in the Asuni sector where some “stream” samples collected during the above mentioned geochemical campaigns showed high Pb, Zn, Cu, and Au values. Besides base metals, precious elements and PGM have been determined in limestone, marble, and black shale samples by ICP-MS and INAA. These new data are reported in Table 2.

The sampled lithological formations outcropping in the area are mostly composed of Silurian-Devonian shales, black shales, marbles, calcschists, and quartz veins (Fig. 2).

4. Discussion

The most important mineral occurrences are around the paleoreliefs, always at the base of the Silurian limestone or in a synchronous stratigraphic level. Important ore deposits occur around the

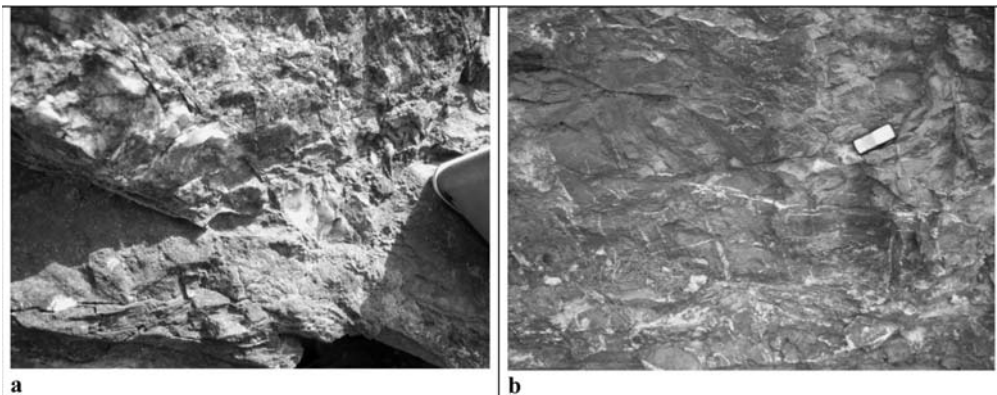


Fig. 2: a) Disseminations of sulfides in silicified limestones, Costa Ualla, Rio Misturatroxiu; b) The “protore” as a tight stockwork of sulfide-bearing quartz veinlets.

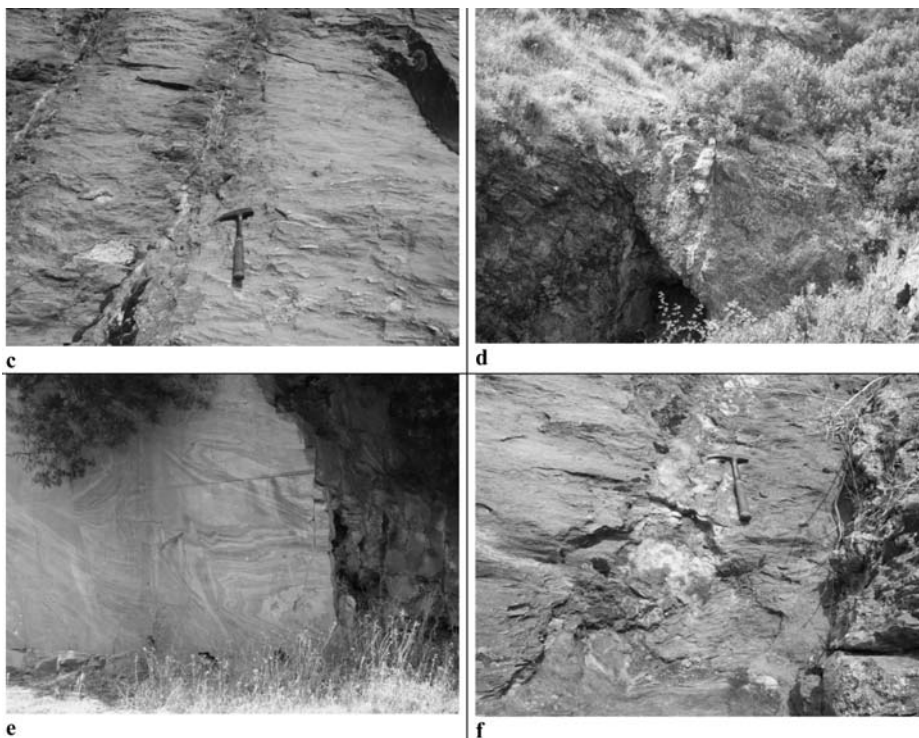


Fig. 2: c) The “protore” as small lenses of squeezed sulfide-bearing quartz. A late mobilization, probably of Hercynian age, formed a sulfide-richer quartz vein; d) Quartz-fluorite-barite-galena vein (an exploration tunnel is visible), as the latest aspect of the ore-level mobilization; e) Asuni marble open pit; f) Oxidized pyrite in quartz vein (in black shales).

thickest volcanic occurrences; they include Fe, Cu, Zn, Ag, and minor amounts of Pb and F. At Funtana Raminosa (chalcopyrite and galena), the ore-bearing horizon reaches its maximum thickness, about 10-15 metres, and the origin of the mineralization has been essentially attributed to concentrations of previous low-grade ores; in fact a fine interpenetration between sulfide and Ca-silicate minerals is present when the ore-content is not very high (Fig. 3).

With increasing ore concentration the structure may become massive and mineralisation assumes the “massive sulfide” structure. In this case the ore bed consists almost exclusively of sulfides; nevertheless a bedding can be frequently recognized in the mineralized layers. Ag was also recovered from the Funtana Raminosa ores. On a microscopic scale the ore occurrences of these areas consist of a mixture of sulfides, sulfosalts and oxides; the main ore minerals are sphalerite, galena, pyrite, chalcopyrite, and magnetite; fluorite also occurs.

The ore-bearing horizon overlies the volcanic system and underlies the Silurian–Devonian sequence; it may represent the result of direct deposition and/or replacement phenomena near the sea floor, around the volcanic centres, where sub-marine fumarolic activity was present. However the mineralising processes represent systems in equilibrium with the environmental evolution and they cannot be interpreted as restricted in time and space. The Ordovician-Silurian mixed sulphides have been subjected to the Hercynian orogenesis and have been reworked; the *Filone Argentifero*, and the ore deposit of Baccu Locci in Sarrabus may represent the result of these remobilisation phenomena (Bakos et al., 1988).



Fig. 3: Ore-bearing horizon made up of garnet, epidotes, quartz. The sulfides are finely disseminated in the rock. Crystallization broadly synchronous with the microfolds is visible; S. Gabriele, Funtana Raminosa Mine.

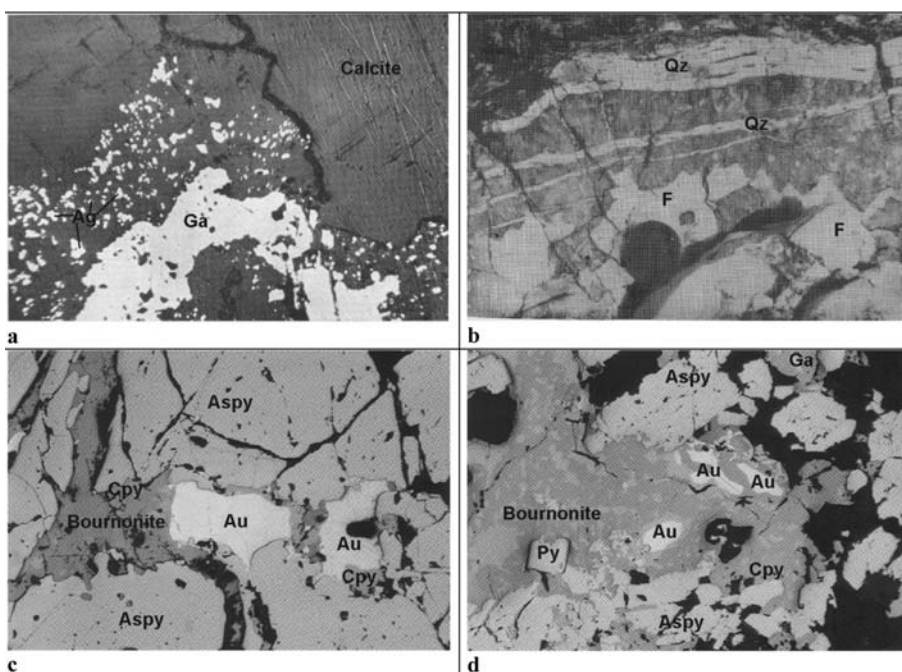


Fig. 4: a) Galena (white) and native silver disseminated in calcite (dark grey), Silver Lode of Tuviois, Sarrabus; b) Fluorite (grey), and quartz, outcrop of Serra S' Angassua, Serra S'Ilixi mine; c) Gold (yellow) accompanying chalcopyrite (brown) and bournonite (grey), galena (medium grey), myrmekitic intergrowth invading fractured arsenopyrite. Reflected light, 660 X (Baccu Locci ore deposit); d) Gold (yellow) in bournonite (grey), galena (medium grey) myrmekitic intergrowth, with chalcopyrite (brown) in fractured arsenopyrite with euhedral pyrite. Black: quartz. Reflected light, 660 X (Baccu Locci ore deposit).

These deposits in fact show a close connection to the Ordovician-Silurian horizon on a regional scale. Fluorine, another element which is likely to have been abundantly supplied by the volcanic activity, often occurs in all the areas from Barbagia to Sarrabus (Fig. 4); the F content in the Or-

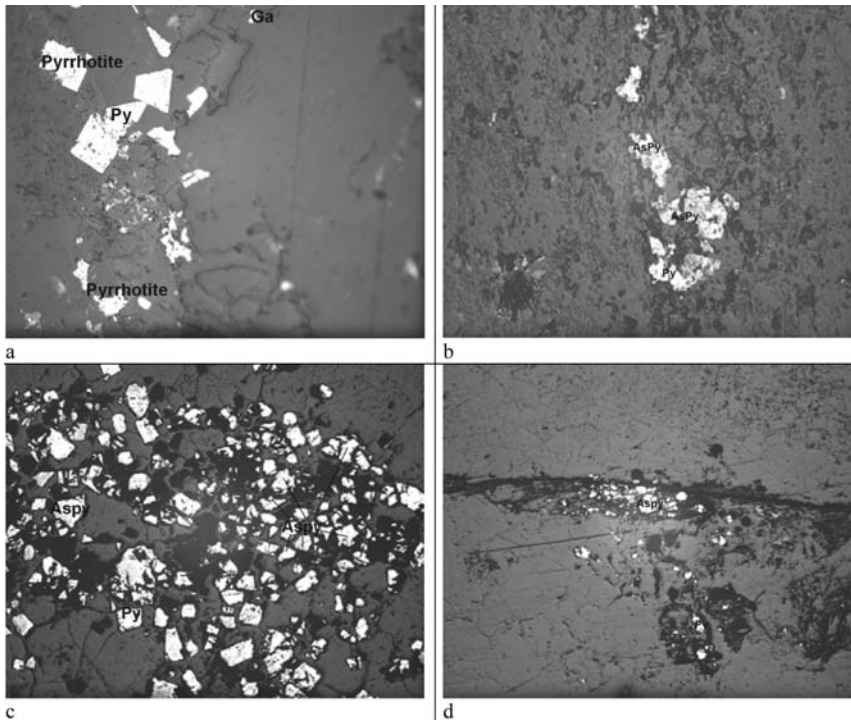


Fig. 5: a) Pyrite, pyrrhotite, and galena in quartz vein in silicified limestone, polished section, 10 X; b) Oxidized arsenopyrite and pyrite in metamorphosed limestone, polished section, 2.5 X; c) Oxidized arsenopyrite disseminated in quartz, polished section, 2.5 X; d) Fine dissemination of pyrite, arsenopyrite in quartz vein, polished section, 2.5 X, Rio Misturadroxii outcrop.

dovician-Silurian rocks might have been utilized by Hercynian magmatism to give rise to the important veins of Silius (Pani et al., 1988). This mine, a large quartz vein with about 40% CaF_2 and 1.5 % PbS , is still operating and is believed to be one of the most valuable fluorite mines in Europe. The previous geochemical data reported in table 1 suggest the following considerations: lead distributions are very similar between the two groups of formations, but it shows high variability within the same group. Zn shows the highest values and the great differences of distribution between the two group of formations. Cu shows an intermediate behaviour.

However the highest geochemical anomalies are localized in the “skarnoid” horizon, which contains a sort of “spots” having high metal contents. The prevailing metal associations in economic ores, i.e. Fe-Zn-Cu and Pb-Zn, were also found at a geochemical level; when positive anomalies of Pb and/or Pb-Zn are present the Cu contents are rather low; on the contrary positive anomalies of Zn and/or Zn-Cu are always associated with very low Pb contents. The analytical results of the samples from the Asuni sector (Table 2) at least would display a negative correlation between Pb and Cu, in good agreement with the above previous data.

5. Conclusions

The occurrence of high-metal content “spots” detected in the area of Asuni could be interpreted as the result of preconcentration phenomena which began during deposition and diagenesis of Pre-

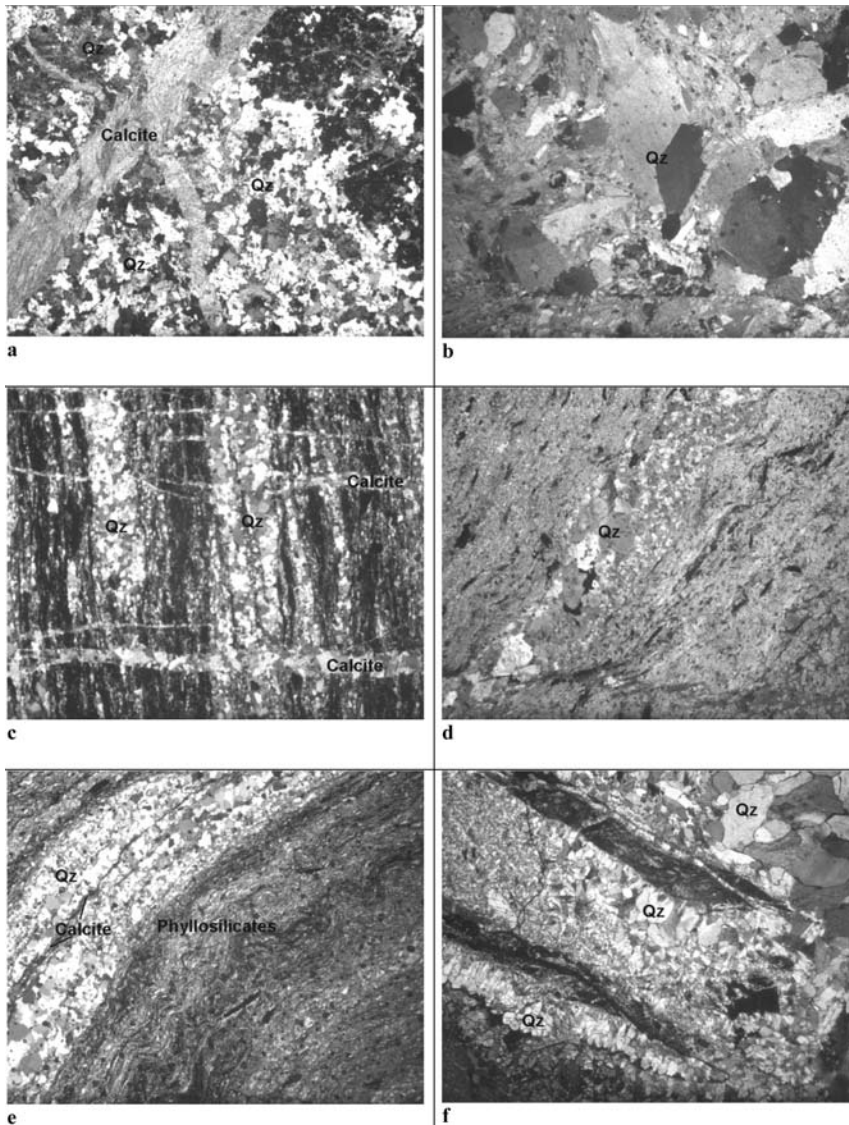


Fig. 6: a) Veinlets of calcite in silicified rock hosting opaque minerals (black), thin section, 2.5 X; b) Quartz veinlet developing idiomorphic crystals in limestone, thin section, 2.5 X; c) Calcite crossing quartz veins and carbonaceous matter, c; d) Quartz and phyllosilicates in limestone; opaque minerals are also visible, thin section, 2.5 X; e) Band of quartz and calcite in phyllosilicate rock that contains the mineralization, thin section, 2.5 X; f) Quartz veinlets, growing in euhedral crystals, alternating with carbonaceous matter bands, thin section, 2.5 X.

Permian, more or less deep sediments, and lasted up to the early Hercynian pulses. These mineralizations (Figs. 5, 6) would represent the Post-Cambrian to Lower Devonian stratabound protore occurrences that mostly formed after a primary volcano-sedimentary metal deposition in a structurally and geodynamically active paleomargin, and then subjected to enrichment phases by several reworking phenomena.

These protores would have been leached, remoulded and remobilised from the older to younger terrains during the Hercynian, by tectonic effects and/or magmatic or post-magmatic fluid circulation phases which contributed greatly to the formation of exploitable ore bodies. However now these deposits in detail exhibit prevalent vein-shaped and other epigenetic features, from pneumatolytic to epithermal, while on a regional scale they show a close connection to the metal-bearing Ordovician-Silurian stratigraphic level.

The “skarnoid” horizon always represents a geochemical anomaly for metals; less mobile elements, such as Pb, Au, Ag, and Bi, were further concentrated by Carboniferous-Permian hydrothermal fluids; on the contrary these fluids dispersed zinc, while barium and fluorine from the Ordovician-Silurian rocks were concentrated as veins of barite and fluorite. Numerous exploration and exploitation works for these industrial minerals are present in the area of Asuni (Bakos et al., 1972). Each mineralising stage seems to be, more or less, connected to the preceding ones. The mineral association of the ores prevailing in Sarcidano and Barbagia, mostly consisting of pyrite-chalcopyrite, sphalerite, and galena, also occur in the area under study even if small variations may occur.

Our recent detailed prospecting in the area of *Castello Medusa* has emphasised the presence of numerous high-metal “spots”. These small ore outcrops probably witness the presence of copper-lead-zinc (-silver, -gold) exploitable mineralizations in the areas neighbouring the exhausted mines, and practically in the whole Central Sardinia, where the same stratigraphic and/or geodynamic environment occurs.

6. Acknowledgements

This study was supported by the Istituto di Geologia Ambientale e Geoingegneria del CNR and the Dipartimento di Geoingegneria e Tecnologie Ambientali (DIGITA), piazza d’Armi, 09123 Cagliari, Italy.

7. References

- Bakos, F., Valera, R., 1972. Il Campo Filoniano di Castel Medusa, (Asuni - Sardegna Centrale) 283-297.
- Bakos, F., Carcangiu, G., Fadda, S., Mazzella, A., Valera, R., 1988. The Au-Ag-As-Fe-Cu-Pb-Zn-Sb-W paragenesis of Baccu Locci (SE Sardinia): an example of multistage evolution from a protore of volcano-sedimentary origin. Zuffar’ Days – Symposium held in Cagliari, October, 10-15, 1988, 9-13.
- Carmignani, L., Marcello, A., Musumeci, G., Oggiano, G., Pertusati, P.C., Pretti, S., Salvadori, I., 1994. Paleozoic sequences, extensional tectonics and talc-chlorite deposits of Central Sardinia. Guide-book to the field excursion of the 16th General Meeting of the IMA, 61-72.
- Garbarino, C., Grillo, M.S., Marini, C., Mazzella, A., Melis, F., Padalino, G., Tocco, S., Violo, M., Maccioni, L., Fiori, M., 1980. The Paleozoic Metallogenic Epochs of the Sardinian Microplate (Western Mediterranean): An Attempt of Synthesis on Geodynamic Evolution and Mineralizing Processes. *Rend. Soc. It. Min. Petr.*, 39: 193-228.
- Marcello, A., Pretti, S., Salvadori, I., 1994. Introduction to the minerogenesis and the economic geology of Sardinia. Guide-book to the field excursion of the 16th General Meeting of the IMA, 37-43.
- Pani, E., Valera, R., 1988. Fluorite in the Sardinian metallogenic history. Zuffar’ Days – Symposium held in Cagliari, October, 10-15, 1988, 71-85.
- Pretti, S., Salvadori, I., Uras, I., Valera, R., Zuffardi, P., 1990. The metallogeny of Sardinia. *Atti Acc. Lincei, serie IX*, 1.

IMMOBILE TRACE ELEMENTS DISCRIMINATION DIAGRAMMS WITH ZEOLITIZED VOLCANICLASTICS FROM THE EVROS - THRACE - RHODOPE VOLCANIC TERRAIN

Kitsopoulos K.

*University of Leicester, Department of Geology, University Road, LE1 7RH Leicester, UK,
kitsopoulos.k@gmail.com*

Abstract

The Rhodope and Evros areas of the Thrace Region in north-eastern Greece and the adjacent areas in Bulgaria are characterized by wide spread volcanic formations of Upper Eocene to Miocene in age. The volcanoclastic materials associated with such formations have, in some cases, undergone inter alia a notable zeolitization process. The mineralogy of the altered volcanoclastics is often dominated by clinoptilolite - heulandite type of minerals. The Winchester and Floyd (1977) plots indicating rhyodacite/dacite to trachyandesite parent materials, while the similar diagram, as modified by Pearce (1986), indicate andesite to trachyandesite precursors. The alkalinity index (Nb/Y ratio) seems to coincide between the two types of diagrams, but, there is a notable difference of the differentiation index, i.e. the Zr/TiO₂ ratio. The Th-Co diagram (Hastie et al., 2007) unfolds a clearer picture for the nature of the precursors and reveals a clear progression of a calc-alkaline to a high-K calc alkaline affinity of the parental volcanic materials.

Key words: *volcanoclastics, zeolitization, zeolite minerals, geochemical classification, trace elements, Thrace - Evros, Greece.*

1. Introduction

Zeolite minerals, such as clinoptilolite and mordenite, are often found worldwide as alteration products in volcanoclastic materials. It is known that the zeolitization involves a diffusion-controlled hydration, mainly of volcanic glass, and an alkali ion exchange procedure. As a result, the zeolitization involves the relative gain and losses of elements initially present, especially alkaline and alkali earths and sometimes Si too. So, because of their zeolitization, these materials usually do not attract any considerable petrological attention, especially on their geochemical nature. The truth is that under this situation, the geochemical nature of the parent materials is extremely difficult to establish. The indiscriminate use of geochemical classification diagrams is not recommended.

The objective of the present study was to choose and apply the most appropriate geochemical tools, for zeolitized rocks, i.e. altered materials, with an ultimate scope to examine their geochemical characteristics and to verify the nature of the parent volcanoclastic materials (i.e. the nature of the precursors for the formation of zeolites).

2. Geological setting

The geological structure of the Western Thrace – Evros area of Greece consists of three distinct units:

1. The Pre - Mesozoic crystalline basement which consist of a high grade metamorphic rocks, such as marbles, gneisses, amphibolites and pegmatites (lower allochthonous unit) to schist- and amphibolitic- gneisses and amhibolites (upper autochthonous unit).
2. The Circum-Rhodope Zone, which, in the wider Thrace and Evros areas, consist of two parts, the Makri Unit and the Drymos-Melia Series.
3. Tertiary basins which are built from: a) volcanic rocks, such as granite bodies, sills and dykes, b) volcanoclastic materials such as tuffs, breccias and lahars, and c) sediments and sedimentary rocks such as conglomerates, sandstones, marls, sandy marls and locally lignite seams. The magmatic activity, of Eocene to Oligocene age is related continental collision that followed the subduction of African - Arabian plate beneath the Eurasian (Yanev et. al. 1998). Marchev et al (2004) have compiled a map of the geology of the Eastern Rhodope area (Figure 1).

3. Materials and Methods

3.1 Materials

The samples we used are zeolite-bearing volcanoclastic materials from the wider Evros - Thrace – Rhodope volcanic terrain of Greece. Typical examples of such type of alteration have been recorded in numerous locations in the above mentioned areas of north-eastern Greece, (Figure 2), as well as in south and southeast Bulgaria (Tsirambides et al., 1989; Kirov et al., 1990; Tsolis-Katagas and Katagas, 1990; Kitsopoulos, 1991; Skarpelis et al., 1993; Djourova and Aleksiev, 1995; Stamatakis et al., 1998; Marantos et al., 2004).

3.2 XRD and XRF

Since the mineralogy of the zeolitized materials of the Tertiary basins of the Thrace – Evros area has been examined in many occasions in the past (Tsirambides et al., 1989; Kirov et al., 1990; Tsolis-Katagas and Katagas, 1990; Skarpelis et al., 1993; Djourova and Aleksiev, 1995; Stamatakis et al., 1998; Marantos et al., 2004), the XRD method was applied, with the sole purpose to confirm the presence of zeolite minerals in the samples chosen to be examined.

The geochemistry was examined by using a PANalytical Axios Advanced PW4400 XRF spectrometer, fitted with a 4kW Rh anode SST-mAX X-Ray tube. Major elements determined on fused glass beads prepared from ignited powders sample to flux ratio 1:5, 80% Li metaborate: 20% Li tetraborate flux. Trace elements analysed on 32mm diameter pressed powder briquettes prepared from 10g fine ground powder mixed with ca 20-25 drops 7% PVA soln and pressed at 10 tons per square inch. Various international standards, as recorded in GeoRem (Jochum et al., 2005, <http://geo-rem.mpch-mainz.gwdg.de>), were run with the samples as control on the quality of the analyses.

4. Data

Data 4.1

The XRD analysis has confirmed the presence, in various amounts, of zeolite minerals in the samples studied. There was no evidence found in their mineralogy in line with any influence of any other significant alteration, i.e. hydrothermal.

Some representative data, on TiO₂, Nb, Zr, Y, Th and Co values from the XRF analyses of the zeolitized volcanoclastics are given in Table 1.

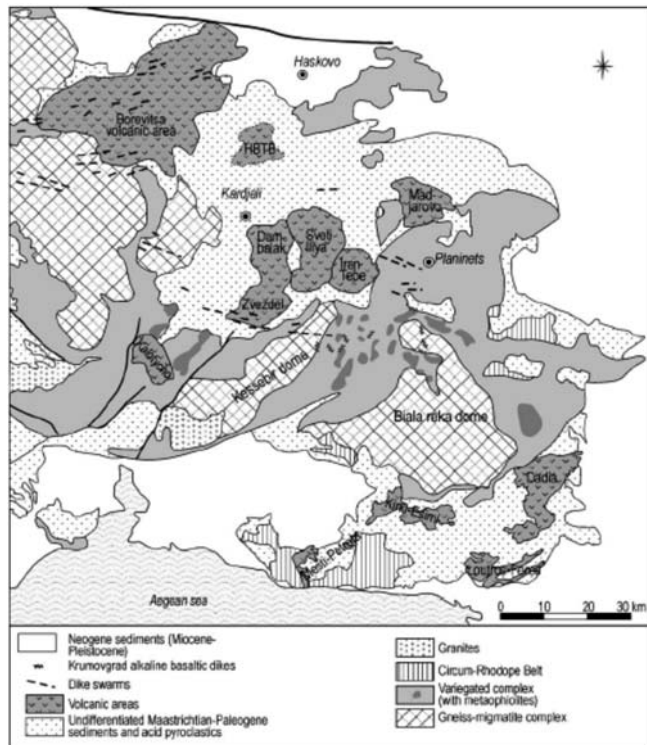


Fig. 1 : Schematic map of the geological structure of Eastern Rhodope (Marchev et al., 2004).



Fig. 2 : Zeolite deposits (Z) and occurrences (z) in Thrace (north eastern Greece), scale 1:1.000.000 (Marantos et al., 2000).

Table 1.

Sample	Locality	TiO ₂	Nb	Zr	Y	Th	Co
		%	ppm				
M1	Metaxades	0.11	28.1	60.8	34.9	21.6	0.9
M2	Metaxades	0.09	27.7	65.9	28.4	22.7	0.9
L1	Lefkimi - Dadia	0.13	10.2	87.8	12.0	15.8	0.8
L2	Lefkimi - Dadia	0.18	8.4	91.6	18.6	14.1	3.0
P1	Petrota	0.16	21.9	145.9	16.5	30.9	0.8
P2	Petrota	0.17	26.6	166.8	22.2	38.3	0.8
F1	Ferres	0.14	8.9	65.4	13.1	12.9	1
F2	Ferres	0.40	6.3	136.2	13.1	12.3	5

The classic SiO₂ vs. K₂O (Peccerillo & Taylor, 1976; Rickwood, 1989) and the SiO₂ vs. Na₂O+K₂O (Le Maitre et al., 1989, 1992) diagrams have been proved unusable with zeolitized materials (Kitsopoulos et al., 2001). In these cases the problems occurred are related to the mobilisation and the redistribution of the alkalis during the zeolitization process. An alternative approach to establish the nature of the parent materials is to use immobile trace elements. As a proxy to the TAS diagram, a discrimination diagram, based on immobile elements, was proposed, which uses the Nb/Y vs. Zr/TiO₂ ratios (Winchester and Floyd, 1977). The Ti, Zr, Nb and Y are considered immobile during post-consolidation alteration and metamorphic processes. In the Winchester and Floyd, the Zr/TiO₂ ratio can primarily act as a differentiation index, as the differentiation of a basaltic magma can be traced by the decrease of TiO₂, and to a less extent as an alkalinity index, as Zr tends to concentrate in alkaline rocks. The Nb/Y ratio acts only as an alkalinity index (Pearce and Cann 1973,) which corresponds with the higher concentrations of Nb in alkaline provinces. The field boundaries of the diagram should be viewed as marking gradational changes rather than sharply defined fields. Also, it should be always taken into account that the diagram was prepared using all types of igneous rocks except for island arc lavas. As the original plot by Winchester and Floyd (1977) has been designed prior to the publication of the TAS diagram by Le Bas et al. (1986, 1992), the field definition has been subsequently modified by Pearce (1996) who used a much larger dataset and also statistically drawn boundaries. The diagram used volcanic arc analyses but it poses the problem of a large overlap displayed by island arc basalts, basaltic andesites, andesites and dacites.

5. Discussion - Conclusions

By using the Winchester and Floyd (1977) it can be seen that the samples examined plot in the field of rhyodacite/dacite to trachyandesite, with one sample be plotted as trachyte (Fig. 3). On the similar diagram as modified by Pearce (1986) they plot on the field of andesite to trachyandesite (Figure 4). Although the alkalinity index (Nb/Y ratio) seems to coincide between the two plots, there is a notable difference of the differentiation index of these plots, i.e. the Zr/TiO₂ ratio.

Koutles et al. (1995) examined the geochemistry of a single zeolitized outcrop, the Metaxades deposit, by using samples which were collected on a vertical mode, of a traverse of visible thickness of 100m, in the Metaxades quarry. Their results are plotted in the Winchester and Floyd (1977) and the similar, but modified, by Pearce (1986) (Figs 5 & 6).

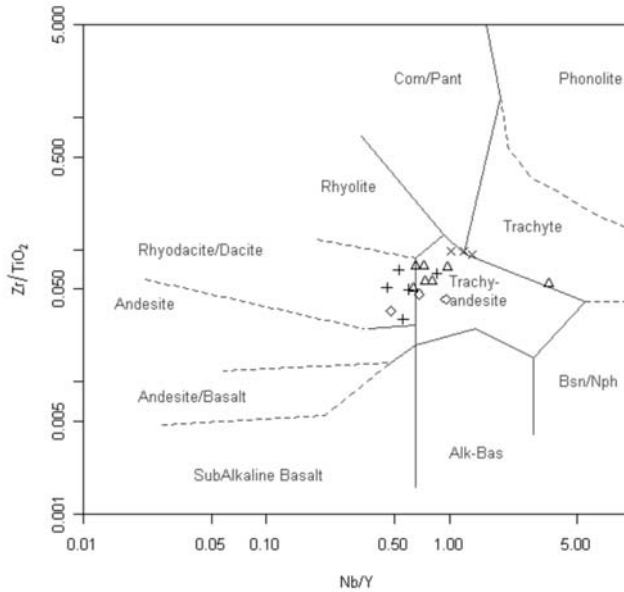


Fig. 3: Nb/Y vs. Zr/TiO₂ plot of XRF analyses of zeolitized materials on the diagram by Winchester and Floyd (1977). +: Dadia-Lefkimi, Δ: Metaxades, X: Petrota, ◊: Ferres.

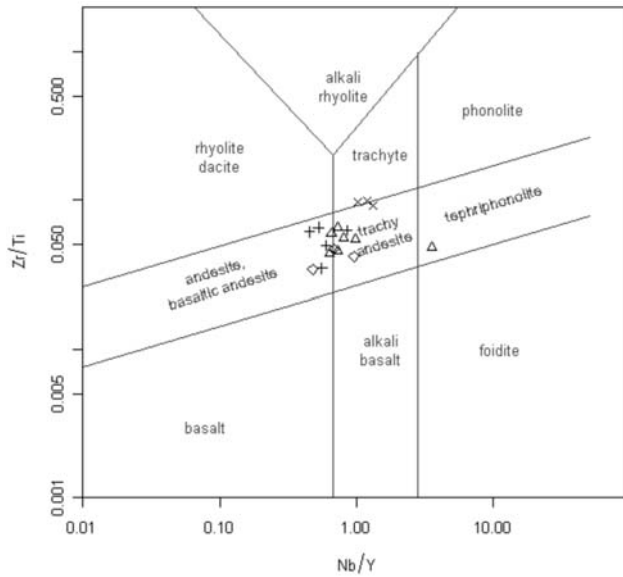


Fig. 4: Nb/Y vs. Zr/Ti plot of XRF analyses of zeolitized materials on the diagram by Winchester and Floyd (1977), as modified by Pearce (1986). +: Dadia-Lefkimi, Δ: Metaxades, X: Petrota, ◊: Ferres.

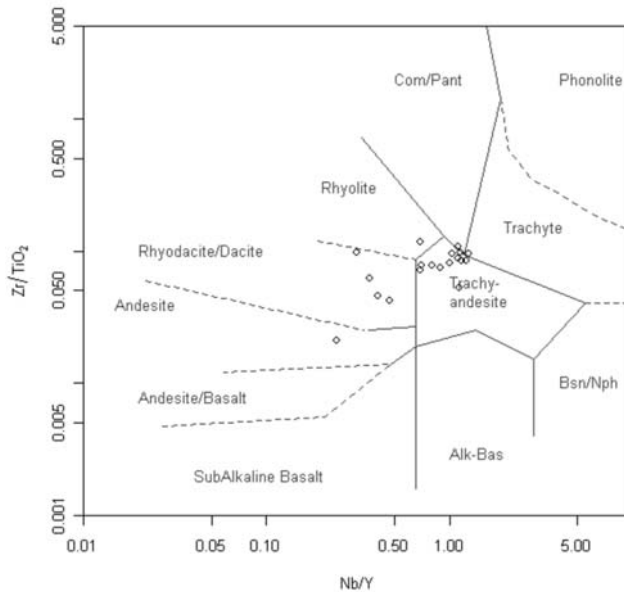


Fig. 5: Nb/Y vs. Zr/TiO₂ plot of XRF analyses of zeolitized materials from Metaxades, Evros, Greece. Diagram by Winchester and Floyd (1977). Data from Koutles et al. (1995).

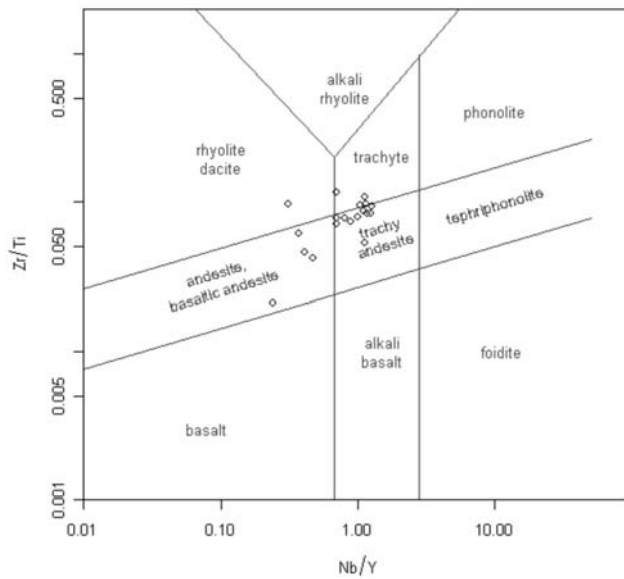


Fig. 6: Nb/Y vs. Zr/Ti plot of XRF analyses of zeolitized materials from Metaxades, Evros County, Greece. Diagram by Winchester and Floyd (1977), as modified by Pearce (1986). Data from Koutles et al. (1995).

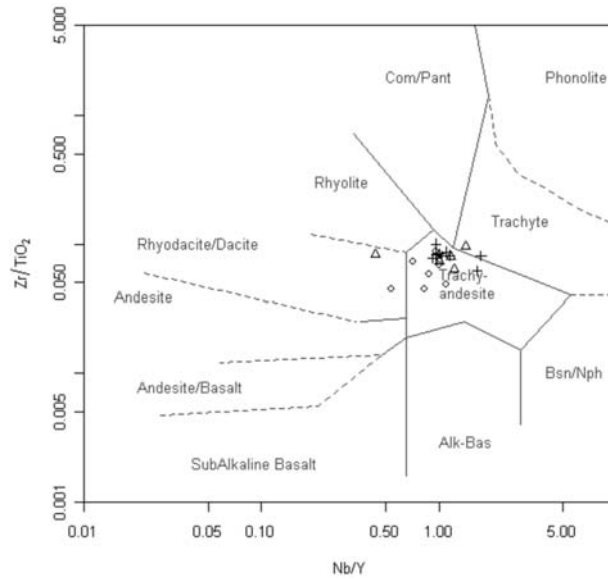


Fig. 7: Nb/Y vs. Zr/TiO₂ plot of XRF analyses of zeolitized materials from Pentalofos, Palestra and Petrotá-Paleochorofa area. Diagram by Winchester and Floyd (1977). Data from Stamatakis et al. (1998).

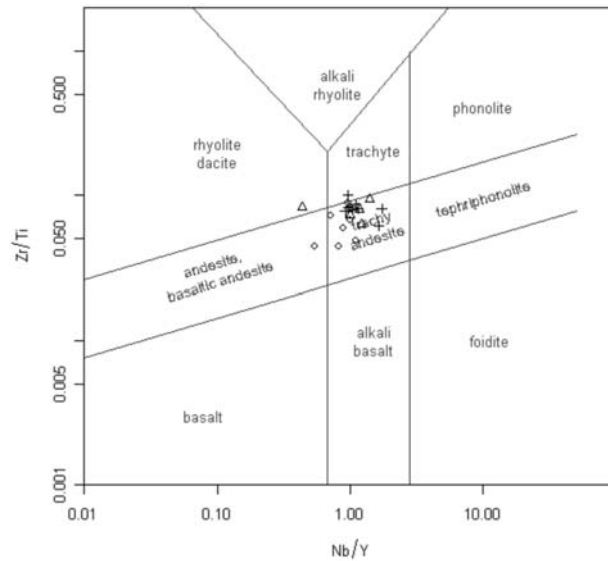


Fig. 8: Nb/Y vs. Zr/TiO₂ plot of XRF analyses of zeolitized materials from Pentalofos, Palestra and Petrotá-Paleochorofa area. Diagram by Winchester and Floyd (1977), as modified by Pearce (1986). Data from Stamatakis et al. (1998).

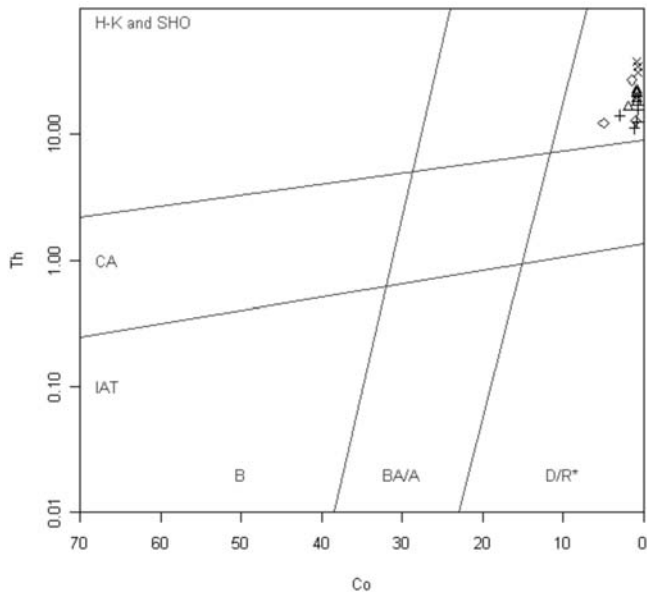


Fig. 9: Th - Co plot of XRF analyses of zeolitized materials on the diagram by Hastie et al. (2007). B, basalt; BA/A, basaltic andesite and andesite; D/R*, dacite and rhyolite (* indicates that latites and trachytes also fall in the D/R fields). IAT, island arc tholeiite; CA, calc-alkaline; H-K, high-K calc-alkaline; SHO, shoshonite. +: Dadia-Lefkimi, Δ: Metaxades, X: Petrota, ϕ: Ferres.

In both diagrams the spreads, in terms of both the differentiation and the alkalinity indexes, and subsequently of the rock types of the precursor material, are notable. By taking into consideration the fact that there is no evidence in the area of the influence of a significant heavy alteration procedure, for example post hydrothermal events, it seems that these spreads, which come from a single pyroclastic unit with a vertical examined thickness of 100m, are to be questioned. Nb shows a mean value of 24.79 (s.d. 6.24), Zr 68.63 (s.d. 8.18), and Y 33.95 (14.31) respectively.

Stamatakis et al examined the geochemistry of zeolitized outcrops from the Pentalofos-Palaistra-Petrota area. In this case the plots in the Winchester and Floyd (1977) and the one modified by Pearce (1986) are clearly showing an almost single parent precursor (Figs 7, 8).

A quite important diagram used to identify rock types and volcanic series of volcanic are rocks is the $K_2O - SiO_2$ diagram, which however is highly susceptible to the effects of alteration. Working with altered volcanic island arc rocks Hastie et al. (2007) have developed a similar diagram by using Th as a proxy for K_2O and Co as a proxy for SiO_2 with a classification success rate of about 80%. They also claimed that they managed to identify the volcanic series of initially hydrothermally altered, then tropically weathered, Cretaceous volcanic arc lavas from Jamaica. There was no indication from the bibliography that the diagram has been ever used with zeolitized volcanics and certainly has not been applied to such materials from Greece. The use of Th and Co has been proved extremely successful with heavily altered, by tropical weathering, hydrothermal and metamorphic processes, lavas comprising of basalts and dacitic tuffs (Hastie *et al.*, 2008; Hastie and Kerr, 2010) as well as in calc-alkaline and alkaline magma mixing geo-petrological terrains (Luhr *et al.*, 2010).

In this case it becomes apparent (Fig. 9) that the rock type of the precursor of the zeolitized material studied is narrowed down to the field of dacites/rhyolites. This is coinciding with the finding of the initial Winchester and Floyd diagram. However, the Hastie diagram also reveals a degree of progression of a almost calc-alkaline to a high-K calc alkaline affinity of the parental volcanic materials.

6. Acknowledgments

The author has been always grateful to the Academic, Technical and Clerical Staff of the Geology Department of Leicester University for their kind host and constant support for almost two decades now. For their master knowledge and their valuable help with the analytical work and the data handling and interpretation, Nick Marsh, Rob Wilson, Rob Kelly, Rod Branson and Collin Cunningham should be specially mentioned. On 14/7/2007 Dr. Tim Brewer was suddenly lost for ever. I shall always remember and be grateful to Tim for proposing and setting up a Fellowship, so I can be able to continue my work in Leicester.

7. References

- Djourova, E., and Aleksiev, B., 1995. Zeolitic rocks in the Northeastern Rhodopes. In: Aleksiev, B (Ed.), *An Excursion to selected Zeolite and Clay deposits in the Eastern Rhodopes. A Guide to the post-Meeting trip, Sofia Zeolite Meeting '95*, 20-30.
- Finlow-Bates, T., and Stumpf, E. F., 1981. The behaviour of so-called immobile elements in hydrothermally altered rocks associated with volcanogenic submarine-exhalative ore deposits. *Mineralium Deposita* 16, 319-328.
- Hastie, A.R., Kerr, A.C., Pearce, J.A., & Mitchell, S.F., 2007. Classification of altered volcanic island arc rocks using immobile trace elements: development of the Th-Co discrimination diagram. *Journal of Petrology* 48, 2341-2357.
- Hastie, A.R., Kerr, A.C., Mitchell, S.F., & Millar, I.L., 2008. Geochemistry and petrogenesis of Cretaceous oceanic plateau lavas in eastern Jamaica. *Lithos*, 101, 323-343.
- Hastie, A.R., and Kerr, A.C., 2010. Mantle plume or slab window?: Physical and geochemical constraints on the origin of the Caribbean oceanic plateau. *Earth Science Reviews*, 98, 283-293.
- Jochum, K.P., Nohl, U., Herwig, K., Lammel, E., Stoll, B., & Hofmann, A.W., 2005. GeoRem: A new geochemical database for reference materials and isotopic standards. *Geostandards & Geoanalytical Research* 29, 333-338.
- Kirov, G., Fillipides, A., Tsirambides, A., Tzvetanov, R., & Kassoli-Fournaraki, A., 1990. Zeolite bearing rocks in Petrota area (Eastern Rhodope Massif, Greece). *Geologica Rhodopica* 2, 500-511.
- Kitsopoulos, K. P., 1991. Volcanic zeolitic tuffs from Greece as an industrial commodity. Useful properties and possible applications. University of Leicester, MSc Thesis, 110 pp.
- Kitsopoulos, K. P., Scott, P.W., Jeffrey, C.A., & Marsh, N.G., 2001. The mineralogy and geochemistry of zeolite-bearing volcanics from Akrotiri (Santorini island) and Polyegos (Milos group of islands) Greece. Implications for geochemical classification diagrams. *Bulletin of the Geological Society of Greece*, vol. XXXIV/3, Proceedings of the 9th International Congress, Athens, 859-865.
- Koutles, Th., Kassoli-Fournaraki, A., Filippidis, A., & Tsirambides, A., 1995. Geology and geochemistry of the Eocene zeolite-bearing volcanoclastic sediments of Metaxades, Thrace, Greece. *Estudios Geologicos*, 51, 19-27.
- Le Bas, M.J., Le Maitre, R.W., Streckeisen, A., & Zanettin, B., 1986. A chemical classification of volcanic rocks based on the total alkali-silica diagram. *Journal of Petrology*, 27, 745-750.
- Le Bas, M. J., Le Maitre, R.W., & Woolley, A. R. (1992). The construction of the total alkali-silica chem-

- ical classification of volcanic rocks. *Mineralogy and Petrology*, 46, 1-22.
- Le Maitre, R. W., Bateman, P., Dudek, A., Keller J., Lameyre, J., Le Bas, M. J., Sabine, P. A., Schimd, R., Sorensen, H., Strckeisen, A., Woolley, A. R., & Zanettin, B., 1989. *A classification of igneous rocks and glossary of terms*. (Blackwell, Oxford).
- Luhr, J. F., Ochoa, C. N., and Savov, I.P., 2010. Tephrochronology, petrology and geochemistry of Late-Holocene pyroclastic deposits from Volcán de Colima, Mexico. *Journal of Volcanology and Geothermal Research*, doi:10.1016/j.jvolgeores.2009.11.007
- Marantos, I., Kosharis, G., Perdikatsis, V., & Karantassi, S., 2000. *Study on the zeolitic tuffs of Skaloma Area, Rodopi Prefecture, Thrace*. Internal Report, I.G.M.E., Athens, 56 pp.
- Marantos, I., Kosharis, G., Karantassi, S., Perdikatsis, V., and Christidis, G., 2004. Preliminary study of altered Tertiary volcanoclastic rocks in the area of Asproula, Nea Santa, Rodopi prefecture, Thrace, NE Greece. *Bulletin of the Geological Society of Greece*, 35, 454-463.
- Marchev, P., Raicheva, R., Downes, H., Vaselli, O., Chiaradia, M., & Moritz, R., 2004. Compositional diversity of Eocene–Oligocene basaltic magmatism in the Eastern Rhodopes, SE Bulgaria: implications for genesis and tectonic setting. *Tectonophysics*, 393, 301-328.
- Pearce, J. A., 1996. A user's guide to basalt discrimination diagrams. In: Wyman, D. A. (ed.) *Trace Element Geochemistry of Volcanic Rocks: Applications for Massive Sulphide Exploration*. Geological Association of Canada, Short Course Notes 12, 79–113.
- Peccerillo, R. and Taylor, S. R., 1976. Geochemistry of Eocene calc-alkaline volcanic rocks from the Kastamonu area, northern Turkey. *Contributions to Mineralogy and Petrology*, 58, 63-81.
- Rickwood, P. C., 1989. Boundary lines within petrologic diagrams which use oxides of major and minor elements. *Lithos*, 22, 247-263.
- Skarpelis, N., Marantos, I., & Christidis, G., 1993. Zeolites in Oligocene volcanic rocks, Dadia-Lefkimi area, Thrace, Northern Greece: mineralogy and cation-exchange properties. *Bulletin of the Geological Society of Greece*, 28, 305.
- Stamatakis, M., Hall, A., Lutat, U., & Walsh, J.N., 1998. Mineralogy, origin and commercial value of the zeolite-rich tuffs in the Petrota-Pentalofos area, Evros county, Greece. *Estudios Geologicos*, 54, 3-15.
- Tsirambides, A., Kassoli-Fournaraki, A., Filippidis, A., & Soldatos, K., 1989. Preliminary results on clinoptilolite containing volcaniclastic sediments from Metaxades area, NE Greece. *Bulletin of the Geological Society of Greece*, 23, 451-460.
- Tsolis-Katagas, P., and Katagas, C., 1990. Zeolitic diagenesis of Oligocene pyroclastic rocks of the Metaxades area, Thrace, Greece. *Mineralogical Magazine*, 54, 95-103.
- Winchester, J. A., and Floyd, P. A., 1977. Geochemical discrimination of different magma series and their differentiation products using immobile elements. *Chemical Geology*, 20, 325-343.
- Yanev, Y., Innocenti, F., Manetti, P., & Serri, G., 1998. Upper Eocene – Oligocene collision – related volcanism in Eastern Rhodopes (Bulgaria) – Western Thrace (Greece): Petrogenetic Affinity and Geodynamic Significance. *Acta Vulcanologica*, 10 (2), 279 – 291.

HUMAN INTERFERENCES TO THE ENVIRONMENT, CONSEQUENCES AND CARE

Lampropoulou P.¹, Tzevelekou Th.², Papamantellos D.², Stivanakis V³,
Papaefthymiou S.²

¹ University of Patras, Department of Geology, Section of Earth Materials, 26500 Patras, Greece, p.lampropoulou@upatras.gr

² Hellenic Center of Metals Research S.A. (ELKEME), 177 78 Tavros, Athens/Greece, dpapamantellos@elkeme.vionet.gr, ftzevelekou@elkeme.vionet.gr, spapaefthymiou@elkeme.vionet.gr

³ University of Patras, Department of Chemical Engineers, Laboratory of Metallurgy, 26500 Patras, Greece

vstivanakis@chemeng.upatras.gr

Abstract

The need to restore the relationship of mankind with the environment led to the designation of measures, terms and processes worldwide for the prevention or reduction to the highest possible degree of the negative consequences to the environment ensuring a high level of protection of human health and the environment. It is general ascertainment that there is a big lack of objective information in Greece regarding the possibilities of modern science and technology for the treatment of Solid Industrial Wastes (SIW), Municipal Solid Wastes (MSW) and biological Sewage Treatment Plants (STP) products safely for the public health and the environment. In Greece the most significant sources of SIW are the big exploitations of "Mineral Ores". On the contrary, the cement industries provide an important way out for the consumption of SIW like fly ash, red mud, et. A big percentage of the total amount of produced alloys of iron, copper, zinc and aluminium do not use "Mineral Resources" as raw materials but recycle scrap metals. At the end, the successful results of pyrometallurgical production of final products by SIW as well as the results of the production of new friendly to the environment and high technology refractory materials are given in this work.

Key words: environment, human interferences, solid industrial and municipal wastes, consumption of wastes.

1. Introduction

The current image of Greece regarding the management of Solid Industrial Wastes (SIW) and especially of the Municipal Solid Wastes (MSW) as well as of the products resulting from the biological Sewage Treatment Plants (STP) is falling behind the European Standards. The hierarchy in waste prevention and management as set in EU Waste Framework Directive (EU Directive 2008/98/EC) should lie on (i) prevention, (ii) preparation for reuse, (iii) recycling, (iv) other recovery (i.e. energy recovery) and (v) disposal. Modern technologies based on Best Available Techniques and on the results of relative scientific studies should be implemented.

2. Municipal Solid Wastes (MSW)

The present Greek MSW production is in the range of ~4.5mil.t/y. The main characteristic of MSW management in Greece is that over 90% results in landfilling as presented in Fig. 1 (Papamantellos et al 2005), and in more than 1300 cases landfilling has been performed illegally (2005 data). Only in Attica, within the next decade the handling of predicted 35-45 mil. tons municipal wastes, taking a production of 7000t/d MSW, will require 7-8 additional landfill sites of 500.000m² area and ~20m height each, while the operation of the already approved landfilling areas in Keratea and Grammatiko have been blocked!

Greece “keeps the negative record” in Municipal Solid Wastes Landfilling and the last place in the energy exploitation of their content in modern WTE (Waste to Energy) plants, Fig. 2, according to 2005 data (Papamantellos, 2007).

This situation of MSW mismanagement, which does not conform to the EU environmental legislation, resulted in sensitive penalties posed by the EU. The current status requires drastic measures under one political and decision making centre ready to adapt and implement modern and efficient techniques. The current decision decentralization to the regions and the municipalities leads to polyphony and endless discussions about the most suitable technologies without implementation.

For solving the hot environmental issues of the Greek Society quick cooperation between involved Ministries is absolutely necessary. Creation of a task force from the Ministers of Environment, Economy, Interior and Development is here proposed. Target of this task force would be the foundation of an independent Authority for determining strategies of Municipal-, Hazardous-, Industrial- Waste - Management and landscape rehabilitation. This independent Authority should decide about technologies to be applied, the structure of the cooperating involved parties (private, state, municipal, etc), their funding including cost-benefit analyses and optimum for each case operation units. This independent Authority should be responsible for making the final decision about the needed measures and actions for the environmental problems under consideration and should assist the funding of the projects, taking also EU grants into consideration. It also could provide technical assistance for the preparation, publication and evaluation of all kind of tenders (public, private). Furthermore, it will supervise the implementation of the relevant projects keeping the time scheduling. In case of landscape rehabilitation the Authority will provide the legal and environmental framework and, then, supervise the execution of the rehabilitation actions taken by private companies after private tender on their responsibility. A very essential task of this independent Authority, in cooperation with Universities, NGOs, etc should be the information of the Society regarding environmental safe MSW management measures. Relevant example of such an independent Authority’s successful activity was the Organization Committee “Athens 2004”.

As an example, the public opinion should be informed that modern applied technologies allow nowadays the safe and clean operation of a WTE unit as shown in Figs. 3, 4. Very impressive is the high volume of gas cleaning systems installation, Fig. 3, so that the gas outlet is completely clean and air pollution is prevented especially from dioxins. A characteristic example of WTE installation is the one operating successfully in Brescia, Italy, Fig. 4, serving the needs of 500.000 people. The sewage sludge from the waste water treatment plant of the city is also incinerated in the plant. The unit produces 50 MW and the producing steam is used for central thermal supply in the city (Papamantellos et al., 2009). The Brescia WTE plant was placed on the area of the old landfill site of the city, which has been rehabilitated.

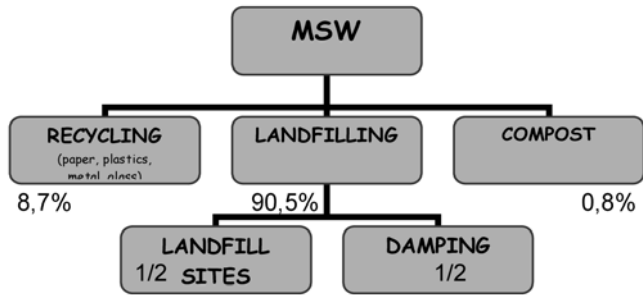


Fig. 1: Breakdown of the MSW management in Greece (Papamantellos et al., 2009).

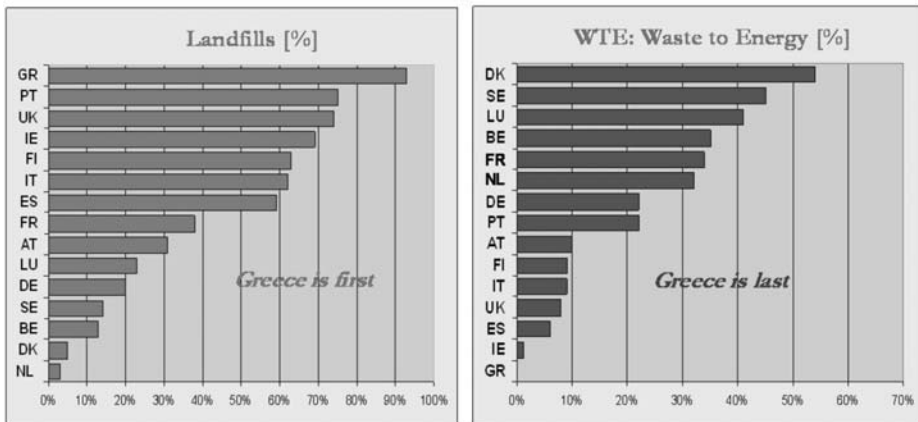


Fig. 2: Municipal Solid Wastes (MSW) management in Greece and EU, 2005 data.

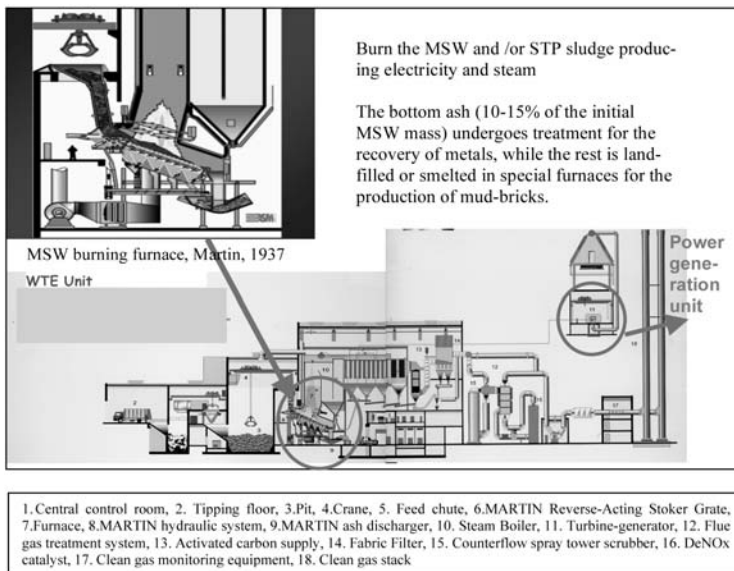


Fig. 3: WTE unit for the MSW management: feeding, burning, steam and power generation.

Solid Industrial Wastes (SIW)

Extended open pits for exploitation of fossil fuels (lignite Figs 5 a, b), ores (nickeliferous laterites (Figs 7a, b), bauxite (Fig. 8), magnesites, limestone (Figs 9a,b) perlite, pumice, etc) is the biggest source of industrial solid waste in Greece. Example of open pit rehabilitation is shown in Fig. 5b including the reforestation and lake creation forming a refreshment area close to urban environment.

The development of the total lignite production (t/y) and the total excavations has been proliferated since the beginning of the mine operation till the year of 2006 (Figs 6a, b) [Papamantellos, 2007].



Fig. 4: WTR facility in Brescia.



Fig. 5a: PPC Lignite mine for el. power generation.



Fig. 5b: Environmental rehabilitation of open pit

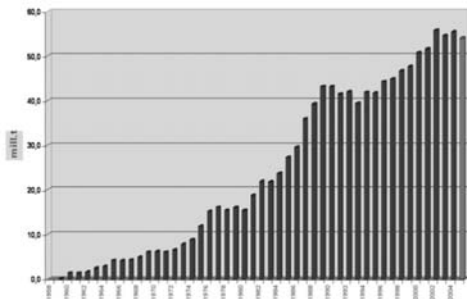


Fig. 6a: Development of lignite production.

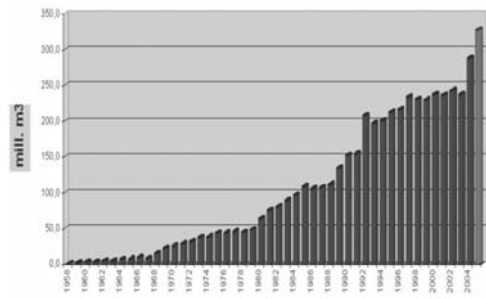


Fig. 6b: Development of excavations of lignite open pits.



Fig. 7a: Nickelferrous laterite mine of LARCO for the production of ferronickel. For the production of 100.000 t/y FeNi 20, ~2.2 mil.t /y of ore are needed.

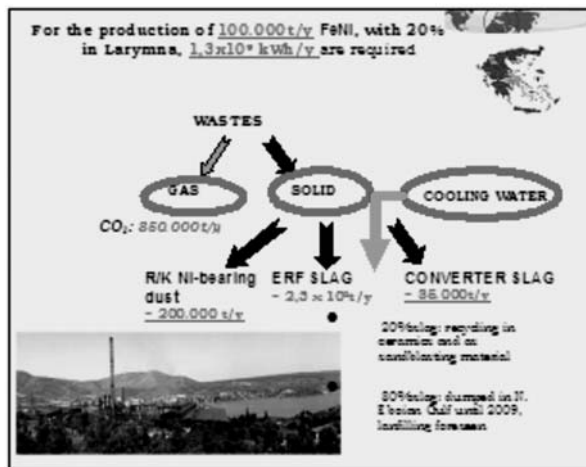


Fig. 7b: The waste (solid, liquid and gas) generation associated with the production of 100.000 t/y ferronickel, 20% Ni, FeNi20 at Larymna.



Fig. 8: Bauxite mine of ALUMINIUM OF GREECE for the production of alumina and primary aluminium. From 1,000,000 t/y bauxite are produced 450,000 t/y alumina, 170,000 t/y aluminium and 650,000 t/y red mud (SIW).



Fig.9a, b: Early and late stage of limestone open pit rehabilitation (Titan, 2009).



Fig. 10: Cement Industry.



Fig. 11: Scrap metals used as raw materials for the production of new metallic products.

It is evident that the reforestation efforts of open pits excavations as well as of burned forests according to international experience should be combined not only with the plantation of trees but also with bushes adjusted to the environment to be rehabilitated. The use of biological STP sludge as well as fly ash of the lignite production could be very helpful in the above efforts as humus and trace elements carriers respectively.

3. Industrial utilization of SIW

The cement industries provide an important way out for the consumption of SIW like fly ash, red mud, etc incorporating them in their high temperature industrial production, Fig. 10. The metallurgical industries in Greece that produce steel, alloys of copper, zinc and aluminium do not use “Mineral Resources” as raw materials but recycle scrap metals which are actually wastes of the consumer society and/or of other small or large scale industrial facilities (Fig. 11).

Table 1. Composition of Plyttalia sludge compared to lignite (Papamantellos et al 2005).

	<i>Psyttalia sludge</i>		<i>Lignite of Megalopolis</i>
	<i>Dewatered</i>	<i>Dry</i>	
<i>Humidity (%)</i>	68	-	60
<i>Inorganic (Ash) (%)</i>	10	60-35	14
<i>Organic Matter (%)</i>	21	40-65	26
<i>Energy content (kcal/kg)</i>	500-750	2200-3200	900

4. Examples of pyrometallurgical production of final products by SIW and of new friendly to the environment basic refractory materials

Successful researches related with production of final products by solid industrial wastes as well as production of new friendly to the environment and high technology refractory materials, have been carried out by researchers in the University of Patras and these examples are referred in this work:

EXAMPLE 1: Production of alumina cement by SIW (slag from the ferronickel production). (Dourounis, 2003).

EXAMPLE 2: Reduction smelting of SIW (E-filter R/K Ni-dust) of ferronickel production for the production of low alloyed steel grades and slagcements (Tzevelekou, 2004).

EXAMPLE 3: Utilization of solid by products resulting from lignite firing in the production of light-weight aggregates (Anagnostopoulos, 2009).

EXAMPLE 4: Production of FeNi and FeV from the reduction smelting of residues resulting from the PPC'S oil firing units for the electrical power generation (Karamoutsos, 2004).

EXAMPLE 5: Production of Greek type portland cement by using fly ash, the SIW of PPC'S lignite firing as a pozzolanic material (Stivanakis, 2003).

EXAMPLE 6: Utilization of red mud, the SIW from the production of alumina for the production of bricks, tiles and as raw material in the production of cement (Pontikes, 2007).

EXAMPLE 7: Mineralogical composition and properties of basic refractories and new magnesia-spinel compositions derived from magnesite of N. Evian (Lampropoulou, 2003).

5. The case of Psyttaleia's Biological Sewage Treatment Plant sludge

The composition of Biological Sewage Treatment Plant sludge, like the one produced on the island of Psyttaleia, Table 1, renders it a very promising solid fuel compared to solid fossil carbonaceous fuels, as lignite, used for electrical energy production due to its high energy content. The disintegrated sludge with thermal capacity of 500-700kcal/kg can be fired in a solid fuel fired boiler for power generation without any previous treatment. The dry sludge is fired nowadays in cement production units. In case a WTE unit existed for the management of MSW, the sludge could be easily co-fired to the unit as well. Provided that, as already mentioned, there are no such installations in Greece today, the sludge could be co-fed to one of the existing coal power plants after proper modifications of the relative units. The PPC unit No 3 in Aliveri was selected as a possible solution for co-firing the sludge

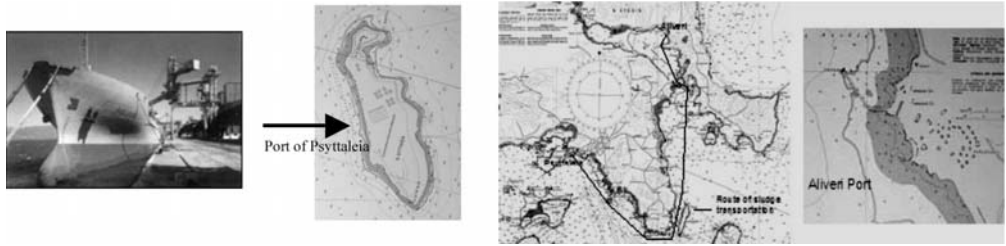


Fig. 12: Transportation of STP sludge from Psyttalia to Aliveri by special ships.

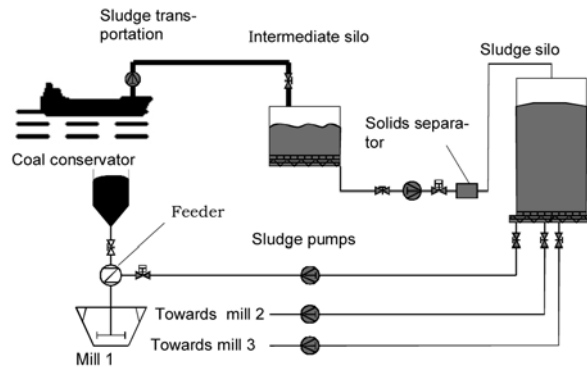


Fig. 13: Flow chart of sludge management in the power plant of PPC in Aliveri.

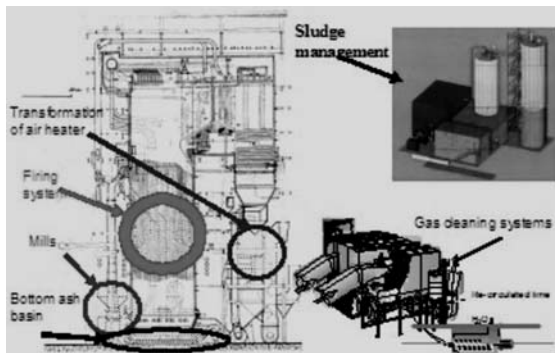


Fig. 14: Transformation areas of No 3 power plant unit in Aliveri.

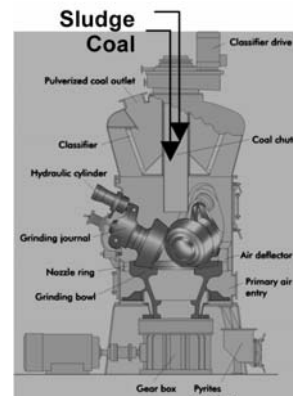


Fig. 15: Co-firing of sludge & hard-coal in hard-coal fired power station.

with solid fuel (steam coal) due to its geographical position, which enables the short marine transportation (~70nm) of the sludge in special ships, Fig. 12, from the port of Psyttaleia to the port of Aliveri (Papamantellos et al., 2005).

Once the sludge arrived to the power plant in Aliveri, the process described in the flow chart of Fig. 13 would follow. Certain modifications of the unit would be necessary in order to co-fire the sludge as presented in Fig. 14 (Heinz et al., 2005). The transformation, gas cleaning systems and sludge drying (optional) expenses were estimated 55 mil.€, which could be depreciated in 2-3 years from the

difference in the fuel cost. This proposal for Aliveri was not realized by PPC. However similar transportation of the sludge and co-firing to a hard-coal fired power station placed on the coast, with maximum distance from Psyttaleia 70-130km, to be constructed in the near future could be examined. The sludge can be pneumatically charged to the hard-coal mills as shown in Fig. 15 (Heinz et al., 2005).

6. Conclusions

1. Pyrometallurgical methods through the utilization of high temperatures comprise an active tool in the environmental management of SIW, MSW and STP products.
2. Development of zero residue industrial production processes can be achieved by combining industrial byproducts of power generation, metals production and cement industry.
3. In a future step it will be shown that considerable benefits will result regarding CO₂ emissions, energy savings, conservation of natural resources and environmental landscape protection from the adaptation of (1) to (4).
4. Closer collaboration among Municipalities, Industry, Government, Research Centres and Universities for the achievement of the aforementioned goals should be enhanced.
5. The lack in the objective information of the society must be covered regarding the possibilities of modern science and technology in the treatment of SIW, MSW and STP products safely for the public health and the environment.
6. The last two decades a lot of discussions have taken place regarding waste management in relative conferences, seminars, etc all over Greece with poor implementation results of modern waste management techniques. The current unsatisfactory situation requires drastic measures under one independent political and decision making umbrella for the whole country. The creation of a task force from the Ministers of Environment, Economy, Interior and Development is proposed with target the foundation of an independent Authority for managing Municipal, hazardous, industrial wastes and landscape rehabilitation.
7. This independent Authority should decide about the optimum technologies to be applied for MSW management, the structure of the cooperating involved parties (private, state, municipal, etc), their funding including cost-benefit analyses and optimum for each case operation units. The Authority should be responsible for making the final decision about the needed measures and actions for the environmental problems under consideration and should assist the funding of the projects, taking also EU grants into consideration. In addition, could provide technical assistance for the preparation, publication and evaluation of all kind of tenders (public, private).
8. Furthermore, this Authority will supervise the implementation of the relevant projects keeping the time scheduling. In case of landscape rehabilitation it will provide the legal and environmental framework and supervise the execution of the rehabilitation actions taken by private companies.
9. A very essential task of this independent Authority, in cooperation with Universities, NGOs, etc should be the information of the Society regarding environmental safe MSW management measures.

7. Acknowledgments

The authors would like to thank the Director of the Earth Engineering Centre of Columbia University, Prof. N. J. Themelis and the President of THERMOGON Mr. N. Mitsos for providing important data for the performance of the relevant studies.

8. References

- Anagnostopoulos I., 2009. Utilization of solid by products resulting from lignite firing in the production of lightweight aggregates. Thesis, University of Patras.
- Directive 2008/98/EC of the European Parliament and of the Council of 19 November 2008 on waste and repealing certain Directives.
- Dourdounis E., 2003. Production of alumina cement by SIW. Thesis, University of Patras.
- Heinz G., H. Brueggemann and B. Svenson of ALSTOM POWER BOILERS GmbH, Stuttgart and Vaxjo, "Private communication", 2005.
- Karamoutsos S., 2004. Production of FeNi and FeV from the reduction smelting of residues resulting from the PPC'S oil firing units for the electrical power generation. Thesis, University of Patras.
- Lampropoulou P., 2003. Mineralogical composition and properties of basic refractories and new magnesia-spinel compositions derived from magnesite of N. Evian. Thesis, University of Patras.
- Papamantellos D.C., Papandreou N. A., Papaefthymiou S. A., Tzeveleku T. V.: Proposal for Recycling and Energy Usage of Municipal Wastes in Greece, [in] Proc. of ISWA APESB "turning waste into ideas" International Conference, Lisbon 12.-15.10.2009.
- Papamantellos D. C., Themelis N. J., Tzeveleku Th., Karamoutsos S. "Proposal for Waste to Energy implementation in Western Greece", Solid Waste Management in Western Greece Prefecture Conference, Patras, 25/02/2005.
- Papamantellos D.C. "At the edge of renewable energy sources", 2nd National Conference of Mechanical and Electrical Engineers, 18/05/2007, Greece.
- Papamantellos D.C., "Metallurgy and wastes – Metallic alloys, oxidic materials and energy" 3rd National Conference on Metallic Materials, Patras, 5-6 Dec. 2007.
- Papamantellos D.C., Heinz G., H. Brueggemann and B. Svenson in cooperation with S. Karamoutsos and Th. Tzeveleku "Proposal for energy exploitation of Psyttaleia sludge by means of co-firing with steam coal", submitted to the Greek Ministries of Environment, Development in December 2004 and PPC in March 2005.
- Pontikes I., 2007. Utilization of red mud, the SIW from the production of alumina for the production of bricks, tiles and as raw material in the production of cement. Thesis, Univ.of Patras.
- Stivanakis V., 2003. Production of Greek type Portland cement by using fly ash, the SIW of PPC'S lignite firing as a pozzolanic material. Thesis, University of Patras.
- Titan, Publ. Issue 110, 2009, URL: <http://www.titan.gr/UserFiles/File/titanes/issue110/26-27.pdf>.
- Tzeveleku Th., 2004. Development of a process for recycling and producing new materials by reduction smelting of gas cleaning systems dusts from the ferronickel industry. Thesis, University of Patras.

“KARYSTÍA LÍTHOS”: A TIMELESS STRUCTURAL ORNAMENTAL STONE

Laskaridis K.¹ and Patronis M.¹

¹ *Institute of Geology and Mineral Exploration, Department of Economic Geology, LITHOS Laboratory, 13766 Athens, Greece, laskaridis@igme.gr, patronis@igme.gr*

Abstract

Karystía Líthos (= Stone of Karystos) is a widely used structural material since archaic times. It has been used in various constructions, considered to date before 700 BC or before the Trojan War or even as early as the Neolithic Age. The term “Karystía Líthos”, mentioned by Strabo, Pliny et al., includes cipollino marble, slates etc. Their main mineralogical constituent is calcite and their colour depends on the secondary and accessory minerals. This paper examines the timelessness of Karystía Líthos, focusing on the determination of its physical - mechanical and aesthetic characteristics. The natural stone properties are classified into those characterizing the material, and those determining the suitability of the stone for various special uses. Those properties were determined according to Standard EN 12326-2 “Slate and stone products for discontinuous roofing and cladding - Part 2: Methods of test”. The results were statistically analyzed, in order to draw relevant practical conclusions. The physical - mechanical properties of Karystía Líthos, on which its endurance through time and under mechanical stresses is depending, and its aesthetics, render it a widely applied ornamental stone to-date.

Key words: *Karystía Líthos, “Karystos Schists”, physical - mechanical properties, EN 12326-2, statistical analysis.*

1. Introduction

Karystía Líthos (= Stone of Karystos) is a widely used structural material since archaic times. It has been employed in the construction of columns, monuments and other buildings of colossal (“cyclopean”) dimensions, used for decorative, ritualistic or other practical purposes. It is considered that those constructions date before 700 BC or before the Trojan War or even as early as the Neolithic Age.

The term “Karystía Líthos” — as it is mentioned by Strabo, Pliny et al. — refers to cipollino marble, slates etc. These stones are still quarried in the southern part of Euboea Island, under the commercial name “Karystos Schists”.

The objective of this paper is to examine the reasons for the timelessness of Karystía Líthos, focusing on the determination of its physical - mechanical properties and its aesthetic characteristics.

Those features were determined according to the test methods specified in Standard EN 12326-2 “Slate and stone products for discontinuous roofing and cladding - Part 2: Methods of test”.

All tests were carried out in the accredited Ornamental Stones Quality Control Laboratory of I.G.M.E., “LITHOS”. The relevant results were evaluated via statistical analysis methods.



Fig. 1: The Mt. Óchi Drakóspito: External view.

2. Historical data

2.1 Euboea Island

Among the extant buildings being made of Karystía Líthos, the most imposing are the “drakóspita” (= dragon houses). That is the name given to some megalithic buildings (20 - 30 of them have been discovered to-date) mainly located in southern Euboea. The most important of them (Fig. 1) is found on the top of Mt. Óchi at an altitude of about 1400 m, overlooking the town of Karystos. Also, rather impressive are the 3 drakóspita near the town of Styra.

The Óchi “drakóspito” (= dragon house) is located on a small plateau formed between the twin tops of the mountain. It has been built with boulders and slabs quarried in the surrounding area. Those building elements have been shaped and they are perfectly matched without any binding material. The drakóspito walls are almost 1,50 m thick and its internal dimensions are about (5 × 10) m. The slab over the entrance measures (4 × 2 × 0,30) m. This structure is thought to be a Dryopic temple built before 700 BC, while other views date its construction before the Trojan War (~ 1300 BC) or even during the Neolithic Age (i.e. before 3000 BC).

The drakóspita roofs are structured following the “ekphorikón” system. This structure demands precise calculations and considerable skill. It is achieved by placing an inwardly protruding row of slabs on one wall of the drakóspito, followed by a second row protruding more, and so on, until the last row meet the relevant row from the opposite wall. If the slabs’ weight calculations are not adequate, the structure’s centre of gravity will be shifted off the walls and the roof will collapse. To avoid this, other boulders have been used as counterbalancing weights over the slabs’ part lying on the walls.

The slabs, the counterbalancing weights and most of the structure’s boulders are of huge (“cyclopean”) dimensions, and some of those elements weigh many tons.

Finally, near Aetos village (to the east of Karystos) there is an ancient quarry with big columns lying abandoned. Most of them are about 1.70 m in diameter and 13.50 m in height.



Fig. 2: The Library of Hadrianus: (a) Three of the columns (close view), (b) The NW wing of the façade propylon, with the seven extant columns.

2.2 City of Athens

An ancient monument of Athens, in the construction of which *Karystía Líthos* has been used, is the Library of Hadrianus (Fig. 2). It was built around 132 AD, during the reign of the Roman Emperor Hadrianus (117 - 138 AD), and takes up an orthogonal area of (122 × 82) m in the northern part of the Roman Agora. This is a big rectangular structure with an open peristyle courtyard measuring about (82 × 60) m and its perimeter was bordered by 100 columns (22 each on the east and the west side and 28 each on the north and the south one). The Library's façade is located on the west side of the building. The entrance, with a propylon of 4 Corinthian columns, was found in the middle of this western wall. The façade wall was decorated with 7 Corinthian columns on each side (i.e. the left and the right wing) of the entrance. The Library was partly destroyed during the Heruli raid (267 AD) and refurbished in the beginning of the 5th century AD. Today, a relatively small part of the façade is still standing (i.e. the NW wing) on Áreos Street, where the modern tourist may have the opportunity to admire the 7 imposing Corinthian columns made of *Karystía Líthos*.

3. Laboratory testing

3.1 Mineralogical - petrographic study of *Karystía Líthos* (commercially “*Karystos schists*”)

The relevant geological survey has located two horizons whose thickness occasionally reaches 10 - 15 m, in which green (“cipollino”) and brown to black marble alternations are observed. *Karystos schists* are quarried in these horizons.

Most of the quarries are located in the areas of Aghios Dimitrios, Melissonas, Stouppaeoi, Paradissi, Aktaion (Marmari Municipality) and Kalyvia, Grambias (*Karystos Municipality*). Out of a recorded quarrying area of 1800 × 103 m², where about 75 quarrying companies are active, the 850 × 103 m² are found in Aghios Dimitrios. The main *Karystos schist* types coming from the above areas are “Green-Grey” (~ 49.5%), “Grey-Black” (~ 48%) and “Brown” (~ 2.5%). The total production of all types reaches 170000 tpa.

The following data were derived from the mineralogical - petrographic study (I.G.M.E., Mineralogy - Petrography Division) of slate samples:

- The material is the same in all the quarries and corresponds to different colour varieties of fine- to ultra fine-grained “cipollino marble” (the calcite crystals’ size is ~ 0,20 mm) with a granoblastic - lepidoblastic fabric, whose main feature is dynamic metamorphism (the secondary fabric type is protomylonitic - mylonitic).
- In all quarries, alternating horizons of various thickness occur, mainly consisting of brownish-black, brown, brownish-green and light green cipollino marble always with a banded texture, while in some sites the marble also exhibits chestnut, orange, violet and emerald-green hues.
- The mineralogical composition of the cipollino marble is as follows:
 - Calcite (main mineral), 83 - 93 % wt
 - Quartz, 1 - 6 % wt
 - Albite, 1 - 4 % wt
 - Muscovite, 2 - 5.5 % wt
 - Chlorite, 1.5 - 5.5 % wt
 - Accessory minerals: titanite, leucoxene, rutile, epidote, glaucophane, biotite, tourmaline, pyrite, iron oxides / hydroxides, organic matter, each of them at very low content ($\leq 1\%$ wt) and at various proportions.
- The colour of Karystos schists depends on their secondary and accessory minerals content. Thus, the brown or brownish-black varieties are characterized by a relatively increased organic matter and Ti-ferous materials content; the greenish ones by their marked muscovite and chlorite content; the chestnut ones by the presence of iron oxides / hydroxides; the violet contain glaucophane or Mn-ferous compounds etc.
- In some cases, layers consisting either of “common” marble or calc-mica schist are intercalated within the cipollino marble. The presence of those layers provides evidence on the composition of the initial sedimentary materials from which this marble was formed via metamorphism.
- All rocks found in the quarries have undergone dynamic metamorphism. This is evident mainly as folding tectonics, being responsible for the modification of the rocks’ initial texture and fabric, as well as for the deformation of their mineralogical constituents (microfolds, cracks, cataclastic fabric formation etc.). According to the microscopic study, the material called “ágrio” in the quarry jargon exhibits mainly cataclastic fabric (protomylonitic or mylonitic), while the so-called “strimméno” is mainly microfolded.
- The schistosity of the cipollino marble and its ability to be readily separated into slabs, hence its exploitability, depend on three basic parameters: (a) the favourable lineation and layer orientation of the sheet-silicates (muscovite, chlorite); (b) the thickness and pureness of the foliaceous banded intercalations; (c) the tectonics.

The average chemical assay of an indicative sample of cipollino marble is given below (Table 1).

Table 1. Average chemical assay of cipollino marble (% in dry substance) (*).

	SiO ₂	Al ₂ O ₃	Fe ₂ O ₃	CaO	MgO	K ₂ O	Na ₂ O	MnO	Ti	Pb	Cr	LOI
Content	7.40	1.75	1.15	47.00	0.65	0.33	0.27	0.10	<0.01	0.02	0.01	40.00

(*)I.G.M.E., Analytical Laboratories Division

3.2 Physical - mechanical properties

The natural stone properties are classified into those characterizing the material, such as the apparent density, the open porosity, the water absorption etc., and those determining the suitability of the stone for various special uses, such as the compressive strength, the flexural strength, the dynamic modulus of elasticity, the effect of thermal and/or freeze-thaw cycles on its strength, the impact strength, the abrasion resistance, etc.

The determination of the above properties was based, in general, upon the test methods specified in Standard EN 12326-2 “Slate and stone products for discontinuous roofing and cladding - Part 2: Methods of test”. Each of those properties is briefly outlined below.

3.2.1 Apparent density, kg/m³

Apparent density is the ratio between the specimen’s mass and its apparent volume (i.e. the volume of specimen’s mass plus the volume of any included voids). It is connected to the structure’s weight and provides information about the compactness of the material. The determination was based upon EN 12326-2, in combination with DIN 52102. Eighty specimens were employed.

3.2.2 Open porosity, % vol

Open porosity is the volume of the specimen’s open voids (pores), as a percentage of its apparent volume. It is mainly connected to the external use of the material under moisture conditions and provides information about its compactness, strength and toughness. The determination was based upon EN 12326-2, in combination with DIN 52102. Eighty specimens were employed.

3.2.3 Water absorption, % wt

Water absorption, a property directly related to open porosity, is the mass of water held within a saturated specimen, as a percentage of its mass. It is mainly connected to the external use of the material under moisture conditions and provides information about its compactness, strength and toughness. The determination was based upon EN 12326-2, in combination with DIN 52103. Eighty specimens were employed.

3.2.4 Dynamic modulus of elasticity, GPa

The dynamic modulus of elasticity, calculated during the flexural strength test, is a significant property when the slabs are going to be used in cladding and roofing. It gives an indication of the material’s ability to resume its initial state after the removal of a potential mechanical stress. The determination was based upon EN 12326-2, in combination with DIN 52112. Forty specimens were employed.

3.2.5 Compressive strength, MPa

Compressive strength is the ratio between the load producing the breakage of the specimen and its cross-sectional area (perpendicular to the loading direction). It is connected to the static loading capacity of the material and provides evidence on its resistance to mechanical stresses. Standard EN 12326-2 does not provide for the compressive strength determination of slates, because due to their anisotropy (schistosity plains, etc.) the relevant results are not considered reliable. This test was performed only for reasons of comparison with other ornamental stones. The determination was based upon DIN 52105. Twenty-four specimens were employed.

3.2.6 Flexural strength, MPa

Flexural strength is the ratio between the bending moment producing the breakage of the specimen and the moment of resistance developed in it. It is connected to the dynamic loading capacity of the material and provides evidence on its resistance to mechanical stresses and contributes in selecting a stone appropriate for use in cladding, roofing, stairs and paving. The determination was based upon EN 12326-2, in combination with DIN 52112. Twenty-four specimens were employed.

3.2.7 Flexural strength after freeze-thaw cycles, MPa

The determination of flexural strength after freeze-thaw cycles, simulating the ageing of the material, is significant in determining its behaviour for external applications in moist and cold climates. The strength thus obtained is compared to that corresponding to specimens having not undergone freeze-thaw cycles. The determination was based upon EN 12326-2, in combination with DIN 52104 and DIN 52112. Forty specimens were employed.

3.2.8 Flexural strength after thermal cycles, MPa

The determination of flexural strength after thermal cycles, simulating the ageing of the material, provides useful information on its behaviour when used externally in moist areas with significantly wide range of temperatures between day and night or between seasons. The strength thus obtained is compared to that corresponding to specimens having not undergone thermal cycles. The determination was based upon EN 12326-2, in combination with DIN 52204 and DIN 52112. Thirty-seven specimens were employed.

3.2.9 Abrasion resistance - Böhme, mm

Abrasion resistance is the height loss of the specimen under abrasion on the appropriate apparatus. It is connected to the differential wear and the finishing ability of the material, being decisive for selecting a stone suitable for paving and stairs. The determination was based upon EN 12326-2, in combination with DIN 52108. Twenty-four specimens were employed.

3.2.10 Impact strength, cm

Impact strength is the minimum height from which a steel ball falling on a slab of a given material causes its breakage. It is connected to the instantaneous dynamic loading capacity of the material, being significant in selecting a stone suitable for paving and stairs. The determination was based upon EN 12326-2, in combination with Italian Standard UNI-U 32.07.248.0. Twenty-four specimens were employed.

4. Statistical analysis of the tests results

4.1 Overview

The considerable number of measurements collected, made it possible to statistically evaluate them in order to calculate the relative confidence intervals for the values of the physical - mechanical properties that were determined.

The “classical” way was followed for this calculation, i.e. the Normal distribution (z-tests) has been employed for large samples ($N_x \geq 30$) and the Student t-distribution (t-tests) for small samples ($N_x < 30$). All the necessary calculations were performed by means of Microsoft® Excel.

4.2 Statistical analysis

4.2.1 Apparent density

Sample size $N_x = 80$, Mean $\bar{x} = 2716 \text{ kg/m}^3$, Standard deviation $\hat{s}_x = 16 \text{ kg/m}^3$

Confidence intervals for the population mean μ_x (z-test):

At a 90% confidence level⁽¹⁾ $\rightarrow 2713.1 \text{ kg/m}^3 < \mu_x < 2718.9 \text{ kg/m}^3$

At a 95% confidence level $\rightarrow 2712.6 \text{ kg/m}^3 < \mu_x < 2719.4 \text{ kg/m}^3$

At a 99% confidence level $\rightarrow 2711.5 \text{ kg/m}^3 < \mu_x < 2720.5 \text{ kg/m}^3$

Those data show that Karystos schists are sufficiently compact and they do not exhibit significant variation in the values of their apparent density.

4.2.2 Open porosity

Sample size $N_x = 80$, Mean $\bar{x} = 0.20 \text{ \% vol}$, Standard deviation $\hat{s}_x = 0.11 \text{ \% vol}$

Confidence intervals for the population mean μ_x (z-test):

At a 90% confidence level $\rightarrow 0.180 \text{ \% vol} < \mu_x < 0.220 \text{ \% vol}$

At a 95% confidence level $\rightarrow 0.176 \text{ \% vol} < \mu_x < 0.224 \text{ \% vol}$

At a 99% confidence level $\rightarrow 0.169 \text{ \% vol} < \mu_x < 0.231 \text{ \% vol}$

Open porosity of the Karystos schists is relatively low, thus rendering them sufficiently tough.

4.2.3 Water absorption

Sample size $N_x = 80$, Mean $\bar{x} = 0.08 \text{ \% wt}$, Standard deviation $\hat{s}_x = 0.04 \text{ \% wt}$

Confidence intervals for the population mean μ_x (z-test):

At a 90% confidence level $\rightarrow 0.072 \text{ \% wt} < \mu_x < 0.088 \text{ \% wt}$

At a 95% confidence level $\rightarrow 0.070 \text{ \% wt} < \mu_x < 0.090 \text{ \% wt}$

At a 99% confidence level $\rightarrow 0.067 \text{ \% wt} < \mu_x < 0.093 \text{ \% wt}$

The toughness of the Karystos schists is also justified by their relatively low water absorption.

4.2.4 Dynamic modulus of elasticity

Sample size $N_x = 40$, Mean $\bar{x} = 25.60 \text{ GPa}$, Standard deviation $\hat{s}_x = 10.57 \text{ GPa}$

Confidence intervals for the population mean μ_x (z-test):

At a 90% confidence level $\rightarrow 22.85 \text{ GPa} < \mu_x < 28.35 \text{ GPa}$

At a 95% confidence level $\rightarrow 22.32 \text{ GPa} < \mu_x < 28.88 \text{ GPa}$

At a 99% confidence level $\rightarrow 21.29 \text{ GPa} < \mu_x < 29.91 \text{ GPa}$

The dynamic modulus of elasticity of the Karystos schists is relatively high and justifies their satisfactory elastic mechanical behaviour.

⁽¹⁾ The term “...at an $\epsilon\%$ confidence level“ practically means that there is an $\epsilon\%$ probability for the mean μ_x of the normal population, from which the certain sample has been drawn, to be included in the relative confidence interval. Furthermore, if **100** random independent samples would be drawn from a normal population (x_1, x_2, \dots, x_n), then **ϵ out of the 100** relevant (i.e. at an $\epsilon\%$ confidence level) confidence intervals $\mathbf{a}_i < \mu_x < \mathbf{b}_i$ ($i = 1$ to 100) being calculated from the above samples will contain the mean μ_x of the population (x_1, x_2, \dots, x_n).

4.2.5 Compressive strength

Sample size $N_x = 24$, Mean $\bar{x} = 52.60$ MPa, Standard deviation $\hat{s}_x = 16.06$ MPa

Confidence intervals for the population mean μ_x (t-test):

At a 90% confidence level $\rightarrow 46.98 \text{ MPa} < \mu_x < 58.22 \text{ MPa}$

At a 95% confidence level $\rightarrow 45.82 \text{ MPa} < \mu_x < 59.38 \text{ MPa}$

At a 99% confidence level $\rightarrow 43.40 \text{ MPa} < \mu_x < 61.80 \text{ MPa}$

Due to their schistosity, the compressive strength of the Karystos schists is expectedly lower than that presented by other more homogeneous stones. Nevertheless, the measured values are satisfactory.

4.2.6 Flexural strength

Sample size $N_x = 24$, Mean $\bar{x} = 24.38$ MPa, Standard deviation $\hat{s}_x = 5.99$ MPa

Confidence intervals for the population mean μ_x (t-test):

At a 90% confidence level $\rightarrow 22.29 \text{ MPa} < \mu_x < 26.47 \text{ MPa}$

At a 95% confidence level $\rightarrow 21.85 \text{ MPa} < \mu_x < 26.91 \text{ MPa}$

At a 99% confidence level $\rightarrow 20.95 \text{ MPa} < \mu_x < 27.81 \text{ MPa}$

Flexural strength of the Karystos schists is high and the measured values do not exhibit significant variation. The very satisfactory mechanical behaviour of Karystos schists in roofing, flooring, etc. is due to this property.

4.2.7 Flexural strength after freeze-thaw cycles

Sample size $N_x = 40$, Mean $\bar{x} = 18.69$ MPa, Standard deviation $\hat{s}_x = 4.86$ MPa

Confidence intervals for the population mean μ_x (z-test):

At a 90% confidence level $\rightarrow 17.43 \text{ MPa} < \mu_x < 19.95 \text{ MPa}$

At a 95% confidence level $\rightarrow 17.19 \text{ MPa} < \mu_x < 20.19 \text{ MPa}$

At a 99% confidence level $\rightarrow 16.71 \text{ MPa} < \mu_x < 20.67 \text{ MPa}$

Though the freeze-thaw cycles test lowers slightly the flexural strength of the Karystos schists (see item 4.2.6.), it still remains sufficiently high and the measured values do not exhibit significant variation. In addition, the specimens having undergone the test do not present any deterioration or alterations. Consequently, the schists are suitable for external applications, particularly in moderately cold and moist climates as in most parts of Hellas.

4.2.8 Flexural strength after thermal cycles

Sample size $N_x = 37$, Mean $\bar{x} = 22.98$ MPa, Standard deviation $\hat{s}_x = 7.26$ MPa

Confidence intervals for the population mean μ_x (z-test):

At a 90% confidence level $\rightarrow 21.02 \text{ MPa} < \mu_x < 24.94 \text{ MPa}$

At a 95% confidence level $\rightarrow 20.64 \text{ MPa} < \mu_x < 25.32 \text{ MPa}$

At a 99% confidence level $\rightarrow 19.91 \text{ MPa} < \mu_x < 26.05 \text{ MPa}$

The effect of the thermal cycles test on the flexural strength of the Karystos schists is negligible (see item 4.2.6.), while the measured values do not exhibit significant variation. In addition, the specimens having undergone the test do not present any deterioration or alterations. Consequently, the schists are suitable for external applications, even in moist areas where the temperature variations are considerable.

Table 2: Confidence intervals for the mean μ_x of each population, at given confidence levels ϵ .

PHYSICAL - MECHANICAL PROPERTIES	CONFIDENCE INTERVALS		
	$\epsilon = 90\%$	$\epsilon = 95\%$	$\epsilon = 99\%$
Apparent density, kg/m ³	2713.1 < μ_x < 2718.9	2712.6 < μ_x < 2719.4	2711.5 < μ_x < 2720.5
Open porosity, % vol	0.180 < μ_x < 0.220	0.176 < μ_x < 0.224	0.169 < μ_x < 0.231
Water absorption, % wt	0.072 < μ_x < 0.088	0.070 < μ_x < 0.090	0.067 < μ_x < 0.093
Dynamic modulus of elasticity, GPa	22.85 < μ_x < 28.35	22.32 < μ_x < 28.88	21.29 < μ_x < 29.91
Compressive strength, MPa	46.98 < μ_x < 58.22	45.82 < μ_x < 59.38	43.40 < μ_x < 61.80
Flexural strength, MPa	22.29 < μ_x < 26.47	21.85 < μ_x < 26.91	20.95 < μ_x < 27.81
Flexural strength after freeze-thaw cycles, MPa	17.43 < μ_x < 19.95	17.19 < μ_x < 20.19	16.71 < μ_x < 20.67
Flexural strength after thermal cycles, MPa	21.02 < μ_x < 24.94	20.64 < μ_x < 25.32	19.91 < μ_x < 26.05
Abrasion resistance - Böhme, mm	2.31 < μ_x < 2.77	2.27 < μ_x < 2.81	2.17 < μ_x < 2.91
Impact strength, cm	52.6 < μ_x < 59.4	51.9 < μ_x < 60.1	50.4 < μ_x < 61.6

4.2.9 Abrasion resistance - Böhme

Sample size $N_x = 24$, Mean $\bar{x} = 2.54$ mm, Standard deviation $\hat{s}_x = 0.65$ mm

Confidence intervals for the population mean μ_x (t-test):

At a 90% confidence level \rightarrow **2.31 mm < μ_x < 2.77 mm**

At a 95% confidence level \rightarrow **2.27 mm < μ_x < 2.81 mm**

At a 99% confidence level \rightarrow **2.17 mm < μ_x < 2.91 mm**

Expressed as the (relatively low, in this case) average thickness of the material's layer abraded from each specimen during the relevant test, the abrasion resistance of the Karystos schists is high and justifies their endurance and appearance stability. The measured values do not exhibit any significant variation.

4.2.10 Impact strength

Sample size $N_x = 24$, Mean $\bar{x} = 56$ cm, Standard deviation $\hat{s}_x = 10$ cm

Confidence intervals for the population mean μ_x (t-test):

At a 90% confidence level \rightarrow **52.6 cm < μ_x < 59.4 cm**

At a 95% confidence level \rightarrow **51.9 cm < μ_x < 60.1 cm**

At a 99% confidence level \rightarrow **50.4 cm < μ_x < 61.6 cm**

Impact strength of the Karystos schists is relatively high and justifies their endurance under significant instantaneous mechanical stresses. The measured values do not exhibit any significant variation.

All the above confidence intervals for the population mean μ_x of each physical - mechanical property are summarized in Table 2, according to their corresponding confidence level ϵ .

5. Conclusions

Karystía Líthos has been widely used since archaic times in the construction of columns, monuments and other buildings of colossal ("cyclopean") dimensions for decorative, ritualistic or other

practical purposes. Those constructions date before 700 BC or before the Trojan War (~ 1300 BC) or even as early as the Neolithic Age (> 3000 BC).

Geological survey has located two horizons whose thickness occasionally reaches 10 - 15 m, in which green and brown to black marble alternations are observed. Karystos schists are quarried in these horizons. About 75 quarrying companies are active in the region. Out of a recorded quarrying area of 1800 × 103 m², the 50% is found in Aghios Dimitrios. The main Karystos schist types quarried are “Green-Grey”, “Grey-Black” and, at a lesser extent, “Brown”. The total production is about 170000 tpa.

All the slate samples examined correspond to a special marble variety (cipollino marble). Their main mineralogical constituent is calcite (85-95 % wt), while the secondary minerals are muscovite + chlorite + quartz + albite (2-5 % wt each). The accessory minerals are epidote, titanite, oxidized pyrite, iron oxides/ hydroxides, tourmaline, organic matter and Mn-ferous compounds. The colour of Karystos schists depends on their secondary and accessory minerals content.

All rocks found in the quarries have undergone dynamic metamorphism. This is evident mainly as folding tectonics, being responsible for the disturbance of the rocks texture and fabric, as well as for the deformation of their mineralogical constituents (microfolds, cracks, cataclastic fabric formation etc.).

The exploitability of cipollino marble relates with its schistosity and its ability to be readily separated into slabs, depending on three basic parameters: (a) the favourable lineation and layer orientation of the sheet-silicates (muscovite, chlorite); (b) the thickness and pureness of the foliaceous banded intercalations; (c) the tectonics.

Karystos schists are compact and tough. They present low water absorption and open porosity.

The values of mechanical properties determined for Karystos schists are much higher than the minimum acceptable for ornamental stones.

Abrasion resistance and impact strength of Karystos schists justify their endurance.

The absence of any deterioration or alterations from the Karystos schists specimens after “environmental” testing (freeze-thaw and thermal cycles) and the slight to negligible effect observed on their flexural strength, render Karystos schists suitable for external applications under various climatic conditions.

The physical - mechanical properties of Karystía Lithos (commercially “Karystos schists”), on which its endurance through time and under mechanical stresses is depending, as well as its aesthetics resulting from its mineralogical composition, render it an attractive structural ornamental stone with a wide range of applications to-date, thus confirming and justifying the timelessness in its use.

6. References

- Himmelblau, D. M. 1970. *Process Analysis by Statistical Methods*, Sterling Swift Publishing Co., Texas, 1970.
- Laskaridis, K., Papaioannou, N., Kousseris, I. 2002. *Mapping and Recording of the Karystos Schists Exploitable Reserves*, Final Report, I.G.M.E., LITHOS Laboratory, Athens, May 2002 (in Hellenic).
- Mastrapas, A. 1999. *Topography of the Ancient Athens monuments*, Kardamitsas Editions, 2nd Ed. Updated, Athens, 1999 (Historical data in “2.2. City of Athens” - in Hellenic).
- Patronis, M. 2002. *Application of Statistical Analysis Methods for Evaluating the Physical Mechanical Properties Determination Tests Results of Karystos Schists*, I.G.M.E., LITHOS Laboratory, Athens, May 2002 (in Hellenic).
- Spiegel, M. R. (Author), Lindstrom, D. P. (Editor) 2000. *Statistics, Schaum's Easy Outlines*, McGraw - Hill, 2000.
- Web Site. <http://www.galaxy.gr/drakospita-01.htm> (Historical data in “2.1. Euboea Island” - in Hellenic).

A CASE STUDY OF DIFFERENT LIMESTONES DURING QUICK LIME AND SLAKED-LIME PRODUCTION

Leontakianakos G.¹, Baziotis I.², Ekonomou, G.³, Delagrammatikas, G.¹, Galbenis, C.T.¹ and Tsimas, S.¹

¹ National Technical University of Athens, School of Chemical Engineering, Laboratory of Inorganic and Analytical Chemistry, 9 Heroon Polytechniou Str., Zografou Campus, 15773, Athens, Greece, gleontakianakos@yahoo.gr

² National Technical University of Athens, School of Mining and Metallurgical Engineering, Department of Geological Sciences, 9 Heroon Polytechniou Str., Zografou Campus, 15773, Athens, Greece, baziotis@metal.ntua.gr

³ Institute of Geological and Mineral Exploration, Department of Mineralogy-Petrography, Spirou Loui Str., Acharnae, 13677, Athens, Greece

Abstract

We have examined 5 different limestones in order to study their behavior i) during calcination at different temperatures (900, 1050 and 1200°C for 30 min) and ii) after hydration of quick limes derived to slaked lime. Quick limes calcined at 900°C show the lower reactivity values. This could be related to the low calcination temperature or to the short calcination time of 30 min which was unable to produce enough lime. The samples calcined at temperatures of 1200°C are less reactive compared to the hydrated limes which were prepared by hydration of quick lime calcined at 1050°C, indicating by parameters such as the $(CaO+MgO)_{Lime}$, the time required to become the temperature maximum and the reactivity rate. These, probably could be due to crystal growth at relative high temperatures.

Key words: Quick lime, calcination temperature, reactivity, hydration.

1. Introduction

Limestones and their varieties represent the most frequently used rocks in industry and are included among the thirty more important raw materials. Carbonate rocks mainly consisted by carbonate minerals of calcium and magnesium (calcite, dolomite, magnesite)(e.g. Oates 1998). The industrial limestones in the world economic market possess the 11th place depending on their value (apart from the industry of cement where they possess 5th place).

In the industry, the more important chemical property of limestones is their calcination due to the following reaction:

$CaCO_3(s) \rightarrow CaO(s) + CO_2(g)$. This reaction is endothermic occurred at very high temperatures (>900°C); in closed systems is highly influenced by the partial pressure of the gas phase (P_{CO_2}). The theoretical dissociation temperatures of $CaCO_3$ to produce lime is around 900°C whereas those of the $MgCO_3$ ranging from 402 to 550°C (e.g. Boynton, 1980; Schwarzkopf, 1994; Moffat and Walmesley, 2004). Thus, the temperature required for calcination process of limestone is not constant and

depends on various factors; the $\text{CaCO}_3/\text{MgCO}_3$ ratio is one of them, also differences on crystallinity (grain size) and the heat rate could also play a significant role in the final quality of the resulted lime (Ar and Dögu 2001).

Another important process is the slaked lime production through the exothermic reaction $\text{CaO(s)} + \text{H}_2\text{O(l)} \rightarrow \text{Ca(OH)}_2\text{(aq)}$. In multivariable systems, relative high MgO content could also react with water to earlier form $\text{Mg(OH)}_2\text{(aq)}$. Both reactions increase the maximum temperature on the added water influencing the observed reactivity values. So, it is important to check the MgO behaviour in such systems. According to various authors, reactivity of lime depends on the presence of admixtures in the used limestones; in particular admixtures like MgO lower the reactivity (Potgieter et al. 2003). As a consequence, the higher the amount of MgO, the lower the lime reactivity reducing the maximum hydration temperature and increasing the hydration time. Another factor that influences the hydration process is the initial temperature of the added water (Boynton 1980). An increase in the initial temperature of the water used for hydration of the lime increases the rate of the hydration reaction due to faster dissolution of the CaO particles.

The aim of this paper is to analyze the physicochemical properties of the studied limestones testing their influence in the quality of lime. Additionally, three datasets, arise from the three different calcination temperatures (at 900, 1050 and 1200°C), of hydrated limes are studied in terms of reactivity changes.

2. Experimental Work-Analytical Methods

Five samples (K1, A2, T3, T4, T5) of limestones from different quarries from Greece were collected for this study. Limestone particles were reacted in a pre-heated oven at three different temperatures (900, 1050 and 1200°C) for 30 min in order to produce lime. The tests were done by heating a 200 g sample of a specific particle size (1.6-2 cm) at the required temperature. Subsequently, 25 gr of the produced lime were hydrated by adding distilled water to produce Ca(OH)_2 through the reaction $\text{CaO(s)} + \text{H}_2\text{O(l)} \rightarrow \text{Ca(OH)}_2\text{(aq)}$. This reaction is highly exothermic, increasing the temperature of the added water. We measured the temperature difference in the water until a maximum value is reached; this value represents the reactivity of the produced slaked lime.

Chemical composition of each limestone was carried out using atomic absorption spectroscopy (AAS) method. We used an Perkin Elmer 3300 spectrometer at the Department of Chemical Engineering, National Technical University of Athens. The mineral chemical analysis of limestone and lime was performed using a JEOL JSM-5600 scanning electron microscope (SEM) at the Institute of Geology and Mineral exploration. The operating conditions were: 15 kV, 5 nA, data acquisition time 100 s and beam diameter 4-8. All samples were measured with energy dispersive system (EDS).

Raman micro-spectroscopy and X-ray diffraction methods were applied in order to identify the carbonate phases (calcite and dolomite) in the studied limestones. Analyses were performed using a Renishaw confocal RM1000B Raman Microprobe and a Siemens D-500 with a graphite crystal monochromator. Raman spectra were excited at room temperature using the 632.817 nm line of the He-Ne laser. The spot at the surface of the sample is about 5 μm using a 100 \times objective with laser power < 5 mW. The diffraction interval was between 2° and 50° 2 θ with a narrow 0.02° step. Raman micro-spectrometer is based at the Department of Geosciences of the National Technical University of Athens and the X-ray diffractometer at the Institute of Geology and Mineral exploration. The modal percentage of each mineral (calcite, aragonite, magnesite, dolomite, others) in 5 limestones was calculated applying a quantitative XRD method. Confirmation of the quality of the XRD results

Table 1. Major element compositions and mineral modes of the studied limestones.

Sample	K1	A2	T3	T4	T5
SiO ₂	0.89	1.21	1.10	0.85	0.99
Al ₂ O ₃	0.38	0.58	0.36	0.33	0.35
FeO	0.20	0.51	0.25	0.08	0.65
MgO	0.61	5.53	5.17	0.36	2.17
CaO	53.20	46.82	48.76	54.17	50.54
Na ₂ O	0.22	0.31	0.25	0.25	0.25
K ₂ O	0.21	0.12	0.12	0.08	0.08
H ₂ O	0.27	0.43	0.18	0.23	0.40
CO ₂	44.00	44.12	44.45	44.35	44.55
Total	99.98	99.63	100.64	100.70	99.98
Calcite	95%	75%	80%	98%	90%
Dolomite	3%	20%	15%	-	8%
Albite	<2%	3%	<2%	<2%	<2%
Quartz	-	<2%	<2%	-	-

-: Only in trace amounts.

Table 2. Chemical composition of the resulted lime at three different calcination temperatures.

at 900°C					
Sample	K1	A2	T3	T4	T5
CaCO ₃	48.1	50.86	47.17	46.76	45.07
MgCO ₃	-	0.52	-	-	-
CaO	11.2	-	7.65	14.34	14.19
MgO	0.71	5.45	5.8	0.4	2.58
CO ₂	37.75	40.18	37.02	36.7	35.37
Other	2.24	2.99	2.35	1.79	2.78
Total	100	100	99.99	99.99	99.99
at 1050°C					
Sample	K1	A2	T3	T4	T5
CaCO ₃	14.73	21.06	7.33	4.29	4.57
MgCO ₃	-	-	-	-	-
CaO	69.41	49.37	74.17	88.95	84.18
MgO	1.04	8.71	9.07	0.62	3.69
CO ₂	11.56	16.53	5.75	3.37	3.59
Other	3.26	4.33	3.67	2.77	3.98
Total	100	100	99.99	100	100.01
at 1200°C					
Sample	K1	A2	T3	T4	T5
CaCO ₃	12.01	21.59	5.4	1.5	2.46
MgCO ₃	-	-	-	-	-
CaO	74.18	48.13	77.52	93.83	87.4
MgO	1.06	8.9	9.14	0.64	3.95
CO ₂	9.42	16.95	4.24	1.17	1.93
Other	3.33	4.42	3.7	2.85	4.25
Total	100	99.99	100	99.99	99.99

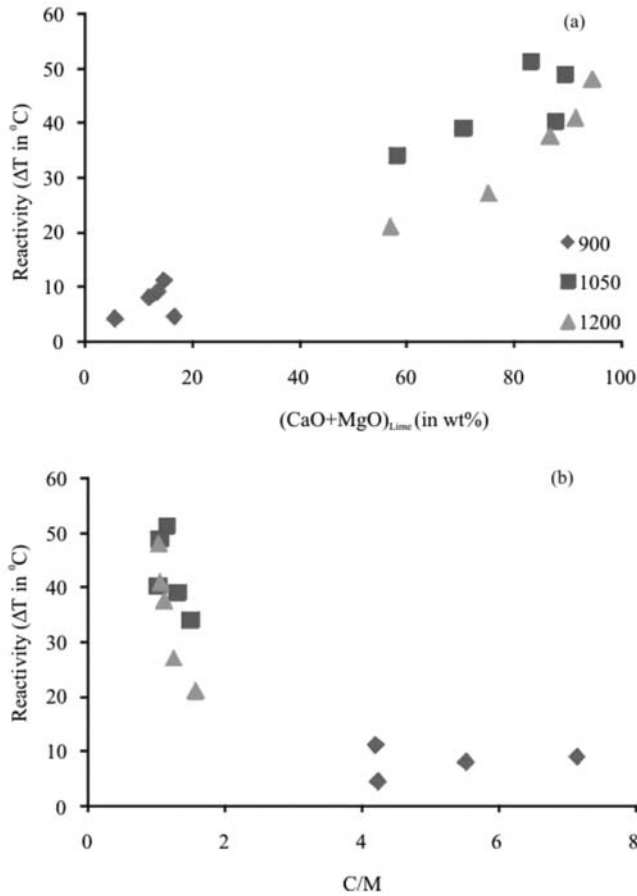


Fig. 1: Variations of Reactivity against (a) $(CaO+MgO)_{Lime}$ and (b) C/M ratio. C/M is expressed as $(CaO_{Rock} \cdot MgO_{Lime}) / (CaO_{Lime} \cdot MgO_{Rock})$.

was established using Raman micro-spectroscopy. Representative whole-rock limestone and lime compositions and mineral mode results are summarized in Table 1 and 2, respectively.

3. Results and Discussion

The reactivity represents a factor that characterizes the quality of the used lime. According to literature, the lower calcination temperature, the higher the reactivity value and the higher the quality of the resulted lime (e.g. Moropoulou et al. 2001). However, our results indicate an inversion of such process at low temperature side. In particular, the 900°C calcinated samples show the lower values of reactivity. An increase in calcination temperature (at 1050°C) indicates a switching in the reactivity behavior and become maximum for all of the studied samples. We construct bivariate plots of reactivity against $(CaO+MgO)_{Lime}$ and $CaO_{Rock}/CaO_{Lime} / MgO_{Rock}/MgO_{Lime} = (CaO_{Rock} \cdot MgO_{Lime}) / (CaO_{Lime} \cdot MgO_{Rock})$ (denoted here as C/M) in order to check, consistent or not, trends of reactivity with composition of limestone or lime. In figure 1a, we observe a systematic increase of reactivity with increasing $(CaO+MgO)_{Lime}$ for all of the calcined samples; however, for a given $(CaO+MgO)_{Lime}$ content, the reactivity is higher in the 1050°C calcined samples indicating that the optimal reactiv-

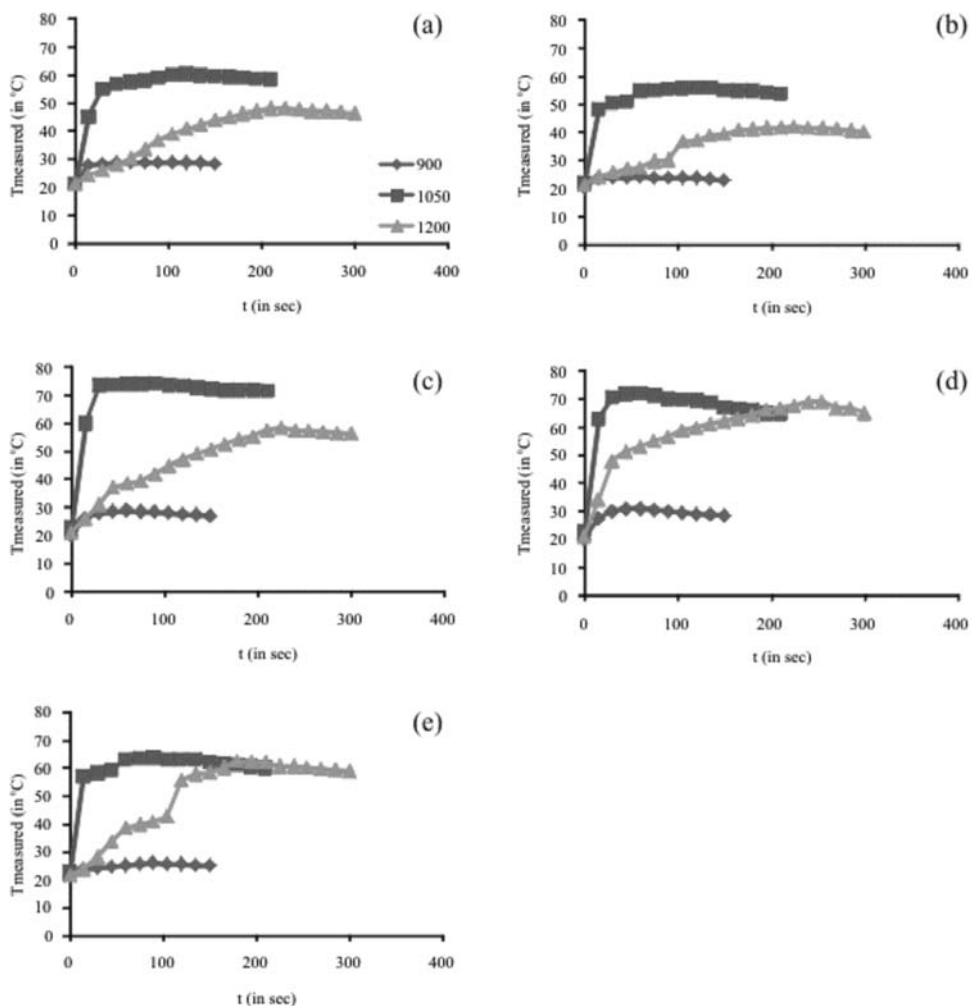


Fig. 2: (a-e) T_{measured} vs time plots showing temperature rise during hydration of quick lime at the three calcination temperatures (900, 1050 and 1200°C). Samples (a) K1, (b) A2, (c) T3, (d) T4 and (e) T5.

ity is observed at 1050°C, perhaps due to hard-burnt phenomena or densification of the quick lime structure at higher temperatures (e.g. Shin et al., 2009). A close inspection of the figure 1b, shows a systematic increase of reactivity with decreasing C/M ratio for the 1050 and 1200°C calcined samples; in oppose, the samples calcined at 900°C show a relative constant reactivity value for decreasing C/M ratios. Regarding that the CaO and MgO in limestone are constant, then the $(\text{MgO}/\text{CaO})_{\text{Lime}}$ ratio could play a potential role in reactivity behavior. Moreover, the low constant values for the samples calcined at 900°C indicates that probably the calcination temperature was rather too low or the calcination time of 30 min was too short to produce enough lime.

The Figure 2 (a-e) shows the temperature rise vs. hydration time of quick lime at temperature 900, 1050 and 1200°C for the studied samples. The limestones calcined at 1050°C shows the maximum temperature rise; at lower/higher calcination temperature the temperature rise is lower. The temper-

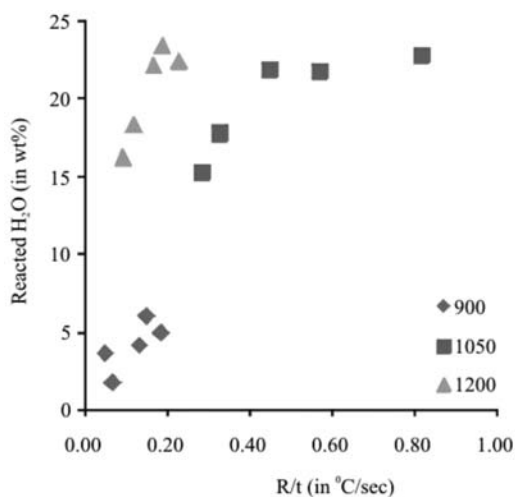


Fig. 3: Variation of reactivity rate of quick limes against the H₂O reacted with the calcined samples at various temperatures.

ature rise of the 1200°C calcined limestone was lower than that of the 1050°C and also the time required for hydration was expanded at later stage. These results confirm that quick limes calcined at temperature of 1050°C have the highest reactivity for hydration and also that the quick lime calcined at 1200°C is less reactive probably due to larger grain size (grain growth during temperature increase) and lower porosity (denser structure). Shin et al., (2009) suggested the temperature of 1100°C as the optimum calcination temperature for the highest reactivity values with the largest specific area. At this temperature seems to formed a lot of pores due to dissociation of carbonates, whereas quick limes calcined at lower temperatures (900 and 1000°C) tend to have less pores and minimum specific surface area due to incomplete lime production and remnants of the original limestone (as we observe in a previous paragraph); at calcination temperatures >1200°C the structure become more dense and compact and the grains become larger leading to minimization of the existing pores so the hydration process itself cannot entirely proceed into the interior mass of the quick lime also requiring more time to accomplished.

The MgO content plays an important role in reactivity rate of the lime due to earlier decompose of MgCO₃ to MgO producing hard burnt samples. As we previously state, the higher the amount of MgO, the lower the lime reactivity reducing the maximum hydration temperature and increasing the hydration time. Besides, in case of non-hard burnt samples, MgO content when it's low in concentration (lower than 2-3 wt%) could accelerate the hydration rate of the unslaked lime. (Potgieter et al., 2003). Three of the studied limestones share a common feature with high MgO content ranging from 2.17-5.53 wt% (samples A2, T3 and T5). These samples also possess the higher MgO content during calcination, thus the quick limes formed by this process also have high MgO content. In practice, the MgO vs. reactivity rate are inversed correlated with the samples calcined at 1200°C share a common, low reactivity rate, with those calcined at 900°C.

To visualize better the hydration process we compare the H₂O that reacted with the free lime against the reactivity rate. Reactivity values are divided by the time required for the T_{max} giving the reactivity rate. Figure 3 shows that at constant reactivity rate values the water needed to complete hydration is lower; for example, the quick lime calcined at temperature of 1050°C need much less

water for hydration relative to the respective samples at 1200°C. Also, the slope of the curve for the samples calcined at 1200°C is steeper compared to the one for lower calcination temperature. Concluding, the higher the reactivity rate the better quality of slaked lime.

4. Conclusions

The results on the behaviour of quick- and slaked- lime are summarized in the following:

- The samples calcined at temperatures of 1050°C have the higher reactivity values.
- The MgO content is not a significant factor on the control of the reactivity; instead the hard-burned effect and the structure of the original limestone and the resulted quick lime are more important. However, the $(\text{CaO}/\text{MgO})_{\text{Lime}}$ ratio plays a potential role, increasing the reactivity of the quick lime.
- For a constant reactivity rate the water required for hydration is lesser for the samples calcined at 1050°C compared to those calcined at 1200°C.

5. Acknowledgments

Sincere thanks are due to Onassis Foundation for the financial support to G. Leontakianakos.

6. References

- Ar, I. and Dögu, G., 2001. Calcination kinetics of high purity limestones. *Chemical Engineering Journal*, 83, 131-137.
- Boynton, R.S., 1980. *Chemistry and Technology of Lime and Limestone* (2nd ed.), New York, Wiley, 5 – 33, 132 -164, 592pp.
- Moffat, W. and Walmsley, M.R.W., 2004. Improving Energy Efficiency of a Lime Kiln. *Proceedings of Joint SCENZ/FEANZ/SMNZI Conference*, Hamilton, 17-24.
- Moropoulou, A., Bakolas, A. and Aggelakopoulou, E., 2001. The effects of limestone characteristics and calcination temperature to the reactivity of the quicklime. *Cement and Concrete Research*, 31, 633-639.
- Oates, J. A. H., 1998. *Lime and Limestone. Chemistry and Technology, Production and Uses*. Wiley – VCH, Weinheim, 9 – 62, 117 - 250.
- Potgieter, J.H., Potgieter, S.S. and DeWaal, D., 2003. An empirical study of factors influencing lime slaking Part II: lime constituents and water composition. *Water SA* 29 (2), 157–160.
- Schwarzkopf, F., 1994. *Lime Burning Technology – a manual for lime plant operators* (3rd ed.). Svedala Industries Kennedy, Van Saun.
- Shin, H.G., Kim, H., Kim, Y.N. and Lee, H.S., 2009. Effect of reactivity of quick lime on the properties of hydrated lime sorbent for SO₂ removal. *Journal of Materials Science and Technology*, 25 (3), 329-332.

METHODOLOGY FOR OPTIMAL DETERMINATION OF NEW DRILLING PROGRAM IN AN ACTIVE OPEN PIT: EXAMPLE FROM AN ACTIVE SULFATE OPEN PIT IN ALTSI, LASITHI PREFECTURE, EASTERN CRETE

Manoutsoglou E.¹, Panagopoulos G.¹, Spyridonos E.² and Georgiou A.³

¹ Technical University of Crete, Department of Mineral Resources Engineering, Research Unit of Geology,
731 00 Chania, Greece, emanout@mred.tuc.gr, gpanag@mred.tuc.gr

² National and Kapodistrian University of Athens, Faculty of Geology and Geoenvironment,
vangelis@zedat.fu-berlin.de

³ TITAN Cement S.A., egeorgiou@titan.gr

Abstract

For the cement industry the minerals gypsum and anhydrite, due to their similar chemical composition, are of the same importance. In cement production line, the energy requirements for grinding anhydrite are different from that of gypsum. Occasionally, the difference in mechanical properties of the extreme members (anhydrite / stiff - gypsum / brittle) can cause problems during grinding procedure. For these reasons it is necessary to be aware of the spatial distribution of these rocks in an active open pit. This knowledge, because of its strict connection with the calculation of the reserves (geological and recoverable), contributes to the direct production planning of the open pit and to the medium and long term planning as well. In order to approach the spatial distribution of sulphate rocks in the active gypsum open pit of INTERBETON S.A. in Altsi (Sitia region, Eastern Crete), new exploration boreholes were drilled. The proposed methodology concerning the determination of the new borehole locations consists of two steps. In the first step detailed geological mapping of the surface sulphate rocks is conducted and in the second step a three-dimensional geological model is constructed. The model's construction is based on data derived from a past drilling program. Those data were enriched with the results of geochemical analysis of 100 new surface samples. The surface samples were taken by means of Wagon Drill accordingly to a predefined grid. Five different drilling scenarios were proposed, contributing to the determination of the optimal drilling program.

Key words: 3D Geological Modelling, Active Open Pit, Sulfate Deposits, Optimal Drilling Program.

1. Introduction

In cement industry, calcium sulfate (either in the form of gypsum or anhydrite), is one of the ingredients of Portland cement which increases the time needed for the setting of cement. But, the difference in stiffness of anhydrite and gypsum can cause problems in crushing and grinding procedure in the open pit. The stiffness of Anhydrite is 3-3.5 in Mohs scale, while for gypsum it is 1.5-2. It is known that gypsum is dehydrated and is transformed to anhydrite as a consequence of geological burial. On the contrary, anhydrite is transformed to gypsum when it comes in contact with fluids during exhumation. These two minerals, are common minerals in evaporitic sequences. Evaporites are

deposits which are created by salt precipitation from aqueous solutions during solar evaporation. The precipitation begins when the aqueous solution's salt concentration exceeds 50‰ (brine). If the brine is saturated in SO_4^{2-} and Ca^{+2} gypsum or anhydrite is formed. These two forms of calcium sulfate usually transit to each other (Warren, 2006).

The knowledge of the quantitative spatial distribution of these two extreme members is essential both for the immediate and the long term programming of the development of the active gypsum open pit in Altsi, Eastern Crete, where INTERBETON S.A. operates. In this study the combination of several methodologies aiming to the determination of the new exploration drilling program in the active open pit is presented. The results of this drilling program are substantial for the accomplishment of the objective.

2. Geological setting

Permian/Triassic evaporites form almost 35% of the global evaporite deposits. In that period palaeogeography and climate produced favourable circumstances for evaporite formation, which reached a peak during Triassic. After the formation of Pangea and the drop of sea level, the marginal basins became shallower and a large number of endocraton basins were created. During Permian, the climate became even more arid, contributing to the increase of evaporation's rate (Trappe, 2000). Evaporites of Extrenal Hellenides comprise a part of the Permian/Triassic evaporitic layers which were formed around Pangea. Evaporites are regarded as the first Alpine deposits of Paxos and Ionian isopic zones. This conclusion is based on field observations, compounded with existing drilling data. Their age is Permian/Triassic, but there are observations of evaporitic intercalations within limestones of lower Liasic and Cretaceous age, as well. Their maximum thickness varies from 1500m to 3000m (Nikolaou, 1986).

The island of Crete exhibits several sulfate outcrops. Many of them were characterized as exploitable deposits and some are still regarded as significant deposits both quantitative and qualitative. Those deposits are discriminated according to their time of genesis in Permian/Triassic and Neogene. The main characteristic of Neogene deposits is the exclusive existence of dihydrate form of calcium sulphate ($\text{CaSO}_4 \cdot 2\text{H}_2\text{O}$) related to the "salinity crisis" or "Messinian event", which affected the whole Mediterranean area during Messinian. (Kanaris, 1989). On the contrary, Permian/Triassic deposits exhibit the two main forms of calcium sulfate: gypsum ($\text{CaSO}_4 \cdot 2\text{H}_2\text{O}$) and anhydrite (CaSO_4) (Raulin, 1869; Cayeux, 1902; Papastamatiou, 1958; Fytrolakis, 1980; Antoniou, 1987). Deposits of Permian/Triassic age are all over the island. One of the most significant is that of Altsi in Eastern Crete. Its extent is 1.25 km² and is an exploitable mineral resource. It is placed above the lower layers of the metamorphic Phyllitic Nappe and it is surrounded by multi-folded schists, which belong to the same nappe, and by younger sediments as well (Kanaris, 1989).

3. Methods

The methodologies followed include field and computational work. In the first stage of our study, all existing data were digitized in order to construct a preliminary three dimensional model of the sulfate deposits of the open pit. Planning of the field works was based on this preliminary 3D model. Results of geological mapping of the open pit's slopes (scale 1:500) and the petrographical study of representative sulfate samples were integrated into the 3D model. Finally, the model was used to formulate alternative scenarios for exploration drilling programs. The aim of this work was to achieve maximum information about the spatial distribution of gypsum and anhydrite in the quarry, while minimizing the cost of the drilling program.

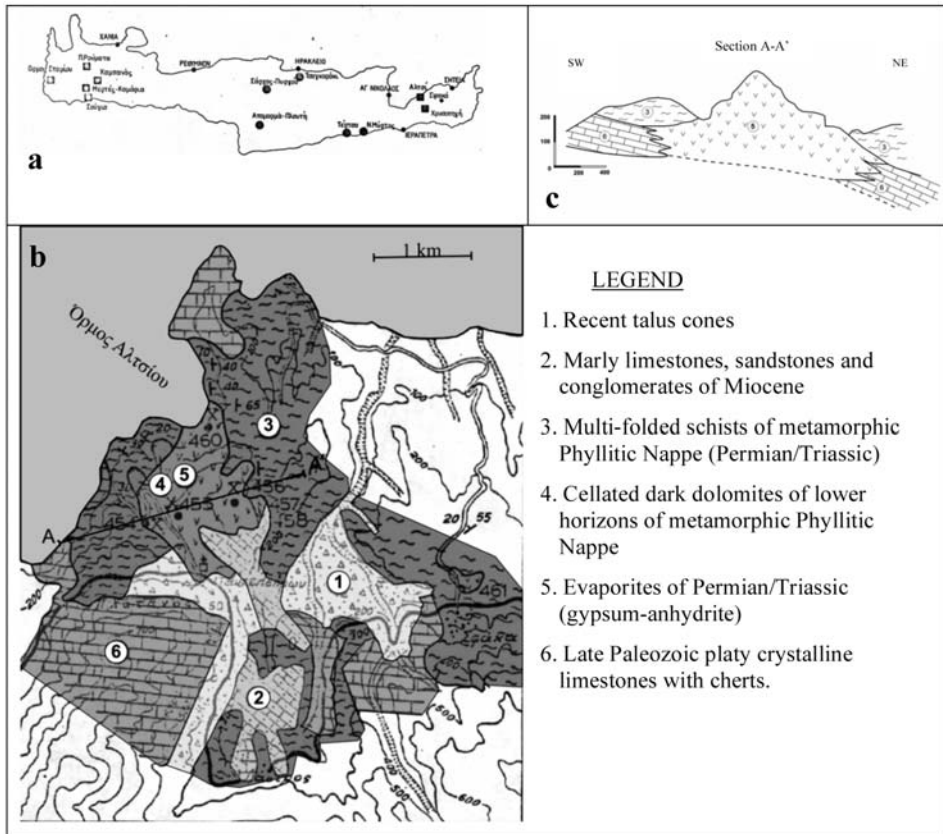


Fig. 1: (left): a) Deposits of Permian/Triassic age (squares) and Neogene age (circles) in Crete island. b), c) Geological map and section of the area where gypsum-anhydrite deposit is located. (after Kanaris, 1989).

3.1 Geological mapping

During geological mapping in scale 1:500, all the geological features observed on the pit's slopes were mapped. According to this mapping, the sulfate deposit of Altsi consists of seven different lithological units. These units are the schists of the bedrock, the light-colored sulfates with dolomitic segments, the light-colored sulfates with dark laminas, the dolomites, the anhydrites, the soft gypsums and the stiff gypsums.

In particular, the light grey sulfates host dark dolomitic fragments of centimeters in size. The light-colored sulfates with dark laminas are white to white ash with dark to light grey laminas. The mineralogical composition of laminas can be either dolomitic or magnesitic or even sulfate. The soft gypsum is white to white ash without any calcitic inclusion. All the above three units are brittle, while the white to white ash coarse crystalline gypsum is rather massive. The hardest sulfate unit is anhydrite. It is coarse crystalline dark grey and often contains dolomitic fragments. The dark dolomites are always observed in the open pit area as fragments of centimeter to meter in size, which are hosted in sulfate formations and never as a distinct layer. The schists belong to Phyllite Nappe (after Dornsiepen et al., 2001) and surround all the aforementioned units. The schists present reddish colour close to their contact with the sulphate deposit.

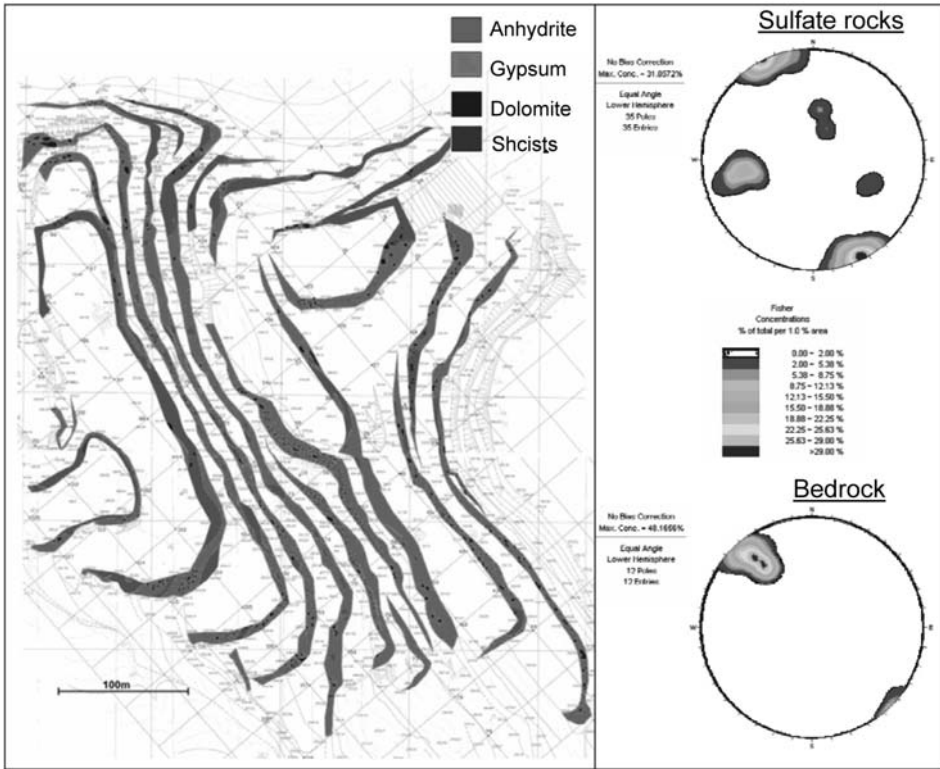


Fig. 2: Geological map of the pit area which depicts the four lithological units. It is also shown two stereonet concerning fault planes' orientation both in the sulphate rocks and the bedrock.

Initially, these units were separated by their macroscopic characteristics. Later, representative samples were taken from each lithological unit and were analyzed geochemically. Lithological units that had similar mineralogical composition were grouped in order to simplify the geological map. This fact resulted in the generation of a new geological map (Fig. 2) distinguishing four lithological units. These are gypsum, anhydrite, dolomite and schist.

The geological map of Figure 2 shows the surface distribution of gypsum and anhydrite on the slopes of the open pit. It is concluded that gypsum outcrops cover the larger area of the pit, while anhydrite outcrops exist in the northern and western part. The dolomitic segments are dispersed throughout the open pit, having size of centimeter to meter. The size and the frequency in appearance of dolomitic segments increase towards the upper levels of the eastern part. The bedrock is observed in the lower level of the pit.

In order to understand the structural regime of the area where the open pit is located, fault planes' orientation measurements were conducted in both the sulfate deposits of the pit and the bedrock. In figure 2 are shown the two major tectonic systems. The first one has an ENE-WSW orientation with almost vertical dip (85°-90°) which is observed in both the sulfate rocks and the bedrock. The second one has an NNW-SSE orientation with 65° dipping angle towards the WSW occurring only in the sulfate rocks.

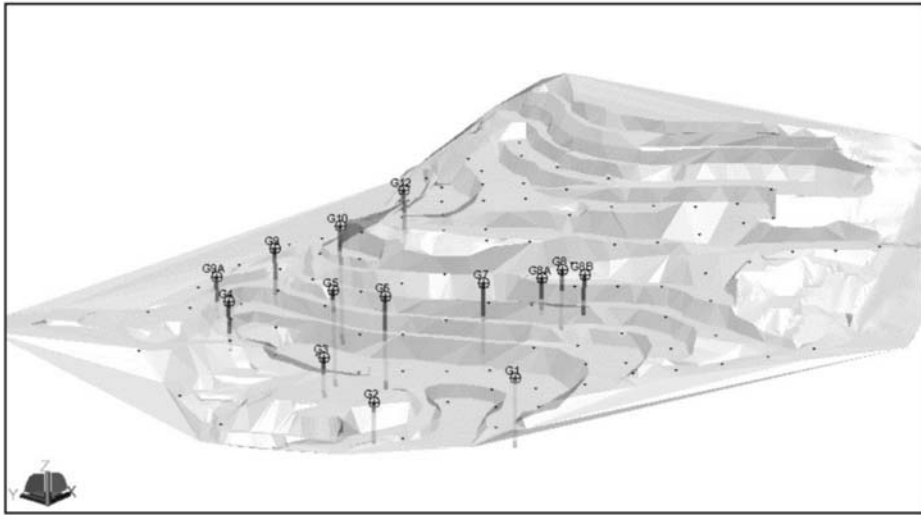


Fig. 3: Digital terrain model of the Altsi Open Pit (transparent), with existing exploration drillholes and surface sampling locations.

3.2 3D Geological modelling

Computer-aided deposit modelling comprises the generation of a geometric model, a property model, as well as a mine model. A more detailed description of the modeling process in mining can be found in Prissang et al. (1996; 1999). In the model which was set up for this study, the following data were integrated (Fig. 3): a) digital terrain models of the pit surface and the future final exploitation surface area, b) results of the geochemical analysis of 100 surface spot samples located on a 40m orthogonal raster and c) 255 samples of drilling cores with an average length of 3m each, from exploration drillholes (843m total length). The drillholes were conducted by the company in 1982, whereas the spot sampling took place during this study. The interpretation of all the geochemical data was the base of the lithological description. The latter was processed with the Surpac Vision mining software package in order to setup the model.

3.3 Geostatistical Structure Analysis

A geostatistical structure analysis was carried out to investigate the spatial correlation of the grade values concerning CaSO_4 and $\text{CaSO}_4 \cdot 2\text{H}_2\text{O}$. These spatial correlation structures can be interpreted as the results of the formation process of the deposit. Empirical variograms indicating the presence of a spatial correlation have been calculated for these parameters. By calculating variograms for the two parameters, anisotropy ellipsoids for the spatial correlation of the grades could be modeled (Table 1). The best variograms were obtained in the vertical direction (Fig. 4).

3.4 Property Modelling

The objective of property modelling is to provide predictions of the spatial distribution of grade values within the deposit. This covers discretisation of the geological body under consideration, grade estimations as well as reliability checks of the results.

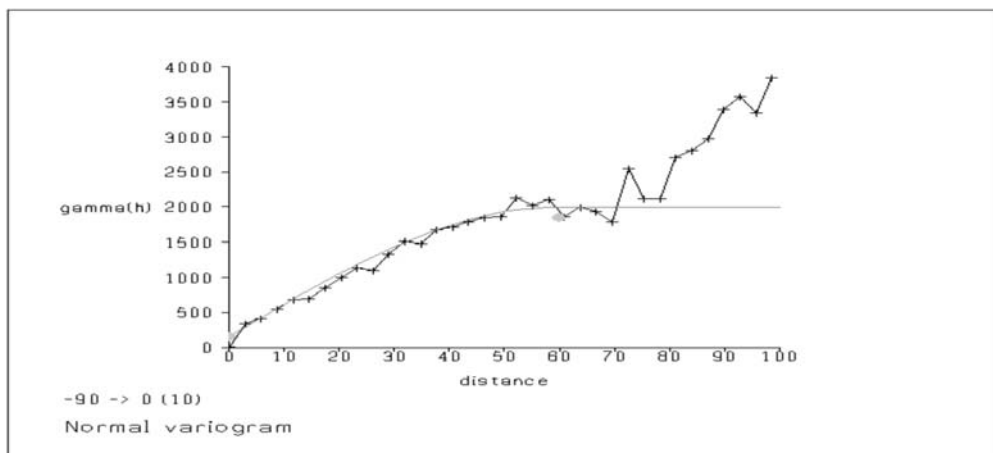


Fig. 4: Variogramm for gypsum in the vertical direction.

Table 1. Parameters of the 3-axis anisotropy ellipsoids for gypsum and anhydrite.

Parameter	Gypsum	Anhydrite
Direction/Dip of major Axis	N190/04	N190/-20
Major axis rotation	0	0
Major / Semi-major axis	1,27	1,05
Major / minor axis	2,10	3,33
Maximum Range	110 m	130 m
Vertical range	40 m	60 m
C (nugget)	60	20
Sill	810	970

3.5 Spatial Discretization

The representation of the spatial distribution of grade values required the subdivision of the gypsum/anhydrite body into cells. From the point of view of the planning engineer, a block size 3.5m x 3.5m x 15m, matching the size of future extraction units (i.e. blasting blocks), was considered as sufficient. For each block, the grade values had to be computed.

3.6 Grade Estimation

The grades for gypsum and anhydrite for the blocks were calculated by the Ordinary Kriging Method. The variogram models described in Table 9 were used during the estimation, and the anisotropy ellipsoids were also used as search ellipsoids for the estimation procedure. The applied parameters were crossvalidated on the sampling location, to check for possible bias on the estimation results. The estimation error distribution for anhydrite shown on Figure 5 indicates that no bias is inserted in the estimations. The results for gypsum are similar.

The estimated concentrations for gypsum can be seen on Figure 6.

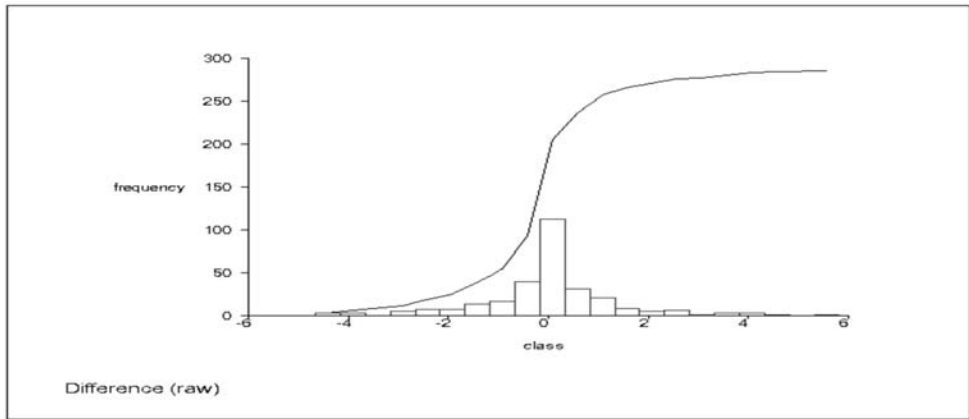


Fig. 5: Estimation error (measured – estimated) for the anhydrite concentrations.

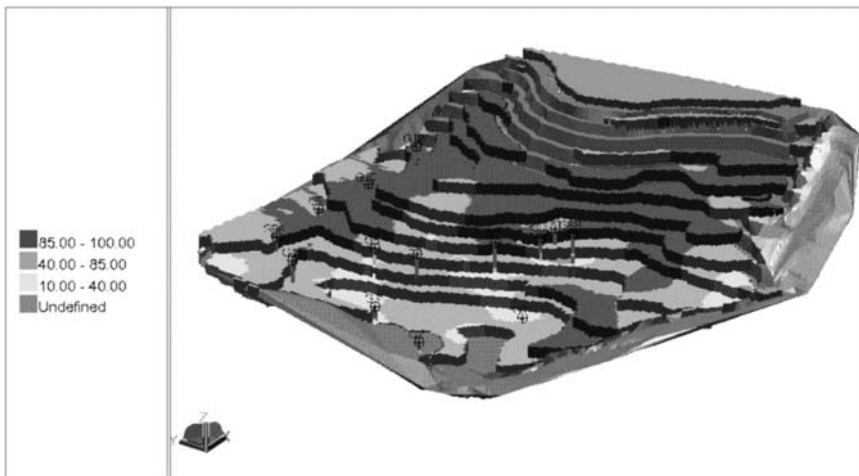


Fig. 6: Block model of the Altsi Open Pit with estimated gypsum values.

4. Conclusions-Results

In order to improve further the precision of the outcomes, 5 exploration scenarios are proposed. Results from the old exploration drillholes and from surface sampling are combined in these scenarios. The usual total depth for each sampling position is 25 m (unless it is stated as less) and the length of each separate sample is 3 m. This option is proposed in order to increase the density of the known spatial information without increasing the total cost of the project. All the proposed scenarios focus on the areas where there is lack of samples/data and, in addition, appear to have the maximum thickness of recoverable material. The drillholes' maximum depths don't exceed the designed final excavation depth of the open pit. As the variogram's vertical range is 40 m for the anhydrite and 60 m for the gypsum, drillholes can be limited at a higher elevation. Regarding the assessment of the spatial distribution of the qualities in the pit, based on the results of the structural geostatistical analysis and, in specific, the 60 m range for the gypsum and the more than 40 m range for the

anhydrite in the horizontal dimension, the distance between the drillholes is approximately 120 m apart. The distance is the same between the new and the existing drillholes. This option contributes to the maximum coverage of the pit's surface area.

From another point of view, if the aim is focused solely on the improvement of the assessment's precision, then some of the new drillholes must be located in a distance of 40 m from the existing ones and between them. This option contributes to the calculation of new variograms and to the redetermination of the anisotropy's ellipsoid.

Because of the fact that the two aforementioned options have different purposes, different scenarios are proposed. All of them maintain the research's cost in acceptable level. These are:

Exploration scenario 1: 5 drillholes, with a total length of 250 m, or 4 drillholes, with a total length of 280 m

Exploration scenario 2: 3 drillholes, of 194 m in total length

Exploration scenario 3: 2 drillholes, of 120m in total length and 19 additional surface samplings

Exploration scenario 4: 37 surface samplings

Exploration scenario 5: 4 drillholes, with a total length of 250 m & and 28 supplementary surface samplings

The first two scenarios offer the most insight in the deeper parts of the quarry, but do not offer any improvement in the recognition of smaller intermediate structures than the ones detected by the surface sampling on the 40m raster

The 3rd scenario tries to combine knowledge from the deeper parts with the advantages of additional surface information from a more dense raster.

The 4th scenario focuses on the extra information from a surface raster, assuming that the information from the older drillholes concerning the deeper parts of the ore body is sufficiently enough.

Finally scenario 5 maximizes information gain both in depth and on the surface raster.

Scenario number 1 was finally selected as the best candidate, because it offered more information concerning the deepest parts of the ore body. As a result, 4 drillholes were drilled with a total drilling length of 297m.

After the cumulative evaluation of the total data occurred during the above mentioned new drilling project in combination with the already existing information from the older drilling and sampling campaigns, it became obvious that:

1. The data occurred from the proposed drilling scenarios were crucial not only for the final calculation of the recoverable gypsum reserves, but also for the calculation of the spatial distribution of gypsum and anhydrite in the ore body.
2. As a further consequence of the above mentioned improvements, these information can be considered as really important for the annual planning of the open pit production, since the main aim of the production (concerning the cement factories feeding with gypsum) is focused on providing a stable and predictable quality of raw material (ratio between gypsum/anhydrite), and keeping at the same time the productive benches fully operational and safe.

5. References

- Antoniou, M., 1987. Contribution to the knowledge of evaporitic deposits in Eastern Crete and Karpathos islands. *Mineral Wealth*, 49, 55-62, (in greek).
- Cayeux, L., 1902. Sur la composition et l'âge des terrains métamorphiques de la Crète. - *C. R. Acad. Sc. Paris*, 134, 1117-1119, Paris.
- Dornsiepen, U.F., Manutsoglu, E. & Mertmann, D. 2001. Permian – Triassic Palaeogeography of the external Hellenides. *Palaeogeography, Palaeoclimatology, Palaeoecology*, 172, 327-338.
- Fytrolakis, N., 1980. The geological structure of Crete. Habil. Thesis, NTUA, Athens, 146 pages, (in greek).
- Kanaris, I., 1989. Gypsum deposits in the island of Crete, Internal Report IGME, Athens, 63 pages, (in greek)
- Nikolaou, K., 1986. Contribution to the knowledge of Neogene and of Geology and delineation of Ionian and Pre-Apoulian zones in relation to petroleum-geological observations performed in the islands of Strofades, Zante, Kefallinia. *PhD thesis, University of Athens*, 228 pages, (in greek).
- Papastamatiou, I., 1958. Report regarding Altsi gypsum deposit in Eastern Crete, Internal Report IGME, Athens, 3 pages, (in greek).
- Prissang, R., Spyridonos, E. & Frentrup, K.-R., 1999. Computer assisted 3D Modelling and Planning for the Cement Industry of El Salvador, *Mathematische Geologie*, 4, 61-72, Dresden.
- Prissang, R., Spyridonos, E., Frommer, Th., Skala, W., 1996. Operational Grade Modelling at the Breitenau Magnesite Mine. In : RAMANI, R.V. (ed.): Proceedings of the 26th Int. Symp. Applications of Computers and Operations Research in the Mineral Industry, *APCOM '96*, University Park, PA.
- Raulin, V., 1869. Description physique de l'île de Crete. *Actes. Soc. Linn. Bordeaux*, T.23, pp. 1-157, 321-444, Bordeaux.
- Trappe, Jorg, 2000. Pangea: extravagant sedimentary resource formation during supercontinent configuration, an overview. *Palaeogeography, Palaeoclimatology, Palaeoecology*, 161, 35-48.
- Warren, John, 2006. Evaporites: Sediments, Resources and Hydrocarbons, pp. 1036, Berlin etc. (Springer).

SUITABILITY ASSESSMENT OF CRETACEOUS LIMESTONES FROM THERMO (AITOLOKARNANIA, WESTERN GREECE) FOR THEIR USE AS BASE AND SUB-BASE AGGREGATES IN ROAD-CONSTRUCTION

Mpalatsas I., Rigopoulos I., Tsikouras B. and Hatzipanagiotou K.

Department of Geology, Section of Earth Materials, University of Patras, 26500 Patras, Greece, mpalatsas@upatras, rigopoul@upatras.gr, v.tsikouras@upatras.gr, k.hatzipanagiotou@upatras.gr

Abstract

This paper focuses on the assessment of mineralogical, petrographical and physico-mechanical properties of limestone formations in order to evaluate their suitability as road construction aggregates. Research focuses on Olonos-Pindos zone limestones of Cretaceous age in Aitolokarnania province, Western Greece. Special emphasis was given on comparing the mechanical properties to the mineral components. The results were evaluated in accordance with Greek and International suitability Standards for road construction aggregates. It was finally concluded that the physical and mechanical properties of the tested rocks are in compliance with the suitability Standards and that they can be used as road-construction aggregates.

Keywords: *Aggregates, limestone, physico-mechanical properties, Thermo Aitolokarnania.*

1. Introduction

The increasing demand for crushed rock aggregates in various applications and especially the requirement for hard aggregates in numerous engineering projects of Greece, have increased the necessity for the detection of carbonate rocks which are suitable for the production of aggregates used for: bases and sub-bases, improvement layers, bituminous mixtures, concrete and embankments. Additionally, carbonate rocks are used in various environmental applications such as for erosion protection, for the stability of natural or artificial slopes and for filters (Spyropoulos, 2005).

This paper investigates potential aggregate resources from the Cretaceous limestone formations of the Olonos-Pindos zone. Six representative samples were examined (AT9A, AT9B, AT13A, AT13B, AT22), in order to determine their suitability as road bases and sub-bases. The quality of the collected limestones was assessed based on their physico-mechanical properties, as well as on their mineralogical and textural features.

2. Geological setting

The studied carbonate rocks of Thermo (Aitolokarnania province, Western Greece) (Fig. 1), cover a total area of 37 km². They comprise part of the lower unit (thickness more than 1000 m) of the Olonos-Pindos zone, which includes pelagic limestones of Triassic to Upper Cretaceous age. These limestones are intercalated with radiolarites of Middle Jurassic to Lower Cretaceous. The Upper

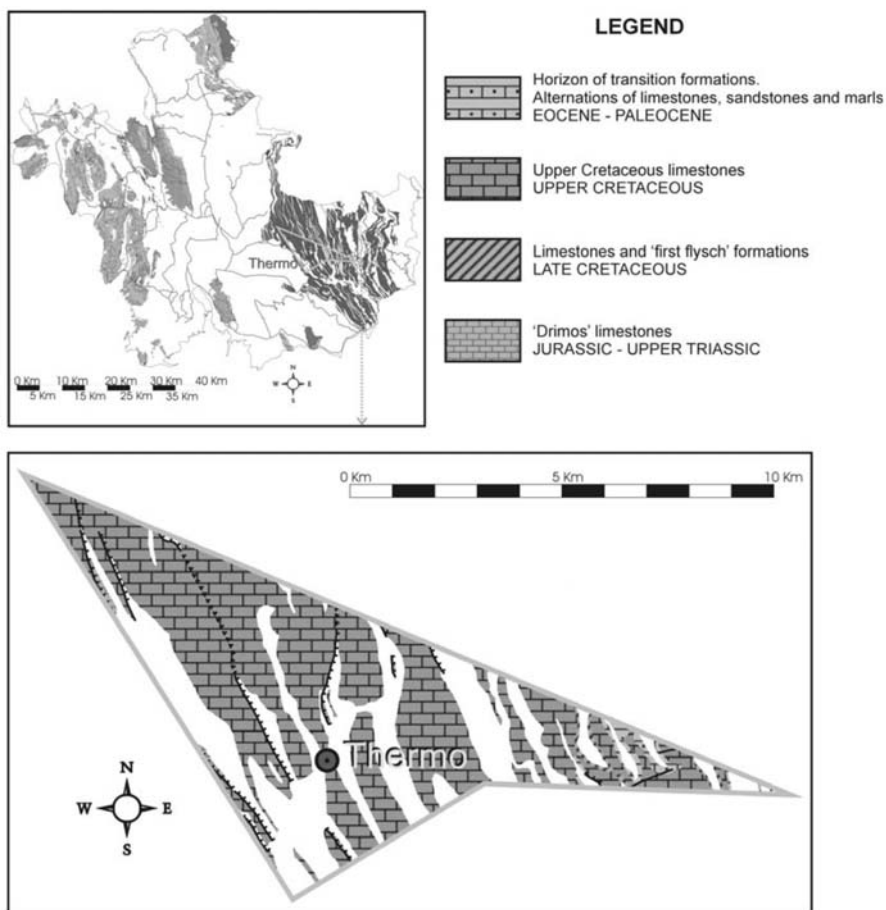


Fig. 1: Geological map of Thermo (Aitolokarnania province). The general map is an extract from the “Thermo” map sheet, I.G.M.E. (1977).

Cretaceous limestones, which comprise the upper part of this lower unit, are biomicritic and medium-bedded with intercalations and nodules of flint. The colour of these limestones varies from gray to whitish and becomes reddish at the lower parts, while their thickness varies from 200 to 400 m (Katsikatsos, 1992; Mountrakis, 1985).

The Cretaceous carbonate rocks (Fig. 1) cover the greatest area (34 km²) among the formations of the Olonos-Pindos zone and occur in beds up to 20 cm thick. The rock slopes of the studied area are cut by joints with opening up to 3-4 cm and are characterized by manifold disruption and intense folding. All these features have led to local destruction of the original structure of these rocks (Fig. 1). Statistical analysis of the strike of the limestone beds revealed that the main direction strikes NNW – SSE and dips 15° to 60° to the ENE or WSW.

3. Petrography

The studied Upper Cretaceous carbonate rocks were collected from representative localities of quarry faces or natural slopes, with a view to be fresh and to represent the full variability of the quarry

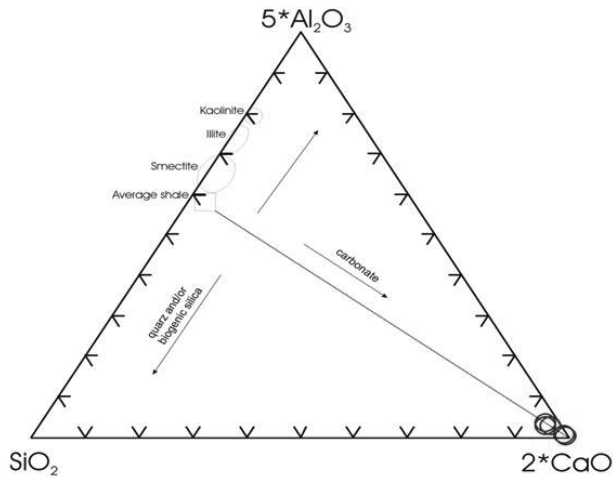


Fig. 2: Plot of the analysed samples on the Al_2O_3 - SiO_2 - CaO diagram for sedimentary rocks.

products. Most of these rocks are macroscopically whitish to gray with a dense network of sparitic veins, except for samples AT9B and AT22B, which have a yellowish pink colour. The microscopic examination was carried out using polarized microscopy at the Laboratory of Research Mineral and Rocks, Department of Geology, University of Patras, as well as at the Laboratory of Electron Microscopy and Microanalysis, University of Patras. Petrographic examination indicated that samples AT9A, AT9B, AT13A and AT22B are micritic limestones and according to Folk (1959, 1962) are classified as packed biomicrites (AT9A) and sparse biomicrites (AT9B, AT13A and AT22B), whereas according to Dunham (1962) are classified as wackestone (AT13A and AT22B), bioclast packstone (AT9A) and bioclast mudstone (AT9B). Samples AT13B and AT22A are sparitic limestones and are classified as sorted biosparites (AT22A) and as sorted endobiosparites (AT13B) according to Folk, and as biograinstone (AT22A) and endobioclast grainstone (AT13B) according to Dunham (1962).

4. Whole-rock geochemistry

Whole-rock analyses in six representative Cretaceous carbonate samples are listed in Table 1. TiO_2 , Fe_2O_3 , MgO , K_2O and P_2O_5 abundances are lower than the Greek and Global average values. Low P_2O_5 is a result of the absence of apatite, which frequently exists in carbonate rocks, while the low TiO_2 values are related to the absence of detrital heavy minerals. SiO_2 in three samples (AT9B, AT13A, AT22B) is higher than the Greek average value (1.80%) whereas samples AT9A, AT13B and AT22A show lower values. Samples AT9B, AT13A and AT22B are richer in Al_2O_3 relative to the Greek average value, most likely reflecting the occurrence of clay minerals. Samples AT9A, AT9B, AT13B and AT22B are richer in Na_2O relative to the Greek and Global average value probably due to the presence of anhydrite and feldspars. All samples are rather rich in MnO with the highest value in sample AT9A (0.07%). Samples with higher SiO_2 values show also lower loss-on-ignition values, reflecting the lower calcite abundances.

On an Al_2O_3 - SiO_2 - CaO diagram (Fig. 2), the analysed samples plot close to the CaO apex, suggesting that they are poor in clay- and silicate-fraction.

5. Physiomechanical properties

Several laboratory tests were performed for the suitability assessment of the Cretaceous limestones from Aitoloakarnania as aggregates (Table 2). These tests were carried out according to the American (ASTM) and Greek (ELOT) Standards. Selection of samples was based on their mineralogical composition that strongly controls the quality of aggregate materials (Zarif & Tuğrul, 2003; Tsikouras et al., 2005; Pomonis et al., 2007). Physicomechanical properties were estimated in six representative samples, which include micritic (AT9A, AT9B, AT13A and AT22B) and sparitic limestones (AT13B and AT22A).

5.1 Physical properties

Apparent density, bulk density (ASTM C-127), water-absorption (ASTM C-128) and sand equivalent (ASTM D-2419) were carried out. Normal density aggregates show values ranging between 2-3 gr/cm³, which are broadly used in several construction works. Light-weighted aggregates have densities <2gr/cm³ whereas heavy aggregates are those with density >3gr/cm³. Apparent density in the analysed samples ranges from 2.68 gr/cm³ to 2.71 gr/cm³ and are classified as normal aggregates.

Water-absorption was estimated after 24 hours immersion of the samples in water and ranges between 0.40% and 1.30%; samples AT9B AT22 have the maximum and minimum values, respectively.

Aggregates with sand equivalent values >50% are considered suitable for base and sub-base aggregates in road constructions. The sand equivalent (AASHTO T176-65) ranges in the analysed samples between 63 % and 78%, suggesting their good quality.

5.2 Mechanical properties

The estimated mechanical properties according to Greek and international standards include the riprap soundness using Na₂SO₄ (ELOT EN 1097-01), the toughness and abrasion resistance using the Los Angeles abrasion test (L.A.A.V.; ASTM C 535), the uniaxial compression strength (ELOT 408), and the maximum Proctor density (E105-86). The results are listed in Table 2. The Los Angeles values range between 23.26% and 27.52%, the riprap soundness (Na₂SO₄) yielded values between 2.70% and 3.70%, the uniaxial compression strength ranges between 49.30MPa and 68.00MPa, and the maximum Proctor density is in the range of 2176-2207 kgr/m³.

Using linear regression analysis (Bevington & Robinson, 2002) it is clearly shown that there is an antipathetic relation between the Los Angeles values and the uniaxial compressive strength values with a correlation coefficient R²=0,8065 (Fig. 3). Los Angeles values also plotted against the whole-rock major oxides. SiO₂ abundance shows positive correlation with the Los Angeles values, indicating that with increasing silica there is a decrease in the rock quality (Fig. 4); similar behaviour is also suggested with increasing Al₂O₃ contents. The Los Angeles values show also significant positive correlation with the riprap soundness values (Fig. 5), revealing that the more durable in toughness and abrasion a rock is the more durable in weathering under variable climatic conditions. Finally, a moderate correlation between the Los Angeles values and the maximum Proctor density values is observed in the analysed (Fig. 6).

6. Discussion

Mineralogical and textural characteristics, as well as the degree deformation and porosity are some critical factors in the quality of aggregates (Hartley, 1974; Kazi & Al-Mansour, 1980; Al-Jassar &

Table 1. Whole-rock geochemical analyses of representative samples from Cretaceous limestones from Thermo (-: below detection limit)

Major elements (wt %)	AT9A	AT9B	AT13A	AT13B	AT22A	AT22B	Global Average Value ¹	Greek Average Value ²
SiO ₂	0.81	3.22	3.33	0.52	0.72	2.29	5.20	1.80
TiO ₂	-	0.02	0.01	-	-	0.01	0.07	-
Al ₂ O ₃	0.14	0.78	0.62	0.08	0.15	0.59	0.80	0.50
Fe ₂ O ₃ ^t	0.08	0.40	0.32	0.10	0.10	0.31	0.50	0.50
MnO	0.07	0.04	0.05	0.05	0.05	0.05	0.05	0.02
MgO	0.40	0.37	0.36	0.31	0.56	0.39	7.90	2.80
CaO	53.96	53.32	53.84	57.34	53.56	53.71	42.60	51.60
Na ₂ O	0.07	0.07	0.05	0.08	0.1	0.07	0.05	0.05
K ₂ O	-	0.19	-	-	0.03	0.08	0.30	0.05
P ₂ O ₅	0.02	0.03	0.03	0.03	0.03	0.03	0.09	-
LOI	43.30	41.77	41.92	40.32	43.57	42.50		
Total	98.83	100.21	100.53	98.81	98.91	100.00		

¹ Mason & Moore (1982), ² I.G.M.E. (1997)

Table 2. Results of the physico-mechanical properties of the analysed samples from Thermo

Sample No.	AT9A	AT9B	AT13A	AT13B	AT22A	AT22B
Bulk density (gr/cm ³)	2.69	2.69	2.71	2.70	2.70	2.68
Apparent density (gr/cm ³)	2.65	2.63	2.66	2.66	2.64	2.66
Water absorption (%)	0.80	1.30	1.10	0.9	1.20	0.40
Los Angeles (%)	23.26	25.79	27.50	24.55	27.11	27.52
Riprap soundness (%)	2.70	3.40	3.70	3.20	3.70	3.50
Uniaxial compressive strength (MPa)	68.00	58.85	49.30	55.00	50.00	51.00
Sand equivalent (%)	68	63	69	70	73	72
Maximum Proctor density (kgr/m ³)	2176	2192	2201	2176	2207	2189

Hawkins, 1991; Smith & Collis, 2001; Jensen et al., 2010).

Apparent and bulk density of the Cretaceous limestones from Thermo show moderate to slightly high values and are within the acceptable limits of aggregates suitability (NBG 1985, Shakoor et al. 1982, Cargill, 1989). Water absorption is another important factor related to durability of the materials. Experimental results have shown that rocks with water absorption values higher than 3% are vulnerable to shock changes of temperature (Shakoor et al., 1982). Samples AT9B (1.3%), AT13A (1.10%) and AT22A (1.20%) show the highest water absorption values compared to the rest samples, most likely due to their higher porosity and participation of clay minerals that strongly absorb

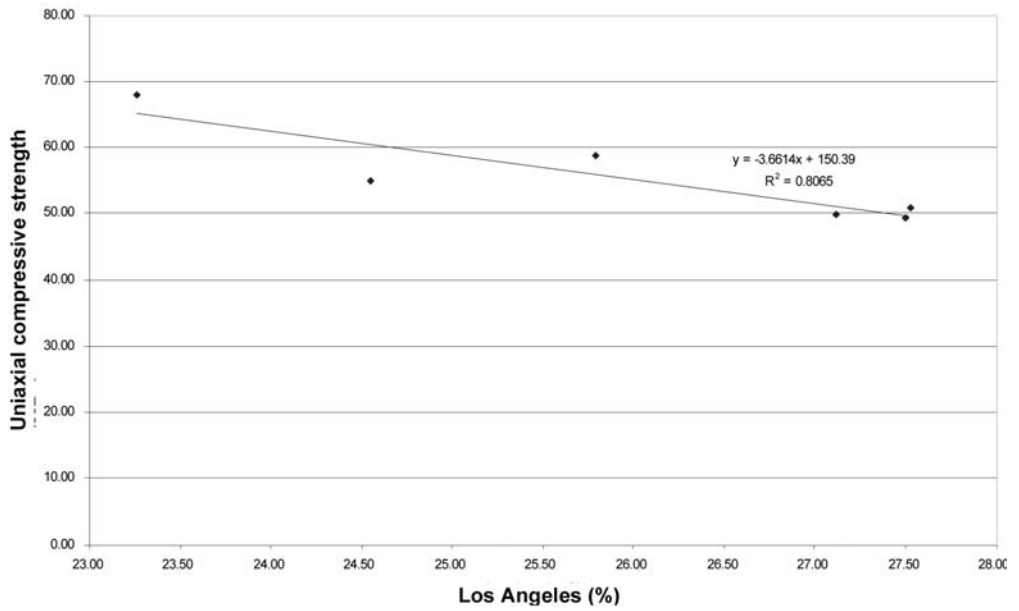


Fig. 3: Plot of Los Angeles values vs. uniaxial compressive strength values of the analysed samples from Thermo.

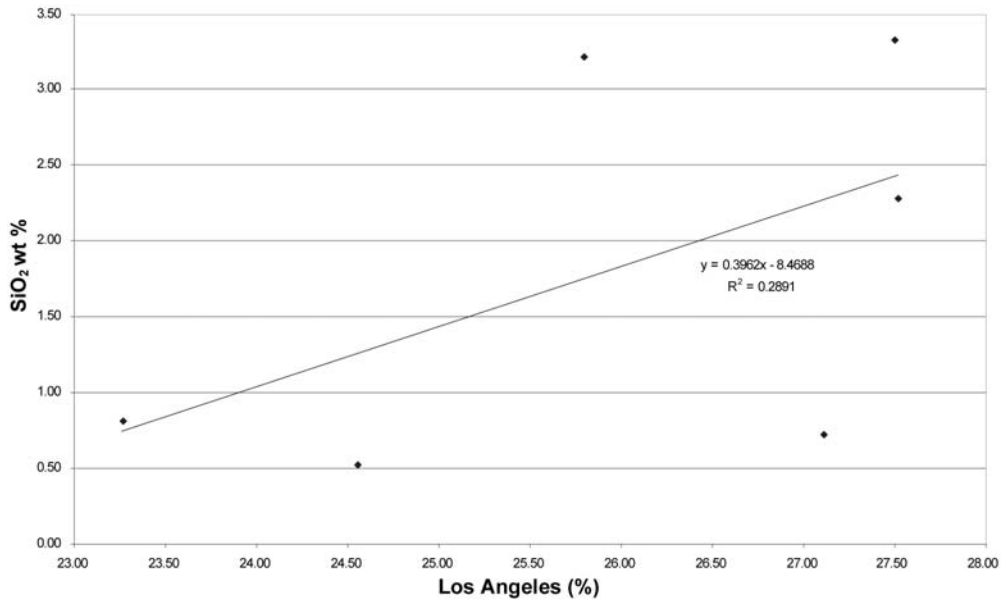


Fig. 4: Plot of Los Angeles values vs. SiO₂ contents of the analysed samples from Thermo.

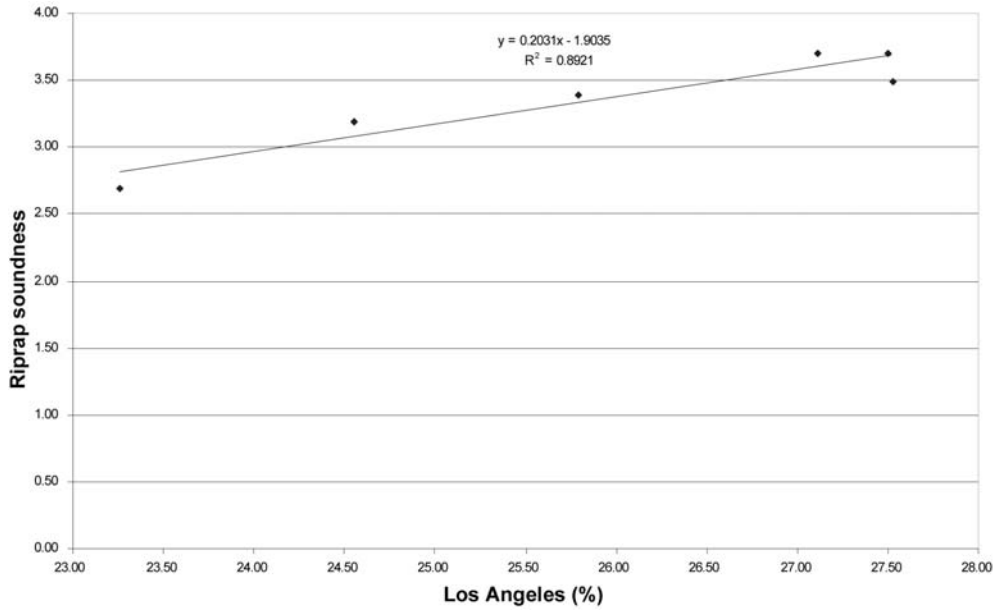


Fig. 5: Plot of Los Angeles values vs. riprap soundness using Na_2SO_4 of the analysed samples from Thermo.

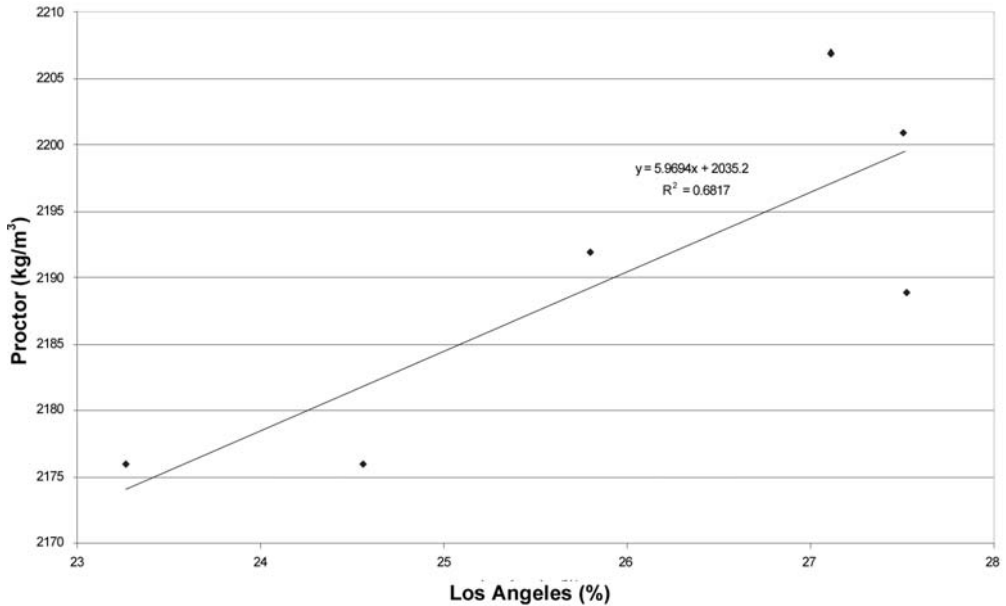


Fig. 6: Plot of Los Angeles values vs. maximum Proctor density of the analysed samples from Thermo.

water. A test that simulates the volume changes of aggregate materials and estimates their durability under climatic variations is the soundness of riprap (Smith & Collis, 2001). For this purpose, it is used Na_2SO_4 or MgSO_4 , which crystallize in the pores and joints of the aggregates and disintegrate them after repeated freeze-thaw and dry-wet cycles (Bloem, 1966). In this study, we used a Na_2SO_4 solution and the obtained riprap soundness values of the Cretaceous limestones are below the limit of 12, for their use as bases and sub-bases in road construction

The Los Angeles values are low whereas the sand equivalent values are high in the analysed Cretaceous limestones from Thermo. According to the standards of the Greek Ministry of Environment the upper limit of Los Angeles and the lower limit of sand equivalent, for the suitability of aggregates for road construction works, are 30 and 50, respectively. Our samples clearly fulfill these prerequisites and hence it is strongly suggested that they are suitable for use as bases and sub-bases aggregates. The somewhat higher Los Angeles values of samples AT22A and AT22B are interpreted as the result of their sparitic texture (e.g. Zarif & Tuğrul, 2003; Sabatakakis et al., 2008).

7. Conclusions

Petrographic investigation in Cretaceous limestones from Thermo showed that they comprise rocks with both micritic and sparitic textures; they are intensely tectonised and frequently they are cut by joints filled with recrystallised calcite. Geochemical analyses reveal that they contain insignificant impurities and are similar to the Greek and Global average limestones. Physicomechanical properties such as Los Angeles, soundness of riprap, uniaxial compressive strength and maximum Proctor density are correlated each other. Moreover, there is a positive correlation of the Los Angeles values with the SiO_2 abundance in the rocks. Therefore, knowledge of some of these parameters can easily predict the quality of the aggregates.

The studied rocks show values of their physicomechanical properties within the acceptable Greek and international limits and hence they are suitable for their use as bases and sub-bases aggregates in road construction works.

8. References

- Al-Jassar, S. & Hawkins, A.B., 1991. The Carboniferous Limestone of the Bristol area: a review of the influence of the lithology and chemistry on its use as a geomaterial. *Quarterly Journal of Engineering Geology and Hydrogeology*, p. 24, 143 - 158.
- Bevington, P.R. & Robinson, D.K., 2002. Data reduction and error analysis for the Physical sciences, 3rd ed., p. 320.
- Bloem, D.L., 1966. Soundness and deleterious substances. ASTM STP 169A, p. 497-512.
- Cargill, J.S., 1989. Evaluation of Empirical Methods of Measuring the Uniaxial Compressive Strength of Rock, Unpublished Thesis, Department of Geology, Kent State University, Kent, OH. p. 80.
- Dunham, R. J., 1962, Classification of carbonate rocks according to depositional texture. In: Ham, W. E. (ed.), Classification of carbonate rocks: American Association of Petroleum Geologists Memoir, p. 108-121.
- Folk, R.L., 1959. Practical petrographic of limestone. *Bull. Am. Ass. Petroleum Geologists*, p. 43, 1-38.
- Folk, R.L., 1962. Spectral subdivision of limestone types. In W.E. Ham (ed), Classification of carbonate rocks. *Am. Assoc. Petroleum Geologists*, Memoir, p. 1, 62-84.
- Hartley, A., 1974. A review of the geological factors influencing the mechanical properties of road surface aggregates. *Quarterly Journal of Engineering Geology and Hydrogeology*, p. 7, 69-100.

- I.G.M.E., 1977. Geological map of Greece, Thermo sheet. I.G.M.E., Athens.
- Jensen, L.R.D., Friis, H., Fundal, E., Møller, P. & Jespersen, M., 2010. Analysis of limestone micromechanical properties by optical microscopy. *Engineering Geology*, p. 110, 43-50.
- Katsikatos, G., 1992. Geology of Greece. University of Patras, p. 451.
- Kazi, A. & Al-Mansour, Z.R. 1980: Influence of geological factors on abrasion and soundness characteristics of aggregates. *Engineering Geology*, p. 15, 195-203.
- Mason, B and Moore, C.B., 1982. Principles of geochemistry, New York, J. Wiley & Sons, p. 344.
- Mountrakis, D., 1985. Geology of Greece. University Studio Press, Thessaloniki, p. 207.
- NBG (Norwegian Group for Rock Mechanics), 1985. Engineering Geology and Rock Engineering. Handbook No. 2, p. 249.
- Pomonis, P., Rigopoulos, I., Tsikouras, B. & Hatzipanagiotou, K., 2007. Relationships between petrographic and physico-mechanical properties of basic igneous rocks from the Pindos ophiolitic complex, NW Greece. Proceedings of the 11th Conference of the Geological Society of Greece, p. 947-958.
- Sabatakakis, N., Koukis, G., Tsiambaos, G. & Papanakli, S., 2008. Index properties and strength variation controlled by microstructure for sedimentary rocks. *Engineering Geology*, p. 97, 80-90.
- Shakoor, A., West, T.R. & Scholer, C.F., 1982. Physical characteristics of some Indiana argillaceous carbonates regarding their freeze-thaw resistance in concrete. Bulletin of the Association of Engineering Geologists, p. 19, 371- 384.
- Smith, M.R. & Collis, L., 2001. Aggregates: Sand Gravel and Crushed Rock aggregates for Construction Purposes, Geological Society, London Eng. Geol., Special Publication, 17, p. 339.
- Spyropoulos, A., 2005. Investigation of the engineering-geological conditions in the Achaia prefecture related to search of aggregates for various uses. PhD Thesis, Univ. Patras, p. 306.
- Tsikouras, B., Pomonis, P., Rigopoulos, I. & Hatzipanagiotou, K. (2005). Investigation of suitability of basic ophiolitic rocks from Mikrokleisoura, Grevena, for their use as antiskid aggregates and railway ballast. Proceedings 2nd Congress of the Committee of Economic Geology, Mineralogy, and Geochemistry of the Geological Society of Greece, p. 347-356.
- Zarif, I.H. & Tuğrul, A., 2003. Aggregate properties of Devonian limestones for use in concrete in Istanbul, Turkey. *Bulletin of Engineering Geology and the Environment*, p. 62, 379-388.

AIR QUALITY IN MINING AREAS: THE CASE OF STRATONI, CHALKIDIKI, GREECE

Papastamatiou D., Skarpelis N. and Argyraki A.¹

¹ *National and Kapodistrian University of Athens, Faculty of Geology and Geoenvironment, Department of Economic Geology and Geochemistry, 157 84 Zografou, Athens, Greece, depapasta@hotmail.com, skarpelis@geol.uoa.gr, argyraki@geol.uoa.gr*

Abstract

Air quality sampling tests are conducted on a 24h basis by “HELLENIC GOLD S.A.” in the Stratoni mining settlement. The settlement is located in the neighbourhood of a flotation plant where galena and sphalerite concentrates are produced after crushing and processing of Pb-Ag-Zn sulfide ore. Old piles of mineral waste occur close to the settlement. The mineralogy of mineral dust collected on filters of 3 air samplers from August to December 2008 was studied. Elemental analysis of mineral dust collected from January to December 2008 was conducted. The purpose of the study was to determine levels of air pollution, type of mineral particles as well as potential sources. Measurements of air quality included PM_{10} . Statistical analysis of the collected data included tests to determine the control on daily particle concentration and mineralogy of fluctuations of temperature, humidity, wind direction and wind speed. Air quality was better than during 1998-2000. Air quality was typically at its worse during hot summer days when wind speed was high. The concentration of PM_{10} particulate matter was quite low when compared to International Air Quality Standards regulations, indicating that levels of air pollution in the area do not pose human health hazards.

Key words: *air quality, mineral dust, PM_{10} , Stratoni, Chalkidiki, Greece.*

1. Introduction

Protection of public welfare from particulate matter in the atmosphere is promulgated by the Greek law and is being monitored by competent agencies based on international air quality standards. Particulate matter is a significant category of pollution with a variety of shapes and sizes, coming from the processing of materials, procedures of combustion and transformation reactions of gas (Cooper & Alley, 2004). Historically, particulate matter (PM) measurements have focused on Total Suspended Particulates (TSP). Last decade the primary air quality standard TSP was replaced with PM_{10} standard. PM_{10} denotes particulate matter which passes through a size-selective inlet as defined in the reference method for sampling and measurement of PM_{10} EN 12341, with a 50% efficiency cut-off at 10 μ m aerodynamic diameter (Directive 2008/50/EC). Recent trends lead to further replacement of PM_{10} by a $PM_{2.5}$ standard. Areas in the country with potential for high levels of mineral particulate matter are those where mining, transportation, deposition, crushing-milling and processing of minerals were conducted (e.g. the Florina – Ptolemais – Kozani lignite basins (Triantafyllou, 2000; Triantafyllou et al., 2000) and Lavrion (Skarpelis et al., 2009).

The examination of the amount and type of the particulate matter is imposed especially in areas

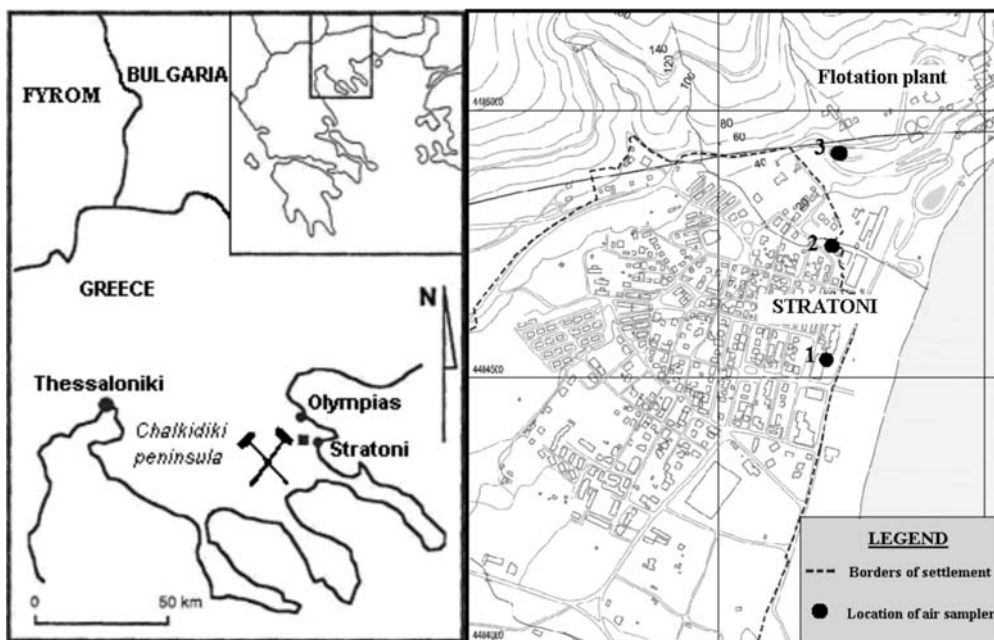


Fig. 1: a: Location of the main mining centers in NE Chalkidiki. b: Location of air samplers. (Ballas & Gazea, 2009).

where grains of minerals with toxic elements load are released by human activities. The mineralogy, chemistry, solubility and oxidation state of the inhaled particles strongly influence human health effects (Posfai & Molnar, 2000; Plumlee et al., 2006).

The wider area that Stratoni settlement belongs to, is well known as “Kassandra Mines” (Fig. 1a). The flotation plant of the mining company “HELLENIC GOLD S.A.” is located at the northeastern part of the Stratoni settlement, producing sphalerite and galena concentrates after processing of Pb-Ag-Zn sulphide ore exploited at the Mavres Petres mine. A crushing-milling facility and condensation-filtration and mineral waste units are associated with the flotation plant. For the protection of the citizens and workers welfare of Stratoni, the company has established and operates three air samplers; location of the samplers is shown in Fig. 1b. Previous studies reported on ambient concentrations of Total Suspended Particulate Matter (TSP) in the wider area of Stratoni (Gaidajis, 2003).

The purpose of this study is to identify the mineral phases of PM_{10} fraction of the dust and search for the source(s) of grains, taking into consideration the chemistry of dust samples and meteorological parameters. Also, there was an evaluation of the impact on air quality at the Stratoni settlement and the data was compared with the conditions during 1998-2000. This data can be used for further assessments of particles dissemination.

2. Geology of the ore deposits

The Kassandra mining district comprises mainly Pb-Zn (Ag-Au) carbonate hosted replacement, skarn and porphyry Cu-Au ore deposits. They are hosted by lithologies of the Serbomacedonian Belt and temporally and spatially related to Tertiary intrusives. The Mavres Petres, Madem Lakkos and Stratoni deposits are structurally controlled by the NW-SE trending Varvara - Stratoni fault and litho-

logically by marble in contact with gneiss of the polymetamorphic Vertiskos Unit. Base metal sulphides, sulphosalts, quartz, rhodochrosite, graphite, kaolinite, sericite are the predominant hypogene minerals (Nikolaou, 1960; Kockel et al., 1977; Nebel et al., 1991; Gilg, 1993; Gilg & Frei, 1994).

3. Materials and Methods

In order to monitor the ambient air quality at Stratoní, air samplers produced by “Thermo Electron” are used (type rp Patrisol –plus model 2025 sequential air sampler). The filters that are used (Pallflex TX40) retain particles PM_{10} , have a diameter of 47mm and are made of glass fiber coated with Teflon and manufactured by Thermo Electron 9. Estimation of the index “Mass Concentration”, indicating the amount of dust deposited on the filter, was made using the formula: $MC = DW \cdot 10^6 / V$, where: MC: Mass Concentration, DW: mass concentration in grams (g) on the surface of the filter and V: volume of air (in m^3) that passed through the filter. Elemental analysis of collected PM_{10} for Pb, Zn, As, Cd, Fe, Cu, Mn, was performed using Inductively Coupled Plasma - Atomic Emission Spectrometry at the laboratories of «HELLENIC GOLD S.A.».

Mineral investigation was carried out with the aid of a reflected light microscope and a JEOL JSM 5600 Scanning Electron Microscope at the Faculty of Geology and Geoenvironment, University of Athens. Mineral examination was conducted on 61 filters, which were chosen based on their high values of mass concentration. Approximately two filters per week were investigated for a six-month period. The mineralogical composition of samples of mineral waste and tailing, stockpiled sulphide ore and dust from the crushing-milling facility, has been also investigated. Emphasis was given on mineral grains of a size $<10\mu m$.

4. Results and Discussion

Based on the measurements of the mass concentration for the year 2008, it is presumed that there is a wide range of values between 2.5 and $79.6\mu g/m^3$ (Table 1).

Although the mass concentration data (Tables 1, 2) refer to PM_{10} and TSP respectively, a trend for reduction of emission of mineral particulates from the time period of 1998-2000 to 2008 is evident. It is worth mentioning that the ratio PM_{10}/TSP is not known; however the mineralogical study of TSP dust collected on the filter of a portable dust sampler during this sampling survey indicates the ratio PM_{10}/TSP is roughly around 0.7.

According to data on Table 1, during 2008, the number of days when mass concentration exceeded the daily limit value of $50\mu g/m^3$, were seven (7) in air sampler SAM 1, two (2) in the air sampler SAM 2 and nineteen (19) in the air sampler SAM 3, indicating that the daily concentration of particulate matter of PM_{10} was quite low when compared to European and International Air Quality Standards. It is worth mentioning – although not directly comparable – that many European cities (e.g. Berlin) cannot comply with the daily limit value for PM_{10} , which is in force since 2005. As stated by Goergen and Lambrecht (2007) Berlin experienced particle episodes in February, March and October during the year 2005 with PM_{10} concentrations up to $130\mu g/m^3$ in two sites, one close to a very busy street downtown and the other at the periphery of the city.

It is noticeable that mass concentration is not always analogous with the amount of mineral grains. This fact can be explained because organic substances from oil combustion as well as particles of biological origin can settle on the surface of the filter.

The examination of the mineralogy of the dust settled on the filters of the air samplers SAM 1-3,

showed that grains of pyrite, galena and sphalerite predominate. At a lower proportion, grains of arsenopyrite, chalcopyrite, barite, cerussite, gypsum, goethite, tennantite, boulangerite and bournotite can be found (Fig. 2a,b and 3b). Furthermore, in some of the filters, grains of halite were identified (Fig. 3a).

Sphalerite, pyrite, galena and arsenopyrite are the predominant minerals in samples collected from mine waste and tailing piles at the vicinity of the processing plant. Minor mineral constituents are gangue minerals (e.g. quartz, sericite, kaolinite). Samples of dust collected within the area of the crushing –milling facility comprise grains of sphalerite, galena and pyrite. Calcite, quartz and feldspars are subordinate.

Table 1. Mass Concentration variation of PM10 dust at Stratoni from January to December 2008.

SAM 1 to SAM 3: Air samplers; Mass Concentration in $\mu\text{g}/\text{m}^3$; NED: Number of Exceedance of regulatory limit Days (35 per year are permitted)

Month	1	2	3	4	5	6	7	8	9	10	11	12	Annual	NED
SAM 1														
min	8.9	18	5.4	8.7	8.3	7.1	8.7	18	12	10	5	2.5	2.5	7
max	38	71	53	64	32	38	29	53	38	50	52	46	70.8	
average	26	33	30	28	17	20	19	31	25	27	24	21	24.6	
median	28	30	28	25	17	20	19	30	23	26	22	17	22.5	
SAM 2														
min	13	20	12	19	11	10	15	13	16	7.5	9.1	3.3	3.3	2
max	27	48	64	29	42	37	27	50	44	52	49	36	63.5	
average	19	29	29	24	22	21	20	34	29	27	24	16	24.8	
median	18	27	29	23	21	19	20	37	29	29	20	15	23.6	
SAM 3														
min	7.6	19	12	9.6	5	11	15	20	6.2	12	3.8	6.7	3.8	19
max	34	55	60	80	75	61	75	63	52	48	46	67	79.6	
average	22	35	33	34	33	33	35	35	28	27	30	23	30.1	
median	20	35	35	30	31	32	31	35	27	27	22	20	27.1	

Table2. Mass concentration of Total Suspended Particulate matter from 1998 to 2000 (Gaidajis, 2003).

Sampler	Mass concentration ($\mu\text{g}/\text{m}^3$)				
	Number of samples	max	min	average	median
SAM 1	20	100.4	19.1	51.4	54.9
A*	13	106.6	23.2	60.1	57.1
B**	14	185.4	4.8	56.3	39.6

* Sampler close to fuel tanks; ** Sampler close to adit +410

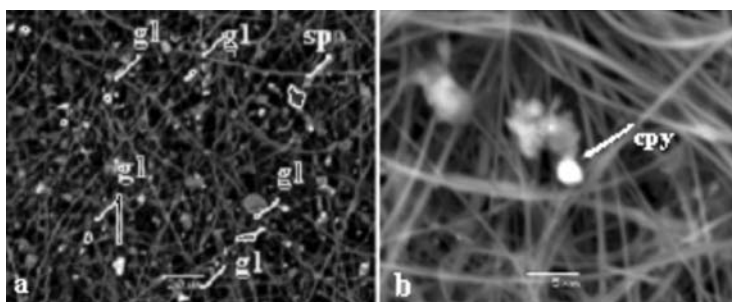


Fig. 2: SEM micrograph of dust grains on air filters: a. “SAM 3 14/9-15/9”, b. “SAM 2 30/9-1/10” (gl: galena, sp: sphalerite, cpy: chalcopyrite).

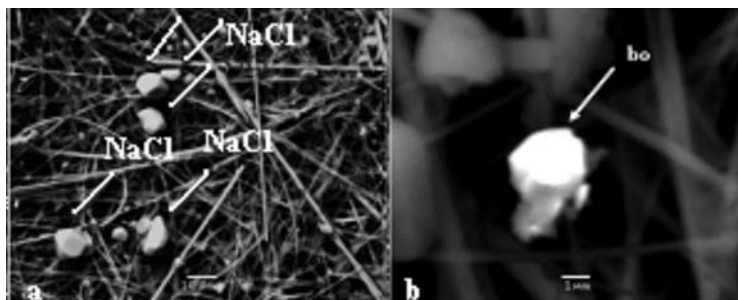


Fig. 3: SEM micrograph of dust grains on air filters: a. “SAM3 14/9-15/9”, b. “SAM3 25/11-26/11” (NaCl: halite, bo: bournonite).

Lead concentration in particulate matter during 2008 can be seen in Table 3. The Pb values are lower than the permitted limit (annual value $0.5 \mu\text{g}/\text{m}^3$; Directive EE 2008/50). It is well-known that due to differential toxicity, various minerals have different impact on human health when inhaled. According to Plumlee et al. (2006), Pb as a constituent of cerussite (a very acid-soluble lead carbonate), Pb oxides, and Pb sorbed onto atmospheric aerosols generated by lead-zinc smelting is substantially more bioaccessible than Pb as a major constituent of galena and various lead-phosphate minerals. Consequently, the dominant presence of galena in the dust acts more positively for the environment rather than other Pb-minerals.

The average concentration of Fe, As, Zn, Cu, Mn and Cd in particulate matter PM_{10} from all air samplers during 2008 is shown in Table 4, whereas the average concentrations of these metals for TSP during 1998-2000 in Table 5. By comparing these concentrations we cannot observe any significant differences. An exception is Fe, which has high levels during 2008 in all air samplers.

Concentrations of the elements Pb, Zn, As, Cd, Fe, Cu, Mn and the Mass Concentration of PM_{10} during 2008 vary widely. It is ascertained that during warm periods the levels of element and mass concentrations are generally higher (Papastamatiou, 2009). This variation can be explained due to high-speed winds, during warm periods and low precipitation, during a major part of the cold period¹.

An effective way to determine the source of metallic minerals in the dust, are wind rose diagrams in connection with the concentrations of chemical elements. In Fig. 4 the average wind direction can

¹ Months from April to October are warm period, whereas November to March are cold period.

Table 3. Pb concentration ($\mu\text{g}/\text{m}^3$) in PM_{10} during 2008.

<i>Sampler</i>	<i>Max</i>	<i>Min</i>	<i>Average</i>	<i>Median</i>
SAM 1	1.116	0.029	0.356	0.257
SAM 2	0.404	0.057	0.184	0.167
SAM 3	0.114	0.013	0.063	0.062

Table 4. Average metal concentration in PM_{10} during 2008

<i>Sampler</i>	<i>Average metal concentration ($\mu\text{g}/\text{m}^3$)</i>					
	<i>Fe</i>	<i>As</i>	<i>Zn</i>	<i>Cu</i>	<i>Mn</i>	<i>Cd</i>
SAM1	1.698	0.174	0.723	0.017	0.167	0.012
SAM2	1.604	0.08	1.178	0.017	0.036	0.011
SAM3	1.379	0.077	0.982	0.009	0.022	0.01

Table 5. Average metal concentration in TSP during 1998-2000 (Gaidajis, 2003)

Location of samplers: A. Close to fuel tanks, B. Close to Adit +410.

<i>Sampler</i>	<i>Average metal concentration ($\mu\text{g}/\text{m}^3$)</i>					
	<i>Fe</i>	<i>As</i>	<i>Zn</i>	<i>Cu</i>	<i>Mn</i>	<i>Cd</i>
SAM 1	0.254	0.012	0.083	0.112	0.055	0.0006
A	0.584	0.045	0.299	0.066	0.121	0.016
B	0.247	0.019	0.051	0.041	0.103	0.0004

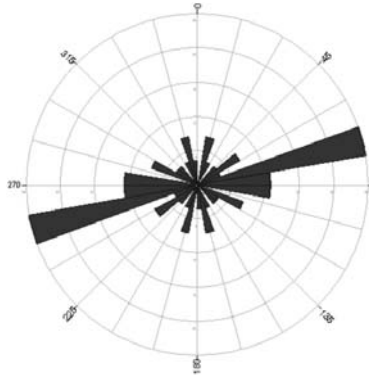


Fig. 4: Wind rose diagram during 2008 in Stratoni (Data from air sampler SAM 1).

be shown as a function of geographical bearings. The length of the bar for a particular direction indicates the time that the wind blows from that direction. It is concluded that the predominant wind direction is ENE and WSW.

Wind rose diagrams were also constructed based on wind data of air sampler SAM 1 and elemental concentrations from chemical analysis of the filters of the same sampler (Fig. 5). The elements Pb and As have the highest concentrations when N-NE directed winds blow, indicating that the main source

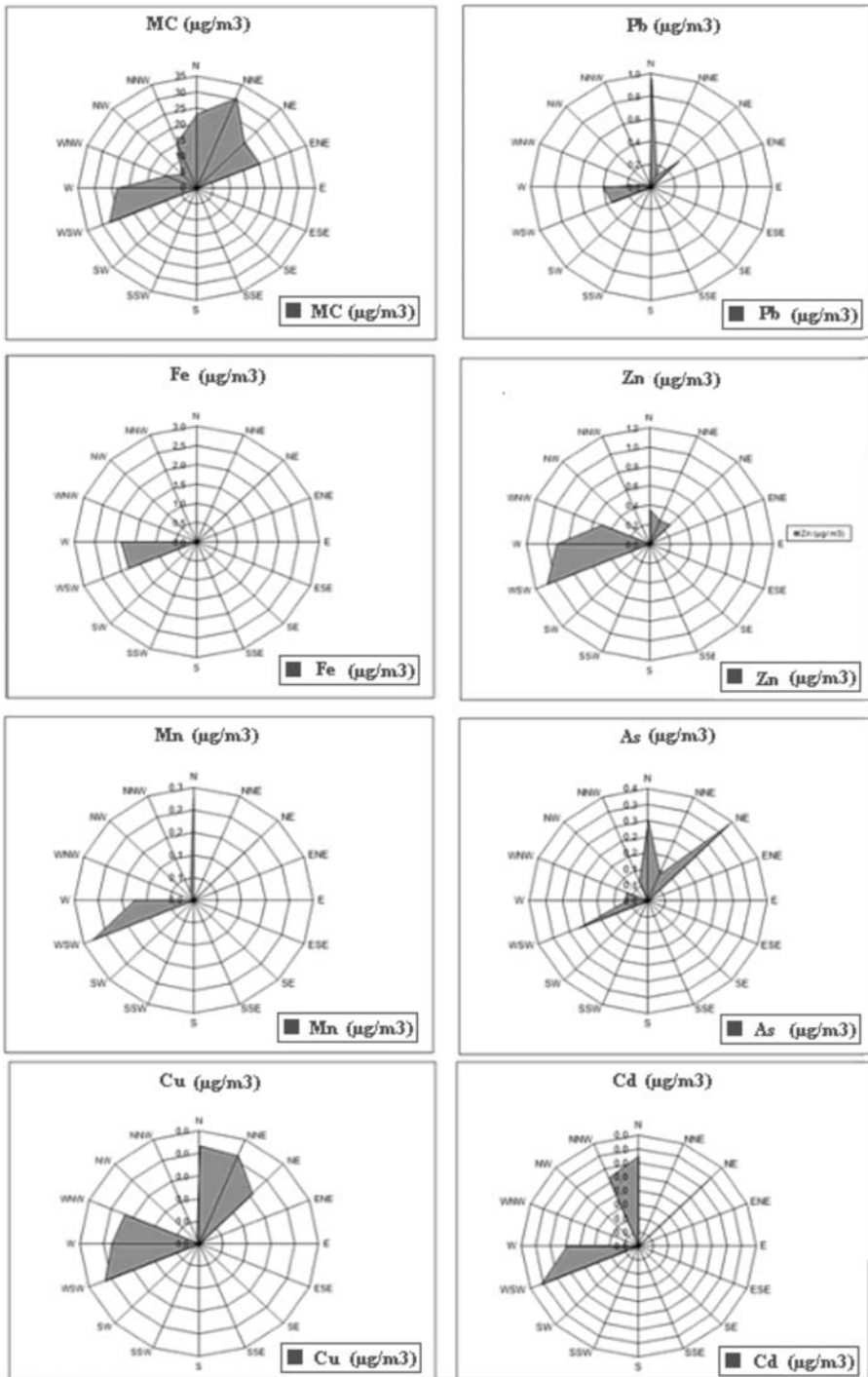


Fig. 5: Wind rose diagrams of PM_{10} , Pb, Fe, Zn, Mn, As, Cu, Cd ($\mu\text{g}/\text{m}^3$) (Data from sampler SAM 1).

of these elements is dust that comes from the processing facilities located on this direction in relation to air sampler SAM1. Wind rose diagrams of Fe, Mn and Zn have high concentrations during W-WSW winds. This observation suggests that the main source of the metal bearing particulate matter is the surface cover of the settlement of Stratoni. Data from previous studies, examining the composition of the soil from gardens of the settlement, confirmed that the main phases are oxides of Fe and Mn (Plakaki, 2006, Argyraki et al., 2007, Nicolaou, 2007). These mineral phases act as collectors for other metals. Finally, Mass Concentration, Cu and Cd, present high concentrations both when NNE and WSW directed winds blow, suggesting a mixed source of the transported particulate matter.

5. Conclusions

Measurements of ambient concentrations of particulate matter of less than 10µm aerodynamic diameter (PM₁₀) are conducted on a 24 hours basis at Stratoni settlement. Evaluation of chemical data from air filters for the year 2008, combined with detailed mineralogical analysis of PM₁₀ fraction leads to the following conclusions:

- a. Mass Concentration of collected dust ranged between 2.5µg/m³ and 79.6µg/m³.
- b. The majority of metal bearing dust grains are metallic minerals that exist in the ore. A mineralogical study of dust settled on filters in the air sampler operating close to the processing facility did not demonstrate variation in the type of metallic minerals. Galena, sphalerite and pyrite dominate, whereas bournotite, boulangerite, chalcopyrite, cerussite, barite, gypsum, goethite and tennantite are subordinate mineral phases. During time periods when winds are of an E-NE direction it seems that seawater droplets are settled on the filters and halite is formed.
- c. The annual limit value PM₁₀ in all stations, as well as the Pb values are lower than the limits permitted by European Standards (40µg/m³ and 0.5µg/m³ respectively).
- d. The number of exceedance days, that is the number of days when Mass Concentration exceeds the daily limit value of 50µg/m³, is significantly lower than the number permitted by European Standards (35 days)². It is worth mentioning that even at the station which is located very close to the processing facilities that number reached a value to 19 during the year 2008.
- e. On the basis of the EU Commission “Thematic Strategy on Air Pollution” published in 2005 the PM₁₀ data at Stratoni pose no risk for human health. However, further research is needed before concluding on the safety of ambient air for the local population. To that end, examination of finer fractions of particulate matter (e.g. PM_{2.5}) as well as collection of data from additional air samplers located within the area of the village of Stratoni is proposed.

² Consultation status in the EU on particulates provisions of the Air Quality Directive (from Goergen & Lambrecht, 2007).

	Commission proposal (09-09-05)	EP first reading (26-09-06)
Limit values for PM ₁₀	a. Daily limit value from 2005 of 50µg/m ³ , which may be exceeded on a max. of 35 days b. Annual limit value from 2005 of 40 µg/m ³	a. Daily limit value from 2005 of 50µg/m ³ , which may be exceeded on a max. of 35 days, but possibility for member States to increase the number of exceedance days to 55 from 2010 b. Annual limit value from 2005 of 40 µg/m ³ in the period from 2005-2010 c. Annual limit value of 33 µg/m ³ from 2010

6. Acknowledgments

This research work would not had been possible without the support of “Hellenic Gold S.A.”. Dr Emmy Gazea, Head of the Department of Environment and Safety of the Company, as well as D. Ballas, A. Gatsios and E. Daftsos are thanked for providing help, for suggestions and discussions. We would like to thank Assoc. Prof. P. Nastos for helpful discussions, and an anonymous reviewer for critical comments which improved the manuscript.

7. References

- Argyraki, A., Plakaki, A., Godelitsas, A., 2007. Characterization of garden soil pollution in the mining vil-
lage of Stratoni, N. Greece. *Bull. Geol. Soc. Greece*, 40, 1331-1342.
- Ballas, D. and Gazea, V., 2009. Measurements of PM₁₀ in the area of Stratoni. Unpublished technical re-
port, February 2009, Eurotechnica EPE, Chalkidiki, Greece.
- Cooper, C.D., Alley, F.C., 2004. Air Pollution Control, A Design Approach, 3rd edition, Waveland Press
Inc., 739p.
- DIRECTIVE 2008/50/EC of the European Parliament and of the Council of May 2008 on Ambient air
quality and cleaner air for Europe. *Official Journal of the European Union*, 11-6-2008, L152/1-44.
- Gaidajis, G., 2003. Ambient Concentrations of Total Suspended Particulate Matter and Its Elemental Con-
stituents at the Wider Area of the Mining Facilities of TVX Hellas in Chalkidiki, Greece. *Journal of
Environmental Science and Health*, A38, 10, 2509-2520.
- Gilg, H.A., 1993. Geochronology (K-Ar), fluid inclusion, and stable isotope (C, H, O) studies of skarn,
porphyry copper, and carbonate – hosted Pb – Zn (Ag, Au) replacement deposits in the Kassandra min-
ing district (Eastern Chalkidiki, Greece). PhD Thesis, ETHZ, Zurich, 153p.
- Gilg, H.A., Frei, R., 1994. Chronology of magmatism and mineralization in the Kassandra mining area,
Greece: The potentials and limitations of dating hydrothermal illites, *Geochemica et Cosmochimica
Acta*, 58, 9, 2107-2122.
- Goergen, R., Lambrecht, U., 2007. Particulate Matter in Ambient Air. *Journal for European Environ-
mental & Planning Law*, 4, 4, 278-288.
- Kockel, F., Mollat H., Walther H. W., 1977. Erläuterungen zur Geologischen Karte der Chalkidiki und an-
grenzender Gebiete 1:100.000 (Nord- Griechenland). Hannover, Bundesanstalt für Geowissenschaften
und Rohstoffe, 119p.
- Nebel, M., Hutchinson R., Zartman, R., 1991. Metamorphism and polygenesis of the Madem Lakkos
polymetallic sulfides deposit, Chalkidiki, Greece. *Economic Geology*, 86, 81-105.
- Nikolaou, M., 1960. The Stratoni - Olympias granitic intrusion and the associated mineralization. *Ann.
Geol. Pays. Hellen.*, 2, 214-265.
- Nikolaou, S., 2007. Spatial distribution of potentially toxic elements in soils at NE Chalkidiki, N. Greece.
MSc Thesis, Department of Economic Geology & Geochemistry, University of Athens, Athens, 168
p. (in Greek with English Abstract).
- Papastamatiou, D., 2009. Inhalable particulate matter PM₁₀ in mining areas: The case of Stratoni,
Chalkidiki, Greece. MSc Thesis, Department of Economic Geology & Geochemistry, University of
Athens, Athens, 142p. (in Greek with English Abstract).
- Plakaki, A., 2006. Mobility of potentially toxic elements in soils of the Stratoni mining area, Chalkidiki,
N. Greece. MSc Thesis, Department of Economic Geology & Geochemistry, University of Athens,
Athens, 150 p. (in Greek with English Abstract).
- Plumlee G., Morman, S., Ziegler, T., 2006. The Toxicological Geochemistry of Earth Materials: An
Overview of Processes and the Interdisciplinary Methods Used to Understand them. *In: Sahai, N. &*

- Schoonen, M.A.A. (eds) Medical Mineralogy and Geochemistry*. Mineralogical Society of America, *Reviews in Mineralogy & Geochemistry*, 64, 5-57.
- Posfai, M., Molnar, A., 2000. Aerosol particles in the troposphere: A mineralogical introduction. *In: Vaughan, D.J. & Wogelius, R.A. (eds)*. EMU Notes in Mineralogy, 2, Eoetvos University Press, Budapest, 197-252.
- Skarpelis, N., Argyraki, A., Grypioti, A., 2009. Characterization of sources of inhalable particulate matter (PM₁₀) in the old processing and smelting site of lavrion, Greece. Goldschmidt 2009, Davos, Switzerland, *Special Supplement Geoch. et Cosmoch. Acta* 73, no 13S, p. A 1324.
- Triantafyllou, A., 2000. Patterns and concentrations of PM₁₀ in a Mountainous Basin Region. *Journal of the Air & Waste Management Association*, 50, 1017-1022.
- Triantafyllou, A., Filippidis, A., Patra, A., Pavlidis, A., Kantiranis, N., 2000. Concentrations, mineralogy and morphology of the suspended particles PM₁₀ in the city of Kozani. Proceedings 1st Congress of the Committee of Economic Geology, Mineralogy and Geochemistry, Geological Society of Greece (Kozani), 452-462 (In Greek with English Abstract).

12ο ΔΙΕΘΝΕΣ ΣΥΝΕΔΡΙΟ ΤΗΣ ΕΛΛΗΝΙΚΗΣ ΓΕΩΛΟΓΙΚΗΣ ΕΤΑΙΡΙΑΣ
ΠΛΑΝΗΤΗΣ ΓΗ: Γεωλογικές Διεργασίες και Βιώσιμη Ανάπτυξη

12th INTERNATIONAL CONGRESS OF THE GEOLOGICAL SOCIETY OF GREECE
PLANET EARTH: Geological Processes and Sustainable Development



ΟΡΥΚΤΟΛΟΓΙΑ ΚΑΙ ΠΕΤΡΟΛΟΓΙΑ
MINERALOGY AND PETROLOGY

GEOCHEMISTRY AND TECTONIC SETTING OF ECLOGITE PROTOLITHS FROM KECHROS COMPLEX IN EAST RHODOPE (N.E. GREECE)

Baziotis I. and Mposkos E.

National Technical University of Athens, Department of Mining and Metallurgical Engineering, Section of Geological Sciences, Heroon Polytechniou 9, 15780, Athens, Greece, mposkos@metal.ntua.gr, baziotis@metal.ntua.gr

Abstract

Eclogites and partially amphibolitized eclogites from the metamorphic Kechros complex in East Rhodope are studied in order to provide the geodynamic framework for the origin of their protoliths. Geochemical evidence from whole-rock major and trace element concentrations shows two distinct protolith groups. The low-Fe-Ti eclogites (Charakoma locality) have low-TiO₂ content (<0.67 wt%), negative Nb anomalies, positive Sr anomalies, small negative Zr and Hf anomalies and variable enrichments in LILE (e.g. Rb and Ba). The REE patterns are characterized by strong LREE enrichment ($La_N/Yb_N=5.45-5.81$), HREE depletion ($Gd_N/Yb_N=1.60-1.63$) and HREE abundance within the range of 9-10 × chondrite. The high-Fe-Ti eclogites (Kovalo and Virsini locality) have variable Sr contents, small to moderate LILE enrichment, HREE's similar to MORB values and absence of Nb anomalies. The REE patterns of the Kovalo and Virsini eclogites are characterized by LREE depletion and relative flat MREE-HREE patterns at approximately 20-30 × chondrite concentrations. Our results suggest that the protoliths of the Low-Ti eclogites show a continental rifting tectonic environment. In contrast, the protoliths of the High-Ti eclogites indicate formation of their protoliths by partial melting in an extensional oceanic environment.

Key words: *eclogites, amphibolitized eclogites, Kechros Complex, Rhodope.*

1. Introduction

Eclogites are high-pressure rocks that consist of omphacite and garnet, have broadly basaltic to intermediate composition and occur in a variety of geotectonic environments. Geochemical investigations are of great importance to elucidate the geotectonic environment of their protoliths and to provide important information on the tectonic evolution of the orogenic belts (e.g. Ernst and Liou, 1995).

The Rhodope high-pressure (HP) Province represents an Alpine synmetamorphic thrust and nappe complex that incorporates several tectonic slivers of ultra-high pressure (UHP) and HP metamorphic rocks formed during the Jurassic to Mid-Tertiary collision of the African and European plates (Burg et al., 1996; Liati and Mposkos, 1990; Mposkos and Krohe, 2000). It offers a great opportunity to study the geochemistry of such HP rocks, since they are common in the most tectonometamorphic complexes of it (Mposkos and Krohe, 2000). In the eastern Rhodope, the structurally uppermost Kimi Complex underwent UHP-HT metamorphism in early Jurassic (Mposkos and Kostopoulos, 2001; Bauer et al., 2007) and exhumed to the surface between 62 and 48 Ma (Krohe and Mposkos,

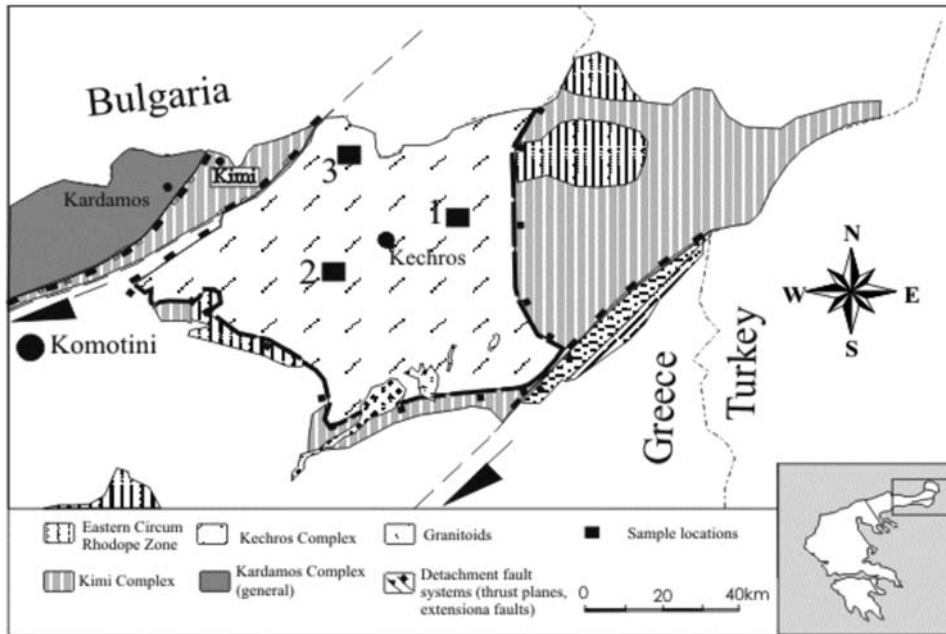


Fig. 1: Geological map of Kechros area showing the locations of the studied eclogites (Mposkos and Krohe, 2000).

2002). The underlying Kechros Complex underwent also Alpine HP metamorphism, documented by the common occurrence of fresh eclogites and amphibolitized eclogites with Permo-Triassic age of gabbroic protoliths (Liati and Mposkos, 1990; Liati, 2005). Exhumation to shallow crustal levels of the Kechros Complex occurred in Oligocene (Wawrzenitz and Mposkos, 1997; Lips et al., 2000).

In the present work we describe the geochemistry of eclogites, amphibolitized eclogites and dyke amphibolites from the Kechros Complex. Our objective is to investigate the nature of the protoliths, to provide a compilation of whole-rock major and trace element data and to place constraints on the petrogenesis and geodynamic history of the protoliths of the studied rocks.

2. Geological setting

In eastern Rhodope, a discrete tectonic contact separates the Kimi Complex from the underlying Kechros Complex (Fig. 1). The Kechros Complex consists of orthogneisses, metamigmatites (containing muscovite metapegmatite lenses, pelitic gneisses, high-alumina metapelites and rare marbles). Within the orthogneisses and metapelites, boudins of eclogites, eclogite amphibolites and amphibolites occur. Large ultramafic bodies are tectonically intercalated.

In the eclogites P-T conditions of ~ 1.5 GPa at $\sim 550^\circ\text{C}$, are estimated by Grt-Omp (Jd_{55}). (Thermobarometry; Liati and Mposkos, 1990). In the orthogneisses and metapelites the HP event is documented by the presence of phengites with maximum 3.5 Si atoms per formula unit (a.p.f.u.) and up to 3.42 Si a.p.f.u. respectively (Mposkos, 1989). Decompression was nearly isothermal from the maximum pressure of 1.5 GPa up to 0.4 GPa. It is recorded in metapelites by the successive formation of staurolite, chlorite and biotite at the expense of chloritoid and phengite (Mposkos, 1989; Mposkos and Liati, 1993, their figure 11a) implying rapid uplift.

Orthogneisses and metapegmatites indicate Variscan protolith ages. U-Pb zircon ages from orthogneisses range between 320-299 Ma (Liati, 2005; Cornelius, 2008). Rb-Sr age of magmatic muscovite in a metapegmatite associated with metamigmatites yielded 334 Ma (Mposkos and Wawrzenitz, 1995). U-Pb ages of magmatic zircons in eclogite yielded 245 Ma for the crystallization time of the gabbroic protolith (Liati, 2005). Rb-Sr and ^{39}Ar - ^{40}Ar white mica ages from mylonitic orthogneisses range between 41-36 Ma, constraining minimum age for the Alpine HP metamorphism (Wawrzenitz and Mposkos, 1997; Lips et al., 2000).

3. Petrography

The selected eclogites and amphibolitized eclogite samples occur in the following three areas: (1) Charakoma, (2) Kovalo and (3) Virsini (Fig. 1).

The eclogites have the mineral assemblage garnet + omphacite (Jd_{35-55}) + tremolite + hornblende \pm glaucophane + epidote \pm kyanite + phengite + rutile + quartz and the retrogressed amphibolitized eclogites tremolite + hornblende + albite + chlorite + epidote + quartz \pm phengite \pm paragonite \pm garnet \pm margarite + rutile. Glaucophane is found as inclusions in garnet from the Kovalo eclogite and kyanite from the Charakoma eclogite. Kyanite is associated with omphacite as inclusions in garnet as well as in the rock matrix. Garnet-clinopyroxene geothermometry yielded 550-620°C at 1.5 GPa (minimum pressure constrained from jadeite content in omphacite). However, the coexistence of kyanite with omphacite (j_{50}) constrains the minimum pressure at 2.1 GPa at least for the Charakoma eclogite.

4. Whole-rock major and trace element analysis

4.1 Methods

Major and trace element compositions of 11 representative samples (Table 1), including eclogites and amphibolitized eclogites, were determined by inductively coupled plasma – emission spectroscopy (ICP-ES). For major and trace element analysis, structural water was removed from sample powders by heating at 1000°C for 1 hour. Loss on ignition (LOI) was determined from the total weight change. Major and trace element analyses were performed on solutions after LiBO_2 fusion and nitric acid digestion of rock powder for ICP-ES analysis and on prepared beads after mixing with Di-Lithium Tetraborate and fusion for XRF analysis. Rare earth element (REE) analyses were determined by inductively coupled plasma-mass spectroscopy (ICP-MS) after LiBO_2 fusion and nitric acid digestion. The detection limits for the REE (in ppm) are <0.5 for La and Ce, <0.02 for Pr, <0.4 for Nd, <0.1 for Sm, <0.05 for Eu, Gd, Dy, Ho, Er, Tm and Yb, <0.01 for Tb and Lu. The whole-rock analyses were carried out at Acme Analytical laboratories in Canada.

4.2 Major elements and compatible trace elements

Based on $\text{Fe}_2\text{O}_3\text{t}$ and TiO_2 contents, two types of eclogites are distinguished: low-Fe-Ti eclogites (LFT) with $\text{Fe}_2\text{O}_3\text{t}$ < 9.9 wt% and TiO_2 < 0.79 wt% and high-Fe-Ti eclogites (HFT) with $\text{Fe}_2\text{O}_3\text{t}$ > 12.3 wt% and TiO_2 > 1.3 wt%.

Low-Fe-Ti eclogites:

The LFT eclogites have SiO_2 contents that range from 51.5 to 52.9 wt%, Al_2O_3 from 14.1 to 15.9 wt %, $\text{Fe}_2\text{O}_3\text{t}$ from 7.9 to 9.9 wt%, CaO from 8.6 to 10.6 wt%, TiO_2 from 0.48 to 0.79 wt% and Na_2O content from 1.75 to 3.14 wt%. Cr, Ni and Co abundances range from 103 to 438 ppm, 18 to 185 ppm and 29 to 44 ppm respectively.

Table 1. Representative major and trace element compositions of Low-Fe-Ti (LFT) and High-Fe-Ti (HFT) eclogites from the high pressure metamorphic Kechros Complex.

Sample	EK-7	At-13	At-13B	EK-6B	EK-9	93A-9	93A-11	B90-3B	KO2	KO4	KO6
Rock	LFT	LFT	LFT	LFT	LFT	HFT	HFT	HFT	HFT	HFT	HFT
<i>Major elements (wt%)</i>											
SiO ₂	52.46	52.86	51.67	51.49	52.04	44.56	43.48	44.55	45.68	44.29	46.01
TiO ₂	0.56	0.79	0.75	0.58	0.56	2.94	2.46	2.76	2.33	2.44	1.35
Al ₂ O ₃	14.56	15.00	14.54	14.71	15.95	13.10	12.71	13.16	11.74	12.27	15.92
Fe ₂ O _{3t}	8.39	9.90	7.90	8.76	8.19	18.70	17.90	17.95	15.50	16.57	12.27
MnO	0.14	0.21	0.09	0.14	0.14	0.27	0.26	0.26	0.24	0.23	0.18
MgO	10.15	6.17	7.54	10.62	8.97	6.76	8.21	7.28	8.19	9.24	8.59
CaO	9.00	8.73	10.57	8.88	9.03	10.87	13.27	10.87	13.28	11.70	12.32
Na ₂ O	2.07	2.23	3.14	1.75	1.80	2.53	0.99	2.50	1.18	1.02	1.72
K ₂ O	1.11	1.44	1.13	0.73	1.18	0.07	0.10	0.08	0.15	0.21	0.28
P ₂ O ₅	0.12	0.22	0.17	0.11	0.13	0.07	0.18	0.08	0.18	0.15	0.11
LOI	1.00	2.10	2.10	1.49	0.95	0.10	0.10	0.10	0.44	0.91	0.96
Total	99.56	99.65	99.60	99.25	98.93	99.97	99.66	99.59	98.91	99.03	99.71
Mg#	0.71	0.55	0.66	0.71	0.69	0.42	0.48	0.45	0.51	0.53	0.58
<i>Trace elements (ppm)</i>											
Ba	183	253	216	144.4	252.2	8	9	14	43.3	85.9	31.5
Cs	2.9	7.4	1.1	<0.1	6.6	0.2	<0.1	0.7	7.5	2.3	<0.1
Pb	4.5	1	2.6	18.5	29.4	0.8	0.4	0.7	<0.1	<0.1	4.1
Rb	37.5	58.1	27.7	25.3	32.3	1.5	1.4	1.6	4.3	4.4	7.6
Sr	409.9	416.6	656.9	466.6	754.3	36.9	45.6	45.2	129.6	33.3	338.1
Ta	0.2	0.5	0.3	<0.1	<0.1	0.3	0.3	0.4	<0.1	<0.1	<0.1
Th	2.9	4	2.7	11.7	6.3	<0.2	<0.2	<0.2	4.9	<0.2	<0.2
U	1	1.8	1.6	<0.1	<0.1	<0.1	<0.1	<0.1	<0.1	<0.1	<0.1
Nb	2.4	5.1	3.9	<0.1	<0.1	4.7	4.4	6.1	<0.1	<0.1	<0.1
Zr	54.1	91.4	69.8	30.2	45	149.5	108.5	215.5	94.9	99.5	40.2
Y	14.5	21.3	17.9	15.1	16.8	61.8	51.5	74	36.9	39.1	27.1
Ni	178	59	83	185.3	133.6	73	68	74	91	171.7	108.2
Cr	417.38	102.63	157.37	207.4	211.9	88.95	116.32	164.21	189.9	167.2	297.4
La	10.4	16.2	13	11.4	11.5	4.9	2.9	6.4	3.40	3.12	3.2
Ce	22.3	33.8	27.9	23.6	24.3	17.5	11.1	21.9	12.29	11.40	9.8
Pr	2.92	4.52	3.68	3.02	2.94	3.21	2.29	3.94	2.41	2.29	1.63
Nd	13.1	19.3	16.2	13.7	13.4	18.1	14.9	22.8	13.41	12.95	9.2
Sm	2.85	4.15	3.73	3.1	3	6.12	4.87	7.26	4.84	4.63	3.4
Eu	0.8	1.05	1.16	0.96	0.86	2.09	1.74	2.3	1.97	1.66	1.3
Gd	2.74	3.86	3.55	2.9	2.8	7.68	6.48	9.15	6.51	6.31	4.5
Tb	0.43	0.6	0.58	0.5	0.46	1.63	1.32	1.86	1.23	1.18	0.84
Dy	2.48	3.68	3.31	2.67	2.6	10.56	8.53	12.03	8.09	7.80	5.27
Ho	0.51	0.73	0.63	0.59	0.58	2.25	1.82	2.61	1.74	1.68	1.2
Er	1.47	2.29	1.87	1.54	1.55	6.84	5.57	8.34	5.10	4.98	3.33
Tm	0.22	0.32	0.24	0.23	0.23	0.99	0.8	1.17	0.75	0.74	0.52
Yb	1.5	2.09	1.55	1.5	1.42	6.51	5.25	7.66	4.81	4.80	3.17
Lu	0.22	0.31	0.23	0.25	0.22	0.97	0.78	1.13	0.70	0.70	0.5
[Gd/Yb]N	1.51	1.53	1.89	1.60	1.63	0.98	1.02	0.99	1.12	1.09	1.17
[La/Yb]N	4.97	5.56	6.02	5.45	5.81	0.54	0.40	0.60	0.51	0.47	0.72
[Eu/Eu*]	0.88	0.80	0.97	0.98	0.91	0.93	0.95	0.86	1.07	0.94	1.02
<: Below the detection limit											

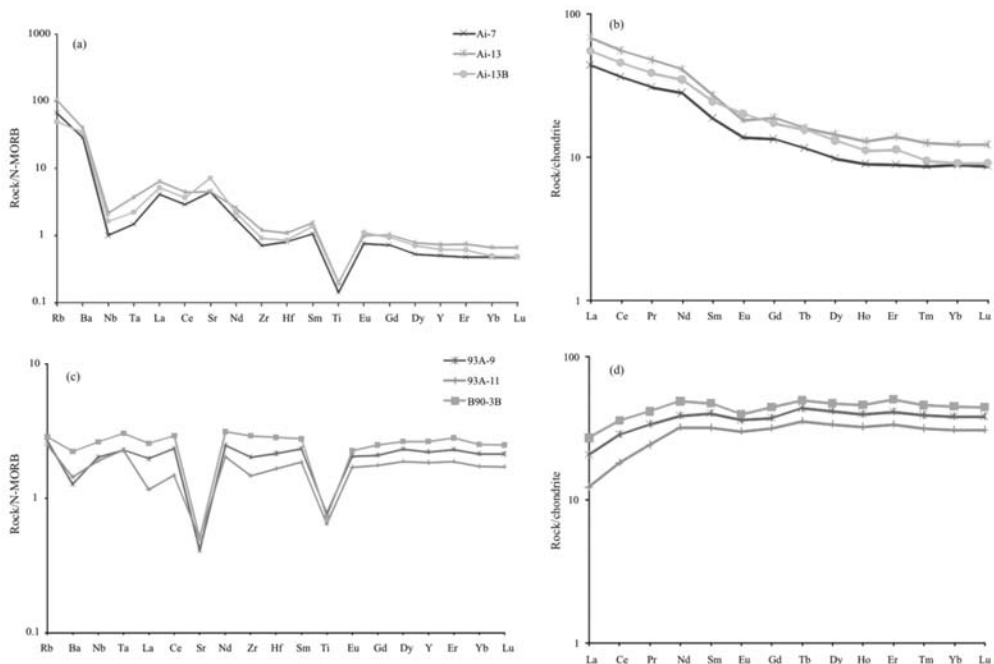


Fig. 2: N-MORB and chondrite-normalized trace-element diagrams for LFT (a,b), and HFT (c,d) eclogites. Normalizing values are from Sun & McDonough (1989).

High-Fe-Ti eclogites:

The HFT eclogites have SiO₂ contents that range from 43.5 to 46.0 wt%, Al₂O₃ from 11.7 to 15.9 wt %, Fe₂O₃t from 12.3 to 18.7 wt%, CaO from 10.9 to 13.3 wt%, TiO₂ from 1.3 to 2.9 wt% and Na₂O content from 1.0 to 2.5 wt%. Cr, Ni and Co abundances range from 89 to 297 ppm, 68 to 172 ppm and 45 to 66 ppm respectively.

4.3 Incompatible trace elements

Low-Fe-Ti eclogites:

N-MORB normalized trace elements patterns (Fig. 2a) are characterized by negative Nb-Ta and Ti anomalies, small positive Sr anomalies, high LILE (Rb, Ba) abundances and relatively flat high field strength elements (HFSE) from Zr-Lu with the exception of Sm which shows small positive anomalies.

The REE patterns normalized to chondrite (Fig. 2b) are characterized by strong LREE enrichment ($La_N/Yb_N=4.97-6.02$), HREE depletion ($Gd_N/Yb_N=1.51-1.89$) and HREE abundance within the range of 8-12 × chondrite.

High-Fe-Ti eclogites:

N-MORB normalized trace element patterns (Fig. 2c) are characterized by very strong negative Sr and Ti anomalies, small to moderate LILE enrichment, HREE's similar to MORB values and absence of Nb anomalies.

The REE patterns normalized to chondrite (Fig. 2d) are characterized by LREE depletion ($La_N/Yb_N=0.40-0.72$), slight negative Eu anomalies ($Eu/Eu^*=0.94-1.07$) and relatively flat MREE-HREE patterns. They fall within the range of 13-45 × chondrite for both LREE and HREE.

5. Discussion

5.1 Compositional modification during metamorphism

Seawater alteration, dehydration during metamorphism and partial melting are the main processes that could affect the composition of the protoliths of the LFT and HFT after their initial formation. Seawater alteration includes two opposite processes; the first is that they gain LILE and alkalis and the second is that they lose Si, Mg and Ca (Jacob et al., 1994).

Dehydration and loss of a melt component during passing from eclogite to amphibolite facies conditions could affect mainly the SiO_2 content and in lesser degree the LILE and LREE contents of the bulk-rock composition (Stalder et al., 1998; Foley et al., 2002). This could be done due to transformation of clinopyroxene to amphibole at high water activity. Besides, the more compatible elements (Cr, Ni, HREE) in eclogitic minerals (e.g. clinopyroxene and garnet) are less mobile and remain at the peak P-T conditions (Jacob and Foley, 1999). The HFSE (Nb, Ta, Zr, Hf) and Th have very low mobility in retrograde fluids and retain at the eclogitic primary or accessory minerals (Elliott et al., 1997; Hebert et al., 2009).

The incompatible elements enrichment of LFT eclogites could be attributed to mineral-fluid interaction at high-pressure conditions or even low-T seawater alteration. Low-T seawater alteration is a mechanism that theoretically is present but is difficult to influence all of the samples in a consistent way producing parallel trace element/REE patterns. Though, the Rb, Ba, K enrichments in our eclogitic samples (especially in LFT) is due to the extensive rehydration mechanism which results in the formation of hornblende (Becker et al., 2000). Petrographic data from the LFT eclogites suggest that the retrograde amphibole is in very high modal content indicating extended water fluxes. During the formation of such amphibole, a fluid phase, rich in Rb, Ba and K, is consumed in order to complete the reaction, by increasing the LILE contents in the eclogites. Another LILE element such as Cs, is positively and more strongly correlated with K (diagram not shown) indicating that retrograde fluids could affect its concentration.

In fact, the REE patterns of both LFT and HFT eclogites vary interconsistently probably reflecting primary composition of the protoliths.

In order to check the relative mobilization of various elements, we investigate the role of the theoretical immobile elements. The HFSE's (Nb, Ta, Zr, Ti) and the REE's are seen to be relative less mobile during retrogression process.

5.2 Bivariate TiO_2 -Mg# vs. Major/trace element plot

Major and trace element vs. TiO_2 plots are shown in Figure 3. They display the following trends with decreasing TiO_2 : (1) The HFT eclogites show CaO, MgO and Cr concentrations which more or less continuous negative trend with TiO_2 whereas Fe_2O_3t is positively correlated; (2) SiO_2 remain nearly constant at decreasing TiO_2 content whereas Na_2O decreasing for $TiO_2 > 2.4$ wt% and increasing for lower TiO_2 contents; (3) CaO, MgO, Fe_2O_3t lie above the MORB field whereas SiO_2 and Na_2O fall below the field defined for MORB-type basaltic rocks; Cr is plotted within the MORB field. In contrast to the HFT eclogites, the LFT ones, display limited range of TiO_2 showing (1) steep negative

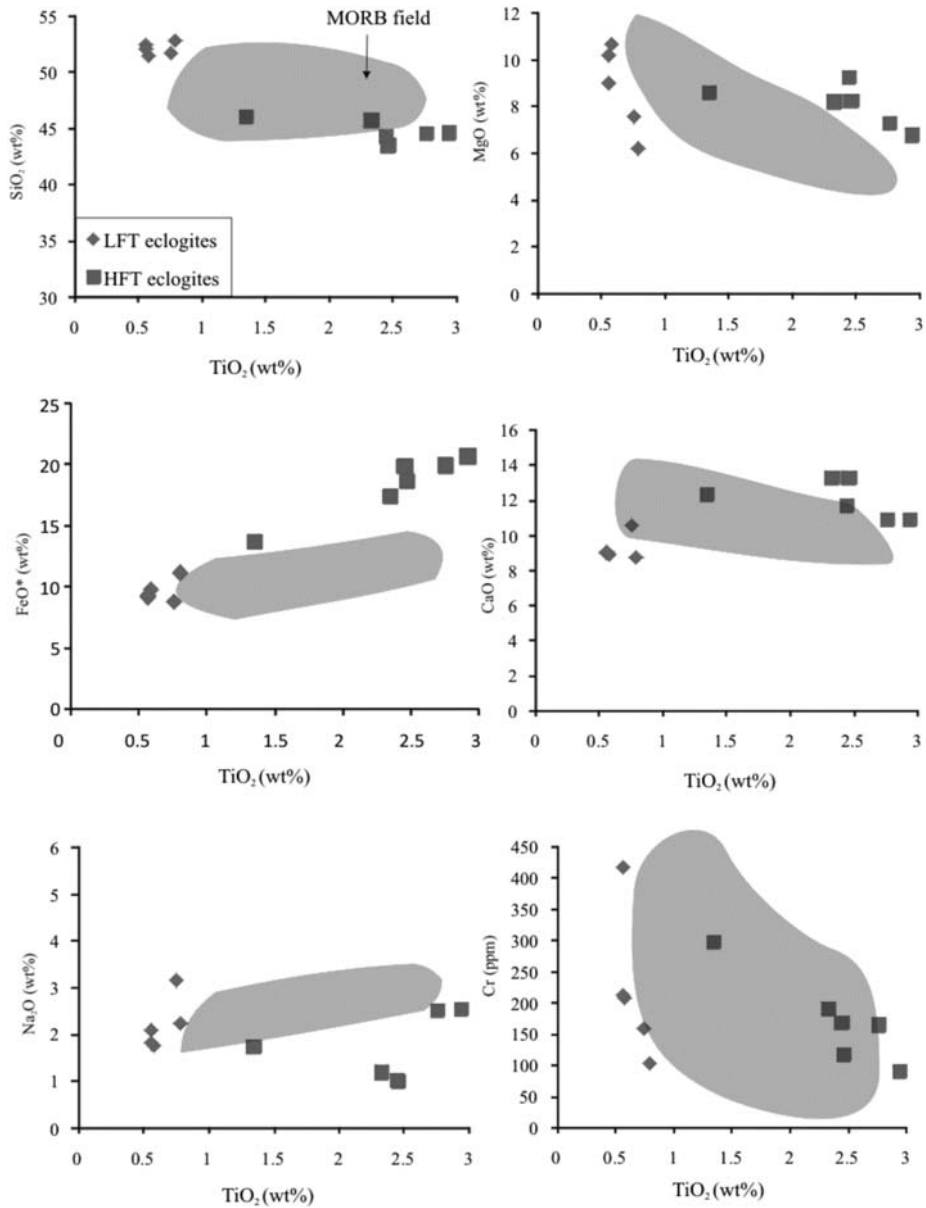


Fig. 3: Selected major and trace elements vs. TiO_2 for both LFT and HFT eclogites. Grey field represents MORB values.

trends for Cr and MgO, whereas the major elements CaO, SiO_2 , FeO^* and Na_2O contents are more scattered without obviously trends; (2) comparing the values of the LFT eclogites, are generally plotted outside the MORB field.

The evolution of the Mg- to Fe-rich gabbroic rocks is well established in bivariate plots of selected major and trace elements vs. Mg# (figure not shown). The compatible elements such as Cr and Ni

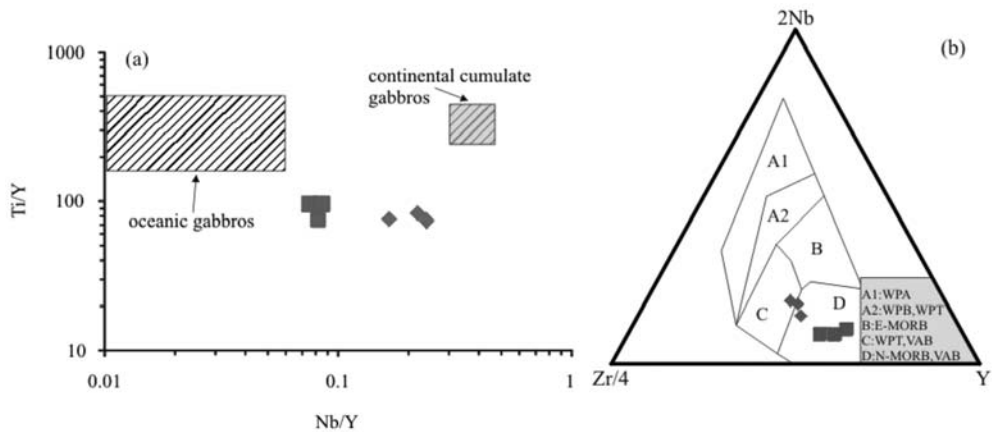


Fig. 4: (a) Nb/Y vs. Ti/Y variation diagram comparing LFT and HFT eclogites with continental and oceanic gabbros. (b) Nb-Zr-Y ternary plot showing the contrasting tectonic signatures of LFT and HFT eclogites. Symbols for both LFT and HFT eclogites as in figure 3.

decrease with decreasing Mg# whereas the elements Zr, P, Ti and Y increase with decreasing Mg# for both LFT and HFT eclogites respectively. However, the LFT eclogites display higher Mg# and do not show coherent and continuous fractionation trends for most of the elements compared with HFT eclogites. Within each sampling area of the study region, the eclogites have parallel REE patterns with systematically increasing REE concentration with decreasing Mg#. The LFT eclogites display LREE-enriched patterns whereas the HFT eclogites generally display LREE-depleted patterns. The above geochemical features suggest that the studied eclogites represent gabbroic rocks having different petrogenetic histories. The gabbroic character of these eclogites is also verified in the LFT eclogite from Charakoma area where relics of the primary gabbro are preserved in the central part of the eclogite body (Liati and Mposkos, 1990).

6. Tectonic setting

As already shown in the geochemistry section, the LFT eclogites have rift-related signatures whereas the HFT eclogites have MORB signatures. Such speculations could be represented in a Ti/Y-Nb/Y variation diagram (Fig. 4a), in which the two types of eclogites are shown; both types of eclogites share similar Ti/Y values (~66-84 for LFT and 75-99 for HFT) but significant different Nb/Y values (0.17-0.22 for LFT and ~0.08 for HFT). The LFT samples are plotted close to the continental cumulate gabbros whereas the HFT close to the oceanic gabbros; however both eclogites are shifted toward lower Ti/Y values.

Low-Fe-Ti eclogites

The LFT eclogites have rift-related enriched-REE patterns. Trace element systematics such as the high Ce/Nb (>6.6) and Th/Yb (1.74-7.80) ratios span over the N-MORB range for the Ce/Nb (~3.2) and Th/Yb (~0.04). Most of the samples are plotted in the C field of the ternary diagram Nb-Zr-Y (Fig. 4b) which corresponds to within-plate or volcanic-arc basalts; though indicates the rift-related signatures of the LFT eclogite protolith. The geochemistry of LFT eclogites suggests formation in a rift-related tectonic setting.

High-Fe-Ti eclogites

The HFT eclogites have typical MORB-type REE patterns. Currently, trace element geochemistry systematics suggest an N-MORB protolith. The Ce/Nb ratios range from 2.52 to 3.72, whereas the Th/Yb ratios are lower than 1.02. The above ratios span over the N-MORB range for the Ce/Nb (~3.2) and Th/Yb (~0.04). All of the samples are plotted within D field of the diagram Nb-Zr-Y, indicating N-MORB signatures for the HFT eclogite protolith (Fig. 4b). Nb and Ti depletion observed in N-MORB-normalized trace element patterns is consistent with fractionation and continuous removal of minor amounts of Ti-bearing phase such as rutile. Besides, all of the analyzed samples show negative Nb-Ta, Sr and Ti anomalies in their N-MORB normalized trace element patterns suggesting that the protolith was oceanic crust, derived from a depleted mantle in a SSZ environment.

7. Conclusions-Results

The eclogites from Charakoma, Kovalo and Virsini areas are the metamorphic equivalents of gabbroic rocks in terms of mineral assemblages, major and trace element geochemistry.

Based on the geochemical data presented on this study, the studied eclogites are divided into two groups. The first group (Charakoma locality-LFT eclogites) displays strong LREE enrichment, HREE depletion, low Ti and Fe contents, variable enrichments in LILE (e.g. Rb and Ba), negative Nb-Ta, Zr and Hf anomalies and positive Sr anomalies. Their protoliths have been formed in a continental rifting tectonic environment. The second group (Kovalo and Virsini locality-HFT eclogites) show LREE depletion and relative flat MREE-HREE on REE patterns, high Ti and Fe contents, small to moderate LILE enrichment, variable Sr contents, HREE's similar to MORB values and absence of Nb anomalies. The protoliths of the HFT eclogites indicate formation by partial melting in an extensional oceanic environment.

8. Acknowledgments

I.B. and E.M. were financially supported by the Special Research project "PEBE 2008" funded by National Technical University of Athens.

9. References

- Bauer, C., Rubatto, D., Krenn, K., Proyer, A. and Hoinkes, G. 2007. A zircon study from the Rhodope metamorphic complex, N-Greece: Time record of a multistage evolution. *Lithos*, 99, 207-228.
- Baziotis, I., Mposkos, E. and Asimow, P.D. 2008. Petrogenesis of ultramafic rocks from the ultrahigh-pressure metamorphic Kimi Complex in Eastern Rhodope (NE Greece). *Journal of Petrology*, 49, 5, 885-909.
- Becker, H., Jochum, K.P. and Carlson, R.W. 2000. Trace element fractionation during dehydration of eclogites from high-pressure terranes and the implications for element fluxes in subduction zones. *Chemical Geology*, 163, 65-99.
- Burg, J.P., Ricou, L.E., Ivanov, Z., Godfriaux, I., Dimov, D. and Klain, L. 1996. Syn-metamorphic nappe complex in the Rhodope Massif: structure and kinematics. *Terra Nova*, 8, 6-15.
- Cornelius, N.K., 2008. UHP metamorphic rocks of the Eastern Rhodope Massif, NE Greece: new constraints from petrology, geochemistry and zircon ages. PhD Thesis, Johannes-Gutenberg Universität, Mainz.
- Elliott, T., Plank, T., Zindler, A., White, W. and Bourdon, B. 1997. Element transport from slab to volcanic front at the Mariana arc. *Journal of Geophysical Research*, 102 (B7), 14991-15019.
- Ernst, W.G. and Liou, J.G., 1995. Contrasting plate-tectonic styles of the Qinling–Dabie–Sulu and Franciscan metamorphics. *Geology* 23, 353–356.

- Foley, S.F., Tiepolo, M. and Vannucci, R. 2002. Growth of continental crust controlled by melting of amphibolite, not eclogite. *Nature*, 417, 837-840.
- Hebert, L.B., Asimow, P.D. and Antoshechkina, P. 2009. Fluid source-based modeling of melt initiation within the subduction zone mantle wedge: Implications for geochemical trends in arc lavas. *Chemical Geology*, 266, 306-319.
- Jacob, D.E. and Foley, S.F. 1999. Evidence for Archean ocean crust with low high field strength element signature from diamondiferous eclogite xenoliths. *Lithos*, 48, 317-336.
- Jacob, D.E., Jagoutz, E., Lowry, D., Matthey, D. and Kudrjavitseva, G. 1994. Diamondiferous eclogites from Siberia: remnants of Archean oceanic crust. *Geochimica et Cosmochimica Acta*, 58, 5191-5207.
- Jacob, D.E. and Foley, S.F., 1999. Evidence for Archean ocean crust with low high field strength element signature from diamondiferous eclogite xenoliths. *Lithos*, 48, 317-336.
- Krohe, A. and Mposkos, E., 2002. Multiple generations of extensional detachments in the Rhodope Mountains (N.Greece): evidence of episodic exhumation of high-P rocks. In: Blundell, D.J., Neubauer, G. and Von Quant, A. (eds.): The timing and location of major ore deposits in an evolving orogen. Geological Society of London, Special Publication, 204, 151-178.
- Liati, A., 2005. Identification of repeated Alpine (ultra) high-pressure metamorphic events by U–pb SHRIMP geochronology and REE geochemistry of zircon: the Rhodope zone of Northern Greece, *Contributions to Mineralogy and Petrology* 150, 608–630.
- Liati, A. and Mposkos, E., 1990. Evolution of the eclogites in the Rhodope Zone of northern Greece, *Lithos*, 25, 89–99.
- Lips, A.L.W., White, S.H. and Wijbrans, J.R. 2000. Middle–Late Alpine thermotectonic evolution of the southern Rhodope Massif, Greece. *Geodinamica Acta*, 13, 281–292.
- Martin, R.F., 1998. Symbols of the rock-forming minerals. The Nomenclature of minerals: A compilation of IMA reports. IMA`98 Toronto, 148-149.
- Mposkos, E., 1989. High-pressure metamorphism in gneisses and pelitic schists in the Eat Rhodope Zone (N. Greece). *Mineralogy and Petrology*, 41, 25-39.
- Mposkos, E. and Krohe, A., 2000. Petrological and structural evolution of continental high pressure (HP) metamorphic rocks in the Alpine Rhodope domain (N.Greece). Proceedings of the 3rd International Conference on the Geology of the Eastern Mediterranean, 221-232.
- Mposkos, E. and Kostopoulos, D., 2001. Diamond, former coesite and supersilicic garnet in metasedimentary rocks from the Greek Rhodope: a new ultrahigh-pressure metamorphic province established. *Earth and Planetary Science Letters*, 192, 497-506.
- Mposkos, E. and Liati, A., 1993. Metamorphic evolution of metapelites in the high-pressure terrane of the Rhodope zone, Northern Greece. *Canadian Mineralogist*, 31, 401-424.
- Mposkos, E. and Wawrzenitz, N., 1995. Metapegmatites and pegmatites bracketing the time of HP-metamorphism in polymetamorphic rocks of the E-Rhodope: Petrological and geochronological constraints. Geological Society of Greece, Special Publication 2(4), 602-608.
- Stalder, R., Foley, S.F., Brey, G.P. and Horn, I. 1998. Mineral-aqueous fluid partitioning of trace elements at 900-1200°C and 3.0-5.7 GPa: new experimental data for garnet, clinopyroxene, and rutile, and implications for mantle metasomatism. *Geochimica et Cosmochimica Acta*, 62, 1781-1801.
- Sun, S.S. and McDonough, W.F., 1989. Chemical and isotopic systematics of oceanic basalts: implications for mantle composition and process. In: Saunders, A.D. & Norry, J.M. (eds) Magmatism in Ocean Basins. Geological Society of London, Special Publications 42, 313-345.
- Wawrzenitz, N. and Mposkos, E., 1997. First evidence for lower Cretaceous HP / HT-metamorphism in the Eastern Rhodope, North Aegean Region, North-East Greece. *European Journal of Mineralogy*, 9, 659-664.

MUNICIPAL WASTEWATER TREATMENT WITH BENTONITE FROM MILOS ISLAND, GREECE

**Bourliva A.¹, Michailidis K.¹, Sikalidis C.², Filippidis A.¹,
and Apostolidis N.³**

¹ Aristotle University of Thessaloniki, Faculty of Sciences, Department of Mineralogy-Petrology- Economic Geology, 54124 Thessaloniki, Greece, annab@geo.auth.gr

² Aristotle University of Thessaloniki, Department of Chemical Engineering, 54124 Thessaloniki, Greece

³ Water & Sewage Municipal Public Utility of Kilkis City, 1st klm. Kilkis-Xirovrisi, 61100 Kilkis, Greece

Abstract

Bentonite clay minerals belonging to the smectite group have a wide range of chemical and industrial uses. The structure and chemical composition, exchangeable ion type and small crystal size of smectite are responsible for several properties, including a large chemically active surface area and a high cation exchange capacity. A wastewater treatment using bentonite from Milos island, Greece, was investigated. Raw wastewater sample (influent) from the wastewater treatment plant (WTP) of the city of Kilkis, Northern Greece was treated using bentonite in conjunction with chemical coagulants (polyaluminium chloride-PAC and cationic polyelectrolyte), in batch type experiments. The removal of suspended solids (SS), chemical oxygen demand (COD), nitrate ion, ammonium ion, phosphate ion, and toxic metals were evaluated. The treatment gave overflowed clear water improved concerning the quality parameters. The bentonite adding prior to flocculation resulted in effective removal of heavy metals such as chromium and copper. Additionally, the bentonite removed nitrogen compounds with relatively high efficiency, while the clay presence highly improved the COD removal. The quality parameters after treatment were improved fulfilling the requirements for disposition as downstream, irrigation, swimming and fish waters.

Keywords: wastewater treatment, bentonite, influent, chemical coagulants.

1. Introduction

Due to the rapid development in technology and urbanization, increasing amounts of industrial, agricultural, and domestic wastes are discharged to receiving waters. Generally, they are discharged to the nearest water sources such as rivers, lakes and seas. Wastewater treatment plants (WTPs) are expected to control the quality of the municipal wastewater (including industrial hazardous wastes) before being discharged into the nearby water sources (Chen et al., 2002).

The need for water re-use has made the effluents from municipal WTPs to be considered as a valuable resource and integrated into the available water supply. The effluents from these plants, however, usually contain some impurities, such as suspended matter, residues of stable organic materials, and refractory matter, which can cause undesirable colour, taste, and odour. Besides they contain nutrients such as phosphates and nitrogenous materials that cause eutrophication in receiving waters.

Table 1. Chemical and mineralogical composition of bentonite with specific surface area and cation exchange capacity value.

Sample	SiO ₂	Al ₂ O ₃	TiO ₂	MnO	Fe ₂ O _{3t}	MgO	CaO	Na ₂ O	K ₂ O	P ₂ O ₅	LOI	
Bentonite	58.75	17.09	0.62	0.035	4.00	3.52	3.56	0.95	0.75	0.08	10.72	
	Ba (µg/g)	Co (µg/g)	Cr (µg/g)	Cu (µg/g)	Ni (µg/g)	Pb (µg/g)	Rb (µg/g)	Sr (µg/g)	Zn (µg/g)			
	386	22	23	26	-	-	49	95	42			
	CEC (meq/100g)		SSA (m ² /g)		Mineralogical Composition							
	104.35		66.41		Smectite, Calcite, Amorphous, Mica (tr), Pyrite (tr)							

Flocculation and adsorption are typical examples of treatment processes. Recently, low cost materials, including rice-husk, maple sawdust, soya cake, coal ash, peat and bone char, have been investigated as adsorbents for wastewater treatment (Ahsan et al., 2001; Daneshvar et al., 2002; Ringqvist et al., 2002; Daifullah et al., 2003; Yu et al., 2003; Kirk et al., 2003). Additionally, the purification of industrial and urban wastewaters using a HEU-type zeolite (clinoptilolite) has been successfully applied (Filippidis et al., 2008a, Filippidis et al., 2008b).

Clay minerals have great potential as inexpensive and efficient adsorbents for wastewater treatment due to their large reserves, chemical and mechanical stability, high specific surface area, and structural properties. Part of the organic matter present in the effluent may be adsorbed on clay minerals, which have a large active surface area available for adsorption, especially for compounds containing amines, amides, and polysaccharides (Greenland, 1965). In this way, the adsorbed complex will cause removal of various compounds from the liquid during a flocculation step.

In the present study raw bentonite samples from Milos island were used in combination with chemical coagulants in the treatment of municipal wastewater. Bentonite is a natural clay formation consisting mainly of montmorillonite which belongs to the 2:1 smectite clay mineral group. The basic structural unit is composed of two tetrahedrally coordinated sheets of silicon ions surrounding a sandwiched octahedrally coordinated sheet of aluminum ions. The isomorphous substitution of Al³⁺ for Si⁴⁺ in the tetrahedral layer and Mg²⁺ for Al³⁺ in the octahedral layer results in a net negative surface charge on the clay (Luckham and Rossi, 1999). Compared with other clay types, it has excellent sorption properties and possesses sorption sites available within its interlayer space as well as on the outer surface and edges (Tabak et al., 2007).

2. Materials and Methods

2.1 Characterization of bentonite

The raw bentonite was kindly provided by the S&B Industrial Minerals S.A., Milos island, Greece. The sample was air-dried, ground and sieved. The <63µm particle size fraction was used in the experiments. The chemical composition of bentonite was determined by AAS (Perkin Elmer 901A). X-ray diffraction (XRD) analysis of the sample was carried out with a Philips PW 1710 diffractometer using CuKα radiation, in the 2θ angle range from 3° to 63°. The cation exchange capacity (CEC) and specific surface area (SSA) were obtained by the ammonium acetate method (Alexiades and Jackson, 1966) and multipoint BET N₂ adsorption method. The mineralogical and chemical

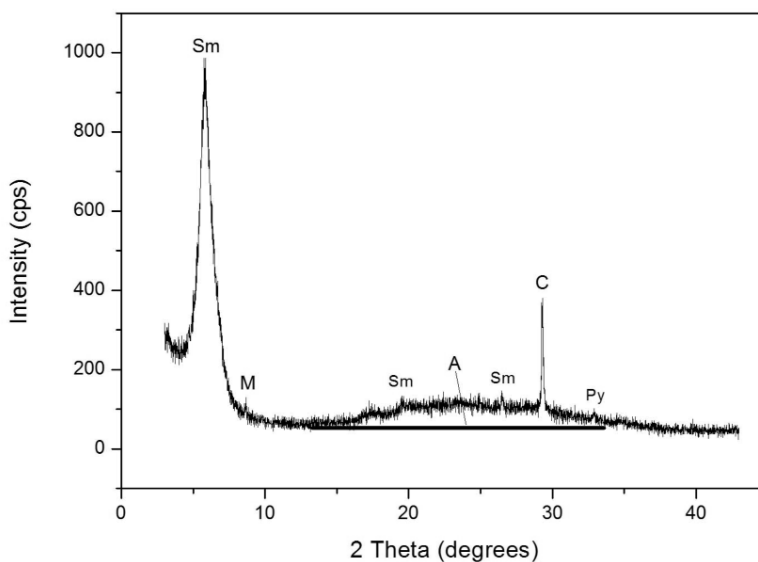


Fig. 1: X-ray diffraction pattern of bentonite sample (A: Amorphous, C: Calcite, M: Mica, Sm: Smectite, Py: Pyrite).

compositions of the bentonite are presented in Table 1. The X-ray diffraction pattern of the bentonite sample is shown in Figure 1.

2.2 Sampling the wastewater samples

The raw wastewater samples (influent) were obtained from the wastewater treatment plant (WTP) of the city of Kilikis. The WTP serves about 26,000 residents by treating daily 7,500-10,000 m³ of municipal wastewaters. About 5–10% of the total flow is contributed by small enterprises. The treatment process includes screening, grit removal, primary sedimentation with the use of chemical coagulants (polyaluminium chloride-PAC and cationic polyelectrolyte), conventional activated sludge treatment, and effluent disinfection with UV-radiation. The quality of the influent is presented in Table 2.

2.3 Treatment Procedure

Municipal wastewaters were treated with bentonitic clay at room temperature, in batch type experiments. The treatment process proceeded with rapid mixing of 300ml raw wastewater samples with 7.5g of bentonite at 400 rpm for 60 min, slow mixing of 40 rpm for 30 min and then standstill for 20 min. Polyaluminium chloride (PAC) and cationic polyelectrolyte were added as coagulant aids during the slow mixing step. For comparison reasons the same process was conducted without the addition of the bentonite. The bentonite amount (7.5g) added was chosen as the optimum (with the higher removal percentage) after experimental trials with various amounts of this material. The supernatant was filtered through 0.45µm and analyzed. All the essays were conducted in triplicate and only mean values are presented.

Table 2. Quality of the raw wastewater (influent) from the Kilkis wastewater treatment plant.

<i>Constituents</i>	<i>Units</i>	<i>Influent (Raw Wastewater)</i>
Temperature	°C	23.6
pH		8.71
Conductivity	µS/cm	1487
Colour	Pt/Co	2375
TSS	mg/L	360
COD	mg/L	742
NO ₃ -N	mg/L	14.2
NO ₂ -N	mg/L	0.043
NH ₄ -N	mg/L	138.50
PO ₄ ³⁻	mg/L	4.77
Cr _{total}	mg/L	0.05
Cu	mg/L	0.30
Mn	mg/L	0.241
Ni	mg/L	0.281
Zn	mg/L	0.67

TSS: Total Suspended Solids, COD: Chemical Oxygen Demand

2.4 Analytical Methods

Electrical conductivity and pH were measured with an electrode (CDM210, Radiometer, Copenhagen) and a combination electrode, respectively, at 25°C. The concentration of total suspended solids was determined by immediately filtering the samples through a 0.45 micron filter paper. The filters were weighed before the filtration and subsequently dried and weighed again after the filtration to determine the concentration of suspended solids. Analysis of colour, phosphate (PO₄³⁻), ammonia (NH₄⁺), nitrate (NO₃⁻), nitrite (NO₂⁻), and the metals Cr(total), Cu²⁺, Mn²⁺ and Ni²⁺ were performed using a HACH DR/2000 spectrophotometer.

3. Results and Discussion

The use of bentonite in conjunction with chemical coagulants in the treatment of municipal wastewaters was investigated. The results are presented in Table 3 and Figure 1. The treated wastewaters resulted in clear overflowed waters, free of odours and highly improved quality parameters.

Treatment of the municipal sewages with pH 8.71 resulted in a decrease of pH value to 6.72 and 6.61 with and without the addition of bentonite in the process, respectively.

Reduction of suspended solids (SS) plays a significant role in modern wastewater treatment, since the SS serves as an adsorbent for heavy metals and polychlorinated biphenyls (PCBs) (Rosenwinkel et al., 2001). Total suspended solids were effectively removed (99%) with no bentonite addition, due to flocculation. The bentonite added in the process made no significant difference in the TSS removal.

Table 3. Quality of the wastewaters after the treatment with and without the addition of bentonite.

Constituents	Treatment Without Bentonite		Treatment With Bentonite		
	Treated Wastewater	±%	Treated Wastewater	±%	±% Difference With the Bentonite Addition
pH	6.61 ± 0.1	-24.11	6.72 ± 0.2	-22.85	+1.3
EC (µS/cm)	1929 ± 3	-29.72	2050 ± 2	-37.86	+8.1
Colour (Pt/Co)	32 ± 0.5	-98.65	6 ± 0.1	-99.75	+1.10
TSS (mg/L)	3 ± 0.1	-99.17	1 ± 0.1	-99.72	+0.56
COD (mg/L)	250 ± 2	-66.31	146 ± 2	-80.32	+14.02
NO ₃ -N (mg/L)	5.40 ± 0.05	-61.97	1.90 ± 0.02	-86.62	+24.65
NO ₂ -N (mg/L)	0.018 ± 0.007	-58.14	0.010 ± 0.003	-76.74	+18.60
NH ₄ -N (mg/L)	126.20 ± 0.05	-30.01	82.40 ± 0.08	-54.30	+24.29
PO ₄ ³⁻ (mg/L)	0.44 ± 0.01	-90.78	0.39 ± 0.01	-91.82	+1.05
Cr _{total} (mg/L)	0.02 ± 0.01	-60.00	0.01 ± 0.01	-80	+20
Cu (mg/L)	0.11 ± 0.01	-63.33	0.07 ± 0.01	-76.67	+13.33
Mn (mg/L)	0.041 ± 0.005	-82.99	0.037 ± 0.005	-84.65	+1.66
Ni (mg/L)	0	-100	0	-100	0
Zn (mg/L)	0.21 ± 0.03	-68.66	0.50 ± 0.03	-25.37	-43.28

Each value is the mean of three readings ± standard deviation.

The discharge of untreated wastewater containing high levels of organic pollutants into river water affects the suitability of river water for human use and it stimulates the growth of algae and aquatic plants (Kuroda et al., 1997). Hence, various treatment methodologies have been used for the removal of organic load from wastewater. Most of them are complicated and time-consuming, except for adsorption methods, which are of low cost and easy to use. A COD removal of about 66% occurs as a result of the treatment with no clay added, due to flocculation. The presence of bentonite notably improves the removal of COD. Almost 80% of the total COD can be removed by treating with chemical coagulants after the addition of clay. The bentonite alone, when added to the influent removed 14% of the total COD. The more efficient removal of COD by bentonite is related to the effective adsorption of organic matter in the large surface area of the clay (Greenland, 1965).

The presence of excess nitrogen and its compounds has a negative impact on the environment. Nitrogenous compounds play an important role in water pollution and it is well known that they cause serious diseases (Balci and Dinçel, 2002). Therefore, the control of them in water has vital importance. In the treatment process without the bentonite, the removal efficiencies of nitrate, nitride and ammonium ion from the wastewater, were relatively low (30-62%). Bentonite adding prior to flocculation highly improved the removal of the nitrogen compounds. The bentonite itself removes 25% of nitrate ion, 19% of nitride ion and 24% of ammonium ion. Consequently, nitrogen compounds are

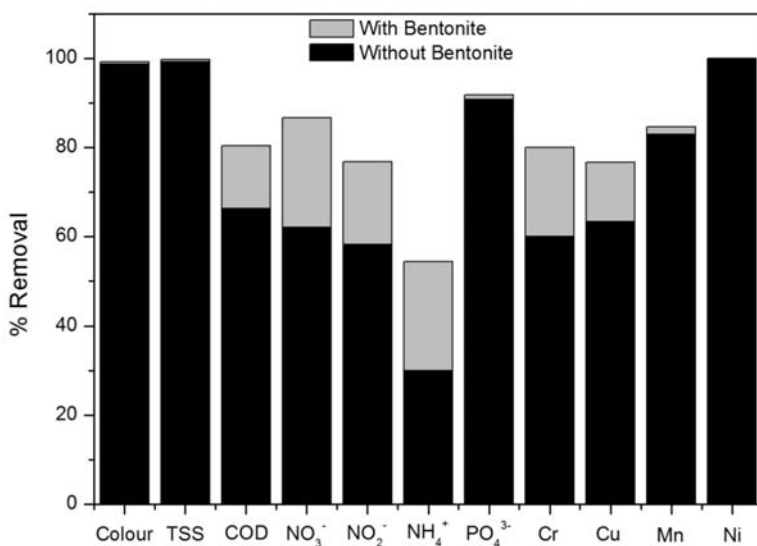


Fig. 2: Removal percentage of influent constituents with and without the presence of bentonite in the treatment process.

effectively removed by the bentonitic clay. NO_3^- and NO_2^- ions were basically removed by ion exchange or by physical adsorption, while NH_4^+ ions were removed by cation exchange processes after bentonite addition (Grimshaw and Harland, 1975; Ahsan et al., 2001).

Phosphorus is a critical nutrient for many biological systems, including the production of food. In a soluble form, phosphate has good surfactant properties and is used extensively in cleaners, detergents and washing soaps. During its widespread commercial use, its ability to stimulate the growth of algae in water systems has become very apparent. Therefore, the amounts of phosphate in domestic and industrial wastewaters need to be controlled using the either chemical or biological techniques (Galarneau and Gehr, 1997; Kirk et al., 2003). The chemical coagulants used in the treatment process showed high efficiencies for removal of phosphate ion. The bentonite addition in the treatment resulted in a slight difference (~1%) in the phosphate ion removal.

Chromium, copper, manganese, nickel and zinc are commonly known toxic heavy metals and tend to concentrate in environmental systems and in humans. Therefore, the effect of bentonite in conjunction with chemical coagulants in the removal of these heavy metals in wastewater treatment was investigated, as presented in Table 3 and Figure 1. The heavy metal removal efficiencies are relatively high (60-100%) for the treatment with no bentonite added. The bentonite addition shows a slight difference in the removal of chromium (20%), copper (13%) and manganese (1.7%). Contrary, the clay addition showed an increase in the zinc concentration in the treated wastewater. However, this increase can be attributed to the exchangeable Zn cation hosted in the bentonitic clay (Table 2). Therefore, for the concentrations of heavy metals tested (<1mg/L), the bentonite addition seems to be effective only for the removal of chromium and copper.

The notable effect of bentonitic clay in improving removal of the various components from the influent can be explained by several mechanisms. This hydrophobic colloid, having a large available surface area, adsorbs the products of the reaction between the chemical coagulants like cationic

polyelectrolyte and anionic components of the influent. The clay particles serve as nuclei for flocculation, resulting in formation of large, rapid settling flocs. Therefore, reaction products that were finely dispersed and could not be made to settle after flocculation (but would be separated by centrifuging) did indeed settle from the suspension in the presence of clay. This means that the main task of the clay is to aid in the settling of the suspended solids. It must also be remind that the clay added to the effluent is in a coagulative state, because of the ionic strength and the high Ca^{2+} concentration in the latter. The clay suspension approaches instability and it can easily be flocculated (Rebhun et al., 1969).

4. Conclusions

The use of bentonite in combination with chemical coagulants for the removal of TSS, COD, nitrogen compounds (NO_3^- , NO_2^- , NH_4^+), phosphate ion and toxic metals in the treatment of municipal wastewaters was investigated. Treatment resulted to clear overflowed waters, free of odours. The quality parameters of the overflowed water were improved. Bentonite adding prior to flocculation was effective for removal of COD, nitrogen compounds and selected heavy metals such as chromium and copper. The quality parameters in the treated wastewaters are fulfilling the requirements for disposition as downstream, irrigation, swimming and fish waters (Andreadakis et al., 2003; EPA, 2004).

5. Acknowledgements

The authors would like to thank the S&B Industrial Minerals S.A. company which kindly provided the raw bentonite applied in this investigation.

6. References

- Ahsan, S., Kaneco, S., Ohta, K., Mizono, T., Kani, K., 2001. Use of some natural and waste materials for waste water treatment. *Water Res.* 35, 3738–3742.
- Alexiades, C.A., Jackson, M.L., 1966. Quantitative clay mineralogical analysis of soils and sediments. *Clays and Clay Minerals* 14, 35-52.
- Andreadakis, A., Gavalaki, E., Mamais, D., Tzimas, A., 2003. Wastewater reuse criteria in Greece. *Global Nest*, 5(1), 9-14.
- Balci, S., Dinçel, Y., 2002. Ammonium ion adsorption with sepiolite: use of transient uptake method. *Chem. Eng. Process.* 41, 79–85.
- Chen, J.P., Chua, M.L., Zhang, B., 2002. Effects of competitive ions, humic acid, and pH on removal of ammonium and phosphorus from the synthetic industrial effluent by ion exchange resins. *Waste Manage.* 22, 711–719.
- Daifullah, A.A.M., Girgis, B.S., Gad, H.M.H., 2003. Utilization of agroresidues (rice husk) in small waste water treatment plans. *Mater. Lett.* 57, 1723–1731.
- Daneshvar, N., Salari, D., Aber, S., 2002. Chromium adsorption and Cr (VI) reduction to trivalent chromium in aqueous solutions by soya cake. *J. Hazard. Mater.* B94, 49–61.
- Filippidis, A., Apostolidis, N., Filippidis, S., Paragios, I., 2008. Purification of industrial and urban wastewaters, production of odorless and cohesive zeo-sewage sludge using Hellenic Natural Zeolite. Proceedings of 2nd Intern. Conf. Decentralized Water and Wastewater Treatment Plants, Skiathos, Greece, 403-408.
- Filippidis, A., Apostolidis, N., Filippidis, S., Paragios, I., 2008. Purification of urban wastewaters, production of odorless and cohesive zeo-sewage sludge using Hellenic Natural Zeolite. Proceedings of

- 8th Hydrogeological Intern. Congr. Of Greece, 9p (in press).
- Galarneau, E., Gehr, R., 1997. Phosphorus removal from wastewater: experimental and theoretical support for alternative mechanisms. *Water Res.* 31, 328–338.
- Greenland J., 1965. Interaction between clays and organic compounds in soils. Part 1. Mechanisms of interaction between clays and defined organic components. *Soils Fertil.* 38, 415–421.
- Grimshaw, R.W., Harland C.E., 1975. Ion-exchange: Introduction to theory and practice. *The Chemical Society*, London, pp.137.
- Kirk, D.W., Charles, Q., Jia, J.Y., Alan, L.T., 2003. Wastewater remediation using coal ash. *J. Mater. Cycles Waste Manage.* 5, 5–8.
- Kuroda, M., Watanbe, T., Umedu, Y., 1997. Simultaneous COD removal and denitrification of wastewater by bio-electro reactors. *Water Sci. Technol.* 35, 161–168.
- Luckham, P.F., Rossi, S., 1999. The colloidal and rheological properties of bentonite suspensions. *Adv. Colloid Interface Sci.* 82, 43–92.
- Rehman, M., Narkis, N., Wachs, A.M., 1969. Effect of polyelectrolytes in conjunction with bentonitic clay on contaminants removal from secondary effluents. *Water Res.* 3, 345-355.
- Ringqvist, L., Holmgren, A., Öborn, I., 2002. Poorly humified peat as an adsorbent for metals in wastewater. *Water Res.* 36, 2394–2404.
- Rosenwinkel, K.H., Weichgrebe, D., Meyer, H., Wendler, D., 2001. Suspended solids from industrial and municipal origins. *Ecotoxicol. Environ. Saf.* 50, 135–142.
- Tabak, A. Afsin, B., Aygun, S.F., Koksal E., 2007. Structural characteristics of organo-modified bentonites of different origin. *J. Therm. Anal. Calorim.* 87, 375–381.
- U.S. Environmental Protection Agency, 2004. Guidelines for water reuse. EPA/625/R-04/108, Washington D.C., U.S.A.
- Yu, L.J., Shukla, S.S., Dorris, K.L., Sukla, A., Margrave, J.L., 2003. Adsorption of chromium from aqueous solutions by mapple sawdust. *J. Hazard. Mater.* 100, 53–63.

PETROLOGICAL INVESTIGATION OF CARBONATE ROCKS FROM THE IONIAN ZONE (ETOLOAKARNANIA, WESTERN GREECE)

Bourouni P., Tsikouras B., and Hatzipanagiotou K.

*University of Patras, Department of Geology, Section of Earth Materials, 26500 Patras, Greece,
bourouni@upatras.gr, v.tsikouras@upatras.gr, k.hatzipanagiotou@upatras.gr*

Abstract

The petrographic features of the carbonate rocks from the Ionian Zone in the Etoloakarnania Prefecture are presented. They are represented by limestones with minor dolomite. The limestones include: (i) wackestones (or sparse micrites), with poor presence of allochems within a mud matrix; (ii) packstones (or packed micrites) with increasing levels of carbonate grains that are still surrounded by micrite matrix, and (iii) grainstones (or sparites) containing allochems that are cemented with sparry calcite crystals, while the mud matrix is absent. Bioclasts are the dominant carbonate components in most of the samples accompanied by infrequent peloids, intraclasts, lithoclasts and ooids. Crystalline limestones were not identified. Quartz, apatite, barite, anhydrite, halite, clay minerals, magnetite and ilmenite have been determined as accessory phases. The results show that mineralogical and petrographic features of the analyzed carbonate rocks are related to their evolution during the development of the Ionian Zone from a shallow-marine platform to a deep-water basin.

Key words: *carbonate rocks, limestone, fabric, Ionian Zone, western Greece.*

1. Introduction

Ranging in age from Precambrian to Holocene, carbonate rocks are present virtually throughout the world. Limestone contains principally calcite, with or without dolomite. Aragonite and magnesian calcite are abundant primary minerals in recent marine carbonate sediments and limestones. Both are metastable, tending to alter to stable calcite or low-magnesian calcite with burial. Limestone is a common sedimentary rock and one of the most useful and versatile of all industrial materials, having variable applications such as in chemical and metallurgical industries, as construction material, for glass and ceramics, in the production of cement, as filler in paper, plastics and paint industry and for soil treatment. Along with dolomite, limestone comprises about 15% of all sedimentary rocks and although they consist only 2% of the whole of crustal rocks per volume, in Greece they cover 70% of its total surface (Carr et al., 1994).

The Etoloakarnania Prefecture consists principally of various series of carbonate rocks. The present study aims in describing the carbonate rocks of the Ionian Zone of Etoloakarnania, to investigate their depositional environment and to evaluate their properties for their uses as industrial rocks.

2. Geological setting

The Etoloakarnania Prefecture is located in continental Western Greece and consists, from West to East, of the Ionian, Gavrovo-Tripolitza and Olonos-Pindos geotectonic Zones (Fig.1). Continuous

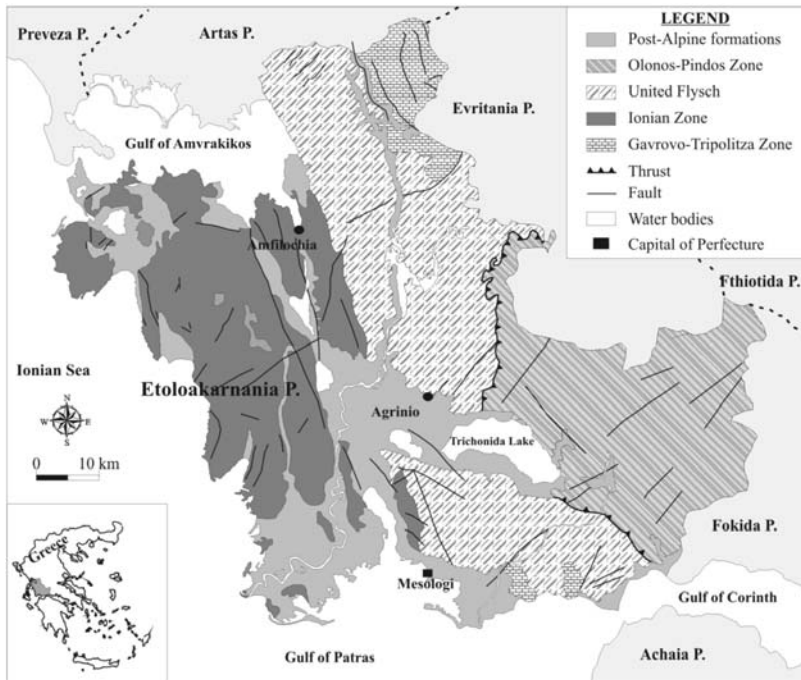


Fig. 1: Map showing the geotectonic units occurring in Etoloakarnania Prefecture (after Bornovas and Rodoyanni-Tsiabaou, 1983).

sedimentation prevailed throughout the Mesozoic and Tertiary; hence thick successions of carbonate rocks cover the major part of the study area. The Gavrovo-Tripolitza Zone includes shallow platform carbonate rocks of Cretaceous-Eocene age which are covered by vast quantities of clastic sediments (De Wever, 1975; Fleury, 1980) whereas the Pindos zone reflects an oceanic basin at the easternmost part of the Etoloakarnania. The Mesozoic series of the Pindos basin consists typically of deep-water sediments which together with the clastic sediments of flysch form a thick succession (Smith et al., 1975, 1979; Jones, 1990; Robertson et al., 1991; Degnan, 1992; Robertson, 1994, Degnan and Robertson, 1998).

During the Mesozoic the Ionian zone corresponded to a vast, intra-platform rift basin bounded on both sides by shallow platforms; the Apulia platform on the west and Gavrovo-Tripolitza platform on the east (Aubouin, 1959; Katsikatsos, 1992; Bosellini and Morsilli, 1997). The early shallow character, of the Ionian basin, during the pro-rift period, is reflected on its older rocks which include the Permian-Triassic evaporites and dolomites, and the neritic Pantokrator limestones of Upper Triassic age, which chiefly extend on the west part of the study area. During the following rift period (Lower Jurassic – Upper Jurassic), the Lower siliceous shales with *Posidonomya*, the red-blue, limestones with ammonites (Ammonitico Rosso), the filamentous limestones and the Upper siliceous shales with *Posidonomya* are deposited (Renz, 1955) (Fig 2). The syn-rift formations are overlain by the Upper Jurassic – Lower Cretaceous pelagic Vigla Limestone Formation (Aubouin, 1959; Karakitsios and Koletti, 1992; Karakitsios et al., 2004), the Upper Cherts (BP 1971, IFP-IGRS 1966) the pelagic and microbrecciated limestones of Senonian and Paleocene-Eocene limestones. The upper members are covered by flysch deposits of Eocene age (Zelilidis et al., 2003) (Fig. 2). West-

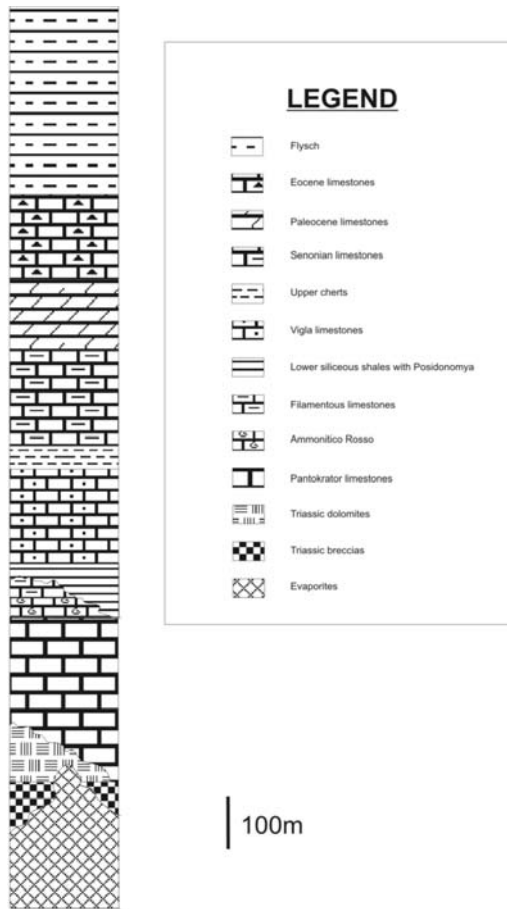


Fig. 2: Stratigraphic column of the Ionian Zone formations in Etoloakarnania area.

wards emplacement and successive overthrust resulted in a series of nappes of Gavrovo-Tripolitza and Pindos Zones onto the Ionian Zone along with deformation of the Pindos and formation of a series of thrust sheets (Robertson and Degnan, 1997).

3. Analytical methods

Electron microanalyses were carried out on polished thin sections at the Laboratory of Electron Microscopy and Microanalysis, University of Patras. All elements were analyzed by an electron-dispersive X-rays (EDX), using EDS and WDS detectors attached to a JEOL JSM-6300 SEM. The calibration of the instrument was made with well characterized reference materials (including natural minerals, synthetic glass and metal). Operating conditions were accelerating voltage 20kV and beam current 0.9 nA with 4 μ m diameter beam. The total counting time was 60 sec and dead time 40%. Detection limits are ~0.1% and accuracy better than 5% was obtained.

Whole rock chemical analyses were performed at ACTLABS, Ancaster, Ontario, by fusion ICP-OES for major elements and combined ICP-MS and INAA for trace elements. Detection limit for major elements is 0.01%, except for TiO₂ which is 0.005%. Replicate analyses suggest accuracy

better than 5% for major elements and most trace elements. The determination of CO₂ was accomplished by coulometry.

4. Macroscopic description

Field work in the carbonate rocks of the Ionian Zone showed that Triassic dolomites are massive and unbedded, with compact, grainy texture and gray colour. The overlying Pantokrator limestones form unbedded to very thick bedded, homogenous outcrops (Fig. 2). It comprises white to whitish or gray to dark gray, fine crystalline rocks with visible carbonate components. Small, window-like, cavities which are filled by secondary, crystalline calcite are frequently observed. The Vigla Limestone formation displays thin to medium platy outcrops with intercalations of grayish to dark-gray nodules or beds of cherts, indicating the change of the depositional conditions from neritic to pelagic, as the Ionian zone evolves to a deep basin. This massive limestone has cream, yellowish, and whitish colors, often with Fe-oxides impregnations. Calcite veins or fracture discontinuities are rare or absent. Bedding is not present in any of these biomicrites. The collected samples from the Senonian limestones show large variability. This is due to variable material deposited during clastic and pelagic processes that operated at the edges and central area of the Ionian zone. Representative samples of this formation comprise: a) cream to whitish, massive micrites, with well shaped dendritic depositions of oxides, stamped on their planar interfaces, b) light gray, grainy limestones with discernible carbonate components, weakly orientated to parallel directions and c) brecciated, light gray to whitish limestones, composed by an agglomerate of grains and fragments of various sizes and shapes which are cemented in a micritic matrix. The Paleocene limestone includes fossiliferous, whitish micrites, accompanied by rare nodules of gray cherts, red-brownish Fe-oxides and stylolites, as well as fine-crystalline, gray limestones. The carbonate succession of the Ionian zone is completed with Eocene limestones, which include cream to whitish, homogenous micrites and light gray, microcrystalline, laminated limestones. Stylolites and rare depositions of opaque minerals occur in both types and cross-cut their almost pure carbonate mass (Fig. 2).

5. Petrography

Thin sections from 30 samples were prepared and observed through a polarizing microscope: the classification schemes by Dunham (1962) and by Folk (1959, 1962) have been used for the description of the microscopic features of the collected samples. For clarity and simplicity, classification according to Folk is given in brackets, below. Although carbonate rocks are variable in composition, their components can be broadly divided into four main groups: non-skeletal grains, skeletal grains, micrite matrix and cement.

Limited outcrops of Triassic dolomites and dolomitic limestones, at the base of the zone, enabled us to collect only one sample. Microscopic examination reveals that the original structure has not been completely obliterated, so these dolomites can be described in terms of Dunham's (1962) and Folk's (1959, 1962) classification (preceded by the word dolomitic). Thus, this sample is a dolomitic peloidal grainstone or a dolomitic unsorted pelsparite, respectively. The majority of carbonate grains constitute pelloids, micritic, rounded to weakly elliptical in cross section, varying in size between 0.05-0.4 mm (Fig. 3a). Minor, thin-walled, bioclasts occur, too; their identification is not always easy because of dolomitization. The grains are cemented with fine (10µm), anhedral dolomite crystals, which form a xenotopic mosaic while micrite matrix is absent (Fig. 3a). Dolomitization is not fabric selective, as allochems and matrix have all been replaced by dolomite; rare calcite crystals have escaped dolomitization. Thin calcite veinlets also cross-cut the rocks.

The Pantokrator limestones include:

- a) Bioclastic wackestones (sparse biomicrites), composed predominately of micrite matrix that supports larger, sparsely distributed bioclasts. Scanning electron microscopic study aims in verifying that the carbonate matrix consists of microspar calcite crystals, ranging in size from 4 μm up to 10 μm , forming a patchy developed, coarser mosaic of anhedral crystals (Fig. 3b). The skeletal fragments possess a dark micrite envelope around the grains, which is produced mostly by the boring activity of endolithic bacteria and they lack well preserved original structure, as their internal chambers are filled by equant, drusy sparite. This fact and their small size renders the identification of bioclasts difficult. The cavities filled with sparry calcite are frequently observed (Fig. 3c). Veinlets of calcite and stylolites are often associated with insoluble material (mainly clay minerals) accumulated as a result of pressure-induced dissolution, interrupt the samples at any orientation.
- b) Oobioclastic grainstones/packstones (unsorted oobiosparites/packed biomicrites). Abundant grains are observed within these limestones, such as bioclasts (e.g. green algae, foraminifera and gastropods with thin micrite walls and not always obvious chambering), ooids, pelloids (wholly micritized equigranular grains), and intraclasts. Although the observed ooids have been micritized they are still recognizable by their almost perfect circular shape, their size (about 0.45 mm) and their weak, residual, concentric structure. Lithoclastic fragments of carbonate rocks, completely different from the host limestone, are rarely detected. The observed grainstones lack carbonate mud and allochems are cemented mostly by equant sparite crystals. However in places, probable micrite matrix exists in interstices. Calcite veins and stylolites occur, too. Small crystals of Fe-oxides are also present in trace amounts.

The Vigla Limestone samples are classified as bioclastic wackestones (sparse biomicrites) and comprise locally porous, well indurated carbonate mud with small bioclasts suspended in it (Fig. 3d). The matrix is not completely dark and has undergone weak aggrading neomorphism leading in a relatively coarser mosaic. The micrite matrix is also loaded with homogeneously, distributed very-fine silica crystals. The bioclasts have circular or elliptic shape and drusy sparite infilling. Small voids are detected within the fossils (intraparticle porosity), whereas in some cases bioclasts have completely dissolved out leaving a biomouldic porosity. No evidence of compaction was observed. Scanning electron microscopic examination confirmed the presence of Fe-oxides and quartz.

The textural variety observed in the Senonian limestones is also expressed in their microscopic features; their classification suggested the presence of:

- bioclastic wackestones (sparse biomicrites), with small bioclasts, mainly multi-chambered foraminifera “floating” in carbonate mud;
- bioclastic grainstones/packstones (unsorted biosparites/packed biomicrites) with bioclasts and intraclasts cemented with crystalline calcite. Tabular-shaped, bioclastic fragments now composed of fibrous calcite occur, probably as a result of calcitization of former aragonite that allowed the preservation of the fibrous structure (Fig. 3e). Minor amounts of anhydrite, apatite, halite and clay minerals were detected by electron microscopic observation (Fig. 3f).
- lithoclastic packstones (packed extramicrites), where fragments of limestones, with texture different relative to their host biomicrite matrix, supporting an out of depositional basin provenance for them.

The Paleocene limestones include bioclastic wackestones (sparse biomicrites) and bioclastic grain-

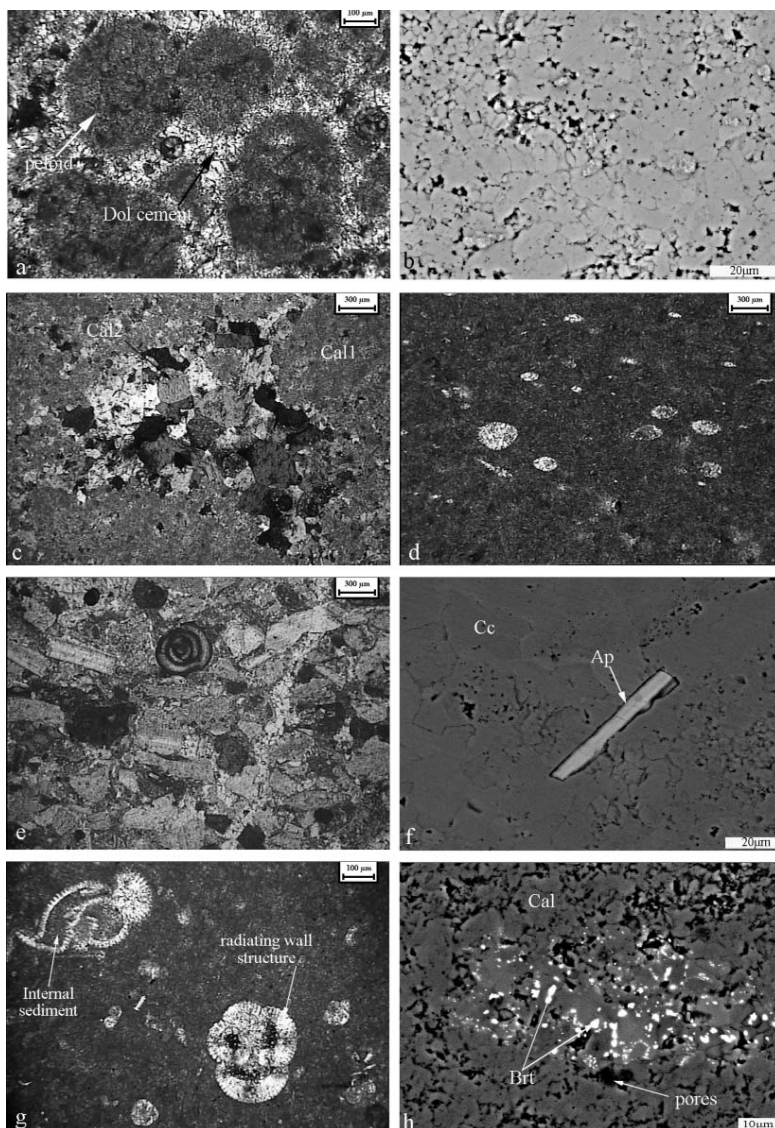


Fig. 3: (a) Photomicrograph showing peloids cemented by fine-crystalline dolomitic cement from sample AIT37 (crossed polarized light). (b) Back scattered electron image illustrating microspar which has resulted from the aggrading neomorphism of the micrite in sample AIT26. The neomorphic spar crystals are characterized by irregular or curved intercrystalline boundaries with embayments and irregular crystal-size distribution. Dark areas represent intercrystalline porosity. (c) Photomicrograph showing the characteristic cavities observed in Pantokrator limestones (sample AIT26). Calcite occupies the cavities (Cal2) exhibits a drusy fabric, characterized by increasing crystal size away from the cavity wall towards the cavity centre. The cavity is surrounded by micrite matrix (Cal1) (crossed polarized light). (d) Wackestone with sparse bioclasts from Vigla limestone formation. Photomicrograph from sample AIT35 (plane polarized light). (e) Photomicrograph showing abundant bioclasts and few endoclasts (dark micrite pieces) that produce a grain supported texture (sample AIT32b) (plane polarized light). (f) Back scattered electron image showing an apatite crystal in sample AIT32b. (g) Well preserved foraminifera floating in opaque micrite matrix. Photomicrograph from sample AIT46a (crossed polarized light). (h) Back scattered electron image showing anhedral barite crystals detected in sample AIT34a.

stones (unsorted biosparites). The wackestones contain bioclasts, dominantly foraminifera rooted in the carbonate mud matrix. The bioclasts may have either thin walls, occasionally broken, filled with internal sediment and/or fine crystalline calcite, or thick walls, displaying well preserved radiating structure of fibrous crystals, with sparite infilling. The micrite matrix is opaque and uniform (Fig. 3g). The grainstones usually contain well-preserved, undamaged, sizeable fossils (mainly mollusks and benthonic foraminifera). Rare ooids showing well concentric structure and uniaxial extinction have been observed. Grains consisting exclusively of micrite probably represent micritized bioclasts. Usually, long axes of fossils are preferentially orientated parallel to sedimentary bedding. The grainstones are totally devoid of micrite matrix and their carbonate constituents produce a poorly sorted, grain supported texture.

The Eocene limestones comprise bioclastic wackestones (sparse biomicrites) and bioclastic packstones (packed biomicrites) with characteristics similar to those rock-types described for the Paleocene limestones. The majority of allochems constitute bioclasts, mainly well-preserved foraminifera, composed of fine-crystalline sparite and carbonate mud. The micrite matrix of the wackestones is not completely dark and exhibits a very-fine-crystalline texture, as a result of aggrading neomorphism. This diagenetic process resulted in the development of fine-crystalline calcite along subparallel zones with fuzzy margins with the micrite matrix. The packstones are sorted and in a few cases potential intraclasts of micrite are rarely detected. Trace amounts of apatite, quartz and micron-sized, anhedral crystals of barite, Fe-oxides and ilmenite are present within the wackestones and packstones (Fig. 3h).

6. Mineral chemistry

Representative microanalyses of the main constituents of the carbonate rocks are given in Table 1. Several grains and crystals were analyzed, and in some cases each grain was analyzed from rim to core. The dominant rock forming mineral calcite may be termed, depending on the magnesium content, as low-Mg calcite with less than 4 mol. % MgCO_3 (molar MgCO_3 ranges typically from 0.45 to 1.80). In a similar way, iron content of the studied samples show Fe-poor calcite compositions, as Fe_2O_3 is below detection limit in most of the samples (with few exceptions), thus the calcite is characterized as non-ferroan.

The analyzed calcite crystals from the collected rocks have CaO contents that range from 53.08 to 56.52 %. Some crystals show limited substitution of Mg for Ca with MgO ranging from 0.18 to 0.72 %. In general, the Pantokrator limestone contains the purest calcite crystals relative to those from the other formations. Calcite crystals from cement and in veins are richer in CaO relative to the calcite analysed in grains and matrix. Few impurities include mainly few amounts of K_2O , MgO, Na_2O and SiO_2 in the analyzed calcites. K_2O content ranges from 0.10 to 0.28 % whereas Na_2O is relatively higher (0.18-0.48 %). SiO_2 ranges from 0.21 to 0.35 % particularly in the micrite carbonate matrix or to a lesser extent in micritized grains, mainly in the Eocene and Vigla Limestones; the higher SiO_2 values may be related to biased results from the presence of clay minerals or micro-crystalline silica. P_2O_5 and SO_3 show a preferential accumulation mostly in calcites from skeletal grains and cement. Dolomites from the Triassic dolomitic rocks were analyzed from cement, skeletal and non skeletal (mainly micritized) grains and generally display coherent compositions. They are non-ferroan and their calcium and magnesium contents range between 30.19-32.11 wt% and 19.81-20.13 wt%, respectively. They are characterized as Ca-rich, with a molar CaCO_3 content ranging from 53.9 to 57.3 (Lumsden and Chimahusky, 1980; and Morrow, 1978, 1982a).

7. Geochemistry

Whole-rock geochemical analyses from the collected carbonate rocks are listed in Table 2. For comparison, the global average chemical composition of limestones (Mason and Moore, 1982) is also given. Our limestone samples have higher CaO and Na₂O and lower MgO and Sr abundances relative to the global average limestone composition. Considering the chemical classification based on CaCO₃ content (Oates, 1998), all samples are characterized as ultra-high calcium limestones (CaCO₃ > 97%), except for the sample AIT 37 which is a magnesian limestone (CaCO₃ = 80.23 %). The total amount of impurities (sum of all oxides excluding CaO and CO₂) for all the limestones except the dolomitic sample AIT 37, ranges between 0.27 and 1.65%. SiO₂ (0.03-0.93%) shows the highest concentrations in the Vigla limestones (Table 2), most likely due to the presence of minute silica grains and/or clay minerals in the carbonate matrix. This is compatible with the higher amounts of insoluble residual measured in these samples. All samples are poor in MgO (<1%), except for sample AIT 37 with high MgO content (19.41%) due to the presence of dolomite. Samples AIT 34a, AIT 34b and AIT 25a exhibit the highest Al concentrations, which along with high amounts in Si reflect the presence of detrital minerals in their carbonate matrix. Most biomicrites are rather rich in Fe most likely related to the occurrence of Fe-oxides and ilmenite, usually found together with clay minerals. Na, Mn, K, and P are insignificant in most of the samples while P is primarily detected in the Senonian and Eocene limestones, probably attributed to the presence of apatite.

Sr is detected in all samples. Eocene and Senonian limestones are the most enriched samples in Sr (except for sample AIT 33 with Sr = 181 ppm). The highest value is shown by the biomicrite sample AIT 34a (518 ppm) which contains also significant apatite amounts. The Pantokrator limestones, which contain the purest calcite, display the lowest Sr concentrations (78-114 ppm), except samples AIT 28a and AIT 24a, which are clearly richer in Sr (234 and 253, respectively). These two samples are also richer in SiO₂ and Al₂O₃. The dolomitic sample AIT 37 has low Sr content compared to the rest analyzed carbonate rocks (82 ppm). Sulfur content is fairly coherent displaying inconsiderable variations between 0.028-0.046 wt%.

The trace elements As, Be, Br, Cd, Cs, Hf, Mo, Rb, Sb, Se, Ta, and Th amounts in the analyzed samples are mostly below detection limits. However, the studied limestones are generally enriched in Ba, Bi, Co, and Cu compared to the global average limestone. The high Ba content in samples AIT 34a, AIT 34b and AIT 25a is most likely the result of the presence of barite in them. The Eocene and Vigla limestones demonstrate higher Cu values compared to the rest samples. The U abundance in sample AIT 37 (5.3 ppm) is higher than the rest samples. Except for calcite, Y is commonly incorporated to apatite, replacing Ca.

8. Discussion and conclusions

The analyzed, Triassic dolomitic rocks generally contain Ca-rich dolomite crystals with coherent compositions and MgO contents ranging from 19.81 to 20.13 wt %. Ca-rich, fine-crystalline dolomites, similar to those observed in the analyzed sample from the Ionian Zone, are thought to be early diagenetic, near surface in origin and usually they are unassociated with evaporites (Tucker and Wright, 1990). However, it has been observed that evaporites occur at the lower members of these dolomitic rocks commonly forming diapiric domes (IGRS-IFP 1966; Underhill, 1988; Karakitsios, 1995). The timing of dolomitization as well as the mineralogy of the precursor carbonate are also important factors in determining the dolomite Sr content. Ancient dolomites have variable Sr contents, a few tens to hundreds of ppm is the typical range. Early dolomitization of marine carbonates will result in Sr-richer dolomites compared to those resulting from later dolomitization of stabilized

Table 2. Whole-rock chemical analyses from the carbonate rocks of the Ionian Zone (-: below detection limits).

Formation	Eocene		Senonian			Vigla		Pantokrator						
	AIT34A	AIT 34B	AIT 32A	AIT 32B	AIT 33	AIT 25A	AIT 35	AIT 26A	AIT 28A	AIT 31A	AIT 31B	AIT 36	AIT 24A	Dolomites AIT 37
Major elements wt%														
SiO ₂	0.75	0.37	0.61	0.10	0.19	0.73	0.93	0.03	0.12	0.07	0.03	0.03	0.14	0.05
TiO ₂	-	-	-	-	-	-	-	-	-	-	-	-	-	-
Al ₂ O ₃	0.24	0.12	0.25	0.03	-	0.20	0.21	-	-	-	-	-	-	-
Fe ₂ O ₃ (T)	0.14	0.10	0.11	0.01	-	0.07	0.12	-	-	-	-	-	-	-
MnO	0.04	0.03	0.04	0.02	-	0.01	0.02	-	-	-	-	-	-	-
MgO	0.36	0.37	0.50	0.34	0.57	0.34	0.29	0.20	0.42	0.22	0.39	0.39	0.46	19.41
CaO	55.30	54.39	53.55	54.43	54.28	55.25	54.13	55.70	56.01	55.84	55.35	54.89	56.05	33.04
Na ₂ O	0.08	0.06	0.04	0.05	0.05	0.07	0.05	0.04	0.05	0.07	0.07	0.05	0.05	0.12
K ₂ O	-	-	-	-	-	0.04	-	-	-	-	0.02	-	-	0.02
P ₂ O ₅	0.04	0.05	0.06	0.01	0.02	0.02	0.02	-	-	-	-	-	0.01	-
LOI	43.28	43.49	43.39	43.73	43.67	43.43	43.22	42.85	43.79	42.80	43.42	43.35	43.48	46.63
Total	100.20	98.94	98.54	98.7	98.83	100.20	98.96	98.78	100.50	98.94	99.29	98.66	100.30	99.30
CO ₂	44.50	44.90	43.80	44.80	45.20	45.40	45.00	45.60	45.30	44.90	44.80	45.90	45.40	47.90
CaCO ₃	98.38	98.93	98.38	99.45	99.11	98.48	98.37	99.77	99.30	99.70	99.48	99.57	99.23	80.23
Trace elements ppm														
S (%)	0.037	0.046	0.038	0.039	0.034	0.039	0.034	0.028	0.034	0.029	0.043	0.034	0.043	0.041
Cr	5	6	6	-	8	5	-	4	5	-	2	4	6	-
Co	5	4	3	4	5	5	3	3	3	4	3	5	4	7
Ni	5	2	4	-	-	-	1	-	1	-	1	-	-	-
Cu	12	11	3	2	3	10	5	-	1	1	3	-	4	1
Zn	7.0	3.0	5.0	-	-	4.0	5.0	-	-	-	-	-	-	-
Rb	-	-	-	-	-	-	-	-	-	-	-	-	-	-
Sr	518	439	415	367	181	191	122	78	234	79	108	114	253	82
Y	7	5	9	-	-	8	4	-	-	2	6	-	2	-
Zr	-	-	3.0	-	-	4.0	-	-	-	-	3.0	-	-	-
Pb	8	10	8	10	7	9	9	9	8	8	6	8	9	-
Ba	38	20	6	-	4	12	10	-	4	-	-	4	3	3
V	-	-	9	-	-	-	-	-	7	-	19	-	-	8
Sc	0.4	0.2	0.7	0.1	0.1	0.5	0.3	-	-	-	-	-	0.1	-
Th	-	-	-	-	-	-	-	-	-	-	-	-	-	-
Ta	-	-	-	-	-	-	-	-	-	-	-	-	-	-
Hf	-	-	-	-	-	-	-	-	-	-	-	-	-	-
As	-	-	-	-	-	-	-	-	-	-	-	-	-	-
Mo	-	-	-	-	-	-	-	-	-	-	-	-	-	-
Ag	-	-	-	-	-	-	1.0	-	-	-	0.5	-	-	-
Cd	-	-	-	-	-	-	-	-	-	-	-	-	-	-
Hg	-	-	-	-	-	-	-	-	-	-	-	-	-	-
Bi	-	-	-	5	-	-	-	-	-	4	-	-	-	9
U	-	-	0.6	-	-	-	-	-	0.7	-	1.4	-	-	5.3
Au (ppb)	11	12	8	-	-	29	25	-	8	-	20	-	-	-
Be	-	-	-	-	-	-	-	-	-	-	-	-	-	-
Br	-	-	-	-	-	-	-	-	-	-	-	-	-	-
Cs	-	-	-	-	-	-	-	-	-	-	-	-	-	-
Ir	-	-	-	-	-	-	-	-	-	-	-	-	-	-
Sb	-	-	-	-	-	-	-	-	-	-	-	-	-	-
Se	-	-	-	-	-	-	-	-	-	-	-	-	-	-

marine carbonates composed of diagenetic low-Mg calcite (Tucker and Wright, 1990). However, based on dolomite stoichiometry and rock microstructure it is suggested that the low-Sr dolomites from the Ionian Zone are interpreted as early diagenetic and are related to dolomitization of original carbonate phases poor in aragonite skeletal components. Ancient dolomites have variable Sr contents, a few tens to hundreds of ppm is the typical range. Early dolomitization of marine carbonates will result in Sr-richer dolomites compared to those resulting from later dolomitization of stabilized marine carbonates composed of diagenetic low-Mg calcite (Tucker and Wright, 1990). However, based on dolomite stoichiometry and rock microstructure it is suggested that the low-Sr dolomites from the Ionian Zone are interpreted as early diagenetic and are related to dolomitization of original carbonate phases poor in aragonite skeletal components.

The Pantokrator limestones are the purest carbonate rocks of the Ionian zone, devoid of non-carbonate impurities. Mineral chemistry is also compatible with this fact since the analyzed calcites from the Pantokrator limestones are the purest in Ca phases. Whole-rock analyses suggest that most minor and trace elements are very low or below detection limits and the analyzed Pantokrator samples are clearly the most enriched in CaO relative to the rest samples. The microspars observed in the Pantokrator limestone samples are the result of aggrading neomorphism of the precursor carbonate mud.

The Vigla limestone belongs to the post-rift sequence of the Ionian Zone (Karakitsios, 1995). The nodular and bedded cherts found within the Vigla limestones indicate the change of the depositional conditions from neritic to pelagic and the evolution of the Ionian Zone from shallow-marine platform to a deep basin. The micrite matrix of the Vigla limestones is loaded with homogeneously distributed very-fine silica crystals, related also to their deep water depositional environment. Whole-rock geochemical results indicate that SiO₂ contents are also higher than the limestones from the other formations, most likely due to the presence of minute silica grains and/or clay minerals in the carbonate matrix. This is consistent with the higher amounts of insoluble residue measured in these samples, and most likely reflects the pelagic depositional conditions which were prevailing during this period.

Most of the biomicrites from Eocene, Senonian and Vigla formations are rather rich in Fe, reflecting the occurrence of Fe-oxides. These opaque minerals are frequently usually found in association with clay minerals of clastic origin. The formation of the Senonian and Paleocene-Eocene limestones mark the post-rift period of the pre-orogenic evolution of the Ionian Zone, and correspond to depositional conditions where pelagic sedimentation (resulted in deposition of biomicrites) and clastic material influx from the basin margins and the neighboring zones (resulted in formation of brecciated lithotypes). The Eocene and Senonian limestones are the most enriched in Sr samples. Sr substitutes greatly for Ca in calcite; however, it is also a significant substitute for Ca and Ba in apatite and barite lattice, respectively. The highest Sr values are shown by the samples which contain also appreciable amounts of apatite and barite, therefore suggesting that calcite, apatite and barite contribute to the concentration of Sr. The low Sr contents in the Pantokrator limestone may be related to diagenetic loss of Sr, and/or to a calcitic rather than an aragonitic original mineralogy, likely in an inner platform environment which are typically poor in aragonite and/or the absence of non carbonate minerals related to Sr.

9. References

Aubouin, J., 1959. Contribution a l' etude géologique de la Grèce septentrional: les confins de l' épire et de la Thessalie, *Ann. Geol. Pays Hell* 10, 403.

- Bosellini, A., and Morsilli, M., 1997. A Lower Cretaceous drowning unconformity on the eastern flank of the Apulian Platform (Cargano Promontory, southern Italy), *Cretaceous Research* 18, 51-61.
- B.P. Co. Ltd., 1971. The geological results of petroleum exploration in western Greece. The Geology of Greece, Institute for Geology and Subsurface Research, Athens, 73p.
- Carr, D. D., Rooney, L. F., and Freas, R. C., 1994. Limestone and dolomite, *Industrial Minerals and Rocks, AIME Soc*, 605-609.
- De Wever, P., 1975. Etude géologique des séries apparaissant en fenêtre sous l'alloctone pindique (série de Tripolitza et série épimetamorphique de Zarouchola). Péloponnèse septentrionale, Grèce, *Thèse 3ème cycle*, Université de Lille.
- Degnan, P.J., 1992. Tectono-Sedimentary Evolution of a Passive Margin: The Pindos Zone of the NW Peloponnese, Greece. *Unpublished PhD thesis*, University of Endinburgh.
- Degnan, P.J. and Robertson, A.H.F., 1998. Mesozoic-early Tertiary passive margin evolution of the Pindos ocean (NW Peloponnese, Greece), *Sedimentary Geology* 117, 33-70.
- Dunham, R.J., 1962. Classification of carbonate rocks according to depositional texture. In: W.E. Ham (ed.), *Classification of carbonate rocks*, *Am. Assoc. Petroleum Geologists, Memoir* 1, 108-121.
- Fléury, J.J., 1980. Evolution d'un bassin dans leur cadre alpin: les zones de Gavrovo-Tripolitza et du Pindos-Olonos, *Soc. Géol. Nord. Spec. Publ.* 4, 651.
- Folk, R.L., 1959. Practical petrographic classification of limestones, *Bull. Am. Ass. Petroleum Geologists* 43, 1-38.
- Folk, R.L., 1962. Spectral subdivision of limestone types. In: W.E. Ham (ed.), *Classification of carbonate rocks*, *Am. Assoc. Petroleum Geologists, Memoir* 1, 62-84.
- IGRS-IFP, 1966. Étude géologique de l'Épire. Institute for Geology and Subsurface Research, Athens, 306p.
- Jones, G., 1990. Tectonostratigraphy and evolution of the Pindos Ophiolite and Associated Units, Northwest Greece, *PhD. thesis*, University of Endinburgh.
- Karakitsios, V., 1995. The influence of preexisting structure and halokinesis on organic matter preservation and tectonic system evolution in the Ionian basin, Northwest Greece, *AAPG Bulletin* 79, 960-980.
- Karakitsios, V., and Kolletti, L., 1992. Critical revision of the age of the basal Vigla limestones (Ionian Zone, western Greece), based on nannoplankton and calpionellids with paleogeographical consequences. In B. Hamrsmid and J. Young (eds), *Proceedings of the Forth International Nannoplankton Association Conference*, Prague 1991, *Knihovnicka ZPN*, 14a, vol. 1, 165-177.
- Karakitsios, V., Tsikos, H., Van Breugel, Y., Bakopoulos, I., Koletti, L., 2004. Cretaceous oceanic anoxic events in western continental Greece, *Bull. of the Geol. Soc. Greece*, XXXVI, 846-855.
- Katsikatsos, G., 1992. The geology of Greece, University of Patras, 451.
- Lumsden, D. N. and Chimahusky, J. S., 1980. Relationship between dolomite nonstoichiometry and carbonate facies parameters. In: *Concepts and Models of Dolomitization* (ED. by D. H. Zenger, J. B. Dunham and R. L. Ethington) *Spec. Publ. Soc. econ. Paleont. Miner.* 28, 123-137.
- Mason, B. H. and Moore, C. B., 1982., *Principles of Geochemistry*, John Wiley, New York, 344.
- Morrow, D. W., 1978. The influence of the Mg/Ca ratio and salinity on dolomitization in evaporite basins, *Bull. Can. petrol. Geol.* 26, 389-392.
- Morrow, D. W., 1982a. Diagenesis I. Dolomite-part I. The chemistry of dolomitization and dolomite precipitation, *Geoscience Canada* 9, 95-107.
- Oates, J. A. H., 1998. Lime and Limestone. Chemistry and Technology, Production and Uses. Willey-VCH Verlag, Germany.

- Renz, C., 1955. Die vorneogene Stratigraphie der normal-sedimentaren Formationen Griechelan. Inst. Geol. Susurf. Res. Athens, 637.
- Robertson, A.H.F., 1994. Role of the tectonic facies concept in orogenic analysis and its application to Tethys in the Eastern Mediterranean region, *Earth. Sci. Rev.* 37, 139-213.
- Robertson, A.H.F., Clift, P.D., Degnan, P.J., and Jones, G., 1991. Palaeogeographic and palaeotectonic evolution of the Eastern Mediterranean Neotethys, *Palaeog. Palaeocl. Palaeoecol.*, 87: 289-343.
- Robertson, A.H.F., and Degnan, P.J., 1997. Kerassia Millia Complex evidence of a Mesozoic-Early Tertiary oceanic basin between the Apulian continental margin and the Parnassus carbonate platform in western Greece, *Bull. Geol. Soc. Greece*.
- Smith, A.G., Hynes, A.J., Menzies, M., Nisbet, E.G., Price, I., Welland, M.J.P., and Ferrière, J., 1975. The stratigraphy of the Othris Mountains, eastern central Greece: a deformed continental margin succession, *Eclogae Geol. Helv.* 86, 463-481.
- Smith, A.G., Woodcock, N.H., and Naylor, M.A., 1979. The structural evolution of a Mesozoic continental margin, Othris Mountains, Greece, *J. Geol. Soc. London* 136, 589-603.
- Tucker, E. M., and Wright V. P., 1990. Carbonate Sedimentology, Blackwell Science, 482, 370-381.
- Underhill, J. R., 1988. Triassic evaporites and Plio-Quaternary diapirism in western Greece, *Journal of the Geological Society*, London 145, 269-282.
- Zelilidis, A., Piper, D. J., Vakalas, I., Avramidis, P., and Getsos, K., 2003. Oil and Gas Plays in Albania: Do Equivalent Plays Exist in Greece?, *Journal of Petroleum Geology* 26, 29-48.

CLAY MINERALOGY OF THE SEDIMENTARY IRON-NICKEL ORE OF AGIOS IOANNIS, NE BOEOTIA: NEW DATA AND IMPLICATION FOR DIAGENETIC MODIFICATIONS

Christidis G.E.¹, and Skarpelis. N.²

¹ Technical University of Crete, Department of Mineral Resources Engineering, 73100 Chania, Greece, christid@mred.tuc.gr

² University of Athens, Department of Geology, 15787 Panepistimioupolis Ano Ilissia, Athens, Greece, skarpelis@geol.uoa.gr

Abstract

The clay mineralogy of the sedimentary Fe-Ni deposit of Agios Ioannis and a Ni-lateritic profile from Pavlos, both in Lokris area, Greece, is investigated. The clay fraction of samples from Agios Ioannis consists mainly of Fe-rich chlorite and Fe-smectite, with minor serpentine, hematite and goethite. Locally, disordered talc (kerolite and/or pimelite), illite, R1 mixed layer illite/smectite and gibbsite are identified. The lateritic profile has different composition and contains mainly Fe-rich smectite (nontronite and/or ferruginous montmorillonite) with minor serpentine, goethite, magnetite, and talc, whereas chlorite is absent. It is suggested that in the Agios Ioannis deposit chlorite has formed from smectite via R0 mixed layer chlorite/smectite with >80% chlorite layers. The source of Al is probably the diagenetic transformation of pedogenic goethite to hematite during burial. The lack of chlorite in the lateritic profile of Pavlos is attributed to the limited presence of goethite. Smectite is believed to be a major mineralogical constituent of the Fe-Ni ores of the broader Lokris area.

Key words: Fe-Ni deposit, Ni-lateritic profile, Fe-smectite, Fe-chlorite, diagenesis, Agios Ioannis, NE Boeotia.

1. Introduction

The Upper Cretaceous Fe-Ni sedimentary deposits of Lokris, have been studied thoroughly over the last 60 years. It is well established that the principal Ni-bearing phases are phyllosilicates, mainly chlorite (Ni-chamosite and nimite), talc serpentine (antigorite and nepouite) and garnierite (Augoustithis 1962; Siegl, 1954; Albandakis, 1974; 1984; Rosenberg, 1984; Valetton et al., 1987; Alevizos, 1997; Skarpelis, 1997; 1999; 2000; Eliopoulos & Economou-Eliopoulos, 2000; Apostolikas, 2007). Albandakis (1974; 1984) reported the presence of Ni-montmorillonite in the deposit of Agios Ioannis and Maksimovic et al. (1993) found smectite in the Marmeiko deposit. Alevizos (1997) and Apostolikas (2007) reported clinocllore in the deposits of Agios Ioannis and Kopais. Ni-free clay minerals such as kaolinite have been reported in the deposits of Agios Ioannis and Marmeiko (Maksimovic et al., 1993; Alevizos, 1997). Similar assemblages of Ni-bearing phyllosilicates have been recorded in the Fe-Ni deposits of Evia (Andoniades & Vgenopoulos, 1989).

Reactions between clay minerals have been widely used as tracers for mineralogical transformations during diagenesis. The most commonly studied diagenetic change is the smectite to illite tran-

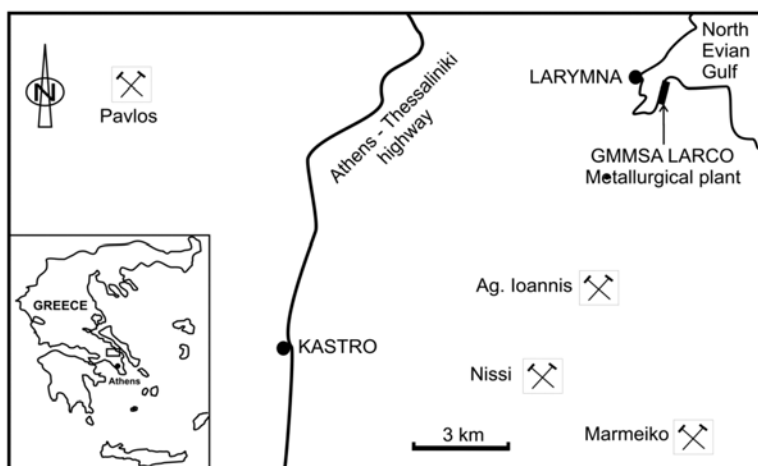


Fig. 1: Location of the lateritic profile at Pavlos and the Fe-Ni ore deposits at Agios Ioannis, NE Boeotia.

sition via mixed-layer illite/smectite (I/S), which has been studied in several sedimentary basins in the world including among others the Gulf Coast (Hower et al., 1976; McCarty et al., 2008 among many others) and several basins in Eastern Europe (Srodon & Clauer, 2001; Srodon et al., 2006). In contrast, there are fewer references on the smectite to chlorite transition via formation of corrensite. A typical example of this transition is observed in off-shore Brazilian sediments (Chang et al., 1986).

Although the main Ni-phases present in the sedimentary Fe-Ni deposits of Lokris are clay minerals, systematic clay mineralogical study has not been carried out so far. Such a study would be important not only from the pure mineralogical point of view, but it would also shed light on the diagenetic processes that have taken place in the Fe-Ni ores. So far only in a limited number of studies the clay minerals have been distinguished into clastic and authigenic (Valeton et al., 1987). It is the purpose of this preliminary contribution to present the first systematic study of the clay mineralogy of the Agios Ioannis Fe-Ni ore deposit, to compare with the mineralogy of the saprolitic and clayey horizons of a Ni-laterite profile and to propose possible diagenetic modifications of the Fe-Ni sediments.

2. Geological setting

Remnants of old weathering crusts on ophiolitic ultramafic rocks are preserved in Lokris area, being a critical lithology, with significance for interpretation of the geological evolution of the ophiolites and the Sub-Pelagonian Belt. They provide evidence on the nature and extent of lateritization processes in pre-Cenomanian - Turonian times. The crusts show large variations in thickness and continuity, mineralogy and chemistry of individual zones. The following lateritic zones are identified (bottom to top) (Skarpelis, 2005): a. Bedrock, b. Saprolite, c. Clayey zone, d. In situ limonite (oxidic zone). Silcrete layers were formed into the clay and goethitic zones. Reworked granular Fe-Ni ore with angular fragments of silcrete overly the lateritic profiles. The uppermost gravelly ferruginous sector, the clayey and goethitic zones, the silcretes and the saprolite were eroded to a major extent and the material reworked and redeposited partly on the bedrock and the lateritic crusts or washed down, transported and redeposited under submarine conditions within mechanical traps on karstified carbonates, forming sedimentary Fe-Ni ore deposits. This is evidenced by the occurrence

into the sedimentary ore of detrital minerals and particles, identical to typical lateritic weathering crusts (e.g. detrital Cr-spinel, chromite, Ti-oxides, magnetite, maghemite, nickeliferous chlorite, ferrous spheroidal particles, detritus of silcrete (Skarpelis, 1999 and references therein). Both the weathering crusts and the karstic Fe-Ni deposits were transgressively covered by Upper Cretaceous (Cenomanian-Turonian) limestones.

3. Sampling and experimental methods

Fifteen samples were collected from the Agios Ioannis sedimentary Fe-Ni deposit and the lateritic profile close to Pavlos village (Fig. 1). Samples collected from the Agios Ioannis deposit belong to fine-grained (argillaceous) Fe-Ni ore type and were collected from the lowermost part of the underground working face of the deposit, close to the contact with the underlying Jurassic limestones. Samples do not represent profiles but were collected randomly, because systematic diagenetic changes in clay minerals due to burial are not expected in the limited thickness of the deposit (4-7 m). In the lateritic profile of Pavlos samples were collected from the saprolite zone and the clayey (nontronitic) zone.

The bulk mineralogy was determined by X-ray powder diffraction (PXRD) (Siemens D500, CuK α radiation, graphite monochromator, 35 kV and 35 mA, using a 0.02° step size and 1 second per step counting time), on randomly oriented samples initially crushed with a fly press and subsequently ground with pestle and mortar. The clay mineralogy was determined in materials dispersed in distilled water using an ultrasonic probe (20 seconds). The less than 2 μ m fractions were separated by settling, dried on glass slides at room temperature and then were solvated with ethylene-glycol vapour at 60°C overnight to ensure maximum saturation. XRD traces of the clay fractions, both air-dried and after ethylene glycol solvation, were obtained using a 0.02° step size and 4 seconds per step counting time. The FWHM of the 002 diffraction maximum of chlorite was determined in those clay fractions which did not contain serpentine.

Infrared (IR) spectra of clay fractions from the Pavlos lateritic profile were obtained using a Perkin Elmer 1000 Fourier Transform Infrared (FTIR) spectrometer in the range 400-4000cm⁻¹. Each spectrum was the average of 50 scans collected at 4 cm⁻¹ resolution. An amount of 1.5 mg of the smectite clay fractions was diluted in 200 mg KBr and pressed in 13mm KBr disks, which were subsequently dried at 150°C.

4. Results

The argillaceous samples from Agios Ioannis deposit consist of hematite, goethite, quartz, calcite, chlorite, serpentine and talc. Locally, gibbsite and gypsum have been identified. In the random oriented samples the presence of smectite is not unambiguous, because the 001 diffraction maximum coincides with that of chlorite. The samples from Pavlos lateritic profile consist of hematite, dioctahedral smectite, calcite, quartz, serpentine, talc, goethite and magnetite. Representative XRD trace of ethylene-glycol solvated clay fraction from the nontronite zone of the Pavlos lateritic profile is shown in Figure 2. The main phase is smectite associated with minor talc, serpentine and goethite, whereas chlorite is absent. Nevertheless, chlorite has been described in other lateritic profiles in the broader area (Skarpelis, 2000). The mineralogical composition of the nontronite zone is relatively homogeneous. Identical XRD traces were obtained from clay fractions in the saprolite zone (not shown). The rational sequence of the higher order basal reflections indicates that mixed-layering is not present.

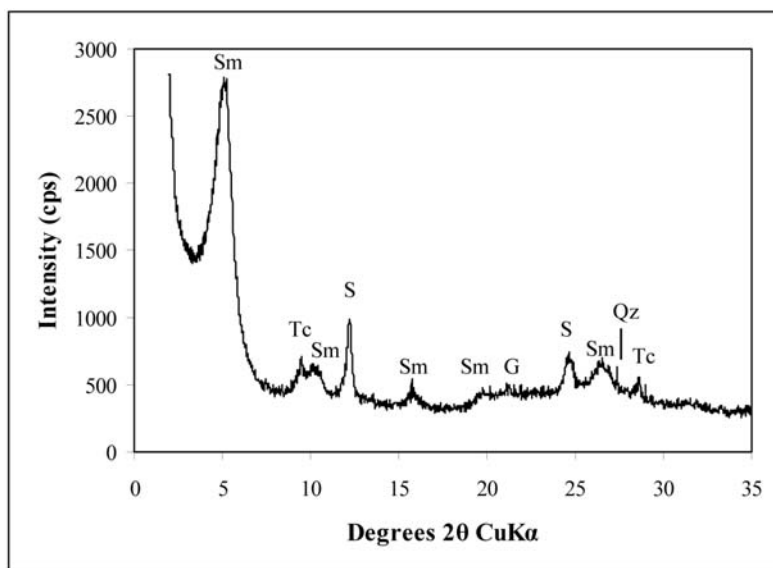


Fig. 2: Glycolated XRD trace of clay fraction from the nontronite zone, Pavlos lateritic profile. Sm= smectite, S= serpentine, Tc= talc, G= goethite, Qz= quartz.

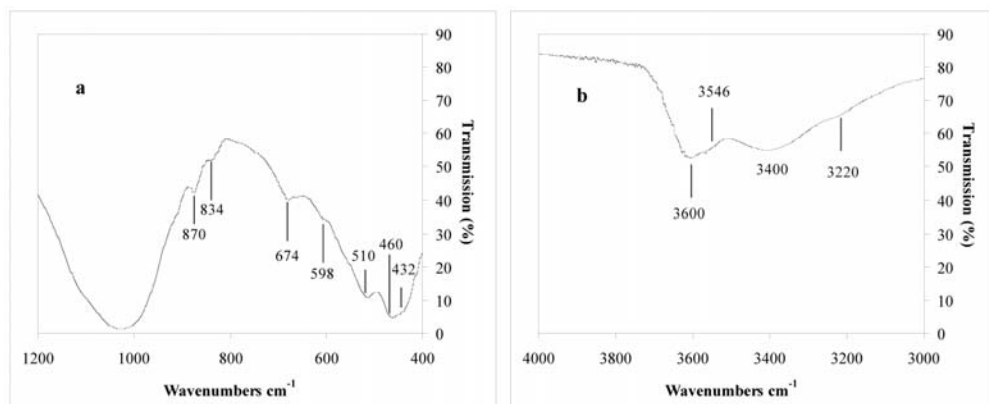


Fig. 3: FTIR spectrum of the smectite from the nontronite zone, Pavlos lateritic profile. a) lattice vibrations, b) –OH stretching vibrations.

The FTIR spectrum of the smectite from the nontronite zone is shown in Figure 3. The spectrum is typical for Fe-rich smectites. The presence of the bands at 870 cm^{-1} and 3600 cm^{-1} (AlFeOH deformation and stretching vibrations respectively) (Fig. 3a), suggests that the smectite may not be true nontronite but ferruginous montmorillonite (Gates, 2005). Nevertheless, the shoulder at 3546 cm^{-1} is indicative of $\text{Fe}_2^{3+}\text{OH}$ linkages. Allocation of the band at 674 cm^{-1} , which could suggest the presence of nontronite, is not unequivocal, because except for Fe-rich dioctahedral smectites, trioctahedral minerals like talc and serpentine, which are present in the sample (Fig. 2), have also their main

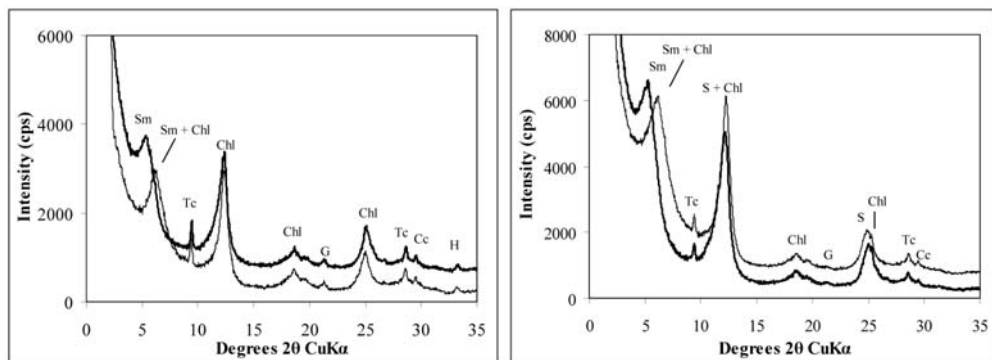


Fig. 4: XRD traces of clay fractions of representative samples from the Agios Ioannis deposit. Sm= smectite, Tc= talc, Chl= chlorite, S= serpentine, G= goethite, H= hematite, Cc= calcite.

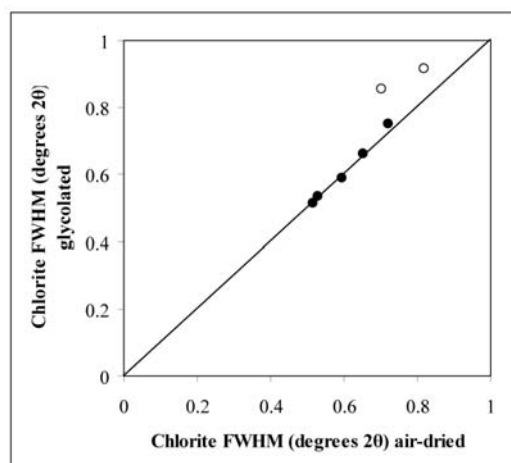


Fig. 5: FWHM of chlorites in ethylene glycol solvated and air-dried clay fractions. Open circles denote samples in which the FWHM of the ethylene glycol solvated samples is significantly greater than the air-dried samples.

M₃OH deformation band in the same area. In the Fe-rich dioctahedral smectites the M-O deformation band at 674 cm⁻¹ suggests that at least 75% of the octahedral cations are Fe³⁺. Note that some of the spectra (not shown here) strongly suggest the presence of nontronite. In any case the results suggest that the smectite present in this sample is a Fe-rich smectite.

Representative XRD traces of clay fractions of samples from Agios Ioannis deposit are shown in Fig. 4. Opposite to the lateritic profile chlorite is the most abundant phase. Nevertheless, most samples are rich in smectite, as it is verified by the shift of the 001 diffraction maximum after exposure in ethylene-glycol vapour. Serpentine, talc and calcite are also present. Finally, goethite and hematite are observed in most of the clay fractions examined. From the relative intensities of the basal reflections it is suggested that chlorite is Fe-rich (odd-order diffraction maxima have considerably lower intensity than even-order diffraction maxima).

In most samples the full width at half maximum (FWHM) of chlorites in the ethylene-glycol solvated clay fractions is comparable to that of the air-dried samples (Fig. 5). In two exceptions the ethylene-glycol solvated samples have greater FWHM (the observed difference is statistically significant)

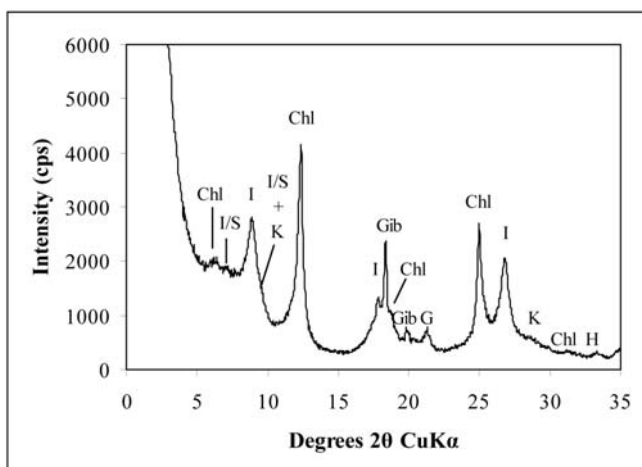


Fig. 6: Illite-gibbsite bearing ethylene glycol solvated clay fraction from the Agios Ioannis Fe-Ni deposit. I= illite, I/S= R1 mixed layer illite smectite, K= kerolite, Chl= chlorite, Gib= gibbsite, G= goethite, H= hematite.

and the diffraction maximum of the 002 maximum shifts to lower angles (i.e. higher d-spacings), suggesting random interstratification (R0) with smectite. In these clay fractions the proportion of smectite in the mixed layer phase does not exceed 20% (Moore & Reynolds, 1997).

Locally, the Agios Ioannis deposit has unusual mineralogical composition and contains also illite, R1 mixed layer illite/smectite, gibbsite and disordered talc (Fig. 6). These samples are smectite-free. Note the differences in talc between the samples from the lateritic profile and those from Agios Ioannis deposit. The former is well crystallized, whereas the latter is disordered. It is thus considered that the talc from Agios Ioannis is kerolite or/and pimelite. Also, the distribution of peak heights of the basal reflections indicates that illite is Al-rich. Had Fe-rich illite been present then the ratio of the odd/even basal diffraction maxima would have been higher than the Al rich illite. Based on the XRD traces the illite-gibbsite bearing samples are rich in Al.

5. Interpretation and discussion

The lateritic profile in Pavlos has significantly different mineralogical composition from the clayey sector of the sedimentary Fe-Ni deposit at Agios Ioannis. The main difference is the predominance of Fe-rich smectite (ferruginous montmorillonite and nontronite) in the former compared to Fe-rich chlorite present in the Fe-Ni deposit. Other important difference is the presence of well crystallized talc in the lateritic profile and kerolite/pimelite and Al-rich minerals (except for chlorite), such as gibbsite, illite and mixed layer illite/smectite (I/S) in the clayey ore. Considering that the weathering of lateritic profiles was the source for the Fe-Ni ores (Skarpelis, 1999), it follows that the observed differences reflect diagenetic modifications or/and additional sources.

An important finding of this contribution is that the clayey Fe-Ni ore contains abundant smectite. The significance of smectite as a critical diagenetic mineral had not been understood and recognized in previous studies, since they were focused mainly on issues on the origin and geochemistry of the ores. Convincing evidence for the presence of smectite has been presented only in Marmeiko deposit (Maksimovic et al., 1993). Moreover the shift from Fe-smectite as main phase in the lateritic profile to Fe-chlorite which is a main phase in the Fe-Ni ore, suggests conversion of smectite to

chlorite after deposition. Diagenetic transformation of smectite to chlorite via intermediate corrensite has been reported in marine sediments off-shore Brazil (Chang et al., 1986). Evidence for this diagenetic transformation in the Fe-Ni deposit of Agios Ioannis is provided by the R0 mixed layer chlorite/smectite (Fig. 5).

Nevertheless, it is surprising that this transformation did not take place in the Fe-smectite of the lateritic profiles. Different depth of burial does not seem to be the main reason for this difference, because the whole area has similar geological evolution. The difference in altitude between the lateritic profiles and the mechanical traps on Jurassic limestones where the laterite-derived material was deposited, does not exceed 200-500 m. Moreover after the Cenomanian-Turonian transgression both areas had the same burial history. It is expected that maximum depth of burial did not exceed 1500-2000 m after deposition of the Upper Cretaceous limestones and the Paleocene flysch. Diagenetic conversion of smectite to chlorite requires temperatures in excess of 150°C (Chamley, 1989), which certainly were not experienced in this area. Similarly, the presence of R1 mixed layer I/S suggests temperatures of 100-110°C. Considering a maximum burial depth of ~2000 m, average surface temperature of 20°C and geothermal gradient 25-30°C per km of burial, the temperature at maximum burial depth should not exceed 70-80°C.

Since burial depth was not the main reason for the observed differences in mineralogy, it follows that the diagenetic transformations in the Fe-Ni ore in Agios Ioannis were triggered by a different geochemical environment. In order for abundant chlorite to form at the expense of smectite a) there must be abundant Al in the system and b) Fe-smectite must be destabilized. Iron in nontronite and ferruginous montmorillonite can be readily reduced with simultaneous change from *trans*-vacant to *cis*-vacant configuration (Manceau et al., 2000; Stucki, 2006). After deposition and burial of the smectite-bearing sediments the Eh decreases with depth and the depositional environment gradually changes from aerobic at the sea floor, to suboxic and finally anaerobic at shallow depths close to the sea floor, even within the area affected by storm reworking (Taylor & Curtis, 1995). This decrease of Eh may well cause reduction of Fe (Rozenon & Heller-Kallai, 1978) and destabilize Fe-rich smectite.

The presence of abundant Al, must be looked for in the source material which was deposited in the karstic cavities along with the weathered lateritic mantles. There is evidence for deposition of bauxitic material in the nearby Fe-Ni deposit of Nissi (Andoniades & Vgenopoulos, 1987). The main Al-oxyhydroxide in the deposit of Nissi is boehmite, associated with hematite, kaolinite and lesser gibbsite. The clayey horizon of Agios Ioannis contains only gibbsite (Fig. 6), the presence of which is attributed to diagenetic mobilization of Al. Aluminum can be mobilized either during dissolution of kaolinite or during conversion of Al-bearing goethite to hematite. Aluminium substitution in goethite - detected by XRD on the basis of (111) reflection - was estimated to be *ca* 13 mol% (Skarpelis, 2005). However, scarce kaolinite has been reported in Agios Ioannis deposit (Alevizos, 1997) and its limited abundance cannot explain the predominance of chlorite. In contrast, the Fe-Ni deposits contain mainly hematite, whereas the original weathered lateritic profiles are expected to have been goethite-rich. Hence transformation of goethite to hematite during diagenesis is a plausible explanation as a source of Al. The lack of a similar Al-source in the lateritic profiles, which nevertheless contain both goethite and hematite, is attributed to the erosion of the uppermost goethite-rich horizons of the lateritic profile (ferruginous zone) which was transported and deposited in the karstified Jurassic limestones.

Finally, the presence of Fe-poor illite and mixed layer I/S is another interesting observation, which is not compatible with the geochemical characteristics of the studied sediments. The fact that these

phases are not widespread in the Fe-Ni sediments strongly indicates that they are diagenetic. Authigenic illite is a common diagenetic phase in argillaceous sediments (Meunier, 2005 and references therein). Both phases may have been formed at the expense of precursor Al-rich phyllosilicates such as kaolinite with supply of K from sea water. This specific topic is currently under investigation.

6. Conclusions

The sedimentary Fe-Ni deposit of Agios Ioannis in Lokris contains Fe-smectite as a main clay mineral phase along with Fe-chlorite. It seems therefore that Fe-rich smectite is a widespread mineral in the Fe-Ni deposits of the broader Lokris area. Although clastic grains of chlorite have been recognized in the past by previous workers, the majority of chlorite is diagenetic and has formed at the expense of smectite via a R0 mixed layer chlorite/smectite with >80% chlorite layers. The source of Al was probably Al-goethite which was converted to hematite after burial.

The lateritic profiles recognized in the broader Lokris area, have a different mineralogical assemblage and consist mainly of Fe-rich smectite (nontronite and/or ferruginous montmorillonite). The lack of authigenic Fe-chlorite in these lateritic profiles is attributed to the erosion of the higher lateritic horizons, which contained abundant Al-goethite. It is not known if these diagenetic mineralogical transformations were associated with mobilization of Ni and REE which has been reported in several Fe-Ni deposits and has been considered as epigenetic (Valeton et al. 1987; Maksimovic et al. 1993).

7. Acknowledgments

The authors would like to thank GMMSA LARKO for their permission to collect samples from the underground works of Agios Ioannis mine.

8. References

- Augustithis, S.S., 1962. Mineralogical and Geochemical Changes in the Diagenetic and Post-Diagenetic Phases of the Ni-Cr-Iron Oolitic Deposit Larymna/Lokris, Greece. *Chemie der Erde* 22, 5-17.
- Albandakis, N. 1974. The nickeliferous Fe-ores of Lokris and Euboea. *Metal. Mining Annals*, 19, 1-41 (in Greek).
- Albandakis, N. 1984. Ni-minerals in the deposits of the Sub-Pelagonian zone. *Mineral Wealth*, 31, 9-32 (in Greek).
- Alevizos, G. 1997. Mineralogy, geochemistry and genesis of sedimentary nickeliferous Fe-ores of Lokris (Central Greece). Unpubl. Ph.D Thesis, Tech. Univ. Crete, Greece, 245 p (in Greek).
- Andoniades, P.A. & Vgenopoulos, A.G. 1987. Study of the nickeliferous bauxitic laterite of the area N. Kokkino-Lokris. *Metal. Mining Annals*, 65, 51-60.
- Andoniades, P.A. & Vgenopoulos, A.G. 1989. Some aspects of the genesis of Ni-Fe-Lateritic ore deposits at Pissona and Katsikiza in the island of Euboea, Greece. In: Augustithis, S.S. (ed) *Metallogeny of basic and ultrabasic rocks (regional presentations)*, Theophrastus Publications, Athens, 519-531.
- Apostolikas, A.G. 2007. The Fe-Ni ore deposit of Kopais Basin, Boiotia Prefecture. Unpubl. Ph.D Thesis, Technical University of Crete, Greece, 179 p (in Greek).
- Chamley, H. 1989. *Clay Sedimentology*. Springer Verlag, Berlin, 623 p.
- Chang, H.K., Mackenzie, F.T. & Schoonmaker, J. 1986. Comparisons between the diagenesis of dioctahedral and trioctahedral smectite, Brazilian offshore basins. *Clays Clay Miner.*, 34, 407-23.
- Eliopoulos, D.G. & Economou-Eliopoulos, M. 2000. Geochemical and mineralogical characteristics of

- Fe-Ni- and bauxitic-laterite deposits of Greece. *Ore Geol. Rev.*, 16, 41-58.
- Gates, W.P. 2005. Infrared spectroscopy and the chemistry of dioctahedral smectites. In: Klopogge J.T. (ed) *The Application of Vibrational Spectroscopy to Clay Minerals and Layered Double Hydroxides*, CMS Workshop lectures, 13, 125-168.
- Hower, J., Eslinger, E.V., Hower, M.E. & Perry, E.A. 1976. Mechanism of burial metamorphism of argillaceous sediments. *Geol. Soc. Amer. Bull.*, 87, 725-737.
- Maksimovic, Z., Skarpelis, N. & Panto, G. 1993. Mineralogy and geochemistry of the rare earth elements in the karstic nickel deposits of Lokris area, Greece. *Acta Geol. Hungarica*, 36, 331-342.
- Manceau, A., Drits, V.A., Lanson, B., Chateigner, G., Wu, J., Huo, D., Gates, W.P. & Stucki, J.W. 2000. Oxidation-reduction mechanisms of iron in dioctahedral smectites. I. Structural chemistry of oxidized reference nontronites. *Amer. Mineral.*, 85, 133-152.
- McCarty, D.K., Sakharov, B.A. & Drits, V.A. 2008. Early diagenesis in Gulf Coast sediments: new insights from XRD profile modeling. *Clays Clay Miner.*, 359-379.
- Meunier, A. 2005. *Clays*. Springer-Verlag, Berlin, 472 p.
- Moore, D.M. & Reynolds, R.C. Jr 1997. X-Ray Diffraction and the Identification and Analysis of Clay Minerals, 2nd ed. Oxford, New York, 378 p.
- Rosenberg, F. 1984. Geochemie und Mineralogie lateritischer Nickel- und Eisenerze in Lokris und auf Euböa, Griechenland. Unpubl. Ph.D Thesis, Univ. Hamburg, Germany, 129 p.
- Rozenson, I. & Heller-Kallai, L. 1978. Reduction and oxidation of Fe³⁺ in dioctahedral smectites-III. Oxidation of octahedral iron in montmorillonite. *Clays Clay Miner.*, 26, 88-92.
- Siegl, W. 1954. Mineralogische Untersuchung der Eisenerze von Lokris und Skyros. I.G.S.R., Athens, 116-134.
- Skarpelis, N. 1997. Eocene nickel laterite deposits in Greece and Albania. In: Papunen H. (ed) *Mineral Deposits: Research and Exploration. Where do they meet?* A.A. Balkema, Rotterdam, 503-506.
- Skarpelis, N. 1999. Lateritic weathering crusts as a source of ferruginous spheroidal particles of sedimentary nickeliferous iron ores, Greece. *Bull. Acad. Serbe Sci. & Arts*, 39, 213-224.
- Skarpelis, N. 2000. Sedimentary nickeliferous iron ores and lateritic weathering crusts in SW Balkan Peninsula: mineralogical textural relationships and genesis. *Proc. 1st Conf. Greek Comm. Econ. Geol. Miner. Geoch.*, 398-412 (in Greek).
- Skarpelis, N. 2005. Lateritization processes of ultramafic rocks in Cretaceous times: The fossil weathering crusts of mainland Greece. *J. Geoch. Explor.*, 88, 325-328.
- Srodon, J. & Clauer, N. 2001. Diagenetic history of Lower Palaeozoic sediments in Pomerania (northern Poland), traced across the Teisseyre–Tornquist tectonic zone using mixed-layer illite-smectite. *Clay Miner.*, 36, 15-27.
- Srodon, J., Kotarba, M., Biron, A., Such, P., Clauer, N. & Wojtowicz, A. 2006. Diagenetic history of the Podhale-Orava Basin and the underlying Tatra sedimentary structural units (Western Carpathians): evidence from XRD and K-Ar of illite-smectite. *Clay Miner.*, 41, 751-774.
- Stucki, J.W. 2006. Properties and behaviour of iron in clay minerals. In: Bergaya, F., Theng, B.K.G. & Lagaly, G. (eds), *Handbook of Clay science*, Elsevier, Amsterdam, 423-475.
- Taylor, K.G. & Curtis, C.D. 1995. Stability and facies association of early diagenetic mineral assemblages: an example from a Jurassic ironstone-mudstone succession, U.K. *J. Sed. Res.*, 65, 358-368.
- Valeton, I., Biermann, M., Reche, R. & Rosenberg, F. 1987. Genesis of nickel laterites and bauxites in Greece during the Jurassic and Cretaceous, and their relation to Ultrabasic parent rocks. *Ore Geol. Rev.* 2, 359-404.

RHEOLOGICAL PROPERTIES OF Palygorskite-Smectite SUSPENSIONS FROM THE VENTZIA BASIN, W. MACEDONIA, GREECE

Christidis, G.E.¹ Katsiki, P.¹ Pratikakis, A.¹ and Kacandes, G.²

¹ Technical University of Crete, Department of Mineral Resources Engineering, 73100 Chania, Greece, christid@mred.tuc.gr, apratik@mred.tuc.gr,

²Geohellas SA, 60 Zephyrou st & Syngrou Av. 17564 Athens, Greece, gkacandes@geohellas.gr

Abstract

In this contribution we examine the rheological properties of palygorskite rich clays from the Ventzia Basin, W. Macedonia, Greece. The clays consist of palygorskite and/or dioctahedral Fe-rich smectite (nontronite) and quartz as main components, and serpentine, amphibole and sepiolite as minor constituents. The apparent and plastic viscosity and yield point increase with increasing concentration of clay in the suspension. Flow is Newtonian for 1% suspensions, becoming gradually Bingham plastic (3% clay suspensions) and then pseudoplastic with yield point described by the Herschel-Bulckley flow model. In the case of suspensions of smectite-free clays Bingham plastic flow behaviour was not observed. Addition of 1M NaCl electrolyte deteriorates the rheological behaviour of the smectite-bearing palygorskite clays but it does not affect significantly the smectite-free, palygorskite rich clays. The different rheological properties of the palygorskite compared to smectite is due to the different morphological and crystal-chemical properties of these two minerals. It is suggested that the palygorskite-rich clays can be used successfully as drilling muds in seawater based drilling fluids, in which smectite-based drilling muds tend to flocculate.

Key words: palygorskite, nontronite, viscosity, yield point, electrolyte, Herschel-Bulckley flow, Ventzia Basin, W. Macedonia.

1. Introduction

Palygorskite is an Mg-rich clay mineral, forming crystals with characteristic fibrous or lath-like habit, which is attributed to their ribbon-like structure. It is considered special clay characterized by microfibrillar morphology (Murray, 2007). The term attapulgite is often used as synonymous to palygorskite, although it is not recommended by the nomenclature committee of AIPEA. In the USA the term fuller's earth, which describes sorptive clays includes also palygorskite rich clays, although in the UK this term describes mainly Ca-rich bentonites.

The rheological properties of suspensions of industrial clays such as bentonites and kaolins have been studied extensively in the past and it is well known that it is affected by particle size and shape, clay concentration, type of exchangeable cation, pH, electrolyte concentration and layer charge (Heath and Tadros, 1983; Brandenburg and Lagaly, 1988; Lagaly, 1989; Permien and Lagaly, 1995; Keren, 1988; 1989). In contrast the rheological properties of palygorskite suspensions have been studied to a lesser degree. In a limited number of studies it has been established that the type of ad-

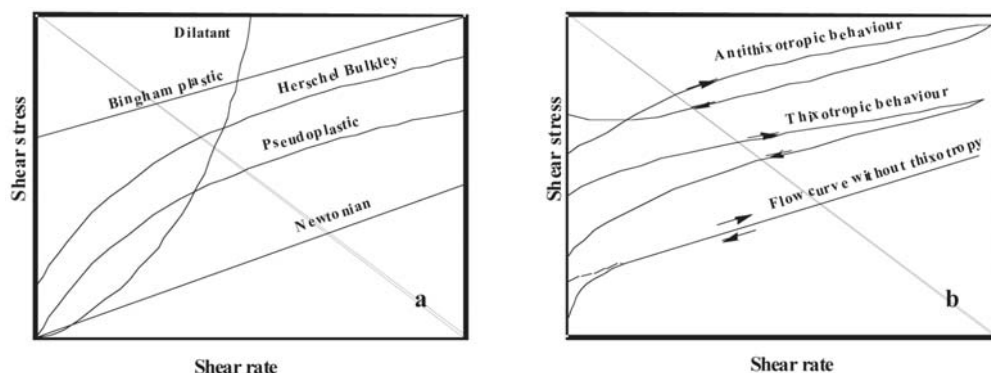


Fig. 1: a) Different types of flow curves observed in clay suspensions. b) Typical flow curves for concentrated thixotropic clay suspensions.

Table 1. Rheological models which describe the rheological behaviour of clay suspensions

Type of suspension	Equation	Type of flow
Newtonian	$\tau = \eta \gamma$	Newtonian
Bingham Plastic	$\tau = \tau_{\beta} + \eta_{pl} \gamma$	Plastic
Power law	$\tau = K \gamma^n$	Shear thickening or shear thinning
Herschel-Bulkley	$\tau = \tau_y + K \gamma^n$	Shear thinning or shear thickening

Where η = viscosity, τ = shear stress, γ = shear rate, τ_{β} = Bingham yield stress and τ_{pl} = plastic viscosity. In the Herschel Bulkley (HB) model, τ_y = HB yield stress and K = HB consistency index

sorbed ions, pH, clay concentration, fibre length and electrolyte addition influence the rheological properties of a series of palygorskite suspensions (Neaman and Singer, 2000; 2004)

In this contribution we study the rheological properties of a series of palygorskite-rich samples from a palygorskite deposit which was recently discovered in Ventzia Basin, Western Macedonia (Kastritis et al., 2003). The deposit formed in a lacustrine environment and displays zonation, with palygorskite occurring at the centre of the basin. Palygorskite is Fe-rich and formed via diagenetic alteration of detrital smectite which originated from the nearby ophiolite complex of Vourinos and the smectite-bearing sands of the Mesohellenic trench (Kastritis et al., 2003). The parameters which were examined are the clay concentration and electrolyte addition. We also examined the influence of smectite in the rheological properties of the suspensions.

2. Theoretical background

Clays are often used in suspensions. For example suspensions of kaolins are used in the slip casting processes during the manufacture of ceramics and in coating paper, whereas smectite and palygorskite are used in drilling fluids. In these applications the flow properties of the suspensions are of primary importance. The science of the deformation and flow of matter is known as *rheology* (Hiemenz & Rajagopalan, 1997). The *viscosity* of a liquid is a measure of the internal resistance offered to the relative motion of different parts of a liquid. Clay suspensions can display Newtonian, Bingham plastic, shear thickening (dilatant) or shear thinning (pseudoplastic) behaviour and may develop yield stress (Fig. 1) (Lyckham & Rossi, 1999). The equations which describe the rheological

behaviour of various types of suspensions are shown in Table 1. Moreover they can develop time-dependent phenomena such as thixotropic or rheopectic (antithixotropic) behaviour (Brandenburg & Lagaly, 1988; Lagaly, 1989; Lyckham & Rossi, 1999) (Fig. 1b). The term *thixotropy* refers to the ability of a suspension to form a gel upon standing and to become fluid when subjected to shear stress i.e. under stirring or agitation.

3. Sampling and experimental methods

Ground palygorskite-rich clayey samples were obtained from Geohellas SA. The received powders were less than 75 μm in size. Bulk mineralogy was determined by X-ray powder diffraction (PXRD) (Siemens D500, CuK α radiation, graphite monochromator, 35 kV and 35 mA, using a 0.02° step size and 1 second per step counting time), on randomly oriented samples, which had been previously gently ground with pestle and mortar in acetone. After grinding the samples were dried at 60°C. The final particle size of the powders was $\sim 10\mu\text{m}$. According to the type of clay mineral present (palygorskite or/and smectite) the clay samples were classified in three groups: clays containing only palygorskite, clays containing only smectite and clays with both minerals.

In as much as only one sample was palygorskite-free, experiments were focused on determination of the rheological properties of clay suspensions of samples containing palygorskite and palygorskite + smectite. Rheological properties (apparent viscosity, plastic viscosity, yield point) were determined with a Couette-type Fann 35S viscometer at 20°C according to the API specifications (API 13A, 1993). Fann viscometers are standard instruments for determination of viscosity of drilling fluids containing bentonite, palygorskite or sepiolite.

The suspensions were prepared according to the API specifications by adding certain amounts of clay to distilled water. The clays were disaggregated with an ultrasonic probe for 20 s prior to stirring with a Hamilton Beach® mixer (see below). 1%, 3%, 5% and 6.42% w/v suspensions were prepared. The 6.42% suspension corresponds to the concentration suggested for industrial drilling fluids (API 13A, 1993). The suspensions were stirred for 20 minutes at 11000 rpm and were left to age for 16 hours. After aging the suspensions were stirred again for 5 min before determination of rheological properties. The measurements were carried out at pH 8. For all samples we constructed complete rheograms (plots of shear rate vs shear stress). No modeling of the rheological curves was attempted using any of the rheological models shown in Figure 1.

4. Results

4.1 Mineralogy

Representative XRD traces of the palygorskite rich samples are shown in Figure 2. The clays consist mainly of palygorskite, smectite, serpentine and quartz. Minor amphibole and sepiolite are present in places. Quartz is biogenic and is related with diatom frustules. The mineralogical composition of the clays varies between palygorskite-free and smectite-free samples. The position of the 060 diffraction maximum is 1.51-1.52 Å, suggesting either the presence of di-trioctahedral phyllosilicates or Fe-rich phases (the 060 diffraction maximum of nontronite is 1.52 Å, Moore and Reynolds, 1997). Note that the diffraction maximum at 1.535 Å belongs to serpentine and indeed it is more intense in trace b which is richer in serpentine. Recent FTIR data of palygorskite-free, smectite bearing samples clearly prove the existence of nontronite (data not shown). Briefly the FTIR spectra are characterized by OH-stretching band at 3548 cm^{-1} and 819 cm^{-1} (FeFeOH stretching and bending respectively), the existence of a Si-Fe-O band at 492 cm^{-1} and the lack of the dominant OH-bend-

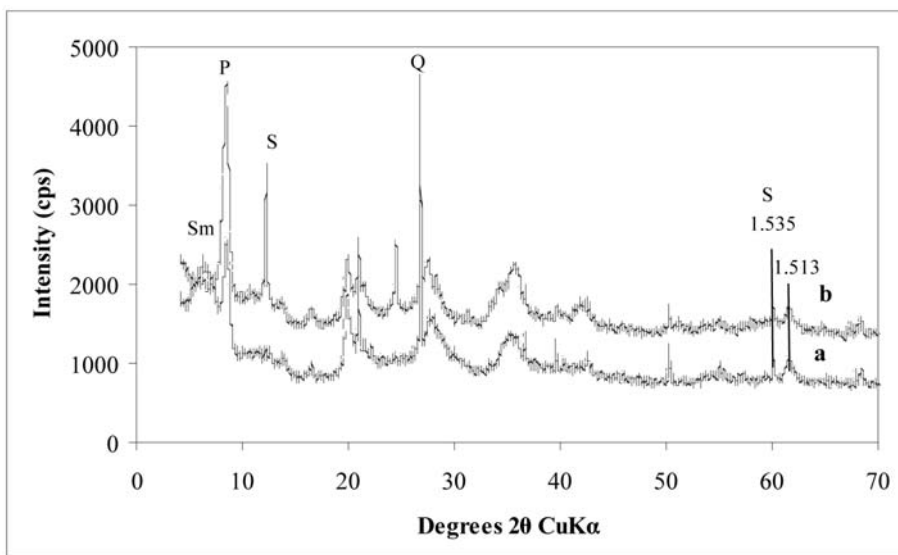


Fig. 2: Representative XRD traces of the palygorskite rich clays from the Ventzia basin. a) Smectite-bearing palygorskite clay, b) Smectite-free palygorskite clay. P= palygorskite, Sm= smectite, S= serpentine, Q= quartz.

Table 2. Rheological properties of the different clay suspensions (according to API 13A, 1993)

Type of clay	Rheological properties	Suspension concentration				
		1%	3%	5%	6.42%	6.42% + 1M NaCl
Clay with smectite + palygorskite	Apparent viscosity (cp)	1.13	3.13	8.13	15	6.25
	Plastic viscosity (cp)	1	1.75	4	2.5	4.5
	Yield point (Pa)	0	0.25	2.5	7	1.5
Clay with palygorskite	Apparent viscosity (cp)	1.88	4.88	17.75	23.75	24.5
	Plastic viscosity (cp)	1.25	1.75	2.25	2.25	6
	Yield point (Pa)	0.1	1.75	14	13.9	10

ing band at 670 cm^{-1} characteristic for trioctahedral phyllosilicates. The Si-Fe-O band at 492 cm^{-1} is indicative of tetrahedral Fe. It is therefore concluded that the predominant smectite present is a Fe-rich smectite dioctahedral smectite (nontronite) not a trioctahedral smectite (saponite).

4.2 Rheological properties

The rheological properties of the representative clays containing palygorskite and palygorskite + smectite are listed in Table 2. In the electrolyte free suspensions viscosity and yield point increases with increasing clay content. Palygorskite suspensions in general develop higher apparent viscosity and yield point than their smectite-bearing counterparts, but the plastic viscosities of the two clay suspensions are comparable (Table 2). In the smectite-bearing clay plastic viscosity decreases for suspension concentration 6.42%. In electrolyte bearing suspensions the two clays display different be-

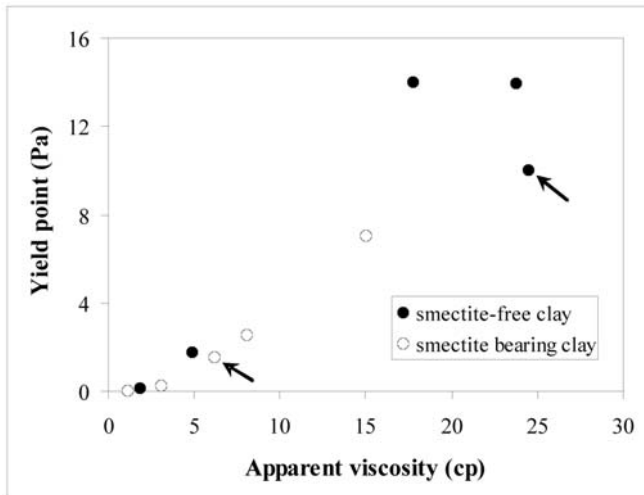


Fig. 3: Relationship between apparent viscosity and yield point for the different clay suspensions. The arrows indicate NaCl suspensions with concentration 6.42%.

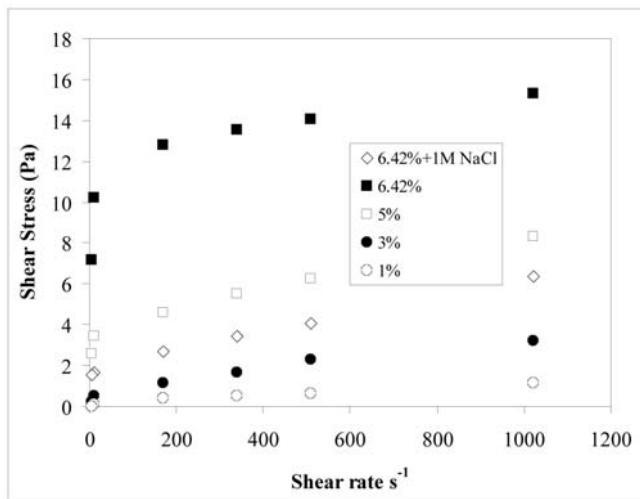


Fig. 4: Rheograms of smectite-bearing clay suspensions with different concentrations. See text for discussion.

behaviour. Palygorskite suspensions are not affected or their rheological properties are improved (e.g. plastic viscosity) after addition of 1M NaCl, whereas smectite-bearing suspensions flocculate and display inferior rheological properties (Table 2).

Therefore palygorskite suspensions are affected to a lesser degree from the presence of electrolytes in accordance with previous reports (Galan, 1996). Finally, yield point is correlated with apparent viscosity but not with plastic viscosity (Fig. 3). This relationship is better expressed for smectite bearing suspensions than for pure palygorskite suspensions.

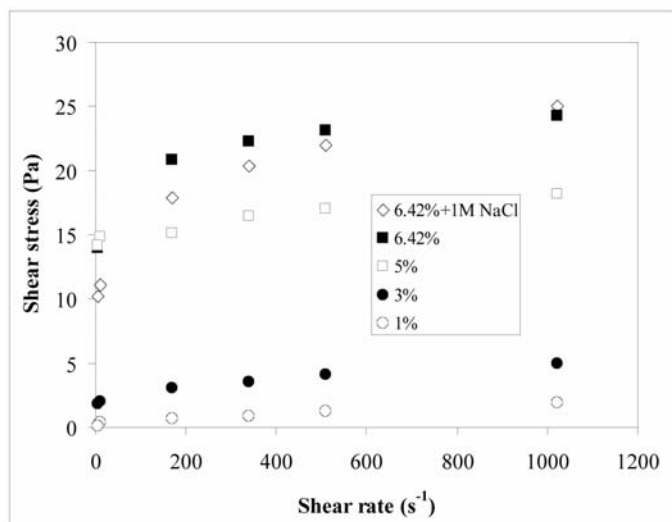


Fig. 5: Rheograms of palygorskite clay suspensions with different concentrations. See text for discussion.

Representative rheograms of smectite-bearing clay suspensions with different concentrations are shown in Fig. 4. The XRD trace of this clay sample is shown in Figure 2a. Electrolyte-free clay suspensions have essentially Newtonian characteristics at 1% concentration (yield point is not observed), which become Bingham plastic for 3% concentration (development of yield point) and Herschel Buckley (shear thinning behaviour with yield point) at higher concentrations. The clay concentration affects both flow resistance (viscosity) and yield point (Table 2, Fig. 4). Both increase with increasing clay concentration. Addition of electrolyte affects the behaviour of the suspension which displays Bingham plastic characteristics. Also the rheogram of the 6.42% suspension with 1M NaCl is between the suspensions with concentration of 3 and 4% clay. Addition of electrolyte decreases both the viscosity and the yield point of the clay suspensions.

Representative rheograms of suspensions of the palygorskite clay with different concentrations are shown in Figure 5. The XRD trace of this clay sample is shown in Figure 2b. The flow is essentially Newtonian for suspension concentration 1%, becoming Herschel-Bulkley type at higher concentrations (Fig. 5). Bingham flow behaviour was not observed at any concentration. Viscosity and yield point increases with increasing suspension concentration, the latter being essentially constant at concentrations higher than 5%. Addition of 1M NaCl to the 6.42% palygorskite suspension does not affect its rheological characteristics significantly. The flow behaviour is described better by the Herschel-Bulkley model, but the plastic viscosity and the yield point are greater than the electrolyte-free suspension. In summary the palygorskite suspensions display better rheological characteristics than their smectite-bearing counterparts and they are affected to a lesser degree by the addition of electrolytes.

5. Discussion

The flow behaviour of suspensions containing palygorskite and mixture of smectite and palygorskite displays some similarities and some important differences. The similarities include the increase of viscosity and yield point with increase of suspension concentration and the Newtonian flow behaviour for suspension concentration 1%. The differences include response in the addition of electrolyte

and the flow characteristics of the suspensions and are attributed to different structures of the suspended clay particles. This in turn is due to the different morphological and structural characteristics of smectite and palygorskite.

Palygorskite forms fibrous crystals often larger than 2 μm in size (Jones & Galan, 1988), whereas smectites form flakes usually smaller than 0.5 μm (Grim & Güven, 1978; Christidis, 1995). Although, nontronite often form ribbon-like crystals (Grim & Güven, 1978; Christidis et al., 1995), their size is considerably smaller than palygorskite fibres. Palygorskite crystals have low layer charge and the viscosity of their suspensions is due to the formation of networks of aggregated fibres. These networks are also responsible for the development of yield point especially at higher clay concentrations. In contrast smectite crystals at this pH form edge-to-edge band-like aggregates rather than card-house structures (Brandenburg and Lagaly, 1988). These aggregates are responsible for the development of viscosity in smectite suspensions.

Palygorskite suspensions develop different flow characteristics than their smectite-bearing counterparts. The rheograms are described by the Herschel-Bulkley model, even at suspension concentrations as low as 3%. This model indicates complex linkages between palygorskite fibres even at low concentrations, at which smectite-bearing clays display Bingham-plastic behaviour. The fact that smectite-bearing suspensions develop Herschel-Bulkley flow characteristics at higher concentrations is in accordance with the complex particle associations and formation of networks between palygorskite fibers.

The different rheological behaviour of the smectite-bearing suspensions in electrolyte bearing suspensions is due to the compression of the diffuse double layers of the smectite particles. In fact the decrease of the rheological properties reflects the presence of smectite. Compression of the double layers causes flocculation of the smectite particles, thus decreasing viscosity. Moreover in cases in which smectite quasicrystals form networks with palygorskite fibers, formation of larger aggregates of smectite crystals is expected to weaken the palygorskite-smectite networks leading to lower yield points. On the other hand, palygorskite has lower layer charge and is expected to develop less extended diffuse double layers, the thickness of which is not affected significantly by the presence of electrolytes. Therefore viscosity and yield point are not affected by the presence of electrolytes. Similar results were obtained from sepiolite suspensions after addition of electrolytes (data not shown). It is not known if the addition of bivalent electrolytes (e.g. CaCl_2 or MgCl_2) will affect the rheological properties of the palygorskite suspensions in a similar manner.

In summary the palygorskite from the Ventzia Basin, Grevena, develops suspensions of high viscosity which meet the API specifications even at concentration of 5%. These suspensions are not affected by the addition of electrolytes. In this manner they perform better than bentonites in seawater based drilling fluids.

6. Acknowledgments

The authors would like to thank Geohellas S.A. for the supply of palygorskite samples from their deposits in Grevena area.

7. References

- API Specifications 13A 1993. *Specification for Drilling Fluid Materials*. American Petroleum Institute.
- Brandenburg, U. & Lagaly, G. 1988. Rheological properties of sodium montmorillonite dispersions. *Appl. Clay Sci.*, 3, 263-279.

- Christidis, G.E. 1995. Mechanism of illitization of bentonites in the geothermal field of Milos Island, Greece. Evidence based on mineralogy, chemistry, particle thickness and morphology. *Clays Clay Miner.*, 43, 567-594.
- Christidis, G., Scott, P.W. and Marcopoulos, T. 1995. Origin of the bentonite deposits of Eastern Milos, Aegean, Greece: Geological, Mineralogical and Geochemical evidence. *Clays Clay Miner.*, 43, 63-77.
- Galan, E. 1996. Properties and applications of palygorskite-sepiolite clays. *Clay Miner.*, 31, 443-453.
- Grim, R.E. and Güven, N. 1978. *Bentonites. Geology, mineralogy, properties and uses*. Elsevier, Amsterdam, 143-155.
- Heath, D. and Tadros, T.F. 1983. Influence of pH, electrolyte and poly(vinyl alcohol) addition on the rheological characteristics of aqueous dispersions of sodium montmorillonite. *J. Colloid Interf. Sci.*, 93, 307-319.
- Hiemenz, P.C. and Rajagopalan, R. 1997. *Principles of colloid and surface chemistry*, 3rd edition. New York: Taylor and Francis.
- Jones, B.F. and Galan, E. 1988. Sepiolite and palygorskite. In: Bailey S.W. (ed.): *Hydrous Phyllosilicates. Rev. Mineral.*, 19, MSA 631-674.
- Kastritis, I.D., Kacandes, G.H. and Mposkos, E. (2003): The palygorskite and Mg-Fe-smectite clay deposits of the Ventzia basin, western Macedonia, Greece. In: Eliopoulos, D. et al., (eds): *Mineral exploration and sustainable development*, Millpress, Rotterdam, 891-894.
- Keren, R. 1988. Rheology of aqueous suspension of sodium/calcium montmorillonite. *Soil Sci. Soc. Am. J.*, 52, 924-928.
- Keren, R. 1989. Effect of clay charge density and adsorbed ions on the rheology of montmorillonite suspension. *Soil Sci. Soc. Am. J.*, 53, 924-928.
- Lagaly, G. 1989. Principles of flow of kaolin and bentonite dispersions. *Appl. Clay Sci.*, 4, 105-123.
- Lyckham, P.F. and Rossi, S. 1999. The colloidal and rheological properties of bentonite suspensions. *Adv. Colloid Interface Sci.*, 82, 43-92.
- Moore, D.M. and Reynolds, R.C. Jr. 1997. *X-ray diffraction and the identification and analysis of clay minerals*, 2nd edition. Oxford: Oxford University Press.
- Murrey, H.H. 2007. *Applied Clay Mineralogy/Developments in Clay Science 2/*. Elsevier, Amsterdam, 180 pp.
- Neaman, A. & Singer A. 2000. Rheological properties of aqueous suspensions of palygorskite. *Soil Sci. Soc. Am. J.*, 64:427-436.
- Neaman, A. & Singer A. 2004. Possible use of the Sacalum (Yucatan) palygorskite as drilling muds. *Appl. Clay Sci.*, 25, 121-124.
- Permien, T. and Lagaly, G. 1995. The rheological and colloidal properties of bentonite dispersions in the presence of organic compounds. V. Bentonite and sodium montmorillonite and surfactants. *Clays Clay Miner.*, 43, 229-236.

MINERALOGY OF THE SAHARAN AEOLIAN DUST IN CRETE: EXAMPLES FROM THE PERIOD 2004-2009

Christidis, G.E.¹, Perdikatsis, V¹ and Apostolaki, Ch¹.

¹ *Technical University of Crete, Department of Mineral Resources Engineering, 73100 Chania, Greece,
vperdik@mred.tuc.gr, christid@mred.tuc.gr, xapostol@mred.tuc.gr*

Abstract

Aeolian dust sediments, which were deposited by spring rainstorms or directly by the dust cloud were collected in the Technical University of Crete during the interval 2004-2009. The samples display remarkable mineralogical homogeneity and consist of illite, quartz, calcite, albite, kaolinite, palygorskite and dolomite. Chlorite or/and smectite is present in samples collected in 2006 and 2009. Gypsum is present in the collected from the airborne dust in 2009, but not from the sample which precipitated from rain in the same day. Mirabilite was traced in the sediment collected in 2005. The presence of palygorskite and dolomite in all samples and gypsum and mirabilite in two of the collected sediments implies formation of the original material in an arid environment characterized by alkaline pH. The mineralogical composition coupled with back trajectory analysis on similar dust clouds indicate that the clouds originated in areas of Western Sahara or/and southern Morocco and that major mixing with fine-grained material from Europe is less probable. The possibility for a Central Algerian source for the airborne dust clouds is rejected because of the lack of smectite.

Key words: *Airborne dust, Crete, Sahara, Sahel, palygorskite, illite, quartz, dolomite, arid alkaline environment.*

1. Introduction

Every year, especially in spring and autumn Greece receives significant amounts of Aeolian dust from Africa. This phenomenon is widespread in all South European countries of the Mediterranean region (Bücher and Lucas, 1984). The dust clouds originate from the Sahara desert and are typically observed as yellowish-brown clouds that are washed out by rains mostly against topographic barriers, which cause uplift of the of the transporting air-masses (Prodi and Fea, 1979; Nihlen and Mattsson, 1989). It is interesting that dust clouds from the Sahara have been traced as far as north Europe namely Germany (Littmann and Steinrücke, 1989) and Scandinavia (Franzén, 1989) as well as in North and South American continent (Prospero, 1999; Stuut et al., 2009). Mineral dust aerosols from desert regions contribute significantly to the total atmospheric aerosol load (Linke et al., 2006). For this reason they have been studied considerably in various places in the world such as the Middle East (Abdul-Wahab et al., 2005) China (Yi et al., 2007).

An Aeolian dust system is described by particle formation (P), particle transportation (T) and particle deposition (D) events, known as the PTD scheme (Smalley et al., 2005). Particle formation events include both determination of the locality of and mechanisms of formation. Determination of the locality of formation is difficult because the exact transportation paths are often not known with cer-

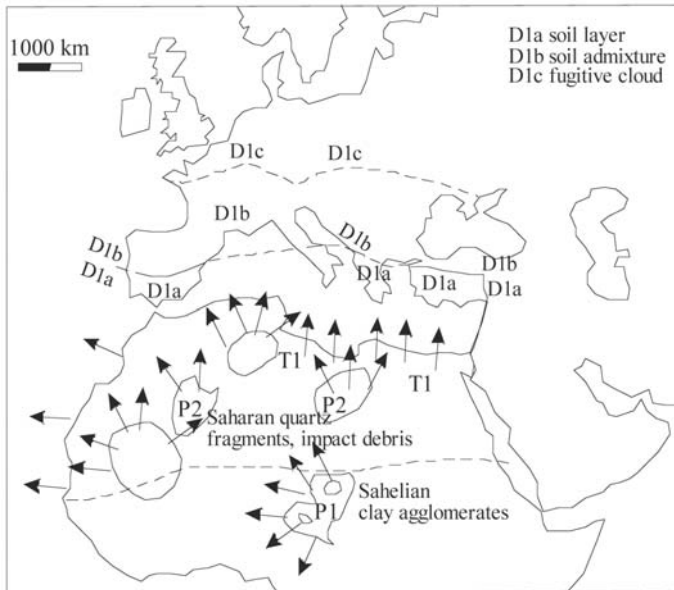


Fig. 1: Source areas and deposition sites of dust clouds, which originate in Saharan and Sahelian areas of North Africa. P denote particle formation areas, T denote transportation and D denote areas of deposition (modified from Stuut et al., 2009).

tainty and multiple sources are often involved in the formation of the cloud. More recently back trajectory analysis and direct satellite image data have been used to determine the sources of the Aeolian Saharan dust (Stuut et al., 2009). Notwithstanding the small deviations between the various authors there is general consent for the existence of a main source in Western Sahara including Morocco and Mauritania, and two additional sources, one in South Libya and Chad and one in Egypt and North Sudan (Fig. 1). The latter two sources located south of the 30° N can be classified as “Sahelian” (see below).

Due to the frequency of the Saharan airborne dusts over Greece including Crete, they have been studied extensively during the past few years. The studies are focused on the optical and physical properties of the airborne clouds (e.g. Fotiadi et al., 2006; Balis et al., 2006 among others). In contrast the mineralogical composition of the dusts has not been studied in the past. In this contribution we present the mineralogical composition of different airborne Saharan dusts which were deposited in the Technical University of Crete, Chania in spring time during the years 2004-2009. Moreover important conclusions about the type of the dust source (single over variable sources) are drawn.

2. Types of Saharan airborne dust

The Saharan dust has been classified according to its particle size into *small dust* and *large dust* (Livingstone and Warren, 1996). According to this classification scheme, large dust has coarse silt (16-31 μm) and very coarse silt (31-63 μm) size, it consists predominantly of quartz crystals and it travels short distances and forms loess deposits. Large dust deposits have been recognized in proximal deposition areas to Sahara such as Sicily, southern Italy and Crete (Correggiari et al., 1989; Guerzoni et al., 1996; di Sarra et al., 2002). Fossil large-dust deposits have also been recognized

Table 1. Mineralogical composition of the airborne dust samples

<i>Sample</i>	<i>Quartz</i>	<i>Illite</i>	<i>Albite</i>	<i>Kaolin-ite</i>	<i>Paly-gorskite</i>	<i>Dolomit-e</i>	<i>Calcite</i>	<i>Chlorite/smectite</i>	<i>Gypsum</i>	<i>TCM**</i>
NLB 5_5_04R	19.3	30	9.3	8.2	6.3	5.8	21.2	-	-	44.5
LB 17_4_05R*	19	29.8	7.4	4.8	4.9	4.7	28.7	-	-	39.5
LB 21_4_06R	15	38.6	12	5.1	3.5	3.2	17	4.6	-	47.2
LB 5_3_09R	25.8	28.7	14	6.9	3.5	4.3	12.7	4.5	-	39.1
LB 5_3_09D	24.5	30	10	8	3	3.5	13	3	5	41

*Sample LB17_4_05 contains traces of mirabilite ($\text{Na}_2\text{SO}_4(\text{H}_2\text{O})_{10}$)

**TCM = Total Clay Mineral content.

across the European continent. In contrast small dust deposits have been traced not only in central and northern Europe but in the American continent and the Middle East and Central Asia as well (Prospero, 1999).

Small dust includes both *Saharan* and *Sahelian* inputs (Stuut et al., 2009). The term Sahelian includes origin from basins in peri-Saharan areas, south of the 30th parallel. Two main types of airborne particles have been recognized in small dust, clay mineral agglomerates (CMA) and monomineralic fragments, mainly quartz and feldspar. The CMA are in fact fine grained lake deposits, which consist of quasicrystals of different clay minerals. Several Sahelian basins have been considered as sources of fine dust, the most important being Lake Chad and areas of Western Sahara and southern Morocco. However, due to the complex trajectories of the dust clouds, which pass over extended *Ergs* (large desert areas consisting of sand dunes known as sea sands) most of them contain both large dust and small components, due to mixing.

3. Sampling and experimental methods

Five airborne dust samples were collected in canisters in spring of 2004, 2005, 2006 and 2009. The first 3 samples were deposited in the canisters by rain. In 2009 we collected two samples, one directly from the dust cloud and the second after rain the same day. Therefore these two samples represent materials which were transported with the same mechanism but were deposited via a different process. The samples are denoted according to the type of deposition (rain or cloud) and date of collection. For example LB5_5_04R indicates that the sample was collected in 5th May 2004 after rain and LB5_3_09D denotes that the sample was collected in 5th March 2009 from the dust cloud. Notation of the samples and sampling dates are listed in Table 1. The deposited dust clouds were collected the next day. The samples were filtered to remove rain water, dried at 105°C and stored in plastic bags.

Bulk mineralogy was determined by X-ray powder diffraction (PXRD) (Siemens D500, CuK α radiation, graphite monochromator, 35 kV and 35 mA, using a 0.02° step size and 1 second per step counting time), on randomly oriented samples initially gently ground with pestle and mortar in acetone. Since all samples were mainly fine grained (fine dust samples) minimum grinding was applied. Quantitative analysis was carried out using Autoquan software using Rietveld refinement and standardless profile fitting. The relative error of the quantitative estimations is $\pm 5\%$ for minerals present in amounts greater than 50% and $\pm 10\%$ for minerals present in amounts less than 10%.

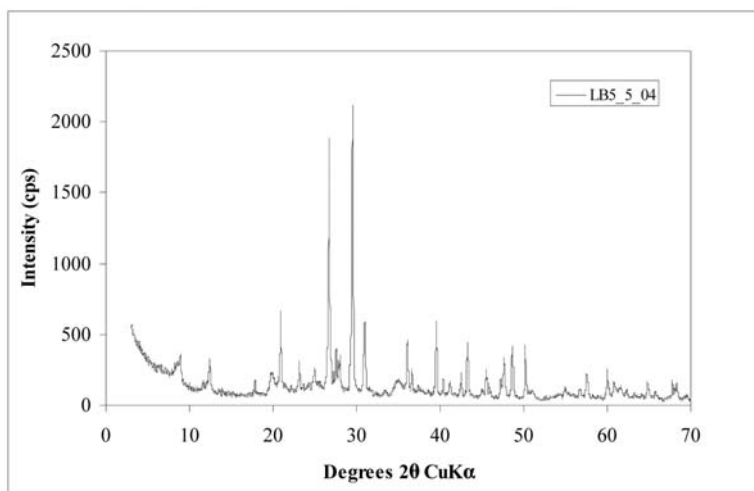


Fig. 2: Representative XRD of Aeolian dust sample LB_5_5_04.

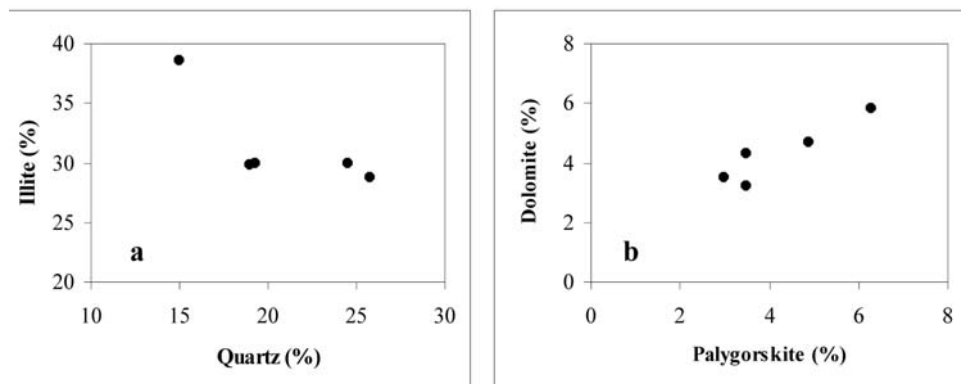


Fig. 3: Compositional trends in the Aeolian dust samples.

4. Results

The mineralogical composition of the samples is listed in Table 1. Representative XRD trace is shown in Figure 2. In general the composition of dust remains constant through time. The main change in the mineralogical composition is the decrease of carbonates and palygorskite and the increase of quartz content towards present. The most widespread phase is illite, the abundance of which remains essentially constant with time and so is the total clay mineral (CM) content. This is expected, because the clay fraction is dominated by illite. Kaolinite is the second most abundant clay minerals, whereas chlorite or/and smectite are present only in the samples from 2006 and 2009 sediments.

The mineralogical composition of samples displays certain mineralogical trends. A clear negative relationship holds between illite and quartz (Fig. 3a). Similar trend is observed between quartz and total clay mineral content (not shown). In contrast a distinct positive trend is observed between dolomite and palygorskite (Fig. 3b) and suggests a possible common origin of the two minerals. This is typ-

ical of alkaline soils frequently found in arid areas, such as the Sahara desert. The composition of samples LB5_3_09R and LB5_3_09D is essentially identical except for the presence of gypsum in the latter (Table 1). The lack of gypsum from sample LB5_3_09R is attributed to the conditions of deposition of the two samples. Deposition from rain water dissolved the small amounts of gypsum initially present in the dust cloud. Dissolution took place in the canister, which was used to collect the samples, because gypsum was in contact with rain water for several hours before collection.

5. Discussion

The Aeolian dust sediments, which were collected over a period of 6 years, display remarkable compositional homogeneity both in terms of the type of minerals present and their abundances. This homogeneity reflects common source areas and transportation paths. The collected sediments have two major characteristics a) they are rich in clay minerals (39.1-47.2 wt %) and b) they contain palygorskite. Potential sources of palygorskite are areas of Western Sahara and southern Morocco (Molinaroli, 1996). Although the northern sectors of Sahara are closer to Crete it seems that the Aeolian clouds follow a different route. The possibility for a source in the Western part of North Africa is supported by the back trajectory analysis of an Aeolian dust cloud, which was traced in August 2003 in northern and central Greece and Crete (Balis et al., 2006). This analysis clearly indicates a Western Saharan source for the cloud, which practically coincides with area P2 (Fig. 1), and trajectory route over Corsica, South Italy and Central Greece.

The well expressed positive relationship between palygorskite and dolomite implies a common origin for the two minerals. Mg-silicates and carbonates are common phases in soils formed in arid or semi-arid climates (Meunier, 2005). In such environments intense evaporation increases significantly the concentration of alkalis and alkaline-earth elements. Salts precipitate a precise soil levels controlled by capillary forces. Soils with crusts of salt or gypsum occur in schots or sahkhass. In such environments the pH is alkaline (~9) favouring precipitation of palygorskite and dolomite. Mg-rich silicates in these environments form at the expense of detrital Al-rich phyllosilicates such as kaolinite, illite or smectite. Both illite and kaolinite, which can act as precursors of palygorskite are present in the samples. Moreover the presence of gypsum and mirabilite in two of the collected sediments strongly suggests an alkaline environment.

In general the presence of quartz, kaolinite dolomite and calcite is considered a good indication of Saharan origin (Chester et al., 1984; Avila et al., 1997). Also palygorskite has been considered as tracer of desert dust. With the exception of calcite, the abundances of these minerals are in accordance with their corresponding abundances in soils from the Moroccan Atlas and Western Sahara (Avila et al., 1997). Calcite is particularly enriched in the dust samples of the present study, although its abundance decreases towards present. This enrichment in calcite may indicate mixing with other soil source areas rich in this mineral. Note that calcite is not systematically related to the precipitation of palygorskite and this is indicated also in the data of our study (Table 1).

An important difference with previous studies on Aeolian dust samples which originated in the Western part of North Africa is the lack of smectite which is virtually absent from our samples or it may be present in trace amounts (Table 1). The reason for the lack of smectite is not known with the existing data. Note that all possible sources in the broader Western North Africa contain smectite, with Central Algeria being richer in this mineral (Avila et al., 1997). This suggests that the Central Algerian soils must be excluded as source materials for the Aeolian dusts. Finally, the lack of chlorite indicates that important mixing with other soils rich in this mineral, such as the Iberian soils (Avila et al., 1997) has not taken place.

6. Conclusions

Aeolian dust sediments which were collected from Crete during spring storms in the interval 2004-2009 display remarkable mineralogical heterogeneity. They are rich in clay minerals and their origin must be sought for in the areas of Western Sahara and/or south Morocco. The lack of smectite from the samples precludes the possibility for origin from Central Algeria. The consistent mineralogical composition over this time interval suggests that the air circulation in the air which is responsible for the transportation of the dust clouds remain essentially unchanged during this time interval. Although mineralogy points towards certain origin for the dust clouds, the study should be complemented with back trajectory analysis, using weather data available for the periods of sampling for verification of the mineralogical data. This will be performed in the near future.

7. References

- Abdul-Wahab, S.A., Worthing, M.A. & Al-Maamari, S. 2005. Mineralogy of atmospheric suspended dust in three indoor and one outdoor location in Oman. *Environ. Monitor. Assess.*, 107, 313-327.
- Avila, A., Queralt-Mitjans, I. & Alarcon, M. 1997. Mineralogical composition of African dust delivered by red rains over northeastern Spain. *J. Geophys. Res.* 102 (D18), 21977-21996.
- Balis, D., Amiridis, V., Karadzis, S., Papayannis, A., Tsaknakis, G., Tzortzakos, S., Kalivitis, N., Vrekoussis, M., Kanakidou, M., Mihalopoulos, N., Chourdakis, G., Nickovic, S., Perez, C., Baldasano, J. & Drakakis, M. 2006. Optical characteristics of desert dust over the East Mediterranean during summer: a case study. *Ann. Geophys.*, 24, 807-821.
- Bücher, A. & Lucas, G. 1984. Sedimentation eolienne intercontinentale, poussières sahariennes et géologie. *Bull. Centres Res. Explor.-Production ELF Aquitaine*, 8, 151-165.
- Chester, R., Sharples, E.J., Sanders, G.S. & Saydam, A.C. 1984. Saharan dust incursion over the Tyrrhenian Sea. *Atmos. Environ. J.*, 18, 929-935.
- Corregiari, A., Guerzoni, L., Lenaz, R., Quarantotto, G. & Rampazzo, G. 1989. Dust deposition in the central Mediterranean (Tyrrhenian and Adriatic Seas): relationships with marine sediments and riverine input. *Terra Nova*, 1, 549-558.
- di Sarra, A., Cacciani, M., Chamard, P., Cornwall, C., DeLuisi, J.J., Iorio di T., Disterhoft, P., Fiocco, G., Fua, D., Monteleone, F. 2002. Effects of desert dust and ozone on the ultraviolet irradiance at the Mediterranean island of Lampedusa during PAUR II. *J. Geophys. Res.*, 107 (D18), 8135.
- Evans, R.D., Jefferson, I.F., Kumar, R., O'Hara-Dhand, K. & Smalley, I.J. 2004. The nature and early history of airborne dust from North Africa; in particular the Lake Chad basin. *J. Afr. Earth Sci.*, 39, 81-87.
- Fotiadi, A., Hatzianastassiou, N., Drakakis, M., Matsoukas, C., Pavlakis, K.G., Hatzidimitriou, D., Gerasopoulos, E., Mihalopoulos, N. & Vardavas, I. 2006. Aerosol physical and optical properties in the Eastern Mediterranean Basin, Crete, from Aerosol Robotic Network data. *Atmos. Chem. Phys.*, 6, 5399-5413.
- Franzén, L.G. 1989. A dustfall episode on the Swedish West Coast, October 1987. *Geogr. Ann. Ser. A, Phys. Geog.*, 71, 263-267.
- Guerzoni, S., Quarantotto, G., Cesari, G., Molinaroli, E., Rampazzo, G. & Le Balloch, O. 1996. Trace metal composition and grain size of the particulates in aerosols and precipitation collected in NW Mediterranean (39°N, 9°E) a multivariate analysis. In: Guerzoni, S. & Chester, R (eds), *The impact of Desert Dust Across the Mediterranean*. Kluwer Academic Publishers, Rotterdam, 333-338.
- Linke, C., Möhler, O., Veres, A., Moracsi, A., Bozoki, Z., Szabo, G & Schnaiter, M. 2006. Optimal properties and mineralogical composition of different Saharan mineral dust samples: a laboratory study. *Atmos. Chem. Phys. Discuss.*, 6, 2897-2922.

- Littmann, T. & Steinrück, J. 1989. Atmospheric boundary conditions of recent Saharan dust influx into Central Europe. *GeoJournal*, 18, 399-406.
- Livingstone, I. & Warren A. 1996. *Aeolian Geomorphology: An introduction*. Longman, London, 211 p.
- Meunier, A. 2005. *Clays*. Springer-Verlag, Berlin, 472p.
- Molinaroli, E. 1996. Mineralogical characterization of Saharan dust with a view to its final destination in Mediterranean sediments. In: Guerzoni S. & Chester, R. (eds) *The impact of Desert Dust Across the Mediterranean*. Kluwer, Rotterdam, 153-162.
- Nihlen, T. & Mattsson, J.O. 1989. Studies on eolian dust in Greece. *Geogr. Ann.*, 71A, 269-274.
- Prodi, F. & Fea, G. 1979. A case of transport and deposition of Saharan dust over the Italian peninsula and southern Europe. *J. Geophys. Res.*, 84 (C11), 6951-6960.
- Prospero, J.M. 1999. Long-range transport of mineral dust in the global atmosphere: Impact of African dust on the environment of the southeastern United States. *Proc. Natl. Acad. Sci. USA.*, 96, 3396-3403.
- Smalley, I.J., Kumar, R., O'Hara-Dhand, K., Jefferson, I.F. & Evans, R.D. 2005. The formation of silt material for terrestrial sediments; particularly loess and dust. *Sed. Geol.*, 179, 321-328.
- Stuut, J-B., Smalley, I. & O'Hara-Dhand, K. 2009. Aeolian dust in Europe: African sources and European deposits. *Quatern. Inter.*, 198, 234-245.
- Yi., S.L., Li, W.J., Yang, S.S., Shi, Z.B. & Lü, S.L. 2007. Mineralogical characteristics of airborne particles collected in Beijing during a severe Asian storm period in spring 2002. *Sci. China Ser. D-Earth Sci.*, 50, 953-959.

MINERALOGY OF CHROMITITE, BULQIZA ULTRAMAFIC MASSIF, ALBANIAN OPHIOLITIC COMPLEX

Çina A.

*Institute of Geosciences, Polytechnic University of Tirana. Str. Don Bosco, Nr. 60.
al_cina@yahoo.com*

Abstract

Ultramafic massif of Bulqiza belongs to Eastern Jurassic Albanian ophiolite belt of IAT-BSV- type. This massif is the most important chromite-bearing ore. The mantle ultramafics have extremely refractory nature. This is due to the high partial fusion of upper mantle which is depleted in CaO and Al₂O₃. The chromitite is situated to different parts of ultramafic pile, from bottom Cpx-harzburgites up to massive dunites and cumulate ultramafic but the mainly chromite potential belongs to mantle harzburgite –dunite level and to transition dunites partly. The chromite is chiefly of Cr-rich metallurgical type. The atomic ratios of chromite, Fo of olivine and some physical properties of them vary according to the chromitite setting and reflects the evolution of Ol-Sp equilibrium process depended of the chromite concentration, from barren dunitic lenses towards dunite envelops of the ore bodies and the interstitial and inclusions of olivine within chromite grains. Two particular chromite deposits are the Bulqiza- Batra tabular folded ore body and Shkalla, pencil –like ore body.

Key words: *Chromitite mineralogy, ultramafic, massif Bulqiza Albania.*

1. Introduction

Widespread ophiolitic rocks in Albania occur along two ophiolitic belts, the Western and the Eastern ones characterized by individual petrological, geochemical and metallogenic features. The Western belt comprises ophiolitic rocks of Jurassic age and MOR-type affinity and includes high – Ti basaltic rocks. On the contrary, the ophiolitic rocks of Eastern belt show IAT type geochemical character and comprise of low-Ti basalts. This belt suggested that it is formed over a subduction zone (SSZ) (Alliu et al., 1994; Shallo et al., 1995; Kodra et al., 1995). This ophiolitic belt is composed by some massifs, with them, the Bulqiza massif is most important for its high chromite-bearing. Many chromite occurrences and some big and very big deposits are situated in this massif related chiefly to harzburgite –dunitic mantle part and partly with super MOHO- dunites. The ore body are folded tabular, podiform, banded – layered and pencil – like even. The principal rock constituent are mantle harzburgites and super MOHO –dunites, whereas the Pl-dunites, lherzolites, wehrlites, pyroxenites and gabbroic rocks, are less abundant. The Bulqiza massif, similarly to other Eastern ophiolitic complexes such the Vurinous and Troodos. (Çina et al., 1986; Econoumu et al., 1986; Panayiotou et al., 1986), has been affected by intensive partial melting of the upper mantle as it is implying by depletion in CaO and Al₂O₃ and enrichment in MgO and Cr₂O₃ of the mantle rocks. The chromite is of Cr-rich, metallurgical type, with a few exceptions, for some occurrences composed by Al-rich chromite – type. It is remarkable that olivine as dunite and chromitite – component is two much forsteritic type. The morphology and textures of ore body as well as the chemical composi-

tion and some physical properties of chromite are subordinated related to their geological setting, from Cpx- harzburgite of deeper part to upwards super MOHO-dunites and ultramafite – mafite sequences. All the same, the composition of olivine is variable related to chromite concentration, as reflection of equilibrium process between ol- sp. The aim of this review is to make known the mineralogy of chromitite of one of the most distinguished chromitite-bearing ultramafic massifs of Bulqiza, and wider for the Eastern ophiolitic complexes in general.

1.1 Analyses' methods and conditions.

The analyses of chromite and olivine are brought out by electronic microprobe CAMEBAX under the conditions accelerating voltage 15 kV and a current of 10 nA, time of capture 10 sec. The correction programme ZAF by Honoc and Tong (1978). The analyses have been conducted in MGA-BRGM, France by Ch. Gilles and D. Ohnenstetter. The parameter of the elementary cell of chromite have been extracted from the Ro-analyse with 4x time camera of Guinier and Wolff, anticathode Cu- Ka1, 36 kV, 20 mA with the assistance of F. Pillard at MGA-Mineralogy Geochemistry Analyses, France.

2. Geology and chromitite-bearing of the massif.

The Bulqiza ultramafic massif is situated at Eastern ophiolitic belt. It covers a surface of 350 km², with a thickness about 5 – 6 km. It is surrounded by different sediments, from Triassic, Triassic – Jurassic limestones, and partly is covered by Cretaceous limestones and Neogenic molassic sediments. This massif consists mainly of mantle harzburgites, Eastern and central part, by super – MOHO dunites, South – Western and Western parts and by ultramafic – mafic intrusive rocks at Western side (Fig.1). This massif is remarkable for its high chromite-bearing mineralization. About 100 occurrences and 15 deposits occur. Among them, some are big and very big as Bulqiza – Batra, Shkalla, Thekna, Ternova, Lugu Gjat, and Krasta deposits. The most important chromite mineralization is situated at central part of massif related to harzburgite – dunites, and partly at South – South – Western part related to super - MOHO dunites. Only from Bulqiza – Batra deposits are extracted about 20 mega ton high grade chromite ore. The ore bodies have tabular concordant and semi concordant folded shapes, podiform and banded-layered, even pencil –like morphology. The exceptional is Bulqiza deposit represented by tabular folded ore bodies, 5000m in strike and 0,5 up to 5-10 m thick. The ore body came out at the height of 1570 m over the sea level and goes down to 300 m under the sea level. The other particular deposit is Shkalla, pencil – like ore bodies. These have oval - shaped surface section from 5 to 25 m² and go up to 1500m downwards. The chromite is Cr-rich metallurgical high grade type. It is situated at different part of ultramafic pile, from that related to deep mantle cpx – harzburgites, towards upper harzburgite – dunite and dunite – harzburgite parts, up to super –MOHO dunites, even to ultramafite – mafite and troctolite sequences. The most chromite –bearing potential is situated at 300 up 1200 m interval below super-MOHO dunites and only low – grade chromite ores are related at middle – deep dunitic sequence (Fig.2). The chromite ore grade concerning its geological setting decreases from mantle harzburgite – dunitic level of high to highest grade from 37% to 45% Cr₂O₃ even 53% Cr₂O₃ for pencil –like ore body, upwards for dunite – harzburgite part (middle grade, from 30% to 35% Cr₂O₃) and particularly for super – MOHO dunites (lower grade, from 18% to 25% Cr₂O₃).

2.1 Petrography

The most common mineral components of chromitites are chromite and olivine, as well as serpentine. In small quantities occur also the other silicate minerals clinopyroxene, orthopyroxene, amphi-

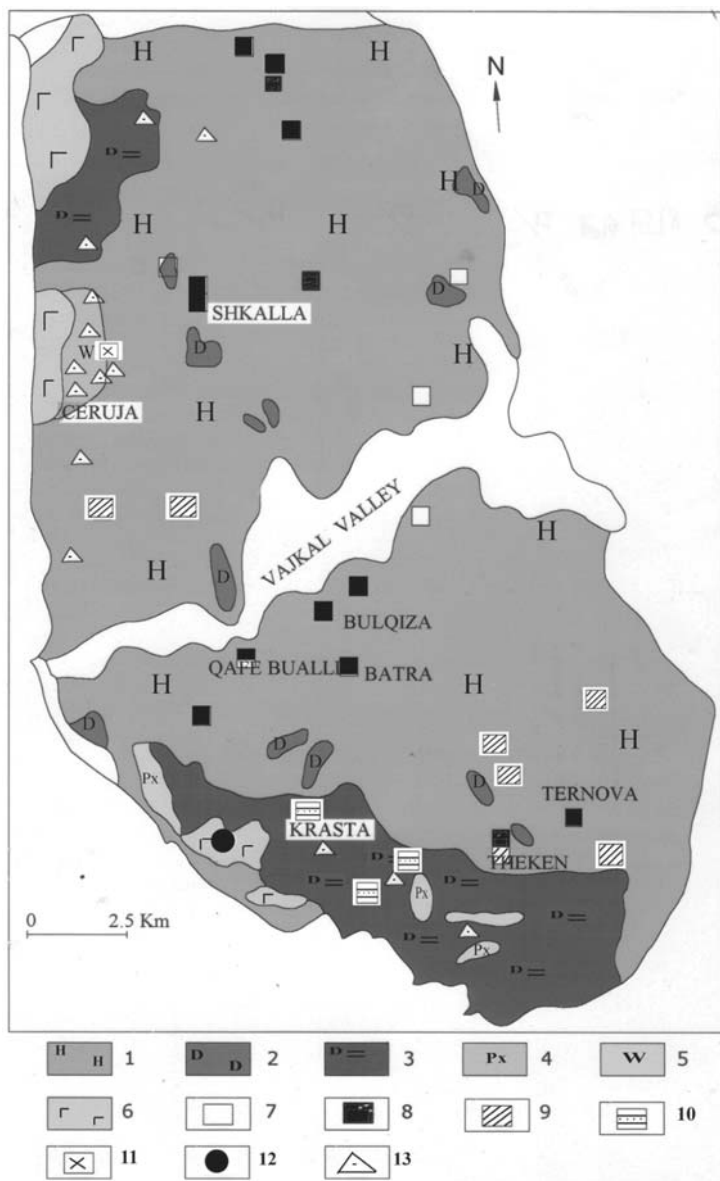


Fig. 1: Geological map of Bulqiza ultramafic massif and related mineralization.

1: Mantle harzburgites; 2: Mantle dunites, 3: Super - MOHO dunites, 4: Pyroxenites, 5: Wehrlites, pl - lherzolites, pyroxenites; gabbros; 6: Gabbro- troctolites.

Chromite mineralization related to:

7: Deep mantle, cpx - harzburgites, Al - rich chromite type. 8: Middle mantle, harzburgite - dunite level, Cr-rich chromite type; 9: Upper mantle, dunite - harzburgite level, Cr- rich chromite type; 10: Super - MOHO dunitic transition zone, Cr- rich chromite type; 11: Ultramafite - mafite, cumulate sequences and intrusive rocks, Al -rich type chromite; 12: Troctolite sequence, Al- rich chromite; 13: Ni and Ni - Cu sulphide mineralization associated by PGM.

	LITHOLOGY	CHROMITE TYPES, GRADE ORE	Cr# (mol. 100xCr / (Cr+Al)	Mg#(mol 100xMg/ (Mg+Fe)	Elementary cell a ₀ Å
CUMUL. SEQUEN.	TROCTOLITE	Al- RICH REFRACTARY TYPE	42.7	79.8	8.198
	WEHLITE	Al- RICH REFRACTARY TYPE MED - GRADE ORE	52.9	68.3	8.239
SUPER- MOHO TRANZITION ZONE	MASSIVE DUNITES	Cr-RICH METALLURGICAL TYPE , LOW- GRADE ORE	81.6 – 83.5	70 -78.5	8.309- 8.326
MANTLE TECTONITES	DUNITE- HARZBURGITE	Cr-RICH METALLURGICAL TYPE , LOW-MED.-GRADE ORE	80.9 -82.7	64.3 – 70.5	8.306
	HARZBURGITE DUNITE	Cr-RICH METALLURGICAL TYPE , HIGH- GRADE ORE	77.3 –81.9	68.8– 75	8.285- 8.303
	Cpx - HARZBURGITE	Al- RICH REFRACTARY TYPE MED - GRADE ORE	59.5	78.7	8.250

Fig. 2: Geological setting, types, grade ores and some significant chemical ratios of chromitites. Eastern ophiolite belt, ultramafite massif of bulqiza, Albania.

boles, Cr- diopside, Cr –garnet, Cr –chlorite, BMS and PGM. The minute grains of these minerals are included within host chromite grains and as interstitial forming between them also. It is interesting to point out the presence of uvarovite and kemmererite related to massive chromitite of vein – like ore body. The sulphide and arsenide of BME as pentlandite, millerite heazlewoodite, nickeline, maucherite, pyrrhotite, cubanite as well as of PGE mainly Ru, Os , Ir alloys and their sulphides, are related to super –MOHO dunites and upper mantle chromitite. The textural features of chromitites of tabular, podiform and vein – like ore bodies are varied, massive, dense dissemination and nodular. For banded – layered ore bodies disseminated and banded texture are characteristic. Some textural features of them testify on magmatic plastic deformation processes, and posmagmatic budinage (Figs 3: a, b, c and d). The chromite grains display euhedral and subhedral shape with 1 to 2mm up to 5mm dimensions (Figs 4: a, b and c). For the disseminated chromitite related to dunites, euhedral shape and less 1 mm size are more characteristic. The chromite grains contain many different inclusions, opx, cpx, ol, BMS and PMG (Figs 4: d and e). The partly metamorphosed chromite grains and transformed into Fe – chromite up to magnetite and its veinlets are observed. (Fig 4: f).

3.1 Chemical composition of chromite in the various chromitite types

The Cr# in spinel can be regarded as a sensitive chemical parameter for the degree of depletion as long as it lies above 15 (Dick and Bullen 1984).The main chromites of Bulqiza massif show high-Cr character (Cr# vary from 77 to 83.5). The most frequent Mg# ratios is from 64.3 to 78. Only a few of them are of Al-rich type, with Cr# from 53 to 59. The associated olivine is of the high

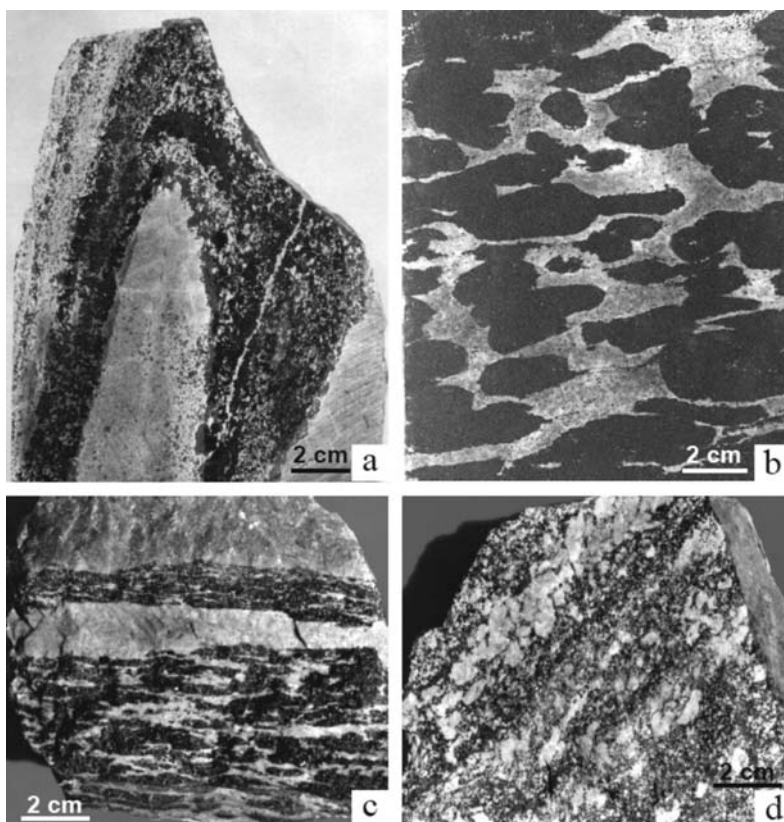


Fig. 3: a: The plastic sindeformed chromitite. The foliation plan of isoclinal fold is parallel to axial plan of folding; b: Nodular chromitite, intensely deformed. The nodules are extended and crushed by strong attraction; Fig. c: The buddined chromitite transformed into banded – like shape. The pull-apart lineation is expressed clearly; d: The chromitite intensely deformed, transformed into lensoid – breccious up to antinodular – shape.

forsteritic type, Fo from 90 to 96. In accordance with chromite composition the physical properties are not so variable. So, among them, the elementary cell parameter a_0 , in average is from 8.285 Å to 8.326 Å, regardless some exceptions for the chromites related to deep Cpx-harzburgites and for these relate to ultramafic cumulates ($a_0=8.25$ and 8.239 Å) (Fig 2.). Nevertheless, a clear tendency is evident regarding the correlation between chemical composition and its geological setting, from bottom Cpx –harzburgites to top super –MOHO dunites and ultramafic – mafic part. So, the Cr# ratios and some physical properties increase, whereas the Mg# decrease from bottom upwards to top ultramafic pile. By the contrast, the chromite related to ultramafic– mafic sequence have lower Cr# and a_0 , and high Mg# especially this related to troctolites (Fig. 2). The chemical composition of chromite for some particular deposits are reported in Table 1. Those compositions are different from less depleted Western ophiolitic belt of Al-rich nature mainly (Fig. 5). The chromite of Bulqiza massif is similar with Vourinos massif in Greece. The chromite of its Xerolivado and Skoumtsa deposits has Cr# from 0.80 to 0.83 and Mg# from 0.65 to 0.68. (Economou et al., 1986). But the similarity to chromite from Troodos (Kokkinoratsos, Kannures and Hadjipavlou) is less evident, because its chemical indicators are lower, Cr# from 0.72 to 0.76 and Mg# from 0.61 to 0.63. (Panayiotou et al., 1986; Dick and Bullen, 1984; Dietrich et al., 1987; Migiros et al., 1988; Konstatopoulou et al.,

Table 1. Chromite deposits: Deep mantle: 1.Takimi Pare, Harzburgit-dunite:2-3 Bulqiza, 4-Batra, 5 Shkalla, 6-Qafe Buall Dunite-harzburgite: 7- Lugu Gjate; 8-Thekna Super MOHO dunite:9-Krasta; Ultramafic -mafic cumulates: 10-Crruja;Troctolite :11- Stavec ; Pensil -like chromite -Cr-diopside :12-Maja Hudres. Cr#= 100x Cr/(Cr+Al) atom.ratio Mg# = 100x Mg/(Mg+Fe²⁺) atom ratio.

	1	2	3	4	5	6	7	8	9	10	11	12
SiO ₂	0.09	0.07	0.07	0.03	0.06	0.16	0.01	0.09	0	0.06	0.2	0.11
TiO ₂	0	0	0.07	0.1	0.07	0.18	0.08	0.16	0.06	0.26	0.16	0.05
Al ₂ O ₃	21.3	9.89	10.38	11.49	8.8	8.6	9.51	8.73	8.98	22.8	31.73	15.22
Cr ₂ O ₃	46.72	59.78	58.5	58.32	59.3	61.4	59.99	59.4	59.56	42.57	35.32	53.12
FeO	8.07	11.13	7.5	9.45	7.51	13.39	10.51	14.55	7.63	12.67	8.07	10.46
Fe ₂ O ₃	5.18	3.84	5.71	4.21	6.43	1.14	3.66	4.7	6.45	4.15	5.05	4.63
MnO	0.31	0.39	0.37	0.27	0.32	0.19	0.34	0.27	0.43	0.17	0.34	0.36
MgO	17.42	14.27	16.72	15.71	16.5	14.11	14.58	11.5	16.51	15.58	18.63	15.22
NiO	0.1	0	0.09	0.11	0.36	0.09	0.05	0.08	0	0.17	0.12	0.05
CaO	0	0	0	0.01	0	0.01	0	0.01	0	0.01	0.01	0
V ₂ O ₃	0.17	0.12	0.15	0.18	0	0.2	0.03	0.09	0.03	0.1	0.35	0.12
CoO	0.02	0.05	0.07	0.04	0	0.02	0	0.03	0	0.02	0.1	0
Total	31.27	29.8	30.61	29.98	31.12	29.15	29.17	31.23	31.05	32.87	32.67	30.84
Si	0.021	0.017	0.018	0.006	0.015	0.036	0.003	0.02	0	0.016	0.045	0.014
Ti	0	0	0.013	0.018	0.012	0.035	0.015	0.032	0.011	0.048	0.028	0.009
Al	6.069	3.01	3.1	3.43	2.66	2.655	2.914	2.717	2.705	6.595	8.563	4.522
Cr	8.931	12.2	11.721	11.68	12.021	12.714	12.328	12.027	12.027	8.261	6.356	10.586
Fe ²⁺	1.632	2.402	1.59	2.003	1.61	2.931	2.285	3.213	1.631	2.6	1.546	2.205
Fe ³⁺	0.943	0.746	1.089	0.802	1.241	0.245	0.715	0.934	1.239	0.768	0.87	4.63
Mn	0.063	0.084	0.079	0.059	0.07	0.042	0.075	0.06	0.093	0.035	0.066	0.077
Mg	6.276	5.429	6.313	5.931	6.306	5.44	5.64	4.491	6.284	5.675	6.358	5.678
Ni	0.02	0	0.017	0.021	0.073	0.02	0.01	0.017	0	0.034	0.022	0.05
Ca				0.003						0.003	0	
V	0.032	0.026	0.031	0.036	0	0.035	0.005	0.016	0.007	0.035	0.065	0.031
Co	0.003	0.01	0.023	0.008	0	0	0	0	0	0	0.019	0
Total	8.969	8.697	9.142	8.863	9.3	8.713	8.73	8.731	9.254	9.15	8.946	12.671
Cr#	0.595	0.802	0.791	0.773	0.819	0.827	0.809	0.82	0.816	0.529	0.427	0.701
Mg#	0.787	0.688	0.791	0.742	0.79	0.643	0.705	0.578	0.785	0.683	0.798	0.708

1990; Georgiou et al., 1990; Gartzos et al., 1990). As is reported by Panayiotou et al. (1986), the variability of chromite composition is also evident concerning their geological setting in main dunites, harzburgite – dunite contact, transition zone and deep harzburgites.

In the Cr# vs. Mg# diagram (Fig. 5) the chromites of Bulqiza massif are compared to the chromites from the other Eastern ophiolitic complexes such as Vourinos and Troodos comparable to the spinels in Tertiary boninites from Western Pacific and Cape Vogel (Papua) and field for spinels in island arc arc-thoeliites (IAT) (Dietrich et al., 1987).

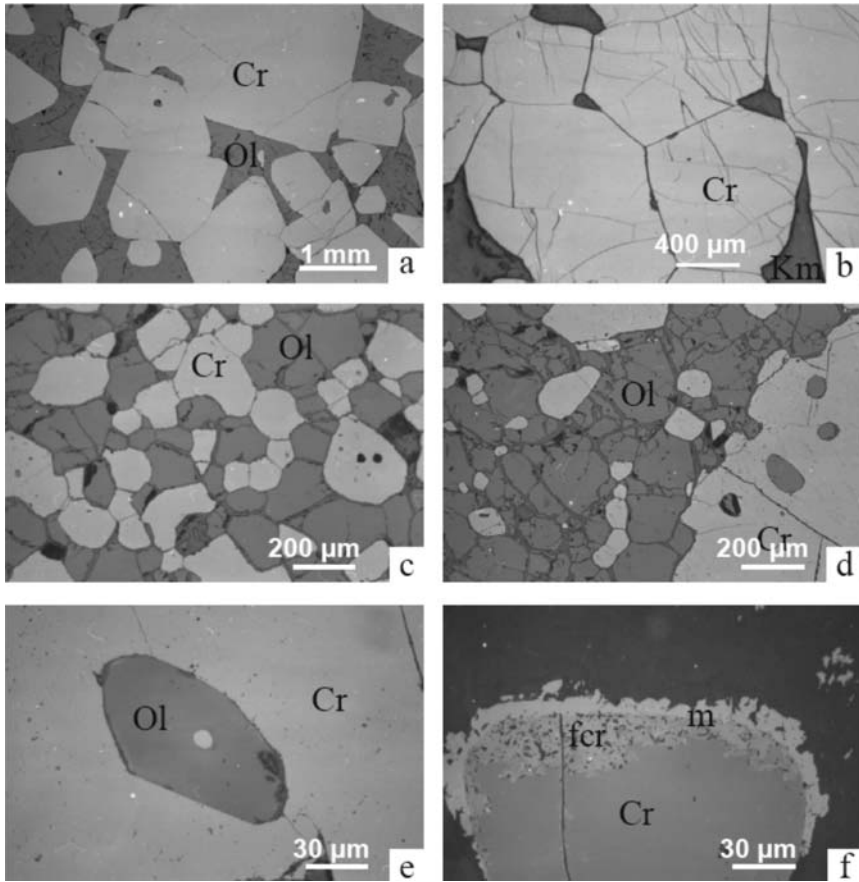


Fig. 4-a: Perfect euhedral chromite crystals (Cr) within olivine (Ol) groundmass; b: Massive chromitite built up by compressed euhedral crystals (Cr). Interstices filled by kemmererite; c: Different euhedral and anhedral chromite grains (Cr) towards olivine ones (Ol); d: The different relation between chromite and olivine: its inclusions (Ol) within chromite (Cr) grains and the contrary; e: The lense shaped olivine inclusions (Ol) within chromite (Cr) grains and the contrary, minute spheric chromite inclusion within bigger olivine inclusion f: The partly metamorphosed chromite grain (Cr) in to Fe – chromite (fCr) and surrounded by magnetite rim (m).

A great part of the chromites of Bulqiza massif, such as those related to harzburgite- dunitic, dunitic-harzburgitic and super MOHO dunites are characterized by high Cr# ratios similarly to those of Troodos, chromites from the main dunite and from southern Vourinos massif. All these chromites are analogues to boninites and IAT environment.

On the contrary, some of the chromites from Bulqiza related to deep Cpx- harzburgites and especially, these related to ultramafic cumulate have low up to very low Cr# ratios similarly to the others from the contact between the harzburgite and the transition zone of Troodos as well as those from Kissavos and Rodiani are characterized by low Cr# ratios.

Regarding to the Mg# ratios, the difference between these complexes is less evident. This parameter varies between narrow limits, 62 up to 78 in average.

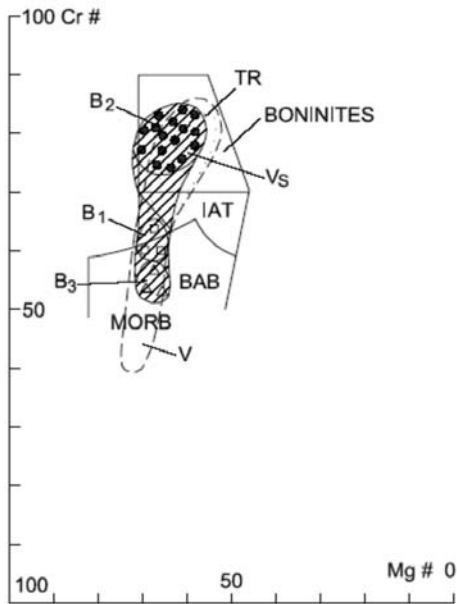


Fig. 5: Cr# versus Mg# for chromites of B-Bulqiza massif, Albania and of similarly, V- Vourinos and TR- Troodos with reference to boninitic lavas from Western Pacific, IAT and MORB environments (Data from Dick and Bullen, 1984; Economou et al., 1986; Panayiotou et al., 1986; Georgiou et al., 1990; Konstantopoulou et al., 1990; Gartzos et al., 1990. Chromite of Bulqiza massif related to: B₁- deep mantle Cpx- harzburgites; B₂- ultramafic cumulates; B₃- mantle harzburgite-dunitic, dunitic-harzburgitic and super MOHO dunitic parts; Vs- Southern Vourinos massif.

3.1.1 The composition of olivine and the equilibrium temperature.

The compositional change of olivine is also very interesting, from barren dunitic lenses towards the dunitic envelops of the ore bodies, interstitial and inclusions of olivine within chromitite, Fo varies in the range from 90 to 96.5 (Table 2). According to xMg and xFe variations in olivine and spinel, the temperatures, calculated on the Ol – Sp thermometer (by Lehmann, 1981) vary widely, from 650 to 750 C⁰ for the chromitite, up to 800°C for accessory chromites (Table 3).

The differences of Fm reflects the evolution of Ol – Sp equilibrium process depended from the grade of chromite concentration. So the chromitite Ol – Sp equilibrium has been more prolonged and was interrupted in lower temperatures. On the contrary, for schiren and especially for accessory chromites this equilibrium has been blocked early, in high temperatures. As suggested by Economou (1984) the systematic variation of olivine composition is probably a result of subsolidus reaction.

4. Conclusions

The Bulqiza ultramafite massif belongs to Eastern ophiolite belt of Albania. It is the most important chromite-bearing in Alpin Mediterranean belt. The rock composition of this massif mainly by mantle harzburgites and super –MOHO dunitic, and by fosteritic olivine and enstatitic orthopyroxene, rock – forming minerals, is distinguished by high magnesian character. This is due to high partial melting of upper mantle and intensively mantle –crust interaction. In the consequence, a thick super-MOHO dunitic sequence is formed. The ultramafic – mafic intrusive rocks are present also. The consequence of high partial melting, the upper part of ultramafic pile is high consumptioned and impoverished by CaO and Al₂O₃ and enriched by MgO and Cr₂O₃. The chromite mineralization is situated at all ultramafic pile, but the most important chromite potential belongs to harzburgite –dunitic and partly to super –MOHO dunitic part, about from 300m down super- MOHO level, to 1200m. The predominant chromitite is of Cr- rich chromite high – grande ore, metallurgical – type. Among

Table 2.

Table 2 Chemical analyses of olivine						
	1	2	3	4	5	6
SiO ₂	40.98	41.53	41.02	40.65	41.08	41.2
FeO	7.85	7.24	4.06	5.08	2.99	2.78
CaO	0.04	0.05	0	0	0.01	0.04
Al ₂ O ₃	0.04	0.02	0	0.01	0	0
MnO	0.33	0.02	0	0.04	0.06	0.01
MgO	49.79	50.87	55.29	55.39	56.46	56.09
Cr ₂ O ₃	0	0.06	0		0.03	0.18
NiO	0.5	0.33	0.67	0.4	0.62	0.67
Total	99.55	100.1	100.66	101.94	101.25	100.97
Si	1	1	0.972	0.97	0.97	0.974
Fe	0.16	0.15	0.081	0.1	0.059	0.055
Mn	0	0	0	0.01	0.01	0
Mg	1.81	1.83	1.963	1.95	1.986	1.977
Cr					0.001	0.003
Ni	0.01	0.01	0.012	0.007	0.012	0.013
Total	2.98	2.99	3.025	3.028	3.029	3.023
Fo	91.1	92.3	95.18	94.7	96.5	96.7
Fa	8.9	7.7	4.82	5.3	3.5	3.3

1-In harzburgite; 2-In dunite; 3 and 4- interstitial in chromite; 5 and 6- inclusions within chromite.

Table 3.

Table 3. The equilibrium temperatures after olivine - spinel couple													
Number of atoms in elementary cell of chromite and olivine													Temp C
	Al	Cr	Fe ³⁺	Fe ²⁺	Mg	FM	CAF	Si	Mg	Fe ²⁺	Fo	Fm	Lehm.
CHROMITE								OLIVINE					
1	0.386	1.471	0.134	0.208	0.78	0.219	0.738	0.97	1.986	0.056	0.965	0.029	673
2	0.31	1.6	0.085	0.362	0.627	0.373	0.802	0.969	1.951	0.1	0.947	0.049	795
3	0.466	1.416	0.107	0.246	0.745	0.256	0.711	0.973	1.971	0.062	0.965	0.031	648
4	0.331	1.548	0.112	0.28	0.707	0.292	0.777	0.971	1.966	0.078	0.957	0.038	750
5	0.418	1.469	0.109	0.267	0.74	0.265	0.732	1.003	1.185	0.073		0.037	704
6	0.364	1.541	0.089	0.286	0.706	0.295	0.772	0.972	1.973	0.07		0.034	693
7	0.319	1.548	0.128	0.243	0.748	0.258	0.775	0.964	1.99	0.068	0.961	0.033	730
8	0.375	1.53	0.091	0.301	0.689	0.31	0.766	0.969	1.963	0.081	0.952	0.04	799
9	0.049	1.418	0.129	359	653	0.355	0.71	1.003	1.843	0.109		0.056	794
10	0.558	1.335	0.101	0.406	0.581	0.417	0.669	0.964	1.888	0.173	0.912	0.085	891
11	0.341	1.611	0.048	0.595	0.411	0.591	0.805	0.96	1.834	0.207		0.101	942

1 to 8; Chromitites; 9; Chromitic dunites; 10 and 11; Harzburgites. FM=Fe²⁺/ (Fe²⁺ Mg) atom., CAF = Cr/(Cr+Al+Fe³⁺) atom.

them the other less important chromitite of Cr-rich metallurgical type also, but low – grade ores are related to super –MOHO dunites. The different restricted chromite ores, Al-rich, refractory type, are related to deep cpx –harzburgites and, in contrary at top of ultramafite – mafite sequences. The intensively partial melting of upper mantle is not fully sufficient argument to explain the high chromite concentration. As is suggested by Nicolas et al., (1991) the slow spreading, oxygen fugacity and the cool action of overlayers crust have played also their role for this concentration. The correlation between geological setting and the morphology, chromite –type, ore grade, chemical composition of chromite and textural features of chromitite, and ol – sp subsolidus reaction, are the arguments for the magmatic origin, complicated by later geodynamic processes.

5. Acknowledgements.

The author would like to express his appreciation to Zdenek Johan, Maryse and Daniel Ohnenstetter for their precious suggestions on chromite mineralization and for assistance with the electron microprobe analyses at BRGM – France. I wish to express my thank to Maria Economou – Eliopoulos, Alexander Panayitou and G. Migiros for their data on investigations about Greece and Cyprus chromite mineralization.

6. References

- Alliu, I., Beccaluva, L., Cina, A., Coltorti, M., et al., 1994. The Skanderbeg and Bulqiza mafic-ultramafic ophiolitic complexes and their relationship with chromititic ore deposits *Working group meeting of IGCP project No 256- field trip B. Ofioliti*, 19(1), 27 – 55.
- Auge, T. and Johan Z., 1988. Comparative study of chromite deposits from Troodos, Vurinous, North. Oman and New Caledonia ophiolites. *Mineral Deposits*, ed by Boissonas and P. Omenetto, Springer-Verlag Berlin. 267-288.
- Burgath, K. P., Krauss, U., Mohr, M., 2002. Chromium ores and platinum – group element occurrences in Europe and Turkey: Inventory, evolution and possibilities *Chron. Rech. No. hors serie.*, 55-77..
- Cina, A., 1986. Some physical properties of the chromitite chromespinels of the ophiolitic ultrabasic massifs of Bulqiza, Albania. *Ofioliti*, 11, Nr.1, 51.
- Cina, A., Casli, H. and Goci, L., 1986. Chromites in the ophiolites of Albanides. In: "Chromites" UNESCO'S -197project, *Metallogeny of ophiolites. Theophrastus Pub. S.A Athens*, 107-126.
- Dick, H.J. Band, Bullen, T., 1984. Chromian spinel as a petrogenic indicator in abyssal and alpine-type peridotites and spatially associated lavas. *Contribution to Mineralogy and Petrology*, v.86, 54-76.
- Dietrich, V., Oberhänsli, R. and Marcolli, J. 1987. A new occurrence of boninite from the ophiolitic mélange in the Pindus-subpelagonian zone. *Ofioliti*, 12, 83-90.
- Economou, M., Dimou, E., Economou, G., Vacandios, I., Grivas E., Rassios, A. and Dabitzias, S., 1986. Chromite deposits of Greece. In: *Chromites UNESCO'S -197project, Metallogeny of ophiolites. Theophrastus Pub. S.A Athens*, 129-159.
- Economou, M. 1984. On the chemical composition of the chromite ores from the Chalkidi peninsula, Greece *ofiolitu*, 9(2), 123-134.
- Gartzos, E., Migiros, G. and Parcharidis, I. 1990. Chromites from ultramafic rocks northern Evia (Greece) and their geotectonic significance. *Schweiz Mineral. Petrogr. Mitt*, 70, 301-307.
- Georgiu, E. and Xenophonos, C. 1990. Chromite occurrences and associated plutonic rocks in the Akapnou Forest. In: *Ophiolites, oceanic crustal analogues. Proc. of the Symp "Troodos 1987". Nicosia Cyprus*. 585-592.
- Karaj, N., 1992. Repartition des platinoïdes, des chromites et sulfures dans le massif de Bulqiza, Alba-

- nie. Incidence sur les processus metallogeniques dans les ophiolites. *These, Univ d'Orleans*, pp.400.
- Kodra, A., Gjata, K. and Bakalli, F., 1995. The Mirdita oceanic basin from rifting to the closure. In: *Workshop on Albanian ophiolites and related mineralizations. Documents du BRGM. 244. Editions BRGM, France* 9-26.
- Konstantopoulou, G. and Economou, M-Eliolopoulos 1990. Geochemistry of the Vourinos chromite ores, Greece. In: *Ophiolites, oceanic crustal analogues. Proc. of the Symp "Troodos 1987". Nicosia, Cyprus. 605-613.*
- Nicolas, A., Bondier, F. and Meshi, A., 1999. A slow spreading accretion in the ophiolite of Mirdita (Albania). *Jurnal of Geophysical Reseacher*. 104, nr.87, 15155-15167.
- Ohnenstetter, M., Karaj, N., Neziraj, A., Johan, Z., Çina, A. 1991: Le potentiel platinifere des ophiolites: Mineralizations en elements du groupe du platine (EGP) dans les massifs de Tropoja et Bulqiza, Albanie. *C.R. Acad. Scie. Fr.*, v .313, ser. II.201-208.
- Panayiotou, A., Michaelides, A.E. and Georgiou, E., 1986. The chromite deposits of the Troodos. Ophiolite complex, Cyprus. *Chromites UNESCO'S IGCP.197 Project Metallogeny of ophiolites. Theophrastus Pub. S.A Athens*. 161-198
- Shallo, M., Çina, A. and Turku, I., 1995. Outline of metallogeny of the Albanian MOR and SSZ- type ophiolites. In: *Workshop on Albanian ophiolites and related mineralization. Documents du BRGM 244. Editions BRGM, France*, 27-46.

MANGANESE MINERALISATIONS AT THE BASE OF MIOCENE SEDIMENTS IN NORTHERN SARDINIA (ITALY)

Fadda S.¹, Fiori M.¹, Pretti S.², and Valera P.²

¹ *Istituto di Geologia Ambientale e Geoingegneria del CNR, 09100 Cagliari, Italy,
sfadda@unica.it, fiori@unica.it*

² *Dipartimento di Geoingegneria e Tecnologie Ambientali, Università di Cagliari, Italy.
paolo@paolov.net*

Abstract

During the eastward drift of the Palaeozoic-Mesozoic block formed by Sardinia and Corsica in the Oligocene-Miocene, calc-alkaline volcanism developed mostly in the western part of the island. Most Tertiary metallogenic phenomena are related to hydrothermal activity associated with this volcanism. Following volcanic and related hydrothermal activity, sediments were deposited during the Oligocene-Miocene as a consequence of a marine transgression. The basal part of this series is clastic and includes elements derived from erosion of unaltered volcanics as well as hydrothermally altered rocks and hydrothermal vein quartz. Inside the Tertiary volcanics manganese ore-minerals occur as nodules, veinlets, and stockworks and mainly include Mn and Fe oxides; quartz in different forms is the most common gangue mineral. The mineralisations at the contact between volcanics and Miocene sediments are the most homogeneous, the ore-minerals occur in the cement, but also as fairly continuous thin beds, nodules and veinlets containing pyrolusite, frequent ramsdellite, less frequent manganite, psilomelane, cryptomelane-manjiroite, rare ranciéite, and todorokite. The nature of the ore-bearing beds indicate a near-shore clastic environment along the ancient coastal lines of the Miocene sea. Genetic considerations point to a supergenic transport and redeposition after erosion of primary dispersion and residual concentrations of Mn in the volcanics.

Key words: *sedimentary manganese, volcanism, metallogeny, Sardinia.*

1. Introduction

During the detachment and eastward drift towards Italy of the Sardinian-Corsican massif, extensive conditions led to an important rifting phase, which opened the presently NS-striking trough, the so called Fossa Sarda, cutting the entire island of Sardinia (Fig. 1). Related to these conditions, and within the resultant graben, an intense volcanic activity took place from the Upper Oligocene to the Middle Miocene in the western half of this island, with mostly extrusive products of calc-alkaline affinity typical of plate convergence zones (Cherchi and Montadert, 1982). Three main volcanic cycles developed, each characterized by initial, mainly andesitic lavas followed by more acidic pyroclastic activity with intervals of epiclastic rocks. The earlier volcanic products occurred in southwestern Sardinia between 29 and 27 My ago, with episodes of basaltic and andesitic lavas forming flows, domes, and dikes. The following, mostly explosive phase lasted from 20 to 18 My ago and developed particularly in central and northern Sardinia with ignimbrites and minor flows

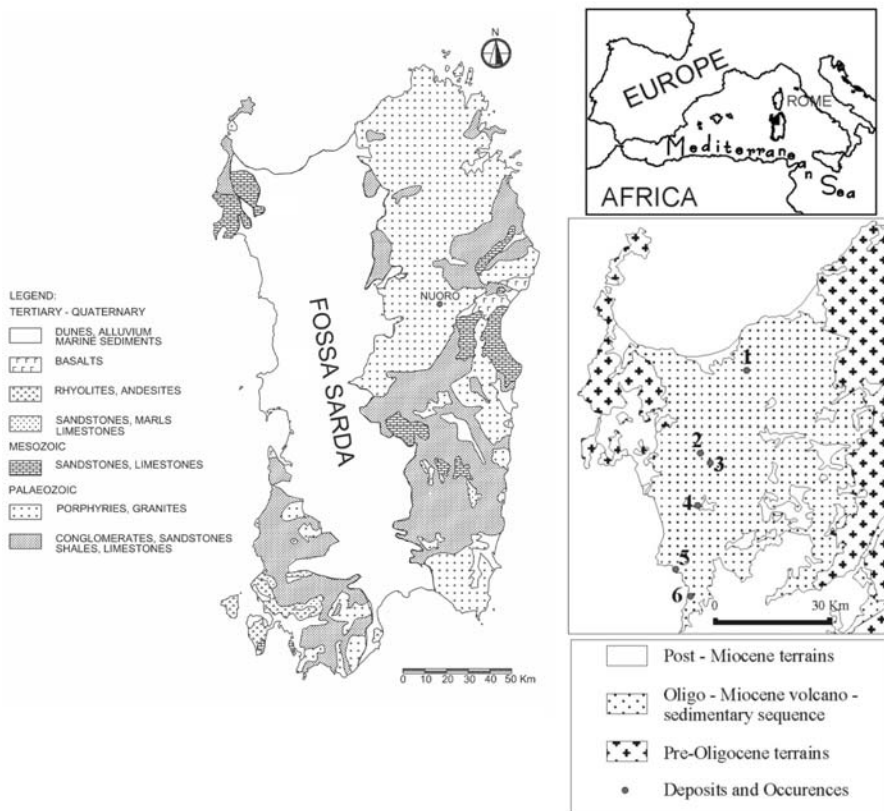


Fig. 1: Left: Geological sketch map of Sardinia showing the Fossa Sarda trough. Right: Geological sketch map of the north-western Sardinia showing the distribution of manganese occurrences: 1) Corona de Corvu, 2) Monte Jorzi, 3) Sos Aghedos, 4) Alghentalzos, 5) Giolzi Moro, 6) Tippiiri.

of rhyolitic and dacitic composition. The latest products of this mostly subaerial volcanism, from 14 to 13 My, are represented by intercalated epiclastic and ash flow beds (Coulon, 1977). During the waning phases of this volcanism, hydrothermal activity developed episodically, producing local alteration and precious- and base-metal mineralizations mainly high- and low-sulfidation epithermal veins and stockworks containing gold, pyrite, sphalerite, galena, and minor chalcopyrite (Garbarino et al., 1991). Closely linked with this calc-alkaline magmatism, manganese deposits also formed, mainly within the volcanic products, and subordinately in the Miocene beds immediately resting upon these volcanics. At the same time, the gradual dipping of the longitudinal trough initiated a marine transgression progressing from the south to the north across the island, and then continental clastic sediments were deposited. The final submarine Tertiary calc-alkaline volcanic rocks (around 11 My) are interbedded with these sediments, especially within the central part of the rift. The terrigenous materials show textural and compositional immaturity, commonly show lenticular bedding and locally exhibit sedimentary structures indicative of low-energy depositional environments, such as lamination. The basal conglomerates and sandstones of the sequence are characterized by erosion products that include metals mobilized from unaltered volcanics as well as from hydrothermally altered rocks and the newly formed hydrothermal deposits. Literature records concerning occurrences

of metallic minerals in Tertiary sedimentary rocks of Sardinia are rare. The best and long-known are manganese oxides bodies in NW Sardinia, only recently recognised as near-shore deposits, which were explored and mined to a minor extent.

2. Geological setting and stratigraphy

The sedimentary basins under study represent the northern part of the Tertiary trough cutting the island of Sardinia from north to south (Fig. 1). In this area, the graben filling is formed of ignimbritic lava flows dipping toward the centre of the trough, with numerous faults connected to tectonic events of Miocene age. The region is characterized by the presence of volcanic rocks generated during the calc-alkaline volcanism, and formed of andesites, dacites, rhyolites and ignimbrites (Coulon, 1977). The sedimentary filling consists of marginal fan conglomerates and central lacustrine sediments. Calc-alkaline volcanics and tuffites are interlayered with continental sediments. The Oligocene-Aquitainian age of the sediments and volcanic rocks confines the development of the basin to this time span. The post-volcanic sedimentary rocks are mixed siliciclastic-carbonate sequences from terrestrial and coastal sands, shelf carbonates and marls. Silty marlstones of Late Burdigalian-Early Langhian age characterize the central part of the main basin, whereas variable siliciclastic and carbonate sequences developed at its margins and at the confluence with the smaller grabens (Martini et al., 1992). The sedimentary sequence rests unconformably upon volcanoclastic beds (tuff and cinder) interlayered with freshwater limestones and black cherts. At the top, the most continuous sections have been preserved either under thick carbonates, or under 5 to 30 m-thick Pliocene-Pleistocene lava flows, which cap the hills. However, the layercake disposition of the strata allows the visual correlation of several Units across the basins and the overall paleosetting of the sediments can be reasonably well reconstructed (Mazzei and Oggiano, 1990). Five informal lithostratigraphic units have been distinguished: the Lower Sands, of continental fluvial-deltaic origin are followed upward by the Lower Limestones which mark the first marine transgression of the whole area during the uppermost Burdigalian. A sudden deepening of the basin is marked by the Marly Arenaceous unit that shows features indicative of an environment deeper than that of the Lower Limestones and occurs primarily in the deepest central part of the main graben; a sandier variety is also present on parts of the basin-edge area. The Upper Sands, again of deltaic-fluvial origin, have been ascribed to the Upper Langhian - Lower Serravallian interval. They rest on the Marly Arenaceous Unit through an erosional contact. Finally, the Upper Limestone lies unconformably on both the Upper Sands and the Marly Arenaceous Unit; this lithostratigraphic unit marks a second marine transgression, which probably occurred during the Lower Messinian.

A major transgression can be established in the lower part of the sequence, from continental sands to marine marly and algal limestone units. The environment represented by these Lower Sands ranges from braided fluvial deposits to lowland paralic settings, to fluvio-lacustrine and fluvio-marine deltas, to barred shores containing fossiliferous banks. The Lower Sands are characterized by the vertical and lateral transitions of gravel to sandy continental facies grading up into marine sands and sandy carbonate. These sandstones may be derived from numerous sources, Tertiary volcanites, Palaeozoic granites, schists and gneisses. Gravel has two types of occurrences: one type consists of reddish, sandy, pebble-to-small-boulder conglomerate, well cemented and locally showing well developed fabric; the other consists of sandy, poorly cemented, fairly well-sorted conglomerate, with plane- and cross-beds. In both cases, the gravels represent braided-stream deposits. Siliciclastic deposits vary from coarse, conglomeratic in places, unfossiliferous, massive to locally cross-bedded lithic sands, to purer quartz-feldspathic sands. Locally, the sands are calcareous and rarely include large-scale foresets. These lower continental facies were gradually drowned by a transgressive sea,

and their topset materials were reworked into bars and plains, and finally a carbonate environment was established.

3. Mode of occurrence, mineralogy and chemistry of Mn-ore

All the exploration and mining operations on Mn ores have long ceased, and the old mining works are seldom accessible. Thus, only a few small excavations and outcrops have been surveyed and sampled, and most of the samples are from old dumps. The mineralisations inside Tertiary volcanics are the most widespread, Mn minerals occur as nodules, veinlets, and stockworks. Besides the dominant pyrolusite, ubiquitous, the ore-mineral assemblages commonly include ranciéite, manjiroite and cryptomelane. Among the Fe minerals goethite, often accompanied by hematite, is highly frequent. The gangue mineral is quartz, that commonly occurs as chalcedony or jasper, finely disseminated in the ore, or as chalcedony veins impregnated with Mn oxides.

The mineralisations at the contact Tertiary volcanics - Miocene sediments are the most homogeneous: their attitude is always stratiform and concordant. Figure 1 shows the distribution of manganese occurrences at the contact Tertiary volcanics - Miocene sediments in the northern regions of Anglona - Logudoro and Meilogu – Planargia (Marcello et al., 2004).

The stratigraphy of the manganese mineralized formations is uniform along the near-shore zones and coastal lines, with only minor variations. The ore minerals are distributed along the shoreline, with the bulk contained in a conglomeratic stratiform layer. The most important character common to all these bodies is their occurrence within clastic (clasts from the underlying volcanics), mainly conglomeratic, suites. Their cover (that is missing only at Giolzi Moro) is a Miocene carbonatic platform series. The ore minerals occur in the cement, but also as fairly continuous thin beds, nodules and veinlets. The Mn-bearing ore minerals occur both well crystallized, compact and of metallic appearance, and earthy, with loose fabric and deep-black colour. To the earthy strata fossiliferous (fish teeth) pelitic lenses are commonly associated. Several “burrows” can be observed. Their cylindrical shape is filled with the ore minerals in fibrous structures with radial symmetry, along with clastic elements.

The ore mineral assemblage is monotonous: ubiquitous pyrolusite (pure MnO_2 tetragonal), frequent ramsdellite (MnO_2 orthorhombic), less frequent the manganese hydroxide manganite (MnOOH), psilomelano ($(\text{Ba}, \text{K}, \text{Mn}, \text{Co})_2 \text{Mn}_5\text{O}_{10} \cdot x\text{H}_2\text{O}$), and cryptomelane-manjiroite ($(\text{Na}, \text{K})_{1-2} \text{Mn}_8\text{O}_{16} \cdot x\text{H}_2\text{O}$), rare ranciéite ($(\text{Ca}, \text{Mn}) \text{Mn}_4\text{O}_9 \cdot 3\text{H}_2\text{O}$) and todorokite ($(\text{Na}, \text{Ca}, \text{K}, \text{Mn}^{2+})(\text{Mn}^{4+}, \text{Mn}^{2+}, \text{Mg})_6\text{O}_{12} \cdot 3\text{H}_2\text{O}$). The nature of the ore-bearing beds indicates a near-shore clastic environment, followed by a slightly deeper one. All points to a supergenic deposition controlled by ancient coastal lines, like in the better known, quite bigger occurrences of Western Europe and Northern Africa.

The tetravalent oxides pyrolusite and ramsdellite are the most common ore minerals for which precipitation involves oxidation of the Mn^{2+} in solution to Mn^{4+} possibly favoured by the presence of a pre-existing surface of iron oxide or hydroxide. In this model, the dissolved metal carried by surface waters under oxidizing conditions, precipitated at the shoreline owing to a rise in pH from 6 to 8, typical of the fresh water to marine transition. The presence of psilomelane, cryptomelane, todorokite and ranciéite suggests that somehow K, Ba, Ca and Na, originated from the erosion of hydrothermally altered volcanic source rocks in the continental drainage area, must have been present at the time of deposition. However, where slightly more reducing conditions prevailed in the muds of even shallow marine environments, tetravalent manganese was gradually reduced to the trivalent state in the manganite-rich ores found in limited parts of these deposits. Trace elements such as Ni, W, Sn, Ag and others may be adsorbed successfully on to hydrated colloidal MnO_2 at pH 7-8. The

Table 1. Major elements were determined by flame atomic absorption and emission spectrometry (FAAS/FAES). Trace elements by inductively coupled plasma-atomic emission spectrometry (ICP-AES). For mineral identification, powdered samples were mounted on glass slides and subjected to X-ray diffractometry (XRD) on a Rigaku Geigerflex fully automated apparatus. The assignments of peaks were from the JCPDS File (1985).

<i>Localities</i>	<i>District</i>	<i>Type</i>	<i>Minerals</i>	MnO %	Fe₂O₃ %	SiO₂ %	Ba %	Ni ppm	W ppm	Sn ppm	Ag ppm	
Corona De Corvu	Turritano	Stratiform	Pyrolusite	50.6 74.36 47.50 68.68	4.58 0.28 0.85 0.86	18.3 2.4 3.5 6.2	2.1 0.20 0.51 0.22	55 45 45 110	<50 <50 <50 <50			
			Ramsdellite									
			Manjiroite									
			Ranciéite Psilomelane* Criptomelane*									
Monte Jorzi	Meilogu	Stratiform	Pyrolusite	52.1 48.6	1.9 0.68	10.4 6.8	0.45 0.45	103 58	<20 <20	80 75	<1.5 <1.5	
			Todorokite*									
Sos Aghe- dos	Meilogu	Stratiform	Pyrolusite	24.2 65.5	1.9 1.0	32.1 8.6	0.42 0.16	21 96	<20 <20	55 110	<1.5 <1.5	
			Manganite Grouitite*									
Alghental- zos	Logudoro	Stratiform	Pirolusite	85.2 66.5 52.3 66	0.14 3.13 1.90 1.2	2.1 5.2 13.2 8.8	0.77 0.09 0.19 0.21	20 330 40 95	<20 <20 <20 <20	15 105 90 100	<1.5 <1.5 <1.5 <1.5	
			Manganite Grouitite*									
Giolzi Moro	Bosano Planargia	Veins and crustiform	Ranciéite	50.33 1.54	1.51 12.58	34.8 61.9	0.25 0.09	15 20	150 50			
			Ematite									
			Pyrolusite Goethite*									
Tippiri	Bosano Planargia	Lentiform	Pyrolusite	51.7 45.15	0.2 2.0	3.1 11.9	0.05 0.14	45 20	<20 <20	85 110	<1.5 <1.5	

* Only XRD detected

absence of Mn carbonate minerals is notable because it shows evidence of no significant burial and post-depositional diagenesis in the metalliferous oxide bands. In fact, these minerals have been reported from reducing and high-pH anoxic environments where Mn was first deposited at the sediment surface as tetravalent oxide and then, during diagenesis, carbonate grew at the expense of the oxides. Table 1 shows the most common manganese ore minerals as detected by X ray diffractometry (XRD) and some chemical data which only concern the main ore-forming elements, and the most significant trace elements.

4. The formation of sedimentary manganese

The genetic study of these sedimentary ores investigated possible sources of ore materials, transport-deposition processes, the paleogeographical conditions and mechanism of ore formation.

4.1 Metal source

Bulk-rock geochemical concentrations of manganese are the most plausible primary source of Mn ions to freshwater and groundwaters of the Logudoro basin. In addition, low-grade, non-economic concentrations of this metal occur in numerous small hydrothermal veins where strong anomalies of Mn are known to exist (Redini, 1940); these examples of mineralization are widespread in the surrounding calcalkaline igneous complex. The Authors support this model of metal release from a “continental” source.

4.2 Transport

After the weathering of primary silicates and disseminated mineralizations in the volcanic and volcanoclastic host rocks of the drainage areas, the soluble load of the descending, near-surface, acidic waters would include metals in ionic solution as well as metals adsorbed on clay particles in colloidal suspension. Furthermore, mechanical transport of clastic particles is also quite possible owing to the proximity of the source area. Percolating solutions could have migrated down along the soils and tectonic structures, faults, fractures, conduits, forming a system of local fluid circulation before and during the Basal Miocene deposition. The surface- and ground-waters rich in free oxygen played an important role in the weathering of the rocks above sea level. Under the local paleoclimatic conditions, warm and semiarid climate (Biondi and Filigheddu, 1990), heavy seasonal rainfall resulted in an acidic and oxidizing medium that promoted metal dissolution and transport into lagoons or bays or lacustrine environments for the sedimentation in near-shore, low-energy environments (Maynard, 1983).

A possible type of low-temperature fluid for mobilizing and transporting the metals from the enclosing rocks to the depositional basins is acid groundwater or streams which commonly arise from the oxidation of pyritic orebodies or other sulfide mineralization (Jambor & Blowes, 1994). These acidic, oxidizing conditions, and high sulfate content, are those which optimise solution transport of both iron and manganese. The principal reactions that generate H^+ in the surface-water, with subsequent infiltration in the underlying aquifers, are the oxidation of pyrite and other sulfide minerals (Lentz, 2003). However, a variety of acidity attenuation reactions occur in the surroundings geological materials, depending on the availability of acid-consuming mineral phases (e.g., carbonate and other base-containing solids) but the widespread presence of disseminated sulfide mineralizations ensures acid generation in the moving water and simultaneous migration of the metals downstream in the direction of ground-water flow. The solubility of manganese is considerably higher than that of iron for any given Eh and acid Ph and preferential leaching of this metal with respect to iron may take place because of its larger ionic size and lower ionic potential (Roy, 1981; Sapozhnikov, 1970). Mn-specific soil bacteria may also lead to dissolution and leaching of the element while Mn organic complexes may form by reaction with humic acid in solution.

4.3 Depositional environment

The earliest deposition of the host sediments in the initial rifts was probably subaerial, not far from the paleocoastal line, and consisted of conglomerates and arkoses. A first marine transgression fol-

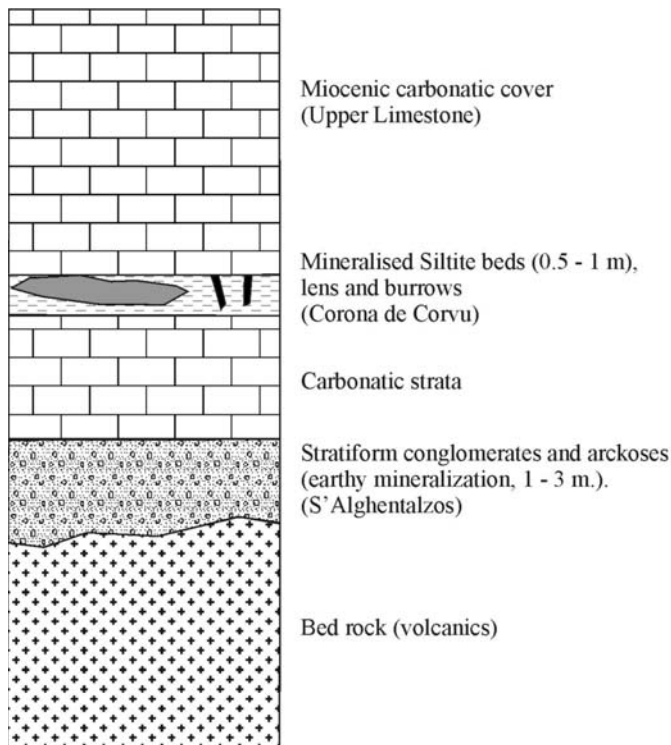


Fig. 2: Schematic lithostratigraphic column of the mineralised series.

lowed and deposited coarse- to very fine-grained sediments. Clastic deposition, mainly arenaceous, was slow, with sands and clay minerals being poured into a restricted-circulation water body in shallow marine and beach environments. Although overall conditions were transgressive, Mazzei & Oggiano (1990) record two main regression and transgression phases during Miocene time. The mineralised lower conglomerate consists of well rounded to sub-angular poorly sorted clasts in a loose coarse sandstone matrix; this conglomerate is rather discontinuous in beach gravels, also consisting at random of feldspathic to impure clayey sands and lens-shaped beds of coarse-grained feldspathic arenite. These conglomerate beds are graded locally and commonly are 0.5 to 3 m thick. The overlying mineralised rock consists of siltite beds containing remnants of plant material (Fig. 2). The sandstones consist of quartz, feldspar, and volcanic rock fragments, thus may be classified as lithic arkose according to Pettijohn et al. (1972), and represent the first-cycle erosion products of a calc-alkaline volcano-plutonic complex. The sandstone beds associated with the conglomerates are texturally immature, first-cycle arkosic wackes, consisting of poorly sorted quartz and plagioclase feldspar of oligoclase-andesine composition, with accessory alkali feldspar; the smectite-illite matrix content is as high as 30%, thus plotting in the sediment compositional field of arkosic wackes.

5. Conclusions

The northwestern part of Sardinia includes zones of stratiform manganese mineralization extending along the margin of the Fossa Sarda rift. Most of these Mn occurrences, although they may be locally concentrated to ore grades, are of subeconomic size. The major control on mineralized sites was the paleotopography, as they are located along ancient coastal lines against basement highs, and re-

lated to permeable sedimentological features. The weathering and erosion of “fertile“ minerals of igneous provenance gives the first link between manganese and the ore occurrences formed in conglomerates in restricted paralic environments.

The main ore-forming event is represented by the arrival of ore constituents released by the continent and transported by gravity-driven ground- and surface-waters in coastal (subaerial to saturated) sediments where the mineralization process took place at very low burial depths. However, restricted locally reducing conditions may indicate temporary subtidal environments or playa flats and lake environments. The syndepositional history was not too complex; most modifications occurred during subaerial exposure or fresh-water environments as shown by the scarcity of marine cements. Synchronous with sedimentation, manganese was precipitated in oxidized low-energy lacustrine (fresh to brackish-water) environments of neutral to alkaline pH values. The regional paleogeographical and geophysical interpretations of the Logudoro basin and of the broader area of northwestern Sardinia, allowed us to evaluate the regional controls on the localizations of this type of possibly economic manganese mineralizations. Constraints on the size of these occurrences include the lateral variability of the enclosing sedimentary rocks, and their permeabilities. The economic potential of these small but high-grade deposits may be important. Exploration should take into account areas containing regionally high Mn values. First of all, the paleogeographic and structural conditions described in this paper should be confirmed. This may be ascertained through a careful preliminary geological mapping program followed by the definition of necessary palaeogeographic and structural controls. If these first studies identify a favourable situation, geochemical and geophysical studies, along with the examination of a possible primary source of the metal, should further reduce the exploration area to one or more prospects. Normal detailed exploration methods would then be applied to evaluate the individual ore concentrations.

6. Acknowledgments

This study was supported by the Istituto di Geologia Ambientale e Geoingegneria, IGAG del CNR and the Dipartimento di Ingegneria e Tecnologie Ambientali (DIGITA), piazza d'Armi, 09123 Cagliari, Italy.

7. References

- Biondi E., Filigheddu, P., 1990. A palm fossil closely related to *Chamaerops humilis* L. from the Lower Miocene of Sardinia. *Giorn. Bot. Ital.* 124, 711-724.
- Cherchi, M. A., Montadert, L., 1982. Il sistema di rifting Oligo-Miocenico del Mediterraneo occidentale e le sue conseguenze Paleogeografiche sul Terziario Sardo. *Mem. Soc. Geol. Ital.* 24, 387-400.
- Coulon, C., 1977. Le volcanisme calco-alkalin Cénozoïque de Sardaigne (Italie): Pétrographie, géochimie, et genèse des laves andésitiques et des ignimbrites: Signification géodynamique; Thèse, Université de Droit, D'Économie et des Sciences D'Aix, Marseille.
- Garbarino, C., Grillo, S. M., Marcello, A., Pretti, S., Uras, I., Fiori, M., 1991. First data on Tertiary epithermal occurrences in Sardinia, Italy. *Proc. Symp. Braz. Gold 91, Belo Horizonte*, 143-150.
- Lentz, D.R., 2003. *Geochemistry of Sediments and Sedimentary Rocks: Evolutionary Considerations to Mineral Deposit-Forming Environments*. Ed. Lentz, D.R., 184pp.
- Jambor, J., L., & Blowes, D., W., 1994. Short course handbook on environmental geochemistry of sulfide mine-wastes. Waterloo Ontario, May, 1994; Ed. Jambor, J., L., & Blowes, D., W., 22, 438.
- JCPDS File, 1985. Powder diffraction file: Inorganic phases. JCPDS International Centre for Diffraction Data, PA, USA, 998 pp.

- Maynard, J., B., 1983. *Geochemistry of Sedimentary Ore Deposits*. Springer-Verlag, New York, Heidelberg, Berlin, 305 pp.
- Marcello, A., Pretti, S., Valera, P., Fiori, M., 2004. Tertiary manganese occurrences in Sardinia (Italy). Proceedings of the interim IAGOD Conference, Vladivostok, Russia, 487-490.
- Martini, I., P., Oggiano, G., and Mazzei, R., 1992. Siliciclastic-carbonate sequences of Miocene grabens of northern Sardinia, western Mediterranean Sea. *Sedimentary Geology*, 76, 63-78.
- Mazzei, R., Oggiano, G., 1990. Messa in evidenza di due cicli sedimentari nel Miocene dell'area di Florinas (Sardegna settentrionale). *Atti Soc. Tosc. Sci. Nat., Mem. Seie A.*, 97, 119-147.
- Pettijohn, F., J., Potter, P., E., & Siever, R., 1972. *Sand and sandstones*. Springer-Verlag, New York-Heidelberg-Berlin, 618 pp.
- Redini, R., 1940. Sul wolframio connesso a minerali manganesiferi e sull'età di talune formazioni terziarie della Sardegna settentrionale. *Boll. R. Uff. Geol. d'It.*, 65, 44 pp.
- Roy, S. 1981. *Manganese Deposits*. Academic press., 418 pp.
- Sapozhnikov, D., G., 1970. *Manganese Deposits of the Soviet Union*. Ed. Sapozhnikov, D., G., 522pp.

PURIFICATION OF URBAN WASTEWATERS BY HELLENIC NATURAL ZEOLITE

**Filippidis A.¹, Papastergios G.¹, Apostolidis N.¹, Filippidis S.¹, Paragios I.¹
and Sikalidis C.²**

¹ Aristotle University, Department of Mineralogy-Petrology-Economic Geology, 54124 Thessaloniki, Greece, anestis@geo.auth.gr

² Aristotle University, Department of Chemical Engineering, 54124 Thessaloniki, sikalidi@eng.auth.gr

Abstract

Treatment of urban wastewaters ($\text{pH}_{\text{initial}}$ 8.2), with 6 g of Hellenic Natural Zeolite (HENZAZE) of an grain-size < 1.5 mm, gave overflowed clear water of pH 7.5, free of odors and improved quality parameters by 87% for the suspended particles, 88% for the color, 91% for the P_2O_5 content, 93% for the chemical oxygen demand (COD) and 97% for the NH_4 content. Compared to previous experiment, the decrease of the amount of HENZAZE by 1.5 g (20%) resulted to the purification worsening only by 1-2%. The HENZAZE comes from Ntrista stream of Petrota village of Trigono Municipality of Evros Prefecture, Northeastern Greece. HENZAZE contains 89 wt.% HEU-type zeolite and exhibit an ammonia ion exchange capacity (sorption ability) of 226 meq/100g. The mineralogical composition and the unique physico-chemical properties, make the HENZAZE suitable material for numerous environmental, industrial, agricultural and aquacultural applications, such as: Animal nutrition, soil amendment for agriculture, pH soil regulation, greenhouse and flowers substrates, durability and health improvement of lawn, purification of industrial and urban wastewaters, treatment of sewage sludge, odor control, fishery and fish breeding, gas purification and drying systems, oxygen enrichment of aquatic ecosystems, improvement of drinking water quality, constructed wetlands and wastewater treatment units. The treatment gave as precipitate an odorless and cohesive zeo-sewage sludge, suitable for safe deposition and also for the reclamation of agricultural soils. The zeo-sewage sludge, produced either from the urban wastewater treatment or from the mixing of HENZAZE and sewage sludge, can be used for the reclamation of agricultural soils. The presence of HENZAZE in the agricultural soils, increases the crops yield by 29-57% and improves the quality of agricultural products by 4-46%, reduces the use of fertilizers by 55-100%, reduces the usage of irrigation water by 33-67%, prevents the seepage of dangerous species into the water environment (e.g., NO_3^- by 55-57%), protecting thus the quality of surface and underground waters. The usage of HENZAZE in vivarium units and in the animal nutrition, increases the production and improves the quality of the relevant products.

Key words: natural zeolite, urban wastewaters, sewage, sewage-sludge, Evros, Greece.

1. Introduction

Zeolite comprises a special solid crystalline microporous material, with open structure and void space. Some high quality HEU-type natural zeolites, displays unique physical and chemical features

and have a great variety of environmental, industrial, aquacultural and agricultural applications. The large natural zeolite deposits and the low cost of mining, gave access to large-scale utilization (e.g., Pond and Mumpton, 1984; Tsitsishvili et al., 1992; Carr, 1994; Collela and Mumpton, 2000; Filippidis and Kassoli-Fournaraki, 2000; Bish and Ming, 2001; Harben, 2002; Savvas et al., 2002; Inglezakis and Grigoropoulou, 2004; Inglezakis et al., 2004, 2005; Filippidis, 2008; Filippidis et al., 2008e-g).

In the Trigono Municipality (Evros Prefecture, Northeastern Greece) and around the villages of Petrota and Pentalofos, eight different occurrences show varying zeolite contents, on average 39-76 wt. % (e.g., Kirov et al., 1990; Marantos and Perdikatsis, 1994; Filippidis et al., 1995; Arvanitidis, 1998; Stamatakis et al., 1998, 2001; Filippidis and Kassoli-Fournaraki, 2000; Hall et al., 2000; Kassoli-Fournaraki et al., 2000; Yannakopoulos et al., 2000; Zorpas et al., 2000a,b; Barbieri et al., 2001; Moirou et al., 2001; Vlessidis et al., 2001; Koshiaris et al., 2002; Kyriakis et al., 2002; Papaioannou et al., 2002a,b; Savvas et al., 2002; Christidis et al., 2003; Katranas et al., 2003; Krestou et al., 2003; Perraki et al., 2003; Fokas et al., 2004; Inglezakis and Grigoropoulou, 2004; Inglezakis et al., 2004, 2005; Perraki and Orfanoudaki, 2004; Kantiranis et al., 2006; Warchol et al., 2006).

In a specific ground of Petrota village (Ntrista stream) has been located a HEU-type zeolite deposit, the Hellenic Natural Zeolite (HENZA) of GEO-VET N. Alexandridis & Co O.E. concession (e.g., Filippidis and Kantiranis, 2002, 2005, 2007; Deligiannis et al., 2005; Filippidis, 2005, 2007; Filippidis et al., 2006, 2007, 2008a-d, 2009). The purification of urban wastewaters, as well as the production of odorless zeo-sewage sludge, using 7.5 g of HENZA and stirring time 5-60 min, has been investigated (Filippidis et al., 2008a-d, 2009). The present study investigates the purification of urban wastewaters, using 6.0 g of HENZA and stirring time of 5 min.

2. Materials and methods

The Hellenic Natural Zeolite (HENAZE) sample used was selected from a vertical profile of the Ntrista stream within the GEO-VET's concession. Petrographic investigation of HENZA was performed on thin and polished thin sections. The morphology and chemistry of the HEU-type zeolite were studied by Scanning Electron Microscopy - Energy Dispersive Spectroscopy (SEM-EDS) with Link-AN 10000 EDS system. To minimize volatilization of alkalis, the electron beam spot size was enlarged and the counting time decreased. The mineralogical composition was determined by X-Ray Powder Diffraction (XRPD). Semi-quantitative estimates were performed using external mixture standards of the identified mineral phases (Filippidis and Kantiranis, 2007). The chemical composition of the HENZA was determined by Atomic Absorption Spectrometry. The ammonia ion exchange capacity (sorption ability) of the HENZA was determined according to the Ammonium Acetate Saturation (AMAS) method. The pH variations and the removal ability of metals and anions were performed through batch-type experiments at RT (Filippidis and Kantiranis, 2002, 2007; Filippidis, 2005; Filippidis et al., 2006).

The typical platy crystals of HEU-type zeolite have a grain-size of 5-25 μm (Fig. 1a, Filippidis and Kantiranis, 2002; Filippidis, 2005, 2007). The chemical formula of the clinoptilolite is $\text{Ca}_{1.5}\text{K}_{1.4}\text{Mg}_{0.6}\text{Na}_{0.5}\text{Al}_{6.2}\text{Si}_{29.8}\text{O}_{72}\cdot 20\text{H}_2\text{O}$. The minerals content of HENZA is 89 wt.% HEU-type zeolite, 3 wt.% mica + clays (92 wt.% microporous minerals), 6 wt.% feldspars and 2 wt.% quartz (Filippidis and Kantiranis, 2002, 2007; Filippidis, 2005). The chemical analysis of HENZA gave: 68.62 wt.% SiO_2 , 11.80 wt.% Al_2O_3 , 2.92 wt.% K_2O , 2.14 wt.% CaO , 1.13 wt.% Na_2O and 0.75 wt.% MgO . HENZA shows a remarkable ammonia ion exchange capacity of 226 meq/100g, as well as an ability to neutralize the pH of basic water (pH 9.5) from the lake Koronia (Prefecture of Thes-

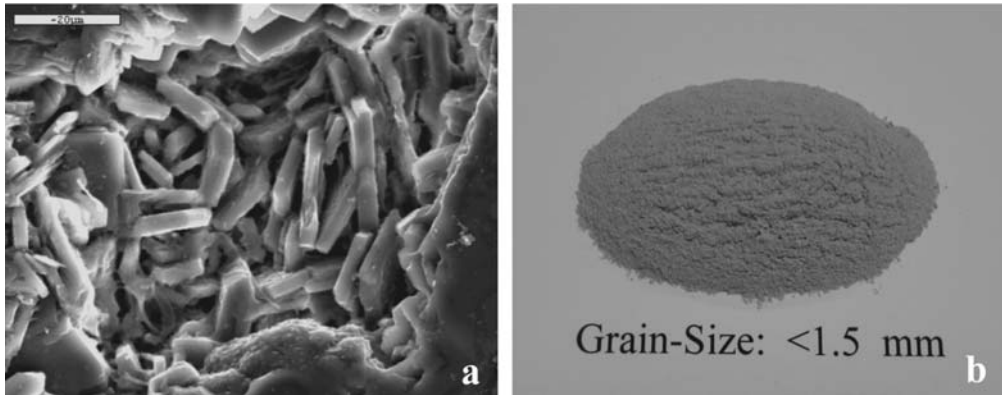


Fig. 1: a) SEM microphotograph of typical platy crystals of HEU-type zeolite of the HENAZE. b) The grain-size < 1.5 mm of HENAZE, used for the batch-type experiments.

saloniki) and of acidic stream mine water (pH 5.5) from NE Chalkidiki Prefecture, exhibiting an amphoteric character (Filippidis and Kantiranis, 2002, 2007; Filippidis, 2005). Also found to remove from their aqueous solutions 74 % of Pb, 79% of Ag and 55-57% of NO_3^- (Filippidis and Kantiranis, 2002, 2007; Filippidis, 2005; Filippidis et al., 2006).

Kilkis City (Northern Greece) urban wastewaters of pH 8.2, were treated at room temperature with < 1.5 mm grain-size HENAZE (Fig. 1b), in batch-type experiment. In 300 ml municipal sewage 6.0 g of HENAZE was added, the whole was stirred for 5 minutes and polyaluminium chloride as well as cationic polyelectrolyte was added. The overflowed clear water and the precipitated zeo-sewage sludge were separated by filtering. The zeo-sewage sludge was dried overnight at room temperature (RT). The starting urban wastewater and the overflowed clear water, were analyzed for (method): pH (electrometric), color (photometric), suspended particles (filtering and centrifugation), COD (method of K_2CrO_6), P_2O_5 and NH_4 (molecular absorption spectrophotometry).

3. Results

Microscopic examination of thin sections reveals a fine-grained vitroclastic texture containing glass shards (Fig. 2), angular to subangular quartz and feldspar, as well as tabular mica crystals.

The lath- or tabular shaped crystals of HEU-type zeolite are very abundant as interstitial cements or as polycrystalline replacements of glass shards. The peripheral zone of the altered glass shards is often a rim containing clay minerals (Fig. 2).

The treatment of urban wastewater of pH 8.2 with the HENAZE gave overflowed clear water (Fig. 3a) of pH 7.5, free of odors and improved quality parameters by 87% for the suspended particles, 88% for the color, 91% for the P_2O_5 content, 93% for the chemical oxygen demand (COD) and 97% for the NH_4 content (Table 1).

Treatment with 7.5 g of HENAZE resulted to pH of 7.3 for the clear water and to improvement by 89% for the suspended particles, 90% for the color, 93% for the P_2O_5 content, 94% for the chemical oxygen demand (COD) and 98% for NH_4 content (Table 1, Filippidis et al., 2009).

Simultaneously, the treatment gave as precipitate odorless and cohesive zeo-sewage sludge, dried overnight at room temperature (Fig. 3b).

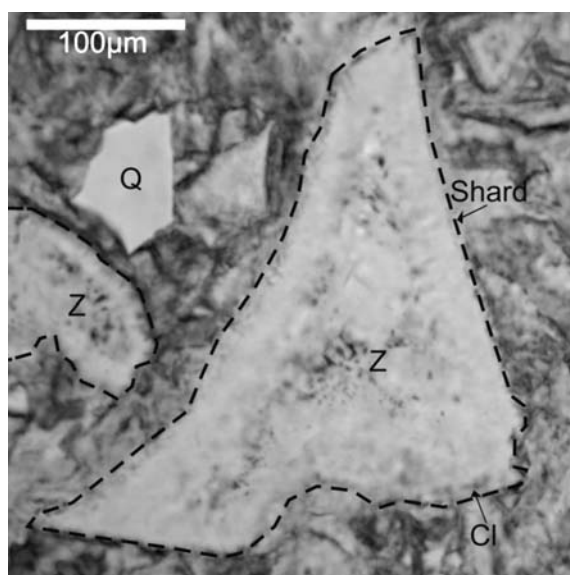


Fig. 2: Photomicrograph of thin section, altered glass shards (discontinuous line), lath-shaped crystals of HEU-type zeolite (Z), angular-subangular quartz crystal (Q) and the peripheral rim of the shards containing clay minerals (Cl).



Fig. 3: a) Left: Starting urban wastewater (SUW), Right: Overflowed clear water (CW) after the HENAZE treatment. b) Odorless and cohesive zeo-sewage sludge, dried overnight at RT.

Table 1. Chemistry of starting urban wastewater (SUW) and overflowed relevant Clear Water treated with 6.0 g (CW-6) and 7.5 g (CW-7.5) of HENAZE at RT.

Quality parameters (detection limit)	SUW	CW-6	± %	CW-7.5*	± %
pH (0.1)	8.2	7.5	- 9	7.3	- 11
Suspended Particles, mg/L (5)	210	28	- 87	23	- 89
Color, mg/L, Pt scale (5)	1180	143	- 88	119	- 90
Chemical Oxygen Demand (COD), mg/L O ₂ (15)	410	29	- 93	26	- 94
P ₂ O ₅ , mg/L (0.02)	9.24	0.80	- 91	0.66	- 93
NH ₄ , mg/L (0.02)	30.52	0.79	- 97	0.51	- 98

* Filippidis et al., 2009.

4. Discussion and Conclusions

The natural zeolites show a remarkable ability to remove inorganic, organic, organometallic compounds, gas species, metals and radionuclides from their aqueous solutions. The sorption of the different species from their solutions by the micro- meso- and macroporous of natural zeolite can be attributed to absorption (mainly ion exchange), adsorption and surface precipitation processes (e.g., Tsitsishvili et al., 1992; Misailides et al., 1993, 1995; Godelitsas et al., 1999, 2001, 2003; Collela and Mumpton, 2000; Bish and Ming, 2001). The sorption of gas phases results to oxygen enrichment of the air and to the remarkable decrease of the malodour. Also, they show an ability to neutralize the pH of acidic and basic waters, acting either as a proton acceptor or donor, exhibiting thus an amphoteric character (e.g., Filippidis et al., 1996; Charistos et al., 1997).

The Hellenic Natural Zeolite (HENZA) is of very high quality (> 85 wt.% HEU-type zeolite), removes inorganic, organic, organometallic, gas species, metals, cations and anions from their aqueous solutions. The mineralogical composition and the unique physico-chemical properties, make the HENZA suitable material for numerous environmental, industrial, agricultural and aquacultural applications, such as: Animal nutrition, soil amendment for agriculture, conditioning of acid and basic soils, greenhouse and flowers substrates, durability and health improvement of lawn, purification of industrial and urban wastewaters, treatment of sewage sludge, odor control, fishery and fish breeding, gas purification and drying systems, oxygen enrichment of aqua ecosystems, improvement of drinking water, constructed wetlands and wastewater treatment units (e.g., Collela and Mumpton, 2000; Harben, 2002; Filippidis, 2007; Filippidis et al., 2007, 2008a-g).

The HENZA treatment of urban wastewater (pH initial 8.2) gave overflowed clear water of pH 7.5, free of odors and improved by 87% for the suspended particles, 88% for the color, 91% for the P_2O_5 content, 93% for the chemical oxygen demand (COD) and 97% for the NH_4 content. Treatment with 7.5 g of HENZA resulted to pH of 7.3 for the clear water and to improvement by 89% for suspended particles, 90% for color, 93% for P_2O_5 , 94% for COD and 98% for NH_4 (Filippidis et al., 2009). The decrease of the amount of HENZA by 1.5 g (20 %) resulted to the purification worsening only by 1-2 %. These final values of the pH and of the previous mentioned quality parameters, measured in the overflowed clear water, are fulfilling the requirements for disposition as downstream, irrigation, swimming and fish waters.

The HENZA treatment gave also as precipitate, odorless and cohesive zeo-sewage sludge, suitable for safe deposition but also for the reclamation of agricultural soils. The same stands for the odorless and cohesive zeo-sewage sludge produced by mixing the sewage sludge and the HENZA. The presence of HENZA in the agricultural soils, increases the yield by 29-57% and improves the quality by 4-46% of agricultural products, reduces the use of fertilizers by 55-100%, reduces the usage of irrigation water by 33-67%, prevents the seepage of dangerous species into the water environment (e.g., NO_3^- by 55-57%), protecting thus the quality of surface and underground waters. The usage of HENZA in vivarium units and in the animal nutrition increases the production and improves the quality of their products (e.g., Filippidis, 2005, 2007; Filippidis et al., 2006, 2007, 2008c).

5. Acknowledgments

We express our gratitude to the GEO-VET N. Alexandridis & Co O.E., for the supply and treatment of HENZA, as well as for their economical support.

6. References

- Arvanitidis, N., 1998. Northern Greece's industrial minerals: production and environmental technology developments. *Journal of Geochemical Exploration* 62, 217-227.
- Barbieri, M., Castorina, F., Masi, U., Garbarino, C., Nicoletti, M., Kassoli-Fournaraki, A., Filippidis, A. and Mignardi, S., 2001. Geochemical and isotopic evidence for the origin of rhyolites from Petrotta (Northern Thrace, Greece) and geodynamic significance. *Chemie der Erde* 61, 13-29.
- Bish, D.L. and Ming, D.W., 2001. Natural Zeolites: Occurrence, Properties, Applications. Mineralogical Society of America, 654 pp., Washington DC.
- Carr, D.D., 1994. Industrial Minerals and Rocks. Braun-Brumfield Inc., 1196 pp., Ann Arbor, Michigan.
- Charistos, D., Godelitsas, A., Tshipis, C., Sofoniou, M., Dwyer, J., Manos, G., Filippidis, A. and Triantafyllidis, C., 1997. Interaction of natrolite and thomsonite intergrowths with aqueous solutions of different initial pH values at 25° C in the presence of KCl: Reaction mechanisms. *Applied Geochemistry* 12, 693-703.
- Collela, C. and Mumpton, F.A., 2000. Natural Zeolites for the Third Millennium. De Frede Editore, 481 pp., Napoli.
- Christidis, G.E., Moraetis, D., Keheyan, E., Akhalbedashvili, L., Kekelidze, N., Gevorkyan, R., Yeritsyan, H. and Sargsyan, H., 2003. Chemical and thermal modification of natural HEU-type zeolitic materials from Armenia, Georgia and Greece. *Applied Clay Science* 24, 79-91.
- Deligiannis, K., Lainas, Th., Arsenos, G., Papadopoulos, E., Fortomaris, P., Kufidis, D., Stamataris, C. and Zygoyiannis, D., 2005. The effect of feeding clinoptilolite on food intake and performance of growing lambs infected or not with gastrointestinal nematodes. *Livestock Production Science* 96, 195-203.
- Filippidis, A., 2005. Mineralogy and physico-chemical characteristics of five natural zeolite samples for N. Alexandridis & Co O.E. Internal report, 10 pp., Thessaloniki, In Greek.
- Filippidis, A., 2007. Zeolites of Trigono Municipality of Evros Prefecture in industrial, agricultural, cattle-raising and environmental technology. *Proceedings, Scientific Meeting on Development Perspectives of Northern Evros*, Petrotta, Greece, 89-107, In Greek.
- Filippidis, A., 2008. Treatment and recycling of municipal and industrial waste waters using Hellenic Natural Zeolite: A Review. *CD-Proceedings, AQUA 2008, 3rd Intern. Conf. Water Science and Technology*, Athens, 5 pp.
- Filippidis, A. and Kantiranis, N., 2002. Morphology, mineralogy, chemistry, mineralchemistry and ion exchange capacity of five natural zeolite samples for N. Alexandridis & Co O.E., Internal report, 5 pp., Thessaloniki, In Greek.
- Filippidis, A. and Kantiranis, N., 2005. Industrial, agricultural and environmental uses of the natural zeolites of Thrace. *Bull. Geol. Soc. Greece* 37, 90-101, In Greek with English summary.
- Filippidis, A. and Kantiranis, N., 2007. Experimental neutralization of lake and stream waters from N. Greece using domestic HEU-type rich natural zeolitic material. *Desalination* 213, 47-55.
- Filippidis, A. and Kassoli-Fournaraki, A., 2000. Environmental uses of natural zeolites from Evros district, Thrace, Greece, *Proceedings, 5th International Conference on Environmental Pollution*, Thessaloniki, 149-155.
- Filippidis, A., Kassoli-Fournaraki, A. and Tsirambides, A., 1995. The zeolites of Petrotta and Metaxades (Thrace) and the kaolins of Leucogia (Macedonia), Greece. In: Aleksiev, B.(ed.) *Field Tripe Guide, International Symposium on Natural Zeolites*, Sofia, 49-62.
- Filippidis, A., Godelitsas, A., Charistos, D., Misaelides, P. and Kassoli-Fournaraki, A., 1996. The chemical behavior of natural zeolites in aqueous environments: Interactions between low-silica zeolites and 1M NaCl solutions of different initial pH-values. *Applied Clay Science* 11: 199-209.

- Filippidis, A., Kantiranis, N., Drakoulis, A. and Vogiatzis, D., 2006. Improvement and protection of the lake Koronia using natural zeolite. *Proceedings, 2nd Congress of Aristotle University Environment Council*, Thessaloniki, 273-279, In Greek with English summary.
- Filippidis, A., Siomos, A., Barbayiannis, N. and Philippidis, S., 2007. Agricultural and environmental applications using Hellenic Natural Zeolite of Petrota (Evros), *Proceedings, Jean Monnet Congress*, Veria, Greece, 557-569, In Greek with English summary.
- Filippidis, A., Apostolidis, N., Philippidis, S. and Paragios, I., 2008a. Purification of industrial and urban wastewaters, production of odorless and cohesive zeo-sewage sludge using Hellenic Natural Zeolite. *Proceedings, Second International Conference on Small and Decentralized Water and Wastewater Treatment Plants*, Skiathos, Greece, 403-408.
- Filippidis, A., Apostolidis, N., Paragios, I. and Philippidis, S., 2008b. Purification of dye-work and urban wastewaters, production of odorless and cohesive zeo-sewage sludge, using Hellenic Natural Zeolite. *CD-Proceedings, 1st International Conference on Hazardous Waste Management*, Chania, Greece, 8 pp.
- Filippidis, A., Apostolidis, N., Paragios, I. and Philippidis, S., 2008c. Safe management of sewage sludge, produced by treatment of municipal sewage with Hellenic Natural Zeolite. *CD-Proceedings, AQUA 2008, 3rd International Conference on Water Science and Technology*, Athens, 5 pp.
- Filippidis, A., Apostolidis, N., Paragios, I. and Philippidis, S., 2008d. Zeolites clean up. *Industrial Minerals*, April, 68-71.
- Filippidis, A., Kantiranis, N., Philippidis, S., Vordogiannis, I., Apostolidis, N. and Paragios, I., 2008e. Purification of Textile-work Waste Waters with Natural Zeolite. Patent Number: 1006140, Industrial Property Organisation, Athens, In Greek.
- Filippidis, A., Kantiranis, N., Philippidis, S., Vordogiannis, I., Apostolidis, N. and Paragios, I., 2008f. Purification of Sewage with Natural Zeolite. Patent Number: 1006145, Industrial Property Organisation, Athens, In Greek.
- Filippidis, A., Kantiranis, N., Philippidis, S., Vordogiannis, I., Apostolidis, N. and Paragios, I., 2008g. Purification of Tanning-work Waste Waters with Natural Zeolite. Patent Number: 1006146, Industrial Property Organisation, Athens, In Greek.
- Filippidis, A., Papastergios, G., Apostolidis, N., Paragios, I., Philippidis, S. and Sikalidis, C., 2009. Odorless and cohesive zeo-sewage sludge produced by Hellenic Natural Zeolite treatment. *Proceedings, 3rd International Conference, AMIREG 2009*, Athens, 96-100.
- Fokas, P., Zervas, G., Fegeros, K. and Zoiopoulos, P., 2004. Assessment of Pb retention coefficient and nutrient utilization in growing pigs fed diets with added clinoptilolite. *Animal Feed Science and Technology* 117, 121-129.
- Godelitsas, A., Charistos, D., Dwyer, J., Tshipis, C., Philippidis, A., Hatzidimitriou, A. and Pavlidou, E., 1999. Copper (II)-loaded HEU-type zeolite crystals: characterization and evidence of surface complexation with N,N-diethyldithiocarbamate anions. *Microporous and Mesoporous Materials* 33, 77-87.
- Godelitsas, A., Charistos, D., Tshipis, A., Tshipis, C., Philippidis, A., Triantafyllidis, C., Manos, G. and Siapakas, D., 2001. Characterisation of zeolitic materials with a HEU-type structure modified by transition metal elements: Definition of acid sites in Nickel-loaded crystals in the light of experimental and quantum-chemical results. *Chemistry European Journal* 7, 3705-3721.
- Godelitsas, A., Charistos, D., Tshipis, C., Misaelides, P., Philippidis, A. and Schindler, M., 2003. Heterostructures patterned on aluminosilicate microporous substrates: Crystallisation of cobalt (III) tris(N,N-diethyl-dithiocarbamate) on the surface of HEU-type zeolite. *Microporous and Mesoporous Materials* 61, 69-77.

- Hall, A., Stamatakis, M. and Walsh, J.N., 2000. The Pentafos zeolitic tuff formation: A giant ion-exchange column. *Annales Geologiques des Pays Helleniques* 38, 175-192.
- Harben, P.W., 2002. The Industrial Minerals HandyBook. Pensord, 409 pp., Blackwood, UK.
- Inglezakis, V.J. and Grigoropoulou, H., 2004. Effects of operating conditions on the removal of heavy metals by zeolite in fixed bed reactors. *Journal of Hazardous Materials* B112,37-43.
- Inglezakis, V.J., Loizidou, M.M. and Grigoropoulou, H.P., 2004. Ion exchange studies on natural and modified zeolites and the concept of exchange site accessibility. *Journal of Colloid and Interface Science* 275, 570-576.
- Inglezakis, V.J., Zorpas, A.A., Loizidou, M.D. and Grigoropoulou, H.P., 2005. The effect of competitive cations and anions on ion exchange of heavy metals. *Separation and Purification Technology* 46, 202-207.
- Kantiranis, N., Chrissafis, C., Filippidis, A. and Paraskevopoulos, K., 2006. Thermal distinction of HEU-type mineral phases contained in Greek zeolite-rich volcanoclastic tuffs. *European Journal of Mineralogy* 18, 509-516.
- Kassoli-Fournaraki, A., Stamatakis, M., Hall, A., Filippidis, A., Michailidis, K., Tsirambides, A. and Koutles, Th., 2000. The Ca-rich clinoptilolite deposit of Pentafos, Thrace, Greece. In: Colella, C. & Mumpton, F.A.(eds) *Natural Zeolites for the Third Millennium*, De Frede Editore, Napoli, 193-202.
- Katranas, Th., Vlessidis, A., Tsiatouras, V., Triantafyllidis, K. and Evmiridis, N., 2003. Dehydrogenation of propane over natural clinoptilolite zeolites. *Microporous and Mesoporous Materials* 61, 189-198.
- Kirov, G.N., Filippidis, A., Tsirambides, A., Tzvetanov, R.G. and Kassoli-Fournaraki, A., 1990. Zeolite-bearing rocks in Petrota area (Eastern Rhodope Massif, Greece). *Geologica Rhodopica* 2, 500-511.
- Koshiaris, G., Marantos, I., Tsirambides, A., Stamatakis, M.G., Kassoli-Fournaraki, A. and Filippidis, A., 2002. The zeolite deposits of Thrace (North-Eastern Greece). *Field Trip Guide, 6th International Conference on Natural Zeolites*, Thessaloniki, 23 pp.
- Krestou, A., Xenidis, A. and Pnias, D., 2003. Mechanism of aqueous uranium (VI) uptake by natural zeolitic tuff. *Minerals Engineering* 16, 1363-1370.
- Kyriakis, S.C., Papaioannou, D.S., Alexopoulos, C., Polizopoulou, Z., Tzika, E.D. and Kyriakis, C.S., 2002. Experimental studies on safety and efficacy of the dietary use of a clinoptilolite-rich tuff in sows: a review of recent research in Greece. *Microporous and Mesoporous Materials* 51, 65-74.
- Marantos, I. and Perdikatsis, V., 1994. Study of the mineralogical composition, dehydration / adsorption of water and ion exchange capacity of zeolitic tuffs from Petrota-Pentafos area, N. Evros. *Bull. Geol. Soc. Greece* 30/3, 311-321, In Greek with English abstract.
- Misaelides, P., Godelitsas, A., Haristos, D., Noli, F., Filippidis, A. and Sikalidis, C., 1993. Determination of heavy metal uptake by the sodium form of heulandite using radiochemical techniques. *Geologica Carpathica - Series Clays* 44/2, 115-119.
- Misaelides, P., Godelitsas, A., Filippidis, A., Charistos, D. and Anousis, I., 1995. Thorium and uranium uptake by natural zeolitic materials. *The Science of the Total Environment* 173/174, 237-246.
- Moirou, A., Xenidis, A. and Paspaliaris, I., 2001. Stabilization Pb, Zn, and Cd- contaminated soil by means of natural zeolites. *Soil and Sediment Contamination* 10/3, 251-267.
- Papaioannou, D.S., Kyriakis, S.C., Papasteriadis, A., Roubies, N., Yannakopoulos, A. and Alexopoulos, C., 2002a. A field study on the effect of in-feed inclusion of a natural zeolite (clinoptilolite) on health status and performance of sows/gilts and their litters. *Research in Veterinary Science* 72, 51-59.
- Papaioannou, D., Kyriakis, S., Papasteriadis, A., Roubies, N., Yannakopoulos, A. and Alexopoulos, C., 2002b. Effect of in-feed inclusion of a natural zeolite (clinoptilolite) on certain vitamin, macro and

- trace element concentrations in the blood, liver and kidney tissues of sows. *Research in Veterinary Science* 72, 61-68.
- Perraki, Th. and Orfanoudaki, A., 2004. Mineralogical study of zeolites from Pentelofos area, Thrace, Greece. *Applied Clay Science* 25, 9-16.
- Perraki, Th., Kakali, G. and Kontoleon, F., 2003. The effect of natural zeolites on the early hydration of Portland cement. *Microporous and Mesoporous Materials* 61, 205-212.
- Pond, W.G. and Mumpton, F.A., 1984. Zeo-Agriculture, Use of Natural Zeolites in Agriculture and Aquaculture, I.C.N.Z., 305 pp., Brockport, NY.
- Savvas, D., Samantouros, K., Paralemos, D., Vlachakos, G., Stamatakis, M. and Vassilatos, C., 2002. Yield and nutrient status in the root environment of tomatoes (*Lycopersicon esculentum*) grown on chemically active and inactive inorganic substrates. *Acta Horticulturae* 644, 377-383.
- Stamatakis, M., Hall, A., Lutat, U. and Walsh, J.N., 1998. Mineralogy, origin and commercial value of the zeolite-rich tuffs in the Petroti-Pentelofos area, Evros county, Greece. *Estudios Geologicos* 54, 3-15.
- Stamatakis, M., Koukouzas, N., Vassilatos, Ch., Kamenou, E. and Samantouros, K., 2001. The zeolites from Evros region, Northern Greece: A potential use as cultivation substrate in hydroponics. *Acta Horticulturae* 548, 93-103.
- Tsitsishvili, G.V., Andronikashvili, T.G., Kirov, G.N. and Filizova, L.D., 1992. Natural Zeolites, Ellis Horwood Ltd, 295 pp., Chichester, West Sussex.
- Warchol, J., Misaelides, P., Petrus, R. and Zamboulis, D., 2006. Preparation and application of organo-modified zeolitic material in the removal of chromates and iodides. *Journal of Hazardous Materials* B137, 1410-1416.
- Vlessidis, A.G., Triantafyllidis, C.S. and Evmiridis, N.P., 2001. Removal and recovery of p-phenylenediamines developing compounds from photofinishing lab wastewater using clinoptilolite tuffs from Greece. *Water Research* 35, 1603-1608.
- Yannakopoulos, A., Tserveni-Gousi, A., Kassoli-Fournaraki, A., Tsirambides, A., Michailidis, K., Filipidis, A. and Lutat, U., 2000. Effects of dietary clinoptilolite-rich tuff on the performance of growing-finishing pigs. In: Colella, C. & Mumpton, F.A.(eds) *Natural Zeolites for the Third Millennium*, De Frede Editore, Napoli, 471-481.
- Zorpas, A.A., Constantinides, T., Vlyssides, A.G., Haralambous, I. and Loizidou, M., 2000a. Heavy metal uptake by natural zeolite and metals partitioning in sewage sludge compost. *Bioresource Technology* 72, 113-119.
- Zorpas, A.A., Kapetanios, E., Zorpas, G.A., Karlis, P., Vlyssides, A., Haralambous, I. and Loizidou, M., 2000b. Compost produced from organic fraction of municipal solid waste, primary stabilized sewage sludge and natural zeolite. *Journal of Hazardous Materials* B77, 149-159.

TEXTURAL AND PETROLOGICAL STUDY OF MODERN SANDS FROM THE VERTISKOS UNIT OF SERBOMACEDONIAN MASSIF (MACEDONIA, GREECE)

Georgiadis I. K.¹, Koronaios A.¹, Tsirambides A.¹ and Stamatakis M.²

¹ Aristotle University of Thessaloniki, School of Geology, Department of Mineralogy-Petrology-Economic Geology, 541 24 Thessaloniki, Greece, iogeorgi@geo.auth.gr, ananias@geo.auth.gr, koroneos@geo.auth.gr

² National and Kapodistrian University of Athens, School of Geology and Geoenvironment, Department of Economic Geology and Geochemistry, 157 84 Athens, Greece, stamatakis@geol.uoa.gr

Abstract

The sediments analyzed are in general coarse grained gravelly sands to slightly gravelly muddy sands poor in mud content and texturally and mineralogically immature to submature. They have been deposited in a fluvial environment. They are feldspathic and in all samples detrital minerals of metamorphic origin are found along with minor amounts of detrital calcite. These sediments are deposited rapidly near their source which comprises the Vertiskos Unit. The mineral constituents of the samples show that Vertiskos Unit is rapidly weathered under a seasonably wet and warm climate. All the samples may be considered as constituting one sedimentary petrologic province, comprised of one mineral association, namely the amphibole-garnet.

Key words: *Vertiskos Unit, metamorphic rocks, fluvial, modern sands.*

1. Introduction

Five are the basic processes that lead to the formation and release of sand-sized grains (Pettijohn et al., 1987); weathering (including both disintegration and decomposition), explosive volcanism, crushing (not including ordinary abrasion), pelletization and precipitation from solution. In general, sands accumulate in environments of high kinetic energy, such as sections of stream channels, alluvial fans and marine environments (Ehlers and Blatt, 1982). Especially the medium of transport and deposition, along with climate and source areas, are the most important factors for the accumulation of a sedimentary deposit (Reineck and Singh, 1986).

Studies on modern sand contribute to our understanding of the effects of processes controlling the composition of sand-size sediment, this information being useful for better paleogeographic interpretations of ancient source area and basin systems (Dickinson, 1985). According to Suttner (1974) the factors that combine to produce detrital assemblages found in modern and ancient sediments include source-rock composition, tectonics, climate and relief. These factors grouped together are referred to as provenance (Dickinson, 1970). In a more descriptive way, Pettijohn et al. (1987) consider provenance of including the paleogeography of a region, the identification of possible source areas for the clastic material under study and the revealing of details about the paleocurrents and the paleoslope. The above mentioned authors also state furthermore that the study of the mineralogy of modern sands may disclose valuable minerals and if the provenance is understood, we may prospect

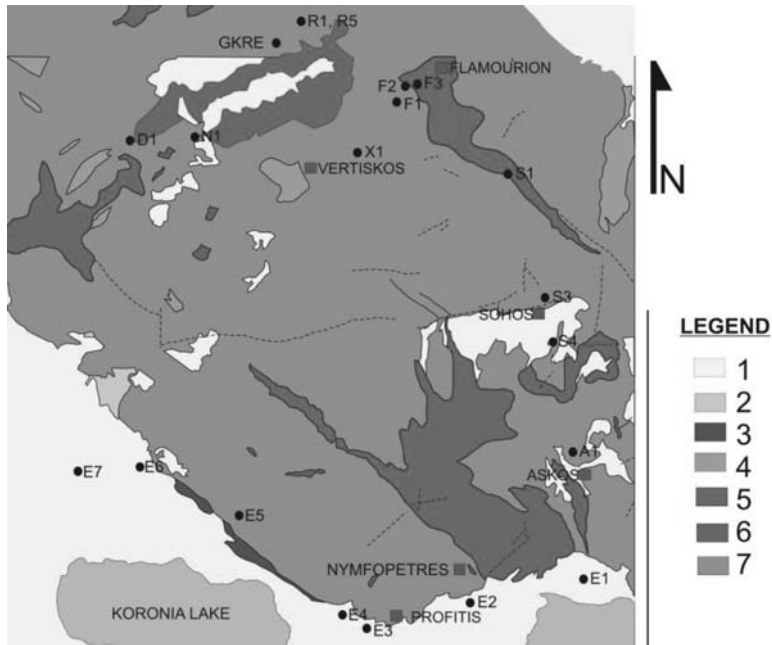


Fig. 1: Petrographic sketch map of the study area (Vertiskos Unit). 1=Quaternary and Neogene gravels, sands and sandy muds, 2= Neogene molassic sediments, 3=Quartzites (Examili Formation), 4=hornblend-quartz diorite, 5=biotite-quartz diorite to granodiorite, 6=two-mica and biotite granite and 7=Alpine metamorphic basement.

them more accurately. Also, sand petrology is helpful in developing a systematic quantitative approach to the problem of optimizing sampling procedures in sedimentary petrography (Weltje, 2004).

Modern sediments from Doirani Lake (NW margin of Vertiskos Unit) are coarse to medium grained and poorly sorted feldspathic wackes and arkoses, deposited in a lacustrine environment with little transportation, since they contained ferromagnesian minerals (Tsirambides, 1997). Drilling cuttings (fluvial sand gravels to gravel sands) from Herso, Kilkis (West margin of Vertiskos Unit) are also mineralogically immature, litharenites to feldspathic litharenites or orthoquartzites, formed under intense physical weathering with rapid transport and deposition, under semi-arid climate or under the influence of a high relief (Georgiadis, 2006; Georgiadis et al., 2007). All the above detrital sediments have as exclusive source, the metamorphic basement of the Unit.

The detrital sediments studied are deposited onto the Vertiskos Plateau, overlying the alpine gneissic basement. These are soil profiles along with generally loose alluvial, fluvial and some lacustrine formations. This study considers the detailed textural, petrological and mineralogical study of modern sands from the Vertiskos Unit. Using mechanical, petrographic and mineralogical techniques it is attempted to indicate the processes under which these sediments were formed, the petrology of the source areas and the current state of weathering of the Vertiskos Unit, Serbomacedonian Massif.

2. Geological setting

The study area belongs to the Serbomacedonian Massif and more specifically comprises the Northern and major part of the Vertiskos Unit. The Vertiskos mountain is located in the centre of this Unit,

Table 1. Peak heights used for mineral semi-quantitative determination (Tsirambides, 2008).

Mineral	Angle (2 θ)	d (Å)	Counts/second
Quartz	20.8	4.26	765
Plagioclase	28.0	3.18	1350
Alkali feldspar	27.5	3.24	1350
Calcite	29.4	3.04	1370
Pyroxene	29.9	2.99	1250
Amphibole	10.5	8.45	1250
Garnet ¹	34.7	2.57	1250
Micas	19.7	4.50	260

¹d-value varies slightly according to composition.

with an altitude of approximately 1,103 m. This mountain is drained from several rivers and torrents. This complex drainage system is generally of dendritic pattern, discharging its detrital load to Galikos and Strymon Rivers (West and East ends of the Massif, respectively), to Doirani and Kerkini Lakes to the North and to Koronia and Volvi Lakes to the South (North and South ends of the Unit, respectively) (Fig. 1).

The Alpine basement of the Vertiskos Unit is mainly comprised of Paleozoic metasediments and metabasic rocks, along with Eocene to Miocene granites. The Unit has been metamorphosed during the Paleozoic to the amphibolite facies, followed by a Cretaceous retrograde metamorphosis to the greenschist facies (Mountrakis, 2002). In detail the petrographic types that consist the Unit (excluding granites, pegmatites and marbles), are (Kourou, 1991; Sidiropoulos, 1991; Chatzidimitriadis et al., 1993): A) Amphibolites, amphibolitic gneisses and banded amphibolites. B) Medium grained pelitic to semi-pelitic mica schists. C) Fine grained meta-arkosic rocks. D) Fine-grained and massive meta-sandstones in bands with migmatitic gneisses. E) Calcic silicic rocks with no typical composition, developed between the contact of the marbles and the semi-pelitic schists. F) Augen gneisses and banded gneisses. G) Medium to coarse grained garnet mica gneisses. H) Small eclogitic bodies. I) Ultrabasic rocks (typical serpentinites and talc-chlorite schists) and J) Poorly sorted Tertiary massive graywackes along with poorly sorted and massive arkoses.

3. Materials and Methods

From different locations of the Vertiskos Unit samples of modern sands were taken. They were analyzed in detail mineralogically by the use of powder X-ray diffraction (PXRD). The samples when moisten were left to dry at room temperature and then separated into consecutive size fractions by sieving in order their textural properties to be studied. Powder X-ray diffraction was performed on a Philips diffractometer with Ni-filtered CuK α radiation. Randomly oriented mounts of the untreated sand sized fraction of the samples were scanned over the interval 3-63° 2 θ at a scanning speed of 1.2° per minute. Semi-quantitative estimates of the minerals present are based on peak heights and intensity factors of XRD patterns (Table 1), using the methods described by Hower et al. (1976), Moore and Reynolds (1997) and Tsirambides (2008). In addition, polarizing microscopy analysis was performed by the use of thin sections prepared from grains of the fractions 1 Φ , 2 Φ , and 3 Φ of samples R1 and G1. In this way the shape of the grains along with the distribution of minerals in each fraction was examined.

Table 2. Statistical parameters of grain size populations for the modern sand samples, according to Folk (1974).

Sample	Mo (Φ)	Md (Φ)	M_z (Φ)	σ_1 (Φ)	Sk ₁	K _G
E1	-1.0 & 2.0	-0.8	-0.49	1.82	0.17	0.83
E2	-1.0 & 2.0	-1.0	-0.41	1.82	0.21	0.92
E3	0.1	-0.5	-0.59	1.33	-0.07	1.06
E4	-0.3	-0.8	-0.62	1.69	0.08	0.88
E5	-2.0 & 0.0	-0.9	-0.93	1.68	0.02	0.86
E6	-2.8 & -0.7	-1.2	-1.35	1.52	-0.02	1.04
E7	0.6	-0.2	-0.21	1.59	0.00	0.97
X1	-2.9 & 0.9	-0.1	-0.41	1.68	-0.29	1.11
A1	-0.1	-0.7	-0.55	1.30	0.10	1.08
S1	-2.0 & 1.0	0.0	-0.17	1.64	-0.18	0.91
S3	-1.1 & 2.0	1.0	-0.75	1.84	0.22	0.93
S4	1.9	-0.2	0.94	1.79	-0.10	1.00
F1	0.1	-0.6	-1.12	1.11	0.16	1.18
F2	-0.1	-0.5	-1.64	0.97	-0.02	1.04
F3	0.0	-0.3	-0.44	1.02	0.07	1.00
N1	0.4	-0.5	-0.26	1.04	0.00	0.98
D1	0.0	0.5	-0.50	0.99	0.05	1.05
R1	5.0	2.1	2.19	2.17	-0.11	0.74
R5	1.0	0.5	0.13	1.83	-0.01	0.95
G1	1.8	1.1	0.94	1.35	-0.30	1.54

Mo=mode, Md=median, M_z =graphic mean, σ_1 =inclusive graphic standard deviation, Sk₁=inclusive graphic skewness and K_G=graphic kurtosis.

4. Results

4.1 Texture and Lithology

Macroscopically all the modern sand samples are generally brown and grey coloured coarse grained loose sands, showing a sandy gravel to gravely sand texture, with little or no mud. Exceptions are the samples R1 and R5, which demonstrate a muddier suite.

All grains macroscopically present low sphericity and are angular to subangular, with easily identified more rounded lithic fragments of metamorphic origin, usually schist, along with some round shaped granite pebbles. The statistical parameters of grain size populations of the modern sand samples analysed are presented in Table 2.

The equations adopted for their calculation along with their interpretation are according to Folk (1974). In figure 2 the lithological classification of the modern sand samples is shown, according to Folk (1974).

According to the variation amplitude of the inclusive graphic standard deviation, the modern sands appear to be moderately sorted to very poorly sorted. The degree of sorting along with the content of mud in the samples, designates them as texturally immature to submature (Weller, 1960; Folk,

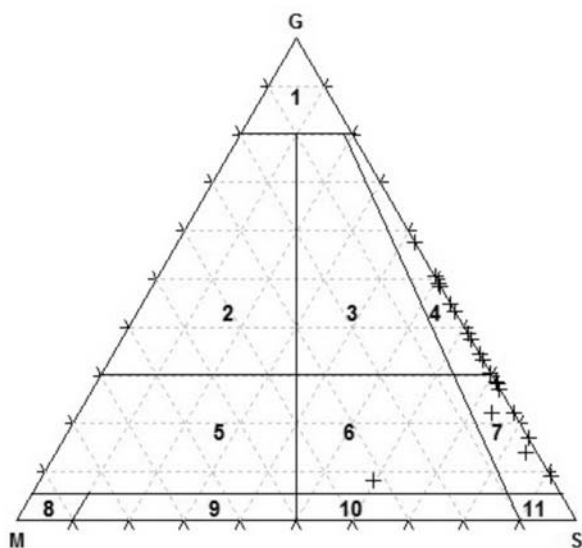


Fig. 2: Textural classification of modern sand samples, according to Folk (1974). G=percentage of gravel, S=percentage of sand, M=percentage of silt+clay, 1=gravel, 2=muddy gravel, 3=muddy sandy gravel, 4=sandy gravel, 5=gravelly mud, 6=gravelly muddy sand, 7=gravelly sand, 8=slightly gravelly mud, 9=slightly gravelly sandy mud, 10=slightly gravelly muddy sand and 11=slightly gravelly sand.

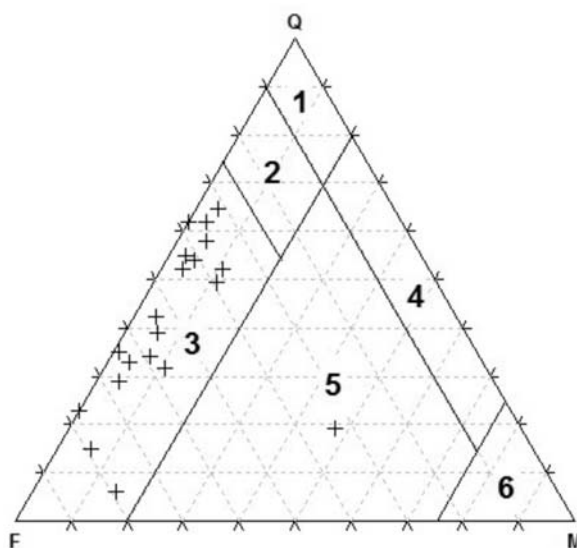


Fig. 3: Ternary diagram for the classification of detrital sediments according to Stewart et al. (1959). 1=orthoquartzite, 2=feldspathic orthoquartzite, 3=arkose, 4=subgraywacke, 5=greywacke (phylarenite), 6=pelite, Q=quartz, F=feldspars and M=micas (+chlorite).

1974). The inclusive graphic skewness implies that they have grain size curves from coarse skewed, to symmetrical and fine skewed. Modern sands have graphic kurtosis with positive value, ranging from 0.74 to 1.54, so being platykurtic to leptokurtic.

According to Folk (1974), the modern sand samples analyzed are classified as sandy gravels to gravelly sands, with the exception of the sample R1 which plots to the field of gravelly muddy sand.

4.2 Mineralogy and Petrology

The powder X-ray diffraction semiquantitative mineralogical composition of the modern sand samples is shown in Table 3. The petrographical classification adopted is that of Pettijohn (1957) and

Table 3. Mineralogical composition (wt. %) of the modern sands analyzed.

Sample	Q	Pl	Kf	M	Am	Px	Grt	Cc	Q _n	F _n	M _n
E1	22	23	49	tr	6	nd	nd	tr	23	77	0
E2	19	33	nd	47	nd	nd	1	nd	19	81	0
E3	55	23	11	tr	10	nd	1	nd	62	38	0
E4	33	37	20	7	nd	2	nd	1	34	59	7
E5	37	49	4	6	2	nd	2	nd	39	55	6
E6	44	26	5	9	7	2	nd	7	52	37	11
E7	61	31	4	3	1	nd	nd	nd	62	35	3
X1	30	18	6	7	33	2	4	nd	53	4	43
A1	45	25	9	4	12	1	1	3	54	41	5
S1	59	13	24	5	nd	nd	nd	nd	58	37	5
S3	17	29	4	6	43	nd	nd	nd	30	60	10
S4	27	42	8	1	19	3	nd	nd	35	64	1
F1	13	63	3	5	15	tr	nd	nd	16	80	4
F2	39	41	9	4	3	3	2	nd	43	53	4
F3	33	40	21	4	3	nd	nd	nd	34	62	4
N1	51	35	8	4	nd	2	nd	nd	52	44	4
D1	54	20	20	3	2	2	nd	1	56	41	3
R1	21	33	15	3	21	1	6	nd	29	67	4
R5	6	66	8	14	3	1	2	nd	7	78	15
G1	57	19	9	4	9	2	nd	nd	64	31	5

Q=quartz, Pl=plagioclase, Kf=alkali feldspars, M=micas including chlorite, Am=amphibole, Px=pyroxene, Grt=garnet, Cc=calcite, Q_n=normalized percentage of quartz, F_n=normalized percentage of total amount of feldspars, M_n=normalized percentage of micas, tr=traces and nd=not detected.

Stewart et al. (1959), shown on figure 3. These authors use the percentages of quartz, total feldspars and micas, avoiding the use of rock fragments, thus making this scheme suitable for bulk X-ray analyses.

In the petrographical classification scheme adopted in this study, the term greywacke is used for sandstones rich in micaceous material. Depending though on the textural examination of the samples which revealed that they are poor in muddy matrix, the term phyllarenites should be adopted according to Folk (1974). Accessory minerals which participate in the assemblage of the samples with percentages greater than 3%, are included as prefixes to the rock naming.

In the modern sand samples analyzed the quartz content varies significantly, ranging from 6% to 61%. The same variation width is observed also in the plagioclase content (13-66%) and the alkali feldspar content (3-49%), with the mica content being also diverse (1-47%). Accessory ferromagnesian minerals (amphiboles and pyroxenes), along with detrital garnet and calcite, are almost always present in the composition of the above samples, sometimes in great amounts.

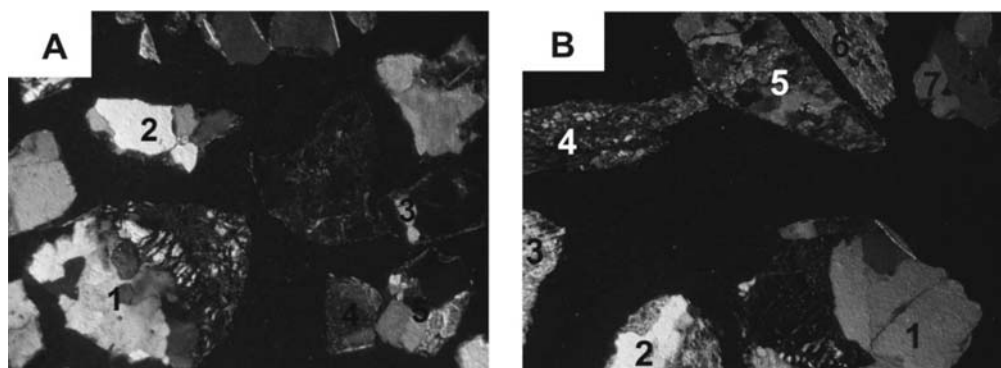


Fig: 4: A) Microphotograph of fraction 1Φ from sample R1. 1=rock fragment with undulatory quartz, biotite and garnet, 2=rock fragment with undulatory quartz and biotite, 3=rock fragment with quartz and biotite crystal showing extinction, 4=monocrystalline biotite and 5=rock fragment with quartz and amphibole. Nicol+. B) Microphotograph of fraction 0Φ from sample G1. 1=rock fragment with undulatory quartz and garnet, 2=rock fragment with undulatory quartz, fine biotite and fine white mica, 3=fragment with fine white mica, 4=rock fragment with biotite and quartz, 5=polycrystalline fine quartz with minor white mica, 6=muscovite fragment and 7=polycrystalline quartz.

All of the samples presented in this study are mineralogically immature according to Weller (1960) since they contain feldspars, ferromagnesian and heavy minerals (i.e. micas, amphibole, pyroxene and garnet). Their high content in lithic fragments and feldspars, is indicative of an adjacent source of the clastic load (Tucker, 2001). From the petrographic examination of the samples it is obvious that the modern sand samples demonstrate controversial composition. This can be attributed to rapid erosion and mixing of sand populations from different but adjacent sources.

According to petrographical classification scheme adopted in this study, the samples may be distributed under seven clans of rocks, namely: A) Arkose: samples E2, E4, E5, A1, S1, F1 and D1, all being rich in feldspars. B) Amphibole arkose: samples E1, E3, E6, E7, S3, F3, N1 and G1 due to their content in amphiboles and feldspars. C) Pyroxene amphibole arkose: samples S4 and F2. D) Garnet amphibole arkose: only the sample R1 is included as being rich in amphibole and garnet. E) Amphibole greywacke: the sample R5 due to its content in amphibole and mica and F) Garnet amphibole subgraywacke: X1 is the only member of this clan, being rich in amphibole and moderately rich in mica.

From the polarized microscopy study (Fig. 4) it is found that the assemblage of the 1Φ fraction of samples R1 and G1 is mainly constituted of monocrystalline and polycrystalline quartz, plagioclase always altered to sericite, few alkali feldspar usually found as orthoclase and individual euhedral crystals of muscovite and biotite or along with quartz. Quartz is present with undulatory extinction and when present in fine quartzose aggregates it shows characteristic lobe sutures. Single crystals of quartz and feldspar are generally angular to subangular. Opaque minerals are always present in small amounts. Rock fragments are generally subangular to subrounded and composed of quartz, biotite, muscovite, amphibole, plagioclase, epidote, kyanite, sillimanite, orthopyroxene and zoisite. Other accessory minerals found are garnet and kyanite in single euhedral crystals and single crystals of orthopyroxene and rutile.

In the fraction of 2Φ the amount of rock fragments decreases and they become more angular, maintaining though their mineral constitution. This fraction is rich in single angular to subangular crystals of muscovite, orthopyroxene, epidote, biotite, kyanite, plagioclase (altered in sericite), quartz,

orthoclase, clinopyroxene, garnet, rutile and some amphibole. Fraction 3Φ is mainly constituted of single angular crystals of the above mentioned minerals, plus minor amounts of zoisite.

5. Discussion

The samples analyzed in general demonstrate unimodal patterns of grain size distribution, except samples E1, E2, E5, E6, X1, S1 and S3 with bimodal pattern. Samples F2 and D1 are moderately sorted, R1 is very poorly sorted, whereas the rest of the samples are poorly sorted. The previous designates them as being immature to submature (Folk, 1974). Folk (1974) and Tucker (2001) interpret this feature as being distinctive of sediments accumulated in loci of the source (rapid deposition), or the current action was weak (i.e. detrital material deposited from a viscous flow, such as a mud flow). The above acceptance also implies that these sediments were deposited under intense to mild tectonic activity (Folk, 1974). Taira and Scholle (1979) studied the origin of bimodal sands in modern environments and found that this feature of sediments in fluvial channels could be attributed to the mixing of two sorting processes, which have different sorting tendencies.

According to Friedman (1961) all samples are fluvial deposits. Fuchtbauer and Muller (1970) suggest that fluvial sediments demonstrate $\sigma_1 > 1.2\Phi$ (or sometimes $> 1.3\Phi$) and $Sk_1 < 1$ (rarely > 1), whereas flood plain sediments demonstrate mostly $\sigma_1 > 2\Phi$ and always $Sk_1 < 1$. This rule is not always followed by the samples studied. In general, the samples studied are poor in mud content (except sample R1), so they have arenitic character.

From the petrographic analysis of the samples it is found that quartz is present in all samples, but its content varies greatly. Its presence is due to its abundance in the surrounding metamorphosed rocks and granites and to its mechanical resistance (Blatt, 1992). When plotting the values acquired for inclusive graphic skewness versus the quartz content, a general trend is obvious with quartz content diminishing with increasing skewness. This is indicative that the bulk of the quartz content is accumulated in the coarse fraction of the sediment. Blatt et al. (1972) consider the mean size of detrital quartz to be approximately 2Φ in sandstones. The texture of the quartzose rock fragments, as revealed from the polarized microscopy, is indicative of a metamorphic gneissic and acid plutonic source: Quartz crystals show undulatory extinction and intercrystalline suturing in polycrystalline grains. Also, assuming a first-cycle origin of the modern sands, the fine monocrystalline quartz grains must have originated from foliated metamorphic rocks (Blatt et al., 1972).

In the modern sands, the content of feldspars follows an increasing trend along with the increase in the values of inclusive graphic skewness, showing that the former mainly contribute to the finer fractions of the samples. According to Blatt et al. (1972) the most altered feldspars in feldspathic sediments are the calcic ones and the freshest are the potassic, a general rule that seems to apply to all the samples studied. According to Pittman (1969) feldspar grains diminish in size by fracture along twin crystal planes, as they are transported in streams of high gradient. In the samples studied, feldspars do accumulate in the finer sand fractions but they also contribute to the coarser ones; this observation also favours the assumption of the accumulation of these sediments near their source.

Micas almost always contribute to the assemblage of the samples but in minor amounts, except sample R1 where it attributes a wacke character. Their abundance is due to the mica presence in the metamorphic parent rocks. Chlorite was also detected in traces in some of the samples along with some kaolinite. Their presence is associated with the alteration of micas and feldspars, respectively.

Detrital calcite was detected in some samples, its content ranging from traces to 7%. This can be attributed to minor contribution in carbonate clastic load from the carbonate rocks outcropping in the

Vertiskos Unit. Pyroxene when detected, always participate as a minor constituent of the samples analyzed. Garnet is a more common accessory mineral in the modern sands. The same is also true for amphiboles. All the three previous mentioned minerals are indicative of a metamorphic source and belong to the metastable group of heavy minerals (Folk, 1974). Morton and Johnsson (1993) showed that the abundances of garnet and pyroxene tend to decline with increased alluvial storage. Morton and Hallsworth (1999) consider heavy mineral assemblages in sandstones to be affected by physical sorting, mechanical abrasion and dissolution. These authors also note that source-area weathering does not significantly affect the diversity of heavy mineral suites prior to incorporation of sediment into the transport system, with the degree of enrichment of stable heavy minerals being greatest in transport-limited erosional regimes.

Suttner et al. (1981) and Suttner and Dutta (1986) correlated the framework composition and compositional maturity of fluvial sandstones with the climate setting, the more feldspathic (immature) being deposited near the source under a warm and dry climate and the more quartzose and mature being deposited under a wet climate. Girty (1991) showed that under semi-arid to mediterranean (hot summer) climate plutonic sands produced are less altered than under temperate and humid. Our samples due to their quartz content, may be considered to have been deposited under a wet climate, where chemical weathering readily acts, whereas according to von Eynatten (2003) the samples studied were deposited under a semi-arid climate with the effect of strong relief. The feldspar and heavy mineral content is more in agreement with the latter hypothesis (temperate and seasonable climate with the action mainly of physical weathering). Tsirambides (1999) also showed that the presence of amphibole and pyroxene in modern sediments is correlated with mild climatic conditions. The presence of unstable minerals (i.e. pyroxene, plagioclase) along with semistable ones (i.e. amphibole, orthoclase) also indicate the absence of chemical weathering (Garzanti et al., 2004).

According to Blatt et al. (1972) all the modern sand samples constitute a distinct petrologic province, correlated by age (modern), origin (the metamorphic basement) and distribution. This province could be furthermore mainly characterized by an amphibole association which includes all the modern sand samples.

6. Conclusions

The majority of the samples are coarse grained gravelly sands.

All samples are poor in mud content, demonstrate arenitic character and are texturally and mineralogically immature to submature. They have been deposited in a fluvial environment.

The sorting degree of the samples, along with their composition, is distinctive of sediments accumulated near the source under intense to mild tectonic activity. Especially, the bimodality of grain size in some of the samples is indicative of rapid weathering and mixing of different detrital populations.

Their assemblage is constituted mainly from quartz, feldspars and micas, along with accessory minerals of metamorphic and granitic origin. The studied sands are feldspathic and rich in heavy minerals. The latter feature verifies that these sands are deposited near their source. All the samples have as source the rocks comprising the Vertiskos Unit.

The mineral abundances described above designate Vertiskos Unit as being rapidly weathered under a seasonably wet and warm climate, with intense physical weathering. It is noticed a general trend of the samples becoming more quartzose and depleted in accessory minerals as they are transported from their source.

All the samples constitute a distinct sedimentary petrologic province on the Unit, comprised of an amphibole-garnet association.

7. References

- Blatt, H., 1992. *Sedimentary petrology*, New York, Freeman & Co, 250pp.
- Blatt, H., Middleton, G. & Murray, R., 1972. *Origin of sedimentary rocks*, New Jersey, Prentice-Hall Inc., 634pp.
- Chatzidimitriadis, E., Tsirambides, A. & Theodorikas, S., 1993. Clay mineral abundance of shales and slates from some Greek regions through geologic time. *Proc. Academy of Athens*, 68, 144-161.
- Dickinson, W.R., 1970. Interpreting detrital modes of greywacke and arkose. *J. Sed. Petrol.*, 40, 695-707.
- Dickinson, W.R., 1985. Interpreting provenance relations from detrital modes of sandstones. In: Zuffa, G.G. (Ed.), *Provenance of Arenites*. Reidel Publ, Dordrecht, 333-361pp.
- Ehlers, E.G. & Blatt, H., 1982. *Petrology: Igneous, sedimentary and metamorphic*, San Francisco, W.H. Freeman and Co, 732pp.
- von Eynatten, H., 2003. Petrography and chemistry of sandstones from the Swiss Molasse Basin: An archive of the Oligocene to Miocene evolution of the Central Alps. *Sedimentology*, 50, 703-724.
- Folk, R.L. 1974. *Petrology of sedimentary rocks*, Hemphill Publ. Co., Texas, 184pp.
- Friedman, G.M., 1961. Distinction between dune, beach and river sands from their textural characteristics. *J. Sed. Petrol.*, 31, 514-529.
- Fuchtbauer, H., & Muller, G., 1970. *Sediment – petrologie. Teil II Sedimente und sedimentgesteine*. E. Schweizerbart'sche Verlagsbuchhandlung, 726pp.
- Garzanti, E., Vezzoli, G., Ando, S., France-Lanord, C., Singh, S.K. & Foster, G., 2004. Sand petrology and focused erosion in collision orogens: The Brahmaputra case. *Earth Plan. Sci. Let.*, 220, 157-174.
- Georgiadis, I.K., 2006. *Petrological and geochemical study of the Quaternary clastic sediments of Herso Basin, Kilkis Prefecture*. M.Sc. Thesis, Aristotle University, Thessaloniki, 127pp.
- Georgiadis, I.K., Tsirambides, A., Kassoli-Fournaraki, A. & Trontsios, G., 2007. Petrology and provenance study of the Quaternary clastic sediments from Herso Kilkis (Macedonia, Greece). *Bull. Geol. Soc. Greece*, 40(2), 747-758.
- Girty, G.H., 1991. A note on the composition of plutoniclastic sand produced in different climatic belts. *J. Sed. Petrol.*, 61(3), 428-433.
- Hower, J., Eslinger, E.V., Hower, M.E. & Perry, E.A., 1976. The mechanism of burial metamorphism of argillaceous sediment. 1. *Geol. Soc. Amer. Bull.*, 87, 727-757.
- Kourou, A.N., 1991. *Lithology, geochemistry, tectonics and metamorphosis of a part of the Western part of Vertiskos group. The area NE of the Lake of Agios Vasilios (Koronia)*, PhD Thesis, Aristotle University, Thessaloniki, 461pp.
- Moore, D.M. & Reynolds, R.C., 1997. *X-ray diffraction and the identification and analysis of clay minerals*, 2nd Ed, Oxford University Press, Oxford, 378pp.
- Morton, A.C. & Johnsson, M.J., 1993. Factors influencing the composition of detrital heavy mineral suites in Holocene sands of the Apure River drainage basin, Venezuela. In: Johnsson, M.J. & Basu, A. (Eds.), *Processes controlling the composition of clastic sediments*. *Geol. Soc. Am., Spec. Pap.* 284, 171-185.
- Morton, A.C. & Hallsworth, C.R., 1999. Processes controlling the composition of heavy mineral assemblages in sandstones. *Sed. Geol.*, 124, 3-29.
- Mountrakis, D., 2002. Tectonic evolution of the Hellenic orogen: Geometry and kinematics of deforma-

- tion. *Bull. Geol. Soc. Greece* 34(6), 2113-2126.
- Pettijohn, F.J., 1957. *Sedimentary rocks*, 2nd Ed. Harper & Row, New York, 718 p.
- Pettijohn, F.J., Potter, P.E. and Siever, R., 1987. *Sand and sandstone*, New York, Springer-Verlag, 618pp.
- Pittman, E.D., 1969. Destruction of plagioclase twins by stream transport. *J. Sed. Petrol.*, 39, 1432-1437.
- Reineck, H.-E. & Singh, I.B., 1986. *Depositional sedimentary environments*, 2nd Ed., New York, Springer-Verlag, 551pp.
- Sidiropoulos, N., 1991. *Lithology, geochemistry, tectonics and metamorphosis of the Northwestern part of Vertiskos group. The area of Mountain Disoro (Kroussia), North of Kilkis*, PhD Thesis, Aristotle University, Thessaloniki, 592pp.
- Stewart, J.H., Williams, G.A., Albee, H.F., Raup, O.B. & Cadigan, R.A. 1959. Stratigraphy of Triassic and associated Formations in part of the Colorado Plateau region. *U.S.G.S. Bull*, 1046-Q, 98 p.
- Suttner, L.J., 1974. Sedimentary petrographic provinces: an evaluation. In: Ross, C.A. (Ed.), *Paleogeographic Provinces and Provinciality*, Special Publ., Soc. Econ. Paleontol. Mineral., vol. 21, 75-84pp.
- Suttner, L.J., Basu, A. and Mack, G.H., 1981. Climate and the origin of quartz arenites. *J.Sed. Petrol.*, 51, 1235-1246.
- Suttner, L.J. & Dutta, P.K., 1986. Alluvial sandstone composition and paleoclimate, I. Framework mineralogy. *J. Sed. Petrol.*, 56(3), 329-345.
- Taira, A. & Scholle, P.A., 1979. Origin of bimodal sands in some modern environments. *J. Sed. Petrol.*, 49(3), 777-786.
- Tsirambides, A.E., 1997. Study of the Quaternary sediments of Doirani basin. *Ann. Geol. Pays Hell.* 37, 907-919.
- Tsirambides, A.E., 1999. Mineralogical composition of soils from Platamonas Pierias (Macedonia, Greece). *Bull. Geol. Soc. Greece*, 33, 99-104.
- Tsirambides, A.E., 2008. *Sedimentary rocks*, Thessaloniki, Giahoudi Publ., 317pp.
- Tucker, M.E., 2001. *Sedimentary petrology*, 3rd Ed., Oxford, Blackwell, 262pp.
- Weller, J.M., 1960. *Stratigraphic principles and practises*, New York, Harper & Row, 725pp.
- Weltje, G.J., 2004. A quantitative approach to capturing the compositional variability of modern sands. *Sedimentary Geology* 171, 59-77.

INSIGHTS INTO HYDROTHERMAL ACTIVITY IN THE ITI OPHIOLITE (CENTRAL GREECE)

**Karipi, S.¹, Tsikouras, B.¹, Rigopoulos, I.¹, Hatzipanagiotou, K.¹,
and Pomonis, P.²**

¹ University of Patras, Department of Geology, Section of Earth Materials, 26500 Patras, Greece, skaripi@upatras.gr, v.tsikouras@upatras.gr, rigopoul@upatras.gr, k.hatzipanagiotou@upatras.gr

² University of Athens, Department of Geology and Geoenvironment, 15784 Athens, Greece, ppomonis@geol.uoa.gr

Abstract

Scarce intensely epidotised doleritic dykes, up to 1.5 m thick, penetrate in sharp contact serpentinised peridotites of the remnant ophiolite nappe of the Iti ophiolite. They are generally whitish rocks characterised by distinct and irregularly distributed, olive-green areas within the rock mass. Petrographic evidence reveals that their assemblage is dominated by quartz and epidote. Albite, chlorite and titanite occur as accessory phases. Minor opaque minerals are represented by magnetite, pyrite and chalcopyrite, as well as relic Cr-spinel. The mineral assemblage of the studied rocks comprises replacement products of the original phases under greenschist facies conditions. Moreover, the almost exclusive bi-mineralic (quartz + epidote) assemblage of the altered doleritic rocks, as well as obliteration of the original doleritic textures imply extensive recrystallisation, controlled by hydrothermal circulation. The compositions of the phases in these dykes mark the most alteration-resistant chemical components that have the potential to remain in their original associations, during such extensive recrystallisation.

Key words: *epidotised dykes, dolerite, hydrothermal activity, Iti ophiolite, Central Greece.*

1. Introduction

Ophiolites provide significant information on the geological, petrological and hydrothermal processes taken place beneath ocean ridges. A major difference between hydrothermal alteration in ophiolites and modern oceanic crust is that the former invariably exhibit evidence of extensive epidotisation relatively to the latter. Various aspects of epidosite-type alteration have been described worldwide from the Troodos (Bettison-Varga et al., 1992; Gillis, 2002; Cann and Gillis, 2004; Jowitt et al. 2007), the Semail (Stakes and Taylor, 1992), the Josephine (Alexander et al., 1993), the Tonga (Banerjee and Gillis, 2001) and the Mirdita (Muehlenbachs et al., 2004) ophiolite complexes. Several studies have also been devoted on the hydrothermal alteration in the Pindos and Othris ophiolites of Greece (Valsami, 1990; Valsami and Cann, 1992; Valsami-Jones and Cann, 1994; Valsami-Jones and Ragnarsdóttir, 1997).

The aim of this study is to describe the evolution of hydrothermally altered dolerite dykes in the Iti ophiolite.

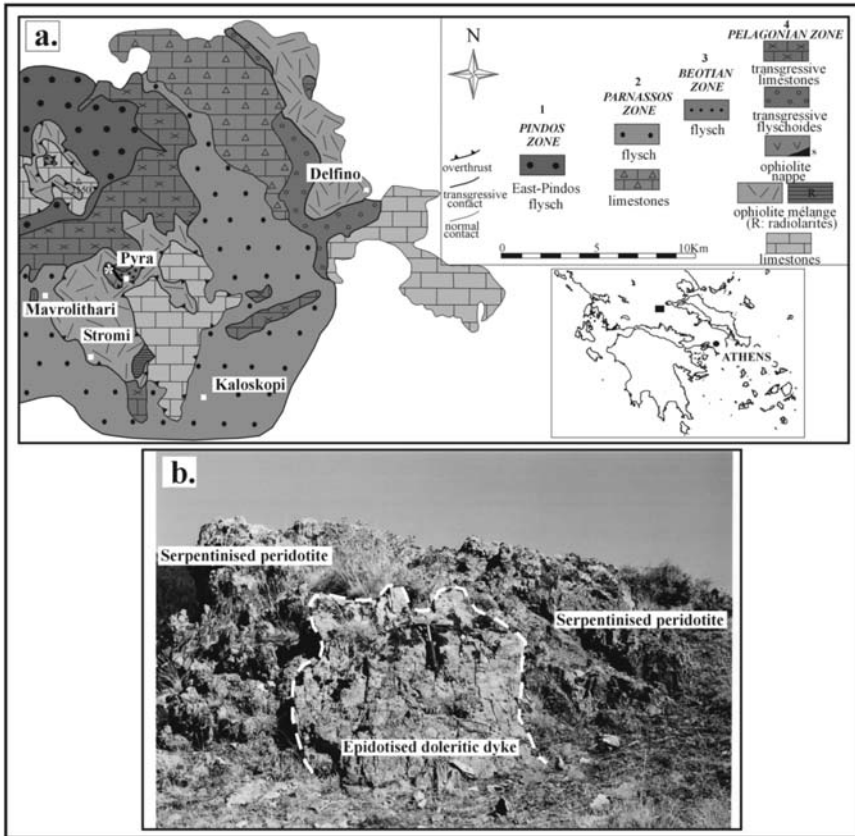


Fig. 1: (a): Simplified geological map of the Iti Mountain; asterisk (*) marks the location of the epidotised doleritic dykes, (b) outcrop of the epidotised doleritic dyke within serpentinised peridotite of the remnant ophiolite nappe.

2. Geological setting

The Iti Mountain lies to the south of Othrys Mountain and the Sperchios River, in continental Central Greece. It belongs to the “Pelagonia terrane” (Stampfli, 1996; Stampfli et al., 1998) a carbonate platform, equivalent to the “Internal carbonate platform” of Papanikolaou (1989). The geological structure of the Iti Mountain includes four westward verging tectono-stratigraphic zones, representing different paleotectonic domains. They comprise, from west to east: the Pindos, Parnassos, Beotian and Pelagonian zones (Wigniolle, 1977). The Iti Mountain (Fig. 1) is composed of a stack of nappe units. From bottom to top, they include: (1) the flysch of the East-Pindos syncline, (2) Mesozoic platform carbonates along with flysch of the Parnassos zone, (3) the Beotian flysch, (4) the Jurassic platform carbonates of the Pelagonian zone, and the overthrust ophiolite unit (Celet, 1976; Celet et al., 1977; Richter et al., 1997). The latter includes a lower ophiolite mélangé, which is locally, tectonically overlain by a sub-ophiolitic metamorphic sole (s). Both formations are overthrust by a remnant ophiolite nappe of upper mantle tectonites (harzburgite and lherzolite; Karipi, 2004; Karipi et al., 2006; Karipi et al., 2008). The ophiolite unit is transgressively overlain by Upper Cretaceous formations (Celet, 1962; Wigniolle, 1977).

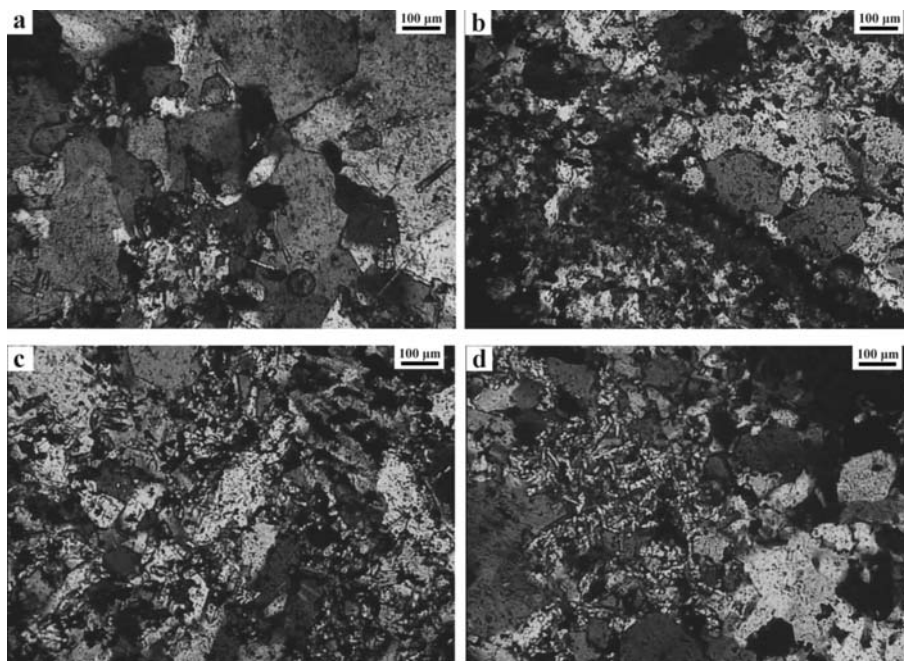


Fig. 2: (a-d): Photomicrographs (XPL) of epidotised doleritic dyke from Iti showing the main mineral constituents, quartz (qz) and epidote (ep), developing granoblastic (qz, ep) and tiny, embryonic crystals (ep).

Rare epidotised dykes, up to 1.5 m thick, trending NNE-SSW crosscut variably serpentinised peridotite, in an area northwest of the Pyra village (Fig. 1a; Mavri Tsouma). The epidotised dykes are in sharp contact with the peridotite host that belongs to the remnant ophiolite nappe (Fig. 1b). They are generally whitish rocks, characterized by distinct and irregularly distributed olive-green patches due to the presence of epidote.

3. Petrography

The epidotised dolerite is mainly composed of quartz, epidote and accessory albite, chlorite and titanite. Minor opaque minerals are represented by magnetite, pyrite, chalcopyrite and relic Cr-spinel. Original textures are obliterated by granoblastic, poikiloblastic and locally cataclastic textures. Typically poikiloblastic epidote forms in a granoblastic matrix of quartz and epidote crystals of variable size (Figs. 2a, b); epidote also shows aggregates of tiny, embryonic crystals filling the quartz interstices (Figs. 2c, d). The poikiloblastic epidote crystals are either homogeneous or inhomogeneous with irregularly distributed rich and poor in pistacite component areas (Figs 3a, b). Local relics of dolerite with subophitic plagioclase and altered clinopyroxene have been observed.

4. Analytical Methods

Electron microanalyses were carried out at the Laboratory of Electron Microscopy and Microanalysis, University of Patras. All elements were analyzed by an electron-dispersive X-Rays (EDX) using EDS and WDS detectors attached to a JEOL JSM-6300 SEM. Operating conditions were accelerating voltage 15 kV and beam current 3.3 nA with 4 µm diameter beam. EDS and WDS spec-

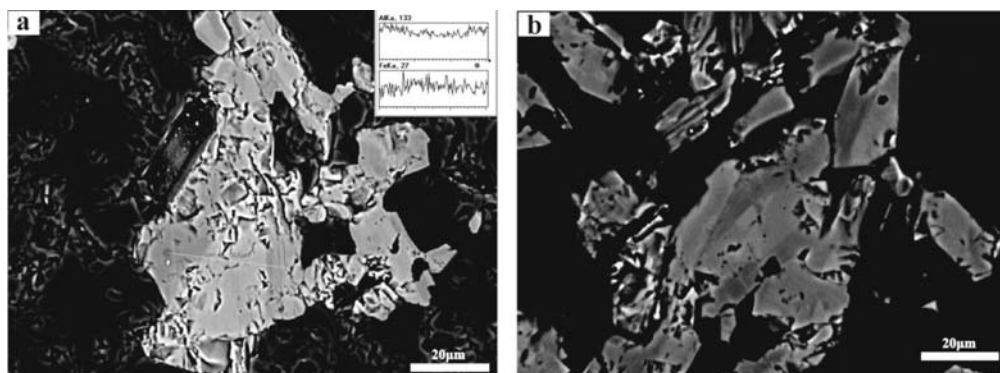


Fig. 3: Back-scatter-electron images (SEM) of inhomogeneous epidote crystals in epidotised doleritic dykes. In (a), line-scan analysis across the different compositions mainly shows variability in Al and Fe contents.

trum information with the ZAF correction software information was used. The total counting time was 60 sec and dead-time 40 %. Synthetic oxides and natural minerals were utilized as standards for our analyses. Detection limits are ~0.1 % and an accuracy better than 5 % was obtained.

5. Mineral Chemistry

Representative microanalyses of epidote, chlorite and plagioclase from the epidotised doleritic dykes of Iti are given in Table 1. The analysed epidotes show variable contents of Fe^{3+} (stoichiometric calculations assuming total Fe as Fe^{3+}) and Al^{VI} (see Table 1 and Fig. 3a). Pistacitic (Ps) contents range from 11.9% to 34.4% (Table 1).

The analysed chlorites plot in the pycnochlorite and clinochlore fields on the classification diagram of chlorites (after Hey, 1954; not shown) and they display a rather broad $\text{Fe}^{\text{I}}/(\text{Fe}^{\text{I}}+\text{Mg})$ variation (Table 1).

The analysed plagioclases are albites with An contents ranging up to 6.8 and negligible Or (Table 1).

6. Hydrothermal alteration of the Iti ophiolite: Discussion and Conclusions

Hydrothermal systems beneath ocean ridges have been summarized by Alt (1995). Hydrothermal circulation beneath ocean ridges is a fundamental process governing the heat transfer and chemical compositions of ocean crust. It was generally considered that penetration of seawater into fast-spread ocean crust is rapidly decreased beneath sheeted dike complex due to closing of fractures by precipitation of minerals (Lister, 1974; Mevel and Cannat, 1991). Chloritisation, sericitisation, silicification, and pyritisation are well-known alteration features associated with volcanogenic massive sulphide ore deposits related to ophiolites and other submarine and non-oceanic contexts (Honnorez et al., 1998). Our knowledge of the deep portions of hydrothermal upflow zones only comes from ophiolites, where epidotes are thought to indicate the root zones of upflow zones at the base of the sheeted dyke complex (Richardson et al., 1987; Schiffman et al., 1987; Harper et al., 1988; Nehlig et al., 1994). Epidotes are well documented in suprasubduction-zone ophiolites (Richardson et al., 1987; Schiffman et al., 1987; Harper et al., 1988; Nehlig et al., 1994) whereas they are rare in rock collections from modern oceanic setting. According to Banerjee et al. (2000), epidotes discovered from the Tonga forearc representing the first documented suite recovered from a modern oceanic set-

Table 1. Chemical variations in representative epidotes, chlorites and plagioclases from epidotised doleritic dykes of Ili.

Epidote	Chlorite							Plagioclase						
	I618/1a	I618/1b	I618/3b	I618/3c	I618/38	Sample	I618/5	I618/12	I618/20	Sample	I618/6	I618/14	I618/44	
SiO ₂	38.76	38.81	38.27	37.49	36.84	SiO ₂	28.02	27.56	32.84	SiO ₂	68.85	68.43	66.83	
TiO ₂	0.42	-	-	-	0.50	TiO ₂	-	0.02	0.17	TiO ₂	-	-	-	
Al ₂ O ₃	26.48	30.02	26.08	22.17	19.82	Al ₂ O ₃	17.21	19.13	20.88	Al ₂ O ₃	19.00	19.16	21.82	
Fe ₂ O ₃	9.60	6.24	10.88	15.30	16.09	Cr ₂ O ₃	0.17	-	-	Fe ₂ O ₃ ^t	0.32	0.33	0.83	
Y ₂ O ₃	-	-	-	-	-	FeOt	19.59	23.72	10.26	MnO	-	-	-	
La ₂ O ₃	-	-	-	-	-	MgO	18.46	16.77	24.70	MgO	-	0.39	-	
MnO	-	-	-	-	-	MnO	0.16	0.59	0.22	CaO	0.04	0.07	1.29	
CaO	23.63	23.96	23.22	23.22	25.06	CaO	0.12	0.29	0.27	Na ₂ O	11.80	11.53	9.82	
Na ₂ O	-	-	0.30	0.09	-	Na ₂ O	0.20	-	0.31	K ₂ O	-	0.12	-	
K ₂ O	-	-	-	-	-	K ₂ O	0.10	0.02	-	Cr ₂ O ₃	-	-	-	
Total	98.89	99.03	98.75	98.27	98.31	Total	84.03	88.10	89.65	Total	100.01	100.03	100.59	
<i>Structural formulae on the basis of 25 O</i>														
Si	6.014	5.937	5.976	5.992	5.962	Si	5.985	5.732	6.170	Si	3.008	2.991	2.904	
Al ^{IV}	-	0.063	0.024	0.008	0.038	Al ^{IV}	2.015	2.268	1.830	Al	0.977	0.986	1.117	
	6.014	6.000	6.000	6.000	6.000		8.000	8.000	8.000	Ti	-	-	-	
Al ^{IV}	4.838	5.345	4.772	4.165	3.739	Al ^{IV}	2.314	2.417	2.790	Fe ³⁺	0.011	0.011	0.027	
Ti	0.049	-	-	-	0.061	Ti	-	0.003	0.024		3.996	3.988	4.048	
Fe ³⁺	1.120	0.720	1.280	1.840	1.960	Fe ²⁺	3.499	4.125	1.612	Mn	-	-	-	
	6.007	6.065	6.052	6.005	5.760	Cr	0.029	-	-	Mg	-	0.025	-	
Mn	-	-	-	-	-	Mn	0.029	0.104	0.035	Ca	0.002	0.003	0.060	
Ca	3.928	3.927	3.885	3.976	4.345	Mg	5.878	5.199	6.918	Na	0.999	0.977	0.828	
Na	-	-	0.091	0.028	-	Ca	0.027	0.065	0.054	K	-	0.007	-	
K	-	-	-	-	-	Na	0.083	-	0.113	Cr	-	-	-	
Y ³⁺	-	-	-	-	-	K	0.027	0.005	-		1.001	1.012	0.888	
La ³⁺	-	-	-	-	-	Sum.Cat.	19.886	19.918	19.546	Sum.Cat.	4.997	5.000	4.936	
	3.928	3.927	3.976	4.004	4.345					Ab	99.8	99.0	93.2	
Sum.Cat.	15.949	15.992	16.028	16.009	16.105	Fet/(Fet+Mg)	0.37	0.44	0.19	An	0.2	0.3	6.8	
Ps	18.8	11.9	21.2	30.6	34.4	Or	-	-	-	Or	-	0.7	-	

ting that may represent a modern analogue for the tectonic setting in which suprasubduction-zone ophiolites formed.

The Iti epidiosites are characterised by metasomatic replacement of primary igneous minerals by granoblastic and poikiloblastic assemblages of quartz + epidote \pm albite \pm chlorite \pm titanite \pm magnetite \pm sulfides. Mineral chemistry reveals that epidote, chlorite and plagioclase from the Iti epidiosites have a range in composition similar to that of ophiolite-hosted epidiosites (e.g. Schiffman and Smith, 1988; Nehlig et al. 1994) and Tonga forearc ones (Banerjee et al., 2000). The above-mentioned mineral assemblage indicates that the Iti dolerites underwent hydrothermal alteration under greenschist facies conditions. According to Banerjee et al., (2000), epidiosites formed by pervasive alteration of basalt at greenschist facies conditions and at high water-rock ratios. The Iti epidiosites could be characterised as true epidiosites as they are mainly composed of quartz and epidote with minor albite and other phases. According to Cowan (1989) and Schiffman et al. (1990), the transformation of basalt to a true epidiosite involves considerable chemical change. On the scale of an epidiosite zone, the sheeted dykes are consistently depleted in Na and K and are enriched in Si. The extent of Mg and Ca mobility is more variable, such that chlorite-rich epidiosites are enriched in Mg and depleted in Ca, whereas chlorite-poor rocks show the opposite trends. In terms of chemical components, the Iti epidiosites are dominated by quartz and Ca-rich minerals such as epidote \pm titanite whereas they contain only minor amounts of albite and Mg(Fe)-rich minerals as chlorite. This almost bi-mineralic assemblage (quartz + epidote) of the Iti epidiosites could imply that the hydrothermal fluids that metasomatically altered precursor dolerite were depleted in Mg and alkalis while enriched in Si and Ca. According to other well-documented ophiolitic epidiosites (e.g. Richardson et al., 1987; Nehlig et al., 1994), these highly focused upflow hydrothermal fluids that circulated in the Iti ophiolite caused intensive alteration at the deeper portion of the dolerite dyke intruded the upper mantle peridotites. The irregular distribution of variable Ps components in the epidote crystal is possibly related to changes of the composition of the fluid phase and different fluid pulses that likely were evolving in composition as they were interacting with the peridotite and the dolerite. Hence, it is probable that the fluid phase was recirculated through the serpentinite, slightly adjusting its composition during chemical modifications that were taking place due to fluid-rock interaction.

The Iti epidiosite could be thus interpreted as has been formed via extreme geochemical and mineralogical transformations at temperatures up to 400°C within reaction zones and deep hydrothermal discharge zones (epidiosite zones). These conditions are also consistent with the frame of epidote formation, as according to Schiffman (1995) and Bird and Spieler (2004), hydrothermal epidote from ophiolite sequences forms during intense fluid-rock interaction at temperatures between 300 and 400°C.

7. References

- Alexander, R.J., Harper, G.D., and Bowman, J.R., 1993. Oceanic faulting and fault-controlled subseafloor hydrothermal alteration in the sheeted dike complex of the Josephine Ophiolite, *Journal of Geophysical Research*, 98, 9731–9759.
- Alt, J.C., 1995. Subseafloor processes in mid-ocean ridge hydrothermal systems. In S. Humphris, J. Lupton, L. Mullineaux and R. Zierenberg (eds.), *Seafloor Hydrothermal System: Physical, Chemical, Biological and Geological Interpretation. Geophysical Monograph*, 91, 85–114. American Geophysical Union, Washington D. C.
- Banerjee, N.R., and Gillis, K.M., 2001. Hydrothermal alteration in a modern suprasubduction zone: The Tonga forearc crust, *Journal of Geophysical Research*, 21, 737–750.
- Banerjee, N.R., Gillis, K.M., and Muehlenbachs, K., 2000. Discovery of epidiosites in a modern oceanic

- setting, the Tonga forearc, *Geology*, 28(2), 151-154.
- Bettison-Varga, L., Varga, R.J., and Schiffman, P., 1992. Relation between ore-forming hydrothermal systems and extensional deformation in the Solea graben spreading center, Troodos ophiolite, Cyprus, *Geology*, 20, 987-990.
- Bird, D.K., and Spieler, A.R. 2004. Epidote in Geothermal Systems, *Reviews in Mineralogy and Geochemistry*, 56(1), 235-300.
- Cann, J., and Gillis, K., 2004. Hydrothermal insights from the Troodos ophiolite, Cyprus. In E.E. Davis and H. Elderfield (eds.), *Hydrogeology of the Oceanic Lithosphere*. 274-310, Cambridge University Press.
- Celet, P., 1962. Contribution à l'étude géologique du Parnasse-Kiona et d'une partie des régions méridionales de la Grèce continentale, *Annales Géologiques des Pays Helléniques*, 13, 446pp.
- Celet, P., 1976. À propos du mélange de type "volcano-sédimentaire" de l'Iti (Grèce méridionale), *Bulletin de la Société Géologique de France*, 18, 299-307.
- Celet, P., Ferrière, J., and Wigniolle, E., 1977. Le problème de l'origine des blocs exogènes du mélange à éléments ophiolitiques au Sud du Sperchios et dans le massif de l'Othrys (Grèce), *Bulletin de la Société Géologique de France*, 19(4), 935-942.
- Cowan, J.G., 1989. Geochemistry of reaction zone source rocks and black smoker fluids in the Troodos ophiolite, *Ph.D. Thesis*, University of Newcastle-upon-Tyne.
- Gillis, K.M., 2002. Root-zones of a fossil oceanic hydrothermal system exposed in the Troodos Ophiolite, *The Journal of Geology*, 110, 57-74.
- Harper, G.D., Bowman, J.R., and Kuhns, R.J., 1988. A field, chemical, and stable isotope study of seafloor metamorphism of the Josephine Ophiolite, California-Oregon, *Journal of Geophysical Research*, 93, 4625-4656.
- Hey, M.H., 1954. A new review on the chlorites, *Mineralogical Magazine*, 224, 277-298.
- Honnorez, J.J., Alt, J.C., and Humphris, S.E., 1998. Vivisection and autopsy of active and fossil hydrothermal alterations of basalt beneath and within the TAG hydrothermal mound. In P.M. Herzig, S.E. Humphris, D.J. Miller and R.A. Zierenberg (eds.), *Proceedings of the Ocean Drilling Program, Scientific Results*, Vol. 158.
- Jowitt, S.M., Jenkin, G.R., Coogan, L.A., Naden, J., and Chenery, S.R.N., 2007. Epidotes of the Troodos Ophiolite: A direct link between alteration of dykes and release of base metals into ore-forming hydrothermal systems? 9th Biennial SGA Meeting, Mineral Exploration and Research: Digging Deeper, 20th – 23rd August 2007.
- Karipi, S., 2004. The ophiolitic outcrops of Iti and Kallidromon. Geological study – Petrogenetic evolution – Geotectonic interpretation, *Ph.D. Thesis*, University of Patras, 417pp.
- Karipi, S., Tsikouras, B., and Hatzipanagiotou, K., 2006. The petrogenesis and tectonic setting of ultramafic rocks from Iti and Kallidromon Mountains, continental Central Greece: vestiges of the Pindos ocean, *Canadian Mineralogist*, 44(1), 267-287.
- Karipi, S., Tsikouras, B., Pomonis, P., and Hatzipanagiotou, K., 2008. Geological evolution of the Iti and Kallidromon Mountains (central Greece), focused on the ophiolitic outcrops, *Zeitschrift der Deutschen Gesellschaft für Geowissenschaften*, 159(3), 549-563.
- Lister, C.R.B., 1974. On the penetration of water into hot rock, *Geophysical Journal of Royal Astronomical Society*, 39, 465-509.
- Mevel, C., and Cannat, M., 1991. Lithospheric stretching and hydrothermal processes in oceanic gabbros from slowspreading ridges. In Tj. Peters et al. (ed.), *Ophiolite Genesis and Evolution of the Oceanic Lithosphere*, Ministry of Petroleum and Minerals, Sultanate of Oman, 293-312.

- Muehlenbachs, K., Banerjee, N.R., Dilek, Y., Furnes, H., and Shallo, M., 2004. Seafloor hydrothermal alteration of the crustal sequence of the Mirdita ophiolite, Albania. 32nd International Geological Congress, Florence, Italy, 20-28/8/2004.
- Nehlig, P., Juteau, T., Bendel, V., and Cotten, J., 1994. The rootzones of oceanic hydrothermal systems: constraints from the Semail ophiolite (Oman), *Journal of Geophysical Research*, 99, 4703–4713.
- Papanikolaou, D., 1989. Are the medial crystalline massifs of the Eastern Mediterranean drifted Godwanian fragments?, *Geological Society of Greece*, Special Publication, 1, 63-90.
- Richardson, C.J., Cann, J.R., Richards, H.G., and Cowan, J.G., 1987. Metal-depleted root zones of the Troodos ore-forming hydrothermal systems, Cyprus, *Earth and Planetary Science Letters*, 84, 243–253.
- Richter, D., Mihm, A., and Müller, C., 1997. Die pelagonischen Deckenreste auf dem Flysch des Ostpindos-Synklinorium (Pindos-Zone) westlich des Itri-Gebirges (Mittelgriechenland), *Zeitschrift der Deutschen Geologischen Gesellschaft*, 148(2), 237-246.
- Schiffman, P., 1995. Low grade metamorphism of mafic rocks. Geological Society of America, Special Paper 296.
- Schiffman, P., Bettison, L.A., and Smith, B.M., 1990. Mineralogy and geochemistry of epidotes from the Solea graben, Troodos ophiolite, Cyprus. In J. Malpas, E. Moores, A. Panayiotou, and C. Xenophontos (eds.), *Ophiolites: Oceanic Crustal Analogues*. Nicosia: Cyprus Geological Survey Department, pp. 673–684.
- Schiffman, P., and Smith, B.M., 1988. Petrology and oxygen isotope geochemistry of a fossil seawater hydrothermal system within the Solea Graben, Northern Troodos Ophiolite, Cyprus, *Journal of Geophysical Research*, 93, 4612-4624.
- Schiffman, P., Smith, B.M., Varga, R.J., and Moores, E.M., 1987. Geometry, conditions, and timing of off-axis hydrothermal metamorphism and ore-deposition in the Solea Graben, *Nature*, 325, 423-425.
- Stakes, D.S., and Taylor, H.P., 1992. The Northern Semail Ophiolite: an oxygen isotope, microprobe and field study, *Journal of Geophysical Research*, 97(7), 43-80.
- Stampfli, G.M., 1996. The Intra-Alpine terrain: A Paleotethyan remnant in the Alpine Variscides, *Eclogae Geologicae Helveticae*, 89(1), 13-42.
- Stampfli, G.M., Mosar, J., De Bono, A., and Vavassis, I., 1998. Late Paleozoic, Early Mesozoic Plate Tectonics of the Western Tethys, Geological Society of Greece, Special Publication, *Bulletin of the Geological Society of Greece*, 32(1), 113-120.
- Valsami, E., 1990. Geochemistry and petrology of hydrothermal discharge zones in the Pindos and Othris ophiolites, Greece, *Ph.D. Thesis*, University of Newcastle upon Tyne, 359pp.
- Valsami, E., and Cann, J.R., 1992. Evidence for the mobility of the rare earth elements in zones of intense hydrothermal alteration in the Pindos ophiolite, Greece. In L.M. Parson, B.J. Murton, and P. Browning (eds.), *Ophiolites and Their Modern Oceanic Analogues*, Geological Society of London, Special Publication, 60, 219-232.
- Valsami-Jones, E., and Cann, J.R., 1994. Controls on the Sr and Nd isotopic compositions of hydrothermally altered rocks from the Pindos ophiolite, Greece, *Earth Planetary Science Letters*, 125, 39-54.
- Valsami-Jones, E., and Ragnarsdóttir, K.V., 1997. Controls on uranium and thorium behaviour in ocean-floor hydrothermal systems: examples from the Pindos ophiolite, Greece, *Chemical Geology*, 135, 263-274.
- Wigniolle, E., 1977. Données nouvelles sur la géologie du massif de l'Itri (Grèce continentale), *Annales de la Société Géologique du Nord*, 47(3), 239-251.

MAGMA GENERATION AND MIXING IN THE EARLIEST VOLCANIC CENTRE OF SANTORINI (AKROTIRI PENINSULA). MINERAL CHEMISTRY EVIDENCE FROM THE AKROTIRI PYROCLASTICS

Kitsopoulos K.

*University of Leicester, Department of Geology, University Road, LE1 7RH Leicester, UK,
kitsopoulos.k@gmail.com*

Abstract

Santorini is a dominant expression of magma generation and subsequent volcanism in the Mediterranean area, where a calc-alkaline, high-alumina, basalt-andesite-dacite type of volcanism was expressed from eight centres. The volcanics of the Akrotiri peninsula are considered to be the products of the earliest (Pliocene-Pleistocene) volcanic centre. The present study has investigated the mineral chemistry of some major pyrogenic phenocrysts, such as plagioclase and Fe-Ti oxides, of the Akrotiri pyroclastics unit, which have undergone a notable zeolitization procedure. The results are compatible with magma mixing mechanism of a primitive mantle derived, saturated, of mafic composition component with silicic magma in shallow crustal depths.

Key words: *pyroclastics, plagioclase, Fe-Ti oxides, mineral chemistry, magma mixing, Santorini, Greece.*

1. Introduction

The petrographic and volcanological characteristics of volcanoclastic material are often thoroughly studied in terms of revealing the magma's physical properties, eruption mechanisms and deposition conditions. On the other hand, detailed petrological studies of such type of materials, for example mineral chemistry of the phases present, are not so usual. Furthermore, in cases where those volcanoclastic materials are thought to have gone under a series of alteration procedures, starting from low grade transformations, such as clay and zeolite alteration, to heavy hydrothermal alteration, then these materials are usually overlooked. However, the knowledge of the chemical composition of the pyrogenic mineral phases present, even in altered pyroclastic materials, could lead to notable conclusions regarding the magma evolution and petrogenetic procedures.

Santorini is situated in the centre of the prominent of the South Aegean Volcanic Arc. Evidence of the influence of the activity of the Arc are widespread in the eastern Mediterranean area. Bathrellos *et al.* (2009) have studied a pumice pebbles-rich sandy horizon, located in Holocene deposits of western Peloponnesus and they suggested an origin for the pumice in the South Aegean Volcanic Arc. It is implied that they related to a paroxysmal event of the arc, floated on the sea and they arrived through the combined action of wind and marine currents.

In Santorini, Greece, the volcanic rocks are the product of a calc-alkaline, high-alumina, basalt-andesite-dacite type of volcanism, which was expressed from eight centres (Pichler and Kussmaul, 1972). The majority of the volcanics around the Akrotiri peninsula of Santorini are considered to be

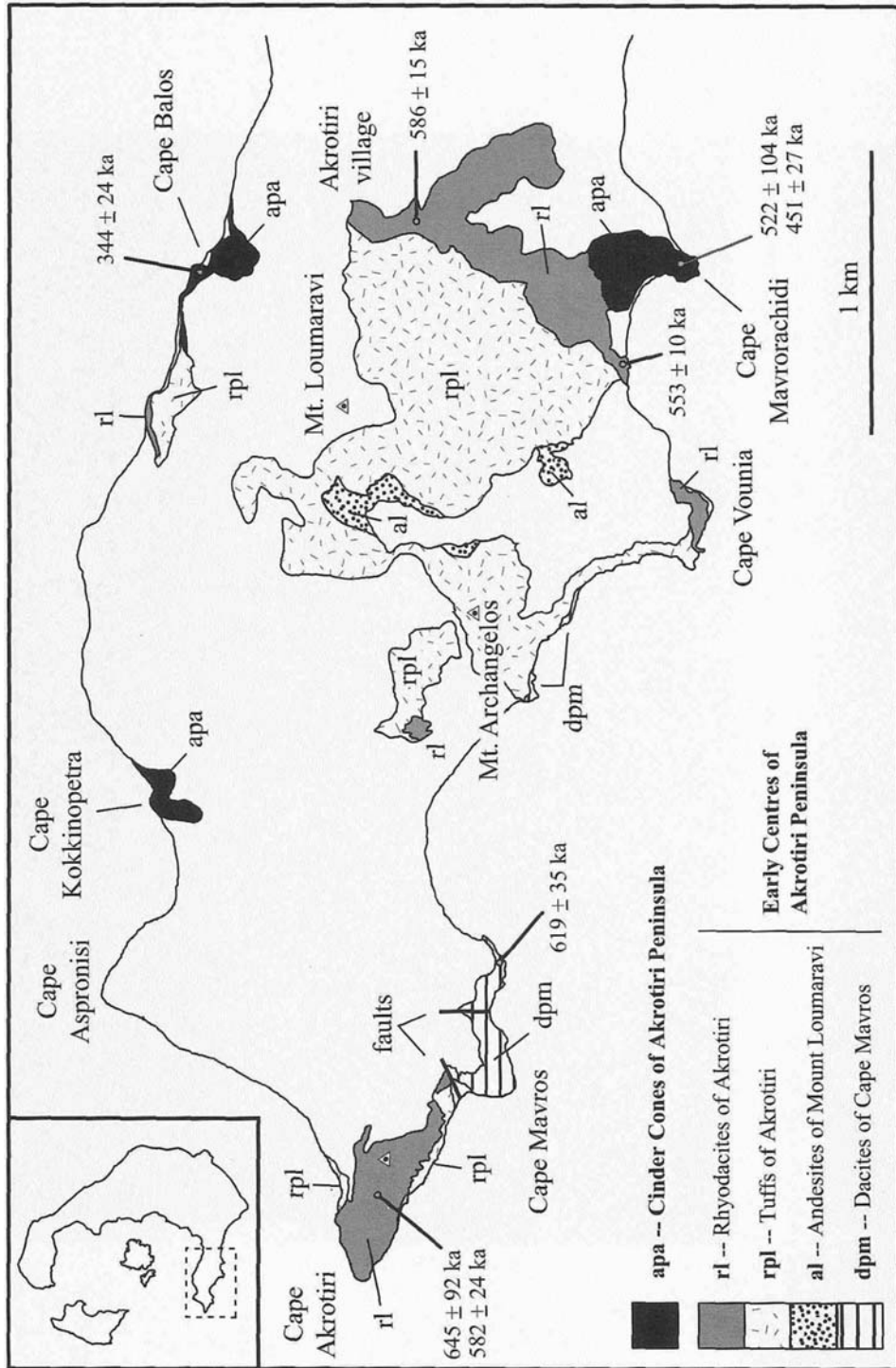


Fig. 1: Geological map of the Akrotiri peninsula (Druitt *et al.*, 1999). Younger volcanic products are omitted.

the first volcanic products in Santorini, with an age of Pliocene to Pleistocene. In this area a predominant feature is a pyroclastic unit, consisting of tuffs, breccias and conglomerates. The mineralogy of the material throughout the outcrop is dominated by zeolite minerals (Tsolis-Katagas and Katagas, 1989 and Kitsopoulos, 1995, 1996).

The present study has examined the mineral chemistry of the major pyrogenic phenocrysts of the Akrotiri pyroclastics unit., with the aim to contribute to the knowledge of magma generation mechanisms in the earliest known eruption period of Santorini Volcano.

2. Geological setting

The three islands of Santorini (Thera) (Santorini), Therasia and Aspronisi are the remnants of the Santorini stratocone, while the Old and New Kameni are the products of a much later volcanism.

The complete evolution of the Santorini volcanic complex has been studied by Druitt *et al.* (1999), while Nichols (1971) and Huijsmans *et al.* (1988) focused mostly on the younger volcanic products. The majority of the volcanics around the Akrotiri peninsula are considered to be the first volcanic products in Santorini (Pliocene-Pleistocene). They have been studied by Davis *et al.* (1998) and Dietrich *et al.* (1998). The geology of the Akrotiri Peninsula is given in Figure 1. Two volcanic suites have been recognised; the silicic Lumaravi-Archangelos and the mafic Akrotiri volcanic suites.

The Lumaravi-Archangelos volcanic suite is composed of submarine domes, coulees, and hyaloclastite aprons (Rhyodacites of Akrotiri, rl in Figure 1) intercalating with vitric tuffs, pumice breccias and conglomerates (Tuffs of Akrotiri, rpl in Figure 1).

The pyroclastic materials are the expression of three different centres. The white to pale green tuffs originally consisted of ash and/or lapilli, which were vitric and crystalline in composition. Agglomerated bands consisting of gray to green dacitic cognate xenoliths up to 15 cm long form tuff breccia. The exposed thickness is about 160m but some borehole investigations recorded at least 220 m. Fouque (1879) found Pliocene marine fossils indicating deposition in shallow water, although no evidence of sorting was reported by him. The mafic Akrotiri volcanic suite is composed of small domes and flows of andesites and basalts.

3. Materials and Methods

3.1 Akrotiri pre-Caldera Zeolitized Pyroclastics

The samples used in this study were collected from the “Tuffs of Akrotiri” unit of Figure 1, which has undergone substantial zeolitization.

The zeolitization of the pyroclastics involved the development of heulandite type of minerals and illite/smectite which have replaced the vitric matrix, forming characteristic pseudomorphs after the inner parts of glass shards. Authigenic opal-CT and cristobalite, halite, and pyrogenic phenocrysts of feldspars, amphiboles and Fe-Ti oxides complete the mineralogy. By using thermal tests the heulandite type of minerals were classified as heulandites type 3, i.e. clinoptilolites.

Tsolis-Katagas and Katagas (1989) proposed that the formation of zeolites resulted from the activity of interstitial water into the pile of the volcanoclastic material. The different mineralogical assemblages and compositions were attributed by the same authors to variations in the heat flow, the ionic activity in the interstitial waters, and the permeability. Kitsopoulos (1996) suggested that the formation of heulandite type of minerals did not exactly follow a “glass dissolution” path, but it involved

a number of continuous reactions. These reactions and their subsequent results were often controlled in numerous small closed sub-systems, even within the area of individual glass particles. The formation of zeolites did not proceed through a form of complete dissolution, but a continuous two end-members equilibrium reaction between the solid and the fluid components of a rather closed system.

The silicic pyroclastics range in SiO₂ from 61-75%, with a mean value of 67.2%, therefore, they could be classified as rhyodacites-dacites to low-Si rhyolites (Kitsopoulos, 1995). Because of the zeolitization process that the pyroclastics had undergone, the trace element discrimination diagram Nb/Y vs. Zr/TiO₂, proposed by Winchester and Floyd (1977), were also applied on the Akrotiri zeolitized pyroclastics. Kitsopoulos et. al., (2001) concluded, that the formation of the zeolites should have been mainly facilitated by an acidic precursor, obviously a rhyodacite-dacite type of rock. A small number of the samples used plotted very close to the rhyodacite-dacite/andesite boundary and one in the andesite field, indicating a more basic origin of their precursor. It was also found that there was no change in the alkaline affinity recorded during the eruption of the Akrotiri tuffs, but at the same time some degree of magma differentiation was evidenced.

3.2 Electron MicroProbe Analysis (EMPA)

EMPA was used to study the composition of the major mineral phases, other than the zeolite minerals, in the zeolitized tuffs. Carbon-coated polished thin sections were prepared from impregnated samples. The instrument used was a JEOL JXA-8600 Superprobe. The specific probe model carries four wavelength spectrometers (WDS) and is also equipped with a LINK 860 Series 1 Energy Dispersive System (EDS) detector with a 158 eV resolution at 5.8 KeV, which is used to analyse crystals with high volatility, and of very small sizes. The beam for the WDS analyses was operated at 15 kV and 30 nA, voltage and current conditions. Wollastonite was used for the standardisation of Si and Ca, rutile for Ti, jadeite for Al and Na, Fe₃O₄ for Fe, rhodonite for Mn, MgO for Mg, CH14 (microcline) for K and pure Cr and Ni for Cr and Ni respectively. All the running conditions, crystals and the values of standard used are described in detail by Kitsopoulos (1995) and they are available in the microprobe laboratory of Geology Department of Leicester University, UK.

4. Data

4.1 Data

More than 600 analyses were taken from plagioclase crystals from the Akrotiri pyroclastics, Some representative analyses are given in Table 1.

Some representative analysis of Fe-Ti oxides are given in Table 2. The analyses are recalculated to allow any Fe⁺³ to be distributed. The magnetite analysis which are given were the best results which could be achieved and they are taken into account, albeit the consideration of having low totals and therefore not to be perfectly reliable for interpretation.

5. Discussion - Conclusions

The majority of the plagioclases from the Akrotiri pyroclastics unit are falling within the region of andesine to labradorite with just a few crystals falling to the oligoclase composition. The plagioclases seem to exhibit a rather intermediate composition in contrast with the overall acidic geochemistry of the samples. The Or content in the plagioclases reach values up to 10-12% and in some cases the percentage is even higher and it can go up to 20-30%. Since a notable number of the analyses consider analyses of crystals' rims, the fact suggests that some of the crystals apparently have a rim of

Table 1.

SiO ₂	56.59	56.61	54.22	58.24	43.69
TiO ₂	0.02	0.01	0.02	0.01	0.04
Al ₂ O ₃	27.07	26.80	27.70	24.94	34.70
FeO	0.28	0.36	0.36	0.36	0.30
MnO	0.01	0.01	0.02	0.05	0.03
MgO	0.01	0.02	0.04	0.01	0.10
CaO	9.66	9.38	11.08	7.88	19.77
Na ₂ O	6.11	6.17	5.28	5.56	0.59
K ₂ O	0.21	0.23	0.17	2.05	0.03
Total	100.15	99.77	99.22	99.21	99.38
Si	10.183	10.222	9.911	10.581	8.173
Ti	0.003	0.001	0.003	0.001	0.006
Al	5.742	5.704	5.968	5.341	7.651
Fe ⁺²	0.042	0.054	0.055	0.055	0.047
Mn	0.002	0.002	0.003	0.008	0.005
Mg	0.003	0.005	0.011	0.003	0.028
Ca	1.863	1.815	2.170	1.534	3.963
Na	2.132	2.160	1.871	1.959	0.214
K	0.048	0.053	0.04	0.475	0.007
An	46.072	45.054	53.174	38.661	94.713
Ab	52.734	53.360	45.854	49.363	51.150
Or	11.925	13.154	0.9714	11.975	0.1711
cations	20.034	20.031	20.058	19.964	20.106
oxygens	32.000	32.000	32.000	32.000	32.000

Table 2.

	Ilmenite analyses				
SiO ₂	0.00	0.00	0.00	0.00	0.03
TiO ₂	38.94	40.11	40.07	38.90	37.99
Al ₂ O ₃	0.27	0.22	0.25	0.32	0.28
Cr ₂ O ₃	0.03	0.04	0.02	0.01	0.03
V ₂ O ₃	0.03	0.02	0.09	0.18	0.08
FeO	30.08	30.83	30.63	29.52	29.15
Fe ₂ O ₃	27.11	24.60	26.56	27.07	28.76
MnO	0.83	0.86	0.82	0.70	0.82
MgO	2.21	2.41	2.49	2.62	2.32
CaO	0.01	0.01	0.01	0.01	0.02
NiO	0.03	0.02	0.02	0.03	0.03

Table 2 (continued).

	Ilmenite analyses				
ZnO	0.13	0.02	0.11	0.04	0.03
Total	99.67	99.17	101.07	99.40	99.54
Si	0.000	0.000	0.000	0.000	0.001
Ti	0.740	0.763	0.749	0.739	0.722
Cr	0.010	0.001	0.000	0.000	0.001
Fe ⁺²	0.635	0.652	0.637	0.632	0.616
Fe ⁺³	0.515	0.468	0.497	0.514	0.547
Mn	0.018	0.018	0.017	0.015	0.018
Mg	0.083	0.091	0.092	0.099	0.087
Ca	0.000	0.000	0.000	0.000	0.001
cations	2.000	2.000	2.000	2.000	2.000
oxygens	3.002	3.001	3.001	3.001	3.001
	Magnetite analyses				Magnesiochromite
SiO ₂	0.05	0.00	0.00	0.03	0.00
TiO ₂	6.50	7.08	6.64	6.98	0.47
Al ₂ O ₃	2.15	1.94	1.78	1.94	20.40
Cr ₂ O ₃	0.04	0.05	0.07	0.03	42.17
V ₂ O ₃	0.32	0.43	0.41	0.42	0.16
FeO	33.00	33.48	33.88	33.47	15.65
Fe ₂ O ₃	51.54	50.81	53.33	51.08	7.89
MnO	0.77	0.83	0.76	0.76	0.29
MgO	1.58	1.56	1.46	1.54	12.71
CaO	0.02	0.04	0.03	0.04	0.00
NiO	0.02	0.01	0.04	0.00	0.15
ZnO	0.05	0.03	0.10	0.17	0.05
Total	96.04	96.26	98.50	96.46	99.94
Si	0.002	0.000	0.000	0.001	0.000
Ti	0.191	0.208	0.191	0.205	0.011
Cr	0.001	0.002	0.002	0.001	1.042
Fe ⁺²	1.077	1.092	1.084	1.091	0.411
Fe ⁺³	1.513	1.491	1.535	1.498	0.184
Mn	0.025	0.027	0.025	0.025	0.008
Mg	0.092	0.091	0.083	0.089	0.592
Ca	0.001	0.002	0.001	0.002	0.000
cations	3.001	3.001	3.001	3.000	3.000
oxygens	4.000	4.000	4.000	4.000	4.000

K-rich part surrounding them, indicating residual liquid rich in K during the crystallisation of the plagioclases.

There is no absolute clear evidence of zoning in the crystals, although techniques such as the Nomarski contrast interferometry (Anderson, 1983; Clark *et al.*, 1986) or laser interferometry (Pearce, 1984) which can help the zoning examination were not applied. Seymour *et al.* (1990) for example applied these techniques in plagioclases from basalts, andesites and dacites, which are younger than the pyroclastic deposits, from the Akrotiri area in Santorini and they concluded that three main categories of plagioclase occur. Here, wherever a positive, clear zoning was observed that was of an anorthitic core to an albitic rim.

With the exception of very few samples, where some extremely calcic plagioclase crystals with An content from An₈₇ up to An₉₅ were found, the overall range of An was recorded in the range An₂₁ up to An₇₂ which is rather wide for the single pyroclastic unit.

From the Fe-Ti oxides analyses two facies were recognised. A magnetite-ulvospinel series and a hematite-ilmenite series.

The magnetite analyses, which are presented in this study, show low totals (from 95.91 to 98.50), but they were the best analytical results could be obtained. The TiO₂ values range from 6.34 to 7.55 % and despite their low totals, they represent a close relationship to the known solid solution of the magnetite-ulvospinel facies. They are poorer in Ti than those recorded by Mitropoulos and Tarney (1992) from the younger Santorini volcanics they have studied, which had a TiO₂ content from 13.4 up to 17.2%. Even if the assumption is made, that the amount missing to makeup the present analyses closer to 100 (an amount from 4.09 to 1.50) is all being attributed to Ti, there is still a gap between the analyses from the younger Santorini volcanics and those from Akrotiri. The titanomagnetites within the Akrotiri volcanics are clearly more oxidised than the titanomagnetites in the above volcanic sequence. These Akrotiri magnetite values are only comparable to the amount of TiO₂ present in magnetite crystals from the western parts of the Aegean Volcanic Arc, which exhibit a TiO₂ content from 4.4 up to 10.2%. Pe-Piper and Piper (2005) have found that the western part of the arc, including Aegina, Methana, and the older rocks of Milos and Santorini, has typical arc-related andesite-dacite volcanism, predominantly of Pliocene age, associated with E-W listric faulting with slow slip rates.

The TiO₂ values of the ilmenite crystals range from 37.94 to 40.80 % and they represent a quite close relationship to the known solid solution of the hematite-ilmenite facies.

The hematite-ilmenite series is almost absent from studies of younger volcanics of Santorini. Mitropoulos and Tarney (1992) have recorded just one analysis of ilmenite. The TiO₂ content of the analyses of the present study is 5.14% up to 8% lesser than the values recorded from the younger volcanics.

The Fe-Ti oxides analyses exhibit a positive correlation for the FeO - TiO₂ pair values and a negative correlation for the FeO - Fe₂O₃ and Fe₂O₃ - TiO₂ pair values. For the hematite-ilmenite facies the correlation coefficients were 0.96, -0.86 and -0.89 respectively. For the magnetite-ulvospinel facies the relevant values were: 0.69, -0.17 and -0.72. The lower values for this group are due probably to the poor analysis available, but this may indicate that the possible analytical problem was due to the Fe and not to Ti.

The positive correlation of FeO to the TiO₂ and the negative correlation of the other two pairs suggests that the increase of ilmenite and possibly of ulvospinel content are related to the decrease of the f_{O_2} within the lavas gave the Fe-Ti oxide facies.

Karberg and Barton (2006) have calculated the fO_2 values from mafic calc-alkaline magmas erupted from four volcanic centers (Akrotiri, Micro Profitis Ilias, Megalo Vouno, and Skaros) on Santorini, Greece, based on the olivine-melt equilibrium and by using microprobe analyses of olivine rims and coexisting groundmass. The fO_2 lie in a fairly narrow range ($\Delta FMQ = 1.06 \pm 0.18$). By combining the results with those obtained for other samples (based on mineral equilibria), have found out that the pre-eruptive oxygen fugacities of the majority of Santorini magmas (including that erupted in the well-known Minoan event) lie slightly above, but close to, values defined by the NNO buffer ($\Delta FMQ = 1.13 \pm 0.26$; $n=86$) and thus, have suggested that the redox states of mafic magmas erupted on Santorini have remained constant over $\sim 400,000$ to $600,000$ years. However, they also stated that a small number of silicic lavas erupted in the Akrotiri region early in the history of the volcanic field evolved at higher fO_2 ($\Delta FMQ = 2.11 \pm 0.15$).

The range of the composition of the plagioclase component, the composition of the Fe-Ti oxides, the occurrence even of magnesiocromite crystals within tuffs of rhyolitic-dacitic composition can be accommodated under the effect of magma mixing procedures, more specifically in the Akrotiri case, of a mixing-mingling mechanism which involves two parts, a mantle derived, saturated mafic composition component and a silicic magma part, in relatively shallow crustal depths. Pyle *et al* (1988) were among the first, using U–Th isotopic data, to suggest mixing between a crystal mush and a magma in an andesite from the island of Santorini, in the Aegean arc. The lava contains crystal populations from two sources of distinct thorium isotope composition: one from a basic cumulate; the other phenocrysts from a dacite magma.

Mixing procedures, such as the emplacement of andesite into a voluminous rhyolite magma in a mid-crustal magma chamber led to the explosive Kos Plateau Tuff super-eruption in the eastern part of the Aegean Arc (Pe-Piper and Moulton, 2008). Also, evidence of magma mixing for the pre-caldera deposits of Nisyros has been presented by Seymour and Vlassopoulos (1992). It is accepted that the injection of mafic magma into a magma reservoir of intermediate composition may trigger eruption due to the combined effects of increased mass, heat and volatile input (Sparks *et al.*, 1977). The abundance of mafic enclaves in andesites and dacites from a number of arc volcanoes, and disequilibrium textures in the host lavas, provide support for this model (Zellmer *et al.*, 2003).

Nevertheless, it has been proved that the understanding of the petrogenetic history of some intermediate arc magmas appears to be rather complicated. Recently, Bailey *et al.* (2009) have suggested, by using elemental and Sr–Nd–Pb isotopic data, that three main (and a fourth, less prominent) magmatic series with sub-parallel trace element patterns for basalts can be distinguished in northern Santorini. The long-lived histories of the three main magmatic series imply repetitive melting of isolated mantle regions, ascent of magmas through independent feeder systems, and their residence in separate crustal magma chambers. It becomes apparent that further investigation of the elemental, mainly of traces, and of the isotopic characteristics of the entire Akrotiri volcanic suite can only unfold a more detailed of the magma evolution and eruption mechanism of the earliest volcanic centre of Santorini.

6. Acknowledgments

The author has been always grateful to the Academic, Technical and Clerical Staff of the Geology Department of Leicester University for their kind host and constant support for almost two decades now. For their master knowledge and their valuable help with the analytical work and the data handling and interpretation, Rob Wilson, Nick Marsh, Rob Kelly, Rod Branson and Collin Cunningham should be specially mentioned. On 14/07/2007 Dr. Tim Brewer was suddenly lost for ever. I shall

always remember and be grateful to Tim for proposing and setting up a Fellowship, so I can be able to continue my work in Leicester. Part of this work has been carried out under the inspired supervision and guidance of Prof Ansel Dunham. Ansel is always be remembered, thanked and honored by his numerous BSc, MSc and PhD students around the world.

7. References

- Anderson, A.T., 1983. Oscillatory zoning of plagioclase: Nomarski interference microscopy of etched polished sections. *American Mineralogist* 68, 125-129.
- Bailey, J.C., Jensen, E.S., Hansen, A., Kann, A.D.J., & Kann, K., 2009. Formation of heterogeneous magmatic series beneath North Santorini, South Aegean island arc. *Lithos* 110, 20-36.
- Bathrellos, G.D., Vasilatos, C., Skilodimou, H.D., & Stamatakis, M.G., 2009. On the occurrence of a pumice-rich layer in Holocene deposits of western Peloponnesus, Ionian Sea, Greece. A geomorphological and geochemical approach. *Central European Journal of Geosciences* 1, 19-32
- Clark, A.H., Pearce, T.H., Roeder, P.L., & Wolfson, I., 1986. Oscillatory zoning and other microstructures in magmatic olivine and augite: Nomarski interference contrast observations on etched polished surfaces. *American Mineralogist* 71, 734-741.
- Davis, E., Gartzos, E., & Dietrich, V.J., 1998. Magmatic Evolution of the Pleistocene Akrotiri Volcanoes. In Casale, R. et al (eds), Proceedings of the 2nd workshop, "The European Laboratory Volcanoes", Santorini, 2-4 May 2-4 1996, 49-68.
- Dietrich, V.J., Davis, E., & Gartzos, E., 1998. Amphibole in rhyodacites and dacites from the Akrotiri volcanoes and the complexities of discontinuous fractional crystallization. In Casale, R. et al (eds), Proceedings of the 2nd workshop, "The European Laboratory Volcanoes", Santorini, 2-4 May 2-4 1996, 69-80.
- Druitt, T.H., Edwards, L., Mellors, R.M., Pyle, D.M., Sparks, R.S.J., Lanphere, M., Davies, M., & Barriero, B., 1999. Santorini Volcano, Geological Society, London, Memoirs, 19, 165pp.
- Fouque, F., 1879. Santorin et ses Eruptions, Paris, G. Masson, 440pp.
- Huijsmans, J.P.P., Barton, M., & Salters, V.J.M., 1988. Geochemistry and evolution of calc-alkaline volcanic complex of Santorini, Aegean Sea, Greece. *Journal of Volcanology and Geothermal Research* 34, 283-306.
- Karberg, S., & Burton, M., 2006. Oxygen fugacities of mafic magmas erupted in the Santorini volcanic field, Aegean Sea, Greece. *GSA Abstracts with Programs* 38 (7), Paper No. 183-13, p. 447.
- Kitsopoulos, K.P., 1995. The mineralogy, geochemistry, physical properties and possible industrial applications of volcanic zeolitic tuffs from Santorini and Polyegos islands, Greece, University of Leicester, PhD Thesis, 442pp.
- Kitsopoulos, K.P., 1996. Zeolitization of the Akrotiri pre-caldera pyroclastics from Santorini island, Greece. Implications for existing zeolitization models as applied with volcanoclastic materials, *GSA Abstracts with Programs* 28 (7), A-104.
- Kitsopoulos, K. P., Scott, P.W., Jeffrey, C.A., and Marsh, N.G., 2001. The mineralogy and geochemistry of zeolite-bearing volcanics from Akrotiri (Santorini island) and Polyegos (Milos group of islands) Greece. Implications for geochemical classification diagrams. *Bulletin of the Geological Society of Greece* XXXIV/3, Proceedings of the 9th International Congress, Athens, 859-865.
- Mitropoulos, P., & Tarney, J., 1992. Significance of mineral composition variations in the Aegean Island Arc, *Journal of Volcanology and Geothermal Research* 51, 283-303.
- Nicholls, I.A., 1971. Petrology of Santorini volcanic rocks. *J Petrol.* 12, 67-119.
- Pe-Piper, G., & Piper, D.J.W., 2005. The South Aegean active volcanic arc: relationships between mag-

- matism and tectonics. *Developments in Volcanology* 7, 113-133.
- Pe-Piper, G., & Mourton, B. 2008. Magma evolution in the Pliocene–Pleistocene succession of Kos, South Aegean arc, Greece. *Lithos* 106, p. 110-124
- Pichler, H., & Kussmaul, S., 1972. The calc-alkaline volcanics rocks of the Santorini Group (Aegean Sea, Greece), *Neues Jahrbuch Mineralogie Abhandlungen*, 116: 268-307N.
- Pyle, D.M., Ivanovich, M., & Sparks, R.S.J., 1988. Magma–cumulate mixing identified by U–Th disequilibrium dating. *Nature* 331, 157-159.
- Seymour, K.St., Vlassopoulos, D., Pearse, T.H., & Rice, C., 1990. The record of magma chamber process in plagioclase phenocryst at Thera volcano, Aegean volcanic arc, Greece. *Contributions to Mineralogy and Petrology*. 104, 73-84.
- Seymour, K.S., Vlassopoulos, D., 1992. Magma mixing at Nisyros volcano, as inferred from incompatible trace-element systematics. *Journal of Volcanology and Geothermal Research* 50, 273–299.
- Sparks, R.S.J., Sigurdsson, & H., Wilson, L., 1977. Magma mixing: a mechanism for triggering acid explosive eruptions. *Nature* 267, 315–318.
- Tsolis-Katagas, P., & Katagas, C., 1989. Zeolites in Pre-Caldera pyroclastic rocks of the Santorini Volcano, Aegean Sea, Greece. *Clays and Clay Minerals* 37, 497-510.
- Winchester, J. A., and Floyd, P. A., 1977. Geochemical discrimination of different magma series and their differentiation products using immobile elements. *Chemical Geology*. 20, 325-343.
- Zellmer, G.F., Sparks, R.S.J., Hawkesworth, C.J., & Wiedenbeck, M., 2003. Magma emplacement and remobilization timescales beneath Montserrat: insights from Sr and Ba zonation in plagioclase phenocrysts. *Journal of Petrology* 44, 1413–1431.

HEAVY METALS IN STREAM SEDIMENTS AFFECTED BY A LANDFILL AND ASSOCIATED IMPACT ON GROUNDWATER QUALITY

Koutsopoulou, E., Tsolis-Katagas, P. and Papoulis, D.

University of Patras, Department of Geology, Section of Earth Materials, 26500 Patras, Greece, ekoutsop@upatras.gr

Abstract

Sanitary landfill facilities are essential to modern societies as repositories for municipal solid wastes. However, they always entrain a certain risk of environmental impact. For this reason monitoring is essential to their operation. In the present work, the environmental impact of such a landfill is studied. Soil samples were collected in and around the landfill and their mineralogy was studied. Top layers of stream sediments were collected to examine possible dispersion of pollutants in the environment. Chemical analyses showed enrichment in As, Cu, Zn, and Pb in the stream sediments compared to uncontaminated samples. The presence of anions such as chloride, sulphate and phosphate adsorbed on clay minerals suggest the interaction of stream sediments with run-off water from the landfill.

The groundwater near the landfill site was characterised as not potable and not suitable for irrigation purposes, because some parameters such as NO_3^- and Cl^- were close or exceeded the permissible limits given by EE, EPA and WHO.

Key words: *sanitary landfill, clay minerals, groundwater, heavy metals, stream sediments.*

1. Introduction

Waste management policies concerning municipal landfills play an important role on preventing the emissions of contaminants, eliminating potential health hazards and preserving the environment. Landfills should hold no risks for the environment and that means that the transport of contaminants should be confined and restricted from reaching the natural environment. As stated by the Swiss Waste Management Standards of 1986 and the legislation in most European countries (Council Directive 99/31/EC), municipal waste deposits have to be compatible with the environment. Sanitary landfills require that a composite liner comprising a geomembrane and a clay mineral liner according to the multi-barrier system should be used at the bottom of the waste disposal site (Stief, 1986; Technical Instructions Hazardous Wastes, 1991; Hermanns Stengele and Plötze, 2000; Kalbe et al., 2002). This concept is essential for the avoidance of leachate migration from the landfill boundaries and its release into the surrounding environment, which may cause ground water pollution and other environmental impacts. Compacted clayey soils are widely used as landfill liners in order to isolate waste materials from surrounding environments, and to prevent the heavy metals commonly found in landfill leachate from migrating into groundwater (Chalermyanont et al., 2009). However, various studies have reported elevated concentrations of metals in stream sediments originating from landfill contamination sources. Studies of increased Cu, Pb, Zn, Cd, Ag, and Ba concentrations in stream sediments from landfills and water treatment facilities have been reported (Mantei and Coon-

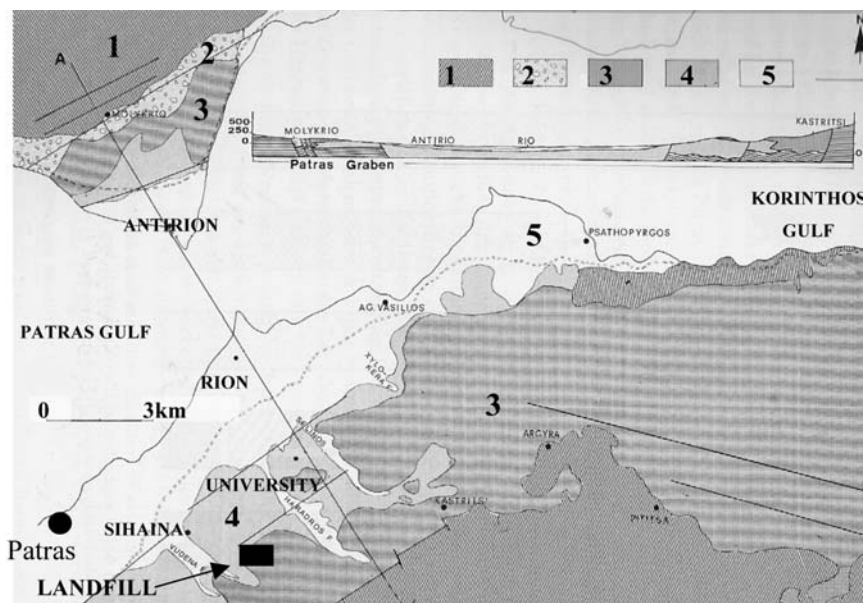


Fig. 1: The location of the sanitary landfill of the Municipality of Patras: 1. limestone, flysch, chert, 2. alluvial deposits, 3. fluvial deposits, 4. undivided Plio-Pleistocene 5. recent deposits (Doutsos et al., 1985).

rod, 1989; Mantei and Foster, 1991; Gonçalves et al., 2004). In the latter study the contamination of the stream sediments was a result of run-off waters from the landfill. Infiltration of water through the top cover of the landfill can also lead to surface and groundwater contamination (Kjeldsen et al., 1993; Fatta et al., 1999).

In the present work, clay materials from an operating waste disposal facility in Patras, NW Peloponnese, Greece, were collected in order to determine the different clay minerals present and to evaluate the consequences of solid waste disposal in the landfill. Stream sediments were examined for the presence of contaminants to examine possible dispersion of pollutants in the environment. Moreover, the extent of the leachate adverse impacts on the groundwater of the area, and the pollution level of groundwater were investigated.

2. The sanitary landfill of Patras

The sanitary landfill of Patras is located near Ano Sihaina village, approximately 10km southeast of the city of Patras (Fig. 1). The total available area of the plant is 400,000m², of which 70,000m² are developed as landfill area.

The geological and hydrogeological conditions of the landfill area are characterized by the presence of thick sequences of Plio-Pleistocene fine sediments (clayey marls, marls and siltstones) with lensoidal intercalation of sandstones and conglomerates, which do not sustain a considerable groundwater table (Zelilidis et al., 1998; Doutsos et al., 1988).

The studied area is located in the southern flanks of the Rio Graben (Fig. 1), which is an extensional structure controlled by ENE-WSW trending normal faults and the main direction of the extension is almost N-S (Doutsos et al., 1985). The landfill has been developed in a natural depression with

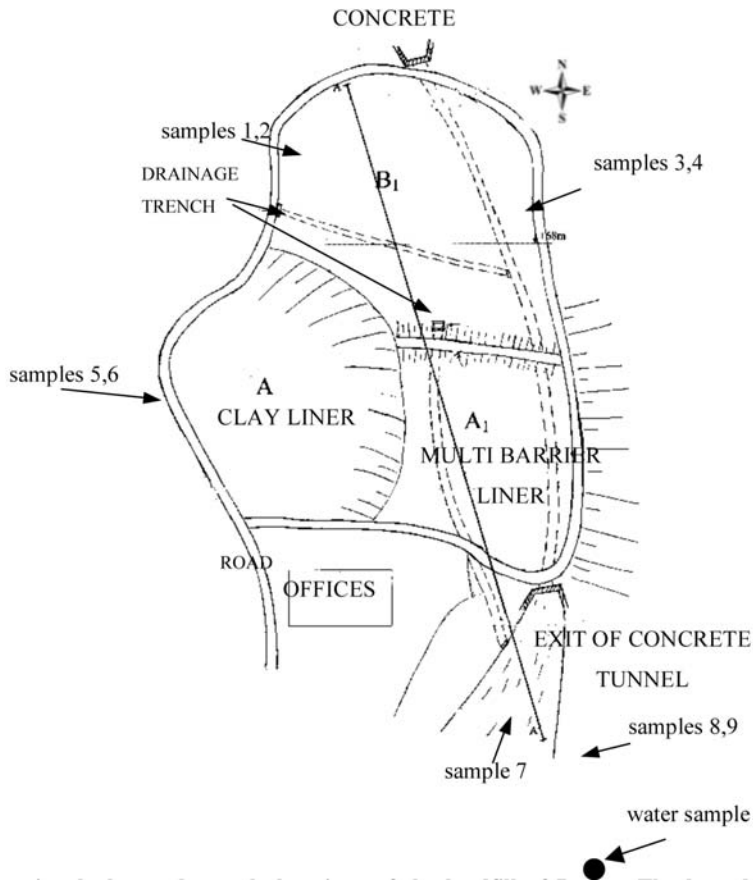


Fig. 2: Sectional plan and sample locations of the landfill of Patras. The boundary of the waste disposal site is outlined by the indication of the perimetrical road.

general axial direction N-S and slope of 10° to the N, bounded to the west by a steep hillslope and to the east by a seasonal stream (Fig. 2).

The filling of the landfill is phased, divided in the areas A_1 , B_1 , A_2 and B_2 . Prior to the construction of the new sanitary landfill, the Municipality of Patras preceded to the preparation of a part of the available area covering $15,000\text{m}^2$ (phase A, Fig. 2). The filling of this phase, which is lined only with compacted clay for the protection of ground and groundwater, was completed in September 1995, when the operation of the new landfill commenced. Phase A is now restored and the landfill gas from the existing waste is extracted and flared.

The new landfill is sealed with a composite lining system that consists of a bottom clay lining layer of compacted clay, and an overlying geomembrane (HDPE) protected by geotextile. The protection of the landfill from surface water run-off and the subsequent decrease in leachate volume was accomplished by the construction of a reinforced concrete tunnel along the riverbed of the stream entering the site from the west in order to collect the streamwater off the site, the diversion of the stream bordering the site from the east and the construction of a drainage trench upgradient (south) and perimetrically of the whole area (KORONIS S.A, 1996).

3. Materials and methods

3.1 Sampling

The landfill is located in clay-rich Pliocene-Pleistocene sediments (Fig. 2). Samples were collected from the material used as capping (samples 1, 2, 3, 4), liner (samples 5, 6) and from the downstream area of the landfill in order to determine the mineralogy and examine possible dispersion of pollutants in the surrounding area (samples 7, 8, 9). One sample was collected from the top layers of a run-off water path since these layers correspond to the volume of sediment which is kept in direct contact with contaminated water for longer time periods (stream sediment – sample 7) (Fig. 2). Finally, a groundwater sample was collected from a downgradient-monitoring borehole in order to detect changes in water quality that may be caused by infiltration of run-off waters or the escape of leachate from the landfill.

3.2 Methods

The mineralogical composition of the clay material was determined by X-Ray Diffraction (XRD), using a Philips diffractometer PW1050/25, with Ni-filtered $\text{CuK}\alpha$ radiation. Briefly, oriented powder mounts of bulk samples were prepared by gently pressing the powder into the cavity holder and were scanned at $1^\circ 2\theta/\text{min}$ from 3 to $60^\circ 2\theta$. The clay minerals were identified from three XRD patterns (i.e., after air-drying at 25°C , with ethylene glycol treatment, and after heating at 490°C for 2 hours).

Clay minerals morphology and chemical composition of coexisting minerals were examined with Scanning Electron Microscopy (SEM), using a JEOL 6300 SEM equipped with an Energy Dispersive Spectrometer (EDS). The chemical composition of the minerals was determined using natural and synthetic standards and 20kV accelerating voltage with 10nA beam current. Microanalyses were performed on epoxy resin-impregnated polished and gold or carbon coated thin sections, and sample powders mounted directly on the sample holder.

Chemical analyses for major and trace elements were carried out in all samples by Instrumental Neutron Activation Analysis (INAA) and by Inductively Coupled Plasma (ICP-MS), using a Thermo Jarrell-Ash ENVIRO II ICP, and a Perkin Elmer Optima 3000 ICP, with the 4-acid (HF , HClO_4 , HNO_3 and HCl) digestion technique (Activation Laboratories, Canada).

Finally, chemical analysis of major and trace elements of the groundwater sample were carried out by Flame Atomic Absorption Spectrometry (FAAS) GBC AVANTA[®] using a HACH DR 4000 Spectrophotometer, and by ICP/MS using an ELAN 6100 Perkin Elmer[®] ICP.

4. Results

4.1 Mineralogy

X-ray diffraction patterns of oriented powder mounts revealed the presence of quartz, calcite, albite and clay minerals in all samples. The clay minerals are chlorite, smectite, illite, kaolinite and mixed-layer chlorite-smectite. Mixed-layer chlorite-smectite is identified by a peak at 14 \AA in the air-dried sample, which shifts to 15.5 \AA after treatment with ethylene glycol and at about 12 \AA after heating at 490°C for two hours. Chlorite is characterised by the presence of peaks at 14.2 \AA , 7.1 \AA , 4.74 \AA and 3.55 \AA which are not affected after ethylene glycol treatment and remain essentially unchanged after heating. Smectite is identified by a reflection at about 16.6 \AA after ethylene glycol solvation that collapses to 10 \AA after heating. Illite is identified by the presence of peaks at 10 \AA , 5 \AA and 3.3 \AA which remain unaffected by ethylene glycol solvation and heating (Moore and Reynolds, 1989).

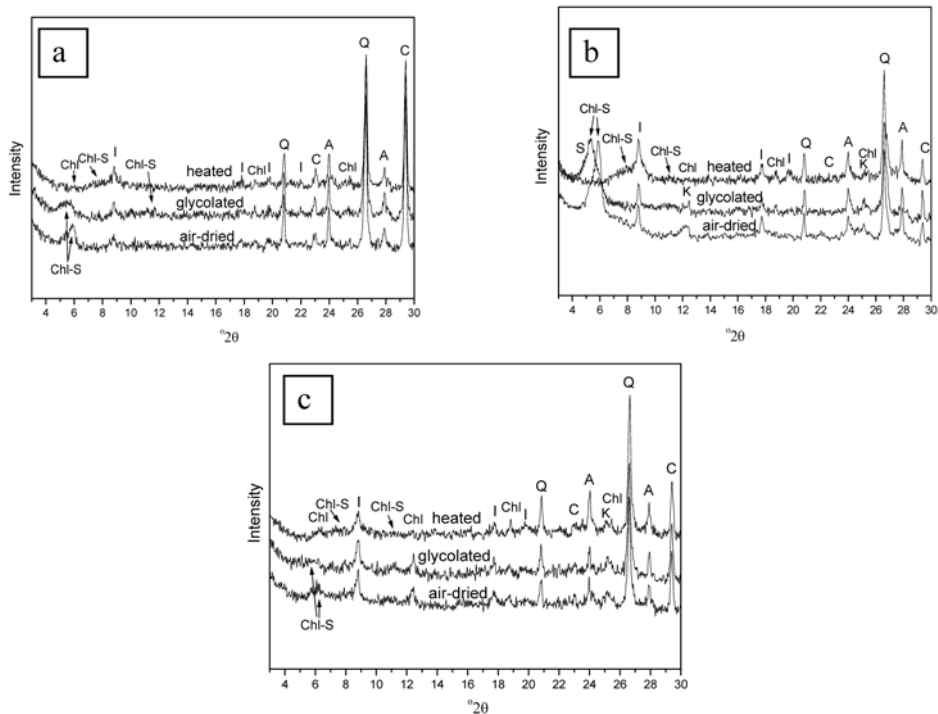


Fig. 3: X-ray diffraction patterns of representative bulk samples: a) material used as capping in the landfill, b) material used as lining in the landfill, c) stream sediment. Chl-S: chlorite-smectite, I: illite, Chl: chlorite, K: kaolinite, Q: quartz, C: calcite, A: albite, S: smectite.

Kaolinite is present in the material used as lining in the landfill and is identified by the (001) and (002) reflections at 7.15 Å and 3.58 Å respectively. The XRD patterns of representative bulk samples collected from the capping material, the lining and the stream sediment are presented in Fig. 3.

Clay minerals and especially smectite and mixed layer chlorite-smectite are more abundant in the material used as a liner in the landfill compared to the samples collected from the capping material and the stream sediment.

4.2 Geochemistry

Bulk sample chemical analyses for major elements were performed in all samples and are listed in Table 1. Samples 5, and 6 used in the liner have the highest K_2O , Na_2O , Al_2O_3 , Fe_2O_3 and SiO_2 content and the lowest CaO and Loss on Ignition (LOI) content, reflecting the abundance in clay minerals and calcite respectively. Trace elements analyses (Table 2) showed that the As, Cu, Zn, Pb and Ni content is higher in the stream sediment (sample 7) compared to the uncontaminated samples. Since stream sediments are in contact with run-off waters from the landfill this could be an indication of contamination from the landfill. Trace elements Ba and Sr are mainly correlated with the presence of calcite and their relatively high content is attributed to the increased calcite content.

The minerals present in the stream sediment were also examined by SEM-EDS. Traces of Cl^- , SO_4^{2-} and PO_4^{3-} were detected in many ED spectra of clay minerals. SEM-EDS analyses also revealed traces of Cu in clay minerals, associated with Cl^- .

Table 1. Bulk sample chemical analyses for major elements (wt%).

<i>sample</i>	<i>SiO₂</i>	<i>TiO₂</i>	<i>Al₂O₃</i>	<i>Fe₂O₃</i>	<i>MnO</i>	<i>MgO</i>	<i>CaO</i>	<i>Na₂O</i>	<i>K₂O</i>	<i>P₂O₅</i>	<i>LOI</i>	<i>Total</i>
1	46.82	0.24	4.44	1.92	0.08	0.80	23.07	0.75	0.69	0.06	20.14	99.00
2	38.94	0.29	5.11	2.14	0.08	0.99	26.47	0.77	0.78	0.08	24.52	100.18
3	54.05	0.35	6.42	2.35	0.09	1.09	16.95	1.12	0.99	0.07	16.69	100.18
4	62.41	0.47	8.30	3.55	0.07	1.37	9.29	1.39	1.26	0.07	11.57	99.75
5	59.20	0.59	9.79	4.27	0.08	1.77	9.68	1.40	1.46	0.13	11.74	100.11
6	59.97	0.56	9.56	4.20	0.10	1.75	8.88	1.46	1.43	0.11	10.76	98.79
7	49.89	0.54	9.33	4.14	0.09	1.98	14.28	1.20	1.63	0.11	16.44	99.63
8	64.34	0.45	7.32	2.77	0.09	1.17	9.72	1.32	1.18	0.08	10.35	98.79
9	46.79	0.25	4.22	1.89	0.07	0.79	23.73	0.83	0.62	0.06	20.38	99.63

Table 2. Bulk sample chemical analyses for trace elements (ppm).

<i>sample</i>	<i>As</i>	<i>Cu</i>	<i>Zn</i>	<i>Pb</i>	<i>Ni</i>	<i>Cr</i>	<i>Ba</i>	<i>Sr</i>
2	<0.5	20	30	11	57	150	135	318
4	3.5	23	47	20	90	260	187	154
5	4	32	61	24	106	292	196	136
6	4.6	34	50	24	96	299	196	163
7	6.5	39	82	18	117	252	420	151

4.3 Groundwater Chemistry

Chemical analyses of major and trace elements of the groundwater sample from the downgradient-monitoring borehole are presented in Tables 3 and 4. The water sample is characterized by a significant enrichment of Ca²⁺, alkalis, HCO₃⁻, NO₃⁻ and Cl⁻. As a result, the groundwater has the characteristics of (Ca²⁺ + Na⁺) - HCO₃⁻ - type water. This type of water is renewed due to continuous dilution by the addition of sporadic precipitation waters (Gibbs, 1970).

The concentrations of potential contaminants such as SO₄²⁻, NO₃⁻ and Cl⁻ were analyzed in order to identify possible human induced contamination. The concentration of SO₄²⁻ is quite high for groundwater that is not related to mining operations but is still below drinkable limits. The NO₃⁻ concentration of the water sample is slightly below the drinking water standard (10 mg/L) and Cl⁻ concentration is quite high for water that is not characterized by seawater intrusion. The concentrations of most toxic elements such as As, Cd, Co, Cr, Cu, Fe, Mn, Ni, Pb, Se and U were in very low values except for Zn which is slightly below drinking limits (95ppb) and could be attributed to human activities (Table 4). Ba and Sr concentrations are also relatively high but this is probably due to the mineralogy of the host rock.

5. Discussion

Fine-grained top layers of stream sediments have been used to study metal contamination in the

Table 3. Selected cation and anion constituents (mg/l) of groundwater).

<i>cation (mg/l)</i>	<i>groundwater (mg/l)</i>	<i>drinkable limits (mg/l)</i>	<i>anion (mg/l)</i>	<i>groundwater (mg/l)</i>	<i>drinkable limits (mg/l)</i>
(Na ⁺)	47.5	150	(HCO ₃ ⁻)	377	-
(K ⁺)	1.7	12	(SO ₄ ²⁻)	44	250
(Mg ²⁺)	15.9	50	(NO ₃ ⁻)	9.68	10
(Ca ²⁺)	192	-	(NO ₂ ⁻)	0	0.1
(NH ₄ ⁺)	0	0.5	(PO ₄ ³⁻)	0.08	-
			(Cl ⁻)	100.4	10

Table 4. Trace elements (µg/l) in groundwater

<i>element</i>	<i>concentration (µg/l)</i>	<i>drinkable limits (µg/l)</i>	<i>element</i>	<i>concentration (µg/l)</i>	<i>drinkable limits (µg/l)</i>
(As)	0	6	(Pb)	0.088	15/0
(Ba)	147.313	-	(Rb)	0.404	-
(Be)	0	4	(Se)	0.772	50
(Cd)	0.044	5	(Sr)	565.13	-
(Cr)	1.113	50	(U)	0.715	30
(Cu)	2.338	-	(V)	0.691	-
(Fe)	0	200	(Zn)	95.965	100
(Ga)	5.936	-	(B)	35.632	1000
(Li)	7.882	-	(Co)	0.57	-
(Mn)	4.625	50	(Mo)	0	-
(Ni)	5.638	50			

vicinity of landfills, since metals generally accumulate on smaller grain fractions of sediment because of the higher surface area-to-grain size ratio (Gibbs, 1973; Harding and Brown, 1978; Ramamoorthy and Rust, 1978; Sinex and Helz, 1981; Rule, 1986; Yanful et al., 1988; Mantei and Coonrod 1989). Therefore, the mineralogy of the material used in the landfill controls the possibility of pollutant escape in the environment (Hermanns Stengele and Plötze, 2000). The material used in the landfill is characterized by the presence of quartz, calcite and clay minerals: chlorite, smectite, illite and the mixed-layer chlorite-smectite. Kaolinite is also present, especially in the samples collected from the liner in the landfill, and in the stream sediment.

The results of the geochemical analyses show the abundance of SiO₂ and Al₂O₃ especially in the samples used as a clay liner and the stream sediment. Samples 5 and 6 (clay liner) are slightly richer in SiO₂ than the stream sediment (sample 7) with SiO₂ ranging to about 60% due to the presence of quartz. The higher percentage of total iron and MgO in the same samples could be ascribed to the presence of chlorite and the mixed layer chlorite-smectite. This was supported by SEM-EDS analyses of chlorite and chlorite-smectite, which showed Mg²⁺ and Fe²⁺ as the commonest divalent cations.

The stream sediment is abundant in most trace elements (As, Cu, Zn, Pb, Ni, Ba) (Table 2). To our knowledge no leakage from the clay barrier has occurred since the operations of the landfill commenced. However, during rainy periods, run-off waters that interact with waste being prepared for storage may flow out downstream. Stream sediments are in direct contact with contaminated water, especially when the flux is low enough (as in the present case), and could show some degree of contamination.

The different clay minerals present, determine the preferential adsorption for cationic heavy metal ions (Churchman et al., 2006) and this adsorption is strongly affected by the pH and the presence of anions in the solution (Cavallaro, 1982; McBride, 1985; Undabeytia et al., 2002). The presence of inorganic ligands such as Cl^- , SO_4^{2-} and PO_4^{3-} may increase metal retention or strongly increase metal mobility depending on the type and amount of metal and ligands present, soil surface properties, soil solution composition, pH and redox conditions (McLean and Bledsoe, 1992). Specific adsorption of ions, such as Cl^- , on the surface with variable charge, could increase the negative charge of the surface, thus enhancing Cu adsorption (Wang et al., 1987; Doula and Ioannou, 2003). In our case, SEM-EDS analyses revealed the presence of Cl^- , SO_4^{2-} and PO_4^{3-} adsorbed on clay minerals in the stream sediment. The presence of Cl^- and other anions seem to have enhanced the adsorption of Cu deriving from run-off waters from the landfill.

Groundwater is enriched in Ca^{2+} and HCO_3^- and can be characterized as fresh water since it is renewed from precipitation waters causing dissolution of salts. The decreasing order of the abundance of major cations in the water is $\text{Ca}^{2+} > \text{Na}^+ > \text{Mg}^{2+} > \text{K}^+$. A comparison between the chemical composition of the groundwater and the catchment rocks indicates that the bedrock types may affect the water chemistry. The high concentration of Ca^{2+} may result from dissolution of calcite, which is one of the main components of the bedrock. Moreover, albite could be a source of Na^+ , and the mixed layer chlorite-smectite for Mg^{2+} and Na^+ . An additional source of Na^+ may also be the landfill. Illite may also be a source of K^+ .

The groundwater is not a source of domestic or drinking water in the area. However, it is used for agricultural irrigation in one case that we are aware of. The high concentrations in NO_3^- in the groundwater sample imply that nitrates could derive from agricultural chemicals or fertilizers in the soil. Nitrate is a naturally occurring chemical that is an important plant nutrient often used in fertilizers. Most human exposure arises from food, and drinking water. Nitrate ends up in drinking water due to agricultural run-off from fertilizer use, erosion of natural deposits, or from animal and human waste via septic tanks and sewage systems. Bacteria in the gut convert nitrate to nitrite, which is mostly responsible for any toxic effects observed (California Environmental Protection Agency, 1997; National Toxicology Program (NTP), 2002).

Chloride is relatively abundant in the water sample and suggests contamination through human activities. Chloride concentration in unpolluted waters is often below 10 mg/litre and sometimes below 1 mg/litre (Department of National Health and Welfare Canada, 1978). In groundwater Cl^- could originate from anthropogenic sources, such as landfill leachate and the use of inorganic fertilizers, since potassium chloride is used in the production of fertilizers (Department of National Health and Welfare Canada, 1978). The mean Cl^- concentration in several rivers in the UK was 11–42 mg/litre during 1974–81 (Brooker and Johnson, 1984). Evidence for a general increase in chloride concentrations in groundwater and drinking-water has been found (WHO, 1978). In the USA, aquifers prone to seawater intrusion have been found to contain chloride at concentrations ranging from 5 to 460 mg/litre (Phelan, 1987), whereas contaminated wells in the Philippines have been reported to have an average chloride concentration of 141 mg/litre (Morales, 1987).

According to drinking water standards, the concentrations of all trace elements in the studied waters were below the maximum contaminant level (MCL) values given by European Council Directive (1980), U.S. EPA (1990) and WHO (1991, 2003). However, the concentration of Zn is quite high, just below drinking limits, and could be a result of contamination from the landfill.

6. Conclusion

Top layers of stream sediments seem to interact with chemically modified run-off waters from the landfill. Trace elements analyses showed that the content of As, Cu, Zn, and Pb is higher in the stream sediment than the uncontaminated samples. Since stream sediments interact with run-off waters from the landfill this is an indication of contamination from the landfill. SEM-EDS analyses revealed the presence of Cl^- , SO_4^{2-} as well as Cu in clay minerals, indicating that clay mineral surfaces adsorb pollutants.

The concentrations of SO_4^{2-} and NO_3^- in groundwater are attributed to agricultural chemicals or fertilizers in the soil. Cl^- concentration is quite high in the groundwater sample and is also attributed to human activities. The Zn content is also high, although just below drinking limits, and is a result of human induced contamination from the landfill.

Special concern should be given during the environmental monitoring of the landfill to ensure that no contaminants that may affect public health and the surrounding environment are released from the landfill.

7. References

- Brooker, MP., and Johnson, PC., 1984. Behaviour of phosphate, nitrate, chloride and hardness in 12 Welsh rivers, *Water Research*, 18(9), 1155-1164.
- Cavallaro, N., 1982. Sorption and fixation of Cu and Zn, and phosphate by soil clays as influenced by the oxide fraction. PhD thesis. Cornell Univ. (Diss. Absr. 82-10799).
- California Environmental Protection Agency, 1997. available at: <http://www.oehha.ca.gov/water.html>
- Chalermyanont, T., Arrykul S., and Charoenthaisong N., 2009. Potential use of lateritic and marine clay soils as landfill liners to retain heavy metals, *Waste Management*, 29, 117-127.
- Churchman, G.J., Gates, W.P., Theng, B.K.G., and Yuan, 2006. Clays and Clay Minerals for Pollution Control. In: Developments in Clay Science Vol.1., *Handbook of Clay Science*, Bergaya, F., Theng, B.K.G. and Lagaly, G. (Eds). 625-676pp.
- Department of National Health and Welfare (Canada), 1978. Guidelines for Canadian drinking water quality. Supporting documentation. Ottawa,
- Doula, M.K., and Ioannou, A., 2003. The effect of electrolyte anion on Cu adsorption-desorption by clinoptilolite, *Microporous Mesoporous Materials*, 58, 115-130.
- Doutsos, Th., Kontopoulos, N., and Ferentinos, G., 1985. *Das westliche Ende des Korinth-Grabens*. (The western end of the Corinth graben.), *Neues Jahrbuch für Geologie und Palaontologie – Abhandlungen*, 1985, 11, 652-666.
- Doutsos, Th., Kontopoulos, N., and Poulimenos, G., 1988. The Corinth -Patras rift as the initial stage of continental fragmentation behind an active island arc (Greece), *Basin Research*, 1, 177-190.
- Environmental Protection Agency (US EPA): 1990, Seminar Publication: *Assessment, Management and Communication of Drinking Water Contamination*. Washington, USA.
- European Council Directive 80/778/EEC concerning Drinking Water Quality of 15/7/1980. <http://ec.europa.eu/environment/enlarg/handbook/water.pdf>

- European Council Directive 1999/31/EC of 26 April 1999 on the landfill of waste. <http://eur-lex.europa.eu/LexUriServ/LexUriServ.do?uri=CELEX:31999L0031:EN:NOT>
- Fatta, D., Papadopoulou A., and Loizidou, M., 1999. A study on the landfill leachate and its impact on the groundwater quality of the greater area. *Environmental Geochemistry and Health*, 21, 175–190.
- Gibbs, R.J., 1970. Mechanisms controlling world water chemistry, *Science*, 170, 1088-1090.
- Gibbs, R.J., 1973. Mechanisms of trace metal transport in rivers, *Science*, 180, 71-73.
- Gonçalves, M.A., Nogueira, J.M.F, Figueiras, J., Putnis, C.V., and Almeida, C., 2004. Base-metals and organic content in stream sediments in the vicinity of a landfill, *Applied Geochemistry*, 19, 137-151.
- Harding, S.C., and Brown H.S., 1978 Distribution of selected trace elements in sediments of Pamlico River Estuary, North Carolina, *Environmental Geology*, 1(2), 181-191
- Hermanns Stengele, R., and Plötze, M., 2000. Suitability of minerals for controlled landfill and containment, *EMU Notes in mineralogy*, 2(8), 291-331.
- Kalbe, U., Müller, W.W., Berger, W., and Eckardt, J., 2002. Transport of organic contaminants within composite liner systems, *Applied Clay Science*, 21, 67-76.
- KORONIS SA., ENVITEC A.E., (1996). ‘Sanitary Landfill Of the Municipality Of Patras’ Booklet for the progress of works in the Landfill of Patras.
- Kjeldsen, P., Bjerg, P., Ruge, K., Pedersen, J. K., Skov, B., Foverskov, A., Wurtz, S., Christensen, T. H., 1993. Assessing the variability in leachate migration from an old municipal landfill, in: R. Cossu, H. T. Christensen and R. Stegmann (eds) *Proceedings Sardinia 93, Fourth International Landfill Symposium*. Sardinia, Italy, 1519–1531pp.
- Mantei, E.J., and Coonrod D.D., (1989), Heavy metal content in the stream sediments adjacent to a sanitary landfill, *Environmental Geology and Water Science*, 13(1), 51-58.
- Mantei, E.J., and Foster M.V., 1991. Heavy Metals in Stream Sediments: Effects of Human Activities, *Environmental Geology and Water Science*, 18, 2, 95-104
- McBride, M.B., 1985. Sorption of Copper(II) on Aluminum Hydroxide as affected by phosphate, *Soil Science Society of America Journal*, 49, 843-846.
- McLean, J. E., and Bledsoe B.E., 1992. Behavior of Metals in Soils. In (eds.): Boulding J.R., *EPA Environmental Assessment Sourcebook*. 19-56 pp.
- Morales, E.C., 1987. Chemical quality of deep well waters in Cavite, Philippines, *Water quality bulletin*, 12(1):43 45.
- Moore, D.M., and Reynolds, R.C.Jr., 1989. *X-Ray Diffraction and the Identification and Analysis of Clay Minerals*. Oxford University Press. New York, 198-269pp.
- National Toxicology Program (NTP) 2002. <http://ntp.niehs.nih.gov/>
- Phelan, D.J., 1987. Water levels, chloride concentrations, and pumpage in the coastal aquifers of Delaware and Maryland. US Geological Survey, 1987 (USGS Water Resources Investigations Report 87 4229; Dialog Abstract No. 602039).
- Ramamoorthy, S., and Rust, B.R., 1978. Heavy metal exchange processes in sediment water systems, *Environmental Geology*, 2(3):165-172
- Rule, J., 1986. Assessment of trace element geochemistry of Hampton Roads Harbor and Lower Chesapeake Bay area sediments, *Environmental Geology*, 8(4):209-219
- Sinex, S.A., and Helz, G.R., 1981. Regional geochemistry of trace elements in Chesapeake Bay sediments, *Environmental Geology*, 3, 315 323
- Stief, K., 1986. Das Multibarrierenkonzept als Grundlage von Planung, Bau, Betrieb und Nachsorge von Deponien, *Müll und Abfall*, 18(1), 15-20.

- Technical Instructions Hazardous Wastes (TA Abfall), (1991). Zweite Allgemeine Verwaltungsvorschrift zum Abfallgesetz, Teil 1: *Technische Anleitung zur Lagerung, chemisch/physikalischen und biologischen Behandlung, Verbrennung und Ablagerung von besonders überwachungsbedürftigen Abfällen vom 12.03.1991*. *Gemeinsames Ministerialblatt*, 8, 139.
- Wang, P.G., Ji G.L., and Yu, T.R., 1987. Adsorption of chloride and nitrate by variable charge soils in relation to electric charge of the soil. *Zeitschrift Fur Pflanzenernahrung Und Bodenkunde*, 150: 17–23.
- WHO Regional Office for Europe, 1978 (EURO Reports and Studies 2). Sodium, chlorides, and conductivity in drinking water: a report on a WHO working group. Copenhagen,
- WHO, World Health Organization, 1991. *Revision of the WHO Guidelines for Drinking Water Quality*, Report of the Second Review Group Meeting on Inorganics, Brussels, Belgium, Geneva, WHO/PEP/91:32, 12 pp.
- WHO, World Health Organization, 2003. Guidelines for drinking-water quality, 2nd ed. Vol. 2. *Health criteria and other supporting information*, WHO/SDE/WSH/03.04/03, Geneva.
- Undabeytia, T., Nir, S., Rytwo, G., Serban, C., Morillo, E., Maqueda, C., 2002. Modeling Adsorption-Desorption Processes of Cu on Edge and Palnar Sites of montmorillonite, *Environmental Science & Technology*, 36, 2677-2683.
- Yanful, E.K., Quigley, R.M., and Nesbitt, H.W., 1988. Heavy metal migration at a landfill site, Sarnia, Ontario, Canada—2: Metal partitioning and geotechnical implications, *Applied Geochemistry*, v. 3, p. 623-629.
- Zelilidis, A., Koukouvelas, I., and Doutsos, Th., 1998. *Neogene paleostress changes behind the forearc fold belt in the Patraikos Gulf area, Western Greece*, *Neues Jahrbuch fur Geologie und Palaontologie – Abhandlungen*, 1998, 311-325.

EPITHERMAL MANGANESE MINERALIZATION, KIMOLOS ISLAND, SOUTH AEGEAN VOLCANIC ARC, GREECE

Lykakis, N.¹ and Kiliias, S. P.²

¹ Grant Institute of Earth Science, School of Geosciences, University of Edinburgh, EH9 3JW, Scotland, UK, nikoslykakis@gmail.com

² Department of Geology and Geoenvironment, University of Athens, 157 84 Zographou, Greece, kiliias@geol.uoa.gr

Abstract

Manganese mineralization is hosted by a marine monomictic, lithic volcanoclastic breccia, possibly an andesitic in situ hyaloclastite, and shallow-marine or subaerial epiclastic conglomerates, in the Korakies area, NE Kimolos, active south Aegean volcanic arc. Old mine workings (in the form of rubble, adit and shaft), and abandoned rail and ship loading facilities, exist in the area. Mineralization occurs as a quartz/chalcedony vein system filling extensional NNE-SSW-trending faults and fractures, of Pliocene age. Maximum vein width reaches 5 m; length may extend to 250 m. The ore shares strong textural analogies with volcanic-hosted epithermal-style deposits, i.e. crustiform banding, vugs, hydrothermal breccias, cockade and comb textures. Vein wall rocks are hydrothermally altered to quartz-adularia±illite, chlorite and barite. Pyrolusite, hollandite, cryptomelane, and coronadite are the main ore minerals, with quartz, chalcedony, jasper and barite gangue. Ore samples contain up to 25.8 % MnO₂, 14.7 % FeO_{TOT}, 2860 ppm Zn, 1132 ppm Pb and 136 ppm Cu; Mn and Zn show mutual positive correlation ($r^2=0.61$). Trace element enrichment (i.e. Zn, Pb, and Cu) may suggest a proximal base metal sulfide mineralization. Concentrations of 4.3 % Na, 0.09 % Mg and barite presence may suggest genetic involvement of sea water. The mineralization studied is similar to volcanic-hosted low-sulfidation epithermal ore deposits deposited from neutral pH fluids. This is a rare example of a vein-type epithermal-style hydrothermal manganese deposit formed in a marine environment.

Key words: *epithermal manganese, Kimolos, South Aegean Volcanic Arc, hollandite, pyrolusite, cryptomelane, epithermal textures.*

1. Introduction

Kimolos volcanic island (36 km²) shares a common geological evolution with Milos, Polyegos and Antimilos the Milos Group of the Pliocene-modern South Aegean volcanic arc (SAVA) (Pe-Piper and Piper, 2002). To date, metallic mineralization has only been reported from Milos, a dormant volcano that documents the transition between the submarine and terrestrial volcanic environments (Fytikas et al., 1986, Stewart and McPhie, 2006). Milos is host to a large inventory of volcanic-hosted metallic deposits (e.g. Hauck, 1984; Plimer, 2000; Liakopoulos et al., 2001; Kiliias et al., 2001; Naden et al., 2005; Alfieris and Voudouris, 2007; Glasby et al., 2005) as well as industrial mineral deposits (Christidis, 2001, and references therein). Recent research on Milos has identified a new metallogenic environment—namely hybrid volcanic-hosted massive sulfide and continental magmato-hy-

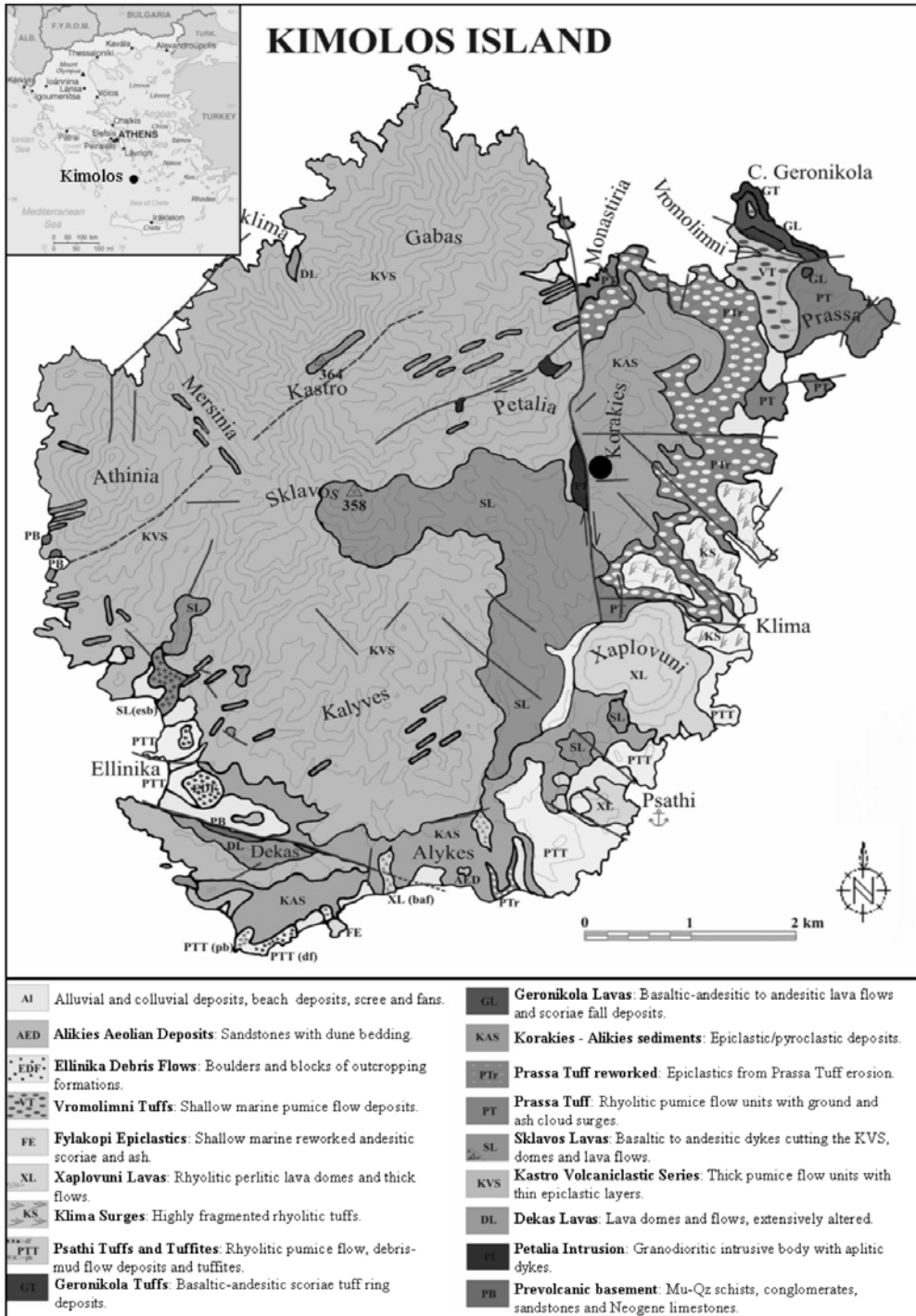


Fig. 1: Geological map of Kimolos Island showing the main structural features and the location of the Mn ore deposit in the Korakies area (black dot) (modified from Francalanci et al., 2007).

drothermal mineralization (i.e. Profitis Ilias–Chondro Vouno Au–Ag–Cu deposit, Naden et al., 2005). In addition, epithermal and sea-floor exhalative textures have been documented in the Vani–Kondaros–Triades Mn–Ba–Pb–Zn–Ag hydrothermal field (Kilias et al., 2007, and unpublished data).

Published reports on the geology and hydrothermal mineralization on Kimolos are very scarce (Fytikas and Vougioukalakis, 1993, Pe-Piper and Piper, 2002; Francalanci et al., 2007); this is the first report on hydrothermal manganese mineralization that occurs in the Korakies area, NE Kimolos.

2. Geological setting

Volcanic centres of the Milos Group are positioned along NE-SW trending regional tectonic lineaments (Francalanci et al., 2007; Pe-Piper and Piper, 2002). Both Kimolos and Milos consist of marine and terrestrial lithologies with composition belonging to the calc-alkaline and high-K calc-alkaline series (Pe-Piper and Piper, 2002; Francalanci et al., 2007, and references therein). Volcanic activity occurred in two periods separated by a long serenity phase. Basaltic to rhyolitic lavas and voluminous pyroclastic rocks were erupted during the first period (3.5–2.0 Ma) in association with NE-SW-trending lineaments, whereas rhyolitic pyroclastic deposits and perlitic lava domes tied to NW-SE structural features, characterize the second period of activity (2.0–0.9 Ma) (Fig. 1). Structurally controlled NE-SW trending, active low-T (~55 °C) geothermal activity, NW Kimolos is recharged mainly by seawater (Pe-Piper and Piper, 2002, Fytikas and Vougioukalakis, 1993).

The host rocks of the manganese mineralization form part of the Korakies-Alikes pyroclastic-epiclastic formation (Fig. 1). This formation consists of a mixture of shallow marine and subaerial pyroclastic and epiclastic lithologies, such as pyroclastic breccias and debris flows, sandstones and siltstones, and epiclastic conglomerates (Fytikas and Vougioukalakis, 1993). The mineralized structures crosscut an ENE-WSW trending monomict, andesitic volcanoclastic lithic breccia, and locally unconformably overlying epiclastic conglomerates. The volcanic rocks show a conspicuous flow texture with individual 2-3 m thick flow-beds trending ENE-WSW. Wallrocks constitute: (1) a clast-supported lithic breccia which contains angular to subangular andesite lava fragments with an average diameter of 20-30 cm, and a matrix of fine grained lava fragments of the same composition (Fig. 2C); this formation is topographically controlled and shows maximum thickness of 30 m best seen along paleo-valleys (Fytikas and Vougioukalakis, 1993). These rocks represent possibly submarine, lithic-rich, volcanoclastic mass-flow deposits, or andesitic in situ hyaloclastites; (2) shallow-marine or subaerial epiclastic sediments which have clasts consisting of basaltic to andesitic Sklavos lavas (see Fig. 1) and Kastro volcanoclastics (see Fig. 1) cemented by hydrothermal silica. Host rocks come to a faulted N-S trending contact with the Kastro volcanoclastics to the east (Fig. 1).

3. Manganese ore: occurrence and textures

Abandoned mine workings (in the form of rubble, adit and shaft) and ship loading facilities, attest to past exploitation of the Mn deposit at Korakies. The deposit occurs in veins hosted exclusively by the Korakies pyroclastic/epiclastic formation. The exploited vein fills NNE-striking normal faults and related extensional fractures within a structural corridor of the regional Pliocene NE trend (Pe-Piper and Piper, 2002). It has maximum width of 5-6 m, a length of at least 250 m and, dips 70° to 90° to the SW; the depth of the vein is unknown (Fig. 2A). The vein displays complex and multi-episodic filling with epithermal-style textures characteristic of open-space precipitation such as crustiform banding, vugs, hydrothermal breccias, and cockade and comb textures (Figs. 2D&E&F, Fig. 3A); breccia mainly occurs on the vein margins (Hedenquist et al., 2000) (Fig. 2E). These textures suggest that vein opening and filling was episodic, with several episodes of fault movement related

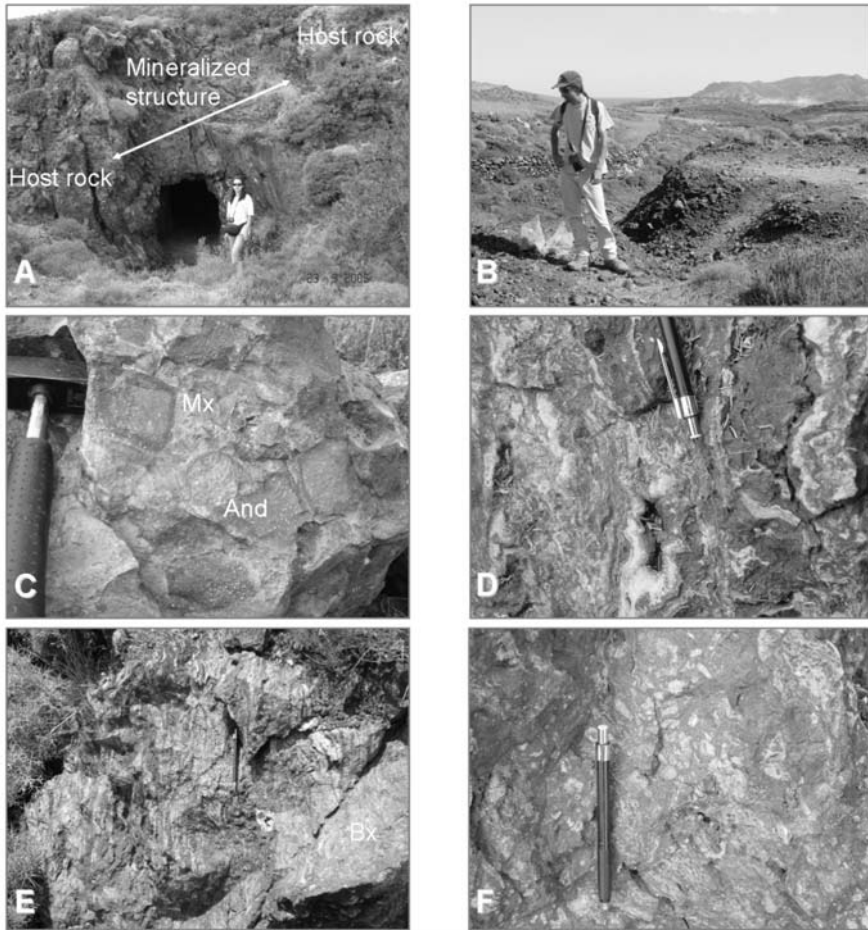


Fig. 2: A. Photo of the Korakies vein in which the banded texture, the width of the mineralized structure and an old mining gallery can be seen. B. Photo of abandoned mine workings close to the vein, where a number of samples were collected. C. Photo of the host rock of Mn mineralization which is a monomict volcaniclastic lithic breccia. Blocky hornblende— and feldspar—phyric andesite clasts (And) are separated by small amounts of millimeter to submillimeter-sized granular matrix (Mx) of the same composition. The matrix includes splinters of andesite and scattered crystal fragments. Group of clasts in the matrix display jigsaw-fit texture. Lithic fragments are surrounded by pinkish jasper. D. Epithermal vein texture displaying: crustiform banded quartz-chalcedony-jasper intergrown with bands of manganese mineralization, and, cockade texture. E. Transitional relationship between banded quartz-Mn ore texture and hydrothermal breccia (Bx) F. Enlargement of (Bx) in previous photo. Hydrothermal fault-breccia structure consists of angular vein material and matrix with Mn-ore. (And: andesite; Mx: matrix; Bx: breccia).

to brecciation and mineralization. Primary Mn ore forms part of these textures. Banding may be related to cyclic pulses of fluid caused by a feeder mechanism in which fluid overpressure caused faulting events during low effective normal stress conditions. A supergene oxidation zone exists of Fe-Mn-oxy-hydroxides, affecting at least 5 m of the upper and exposed parts of the vein.

4. Methods

Thirty two mineralized, host rock and vein wallrock samples were collected both in-situ and from old nearby mine rubble (Fig. 2B). The samples were examined under transmitted and reflected light microscopes, and analysed by SEM-EDS, AAS and XRD methods in the laboratories of the Dept. of Economic Geology and Geochemistry, University of Athens. We used an SEM-EDS Jeol Jsm-5600 (Oxford ISIS 300 microanalysis system) with 20 kV voltage, current of 0.5 nA, analysis time of 50 sec and bundle diameter <2 μ . For the XRD studies, a Siemens D5005 CuK α radiation diffractometer was used, with 1.54 Å wavelength and 40 kV voltage. The concentrations of K and Na were measured with a Jenway PFP7 flamephotometer.

5. Mineralogy and mineral chemistry

Hydrothermal alteration: Due to overprint of supergene oxidation, hydrothermal alteration of the host rocks is not easily discernible. It seems that it is limited to the vicinity of the main vein, to an unknown extent. The most common minerals present in altered wall rock are quartz, adularia, Ba-adularia, illite (sericite), chlorite, and Fe-oxides. The main alteration type is quartz-adularia+chlorite \pm illite. Quartz is mainly present as a pervasive replacement of the volcanic host rock matrix, whereas adularia, illite and chlorite grow over feldspar and hornblende clasts and crystal fragments of the groundmass (Fig. 3B). Traces of Mn-ilmenite were also found.

Manganese minerals: Primary manganese ore essentially consists of pyrolusite and intermixed hollandite-group Mn-oxide minerals (hollandite-cryptomelane-coronadite). Gangue minerals are quartz, chalcedony, jasper, barite, minor adularia and illite. Supergene minerals are iron oxides and hydroxides, and Mn-Fe wad. Formation of manganese, and iron, minerals may have been controlled by Eh changes, under either hypogene and/or supergene oxidizing conditions, or both (i.e. ascending and/or descending fluids) (see Figure 3C&D); temperature and Eh (oxidized sulfur) changes, may have caused gangue precipitation, and barite, respectively (e.g. Leal et al., 2008). Pyrolusite appears as masses of well-formed rhombohedral to prismatic and needle-like crystals that may reach a few millimeters in size. Hollandite-group minerals occur mainly as repetitive colloform microbands with variable grain size and porosity that commonly follow the same succession of precipitation (Fig. 3C), or vug filling wad (Fig. 3D&E). Goethite is the most common iron oxide; it is present as a botryoidal aggregate and usually occurs with hematite. Electron microprobe analyses of Mn minerals are shown in Table 1.

6. Geochemistry

Whole rock chemical analyses of manganese ores are shown in Table 2. The ore samples may contain up to 25.83% Mn, 14.7% Fe, 2860 ppm Zn, 1132 ppm Pb, 136 ppm Cu and 3780 ppm Ba, while concentrations in Ni and Co are very low. In addition, concentrations of 4.3 % Na, 0.75 % K, 0.77% Ca, and 0.09 % Mg have been measured. According to the correlations between all elements, they can be subdivided into different groups; Mn and Zn show mutual positive correlation (correlation coefficient $r^2=0.61$) indicating that Zn is associated with the manganese oxide phase; Fe-Pb-Cu-Zn and Cr show mutual positive correlation ($r^2=0.74-0.99$), suggesting that some of these elements may be adsorbed onto supergene goethite and hematite, however, association with Mn minerals cannot be excluded. Na, K, Al and Ca show positive mutual correlations but do not have a statistically significant correlation with Fe, Mn, or Si-Al. These elements are probably partitioned among all those phases, but predominantly with an aluminosilicate phase. The high Na content may suggest involvement of seawater (Hein et al., 2008); Mg does not correlate with any other element and may also originate from seawater. The Ca content probably reflects a carbonate sediment source.

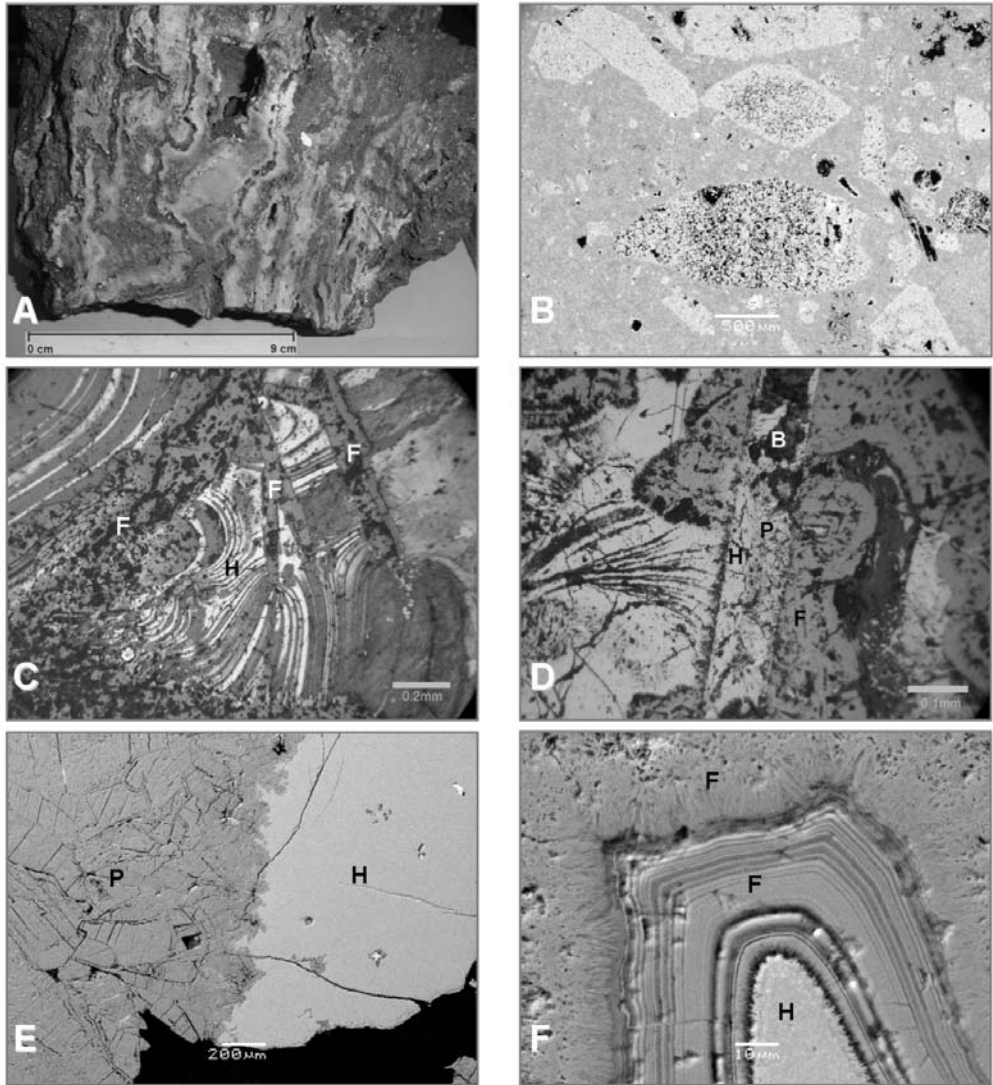


Fig. 3: A. Polished section showing Mn-ore forming part of epithermal-style crustiform banding, vugs and cockade structures. B. Back-scattered electron image of hydrothermally altered wallrock. Equant to cuneiform andesite clasts are packed in a matrix that contains scattered crystal fragments. The clasts consist of feldspar and hornblende altered to Ba-adularia, chlorite, illite, and quartz; groundmass comprises fine-grained silica and altered feldspar and hornblende. C. Microphotograph of colloform hollandite (light grey) cut by hematite and goethite. D. Microphotograph of hollandite wad and pyrolusite within an older elongate barite crystal; goethite-hematite are the supergene phase E. Back-scattered electron image illustrating primary assemblages of pyrolusite (P) and hollandite/coronadite (H). F. Back-scattered electron image of finely laminated bulbous and smooth undulating aggregates of Fe-rich (goethite-hematite) phases, of possible biogenic (microbial) origin (P:pyrolusite; H:hollandite/coronadite; B: barite; F: goethite-hematite)

Table 1. Electron microprobe analyses (wt%) of selected manganese oxides from Korakies. Samples 1-13: hollandite – cryptomelane, 14-17: hollandite – coronadite, 18-26: pyrolusite, 27-36: goethite – hematite (n.d= not detected).

	MgO	Al ₂ O ₃	SiO ₂	K ₂ O	CaO	MnO ₂	Fe ₂ O ₃	ZnO	BaO	PbO	As ₂ O ₃	TOTAL
1	0.5	n.d	n.d	4.5	n.d	80.4	1.7	n.d	5.8	n.d	n.d	93.3
2	1.0	n.d	0.3	1.5	0.2	81.1	n.d	0.7	6.2	n.d	n.d	91.1
3	n.d	n.d	0.4	2.8	n.d	76.9	2.2	n.d	7.2	0.6	n.d	90.5
4	3.2	n.d	n.d	2.4	0.3	81.9	n.d	n.d	7.2	n.d	n.d	95.3
5	1.0	n.d	n.d	2.3	n.d	79.0	n.d	n.d	7.2	n.d	n.d	90.4
6	3.3	n.d	n.d	2.5	n.d	83.1	n.d	0.6	7.3	n.d	n.d	97.3
7	n.d	n.d	n.d	2.0	0.2	80.3	n.d	n.d	7.4	n.d	n.d	90.8
8	1.1	n.d	n.d	1.3	n.d	79.7	n.d	0.8	7.5	0.1	n.d	90.5
9	3.2	n.d	n.d	2.5	0.4	82.5	n.d	n.d	7.5	n.d	n.d	96.7
10	n.d	n.d	0.8	0.7	0.6	65.2	3.6	0.8	10.8	n.d	n.d	82.6
11	n.d	n.d	0.3	1.7	0.3	75.9	1.9	n.d	9.9	n.d	n.d	91.2
12	n.d	n.d	n.d	1.0	n.d	77.6	n.d	0.8	12.5	n.d	n.d	92.8
13	n.d	n.d	n.d	1.2	n.d	76.8	0.9	n.d	12.7	n.d	n.d	92.5
14	n.d	n.d	0.8	0.3	n.d	68.3	n.d	0.8	1.5	28.0	n.d	99.7
15	n.d	n.d	0.7	0.2	n.d	68.0	n.d	0.7	1.5	28.1	n.d	99.2
16	n.d	n.d	0.8	n.d	n.d	66.1	n.d	0.9	1.3	28.5	n.d	97.8
17	n.d	n.d	0.8	n.d	n.d	65.8	n.d	0.8	1.1	28.7	n.d	97.2
18	n.d	n.d	0.7	0.2	0.3	87.0	n.d	0.7	2.2	n.d	n.d	91.7
19	n.d	n.d	1.2	0.2	n.d	87.2	0.6	n.d	1.7	n.d	n.d	91.7
20	0.4	n.d	0.6	n.d	n.d	89.2	n.d	0.6	n.d	n.d	n.d	91.4
21	n.d	n.d	0.5	n.d	n.d	89.3	n.d	n.d	n.d	n.d	n.d	90.3
22	n.d	n.d	0.7	n.d	n.d	89.4	n.d	1.1	n.d	n.d	n.d	91.6
23	n.d	n.d	n.d	n.d	n.d	89.9	n.d	n.d	n.d	n.d	n.d	91.1
24	1.1	n.d	0.8	n.d	n.d	90.0	n.d	n.d	n.d	n.d	n.d	92.7
25	n.d	n.d	0.7	0.0	n.d	90.6	n.d	0.7	n.d	n.d	n.d	92.7
26	n.d	n.d	1.1	n.d	n.d	90.7	n.d	0.9	n.d	n.d	n.d	92.3
27	n.d	n.d	3.0	n.d	n.d	3.5	87.3	n.d	n.d	n.d	1.0	95.2
28	n.d	n.d	5.7	n.d	0.2	21.1	58.2	3.0	0.5	n.d	1.7	90.8
29	n.d	0.4	6.5	n.d	0.2	18.2	61.3	2.9	0.5	n.d	2.2	91.8
30	n.d	n.d	2.8	n.d	0.8	4.1	73.7	1.1	n.d	n.d	4.8	87.7
31	1.4	n.d	6.5	n.d	n.d	1.7	74.4	2.0	n.d	0.2	n.d	86.5
32	n.d	n.d	7.5	n.d	0.2	2.5	74.7	1.2	n.d	n.d	n.d	85.7
33	n.d	n.d	5.2	n.d	n.d	n.d	73.8	1.2	n.d	n.d	n.d	83.0
34	1.2	n.d	6.5	n.d	n.d	1.4	74.7	1.4	n.d	n.d	n.d	85.6
35	n.d	n.d	6.7	n.d	0.4	2.9	67.1	1.5	n.d	n.d	n.d	79.7
36	n.d	0.5	4.2	n.d	n.d	0.7	79.5	1.3	n.d	n.d	n.d	86.1

Table 2. Major element (wt%) and selected trace element (ppm) content with the resulting Mn/Fe ratios of the Mn ore samples.

Sample	1	2	3	4	5	6	7	8	9	10	11	12
(wt %)												
Mn	4.88	9.57	4.49	3.76	17.08	25.75	18.02	1.18	17.91	25.83	10.20	10.97
Fe	2.68	3.06	5.33	1.57	14.70	4.84	4.79	1.64	1.93	3.97	1.82	7.77
Na	4.30	2.07	1.26	1.78	2.09	1.25	3.02	0.87	1.99	0.35	0.46	0.33
K	0.53	0.35	0.24	0.31	0.50	0.17	0.75	0.13	0.29	0.28	0.14	0.21
Al	2.29	0.91	0.56	0.79	0.85	0.50	1.13	0.23	0.22	0.24	0.23	0.12
(ppm)												
Zn	860	651	1045	336	2860	2835	1962	202	488	1047	657	1796
Pb	296	375	136	69	1132	174	189	87	60	626	121	447
Ni	57	79	39	30	70	48	47	77	50	20	30	49
Co	48	30	19	20	60	48	94	38	40	29	30	29
Cu	29	49	39	40	119	29	75	29	30	78	61	136
Cr	96	108	194	59	447	183	160	58	70	127	71	252
Mg	783	335	261	633	715	646	547	366	507	695	848	330
Ca	7727	740	823	742	1549	1080	3745	558	617	1321	646	553
Ba	2259	2395	1983	1294	3780	1995	1894	1629	1450	2458	1970	2109

The relatively high amount of some elements, such as Pb, Zn, Cu, and Ba, provides evidence of the genetic role of hydrothermal solutions (Nicholson, 1992). Some of the elements permit differentiation between manganese oxides formed in fresh water, shallow-marine and marine environment, whereas others distinguish between manganese oxides formed under surface conditions and those precipitated at deeper levels (Nicholson, 1992). For the manganese deposit described in this paper, the oxides must have precipitated under hydrothermal conditions (Fig. 4B), from fluids with a marine component, possibly in a sub-seafloor environment (Fig. 4A).

Hydrothermal enrichment of Zn in manganese deposits has been mentioned from the Galapagos area (Moore and Vogt, 1976, Cronan, 1986, Rogers, 1996), the Mariana-Bonin arc (Hein et al., 2008) and the Tonga-Kermadec Ridge and Lau Basin (Rogers et al., 2001). According to Cronan (1986), Hein et al. (2000), and Rogers et al. (2001), Zn enrichment in manganese deposits may represent the proximity of sulfide deposits that may be located near or below the Zn rich zones.

In terms of the geological, geochemical and mineralogical characteristics, Kimolos shares similarities with volcanic-hosted epithermal systems (Hedenquist et al., 2000). This is a rare example of a vein-type epithermal-style hydrothermal manganese deposit formed in a submarine environment (Roy, 1968, 1997; Canet et al., 2005; Leal et al., 2008).

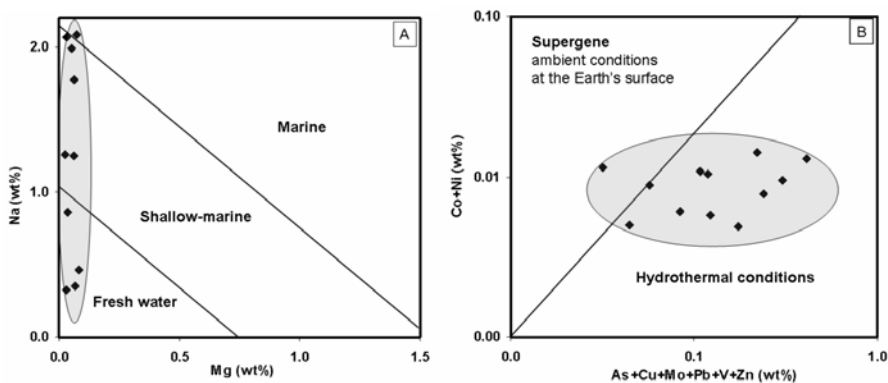


Fig. 4: A. Geochemical signature of manganese oxides from Korakies. A. Marine signature. B. Hydrothermal signature (after Nicholson, 1992).

8. Conclusions

As a result of the present study the following conclusions can be drawn:

1. Base metal-rich manganese oxide mineralization is hosted by a possibly subaqueous monomictic andesitic volcanoclastic lithic breccia, possibly an andesitic in situ hyaloclastite, and shallow-marine or subaerial epiclastic conglomerates, in the Korakies area in NE Kimolos. The deposit has been exploited in the past. Exploitation was centered in a main vein that fills extensional NNE-SSW tectonic lineaments; it has maximum width of 5-6 m, extends for ~250 m, and has unknown depth. The distribution of the mineralized structures coincides with Pliocene NE-SW regional tectonic lineaments, along which the volcanic centres of the island were developed.
2. The vein displays complex and multiepisodic filling with textures characteristic of epithermal open-space precipitation such as crustiform banding, asymmetric banding, vugs, hydrothermal breccias, and cockade and comb textures. The Mn ore forms part of these textures. Ore formation occurred by hydrothermal solutions at shallow depths and at low temperatures.
3. Hydrothermal alteration associated with the mineralization is weak and confined to less than 2 m around the vein, and includes silicification (quartz-adularia and quartz-illite) and propylitization (chlorite-illite). Metallic ore minerals include basically primary pyrolusite and oxides of the isostructural series hollandite-cryptomelane-coronadite, and supergene goethite and hematite. Gangue minerals include quartz, chalcedony, jasper, barite and adularia.
4. The ore contains up to 25.83 % Mn, 14.7 % Fe, 2860 ppm Zn, 1132 ppm Pb, 136 ppm Cu, and 3780 ppm Ba. In addition, concentration of 4.3 % Na, 0.75 % K, 0.77% Ca and 0.09 % Mg has been measured.
5. Seawater together with subordinate contribution of meteoric sources could have been the source(s) for the mineralizing fluids, which formed the deposit in a subseafloor environment.
6. All geological, geochemical and mineralogical evidence compiled in this paper indicate that the Mn deposit of Korakies is similar to volcanic-hosted low-sulfidation epithermal ore deposits, deposited by neutral pH fluids. This is a rare example of a vein-type epithermal-style hydrothermal manganese deposit formed in a marine environment (Canet et al., 2005, Leal et al., 2008).

9. Acknowledgements

This work is based on the first author's B.Sc. thesis. E. Michailidis, I. Mitsis, V. Skounakis and D. Alexakis are all thanked for providing technical support. Many thanks to K. Detsi for her help in this study. Financial support from the University of Athens, Special Account for Research Grants S. P. Kilias (KA 70/4/3373, 70/4/6425) is gratefully acknowledged.

10. References

- Alfieris, D., and Voudouris, P., 2007. High- and intermediate sulphidation Au-Ag-Te mineralization in a shallow submarine setting, Milos island, Greece: Mineralogy and geological environment of formation. In "Digging Deeper" C.J. Andrew et al (editors), v. 2, p. 893-896.
- Canet, C., Prol-Ledesma, R.M., Proenza, J.A., Rubio-Ramos, M.A., Forrest, M.J., Torres-Vera, M.A., and Rodriguez-Diaz, A.A., 2005. Mn-Ba-Hg mineralization at shallow submarine hydrothermal vents in Bahia Concepcion, Baja California Sur, Mexico, *Chemical Geology*, v. 224, I. 1-3, p. 96-112.
- Christidis, G.E., 2001. Formation and growth of smectites in bentonites, a case study from Kimolos Island, Aegean, Greece, *Clays and Clay Minerals*, v. 49, p. 204-215.
- Cronan, D.S., 1986. Geochemical exploration for deep sea mineral deposits. In Thornton, I., Howarth, R., Graham and Trotman (eds), *Applied Geochemistry in the 1980's, London*, p. 241-259.
- Francalanci, L., Vougioukalakis, G.E., and Fytikas, M., 2007. Petrology and volcanology of Kimolos and Polyegos volcanoes within the context of the South Aegean arc, Greece, *GSA Special Papers*, v. 418, p. 33-65.
- Fytikas, M., Innocenti, F., Kolios, N., Manetti, P., Mazuolli, R., Poli, G., Rita, F., and Villari, L., 1986. Volcanology and petrology of volcanic products from the island of Milos and neighbouring islets, *J.volcanol.geotherm*, Res. 28, p. 297-317.
- Fytikas, M., and Vougioukalakis, G., 1993. Volcanic structure and evolution of Kimolos and Polyegos (Milos Island Group), *Bull.Geol.Soc.Greece*, v. 28, p. 221-237.
- Gasby, G.P., Papavassiliou, C.T., Mitsis, J., Valsami-Jones, E., Liakopoulos, A., and Renner, R.M., 2005. The Vani manganese deposit, Milos Island, Greece: A fossil stratabound Mn-Ba-Pb-Zn-As-Sb-W-rich hydrothermal deposit. In Fytikas, M. and Vougioukalakis, G.E. (eds), *Developments in Volcanology*, Elsevier, Amsterdam, v. 7, p. 255-288.
- Hauck, M., 1984. The barite deposits of Milos Island Greece. *Unpubl. PhD Thesis, Univ. Karlsruhe*, 241 pp (in German).
- Hedenquist, J.W., Arribas, A., and Conzalez-Urien, E., 2000. Exploration for epithermal gold deposits, *Reviews in Economic Geology*, v. 13, p. 245-278.
- Hein, J.R., Stamatakis, M.G., and Dowling, J.S., 2000. Trace metal-rich Quaternary hydrothermal manganese oxide and barite deposit, Milos Island, Greece, *Applied Earth Science*, section B, v. 109, p. 67-76.
- Hein, J.R., Schulz, M.S., Dunham, R.E., Stern, R.J., and Bloomer, S.H., 2008. Diffuse flow hydrothermal manganese mineralization along the active Mariana and southern Izu-Bonin arc system, western Pacific, *J. Geophys. Res.*, v. 113, B08S14.
- Kilias, S.P., Naden, J., Cheliotis, I., Shepherd, T.J., Constandinidou, H., Crossing, J., and Simos, I., 2001. Epithermal gold mineralization in the active Aegean volcanic arc: The Profitis Ilias deposit, Milos Island, Greece, *Mineralium Deposita*, v.36, p. 32-44.
- Kilias, S.P., Detsi, K., Godelitsas, A., Typas, M., Naden, J., and Marranitos, Y., 2007. Evidence of Mn-oxide biomineralization, Vani Mn deposit, Milos, Greece. In "Digging Deeper" C.J. Andrew et al (editors), v. 2, p. 1069-1072.

- Leal, P.R., Correa, M.J., Ametrano, S.J., Etcheverry, R.O., Milka, K., and de Brodtkorb, 2008. The manganese deposits of the Pampean Ranges, Argentina, *Canadian Mineralogist*, v. 46, p. 1215-1233.
- Liakopoulos, A., Glasby, G.P., Papavassiliou, C.T., and Boulegue, J., 2001. Nature and origin of the Vani manganese deposit, Milos, Greece: an overview, *Ore Geology Reviews*, v. 18, p. 181–209.
- Moore, W.S., and Vogt, P.R., 1976. Hydrothermal manganese crusts from two sites near the Galapagos spreading axis: Earth Planet, *Sci. Lett.* v. 29, p. 349–356.
- Naden, J., Kiliyas, S.P., Leng, M.J., and Cheliotis, I., 2003. Do fluid inclusions preserve $\delta^{18}\text{O}$ values of hydrothermal fluids in epithermal systems over geological time? Evidence from paleo- and modern geothermal systems, Milos Island, Aegean Sea, *Chemical geology*, v. 197, p. 143-159.
- Naden, J., Kiliyas, S.P., and Darbyshire, D.P.F., 2005. Active geothermal systems with entrained seawater as analogues for transitional continental magmato-hydrothermal and volcanic-hosted massive sulfide mineralization-the example of Milos Island, Greece, *Geology*, v. 33, p. 541-544.
- Nicholson, K., 1992. Contrasting Mineralogical-Geochemical Signatures of Manganese Oxides: Guides to Metallogenesis, *Economic Geology*, v. 87, p. 1253-1264.
- Pe, G.G., and Piper, D.J.W., 1972. Volcanism at subduction zones; The Aegean area, *Bull. Geol. Soc. Greece*, v. 9, p. 113-144.
- Pe-Piper, G., and Piper, D.J.W., 2002. The Igneous rocks of Greece, Berlin, *Gebruder Borntraeger*, 573 pp.
- Plimer, I., 2000. Milos Geologic history, *KOAN Publishing House, Athens*, 262 pp.
- Post, J.E., 1999. Manganese oxide minerals: Crystal structures and economic and environmental significance, *Proc. Natl. Acad. Sci. USA*, v. 96, p. 3447–3454.
- Rogers, T.D.S., 1996. The geochemistry of ferromanganese crusts and sediments from the southern Pacific, *Ph.D. Thesis, University of London*.
- Rogers, T.D.S., Hodgkinson, R.A., and Cronan D.S., 2001. Hydrothermal Manganese Deposits from the Tonga-Kermadec Ridge and Lau Basin Region, Southwest Pacific, *Marine Georesources and Geotechnology*, v. 19, p. 245-268.
- Roy, S., 1968. Mineralogy of the different genetic types of manganese deposits, *Econ. Geol.*, v. 63, p. 760–786.
- Roy, S., 1997. Genetic Diversity of Manganese Deposition in the Terrestrial Geological Record. In Nicholson, K., Hein, J.R., Bihl, B. and Dasgupta, S. (eds), *Manganese Mineralization: Geochemistry and Mineralogy of Terrestrial and Marine Deposits, Geological Society Special Publication*, No. 119, p. 5-27.
- Skarpelis, N., and Koutles, T., 2004. Geology of epithermal mineralization of the NW part of Milos Island: Greece, *5th International Symposium on Eastern Mediterranean Geology*, Thessaloniki, Greece.
- Stewart, A.L., and McPhie, J., 2006. Facies architecture and Late Pliocene – Pleistocene evolution of a felsic volcanic island, Milos, Greece, *Bulletin Volcanology*, v. 68, p.703-726.

CHEMICAL AND MINERALOGICAL ASSESSMENT OF CLAYS FROM PELOPONNESE (S. GREECE) AND THEIR EVALUATION FOR UTILIZATION IN CERAMICS INDUSTRY

Michailidis K., Trontzios G. and Sofianska E.

Aristotle University, Department of Mineralogy-Petrology-Economic Geology 54124 Thessaloniki, Greece, kleopas@geo.auth.gr

Abstract

Mineral constituents, particle size and chemistry of ceramic raw materials may control the way ceramic products are formed and fired. Three compound (combined mixtures of 20 raw samples) clay samples from Chanakia area, Peloponnese (S. Greece), were mineralogically and chemically investigated and their utilization as raw materials for the ceramic industry was evaluated. These samples come from different clay formations, they have red, blue and green colors and constitute the raw materials for a local brick plant. Particle size distribution analysis showed that the percentage of clay size fraction ($d < 2\mu\text{m}$) ranges from 28.3 to 36.3 wt.%. X-ray diffraction analysis revealed that the main mineral constituents are quartz, micas, feldspars (plagioclases, orthoclase), calcite (except the red - clay) and clay minerals (discrete illite, mixed - layered illite/smectite, chlorite and traces of smectite and vermiculite). Projection of their bulk chemistry on some triangular discrimination diagrams has aided us to evaluate their suitability for ceramics production, namely majolica (earthenware), cottoforte, gres and bricks were evaluated. In conclusion, all the studied materials are proved unsuitable for high quality ceramic products. Specifically, the blue and green clays were found suitable for earthenware ceramics as are high porosity building bricks, roofing tiles and similar products, while the red clay is appropriate for gres ceramics as are the low porosity tiles and bricks.

Key words: *Clays, mineralogy, chemistry, bricks, tiles, ceramics.*

1. Introduction

A ceramic product is a material that has been fired to at least 468.3° C (Mitchell, 1983). In addition to being one of our earliest manufacturing and construction materials, ceramic products are among the earliest records of civilization (Austin, 1994). At present, many ceramics are manufactured from mixtures of earth materials which are shaped by compaction and sintered at high temperature.

A wide range of such materials can be transformed into ceramic products, although relatively only few of them make up most of the available resources used for the production of the ceramics offered in today's markets (Burst, 1991). The utilization of specific and well defined materials is a prerequisite for the production of high quality ceramic products (Kromer, 1982; Buhmann et al., 1988; Nakagawa, 1994). Natural clays having specific properties are used for the production of earthenware (faience), semigres (cottoforte) and gres ceramics, as these products are described by the International Association for the study of clays (Veniale and Palmonari, 1974). Water absorption (WA) is the parameter which, according to EN 100 (AFNOR EN 100, 1982), defines the class to which

any ceramic ware belongs. Thus, the fired ceramics (end products) are classified as “faïence” with 16-22 wt.% WA, “semigres” with 12-19 wt.% WA and “gres” with WA<4 wt.%. In the category of faïence and semigres ceramics, are included, among other products, building bricks as well as roof and floor tiles, while in the category of gres, the low porosity tiles and bricks.

Clays and shales are the most widespread ceramic materials in terms of both occurrence and number of mines and plants. Clays that are commonly used for building ceramic products (bricks, roof and floor tiles etc) and coarse earthenwares are usually lean continental sediments, containing different proportions of silt and fine sand, while their clay fraction is usually less than 25% of the total material (Veniale and Palmonari, 1974). The characteristics of clays for building ceramics are not easily defined since they have wide tolerances in their chemical and physical properties. Although the range of natural clays is wide, there are certain requirements concerning their ingredients, in relation to their application. To select the appropriate raw materials, users are always looking for specific criteria, which are related either to the behaviour during the various stages of manufacturing and/or to the overall mineral and chemical composition. Generally, clay-based ceramic raw materials must contain a certain proportion of clay minerals to develop the required plasticity, a proportion of filler (or skeleton formers) materials as quartz, clay, or large fragments of feldspars to prevent excessive shrinkage on drying and firing, and a proportion of fluxes (or glass formers) as are some minerals containing alkalis, magnesium, calcium or iron as fine particles (Mitchell, 1983).

Each ceramic product requires clays having particular and appropriate characteristics. They must not contain a swelling phase and their loss of weight and shrinkage, after drying and firing, have to be low (Austin, 1994; Nahdi et al., 2001). The knowledge of the mineralogical phase composition and especially the clay fraction of the raw materials used for the preparation of ceramic mixtures is of paramount importance for understanding of the technological properties of ceramic products and optimization of firing cycles in production (Teixeira et al., 2001, 2004; Aras, 2004; Ferrari and Gualtieri, 2006)

The mineral content of natural ceramic raw materials controls the way ceramic products are formed and fired. Besides, both the chemical content and crystallite size of constituent minerals affect the response of materials to the firing process, while the elemental composition and the distribution of these elements within raw materials affect the nature of fired products. During the firing process of ceramic raw materials, a series of transformations occur on mineral that will be decisive for establishing the final properties of the ceramic products (Burst and Hughes, 1994; Jordán et al., 2001). Thus, mineral constituents, particle size and chemistry of ceramic raw materials may control the way ceramics are formed and fired (Teixeira et al., 2001). For this purpose, different diagrams have been empirically established on the basis of the grain size or the bulk chemistry to discriminate the suitability of a raw material for the production of various ceramics (Sandrolini and Palmonari, 1974; Vincezini and Fiori, 1976; Schmidt-Reinholz and Schmidt, 1985).

As a function of the extraction process, several raw materials, stemming from different sites of the clay deposits are mixed together in the formulation of ceramic pastes. This may originate a wide range of technical, and industrial problems, since the properties of green bodies and ceramics such as color, mechanical strength, water adsorption, linear contractions during drying and firing cycles is affected by both physical and chemical characteristics as average texture and mineralogical composition (Teixeira et al., 2001). Thus, a detailed characterization of these clay deposits may provide a good help to the local ceramic industries.

Previous investigations (Perraki, 1987; 1990; Perraki and Orfanoudaki 1996; Sikalidis and Minopoulos, 1998; Kastinaki et al., 2004) referred on the evaluation of some Greek clays and mudstones for

the ceramic industry. In W. Peloponnese extensive sedimentary clay deposits are widely used as raw materials for structural red ceramics by local ceramic industries. Furthermore, although there is a great commercial interest in ceramic faience no research has conducted on these clay deposits.

The aim of this study is to investigate the potential use of these clays for the production of ceramic wares on the basis of their particle size, mineral constituents and bulk chemistry.

2. Materials and methods

Samples studied in the present work come from clay formations which are under exploitation by the "ARISTEIDOPOULOS BRICK" local brick factory, at Chanakia (9km on the national road Pyrgos-Patras). These formations are shallow water sediments and typically constitute the lower parts of a Pliocene sedimentary sequence, including fine sands, sandy and clayey deposits. Field observations at the quarry revealed that the clay formations are differentiated, as regard the color, along the depth varying from red at the upper parts to green in the middle and blue at the deeper parts. This distinction in color is attributed to the oxidation state of the iron minerals.

Three compound samples (combined mixtures of 20 raw samples) from the different color clays were collected. In order to assure representative samples, not less than 10Kg were collected. The raw clays from the quarry were preliminary well homogenized. The three clays are referenced on the basis of their color and labelled as RC (red), GC (green) and BC (blue).

Prior to mineralogical and chemical analyses aliquots of about 0.5Kg from each well homogenized sample were disaggregated by grinding in a tungsten mortar for only one minute (Jackson, 1974; Brown and Brindley, 1980). Consequently, 20g splits of each sample were chemically treated, according to the method of Jackson (1974, see also Michailidis et al., 1993), for particle size distribution analyses. Eight size fraction ($>125\mu\text{m}$, 125-63, 63-32, 32-20, 26-16, 8-4, 4-2 and $d < 2\mu\text{m}$) were separated by gravity and centrifugation (Tanner and Jackson, 1947) and estimated as wt.%.

In the sequence, random and oriented mounts were prepared, from bulk clay and the different size fractions for XRD analysis. All the oriented mounts were reanalyzed after ethylene-glycol solvation and heating at 550° C for 2h to distinguish the expandable mineral phases and some were treated with dimethylsulphoxide (DMSO) to resolve kaolinite and chlorite peaks. XRD analysis was done using a Philips X-ray diffractometer (PW 1730) with Ni-filtered Cu K α radiation. Semi-quantitative estimate of the abundances of the minerals were made from the XRD data using the methods of Moore and Reynolds (1997)

The chemical analysis of the bulk clays was performed by atomic absorption spectrophotometry (AAS) using a Perkin Elmer model 3000 apparatus. International geostandards (clay IPT-28, terrigenous clay OOPE-101) provided by Centre de Recherches Pétrographiques et Géochimiques (CRPG) were used as reference materials. Ignition loss was calculated by firing the clays in an oven at 1100° C.

3. Results and discussion

3.1. Particle size distribution analysis

From the particle size distribution analysis of the studied clays (Table 1) results that the blue clay has the higher amount in the clay size fraction (36.3 wt.%) and the lower (0.8 wt.%) in the sand fraction. This feature may increase the plasticity of this clay. In general, the flexural strength and other mechanical properties of ceramics are a function of the particle size distribution and clay com-

Table 1. Grain size distribution (wt.%) of the three compound clay samples

Sample	$d > 63 \mu\text{m}$ (sand)	$d = 63 - 2 \mu\text{m}$ (silt)	$d < 2 \mu\text{m}$ (clay)	C.O.I. ¹ %
RC (red)	7.7	60.2	32.1	2.0
GC (green)	7.9	63.8	28.3	15.3
BC (blue)	0.8	62.9	36.3	16.0

¹Total percentage of carbonates + organics + iron oxides

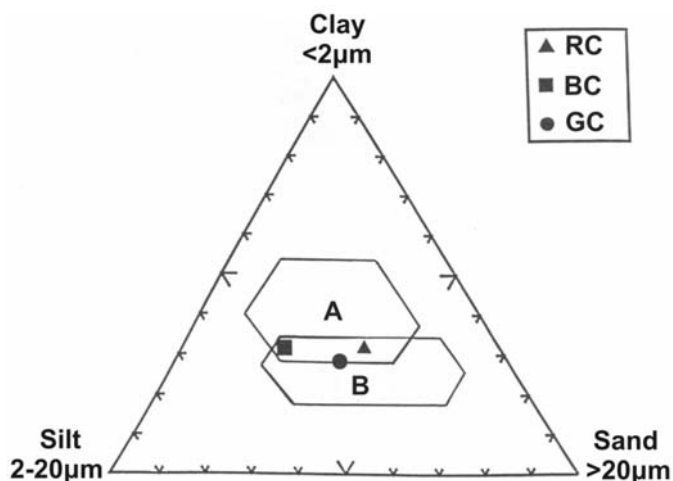


Fig. 1: Evaluation of the clay samples on the basis of their grain size distribution. The fields of roof tiles (A) and bricks (B) are also depicted (after Schmidt-Reinholz and Schmidt, 1985).

position. A low sand concentration is a determining factor to obtain ceramics with high flexural strength (Teixeira et al., 2001). All samples have nearly the same amounts of the silt-size fraction ($d = 32 - 2 \mu\text{m}$) - 60.2 to 63.8 wt.%. Coarse-grained materials increase drying rate, decrease excessive plasticity, and reduce shrinkage and cracking (Mitchell, 1983).

The data of the particle size distribution analysis for the studied clays were depicted in the ternary diagram of Schmidt-Reinholz and Schmidt (1985). From this diagram (Fig. 1) results that all the three clays are suitable for bricks and roof tiles because they are plotted in the overlapping fields of these ceramic wares.

3.2. Mineralogical composition of clay samples

X-ray diffraction analyses of whole rock samples (Fig. 2A) as well as for the $32 - 20 \mu\text{m}$, $20 - 2 \mu\text{m}$ and $< 2 \mu\text{m}$ size fraction showed that the major minerals constituents are quartz, micas, calcite (except RC), feldspars (plagioclases and orthoclase), and clay minerals. Iron minerals are present in the form of pyrite and/or goethite in the three clays. Clay-size particles of the three clays consist dominantly (Fig. 2B) of discrete illite and mixed layered illite/smectite (I/S). Chlorite was identified in the GC and BC clays, while smectite and vermiculite were found in the RC. Semi-quantitative abundances of the minerals (Table 2) show that the RC clay is more quartzitic, while the GC and BC clays are more calcareous.

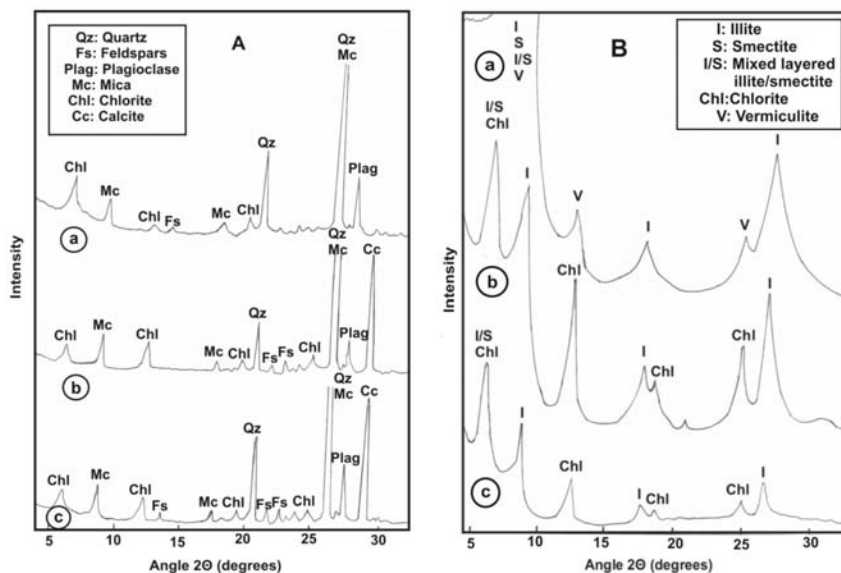


Fig. 2: X-ray diffractograms of the total clay samples (A) and the <2 μm fraction (B) of the studied clays (a: red clay, b: green clay, c: blue clay).

Table 2. Semiquantitative mineralogical analyses of the three compound clay samples

Sample	Qz	Fs	Plag	Mc	Chl	Cc	I	I/S	S	Chl	V
Red Clay (RC)											
Total sample	****		**	**	**	Tr					
32-20μm	****	*	***	**	Tr	//					
20-2μm	****	*	**	**	**	//					
<2μm							+	+	+	±	+
Green Clay (GC)											
Total sample	***		***	**	**	***					
32-20μm	****	*	***	***	*	//					
20-2μm	****	*	**	***	***	//					
<2μm							+	+	-	+	-
Blue Clay (BC)											
Total sample	**	***	**	**	***						
32-20μm	****	*	***	***	*	//					
20-2μm	****	*	**	***	***	//					
<2μm							+	+	-	+	-

Key

*: 1-10%	+: present	Qz: quartz	Chl: chlorite
** : 10-20%	-: not present	Fs: feldspar	I: illite
***: 20-30%	Tr: traces	Plag: plagioclase	I/S: mixed layered (illite/smectite)
****: 30-40%	//: chemically destroyed	Mc: micas	S: smectite
*****:40-50%		Cc: calcite	V: vermiculite

Quartz serves as a non-plastic, in part as filler and in part as glassformer material, decreases the plasticity, facilitates the defloculation and increases the permeability of the ceramic product. The amount of quartz influences the quantity of the amorphous phase after sintering and according to Buhmann et al. (1988), Mitchell (1983), Teixeira et al. (2001) and Das et al. (2005) more quartzitic clays show less shrinkage, with adequate densification and strength values on the ceramic products.

Calcite may provide disadvantages or advantages according to their particle size (Varsos and Sikalidis, 1993). Calcite produces on firing lime (CaO) which slakes in moist air and may crack or “blow” the ceramic product (brick, roof or floor tile). This can be largely avoided in the studied clays because of the fine particle size ($<300\mu\text{m}$, Sikalidis and Minopoulos, 1998). Further more, the finely divided CaCO_3 provides advantages in iron rich clays improving on firing the dark red-brown colour of the product. Calcium compounds act also as binders by glass formation on firing but in excess they may cause premature fusion resulting to distortion of the product. The decomposition of CaCO_3 during firing and the evolution of CO_2 outside the structure of the fired samples tend to create a more porous structure (Darweesh, 2001; Baccour et al., 2009). Thus, the main effect of the calcareous content, and its decomposition on firing, is to increase the porosity, the water absorption and decrease the linear shrinkage (Sousa and Holanda, 2005). Besides, carbonates form a fusible eutectic with alumina and silica (Yatsenko et al., 1998) and also act as fluxing minerals (Andreola et al., 2009).

Feldspars content proportion is moderate ($<20\%$) in RC and moderately high (20-30%) in the GC and BC clays. Plagioclases predominate over K-feldspars, in all clay samples. Feldspars are of major importance in reducing melting points (Mitchel, 1983) promoting vitrification (Buhmann and Fey, 1988). They act as a fluxing material, dissolving first the clay substance and finally the flint particles to form mullite in sufficient quantities to improve ware properties. The feldspar type dictates the content of soda (Na_2O), potash (K_2O) and/or lime (CaO), which in turn influences certain characteristics in the ceramic firing process (Harben, 2002).

Clay minerals along with silica perform a filler function (skeleton formers) of the ceramic articles. Clay size particles of the three clays studied (Table 2) consist of about equal parts of nonexpandable clay minerals (illite and chlorite) and expandable ones (mixed layer illite/smectite, smectite, vermiculite). Illite is one of the major components of clays used in traditional ceramics for the production of cooking pots, plates, tiles and bricks (Ferrari and Gualtieri, 2006). Experimental work by Ferrari and Gualtieri (2006) showed that illite content may determine the percentage of glass phase formed on firing, the linear shrinkage and the water absorption of the fired articles.

3.3. Chemistry of the clay samples

The chemical composition and the ignition loss of the investigated clays are shown in Table 3. These clays consist mainly of SiO_2 and Al_2O_3 which correspond to 58.64-81.38 wt. %.

Since a large quantity of alkalis ($\text{K}_2\text{O} + \text{Na}_2\text{O}$) is present (3.42-4.35 wt.%), these clays may have an important fluxing action and reach the melting point at lower firing temperatures (Darweesh, 2001; Ferrari and Gualter, 2005).

The wt.% of Fe_2O_3 is relatively high (5.04 to 6.50 wt.%) but regarded as acceptable for use in ceramics. Iron is recognised to possess good fluxing properties and the iron oxide content influences the mechanical strength of the ceramics (Anderson et al., 2009; Andji et al., 2009 and Samara et al., 2009).

Projection of the chemical composition of the studied clays on the ternary (empirical) discriminant

Table 3. Chemical analyses of the three compound clay samples

<i>Oxide content</i> <i>wt.%</i>	<i>Clays</i>		
	<i>RC</i>	<i>GC</i>	<i>BC</i>
SiO ₂	67.29	45.57	53.38
Al ₂ O ₃	14.09	13.07	10.49
TiO ₂	0.76	0.68	0.52
MnO	0.15	0.11	0.10
Fe ₂ O ₃ ¹	6.50	6.04	5.04
MgO	1.89	3.42	3.01
CaO	1.02	13.20	11.73
Na ₂ O	1.24	1.92	2.26
K ₂ O	2.18	2.50	2.09
P ₂ O ₅	0.01	0.02	0.02
L.O.I. ²	4.94	13.39	11.20
Total	100.07	99.92	99.84

¹Total iron as Fe₂O₃²Loss on ignition

diagrams proposed by Sandrolini and Palmonari (1974) and Vincenzini and Fiori (1976) elucidates their suitability for ceramic products (Fig. 3). The BC and GC clays were found to be suitable for faience (earthen ware) ceramics which are products with comparatively high values of apparent porosity. This can be explained by the high calcite contents which after firing decompose to lime and volatile CO₂ (Darweesh, 2001; Baccour et al., 2009). The RC having higher quartz content is suitable for gres ceramics.

However, it must be emphasized that conclusions based only on chemical characteristics may lead to misjudgement concerning the suitability of clays for ceramic application. Mineralogical and mainly technological characteristics (e.g. firing tests) are necessary for correct conclusions.

4. Conclusions

The need of technologically accepted raw materials for manufactures of building ceramics (bricks, roof and floor tiles etc) or other clay ceramic products, dictates the investigation, study, and evaluation of local clays towards these applications.

Three compound clay samples (red-blue-green) from a quarry in W. Peloponnese were characterized by particle size analysis, mineralogy and bulk chemistry. The clay size fraction ($d < 2\mu\text{m}$) percentage ranges from 28.3 to 36.3 wt.%.

The clays are of illitic type containing substantial amounts of quartz and calcite (blue and green). The major mineral constituents are quartz, micas, calcite, feldspars and clay minerals. The clay fraction consist mainly of discrete illite and mixed layered I/S.

On the basis of their grain size and specifically on their chemical composition the green and blue clays were found suitable for earthen ware ceramics as are high porosity building bricks, roofing tiles and similar products, while the red clay suitable for gres ceramics.

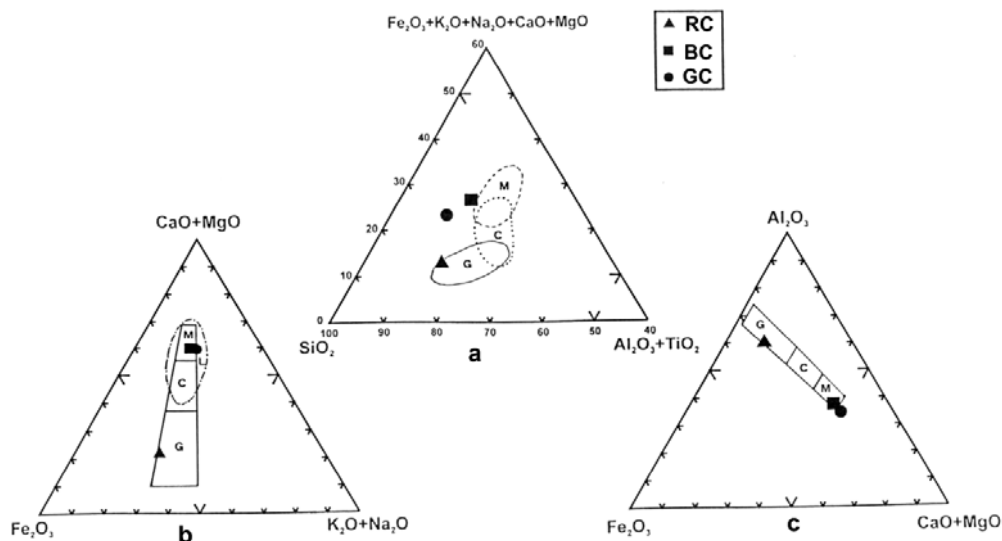


Fig. 3: Projection of the chemical composition of the three compound clay samples on the diagrams: a) SiO₂-(Fe₂O₃+K₂O+Na₂O+CaO+MgO)-(Al₂O₃+TiO₂), b) Fe₂O₃-(MgO+CaO)-(K₂O+Na₂O) and c) Fe₂O₃-Al₂O₃-(CaO+MgO) (after Sandrolini and Palmonari, 1974; Vincenzini and Fiori, 1976). M: majolica, C: cottoforte (semigres), G: gres, F: faïence (earthenware).

5. Acknowledgments

Special thanks are due to Dr. D. Papoulis for his constructive comments, resulting in significant improvement of this paper.

6. References

- AFNOR EN 100, 1982. Careaux et dalles céramiques. Détermination de la résistance à la flexion. 12 pp.
- Anderson, M., Elliott and M., Hickson, C., 2002. Factory scale trials using combined mixtures of three by-product wastes (including incinerated sewage sludge ash) in clay building bricks. *Journal of Chemical Technology and Biotechnology*, 77, 345-351.
- Andji, J., Abba Toure, A., Kra, G., Jumas, J., Yvon, J. and Blanchart, P., 2009. Iron role on mechanical properties of ceramics with clays from Ivory Coast. *Ceramics International*, 35, 571-577.
- Andreola, F., Siligardi, C., Manfredini, T. and Carbonchi, C., 2009. Rheological behaviour and mechanical properties of porcelain stoneware bodies containing Italian clay added with bentonites. *Ceramics International*, 35, 1159-1164.
- Aras, A., 2004. The change of phase composition in kaolinite- and illite- rich clay-based ceramic bodies. *Applied Clay Science*, 24, 257-269.
- Austin, G., 1994. Adobe and Similar Materials. In: D. D. Carr (ed.). *Industrial minerals and rocks 6th ed.* Society for Mining, Metallurgy and Exploration, Inc. Littleton, Colorado, 279-286 p.
- Baccour, H., Medhioub, M., Jamoussi, F. and Mhiri, T., 2009. Influence of firing temperature on the ceramic properties of Triassic clays from Tunisia. *Journal of Materials Processing Technology*, 209, 3812-2817.

- Brown, G. and Brindley, G., 1980. X-ray diffraction procedures for clay mineral identification. In: G.B. Breindley and G. Brown (Editors), *Crystal Structures of Clay Minerals and Their X-ray Identification*. Mineral. Soc., London, 305-360 p.
- Buhmann, C., De Villiers, J. and Fey, M., 1988. The mineralogy of four heaving clays. *Applied Clay Science*, 3 (3), 219-236.
- Burst, J., 1991. The application of clay minerals in ceramics. *Journal Applied Clay Science*, 5, 421-443
- Burst, J. and Hughes, R., 1994. Clay-based ceramic raw materials. In: D. D. Carr (ed.), *Industrial minerals and rocks 6th ed.* Society for Mining, Metallurgy and Exploration, Inc. Littleton, Colorado, 317-324 p.
- Darweesh, H., 2001. Building materials from siliceous clay and low grade dolomite rocks. *Ceramics International*, 27, 45-50.
- Das, S., Dana, K., Singh, N. and Sarkar, R., 2005. Shrinkage and strength behaviour of quartzitic and kaolinitic clays in wall tile compositions. *Applied Clay Science* 29, 137-143.
- Ferrari, S. and Gualtieri, A., 2006. The use of illitic clays in the production of stoneware tile ceramics. *Applied Clay Science*, 32, 73-81.
- Harben, P. W., 2002. *The Industrial Minerals. Handy Book A guide to markets, specification and prices.* 4th edition. Industrial Mineral Information, London, 409pp.
- Jackson, M., 1974. *Soil Chemical Analysis*. Adv. Course. 2nd ed. Madison, WI, 690pp.
- Jordán, M., Sanfeliu, T. and De la Fuente, C., 2001. Firing transformation of Tertiary clays used in the manufacturing of ceramic tile bodies. *Applied Clay Science*, 20, 87-95.
- Kastrinaki, A., Tsirambides, A., Michailidis, K. and Trontzios, G., 2004. Evaluation of mudstone formations and their suitability for ceramics production. *Bulletin Geological Society Greece*, 10th International Congress, XXXVI (1), 19-27.
- Kromer, H., 1982. *Mineralogical and technological characteristics of ceramic clays*. International Clay Conference, 685-697 p.
- Michailidis, K., Tsirambides, and Tsamantouridis, P., 1993. Kaolin weathering crusts on gabbroic rocks at Griva, Macedonia, Greece. *Applied Clay Science*, 8, 19-36.
- Mitchel, L., 1983. Ceramic Raw Materials. In: S.J. Lefond, ed. *Industrial Minerals and Rocks*, 5th (ed.), Vol. 1, AIME, New York, 33-39 p.
- Moore, D. M. and Reynolds R. C. Jr., 1997. *X – Ray Diffraction and the Identification and Analysis of Clay Minerals*. 2nd ed. Oxford Univ. Press, New York, 378 pp.
- Nahdi, K., Gasmí, N. and Trabelsi Ayedi, M., Kbir-Arigoib, N., 2001. Characterization and thermal behaviour of Jebel Ressas clay. *Journal of Societe Chimique de Tunisie*, 4, 125-134.
- Nakagawa, M., 1994. Clay mineral associations and mineralogical properties of quartz in some pottery of western Kyushu, Japan. *Applied Clay Science*, 8 (5), 331-347.
- Perraki, T., 1987. Study of the mineralogical and technological characteristics of ceramic clays from Attiki, Chalkida and Viotia, Ph. D. Thesis, Nat. Tech. Univ. Athens, Athens.
- Perraki, T., 1990. Characteristic of ceramic clays from areas Perivolia and Stalos of Chania Region. *Mineral Wealth*, 64, 41-47.
- Perraki, T. and Orfanoudaki, A., 1996. Evaluation des pates argileuses, en fonction de leur composition chimique en vue de leur utilisation dans la fabrication d'objets ceramiques. *Mineral Wealth*, 100, 15-22.
- Samara, M., Lafhaj, Z. and Chapiseau, C., 2009. Valorization of stabilized river sediments in fired clay bricks: Factory scale experiment. *Journal of Hazardous Materials*, 163, 701-710.

- Sanrdolini, F. and Palmonari C., 1974. Variazioni strutturali e dimensionali durante la cottura di argille italiane per materiali da costruzione. *La Ceramica*, 17, 6-12.
- Schmidt-Reinholz, C. and Schmidt, H., 1985. Suitability tests on raw materials, heavy clay bodies and structural ceramic products. *Interbrick*, 1, 38-42.
- Sikalidis, C. and Minopoulos, P., 1998. Chemical, mineralogical and technological characteristics of natural clays from Macedonia (N. Greece) and their evaluation for utilization in ceramics industry. *Mineral Wealth*, 107, 47-54
- Sousa, S. and Holanda, J., 2005. Development of red wall tiles by the dry process using Brazilian raw materials. *Ceramics International*, 35. 215-222.
- Tanner, C. B. and Jackson, M.L., 1947. Nomographs of sedimentation times for soil particles under gravity or centrifugal acceleration. *Soil Science Society Proceedings of America*, 60-65.
- Teixeira, S., de Sousa, S. and Moura, A., 2001. Mineralogical characterization of clays used in the structural ceramic industry in west of S. Paulo state, Brasil. *Cerâmica*, 47, 204-207.
- Teixeira, S., de Sousa, S. and Nobre, M., 2004. Physical and mechanical properties of ceramics from clays of the west of S. Paulo State, Brasil. *Cerâmica*, 50, 268-273.
- Veniale, F. and Palmonari, C., 1974. Giacimenti di Argolle Ceramiche in Italia. *International Association for clay Research*. Gruppo Italiano A.I.P.E.A. Bologna, 310 pp.
- Varsos, D. and Sikalidis, C., 1993. The preparation of ceramic raw materials through the dry process. *International Journal of Tile and Brick*, 19 (3), 137-140.
- Vincenzini, P and Fiori C., 1976 Italian clays for the production of building material. Their characteristics and some technical properties. *Ceramurgia*, 7 (3), 119-134.
- Yatsenko, N., Zubekhin, A. and Rakova, V., 1998. Low shrinkage ceramic tiles. *Glass Ceramics* 55 (7-8), 255-257.

STUDY OF THE METAMORPHIC EVOLUTION OF A CARBONATE-BEARING METAPERIDOTITE FROM THE SIDIRONERO COMPLEX (CENTRAL RHODOPE, GREECE) USING P-T AND P(T)-X_{CO₂} PSEUDOSECTIONS

Mposkos E. and Baziotis I.

National Technical University of Athens, Department of Mining and Metallurgical Engineering, Section of Geological Sciences, Heroon Polytechniou 9, 15780, Athens, Greece, mposkos@metal.ntua.gr, baziotis@metal.ntua.gr

Abstract

The carbonate-bearing metaperidotite from Sidironero Complex, north of the Xanthi town is composed primarily of olivine and orthopyroxene megacrysts and of Ti-clinohumite, tremolite, chlorite, dolomite, magnesite, talc, antigorite and spinel group minerals. The metaperidotite underwent a prograde HP metamorphism probably isofacial with the neighboring amphibolitized eclogites. Calculated P-T and P(T)-X_{CO₂} phase diagram sections (pseudosections) for the bulk rock composition showed that X_{CO₂} in the fluid phase was extremely low (≤ 0.008) at the first stages of the metamorphism and increased up to 0.022 at the peak P-T conditions ~ 1.5 GPa and 690 °C. The prograde metamorphism probably started from a hydrated and carbonated assemblage including talc+chlorite+magnesite+dolomite and proceeded with tremolite and antigorite formation before olivine growth, and orthopyroxene formation after olivine growth (Ol-1). Matrix dolomite, breakdown of chlorite (Chl-1) to Cr-spinel+olivine and of Ti-clinohumite to olivine+Mg-ilmenite occurred during decompression. The P-T path is constrained by the absence of clinopyroxene in the metaperidotite.

Key words: Carbonate-bearing metaperidotite, pseudosections, Rhodope, Sidironero.

1. Introduction

Carbonate-bearing peridotites in metamorphic terrains provide excellent information about P-T regimes and fluid phase composition. Phase relationships for carbonate-bearing peridotites of lherzolitic bulk compositions are very useful for deciphering details of the metamorphic evolution of a terrain. Thus, peridotites can bear important geodynamic implications that are mostly obscure in other rock types.

The objective of this paper is to describe the successive formation of mineral phase assemblages in the frame of the metamorphic evolution of a carbonate-bearing chlorite-spinel metaperidotite from the HP/UHP Sidironero Complex in the area of Gorgona, north of Xanthi. We calculate P-T-X_{CO₂} pseudosections in the CaO-FeO-MgO-Al₂O₃-SiO₂-CO₂-H₂O (CFMAS-fluid) system using the Perplex software (ver.06 Jul 2006; Connolly, 2009) and the internally-consistent thermodynamic database (Holland and Powell 1998, revised 2002). Calculated P-T (for fixed X_{CO₂}) and P(T)-X_{CO₂} (for specific geothermal gradient) pseudosections for the bulk-rock composition of the studied metaperidotite are able to illustrate the stability fields of certain mineral assemblages and to evaluate the composition of the fluid phase in the successive stages of the metamorphic evolution of the metaperidotite.

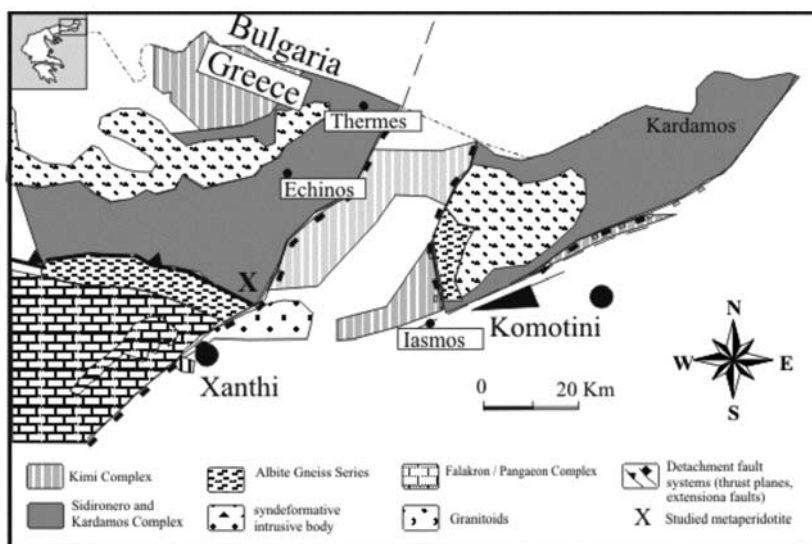


Fig. 1: Geological map of Xanthi area showing the location of the carbonate-bearing metaperidotite (Krohe and Mposkos, 2002).

2. Geological setting

The Rhodope HP Domain extends over large areas of northern Greece and southern Bulgaria. The Greek part of Rhodope is subdivided by Mposkos and Krohe (2000) into several tectonometamorphic complexes that are bounded by thrust and normal faults. These segments differ in P-T conditions during their HP metamorphism, shape of P-T paths and timing of exhumation. The Sidironero complex, where the studied carbonate-bearing metaperidotite occurs, consists predominantly of migmatitic pelitic gneisses and orthogneisses, with intercalations of amphibolitized eclogites, marbles and rare serpentized peridotites. The least serpentized lense of ultramafic rocks from Sidironero Complex in the Xanthi area is the carbonate-bearing metaperidotite from Gorgona location (Fig. 1). It is a small body ~200m wide and ~500m long, surrounded by orthogneisses. The Sidironero Complex records a Late-Jurassic HP/UHP metamorphism similar to the overlying Kimi Complex documented by the presence of partially amphibolitized eclogites and diamond inclusions in garnet from pelitic gneisses (Mposkos and Kostopoulos, 2001; Perraki et al., 2004, 2006; Liati, 2005; Liati and Mposkos, 1990), but experienced an additional weaker Eocene metamorphic overprint (Liati, 2005; Bosse et al., 2009).

3. Petrography and mineral chemistry

The metaperidotite is composed primarily of coarse grained (3-20 mm in size) olivine and orthopyroxene and medium to fine grained (0.9-0.01mm in size) Ti-clinohumite, tremolite, chlorite, dolomite, magnesite, talc, antigorite, light brown to opaque minerals of the spinel group and pentlandite. Anthophyllite replacing orthopyroxene is reported by Kassoli-Fourmaraki et al. (1995).

Olivine (Fo₉₀₋₉₂) occurs in two generations that overgrow each other. The first generation (Ol-1; abbreviations after Martin, 1998) forms irregularly shaped megacrysts commonly rich in fluid inclusions 2 to 5 μm in size. Most of the inclusions are composite and contain one or two solid phases. Micro-Raman spectroscopy showed that the solid phases are talc and magnesite. Ol-1 contains in-

clusions of tremolite, dolomite, talc, magnesite, chlorite, Cr-magnetite and ferrit-chromite (Fig. 2a). The second olivine generation (Ol-2) contains inclusions of light brown Cr-spinel, dolomite and Al-bearing tremolite (Al_2O_3 up to 5.4 wt%). In places Ol-2 overgrows Ol-1 as indicated by inclusions of spinel at the outer parts of some olivine megacrysts (Fig. 2b). These inclusions of light brown chromian-spinel are commonly oriented in the olivine host suggesting simultaneous crystallization of chromian-spinel and host olivine, probably as decomposition products of chlorite. Ol-2 and light brown chromian-spinel are replaced by retrograde diablastic chlorite and magnesite (Fig. 2c).

Orthopyroxene (En_{89-90}) forms sub-idiomorphic prismatic megacrysts. Inclusions of chlorite, tremolite, dolomite, magnesite and olivine in orthopyroxene are common (Figs. 2d). Olivine inclusions in orthopyroxene show corroded edges (Fig. 2e), indicating that orthopyroxene grew from olivine (Ol-1). Cr-magnetite and ferrit-chromite also occur as inclusions in orthopyroxene; but light brown chromian-spinels which are common inclusions in Ol-2 were not observed. This suggests that the formation of orthopyroxene preceded that of the Ol-2. Rarely orthopyroxene occurs also as inclusions in olivine (Fig. 2f).

Ti-clinohumite occurs as inclusions in olivine, orthopyroxene, tremolite and ferrit-chromite. Matrix Ti-clinohumite forms granoblastic megacrysts up to 0.8 mm in size in epitaxial intergrowth with olivine, both minerals showing contemporaneous extinction in thin section. Segments of the clinohumite megacryst are decomposed to olivine and lamellar Mg-ilmenite (Fig. 3a). Representative composition of Ti-clinohumite is given in table 1. TiO_2 content ranges from 4.07 to 4.69 wt% and F content from 1.33 to 1.67 wt%.

Two generations of chlorite are distinguished. The first generation (Chl-1) occurs as inclusions in orthopyroxene, olivine, Ti-clinohumite, dolomite and ferrit-chromite (Fig. 2d). The second generation (Chl-2) is retrograde and forms diablastic flakes replacing olivine (Ol-2) and light brown chromian spinel. It is associated with retrograde talc, magnesite and tremolite (Fig. 2c). Olivine grains with corroded edges and rods of spinel aggregates are included in Chl-2. The two generations of chlorite distinguished on textural criteria show remarkable differences in their chemical composition. Chl-1 shows higher Cr_2O_3 and lower Al_2O_3 contents compared to Chl-2 (Tab. 1). The Cr_2O_3 and Al_2O_3 contents in Chl-1 range from 2.33 to 5.79 wt% and 12.07 to 13.68 wt% and in Chl-2 from 0.71 to 1.63 wt% and 16.99 to 20.33 wt% respectively.

Inclusions of tremolite (Tr-1) in olivine (Ol-1), orthopyroxene and dolomite are common (Fig. 2c,3b). Al-bearing tremolite (Tr-2) occurs as inclusions in Ol-2 and in the matrix. It is associated with Ol-2 and light brown chromian spinel, and commonly overgrows tremolite-1 as indicates the increase in Al_2O_3 content from the core (0.2 wt%) to the rim (5.36 wt%, Tab.1). Retrograde matrix tremolite (Tr-3) is associated with matrix chlorite (Chl-2), magnesite (Mgs-2) and talc and replaces orthopyroxene, olivine and dolomite. Tr-1 is low in aluminum. Most tremolite inclusions in Ol-1 and orthopyroxene have Al_2O_3 contents less than 0.15 wt% and those included in matrix dolomite of less than 0.6 wt%. In Tr-2, which is associated with Ol-2 and light brown spinel, the Al_2O_3 content ranges from 3.2 to 5.4 wt%. Retrograde tremolite (Tr-3) again contains less than 0.10 wt% Al_2O_3 . The $\text{Mg}/(\text{Mg}+\text{Fe})$ ratio in all tremolites ranges from 0.94 to 0.95.

Dolomite inclusions in Ol-2 contain inclusions of magnesite, commonly with corroded edges (Fig. 3c). Matrix dolomite is in textural equilibrium with olivine and orthopyroxene. It contains inclusions of tremolite (Tr-1), chlorite (Chl-1), magnesite (Mgs-1) and olivine (Ol-1) (Fig. 3b). Dolomite contains FeO 1.4-1.6 wt%. Two magnesite generations are distinguished based on textural criteria. Mgs-1 occurs as inclusions in olivine, orthopyroxene and dolomite. Matrix magnesite (Mgs-2) is associated with matrix chlorite (Chl-2); both minerals are formed during replacement of olivine and

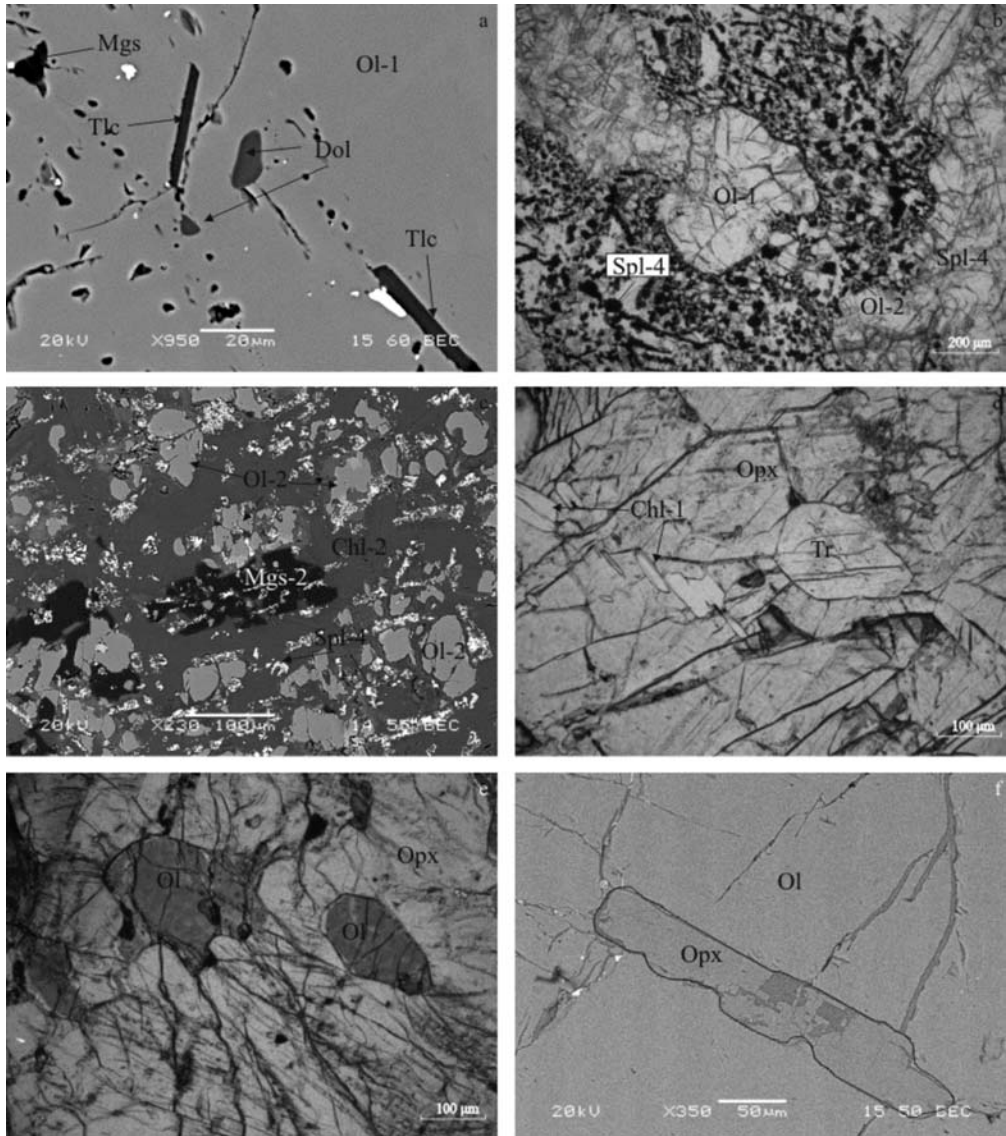


Fig. 2: (a) Inclusions of talc (Tlc), dolomite (Dol) and magnesite (Mgs) in olivine (Ol-1). (b) Two generations of olivine. Ol-2 with inclusions of Cr-spinel (Spl-4) is overgrown Ol-1, which is free of spinel inclusions. (c) Spinel aggregates (Spl-4) and olivine (Ol-2) are replaced by secondary chlorite (Chl-2) and magnesite (Mgs-2). (d) Inclusions of chlorite (Chl-1) and tremolite (Tr) in orthopyroxene. (e) Inclusions of olivine (Ol-1) in orthopyroxene (Opx). The inclusions show corroded edges. (f) Inclusion of orthopyroxene in olivine. (a), (c), (f): Backscattered electron (BSE) image . (b), (d), (e): Microphotographs.

Table 1. Representative mineral compositions of tremolite (Tr), chlorite (Chl), Ti-clinohumite (Ti-Chu) and spinel group minerals (Spl) of the carbonate-bearing metaperidotite from Gorgona (N Xanthi area).

A/A	1	2	3	4	5		6	7	8	9	10
	Tr-1 ^c	Tr-2	Chl-1	Chl-2	Ti-Chu		Spl-1 ^c	Spl-4 ^r	Spl-2	Spl-3 ^c	Spl-4 ^r
SiO ₂	58.30	55.09	32.54	31.02	35.88	TiO ₂	-	-	-	2.49	-
TiO ₂	-	-	-	-	4.69	Al ₂ O ₃	35.69	54.07	1.45	13.71	61.57
Al ₂ O ₃	0.12	5.36	13.30	20.33	-	Cr ₂ O ₃	29.33	14.42	9.88	35.71	4.25
Cr ₂ O ₃	-	0.04	5.79	0.71	-	Fe ₂ O ₃	3.871	1.221	58.991	15.681	5.221
FeOt	2.24	1.78	1.05	2.48	8.41	FeO	19.731	11.241	24.891	25.331	4.251
MnO	0.04	-	0.02	0.02	0.09	MnO	0.04	-	0.02	0.02	-
MgO	23.0	21.27	33.35	32.65	48.08	MgO	11.77	19.20	3.27	7.15	23.54
NiO	0.03	0.05	0.25	0.18	0.37	NiO	-	-	1.54	0.02	-
CaO	13.52	13.52	-	-	1.59*	CaO	-	-	-	-	-
Total	97.2	97.02	86.30	87.40	99.1	Total	100.47	100.15	100.04	100.23	100.54
O	23	23	14	14	+	O	4	4	4	4	4
Si	8.002	7.572	3.115	2.900	3.777	Ti	-	-	-	0.062	-
Ti	-	-	-	-	0.371	Al	1.234	1.676	0.063	0.539	1.818
Al	0.020	0.868	1.501	2.241	-	Cr	0.680	0.299	0.290	0.942	0.084
Cr	-	0.010	0.438	0.053	-	Fe ³⁺	0.085	0.024	1.647	0.394	0.098
Fe ²⁺	0.257	0.204	0.084	0.194	0.740	Fe ²⁺	0.484	0.247	0.771	0.706	0.121
Mn	0.005	-	0.002	0.002	0.01	Mn	0.001	-	-	-	-
Mg	4.709	4.357	4.758	4.550	7.545	Mg	0.515	0.753	0.181	0.355	0.879
Ni	0.003	0.005	0.019	0.014	0.031	Ni	-	-	0.047	-	-
Ca	1.990	1.997	-	-	0.528	Ca	-	-	-	-	0.007

spinel at a retrograde stage of metamorphism (Fig. 2c). Matrix magnesite is also associated with talc, replacing olivine and orthopyroxene, or with tremolite, replacing olivine and dolomite. The FeO content in magnesite ranges from 4.2-5.2 wt%, the MnO content from 0.23-0.24 wt% and the CaO content from 0.45-0.50 wt%.

Four types of spinel group mineral are recognized. Spl-1 is dark-brown and occurs only as cores in zoned crystals (Fig. 3d). Spl-2 and -3 are Cr-magnetite and ferrit-chromite respectively and occur as single grains, or grain aggregates, in the matrix and as inclusions in olivine, orthopyroxene, tremolite and chlorite. Spl-4 is light brown, more or less chromian spinel and associated with olivine (Ol-2) and rarely with tremolite (Tr-2). It is also enclosed in matrix chlorite (Chl-2) and matrix magnesite (Mgs-2)(Fig. 2c). In zoned chromite grains, Spl-4 always forms the outer zone, with cores consisting of type-1 or type-3 spinel (Figs. 3d,e). However, zoning with Spl-4 core and Spl-3 rim also occurs as an alteration product.

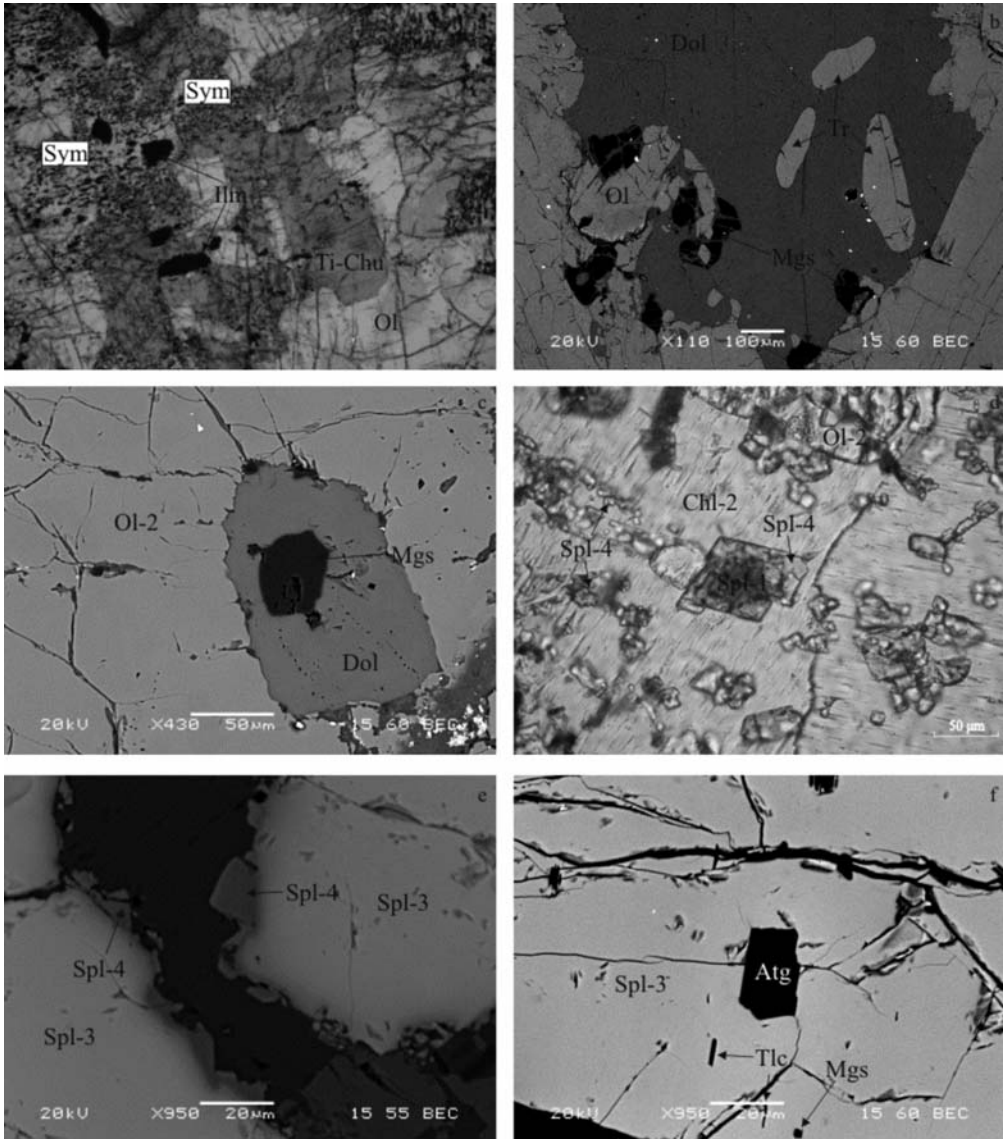


Fig. 3: (a) Ti-clinohumite (Ti-Chu) and olivine (Ol-1) intergrowth. Ti-clinohumite in part is decomposed to olivine+Mg-ilmenite (Sym). (b) Matrix dolomite (Dol) with inclusions of tremolite (Tr), magnesite (Mgs) and olivine (Ol). (c) Inclusion of dolomite in olivine (Ol-2). The dolomite inclusion contains inclusion of magnesite (Mgs) (d) Chromite (Spl-1) overgrown by Cr-spinel (Spl-4) is included in retrograde chlorite (Chl-2). (e) Ferrite-chromite (Spl-3) is overgrown by Cr-spinel (Spl-4). (f) Inclusions of talc (Tlc), magnesite (Mgs) and antigorite (Atg) in ferrite-chromite (Spl-3). (a), (d): Microphotographs. (b), (c), (e), (f): BSE image.

The four types of Cr-spinel minerals distinguished by textural criteria also show remarkable differences in their chemical compositions, indicating growth of spinel minerals at different metamorphic conditions (Tab. 1). Spinel-1 has a Cr# [$\text{Cr}/(\text{Cr}+\text{Al}+\text{Fe}^{3+})$] ratio ranging from 0.34 to 0.43 and a Mg# [$\text{Mg}/(\text{Mg}+\text{Fe}^{2+})$] ratio from 0.38 to 0.51. It probably represents relics of the mantle protolith. Spinel-2 is Cr-magnetite with a Cr# ranging from 0.17 to 0.18. Spinel-3 is ferrit-chromite, with magnetite component ($\text{Fe}^{3+}/\text{R}^{3+}$) ranging from 28 to 43 % and Al-spinel component from 0.03 to 38.3 %. It is characterized by low Mg-contents with Mg# ranging from 0.11 to 0.30. Spinel-4 is chromian spinel with Cr# and Mg# ranging from 0.04 to 0.24 and from 0.67 to 0.91 respectively. The compositional variation in spinel group minerals from Cr-magnetite to ferrit-chromite and chromian spinel, and the compositional zoning with increasing Al content, from the core to the rim in zoned grains suggest a prograde metamorphic evolution of the Gorgona metaperidotite from lower to higher grade conditions. Cr-magnetite is common in serpentized peridotites at greenschist and ferrit-chromite at amphibolite facies conditions (Evans and Frost, 1975).

Talc is found as inclusions in Ol-1 and ferrit-chromite (Figs. 2a, 3f). Secondary talc forms unoriented flakes in the matrix and is associated with matrix magnesite and chlorite replacing olivine and orthopyroxene. Talc has the highest Mg/(Mg+Fe) ratio (0.97) of all the silicate minerals in the metaperidotite. The Al_2O_3 content is up to 0.10 wt% and Cr_2O_3 up to 0.06 wt%. Primary antigorite is rare and is found only as single grain inclusions in ferrit-chromite (Fig. 3f) and olivine. Retrograde serpentine replaces olivine megacrysts along fractures and is associated with retrograde chlorite and talc. The antigorite inclusions in ferrit-chromite have FeO contents ranging from 1.15 to 5.13 and Cr_2O_3 contents up to 0.75 wt%. Mg-Ilmenite (MgO 7.60-8.43 wt%) occurs as inclusions in ferrit-chromite and Ti-clinohumite and as oriented laths in olivine; the latter are decomposition products of former Ti-clinohumite (Fig. 3a).

4. Discussion

4.1 Metamorphic evolution

The inclusions of magnesite, dolomite, chlorite, talc, tremolite, antigorite in ferrit-chromite, olivine and orthopyroxene and the chemical compositions of zoned spinel minerals with increasing Al content toward the rim (Table 1) demonstrate very convincingly the prograde metamorphic character of the Gorgona metaperidotite. The prograde metamorphic evolution probably started from hydrated and carbonated assemblage including talc + chlorite + magnesite + dolomite (+ antigorite) + Cr-magnetite. We assume that the metamorphic evolution occurred in a subduction related environment as is suggested by the presence of amphibolitized eclogites in the same locality (Liati and Mposkos, 1990). Minimum pressures of 1.3 GPa and temperatures of 650-700°C are obtained from the amphibolitized eclogites for the HP event (Liati and Mposkos, 1990). In the tectonometamorphically equivalent Kimi area (eastern Rhodope) P-T conditions of ~700°C and >1.75 GPa are reported for the eclogite stage followed by a temperature increase (~750°C) during the first stage of decompression (Bauer et al., 2007). Therefore, a relatively cool subduction gradient of around 12°C/km was logically assumed for the prograde part of the P-T path.

In order to assess the P-T stability fields and the fluid behavior of the metaperidotite along the selected P-T path, we calculated P-T and P(T)- X_{CO_2} phase diagram sections (pseudosections) for the bulk rock composition 1.95 CaO:5.29 FeO:52.67 MgO:0.81 Al_2O_3 :39.67 SiO_2 (in weight amount) in the system CFMASCHO (CaO-FeO-MgO- Al_2O_3 - SiO_2 - CO_2 - H_2O) (Figs 4, 5) and the results compared with observed phase relationships in the rocks. Calculations were performed with the software Perplex (ver.06 Jul 2006). The thermodynamic database of Holland and Powell (1998, revised 2002)

Inspection of the figure 4 shows that the main reactions, represented by narrow trivariant and divariant fields and some univariant lines, delimit the stability of antigorite, talc, tremolite, orthopyroxene, olivine and spinel. With increasing temperature the successive formed minerals are tremolite, orthopyroxene, clinopyroxene, olivine and dolomite at high pressures and antigorite, tremolite, olivine, dolomite and spinel at lower pressures. Chlorite is stable at a wide P-T field and is decomposed to spinel+olivine at high temperatures. At $X_{\text{CO}_2}=0.02$ the coexistence of orthopyroxene + olivine imply minimum pressure of 1.46 GPa at 635°C (Fig. 4b). With decreasing X_{CO_2} in fluid phase the orthopyroxene stability field is shifted toward higher pressures (Fig. 4a).

The presence of talc, chlorite, magnesite, dolomite and antigorite inclusions in ferrite-chromite, of magnesite, dolomite, chlorite, tremolite, talc and ferrite-chromite inclusions in olivine, and of magnesite, dolomite, chlorite, tremolite and olivine (Ol-1) inclusions in orthopyroxene indicate that the earliest assemblage was talc + chlorite + magnesite + dolomite, with tremolite and antigorite formation before olivine growth and orthopyroxene formation after olivine growth (Ol-1).

For the selected P-T path and for $X_{\text{CO}_2}<0.008$ in the fluid phase, the formation of orthopyroxene in the Gorgona metaperidotite is not expected (see figure 4a). Orthopyroxene can be expected if we assume an increase in X_{CO_2} in the fluid phase. The selected P-T path crosses the orthopyroxene stability field if $X_{\text{CO}_2}>0.02$ (Fig. 4b). However, at $X_{\text{CO}_2}>0.02$ (Fig. 4b) the antigorite is not expected and orthopyroxene comes earlier than olivine, but this is not in accordance with our petrographic observations.

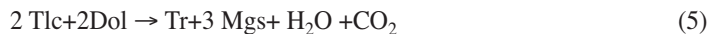
In closed system, the X_{CO_2} value increases by the antigorite and olivine forming reactions 3 and 4. Reaction 3 produces only CO_2 whereas reaction 4 produces more CO_2 than H_2O .

Based on the textural relationships, P-T path and P(T)- X_{CO_2} estimation, it seems that the mineral assemblages in the Gorgona metaperidotite, are formed in two equilibrium stages; a prograde stage and a decompression stage of metamorphism.

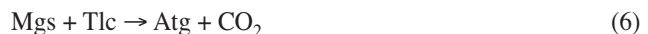
Prograde stage:

The inclusions of magnesite, dolomite, chlorite, talc tremolite in olivine, and magnesite, dolomite, chlorite, tremolite in orthopyroxene indicate that the prograde path of metamorphism crossed the stability fields of Dol+Mgs+Tlc+Chl and Tr+Tlc+Mgs+Chl before the formation of olivine and orthopyroxene. The rare inclusions of antigorite in ferrite-chromite inclusions in olivine show that the prograde path also crossed the antigorite stability field.

For the selected geothermal gradient of 12°C/km, the prograde path crosses the stability field of Tr+Mgs+Tlc+Chl if $X_{\text{CO}_2} \geq 0.0075$ (Fig. 5a). Tremolite is formed by the reaction:



without changes in the mole fraction of the primary X_{CO_2} value. With increasing pressure and temperature, the P-T path meets the boundary of the trivariant Chl+Mgs+Tr+Tlc and the divariant Chl+Tlc+Tr+Atg+Mgs field and antigorite is formed at the expense of talc and magnesite according to the divariant reaction:



As the P-T path moved along this boundary, the modal antigorite increases up to the pseudo-invariant point A, where Chl+Tr+Tlc+Mgs+Atg+Ol is stable and olivine is formed according to the univariant and divariant reactions respectively:

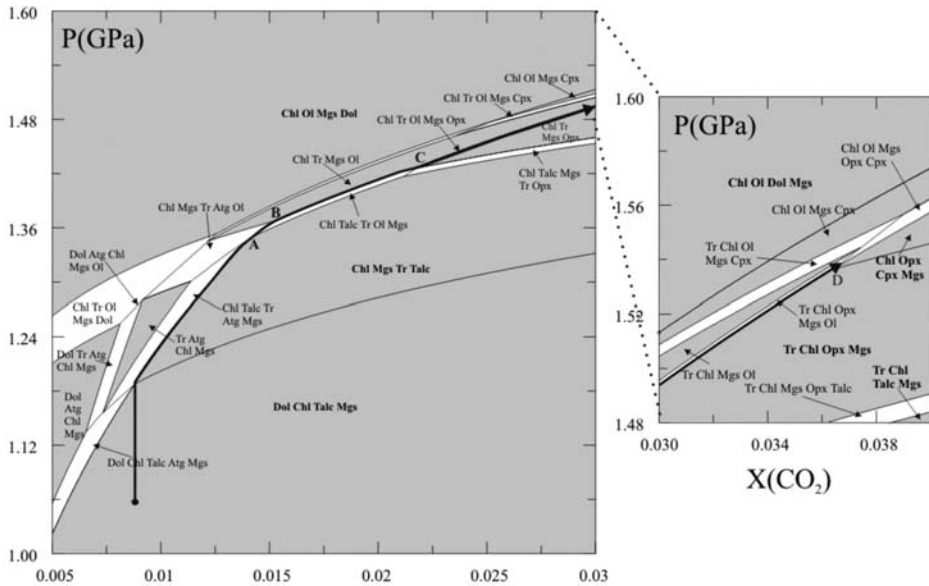
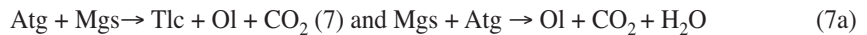
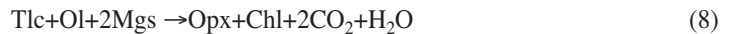


Fig. 5: P/T-X sections for (a) X_{CO_2} 0.005-0.03 and (b) X_{CO_2} 0.03-0.04 in the system CFMASCH. The internal buffering fluid evolution (bold arrow) and the divariant reactions along the prograde P-T path shown in Fig. 4 are illustrated. Assemblages' stability fields as in figure 4. A geothermal gradient of 12°C/km is considered along the vertical axes.



With further increase of pressure and temperature the reactions move along the boundary of the divariant $\text{Chl} + \text{Mgs} + \text{Tr} + \text{Atg} + \text{Ol}$ and $\text{Chl} + \text{Tlc} + \text{Tr} + \text{Mgs} + \text{Ol}$ fields where antigorite and magnesite are consumed to form more olivine and talc up to the pseudo-invariant point B which records the maximum P-T- X_{CO_2} conditions for the antigorite stability in the metaperidotite along the selected P-T path. As prograde metamorphism advances, the reactions move along the boundary of the divariant $\text{Chl} + \text{Tlc} + \text{Tr} + \text{Ol} + \text{Mgs}$ and trivariant $\text{Chl} + \text{Tr} + \text{Mgs} + \text{Ol}$ fields consuming magnesite and talc and forming more olivine up to the pseudo-invariant point C. At the pseudo-invariant point C (Fig. 5a) at P (1.42 GPa), T (635°C) and X_{CO_2} (0.022) talc, olivine and magnesite react to form orthopyroxene, chlorite and fluid phase according to the reaction:



which is in accordance with the textural relationship where olivine inclusions in orthopyroxene show resorbed edges and chlorite inclusions are common in orthopyroxene megacrysts. With continuing prograde path the reactions proceed along the boundary of the trivariant assemblages $\text{Chl} + \text{Tr} + \text{Mgs} + \text{Opx}$ and $\text{Chl} + \text{Tr} + \text{Mgs} + \text{Ol}$ and olivine is formed consuming orthopyroxene. Rare orthopyroxene inclusions in olivine (Fig. 2f) indicate that the prograde path exceeded the P-T- X_{CO_2} conditions of point C (Fig. 5).

P-T- X_{CO_2} conditions did not reach the pseudo-invariant point D (Fig. 5b), where the assemblage $\text{Tr} + \text{Chl} + \text{Ol} + \text{Opx} + \text{Mgs} + \text{Cpx}$ is stable as clinopyroxene is not formed in the metaperidotite. For the selected P-T path the peak metamorphic conditions are constrained between 1.42 GPa and 640°C and 1.53 GPa and 688 °C (points C and D respectively in figure 5).

Decompression stage:

As discussed above, at the maximum P-T conditions, the prograde path crossed neither the Ol+Dol+Mgs+Spl nor the Chl+Ol+Mgs+Dol trivariant field. However matrix dolomite and spinel are common phases in the metaperidotite. Both mineral phases can be formed during decompression. In eclogites, the first stage of decompression is indicated by a temperature increase up to 750°C (Bauer et al. 2007). Following a decompression path similar to that recorded in the associated eclogites, dolomite is formed before the decomposition of chlorite to olivine+spinel (Fig. 4b). This is in accordance with textural relations as commonly matrix dolomite contains inclusions of chlorite (Chl-1). Spinel is formed as the decompression path crosses the univariant reaction:



However textural relationships indicate that spinel associates with olivine (Ol-2) and Al-tremolite and not with primary magnesite (Mgs-1). We propose that in the spinel forming reaction dolomite is involved in the reacting phases with the most possible reaction



Amphibole is not stable with spinel in the calculated pseudosections with the bulk rock composition of the studied metaperidotite. However, amphibole can coexist with olivine and spinel if we take into account the effective bulk composition (richer in SiO₂ content) obtained by subtracting clinohumite, ilmenite and the inclusions in olivine and orthopyroxene megacrysts. Ti-clinohumite with X_{F0.12-0.14} was stable at the peak P-T metamorphic conditions (Fig. 4b) and was decomposed to olivine+Mg-ilmenite (Fig. 3a) during decompression according to the reaction:



4.2 Tectonic implications

The inclusions of magnesite, chlorite, talc, antigorite, tremolite and Cr-magnetite in olivine, orthopyroxene and ferrite-chromite and the chemical composition of zoned spinel minerals with increasing Al-content from the core to the rim indicate that the carbonate-bearing metaperidotite from Gorgona underwent a prograde (HP) metamorphism in a subduction-related setting.

A major concern is the way in which this mantle fragment was incorporated into the subducting slab. Two scenarios can be invoked. Either it represents a piece of former ophiolite mélange and was tectonically incorporated into the crustal assemblage prior to subduction, or it represents a piece of former mantle wedge above an early Jurassic subduction zone incorporated into the subduction channel by a tectonic erosion mechanism, because of hydration from fluids liberated from the subducting oceanic slab (Von Huene et al., 2004). The subcontinental mantle origin is preferred, because the Gorgona metaperidotite is surrounded by gneissic rocks with no sign of oceanic affiliation. The prograde P-T path is clearly constrained to pressure and temperature below 1.5-1.7 GPa and 690-720 °C by the absence of the clinopyroxene. This indicates that peak P-T conditions were lower than those recorded in the Jurassic eclogites (>1.75 GPa and 700°C, Bauer et al. 2007) and much lower than those recorded in the Jurassic diamond-bearing Grt-Ky gneisses (> 4 GPa and ~1000°C, Mposkos and Krohe, 2006). If the mineral assemblage of the Gorgona metaperidotite was formed during the Mesozoic metamorphic cycle then it was subducted to (much) lower depth within the subduction channel than the associated eclogites and diamond-bearing gneisses.

5. Conclusions

Mineral textures and compositions, P-T and P(T)- X_{CO_2} phase diagram calculations show that the Gorgona carbonate-bearing metaperidotite is a mantle-derived, metamorphosed tectonic slice, which was subjected to a prograde HP metamorphism. The prograde path crossed successive the stability fields of Dol+Tlc+Mgs+Chl, Tr+Tlc+Mgs+Chl, Tr+Atg+Tlc+Mgs+Chl, Tr+Mgs+Atg+Ol+Chl, Tr+Chl+Mgs+Ol and at the maximum P-T conditions the field of Ol+Opx+Mgs+Tr+Chl. The intruded fluids had a composition rich in H_2O with $X_{\text{CO}_2} \leq 0.008$. During the prograde metamorphism the X_{CO_2} in the fluid phase increased as magnesite consuming and antigorite, olivine and orthopyroxene forming reactions produced much more CO_2 than H_2O . The increase in X_{CO_2} in the fluid phase was responsible for the orthopyroxene formation. Decomposition of Ti-clinohumite to olivine and Mg-ilmenite and of chlorite to olivine and high Al-chromite occurred during decompression. Retrograde chlorite (Chl-2) associated with magnesite (Mgs-2) and replacing spinel and olivine (Fig. 2c) and retrograde talc and tremolite are formed by a second metamorphic event according to reactions 4, 9 and 10 within the stability field of Tr+Chl+Tlc+Mgs. The reactions require intrusion of a fluid phase. Such fluids can be derived from metamorphic reactions occurred in the underlying Albite-Gneiss Series which underwent prograde HP metamorphism in early Tertiary (Mposkos and Krohe, 2000; Lips et al., 2000).

We suggest that the Gorgona carbonate-bearing metaperidotite represents a fragment of the hydrated mantle wedge and it was incorporated into the subduction channel with a tectonic erosion mechanism in early Jurassic.

6. References

- Bauer, C., Rubatto, D., Krenn, K., Proyer, A. and Hoinkes, G. 2007. A zircon study from the Rhodope metamorphic complex, N-Greece: Time record of a multistage evolution. *Lithos*, 99, 207-228.
- Bosse, V., Boulvais, P., Gautier, P., Tiepolo, M., Ruffet, G., Devidal, J.L., Cherneva, Z., Gerdjikov, I. and Paquette, J.L., 2009. Fluid-induced disturbance of the monazite Th-Pb chronometer: In situ dating and element mapping in pegmatites from the Rhodope (Greece, Bulgaria). *Chemical geology* 261, 3-4, 286-302.
- Connolly, J. A. D. 2009. The geodynamic equation of state: what and how. *Geochemistry, Geophysics, Geosystems*, 10, QXXXX. DOI: 10.1029/2009GC002540.
- Evans, B.W. and Frost, B.R. 1975. Chrome-spinel in progressive metamorphism-a preliminary analysis. *Geochimica et Cosmochimica Acta*, 39, 959-972.
- Holland, T., Baker, J. and Powell, R. 1998. Mixing properties and activity-composition relationships of chlorites in the system MgO-FeO-Al₂O₃-SiO₂-H₂O. *European Journal of Mineralogy*, 10, 395-406.
- Holland, T. J. B. H. and Powell, R. 1996. Thermodynamics of order-disorder in minerals.2. Symmetric formalism applied to solid solutions. *American Mineralogist*, 81, 1425-1437.
- Holland, T. J. B. H. and Powell, R. 1998. An internally consistent thermodynamic data set for phases of petrological interest. *Journal of Metamorphic Geology*, 16, 309-343.
- Kassoli-Fournaraki, A., Filippidis, A., Kolcheva, K., Hatzipanayotou, K., Koepke, J. and Dimadis, E. 1995. Multi-stage alteration of the Gorgona ultramafic body, Central Rhodope Massif, Greece. *Chemie der Erde*, 55, 331-340.
- Krohe, A. & Mposkos, E. 2002. Multiple generations of extensional detachments in the Rhodope Mountains (N.Greece): evidence of episodic exhumation of high-P rocks. In: Blundell, D.J.,

- Neubauer, G. and Von Quant, A. (eds.): The timing and location of major ore deposits in an evolving orogen. Geological Society of London, Special Publication, 204, 151-178.
- Liati, 2005. Identification of repeated Alpine (ultra) high-pressure metamorphic events by U–pb SHRIMP geochronology and REE geochemistry of zircon: the Rhodope zone of Northern Greece, *Contributions to Mineralogy and Petrology*, 150, 608–630.
- Liati, A. and Mposkos, E. 1990. Evolution of the eclogites in the Rhodope Zone of northern Greece, *Lithos*, 25, 89–99.
- Lips, A.L.W., White, S.H. and Wijbrans, J.R. 2000. Middle–Late Alpine thermotectonic evolution of the southern Rhodope Massif, Greece. *Geodinamica Acta*, 13, 281–292.
- Martin, R.F. 1998. Symbols of the rock-forming minerals. The Nomenclature of minerals: A compilation of IMA reports. IMA`98 Toronto, 148-149.
- Mposkos, E. and Kostopoulos, D. 2001. Diamond, former coesite and supersilicic garnet in metasedimentary rocks from the Greek Rhodope: a new ultrahigh-pressure metamorphic province established. *Earth and Planetary Science Letters*, 192, 497-506.
- Mposkos, E. and Krohe, A. 2000. Petrological and structural evolution of continental high pressure (HP) metamorphic rocks in the Alpine Rhodope domain (N.Greece). Proceedings of the 3rd International Conference on the Geology of the Eastern Mediterranean, 221-232.
- Mposkos, E. and Krohe, A. 2006. P-T-deformation paths of closely associated UHP (diamond-bearing) crustal and mantle rocks of the Kimi Complex: Implications for the tectonic history of the Rhodope Mountains, northern Greece. *Canadian Journal of Earth Sciences*, 43, 1755-1776.
- Perraki, M., Proyer, A., Mposkos, E., Kaindl, R., Baziotis, I. and Hoinkes, G. 2004. Micro- and nanodiamonds in garnets of metapelitic rocks from the Greek Rhodope : an in situ micro-Raman study. Proceedings of the 5th International Symposium for Eastern Mediterranean Geology, 1216-1219.
- Perraki, M., Proyer, A., Mposkos, E., Kaindl, R. and Hoinkes, G. 2006. Raman micro-spectroscopy on diamond, graphite and other carbon polymorphs from the ultrahigh-pressure metamorphic Kimi Complex of the Rhodope Metamorphic Province, NE Greece. *Earth and Planetary Science Letters*, 241, 672-685.
- Von Huene, R., Ranero, C.R. and Vannucchi, P. 2004. Generic model of subduction erosion. *Geology*, 32, 913-916.

RADIOACTIVITY OF GRANITIC ROCKS FROM NORTHERN GREECE

Papadopoulos A.¹, Christofides G.¹, Papastefanou C.², Koroneos A.¹
and Stoulos S.²

¹ Department of Mineralogy-Petrology-Economic Geology, School of Geology, Aristotle University of Thessaloniki, 541 24, Thessaloniki, argpapad@geo.auth.gr, christof@geo.auth.gr, koroneos@geo.auth.gr.

² Laboratory of Atomic and Nuclear Physics, Aristotle University of Thessaloniki, 541 24, Thessaloniki, papastefanou@physics.auth.gr, stoulos@auth.gr.

Abstract

Forty-nine samples from several plutons in northern Greece have been studied for their activity concentrations of ⁴⁰K, ²²⁶Ra and ²³²Th by using gamma-ray spectroscopy. The activities of ⁴⁰K, ²²⁶Ra and ²³²Th of the majority of the samples exceed the average level of these radionuclides in soil and building materials. Samples of basic composition have very low concentrations of radionuclides while intermediate and acid rocks are more enriched in ⁴⁰K, ²²⁶Ra and ²³²Th and their decay products. In order to assess the radiological impact from the investigated rocks, absorbed gamma dose rate (D_a), annual effective dose (H_E), activity index (AI) and gamma-ray index (I_γ) were estimated. The activity concentrations and hazard indices were compared to those of plutonic rock samples from all over the world, as well as other building materials. The average of hazard indices of Greek granites is below 'world' average in all cases. Moreover, it is still below the criteria of UNSCEAR (2000). Therefore, at least from radiological point of view and for the investigated rocks, the use of granites from northern Greece as building materials is recommended.

Key words: granite, natural radioactivity, radiation, dose assessment, northern Greece.

1. Introduction

In igneous petrology, granite is a prevailing rock-type describing acid plutonic rocks having a particular mineralogy and geochemistry. However, in dimension stone market the term granite includes a variety of igneous and metamorphic rock-types, used as building materials. In recent years, use of granite as a decor material in buildings (indoors and outdoors) and monuments has globally increased, due to its durability and appearance. In this paper, the term "granite" is used for the plutonic rocks under study including granitic and monzonitic as well as gabbroic rocks.

Radioisotopes that are found in the environment can be classified as naturally occurring radionuclides that are components of the earth's crust since its formation (e.g. ²³⁸U, ²³⁵U, ²³²Th and ⁴⁰K and their decay products), cosmogenic radioisotopes (radioisotopes that are produced by the interaction between cosmic radiation and the atmosphere (e.g. ¹⁴C, ¹⁰Be, ⁴⁴Ti and ²²Na) and finally artificially produced radionuclides that are produced in nuclear reactors (e.g. ⁹⁰Sr and ¹³⁷Cs). Natural radionuclides can be found in soil, rocks, water, air, food, building materials, etc.

The study of natural radioactivity present in rocks and ornament stones, such as granite, is an im-



Fig. 1: Sketch map of northern Greece, presenting the location of plutons from which the granite samples were obtained.

portant subject in environmental radiological protection (Anjos et al., 2005) as it provides the possibility to assess any associated health hazard. This contribution aims at investigating the natural radioactivity level of selected granites from north Greece in order to assess their radiation dose exposure and give information about the potential use of them as building materials.

2. Materials and methods

The samples studied were taken from Pelagonian zone (Varnountas and Kastoria plutons), Circum Rhodope Zone (Sithonia and Maronia plutons), Serbomacedonian Massif (Mouries pluton) and Rhodope Massif (Vrontou, Elatia, Granitis, Panorama, Xanthi, Philippi, and Leptokaria-Kirki plutons) (Fig. 1). The mineralogy of the selected samples is presented in Table 1, while the rock-type along with the location of plutons from which the samples were obtained, is presented in Table 2. The petrographic classification was based on the QAP tertiary diagram (I.U.G.S., 1973).

Details on the petrography and geochemistry of the above plutonic rocks can be found in Christofides et al., 1998 and references therein, Koroneos, 1991; Grigoriadou et al., 2003; D' Amico et al., 1990 and Christofides et al., 1999.

The activity concentration of natural radionuclides was measured by gamma-ray spectrometry for 20 granite samples. Additionally, 29 samples from the same area were used from the literature (Karavasili et al., 2005).

In particular, the content of ^{226}Ra , ^{232}Th and ^{40}K of each sample was measured, as these occur in relatively high levels in the majority of the building materials and they represent the main external source of irradiation to the human body.

All samples were crushed into grains less than 400 μm in diameter, oven-dried at 60 °C to constant weight, well blended and measured using two different high-resolution gamma ray spectrometry systems. The first one consisted of a high purity (HP) Ge coaxial detector with 42% efficiency and 2.0 keV resolution at 1.33 MeV gamma-ray photons, shielded by 4'' Pb, 1 mm Cd and 1 mm Cu and the second one consisted of a low energy (LE) Ge planar detector with 0.7 KeV resolution at 122 keV gamma-ray photons, shielded by 1.3'' Pb, 1mm Cd and 1 mm Cu. The efficiency calibration of

Table 1. Mineralogy (modal composition) of selected samples

sample	Qz	Kf	Pl	Hb	Bi	Mu	Px	Oth	Tot
MP-6	1.2	20.2	50.5	8.8	12.7	0.0	1.1	5.5	100.0
MP-77	14.4	37.0	28.2	16.4	0.1	0.0	0.0	3.9	100.0
XMZ-501	4.1	39.4	28.2	0.2	11.3	0.0	16.0	0.8	100.0
MP-3	6.6	31.0	35.9	11.0	12.4	0.0	0.0	3.1	100.0
MP-38	2.3	31.0	40.6	0.7	9.5	0.0	15.0	0.9	100.0
MP-53	1.8	20.6	28.4	14.7	7.5	0.0	21.5	5.5	100.0
STH-162	35.4	22.9	24.3	0.0	9.4	7.8	0.0	0.2	100.0
MP-90	17.1	33.3	31.6	7.8	3.6	0.0	2.1	4.5	100.0
X-270	17.8	20.0	42.2	7.0	8.3	0.0	0.0	2.2	100.0
MP-501*	37.4	45.9	8.5	5.5	1.7	0.0	0.0	0.9	100.0
P-5**	23.5	42.5	24.6	7.5	0.0	0.1	0.0	1.8	100.0
I-3**	43.7	23.9	24.4	4.4	0.0	0.0	0.0	2.6	100.0
STH-5*	44.0	14.7	34.1	3.9	3.1	0.0	0.0	0.2	100.0
STH-13*	30.4	23.8	41.4	2.3	1.3	0.0	0.0	0.8	100.0
STH-118	38.0	7.1	45.6	9.0	0.0	0.0	0.0	0.3	100.0
STH-450	30.0	12.2	35.5	11.3	0.0	6.7	0.0	4.3	100.0
D-8b***	16.4	0.8	60.4	15.6	0.0	0.0	0.0	6.8	100.0
D-15***	26.2	35.6	32.2	2.0	1.2	0.0	0.0	2.8	100.0
DSK-17***	18.8	0.0	56.5	22.0	0.0	0.2	0.0	2.5	100.0
A-13***	28.7	24.7	37.0	0.0	3.0	0.0	0.0	6.6	100.0
G-2***	34.8	44.7	18.1	2.0	0.0	0.0	0.0	0.4	100.0
YD-12*	11.2	22.3	45.5	7.8	0.0	8.8	0.0	4.3	100.0

(Qz: Quartz, Kf: K-feldspars, Pl: Plagioclase, Hb: Hornblende, Bi: Biotite, Mu: Muscovite, Px: Pyroxenes, Oth: Others, Tot: Total)

* (Karavasili, 2004), ** (Koroneos, 1991), *** (Soldatos, 1985).

the gamma-ray spectrometry systems was performed with the radionuclide specific efficiency method in order to avoid any uncertainty in gamma ray intensities, as well as the influence of coincidence summation and self-absorption effects of the emitting gamma-ray photons. A set of high quality certified reference materials (IAEA, RG-sets) was used, with densities similar to the building materials measured after pulverization. Cylindrical geometry (\varnothing : 55 mm, h = 20 mm) was used assuming that the radioactivity is homogeneously distributed in the measuring samples. The measurement duration was up to 200.000 s and was carried out in the Laboratory of Atomic and Nuclear Physics, Department of Physics, Aristotle University of Thessaloniki.

3. Results and discussion

The specific activities of ^{40}K , ^{226}Ra and ^{232}Th measured in the granite samples are presented in Table 2. The specific activity of ^{40}K has a much wider range (64-1632 $\text{Bq}\cdot\text{kg}^{-1}$) than those of ^{226}Ra and ^{232}Th , which are respectively 1,4-315,4 and 2-372,2 $\text{Bq}\cdot\text{kg}^{-1}$. The average values of ^{40}K , ^{226}Ra and ^{232}Th are 929,3, 77,3 and 91,4 $\text{Bq}\cdot\text{kg}^{-1}$, respectively.

The worldwide average and range (within brackets) of natural radioactivity background levels in soil are 400 (140-850), 35 (17-60) and 30 (11-64) Bq·kg⁻¹, respectively for ⁴⁰K, ²²⁶Ra and ²³²Th (UNSCEAR, 2000). As it was expected, the average activity mass concentrations of the radionuclides measured in the granites from northern Greece are above the average activity levels given in the above UNSCEAR, 2000 report for soil (Pavlidou et al., 2006; Karavasili et al., 2005; Stoulos et al., 2003).

According to UNSCEAR (1993), the world average of natural radioactivity levels of ⁴⁰K, ²²⁶Ra and ²³²Th in building materials is 500, 50 and 50 Bq·kg⁻¹, respectively. Taking into account the measured levels of natural radioactivity in Greek building materials by this study as well as by other Greek researchers (Siotis and Wrixon, 1984, Papastefanou et al., 1984; Pakou et al., 1994; Savidou et al., 1995; Petropoulos et al., 2002) and considering that most of Greek dwellings were constructed mainly by clay bricks and concrete in weight proportion 40–60%, the specific activities of natural radionuclides in building materials that appeared in a typical Greek room are the following: ⁴⁰K, 550 Bq·kg⁻¹; U-series, 35 Bq·kg⁻¹ and Th-series, 32 Bq·kg⁻¹ (Stoulos et al., 2003). This means that granites contain a much higher amount of radionuclides presumably caused by the presence of U- and Th-rich minerals in them. For example, tetravalent Th and U may be isomorphously substituting in the Ca position in allanite, sphene and apatite. Ce-rich monazite rivals zircon in common rocks as a ubiquitous and important carrier of Th. To a much lesser extend U, was also found in monazite, apparently also in isomorphic substitution. The situation is reversed in xenotime, where U was generally more abundant than Th. Uraninite and thorianite are two other minerals found in common rocks that are believed to contain Th and U as essential components in regular crystal structural positions (Adams et al., 1959). According to Faure (1986), U- and Th-rich minerals can be found in acid igneous rocks than in basic rocks. This can be explained by the incompatibility of both U and Th during partial melting and fractional crystallization processes ($K_d < 1$), leading thus in the remaining of U and Th in the melt and their incorporation in minerals of acid rocks.

Activity concentrations of ⁴⁰K, ²²⁶Ra and ²³²Th in granite samples from various countries of the world, including Greece, have been compiled from literature and are presented in Table 3 for comparison. The ‘world’ weighted average calculated from the above measurements has also been used for comparison. The activity concentrations of these radionuclides vary over a wide range. Their average activity concentration in Greek granite samples is below the ‘world’ average in all cases. The minimum and maximum ⁴⁰K were found in the granite from Wadi Karim and Gable El Aradiya in Egypt, respectively. The granite of Gable Gattar II in Egypt contains the maximum and that of Africa has the minimum ²²⁶Ra. The maximum ²³²Th was found in the Pakistani granite and the minimum in the granite of Gable El Aradiya in Egypt.

In order to assess the radiological impact of granites used as building materials, the model of a rectangular parallelepipedon house building 3 m X 3 m X 3m, with infinite thin walls and no doors and windows (standard room model) was commonly considered (UNSCEAR, 1993)

A variety of radiation hazard indices representing different methods to assess the collective effect of mass concentrations of ⁴⁰K, ²²⁶Ra and ²³²Th was used:

1) Absorbed gamma dose rate (D_a). The measured activity concentrations of ²³⁸U (²²⁶Ra), ²³²Th and ⁴⁰K is converted into doses (nGy·h⁻¹·Bq⁻¹·kg⁻¹) (where Gy=Gray and Bq=Becquerel) by applying the factors 0.462, 0.604 and 0.0417 for U (²²⁶Ra), Th and K, respectively (UNSCEAR, 1993). These factors were used to calculate the total absorbed gamma dose rate in air at 1 m above the ground level using the following equation:

$$D_a \text{ (nGy·h}^{-1}\text{)} = 0.462C_U + 0.604C_{Th} + 0.0417C_K$$

Table 2. Activity concentrations of ^{40}K , ^{226}Ra and ^{232}Th in $\text{Bq}\cdot\text{kg}^{-1}$ along with their total uncertainties of the studied samples.

Sample	Location	Rock-type	^{226}Ra	^{232}Th	^{40}K
GAE-1	Xanthi	gabbro	15.6±0	18.2±0	291.0±5
GAE-9	Xanthi	gabbro	42.7±1	50.7±1	685.0±9
GAE-11	Xanthi	gabbro	5.3±0	6.5±1	175.0±4
SB-55*	Vrondou	gabbro	1.4±0	2.0±0	68.0±4
NG-5*	Xanthi	gabbro	2.5±0	6.5±0	64.0±3
MP-6	Maronia	hb-bi monzogabbro	65.9±1	71.8±1	810.0±10
MZ-500*	Xanthi	bi-px-qz-monzodiorite	170.0±2	189.0±3	1304.0±22
MP-5	Varnountas	hb-bi-qz-monzonite	61.4±1	79.5±1	1027.0±12
KR-9*	Varnountas	hb-bi-qz-monzonite	50.0±1	78.0±1	956.0±14
SB-41*	Vrondou	hb-qz-monzonite	109.0±1	113.0±2	1110.0±14
YD-12*	Philippi	bi-hb-qz-monzodiorite	28.0±1	39.0±1	709.0±10
L-23*	Leptokaria-Kirki	bi-px-hb-qz-monzonite	64.0±1	59.0±1	882.0±13
MP-77	Maronia	hb-qz-monzonite	123.4±1	124.9±2	1146.0±13
P-6*	Panorama	qz-monzonite	122.0±1	143.0±2	1177.0±16
XMZ-501	Xanthi	bi-px-qz-monzonite	169.2±1	188.2±2	1172.0±14
MP-3	Maronia	hb-bi-qz-monzonite	106.7±1	110.0±1	954.0±12
MP-38	Maronia	bi-px-monzonite	146.2±1	148.5±2	924.0±11
MP-53	Maronia	bi-hb-px-monzonite	51.4±1	50.0±1	663.0±10
MR-11*	Maronia	hb-bi-px-mozonite	97.0±1	99.0±1	1051.0±14
SB-36*	Vrondou	hb-syenite	136.0±1	152.0±2	1466.0±17
DSK-17*	Elatia	bi-tonalite	41.0±1	80.0 ±1	524.0±10
D-8b*	Elatia	bi-tonalite	44.0±1	82.0 ±1	748.0±10
STH-162	Sithonia	two mica granite	45.2±1	28.8 ±1	751.0±10
STH-170	Sithonia	two mica granite	29.0±1	29.4 ±1	603.0±10
STH-5*	Sithonia	granodiorite	38.0±1	43.0 ±1	693.0±9
STH-118*	Sithonia	bi-granodiorite	69.0±1	80.0 ±1	777.0±10
STH-450*	Sithonia	hb-bi-granodiorite	56.0±1	77.0 ±1	754.0±14
D-5*	Elatia	bi-granodiorite	41.0±1	77.0 ±	546.0±11
MP-501*	Mouries	bi-granite	73.0±1	95.0 ±1	1386.0±15
P-5	Varnountas	bi-granite	44.0±1	88.1 ±1	1104.0±13
SB-50*	Vrondou	hb-granite	69.0±1	70.0 ±1	717.0±12
L-4*	Vrondou	hb-granite	54.0±1	75.0 ±1	919.0±12
TS-10*	Vrondou	hb-granite	90.0±1	138.0±2	1460.0±16
G-6*	Granitis	hb-bi-granite	106.0±1	100.0±1	1060.0±13
MP-90	Maronia	hb- granite	315.4±1	372.2±4	1420.0±16
STH-6*	Sithonia	granite	68.0±1	64.0±1	689.0±11
B-7*	Vrondou	granite	88.0±1	123.0±2	993.0±13
D-15*	Elatia	granite	46.0±1	130.0±2	1448.0±19
A-13*	Elatia	granite	231.0±1	49.0±1	1232.0±16

Table 2. Continued

Sample	Location	Rock-type	²²⁶ Ra	²³² Th	⁴⁰ K
G-2*	Granitis	granite	141.0±1	195.0±3	1632.0±21
PR-27*	Panorama	granite	56.0±1	66.0±1	987.0±14
PE-11	Kastoria	granite	44.7±1	50.2±1	973.0±12
TH-5	Kastoria	granite	70.0±1	68.6±1	1099.0±13
X-270	Xanthi	bi-hb-granite	79.6±1	73.1±1	915.0±11
T-10	Varnountas	granitic gneiss	73.2±1	100.1±1	970.0±12
H-9*	Elatia	alkaligranite	33.0±1	124.0±2	1111.0±14
STH-13*	Sithonia	leucogranite	16.4±1	18.0±1	892.0±11
L-13	Varnountas	leucogranite	58.7±1	115.6±2	1113.0±13
I-3	Varnountas	leucogranite	97.3±1	104.9±1	1386.0±15
Average			77.3±1	91.4±1	929.3±12

(qz: quartz, px: pyroxene, bi: biotite, hb: hornblende), * (Karavasili, 2004)

Table 3. Average values of activity concentrations of ⁴⁰K, ²²⁶Ra and ²³²Th in Bq·kg⁻¹ of granite samples from different countries of the world.

Country/origin	No. of samples	⁴⁰ K	²²⁶ Ra	²³² Th	Reference
Austria	1	1340	40	253	(Chen & Lin 1996)
Belgium	1	1129	68	77	(Tzortzis et al., 2003)
Brazil	14	1297	82	168	(Tzortzis et al., 2003)
Brazil	1	1819	91	152	(Chen & Lin 1996)
China	8	1256	95	158	(Chen & Lin 1996)
Egypt/Wadi Karim	10	4819	56	54	(El-Arabi, 2007)
Egypt/Um Taghir	39	3918	558	359	(El-Arabi, 2007)
Egypt/Gable Gattar II	10	1140	6018	113	(El-Shershaby, 2002)
Egypt/Gable El Majai	10	681	198	30	(Arafa, 2004)
Egypt/Gable El Misikat	9	705	1184	40	(Arafa, 2004)
Egypt/Gable El Aradiya	10	480	126	25	(Arafa, 2004)
Egypt/Homert Waggat North	10	1590	489	109	(Arafa, 2004)
Egypt/Homert Waggat South	10	2302	787	163	(Arafa, 2004)
Finland	3	1223	94	163	(Chen & Lin
Greece	49	929	77	91	(Karavasili et al., 2005 & Present work)
Holland	1	1540	162	490	(Tzortzis et al., 2003)
India	4	1082	119	172	(Chen & Lin 1996)
Italy	4	1206	64	91	(Menager et al., 1993)
Malaysia	1	1019	86	134	(Chen & Lin 1996)

Table 3. Continued

Country/origin	No. of samples	⁴⁰ K	²²⁶ Ra	²³² Th	Reference
Portugal	1	1490	117	105	(Chen & Lin 1996)
S. Africa	1	1151	92	153	(Chen & Lin 1996)
Spain	1	1289	80	123	(Chen & Lin 1996)
Sweedeen	2	1226	107	110	(Chen & Lin 1996)
Turkey/Kaymaz	7	1266	306	248	(Orgun & Altinsoy, 2005)
Turkey/Sivrihisar	7	1058	67	153	(Orgun & Altinsoy, 2005)
Pakistan/Ambela	20	1203	659	598	(Asghar et al., 2008)
	Maximum	4819	6018	598	
	Minimum	480	23	25	
	Weighted				
	Average	1749	567	194	

where C_U , C_{Th} and C_K are the activity concentrations ($Bq \cdot kg^{-1}$) of U, Th and K in the samples. The limiting value of this index is $80 \text{ nGy} \cdot h^{-1}$ (EC, 1999).

2) Annual effective dose (H_E). The effective dose rate indoors in $mSv \cdot y^{-1}$ (Sv =Sievert), is calculated by the following formula:

$$H_E = 10^{-6} \times D \times T \times F$$

where D is the calculated dose rate in $nGy \cdot h^{-1}$, T is the indoor occupancy time, which implies that 20% of time is spent outdoors, and is equal to 7000 h, and F is the doses conversion factor equal to $0.7 \text{ Sv} \cdot y^{-1}$. H_E should be $< 1 \text{ mSv} \cdot y^{-1}$ (UNSCEAR 1993, 2000).

3) Activity index (AI). Several authors have proposed formulae to estimate this index. In this study it is calculated on the basis of former USSR and W. Germany criterion (Chen & Lin, 1996):

$$AI = C_{Ra} / 370 + C_{Th} / 259 + C_K / 4810$$

AI should be less than 1 mSv.

4) Gamma-ray index (I_γ). European Commission (EC, 1999) has proposed this index which is calculated by the formula:

$$I_\gamma = C_{Ra} / 300 \text{ Bq} \cdot \text{kg}^{-1} + C_{Th} / 200 \text{ Bq} \cdot \text{kg}^{-1} + C_K / 3000 \text{ Bq} \cdot \text{kg}^{-1}$$

and is correlated with the annual dose rate due to gamma radiation. Materials having $I_\gamma < 2$ would increase the annual effective dose by 0.3 mSv, while for $2 < I_\gamma < 6$, the gamma-ray index corresponds to an increase in effective dose by $1 \text{ mSv} \cdot y^{-1}$. Building materials used superficially rather than in bulk amounts (tiles, boards, etc.) should be exempted from all restrictions concerning radioactivity, if the excess of gamma radiation originating from them increases the annual effective dose of a member of public by 0,3 mSv at the most. On the other hand, dose rates higher than $1 \text{ mSv} \cdot y^{-1}$ are allowed only in exceptional cases, where materials are locally used. Finally, samples with $I_\gamma > 6$ cannot be recommended for use in buildings (EC, 1999).

Table 4. Absorbed gamma dose rate (D_a), annual effective dose (H_E), activity index (A_I) and gamma-ray index (I_γ) for the granites examined.

sample	D_a (nGy·h ⁻¹)	HE (mSv·y ⁻¹)	AI (Bq·kg ⁻¹)	I_γ
GAE-1	31.20	0.15	0.18	0.2
GAE-9	80.19	0.39	0.46	0.6
GAE-11	13.18	0.06	0.07	0.1
SB-55*	4.58	0.02	0.02	0.0
NG-5*	7.85	0.04	0.05	0.1
MP-6	110.95	0.54	0.64	0.9
MZ-500*	243.25	1.19	1.42	1.9
MP-5	122.41	0.60	0.70	1.0
KR-9*	110.60	0.54	0.63	0.9
SB-41*	169.09	0.83	0.98	1.3
YD-12*	65.93	0.32	0.37	0.5
L-23*	100.28	0.49	0.57	0.8
MP-77	182.58	0.89	1.05	1.4
P-6*	192.81	0.94	1.12	1.5
XMZ-501	245.64	1.20	1.44	1.9
MP-3	157.53	0.77	0.91	1.2
MP-38	200.35	0.98	1.17	1.6
MP-53	81.73	0.40	0.47	0.6
MR-11*	146.79	0.72	0.84	1.1
SB-36*	218.71	1.07	1.26	1.7
DSK-17*	88.57	0.43	0.52	0.7
D-8b*	102.34	0.50	0.59	0.8
STH-162	70.43	0.35	0.39	0.5
STH-170	58.08	0.28	0.33	0.5
STH-5*	73.00	0.36	0.41	0.6
STH-118*	113.82	0.56	0.66	0.9
STH-450*	104.38	0.51	0.60	0.8
D-5*	88.85	0.44	0.52	0.7
MP-501	150.22	0.74	0.85	1.2
P-5	122.62	0.60	0.70	1.0
SB-50*	104.48	0.51	0.60	0.8
L-4*	108.42	0.53	0.62	0.9
TS-10*	192.27	0.94	1.10	1.5
G-6*	155.67	0.76	0.90	1.2
MP-90	438.12	2.15	2.59	3.4
STH-6*	97.88	0.48	0.56	0.8
B-7*	165.16	0.81	0.96	1.3
D-15*	163.39	0.80	0.93	1.3
A-13*	188.02	0.92	1.07	1.4
G-2*	259.03	1.27	1.50	2.0
PR-27*	105.93	0.52	0.60	0.8
H-9*	139.71	0.68	0.80	1.1
STH-13*	56.33	0.28	0.30	0.4
L-13	147.59	0.72	0.85	1.2
I-3*	171.01	0.84	0.98	1.3
T-10	135.33	0.66	0.78	1.1

Table 4. Continued

sample	D_a (nGy·h ⁻¹)	HE (mSv·y ⁻¹)	AI (Bq·kg ⁻¹)	I_γ
PE-11	92.16	0.45	0.52	0.7
TH-5	119.01	0.58	0.67	0.9
X-270	122.61	0.60	0.70	1.0
Lim. Values	80	1	1	6

Table 5. Comparison of radiological parameters based upon data available for granite samples from different countries of the world (Asghar et al., 2008).

Country/origin	D_a (nGy·h ⁻¹)	HE (mSv·y ⁻¹)	AI (Bq·kg ⁻¹)	I_γ
Africa	70	0.5	0.4	0.6
Austria	227	0.8	1.4	1.8
Belgium	125	1.2	0.7	1.0
Brazil	193	1.2	1.1	1.5
Brazil	210	1.4	1.2	1.7
China	192	1.2	1.1	1.5
Egypt/Wadi Karim	259	1.7	1.4	2.1
Egypt/Um Taghir	638	0.5	3.7	5.0
Egypt/Gable Gattar II	2896	17.8	16.9	21.0
Egypt/Gable El Majai	138	0.5	0.8	1.0
Egypt/Gable El Misikat	601	3.7	3.5	4.4
Egypt/Gable El Aradiya	93	0.6	0.5	0.7
Egypt/Homert Waggat North	358	2.3	2.1	2.7
Egypt/Homert Waggat South	558	3.5	3.2	4.2
Finland	193	1.2	1.1	1.5
Greece*	131	0.6	0.8	1.0
Holland	435	2.8	2.6	3.5
India	204	1.3	1.2	1.6
Italy	135	0.9	0.8	1.1
Malaysia	163	1.0	1.0	1.3
Portugal	180	1.2	1.0	1.4
S. Africa	183	1.2	1.1	1.5
Spain	165	1.1	1.0	1.3
Sweedden	166	1.1	1.0	1.3
Turkey/Kaymaz	344	2.2	2.0	2.7
Turkey/Sivrihisar	167	1.1	1.0	1.3
Pakistan/Ambela	716	4.5	4.3	5.6
Limits	80	1	1	6
Average	455	2.2	2.7	3.4
Maximum	2896	17.8	16.9	21.0
Minimum	70	0.5	0.4	0.6

*present study/

The D_a , H_E , AI and I_γ values obtained for the samples of the present study along with their limiting values are presented in Table 4.

The radiological parameters of the basic samples studied (GAE-1, GAE-9, GAE-11, SB-55, NG-5 and MP-6) seem to be below the international dose limiting values. On the other hand, the radiological parameters for two granite samples (MP-90 and G-2 from Maronia and Granitis, respectively) appear to be above limits in all cases except for I_γ .

From the worldwide activity concentration data given in Table 3, hazard indices, as defined above, have been calculated and are given in Table 5.

Among the 27 countries/locations selected for comparison, granite of 7 countries (including Greece) fulfill the criterion of $H_E < 1$ to be used as building materials. Moreover, the average H_E of Greek samples is very close to the minimum H_E found. However, since granites are usually used in small quantities in house buildings, they do not induce an activity level exceeding the $1 \text{ mSv}\cdot\text{y}^{-1}$ dose limit (Pavlidou et al., 2006). As far as the AI is concerned, the average value of the samples studied is half than the 'world' average as it was calculated in this report. Finally, considering the values of gamma-ray index granites from Greece have the fourth lowest value. Only one of the selected countries/locations does not fulfil the criterion of $I_\gamma < 6$, and consequently, its use as building material is not recommended. This is the case of Gable Gattar II granite in Egypt, where there is U mineralization with high economic potential (El-Shershaby, 2002).

As the research on the natural radioactivity of the greek granites is in progress it must be noted here that the present results are considered as preliminary.

4. Conclusions

Twenty granite samples from northern Greece have been measured for their natural radioactivity in order to assess the radiological impact in case they are used as building materials, while 29 more samples were obtained from a previous study. The activities of ^{40}K , ^{226}Ra and ^{232}Th of the majority of the samples exceed the average level of these radionuclides in soil and building materials. That is because granites contain U and Th-rich minerals in them. Samples of basic composition have very low concentrations of radionuclides, which reflect to the values of their hazard indices that are below limits. On the other hand, intermediate and acid rocks are more enriched in ^{40}K , ^{226}Ra and ^{232}Th and their decay products. Four hazard indices were calculated in order to assess the health risk of using the above samples as building materials. The average of hazard indices of Greek granites is below 'world' average in all cases. Moreover, it is still below the criteria of UNSCEAR (2000). Therefore, at least from radiological point of view and for the investigated rocks, the use of granites from northern Greece as building materials is recommended.

5. References

- Adams J.A.S., Osmond Y.K. and Rogers J.J.W., 1959. The geochemistry of uranium and thorium. *Phys. Chem. Earth* 3, 298-343.
- Anjos R.M, Veiga R., Soares T., Santos A.M.A, Aguiar J.G., Frasca M.H.B.O., Brage J.A.P., Uzeda D., Mangia L., Facure A., Mosquera B., Carvalho C., Gomes P.R.S., 2005. Natural radionuclide distribution in Brazilian commercial granites. *Radiation Measurements* 39, 245 – 253.
- Arafa W., 2004. Specific activity and hazards of granite samples collected from the eastern desert of Egypt. *J. Environ. Radioactivity*. 75, 315-327.
- Asghar M., Tufail M., Javied S., Abid A. and Waqas M., 2008. Radiological implications of granite of

- northern Pakistan. *Journal of Radiological Protection* 28, 387-399.
- Chen C.J., Lin Y.M., 1996. Assessment of building materials for compliance with regulations of ROC. *Environment International* 22, 221-226.
- Christofides, G., Soldatos, T., Eleftheriadis, G. and Koroneos, A., 1998. Chemical and isotopic evidence for source contamination and crustal assimilation in the Hellenic Rhodope plutonic rocks. *Acta Vulcanologica*, 10(2), 305-318.
- Christofides G., Koroneos A., Pe-Piper G., Katirtzoglou K., Chatzikirkou, 1999. Pre-Tertiary A-Type magmatism in the Serbomacedonian massif (N. Greece): Kerkini granitic complex. *Bulletin of the Geological Society of Greece* vol. XXXIII, 131-148.
- D'Amico C., Christofides G., Eleftheriadis G., Bargossi G.M., Campana R., Soldatos T., 1990. The Sithonia Plutonic Complex (Chalkidiki, Greece). *Miner. Petrogr. Acta* vol. XXXIII, 143-177.
- El-Arabi A.M., 2007. Ra, Th, K concentrations in igneous rocks from eastern desert Egypt and its radiological implications. *Radiat. Meas.* 42, 94-100.
- El-Shershaby A., 2002. Study of radioactivity levels in granite of Gable-Gattar II in the north eastern desert of Egypt. *Appl. Radiat. Isot.* 57, 131-135.
- European Commission (EC), 1999. Radiation Protection 112 : Radiological Protection Principles Concerning the Natural Radioactivity of Building Materials Directorate –General Environment, Nuclear Safety and Civil Protection.
- Faure G., 1986. Principles of Isotope Geology, second ed. John Wiley & Sons, London, 464 pp.
- Grigoriadou A., Koroneos A., Eleftheriadis G., 2003. Mineralogy of Kastoria pluton, *Bulletin of the Geological Society of Greece* vol. XXXV, 46-60.
- International Union of Geological Sciences (I.U.G.S.), 1973. Subcommission on the systematic of igneous rocks. Classification and nomenclature of plutonic rocks. *N. Jb. Min. Mh.*, 1973, 149-163.
- Karavasili E., 2004. Mineralogy, Petrology and Radioactivity of Greek granitic rocks. MSc Thesis, School of Geology, Aristotle University of Thessaloniki, 98 pp. (in Greek).
- Karavasili E., Christofides G., Papastefanou C., Koroneos A. and Stoulos S., 2005. Mineralogy, Petrography and Radioactivity of Greek Granites. Proceedings of the 2nd Congress of the Committee of the Economic Geology, Mineralogy & Geochemistry of the Geological Society of Greece, Thessaloniki, 123-132.
- Koroneos A., 1991. Mineralogy, petrology and geochemistry of the Eastern Varnountas plutonite (NW Macedonia). Ph.D. thesis, University of Thessaloniki, 450pp (in Greek with English abstract).
- Menager M.T., Heath M.J., Ivanovich M., Montjotin C., Barillon C.R., Camp J. and Hasler S.E., 1993. Migration of uranium from uranium-mineralised fractures into rock matrix in granite: implications for radionuclide transport around a radioactive waste repository. *Radiation Environ. Biophys.* 34, 47-83.
- Orgun Y. and Altinsoy N., 2005. Natural radioactivity levels in granitic plutons and groundwaters in southeast part of Eskisehir, Turkey. *Appl. Radiat. Isot.* 63, 267-275.
- Pakou A.A., Assimakopoulos P.A. and Prapidis M., 1994. Natural radioactivity and radon emanation factors in building materials used in Epirus (north-west Greece). *Science of the Total Environment* 144, 255-260.
- Papastefanou C., Manolopoulou M. and Charalambous S., 1984. Exposure from the radioactivity in building materials. *Health Physics* 47, 775-783.
- Pavlidou S., Koroneos A., Papastefanou C., Christofides G., Stoulos S., Vavelides M., 2006. Natural radioactivity of granites used as building materials. *Journal of Environmental Radioactivity* 89, 48-60.
- Petropoulos N.P., Anagnostakis M.J. and Simopoulos S.E., 2002. Photon attenuation, natural radioactivity content and radon exhalation rate of building materials. *Journal of Environmental Radioactivity*

61, 257–269.

- Savidou A., Raptis C. and Kritidis P., 1995. Natural radioactivity and radon exhalation from building materials used in Attica region, Greece. *Radiation Protection Dosimetry* 59, 309–312.
- Siotis I. and Wrixon A.D., 1984. Radiological consequences of the use of fly ash in building materials in Greece. *Radiation Protection Dosimetry* 7, 101–105.
- Soldatos T., 1985. Petrology and geochemistry of the Elatia pluton. *Ph.D. Thesis, University of Thessaloniki, Greece*, 303 p., (in Greek with English abstract).
- Stoulos S., Manolopoulou M., Papastefanou C., 2003. Assessment of natural radiation exposure and radon exhalation from building materials in Greece. *Journal of Environmental Radioactivity* 69, 225–240.
- Tzortzis M., Tsertos H., Christofides S., Christodoulides G., 2003. Gamma measurements and dose rates in commercially used tiling rocks (granites). *Journal of Environmental Radioactivity* 70, 223–235.
- United Nations Scientific Committee on the Effects of Atomic Radiation (UNSCEAR), 1993. Sources and Effects of Ionizing Radiation. United Nations, New York.
- United Nations Scientific Committee on the Effects of Atomic Radiation (UNSCEAR), 2000. Sources and Effects of Ionizing Radiation, Vol. I. United Nations, New York.

THE GENETIC HYPOTHESIS OF THE URANIFERUS MINERALIZATION, EASTERN CHALKIDIKI (NORTHERN GREECE)

D. Persianis¹, J. Katsikis¹, D. E. Karageorgiou¹

¹ *Institute of Geology and Mineral Exploration, Olympic Village, Entrance C 136 77 Acharnae, Greece, persianis@igme.gr, johncats11@igme.gr, dek@igme.gr*

Abstract

This paper presents the genetic hypothesis of an uranium mineralization observed in Eastern Chalkidiki-Greece.

In the area of Stratoní (location Asprochomata) a uranium mineralization is expressed by disseminated primary (orthobrannerite) and secondary (torbernite) U minerals, in the granodioritic body of this area. Genetically it may be the result of uranium redistribution, which occurs in the resisting accessory minerals (e.g. monazite) of the granodiorite, by magmatic or meteoric hydrothermal fluids of low temperature. The mineralized granodiorite of Stratoní gives no evidence of a metalliferous pluton, based on the study of hydrothermally altered samples and this ascertainment is a fact that should be confronted with a lot of careful thought.

In the granite of Arnea area, uranium mineralization is generally absent, excluding some poor ones, located along the contacts of the granite with small remnants of the hosting rock, expressed in the form of impregnations or veinlets. The possible cause for its formation being the interaction of a secondary low temperature hydrothermal system mainly of meteoric water participation (convective hydrothermal system) with the granite and the hosting wall-rock minerals. The granite of Arnea indicates all the characteristics of a metalliferous granitoid.

Key words: *Uranium redistribution, orthobrannerite, metalliferous granitoid, hydrothermal fluids, Chalkidiki, Northern Greece.*

1. Introduction

In Chalkidiki area, in the granodiorite of Stratoní, which does not present the characteristics of one metalliferous magmatic body, are observed a primary (orthobrannerite), as well as a secondary (torbernite) uranium mineralization resulting from the redistribution of uranium existing in the granodiorite accessory minerals (e.g. Monazite), by low temperature, magmatic or meteoric, hydrothermal fluids. On the contrary, the Arnea area's granite, although this magmatic intrusion presents characters of a metalliferous granitoid, uranium mineralization is not observed.

This study attempts the presentation of the uranium mineralization and the determination of its genesis. The mineral composition, the geochemical characteristics, the age, the geotectonic environment and the metallogenetic evolution of the two plutonic bodies are examined. For this reason thin polished sections of the samples from these areas were prepared, on which was used the method of



Fig. 1: Geological map of Chalkidiki.

autoradiography, with the purpose to detect and study the uraniferous minerals concentration.

2. Petrography - Mineralogy

The magmatic body of Stratoni area, known as Stratoni granodiorite, is a fine to coarse-grained rock with a composition changing from quartz diorite – monzonite to granodiorite – adamellite, with most common phase the granodiorite (Kalogeropoulos et al., 1988; Gerouki et al., 1988).

The main minerals are quartz, potassium feldspar, plagioclase, titaniferous biotite and as secondaries muscovite (sericite), hornblende, pyroxene (diopside), epidote, titanite, calcite, magnetite and pyrite are found. The main hydrothermal alterations are the biotite chloritization and the sericitization of the plagioclases.

The magmatic body of Arnea is a medium to coarse-grained leucogranite, which the composition presents small fluctuations. The main minerals are quartz, plagioclase, potassium feldspar, muscovite and biotite. As secondary minerals chlorite, epidotes, magnetite, +/-titanite, +/-allanite are found.

The comparison of the mineral composition of these two bodies shows that: a) the quartz is more abundant in the leucogranite of Arnea, b) the plagioclases are more abundant and more basic in the Stratoni granodiorite than in the Arnea leucogranite, while alkali feldspar are more abundant in the Arnea body, c) the micas content is low in both bodies, d) in the Arnea, leucogranite the content of muscovite and biotite is the same, but in the Stratoni granodiorite biotite is prevailing, e) the biotites of the Stratoni's granodiorite are rich in titanium, while those of the Arnea's leucogranite, are poor ones, f) femic minerals, like hornblende and pyroxenes, are observed only in the Stratoni body.

3. Chemism – Geotectonic environment – Age

The changing composition of the Stratoni granodiorite means complex magmatic conditions of genesis. In combination with the fact that it presents a metaluminous and a peraluminous character, this signifies a hybrid origin with the participation of both, mantle's components (I - type) as well as sialic components (S - type). Its composition is also fluctuating from cafemic to alumino-cafemic types.

It presents a wide range of SiO_2 values and a differentiation tendency which is expressed with an almost linear negative correlation for $\text{SiO}_2 / \text{TiO}_2$, Al_2O_3 , Fe_2O_3 , FeO , MnO , MgO , CaO , Na_2O ratios and a positive one for $\text{SiO}_2 / \text{K}_2\text{O}$. The dispersion of the values is due to the hydrothermal alterations.

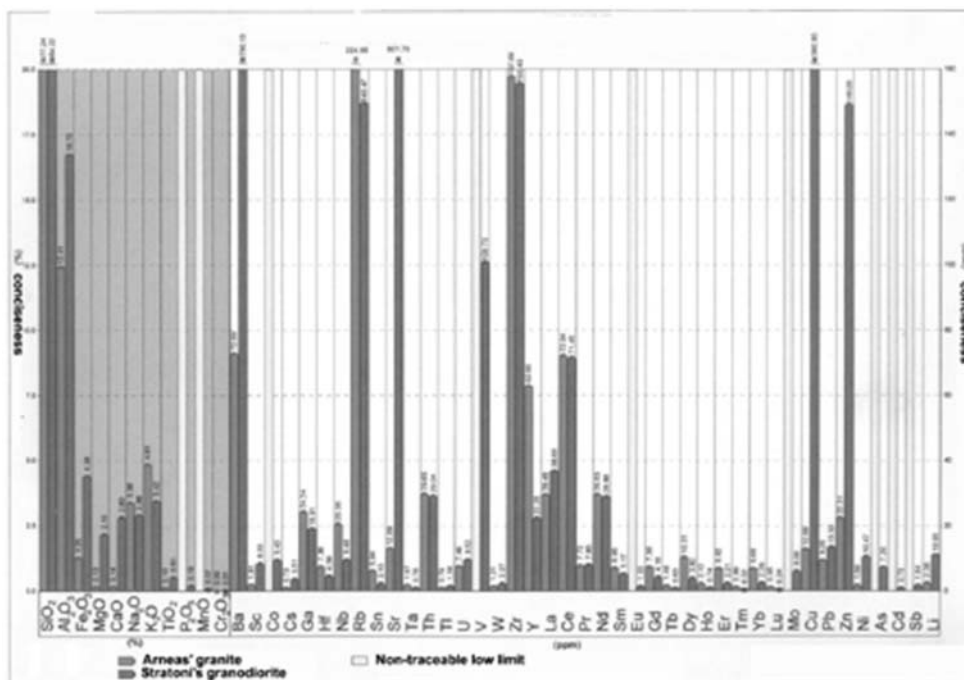


Fig. 2: Standard deviation graph for majors and trace elements in samples of Arneas' granite and Stratoni's granodiorite.

The leucogranite of Arnea has mainly a peraluminous character and presents small fluctuations of its composition, meaning that sialic components (S - type) have the major role in its genesis, but, on the other hand, the presence of magnetite indicates the participation also of a mantle's component (I - type).

Both bodies present a calcalkaline character and it seems that are formed in a subduction environment of high pressure.

The method of K/Ar in biotite gives an age of $29,6 \pm 1,4$ million years (Tertiary) for the Stratoni area granodiorite, (Alther et al., 1976), while the granite of Arnea's area, dated with the method of U/Pb in zircon, gives a Mesozoic age of 212 million years, (Frei, Gerouki pers. com., 1987).

4. Depth and temperature of emplacement.

The granodioritic magma of Stratoni was placed at a temperature of about 900° C and was solidified at a pressure between 1 and >5 kb. It presents a potassium tendency, fact meaning that the magma was firstly saturated in water. The wide range of pressure's values proves a gradual, slow crystallization of this granodiorite. So, the gradual falling of the pressure during the crystallization, would free water and metallic elements in the fluid phase, and this would help the magma ascent to highest levels in the crust (Eugster, 1985).

The leucogranite of Arnea seems to be crystallized in pressures values between ~1kb to <0.5 kb, meaning that its crystallization took place nearest to the crust surface, than the Stratoni body, and for this reason it was not characterized by sufficient water content.

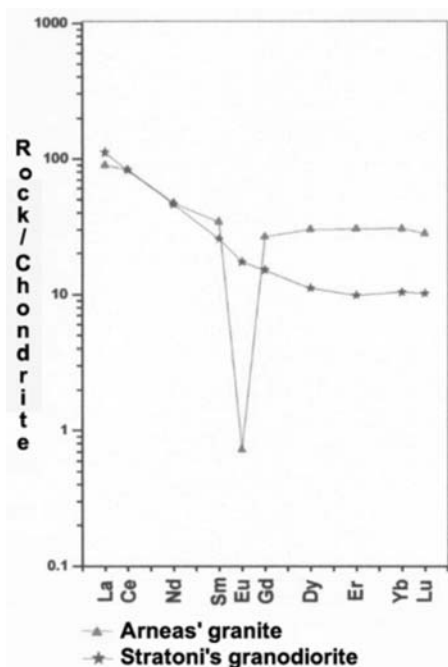


Fig. 3: The REE patterns of Arnea's granitic and Stratoní's granodioritic samples, normalized for 10 ordinary chondrites.

5. Geochemical characteristics

The L.O.I. of the Stratoní samples is great (2.8), in contrary with these of Arnea samples (0.8), fact that is due to the hydrothermal alteration of the Stratoní's samples, which must be examined with care.

The comparison of the mean concentration values of the major, as well as for the trace elements, make obvious the differences of the two bodies, (Fig.2).

The uranium content in the Arnea's granite fluctuates between 5 and 14 ppm, with a mean value of 7,5 ppm ($\sigma=2$), while the Th content changes from 23 to 40 ppm with a mean value of 29,6 ppm ($\sigma=3,8$). In the Stratoní granodiorite, the U content changes between 4-19 ppm with a mean value of 9,5 ppm ($\sigma=3,4$), and respectively the Th between 11-36 ppm with a mean value 29 ppm ($\sigma=6$). These values are higher than those usually found in the granites, (3-5 ppm U and 10-12 ppm Th – Adams et al., 1959).

The granite of Arnea, except the high content of U and Th, also presents high values of other incompatible elements, like the Rb, K, Sn, Nb, Y, Ta, while the content in Ba, Sr, Mg and Ti are low, so the ratios Rb/Sr, K/Ba, Cs/Ba are high and the ratio Sr/Y low.

The Stratoní granodiorite presents exactly the opposite image, with just a little augmentation in Cs and Li content. This results in high values of the Cs/K ratio and a small augmentation in this of U/Th.

In Figure 3 the REE patterns of Arnea's granitic and Stratoní's granodioritic samples, normalized for 10 ordinary chondrites (Nakamura, 1974), are shown. It is observed: a) the enrichment of the light Rare Earth Elements in both plutonic bodies, b) the granite of Arnea presents an augmentation of the heavy Rare Earth Elements values and a significant negative Eu anomaly, c) in the contrary, the granodiorite of Stratoní presents just a little increase in the values of the heavy Rare Earth Elements and a small negative irregularity in Eu.

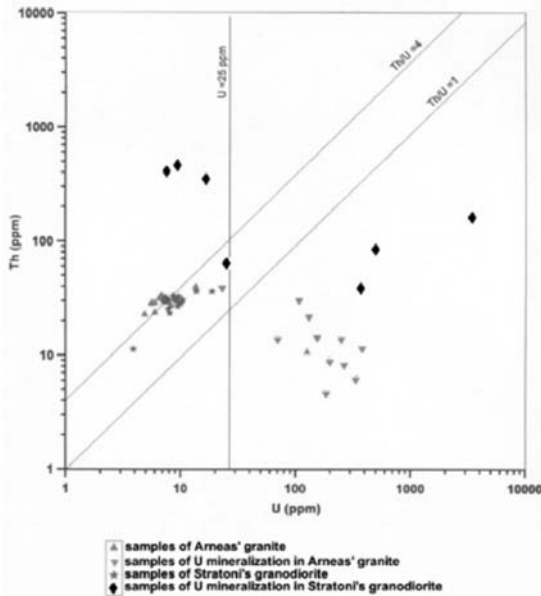


Fig. 4: Th versus U, for mineralized, unaltered and U mineralised samples from Arneas' granite and Stratoni's granodiorite.

The comparison of the chemical data from the two bodies shows that the granite of Arnea, except the Li content, presents all the characteristics of a metalliferous granitoid. On the contrary, the Stratoni granodiorite, except for the U and the Th, seems that does not present this tendency (Howarth et al., 1981).

6. Metallogenic evolution

It is considered that the main supply sources for metallic elements are three. A) The magmatic fluids, which contribute to the circulating hydrothermal fluids, combined with events in the silicate melt, like freezing, crystallization, and pressure or permeability changes. B) The reactions between the hydrothermal fluids (magmatic or meteoric), and the solidified crust of the plutonite and C) the interaction between hydrothermal fluids and the minerals of the hosting rock. The temperatures related with the hydrothermal events B and C, usually does not exceed the 500°C (Eugster, 1985).

This hydrothermal action may be primary or secondary. The primary (magmatic) is related with the last phases of the plutonite crystallization, especially, if this one is saturated in water, while the secondary is developed by the meteoric waters with the creation of an hydrothermal convective system, usually inside an extended system of discontinuities, like the faults, which facilitate the heating and the water circulation. The high concentrations of the radioactive elements, U, Th and K, which heat some parts of the rock, can maintain such hydrothermal systems. In these metal-bearing systems, underground waters are leaching metals and volatic componets from the granite, after his emplacement, especially during periods of higher thermal flows from the mantle, like the Tertiary (Simpson et al., 1979).

The metal bearing granite of Arnea does not present a marked Uranium mineralization, except a small one, observed at the contacts of the granite with some remnants of the hosting rocks inside the granite (of some decade meters), which have a composition of two micas gneisses, or two micas schists with garnet, or phyllites. These contacts sometimes are of tectonic origin and the mineral-

ization is developed at the crossing of NW-SE faults, with faults of E-W direction. The type of this mineralization depends from the kind of the hosting rock and usually it is expressed like veinlets or like impregnations, but always inside the hosting rock and near the contact. The absence of mineralization in the granite is probably due to a lack of water, caused by the high or medium degree of metamorphism of the hosting rocks. On the contrary at the contacts of the granite with the hosting rocks, with the help of the faults and the high concentration of radioactive elements (U, Th, K), seems that a secondary hydrothermal system was developed and maintained, from waters of meteoric origin or waters from the hosting rock. The interaction of the hydrothermal fluids with the solidified part of the granite and the minerals of the hosting rock, probably is the formation source of the uranium mineralization in the area.

The mineralization in the Straton area appears inside the granodiorite at the crossing of two fault systems, of NNW-SSE and NW-SE directions respectively. It is expressed by disseminated primary and secondary uranium mineralizations, located in a small surface of Asprochomata in Straton area. This mineralization seems resulting from the redistribution of the uranium included inside the granodiorite's secondaries resistant minerals. It is accomplished with the help of magmatic and meteoric hydrothermal fluids. These fluids result from the water sufficiency characterizing the granodiorite, the high concentration of radioactive elements (U, Th, K) and the faults, which cut the area.

Comparing the U/Th ratio in samples from the granite of Arnea and the granodiorite of Straton, as well as in uraniferous samples from these two areas, it is observed (fig.4) that the samples from the granite of Arnea and the granodiorite of Straton are projected along the line which is defined from the ratio $Th/U=4$ and till the limit of 25ppm with a positive correlation of the two elements (Wenrich, 1985). This indicates a magmatic differentiation with the uranium hosted to someone of the resistant primary minerals (monazite) and not in the uraninite. The uraniferous samples from Arnea and Straton are projected mainly in the field where the ratio Th/U is less than 1, with just a little bigger value for the Straton samples. This means that either, U rich fluids but not in thorium enriched the samples, or that the Th was removed. Because the Th is a relatively immobile element, is in generally accepted the first process for the mineralization, in which the mineralization was produced from low temperature hydrothermal fluids, usually of meteoric origin. Three samples of the uranium mineralization from Straton area, are projected in the field, where the ratio Th/U is bigger than 4 (values between 21 and 54), and the U concentration has a value less than 25ppm. This means that high temperature hydrothermal fluids redistribute the Th, in the same time the U was leached by the hydrothermal alteration.

7. The Uranium Mineralization (Autoradiographies– mineralogy – mineral chemistry).

The study of the uranium mineralization was completed with the construction of a sufficient number (20) of polished thin sections from uraniferous samples, the examination of their autoradiographies, targeting to charting the α -radiation, which is mainly radiated from the U and Th minerals, and after their localization on the thin section surface, with their examination in the electronic microscope combined with electron microprobe analyser, aiming to determine the chemical composition of these minerals.

The method of the autoradiography is based on the registration of the α -radiation traces from the radioactive elements on a specialized detector. In the present study the used detector was a plastic material, known as CR-39, which was in a stable and constant contact with the thin polished sections surface for one month. After the month, to observe the radiation traces, the pieces of the detector were etching with NaOH 6N in a temperature of 80° C for 3 hours. From the whole number of the sam-

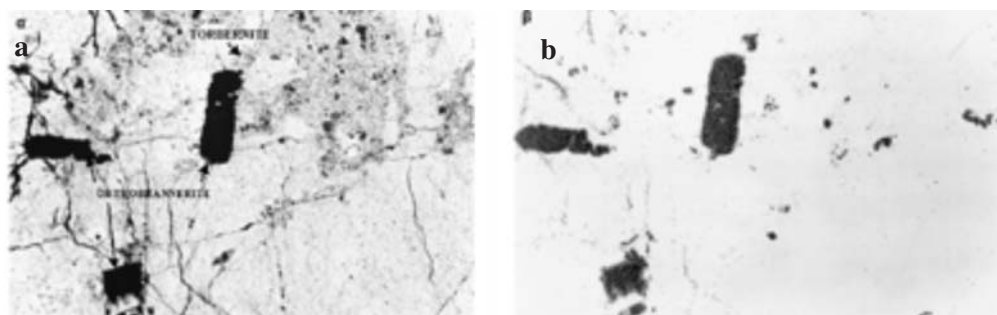


Fig. 5: Specimen AS-3 (thin section AS-3B) a. Microphotography of a thin section from Aspro-chomata, Straton area – East Chalikidiki, with Orthobrannerite and Torbernite crystals (Magnification x16. Nicols//). b. Microphotography of the autoradiography, on CR-39, of the thin section's same area (as the previous foto a), where the traces of a-particles from Orthobrannerite and Torbernite crystals are registered (Nicols //).

les, only seven autoradiographies, the more representatives, were selected, (with the corresponding thin polished sections). After the detection and localization of the radioactive minerals on the sections, it followed their study to the polarizing microscope as well as their electron microprobe analysis, mainly in the laboratories of N.C. S. R. “DEMOCRITOS”, (SEM system PHILIPS 515 coupled with EDAX 9900). For the analysis were used an acceleration voltage of 25KeV, a ZAF correction program and the total error was less than 10% for the major elements. A smaller number of thin sections were examined in the SEM laboratory of IGME, (S.E.M. system JEOL JSM-5600 coupled with an E.D.S system of OXFORD INSTRUMENTS), where the analysis conditions were 30KeV acceleration voltage, 3nA beam current and a spot diameter of 10-30 μm .

For each of the two studied areas the results are the following:

A. Straton area

In the area were observed the uranium minerals Orthobrannerite, Torbernite, Uranothorite and Cheralite. An opaque Fe-P uraniferous mineral, red in color, and coupled with the Cryptomelan was also found.

The radioactivity in the places of sampling reaches 2.500 c/s, while the sample from this area gave a content of 3428 ppm U and 162 ppm Th.

The Orthobrannerite is a primary U mineral with chemical formula $\text{U}^{4+}\text{U}^{6+}\text{Ti}_4\text{O}_{12}(\text{OH})_2$ crystallizing in the orthorhombic system, which does not contain Rare Earth Elements, while the Brannerite (U, Ca, Y, Ce) $(\text{Ti, Fe})_2\text{O}_6$ contains Rare Earth Elements and crystallizes in the monoclinic (Perroud, 1986, 1994, 1998). Standartless semiquantitative spot analysis of an Orthobrannerite crystal in the Electronic Microanalyser gave the following content in oxides (%): $\text{Al}_2\text{O}_3=0.6$ $\text{SiO}_2=0.4$ $\text{UO}_2=54.4$ $\text{TiO}_2=37.4$ $\mu\alpha$ $\text{FeO}=3.7$.

The Torbernite is a secondary U mineral with chemical formula $\text{Cu}(\text{UO}_2)_2(\text{PO}_4)_2 \cdot 12\text{H}_2\text{O}$, which crystallizes in rhombic system. Standartless semiquantitative spot analysis in the Electronic Microanalyser gave the following content in oxides (%): $\text{Al}_2\text{O}_3=0.3$ $\text{SiO}_2=1.8$ $\text{P}_2\text{O}_5=20.1$ $\text{UO}_2=67.7$ $\text{FeO}=0.7$ $\text{CuO}=7.8$ $\mu\alpha$ $\text{As}_2\text{O}_3=1.6$.

The Uranothorite is a thorite (ThSiO_4) with more than 5% U content. Standartless semiquantitative

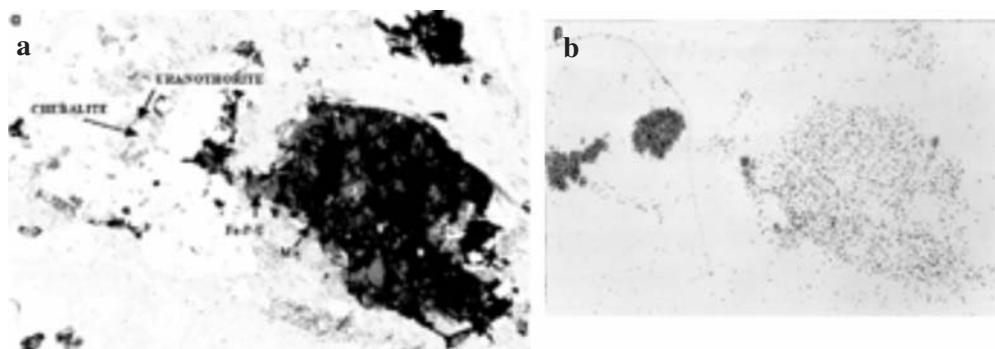


Fig. 6: Specimen AS-3 (thin section AS-3A) a. Microphotography of a thin section from Asprochomata, Stratoni area – East Chalikidiki, with Cheralite and Uranothorite crystals, as well as with uraniferous Fe-P-minerals closely linked with Mn minerals (Magnification x36. Nicols//). b. Microphotography of the autoradiography, on CR-39, of the thin section's same area (as the previous foto a), where the traces of a-particles from the Cheralite and Uranothorite crystals, as well as from the uraniferous Fe-P-minerals closely linked with Mn minerals are registered (Nicols //).

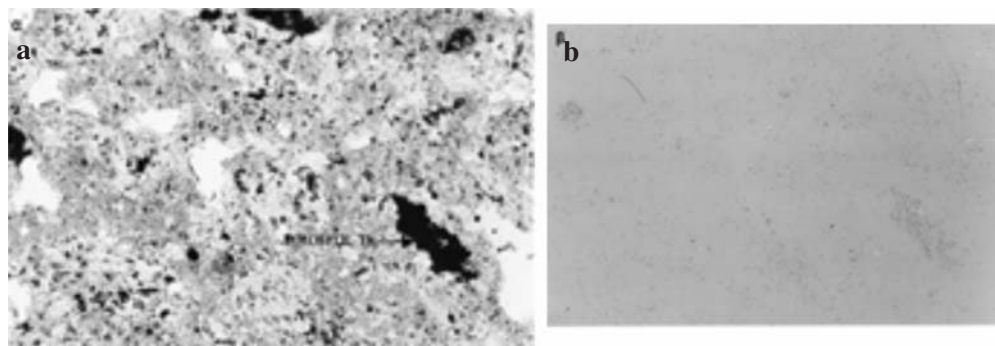


Fig. 7: Specimen AS-6 a. Microphotography of a polished thin section from Asprochomata, Stratoni area – East Chalikidiki, where we can see Jarosite crystals with Th (Magnification x16. Nicols//). b. Microphotography of the autoradiography, on CR-39, of the thin section's same area (as the previous foto a), where the traces of a-particles from the Jarosite crystals containing a little Th concentration are registered (Nicols //).

spot analysis in the Electronic Microanalyser gave the following content in oxides (%): $\text{SiO}_2=13.8$ $\text{ThO}_2=57.8$ $\text{UO}_2=28.3$. Because its great UO_2 content it may be a Thorogoumitte ($\text{Th}(\text{SiO}_4)_{1-x}(\text{OH})_{4x}$), which contains UO_2 between 2.5-31.5% and ThO_2 from 18.2 to 50.8%.

The Cheralite has a chemical formula $(\text{Ce, La, Th, Ca, U})\text{PO}_4 \text{SiO}_4$ with UO_2 content of 3.5-5.5% and ThO_2 between 25.9-27.7%. It is a mineral appartaining in the group of Monazite (they have the same structure), like the Huttonite (ThSiO_4) and the Brabantite ($\text{CaTh}(\text{PO}_4)_2$). Standartless semiquantitative spot analysis in the Electronic Microanalyser gave the following content in oxides (%): $\text{SiO}_2=2.6$ $\text{P}_2\text{O}_5=29.4$ $\text{ThO}_2=27$ $\text{UO}_2=7.9$ $\text{CaO}=4.9$ $\text{La}_2\text{O}_3=11.4$ $\text{Ce}_2\text{O}_3=16.8$.

The standartless semiquantitative spot analysis of the red opaque mineral with Fe and P, gave the following content in oxides (%): $\text{Al}_2\text{O}_3=1.2\%$ $\text{SiO}_2=1.5\%$ $\text{P}_2\text{O}_5=14.2\%$ $\text{SO}_3=3\%$ $\text{UO}_2=0.5$ $\text{CaO}=1$ $\text{MnO}=1.5$ $\text{FeO}=75.8$ and $\text{CuO}=0.8$. Probably the uranium is adsorbed in this mineral, or dispersed in the crystal lattice in a small quantity.

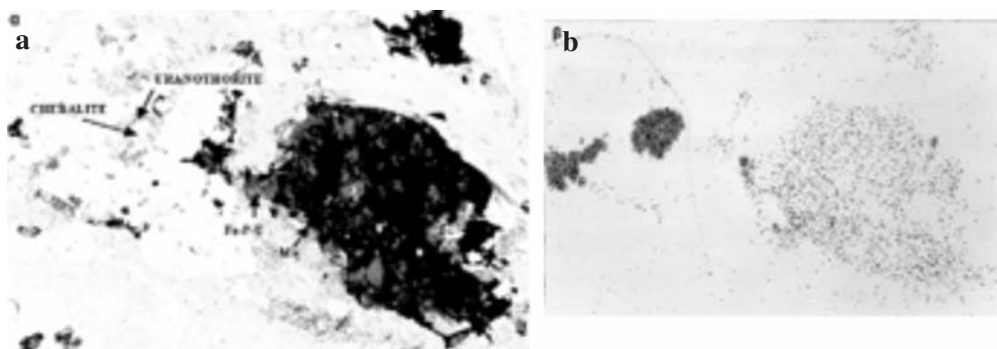


Fig. 8: Specimen AP-1 (thin section AP-1A) a. Microphotography of a thin section from Arnea area – East Chalikidiki, where we can see U-Ti-Fe-Mg oxides inside the cleavage surfaces of a mica crystal (Magnification x36. Nicols//). b. Microphotography of the autoradiography, on CR-39, of the thin section's same area (as the previous foto a), where the traces of a-particles from the U-Ti-Fe-Mg oxides inside the cleavage surfaces of the mica are registered (Nicols //).

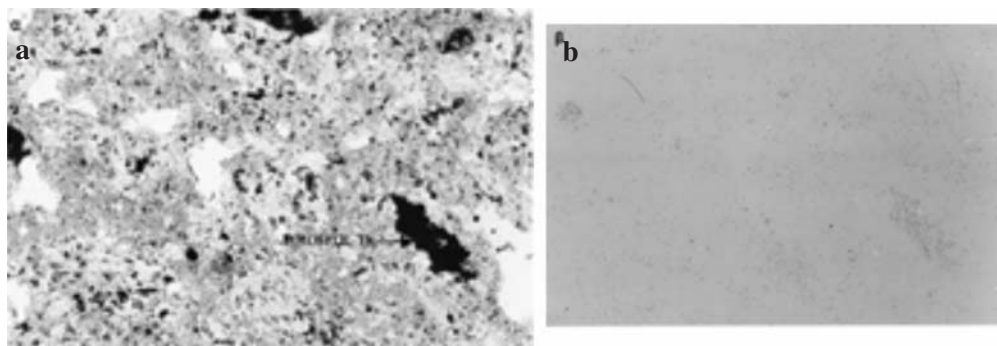


Fig. 9: Specimen AP-4 (thin section AP-4A) a. Microphotography of a polished thin section from Arnea area – East Chalikidiki, where we can see Xenotime crystals (Magnification x40. Nicols//). b. Microphotography of the autoradiography, on CR-39, of the thin section's same area (as the previous foto a), where the traces of a-particles from the Xenotime crystals are registered (Nicols //).

Finally at the sampling place AS-6 (thin polished section AS-6) was measured a radioactivity of 1200 c/s and a content of 9 and 451 ppm of U and Th respectively. The examination of the thin polished section in the E/M demonstrates that the Th, which is contained in the mineral Jarosite, causes the radioactivity. This mineral with chemical formula $KFe_3(SO_4)_2(OH)_6$ is very widespread and it appears in the oxidation zone of the iron sulfide deposits and especially of pyrite. Semiquantitative spot analysis in the Electronic Microanalyser gave the following content in oxides (%): $P_2O_5=3.8$ $SO_3=34.6$ $ThO_2=0.7$ $K_2O=8.3$ $TiO_2=0.5$ $\mu\alpha$ $FeO=51.6$.

B. Arnea area

In the Arnea's area the radioactivity was detected from:

From crystals of Xenotime (YPO_4) in which the standartless semiquantitative analysis in the E/M gave the following contents in oxides (%): $Al_2O_3=3.8$ $SiO_2=9.3$ $P_2O_5=42.2$ $UO_2=1.1$ $CaO=1.2$ $TiO_2=0.7$ $Gd_2O_3=1.3$ $Dy_2O_3=5.2$ $Er_2O_3=3.3$ $\mu\alpha$ $Y_2O_3=30.8$. The radioactivity on the sampling

place was measured at 1000 c/s and the chemical analysis of the sample gave 262 ppm U and 8 ppm Th.

From U-Ti of Ferromanganese oxides in the clivage surfaces of the mica.

From a radioactive veinlet composed of P-Fe-Si-Y-U-Al-Ca-La-Nd oxides with a changing composition from point to point. The standartless semiquantitative spot analysis in a point of the veinlet gave the following content in oxides (%): $\text{Al}_2\text{O}_3=1$ $\text{SiO}_2=32.3$ $\text{P}_2\text{O}_5=24.2$ $\text{UO}_2=7.5$ $\text{CaO}=1.6$ $\text{Nd}_2\text{O}_3=0.7$ $\text{Fe}_2\text{O}_3=11.9$ and $\text{Y}_2\text{O}_3=18.8$. The radioactivity in the place where the sample was taken (1400c/s) is the bigger observed in the area of Arnea. The chemical analysis gave 343ppm for U and 6ppm for Th.

8. Conclusions

In the area of Stratoni (location Asprochomata) the Uranium mineralization is expressed in the granodioritic body of the area by disseminated primary (orthobrannerite) and secondary (torbernite) U minerals.

In the area of Arnea uranium mineralization is in generally not observed in the granite, except this poor one located along the contacts of the granite with small remnants of the hosting rock.

9. References

- Adams, J.A.S., Osmond, J.K., and Rogers, J.J.W., 1959. The geochemistry of thorium and uranium: *Phys. Chem. Earth*, 3: 298-348.
- Alther, R., Keller, J., Harre, W., Moehndorf, A., Kreuzer, H., Lenz, H., Raschka, H., and Wendt, J., 1976. Geochronological data on granitic rocks of the Aegean Sea. Preliminary results : Hist. Struct. Bass. Mediterr, RAP CIESMM 24/7a, p. 71-72.
- Eugster, H.P., 1985. Granites and hydrothermal ore deposits: a geochemical framework: *Min. Mag.* V. 49, p. 7-23.
- Gerouki, F., Karamanou, E., Kalogeropoulos, S.H., Oikonomou, G., and Kougoulis, Ch., 1988: Granites in the area of Serbomacedonian maze. Their mining in the Geology and the Mineral Exploration. Athens I.G.M.E. (in Greek).
- Howarth, R.J., Koch, G.S., Plant, J.A., and Lowry, R.K., 1981. Identification of uraniferous granitoids in the USA using stream sediment geochemical data: *Mineralogical Magazine*, V. 44, p. 455-470.
- Kalogeropoulos, S.H., Oikonomou, G., Gerouki, F., Karamanou, E., Kougoulis, Ch. and, Perlicos, P., 1988. The granodiorite of Stratoni, N. Grece, the mineralogy, the geochemistry and the mineralization mining. Athens, I.G.M.E. (in Greek).
- Nakamura, N., 1974. Determination of REE, Ba, Fe, Mg, Na and K in carbonaceous and ordinary chondrites: *Geochim. Cosmochim. Acta* 38, p.p 757-775.
- Perroud, P., 1986, 1994, 1998. Athena Mineralogy: Mineral Data Base into Internet.
- Rong, J., Han, Z. and Xia, Y., 1989: Uranium metallogenesis of coarse-grained granite in areas H, China: In "Uranium deposits in magmatic and metamorphic rocks". IAEA-TC-571/7, Vienna, p. 93-112.
- Simpson, P.R., Brown, G.C., Plant, J., and Ostle, D., 1979. Uranium mineralization and granite magmatism in the British Isles: *Phil. Trans. R. Soc. London, A.* 291, p. 385-412.
- Wenrich, K.J., 1985. Geochemical characteristics of uranium – enriched volcanic rocks. "Uranium deposits in volcanic rocks". IAEA-TC-490/1, Vienna, p. 29-51.

GEOLOGICAL, PETROLOGICAL AND TECTONIC FEATURES CHARACTERIZING THE COMMERCIALITY OF THE MARBLES OF SOUTHERN VERMION MOUNTAIN

Ploumis P. and Chatzipanagis I.

*Institute of Geology and Mineral Exploration (IGME), Fragon 1, 54626 –Thessaloniki,
ploumis@thes.igme.gr, ixatzipanagis@gmail.com*

Abstract

The southern Vermion mountain is composed of Pelagonian metamorphic rocks. Two different lithologic units are distinguished in this area. The first one consists of the highly metamorphosed rocks of Paleozoic age (migmatites, gneisses with marble intercalations and anatectic granites). The second unit comprises two series: the lower with schists, gneisses and marbles (200 m thick) and the upper with marbles (more than 2500m thick). The age of the rocks in the second unit is Triassic – Jurassic and these are metamorphosed in greenschist facies.

During the last 40 years, the marbles of the second unit are being exploited for ornamental purposes in more than 100 quarries. Variations in chemical and mineralogical composition, grain size as well as some structural characteristics result to the 5 marble qualities – commercial types of Vermion mountain: a) White marbles, b) “Rigota” marbles, c) “Pitsilota” marbles, d) “Louloudata” marbles, e) Sipoline marbles.

Key words: *White marbles, Pitsilota marbles, Rigota marbles, Louloudata marbles, Cipoline marbles, Pelagonian zone, south Vermion mountain, Central-North Greece.*

1. Introduction

The studied area is located in the south Vermion mountain, between Aliakmon river, Polymylos, Tetralofos, Koumaria and Eripiá Tormanis villages (Fig. 1). The bigger part of the studied area is occupied by marbles, some of which are exploited since the mid '60. More than 100 quarries are open in five areas. These areas are: Koumaria (15 quarries), Eripiá Tormanis (16 quarries), Kastania (15 quarries), Arapis (23 quarries) and Zoodochos Pigi with more than 30 quarries. (Χατζηπαναγής κ. α., 2009). Today only 6 of them are active. The exploitation has been considerably restricted because of various problems that appear to the marbles such as their colour, the tectonic strain, the ability of their polishing etc. In the south Vermion region, $1,4 \times 10^6$ m³ of marbles have been quarried and about 50.000 m³ of them have been exploited (Χατζηπαναγής, 2009β). This work identifies the commercial types of the south Vermion marbles according geological, mineralogical, petrological, structural - textural, chemical and aesthetic (colour, impurities) criteria.

2. Geological setting

2.1 Geology - lithostratigraphy

The south Vermion mountain region is mainly composed of pelagonian metamorphic rocks which are partly covered by almopic nappes (Fig. 1). The pelagonian rocks are composed of two units of metamorphic rocks. The first, of Paleozoic age, is characterized of middle to high grade metamorphism. It is composed by schists, gneisses, augen gneisses, migmatized gneisses and thin bangs of marbles. Granite bodies of anatectic character, mainly related with the migmatites are exposed in some areas. This unit of thickness > 2000m (Fig. 2) defines the basement of Pelagonian zone.

The second, younger unit, is of Triassic – Jurassic age (Mercier, 1968). It is composed primarily of marbles and gneisses and schists of middle - low grade metamorphism (greenschist facies). This unit is named the Eastern Carbonate Cover of Pelagonic zone (Kilias & Moundrakis, 1989). Its basis of about 100m thickness is composed of alternating suite of metaquartzites, schists (\pm garnet) and albite gneisses. On this basis lie a series of white calcitic marbles (lower marbles series), called as the series of Zoodochos Pigi (Γαλανάκης & Πλουμής, 2000) with the maximum thickness of 180m. A series of gneisses of ~200m follow these marbles (Fig. 2).

A thick carbonatic series (upper marbles series) called as the series of Angkathi-Tsekouri (Γαλανάκης & Πλουμής, 2000) - of 2.500m in all is composed of semi white, banded, stripped, grey banded, and cipoline marbles, with intercalations of white marble bangs (Χατζηπαναγής, 2009 α).

The Transgressive Carbonate Cover (Kilias & Moundrakis, 1989) and the flysh, are found to be overthrust on the metamorphic rocks of the Pelagonian zone in all their outcrops – always connected with ophiolites (Χατζηπαναγής, 2009α).

2.2 Structural observations in marbles

More or less, related with respectively metamorphic episodes, 4 or 5 deformation events are determined in the Pelagonian zone (Μουντρακης, 1983, Spyropoulos at al., 1988, Kilias & Moundrakis, 1987). Beyond the first deformation event of Paleozoic age which take place only in the basement rocks, all other episodes affect both units creating isoclinal folds, mylonitic zones, faults and overthrusts. The eastern Pelagonian part of the carbonatic cover is thrust on the crystalline basement through a series of thrusts. Field observations in the frame of this work as well as the detailed studies of the south Vermion rocks (Χατζηπαναγής, 2009α) suggest that the pelagonian basement has been affected by plastic deformation episodes, such as isoclinal folds, open folds, mylonites as well as by brittle deformation episodes such as shear zones and cataclastites while the carbonatic cover has been affected only by plastic deformation. Such brittle deformation evidences affect substantially the coherence and the aesthetic (texture, colour) of the marbles.

3. Methods

According to the chemical – mineralogical composition, the colour and even some tectonic deformation features, 5 commercial types of marbles are distinguished:

3.1 White marbles

They occupy the lower series of marbles (Zoodochos Pigi) as a single bang of a maximum thickness of 180 m, between schists in Arapi and Zoodochos Pigi regions and as bangs of 10 to 15m thickness

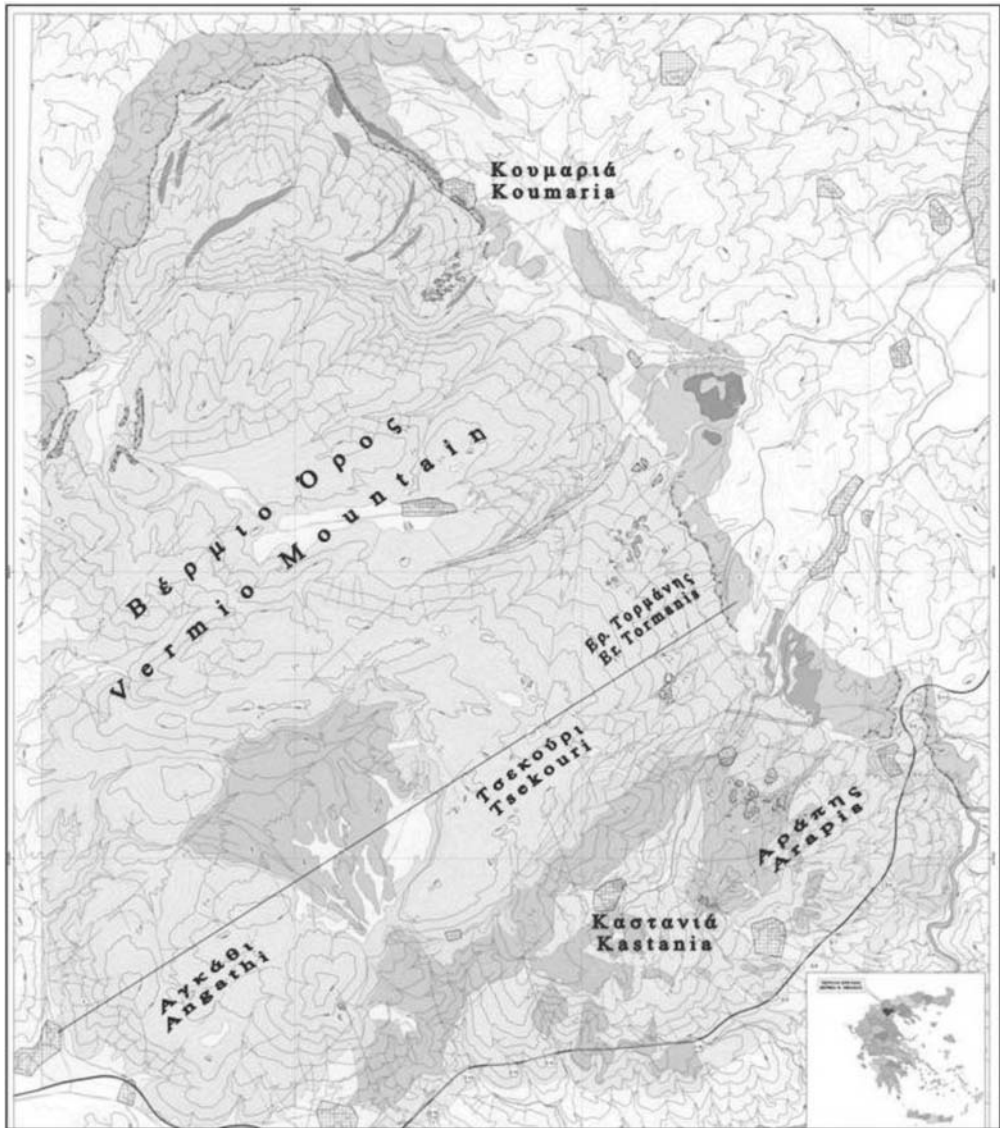


Fig. 1: Geological map of south Vermion mountain.

LEGEND

-  Discard materials
-  Quaternary deposits

ALMOPIAN NAPPES

-  Conglomerates
-  Limestones, schists, phyllites
-  Ophiolites

CARBONATE COVER OF PELAGONIAN ZONE

-  Upper series of marbles
-  Schists
-  Intermediate schists
-  Lower series of marbles
-  Schists, gneisses, metaquarzites

PALAEOZOIC BASAMENT OF PELAGONIAN ZONE

-  Gneisses +/- migmatized, migmatites
-  Lenses of marbles
-  Granites

 Faults with tectonic breccias

 Thrusting

 Normal faults

 30
Strike and dip of foliation

 Quarries

Cross section I – I'



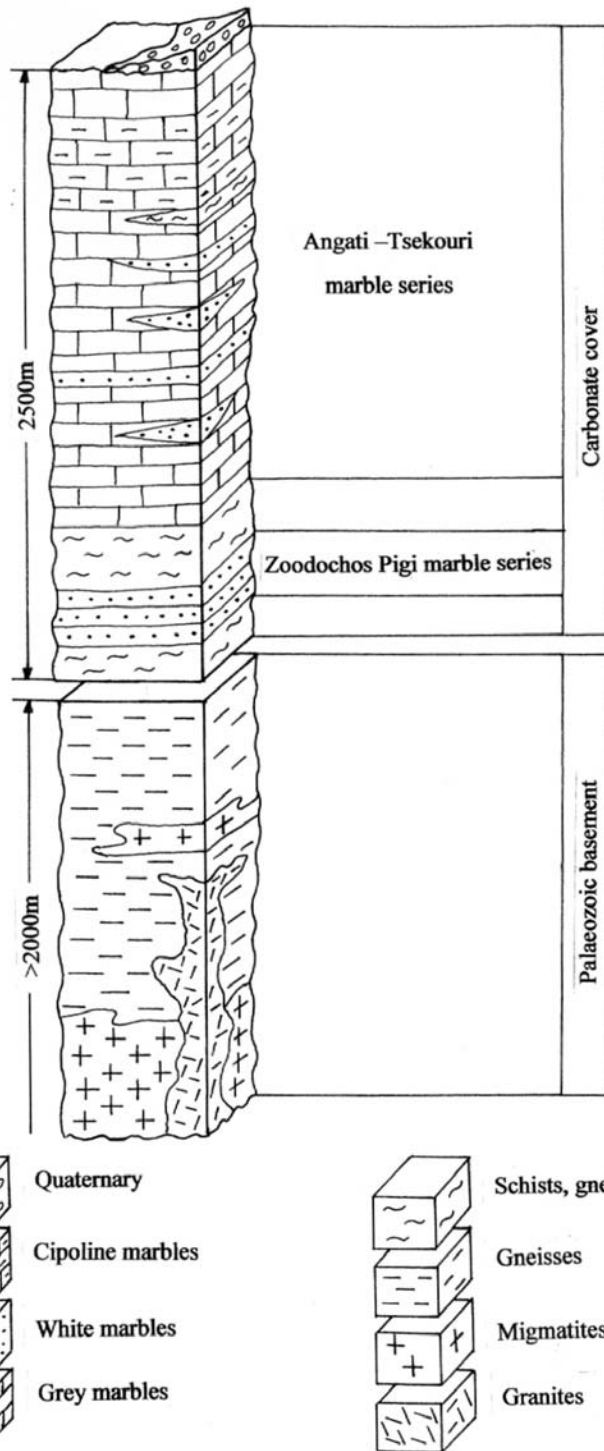


Fig. 2: Lithostratigraphic column of south Vermion mountain

in the semi grey to grey, calcitic marbles of the upper series of marbles (Angathi –Tsekouri) in the Kastania, Eripiá Tormanis and Koumaria reagións (Fig. 3).

At least 7 of those bangs of about 2.000m length have been mapped in the Koumaria region, 5 in Eripiá Tormanis region and 4 in the Kastania region (Χατζηπαναργής κ. α., 2009).

The white marbles of the upper series are characterized by the equigranular granoblastic texture with 0.2 – 0.5 mm crystal size (Fig. 4) (Πλουμής Π., 2009).

In the lower series, the marbles are characterized by their inequigranular texture and deformation features.

The initial crystals are broken in their periphery to smaller, creating two different crystal sizes (0.5 -0.8 and 0.1-0.3mm respectively) (Fig. 5). Bended and broken calcite lamellas of the initial crystals are often observed.

These marbles are pure calcitic and only in some locations, Fe-oxides/hydroxides impregnations are observed.

3.2 Pitsilota (flaked) marbles

Pitsilota marbles are mainly located in Koumaria and Eripiá Tormanis areas.

It is the case of white to semi white calcitic marbles with grey to black elongated flecks which are aggregates rich in Fe-oxides/hydroxides and relict organic material (Figs. 6, 7), (Πλουμής, 2009).

Usually, these flecks are discintiguous and spread but in some cases flecks of 15 – 20 cm in length and 1 – 2 mm thick are even observed. According to the mineralogical study of these flecks, beyond calcite, elongate aggregates of fine grain dolomite, relict organic material (amorphous – cryp-tokrystalline graphite), pyrite, Fe-oxides/hydroxides, mica, quartz, albite, zircon, rutile and apatite, have been identified.

3.3 Rigota (stripped) marbles

Rigota marbles are mainly located in Kastania and Eripiá Tormanis regions. They are semi white, semi grey to grey calcitic marbles with contiguous white stripes of 0.5 – 3mm in thickness. (Figs. 8, 9). These white stripes consist of fine grained (0.2 – 0.4mm) calcite with 0.6-0.7% MgO . Along the cores of some stripes occur ultra fine grained (0.05 – 0.1mm) dolomite aggregates (Fig. 10), (Πλουμής Π., 2009). In some cases, along these stripes are observed evidences of slight deformation of the crystals.

In addition, in frame of late brittle tectonic, thin (1 – 3mm) shear zones are detected. Along them, the calcite crystals are ultra fine grained (Figs. 11, 12). Along these zones with the ultra fine grained material, some vestigial calcite crystals of the initial size with strongly bended lamellas can be seen (Fig. 13). The macroscopic evidence of the shear zones is also a white stripe cross cutting the older, contiguous white stripes (Fig. 11).

3.4 Loulooudata (flowered) marbles

They are located in the lower marble series, called as the Zoodochos Pigi series in the region of Arapi. The main mass (matrix) is a white to semi white marble with inequigranular granoblastic texture. Spread, separated, grey, big, idiomorphic monocrystals of calcite (Fig. 14) or aggregates of

these crystals form shapes of flower or bunch of flowers spread in the white matrix (Πλουμης, 2009), (Fig. 15). This commercial type of marble is named after this secondary creation “loulouda” (flowerd).

There have been found calcite monocrystals bigger than 5cm (Fig. 16) and even bigger, elongate calcite aggregates. The aggregates consist either from elongate crystals in wavy order (Fig. 17) or from crystals with uneven contacts (sutured texture). All these crystals of the “flowers” are secondary formation of calcite which fill cavities due to the dilution of the carbonates. Previous and late formations of dolomite and calcite have also been detected. (Fig. 17).



Fig. 3: White marble of Arapi area.

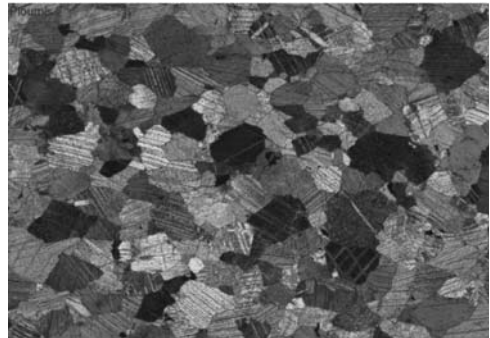


Fig. 4: Equigranular marble of Agathi - Tsekouri series (+Nic., x2.5).

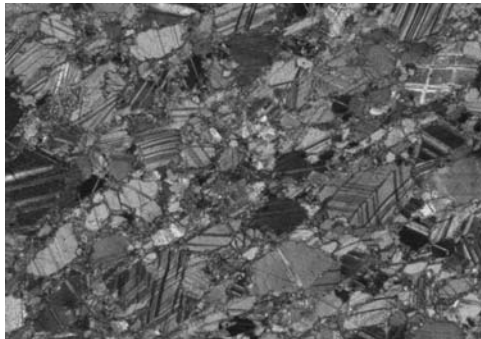


Fig. 5: Inequigranular marble of Zoodochos Pigi series (+Nic., x2.5)

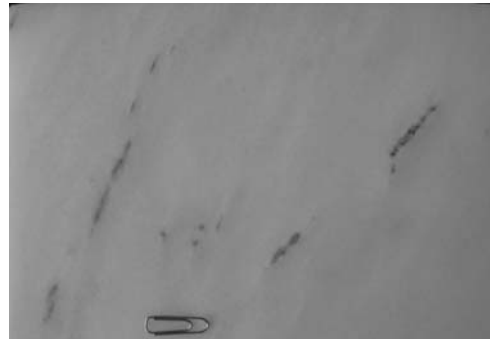


Fig. 6: Pitsilota marble of Koumaria area

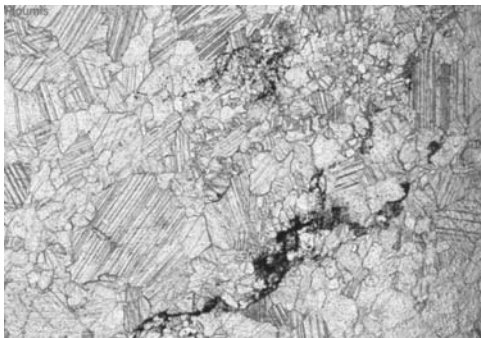


Fig. 7: Pitsila (fleck) in pitsilota marble of Koumaria area (//Nic., x5)

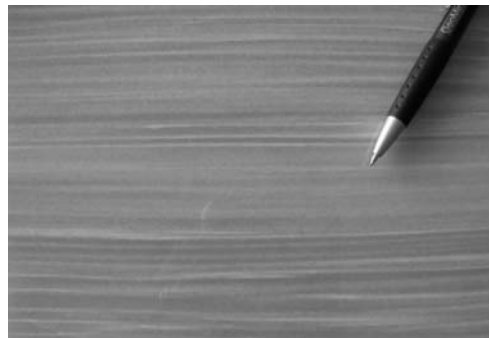


Fig. 8: Rigota marble of Er. Tormanis

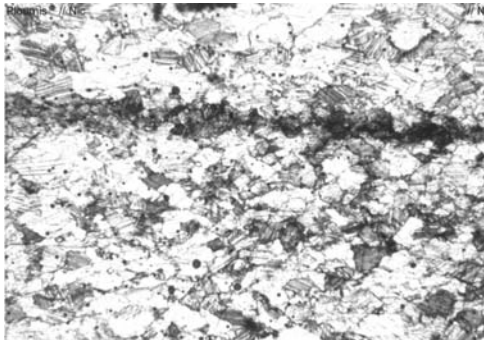


Fig. 9: The white stripe (dark in microscope image) of Koumaria area (//Nic., x1.25).

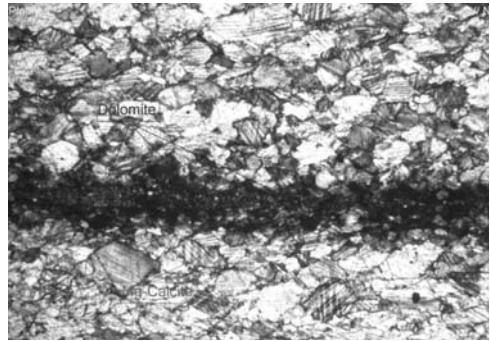


Fig. 10: White stripe with ultra fine dolomite in the core of the stripe (//Nic., x1.25).



Fig. 11: Sheared Rigota marble of Er. Tormanis.

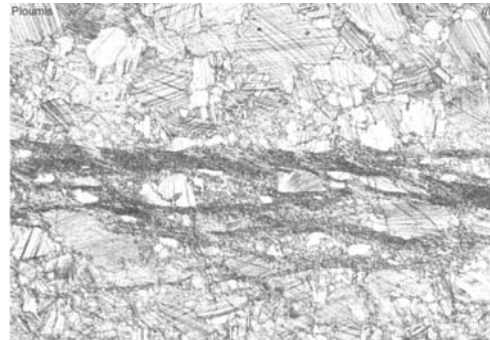


Fig. 12: Microscopic image of white stripe caused of shear (//Nic., x2.5).



Fig 13: Initial size calcite crystals with bended lamellas in shear zone (detail of Fig. 12) (//Nic., x10).

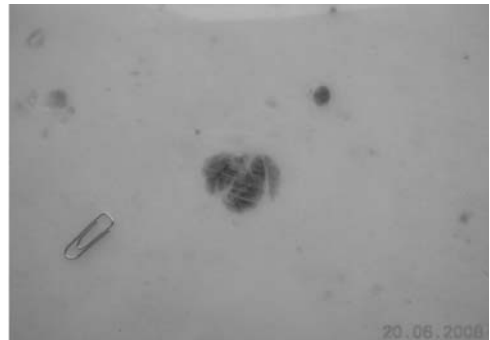


Fig 14: Calite monocrystal in louloudata marble of Arapi area.

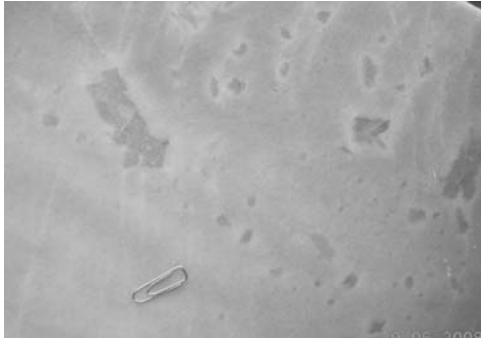


Fig. 15: Louloudata marble of Arapi area.

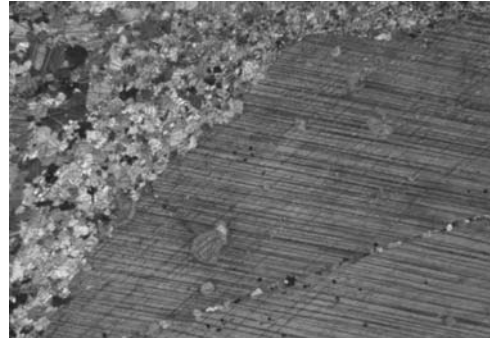


Fig. 16: Calcite monocrystal (+Nic., x1.25).

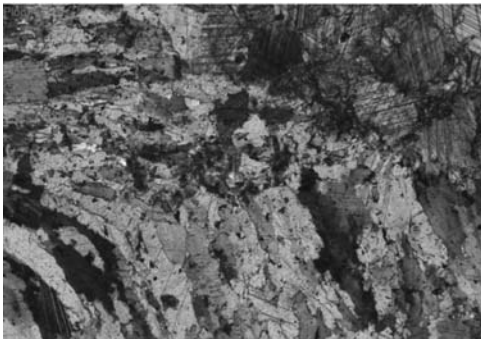


Fig. 17: Elongate calcite crystals in wavy order (+Nic., x2.5).

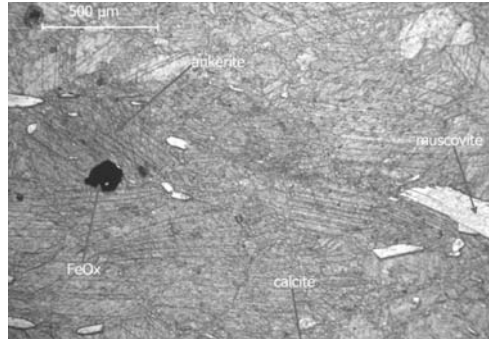


Fig. 18: Ankeritisation of calcite in the pyrite vicinity of Koumaria area cipoline marble.

3. 5. Cipoline marbles

Thin bangs of cipoline marbles occur in the region of Koumaria. Their maximum thickness is 400m. They are semi grey to grey, fine to middle grain equigranular and inequigranular calcitic marbles. Long mica crystals (~ 5%), quartz, albite, pyrite, dolomite (in amounts in some locations), rutile, Fe oxides/hydroxides and ankerite (Fig. 18) are the impurities (Πλουμής, 2009). The high percentage of mica in this marble creates serious problems to the face and shine of the plates.

4. Conclusions -Results

According to geological, mineralogical, petrological, structural - textural, chemical and aesthetic (colour, impurities) criteria, five (5) commercial marble types are being exploited in the south Vermion mountain:

- The pure calcitic (99.5%) white marbles with inequigranular texture in the lower marble series, called as the series of Zoodochos Pigi and inequigranular in the upper series, called as the series of Angathi -TsekouriA. Some impurities of metallic oxides/hydroxides are localized in the bottom and top of the lower marble series and locally in the upper marble series.
- The calcitic, white to semi white pitsilota marbles of Angathi -Tsekouri series with grey to black elongated flecks which are aggregates rich in Fe-oxides/hydroxides and relict organic material.

- The calcitic, semi white, semi grey to grey rigota marbles with contiguous white stripes of 0.5 – 3mm thickness. These white stripes consist of fine grained (0.2 – 0.4mm) calcite with 0.6-0.7% MgO. Wavy cross cutting white stripes of 1 – 3mm thickness are shear zones, creating undulation forms to the striped marble. They occur in the Agathi – Tsekouri series.
- The, calcitic louloudata marbles with white to semi white, inequigranular granoblastic clitic matrix texture with spread, separated, secondary grey, big, idiomorphic, calcite monocrystals or aggregates of these filling cavities after delusion of primary carbonates. This secondary creation forming shapes of flower or bunch of flowers gives the name to this commercial type of marble “louloudata” (flowerd) They occur in the lower marbles series (Zoodochos Pigi series).
- The semi white, semi grey to grey, calcitic cipoline marbles of the Zoodochos Pigi series with impurities of more than 5%.

5. Note

This work is part of ongoing phd of Ploumis Panayiotis.

6. References

- Γαλανάκης Δ. & Πλουμής Π., 2000. Γεωλογική-Κοιτασματολογική Μελέτη των εμπορικών τύπων μαρμάρου στη λατομική περιοχή Ζωοδόχου Πηγής Βερμίου (Δυτική Μακεδονία). Έκθεση Ι.Γ.Μ.Ε., Αθήνα, σ. 28.
- Κίλιας Α. & Μουντράκης Δ., 1989. Το τεκτονικό κάλυμμα της Πελαγονικής. Τεκτονική Μεταμόρφωση και Μαγματισμός. Δελτ. Ελλ. Γεωλ. Εταιρ. XXIII/1, 29-46
- Kilias A. & Mountrakis D. 1987. Zum tektonischen Bau der Zentral Pelagonischen Zone (Kamvounia Gebirge, N. Griechenland). Z. dt. Geol. Ges., 138, 211-237.
- Mercier J., 1968. Étude géologique des zones internes des Hellénides en Macédoine central (Grèce). Contribution á l' étude du metamorphisme et de l' evolution magmatique des zones internes des Hellénides. Thésés, Paris, 1966, *Ann. Geol. Pays Hellen.*, 20, 1-792.
- Μουντράκης Δ., 1983. Η γεωλογική δομή της βόρειας Πελαγονικής ζώνης και η γεωτεκτονική εξέλιξη των εσωτερικών Ελληνίδων. Προγραμματική για υφηγεσία Αριστοτελείου Πανεπιστημίου Θεσσαλονίκης, σ. 289.
- Πλουμής Π., 2009. Πετρογραφία – πετρολογικά στοιχεία του Νοτίου Βερμίου όρους. Γ'Κ.Π.Σ. Επιχειρησιακό πρόγραμμα «Ανταγωνιστικότητα» Μέτρο 7. 3., Δράση 7. 3. 1. Έκθεση Ι.Γ.Μ.Ε., Θεσσαλονίκη, σ.3-39.
- Spyropoulos N., Kilias A., Mountrakis D., 1988. Contribution to the study of the Structural Geology of the Pelagonian Zone in the Askion Mountains, W. Macedonia. Bull. Geol. Soc. Greece, Athens, xx, 121-138.
- Χατζηπαναγής Ι., Σταϊκόπουλος Γ. και Χρυσστομίδης Π., 2009. Η λατομική δραστηριότητα του ΝΑ Βερμίου όρους. Γ'Κ.Π.Σ. Επιχειρησιακό πρόγραμμα «Ανταγωνιστικότητα» Μέτρο 7. 3., Δράση 7. 3. 1. Έκθεση Ι.Γ.Μ.Ε., Θεσσαλονίκη, σ. 67
- Χατζηπαναγής Ι. 2009 (a). Γεωλογία, λιθοστρωματογραφία, τεκτονική και κοιτασματολογία του Νοτίου Βερμίου όρους. Γ'Κ.Π.Σ. Επιχειρησιακό πρόγραμμα «Ανταγωνιστικότητα» Μέτρο 7. 3., Δράση 7. 3. 1. Έκθεση Ι.Γ.Μ.Ε., Θεσσαλονίκη, σ. 61
- Χατζηπαναγής Ι. 2009 (b). Διαχειριστική μελέτη μαρμάρων και λοιπών διακοσμητικών πετρωμάτων. Συμπεράσματα – προτάσεις. Γ'Κ.Π.Σ. Επιχειρησιακό πρόγραμμα «Ανταγωνιστικότητα» Μέτρο 7. 3., Δράση 7. 3. 1. Έκθεση Ι.Γ.Μ.Ε., Θεσσαλονίκη, σ. 16.

QUANTITATIVE ANALYSIS OF ASBESTOS FIBRES IN OPHIOLITIC ROCKS USED AS AGGREGATES AND HAZARD RISK ASSESSMENT FOR HUMAN HEALTH

**Rigopoulos I.¹, Tsikouras B.¹, Pomonis P.², Karipi S.¹,
and Hatzipanagiotou K.¹**

¹ University of Patras, Department of Geology, Section of Earth Materials, 26500 Patras - Greece, rigopoul@upatras.gr, v.tsikouras@upatras.gr, skaripi@upatras.gr, k.hatzipanagiotou@upatras.gr

² University of Athens, Department of Geology and Geoenvironment, 15784 Athens, Greece, ppomonis@uoa.geol.gr

Abstract

This study focuses on the quantification of asbestiform minerals in basic and ultrabasic rocks from ophiolite suites of central and northern Greece. A combination of different methods were used for the detailed investigation of the samples, conducted in the following stages: (i) petrographic examination of thin sections with a polarizing microscope, (ii) mineral phase analysis using X-ray diffraction, (iii) determination of the fibrous mineral composition on polished thin sections using scanning electron microscopy, (iv) image analysis of back-scattered electron images and secondary electron images, to quantify the dangerous asbestiform crystals. SEM is proved to be the most powerful tool for the detailed investigation of fibrous minerals, although polarized microscopy and XRD are necessary tools for a preliminary identification of these minerals.

Basic rocks contain various amounts of actinolite, however not all crystals comprise asbestiform fibres. A conspicuous feature observed during careful petrographic analysis is that many of the non-asbestiform actinolite crystals are broken up along their cleavage planes. Rocks with such features need specific consideration since these crystals may subsequently release numerous fibrous cleavage fragments during the production processes and in-service deterioration of aggregates. Among the serpentinized ultrabasic samples, only one contains chrysotile, while the other samples contain antigorite and lizardite.

Key words: *asbestos, image analysis, ophiolitic rocks, petrography, scanning electron microscopy, X-ray diffraction.*

1. Introduction

The term asbestos (from the Greek “asbestos”= inextinguishable) is a general commercial-industrial term used to describe a group of naturally occurring silicate minerals of fibrous or asbestiform habit. These minerals can be divided into two basic groups: (i) the serpentines, which include only the asbestiform chrysotile and (ii) the amphiboles, which include the asbestiform varieties of actinolite, tremolite, anthophyllite, crocidolite (riebeckite) and amosite (cummingtonite-grunerite). They have been used since ancient times as raw materials for the production of a large variety of materials and objects due to their exceptional attributes (high tensile strength, flexibility, chemical and heat re-

sistance). The inherent properties of asbestos fibres appear to contribute to the toxicity of these mineral particles when lodged inside the human respiratory system (Stanton et al., 1981; Wylie et al., 1993). Occupational exposures to asbestos have been linked to asbestosis, lung cancer, malignant mesothelioma and various cancers of digestive tract (Mossman et al., 1990; Nolan et al., 2001; Constantinopoulos, 2008; Murray and Nelson, 2008).

Ophiolitic rocks may contain various amounts of asbestos minerals (e.g. Skarpelis and Dabitzias, 1987; Ross and Nolan, 2003; Rigopoulos et al., 2008). Chrysotile is usually the most common of these minerals in ophiolitic rocks, since it is possible to be found in any type of serpentinized ultrabasic rock, either as alteration product of olivine and/or orthopyroxene or as veins crosscutting the rock. Basic ophiolitic rocks may also contain considerable percentages of amphibole asbestos fibres, principally actinolite and/or tremolite, which represent alteration products of clinopyroxene (e.g. Tsikouras et al., 2005; Rigopoulos et al., 2006).

Asbestos fibres are thin, needle-like crystals that may vary widely in diameter within the millimetre to micron range. The biologically more important so-called “critical” fibres are those with the following shape criteria: length $\geq 5 \mu\text{m}$, diameter (width) $\leq 3 \mu\text{m}$ and length to diameter ratio (aspect ratio, AR) $\geq 3:1$ (World Health Organization, 1986). Asbestos crystals in ophiolitic rocks used as aggregates for road construction, railway ballast, concrete and other applications, are particularly dangerous for public health, since fibres of the above mentioned sizes may be released into the air during in-service deterioration of aggregates, becoming dangerous for public health. In this study, the proportions of asbestiform minerals were determined in basic and ultrabasic rock samples collected from ophiolite suites of central and northern Greece, using a combination of different techniques.

2. Geological setting

Sampling was performed to the Guevgueli, Pindos, Vourinos and Koziakas ophiolites, which are among the most well-known ophiolitic complexes of Greece (Fig. 1).

The Guevgueli ophiolite (Mercier, 1966; Bebien, 1982; Ivanov et al., 1987), occupies the northern part of the “Innermost Hellenic Ophiolite Belt” (IMHOB) in Greece. It comprises a parautochthonous, Jurassic complex, comprising gabbroic cumulates, diorites associated with plagiogranites, a hypabyssal sheeted dyke complex and mafic lavas. Sampling was performed to the eastern part of the ophiolite, in a sheeted dyke complex, which includes dolerites and minor gabbros.

The Pindos and Vourinos Jurassic ophiolites belong to the western Greek ophiolitic belt and are thought to be continuous beneath the Cenozoic molasse of the Mesohellenic trough (Jones et al., 1991; Rassios and Smith, 2000). Sampling was performed to the eastern part of the Pindos ophiolite, in a well preserved sheeted dyke complex. This area has been further divided into three subunits, which comprise the following lithologies (Rigopoulos et al., 2010): (i) dolerite and minor gabbro, (ii) dolerite, (iii) pillow lavas and minor dolerite. In the Vourinos complex sampling was focused on a dolerite exposure, located to the western part of the ophiolitic occurrences. Two types of dolerites have been distinguished according to their macroscopic characteristics (Rigopoulos et al., 2010): the first group displays significant amounts of chlorite (dark green-coloured), while the second is characterized by the presence of actinolite in high percentages (pale green-coloured). Serpentinized ultrabasic samples were also collected from the mantle section of the Pindos and Vourinos ophiolites.

The Koziakas Jurassic ophiolite belongs to the western Greek ophiolitic belt and it was probably developed, together with the Pindos, Vourinos and Othris ophiolite suites, in the same marginal basin volcanic arc regime in the Pindos ocean (Pomonis et al., 2005; Pomonis et al., 2007). Sampling was

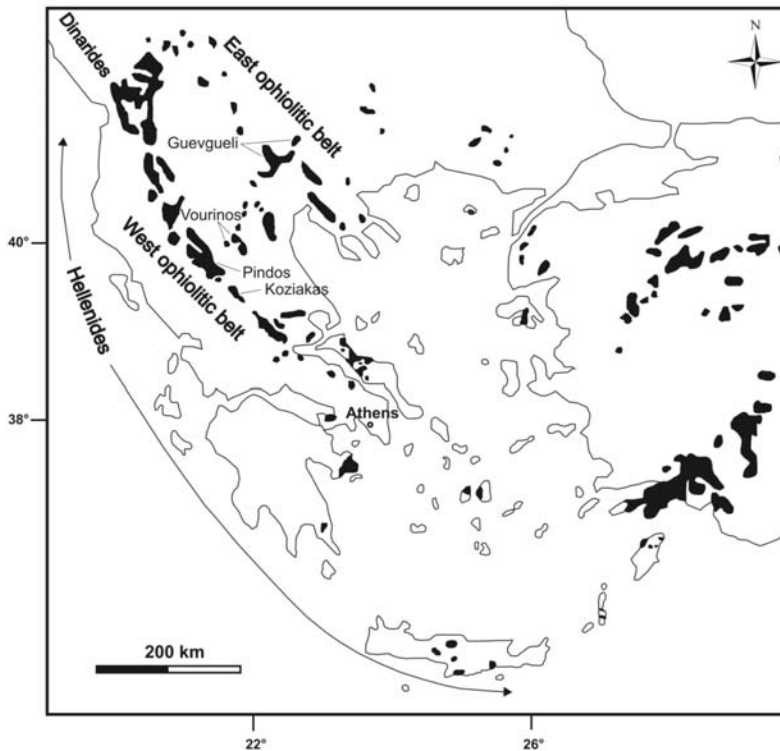


Fig. 1: Simplified map showing the studied areas and the distribution of the ophiolitic outcrops of Greece and neighbouring countries.

performed to the northern part of the ophiolite, which comprises mantle peridotites with various degrees of serpentinization. These are predominantly harzburgites and secondarily plagioclase-bearing lherzolites.

3. Methods and results

3.1 Petrography

A preliminary qualitative analysis of thin sections with a polarized microscope was first accomplished in order to determine the general mineralogical and textural characteristics of the studied rock types. Quantitative measure of the concentration of the constituent minerals was then carried out using a point-counting system.

3.1.1 Basic lithotypes

Dolerites from the Guevgueli, Pindos and Vourinos ophiolites are fine-grained isotropic rocks with subophitic texture (Fig. 2a). Laths of subhedral plagioclase and interstitial anhedral clinopyroxene of augite composition comprise the subophitic groundmass. They are in general equigranular rocks but locally become porphyritic, with subhedral to euhedral plagioclase and clinopyroxene phenocrysts set in a fine-grained matrix with subophitic texture (Fig. 2b). Opaque minerals include various percentages of magnetite, pyrite and chalcopyrite. Titanite is also present in small amounts. Secondary products are actinolite, chlorite, quartz, epidote and clinozoisite. Actinolite and chlorite

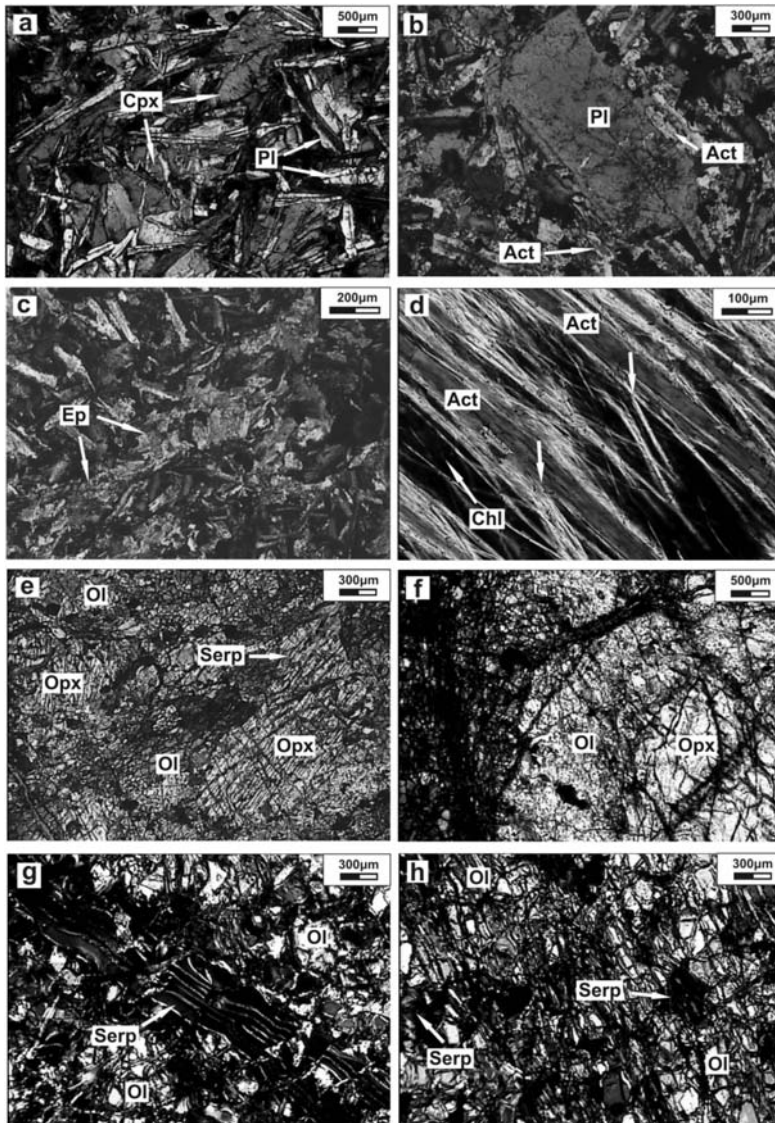


Fig. 2: Photomicrographs (XPL) of the studied basic rocks: a) dolerite with typical subophitic texture (sample PVN2a), b) plagioclase phenocryst in a fine-grained matrix with subophitic texture (sample G1), c) vein filled with epidote (sample B4), d) actinolite crystals broken up along their cleavage planes (arrows indicate characteristic fractures - sample PVN1b). Photomicrographs (XPL) of the studied ultrabasic rocks: e,f) cataclastic and porphyroclastic texture in serpentized harzburgites (samples VVDSR1 and KOZ2, respectively), g) ribbon texture and h) preferred orientation of olivine grains in serpentized harzburgites (sample PKZSR1), (Pl: plagioclase, Cpx: clinopyroxene, Act: actinolite, Chl: chlorite, Ol: olivine, Opx: orthopyroxene, Serp: serpentine).

represent alteration products of clinopyroxene. Actinolite is found either as short prismatic or as fibrous, asbestiform crystals. Epidote and clinozoisite are detected as fine-grained alteration products in saussuritized plagioclase and quartz crystals usually occupy spaces between the other grains, however these minerals also fill veins crosscutting the rock (Fig. 2c). Additionally, calcite commonly fills veins in the Guevgueli and Vourinos dolerites. Another feature observed during the pet-

Table 1. Mineralogical composition (in vol%) of the studied basic rocks (Pl: plagioclase, Cpx: clinopyroxene, Act: actinolite, Chl: chlorite, Qz: quartz, Ep: epidote, Cc: calcite, Op: opaque minerals).

<i>Sample code/locality</i>	<i>Pl</i>	<i>Cpx</i>	<i>Act</i>	<i>Chl</i>	<i>Qz</i>	<i>Ep</i>	<i>Cc</i>	<i>Op</i>
*G1/Guevgueli	44.3	15.6	11.9	12.4	1.9	7.1	1.4	5.4
~G2/Guevgueli	48.6	32.7	10.8	3.6	0.4	1.9	1.2	0.8
*PVN1a/Pindos	47.7	13.7	23.3	4.3	7.7	1.3	-	2.0
*PVN1b/Pindos	49.3	15.3	21.0	3.0	7.0	1.7	-	2.7
*PVN2a/Pindos	50.7	38.0	0.3	7.3	1.0	0.7	-	2.0
*PVN2b/Pindos	46.7	36.0	2.0	10.3	0.7	2.0	-	2.3
*B4/Vourinos	48.8	2.3	5.6	17.0	11.3	7.1	3.3	4.6
*B5/Vourinos	51.8	3.7	26.1	1.8	3.5	7.6	2.1	3.4

(*: dolerite, ~: gabbro)

Table 2. Mineralogical composition (in vol%) of the studied ultrabasic rocks (Ol: olivine, Opx: orthopyroxene, Cpx: clinopyroxene, Pl: plagioclase, Sp: spinel, Serp: serpentine, Ox: oxides, Tc: talc, Chl: chlorite, Tr/Act: tremolite/actinolite, Cc: calcite).

<i>Sample code/locality</i>	<i>Ol</i>	<i>Opx</i>	<i>Cpx</i>	<i>Pl</i>	<i>Sp</i>	<i>Serp</i>	<i>Ox</i>	<i>Tc</i>	<i>Chl</i>	<i>Tr/Act</i>	<i>Cc</i>
*PKZSR1/Pindos	35.5	4.5	0.5	-	0.5	47.5	8.5	0.5	1.5	0.5	0.5
*VVDSR1/Vourinos	39.0	12.5	-	-	1.0	38.0	9.0	-	-	-	0.5
~KOZ1/Koziakas	41.5	10.5	4.0	1.0	1.0	28.5	3.0	1.5	1.5	7.5	-
*KOZ2/Koziakas	47.0	16.0	-	-	1.0	30.5	2.5	2.0	1.0	-	-

(*harzburgite, ~: plagioclase-bearing lherzolite)

Table 3. Mineral phases detected in the investigated rock samples using X-ray diffraction (Chl: chlorite, Act: actinolite, Pl: plagioclase, Aug: augite, Qz: quartz, Ep: epidote, Cc: calcite, Mt: magnetite, Tit: titanite, Lz: lizardite, Ant: antigorite, Chry: chrysotile, Fo: forsterite, En: enstatite, Di: diopside, Sp: spinel).

<i>Sample code/locality</i>	<i>Mineralogical composition</i>
G1/Guevgueli	Chl, Act, Pl, Aug, Qz, Ep, Mt
G2/Guevgueli	Chl, Act, Pl, Aug, Qz, Ep, Cc, Tit
PVN1a/Pindos	Chl, Act, Pl, Aug, Qz, Ep, Mt
PVN1b/Pindos	Chl, Act, Pl, Aug, Qz, Ep, Mt
PVN2a/Pindos	Chl, Pl, Aug, Qz, Ep, Mt
PVN2b/Pindos	Chl, Act, Pl, Aug, Qz, Ep, Mt
B4/Vourinos	Chl, Act, Pl, Aug, Qz, Ep, Cc, Mt
B5/Vourinos	Chl, Act, Pl, Qz, Ep, Cc, Mt
PKZSR1/Pindos	Lz, Ant, Fo, En, Sp, Mt
VVDSR1/Vourinos	Lz, Ant, Fo, En, Mt
KOZ1/Koziakas	Lz, Ant, Chry, Fo, En, Act, Di, Sp
KOZ2/Koziakas	Lz, Ant, Fo, En, Sp

rographic analysis, is that many of the actinolite crystals are broken up along their cleavage planes (Fig. 2d). The percentages of the mineral phases are shown in Table 1.

Regarding the gabbroic rocks collected from the Guevgueli ophiolite suite, they have subhedral to anhedral granular to ophitic texture, most commonly medium- to coarse-grained. Their primary and secondary mineral phases are the same as those of the studied dolerites (Table 1).

3.1.2 Ultrabasic lithotypes

The studied ultrabasic rocks from the Pindos, Vourinos and Koziakas ophiolites include harzburgites with various degrees of serpentinization and deformation. A sample of plagioclase-bearing lherzolite was also collected from the Koziakas mantle section. These rock types mainly display cataclastic and locally porphyroclastic texture (Figs 2e,f). The primary mineralogy of the harzburgites comprises olivine, orthopyroxene (enstatite) with exsolution lamellae of clinopyroxene (diopside) and disseminated spinel (Table 2). The plagioclase-bearing lherzolites also contain clinopyroxene (diopside) and interstitial plagioclase (bytownite-anorthite). Olivine and orthopyroxene occur both as porphyroclasts and neoblasts. Due to hydrothermal alteration, the primary minerals are transformed into secondary products (olivine into hydrated associations of serpentine minerals, orthopyroxene mainly into bastite and talc, clinopyroxene into actinolite, tremolite and chlorite, and spinel into ferrian chromite and magnetite). Some of the samples are crosscut by veins of calcite. The areas occupied by serpentine usually display pseudomorphic mesh and ribbon textures (Fig. 2g) (O'Hanley, 1996). Evidence of plastic deformation is shown in strained olivine and orthopyroxene porphyroclasts, which display well-developed undulatory extinction and kink-bands. Intense deformation results locally in a preferred orientation of the olivine grains (Fig. 2h).

3.2 X-Ray Diffraction

X-ray diffraction (XRD) is a widely used analytical technique for identifying minerals and characterizing their crystal structure. It is generally a semi-quantitative method, although it is possible to estimate the amounts of minerals present in a rock using complicated special procedures (Snyder and Bish, 1989; Addison and Davies, 1990; Williams-Jones et al., 2001).

In the present study, XRD was performed on powdered samples in order to determine asbestos minerals. The weight percent of every mineral in a sample must typically be present in at least 2-3% to be detected. Asbestos minerals (actinolite and serpentine in basic and ultrabasic samples respectively) were detected in almost all samples (except for the dolerite PVN2a). Regarding the ultrabasic lithotypes, chrysotile was detected only in the plagioclase-bearing lherzolite (see Table 3).

3.3 Scanning Electron Microscopy

Scanning Electron Microscope (SEM) is of particular value in identifying asbestiform minerals, since it allows much greater magnifications than polarized microscope and also allows semi-quantitative or quantitative chemical analysis of the imaged material. Hence, it is feasible to analyse and record the length and diameter of individual fibres in any rock type. Elemental analysis of individual separated fibres is ordinarily semi-quantitative but is often sufficient for mineral identification.

Standard analytical methods for quantitative analysis of asbestos have been difficult to develop, primarily due to the difficulty in standardizing the many operating parameters that are controlled in SEM (Clinkenbeard et al., 2002). However, in this study the following procedure is proposed for the quantification of asbestiform crystals:

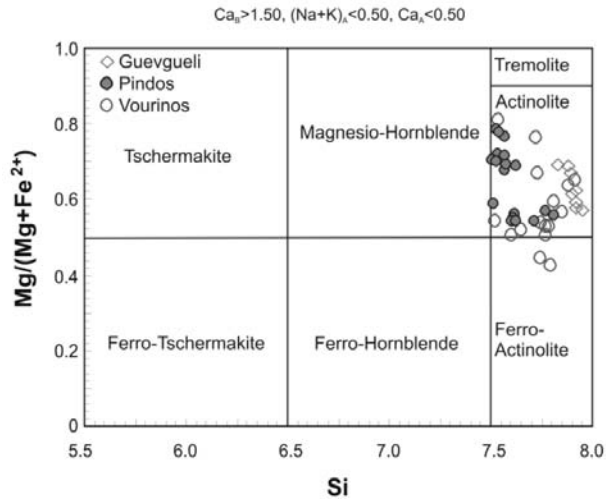


Fig. 3: Plot of the analyzed amphibole crystals from the studied basic rocks on their classification diagram (after Leake et al., 1997).

- Elemental analysis of the constituent minerals – identification of the asbestiform mineral phases.
- Imaging of the studied polished thin sections at several magnifications, depending on the grain size of each lithotype (the images are equally distributed on each thin section). In this study, two polished thin sections were investigated for each sample and six back-scattered electron (BSEI) or secondary electron (SEI) images were acquired from each one.
- Measurement of the dimensions (length and diameter) of the fibrous and non-fibrous crystals which belong to the group of asbestos minerals. The images were analysed using the Leica QWin image analysis software.
- The measurements are statistically analyzed. This process includes: (i) discrimination of the dangerous asbestiform crystals, which fulfil the shape criteria referred to the introduction, (ii) calculation of the area occupied by the dangerous asbestiform crystals, (iii) calculation of the total percentage (vol%) of the dangerous asbestiform crystals.
- Representative compositions of amphibole and serpentine from the investigated basic and ultrabasic samples are listed in Table 4. According to the classification of Leake et al. (1997), the analyzed amphiboles from the Pindos, Vourinos and Guevgueli basic igneous rocks are actinolite (Fig. 3). In the ultrabasic samples, chrysotile is not feasible to be detected by elemental analysis due to its similar chemical composition with the other polymorphs of serpentine (antigorite and lizardite).

The back-scattered electron images (BSEI) acquired for the basic igneous rocks indicated that actinolite participates in various percentages. Among the collected rocks, samples B5, PVN1a, PVN1b, G1 and G2 contain the highest percentages of actinolite, which is detected in various sizes. One generation of larger crystals comprises non-asbestiform, short prismatic crystals and represents the main percentage of actinolite (Fig. 4a-c). Locally, a second generation of asbestiform crystals is present (Fig. 4b-d). It is also mentioned that specific areas of the polished thin sections are totally

Table 4. Representative microanalyses of (a) amphiboles and (b) serpentines from the studied basic and ultrabasic samples (-: below detection limit).

a.	Sample	G1	G2	PVN1a	PVN1b	PVN2a	PVN2b	B4	B5
	Analysis	1	12	17	11	26	30	19	32
	SiO ₂	55.90	55.70	52.45	52.03	52.97	52.79	54.02	55.79
	TiO ₂	-	-	-	-	-	-	-	0.04
	Al ₂ O ₃	3.47	3.45	5.43	2.81	2.35	1.78	2.79	3.51
	FeO ⁱ	14.25	15.90	16.46	25.03	10.56	14.89	15.75	15.80
	MnO	-	-	-	0.65	-	0.72	0.67	-
	MgO	13.54	11.87	11.23	8.81	13.13	10.61	12.12	12.30
	CaO	11.11	11.84	11.79	8.96	19.80	16.45	10.43	9.68
	Na ₂ O	-	-	0.73	-	-	-	-	0.52
	K ₂ O	-	-	-	-	-	-	0.43	-
	Cr ₂ O ₃	-	-	-	-	-	-	-	0.25
	Total	98.27	98.76	98.09	98.29	98.81	97.24	96.21	97.89
Structural formulae on the basis of 23 O and cat. sum-Ca-Na-K=13									
	Si	7.890	7.950	7.618	7.519	7.628	7.822	7.880	7.909
	Al ^{IV}	0.110	0.050	0.382	0.479	0.372	0.178	0.120	0.091
	Fe ³⁺	-	-	-	0.002	-	-	-	-
	Ti	-	-	-	-	-	-	-	-
		8.000	8.000	8.000	8.000	8.000	8.000	8.000	8.000
	Al ^{VI}	0.470	0.530	0.548	-	0.027	0.133	0.360	0.495
	Ti	-	-	-	-	-	-	-	0.004
	Fe ³⁺	0.280	-	-	1.706	-	-	0.419	0.479
	Cr	-	-	-	-	-	-	-	0.027
	Mg	2.850	2.530	2.432	1.898	2.819	2.344	2.636	2.600
	Fe ²⁺	1.400	1.900	1.999	1.316	1.272	1.845	1.502	1.395
	Mn	-	-	-	0.080	-	0.090	0.083	-
		5.000	4.950	4.979	5.000	4.117	4.411	5.000	5.000
	Mg	-	-	-	-	-	-	-	-
	Fe ²⁺	-	-	-	-	-	-	-	-
	Mn	-	-	-	-	-	-	-	-
	Ca	1.680	1.810	1.835	1.387	2.000	2.000	1.630	1.470
	Na	-	-	0.165	-	-	-	-	0.143
		1.680	1.810	2.000	1.387	2.000	2.000	1.630	1.613
	Ca	-	-	-	-	1.055	0.611	-	-
	Na	-	-	0.040	-	-	-	-	-
	K	-	-	-	-	-	-	0.038	-
		-	-	0.040	-	1.055	0.611	0.038	-

Table 4 continued.

b.	Sample	PKZSR1	VVDSR1	KOZ1	KOZ2
	Analysis	15	10	14	1
	SiO ₂	39.55	40.63	38.26	41.41
	TiO ₂	-	-	0.05	-
	Al ₂ O ₃	1.45	-	3.58	1.06
	Fe ₂ O ₃ ³⁺	6.23	2.05	6.61	4.28
	MnO	0.11	0.04	-	0.06
	MgO	39.22	38.45	34.77	38.01
	CaO	-	0.08	0.03	-
	NiO	-	-	-	0.3
	Cr ₂ O ₃	0.17	-	-	0.14
	Total	86.73	81.25	83.30	85.26
Structural formulae on the basis of 28 O					
	Si	7.510	8.068	7.531	7.907
	Ti	-	-	0.008	-
	Al	0.324	-	0.830	0.239
	Fe ³⁺	0.890	0.306	0.979	0.615
	Fe ²⁺	-	-	-	-
	Mn	0.018	0.007	-	0.010
	Mg	11.102	11.382	10.203	10.819
	Ca	-	0.017	0.007	-
	Ni	-	-	-	0.046
	Cr	0.026	-	-	0.021

Table 5. Content of asbestiform actinolite crystals in the studied basic ophiolitic rocks (in vol%).

<i>Sample code/locality</i>	<i>Asbestiform actinolite (vol%)</i>	<i>Sample code/locality</i>	<i>Asbestiform actinolite (vol%)</i>
G1/Guevgueli	0.10	G1/Guevgueli	0.04
G2/Guevgueli	0.05	G2/Guevgueli	0.07
PVN1a/Pindos	1.58	PVN1a/Pindos	0.12
PVN1b/Pindos	1.44	PVN1b/Pindos	0.97

consist of dangerous, asbestiform crystals (Figs 4e f). The percentages of the latter were calculated according to the procedure described above (Table 5).

All peridotite samples of this study contain significant amounts of serpentine, however only the plagioclase-bearing lherzolite contains fibrous chrysotile. These crystals become identifiable only in

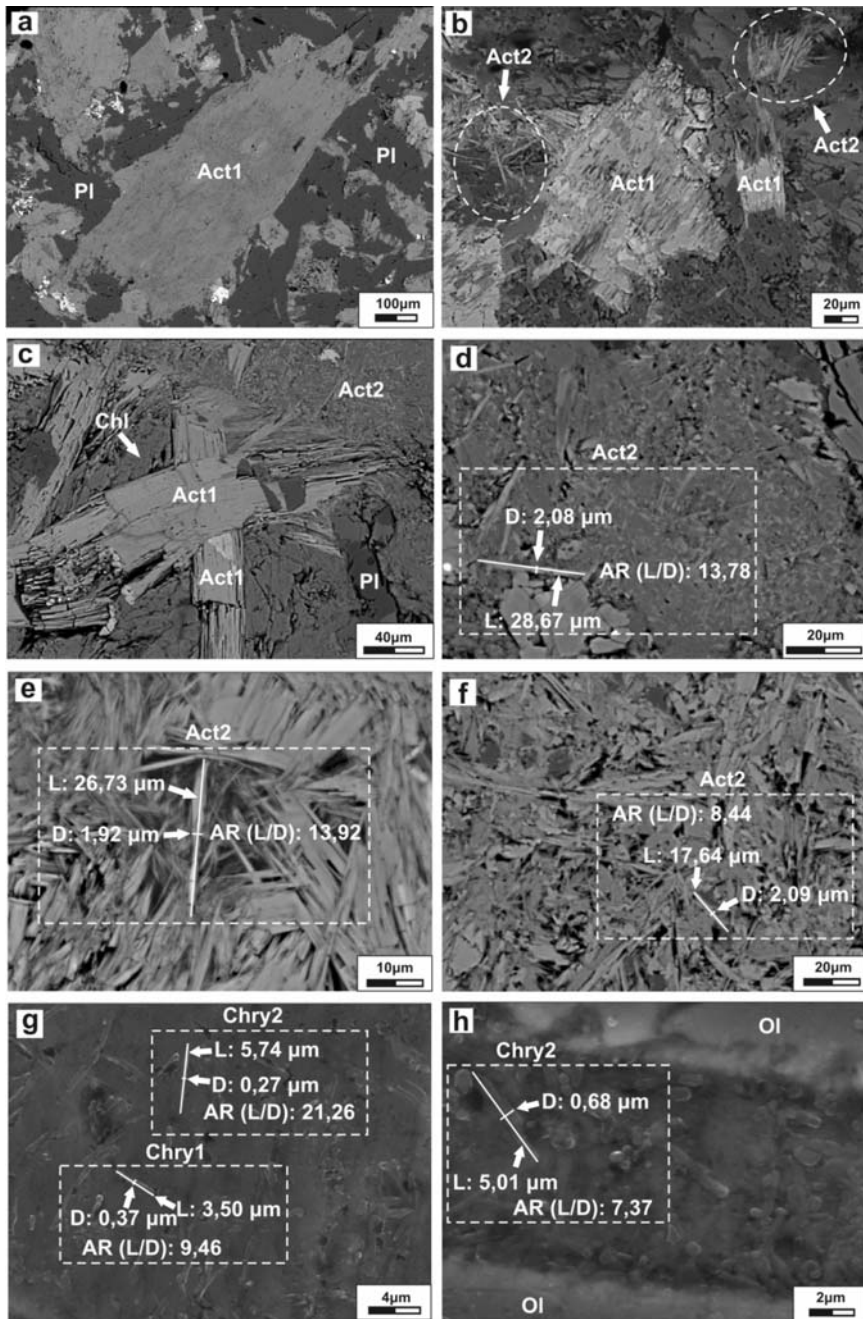


Fig. 4: Back-scattered electron images showing: a) short prismatic crystals of actinolite (sample B5), b,c) asbestiform and non-asbestiform actinolite crystals (samples PVN1a and G1, respectively), d) an area with significant percentage of asbestiform actinolite (sample B5) and e,f) areas totally consisting of dangerous, asbestiform crystals (samples PVN1b and B5, respectively), (Act1: non-asbestiform and Act2: asbestiform actinolite crystals). Secondary electron images showing: g) a whole area and h) a vein occupied by asbestiform chrysotile (sample KOZ1), (Chry1: non-asbestiform and Chry2: asbestiform chrysotile crystals).

secondary electron images (SEI) and they are detected either in areas occupied totally by serpentine (Fig. 4g) or in veins crosscutting the rock (Fig. 4h). The calculated percentage of the dangerous asbestiform crystals of chrysotile in sample KOZ1 is 0.69 vol%.

4. Discussion

Various methods have been proposed for the quantification of asbestos minerals (e.g. Plater et al., 1992; Schneider et al., 1998). In this study, a combination of different methods is proposed for the detailed investigation of basic and ultrabasic ophiolitic rocks used as aggregates.

Polarized light microscopy (PLM) is the most familiar analytical technique to geologists, however it considerably limits the lower limit of visibility of asbestos fibres. This method offers the ability to generally differentiate the non-asbestiform and asbestiform habits of a mineral (Clinkenbeard et al., 2002). Using PLM, two types of actinolite crystals were detected in basic rocks according to their crystal habit: asbestiform and non-asbestiform; however the percentage of the measured dangerous fibres may be underestimated, due to the existence of extremely fine, undetectable crystals. A conspicuous feature observed during careful petrographic analysis is that many of the non-asbestiform actinolite crystals are broken up along their cleavage planes. Rocks with such features need specific consideration, since these crystals may subsequently release numerous fibrous fragments during the production processes and in-service deterioration of aggregates (Rigopoulos et al., 2008). These cleavage fragments may have a similar microscopic appearance to that of true asbestos fibres. On the other hand, the potential existence of chrysotile in the ultrabasic samples was not possible to be designated. This is in consistence with Schneider et al. (1998), who noted that PLM is unreliable for materials containing chrysotile. In this study, a quantitative measure of the total percentage of actinolite and serpentine in each sample was carried out using the point-counting procedure. This technique provides relatively accurate and precise estimates of the asbestos concentration (Perkins, 1990). However, it should be mentioned that although the total percentage of actinolite is a major determinant for the potential danger of basic ophiolitic rocks used as aggregates, the total amount of serpentine in ultrabasic rocks is not considered to be of great importance. In the latter case, XRD and SEM analyses are required in order to investigate the potential existence of asbestiform chrysotile.

XRD can be used to determine the mineral phases that are present in a sample; however it provides no information about their crystal habit (Clinkenbeard et al., 2002). The dimensions of the fibres of asbestos minerals is the main factor of health hazard, hence XRD patterns are not diagnostic for the quantification of fibrous crystals. However, this method is useful for the determination of the asbestos mineral type. In the present study, the XRD method indicated the presence of actinolite in basic rocks. Among the ultrabasic samples, only the plagioclase-bearing lherzolite contains chrysotile, while the other samples contain antigorite and lizardite.

SEM allows imaging and identification of much smaller fibres than PLM and it can be used to evaluate both the morphological and chemical composition of asbestiform minerals. Unlike PLM, the ability of the SEM to utilize reflected energy for imaging, allows fibres adhering to other mineral surfaces to be easily observed. The asbestiform crystals are clearly identifiable since high magnifications can be obtained. However, there is much difficulty in obtaining adequate images of unit fibrils (Clinkenbeard et al., 2002). In this paper, a simplified procedure is proposed for the quantification of asbestiform crystals. BSEI or SEI images, depending on the mineral type, were acquired and analyzed using an image analysing system. The fibres of chrysotile in the ultrabasic samples are identifiable only in SEI images. Statistical analyses of measurements of length, diameter and aspect ratio of asbestos minerals led to the calculation of the amount of crystals with asbestiform habit occur-

ring in the investigated ophiolitic rocks. As already mentioned, the investigated basic lithotypes contain various amounts of actinolite, while among the ultrabasic samples only the plagioclase-bearing lherzolite contains chrysotile. Nevertheless, none of these samples contains asbestiform crystals over 1.6 vol%. In terms of chrysotile, it is mentioned that its chemical composition is similar with that of antigorite and lizardite, thus it is obvious that chemical analysis by SEM may not be sufficient for distinguishing the different polymorphs of serpentine. This discrimination is possible to be made by determining the crystal structure. Although SEM analysis does not allow determination of crystal structure, this information has been acquired using XRD.

5. Conclusions

Due to the possible adverse health effects of asbestos containing rocks used for construction purposes, standardized procedures are required for determining low levels of asbestos in raw materials. The method proposed in this paper is a combination of different techniques and is based on the investigation of various samples of basic and ultrabasic rocks from the Guevgueli, Pindos, Vourinos and Koziakas ophiolites.

The low cost and widely available PLM analysis is very useful for a preliminary identification of asbestos minerals. The quantitative analysis of the mineralogical composition indicated that the basic lithotypes contain various amounts of asbestiform and non-asbestiform actinolite crystals. A noticeable feature observed during the petrographic analysis is that many of the non-asbestiform actinolite crystals are broken up along their cleavage planes. This feature indicates that short prismatic actinolite crystals may subsequently release numerous fibrous fragments during the production processes and in-service deterioration of aggregates. In the ultrabasic samples, which contain various amounts of serpentine, the potential existence of chrysotile was not possible to be designated. Using XRD, it was found that only the plagioclase-bearing lherzolite contains chrysotile. This method also verified the presence of actinolite in basic rocks.

A simplified method was proposed for the quantification of asbestiform crystals using SEM. During this procedure, BSEI or SEI images were acquired and analyzed using an image analysing system. The fibres of chrysotile in the ultrabasic samples are identifiable only in SEI images. Statistical analyses of measurements of length, diameter and aspect ratio of asbestos minerals led to the calculation of the amount of crystals with asbestiform habit occurring in the investigated ophiolitic rocks. The studied basic lithotypes contain variable proportions of actinolite, while among the ultrabasic samples only the plagioclase-bearing lherzolite contains chrysotile. However, none of the collected rocks contains asbestiform crystals over 1.6 vol%.

Considering the advantages and disadvantages of all the methods used in this study, it becomes clear that the image analysis of SEM images is the most powerful tool for quantifying asbestos, although polarized microscopy and XRD are necessary tools for a preliminary identification of these minerals.

6. Acknowledgements

We thank the European Social Fund (ESF), Operational Program for Educational and Vocational Training II (EPEAEK II), and particularly the Program PYTHAGORAS, for funding the above work.

7. References

Addison, J., and Davies, L.S.T., 1990. Analysis of amphibole asbestos in chrysotile and other minerals.

Annals of Occupational Hygiene, 34, 159-175.

- Bebien, J., 1982. L' association ignee de Guevgueli (Macedoine Greque). Expression d' un magmatisme ophiolitique dans une dechirure continentale. *These d' Etat*, Univ. Nancy 467pp.
- Clinkenbeard, J.P., Churchill, R.K., and Lee, K., 2002. Guidelines for geologic investigations of naturally occurring asbestos in California. *California Department of Conservation, California Geological Survey Special Publication 124*.
- Constantopoulos, S.H., 2008. Environmental mesothelioma associated with tremolite asbestos: Lessons from the experiences of Turkey, Greece, Corsica, New Caledonia and Cyprus. *Regulatory Toxicology and Pharmacology*, 52(1), 110-115.
- Ivanov, T., Misar, Z., Bowes, D.R., Dudek, A., Dumurdzanov, N., Jaros, J., Jelinek, E., and Pacesova, M., 1987. The Demir Kapija-Gevgelija ophiolite massif, Macedonia, Yugoslavia. *Ophioliti*, 12, 457-478.
- Jones, G., Robertson, A.H.F., and Cann, J.R., 1991. Genesis and emplacement of the supra-subduction zone Pindos ophiolite, northwestern Greece. In: Tj Peters et al. (Eds), *Ophiolite Genesis and Evolution of the Oceanic Lithosphere*, 771-799.
- Leake, B.E., Wooley, A.R., Arps, C.E.S., Birch, W.D., Gilbert, M.C., Grice, J.D., Hawthorne, F.C., Kato, A., Kisch, H.J., Krivovichev, V.G., Linthout, K., Laird, J., Mandarino, J., Maresch, W.V., Nickel, E.H., Rock, N.M.S., Scumacher, J.C., Smith, D.C., Stephenson, N.C.N., Ungaretti, L., Whittaker, E.J.W., and Youzhi, G., 1997. Nomenclature of amphiboles; report of the Subcommittee on amphiboles of the International Mineralogical Association, Commission on New Minerals and Mineral Names. *American Mineralogist*, 82, 1019-1037.
- Mercier, J.L., 1966. Sur l'existence et l'age de deux phases regionales du metamorphism alpin dans les zones internes des Hellenides en Macedoine centrale (Grece). *Bull. Soc. Geol. France*, 8, 1020-1049.
- Mossman, B.T., Bignon, J., Corn, M., Seaton, A., and Gee, J.B.L., 1990. Asbestos: scientific developments and implications for public policy. *Science*, 247, 294-301.
- Murray, J., and Nelson, G., 2008. Health effects of amosite mining and milling in South Africa. *Regulatory Toxicology and Pharmacology*, 52(1), 75-81.
- Nolan, R.P., Langer, A.M., Ross, M., Wicks, F.J., and Martin, R.F., 2001. The health effects of chrysotile asbestos: contribution of science to risk-management decisions. *The Canadian Mineralogist Special Publication 5*, 304pp.
- O'Hanley, D.S., 1996. Serpentinites: Records of Tectonic and Petrological History. *Oxford University Press*, New York, 277pp.
- Perkins, R.L., 1990. Point-counting technique for friable asbestos-containing materials. *Microscope*, 38, 29-39.
- Plater, S.F., Riley, R.D., and Simon, S.D., 1992. The classification of asbestos fibres by scanning electron microscopy and computer digitizing tablet. *Annals of Occupational Hygiene*, 36(2), 155-171.
- Pomonis, P., Tsikouras, B., and Hatzipanagiotou, K., 2005. Geological evolution of the Koziakas ophiolitic complex (western Thessaly, Greece). *Ophioliti*, 30(2), 77-86.
- Pomonis, P., Tsikouras, B., and Hatzipanagiotou, K., 2007. Petrogenetic evolution of the Koziakas ophiolite complex (W. Thessaly, Greece). *Mineralogy and Petrology*, 89, 77-111.
- Rassios, A., and Smith, A.G., 2000. Constraints on the formation and emplacement age of western Greece ophiolites (Vourinos, Pindos and Othris) inferred from deformation structures in peridotites. In: Dilek Y, Moores EM, Elthon D, Nicolas A (Eds), *Ophiolites and ocean crust: new insights from field studies and the Ocean Drilling Program*, *Geol. Soc. Am. Spec. Pap.*, 349, 473-483.
- Rigopoulos, I., Pomonis, P., Tsikouras, B., and Hatzipanagiotou, K., 2006. Comparative evaluation of dolerites from the Pindos and Vourinos ophiolitic rocks for their use as aggregates. *Tech. Chron. Sci.*

- Rigopoulos, I., Tsikouras, B., Pomonis, P., and Hatzipanagiotou, K., 2010. The influence of alteration on the engineering properties of dolerites: The examples from the Pindos and Vourinos ophiolites (northern Greece). *International Journal of Rock Mechanics & Mining Sciences* 47, 69-80.
- Rigopoulos, I., Tsikouras, B., Pomonis, P., Karipi, S., and Hatzipanagiotou, K., 2008. Quantification methods of asbestos fibres in ophiolitic rocks used as aggregates and hazard risk assessment for human health. *26th European Conference of the Society of Environmental Geochemistry and Health*, SEGH 2008, Athens, Hellas, 31/3/2008-2/4/2008, Abstracts, 48.
- Ross, M., and Nolan, R.P., 2003. History of asbestos discovery and use and asbestos-related disease in context with the occurrence of asbestos within ophiolite complexes. *Geological Society of America, Special Paper* 373, 447-470.
- Schneider, T., Davies, L.S.T., Burdett, G., Tempelman, J., Puleda, S., Jørgensen, O., Buchanan, D., and Paoletti, L., 1998. Development of a method for the determination of low contents of asbestos fibres in bulk material. *Analyst*, June 1998, 123, 1393-1400.
- Skarpelis, N., and Dabitzias, S., 1987. The chrysotile asbestos deposit at Zidani, northern Greece. *Ofioliti*, 12(2), 403-410.
- Snyder, R.L., and Bish, D.L., 1989. Quantitative Analysis, in Bish, D.L. and Post, J.E., eds., *Modern Powder Diffraction, Reviews in Mineralogy*, Washington, D.C., *Mineralogical Society of America*, 20, 101-144.
- Stanton, M.F., Layard, M., Tegeris, A., Miller, E., May, M., Morgan, E., and Smith, A., 1981. Relation of particle dimensions to carcinogenicity in amphibole asbestoses and other fibrous minerals. *J National Cancer Institute*, 67, 965-975.
- Tsikouras, B., Pomonis, P., Rigopoulos, I., and Hatzipanagiotou, K., 2005. Investigation for the suitability of basic ophiolitic rocks from the Mikroklioussa Grevena area as anti-skid aggregate material and railroad ballast. *Proc. of the 2nd Conference of the Committee of Economical Geology, Mineralogy and Geochemistry*, 347-356.
- Williams-Jones, A.E., Normand, C., Clark, J.R., Vali, H., Martin, R.F., Dufresne, A., and Nayebzadeh, A., 2001. Controls of amphibole formation in chrysotile deposits: evidence from the Jeffrey Mine, Asbestos, Quebec. In: Nolan, R.P., Langer, A.M., Ross, M., Wicks, F.J. and Martin, R.F. (Eds), *The health effects of chrysotile asbestos: Contribution of science to risk-management decisions*, *The Canadian Mineralogist, Special Publication* 5, Part 2, Exposure to commercial chrysotile - mineralogy, modern products and exposures, 89-104.
- World Health Organization, 1986. Asbestos and other natural mineral fibres. *Environmental Health Criteria*, No. 53. Geneva.
- Wylie, A.G., Bailey, K.F., Kelse, J.W., and Lee, R.J., 1993. The importance of width in asbestos fiber carcinogenicity and its implications for public policy. *American Industrial Hygiene Association J*, 54, 239-252.

MODELLING OF VOLCANIC ERUPTIONS ON TITAN

Solomonidou A.^{1,2,3}, Fortes A.D.³, Kyriakopoulos K.¹

¹ National & Kapodistrian University of Athens, Department of Geology and Geoenvironment,
Athens, Greece (asolomonidou@geol.uoa.gr),

² LESIA, Observatoire de Paris – Meudon, Meudon Cedex, France (Athena.Coustenis@obspm.fr),

³ University College London, Department of Earth Sciences, London, UK.

Abstract

Observations by the Visual Infrared Spectrometer instrument (VIMS) aboard the Cassini mission have indicated the possible presence of CO₂ ice on the surface on Titan, in areas which exhibit high reflectance in specific spectral windows (McCord et al., 2008). Two of the bright spots of significance are located within the Xanadu region – Tui Regio (located at 20°S, 130°W) and Hotei Regio (located at 26°S, 78°W), and there is a further spot situated in proximity to Omacatl Macula (Hayne et al., 2008). Explosive volcanic eruptions of a cryomagma containing H₂O and CO₂ are modelled for several potential scenarios regarding entrained CO₂ clathrates. The model yielded a range of values corresponding to the fragmentation pressure in the lava conduit, the velocity of the exploding cryomagma, the height of the associated lava fountain and the potential distance covered by ejecta. The results show that a single vent source does not possess the force required to cover an area resembling Hotei Regio or Tui Regio. Therefore, we consider alternative origins: the area may have been resurfaced by small CO₂ grains resulting from multiple explosive eruptions emanating from a zone of weakness (Hayne et al., 2008); the characteristics of the area are consequential of an eruption of cryomagma with CO₂ and NH₃ components (McCord et al., 2008); or finally, long term seasonal winds transferred small CO₂ grains and distributed them within the limits of Tui Regio area.

1. A brief introduction to Icy Moons

A significant proportion of the planetary bodies found within our solar system have been subject to observation, analysis, and mapping as well as classification, based on their characteristics. These achievements were the result of observations dating from ancient times until the present day but were accomplished predominantly through exploratory missions such as Voyager, Galileo, Cassini and many more. The three aforementioned missions provided information about the moons of several planets situated beyond the orbit of Mars. These 'icy moons' have distinctive characteristics, which are unique in our solar system (Lorenz, 2006).

Icy moons are small celestial bodies whose surfaces are partially, if not principally, covered by ice. They exhibit some features similar to planets (Johnson, 2004). Representative bodies of this category include several satellites of Jupiter, Saturn, Uranus, Neptune (Fig.1). The most remarkable icy moons are, respectively to the planets mentioned, Ganymede, Triton, Miranda and Titan with a variety of size, composition and temperature (Johnson, 2004). In recent times, it has been confirmed that the majority of satellites orbiting the outer planets have an icy appearance with a combined structure of rock and H₂O ice and/or NH₃ ice and/or CO₂ ice. It was thought that, due to the abun-

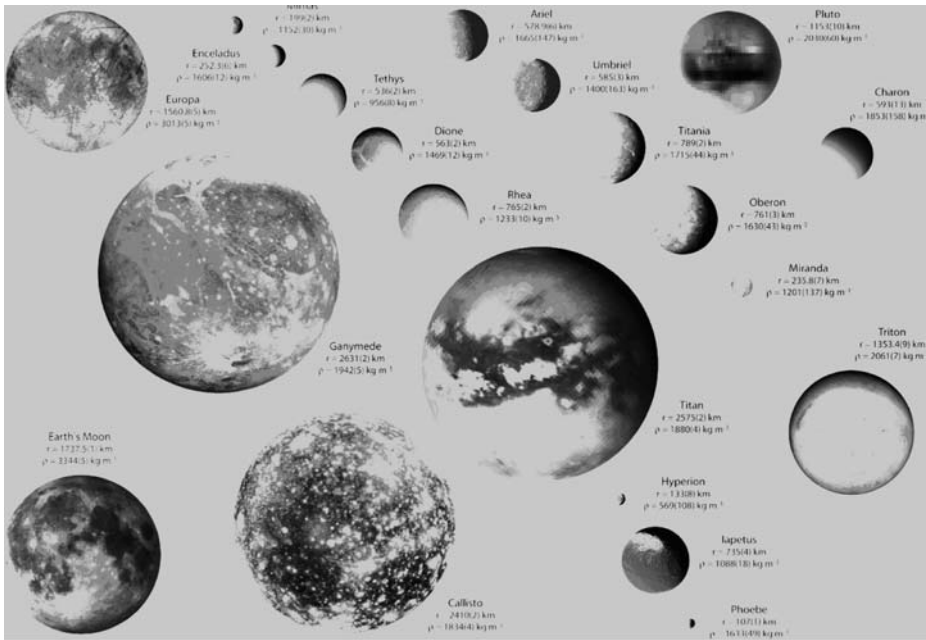


Fig. 1: Icy satellites

dance of water ice, the geology of these bodies would be simple, or rather simpler than Earth's; however, subsequent images have shown complex surfaces with several notable morphological formations. Furthermore, the composition as well as the structure of the surfaces of the icy moons is dependent upon geological and geophysical factors (Johnson, 2004).

2. The Saturnian moons

Long-lasting investigations showed that one of the most fascinating characteristics of the Saturnian icy worlds is their complex, dynamic and Earth-like geology. Intervent and layered plains, icy flows, impact units, extensive ridges and grooves are the effects of endogenous and exogenous intense dynamic processes. On the surfaces of Titan and Enceladus, which geologically are the most interesting satellites, these processes are expressed in the form of cryovolcanoes, geysers and tectonic features. The activity of cryovolcanism on Titan can be described analogous to Earthly volcanism, where methane, as a product of the volcanic activity, is the main component of Titan's unique organic chemistry laboratory (Johnson, 2004). In particular, Titan's atmosphere is mostly nitrogen but there are also methane and many other organic compounds. The problem that arises regarding the presence of methane on Titan is the source that feeds and maintains the surface as well as the atmosphere. On Earth today, it is life itself that refreshes the methane supply through the metabolism of many organisms. On Titan there is no living life that could provide the satellite with methane as a by-product, suggesting that there should be a reservoir of methane within Titan that interacts with the atmosphere.

Methane outgassing from the interior or from the subsurface could constitute the missing reservoir to explain the presence of gaseous methane in today's atmosphere. On the southern limb of Enceladus an impressive phenomenon of icy geysers is present. Instruments on the Cassini spacecraft discovered these icy plumes during close encounters with Enceladus (Matson et al., 2007). They could

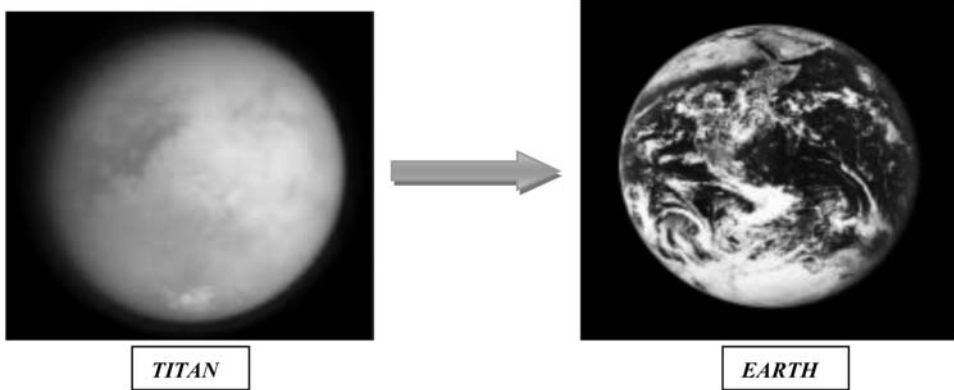


Fig. 2: Earth-like Titan (retrieved from NASA / Goddard Space Flight center).

be due to condensation of the vapor escaping from a water source and stream through the cracks in the ice crust before heading into space and supposedly populate Saturn's E-ring (Kempf et al., 2008). Another moon that displays fascinating geological features is Iapetus, presenting a phenomenon called 'two-tone' coloration due to intense color differences of the leading (dark) and trailing (bright) hemispheres. The dark material is believed to be a residual product of the water ice evaporation on the surface. The event that caused this could be the exposure to sunlight. Alternatively, thermal anomalies after bombardment of micrometeorites that crossed Iapetus's orbit emanating from Phoebe could have caused the evaporation. Iapetus's surface morphology is exceptionally interesting as it presents a high equatorial ridge and impact craters with variety in size on both dark and bright sides. The ridge is a unique geomorphological feature as it rises more than 20km above the plains and consists of a complex system of parallel ridges, surrounding plains and isolated peaks (Porco et al., 2005). Another Saturnian icy moon that is heavily bombarded and grooved, is Rhea (Wagner et al., 2007). This moon geologically is similar to Dione and there are in both potential areas of past cryovolcanic activity. Cassini's spacecraft investigation implied that the level of active endogenic process is extremely low, although the surficial features suggest a world that in the past was geologically active similar to the present situation on Titan and Enceladus. The Saturnian moons suggest unique areas of geological research due to their active interiors or/and their complex formed surfaces. Almost every geological activity and feature present on Earth has so far been observed on these fascinating worlds, acting more dynamically, creating extremely active and powerful systems.

3. Titan

Titan is the largest moon of Saturn and the second largest in the Solar System after Jupiter's Ganymede. It is primarily composed of rocky material and water ice and exhibits a variety of surface formations such as mountains, lakes, craters, dunes and many more (Johnson, 2004). One of the moon's exceptional characteristics, that enhance its allure for exploration, is the existence of stable bodies – lakes – of surface liquid (Stofan et al., 2007). Previous to this discovery, such features had only been identified on Earth's surface (Fig.2). The atmosphere of Titan is also unique, as it is the only moon known to have an atmosphere with a greater density than that of Earth (Coustenis and Taylor, 1999), and the only object that shows stable bodies of surface liquid (Stofan et al., 2006). Of even more importance is the recent discovery of cryovolcanism as an outstanding characteristic of Titan, as well as the possibility that the moon harbours a prebiotic environment rich in complex organic chemistry (Fortes et al., 2007).

Instrument: Descent Imager/Spectral Radiometer (DISR)

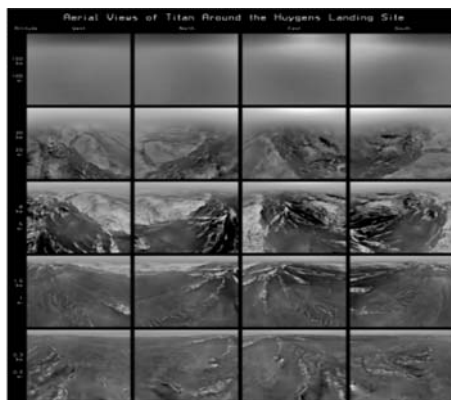


Fig. 3: Huygens's view of Titan's surface from five altitudes (retrieved from NASA).

Titan has been under detailed investigation for the past 17 years. Initially this was carried out by NASA's Hubble Space Telescope, which showed for the first time that an extensive bright continuous land exists on the leading hemisphere. Likewise, observations using several land-based telescopes shed light on additional information concerning the atmosphere and the surface (Coustenis and Taylor, 1999).

The most recent and crucial approach to Titan remains in commission – NASA's Cassini-Huygens spacecraft, on mission to the Saturn system. The data from instruments aboard this craft supplied information regarding Titan's atmosphere, surface composition and structure (Fig.3) as well as concerning the possible existence of evidence of life on this icy satellite (Lorenz and Mitton, 2008).

4. Geological processes on Titan

Titan's surface demonstrates a variety of geological features and formations, which frequently contain water ice or elements that render their presence particularly interesting. Chronologically the surficial geological features are young as well as complicated and unique for a celestial satellite (Mahaffy, 20005). Before 1997, several hypotheses predicted cryovolcanic activity, impact craters and even large stable liquid bodies. Further to the data collected by the Cassini mission, these assumptions were confirmed. In general, Titan's surface appears to have smooth and rough areas of various altitudes, which include volcanic features such as cryovolcanoes and impact craters that are intermittently filled by atmospheric precipitations. In addition, the satellite exhibits topographic features such as rims and edges and tectonic features filled with material by means of thermodynamic processes (Johnson, 2004). These features and formations will be examined individually forthwith.

Cryovolcanism: Cryovolcanism is considered to be one of the principal geological processes that have shaped several of the icy moons' surfaces. This activity can be described as ice-rich volcanism, while the cryovolcanic ejecta is referred to as cryomagma. This volcanic melt appears in the form of icy cold liquid and, in some cases, as partially crystallised slurry (Kargel, 1994). Cryovolcanic activity on icy satellites presents a controversial scientific issue and interest within the scientific community is ever increasing, almost certainly due to the postulation that cryomagma may be relevant to the formation of prebiotic compounds (Fortes, 2000). As a pre-life indicator, prebiotic compounds can possibly be connected to, and considered as evidence for, the existence of extraterrestrial life (Lopes et al., 2007). The composition of cryomagma is still unknown, due to the lack of in situ measurements. The general opinion suggests that the composition of cryomagma on Titan is likely primarily a mix-

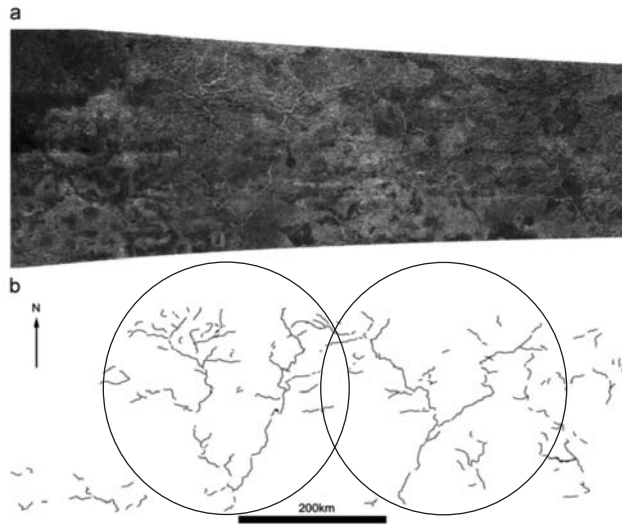


Fig. 4: Fluvial Network Dendritic drainages (Lorenz et al., 2008).

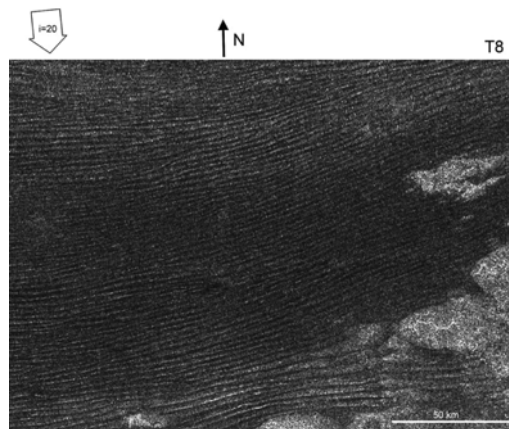


Fig. 5: Equatorial sand sea on Titan (Radebaugh, 2009).

ture of water ice and ammonia (Lopes et al., 2007). Other theories suggest mixtures of a/ H_2O and $(\text{NH}_4)_2\text{SO}_4$ (Mahaffy, 2005) and b/ H_2O and CO_2 (McCord et al., 2008). The icy moons on which features of cryovolcanism have been identified are Europa, Ganymede, Enceladus and Titan.

Geomorphology: Fluvial processes. The Cassini radar observations presented the fluvial features and their flow directions on the Xanadu area of Titan (Fig. 6). The fluvial processes on Titan's surface present a major geodynamic activity that contributes to the satellite's morphology. This fluvial network extends over 400km while it presents a dendritic morphology (Fig. 4). The dendritic network drainage is the pattern formed by the streams, rivers and lakes in a particular "watershed". In this case incisions were not observed but a well-developed branching structure on both channels (red and green circle) is present (Lorenz et al., 2008).

Aeolian processes: A sand dune is a semi-permanent accumulation of loose sand that forms in areas

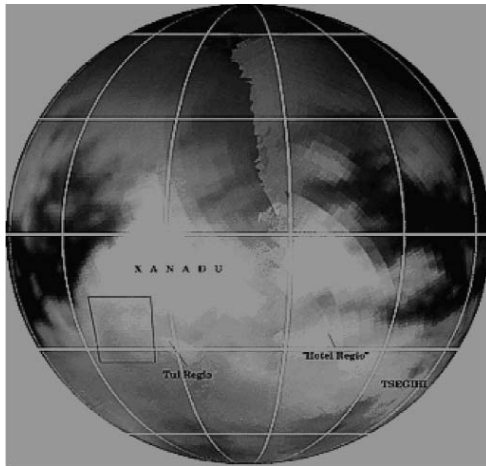


Fig. 6: Titan's possibly active cryovolcanic regions (Barnes et al., 2006).

where the wind tends to blow in one direction, at velocities high enough to move sand, across a land surface that permits sand to amass in a regular and consistent form. The sand composition is possibly a mixture of organic materials and ice grains (Radebaugh et al., 2008).

This geological phenomenon presents two kinds of linear features (Fig. 5). A Cassini Radar image (8° S, 264° W) where dark linears are the sides of dunes facing away from the radar and bright linears are due to direct reflection of a radar-facing slope (Radebaugh, 2009).

5. Instrumentation

The visual and infrared mapping spectrometer is the primary instrument that brought evidence for the CO_2 presence on Titan's surface. In the Cassini-Huygens mission, the visual and infrared mapping spectrometer was used to perform a multidisciplinary investigation of the Saturnian system including the surface and atmosphere of Titan (Brown et al., 2004). Essentially, the observations were made using techniques of spectroscopy (near-infrared imaging) and spectrophotometry (high speed) (Brown et al., 2004).

6. Cryovolcanic Areas of Interest

6.1 Tui Regio

The Tui Regio, also referred to as 'The Smile' (Fig.6), is one of the areas where an anomalously bright spot was observed, and therefore constitutes a component of the most reliable evidence yet obtained concerning the presence of carbon dioxide on Titan's surface. It is circa 150 km wide, extends 1500 km in an east-west direction and is situated near 125° W 24° S (Barnes et al., 2006). Nelson et al. (2007) suggest that this region may be associated with zones of fluctuating brightness while Hayne et al. (2008) propose that the Tui Regio could be an active centre of cryovolcanism. The evidence stands that the spectral reflectance in the $5\mu\text{m}$ window is compatible to CO_2 (Barnes et al., 2006) while other spectral images of candidate materials (ices) such as H_2O and CH_4 seems incompatible (Grundy et al., 2002). Although the presence of CO_2 on the surface has not yet been confirmed.

6.2 Hotel Regio

Other than 'The Smile' bright spot on Titan's surface, telescope investigations and Cassini VIMS data showed another bright spot, lying between the mid-latitude zone and the equatorial zone south of Xanadu

(110° W 15° S). Hotei Regio (Fig. 6) extends over 450 km (N-S) and 400 km (W-E) (Barnes et al., 2006). The region is particularly conspicuous as it is brighter than the whole area of Xanadu at all wavelengths, especially those greater than 1.6µm (Roe et al., 2004). In addition, whilst the Keck Observatory imaged this unusual feature on Titan's surface at 2 µm, the VIMS team presented collected data through the use of colour composites, demonstrating its striking bright characteristics. In the maps created by combining these colour composites, using data from the 5 µm atmospheric window, the feature of Hotei Regio is bright red (Barnes et al., 2006).

7. Modelling

On Earth, the concentrations of different volcanic gases can vary considerably from one volcano to the next. Typically, water vapour is the most abundant volcanic gas, followed by carbon dioxide and sulphur dioxide. Other principal volcanic gases include hydrogen sulphide, hydrogen chloride, N₂, O₂ and hydrogen fluoride (Rosi et al., 2003). Also, noble gases and helium from primordial Earth degassing. A large number of minor and trace gases are also found in volcanic emissions. These include hydrogen, carbon monoxide, halocarbons, organic compounds, and volatile metal chlorides (Bryson and Goodman, 1980).

Fortes et al. (2007) suggest methane gas, carbon monoxide and nitrogen as possible volatile volcanic gases candidates in Titan's magma. In this study, employing a model that we named the 'CO₂ model', we suggest one more candidate – carbon dioxide.

The presence of the 'bright spots' on Titan's surface comprise the evidence that has generated the assumption of CO₂ as a component of Titan's interior as well as the possible origin of cryovolcanism. The modelling of CO₂ imparts substantial amounts of data that, in combination with surface observation, could show whether or not a possible cryovolcanic activity involving a mixture of CO₂ and H₂O could have created the observed 'CO₂ ice' products. These data include; calculations of fragmentation depths, possible velocities according to the amount of clathrates in the mixture, approximate calculations of the maximum height reached by the lava fountain, and the distance at which ejecta could be deposited. The results will contribute to the correlation of the mathematical data with the observation evidence present on Titan's surface. The identification of CO₂ as a component of the surface will further our understanding of the satellite's composition and impose boundary conditions on its evolution. More specifically, such research will provide a holistic overview of cryovolcanism and its role on Titan.

List of properties:

Equations:

- $P = \rho gh$ (1) (P is the difference between the pressure and the initial pressure within the volcanic conduit)
- $\beta^{-1} = [(n_c RT)/mP] + [(1-n_c)/Q_{H_2O}]$ (2) (Density of the bulk magma)
- $V_b = 1 - \beta [(1-n_m)/Q_{H_2O}]$ (3) (Bubble volume fraction)
- $(g h) = (P_f - P_v) / \rho_{crust}$ (4) (Potential energy change per unit mass of magma)
- $0.5 u_v^2 = (n_m RT/m) \ln (P_f/P_v) + \Delta P [(1-n_m/Q_{magma}) - 1/Q_{crust}]$ (5) (Kinetic energy per unit mass)
- $H = u^2/2g$ (6) (Lava fountain height)
- $d = u^2 \sin(2\theta)/g$ (7) (Total horizontal distance).

Using equations we have calculated the horizontal distance, d, that ejecta could cover after an eruption for a range of velocities (Table 1). The angle of ejecta trajectory is considered in the range of 0-80° and g is 1.354 m/s². Plot 1 shows the trajectory of ejecta, which extrudes from an eruption with a velocity

Table 1. Integral table with values resulted from all the possible scenarios

Dissolved CO ₂ clathrate scenarios				
Volume Fraction of exsolved CO ₂	Entrained clathrates (wt%)	Fragmentation depth (m)	Eruption velocity (m/s)	Lava fountain height (m)
0	0		0	0.00
0.75	44	0	5.2	9.82
0.75	50	6.25	12.5	57.85
0.75	55	22.93	24	213.02
0.75	60	44.31	35.2	457.80
0.75	65	46.56	39.3	571.45
0.75	70	64.43	48.3	862.12
0.75	75	90.06	58.6	1270.18
0.75	80	107.62	66.3	1625.65
0.75	85	111.56	70.8	1850.89
0.75	90	136.25	79.6	2338.90

Table 1 summarizes the results of the equations used after the appropriate processing in our model.

List of properties:

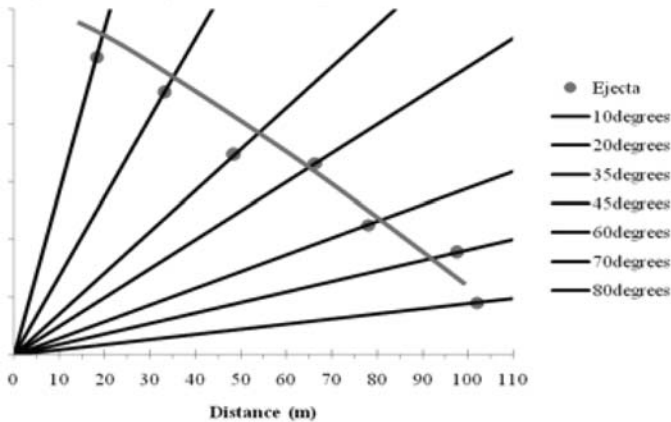
CO ₂ Model	TITAN	Values
Density of the crust		1000 kg/m ³
Density of the cryomagma		1000 kg/m ³
Density of CO ₂ gas		1,87 kg/m ³
Molecular mass of CO ₂		0,044 kg/mol
Gas constant		8,314 kg/mol
Magma Temperature		273 K
Mass of Titan		1,345E+23 kg
Surface gravity		1,354 m/s ²

of 5.2 m/s – the slowest eruption velocity calculated for a potential eruption in the ‘CO₂ model’.

9. Discussion and Modelling

The Visual and Infrared Mapping Spectrometer data suggesting the CO₂ presence on the surface of Titan (‘bright-spots’) generated the assumption of CO₂ being a component of the satellite’s interiors and therefore the possible origin of cryovolcanism. Since exsolution of volatiles, mainly H₂O and CO₂ as well as other volcanic gas species are common during volcanic activity on Earth we have used similar ‘explosivity’ modelling to predict cryovolcanic activity results on Titan (Table 1) assuming a constant volume fraction of exsolved CO₂ and an increasing by 5 wt% amount of clathrate (which is a chemical substance

Ejecta's trajectory (eruption velocity 5.2 m/s)



Plot 1: Trajectory of extruded ejecta and its path to the surface.

consisting of a lattice of one type of molecule trapping and containing a second type of molecule). This ‘‘modelling of CO₂’’ imports substantial amounts of data that, in combination with surface observations, could show whether or not possible cryovolcanic activity involving a mixture of CO₂ and H₂O could have created the observed ‘‘CO₂-ice’’ products. These data include: calculations of fragmentation depths, estimations of eruption velocities as well as the height of the lava fountain for every case scenario.

10. Conclusions

This study has focused on evidence from ‘Hotei Regio’ and Tui Regio, in order to correlate the data provided from the ‘CO₂ model’ with observed data, gathered via VIMS imaging. The variety of possible eruptions was limited because of restrictions on the likely cryomagmatic composition, since it is doubtful that large quantities of ‘‘CO₂-ice’’ are present at the observed bright spots (Sotin et al., 2005). Therefore, the results support a conclusion of rapid eruptions and ejecta that travels within a range of 9-24km (Appendix: Table A) from the vent. It is possible that the remaining area of Hotei Regio, which extends approximately 400km in the latitudinal direction and 450km longitudinally (Barnes et al., 2006), is covered by products of multiple episodic eruptions of cryomagma containing a mixture of NH₃ and CO₂ (Hayne et al., 2008). An alternative origin of the deposits could be provided by seasonal winds that transport and disperse small CO₂ grains within the area.

11. Future work

Since the ‘‘Cassini-Huygens’’ mission at Titan, interest in future missions has increased continuously. Currently, the ‘‘Cassini Equinox mission’’ remains operational with frequent flybys over Titan. Future flybys will bring in additional observations and spectral data from the VIMS instrument and also allow a continuous observation of the bright spots, thus aiding interpretation of the current data. A potential further extension of the Cassini mission will offer valuable supplementary data and observations on the seasonal variations of Titan’s atmosphere and surface. As aforementioned, this will prove helpful in understanding the behaviour of ejecta resulting from a potential eruption and elucidate its relationship with surface winds. Titan has so intrigued the scientific community that several other proposals for future missions have been made by scientists all over the world. Coustenis et al. (2009) suggest a new study of Titan with a combination of two missions. The design of the Titan Saturn System Mission (TSSM), which will study Titan as a system, is based on the scientific and technological achievements of the Cassini-Huy-

gens mission. It aims to investigate Titan specifically, by obtaining measurements that Cassini-Huygens was unable to, via full close-up and *in situ* coverage over long periods of time (Coustenis et al., 2009). The high-resolution coverage of the surface could provide valuable data of increased detail regarding the presence of CO₂ on the surface and the morphology of the CO₂ products, such as flows or ejecta.

12. References

- Barnes, J.W., Brown, R. H., Turtle, E.P., McEwen, A.S., Lorenz, R. D., Janssen, M., Schaller, E.M., Brown, M.E., Buratti, B.J., Sotin, C., Griffith, C., Clark, R., Perry, J., Fussner, S., Barbara, J., West, R., Elachi, C., bouchez, A.H., Roe, H.G., Baines, K.H., Bellucci, G., Bibring, J.P., Capaccioni, F., Cerroni, P., Combes, M., Coradini, A., Cruikshank, D.P., Drossart, P., Formisano, V., Jaumann, R., Langevin, Y., Matson, D., McCord, T.B., Nicholson, P.D., Sicardy, B., 2005. A 5-Micron-Bright Spot on Titan: Evidence for Surface Diversity. *Science*, 310, 92-95.
- Barnes, J.W., Radebaugh, J., Buratti, B.J., Sotin, C., Le Mouelic, S., Rodriguez, S., Turtle, E.P., Perry, L., Clark, R., Baines, K.H., Nicholson, D., 2006. Cassini observations of flow-like features in western Tui Regio, Titan. *Geophys. R. Lett.*, 33, L16204.
- Brown, R.H., Baines, K.H., Bellucci, G., Borbing, J.P., Buratti, B.J., Capaccioni, F., Cerroni, P., Clark, R.N., Coradini, A., Cruikshank, D.P., Drossart, P., Formisano, V., Jaumann, R., Langevin, Y., Matson, D.L., McCord, T.B., Mennella, V., Miller, E., Nelson, R.M., Nicholson, P.D., Sicardy, B. and Sotin, C., 2004. The Cassini visual and infrared mapping spectrometer (VIMS) investigation. *Space Science Reviews*, 115, 112-168.
- Bryson, R.A., Goodman, B.M., 1980. Volcanic Activity and Climatic Changes. *Science*, 207, 1041-1044.
- Coustenis, A., Taylor, F., 1999. Book: Titan: The Earth-Like Moon. Series on Atmospheric, Oceanic and Planetary Physics – Vol. 1.
- Coustenis, A. et al., 2009. THE JOINT NASA-ESA TITAN SATURN SYSTEM MISSION (TSSM) STUDY. 40th Lunar and Planetary Science Conference, id:1060.
- Fortes, A.D., 2000 Exobiological implications of a possible subsurface ocean inside Titan. *Icarus*, 146, 444–452.
- Fortes, A.D., Grindrod, P.M., Trickett S.K, Vořadlo L., 2007 Ammonium sulfate on Titan: Possible origin and role in cryovolcanism. *Icarus*, 188, 139–153.
- Grundy, W.M., Schmitt, B., Quirico, E., 2002. The temperature-dependent spectrum of methane ice I between 0.7 and 5 μ m and opportunities for nearinfrared remote thermometry. *Icarus*, 155, 486–496.
- Hayne, P., McCord, T.B., Sotin, C., Barmatz, M., Mielke, R., Combe, J.P., Hansen, G. B., 2008. Titan: Observational Constraints on Cryovolcanism. 39th LPSC, LPI Contribution No. 1391, 2010.
- Johnson, T., 2004. Geology of the icy satellites. *Space science reviews*, 166, 401-420.
- Kargel, J.S., 1994. Cryovolcanism on the icy satellites. *Earth, Moon, and Planets*, 67, 1-3.
- Kempf, S., Beckmann, U., Schmidt, J., 2008. The E ring in the vicinity of Enceladus. *Icarus*, 193, 420-437.
- Lopes, R.M.C., Mitchell, K.L., Stofan, E.R., Lunine, J.I., Lorenz, R., Paganelli, F., Kirk, R.L., Wood, C.A., Wall, S.D., Robshaw, L.E., Fortes, A.D., Neish, C.D., Radebaugh, J., Reffet, E., Ostro, S.J., Elachi, C., Allison, M.D., Anderson, Y., Boehmer, R., Boudin, G., Callahan, P., Encrenaz, P., Flamini, E., Francescetti, G., Gim, Y,m Hamilton, G., Hensley, S., Janssen, M.A., Johnson, W.T.K., Kelleher, K., Muhleman, D.O., Ori, G., Orosei, R., Picardi, G., Posa, F., Roth, L.E., Seu, R., Shaffer, S., Soderblom, L.A., Stiles, B., Vetrella, S., West, R.D., Wye, L., Zebker, H.A., 2007. Cryovolcanic features on Titan's surface as revealed by the Cassini Titan Radar Mapper. *Icarus*, 186, 395–412.
- Lorenz, R.D., 2006. The exploration of Titan. Johns Hopkins APL Technical Digest, 27, 113-144.
- Lorenz, R.D. and Mitton, J., 2008. Book: Titan Unveiled. Princeton University Press.
- Lorenz, R.D., Mitchell, K.L., Kirk, R.L., Hayes, A.G., Aharonson. O., Zebker, H.A., Paillou, P., Radebaugh, J., Lunine, J., Janssen, M.A., Wall, S.D., Lopes, R.M., Stiles, B., Ostro, S., Mitri, G., Stofan, E.R. and the Cassini

- RADAR team. 2008a. Titan's inventory of organic surface materials. *Geophysical research letters*, 38, 2-17.
- Mahaffy, R., 2005. Intensive Titan Exploration Begins. *Science*, 308, 969–970.
- Matson, D.L., Castillo, J.C., Lunine, J., Johnson, T., 2007. Enceladus' plume: Compositional evidence for a hot interior. *Icarus*, 187, 569-573.
- McCord, T.B., Hayne, P., Combe, J.P., Hansen, G. B., Barnes, J. W., Rodriguez, S., Le Mouelic, S., Baines, E., Buratti, B. J., Sotin, C., Nicholson, P., Jaumann, R., Nelson, R., and the Cassini VIMS TEAM. 2008. Titan's surface: Search for spectral diversity and composition using the Cassini VIMS investigation. *Icarus*, 194, 212–242.
- Nelson, R.M., Kamp, L., Matson, D.L., Irwin, P.G.J., Baines, K.H., Boryta, M.D., Leader, F.E., Jaumann, R., Smythe, W.D., Sotin, C., Clark, N., Cruikshank, D.P., Drossart, P., Pearl, J.C., Hapke, B.W., Lunine, J., Combes, M., Bellucci, G., Bibring, J.P., Capaccioni, F., Cerroni, P., Coradini, A., Formisano, V., Filacchione, G., Langevin, R.Y., McCord, T.B., Mennella, V., Nicholson, P.D. and Sicardy, B., 2007. Saturn's Titan: Searching for Surface Change. AGU Fall Meeting, #P22B-03.
- Porco, C.C., Baker, E., Barbara, J., Brahic, A., Burns, J.A., Charnoz, S., Cooper, N., Dawson, D.D., Del Genio, A.D., Denk, T., Dones, L., Dyudina, U., Evans, M.W., Giese, B., Grazier, K., Helfenstein, P., Ingersoll, A.P., Jacobson, R.A., Johnson, T.V., McEwen, A., Murray, C.D., Neukum, G., Owen, W.M., Perry, J., Roatsch, t., Spitale, J., Sqyures, S., Thomas, P.C., Tiscareno, M., Turtle, E., Vasavada, A.R., Veverka, J., Wagner, R. and West, R., 2005. Cassini Imaging Science: Initial Results on Phoebe and Iapetus. *Science*, 307, 1237–1242.
- Radebaugh, J., et al., 2008. Dunes on Titan observed by Cassini Radar. *Icarus*, 194, 690–703.
- Radebaugh, J., 2009 Linear dunes on Titan and earth: Initial remote sensing comparisons. GEOMOR-02903(IN PRESS).
- Roe, H.G., Pater, I., Gibbard, S.G., Macintosh, B.A., Max, C.E., Young, E.F., Brown, M.E and Bouchez, A.H., 2004. A new 1.6-micron map of Titan's surface. *Geophysical research letters*, 31, L17S03.
- Rosi, M., Lupi, L., Papale, P., Stoppato, M., 2003. Volcanoes. Firefly Books.
- Sotin, C., buratti, B.J., Brown, R.H., Clark, R.N., Soderblom, L.A., Baines, K.H., Bellucci, G., Bibring, J.P., Capaccioni, F., Cerroni, P., Combes, M., Coradini, A., Cruikshank, D.P., Drossart, P., Formisano, V., Langevin, Y., Matson, D.L., McCord, T.B., Nelson, R.M., Nicholson, P.D., Sicardy, B., Lemouelic, S., Rodriguez, S., Stephan, K and Scholz, C.K., 2005. Release of volatiles from a possible cryovolcano from near-infrared imaging of Titan. *Nature*, 435, 786-789.
- Stofan, E.R., Lunine, J.I., Lopes, R., Paganelli, F., Lorenz, R.D., Wood, C.A., Kork, R., Wall, S., Elachi, C., Soderblom, L.A., Istro, S., Janseen, M., Radebaugh, J., Wye, L., Zebker, H., Anderson, Y., Allison, M., Boehmer, R., Callahan, P., Encrenaz, P., Flamini, E., Francescetti, G., Gim, Y., Hamilton, G., Hensley, S., Jonson, W.T.K., Kelleher, K., Muhleman, D., Picardi, G., Posa, F., Roth, L., Seu, R., Shaffer, S and Stiles, B., 2006. Mapping of Titan: Results from the first Titan radar passes. *Icarus*, 185, 443-456.
- Stofan, E.R., Elachi, C., Lunine, J.I., Lorenz, R.D., Stiles, B., Mitchell, K.L., Ostro, S., Soderblom, L., Wood, C., Zebker, H., Wall, S., Janssen, M., Kirk, R., Lopes, R., Paganelli, F., Radebaugh, J., Wye, L., Anderson, Y., Allison, M., Boehmer, R., Callahan, P., Encrenaz, P., Flamini, R., Francescetti, G., Gim, Y., Hamilton, G., Hensley, S., Johnson, W.K.T., Kelleher, K., Muhleman, D., Paillou, P., Picardi, G., Posa, F., Roth, L., Seu, R., Shaffer, S., Vetrella, S., West, E., 2007. The lakes of Titan. *Nature*, 445, 61-64.
- Wagner, R. J., Neukum, G., Giese, B., Roatsch, T. and Denk, T., 2007. Geology and Geomorphology of Rhea: a First Look at the High-Resolution Cassini ISS Images from the Targeted Flyby on Aug. 30, 2007. AGU Meeting abstract #P12B-06.

APPENDIX

Table A. Horizontal distances of ejecta for angles 0-80° and several values of velocity range.

Eruption velocity (m/s)	Angle of ejecta trajectory	Distance (m)	Total distance (m)
35,2	0	0	0
	10	835,43	835,43
	20	681,85	1517,28
	35	708,18	2225,47
	45	818,09	3043,56
	60	531,31	3574,87
	70	897,01	4471,89
	80	200,80	4672,68
	39,3	0	0,00
10		1041,38	1041,38
20		849,94	1891,33
35		882,77	2774,09
45		1019,77	3793,86
60		662,30	4456,16
70		1118,15	5574,30
80		250,30	5824,60
48,3		0	0,00
	10	1572,97	1572,97
	20	1283,80	2856,77
	35	1333,38	4190,15
	45	1540,32	5730,48
	60	1000,37	6730,85
	70	1688,92	8419,76
	80	378,06	8797,82
	58,6	0	0,00
10		2315,37	2315,37
20		1889,73	4205,10
35		1962,71	6167,81
45		2267,32	8435,13
60		1472,52	9907,65
70		2486,04	12393,70
80		556,50	12950,19
66,3		0	0,00
	10	2963,83	2963,83
	20	2418,97	5382,80
	35	2512,40	7895,20
	45	2902,31	10797,51
	60	1884,92	12682,43
	70	3182,30	15864,73
	80	712,35	16577,08

Eruption velocity (m/s)	Angle of ejecta trajectory	Distance (m)	Total distance (m)
70,8	0	0	0
	10	3379,81	3379,81
	20	2758,48	6138,29
	35	2865,02	9003,31
	45	3309,66	12312,98
	60	2149,48	14462,45
	70	3628,94	18091,40
	80	812,33	18903,73
79,6	0	0,00	0,00
	10	4272,21	4272,21
	20	3486,82	7759,03
	35	3621,49	11380,52
	45	4183,53	15564,05
	60	2717,02	18281,07
	70	4587,12	22868,19
	80	1026,82	23895,01

THE USE OF DIATOMACEOUS ROCKS OF GREEK ORIGIN AS ABSORBENTS OF OLIVE-OIL WASTERS

Stamatakis M.¹ and Stamatakis G.²

¹ National & Kapodistrian University of Athens, Faculty of Geology & Geoenvironment, Department of Economic Geology & Geochemistry, Panepistimiopolis, Ano Ilissia, 157 84 Athens, Greece, stamatakis@geol.uoa.gr

² National & Kapodistrian University of Athens, Faculty of Chemistry, Department of Biochemistry, Panepistimiopolis, Ano Ilissia, 157 84 Athens, Greece, stamatakisgeo@gmail.com

Abstract

Diatomite is a multifunctional industrial mineral, having commercial interest in the food/agricultural and the construction sectors and also in environmental applications. Certain diatomite deposits worldwide are used as absorbents and filtering media in industrial scale. In Greece, several types of diatomaceous deposits (calcareous, clayey or amorphous phases-rich) occur in marine or lacustrine Tertiary basins. Bulk samples originated from western Macedonia, Thessaly and the islands of Samos and Milos were characterized, tested and compared concerning their absorption ability against olive mill wastes. The results of the current research show insignificant variations in the absorption ability of the tested Greek diatomites exhibiting equal or better behavior than some of the commercially used absorbents, either diatomaceous, or clayey. Hence, the Greek raw materials could find applications in the prevention of seashores and river banks pollution from the acidic olive-oil wastes.

Key words: diatoms, olive-oil wastes, opaline silica, absorption, clay minerals.

1. Introduction

Biogenic amorphous silica (opal-A) sedimentary deposits characterized as diatomaceous rocks or diatomaceous earth are represented by accumulations of diatom frustules, sponge spicules, radiolarian cells and/or silicoflagellate skeletons. Besides opal-A, diatomaceous rocks may contain carbonate and clay minerals, quartz, feldspars, micas and volcanic glass.

The physical and chemical properties which make diatomite a multifunctional industrial mineral include its low density, high porosity, high specific surface area, abrasiveness, insulating properties, inertness, absorptive capacity, brightness, and high silica content.

Almost all types of the diatomites have found industrial applications, utilized as chemicals, filter aids, fillers, absorbents, construction materials, environmental protection, civil engineering, agriculture, paint additives and catalysts.

Current world statistics show that the absorption applications of diatomite are about 13% of their total consumption (Crosley, 2002; Leahy, 2006). The last 50 years, clayey diatomite or diatomite-bentonite/zeolite mixtures are used to absorb industrial liquid spills. The material is used as granules

and/or powders of various grades. Sometimes the natural samples are calcined to increase the hardness of the grains, to improve durability after absorbing a fluid, and to eliminate dust production.

In Greece, even though several diatomite deposits have been identified in the mainland and several islands of the Aegean and Ionian seas, only one deposit located in SW Milos Island is accidentally used as pozzolana, along with the interbedded tuffs (Fragoulis *et al.*, 2002).

During the production of olive oil, a large volume of waste water is generated and subsequently discarded. It is estimated that in the Mediterranean Basin alone, OOW accounts 10-12×10⁶ m³ each year (Cabrera *et al.*, 1996). OOW is considered one of the “heaviest” biomechanical byproducts mostly due to its organic load, with Biochemical Oxygen Demand (BOD) and Chemical Oxygen Demand (COD) that can reach up to 100 and 220 g/L, respectively (Stamatakis *et al.*, 2009).

Many different methods for the degradation of the wastes have been proposed, the majority of them involving physicochemical and microbial treatment of the wastes (Niaounakis and Halvadakis, 2006; McNamara *et al.*, 2008).

Diatomite and bentonitic clays have been successfully used as absorbent of olive oil wastes (OOW) (Al-Malah *et al.*, 2000; Makri and Stamatakis, 2005; Stamatakis *et al.*, 2009). More specifically, Greek origin calcareous diatomite retains about 86% of the phenolic compounds present in the OOW, whereas its ability to absorb the total dissolved salts is 82% and of the residual solid up to 74% (Makri and Stamatakis, 2005). Diatomites also increase the originally acidic pH of these wastes.

In general, the composition of the OOW varies according to the olive tree species, the harvesting period, the maturity of the olives, the climatic conditions in the specific area, the machinery and the technology of each olive processing plant is equipped (Borja-Padilla *et al.*, 1990; Fiestas Ros de Ursinos and Borja-Padilla, 1992).

According to literature data, the organic compounds may reach up to 18%, followed by inorganic substances, mainly phosphates and potassium salts 2%, whereas 60% of the solids are sugars mainly fructose and mannose (Niaounakis and Halvadakis, 2006).

The aim of the present paper is to characterize and test the OOW absorption capacity of diatomaceous rocks originated from four Greek deposits, namely Kleidi-Florina [western Macedonia], Sarantaporo-Elassona [Thessaly], Chora, Samos Island and Xylokeratia, Milos Island [Aegean Sea]. In addition, a commercial pure diatomite sample was also tested and compared to the aforementioned samples. The sample was collected from a processing plant of filter-aid diatomite, based at Albacete, Andalusia Spain. The samples were also compared to literature data, in order to point out the sufficiency significance of the Greek diatomaceous deposits in industrial applications as absorbents.

2. Materials and Methods

2.1 Geological data

2.1.1 Kleidi, Florina lignite basin, western Macedonia

In western Macedonia, the Komnina, Vegora and Klidi-Florina basins host commercial grade lignite deposits of Upper Miocene age. Vegora deposit was mined in the past, whereas the Kleidi deposit is currently mined, even though there are a series of technical problems. The Komnina deposit is not exploited so far. In all three deposits clayey diatomite is developed as overburden. As a result, in both areas Vegora and Kleidi significant quantities of mining wastes are exposed, which have specific mineralogy and technical characteristics (Owen *et al.*, 2010).

The Kleidi area is part of a broader chain of Neogene basins in western Macedonia. The basin extends from southern Serbia, in a NNW-SSE direction, up to the hills of Kozani through the cities of Florina, Amynteo and Ptolemais. The specific chain of basins is almost 100 km long and 15 - 20 km wide (Ilia *et al.*, 2009).

Fe and Fe-Ca phosphates such as vivianite and anapaite occur, locally in abundance, in the quarry faces as replacements of plant debris and leaves, and spherical faecal pellets <1cm in size respectively.

2.1.2 Sarantaporo-Elasson Basin, Thessaly

Upper Miocene clayey diatomite rocks with thickness of more than 100m occur near Giannota and Lykoudi villages, north of Ellassona town in Thessaly (Stamatakis and Koukouzas, 2001; Stamatakis, 2004). Bulk samples extracted from certain places of the basin have been tested for their suitability as a pozzolanic additive and the production of lightweight aggregates (LWA) (Fragoulis *et al.*, 2004).

The basin is part of the SE extension of the western Macedonian basins of Upper Miocene age and is associated with the Drymos-Elassona Basin that lies southern and contains also clayey diatomaceous rocks (Ilia *et al.*, 2009).

Fe-Ca phosphates such as anapaite and mitridatite (surface samples) and Fe-phosphates such as vivianite (borehole samples) occur in both basins in the form of organic material replacements (Stamatakis and Koukouzas, 2001).

2.1.3 Samos Island, east Aegean Sea

Diatomaceous rocks (opal-A-rich) are present in the uppermost beds of the Late Miocene sedimentary rocks of Mytilinii Basin, east Samos (Stamatakis *et al.*, 1989). At lower stratigraphic levels diatomite has been transformed to porcelanite (opal-CT-rich) as a result of the action of diagenetic alterations in a saline-alkaline environment. Most of the deposits are CaO-rich with medium silica polymorphs content (25-40%) such as those of Chora, Mavratzei and Kakkari stratigraphic sections (Stamatakis *et al.*, 1989). Some of the Samos deposits were evaluated as cement additives and for the production of synthetic wollastonite (CaSiO₃), because of their mineralogical and chemical composition and sufficient reserves (Bedelean *et al.*, 1998; Stamatakis *et al.*, 2000)

The opal-A and opal-CT-rich beds overlie a porcelaneous limestone that is rich in opal-CT (Stamatakis, 1988). Greenish tuff up to 20m thick partially covers the opaline rocks (Stamatakis *et al.*, 1989).

2.1.4 Milos Island central Aegean Sea

Milos Island is located in the Central Aegean Sea, representing an active member of the South Aegean Volcanic Arc. The substrate of the island is mainly composed of lavas and volcanoclastic rocks. Diatomaceous rocks of Upper Pliocene through Lower Pleistocene age, ranging in thickness from few centimeter up to ~20 meters have been located successively alternated and interbedded with ash, pumice and lapilli tuffs in various parts of Milos, such as in Xylokeratia and Frago in the SW coast, in Adamas Bay and in Alimia-Sarakiniko-Agia Irini located at the north coast of Milos. Some of the deposits have been tested as pozzolanic additive, due to their dual yielding of reactive silica phases, namely opal-A and volcanic glass (Fragoulis *et al.*, 2002; Stamatakis *et al.*, 2003)

In the active quarry of pozzolanic rocks, where dark-colored marlstone and lapilli tuffs are co-extracted with light grey pumice tuffs and yellowish-white diatomaceous rocks, two distinct snow-white



Fig. 1: The sampling sites (red diamonds)

diatomite beds with total thickness of 5m are developed. A black lava sill laterally penetrates the diatomite beds altering the amorphous opal-A to poorly crystallised opal-CT (Stamatakis *et al.* 2009).

2.2 Samples

2.2.1 Diatomaceous Rocks

Four bulk diatomaceous rock samples of 70 kg each were collected from Kleidi-Florina, Sarantaporo-Elassona, Chora-Samos and Xylokeratia-Milos. The Kleidi-Florina sample was extracted from the currently exposed 30m thick overburden of the lignite deposit, located north of Kleidi village, the Sarantaporo-Elassona sample was collected from currently developed trenches of 5m thick and 50m long, about 1km west of Lykoudi village, the Samos sample was collected from a technical outcrop up to 100m thick, ~ 1km north of Chora village, whereas the Milos sample is the thinnest among the others, having a total thickness of ~3m and was extracted from the interbedded tuffs in the TITANs Xylokeratia Quarry of Pozzolanas located in the SW part of the island, (Fig. 1). The Spanish sample is a very fine-grained snow-white industrial product that is widely used as filter-aid for filtering of beer and oils.

2.2.2 Olive oil wastes (alpechin)

The OOW used in this experiment was collected from a three-phase centrifugal olive processing plant (olive mill), located at Kyparissia, Messenia Prefecture, Greece.

All samples were fine-grained and homogenous. Their colour varied according to their mineral content; the Samos and Milos samples being poor in common clays have off-white colour, whereas the Kleidi and Sarantaporo samples are dark coloured due to their high clay minerals content.

2.3 Analytical Techniques

2.3.1 X-Ray Diffraction (XRD)

The mineralogy of two sieved fractions [$<0.3\text{mm}$ and 0.3 to 1.7mm] of the crushed, milled [1min] and homogenized diatomaceous rocks was studied by X-ray diffraction, on a Siemens Model 5005 X-ray diffractometer in combination with the DIFFRACplus software package. The diffractometer was operated using CuK α radiation at 40 kV and 40 mA and employing the following scanning parameters: 0.020°/s step size. The raw files were evaluated by use of the EVA 10.0 program of the Siemens DIFFRACplus-D5005 software package.

2.3.2 Scanning Electron Microscopy (SEM)

SEM techniques were performed on a SEM-EDS JEOL-JSM5600. The SEM was performed on diatomite rock chips on a JEOL JSM-5600 microscope with an OXFORD LINK™ ISIS™ energy dispersive X-Ray Microanalyzer. Conditions: Acceleration Voltage 20 KV, Beam current 0.5 nA, Livetime 50 s, Beam diameter $< 2 \mu\text{m}$.

2.3.3 Chemical analysis and grain size

Chemical analysis by X-Ray fluorescence was performed on a XRF PHILIPS PW1010 XRF spectrometer and grain size measurements were performed by the SILAS granulometer at TITAN SA laboratories, based in Kamari Viotia Cement Plant.

2.3.4 Determination of oil absorption values

The absorption capacity of the samples was measured by a technique (oil absorption) followed by the British Geological Survey analytical laboratories at Keyworth (Inglethorpe 1992). Through a burette OOW is added drop wise to 1g of dry sample in a glass plate and mixed using a palette knife. The addition of oil ceases when a smooth paste is formed. The paste should spread without cracking or crumbling and should only adhere to glass plate. The aforementioned method was scaled up in order to simulate a semi-industrial trial trying the absorption capacity of up to 100g of dried raw material. The absorption experiments were conducted on the same day of the OOW sample collection.

3. Results

3.1 Mineralogy

All samples studied contain, besides the crystalline constituents, an amorphous silica phase (opal-A) as shown by the presence of a broad peak (hump) between 20° and 26° 2θ in the X-ray diffractogram. Sieving of the samples in two fractions ($<0.3\text{mm}$ and 0.3 to 1.7mm) resulted to samples with no mineralogical variation (Table 1). The main mineral phases of all diatomaceous rocks studied is the amorphous phase opal-A that is predominantly represented by diatom frustules of various sizes and degree of preservation and secondarily by silicoflagellate skeletons and sponge spicules (Fig. 2) (Stamatakis *et al.*, 2009).

The Kleidi-Florina deposit is characterized by its high non-expandable clay content and traces of dolomite. The Sarantaporo-Elassona deposit has the most peculiar mineralogy as it contains expandable clays such as smectite and vermiculite, and also micro-particles of biogenic opal-A.

The Chora-Samos deposit is characterized by its high calcite and aragonite content and the absence

Table 1. The main mineral phases in the diatomitic deposits.

Sample	Mineralogical Composition										
	O-A	Cc/Ar	VG	Ver	Chl	Qtz	Fld	Ill/Mc	Dol	Ka	Sm/Sap
SRD-1	MJ			MD	TR	MD	MD	MD			MD
SRD-2	MJ			MD	TR	MD	MD	MD			MD
KLF-1	MD				MD	MD	MD	MJ	TR	TR	
KLF-2	MD				MD	MD	MD	MJ	TR	TR	
SMS-1	MD	MJ				TR		TR			
SMS-2	MD	MJ				TR		TR			
MLS-1	MJ		TR			TR	MD	TR			MD
MLS-2	MJ		TR			TR	MD	TR			MD
SPN-1	MJ					TR					

O-A: opal-A, VG: volcanic glass, Cc: calcite, Dol: dolomite, Ar: aragonite, Qtz: quartz, Fld: feldspar, Chl: chlorite, Sap: saponite, Ill: illite, Mc: muscovite, Ka: kaolinite, Sm: smectite, Ver: vermiculite. MJ: major, MD: medium, TR: minor-trace component.

SMS: Samos, SRD: Sarantaporo-Elassona, KLF: Kleidi-Florina, MLS: Milos, SPN: Alba-cete, Spain. Opal-A and volcanic glass [amorphous phases] were distinguished by SEM analysis.

of clay minerals. Apart from traces of quartz, detrital minerals such as micas and feldspars are also absent. The Xylokeratia-SW Milos sample is characterized by its relatively high feldspar and saponite content and the presence of volcanic glass. All these minerals are most likely related to the weathering and alteration of volcanic derived parent rocks. The Spanish sample, being pure diatomite, is almost exclusively composed of opal-A.

Conclusively, Samos and Florina deposits are the poorest in opal-content, whereas the Spanish sample is the richest.

3.2 Texture of the amorphous phases

SEM analysis of several chip samples from each deposit revealed the differences in texture and degree of preservation of the diatom frustules and the other biogenic phases, a factor that might have a significant role in their absorption ability. The major differences are the following:

- Opal-A in Sarantaporo-Elassona deposit is almost exclusively composed of cylindrical diatom frustules, whereas few layers contain disk-shaped diatom species. The degree of preservation is high, as they retain their minute structure (Fig 2: A & B).
- The Kleidi-Florina deposit contains small amounts and sporadically disseminated disk-shaped diatom frustules in a clayey matrix. The degree of preservation is good to medium (Fig 2: C & D).
- The Xylokeratia-Milos deposit contains mostly broken diatom frustules and sponge spicules, most likely due to their detrital nature in a near shore environment (Fig 2: E & F).

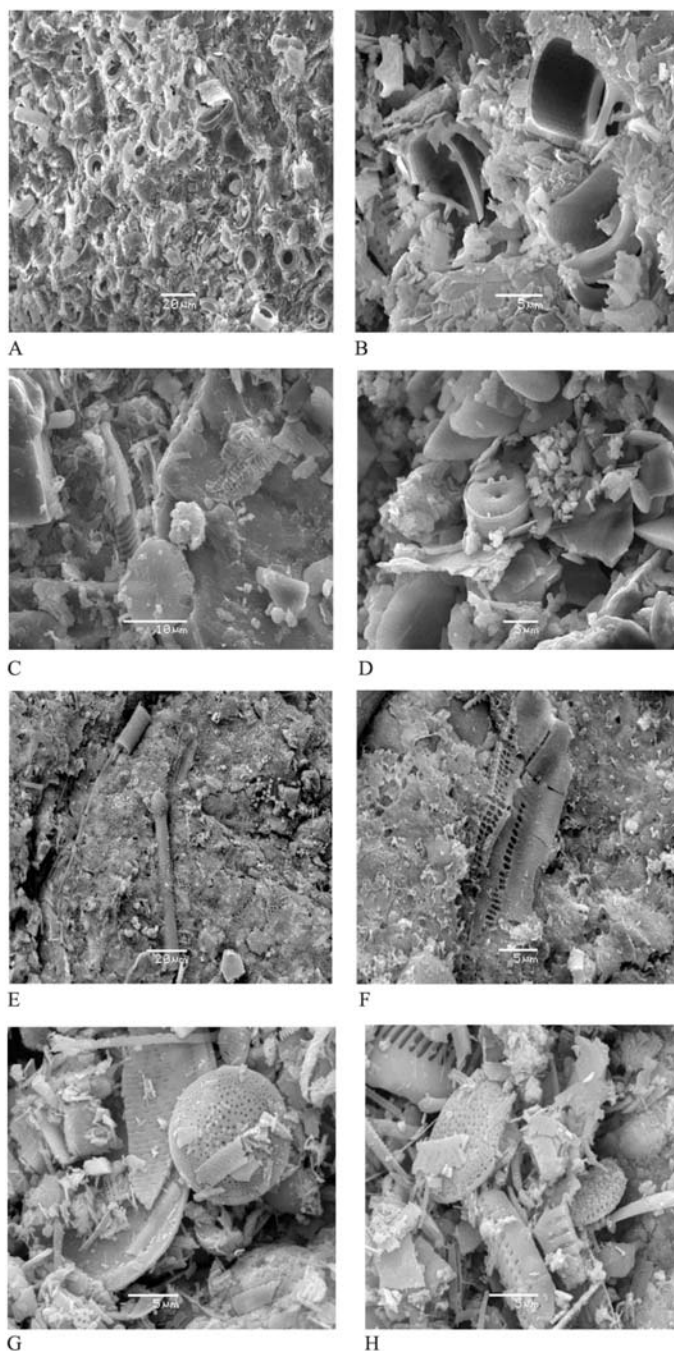


Fig. 2: SEM images of the samples studied. The Sarantaporo-Elassona sample is very rich in cylindrical diatom frustules [A, B]. Kleidi-Florina sample contains scattered diatom frustules in a clayey matrix [C, D]. Xylokeratia Milos sample contains reworked, broken diatom frustules and sponge spicules hosted in a glassy and clayey matrix [H, F]. Chora-Samos is composed of disk shaped and boat-like diatom frustules that exhibit medium degree of preservation [G, H].

Table 2. Major element chemistry of bulk samples of the diatomaceous rocks studied.

Sample	SRD	KLF	SMS	MLS	SPN
	Content%				
Na ₂ O	0.62	1.26	0.19	2.55	<0.1
K ₂ O	2.58	1.93	0.23	0.82	<0.1
CaO	1.82	3.34	29.60	2.72	0.82
MgO	0.95	1.86	1.09	1.11	0.12
Fe ₂ O ₃	8.08	8.90	0.65	5.80	<0.1
Al ₂ O ₃	17.83	15.40	4.36	6.42	0.15
SiO ₂	61.11	63.60	36.84	70.83	95.85
LOI	7.37	3.78	26.62	9.50	3.20
Total	100.36	100.07	99.58	99.75	100.14

- The Chora-Samos deposit contains well preserved to intensely dissolved and broken disk-shaped and boat-like diatom frustules, due to diagenetic alterations at the lowermost part of the succession (Fig 2: G & H).

3.3 Chemical analysis

Major element analysis of the studied samples (Table 2) reflects their mineralogical composition. Hence, the carbonate minerals-rich sample of Samos has the highest CaO and LOI content. Alumina represents small amounts of clay minerals present. Silica is mostly applied to the opal-A silica polymorph. The high iron content of Sarantaporo-Elassona, Kleidi-Florina and Xylokeratia-Milos reflects their high amounts of clay minerals they contain. The higher MgO content of the Kleidi-Florina sample reflects its dolomite content. The highest alumina content of the Sarantaporo-Elassona and the Kleidi-Florina reflects their high content of aluminosilicate minerals (Tables 1 & 2). The chemically purest sample, concerning its total silica content is that of Albacete, Spain. The highest amount of potassium recorded in the Sarantaporo-Elassona sample is attributed to the presence of significant amounts of vermiculite and illite/muscovite.

3.4 Absorption capacity

In general, in various applications diatomite is used in natural, calcined or flux-calcined form. For absorption applications, diatomite is used in natural form and also calcined at temperatures from 400 up to 850°C (Georgiades and Stamatakis, 2010; Ilia *et al.*, 2009).

After their characterization, all samples were tested for their efficiency to absorb olive-oil wastes. Even though most of the currently used techniques grind the samples to obtain the <75µm fraction, we tested the industrially used size fraction of 0.3mm to 1.7mm, as well as the fine residual that has diameter <0.3mm. The samples absorption capacity was measured as described in Materials and Methods. The apparent density of the absorbent, as well as the specific gravity of the olive-oil wastes were measured and calculated respectively. The results are shown in Table 3.

Table 3. Technical characteristics of the samples studied and the olive-oil wastes.

	Sarantaporo		Spain	Milos		Samos		Kleidi	
Grain size [mm]	<0.3	0.3-1.7	<0.3	<0.3	0.3-1.7	<0.3	0.3-1.7	<0.3	0.3-1.7
Absorbent									
Mass [g]	27.5	34.0	4.6	25.7	28.4	29.1	34.5	40.2	36.0
Volume [mL]	49.5	51	31.0	50	50	50	52.5	53.5	46.0
Apparent Density [g/mL]	0.56	0.67	0.15	0.51	0.57	0.58	0.65	0.75	0.78
Olive oil wastes									
Volume [mL]	49.3	48.0	25.0	45.0	37.0	42.5	42.0	58.0	47.2
Mass [g]	50.2	48.9	25.5	45.8	37.7	43.3	42.7	58.7	48.9
Absorption %									
v/v	99.6	94.2	80.6	90.0	74.0	85.0	79.8	109.7	92.5
w/w	182.5	144.0	551	178.4	132.7	148.5	124.0	146.0	135.8

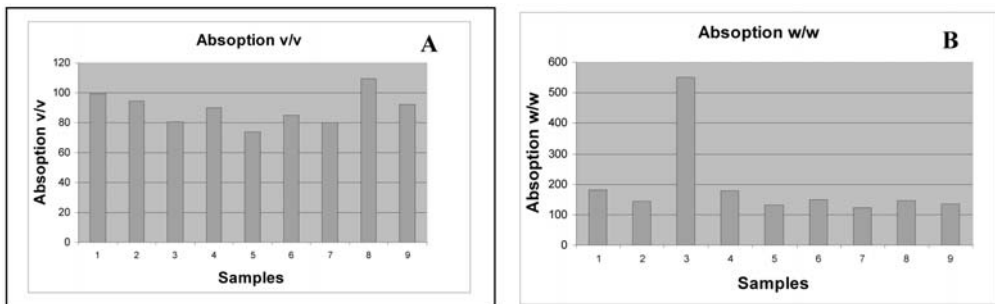


Fig. 3: Absorption capacity v/v% (A) and w/w% (B) of the studied samples [1 & 2 = Sarantaporo fine and coarse fraction, 3 =Spanish commercial sample [filter-aid], 4 & 5 = Milos fine and coarse fraction, 6 & 7 = Samos fine and coarse fraction, 8 & 9 = Kleidi fine & coarse fraction].

4. Discussion

As shown in Table 3 and Figure 3, the finest fraction of the samples [$<0.3\text{mm}$] has better absorption capacity than the $0.3\text{-}1.7\text{mm}$ fraction of all the Greek samples studied. This experimental observation can be attributed to the lower apparent density of the samples, and hence to their higher porosity. In Table 4 is pointed out the relation of the fineness of the particle sizes with the absorption capacity, whereas the amount of the wastes absorbed from each sample are presented in Figures 4 and 5, where it is clearly shown the association of the absorption capacity with the apparent density and the fineness of the sample. The higher absorption capacity of the finest fractions is due to both the finest particles of the clay minerals and the diatom frustules present in the samples. However, the highest absorption capacity of the Spanish sample is exclusively due to the diatom frustules absorption efficiency, as any clay or detrital minerals are practically absent.

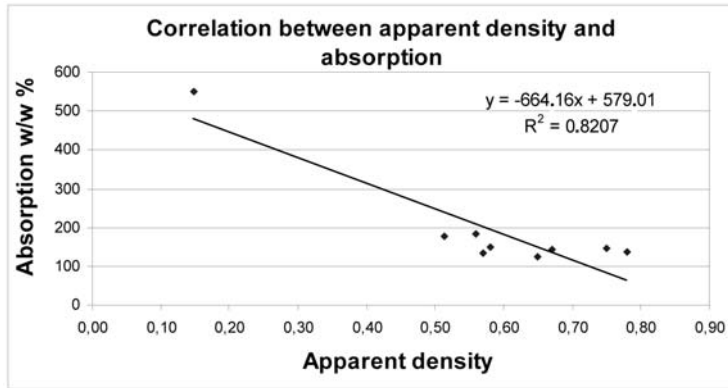


Fig. 4: Correlation between the apparent density and the absorption capacity of the samples studied.

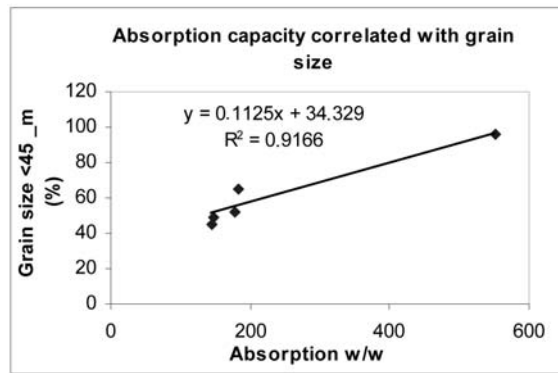


Fig. 5: The relation of the fineness at <45μm passing grain size and the absorption capacity [$<0.3\text{mm}$ fraction].

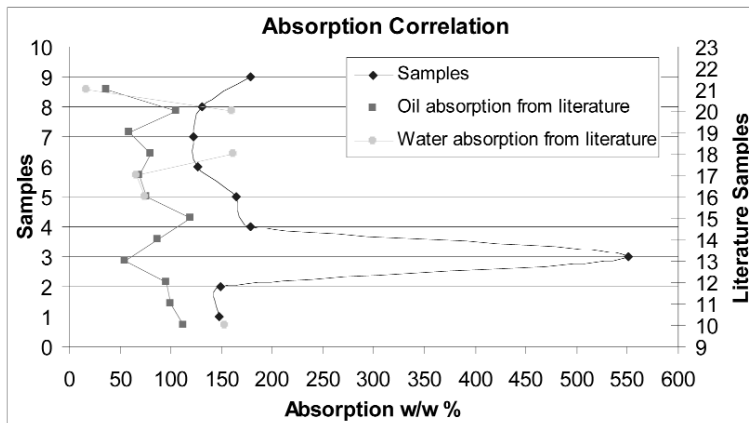


Fig. 6: Correlation of the Absorption Capacity of the nine samples measured [blue points] with literature data [red and yellow points] obtained from testing on oil and water absorption of commercial and laboratory samples of clayey and/or diatomaceous rocks (Makri and Stamatakis 2005; Georgiades and Stamatakis 2010; Ilia *et al.* 2009), Ediafilt kft – Hungarian data sheet, 2009).

Table 4. Correlation of the fineness at <45 μ m passing grain size % and the absorption capacity [<0.3 mm fraction]

absorption w/w	182.5	551	178.4	148.5	146
Grain size passing 45 μ m %	65	95.6	52.3	49	45.5

A correlation of the absorption capacity of the samples studied with literature data obtained from testing on oil and water absorption of commercial and laboratory samples of clayey and/or diatomaceous rocks is presented in Figure 6 (Makri and Stamatakis, 2005; Georgiades and Stamatakis, 2010; Ilia *et al.*, 2009).

In general, the samples studied as olive-oil waste absorbents exhibit equal or even better behaviour than the commercial or laboratory produced absorbents of reference oil and water, based on opal-A and/or clayey constituents. This is an indicator that the Greek diatomaceous rocks either clayey or calcareous might be tested in pilot-plant or an industrial scale to utilize them as industrial absorbents.

4. Conclusions

The olive-oil waste waters Absorption Capacity of the Greek studied diatomaceous rocks, ranges from 182.5% w/w to 124% w/w for Sarantaporo (<0.3mm) to Samos (0.3-1.7mm) samples respectively. The Spanish sample being a high added value specialty used commercially as filter-aid, has much higher absorption capacity. The higher absorption capacity of the Sarantaporo Ellassona sample most likely is attributed to the predominance of expanded clay minerals that have high absorption capacity such as smectite and vermiculite, and cylindrical diatom frustules in that sample, whereas the other samples are richer in other clay minerals and/or detrital constituents and carbonates.

The given measurements indicate that all the examined diatomite bulk samples are appropriate for use as absorption materials in an industrial scale. Literature data classifies as efficient absorbents powder samples that have an efficiency to absorb up to 60-70% of their weight in liquid, hence the samples studied are appropriate for such applications (Crosley, 2002).

A realistic price for such an industrial absorbent might be ~100\$/tn. Hence techno/economic assessment on certain diatomaceous deposits located close to olive-oil producing plants has to be carried out [i.e. in Samos, Lesbos, Zakynthos Crete and Milos islands, and also in Thessaly and in southernmost areas, where the major olive-oil industries and diatomaceous rocks have already been located. The used material could be used in local brick-making factories as source of silica, alumina and burnable matter. Trials on the efficiency of the diatomaceous rocks studied as absorbents of cheese waste-waters are currently being in progress.

5. Acknowledgements

Thanks are expressed by the authors to the Municipality of Sarantaporo-Ellassona (Major Mr, Klisiaris A.) for funding the NKUA for the current research (Contract No 70/3/10014). We also thank Emm. Chaniotakis, R&D Manager of TITAN Cement Company, Kamari Viotia Plant, Greece, for his helping in XRF and particle size analysis.

6. References

- Al-Malah, K., M. O. J. Azzam and N. I. Abu-Lail 2000. Olive mills effluent (OME) wastewater post-treatment using activated clay. *Separation and Purification Technology* 20(2-3): 225-234.
- Bedelean, I., D. Pop and H. Bedelean 1998. The usage of amorphous silica and hydrous aluminosilicates for the production of construction materials with improved mechanical properties. *INCO-Copernicus Project*: 68.
- Borja-Padilla, R., A. Martin-Martin and J. A. Fiestas Ros de Ursinos 1990. Effect of the inhibition of olive mill wastewater biomethanation in bioreactors with microorganisms immobilized on various types of support. *Grasas y Aceites* 41: 397-403.
- Cabrera, F., R. Lopez, A. MartinezBordiu, E. D. deLome and J. M. Murillo 1996. Land treatment of olive oil mill wastewater. *Int. Biodeterior. Biodegrad.* 38(3-4): 215-225.
- Crosley, P., 2002. Diatomite. *The Industrial Minerals: Thrills and Spills. Swell Times for absorbent minerals*. Surrey, UK, IMI Publication: 34-41.
- Fiestas Ros de Ursinos, J. A. and R. Borja-Padilla 1992. Use and treatment of olive mill waste water: current situation and prospects in Spain. *Grasas y Aceites* 43 (2): 101-106.
- Fragoulis, D., M. Stamatakis, D. Papageorgiou, L. Pentelenyi and G. Csirik 2002. Diatomaceous earth as a cement additive - A case study of deposits from North-eastern Hungary and Milos island, Greece. *ZKG Int* 55(1): 80-85.
- Fragoulis, D., M. G. Stamatakis, E. Chaniotakis and G. Columbus 2004. Characterization of lightweight aggregates produced with clayey diatomite rocks originating from Greece. *Materials Characterization* 53(2-4): 307-316.
- Georgiades, G. and M. G. Stamatakis 2010. Clayey Diatomite from a Deposit in Central Greece –A Multifunctional Raw Material for Absorption and Insulation. *Refractories Worldforum* 2 [1]: 82-88.
- Iliá, I. K., M. G. Stamatakis and M. Perraki 2009. Mineralogy and technical properties of clayey diatomites from north and central Greece. *Cent. Eur. J. Geosci.* 1(4): 393-403.
- Inglethorpe, S. D. J., 1992. Diatomite. *Industrial Minerals Laboratory Manual*. Keyworth, Nottingham, UK, British Geological Survey Technical Report WG/92/39: 1-36.
- Leahy, P. P., 2006. Diatomite. *Mineral Commodities Summary*. Reston, Va, USA, USGS, US Department of the Interior: 60-62.
- Makri, E. and M. Stamatakis 2005. The utilization of microporous materials in environmental applications. An example of use natural and calcined calcareous diatomite on the cleaning of fluid olive-oil-press waste, fluid animal waste and waste rich in phosphates. *Book of Proceedings, 2nd Congress of the Committee of Economic Geology, mineralogy and Geochemistry*: 199-208.
- McNamara, C. J., C. C. Anastasiou, V. O'Flaherty and R. Mitchell 2008. Bioremediation of olive mill wastewater. *Int. Biodeterior. Biodegrad.* 61(2): 127-134.
- Niaounakis, M. and C. P. Halvadakis 2006. *Olive Processing Waste Management - Literature Review and Patent Survey*. Oxford UK, Elsevier.
- Owen, R. B., R. W. Renaut and M. G Stamatakis 2010. Diatomaceous sedimentation in late Neogene lacustrine basins of western Macedonia, Greece. *Journal of Paleolimnology*: 1-17.
- Stamatakis, G., N. Tsantila, M. Samiotaki, G. N. Panayotou, A. C. Dimopoulos, C. P. Halvadakis and C. A. Demopoulos 2009. Detection and Isolation of Antiatherogenic and Antioxidant Substances Present in Olive Mill Wastes by a Novel Filtration System. *Journal of Agricultural and Food Chemistry* 57(22): 10554-10564.
- Stamatakis, M. G., 2004. Phosphate deposits of Neogene age in Greece. Mineralogy, geochemistry and genetic implications. *Chem Erde-Geochem* 64(4): 329-357.

- Stamatakis, M. G., D. Fragoulis, S. Antonopoulou and G. Stamatakis 2009. The opaline silica-rich sedimentary rocks of Milos Island, Greece I and their behavior as pozzolanas in the manufacture of cement. *Advances in Cement Research* Accepted.
- Stamatakis, M. G., D. Fragoulis, G. Csirik, I. Bedelea and S. Pedersen 2003. The influence of biogenic micro-silica-rich rocks on the properties of blended cements. *Cement Concrete Comp* 25(2): 177-184.
- Stamatakis, M. G., D. Fragoulis, A. Papageorgiou, E. Chaniotakis, J. Bedelea and G. Csirik 2000. Clinoptilolite-rich tuffs from Greece, Romania and Hungary and their industrial potential as cement additive. *3rd Congress of Mineral Wealth* 3: 451-457.
- Stamatakis, M. G., J. R. Hein and A. C. Magganas 1989. Geochemistry and Diagenesis of Miocene Lacustrine Siliceous Sedimentary and Pyroclastic Rocks, Mytilinii Basin, Samos Island, Greece. *Sediment Geol* 64(1-3): 65-78.
- Stamatakis, M. G. and N. K. Koukouzas 2001. The occurrence of phosphate minerals in lacustrine clayey diatomite deposits, Thessaly, Central Greece. *Sediment Geol* 139(1): 33-47.

COMPARATIVE FOURIER TRANSFORM INFRARED AND X-RAY POWDER DIFFRACTION ANALYSIS OF NATURALLY OCCURRED K-FELDSPARS

Theodosoglou E.¹, Koroneos A.¹, Soldatos T.¹, Zorba T.²,
and Paraskevopoulos K. M.²

¹ School of Geology, Aristotle University of Thessaloniki, 54124 Thessaloniki - Greece,
eltheod@geo.auth.gr, koroneos@geo.auth.gr, soldatos@geo.auth.gr

² Department of Physics, Aristotle University of Thessaloniki, 54124 Thessaloniki - Greece,
zorba@auth.gr, kpar@auth.gr

Abstract

Natural K-feldspars from igneous rocks have been examined by means of X-ray powder diffraction (XRPD) and Fourier transform infrared (FTIR) spectroscopy in the spectral range 400-1400 cm^{-1} , where the Si-Al-O bonds exhibit the dominant vibrations. From the XRPD analysis three species have been distinguished, i.e. microclines (3 samples), orthoclases (4 samples) and sanidines (3 samples); their unit cell parameters were calculated. The FTIR transmittance spectra of all samples have common bands at 426, 463, 584, 604, 726 and 772 cm^{-1} and some additional features. The spectra of sanidine and orthoclase exhibit fewer and broader bands than the microclines', especially in the area 1000-1200 cm^{-1} . The differences in their spectra are located in four bands. The bands at around 536-538 and 646-648 cm^{-1} in the spectrum of microcline, are shifted at around 542-544 and 640-642 cm^{-1} in the spectrum of orthoclase and at around 546 and 636 cm^{-1} in the spectrum of sanidine. Four bands at 1010, 1050, 1090 and 1136 cm^{-1} in the spectra of microcline are substituted with two quite broad bands at about 1030 and 1125 cm^{-1} in the spectra of orthoclase and sanidine. These differences are attributed to different degree of Al-Si ordering in the structure of K-feldspars.

Keywords: microcline, orthoclase, sanidine, FTIR, XRPD.

1. Introduction

One of the most common and well-examined mineral groups is feldspars. Several studies have been carried out concerning their structure, with various methods as X-ray powder diffraction (XRPD) and Fourier transform infrared spectroscopy (FTIR) and plenty of data have been produced (Barth, 1964; Hovis, 1986; Harris et al., 1989; Kronenberg et al., 1996; Zhang et al., 1997). However, the majority of the FTIR research has been focused on synthetic and/or single crystals. A small number of natural feldspar FTIR studies have been focused on single crystals and even fewer on powdered material. In this paper, naturally occurring K-feldspars from igneous rocks of Northern Greece are identified and classified with the X-ray diffraction techniques and their FTIR spectra are investigated. The aim of this paper is to present the first results of a comparative XRPD-FTIR study of the structure (unit cell parameters) and FTIR spectra of the K-feldspars.

Table 1. Classification of the samples.

Sample	Origin	Rock	Identification based on XRPD	
S 1	N. Almopia	Latite	Sanidine	
S 2	Samothraki	Rhyodacite	Sanidine	sample BR-02 Koroneos and Christofides (1985)
S 3	Samothraki	Rhyodacite	Sanidine	sample BR-03 Koroneos and Christofides (1985)
O 1	Xanthi	Granodiorite	Orthoclase	sample 162 (Christofides, 1977)
O 2	Xanthi	Monzonite	Orthoclase	sample 232 (Christofides, 1977)
O 3	Maronia, Komotini	Qtz Monzogab- bro	Orthoclase	sample MR-62 (Papadopoulou, 2002)
O 4	Maronia, Komotini	Qtz Monzogab- bro	Orthoclase	sample MR-74 (Papadopoulou, 2002)
M 1	Elatia, Drama	Bi Granodiorite P.	Microcline	sample 162 (Soldatos, 1985)
M 2	Kastoria	Hb-Bi Granodior- ite	Microcline	sample TH-17 (Grigoriadou, 2001)
M 3	Sithonia	Two Mica Gran- ite	Microcline	sample 100 (D'Amico et al., 1990)

2. Materials and Methods

2.1 Samples

The samples studied here are K-feldspars from various plutonic and volcanic rocks of Northern Greece (Table 1).

The K-feldspars were separated from the mafic minerals of the igneous rocks using a Franz model L-1 magnetic separator. Then, the K-feldspars were separated from the rest silic minerals using the Sodium Polytungstate (SPT) heavy liquid with a density of 2.58. Quartz, plagioclases and most of the perthitic phase were sunk and all the floating material was pure K-feldspar including some microperthitic phase. In cases where zeolites were present their separation was succeeded with the SPT heavy liquid having density 2.54. The grain size used for the separations was 100 to 150 μm . The pure K-feldspar concentrates were prepared by grinding them in an agate mortar to a size less than 63 μm . Concentrates with grain size between 20 and 63 μm were used for FTIR analysis and concentrates with size less than 20 μm were used for the XRPD analysis.

2.2. X-Ray Powder Diffraction (XRPD)

XRPD patterns were obtained on a PHILIPS PW 1820/00 X-ray diffractometer of the Department of Mineralogy-Petrology-Economic Geology, School of Geology, A.U.Th., equipped with a PW 1710 microprocessor and using PC-APD software. Operating conditions for all samples were 35 kV and 25 mA using Ni-filtered $\text{CuK}_{\alpha\text{ave}}$ radiation. The 2θ scanning range was between 3 and 63° and the scanning speed was $0.6^\circ/\text{min}$. The identification of the samples was made using the JCPDS-ICDD 2003 database. The calculations of the unit cell parameters (Table 2), as well as the refinements were made with CHECKCELL software. Silicon was used as external standard. The probability of Al-cation to occupy one of the T1 sites ($t_{10}+t_{1m}$) was calculated from Luth's equation (eq. 1) (Stewart and Wright, 1974).

$$T_1 = t_{10} + t_{1m} = \frac{c - 0.45132 * b - 1.22032}{1.6095 - 0.11252 * b} \quad (1)$$

2.3. Fourier Transform Infrared Spectroscopy (FTIR)

For the FTIR analysis the sample was homogenized with KBr with a ratio 1:100 (1.8 mg of the sample was homogenized with 180 mg KBr). The mixture was pressed for 3 minutes at 4 tn and for 10 minutes at 7 tn using a hydraulic hand press in an evacuated die into a 13 mm pellet. The pellets were dried at 110°C for 48 hours just before the collection of the spectra to avoid taking the spectra of the atmospheric water. The FTIR spectra in transmittance mode were recorded in the region of mid IR (MIR, 400 to 1400 cm^{-1}) and represent the average of 128 scans with resolution 2 cm^{-1} with a PERKIN-ELMER FTIR Spectrometer Spectrum1000 of the Solid State Physics Section, Physics Department, A.U.Th. As a reference was used a pure KBr pellet weighted 180 mg.

3. Results

3.1. XRPD

Representative XRPD patterns of the samples are presented in Fig. 1, their identification based on the ICCD patterns and their calculated unit cell parameters are presented in Tables 1 and 2, respectively. According to the XRPD patterns of the samples they are divided in three species: sanidines (S1, S2, S3), orthoclases (O1, O2, O3, O4) and microclines (M1, M2, M3). It must be noted here that in some samples a small amount of albite is observed. This is due to the concentration of albite in a perthitic form. Perthitic and microperthitic textures were observed under the petrographic microscope in the studied samples. In a better look this amount is present in the samples which had microperthites whereas the samples with perthites present almost pure K phase. The cause is the grain size of the samples during the heavy liquid separation. The rich-in-perthites particles were sunk but the poor-in-perthites ones were floated and mixed with the pure K end-member phase.

3.2. FTIR

In the mid-FTIR spectra (400 - 1400 cm^{-1}), the vibrations of Si and Al bonds with O in the structure of minerals (Si-O, Si-O-Si, Si-O-Al, etc.) are mainly observed (Figs 2a, b, c).

The spectra of all samples (Figs 2a, b, c) present six common bands at around 426 , 463 , 584 , 604 , 726 and 772 cm^{-1} (Table 3). In the spectral region from 1000 to 1200 cm^{-1} there are two quite broad bands, which in some samples appear to be split into four. The band at about 426 cm^{-1} in all sam-

Table 2. Unit cell parameters of the examined samples calculated from the XRPD data.

Sample	$A(\text{\AA})$	$b(\text{\AA})$	$c(\text{\AA})$	$\alpha(^{\circ})$	$\beta(^{\circ})$	$\gamma(^{\circ})$	$t,0+t,m$
S 1	8.3586	13.0021	7.1627	90.00	116.23	90.00	0.507
S 2	8.3661	13.0027	7.1620	90.00	116.29	90.00	0.501
S 3	8.4714	12.9891	7.1716	90.00	116.13	90.00	0.602
O 1	8.5546	12.9706	7.1737	90.00	116.02	90.00	0.663
O 2	8.5585	12.9680	7.1686	90.00	116.00	90.00	0.636
O 3	8.5412	12.9662	7.1683	90.00	115.99	90.00	0.638
O 4	8.5593	12.9838	7.1954	90.00	116.01	90.00	0.776
M 1	8.5230	12.8981	7.1940	90.39	115.88	88.85	0.964
M 2	8.5685	12.9452	7.2177	90.67	115.96	87.78	1.013
M 3	8.5571	12.9635	7.2172	90.73	115.93	87.75	0.969

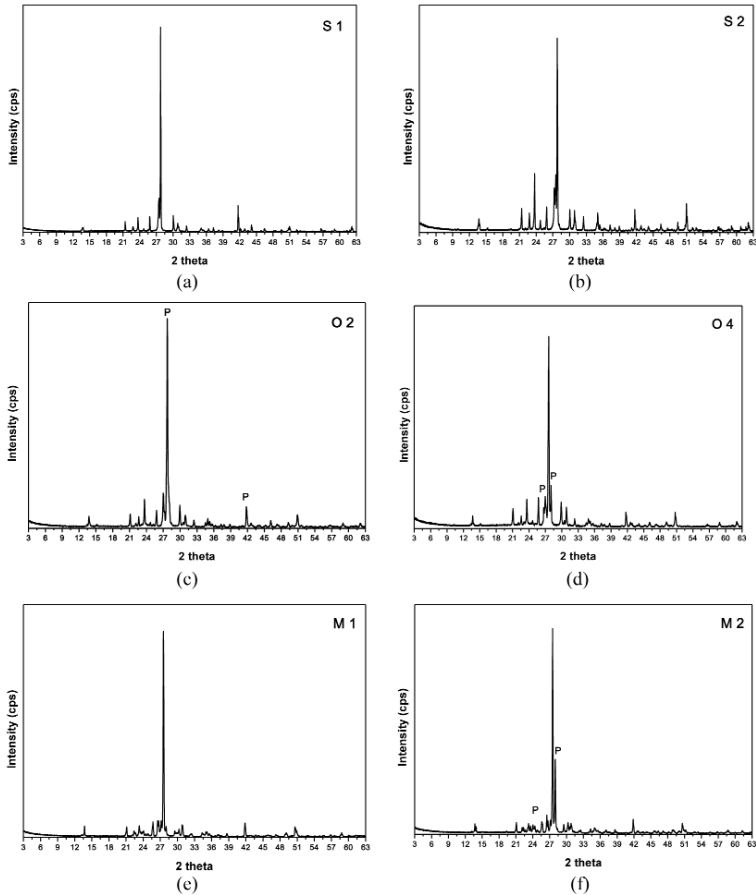


Fig. 1: Representative XRPD patterns (S: sanidine, O: orthoclase, M: microcline, P: Perthite)

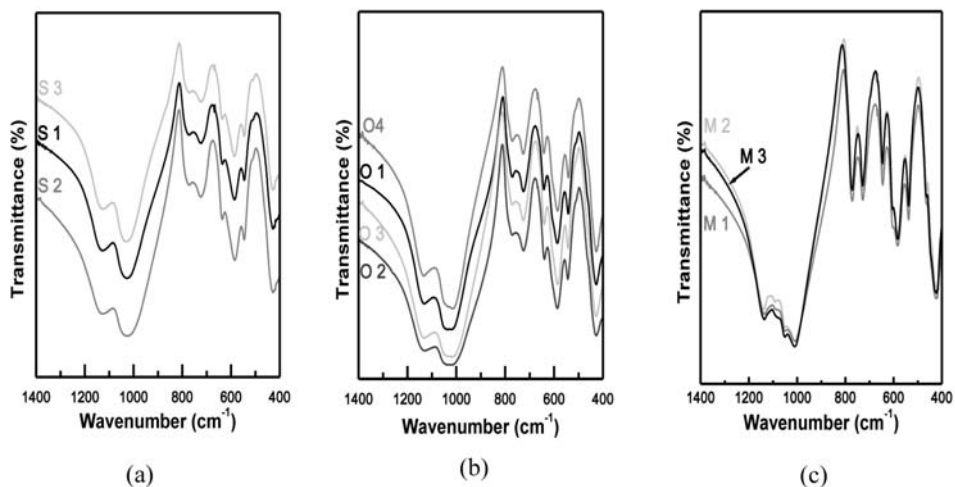


Fig. 2: FTIR spectra of the examined samples (S: sanidine, O: orthoclase, M: microcline).

ples is attributed to the O-Si-O deformation (Iiishi et al., 1971; Matteson and Herron, 1993). The band observed at about 463 cm^{-1} is due to the coupling of O-Si-O bending and the K-O stretching vibrations (Iiishi et al., 1971; Matteson and Herron, 1993). The bands at about 584 and 604 cm^{-1} are correlated to the O-Si(Al)-O bending vibrations of the three species. The bands at about 463 and 604 cm^{-1} appear as weak bands in all microcline spectra and as shoulders in all orthoclase spectra; in the sanidine spectra they are hardly distinguished. The bands at 726 and 772 cm^{-1} are, respectively, attributed to the Si-Al(Si) and the Si-Si stretching vibrations of the three species (Iiishi et al., 1971; Matteson and Herron, 1993). Also, in all samples two broad bands in the spectral areas 1010 - 1050 cm^{-1} and 1090 - 1136 cm^{-1} occur. Besides the afore-mentioned common bands, each K-feldspar species exhibits the following additional features:

Sanidine

The spectra of sanidines reveal two additional bands at around 546 and 636 cm^{-1} , not present in the spectra of orthoclases and microclines (Fig. 3, Table 3). The band at around 546 cm^{-1} is attributed to the coupling between the O-Si-O bending vibration and the K-O stretching vibration, whereas the band at 636 cm^{-1} corresponds to the O-Si(Al)-O bending vibrations (Iiishi et al., 1971; Matteson and Herron, 1993). Two quite broad bands are observed at about 1030 and 1125 cm^{-1} . These bands are due to the Si-O stretching vibration and especially the band at 1030 cm^{-1} may, also, be attributed to the Si(Al)-O stretching vibrations.

Orthoclase

In the spectra of all orthoclases, the 546 cm^{-1} band appeared in the spectra of sanidines is slightly shifted to lower wavenumbers at about 543 cm^{-1} (Fig. 3, Table 3). This band is due to the coupling between the O-Si-O bending vibration and the K-O stretching vibration (Iiishi et al., 1971; Matteson and Herron, 1993). Concerning the 636 cm^{-1} band in sanidines, it is shifted to higher wavenumbers at about 640 - 642 cm^{-1} in the spectra of all orthoclase samples. This band is attributed to the O-Si(Al)-O bending vibrations (Iiishi et al., 1971; Matteson and Herron, 1993). Additionally, there

Table 3. Observed frequencies (cm^{-1}) of the FTIR spectra for sanidine, orthoclase and microcline samples and their attribution.

	<i>Common</i>	<i>Sanidine</i>	<i>Orthoclase</i>	<i>Microcline</i>
426	O-Si-O deformation			
463	coupling between O-Si-O bending and K-O stretching vibrations			
536-538				coupling between O-Si-O bending and K-O stretching vibrations
542-544			coupling between O-Si-O bending and K-O stretching vibrations	
546		coupling between O-Si-O bending and K-O stretching vibrations		
584-604	O-Si(Al)-O bending vibrations			
636		O-Si(Al)-O bending vibrations		
640-642			O-Si(Al)-O bending vibrations	
646-648				O-Si(Al)-O bending vibrations
726-772	Si-Si(Al) and Si-Si stretching vibrations			
1010				Si(Al)-O stretching vibration
1030		Si(Al)-O and Si-O stretching vibrations	Si(Al)-O and Si-O stretching vibrations	
1050				Si(Al)-O stretching vibrations
1090				Si-O stretching vibration
1125		Si-O stretching vibration	Si-O stretching vibration	
1136				Si-O stretching vibration

are two broad bands, one at about 1030 cm^{-1} attributed to the Si-O and Si(Al)-O stretching vibrations and a second one at about 1125 cm^{-1} due to the Si-O stretching vibration.

Microcline

The spectra of microclines present a band at about 536-538 cm^{-1} (Fig. 3, Table 3) which is attributed to the coupling between the O-Si-O bending vibration and the K-O stretching vibration and it is shifted to lower wavenumbers than the bands in orthoclases and sanidines attributed to the same vibrations (Iiishi et al., 1971; Matteson and Herron, 1993). An inverse behavior presents the band that is appeared at about 646-648 cm^{-1} in the spectra of microclines. This band is attributed to the O-Si(Al)-O bending vibrations and is shifted to higher wavenumbers than the bands attributed to the same vibrations in the spectra of orthoclases and sanidines (Iiishi et al., 1971; Matteson and Herron, 1993). Another important difference in the spectra of microclines is the presence of four sharp bands in the region between 1000 and 1200 cm^{-1} instead of only two broad bands in the spectra of orthoclases and sanidines. The bands at around 1010 and 1050 cm^{-1} are both attributed to the Si(Al)-O stretching vibrations. The broad band at around 1090 cm^{-1} and a sharper one at around 1136 cm^{-1} are attributed to the Si-O stretching vibration (Iiishi et al., 1971; Couty and Velde, 1986).

4. Discussion

The basic structure of an alkali-feldspar consists of a three dimensional array of corner-sharing tetrahedra. Three of the four cation sites in their unit cell are occupied by Si-cation and the fourth by Al-cation. The high temperature forms of KAlSi_3O_8 , sanidine and perhaps orthoclase are monoclinic ($C2/m$) and the low temperature form, microcline, is triclinic ($C\bar{1}$). The K-feldspars rarely approximate the end-member composition and usually have a relatively high content of $\text{NaAlSi}_3\text{O}_8$. Although K and Na form a continuous solid solution series at high temperatures, on slow cooling unmixing takes place and the isomorphous series is destroyed. The solid solution is separated into two phases, a K-rich phase and a Na-rich one. The new texture generated from this unmixing is called cryptoperthitic, microperthitic or perthitic, depending on the size of the Na-rich areas. The new Na-rich phase into the K-rich phase is called cryptoperthite, microperthite or perthite, respectively (Deer et al., 1971; Smith and Brown, 1988). In some of the examined samples the presence of perthite is obvious, as revealed by the XRPD analysis combined with the petrographical data.

The infrared spectra of the investigated samples show quite common features. This observation is in agreement with Laves and Hafner (1956), Hafner and Laves (1957) and Martin (1970) observation for the infrared spectra of alkali-feldspars. The low temperature microclines and consequently highly ordered, show spectra with sharp and easily distinguished bands. On the other hand, the high temperature and presumably disordered sanidines have spectra with much broader and fewer bands, observed also by White (1974) and Moenke (1974). These aspects are correlated with the Al/Si disorder of the K-feldspars (Laves and Hafner, 1956; Hafner and Laves, 1957; Moenke, 1974). These, also, are observed in the spectra of the examined samples. All of the sanidine spectra have broader bands than the orthoclases and they have less and broader bands than the microclines.

All of the investigated samples present six common bands at 426 cm^{-1} (O-Si-O bending vibration), 584 cm^{-1} [O-Si(Al)-O bending vibrations], 726 cm^{-1} [Si-Si(Al) stretching vibrations] and 772 cm^{-1} (Si-Si stretching vibration). Of special interest and further investigation is the presence of two bands at around 463 and 604 cm^{-1} . In the spectra of microclines, these two bands appear as sharp and weak bands. The spectra of orthoclases present shoulders in the 463 and 604 cm^{-1} , whereas in the spectra of sanidines there is only an indication of the presence of these two bands. This behavior may be at-

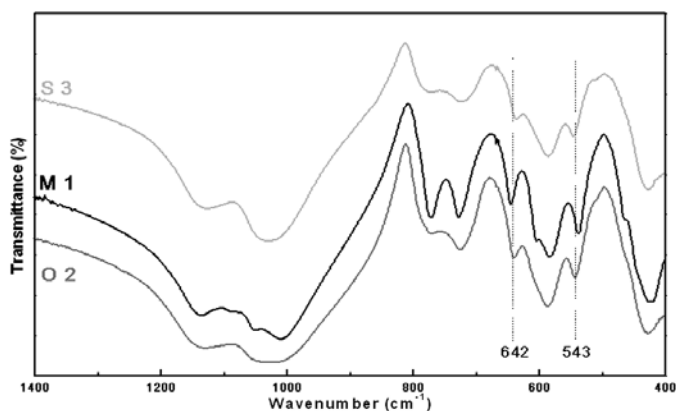


Fig. 3: FTIR spectra of representative samples of each species. The two vertical lines represent the exact positions of 542-544 and 640-642 cm^{-1} bands of orthoclase. Samples as in Fig. 1.

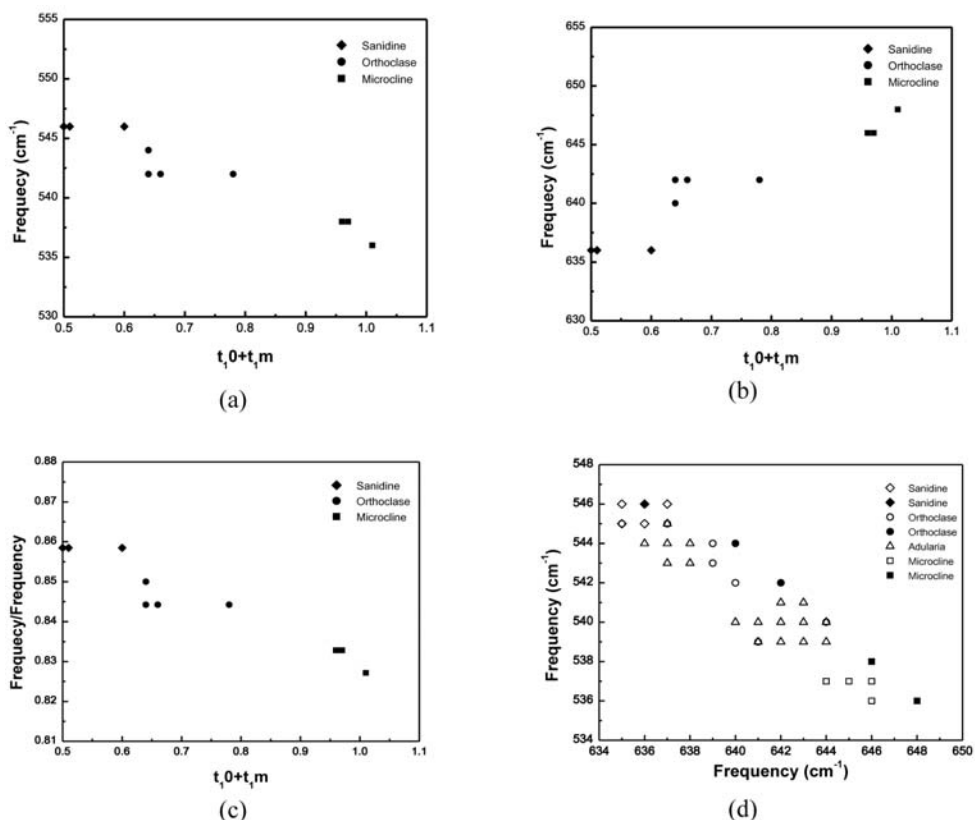


Fig. 4: a. First order-sensitive band versus $t_{10}+t_{1m}$. b. Second order-sensitive band versus $t_{10}+t_{1m}$. c. Ratio of the first to second order-sensitive band versus $t_{10}+t_{1m}$. d. Frequency/frequency diagram, after White (1974), showing the relation of the two sharp order-sensitive bands in the FTIR spectra of the samples. Data of the open symbols from Hafner and Laves (1957) are plotted for comparison along with the investigated samples (filled symbols).

tributed to the degree of ordering in the samples. Microclines, which present a good degree of ordering, exhibit sharper and distinct bands, whereas sanidines, which present the most disordered structure of the K-feldspars, appear only indications of their presence. Orthoclases, an intermediate phase, present shoulders in their spectra in these wavenumbers making certain their presence. Two common but very broad bands in the range of 1000 to 1200 cm^{-1} are attributed mainly to the Si-O stretching vibration.

The main differences in the spectra of the three species are the position of two bands that are shifted and associated with the O-Si-O bending vibration. These bands are correlated with the degree of ordering in the feldspars (Hafner and Laves, 1957; Harris et al., 1989; Matteson and Herron, 1993). The first order-sensitive band, appeared at around 546 cm^{-1} in the spectra of sanidines, is attributed to the coupling of O-Si-O bending and the K-O stretching vibrations and is shifted to lower wavenumbers at around 542-544 cm^{-1} in the spectra of orthoclases and at around 536-538 cm^{-1} in the spectra of microclines. The second order-sensitive band is observed at around 636 cm^{-1} in the spectra of sanidines and is attributed to the O-Si(Al)-O bending vibrations. This band is shifted to higher wavenumbers at around 640-642 and 646-648 cm^{-1} in the spectra of orthoclases and microclines, respectively. The plot of each order-sensitive band versus $t_{10}+t_{1m}$ is presented in Figures 4a and b. In Figure 4a it is observed that as the probability of Al-cation to occupy the T1 site increases, the first order-sensitive band shifts to lower wavenumbers. The opposite trend is observed in Figure 4b where the probability of T1 site to be occupied by Al-cation increases when the second order-sensitive band shifts to higher wavenumbers. In Figure 4c is presented the ratio of the first to second order-sensitive band versus $t_{10}+t_{1m}$. Increasing the $t_{10}+t_{1m}$, the ratio of these bands is decreasing. This observation is in agreement with the aspects of Hafner and Laves (1957), Harris et al. (1989) and Matteson and Herron (1993). In Figure 4d are presented the two order-sensitive bands in a frequency-frequency diagram. In the same diagram are presented data from natural K-feldspars from Hafner and Laves (1957) to compare the samples from Northern Greece to K-feldspars of other igneous rocks all around the world. The plot of the samples from Hafner and Laves (1957) is in agreement with the results of the samples investigated in this paper.

From the diagram of Figure 4d it is concluded that the frequency/frequency ratio is higher in the most disordered K-feldspars (sanidines), with the lowest $t_{10}+t_{1m}$, and lower in the most ordered ones (microclines), with the higher $t_{10}+t_{1m}$. Orthoclases which are an intermediate form, have ratios in between those of sanidines and microclines.

5. Acknowledgments

We would like to thank G. Christofides, G. Eleftheriadis and L. Papadopoulou who offered the samples from Xanthi, Almopia and Maronia respectively, as well as the anonymous reviewer for the very constructive comments, improving the quality of the paper. Also, the first author would like to thank the State Scholarships Foundation of Greece for financial support.

6. References

- Barth, T.F.W., 1964. On the constitution of the alkali-feldspars. *Tschermaks min. u. petr. Mitt.*, Bd. 10, H. 1-4, 14-33.
- Christofides, G., 1977. Contribution to the study of the plutonic rocks of Xanthi area. *PhD Thesis*, Aristotle University of Thessaloniki, 249pp.
- Couty, R., & Velde, B., 1986. Pressure-induced band splitting in infrared spectra of sanidine and albite. *Am. Mineral.*, 71, 99-104.

- D' Amico, C., Christofides, G., Eleftheriadis, G., Bargossi, G. M., Campana, R. & Soldatos, T., 1990. The Sithonia Plutonic Complex (Chalkidiki, Greece). *Miner. Petr. Acta*, XXXIII, 177.
- Deer, W.A., Howie, R.A. & Zussman, J., 1971. *Rock forming minerals, Vol. 4. Framework silicates*. London, Longman Group, 435pp.
- Grigoriadou, A., 2001. Mineralogy of Kastoria pluton. *Diploma Thesis*, Aristotle University of Thessaloniki, 57pp.
- Hafner, S. & Laves, F., 1957. Ordnung/Unordnung und Ultrarotabsorption II. Variation der Lage und Intensität einiger Absorptionen von Feldspäten. *Z. Kristallogr.*, 109, 204-225.
- Harris, M.J., Salje, E.K.H., Güttler, B.K. & Carpenter, M.A., 1989. Structural states of natural potassium feldspar: An infrared spectroscopic study. *Phys. Chem. Minerals*, 16, 649-658.
- Hovis G.L., 1986. Behavior of alkali feldspars: Crystallographic properties and characterization of composition and Al-Si distribution. *Am. Mineral.*, 71, 869-890.
- Iiishi, K., Tomisaka, T., Kato, T., Yamaguchi & Umegaki, Y., 1971. Isomorphous substitution and infrared and far infrared spectra of the feldspar group. *N. Jb. Miner. Abh.*, 115, 1, 98-119.
- Koroneos, A. & Christofides, G., 1985. Preliminary investigation on Al, Si distribution in K-feldspars from Samothraki island (N. Aegean Sea). *Mineral Wealth*, 37, 27-32.
- Kronenberg, A.K., Yund, R.A. & Rossman, G.R., 1996. Stationary and mobile hydrogen defects in potassium feldspar. *Geochim. Cosmochim. Acta*, 60, 4075-4094.
- Laves, F. & Hafner, S., 1956. Ordnung/Unordnung und Ultrarotabsorption I. (Al,Si)-Verteilung in Feldspäten. *Z. Kristallogr.*, 108, 52-63.
- Martin, R.F., 1970. Cell parameters and infrared absorption of synthetic high to low albites. *Contr. Mineral. Petrol.*, 26, 62-74.
- Matteson, A. & Herron, M.M., 1993. End-member feldspar concentrations determined by FTIR spectral analysis. *Journal of Sedimentary Petrology*, 63(6), 1144-1148.
- Moenke, H.H.W., 1974. Silica, the three-dimensional silicates, borosilicates and beryllium silicates. In Farmer, V. C. (ed). *The infra-red spectra of minerals*. 365-382, London, Mineralogical Society, 539pp.
- Papadopoulou, L., 2002. Mineral phase equilibria, crystallization condition and evolution of Maronia pluton, Thrace, Greece. *PhD Thesis*, Aristotle University of Thessaloniki, 336pp.
- Smith, J.V. & Brown, W.L., 1988. *Feldspar minerals, Vol. 1. Crystal structures, physical, chemical and microtextural properties*. Berlin, Springer Verlag, 828pp.
- Soldatos, T., 1985. Petrology and Geochemistry of the Elatia Plutonite (Central Rhodope, Macedonia, N. Greece). *Ph. D. thesis*, Univ. of Thessaloniki, 320 pp.
- Stewart, D.B & Wright, T.L., 1974. Al/Si order and symmetry of natural alkali feldspars, and the relationship of strained cell parameters to bulk composition. *Bull. Soc. Minéral. Cristallogr.*, 97, 356-377.
- White, W.B., 1974. Order-Disorder effects. In Farmer, V. C. (ed). *The infra-red spectra of minerals*. 87-110, London, Mineralogical Society, 539pp.
- Zhang, M., Salje, E.K.H., Carpenter, M.A., Parsons, I., Kroll H., Reed, S.J.B. & Graeme-Barber, A., 1997. Exsolution and Al-Si disorder in alkali feldspars: Their analysis by infrared spectroscopy. *Am. Mineral.*, 82, 849-857.

UPTAKE ABILITY OF ZEOLITIC ROCK FROM SOUTH XEROVOUNI, AVDELLA, EVROS, HELLAS

**Tzamos E.¹, Filippidis A.¹, Kantiranis N.¹, Sikalidis C.², Tsirambidis A.¹,
Papastergios G.¹, Vogiatzis D.³**

¹ School of Geology, Dept. of Mineralogy-Petrology-Economic Geology, Aristotle University, 54124 Thessaloniki, tzamos@geo.auth.gr, anestis@geo.auth.gr, kantira@geo.auth.gr, ananias@geo.auth.gr, gpapaste@geo.auth.gr

² Dept. of Chemical Engineering, Aristotle University, 54124 Thessaloniki, sikalidi@eng.auth.gr

³ School of Geology, Dept. of Geology, Aristotle University, 54124 Thessaloniki, dvogias@geo.auth.gr

Abstract

Zeolitic rock samples from South Xerovouni contain on average, 57 wt.% HEU-type zeolite, 6 wt.% clay minerals, 3 wt.% mica (total of 66 wt.% microporous minerals), 19 wt.% feldspars, 10 wt.% cristobalite and 5 wt.% quartz (total of 34 wt.% non-microporous minerals). Chemically the zeolitic rock consists mainly of 69.9 wt.% SiO₂, 13.2 wt.% Al₂O₃, 1.2 wt.% Fe₂O₃, 1.0 wt.% MgO, 3.0 wt.% CaO, 1.5 wt.% Na₂O and 2.2 wt.% K₂O. The zeolitic rock shows an average ammonia ion exchange capacity of 150 meq/100g. HEU-type zeolite accounts for the most of the uptake ability, while clay minerals and mica contribute to a relative small extent only. The uptake ability of the five zeolitic rock samples showed positive correlations with the content of HEU-type zeolite as well as with the total content of microporous minerals (zeolite + mica + clay minerals). Such materials could be used in a wide range and scale of agricultural, aquacultural, and environmental applications.

Key words: zeolite, HEU-type, Xerovouni, CEC, mineralogy.

1. Introduction

Zeolites constitute a major class of crystalline hydrated aluminosilicate microporous minerals including both natural and synthetic species (Breck, 1974). The crystalline framework of the zeolites is based on a three dimensional network of (Si,Al)O₄ tetrahedral and extra-framework alkali and alkaline-earth cations, which are loosely bound to the anionic charges within this framework structure and can be exchanged for other cations, including H⁺. High quality natural zeolites have many applications in industry, agriculture and the environment (e.g., Merkle and Slaughter, 1968; Barrer, 1978; Mumpton, 1978; Pond and Mumpton, 1984; Gottardi and Galli, 1985; Dyer, 1988; Tsitsishvili et al., 1992; Misaelides et al., 1993; Holmes, 1994; Ming and Mumpton, 1995; Misaelides et al., 1995a,b; Filippidis et al., 1996; Godelitsas et al., 1996a,b; Filippidis and Kassoli-Fournaraki, 2000; Bish and Ming, 2001; Kantiranis et al., 2002; Filippidis, 2008; Filippidis et al., 2008, 2009). The great majority of these applications employs their cation exchange capabilities and involves the replacement of the existing extra-framework cations with other cations from the surrounding environment. Due to the favourable ion-exchange selectivity of natural zeolites for certain cations, these minerals have been studied for potential use in the treatment of nuclear, municipal and industrial

wastewaters and acid mine drainage waters. It is of economic importance that natural zeolites are used in their natural state so that expensive purification is avoided.

Zeolite-bearing rocks occur in a variety of geologic settings; mostly as alteration or authigenic minerals, low temperature-pressure minerals in metamorphic systems, secondary minerals in weathering zones or in vein-deposits. Commercially interesting zeolites are presently limited to authigenic and alteration settings in finely crystalline sedimentary rocks (Mumpton, 1978). Zeolites are widespread in Greece and clinoptilolite is the most common type (e.g., Tsolis-Katagas and Katagas, 1989, 1990; Stamatakis et al., 1996; Filippidis and Kassoli-Fournaraki, 2000; Kantiranis et al., 2002). Clinoptilolite is a high silica member of the heulandite group of natural zeolites and occurs in abundant and easily mined, sedimentary deposits in many parts of the world (Mumpton, 1988). The composition and purity of natural clinoptilolites and therefore their physicochemical properties vary widely between deposits and may even vary within the same deposit (Mercer and Ames Jr, 1978; Kassoli-Fournaraki et al., 2000).

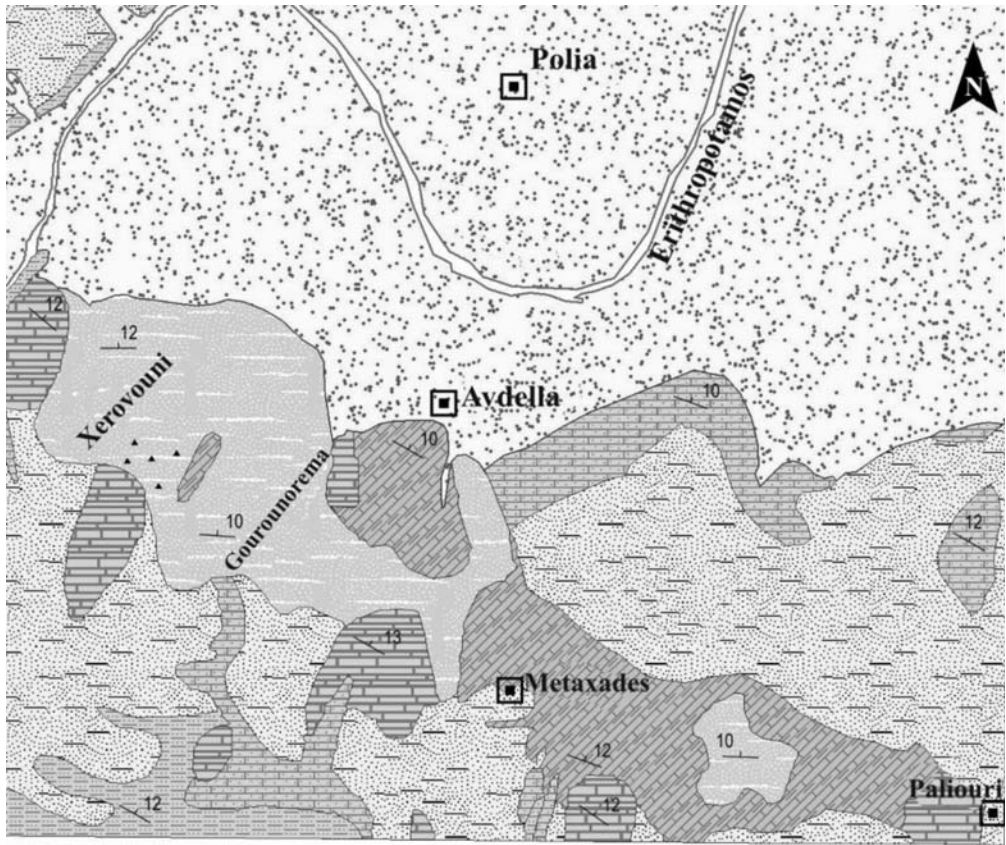
The present study investigates the relationship between the mineralogy and the uptake ability of HEU-type zeolite-bearing tuffs from south Xerovouni, Avdella, Evros, Hellas.

2. Geological setting

The Metaxades upper Eocene zeolite-bearing volcanoclastic sediments belong to the Orestias Tertiary molassic basin of the northeastern Thrace in Greece. This meta-Alpine basin has an elongated shape and extends into Bulgaria. It is dominated by sediments of Eocene to Pleistocene age, deposited unconformably on the crystalline basement of the Rhodope massif. In the investigated area (Fig. 1) the formations recognized are (Koutles et al., 1995): Eocene formations consisting of: a) breccias-conglomerates (10-15 m thick), which lie unconformably upon the metamorphosed basement. Their composition is phyllitic, gneissic, amphibolitic, quartzitic or andesitic; they display a grading from coarser to finer fragments upwards, b) gray siltstones (~100 m thick) with psammitic and marly interlayers, c) mostly semi-loose sandstones (40-50 m thick) of varying grain-size, including very thin clayey interlayers, d) white to pale gray, yellow or green zeolite-bearing volcanoclastic tuffs (20-25 m of visible thickness) conformably deposited on the sandstones or siltstones; a thin layer of gray marl is discernible on the upper part of the tuffs, e) loose white-yellowish marly limestone (510 m thick) and f) limestone (less than 30 m thick) rich in fossils. Oligocene formations of relatively great thickness, unconformably deposited on the Eocene formations. They consist of gray clays, red-yellowish sandstones, white-yellow siltstones and interlayers of marly limestone. Quaternary sediments of varying thickness, deposited over all previous formations. The complete sequence of the above formations is not always present in all sites of the basin. One or more formations may be locally absent due to tectonic activity, erosion or non-deposition. In the broader area, two main visible faults and several fractures have been observed.

3. Materials and Methods

Five zeolitic tuff samples were taken from South Xerovouni of Avdella-Metaxades area (Fig. 1), in order to determine their mineralogical and chemical composition, petrographic characteristics, and uptake ability. The samples were studied in their bulk form, ground (<125 μm) and homogenized. Samples for mineralogical and chemical analyses were ground further in an agate mortar, while thin sections were prepared for microscopic study. Chemical analyses of samples were carried out by AAS on a Perkin Elmer 5000 spectrometer equipped with a graphite furnace.



LEGEND

-  Holocene fluvio-terrestrial formations
-  Plio-Pleistocene formations
-  Limestones
-  Marly limestones
-  Volcaniclastic tuffs
-  Sandstones
-  Siltstones
-  15 Strike and dip of beds
-  Samples location
-  Village

0 300 600 m



Fig. 1: Geological map and samples locations (modified, Koutles et al., 1995).

The mineralogical composition of the samples was determined by X-ray Powder Diffraction (XRPD) method. The XRPD analysis was performed using a Philips PW1710 diffractometer with Ni-filtered CuK_α radiation on randomly oriented samples. The counting statistics of the XRPD study were: step size: $0.01^\circ 2\theta$, start angle: 3° , end angle: 63° and scan speed: $0.02^\circ 2\theta/\text{sec}$. Quantitative estimates of the abundance of the mineral phases were derived from the XRPD data, using the intensity of certain reflections and external standard mixtures of minerals (Kantiranis et al., 2004).

In order to determine the sorption ability of each zeolite-rich sample, the samples were treated with 1M ammonium acetate (NH_4OAc) aqueous solution, according to the AMAS method (Bain and Smith, 1987). Approximately 125 mg of each $<125 \mu\text{m}$ sample was added to a centrifuge tube with 10 mL of the 1N NH_4OAc solution. The suspensions were well shaken, agitated for 24 hours, and then centrifuged. The clear liquid was discarded and the NH_4OAc -saturation procedure repeated 9 times, adding fresh 10 mL of NH_4OAc solution each time. After the completion of the 10-day NH_4OAc -saturation, the excess NH_4OAc was washed with 10 mL of 99% isopropyl alcohol, well shaken, and centrifuged. The clear supernatant liquid was discarded and the procedure repeated five times. The samples then were dried in room temperature. Following the NH_4OAc saturation, the NH_4^+ ions retained by the zeolite-rich samples, are converted using a strong base to NH_3 and analysed by an ammonia electrode. The NH_3 concentration was determined using an Orion potentiometric ammonia gas electrode combined with a Jenway 3045 pH/mV/ion analyser. Each air-dried NH_4^+ -saturated sample was placed in a 100 mL Pyrex beaker containing a Teflon covered stirring bar. Deionised nitrogen-free water (50 mL) was added and the solution was stirred to suspend the sample. The electrode was immersed into the suspension taking care to prevent entrapment of air under the concave tip. By addition of 0.5 mL of 10M NaOH, the NH_3 measurements were taken at constant level achievement. The electrode calibration was performed daily using ammonium calibrating solutions of 10, 100 and 1000 ppm provided by Jenway and hourly using the 10 ppm ammonium solution.

4. Results and Discussion

The study of the thin sections show the presence of zeolite, mica (biotite), clay minerals (mainly smectite), feldspars, quartz and amorphous material (Fig. 2). Also, were recognized glass shards, i.e. sites of altered volcanic glass, which consist from outer to inner of clay minerals and fine zeolite crystals (Fig. 3).

The semi-quantitative mineralogical composition (wt. %), the total micro-porous mineral content (wt. %) and the uptake ability of all samples are presented in Table 1. The major mineral phase present in the studied samples is found to be HEU-type zeolite, with percentages varying from 42 wt.% (sample X1) to 67 wt.% (sample X4), with an average amount of 57 wt.%. These results are in good agreement with previous studies on the zeolitic tuffs of Metaxades Area, which report an average amount of 58 wt.% in HEU-type zeolite (Marantos et al., 1989; Tsirambides et al., 1989, 1993; Tsirambides, 1991; Filippidis, 1993; Misaelides et al., 1994a,b, 1995a,b; Koutles et al., 1995; Symeopoulos et al., 1996; Haidouti, 1997; Tserveni-Gousi et al., 1997; Sikalidis, 1998; Yannakopoulos et al., 1998; Vlessidis et al., 2001; Filippidis and Kassoli-Fournaraki, 2002; Katranas et al., 2003; Papadopoulos et al., 2004; Filippidis and Kantiranis, 2005; Kantiranis et al., 2006; Filippidis et al., 2007). In minor amounts plagioclase (5-21 wt.%), K-feldspar (4-19 wt.%), cristobalite (3-17 wt.%), quartz (3-8 wt.%), micas (3-4 wt.%) and clay minerals (4-11 wt.%), were also determined. The total percent of micro-porous minerals (zeolite + micas + clays minerals) vary from 49 wt.% (sample X1) to 75 wt.% (sample X4), while feldspars + quartz + cristobalite constitute the non-microporous content of the samples varying between 25 wt.% (sample X4) and 51 wt.% (sample X1).

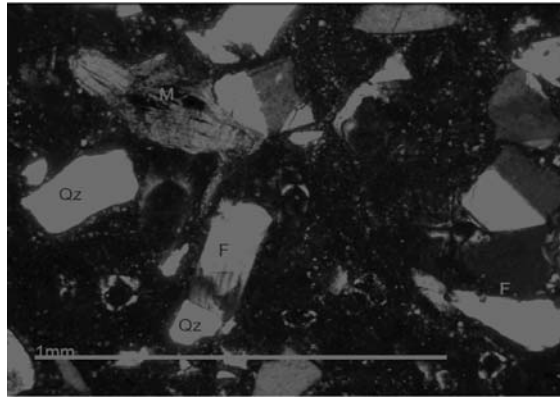


Fig. 2: Representative microphotograph of the studied samples. Qz=Quartz, M=Mica (biotite), F=Feldspars (Nicols +).

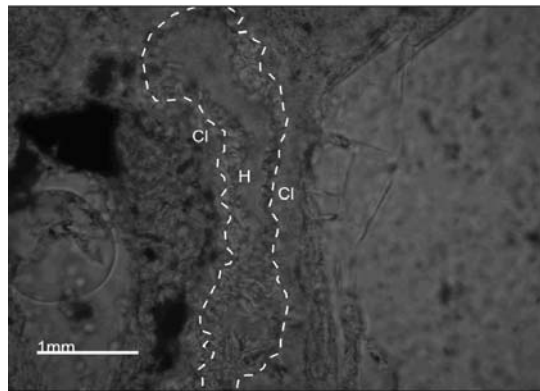


Fig. 3: A glass shard (white line). H=HEU-type zeolite, Cl=Clay minerals (Nicols //).

The chemical compositions of the zeolite-bearing rock samples are presented in Table 2. All samples contain high amounts of SiO₂ varying between 69.24 wt. % (sample X1) and 70.63 wt. % (sample X4). The Al₂O₃ content measured from 12.12 wt. % (sample X4) to 14.57 wt. % (sample X1). Low amounts of TiO₂, MnO and Fe₂O_{3T} were also found. The total percentage of oxides of the exchangeable cations Mg, Ca, Na, and K vary between 6.84 wt. % (sample X4) and 9.11 (sample X1) with a mean value of 7.75 wt.%. These cations mainly came from the zeolite framework, but also high amounts of feldspars and /or micas + clays may affect their content, especially in sample X1. Loss of ignition varies between 6.07 wt.% (sample X1) and 9.42 wt.% (sample X4).

The chemical formula of the HEU-type zeolite in the studied area, calculated from microprobe analyses of prior studies (Tsirambides et al., 1993; Koutles et al., 1995; Kantiranis et al., 2006) is Ca_{2.1}K_{0.5}Mg_{0.3}Na_{0.3}Al_{6.3}Si_{29.9}O₇₂·18.9H₂O.

The measured uptake ability varies between 111 meq/100g (sample X1) and 176 meq/100g (sample X4), with an average value of 150 meq/100g for all five samples (Table 1). This value is in very good agreement with the theoretical value of 152 meq/100g calculated taking in considerations the mineralogical composition of the samples and the theoretical ion exchange capacity values of clinop-

Table 1. Semi-quantitative mineralogical composition (wt.%) and uptake ability (meq/100g) of the South Xerovouni samples.

Sample	X1	X2	X3	X4	X5	Average
HEU-type zeolite	42	62	52	67	59	57
Micas (Biotite)	3	3	4	3	4	3
Clay Minerals	4	6	11	5	5	6
K-Feldspars	19	8	9	6	4	9
Plagioclases	21	8	9	6	5	10
Quartz	8	3	4	3	6	5
Cristobalite	3	10	11	10	17	10
Micro-porous minerals	49	71	67	75	68	66
Uptake ability	111	164	143	176	156	150

Table 2. Whole rock chemical analyses (wt.%) of South Xerovouni samples.

Sample	X1	X3	X4	Average
SiO ₂	69.24	69.91	70.63	69.93
TiO ₂	0.08	0.10	0.07	0.08
Al ₂ O ₃	14.57	12.81	12.12	13.17
Fe ₂ O ₃ t	1.25	1.30	0.92	1.16
MnO	0.09	0.09	0.11	0.10
MgO	0.89	1.22	0.92	1.01
CaO	2.75	2.89	3.33	2.99
Na ₂ O	2.47	1.21	0.90	1.53
K ₂ O	3.00	1.98	1.69	2.22
L.O.I.*	6.07	8.63	9.42	8.04
<i>Total</i>	<i>100.41</i>	<i>100.13</i>	<i>100.10</i>	<i>100.23</i>

*LOI=Loss of Ignition

tilolite (254 meq/100g, Mumpton, 1977), smectite (100 meq/100g, Deer et al., 1992) and biotite (25 meq/100g, Deer et al., 1992).

The comparison between the mineralogical composition and the uptake ability, results in positive correlation between the uptake ability and the wt.% composition in zeolite and total micro-porous minerals. The correlation coefficients were found 0.99 and 0.95 respectively (Figs 4 and 5).

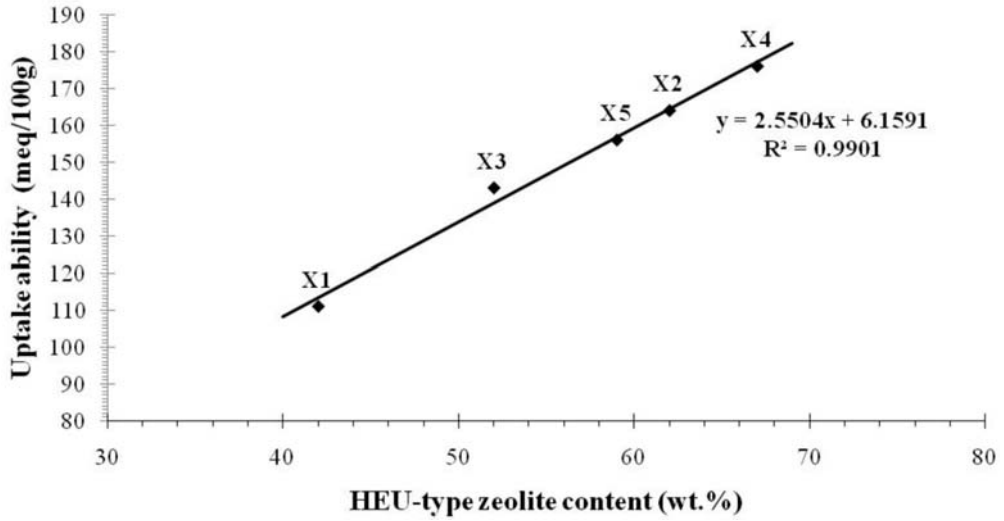


Fig. 4: Correlation of HEU-type zeolite content vs uptake ability of South Xerovouni samples.

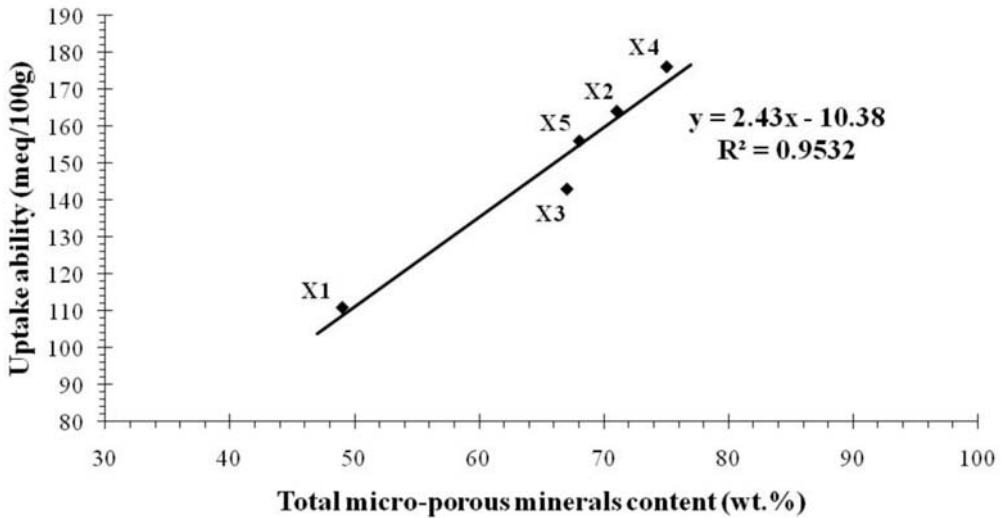


Fig. 5: Correlation of total micro-porous minerals content vs uptake ability of South Xerovouni samples.

The measured uptake abilities gives the opportunity of utilizing the studied South Xerovouni zeolitic tuffs in a wide range of environmental applications, such as: improvement of drinking water, purification of municipal and industrial wastewaters and wastewater treatment units, conversion of sewage sludge and manure to odourless fertilizer, oxygen enrichment of aqua, fishery and fish breeding for production of healthier food, soil amendment, odour control and gas purification and drying systems.

5. Conclusions

Five zeolitic tuff samples were taken from South Xerovouni of Avdella-Metaxades area, in order to determine their mineralogical and chemical composition, petrographic characteristics, and uptake ability. The major mineral phase present in the studied samples is found to be HEU-type zeolite, with an average amount of 57 wt.%. In minor amounts plagioclase, K-feldspar, cristobalite, quartz, micas and clay minerals, were also determined. The total percent of micro-porous minerals (zeolite + micas + clay minerals) vary from 49 to 75 wt.%, while the non-microporous content between 25 and 51 wt.%. All samples contain high amounts of SiO₂ varying between 69.24 and 70.63 wt. %. The Al₂O₃ content measured from 12.12 to 14.57 wt. %, while low amounts of TiO₂, MnO and Fe₂O_{3T} were also found. The total percentage of oxides of the exchangeable cations Mg, Ca, Na, and K vary between 6.84 and 9.11 wt.% with a mean value of 7.75 wt.%. These cations mainly came from the zeolite framework, but also high amounts of feldspars and /or micas + clays may affect their content. Loss on ignition vary between 6.07 and 9.42 wt.%. The measured uptake ability varies between 111 and 176 meq/100g, with an average value of 150 meq/100g for all five samples, showing a positive correlation with the zeolite and total micro-porous minerals content.

6. References

- Bain, C. & Smith, L., 1987. Chemical analysis. In: Wilson M. (ed.), A handbook of determinative methods in clay mineralogy, Glasgow, Blackie, 248-274.
- Barrer, R.M., 1978. Zeolite and Clay Minerals as Sorbents and Molecular Sieves, New York, Academic Press, 499pp.
- Bish, D.L. & Ming, D.W., 2001. Natural Zeolites: Occurrence, Properties, Applications. Mineralogical Society of America, *Reviews in Mineralogy and Geochemistry*, vol. 45, Washington DC, 654 p.
- Breck, D.W., 1974. Zeolite Molecular Sieves, Structure, Chemistry and Use, New York, J. Wiley, 771pp.
- Deer, W.A., Howie, R.A. & Zussman, J., 1992. An Introduction to the Rock-Forming Minerals, 2nd edn. London, Longman, 696pp.
- Dyer, A., 1988. An Introduction to Zeolite Molecular Sieves, Chichester, J. Wiley, 149pp.
- Filippidis, A. 1993. New find of moissanite in the Metaxades zeolite-bearing volcanoclastic rocks, Thrace County, Greece. *Neues Jahrbuch fur Mineralogie Monatshefte*, 11, 521-527.
- Filippidis, A. 2008. Treatment and recycling of municipal and industrial waste waters using Hellenic Natural Zeolite: A Review. AQUA 2008, 3rd Intern. Conf. Water Science and Technology (Athens, 16-19/10), CD-Proceedings, 5p.
- Filippidis, A. & Kantiranis, N., 2005. Industrial, agricultural and environmental uses of the natural zeolites of Thrace. Proc. Sci. Meet. of G.S.G. (Samothraki, 2-4/9), *Bull. Geol. Soc. Greece*, 37, 90-101 (in Greek with English summary).
- Filippidis, A. & Kassoli-Fournaraki, A., 2002. Management of aquatic ecosystems using Greek natural zeolites. 12th Sem. Environmental Protection (Thessaloniki, 2-5/12), Proceedings, 75-82 (in Greek).
- Filippidis, A. & Kassoli-Fournaraki, A., 2000. Environmental uses of natural zeolites from Evros district, Thrace, Greece. In: Anagnostopoulos A. (Ed.), Proc. 5th Int. Conf. on Environ. Pollution. 149-155, Thessaloniki, G. Korakidis Press, 1026pp.
- Filippidis, A., Godelitsas, A., Charistos, D., Misaelides, P. & Kassoli-Fournaraki, A., 1996. The chemical behavior of natural zeolites in aqueous environments; interaction between low-silica zeolites and 1M NaCl solutions of different pH-values, *Applied Clay Science* 11, 199-209.
- Filippidis, A., Kantiranis, N., Stamatakis, M., Drakoulis, A. & Tzamos, E., 2007. The cation exchange capacity of the Greek zeolitic rocks. *Bull. Geol. Soc. Greece*, 40(2), 723-735.

- Filippidis, A., Apostolidis, N., Paragios, I. and Filippidis, S. 2008. Zeolites clean up. *Industrial Minerals*, April, 68-71.
- Filippidis, A., Papastergios, G., Apostolidis, N., Paragios, I., Filippidis, S. and Sikalidis, C. 2009. Oderless and cohesive zeo-sewage sludge produced by Hellenic Natural Zeolite treatment. 3rd AMIREG Intern. Conf. Assessing the Footprint of Resource Utilization and Hazardous Waste Management (Athens, 7-9/9), Proceedings, 96-100.
- Godelitsas, A., Misaelides, P., Charistos, D., Filippidis, A. & Anousis, I., 1996a. Interaction of HEU-type zeolite crystals with Thorium aqueous solutions. *Chem. Erde* 56, 143-156.
- Godelitsas, A., Misaelides, P., Filippidis, A., Charistos, D. & Anousis, I., 1996b. Uranium sorption from aqueous solutions on sodium-form of HEU-type zeolite crystals. *J. Radioan. Nucl. Ch. Ar.* 208, 393-402.
- Gottardi, G. & Galli, E., 1985. *Natural zeolites*, Berlin, Springer, 409pp.
- Haidouti, C., 1997. Inactivation of mercury in contaminated soils using natural zeolites. *The Science of the Total Environment*, 208, 105-109.
- Holmes, D.A., 1994. Zeolites. In: *Industrial Minerals and Rocks* (D.D. Carr, ed.), Braun-Brumfield, Michigan, 1129-1158.
- Kantiranis, N., Chrissafis, C., Filippidis, A. & Paraskevopoulos, K., 2006. Thermal distinction of HEU-type mineral phases contained in Greek zeolite-rich volcanoclastic tuffs. *European Journal of Mineralogy*, 18(4), 509-516.
- Kantiranis, N., Stamatakis, M., Filippidis, A. & Squires, C. 2004. The uptake ability of the clinoptilolitic tuffs of Samos Island, Greece. *Bull. Geol. Soc. Greece*, 36(1), 89-96.
- Kantiranis, N., Filippidis, A., Mouhtaris, Th., Charistos, D., Kassoli-Fournaraki, A. & Tsirambides, A., 2002. The uptake ability of the Greek natural zeolites, ZEOLITE '02, 6th Int. Conf. on the Occurrence, Properties and Utilization of Natural Zeolites, Thessaloniki (June, 3-7 2002), 155-156.
- Kassoli-Fournaraki, A., Stamatakis, M., Hall, A., Filippidis, A., Michailidis, K., Tsirambides, A. & Koutles, Th., 2000. The Ca-rich clinoptilolite deposit of Pentalofos, Thrace, Greece. In: Collela C. & Mumpton F.A. (Eds.), *Natural Zeolites for the Third Millennium*, Napoli, De Frede Editore, 193-202.
- Katranas, T.K., Vlessidis, A.G., Tsiatouras, V.A., Triantafyllidis, K.S. & Evmiridis, N.P., 2003. Dehydrogenation of propane over natural clinoptilolite zeolites. *Microporous and Mesoporous Materials*, 61, 189-198.
- Koutles, Th., Kassoli-Fournaraki, A., Filippidis, A. & Tsirambides, A. 1995. Geology and geochemistry of the Eocene zeolitic-bearing volcanoclastic sediments of Metaxades, Thrace, Greece. *Estudios Geologicos*, 51, 19-27.
- Marantos, I., Koshiaris, G., Karantasi, S. & Gregoriadis, G., 1989. A study on zeolitic alteration of Tertiary pyroclastics from Metaxades area, Evros County, Greece. *Bull. Geol. Soc. Greece*, 23(2), 443-450 (in Greek with English abstract).
- Mercer, B.W. & Ames, Jr.L.L., 1978. Zeolite Ion Exchange in Radioactive and Municipal Wastewater treatment. In: Sand L.B. & Mumpton F.A. (Eds.), *Natural Zeolites, Occurrence, Properties, Uses*, Oxford, Pergamon Press, 451-459.
- Merkle, A.B. & Slaughter, M., 1968. Determination and refinement of the structure of heulandite. *American Mineralogist* 53, 1120-1138.
- Ming, D.W. & Mumpton, F.A., 1995. *Natural zeolites '93: Occurrence, Properties, Use*, International Committee on Natural zeolites, New York, Brockport, 622pp.
- Misailidis, P., Godelitsas, A. & Filippidis A., 1994a. Cesium uptake by zeoliferous rocks from Metaxades, Thrace, Greece. 15th Pan-Hellenic Chemistry Congress, Thessaloniki, Proc. A, 218-221 (in Greek with English summary).

- Misaelides, P., Godelitsas, A. & Filippidis A. 1995a. The use of zeoliferous rocks from Metaxades-Thrace, Greece, for the removal of caesium from aqueous solutions. *Fresenius Environmental Bulletin*, 4, 227-231.
- Misaelides, P., Godelitsas, A., Charistos, V., Ioannou, D. & Charistos, D., 1994b. Heavy metal uptake by zeoliferous rocks from Metaxades, Thrace, Greece: An exploratory study. *Journal of Radioanalytical and Nuclear Chemistry*, Articles, 183, 159-166.
- Misaelides, P., Godelitsas, A., Filippidis, A., Charistos, D. & Anousis, I., 1995b. Thorium and uranium uptake by natural zeolitic materials. *The Science of the Total Environment*, 173/174, 237-246.
- Misaelides, P., Godelitsas, A., Haristos, D., Noli, F., Filippidis, A. & Sikalidis, C., 1993. Determination of heavy metal uptake by the sodium form of heulandite using radiochemical techniques. *Geol. Carpath.-Ser. Clays* 44, 115-119.
- Mumpton, F.A., 1977. Mineralogy and geology of natural zeolites, Mineralogical Society of America, vol. 4, Virginia Blacksburg.
- Mumpton, F.A., 1978. Natural zeolites: A new industrial mineral commodity. In: Sand B.L. & Mumpton F.A. (eds.), *Natural zeolites: Occurrences, Properties, Uses*. New York, Pergamon Press, 3-27.
- Mumpton, F.A., 1988. Development and uses for natural zeolites: a critical commentary. In: Kallo D. & Sherry H.S. (Eds.), *Occurrence, Properties and Utilization of Natural Zeolites*, Budapest, Akademiai Kiado, 333-365.
- Papadopoulos, A., Fatta, D., Parperis, K., Mentzis, A., Haralambous, K.J. & Loizidou, M., 2004. Nickel uptake from a wastewater stream produced in a metal finishing industry by combination of ion-exchange and precipitation methods. *Separation and Purification Technology*, 39, 181-188.
- Pond, G.W. & Mumpton, F.A., 1984. *Zeo-Agriculture: Use of Natural Zeolites in Agriculture and Aquaculture*, Colorado, Westview Press, 305pp.
- Sikalidis, C.A., 1998. Heavy metals and toxic elements removal from contaminated waters by clay minerals and zeolite bearing rocks. Fourth Int. Conf. on Environmental Pollution, Thessaloniki, Proceedings, 102-110.
- Stamatakis, M., Hall, A. & Hein, R., 1996. The zeolite deposits of Greece. *Mineralium Deposita* 31, 473-481.
- Symeopoulos, B., Soupioni, M., Misaelides, P., Godelitsas, A. & Barbayiannis, N. 1996. Neodymium sorption by clay minerals and zeoliferous rocks. *Journal of Radioanalytical and Nuclear Chemistry*, Letters, 212, 421-429.
- Tservedi-Gousi, A.S., Yannakopoulos, A.L., Katsaounis, N.K., Filippidis, A. & Kassoli-Fournaraki, A., 1997. Some interior egg characteristics as influenced by addition of Greek clinoptilolitic rock material in the hen diet. *Archiv fur Getrugelkunde*, 61, 291-296.
- Tsirambides, A., 1991. Study of zeoliferous volcanoclastic sediments of Metaxades Evros. *Mineral Wealth*, 72, 41-48 (in Greek with English summary).
- Tsirambides, A., Filippidis, A. & Kassoli-Fournaraki, A., 1993. Zeolitic alteration of Eocene volcanoclastic sediments at Metaxades, Thrace, Greece. *Applied Clay Science*, 7, 509-526.
- Tsirambides, A., Kassoli-Fournaraki, A., Filippidis, A. & Soldatos, K., 1989. Preliminary results on clinoptilolite-containing volcanoclastic sediments from Metaxades, NE Greece. *Bull. Geol. Soc. Greece*, 23, 451-460.
- Tsitsishvili, G.V., Andronikashvili, T.G., Kirov, G.N. & Filizova, L.D., 1992. *Natural zeolite*. New York, Ellis Horwood, 274pp.
- Tsolis-Katagas, P. & Katagas, C., 1989. Zeolites in pre-caldera pyroclastic rocks of the Santorini volcano, Aegean sea, Greece. *Clays and Clay Minerals* 37, 497-510.
- Tsolis-Katagas, P. & Katagas, C., 1990. Zeolitic diagenesis of Oligocene pyroclastic rocks of the Metax-

ades area, Thrace, Greece. *Mineralogical Magazine* 54, 95-103.

Vlissidis, A.G., Triantafillidis, C.S. & Evmiridis, N.P., 2001. Removal and recovery of p-phenylenediamines developing compounds from photofinishing lab washwater using clinoptilolite tuffs from Greece. *Water Research*, 35, 1603-1608.

Yannakopoulos, A., Tserveni-Gousi, A., Kassoli-Fournaraki, A., Tsirambides, A., Michailidis, K., Filipidis, A. & Lutat, U., 2000. Effects of dietary clinoptilolite-rich tuff on the performance of growing-finishing pigs. In: Collela C. & Mumpton F.A. (Eds.), *Natural Zeolites for the Third Millennium*, Napoli, De Frede, 471-481.

ON THE OCCURRENCE OF A VOLCANIC ASH LAYER IN THE XYLOKASTRO AREA, NORTH PELOPONNESUS, GREECE: MINERALOGY AND GEOCHEMISTRY

Vasilatos Ch.¹, Vlachou-Tsipoura M.², and Stamatakis M.G.¹

¹ National & Kapodistrian University of Athens, Faculty of Geology & Geoenvironment,
Department of Economic Geology & Geochemistry, Panepistimiopolis, Ano Ilissia, 157 84 Athens, Greece,
vasilatos@geol.uoa.gr, stamatakis@geol.uoa.gr

² National & Kapodistrian University of Athens, Faculty of Geology & Geoenvironment,
Department of Mineralogy & Petrology, Panepistimiopolis, Ano Ilissia, 157 84 Athens, Greece,
mvlachou@geol.uoa.gr

Abstract

This paper reports, for the first time, the occurrence of an ash layer intercalated within the Plio-Pleistocene lacustrine deposits near Xylokastro area, North Peloponnesus, Greece. Petrographic and geochemical characteristics of the ash layer are the basis of this study. An attempt was made to correlate the present findings to the reported data from other ash deposits. The composition of the ash bed showed a dacitic to rhyolitic calc alkaline suit. The geochemistry of the volcanic ash indicates high crustal contamination of the lava and points to an origin from the northwest part of the Aegean volcanic arc.

Key words: Volcanic ash, glass shards, pumice, traces element geochemistry, tephrostratigraphy, western Aegean Volcanic Arc, Greece.

1. Introduction

Tephrochronology in its original sense is the use of tephra layers as time-stratigraphic marker beds to establish numerical or relative ages (Lowe et al., 2002). Tephra layers have been described and studied in Greece.

Because tephra beds provide essentially instantaneous chronostratigraphic marker horizons, or isochrons, that can be correlated between sites independently of radiometric dating, they provide a way of circumventing the various interpretative difficulties associated with radiocarbon dating very recent (last millennia) archaeological and paleoenvironmental (natural) sites. Because tephra deposits are found in both archaeological and natural sites, they have the capacity for linking such sites in an unambiguous manner unparalleled by other dating or correlative techniques (Lowe et al., 2000).

Identification of distinct tephra horizons in regions not traditionally associated with tephrochronological research has considerably extended the geographical distribution of some tephtras, thus emphasizing the potential of using such time-parallel marker horizons for correlation of sequences on a wide scale (e.g., Turney et al., 2004).

In Northern Peloponnesus, Greece, a series of Upper Pliocene through Quaternary rocks have been deposited on a Mesozoic substrate (Koutsouveli et al., 1989). Recently, a volcanic ash layer has

been identified by the authors, hosted in clayey rocks and sandstone of Upper Pliocene to Lower Pleistocene age, located close to the eastern slopes of the Koutsa block (Place et al., 2007).

Volcanic ash beds of 4cm thick have been reported in Quaternary offshore deposits, north of the studied area (Cramp et al., 1989). Volcanic ash/tephra layers/beds have been found in sedimentary rocks of the same age in several places in eastern Mediterranean Region (Keller et al., 1978; Vinci, 1985; Stamatakis, 1995; Stamatakis et al., 2001). The majority of the Late Neogene to Recent tephra layers has their origin as either the Campanian volcanic area, or the eastern extension of the Hellenic Arc (Keller & Ninkovitch, 1972; Richardson & Ninkovitch, 1976). The aim of the present paper is to characterise the newly found volcanic ash and to consider any genetic relationship with the volcanic centers of the region.

1.1 Geological setting

The studied area is part of the Gulf of Corinth rift, which has undergone N-S extension strain, from Late Miocene through Late Quaternary (Fig. 1) (Armijo et al., 1996; Lykoussis, et al., 2007; Bell et al., 2008). Steep extensional faults (40° – 50°) crop out south of the gulf, in northern Peloponnesus, mainly trending E–W, which clearly controlled the morphology of the two rift-shoulders (Sorel 2000, Place et al., 2007). The rift was created in two phases, a proto-rift stage that is well developed in the eastern part and a younger rift stage that is mostly developed in the western part (Ori, 1989).

On the Mesozoic substrate of the area which belongs to the Pindos Geotectonic Zone, clastic sediments of fluvial, lacustrine and marine origin have been deposited, having Upper Pliocene – Lower Pleistocene age (Koutsouveli et al., 1989; Doutsos and Piper, 1990). The Upper Pliocene lithostratigraphic succession is mainly composed of conglomerates, sandstones, claystones/mudstones and locally sandy marls up to 600m thick (Fig. 2). In general, the lowermost part of the deposits is more fine-grained, whereas sandstone and conglomerates predominate upwards.

The volcanic ash bed is located in the lower part of the 600m thick clastic succession, having 400m overburden sandy marls and conglomerates of the Reithio-Dendro formation (Koutsouveli et al., 1989) (Fig. 3 & 4).

2. Materials and methods

Five samples from the volcanic tephra horizon were collected from an outcrop of 15m X 50m (Fig. 2) for geochemical and mineralogical analyses. To identify the mineralogy of the host rock, five more representative samples of overlying and underlying sandstone and claystone have been collected. The sample XLK1 is the stratigraphically uppermost among the studied samples.

Grain size analyses of the bulk ash layer were performed using the sieves of 450, 320, 224, 80, 40 and 32 μ m. Bulk Mineralogical analysis was carried out by using an X-Ray powder Diffractometer of Siemens D-5005 type, with copper tube and graphite monochromatographer. The mineralogical phases were determined by using computer and the software of SOCRIM Company (DIFRAC PLUS 2004, EVA ver. 10) and the files of JCPDS, at the laboratories of the NKUA, Faculty of Geology and Geoenvironment.

Major and trace element chemical analysis of the bulk volcanic ash samples was implemented by ME - XRF06 (major elements) and ME - MS81 (trace and rare earth elements) methods in the laboratories of ALS Chemex Labs, Saskatchewan, Canada. Primitive mantle normalized ratios were calculated from the values of Sun & McDonough (1989).

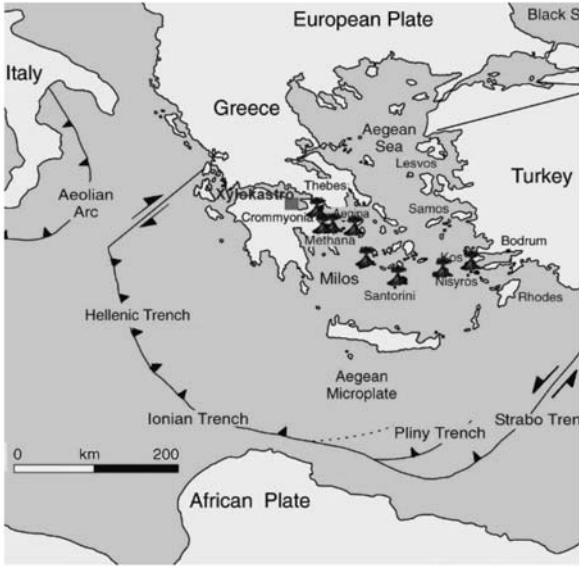


Fig. 1: Location map of the volcanic ash layer (rectangular red). Simplified regional geotectonic map of the eastern Mediterranean. The main volcanic centres of Southern Aegean Volcanic Arc [SEVA] are shown.

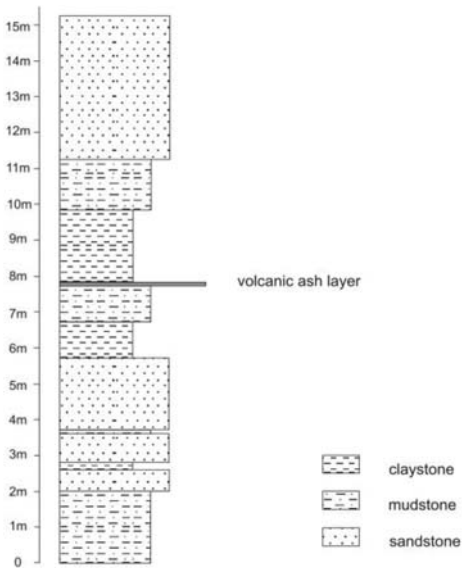


Fig. 2: Lithological column of the sedimentary succession that hosts the volcanic ashbed, Xylokaastro area, Corinth.

Mineralogical, and a petrographic/scanning electron microscope survey for the volcanic ash components, i.e. glass shards, pumice particles and feldspars was performed in thin sections, using optical microscope and scanning electron microscope at the laboratories of the NKUA, Faculty of Geology and Geoenvironment. The scanning electron microscope was a JEOL JSM-5600 equipped with Oxford Link ISIS 300 Energy Dispersive microprobe analytical system. The beam current was 0.5nA and diameter 2 μ m. SEM and microprobe analysis were performed on slides as well as on natural samples.



Fig. 3: The ash-bed hosted in the claystone host rock. Note the tectonic deformation of the bed, due to neo-tectonic manifestations. Scale in inches.



Fig. 4: A closer view of the 10cm thick ash bed showing bedding of off-white to dark grey layers.

Table 1. XRD mineralogical analysis of the volcanic ash bed and the host rock, Xylokaastro area, Corinth

	<i>Description</i>	<i>VG</i>	<i>Fl</i>	<i>Qtz</i>	<i>Cc</i>	<i>Chl</i>	<i>ill-sm</i>
XLK-1	sandstone		MD	MJ	MD		
XLK-2	claystone		MD	MD	MD	MD	MD
XLK-3	claystone just above ash	MJ	MD	MD	TR		
XLK-4	volcanic ash	MJ	MD	TR	TR		
XLK-5 (2)	volcanic ash	MJ	MD	TR			
XLK-6 (1)	volcanic ash	MJ	MD	TR	TR		
XLK-7	volcanic ash	MJ	MD	TR			
XLK-8	volcanic ash	MJ	MD	TR			
XLK-9	claystone just below ash	MJ	MD	MD	TR		
XLK-10	mudstone		MD	MD	MD	MD	MD

Explanatory notes: VG=volcanic glass, Fl=anorthoclase and/or sanidine, Chl=chlorite, ill-sm=illite-smectite, Cc=calcite, Qtz=quartz, MJ=major constituent, MD=medium constituent, TR=minor/trace constituent

3. Results

The XRD analysis revealed that sandstone is mostly composed of quartz, feldspars and calcite, whereas mudstone and claystone contain variable amounts of calcite, quartz, feldspars, smectite, and mixed-layers. The volcanic ash bed is mostly composed of amorphous phase as it is determined by its characteristic hump at 20-26° degrees. Other components that occur in minor or trace amounts are: feldspars, mostly sanidine and anorthoclase, calcite and quartz (Table 1).

The grain size distribution in the bulk ash layer is presented in Fig. 5. Chemical analyses of the volcanic ash samples revealed that they are composed primary of silica (55.80-60.74%) and alumina, (14.42-15.74%). Iron and alkalies occur in minor amounts, whereas Mg and Mn occur in trace amounts (Table 2a & b). The Harker plots (Fig. 6) shows the variation of the composition of the

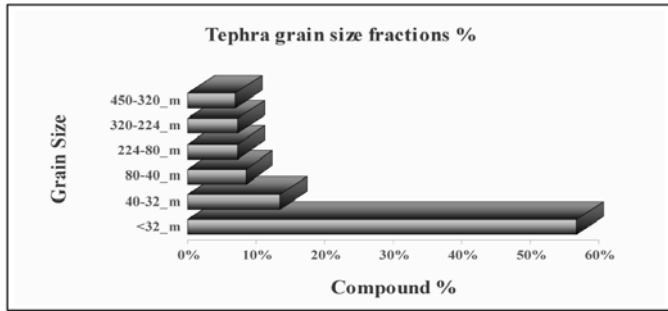


Fig. 5: Grain size distribution in the Xylokastro volcanic ash bed.

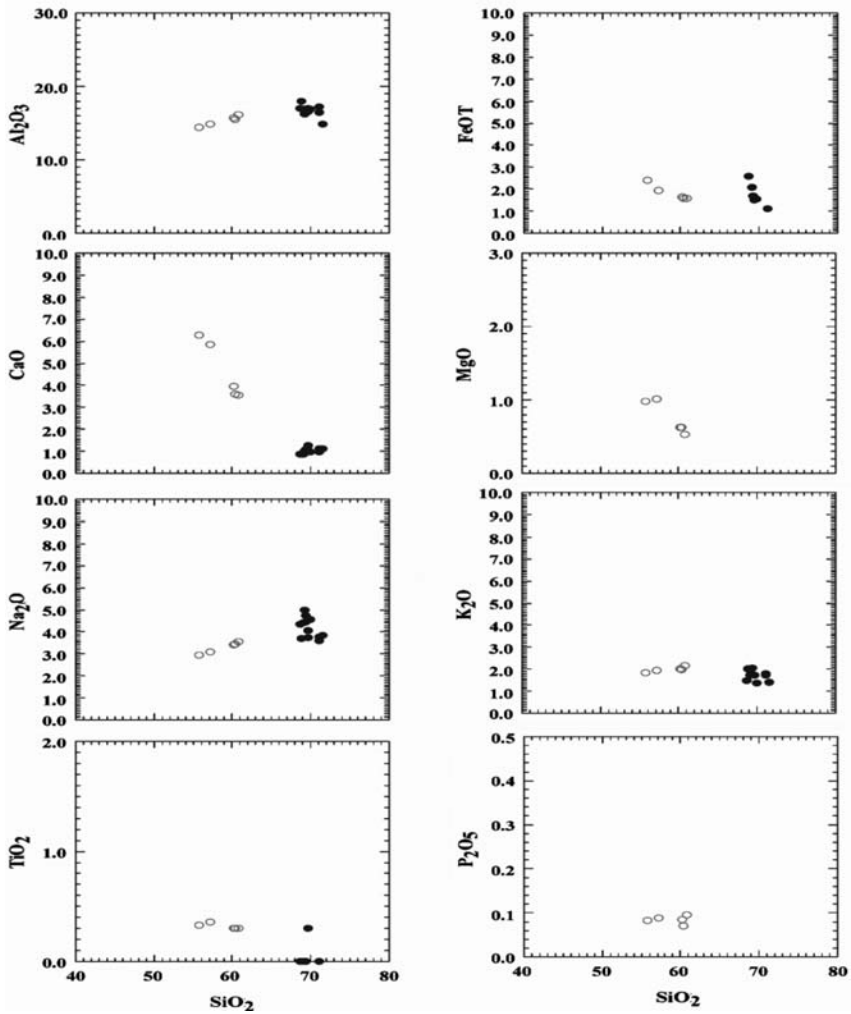


Fig. 6: Harker plots for the major elements, of the Xylokastro volcanic ash bulk samples and glass showing the variations in their composition. (The empty cycles represent the bulk sample compositions and the full cycles the glass microprobe analyses).

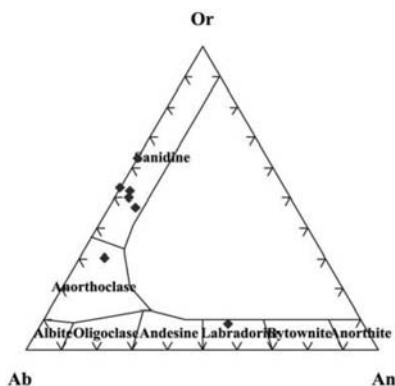


Fig. 7: Classification of the feldspars from the Xylokastro volcanic ash layer.

Table 2a. Major element analyses of bulk samples from Xylokastro tephra layer.

Sample	XLK1	XLK 1W	XLK2	XLK3	XLK4
SiO ₂	57.18	60.34	55.8	60.74	60.19
TiO ₂	0.36	0.3	0.33	0.3	0.3
Al ₂ O ₃	14.84	15.5	14.42	16.11	15.74
Fe ₂ O ₃	2.14	1.78	2.66	1.75	1.83
MnO	0.06	0.07	0.07	0.07	0.07
MgO	1.01	0.62	0.98	0.53	0.62
CaO	5.86	3.57	6.28	3.56	3.96
Na ₂ O	3.07	3.43	2.95	3.56	3.42
K ₂ O	1.94	1.96	1.83	2.14	2.03
P ₂ O ₅	0.088	0.07	0.083	0.096	0.085
LOI	13.10	11.40	13.40	10.95	11.45
Total	99.65	99.04	98.80	99.81	99.69

Table 2b. Trace element analyses of bulk samples from Xylokastro tephra layer.

Sample	XLK1	XLK 1W	XLK2	XLK3	XLK4
Ba	650	670	560	660	680
Rb	91.7	75.4	93.7	83.3	80.6
Sr	353	324	387	390	342
Y	18.6	16.5	18.5	16.5	15.3
Zr	307	347	299	337	337
Nb	32.4	36.2	31.6	35.5	35.3
Th	88.1	87.5	89.6	86.6	79.2
Pb	125.5	136	123.5	137.5	137
Ga	21.9	23.2	20.6	21.8	22
Zn	56	49	56	46	49
Cu	21.4	11.1	23.4	9.6	11.5
Ni	56.3	28.8	59.9	19.3	28.4
V	36	29	36	26	28
Cr	39	19	33	9	17
Hf	9.6	10.9	9.4	10.6	10.6
Cs	37	40.3	35.7	39.6	39.4
Sc	3.3	2.1	3.2	1.6	1.9
Ta	1.56	1.72	1.54	1.73	1.73
Co	7.2	4.5	7.5	3.5	4.4
Li	22.6	12.8	21.8	11.5	12.2
Be	11.95	13.55	11.5	13.2	13.1
U	21.3	22.3	20.6	21.7	21
W	11	12.7	10.5	12.3	12.2
Sn	3.4	3.9	3.4	3.7	3.6
Mo	7.87	8.32	7.3	7.36	7.39
La	86.1	71.3	91	70.3	63.6
Ce	145.5	127	150	125.5	113.5
Th/U	4.14	3.92	4.35	3.99	3.77

Table 3. Representative microprobe analyses of volcanic glass particles.

Analysis	S4	S7	X10	X11	X6	X7	X8	X9
SiO ₂	68.77	71.59	69.26	69.04	68.68	69.43	71.07	69.65
TiO ₂	0.00	0.00	0.00	0.00	0.00	0.00	0.00	0.30
Al ₂ O ₃	17.95	14.89	16.25	16.85	17.00	16.48	16.46	17.00
FeO	1.75	1.98	1.69	2.08	2.60	1.51	1.12	1.55
CaO	0.85	1.10	1.02	0.88	0.88	1.08	0.99	1.04
Na ₂ O	3.69	3.83	5.00	4.40	4.35	4.44	3.57	3.73
K ₂ O	2.00	1.42	1.78	1.74	1.49	2.06	1.80	1.73
Total	95.01	94.81	95.00	94.99	95.00	95.00	95.01	95.00

Table 4. Representative microprobe analyses of feldspars from the ash layer.

Analysis	S10	S12	S13	S5	S6	S9	X5	X5A
SiO ₂	69.04	66.45	62.89	67.55	69.06	68.73	68.73	69.87
Al ₂ O ₃	17.64	19.63	17.99	17.98	17.62	17.12	17.98	17.1
FeO	0.00	0.00	4.11	0.00	0.00	0.87	0.00	1.88
CaO	0.00	1.45	8.46	0.86	0.00	0.00	0.61	1.15
Na ₂ O	4.86	4.87	3.38	5.11	4.86	3.67	4.56	5.56
K ₂ O	8.46	7.60	1.17	8.49	8.46	9.56	8.12	4.08
Total	100.00	100.00	98.00	99.99	100.00	99.95	100.00	99.64

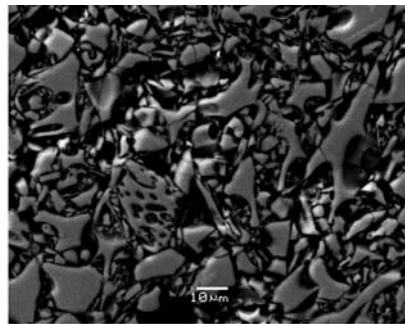
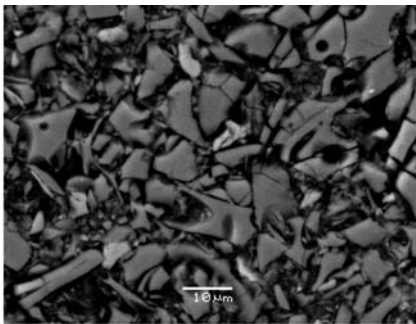


Fig 8a: SEM images of the Xylokastro ash bed: Glass shards. Note the fineness of the particles [size <20μm].

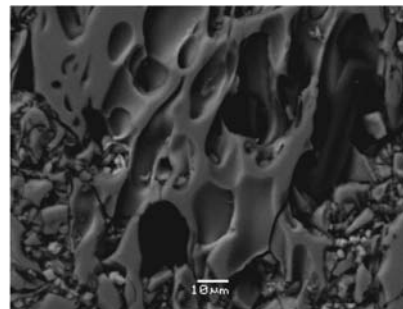
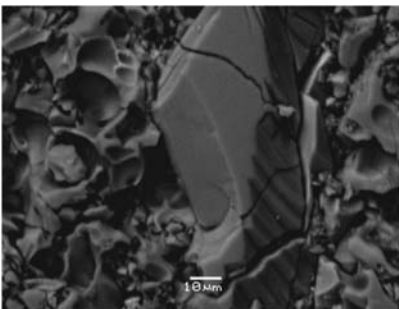


Fig. 8b: SEM images of the Xylokastro ash bed: Pumice and feldspar fragments [left image]. The particle size of both components is higher than that of the glass shards.

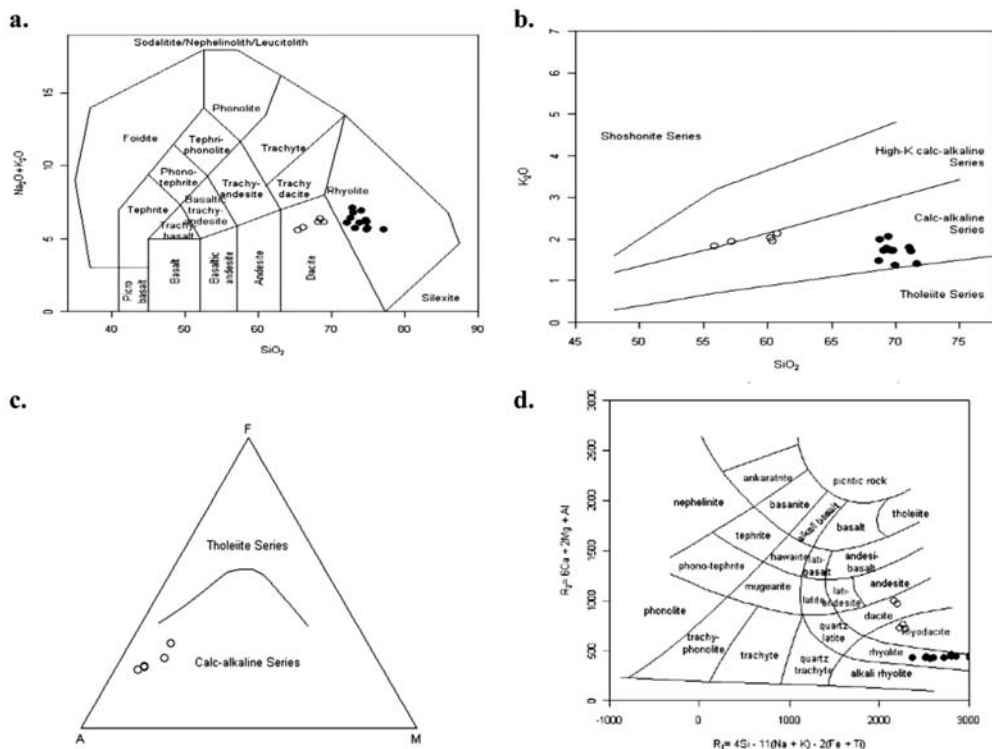


Fig. 9: Geochemical discrimination dia-grams for the Xylokastro volcanic ash bulk samples and glass: a. TAS classification diagram (Middlemost, 1994), b. SiO_2 - K_2O binary classification diagram of Pecerillo & Taylor, (1976), c. AFM ternary classification diagram of Irvine & Baragar, (1971). A.: $\text{Na}_2\text{O} + \text{K}_2\text{O}$, F: FeOt, M: MgO, d. R1-R2 binary classification plot (De la Roche et al, 1980). The empty cycles represent the bulk sample compositions and the full cycles the glass microprobe analyses.

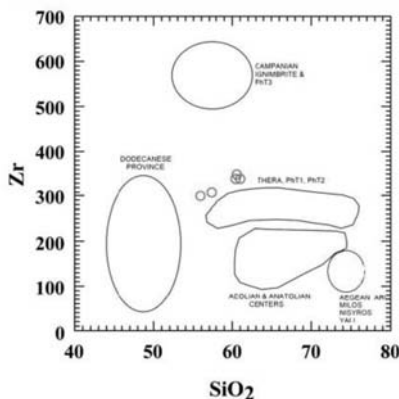


Fig. 10: The Xylokastro ash-bed [red circles] in the Zr vs. SiO_2 systematics (after Seymour et al., 2004).

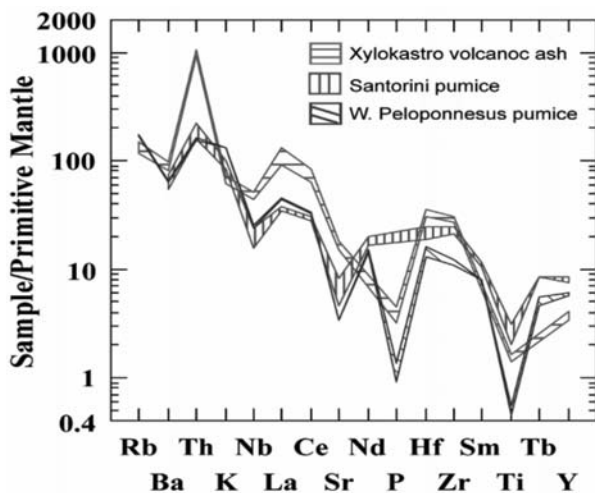


Fig. 11: Trace element spider plots of the Xylokaastro volcanic ash bulk samples, Thera [Santorini] pumices (data from Vitaliano et al., 1989), and pumices from western Peloponnesus (data from Bathrellos et al., 2009).

Xylokaastro volcanic ash bulk samples and glass for the major elements. The higher CaO values in the bulk samples is most likely due to trace amounts of calcite (Table 1), but mainly to an early crystallization of Ca- and Mg-rich mafic minerals in the melting lava. This suggestion is supported by the simultaneous negative trend of MgO versus SiO₂ (Fig. 6).

The study of the samples by SEM presented good sorting, without any evidence of compaction and restricted transportation, as there is no abrasion evidence on grains, fragmentation of glass shards. The diatom frustules that rarely occur in the ash bed retain their minute structure, being preserved unbroken. Microprobe analyses of volcanic glass particles and feldspar crystals are shown in Tables 3 & 4 respectively. The classification of the feldspars of the samples is presented in Fig. 7. showing that the dominant feldspar is sanidine and also the presence of anorthoclase and plagioclase. The SEM-EDS observations suggested slight alteration of both the glass shards and the pumice particles (Fig. 8a & b). The common alteration sequence detected, is the following: 1) etching on glass-grain surfaces 2) formation of silica spheres and quartz overgrowths 3) precipitation of very thin, individual flakes of illite-smectite on glass shards or development of illite-smectite aggregates filling pores 4) formation of Fe-oxides rim along cracks and in voids 5) alteration on plagioclase crystals. The glass fractions consist of shards, bubble wall fragments and micro-particles of pumices. Glass shards show typical conchoidal fracture and different particle shape. Many shards exhibit characteristic U- and Y-shapes (tri-cusate) that have resulted from disruption of highly vesicular pumices that were formed where three bubbles were in close proximity. Other shard derived of double-concave plates that formed the wall between two adjoining bubbles, whereas some particles are angular and lenticular, or highly vesicular. The vesicles, spherical or elongated, have been arranged in groups and in some cases they are curved.

4. Discussion and Conclusions

Mineral and chemical composition is used in the description of volcanic ash deposits. Description of particle size and shape as well as the types of vesicles are also used in ash petrography. The type of material present in volcanic ash is a function of a) the kind of source rock emitted, b) the modification by transport and contamination during transport or deposition c) the alteration processes (devitrification and/or weathering).

The studied samples of the distinct volcanic ash layer, reported for the first time in the studied area, seem to have been deposited in a lacustrine environment displaying parallel-laminated fine tuff layers, possibly formed by subaqueous pyroclastic flows that are generated by eruptions in shallow water or close to a shore. The lacustrine nature of the deposit is determined by the examination of the diatom species found in the volcanic ash and the host rock (*Cyclotella Sp.*, Prof. B. Owen). Its main components are glass shards and pumice particles. According to Izett et al (1981), pumice shard develop from relatively high viscous rhyolitic magmas with temperature <850° C, whereas the bubble wall and bubble junction shards develop from low viscosity rhyolitic magmas at temperature >850° C. Their coexisting in the ash layer could be attributed to successive eruptions, or settling velocity or/and disturbance. The cooling-contraction fragmentation of shard glass points out to ash/water interaction Kokelar (1986). The homogeneous fine-grained, well-sorted and parallel laminated ash layers are products of either a single volcanic event from a subaqueous flow that dispersed in the water column, or distant eruption. In the latter case, the homogeneity is produced by winnowing during aerial transport. The Xylokaastro ash has shown a greater percentage of bubble wall shards with the co-occurrence of blocky types as compared to pumice shard. Rose and Chesner (1987) have pointed to the high drag coefficient of the bubble wall shard which resulted in its preferential dispersal over great distances.

The XRD analysis of the finest [$<32\mu\text{m}$, off-white] and the coarser fraction [$450\text{--}320\mu\text{m}$ dark grey] of the volcanic ash particles showed that there does no any difference in their mineralogy, hence the difference in the color is attributed to differential grain size. The lamination observed in the field is due to the alternation of coarse-rich and fine-rich intercalations in the ash. The thickness of each micro-layer is variable but always $<2\text{cm}$, comparing the dark and bright intervals. Moreover, the bright and dark layers themselves most likely propose repetitive volcanic manifestations in a certain/short period of time, or almost simultaneous manifestations of neighbouring volcanoes that fed the area with successively deposited sheets of ash.

The ash layers have undergone and early alteration processes that refer to the effects of devitrification and/or weathering. Altered glass shards are characterized by silica remobilization and development of sorptive phases as clay minerals. The devitrification process is not intense, as the surfaces of glass shards remain relatively fresh, and the alteration products are rare. It is also confirmed by the Th/U ratio [~ 4] which displays no uranium-loss attributed to devitrification (Table 2).

The composition of the bulk samples showed a dacitic to rhyodacitic calc alkaline suit with relative high potassium (fig. 9). The glass itself has more silicic composition than the bulk sample (fig. 6) indicating a rhyolitic, calc alkaline suit as well (fig. 9). This difference is probably due to the mineralogy of the bulk samples, which contain minerals with variable SiO_2 content (Table 1).

In the binary diagram Zr versus SiO_2 - systematics proposed by Seymour et al. (2004), the bulk sample composition is plotted a little above the field of Santorini pyroclastics (fig. 11). The fineness of the glass and pumice particles (fig. 5), judges for a rather long distance source of the volcanic material.

As it was pointed out by Fischer (1965), in areas of successive eruptions and water sedimentation feldspar or quartz may reach the water bottom at the same time as glass shards from a previous eruption, due to differential settling velocity. The spider area plots for the trace element composition (Fig. 11) shows similarity with the trace element area plots of Santorini pumices and the newly found western Peloponnesus pumices which are assumed to originate from the Aegean volcanic arc (Bathrellos et al., 2008). The differences between those plots are due to a) the lack of analytical date for some elements in each group, b) the higher thorium content of the Xylokaastro tephra, which is

accompanied by high uranium value (Table 2) and c) Xylokaastro tephra shows higher enrichment in LIL elements than the others. Magma-crust interaction is an explanation for the high LIL/HFS element in calc-alkaline magmas (Mitropoulos et al., 1987). Differential crustal assimilation could account for the geochemical differences between the Aegean volcanic centers and may be interpreted as evidence for slightly higher sediment input in the western parts of the arc. Among the volcanic centers of the SEVA, Santorini is situated in the region which has suffered maximum crustal thinning and lithosphere extension, and where asthenospheric mantle may be uprising to replace existing sub-continental mantle. The crust and lithosphere thickness is higher in the margins of SAVA. Xylokaastro volcanic ash having enrichment in LIL elements indicates high crustal contamination of the lava and points to an origin from the northwest part of the Aegean volcanic arc (Methana, Aegina, Poros, Sousaki (Cromyonia) or neighbouring volcanic centers, not exposed today). However, among the possible feeding centers is the Soussaki volcanic terrain is the closest, lying 50 Km eastwards.

5. Acknowledgments

The authors would like to thank Prof. P. Mitropoulos of the University of Athens and Assoc. Prof. K. Seymour of the University of Patras, Geochemists, for their useful remarks for the interpretation of the geochemical data. Also thanks, to Dr K. Kouli for her help in electronic drawing the lithostratigraphic column of the study area.

6. References

- Armijo, R., Meyer, B., King, G.C.P., Rigo, A., Papanastasiou, D., 1996. Quaternary evolution of the Corinth rift and its implications for Late Cenozoic evolution of the Aegean. *Geophys. J. Int.* 126, 11–53.
- Bathrellos D.G., Vasilatos Ch., Skilodimou D.H., Stamatakis G.M., 2009. On the occurrence of a pumice-rich layer in Holocene deposits of western Peloponnesus, Ionian Sea, Greece. A geomorphological and geochemical approach. *Cent. Eur. J. Geosci.*, 1(1), 19-32.
- Bell R. E., McNeill L.C., Bull M.G. and Henstock J.T. 2008. Evolution of the offshore western Gulf of Corinth. *Geological Society of America Bulletin*, V. 120, p. 156-178.
- Cox, K.G, Bell, J.D, Pankhurst, R.J., The interpretation of igneous rocks. Allen and Unwin, London, UK, 1979.
- Cramp A., Vitaliano J. C. Collins B. M. 1989. Identification and Dispersion of the Campanian Ash Layer (Y-5) in the Sediments of the Eastern Mediterranean. *Geo-Marine Letters* V. 9, p. 19-25
- De La Roche, H., 1980. A classification of volcanic and plutonic rocks using R1–R2 diagrams and major element analyses—its relationships and current nomenclature, *Chem. Geol.* 29, pp. 183–210.
- Doutsos, T., Piper, D.J.W., 1990. Listric faulting, sedimentation and morphological evolution of the Quaternary eastern Korinth rift, Greece; first stages of continental rifting. *GSA Bull.* 102, 819–879.
- Irvine, T.N., Baragar, W.R.A., 1971. A guide to the chemical classification of the common volcanic rocks, *Canadian Journal of Earth Science*, 8, 523 – 548.
- Izett, G.A., 1981. Volcanic ash beds: recorders of upper Cenozoic silicic pyroclastic volcanism in the western U.S. *Journal of Geophysical Research* 86, pp. 10,200–10,222.
- Fischer R.V. 1965. Settling velocity of shard glass. *Deep Sea Research and Oceanographic Abstracts.* 12,3, 345-346.
- Ori, G.G., 1989. Geological history of the extensional basin of the gulf of Corinth (?Miocène–Pleistocène), Greece. *Geology* V. 17, p. 918–921.
- Pecerillo, A. and Taylor, S.R., 1976. Geochemistry of Eocene calc-alkaline volcanic rocks from the Kas-

- tamonu area, northern Turkey. *Contrib. Mineral. Petrol.* 58, pp. 63–81.
- Place J., Géraud Y., Diraison M., Warr L. 2007. North-south transfer zones and paleo-morphological reconstruction of the Xylokaastro area (Corinth Gulf, Greece). *Tectonophysics* V. 440, p. 121–139
- Richardson and D. Ninkovich, 1976. Use of K₂O, Rb, Zr and Y versus SiO₂ in volcanic ash layers of the Eastern Mediterranean to trace their source, *Geol. Soc. Am. Bull.* 87, pp. 110–116.
- Sorel D. 2000. A Pleistocene and still-active detachment fault and the origin of the Corinth-Patras rift, Greece. *Geology*, V. 28; no. 1; p. 83-86.
- Keller and D. Ninkovich, 1972. Tephra-Lagen in der Agäis. *Z. Dtsch. Geol. Ges.* 123, pp. 579–587.
- Keller, W.B.F. Ryan, D. Ninkovich and R. Altherr, 1978, Explosive volcanic activity in the Mediterranean over the past 200,000 yr as recorded in deep-sea sediments, *Geol. Soc. Am. Bull.*, 89 pp. 591–604.
- Kokelar P. 1986, Magma-water interactions in subaqueous and emergent basaltic volcanism. *Bull. of Volcanology* 48, 275-289.
- Koutsouveli, A., Mettos, A., Tsapralis, V., Tsaila-Monopoli S., Ioakim, C., 1989. Geological Map of Greece, scale 1:50000, Xylokaastro sheet, IGME publications, Greece.
- Lowe, D.J., Newnham, R.M., McFadgen, B.G. and Higham, T.F.G., 2000: Tephros and New Zealand archaeology. *Journal of Archaeological Science*, 27, 859-870.
- Lowe, D.J., Newnham, R.M. and McCraw, J.D., 2002: Volcanism and early Maori society in New Zealand. In: Natural Disasters and Cultural Change; Torrence, R. and Grattan, J. (eds), Routledge, 126-161
- Lykousis V. Sakellariou D., Moretti I, and Kaberi H., 2007. Late Quaternary basin evolution of the Gulf of Corinth: Sequence stratigraphy, sedimentation, fault–slip and subsidence rates. *Tectonophysics*, V, 440, issues 1-4, p. 29-51.
- Middlemost, K.A.E., 1994. Naming materials in the magma/igneous rock system, *Earth-Science Reviews* 37, pp. 215–224.
- Mitropoulos P., Tarney J., Saunders A. D., and Marsh N. G., 1987. Petrogenesis of Cenozoic volcanic rocks from the Aegean island arc. *Journal of Volcanology and Geothermal Research* 32, p. 177-193.
- Ori, G.G., 1989. Geological history of the extensional basin of the gulf of Corinth (?Miocène–Pleistocène), Greece. *Geology* V. 17, p. 918–921.
- Rose W.I. and Chesner C.A. 1987: Dispersal of ash in the great Toba eruption. *Geology* 15, 913-917.
- Sun S.S., McDonough W.F., 1989. Chemical and isotopic systematics of oceanic basalts: implications for mantle composition and processes. In: Saunders, A.D., Norry, M.J. (Eds.), *Magmatism in the Ocean Basins. Geological Society Special Publications*, pp. 313–345.
- Seymour, K., Christanis, K., Bouzinos, A., Papazisimou, St., Papatheodorou, G., Moran, E. & Denes, G., 2004. Tephrostratigraphy and tephrochronology in the Philippi peat basin, Macedonia, Northern Hellas (Greece), *Quatern. Internat.*, 121, 53 – 65.
- Stamatakis M.G. 1995. Occurrence and genesis of huntite-hydromagnesite assemblages, Kozani basin, Greece - important new white fillers and extenders. 1995. IMM, *Transactions B*, V 104, p. 179-186.
- Stamatakis M.G., Papageorgiou A., Fragoulis D. & Chaniotakis E. 2001. The nature of volcanic glass and its effect in the pozzolanic activity of tuffaceous rocks originated from Macedonia, Northern Greece. Proceedings of the 8th Euroseminar on Microscopy Applied to Building Materials. V. 1, p. 271-280.
- Turney, C.S.M., Lowe, J.J., Davies, S.M., Hall, V.A., Lowe, D.J., Wastegård, S., Hoek, W.Z., Alloway, B., SCOTAV and INTIMATE members, 2004: Tephrochronology of Last Termination sequences in Europe: a protocol for improved analytical precision and robust correlation procedures (a joint SCOTAV-INTIMATE proposal). *Journal of Quaternary Science* 19, 111-120.

- Vinci, A., 1985. Distribution and chemical composition of tephra layers from Eastern Mediterranean abyssal sediments. *Marine Geology*, Volume 64, Issues 1-2, pp 143-155
- Vitaliano, C.J., Taylor, S.R., Norman, M.D., McCulloch, M.T., Nicholls, I.A., 1989 Ash layers of the Thera volcanic series: stratigraphy, petrology, and geochemistry. Thera and the Aegean World III. Papers to be presented at the 3rd International Congress, Santorini, Greece 3-9 September 1989. Volume I sessions 1-3, pp. 115-150.

MINERALOGICAL CONSTRAINTS TO THE FORMATION OF VEIN-TYPE ZEOLITES FROM KIZARI AREA, THRACE NORTHERN GREECE

Voudouris P.¹, Magganas A.¹, Kati, M.¹, Gerogianni N.¹
Kastanioti G.¹, and Sakelaris, G.

¹ University of Athens, Department of Mineralogy-Petrology, 15784 Athens, Greece
voudouris@geol.uoa.gr, amagganas@geol.uoa.gr, kati@geol.uoa.gr

Abstract

Vein-type zeolites in Kizari area, (western Thrace) are found within fresh to zeolitic altered volcanic rocks of andesitic to dacitic composition. The zeolites stilbite-Ca, Sr-bearing heulandite-Ca and laumontite occur in epithermal-style crustiform quartz/chalcedony-calcite veins crosscutting lavas and volcanic breccias. Open-space filling is common and well-shaped crystals (up to 3cm) were observed. Smectite, feldspar, magnetite, pyrite and rutile occur in minor amounts in the veins. Halite and barite grains are included in stilbite-Ca. SEM-EDS data indicate high Sr (up to 4.4 wt. % SrO) and Ba (up to 2.9 wt. % BaO) contents for heulandite-Ca. It is suggested that the studied zeolites are intergral parts of the porphyry-epithermal mineralizing systems which operated in the area during the Oligocene. Their formation took place in the outmost transitional propylitic to fresh zones of the porphyry-epithermal systems and in a submarine environment as indicated by the geological and mineralogical evidence.

Key words: vein-type zeolites, stilbite-Ca, Sr-bearing heulandite-Ca, laumontite, submarine.

1. Introduction

Exploration activities during the last two decades in western Thrace resulted in the discovery of several zeolites deposits hosted mainly in Tertiary volcanoclastic rocks at Petrota, Pentalofofos, Metaxades, Lefkimi, Ferres and Skaloma regions (Kossiaris et al., 1987; Marantos et al., 1989; Tsohis-Katagas & Katagas, 1990; Karafoti & Arikas, 1990; Tsirambides et al., 1989, 1993; Filippidis, 1993; Skarpelis et al., 1993, 1995; Kitsopoulos & Dunham, 1994; Stamatakis et al., 1996, 1998; Kirov et al., 1999; Hall et al., 2000; Kassoli-Fournaraki et al., 2000; Marantos, 2004; Perraki & Orfanoudaki, 2004; Filippidis and Kantiranis, 2005). The most common zeolites present in western Thrace are of HEU type (heulandite-clinoptilolite), but minor amounts of mordenite, analcime, stilbite and laumontite also occur. According to the above authors, the zeolites were formed from the alteration of volcanic glass, and are accompanied by clays, silica polymorphs (quartz, cristobalite), feldspars and calcite.

In addition, vein-type zeolites occur in a few localities (e.g. Virini, Feres, N. Santa and Vathi/Kilkis) (Michael et al., 1984; Filippidis et al., 1988; Marantos et al., 2004, 2007), and show similarities to hydrothermal zeolites found in many parts of the world (e.g. Ferroe islands/Danemark, Nova Scotia/Canada, Fassatal/Italy, Baical/Siberia, Andreasberg/Germany, Teschen/Czech Republik, Kongs-

berg/Norway, Tergahorn/Island, Troodos Complex/Cyprus and Nasik, Poona/India (Extra Lapis, 2007).

Contrary to the papers published on the mineralogy, petrology and geochemistry of western Thracian zeolitized volcanoclastic deposits, there is limited information on the formation of vein-type zeolites in Thrace and in Greece in general. This study describes a new occurrence of vein-type zeolites in western Thrace, located within an andesite quarry at Kizari/Sapes in Rhodope prefecture, and present a model for their genesis based on mineralogical, mineral-chemical and geological data.

2. Regional geology

The geodynamic evolution of northeastern Greece includes an early oceanic-continental subduction/collision, growth of the thickness of the crust, and post-collisional extensional collapse of the orogen resulting in the formation of several supra-detachment basin-controlled volcanosedimentary formations from the Lutetian (48 - 43Ma) through the Oligocene up to the Pliocene (Krohe & Mposkos, 2001; Papadopoulos & Anastasiadis, 2003). Slab break-off and/or slab delamination were principal mechanisms for the generation of extensive post-collisional magmatism in the area (Pe-Piper et al., 1998). The resulting plutonic-subvolcanic and volcanic rocks in Evros-Rhodopi region show calc-alkaline, high-K calc-alkaline, to shoshonitic affinity (Papavasiliou & Sideris, 1984; Innocenti et al., 1984; Eleftheriadis, G., 1995; Christofides et al., 2004; Magganas et al. 2004). For the basic to intermediate and acid magma generation an enriched mantle source region, extensive differentiation within the crust, subordinate magma mixing and/or a partial melting of crustal material has been documented. The main phase of the Tertiary magmatism took place during the Oligocene and is represented by submarine/terrestrial volcanics and subvolcanic rocks associated with volcanosedimentary series composed of marls, sandstones, clays and intercalations of volcanic rocks (lavas, tuffs, pyroclastics).

Numerous porphyry Cu-(Mo) and epithermal Au-Ag-type systems formed during the Tertiary magmatic event in northeastern Greece, and are genetically related to microdiorite, microgranite, andesite and the dacite porphyries (Arikas & Voudouris, 1998; Melfos et al., 2002). Faults and veins trending NW-SE, NE-SW and NNW-SSE influenced the distribution of magmatic rocks and spatially related magmatic-hydrothermal mineralization.

3. Local Geology

The Kizari area belongs to the eastern part of Komotini basin and also forms the northern extension of the eroded Tertiary volcanic edifice of Konos/Sapes: the Tertiary volcanosedimentary formations consist of M-U Eocene conglomerates, sandstones, marls, tuffs and tuffites, overlain by an Oligocene volcanic sequence dominating the entire area of Konos-Kizari (Fig. 1). The later consists of pyroclastics, lava flows and domes of andesitic to dacitic composition. Two types of intrusive stocks have been recognized in the broad area: an older, hydrothermally altered dacite stock with porphyry/epithermal-type mineralization at Konos area (Voudouris et al., 2006; Ortelli et al., 2009) and the 32 Ma (Del Moro et al., 1988) quartz monzodiorite of Kirki. The majority of magmatic rocks in the Kizari-Konos area are hydrothermally altered as a result of repeated hydrothermal activity during the lifespan of the above mentioned porphyry-epithermal system. Alterations typical of both high-sulfidation- and low-sulfidation epithermal gold deposits are the products of interaction between rocks and fluids of acid and near-neutral to alkaline pH respectively (Voudouris, 1993). These alterations are fault-controlled and related mainly to the N-S and E-W trending faults in the area. The western part of the studied area is covered by the Silver Hill conglomerate (Shaw & Constan-

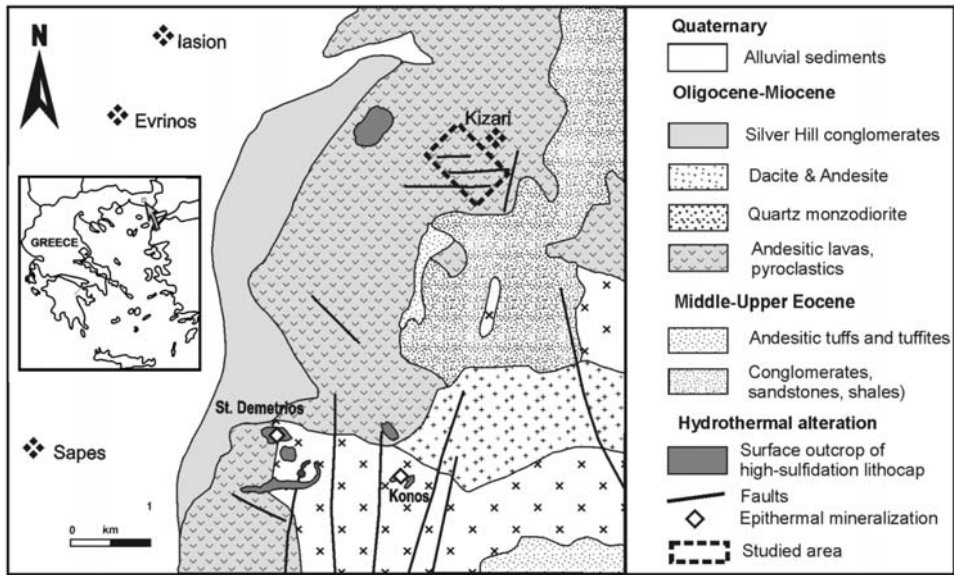


Fig. 1: Simplified geological map of Sapes-Kizari area and location of studied area (open square) (modified after Bitsios, 1973; Arikas, 1980; Greenwich Resources plc, 2004; Ortelli et al. 2009).

tinides, 2001), composed of angular to subrounded fragments of advanced argillic altered volcanic rocks and quartz-amethyst veins within an argillic matrix (Fig. 1). According to Shawh & Constantinides (2001) the Silver Hill conglomerate represents a mass flow deposited marginal to the Komotini Graben during its subsidence.

4. Description of the vein-type zeolite occurrences

The dominant rock types in the studied area are pyroxene-hornblende-bearing andesites, as well as volcanic breccias. The zeolite-bearing veins are fault-related and occur within E-W and N-S trending veins, which crosscut andesitic lavas and volcanic breccias in the broad area (Fig. 2). Fresh andesitic lavas consist of plagioclase, clinopyroxenes and hornblende phenocrysts embedded within a groundmass (up to 70 vol. %) containing microliths of the above minerals surrounded by a glassy matrix. Magnetite occurs both as phenocrysts and disseminated in the matrix. The volcanic breccias contain up to dm andesite angular to subrounded fragments within a fine-grained tuffitic matrix. The breccia fragments are identical to the above mentioned porphyritic lavas, whereas the matrix of the breccias is holocrystalline but finer grained compared to the fragments. Both the groundmass of the fragments and the matrix, consist of plagioclase and pyroxene microliths, few K-feldspar and devitrification products of the glassy matrix.

The volcanic rocks are relatively fresh and only in the vicinity of the zeolite-bearing veins, are partially altered to smectite, pyrite, magnetite, calcite, silica polymorphs and zeolites. The above secondary minerals occur either finely disseminated in the groundmass or as replacement of the phenocrysts. The veins show typical epithermal structures as open space filling and crustification banding. They reach lengths of up to several meters and are up to 50cm wide. Vein mineralogy greatly varies within the studied area and mainly two types of veins are distinguished: quartz-chalcedony±stilbite (Fig. 2b), and carbonate-rich stilbite-laumontite veins (Fig. 2c to f). The last vein-

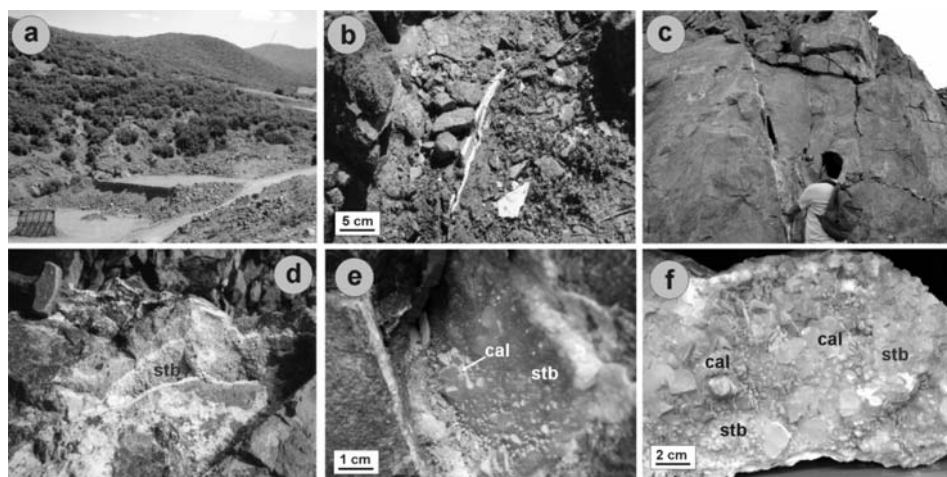


Fig. 2: (a) Panoramic view of lava quarry at Kizari (August 2006); (b) Chalcedony-stilbite veins crosscutting zeolitic altered lavas at Kizari (August 2006); (c) Stilbite-calcite veins with open-space filling crosscutting lavas (August 2009); (d, e) Stilbite (stb) and calcite (cal) filling fissures within lavas; (f) Hand-specimen with orange-colored stilbite (stb) and green-colored calcite (cal).

type may also be monomineralic (stilbite- or laumontite only) or may contain alternating bands with the above mentioned minerals. The quartz-chalcedony-rich veins (up to 5cm wide) are banded with initial deposition of white-colored chalcedonic silica and final deposition of colourless chalcedony and fine-grained quartz. Open spaces are filled by pale orange to beige-colored idiomorphic stilbite crystals and very minor calcite.

In the carbonate-rich veins the silica polymorphs are missing and vein deposition starts with minor calcite, followed by laumontite, stilbite and finally by green-colored calcite (Fig. 2e, f). Hydrothermal breccias are common and consist of fragments of volcanic rocks surrounded by a stockwork of zeolite-bearing veinlets and veins.

5. Methods

Twenty three thin and polished thin sections of host rocks and zeolite assemblages were studied with an optical microscope and a JEOL JSM 5600 scanning electron microscope equipped with back-scattered imaging capabilities, at the Department of Mineralogy and Petrology, University of Athens, Greece. Analytical methods also included X-powder diffraction measurements obtained using a SIEMENS type D-500 diffractometer with Cu tube and Co filter at the Department of Mineralogy and Petrology, University of Athens, Greece. The definition of the studied zeolites is based on the nomenclatures for zeolite minerals proposed by Coombs et al. (1998).

6. Mineralogy and mineral-chemistry

6.1 Zeolite minerals

Stilbite: Stilbite with ideal formula $\text{Na,Ca}_4(\text{Al}_9\text{Si}_{27}\text{O}_{72})\cdot 30\text{H}_2\text{O}$ is the most abundant mineral in the veins at Kizari quarry. It occurs in both silica- and carbonate-rich veins as euhedral crystals up to 3cm

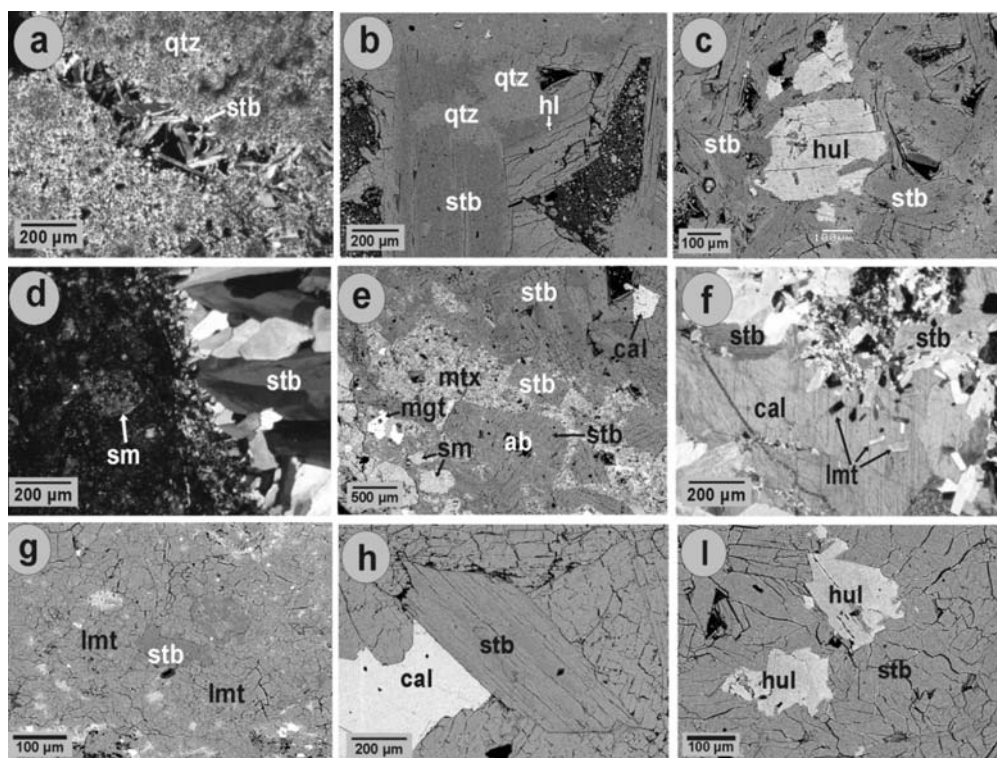


Fig. 3: Microphotographs of the quartz-chalcedony±stilbite veins (a-c) and carbonate-rich stilbite-laumontite veins (d-i) at Kizari (a) Stilbite (stb) filling vugs in quartz (qtz) veinlet (polarizing microscope image, +nicols); (b) Stilbite (stb) with halite (hl) inclusions, surrounds quartz (qtz) (SEM-BSE image); (c) Sr-bearing heulandite-Ca (hul) replaced by stilbite (stb) (SEM-BSE image); (d) Stilbite (stb) veinlet in weakly altered andesite. Smectite (sm) is pseudomorph after pyroxene phenocrysts (polarizing microscope image, +nicols); (e) Stilbite (stb), smectite (sm), albite (ab) and magnetite (mgt) replace plagioclase and clinopyroxene phenocrysts of andesite and also occur in the recrystallized groundmass (mtx). Stilbite and calcite (cal) also occur in veinlets (SEM-BSE image); (f) Laumontite (lmt) postdates stilbite (stb) and is surrounded by calcite (cal) (polarizing microscope image, +nicols); (g) Laumontite (lmt) replaces stilbite (stb) (SEM-BSE image); (h) Idiomorphic stilbite (stb) crystals overgrown by calcite (cal) (SEM-BSE image); (i) Sr-bearing heulandite-Ca (hul) replaced by stilbite (stb) (SEM-BSE image).

with well developed {110}, {010} and {001} faces. In the quartz-chalcedony veins stilbite post-dates silica polymorphs deposition, and filling fractures and open spaces in quartz or is overgrown on quartz (Fig. 3a to c). It contains small inclusions of halite (Fig. 3b) and barite and also replaces Sr-Ba-bearing heulandite-Ca (Fig. 3c). In the carbonate-rich veins stilbite surrounds albite in pseudomorphs after plagioclase (Fig. 3e), replaces and is replaced by laumontite (Fig. 3g) and similarly to the quartz-chalcedony veins also replaces Sr-Ba-bearing heulandite-Ca (Fig. 3i). Stilbite is overgrown by calcite (Fig. 3f, h). Its composition is close to stoichiometry with some K and Sr (up to 0.4 apfu) substituting for Na and Ca in the extra-framework sites (Table 1, Fig. 4). XRD patterns of stilbite are shown in Figure 5.

Table 1. Representative EPMA data of laumontite (1-2), stilbite (3-6), heulandite (7-10) and smectite (11-12)

	1	2	3	4	5	6	7	8	9	10	11	12
SiO ₂	52.38	52.72	55.91	58.03	58.77	56.83	55.66	56.36	57.42	57.66	34.82	33.51
Al ₂ O ₃	20.06	20.64	14.88	15.25	14.61	15.15	16.80	14.92	15.55	15.14	13.57	13.64
Fe ₂ O ₃	0.09	0.18	bd	bd	bd	bd	bd	bd	bd	bd	18.10	19.27
MgO	0.13	0.10	0.04	bd	0.12	bd	bd	bd	bd	bd	18.77	18.67
MnO	0.03	0.05	0.06	bd	0.07	0.01	bd	0.05	0.02	bd	0.31	0.23
CaO	9.54	9.56	6.83	7.32	7.03	7.79	4.89	4.23	4.62	3.99	1.65	1.02
Na ₂ O	0.84	1.14	1.56	0.76	1.22	0.94	1.20	0.75	1.13	1.15	0.39	0.34
K ₂ O	0.72	0.69	0.52	0.08	0.24	0.03	0.53	1.02	0.59	1.33	0.14	0.18
SrO	1.28	0.81	0.57	1.05	0.39	1.39	4.42	2.83	3.67	2.98	0.30	1.08
BaO	0.01	bd	bd	0.01	bd	bd	1.27	2.89	0.75	1.56	0.11	bd
Total	85.08	85.83	80.37	82.50	82.46	82.14	84.77	83.06	83.75	83.81	86.43	86.01
	48(O)	48(O)	72(O)	72(O)	72(O)	72(O)	72(O)	72(O)	72(O)	72(O)	22(O)	22(O)
Si	16.44	16.38	27.27	27.45	27.72	27.27	26.64	27.45	27.27	27.54	5.56	5.42
Al	7.44	7.56	8.55	8.55	8.10	8.55	9.45	8.55	8.73	8.55	2.56	2.61
Fe	-	0.06	-	-	-	-	-	-	-	-	2.17	2.34
Mg	0.06	0.06	-	-	0.09	-	-	-	-	-	4.45	4.51
Mn	-	-	-	-	-	-	-	-	-	-	0.06	0.03
Ca	3.24	3.18	3.60	3.69	3.60	3.96	2.52	2.25	2.34	2.07	0.28	0.17
Na	0.54	0.66	1.44	0.72	1.08	0.90	1.08	0.72	1.08	1.08	0.11	0.11
K	0.30	0.30	0.36	0.09	0.18	-	0.36	0.63	0.36	0.81	0.03	0.03
Sr	0.24	0.12	0.18	0.27	0.09	0.36	1.26	0.81	0.99	0.81	0.03	0.11
Ba	-	-	-	-	-	-	0.27	0.54	0.18	0.27	0.00	-

bd: below detection limit, Number of cations on the basis of oxygen (O)

Laumontite: Laumontite with ideal formula $\text{Ca}_4(\text{Al}_8\text{Si}_{16}\text{O}_{48}) \cdot 18\text{H}_2\text{O}$ is a very common constituent at Kizari quarry. It is found in the matrix of hydrothermal breccias, surrounding angular fragments of andesites, and in the carbonate-rich stilbite veins. It forms white-colored acicular crystals (up to 1cm) with well-developed the {110}, {100} and {001} faces. Laumontite predates and also postdates the deposition of stilbite-Ca. The chemistry of the analyzed laumontites is very close to the stoichiometric formula. The chemical analyses show a constant Si/Al ratio (Fig. 4). Small amounts of extra-framework cations (Na up to 0.7 apfu, K up to 0.3 apfu and Sr up to 0.24 apfu) substitute for Ca (Table 1, Fig. 4). An XRD pattern of laumontite is shown in Figure 5b.

Heulandite: Heulandite series minerals with general formula $(\text{Ca}_{0.5}, \text{Sr}_{0.5}, \text{Ba}_{0.5}, \text{Mg}_{0.5}, \text{Na}, \text{K})_9$

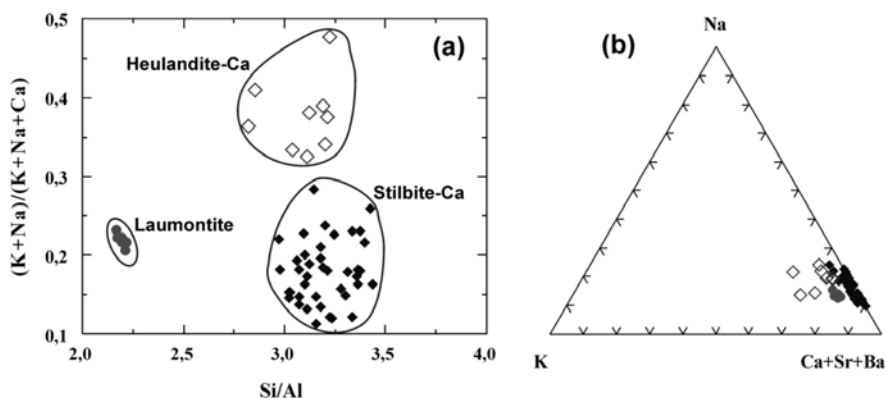


Fig. 4: Plot of zeolite compositions in terms of (a) $(K+Na)/(K+Na+Ca)$, and (b) in the ternary Na-K-(Ca+Sr+Ba) diagram.

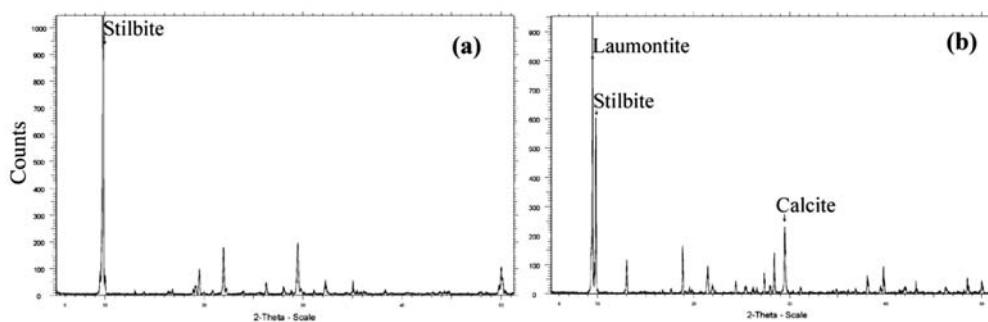


Fig. 5: X-ray diffractograms of (a) stilbite and (b) laumontite-stilbite-calcite association from Kizari.

$(Al_9Si_{27}O_{72}) \cdot 24H_2O$ display highly variable cation content, whereas Ca-, Na-, K-, Sr- and Ba-dominant compositions are known as heulandite-Ca, heulandite-Na, heulandite-K and heulandite-Sr and heulandite-Ba respectively (Coombs, et al. 1998; Larsen et al., 2005). Minerals with the same framework topology but with $Si:Al \geq 4.0$ are distinguished as clinoptilolites (Coombs et al., 1998). In both quartz-chalcedony±stilbite, and carbonate-rich stilbite-laumontite veins heulandite occurs as inclusions (up to 400 μ m) in stilbite (Figs 3c, i). The analyzed heulandites contain up to 1.2 apfu Na, 0.8 apfu K, 1.3 apfu Sr and 0.5 apfu Ba, and are characterized as Sr-Ba-rich heulandites-Ca (Table 1, Fig. 4).

6.2 Smectite

Smectite is a common constituent of the altered volcanics, forming pseudomorphs after pyroxene and hornblende, together with magnetite, pyrite, rutile, calcite and stilbite (Fig. 3d, e). It is also disseminated in the recrystallized groundmass. Representative chemical analyses are given in Table 1. The analyzed smectites contain 13.9-18.77 wt. % MgO (corresponding to 3.55-4.51 apfu Mg) and 16.16-19.67 wt. % FeO (2.03-2.83 apfu Fe).

6.3 Carbonates, Sulfates

In the carbonate-stilbite-laumontite veins, calcite postdates zeolite deposition in open spaces (Fig. 3f,

h). Calcite in green colored crystals up to 5cm is common with both skalenohedral and rhombohedral habits present. In the quartz-chalcedony±stilbite veins minor calcite predates and also postdates quartz and stilbite deposition. In the volcanic wallrocks calcite occurs in phenocryst phudomorphs as well as finely disseminated in the groundmass. Microprobe analyses indicate very minor amounts of Mn, Fe and Mg (<0.1 wt. %). Barite is present as small inclusions in stilbite crystals in the same veins.

7. Discussion-Conclusions

Zeolites occur in rocks of different mineralogical composition, age and geological environment. According to their mode of occurrence and formation environment, mainly two groups of zeolite occurrences have been distinguished (Iijima 1980; Gottardi & Galli, 1985; Hay and Sheppard 2001): (a) those formed under diagenesis to very low-grade metamorphism and (b) hydrothermal genesis. According to Hay (1966), Bargar & Keith (1995), Chipera and Apps (2001), Sheppard and Hay (2001), Utada (2001), and Marantos et al. (2007), the formation and distribution of zeolites is controlled by three main factors: a) the composition of the hostrocks, b) the variation in temperature and pressure, and c) the chemistry of pore water. In general, zeolites are formed under relatively high activity of alkalis and alkali earth elements and high pH values.

Recent studies on southeastern Rhodope zeolites in Bulgaria and Greece suggested a hydrothermal model, where the zeolitization of the volcanoclastic rocks was caused by low-temperature open hydrothermal systems in a shallow-marine environment (Raynov et al., 1997; Sheppard and Hay, 2001; Yanev et al., 2006; Marantos et al., 2007).

The present study describes stilbite-Ca, Sr-bearing heulandite-Ca and laumontite in euhedral crystals up to 3cm associated with smectite, albite, magnetite, pyrite and rutile, within epithermal-style crustiform quartz/chalcedony-calcite veins crosscutting lavas and breccias. Based on geological, petrographical, mineralogical and geochemical data the studied zeolites are of hydrothermal origin and can be regarded as integral parts of the porphyry/epithermal systems in the area. The Kizari zeolites are considered to have been formed in the transitional zone between propylitic alteration and fresh rocks and in a submarine environment as indicated by the presence of halite. The fluids were supersaturated in SiO₂ as can be deduced from the presence of chalcedony and quartz in vugs and veins of the rocks. The observed rhythmic zoning suggests alternated/repeated deposition of zeolites, calcite and smectite at several stages.

The chemical composition of zeolites at Kizari (Ca-dominant) and the absence of Na-rich zeolites (e.g. analcime) may suggest a deeper environment of formation, since at depth the impact of sea water with Na as the main constituent was rather low during zeolitic alteration as in similar zeolite occurrences in basic igneous rocks of Troodos Complex, Cyprus (Dill et al., 2007). The formation of laumontite and stilbite at Kizari may be resulted from the nature of the hydrothermal fluids, which were more enriched in Ca, Ba and Sr. Minor K and Na amounts in the zeolites at Kizari, are derived from glass present in the groundmass of the volcanics. Laumontite and stilbite formation together with albite is attributed to Ca release during breakdown of plagioclase in the rocks. In addition calcium released by the decomposition of An-rich plagioclase was taken up by calcite. This mechanism is also proposed for the laumontite-stilbite association present in stockwork-like zeolitization in the basic igneous rocks of the Troodos Complex (Dill et al., 2007). According to Dill et al. (2007), laumontite is formed at low PH₂O, whereas at higher PH₂O stilbite may crystallize according to the following reactions: anorthite + quartz + 4H₂O → laumontite and anorthite + quartz + 7H₂O → stilbite. The studied zeolites were formed at relatively low temperatures (<140°C), since stilbite coexists with heulandite and laumontite between 110 and 120 °C (Bargar 1994), and in the Troodos Complex

stilbite has derived from laumontite as temperature and pressure dropped below about 140 °C (Dill et al. 2007). In zoned sequences of zeolites in amygdales and veins in the North Mountain Basalt, Nova Scotia, the succession of mordenite → heulandite → stilbite are interpreted as developing under falling temperatures by active hydrothermal circulation (Pe-Piper, 2000).

The amount of the Kizari zeolites is not feasible for exploitation, however the broad area should be considered as target for future exploration. Under consideration of their abundant zeolitic veins and alteration, the quarried lavas are probably not much suitable materials for construction purposes. Nevertheless, the studied zeolites may provide valuable mineralogical specimens suitable for museum collections and educational purposes. Based on this assumption, the Kizari quarry should be protected and considered as a visiting site in a broad Mineralogical-Petrological geotope in Rhodopi region.

8. References

- Arikas, K., 1980. Geologische und petrographische Untersuchungen in Umgebung von Kirki (Thrazien, Griechenland), *Mitteilungen aus dem Geologisch-Paläontologischen Institut der Universität Hamburg*, 49, 1-26.
- Arikas, K., and Voudouris, P., 1998. Hydrothermal alterations and mineralizations of magmatic rocks in the southern Rhodope Massif. *Acta Volcanologica*, 10, 353-365.
- Bargar, K.E., 1994. Hydrothermal alteration in the SUNEDCO 58-28 geothermal drill hole near Breitenbush Hot Springs, Oregon. *Oregon Geol. Soc.*, 56, 75-87.
- Bargar, K.E. and Keith, T.E.C., 1995. Calcium zeolites in rhyolitic drill cores from Yellowstone national park, Wyoming. In D.W. Ming, and F.A. Mumpton (eds), *Natural Zeolites*, International Committee on Natural Zeolites, Brockport, New York, 69-86.
- Bitsios, D., 1973. *La géologie et métallogénie de la région de Kirki* (Thrace Occidentale - Grèce). Thèse 3. Cycle, Univ. Paris VI, 100pp.
- Chipera, S.J., and Apps, J.A., 2001. Geochemical stability of natural zeolites. In D.L. Bish and D.W. Ming (eds) *Natural Zeolites: Occurrence, Properties, Applications. Rev. Mineral. Geochem.*, Mineralogical Society of America and the Geochemical Society, 45, 117-161.
- Christofides, G., Pecskey, Z., Soldatos, T., Eleftheriadis, G., and Koroneos, A., 2004. The Tertiary Evros volcanic rocks (Greece): Petrology, K/Ar geochronology and volcanism evolution. *Geologica Carpathica*, 55, 397-409.
- Coombs, D.S., Alberti, A., Armbruster, T., Artioli, G., Colella, C., Galli, E., Grice, J.D., Liebau, F., Mandarino, J.A., Minato, H., Nickel, E.H., Passaglia, E., Peacor, D.R., Quartieri, S., Rinaldi, R., Ross, M., Sheppard, R.A., Tillmanns, E., Vezzalini, G., 1998. Recommended nomenclature for zeolite minerals: Report of the Subcommittee on Zeolites of the Mineralogical Association, Commission on New Minerals and Mineral Names. *European Journal of Mineralogy*, 10, 1037-1081.
- Del Moro, A., Innocenti, F., Kyriakopoulos, C., Manetti, P. and Papadopoulos, P., 1988. Tertiary granitoids from Thrace (Northern Greece): Sr isotopic and petrochemical data. *Neues Jahrbuch für Mineralogie Abhandlungen*, 159, 113-135.
- Dill, H.G., Füssl, M., and Botz, R., 2007. Mineralogy and (economic) geology of zeolite-carbonate mineralization in basic igneous rocks of the Troodos Complex, Cyprus. *Neues Jahrbuch für Mineralogie Abhandlungen*, 183, 251-268.
- Eleftheriadis, G., 1995. Petrogenesis of the Oligocene volcanics from the Central Rhodope massif (N. Greece). *European Journal of Mineralogy*, 7, 1169-1182.
- Extra Lapis 2007. *Zeolithe. Mineralien-zugleich nützlich und wunderschön*, Christian Weise Verlag,

München, 97pp.

- Filippidis, A., 1993. New find of moissanite in the Metaxades zeolite-bearing volcanoclastic rocks, Thrace county, Greece. *Neues Jahrbuch für Mineralogie Monatshefte*, 11, 521-527.
- Filippidis, A., Kougoulis, C., Michailidis, K., 1988. Sr-bearing stilbite in a quartz-monzonite from Vathi, Kilkis, Northern Greece. *Schweizerische Mineralogische und Petrographische Mitteilungen*, 68, 67-76.
- Filippidis, A., and Kantiranis, N., 2005. Industrial, agricultural and environmental uses of the natural zeolites of Thrace. *Bull. Geol. Soc. Greece*, 37, 90-101.
- Gottardi, G., and Galli, E., 1985. *Natural Zeolites*. Springer-Verlag, Berlin, Germany, 409pp.
- Greenwich Resources plc (2004) *The Sapes project – simplified regional geology*.
- Hall, A., Stamatakis, M., and Walsh, J.N., 2000. The Pentalofos zeolitic tuff formation: a giant ion-exchange column. *Annales Geologiques des Pays Helleniques*, 38, 175-192.
- Hay, R.L., 1966. Zeolite and zeolite reactions in sedimentary rocks. *Geological Society of America Special Paper*, 85, 130pp.
- Hay, R.L., Sheppard, R.A., 2001. Occurrence of zeolites in sedimentary rocks: An overview. In D.L. Bish and D.W. Ming (eds), *Natural zeolites: occurrence, Properties, Applications*, *Rev. Mineral. Geochem.*, Mineralogical Society of America and the Geochemical Society, 45, 217-234.
- Iizima, A., 1980. Geology of natural zeolites and zeolitic rocks. *Pure and Applied Chemistry*, 52, 2115-2130.
- Innocenti, F., Kolios, N., Manetti, O., Mazzuoli, R., Peccerillo, G., Rita, F., and Villari, L., 1984. Evolution and geodynamic significance of the Tertiary orogenic volcanism in northeastern Greece. *Bulletin of Volcanology*, 47, 25-37.
- Karafoti, M. and Arikas, K. 1990. Petrography and geochemistry of Tertiary volcanic rocks between Lutra and Fere (Thrace, Northeastern Greece). *Geologica Rhodopica*, 2, 227-240.
- Kassoli-Fournaraki, A., Stamatakis, M., Hall, A., Philippidis, A., Michailidis, K., Tsirambides, A., and Koutles, Th., 2000. The Ca-rich clinoptilolite deposit of Pentalofos, Thrace, Greece. In C Collela and F.A. Mumpton (eds), *Natural Zeolites for the Third Millennium*, DeFredda Editore, Naples, Italy 193-202.
- Kirov, G.N., Filippides, A., Tsirambidis, A., Tzvetanov, R.G. and Kassoli-Fournaraki, A., 1999. Zeolite-bearing rocks in Petrota area (Eastern Rhodope Massif, Greece). *Geologica Rhodopica*, 2, 500-511.
- Kitsopoulos, K., Dunham, A., 1994. Application of zeolitic volcanic tuffs from Greece (Lefkimi-Dadia, Metaxades and Santorini island, Greece, as pozzolanic materials. *Bull. Geol. Soc. Greece*, 30, 323-333.
- Koshariis, G., Karantassi, S. and Gregoriades, G., 1987. *Zeolite Occurrences in West Thrace*. I.G.M.E. Internal report, 30pp.
- Krohe, A., and Mposkos, E., 2001. Structural evolution and exhumation history of the Rhodope UHP-HP metamorphic province (Northern Greece). *Bull. Geol. Soc. Greece*, 34, 75-82.
- Larsen, A.O., Nordrum, F.S., Döbelin, N., Armbruster, T., Petersen, O.V., and Erambert, M., 2005. Heulandite-Ba, a new zeolite species from Norway. *European Journal of Mineralogy*, 17, 143-153.
- Magganas A., Kyriakopoulos K., Sideris C. and Eleftheriadis G., 2004. Petrological and Geochemical Variations of the Tertiary Convergent Volcanism in North-Eastern Greece. *Annales Geologiques des Pays Helleniques*, 40, 99-116.
- Marantos, I., Koshariis, G., Karantassi, S. and Gregoriades, G., 1989. A study on zeolitic alteration of Tertiary pyroclastics from Metaxades area, Evros county, Greece. *Bull. Geol. Soc. Greece*, 23, 443-450.

- Marantos, I., Koshiaris, G., Karantassi, S., Perdikatsis, V. and Christidis, G., 2004. Preliminary study of altered Tertiary volcanoclastic rocks in the area of Asproula, Nea Santa, Rodopi prefecture, Thrace, NE Greece. *Bull. Geol. Soc. Greece*, 35, 454-463.
- Marantos, I., 2004. *Study of the Tertiary volcanic rocks alteration in the Feres basin of Evros prefecture, emphasizing on the genesis of zeolites and their possible applications*. PhD thesis, Technical University of Crete, Department of Mineral Research Engineering, Chania, Greece. 264pp.
- Marantos, I., Markopoulos, T., and Christidis, G.E., 2007. Zeolitic alteration in the Tertiary Feres volcano-sedimentary basin, Thrace, NE Greece. *Mineralogical Magazine*, 71, 327-345.
- Melfos, V., Vavelidis, M., Christofides, G., and Seidel, E. 2002. Origin and evolution of the Tertiary Maronia porphyry copper–molybdenum deposit, Thrace, Greece. *Mineralium Deposita* 37, 648-668.
- Michael, K., Dimitriades, A., Mastrogiannidou, K., and Angelopoulos, A. 1984. *Ore deposits study at Virini-Pessani-Lefkimi area, Evros prefecture*, IGME internal report, 64pp (in Greek).
- Ortelli, M., Moritz, R., Voudouris, P., Spangenberg, J., 2009. Tertiary porphyry and epithermal association of the Sapes-Kassiteres district, eastern Rhodopes, Greece, In Williams et al. (eds) Smart Science for exploration and mining, *Proc. of the 10th Biennial SGA meeting, Townsville*, 536-538.
- Papadopoulos, P., and Anastasiadis, I., 2003. *Geology of Tertiary basins of SE Rhodope, Thrace*. IGME internal report, 20 pp. (in Greek).
- Papavasiliou, K.T, and Sideris, K., 1984. Geochemistry and mineralogy of Tertiary lavas of Sappai-Ferai area (W-Thrace)-Greece. Implications on their origin. IGME - *Geochemical Research*, 4, 21pp.
- Pe-Piper, G., 2000. Mode of occurrence, chemical variation and genesis of mordenite and associated zeolites from the Morden area, Nova Scotia, Canada. *Canadian Mineralogist*, 38, 1215-1232.
- Pe-Piper, G., Christofides, G., and Eleftheriadis, G., 1998. Lead and neodymium isotopic composition of Tertiary igneous rocks of northeastern Greece and their regional significance. *Acta Volcanologica*, 10, 255-263.
- Perraki, T., and Orfanoudaki, A., 2004. Mineralogical study of zeolites from Pentalofos area, Thrace, Greece. *Applied Clay Science*, 25, 9-16.
- Raynov, N., Popov, N., Yanev, Y., Petrova, P., Popova, T., Hristova, V., Atanasova, R. and Zankarska, R. 1997. Geological, mineralogical and technological characteristics of zeolitized (clinoptilolitized) tuff deposits in the Eastern Rhodopes, Bulgaria. In G. Kirov, L. Filizova and O. Petrov (eds), *Natural zeolites - Sofia '95*. Pensoft, Sofia, 263-275.
- Shawh A.J, Constantinides D.C, 2001. The Sappes gold project. *Bull. Geol. Soc. Greece* 34, 1073-1080.
- Sheppard, R.A. and Hay, R.L., 2001. Formation of zeolites in open hydrologic systems. In D.L. Bish and D.W. Ming (eds). *Natural Zeolites: Occurrence, Properties, Applications*. Rev. Mineral. Geochem., Mineralogical Society of America and the Geochemical Society, 45, 261-276.
- Skarpelis, N., Marantos, I., Christidis, G., 1993. Zeolites in Oligocene volcanic rocks, Dadia-Lefkimi area, Thrace, Northern Greece: Mineralogy and cation exchange properties, *Bull. Geol. Soc. Greece*, 28, 305-315.
- Stamatakis, M., Hall, A., Hein, J.R, 1996. The zeolites deposits of Greece. *Mineralium Deposita*, 31, 473-481.
- Stamatakis, M., Hall, A., Lutat, U., and Wlsch, J.N. 1998. Mineralogy, origin and commercial value of the zeolite-rich tuffs in the Petrota-Pentalofos area, Evros county, Greece. *Estudios Geologicos*, 54, 3-15.
- Tsirambides, A., Kassoli-Fournaraki, A., Filippidis, A., and Soldatos, K. 1989. Preliminary results on clinoptilolite-containing volcanoclastic sediments from Metaxades, NE Greece. *Bull. Geol. Soc. Greece*, 23, 451-460.

- Tsirambides, A., Filippidis, A., and Kassoli-Fournaraki, A., 1993. Zeolitic alteration of Eocene volcaniclastic sediments at Metaxades, Thrace, Greece. *Applied Clay Science*, 7, 509-526.
- Tsolis-Katagas, P., and Katagas, C., 1990. Zeolitic diagenesis of Oligocene pyroclastic rocks of Metaxades area, Thrace, Greece. *Mineralogical Magazine*, 54, 95-103.
- Voudouris, P., 1993. *Mineralogical, geochemical and fluid inclusion studies on epithermal vein type gold-silver mineralizations at Kassiteres/Sapes, (NE- Greece)*. Ph.D. thesis, Univ. Hamburg, 218pp.
- Voudouris, P., Tarkian, M., Arikas, K., 2006. Mineralogy of telluride-bearing epithermal ores in Kassiteres-Sappes area, western Thrace, Greece. *Mineralogy and Petrology*, 87, 31-52.
- Utada, M., 2001. Zeolites in hydrothermally altered rocks In D.L. Bish and D.W. Ming (eds). *Natural zeolites: Occurrence, properties, applications*. *Rev. Mineral.Geochem.*, Mineralogical Society of America and the Geochemical Society, 45, 305-319.
- Yanev, Y., Cochemé J.J., Ivanova R., Grauby, O., Burlet E., and Pravchanska, R., 2006. Zeolites and zeolitization of acid pyroclastic rocks from paroxysmal Paleogene volcanism, Eastern Rhodopes, Bulgaria. *Neues Jahrbuch für Mineralogie Abhandlungen*, 182, 265-283.

ΕΥΡΕΤΗΡΙΟ ΣΥΓΓΡΑΦΕΩΝ AUTHOR INDEX



- Adamaki A.K.: 1984
Agalos A.: 2005
Aidona E.: 1888
Albanakis K.: 2383
Alexandratos V.G.: 2310
Alexandri M.: 1056
Alexandropoulou S.: 989
Alexandrou M.: 1888
Alexopoulos A.: 1792
Alexopoulos J.D.: 1898
Alexouli-Livaditi A.: 737
Alkalais E.: 1286
Amerikanos P.: 1149
Anagnostou Ch.: 2426
Anagnostoudi Th.: 548
Angelopoulos A.: 1094
Antonakos A.: 1821
Antonarakou A.: 568, 613, 620, 763
Antonelou A.: 876
Antoniu A.A.: 1104
Antoniu Var.: 320
Antoniu Vas.: 320
Apostolaki Ch.: 2570
Apostolidis Em.: 1418, 1619, 1850
Apostolidis N.: 2532
Apostolidis N.: 2597
Arapogiannis E.: 2229
Argyraki A.: 1737, 2319, 2510
Argyriadis I.: 264
Arvanitidis N.D.: 2437
Arvanitis A.A.: 1907, 2246
Astiopoulos A.C.: 1994
Athanasoulis E.: 939
Avgerinas A.: 276
Avramidis P.: 558, 654
Ballas D.: 1056, 1737
Baltzois V.: 1149
Bantekas I.: 829
Barbera G.: 663
Barbu O.: 594
Baskoutas I.: 2125
Bathrellos D.G.: 1637
Bathrellos G.D.: 1572
Batsalas A.: 697
Baziotis I.: 2485, 2522, 2667
Behrends T.: 2310
Bel-lan A.B.: 2338
Bellas M.: 1619
Bellas S.: 579
Beshku H.: 1777
Birke M.: 2338, 2350
Bizoura A.: 1314
Bloukas S.: 1149
Bonsall T.A.: 2406
Bourliva A.: 2532
Bourouni P.: 2540
Brachou C.: 907
Brauer R.: 1267
Brusca L.: 2327
Burgess W.: 1716
Caputo R.: 400, 486
Carey S.: 1056
Catalano S.: 400
Chailas S.: 1919
Chalkias D.: 1335
Charalambopoulos S.: 1878
Chatzaras V.: 387
Chatziangelou M.: 1112
Chatzipanagis I.: 2702
Chatzipetros Al.: 486, 1131, 1383
Chiotis E.: 1539, 1549
Chousianitis K.G.: 1572, 2005
Christanis K.: 224, 2218
Christaras B.: 1112, 1122, 1131, 1267, 1672
Christidis G.E.: 2553, 2562, 2570
Christofides G.: 2680
Christoforidou P.: 1678
Çina A.: 2577
Codrea V.: 594
D' Alessandro W.: 2327
Daftsis E.: 1737
Dasaklis S.: 737
De Vos W.: 2350
Delagrammatikas G.: 2485
Delimani P.: 1074
Demetriades A.: 2338, 2350
Depountis N.: 1138, 1210
Dermitzakis M.D.: 86, 978
Diakakis M.: 1323
Diamantis I.: 1697
Diasakos N.: 1149
Dilalos S.: 1898
Dimitrakopoulos D.: 1688
Dimitriou D.: 2229
Dimiza M.D.: 602, 763
Dominic Fortes A.: 2726
Dotsika E.: 886, 958, 1840, 2265, 2383
Doutsou I.: 1350
Doveri M.: 1840
Drakatos G.: 1994
Drinia H.: 613, 620, 763
Dunkl I.: 276
Duris M.: 2338
Economou G.: 804, 2485
Economou N.: 1802
Eikamp H.: 918
Epitropou N.: 939
EuroGeoSurveys Geochemistry Expert Group: 2338, 2350
Exioglou D.: 1230
Fadda S.: 2446, 2588
Fakiris E.: 1064
Falalakis G.: 276
Fassoulas C.: 746
Fassoulas C.: 781, 896, 918
Ferentinos G.: 176, 1018, 1064
Fermeli G.: 978, 989
Fernandez-Turiel J.L.: 2373
Fikos I.: 1953
Filippidis A.: 2373, 2532, 2597, 2762
Filippidis S.: 2597
Fiori M.: 2446, 2588
Foscolos A.E.: 8, 2294
Fotopoulou M.: 2218
Foumelis M.: 1301
Foundas P.: 989
Fountoulis I.: 1046
Frisch W.: 276
Gaki-Papanastassiou K.: 409, 418, 506
Galanakis D.: 1428, 1465
Galbenis C.T.: 2485
Ganas A.: 1607
Garver J.J.: 309
Gawlick H-J.: 276
Georgakopoulos A.N.: 1230, 2236, 2274
Georgiadis I.K.: 2606
Georgiadis P.: 1406
Georgiou A.: 2492
Georgiou Ch.: 1428

Georgiou P.: 1056
 Georgoulas A.: 1074
 Geraga M.: 1018, 1064
 Germenis N.: 989
 Gerogianni N.: 2786
 Gerolymatou E.: 1438
 Gialamas J.: 1777
 Giannakopoulos A.: 958
 Giannouloupoulos P.: 1438, 1447
 Gimeno D.: 2373
 Gioti Ev.: 1627
 Gkadi E.: 548
 Gkiolas A.: 1272
 Gkiougkis I.: 1697
 Golubović Deligani M.: 1582
 Gospodinov D.: 1994
 Gournelos Th.: 1335, 1647
 Hademenos V.: 1539
 Hagiou E.: 1157
 Haidarlis M.: 907
 Hamdan H.: 1802
 Handler R.: 299
 Hatzipanagiotou K.: 876, 2501, 2540, 2617, 2712
 Helly B.: 845
 Iatrou M.: 1018
 Ili I.: 1590, 1688
 Iliopoulos G.: 746, 781, 918
 Īnaner H.: 2218
 Ioakim Chr.: 1035
 Ioannidis N.: 1888
 Janikian Z.: 939
 Jenkyns H.C.: 627
 Jipa-Murzea C.: 594
 Kacandes G.: 2562
 Kadetova A.V.: 1341
 Kafkala I.G.: 2390
 Kafousia N.: 627
 Kalantzi F.: 1350
 Kalisperi D.: 654
 Kallergis G.: 1821
 Kallioras A.: 69, 1697
 Kalogerogiannis G.: 1149
 Kamberis E.: 289, 715
 Kanaris D.: 1202, 1230
 Kantiranis N.: 2762
 Kapetanidis V.: 2015
 Karageorgiou D.E.: 1457, 1601, 2229, 2236, 2274, 2692
 Karageorgiou M.M.D.: 1601, 2236, 2274
 Karagianni A.: 1165
 Karagianni E.: 495
 Karakaisis G.F.: 46, 2026
 Karakitsios V.: 627, 634, 663
 Karakonstantis A.: 2043
 Karakostas V.G.: 1984, 1994, 2053, 2064, 2075, 2093, 2114
 Karalemas N.: 1707
 Karamanos Ch.K.: 2053, 2075
 Karapanos E.: 1716
 Karastathis V.K.: 1438
 Karfakis J.: 1619
 Kargiotis E.: 2257
 Karipi S.: 2617, 2712
 Karmis P.D.: 1393, 1438, 1447, 1919
 Karoutzos G.: 1165
 Karydakias Gr.: 2246, 2265
 Karymbalis E.: 409, 418, 1601
 Kastanioti G.: 2786
 Kastanis N.: 169
 Katagas Ch.: 247
 Kati M.: 2786
 Katrivanos D.E.: 999
 Katsanou K.: 1726, 1878, 2218
 Katsiki P.: 2562
 Katsikis J.: 2692
 Katsonopoulou D.: 812
 Kaviris G.: 2084
 Kelepertsis A.: 1858
 Kelepertzis E.: 1737
 Kementzetzidou D. A.: 2053
 Keupp H.: 579
 Khak V.A.: 1192
 Kidd W.S.F.: 309
 Kilias A.: 276, 2075, 2114
 Kilias S.P.: 2646
 Kiratzi A.: 2135, 2144
 Kitsopoulos K.: 2455, 2625
 Kokinou E.: 289
 Kokkalas S.: 368, 428
 Kokkidis N.: 548
 Kolaiti E.: 1286
 Kolios N.: 2246
 Kondopoulou D.: 1888, 1972
 Konstantinidi-Syvridi E.: 804
 Konstantopoulou G.: 1157, 1619
 Kontakiotis G.: 763
 Kontogianni V.: 886, 1202
 Kontopoulos N.: 558, 643, 654
 Koravos G.Ch.: 2193
 Koroneos A.: 2606, 2680, 2752
 Koskeridou E.: 613
 Kosmidis E.: 1812
 Kossiaris G.: 939
 Kostopoulou V.: 726
 Kotsovinos N.: 1074
 Kougemitrou I.: 804
 Kouki A.: 1169, 1177, 1184
 Koukidou I.: 1747
 Koukis G.: 1138, 1165, 1210, 1508, 1619
 Koukoulis A.: 1457
 Koukouvelas I.: 368, 1350
 Koulouris S.: 1210
 Koumantakis I.: 1590, 1656
 Kounis G.D.: 1758, 1767, 1821
 Kounis K.G.: 1758, 1767
 Kourkouli P.: 1301
 Kourkounis S.: 643
 Koutsinos S.: 2246
 Koutsios A.: 654
 Koutsopoulou E.: 2635
 Koutsouveli An.: 1418, 1619
 Kozireva E.A.: 1341
 Kozyreva E.A.: 1192
 Kranis H.: 1919
 Kritikou S.: 1007
 Ktena S.: 1165
 Ktenas D.: 548
 Kurz W.: 299
 Kynigalaki M.: 1202, 1619
 Kyriakopoulos K.G.: 309, 663, 2327, 2361, 2726
 Kyrousis I.: 1406
 Lagios E.: 344, 2005
 Lainas S.: 1138, 1210
 Lalechos N.S.: 442
 Lalechos S.N.: 442
 Lambrakis N.: 1716, 1726, 1878, 2218
 Lampropoulou P.: 2465
 Laskaridis K.: 2475
 Lasocki S.: 2114
 Lazaridis A.: 1840, 2383
 Lazaris S.: 2390
 Lehmann P.: 1831
 Leivaditi A.: 1406
 Lekkas E.: 1361
 Lekkas S.: 1707
 Lelli M.: 1840
 Lemesios I.: 1878
 Leone G.: 886
 Leontakianakos G.: 2485
 Leptokaropoulos K.M.: 2093
 Liakopoulos S.: 1438
 Limnios N.: 2200
 Locutura J.: 2338
 Lois A.: 2183
 Loukaidi V.: 737
 Loupasakis C.: 1219, 1230, 1465, 1619, 1850
 Lycourghiotis S.: 1029
 Lykakis N.: 2646
 Lykoudi E.: 1314, 1406
 Lykousis V.: 1046
 Magganas A.: 2786

Makri K.: 169, 999
 Makris J.: 32, 357
 Makrodimitras G.: 675
 Makropoulos K.C.: 216, 2005, 2015, 2084, 2104, 2163
 Malandraki V.: 1094
 Malandrakis E.: 1149
 Malegiannaki I.: 1007
 Maneta V.: 685
 Manoutsoglou E.: 697, 1314, 2492
 Maramathas A.: 1777
 Marinos P.V.: 1238, 1248, 1259
 Marinov S.P.: 2398
 Mariolakos I.D.: 92, 821, 829, 1785
 Markantonis K.: 1406
 Maroukian H.: 409, 418, 506
 Marsellos A.E.: 309
 Martelli M.: 2327
 Matiatos I.: 1792
 Mavromatis T.: 1131
 Mazzoleni P.: 663
 Melfos V.: 845, 948
 Mertzaniides Y.: 1802, 1812, 1962, 2257
 Metaxas A.: 2229, 2236, 2265, 2274
 Metaxas Ch.P.: 442
 Michail K.: 939
 Michailidis K.: 2532, 2657
 Midoun M.: 264
 Migiros G.: 320
 Mirek J.: 2114
 Mitropoulos A.: 2257
 Mitropoulos D.: 1474
 Monaco C.: 400
 Moraiti E.: 1267
 Moshou A.: 2104
 Moumou Ch.: 706
 Mountrakis D.M.: 276, 495
 Mourtzas N.D.: 453, 1272, 1286
 Mpalsats I.: 2501
 Mposkos E.: 2522, 2667
 Mwila G.: 1697
 Nastos P.T.: 1335
 Neuweiler I.: 1831
 Nicolaou E.: 939
 Nikas K.: 1821
 Nikolaidis A.: 989
 Nikolakopoulos K.: 1486, 1627, 1647
 Nikolaou N.: 1202, 1393, 1619
 Nikolaou P.: 706
 Nikolopoulos V.: 829
 Nomikou P.: 464, 1056
 Novikova T.: 1438
 Ntontos P.: 264
 Oikonomopoulos I.: 2284
 Or D.: 1831
 Orlecka-Sikora B.: 2093
 Palyvos N.: 829
 Pambuku A.: 1777
 Panagiotakopoulou O.: 643
 Panagiotaras D.: 558
 Panagiotopoulos V.: 548
 Panagopoulos A.: 1678, 1747
 Panagopoulos G.: 2492
 Panoussi P.: 634
 Pantelaki O.: 697
 Papadimitriou E.: 1994, 2200
 Papadimitriou E. E.: 1984, 2053, 2064, 2075, 2093, 2114
 Papadimitriou P.: 2005, 2015, 2043, 2084, 2104
 Papadopoulos A.: 2680
 Papadopoulos G.A.: 1438
 Papadopoulou L.: 845
 Papadopoulou S.: 548
 Papaefthymiou S.: 2465
 Papafotiou A.: 1831
 Papageorgiou E.: 331, 344
 Papakonstantinou K.: 1840
 Papamantellos D.: 2465
 Papamarinopoulos S.P.: 105
 Papanastassiou D.: 1438
 Papanicolaou C.: 2294
 Papanikolaou D.: 72, 464, 475
 Papanikolaou G.: 2236, 2265, 2274
 Papanikolaou I.: 320
 Papanikolaou M.: 475
 Papanikos D.: 939
 Papastamatiou D.: 2510
 Papastefanou C.: 2680
 Papastergios G.: 2373, 2597, 2762
 Papathanassiou G.: 486, 1122, 1131, 1373, 1383
 Papatheodoropoulos P.: 989
 Papatheodorou G.: 1018, 1064
 Papazachos B.C.: 46
 Papazachos C.B.: 46, 495, 1930, 2026, 2064
 Papoulia J.: 357
 Papoulis D.: 558, 876, 2635
 Paradisopoulou P.M.: 2114
 Paragios I.: 2597
 Paraskevopoulos K.M.: 2752
 Parcharidis I.: 1301, 1582
 Parpodis K.: 2390
 Pasadakis N.: 2294
 Pashos P.: 939
 Passas N.: 1286
 Patronis M.: 2475
 Pavlides S.: 169, 486, 1122, 1373, 1383, 1607
 Pavlides Sp.: 1131
 Pavlidou S.: 939
 Pavlopoulos A.: 715
 Pavlopoulos K.: 1582
 Pechlivanidou S.: 706
 Perdikatsis V.: 2570
 Perissoratis C.: 1035
 Perraki M.: 804
 Perraki Th.: 2284
 Persianis D.: 2692
 Petrakaki N.: 2319
 Photiades A.: 726, 1495
 Pikoulis V.E.: 2183
 Pitsonis I.S.: 2193
 Plessa A.: 2193
 Pliakas F.: 1697
 Ploumis P.: 2702
 Pomoni-Papaioannou F.: 620, 726, 793
 Pomonis P.: 2617, 2712
 Pontikes Y.: 856
 Popandopoulos G.: 2125
 Poulakis N.: 1149
 Poulos S.E.: 506
 Poutoukis D.: 886, 2383
 Poyiadji El.: 1393, 1619
 Pratikakis A.: 2562
 Pretti S.: 2446, 2588
 Psarakis E.Z.: 2183
 Psomiadis D.: 886, 958, 1840, 2383
 Puglisi D.: 663
 Pyliotis I.: 548
 Pyrgakis D.: 1138
 Pyrgiotis L.: 1619
 Raco B.: 1840
 Rathossi C.: 856
 Rausch R.: 69
 Reimann C.: 2350
 Rigopoulos I.: 2501, 2617, 2712
 Rizzo A.: 2327
 Romagnoli G.: 400
 Rondoyanni Th.: 379, 1406
 Roumelioti Z.: 1438, 2135, 2144
 Rousakis G.: 1056
 Rozos D.: 1177, 1184, 1219, 1406, 1465, 1590, 1637, 1656, 1850
 Sabatakakis N.: 1138, 1165, 1210, 1619
 Sabatakakis P.: 1508
 Sakelaris G.: 2786
 Sakellariou D.: 1046, 1056
 Salminen R.: 2350
 Sarris A.: 289
 Sboras S.: 486, 1607
 Schüth C.: 69

- Schütz C.: 1831
 Scordilis E.M.: 46, 2026, 2154
 Sdrolia S.: 845
 Seeber L.: 2075
 Segou M.: 2163
 Serelis K.G.: 2390
 Serpetsidaki A.: 2174
 Siavalas G.: 2218
 Sideri D.: 1850
 Sifakis A.: 907
 Sigalos G.: 737
 Sigurdsson H.: 1056
 Sikalidis C.: 2373, 2532, 2597, 2762
 Skarlatoudis A.A.: 1930
 Skarpelis N.: 2417, 2510, 2553
 Skianis G.Aim.: 1627, 1647
 Skilodimou H.D.: 1572, 1637
 Skordas K.: 1858
 Smith D.C.: 804
 Sofianska E.: 2657
 Sokos E.: 989, 2174, 2183
 Soldatos T.: 2752
 Solomonidou A.: 2726
 Sotiropoulos P.: 344
 Sotiropoulos S.: 715
 Soulios G.: 196
 Soulis V.J.: 1094
 Soupios P.: 654
 Spanos D.: 368
 Spanou N.: 1230, 1619
 Spassov S.: 1972
 Spry P.G.: 2406
 Spyridonos E.: 1314, 1785, 2492
 Spyropoulos N.: 886
 St. Seymour K.: 2406
 Stamatakis G.: 2739
 Stamatakis M.: 2606, 2739, 2773
 Stamatis G.: 1868, 1878
 Stamboliadis E.: 697
 Stampolidis A.D.: 1907
 Stefanova M.: 2398
 Stiros S.: 886, 1029
 Stivanakis V.: 2465
 Stoulos S.: 2680
 Stoykova K.: 675
 Stratikopoulos K.: 1726
 Svana K.: 746
 Symeonidis K.: 1286
 Syrides G.: 1131
 Tagkas Th.: 1149
 Tarvainen T.: 2350
 Tassiou S.: 1520
 Theocharis D.: 821
 Theodorou D.: 1335
 Theodorou G.: 763
 Theodosiou Ir.: 926, 939
 Theodosoglou E.: 2752
 Thomopoulos Ach.: 1112
 Thomopoulos K.: 1064
 Tombros S.F.: 2406
 Tortorici G.: 400
 Tortorici L.: 400
 Tougiannidis N.: 2284
 Tranos M.D.: 495, 2064
 Triantafyllidis S.: 2417
 Triantafyllou G.: 2294
 Triantaphyllou M.: 475, 602, 634, 715, 754, 763,
 Trontzios G.: 2657
 Tryfonas G.: 1149
 Tsagas D.: 1335
 Tsaklidis G.M.: 1984, 2200
 Tsanakas K.: 418, 506
 Tsangaratos P.: 1406, 1590, 1656, 1688
 Tsapanos T.M.: 2193
 Tsaparas N.: 620
 Tselentis G–A.: 2174
 Tselepidis V.: 379
 Tsiambaos G.: 183, 1104, 1259
 Tsikouras B.: 876, 2501, 2540, 2617, 2712
 Tsimas S.: 2485
 Tspoura–Vlachou M.: 663
 Tsirambides A.: 2606, 2762
 Tsirigotis N.: 1149
 Tsobanoglou C.: 1812
 Tsokas G.N.: 1907
 Tsolakis E.: 763
 Tsolis–Katagas P.: 856, 2635
 Tsombos P.: 1438, 1447, 1486, 1528, 1539, 1547, 1539, 1548, 1559
 Tsoukala E.: 958
 Tsourlos P.: 1962
 Tzamos E.: 2762
 Tzanaki I.: 289
 Tzani A.: 344, 1919, 1941
 Tzavidopoulos I.: 886
 Tzevelekou Th.: 2465
 Tziritis E.: 1858
 Tzortzaki E.: 613
 Vafidis A.: 1802
 Vagenas N.: 1165
 Vagenas S.: 1210
 Vagioteu E.: 1149
 Vaiopoulos D.: 1627, 1647
 Vakalas I.: 675, 697
 Vako E.: 1777
 Valera P.: 2446, 2558
 Valiakos I.: 965
 Valkaniotis S.: 486, 1383
 Vamvakaris D.: 495
 Van Cappellen P.: 2310
 Varaggouli E.: 1074
 Vargemezis G.: 1953, 1962
 Varnavas S.: 234
 Varvarousis G.: 2229, 2265
 Vasilatos Ch.: 2773
 Vassiliades E.: 1520
 Vassiliou E.: 1688
 Vassilopoulou S.: 516
 Vaxevanopoulos M.: 948
 Vitsas T.: 989
 Vlachopoulos I.: 1165
 Vlachou–Tspoura M.: 2773
 Vogiatzis D.: 2762
 Vontobel P.: 1831
 Votsi I.: 2200
 Voudouris K.: 1678
 Voudouris P.: 685, 845, 2786
 Vougioukalakis G.: 939
 Voulgaris N.: 2163
 Vouvalidis K.: 706, 1122
 Vrettos K.: 2236
 Vythoulkas N.K.: 2193
 Wölfler A.: 299
 Xeidakis G.: 1074
 Xypolias P.: 368, 387
 Zagana E.: 1726, 1878
 Zambetakis–Lekkas A.: 773
 Zananiri I.: 1474, 1539, 1549, 1972
 Zanchetta G.: 886
 Zelilidis A.: 643, 675, 697, 793
 Zerefos C.S.: 2
 Zervakou A.D.: 1528, 1539, 1549, 1559
 Zevgitis T.: 989
 Ziannos V.: 1812
 Zidianakis G.: 781
 Zisi N.: 958, 1840, 2383
 Zorba T.: 2752
 Zoumpoulis E.: 793
 Zouridakis N.: 1792
 Zouros N.: 159, 896, 965
 Zygouri V.: 527